2011 IEEE International Ultrasonics Symposium
(IUS 2011)

including Short Courses and Exhibition

Caribe Royale All-Suite Hotel & Convention Center

Orlando, Florida, USA

October 18-21, 2011

Sponsored by the IEEE Ultrasonics, Ferroelectrics and Frequency Control Society (UFFC-S)

Table of Contents

Oral Sessions, Wednesday, October 19, 2011:

Poster Sessions, Wednesday, October 19, 2011:

Oral Sessions, Thursday, October 20, 2011:

Poster Sessions, Thursday, October 20, 2011:

Oral Sessions, Friday, October 21, 2011:

Poster Sessions, Friday, October 21, 2011:

Welcome from the General Co-Chairs

Ken-ya Hashimoto
Chiba University

Clemens Ruppel
EPCOS AG,

The 2011 IEEE International Ultrasonics Symposium will be held in Orlando at the Caribe Royale from October 18 - 21, 2011. In March 2011, based on extensive uncertainty resulting from the M-9 earthquake that devastated part of Japan, the IEEE UFFC AdCom approved the grave decision to move venue from the original choice (Kobe, Japan) to a backup venue in the USA. The decision to shift the venue was supported by the central Conference Management function within the entire IEEE and many of the local Japanese representatives associated with planning the meeting. The IEEE UFFC society is committed to returning the conference to Japan in 2014, approval of UltraCom and AdCom is pending though.

When you think of Orlando, the first thing that probably comes to mind is Disney. The Walt Disney World® Theme Parks offer vacationers a magical and memorable experience. THE CARIBE™ provides complimentary scheduled shuttle service to the parks, and evening shuttles to the Downtown Disney® area–both located 1.5 miles from the hotel. But there are more theme parks like Universal Studios, and Seaworld.

Aside from the amusement parks and themed attractions, Orlando plays host to a wealth of significant cultural and artistic events. Enjoy the selected works of prominent masters as well as local artisans at one of the many galleries, museums and theaters located within the city. Delight your senses with a tour through a southern style garden at the Harry P. Leu Gardens.

For a pre or post symposium tour we recommend Kennedy Space Center. The launching pad of America's space program, the Kennedy Space Center invites guests to experience the wonders of space firsthand at their state-of-the-art facility near Orlando. Featuring a captivating array of informative exhibits and multimedia presentations, the Center will delight visitors of all ages as it leads them on a journey from the very first space mission to next scheduled shuttle excursion.

Florida and especially Orlando has a lot of attractions for everybody at every age.

Please come to Orlando and attend the 2011 IEEE International Ultrasonics Symposium, 18-21 October, 2011!

Ken-ya Hashimoto and Clemens Ruppel

Welcome from the Technical Program Chair

Yook-Kong Yong,
Rutgers University

Ultrasonics is on the Move! We look forward to an increasing impact of Ultrasonics in numerous emerging technical disciplines. The research community, the industry, and the universities are challenged to invent and develop improved and innovative concepts to efficiently address and solve the many new problems associated with a growing number of novel applications.

We welcome you to the 2011 IEEE International Ultrasonics Symposium which will be held in Orlando, Florida, USA, October 18-21, 2011 to bring together experts in theory and techniques of Medical Ultrasonics, Sensors, NDE & Industrial Applications, Physical Acoustics, Surface Acoustic Waves, and Transducers & Transducer Materials from all over the world.

The IEEE International Ultrasonics Symposium has a tradition of fostering direct, personal contact among the attendees thanks to its unique format with educational short courses, a plenary opening session, open forum presentations, focused sessions, and five sets of parallel sessions. A special student paper competition will be held. The Technical Program Committee will choose twenty-one student paper finalists to join the final competition at the Symposium. Seven winners will be chosen to receive a Best Student Paper award.

Yook-Kong Yong

Symposium Organizing Committee

Finance Co-Chairs

Daniel Stevens, Vectron International

Short Course Chair

Pai-Chi Li, National Taiwan University

Proceedings Chair

Robert Weigel, Friedrich-Alexander University of Erlangen-Nuremberg

Exhibition Chair

C.S. Lam, TXC Corp.

Web Co-Chairs:

Tsung-Tsong Wu, National Taiwan University
Amelie Hagelauer, Friedrich-Alexander University of Erlangen-Nuremberg

Publicity Co-Chairs

Shuji Tanaka, Tohoku University
Helmut Ermert, Ruhr University
Ji Wang, Ningbo University
Jan Kuypers, Sand 9

Local Arrangements Co-Chairs

Ben Abbott, Triquint

Kimon Anemogiannis

Shen Jen, CPI

Guest Program Chair

Mei Yuin (Hanna) Foo

Symposium Management

YesEvents
Mira Digital Publishing
Gerotron

Exhibitors

Exhibition Schedule:

Wednesday, October 19, 2011: 8:00 a.m. – 5:00 p.m.
Thursday, October 20, 2011: 8:00 a.m. – 5:00 p.m.
Friday, October 21, 2011: 8:00 a.m. – 12:00 noon

List of Exhibitors at the 2011 IEEE International Ultrasonics Symposium, as of July 20, 2011:

1	Electronics & Innovation	USA
2	Meggitt Sensing Systems	Switzerland
3	IEEE Ultrasonics, Ferroelectrics and Frequency Control Society	
4	Imasonic	France
5	Polytec	USA
6	Shanghai Apex Electronics Technology Co., Ltd	China
7	Weidlinger Associates - PZFlex	USA
8	Winprobe	USA
9	Texas Instruments - Medical Imaging Group	USA
10	Lecoeur Electronique	France
11	Verasonics	USA
12	Precision Acoustics	UK
13	ONDA Corp.	USA
14	Sonic Concepts	USA
15	ALPINION US (formerly VimedUS)	USA

Plenary Session

8:00 a.m. – 9:30 a.m., Wednesday, October 19, 2011
Carribean Ballroom

Welcome:
Conference organizers and others
UFFC-S President

Awards and Recognitions:

IEEE Awards:
IEEE Fellow Award 2011

IEEE UFFC Society Awards:
Achievement Award 2011
Distinguished Service Award 2011
Outstanding Paper Award 2010
2011-2012 Distinguished Lecturer Award

Ultrasonics Award:
Rayleigh Award 2011

Plenary Speaker:
Title of Presentation: Single Crystals for Medical Applications
Author: Bruce Chai
Crystal Photonics

Abstract: Single crystal is really not the desirable form of materials for any medical application unless there is really no other form of material that can offer the same or comparable performance at lower cost. The reason is simple. Crystals are expensive to make and it has limited physical dimensions. Still, single crystals are being used in both therapeutical and diagnostic applications.

The most common use of single crystals for therapeutical purpose is solid-state lasers. It is based on its unique property to deliver high peak power, short pulses under either Q-switched or mode-locked conditions. Single crystals used for this purpose include Nd-YAG, Er-YAG, CTH-YAG, Ruby, T-sapphire and Alexandrite. All these crystals are produced by CZ melt pulling technique under high temperatures near and over 2,000°C. The primary usage is for surgery, ophthalmology as well as for skin treatment. Even though the total number of laser systems is large, the total quantity (or net volume) of crystal materials used in these instruments is relatively small.

Single crystals used for diagnostic purpose are based either on its piezoelectric properties or scintillating properties. Ultra-sound scanner is one of the most common equipment in all hospitals PZT ceramics were the primary materials used as transducers in these scanners in the past. In recent years, it is gradually replaced by the lead-based single crystals such as PZN-PT and PMN-PT primarily for the high-end scanners. Both of these crystals were grown by vertical Bridgman techniques in sealed Pt-capsules. Again, the total number of ultrasonic scanners can be very large, but the amount (or net volume) of material used in each scanner is quite small.

The only medical application that uses fairly large quantity of single crystals is in medical imaging process based on the scintillating properties for gamma-ray radiation detection. X-ray has such a low energy (< 100 KeV) so that thin film (sub-mm in thickness) of scintillating ceramics is more than enough to capture the radiation. Gamma-ray has much higher radiation energy (> 500 KeV), it is necessary to use thick (cm in thickness) and high density materials in order to have sufficient stopping power. Moreover, once the gamma-ray is captured and scintillating emission is generated, it is needed to transmit the light to the photo-detectors. On cm scale in thickness, the best material to have the least scatter and highest transparency is single crystals. Today, SPECT uses large size (over 40 x 50 cm^2 in area) NaI(Tl) single crystal screen, while PET uses more than ten thousand cm long pixilated detectors to form a detector ring for each scanner. While BGO has been the crystal for PET scanners in the past, the new generation ToF scanners have all but replacing BGO detectors with LSO or LYSO detectors.

Single crystals will continue to be used in medical application but in constant threat to be replaced by other cheaper form materials. It is a very uncomfortable position to be in this business. For the specific examples mentioned here, it appears that they may stay in business for some time since there is really no known new materials on the horizon to replace them yet.

Biography of the Author:

Bruce Chai
Crystal Photonics

Dr. Bruce Chai is currently the President and CEO of Crystal Photonics. He is also the founder of the company.

Dr. Chai was born in 1947 in Shanghai and then moved to Taiwan with his parents. He got his B.S. degree in 1969 from National Taiwan University major in Geology. He then went to Yale University in 1970 for graduate studies and got his Ph.D. degree in 1975 major in Geology and Geophysics.

After a brief period as Post Doctor at Yale, he was recruited by Allied Chemical Corporation (now Honeywell Corporation) and joined the company in 1977. At the company, he is responsible for the research on single crystals for optics, acoustics and other applications. He was recruited again by CREOL (Center for Research in Electro-Optics and Lasers) of University of Central Florida (UCF) in 1988 and joined UCF as Professor of Physics, Electric Engineering and Mechanical Engineering in 1989.

In 1995, Professor Chai found Crystal Photonics, Inc. The Company is an OEM specialized in manufacture of optical single crystals for sensors, detectors, lasers and electro-optical applications. Currently, the company's primary product is the customized gamma-ray scintillating detector for high-end PET (Positron Emission Tomography) and PET/CT scanners. He also set up a plant in China for crystal fabrication and detector assembling.

Professor Chai is a Fellow of the Optical Society of America, a foreign member of the Russia Academy of Engineering and a honorary Professor of Shanghai Institute of Optics and Fine Mechanics, Chinese Academy of Sciences and also Fujian Institute of Structural Matters, Chinese Academy of Sciences. Over his career, Professor Chai has published more than 200 papers and has awarded over 35 U.S. patents.

Closing Ceremony

18:30 – 19:30, Friday, October 21, 2011, Carribean Ballroom

IUS 2011 will hold a Closing Ceremony on Friday, October 21, 2011, 18:30-19:30 in the Carribean Ballroom. The Closing Ceremony will mark the official close of the contributed Technical Program of IUS 2011. We invite all participants of the Ultrasonics Symposium to join us and enjoy some refreshments which are sponsored by PZFlex (www.pzflex.com/). The highlight of the Closing Ceremony will be a presentation by Prof. Hunt from Georgia Tech on Application of SAW Devices for Bio and Medical Sensing.

The Closing Ceremony presents an opportunity for the IUS 2011 Organizing Committee to thank all the attendees for their contributions to making IUS 2011 a success. We will also introduce the IUS2012 Organizing Committee so that they can tell you all about next year's IUS 2012 in Dresden, Germany.

For updates on the agenda please check the symposium website (http://ewh.ieee.org/conf/ius_2011/).

Conference Venue

Caribe Royale All-Suite Hotel & Convention Center

The Caribe Royale is located on more than 53 lush, tropical acres. Guests will discover 1,218 spacious, well-appointed one-bedroom suites, 120 luxurious two-bedroom lakeside villas, expansive state-of-the-art meeting and event facilities, unmatched hospitality and service, and a wealth of desirable dining options and hotel amenities that will appeal to both families and business professionals alike. And it all can be found just minutes from the area's world famous theme parks and attractions.

Caribe Royal Orlando
8101 World Center Drive
Orlando, FL 32821, USA
Tel. +1 407-238-8000
Fax. +1 407-238-8050
http://www.thecaribeorlando.com

Conference Registration

Registration Type	By Sept 18, 2011	After Sept 18, 2011
IEEE Member	$600	$750
Non-IEEE Member	$800	$950
Student (Show Student ID at Conference)	$175	$275
Retiree	$175	$275
One-Day Registration*	$350	$425
Life IEEE Member**	$90	$90
Exhibitor ***	free	free
Visitor for Exhibition	$25	$25
Guests/Additional Exhibitors	$100	$100
A Registrant May Add: - Additional DVD Proceedings: **** - Short Courses: Regular Student/Retiree	 $75 each $200 each $75 each	 $75 each $300 each $125 each

Notes:

- * One-Day Registration includes sessions for the day of registration only. The Wednesday Reception and the Thursday Dinner are optional at $45.00 and $60.00, respectively. DVD proceedings are not included.
- ** Life Member is defined by IEEE as at least 65-year old and the age plus years of IEEE membership should be equal or greater than 100. Life members should show their IEEE Life Member card or evidence of Life Membership when getting registration materials. The Wednesday Reception and the Thursday Banquet are optional at $45.00 and $60.00, respectively. (See the registration form).
- *** One Exhibitor per booth gets a full free registration for the symposium. Additional exhibitors (up to 4 per booth) have to be registered, either as a full registrant or as an additional exhibitor.
- A Full Registration will also include The Wednesday Reception and Thursday Banquet (October 19-20, 2011).
- Guest/Additional Exhibitors Registration includes the Wednesday Reception and three guest meetings. Guests are NOT allowed to attend any technical sessions except for the Wednesday morning plenary session.
- For those who register for Short Courses Only, they will NOT get a badge or any conference materials such as books and meal/show tickets, and will NOT be allowed to register for guests or to attend any technical sessions.
- As indicated in the table above, students are required to show their valid identifications (IDs) to the registration desks to qualify for the student rates and get any registration materials.
- **IMPORTANT NOTICE:** Because arrangement for the Wednesday Reception and Thursday Banquet must be fixed one month before the Symposium, late on-site registration may result in disable to join the occasion. Thus advance registration is strongly recommended.
- **** A Full Registration (IEEE Member, Non-IEEE Member, Student, Retiree, or Life IEEE Member) will include one DVD conference proceedings. If you need additional DVD proceedings, you may order them when you register. A printed version of the Proceedings will only be available by ordering directly from the IEEE after the Symposium.

Introduction:

The deadline for early conference registration with discount registration fees is September 18, 2011 (midnight, Pacific Standard Time). After September 18, 2011, attendees with credit cards (Visa, Master, or American Express) can continue to register on-line at higher fees until October 1, 2011 after which on-line registration ends. Also, registrations via fax or mail will not be accepted after October 1, 2011 (9:00 a.m., Eastern Standard Time), and these attendees are requested to register on-site.

Registration Cancellation and Refund Policy:

There will be a $25.00 USD service charge to process refunds for those who have pre-registered but who are unable, for whatever reason, to attend the conference, or those who would like to make changes to the registration resulting in a refund. A letter requesting the refund should state the registrant's name and to whom the refund check should be made payable. No refunds will be given for requests RECEIVED after September 27, 2011 (9:00 am, Eastern Standard Time). FAX the letter to 2011 IEEE International Ultrasonics Symposium at

1-410-559-2217

Online Registration Link:

https://www.yesevents.com/ius/

Visa Application

Visa requirements: The US has updated its visa policies to increase security, so it may take you 3-6 months to apply for and receive your visa. For details that apply specifically to your country, please go immediately to your nearest US Consulate or Embassy. Review your visa status now to determine if you need a US visa or visa renewal and to find out how to schedule an interview appointment, pay fees, and other vital instructions. If you need a personal letter of invitation to attend the Conference, contact the Conference Coordinators by email at: IUSInfo@yesevents.com. Please provide the following information: complete name, mailing address, and any other details that your country of residence requires for your visa application. Only an original copy (not faxed or email version) of the letter of invitation may be accepted with your visa application. The Symposium cannot contact or intervene with any U.S. Embassy or Consulate office abroad on your behalf, so please begin your visa application process as soon as you determine that you want to attend the 2011 International Ultrasonics Symposium. All nationals and citizens of countries included in the Visa Waiver Program (VWP) who plan to travel to the U.S. for temporary business or pleasure for 90 days or less are not required by law to obtain a Visa prior to initiating travel to the United States, but must meet eligibility requirements to travel without a visa on VWP and, therefore, some travelers from VWP countries are not eligible to use the program. VWP travelers are required to have a valid authorization through the Electronic System for Travel Authorization (ESTA) prior to travel, are screened at the port of entry into the United States, and are enrolled in the Department of Homeland Security's US-VISIT program. This authorization can be obtained online through the **Electronic System for Travel Authorization** (ESTA), an Internet application administered by the U.S. Department of Homeland Security. For additional information about the ESTA please visit http://www.cbp.gov/esta. Travelers from countries not in the VWP are still required to obtain a Visa prior to entry into the United States.

Local Transportation

From Orland International Airport
Taxis, rental cars, buses, and shuttles are available for transportation between the Orlando International Airport (MCO) to International drive. Please refer to the link below for detailed information.

http://www.orlandoairports.net/transport/local_transport.htm

For Travelers arriving by Car
For individuals arriving by car, The Caribe Royale's website provides additional directions.

http://www.thecaribeorlando.com/area-directions

Local Shuttle Buses
After arriving at the conference hotel, the hotel provides a complimentary shuttle bus to near-by destinations. From the nearby Orlando Premium Outlet Mall, the I-Drive shuttle service is also available for transportation to additional local destinations for a low fee. I-Drive Shuttle passes for one to 14 days may be purchased in advance at the hotel. A single fare may be purchased for $1.25 when boarding the trolley. Please provide exact change.

Nearby Food and Shopping

The area near the Caribe Royal offers many options for dining and shopping. The hotel is home to nine restaurants and cafes, with additional dining options within walking distance.

http://www.thecaribeorlando.com/caribe-royale/dining/

The hotel's complimentary shuttle service, and the I-Drive Shuttle (see local transportation) provide transportation to other dining options and popular shopping destinations.

Orlando Weather

Typical Orlando Weather

The rainy season for Orlando is normally over by early October and temperatures begin to drop. Daily temperatures typically vary from a low of 19°C to a high of 23°C (75F to 84F). Precipitation for the month of October is generally light with fewer than 5 days having greater than 3mm (0.1in) of rainfall.

Wednesday Reception & Thursday Banquet

The Reception On Wednesday October 19th and the Banquet on Thursday October 20th are for all full registration guests and others who paid separately for this event will be welcome with their ticket. The Reception and the Banquet will be held in the Grand Sierra A-D and will start at 19:00 p.m. and 21:00 p.m., respectively. If you would like a vegetarian menu please let the registration desk know.

Guest Program

Excursions to local attractions are available daily. Popular attractions include The Walt Disney World Magic Kingdom, Epcot Center, Animal Kingdom, Sea World, Universal Studios and others. No reservations are required. Admission tickets may be purchased upon arrival to the theme parks, or purchased at any of the four Guest Service Desks in the hotel. A complimentary shuttle provides transportation, between the hotel and these destinations (See Local Transportation above).

For a detailed list of excursion choices, refer to the link below.

http://www.thecaribeorlando.com/things-to-do/

A tour of the Kennedy Space Center is also available. You may register for the tour prior to or during the conference, provided there are seats available on the bus. Tours are available each day. Registration may be done on line or by phone. See the link below for further details.

http://www.kennedyspacecentertours.net/?event=offer.detail&offerId=5831

The tour includes transportation between International drive and Kennedy Space Center in Cape Canaveral, and admission to the visitor center complex. The more convenient pick-up/drop-off location for the bus is the Crossroads Plaza.

Crossroads of Lake Buena Vista
12521 St. Rd 535
Orlando, FL 32821, USA

The Crossroads of Lake Buena Vista is about 2.3 miles from the conference hotel. The hotel's complimentary shuttle is able to provide transportation to the Crossroads plaza. Seating on the shuttle is limited so please plan to arrive early. The bus departs The Double Tree at 8:30 am, and returns at about 7:00 pm. Other pick-up/drop-off locations are available. See the like below for more information.

http://www.kennedyspacecentertours.net/?event=page.pickup&offerId=5831

Other tours may become available. The hotel management is attempting to arrange for additional destinations.

Speaker Ready Room

The schedule of the Speaker Ready Room (Regents Board Room) is as follows:

Tuesday (Oct. 18): 2:00 p.m. – 5:00 p.m. (for short courses)
Wednesday – Friday (Oct. 19-21): 7:30 a.m. – 5:00 p.m.

Please follow closely the instructions on the "Oral Presentation Guide" at the conference website to prepare your presentation and to avoid any technical difficulties.

Oral Presentation Guide

The Oral Presentation Guide on the conference website provides detailed instructions, tips to avoid technical difficulties, and good practices for your presentations. It is accessible via the link "Oral Presentation Guide" at the conference website http://ewh.ieee.org/conf/ius_2011. It is the responsibility of authors to follow the guide closely.

Poster Presentation Guide

The Poster Presentation Guide on the conference website provides information needed to prepare your presentation. It also gives a detailed description of poster labels and their use in finding the location of poster boards. The layout of the poster boards is shown on the floor plan near the end of this booklet. Please check the link "Poster Presentation Guide" at the conference website http://ewh.ieee.org/conf/ius_2011 for details.

Session Chairs / Session Summary Forms

Duties of Session Chairs of both oral and poster sessions can be viewed on the conference website via the link "Session Chairs". Session Summary Forms will be available at the Registration Desk. Session Chairs should fill out a form after each session and return it to the Registration Desk.

Technical Program Committee

The Technical Program Committee consists of the following 149 members:

Group 1: Medical Ultrasonics

Vice Chair of TPC:
Jan D'hooge
Catholic University of Leuven
Leuven, Belgium

Members:
1. **Olivier Basset:** *CREATIS, Université Lyon I, France*
2. **Ayache Bouakaz:** *INSERM, Université Tours, France*
3. **Lori Bridal :** *Univ. Pierre and Marie Curie, France*
4. **Charles Cain:** *University of Michigan, USA*
5. **Jean-Yves Chapelon:** *INSERM, France*
6. **Greg Clement:** *Harvard Medical School, USA*
7. **Paul Dayton:** *UNC Chapel Hill and NC State University, USA*
8. **Emad Ebbini:** *University of Minnesota, USA*
9. **Stanislav Emelinov:** *University of Texas at Austin, USA*
10. **David Evans:** *University of Leicester, UK*
11. **Kathy Ferrara:** *University of California Davis, USA*
12. **Stuart Foster:** *University of Toronto, Canada*

13. **James Greenleaf:** *Mayo Clinic College of Medicine, USA*
14. **Anne Hall:** *General Electric Medical Systems, USA*
15. **Christopher Hall:** *Philips Research North America, USA*
16. **Peter Hoskins:** *The University of Edinburgh, UK*
17. **John Hossack:** *University of Virginia, USA*
18. **Kullervo Hynynen:** *University of Toronto, Canada*
19. **Jorgen Jensen:** *Technical University of Denmark, Denmark*
20. **Nico de Jong:** *Erasmus Medical Centre and University of Twente, The Netherlands*
21. **Hiroshi Kanai:** *Tohoku University, Japan*
22. **Jeff Ketterling:** *Riverside Research Institute, USA*
23. **Michael Kolios:** *Ryerson University, Canada*
24. **Elisa Konofagou:** *Columbia University, USA*
25. **Chris de Korte:** *Catholic Univ. of Nijmegen, The Netherlands*
26. **Nobuki Kudo:** *Hokkaido University, Japan*
27. **Pai-Chi Li:** *National Taiwan University, Taipei, Taiwan R.O.C.*
28. **Jian-yu Lu:** *University of Toledo, USA*
29. **Leonardo Masotti:** *Università degli Studi di Firenze, Italy*
30. **Tom Matula:** *University of Washington, USA*
31. **James G. Miller:** *Washington University in Saint Louis, USA*
32. **Kathy Nightingale:** *Duke University, USA*
33. **Svetoslav Nikolov:** *BK Medical, Denmark*
34. **William O'Brien:** *University of Illinois, Urbana-Champaign, USA*
35. **Georg Schmitz:** *Ruhr-Universität Bochum, Germany*
36. **Ralf Seip:** *Philips Research North America, USA*
37. **Mickael Tanter:** *INSERM, France*
38. **Tom Thomas:** *Boston Scientific, Inc., USA*
39. **Kai Thomenius:** *General Electric's Corporate R&D, USA*
40. **Hans Torp:** *Norwegian University of Science and Technology, Norway*
41. **Piero Tortoli:** *Università degli Studi di Firenze, Italy*
42. **Ton van der Steen:** *Erasmus Medical Centre, Rotterdam, The Netherlands*
43. **Kendall Waters:** *Silicon Valley Medical Instruments, USA*
44. **Keith Wear:** *US Food and Drug Administration, USA*
45. **Wilko Wilkening:** *Siemens Medical Solution, USA*

Group 2: Sensors, NDE, and Industrial Application

Vice Chair of TPC:
Jafar Saniie
Illinois Institute of Technology
Chicago, Illinois, U.S.A.

Members:

1. **Robert C. Addison:** *Rockwell Science Center, USA*
2. **Walter Arnold:** *Fraunhofer Institute for Nondestructive Testing, Germany*
3. **Michal Bezdek:** *Endress+Hauser Flowtec AG, Switzerland*
4. **Ramazan Demirli:** *Villanova University, USA*
5. **James Friend:** *Monash University, Australia*
6. **Eric S. Furgason:** *Purdue University, USA*
7. **David Greve:** *Carnegie Mellon University, USA*
8. **Edward Haeggstrom:** *University of Helsinki, Finland*
9. **Mitsutaka Hikita:** *Kogakuin University, Japan*
10. **Jacqueline Hines:** *Applied Sensor Research and Development Corporation, USA*
11. **Patrick Johnston:** *NASA Langley Research Center, USA*
12. **Fabien J. Josse:** *Marquette University, USA*
13. **Lawrence W. Kessler:** *Sonoscan Inc., USA*
14. **Pierre T. Khuri-Yakub:** *Stanford University, USA*
15. **Mario Kupnik:** *Stanford University, USA*
16. **Jun-ichi Kushibiki**: *Tohoku University, Japan*

17. **Roman Maev:** *University of Windsor, Canada*
18. **Kentaro Nakamura:** *Tokyo Institute of Technology, Japan*
19. **Massimo Pappalardo:** *University di Roma TRE, Italy*
20. **Tony Sinclair:** *University of Toronto, Canada*
21. **Bernhard Tittman:** *Pennsylvania State University, USA*
22. **Jiromaru Tsujino:** *Kanagawa University, Japan*
23. **John F. Vetelino:** *University of Maine, USA*
24. **Paul Wilcox:** *University of Bristol, UK*
25. **William M. D. Wright**: *University College Cork, Ireland*
26. **Donald E. Yuhas**: *Industrial Measurement Systems, Inc., USA*

Group 3: Physical Acoustics

Vice Chair of TPC:
Vincent Laude
Institut FEMTO-ST
Besançon, France

Members:
1. **Manabu Aoyagi:** *Muroran Institute of Technology, Japan*
2. **Art Ballato:** *U.S. Army, USA*
3. **Jan Brown:** *JB Consulting, USA*
4. **Fred Hickernell:** *Retired from Motorola, USA*
5. **Takefumi Kanda:** *Okayama University, Japan*
6. **Eun Sok Kim:** *University of Southern California, USA*
7. **Yonkee Kim:** U.S. Army, USA
8. **Minoru Kuribayashi Kurosawa:** *Tokyo Institute of Technology, Japan*
9. **Amit Lal:** *Cornell University, USA*
10. **John Larson:** *Avago Technologies, USA*
11. **George Mansfeld:** *Russian Academy of Sciences, Russi*a
12. **Roy H. Olsson III:** *Sandia National Laboratories, USA*
13. **Mihir Patel:** *Schlumberger-Doll Research, USA*
14. **Edgar Schmidhammer:** *TDK-EPC, Germany*
15. **Susan Schneider:** *Marquette University, USA*
16. **Bikash Sinha:** *Schlumberger-Doll Research, USA*
17. **Ji Wang:** *Ningbo University, China*
18. **Tsung-Tsong Wu:** *National Taiwan University, Taiwan R.O.C.*
19. **Yook-Kong Yong:** *Rutgers University, USA*
20. **Jiun Der Yu:** *Epson Research and Development, USA*

Group 4: Microacoustics - SAW, FBAR, MEMS

Vice Chair of TPC:
Karl Wagner
TDK-EPC
Munich, Germany

Members:
1. **Ben Abbott:** *Triquint, USA*
2. **Robert Aigner:** *Triquint, USA*
3. **Ivan Avramov:** *Institute of Solid State Physics, Bulgaria*
4. **Sylvain Ballandras:** *FEMTO-ST, France*
5. **Kushal Bhattacharjee:** *RF Micro Devices, USA*
6. **Sunil Bhave:** *Cornell University, USA*
7. **Sergey Biryukov:** *IFW Dresden, Germany*
8. **Paul Bradley:** *Avago Tech, USA*
9. **Jidong Dai:** *RF Monolithics, USA*
10. **Omar Elmazria:** *Universié de Nancy--CNRS, France*

11. **Gernot Fattinger:** *Triquint, USA*
12. **Gerhard Fischerauer:** *University of Bayreuth, Germany*
13. **James Friend:** *Monash University, Australia*
14. **Ken-ya Hashimoto:** *Chiba University, Japan*
15. **Shitang He:** *IACAS, China*
16. **Chunyun Jian:** *Ericsson, Canada*
17. **Michio Kadota:** *Murata, Japan*
18. **Jyrki Kaitila:** *Avago Tech, Germany*
19. **Ilia Katardjiev:** *Uppsala University, Sweden*
20. **Kimmo Kokkonen:** *Aalto University, Finland*
21. **Jan Kuypers:** *Sands 9, Inc., USA*
22. **Ken Lakin:** *Consultant, USA*
23. **Don Malocha:** *University of Central Florida, USA*
24. **Natalya Naumenko:** *Technological University Moscow, Russia*
25. **Hiroyuki Odagawa:** *Kumamoto National College of Technology, Japan*
26. **Takeo Oita:** *Retired from NDK, Japan*
27. **Tuomas Pensala:** *VTT, Finland*
28. **Mauricio Pereira da Cunha:** *University of Maine, USA*
29. **Maximilian Pitschi:** *TDK-EPC AG, Germany*
30. **Viktor Plessky:** *GVR Trade SA, Switzerland*
31. **Leonard Reindl:** *Albert-Ludwigs-University Freiburg, Germany*
32. **Richard Ruby:** *Avago Tech, USA*
33. **Clemens Ruppel:** *TDK-EPC, Germ*any
34. **Takahiro Sato:** *Panasonic Electronic Devices, Japan*
35. **Marc Solal:** *Triquint, USA*
36. **Masanori Ueda:** *Taiyo Yuden, Japan*
37. **Robert Weigel:** *Friedrich-Alexander University of Erlangen Nuremberg, Germany*
38. **Sergei Zhgoon:** *Moscow Power Engineering Institute, Russia*

Group 5: Transducers and Transducer Materials

Vice Chair of TPC:
Paul Reynolds
Weidlinger Associates, USA

Members:

1. **Sandy Cochran:** *University of Dundee, UK*
2. **Christopher Daft:** *Samplify Systems, USA*
3. **Levent Degertekin:** *Georgia Institute of Technology, USA*
4. **Charles Emery:** *Mirabilis Medica, USA*
5. **John Fraser:** *Philips Medical Systems, USA*
6. **Steven Freear:** *University of Leeds, UK*
7. **Jean-Francois Gelly:** *GE Healthcare, France*
8. **Reinhard Lerch:** *Friedrich-Alexander-Universität Erlangen-Nuremberg, Germany*
9. **Geoff Lockwood:** *Queen's University, Canada*
10. **Richard O'Leary:** *University of Strathclyde, UK*
11. **Omer Oralkan:** *Stanford University, USA*
12. **Yongrae Roh:** *Kyungpook National University, Korea*
13. **Ahmad Safari:** *Rutgers University, USA*
14. **Mark Schafer:** *Sonic Tech Inc., USA*
15. **Scott Smith:** *GE Global Research, USA*
16. **Stephen Smith:** *Duke University, USA*
17. **Wallace Smith:** *Office of Naval Research, USA*
18. **Yasuhito Takeuchi:** *Kagoshima University, Japan*
19. **Jian Yuan:** *Boston Scientific, USA*
20. **Qiming Zhang:** *Pennsylvania State University, USA*
21. **Qifa Zhou:** *University of Southern California, USA*

Short Courses

There will be 10 short courses offered on Tuesday, October 18, 2011. These are listed below. More information on the course and on the authors can be found on the symposium web site at http://ewh.ieee.org/conf/ius_2011.

8:00 a.m. - 12:00 noon:

Short Course 1A (Boca Rooms IV):
Ultrasound contrast agents: Theory and experiment
Nico de Jong, Erasmus MC, Rotterdam, The Netherlands

Short Course 2A (Boca Rooms V):
Ultrasonic Motors: vibration generation, friction drive and energy harvesting
Minoru Kuribayashi Kurosawa, Department of Information Processing, Tokyo Institute of Technology, Japan

Short Course 3A (Boca Rooms VI):
Medical Ultrasound Transducers
Douglas G. Wildes and **L. Scott Smith**, GE Global Research, Niskayuna, NY, USA

Short Course 4A (Boca Rooms VII):
Phonoic crystals
Vincent Laude, Institut FEMTO-ST, Université de Franche-Comté and CNRS, France
Tsung-Tsong Wu, Institute of Applied Mechanics, National Taiwan University, Taiwan, R.O.C.

Short Course 5A (Boca Rooms VIII):
Elasticity Imaging: Methods and Applications
Kathy Nightingale and **Mark Palmeri**, Department of Biomedical Engineering, Duke University, USA

1:00 p.m. - 5:00 p.m.:

Short Course 1B (Boca Rooms IV):
Acoustic Microfluidics: Microscale Acoustics and Ultrasonics for Driving Fluids
James Friend, MicroNanophysics Research Lab., Dept. of Mechanical and Aerospace Engineering, Monash University, Melbourne Centre for Nanofabrication, Melbourne, Australia

Short Course 2B (Boca Rooms V):
Ultrasonic Signal Processing for Detection, Estimation and Compression
Jafar Saniie, Department of Electrical and Computer Engineering at Illinois Institute of Technology, IL, USA
Ramazan Demirli, Center for Advanced Communications, Villanova University, Villanova, PA, USA
Erdal Oruklu, Department of Electrical and Computer Engineering, Illinois Institute of Technology, IL, USA

Short Course 3B (Boca Rooms VI):
Processing and Characterization Challenges for Integrated Ferroelectric/Piezoelectric Devices
Glen Fox, Fox Materials Consulting, LLC, Colorado Springs, CO, USA

Short Course 4B (Boca Rooms VII):
Ultrasound Imaging Systems: from Principles to Implementation
Kai E. Thomenius, Diagnostics and Biomedical Technologies, General Electric Global Research, Niskayuna, NY, USA

Short Course 5B (Boca Rooms VIII):
Quantitative Ultrasound, Theory and Practice
William D. O'Brien, Jr., Department of Electrical and Computer Engineering, University of Illinois at Urbana-Champaign, IL, USA
Timothy J. Hall, Medical Physics Department, University of Wisconsin-Madison, WI, USA
Michael L. Oelze, Department of Electrical and Computer Engineering, University of Illinois at Urbana-Champaign, IL, USA
Timothy A. Bigelow, Departments of Eletrical and Computer Engineering and Mechanical Engineering, Iowa State University, USA
James A. Zagzebski, Medical Physics Department, University of Wisconsin-Madison, WI, USA

Invited Speakers

There are 18 Invited Talks at this year's Symposium.

Group 1: Medical Ultrasonics

1. "Contrast Ultrasound: Recent Developments and the Battle for Regulatory Approval," Francois Tranquart (Bracco, Switzerland)
2. "Dosimetry and Therapeutics," Gail Ter Haar (Institute of Cancer Research, UK)
3. "Recent Advances in Blood Flow Measurement," Jorgen Arendt Jensen (Technical University of Denmark, Denmark)
4. "New Developments in CMUT Technology," Pierre Khuri-Yakub (Stanford University, USA)
5. "Photo-Acoustics in Biomedicine," Srirang Manohar (University of Twente, The Netherlands)
6. "Optimization of Delivery across the Blood-Brain Barrier," Elisa Konofagou (Columbia University, USA)

Group 2: Sensors, NDE & Industrial Applications

1. "Acoustic Tomography: Promise versus Reality," Neb Dunic (Wayne State University, USA)
2. "Ultrasonic Welding Using Complex and High Frequency Vibration systems," Jiromaru Tsujino (Kanagawa University, Japan)

Group 3: Physical Acoustics

1. "Ultrasonic Fields for Cell Levitation and Manipulation," Martyn Hill (University of Southampton, UK)
2. "Guided Acoustic Waves Propagating at Surfaces, Interfaces and Edges," Andreas P. Mayer (HS Offenburg, Germany)
3. "Micro and Nano Fabricated Phononic Crystals: Technology and Applications," Roy H. Olsson III (Sandia National Laboratories, USA)

Group 4: Microacoustics – SAW, FBAR, MEMS

1. "Electrostrictive Thin Films: an Alternative to Piezoelectricity," Emmanuel Defay (CEA-LETI, France)
2. "Status of Temperature Compensated SAWs in Japan," Ken-ya Hashimoto (Chiba University, Japan)
3. "Wireless Physical SAW Sensors for Automotive Applications," Victor Kalinin (Transense Technologies, UK)
4. "Applying BAW Methods to Reduce Losses in RF SAW Resonators," Marc Solal (Triquint, USA)

Group 5: Transducers and Transducer Materials

1. "Ultrasonic Inspection of Nuclear Reactor Primary Components," Jean-Francois Saillant (Areva, France)
2. "Low Power Embedded Processors for Ultrasonics Signal Chain," Murtaza Ali (Texas Instruments, USA)
3. "Growth of Relaxor Based Single Crystal by Continuous Growing Method," Kazuhiko Echizenya (JFE Mineral, Japan)

Invited Clinical Speakers (Session 1E)

The 2011 International Ultrasonics Symposium will have a special clinical session to show how medical ultrasonic technologies are used in clinical practices. This special session, which will take place on Thursday at 10:30 in the Boca Room II-IV, consists of the following three invited presentations.

1. "IVUS and IVUS Elasticity Related Imaging," Yoshifumi Saijo (Tohoku University, Japan)

2. "OCT, NIR/IVUS and Other Optical Techniques," Evelyn Regar (Erasmus Medical Center, The Netherlands)

3. "Plaque Characterization by IVUS Tissue Characterization, NIR, FFR and Other Emerging Techniques," Akiko Maehara (Cardiovascular Research Foundation, USA)

Student Paper Competition

This is the 11th year of the Student Paper Competition. 19 Student Paper Competition finalists have been selected by the Technical Program Committee. These finalists will present a Poster of their work (in addition to their scheduled Oral presentation, if any) during the Poster Session on the Wednesday afternoon. Please refer to the Poster Presentation Guide to see what is required. A team of judges will discuss the work with the student in attendance and will select the winners of the Competition. The winners will be announced on Thursday evening. The winners of the student paper competition will receive a cash prize and a certificate.

Group 1: Medical Ultrasonics

1. "In-Vivo Pulsed Magneto-Motive Ultrasound Imaging of Tumor Bearing Small Animals," [1]**Mohammad Mehrmohammadi**, [1]Seungsoo Kim, [1]Min Qu, [1]Ryan Truby, [2]Pieter Kruizinga, [1]Stanislav Emelianov ([1]University of Texas at Austin, USA, [2]Erasmus MC., The Netherlands)

2. "Generalized Bayesian Speckle Tracking Applied to Strain and ARFI Displacements," **Brett Byram**, Gregg Trahey, Mark Palmeri (Duke University, USA)

3. "Improving Shear Wave Speed Estimation Precision in Homogeneous Media by Tracking Shear Wave Propagation in 3D Using a Real-Time Volumetric Imaging Transducer," **Michael Wang**, Brett Byram, Mark Palmeri, Ned Rouze, Kathryn Nightingale (Duke University, USA)

4. "Optical Characterization of Individual Liposome Loaded Microbubbles," [1]**Ying Luan**, [1]Telli Faez, [2]Erik Gelderblom, [1]Ilya Skachkov, [3]Bart Geers, [3]Ine Lentacker, [1]Antonius van der Steen, [2]Michel Versluis, [1]Nico de Jong ([1]Erasmus Medical Center, The Netherlands, [2]University of Twente, The Netherlands, [3]University of Gent , Belgium)

5. "In Vivo Monitoring of Nanoparticle Delivery Using Spectroscopic Photoacoustic Imaging," **Seungsoo Kim**, Geoffrey Luke, Yun-Sheng Chen, Stanislav Emelianov (University of Texas at Austin, USA)

6. "Intravascular Ultrasound Chirp Imaging of Atherosclerotic Plaque Pathology and Neovascularization," [1]**David Maresca**, [1]Krista Jansen, [1]Guillaume Renaud, [1]Wijnand den Dekker, [1]Gijs van Soest [2]Xiang Li, [2]Qifa Zhou, [2]Jonathan Cannata, [1]Antonius F.W. van der Steen ([1]Erasmus MC, The Netherlands, [2]University of Southern California, USA)

7. "Real-Time Handheld Optical Resolution Photoacoustic Microscopy," **Parsin Hajireza**, Wei Shi, Roger Zemp (University of Alberta, Canada)

Group 2: Sensors, NDE & Industrial Applications

1. "Precise Transportation of Single Cell by Phase-shift Standing Surface Acoustic Wave," **Long Meng**, Feiyan Cai, Qiaofeng Jin, Lili Niu, Hairong Zheng (Shenzhen Institutes of Advanced Technology, China)

2. "Guided Wave Temperature Compensation with the Scale-Invariant Correlation Coefficient," **Joel B. Harley**, Jos M.F. Moura (Carnegie Mellon University , USA)

3. "Acoustic and Optical Investigation of Microbubble Contrast Agents Designed for Oil Exploration at High Pressures," **Aleksandr Zhushma**, Natalia Lebedeva, Michael Rubinstein, Paul Dayton, Sergei Sheiko (University of North Carolina at Chapel Hill, USA)

Group 3: Physical Acoustics

1. "Confined Acoustic Phonons in Ultra-Thin Silicon Membranes," [1]**John Cuffe,** [1]Emigdio Chavez [1]Jordi Gomis Bresco, [1]Pierre-Olivier Chapuis, [1]Francesc Alzina, [2]Andrey Shchepetov, [2]Mika Prunnila, [2]Jouni Ahopelto, [3]Olivier Ristow, [3]Mike Hettich, [3]Thomas Dekosry, [3]Clivia M. Sotomayor Torres ([1]Catalan Institute of Nanotechnology, Spain, [2]VTT Technical Research Centre of Finland, Finland, [3]University of Konstanz, Germany)

2. "Experimental Evidence of Locally Resonant Sonic Band Gap in 2D Stubbed Plates," [1]**Mourad Oudich**, [2]Matteo Senesi, [1]Badreddine Assouar, [2]Massimo Ruzzene, [3]Jia-Hong Sun, [1]Brice Vincent, [4]Zhilin Hou ([1]Nancy University, France, [2]Georgia Institute of Technology, USA, [3]National Taiwan University, Taiwan R.O.C., [4]South China University of Technology , China)

3. "Experimental Study on High Efficiency Ultrasonic Motors Using Lubricant," **Wei Qiu**, Yosuke Mizuno, Daisuke Koyama, Kentaro Nakamura (Tokyo Institute of Technology, Japan)

Group 4: Microacoustics – SAW, FBAR, MEMS

1. "A Modular SAW Filter Design Approach for Multiband Filtering," [1]**Xiaoming Lu**, [2]Jeffery Galipeau, [1]Koenraad Mouthaan ([1]NUS, Singapore, [2]TriQuint Semiconductor Florida, USA)

2. "Impact of High-Temperature Dielectric and Piezoelectric Behavior on LGT Acoustic Wave Properties up to 900^{o}C," **Peter Davulis**, Mauricio Pereira da Cunha (University of Maine, USA)

3. "C-axis Parallel Oriented AlN Film Resonator Fabricated by Ion-Beam Assisted RF Magnetron Sputtering," **Masashi Suzuki**, Takahiko Yanagitani (Nagoya Institute of Technology, Japan)

Group 5: Transducers & Transducer Materials

1. "An All-optical Thin-film High-frequency Ultrasound Transducer," **Clay Sheaff**, Shai Ashkenazi (University of Minnesota-Twin Cities, USA)

2. "Radiation Impedance of an Array of Circular Capacitive Micromachined Ultrasonic Transducers in Collapsed State," **Alper Ozgurluk,** Abdullah Atalar, Hayrettin Koymen, Selim Olcum (Bilkent University, Turkey)

3. "Cell Characterization Using High Frequency Ultrasound," **Saurabh Bakshi**, John Williams, Xiaoning Jiang, Elizabeth Loboa (North Carolina State University, USA)

Student Travel Support

Some of the students will receive travel support to attend the conference. These students were selected based on need, whether they received support last year, and their group affiliation. Students that receive this support must register normally and will receive the monies at the conference. **They must show proof of their student status and of their membership in the IEEE and UFFC to receive their monies.**

Wednesday Oral Sessions

1A - Ultrasound Drug or Gene Delivery and Enhancement

Boca Rooms II-IV

Wednesday, October 19, 2011, 10:30 am - 12:00 pm

Chair: **Christopher Hall**
Philips Research

1A-1

10:30 am Ultrasound drug targeting to tumors with thermosensitive nanoparticles

Mark Ernsting[1], Arthur Worthington[2], Jonathan May[1], Tatsuaki Tagami[1], **Michael Kolios[2]**, Shyh-Dar Li[1]; [1]Drug Delivery and Formulation, Ontario Institute for Cancer Research, Toronto, Ontario, Canada, [2]Physics, Ryerson University, Toronto, Ontario, Canada

Background, Motivation and Objective

Thermosensitive liposomes that release a drug when exposed to mild hyperthermic temperatures have demonstrated antitumor efficacy. A doxorubicin (DOX) formulation has reached clinical phase III trials (ThermoDox®). However, a faster localized release of the drug is required for increased effectiveness. The objectives of the study were to couple a novel fast release liposomal formulation with ultrasound heat triggering, and demonstrate efficacy in a mouse tumor model.

Statement of Contribution/Methods

Novel Hyperthermia-activated-cytoToxic (HaT) liposomes were made by replacing the function of lysolipid and DSPE-PEG currently used in ThermoDOX liposomes with a polyethoxylated surfactant (Brij). Liposomes were loaded with doxorubicin (DOX) by a pH gradient method. EMT-6 cells (2×10^5 cells/50 µl medium) were inoculated into the mouse footpad of female BALB/c mice. Mice (n=5 per group) were i.v. injected with 200 µL HAT DOX (10 mg/kg), free DOX (10 mg/kg), or saline (control), were anesthetised, and were secured to a customized platform. The tumors were heated with a 10mm planar ultrasound transducer. A frequency generator sine wave output (TEK AFG, 3.9MHz) was amplified by a custom RF amplifier to drive the transducer. Tumor and body temperature were measured by an Omega HH309 thermometer with type K thermocouples. The tumor temperature was maintained at ~42^{o}C for 20 min., after which the mice were placed in recovery. Tumor dimensions before heating and post therapy were taken by caliper measurements.

Results

The data in Figure 1 demonstrate that the ultrasound system was able to rapidly increase the tumor temperature to the target temperature of 42^{o}C, and maintain this for 20 minutes. Treatment of mice with free DOX did not retard tumor growth compared to the control group. Mice treated with HaT DOX demonstrated a significant response, with complete tumor regression for all mice.

Discussion and Conclusions

An ultrasonic heating system was developed to achieve an intratumoral target temperature of 42^{o}C to trigger the release of doxorubicin delivered in a novel HaT liposome formulation. Heated tumors treated with HaT demonstrated complete regression in all cases. The data clearly demonstrate the potential of the approach, which is critically dependent on the formulation stability at non-hyperthermic temperatures and rapid drug release at 42^{o}C.

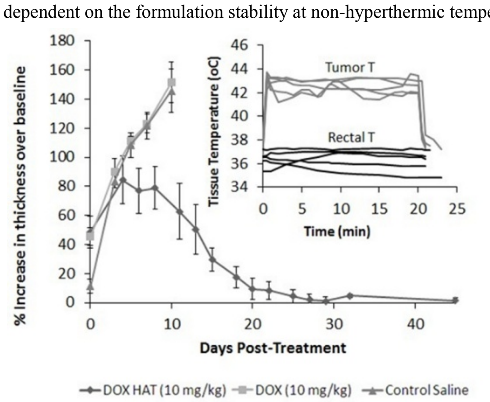

1A-2

10:45 am Investigation of Image-guided Sonothrombolysis in a Porcine Acute Ischemic Stroke Model

William Shi[1], Thomas Porter[2], Francois Vignon[1], Jeffry Powers[3], Shunji Gao[2], Jinjin Liu[2], Feng Xie[2], Lucas Drvol[2], John Lof[2], Carr Everbach[4]; *[1]Philips Research North America, Briarcliff Manor, New York, USA, [2]University of Nebraska Medical Center, Omaha, Nebraska, USA, [3]Philips Healthcare, Bothell, Washington, USA, [4]Swarthmore College, Swarthmore, Pennsylvania, USA*

Background, Motivation and Objective

Stroke is the #3 cause of death and #1 cause of disability worldwide. Although the thrombolytic drug tPA (Genetech) is an approved treatment for acute ischemic stroke (AIS), less than 5% of stroke patients actually receive thrombolytic therapy, due to concerns about the safety, efficacy, and the limited time window for its use. Ultrasound and intravenous microbubbles (MBs) have been used in recanalizing intravascular thrombi which cause stroke, myocardial infarction, deep vein thrombosis, and other vascular occlusions, and this non-invasive treatment modality may be especially useful in rapidly treating AIS patients. The objective of this study was to evaluate the effectiveness and safety of image-guided sonothrombolysis in the presence of contrast MBs for AIS therapy. A porcine AIS model was employed because the ultrasound attenuation of the porcine temporal bone is similar to that for human's.

Statement of Contribution/Methods

An ultrasound system (iE33; Philips Healthcare) was modified with the additional capability of transmitting 1.6 MHz long pulses (via a sector imaging probe S5-1) in new thrombolysis modes. AIS was created in 24 pigs by thrombotic occlusion of bilateral internal carotid arteries. In addition to aspirin, pigs were randomized to 3 sonothrombolysis treatment groups: high MI (2.3) short pulse (5μs) transtemporal ultrasound (TTU) alone, or a systemic microbubble infusion (2% Definity; Lantheus Medical) with guided high MI (2.3) short pulse (5μs) TTU and guided intermediate MI (1.7) long pulse (20μs) TTU. In the 2nd and 3rd groups, TTU impulses were delivered only when low MI imaging detected MBs within the large and small vessels of the ipsilateral cerebrum. Treatments were applied for 30 minutes. Ascending pharyngeal angiography was performed to examine for recanalization at 30 minutes into treatment.

Results

The 30 minute complete angiographic recanalization was 100% (8/8) for guided high MI short pulse TTU/MB treatment group, 38% (3/8) for guided intermediate MI long pulse TTU/MB treatment group, and 50% (4/8) for the high MI short pulse TTU alone treatment group ($p<0.05$ for guided high MI short pulse TTU/MB group versus other groups). There was no gross evidence of intracranial hemorrhage with any treatment.

Discussion and Conclusions

The study limitations are that neurologic outcome and infarct size were not assessed. Nonetheless, a modified diagnostic imaging system can be utilized with systemic MB infusion to rapidly restore cerebral blood flow in AIS. Image-guided high MI TTU and intravenous MBs, combined with aspirin, may be an effective alternative of treating AIS, without the need for fibrinolytic agents.

1A-3 ___

11:00 am Chemo-thermal approach for efficient ultrasonic tumor treatment with phase change nano droplet

Ken-ichi Kawabata[1], Rei Asami[1], Shin-ichiro Umemura[2]; [1]Central Research Laboratory, Hitachi, Ltd., Japan, [2]Graduate School of Bioengineering, Tohoku University, Japan

Background, Motivation and Objective

HIFU therapy is one of promising minimally invasive treatments of tumors and already used in clinical settings. To expand HIFU-applicable clinical situations, improvements in therapy time, targeting, and real time coagulation monitoring are important. For developing such improved therapy, we are proposing a novel approach utilizing nano droplets which turn into microbubbles by a phase change when exposed to triggering ultrasound pulses. The droplets and generated bubbles have been revealed to be capable of promoting cavitation and further enhancing thermal effects of ultrasound. In this paper, ultrasound exposure sequences enabling simultaneous generation of chemical and thermal effects of cavitation with our droplets for a tumor treatment with multidisciplinary mechanism is discussed.

Statement of Contribution/Methods

The nano-droplets which can provide microbubbles by ultrasound pulses were prepared by high-pressure (20 MPa) homogenizing of the mixture of phospholipid liposome and volatile perfluorocarbon molecules. A reaction vessel consisted of very thin (0.03-mm thick) polyethylene film was used for minimizing the influence of standing wave fields. In continuously degassed water kept at 37 °C, aliquots of aqueous solutions containing nano-droplet and indicators for radical generation were exposed to 1.1MHz ultrasound (200 – 500 W/cm^2) generated with a focused transducer (F number: 1, diameter: 48 mm). Acoustic signals from reactants were monitored with a wideband focused hydrophone. For generating microbubbles, triggering ultrasound pulses (1.3 kW/cm^2, 50 cycles) were applied periodically during ultrasound exposure.

Results

The intensity of acoustic signals from reactants, a widely used measure of cavitation significance, was almost independent of the repetition frequency of the triggering pulse in the range of 5 – 300 Hz. However, the induction of chemically active cavitation was highly dependent on the repetition frequency. The frequency was found to be more than 50 Hz to yield radicals in the reactant. It was further found that about 10 Hz was enough for obtaining thermal coagulation of proteins in gels. The effects of other acoustic parameters will also be discussed.

Discussion and Conclusions

Results obtained suggested that conditions for obtaining chemically active cavitation are more severe than those for thermally active one. Presumably, cavitating bubbles generate radicals only immediately after they are born. From the required repetition frequency of trigger, the ‘active time’ of bubbles can be estimated to be approximately 20 ms. Our results further indicated that an ultrasound exposure sequence for performing chemo-thermal therapy is possible by optimizing acoustic parameters.

Part of this work was supported by the Japan Society for the Promotion of Science (JSPS) through its "Funding Program for World-Leading Innovative R&D on Science and Technology (FIRST program).

1A-4 ___

11:15 am Antitumor effects of combining antiangiogenic therapy with the antivascular effects of ultrasound stimulated microbubbles

Margarita Todorova[1,2], Omid Mortazavi[1], Xuan Huo[1], Kullervo Hynynen[1,2], David Goertz[1,2]; [1]Imaging Research, Sunnybrook Research Institute, Toronto, Canada, [2]Medical Biophysics, University of Toronto, Canada

Background, Motivation and Objective

Considerable effort is being directed towards investigating the use of ultrasound (US) approaches to promote the local delivery or uptake of anticancer agents in tumors. In this study we investigate a different approach, which is to combine the vascular damaging effects of US stimulated microbubbles (MBs) with an antiangiogenic drug. In recent work we demonstrated that clinically viable concentrations of microbubbles can, at relatively low intensities, cause vascular damage in tumours, shutting down blood flow and inducing growth delays in tumour models. In these experiments, it was observed that the vascular shutdown was transient and by the 1 wk time point flow was re-established in tumours, suggesting a vascular ‘rebound’ effect. Motivated by previous work combining antiangiogenic and vascular disrupting agents (VDAs), the purpose of this study was to determine if the effectiveness of the vascular disrupting properties of US stimulated microbubbles could be enhanced by combination with an antiangiogenic treatment to suppress the apparent vascular rebound effect.

Statement of Contribution/Methods

Tumor growth inhibition studies were performed with the MDA-MB-231 breast cancer xenograft model. The four experimental groups were: control, drug (cyclophosphamide), US+MBs, and combined US+drug+MBs (n=4-6 per group). Cyclophosphamide was administered continuously in the drinking water, a metronomic dosing scheme that has been shown to act through antiangiogenic mechanisms. US treatments were performed on a weekly basis for a total of 4 weeks and the drug was administered for up to 10 weeks. The US treatment scheme (1MHz, 860 kPa) consisted of a series of fifty 100 microsecond bursts sent at 1ms intervals, repeated at 20s intervals for a duration of 2 minutes following the bolus injection of Definity MBs (60μl/kg). These conditions were found to induce inertial cavitation. Blood flow within the tumors was monitored during the experiments with an imaging transducer operating in contrast mode.

Results

The exposure conditions were confirmed to induce a vascular shut-down within the tumors, as indicated by contrast imaging results. Control tumours grew rapidly and by the 3-4 wk point required sacrifice due to tumor burden (>700 mm3). Drug-only tumor growth leveled off between wks 3-6 before increasing, consistent with previously reported results. US only treatments significantly reduced tumour growth until the 4-5 week stage, at which point growth accelerated. For the combined treatment group, growth leveled off by the 4-5 week point and then tumours began to shrink until the 10 week point.

Discussion and Conclusions

These results indicate that US stimulated microbubbles can be used in combination with antiangiogenic drugs to achieve pronounced antitumor activity. This approach would obviate the need for systemically injected VDAs and their associated side effects, such as myocardial toxicities.

1A-5

11:30 am Targeted delivery of neural stem cells using MRI-guided focused ultrasound

Alison Burgess[1], Carlos Ayala-Grosso[2,3], Milan Ganguly[1], Jessica Jordao[2,4], Isabelle Aubert[2,4], Kullervo Hynynen[1,5]; [1]Imaging Research, Sunnybrook Research Institute, Canada, [2]Brain Sciences, Sunnybrook Research Institute, Canada, [3]5. Laboratorio de Patologia Celular y Molecular. Centro de Medicina Experimental, Instituto Venezolano de Investigaciones Cientificas, Venezuela, [4]Laboratory Medicine and Pathobiology, University of Toronto, Canada, [5]Medical Biophysics, University of Toronto, Canada

Background, Motivation and Objective

Stem cell therapy is promising to treat neurodegenerative diseases, traumatic brain injury, and stroke. For stem cells to progress towards clinical use, the associated risks of current methods for delivery need to be reduced. Here, we introduce focused ultrasound (FUS) as a novel method for non-invasive delivery of neural stem cells to the brain.

Statement of Contribution/Methods

Magnetic resonance imaging (MRI) was used to target the striatum and the hippocampus on the left side for disruption of the blood-brain barrier (BBB). Definity microbubble contrast agent was injected intravenously at the onset of sonication using a 558kHz transducer (0.24MPa estimated in situ pressure, 10ms bursts, 1Hz pulse repetition frequency, 120 s total exposure duration). Following BBB-disruption, iron-labeled, green fluorescent protein (GFP)-expressing neural stem cells were injected into the carotid artery. MRI and standard post-mortem immunohistochemistry were used to detect the cells in vivo.

Results

Contrast-enhanced T1 weighted images confirmed FUS can increase the permeability of the BBB and subsequent imaging detected the entry of the iron-labeled cells in the targeted regions. Immunohistochemistry revealed that the cells crossed the BBB and that they were localized to the left striatum and left hippocampus. Twenty four hours after sonication, GFP-positive cells exhibited a neuronal phenotype and expressed nestin, polysialic acid and doublecortin.

Discussion and Conclusions

Together these results demonstrate that MRI-guided FUS is an effective tool for delivery of cells to the brain. This technique may be the key to reducing the risks of cell transplantation and leading to improvements in stem cell therapy in the clinical setting.

1A-6

11:45 am Release and monitoring of composite droplets in rats liver and brain with imaging pulses

Olivier Couture[1], Alice Bretagne[2], Alan Urban[2], Patrick Tabeling[1], Mickael Tanter[3]; *[1]CNRS / ESPCI, France, [2]ESPCI, France, [3]INSERM, France*

Background, Motivation and Objective

Composite droplets formed by enclosing an aqueous nanoemulsion within a matrix of perfluorocarbon oil can carry a large payload (2/3 of their volume) [Couture et al., IEEE 2009 and Medical Physics 2011]. This payload can be released with low ultrasound power (short pulses at MI=0.75), attainable by conventional ultrasound scanners. Hence, with the same clinical instrument, both imaging and drug delivery can be performed. A potential application would be to tattoo tissues to be resected under radiological guidance before surgery. Our objective is to demonstrate the release of fluorescein in rats at sufficient concentrations to be macroscopically observable, along with its ultrasound targeting and monitoring

Statement of Contribution/Methods

The femoral vein of Sprague-Dawley rats was catheterized and craniotomy was performed. A 5MHz array was connected to an ultrasound system (Aixplorer, Supersonic Imagine, France) and mounted over the liver or the brain. A bolus of 100 uL of composite droplets filled with fluorescein (monodispersed at 4 um in diameter) was injected in the femoral vein. Then, a series of 5 cycle pulses were focused in three regions at a focal distance of 2 cm, interleaved with imaging plane waves at a frame rate of 6000 Hz. Monitoring of the resulting hyperechoic regions was done for 60 minutes afterward. Then, the liver and the brain were harvested and fixed overnight in 4% PAF solution. The samples were sliced in 100 um slices and observed using confocal laser microscopy.

Results

The release within the liver and the brain was observable after a single 5 cycles pulses at a MI of 1.25. This observation was done by differential imaging between plane-wave insonifications performed before and 150 µs after the release focused pulse (left figure), which showed a contrast of 27 dB. This hyperechoic region could be induced by the conversion of the droplets to gas, which was then monitored using conventional Bmode for several minutes after the release (centre figure). After exposition of the liver, the most superficial release site was observable by eye under blue illumination with orange filters (right figure).

Discussion and Conclusions

This study demonstrates that large amount of optical marker can be delivered within the brain and the liver with composite particles. Moreover, this release can be monitored through ultrafast imaging even after a single release pulse.

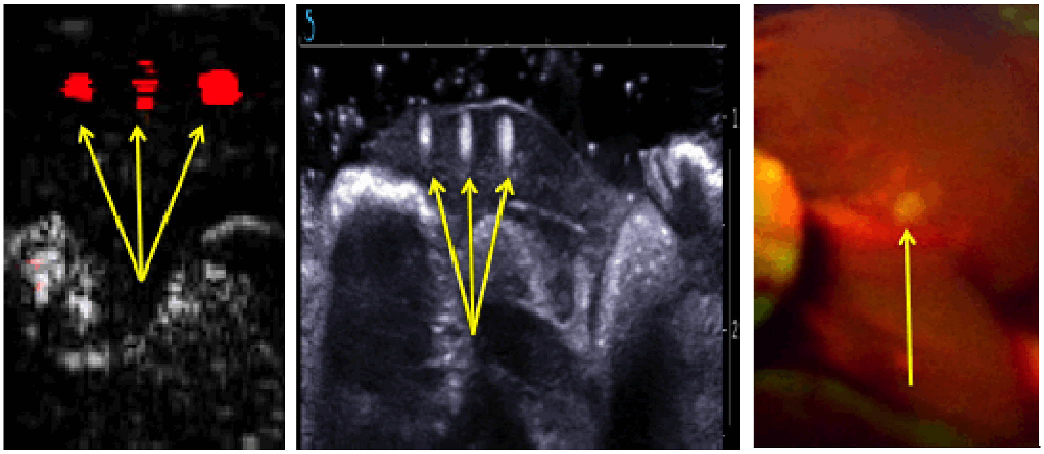

2A - Cardiac Visco-Elasticity and Strain Imaging

Boca Rooms VI-VII

Wednesday, October 19, 2011, 10:30 am - 12:00 pm

Chair: **Jan D'hooge**
Katholieke Universiteit Leuven

2A-1

10:30 am In Vivo Open and Closed Chest Measurements of Myocardial Viscoelasticity through a Heart Cycle Using Lamb wave Dispersion Ultrasound Vibrometry (LDUV)

Ivan Nenadic[1], Matthew Urban[1], Cristina Pislaru[1], Miguel Bernal[1], James Greenleaf[1]; [1]*Mayo Clinic, Rochester, MN, USA*

Background, Motivation and Objective

Diastolic dysfunction accounts for half of heart failures and is accompanied by the stiffening of the left-ventricular (LV) myocardium. Our lab has been investigating the use of Lamb wave Dispersion Ultrasound Vibrometry (LDUV), a technique for measuring mechanical properties of the LV myocardium. LDUV uses focused radiation force to excite harmonic anti-symmetric Lamb waves in the medium of interest and a pulse-echo transducer to track the resulting deformation and measure Lamb wave velocity. Change in Lamb wave velocity as a function of frequency (dispersion) is used to estimate the elasticity and viscosity of the myocardium by fitting the Lamb wave dispersion equation. In this study, we report open and closed chest measurements of elasticity and viscosity of a porcine LV free wall myocardium.

Statement of Contribution/Methods

An open-chest and a closed-chest protocol approved by our Institutional Animal Care and Use Committee were used for in vivo studies of Lamb wave propagation in pig hearts. A programmable ultrasound imaging platform produced by Verasonics (VSX), Inc. (Redmond, WA, USA) was used to excite and track mechanical waves. The VSX system linear array transducer was used to excite 1 ms long impulse in the myocardium and to track the wave propagation using a flash imaging mode scheme with pixels on the order of tenths of millimeters and frame rates of 6 kHz. Wave excitation from the VSX probe was triggered by the ECG R-wave and the data were acquired for 600 ms to capture an entire heart cycles. The slope of impulse propagation as a function of time was used to calculate the group velocity through a heart cycle at every 50 ms.

Results

An impulse contains all the frequency components up to the inverse of the time length of the impulse. Two-dimensional discrete FFT of the displacement versus time data resulted in the k-space whose axes are frequency (f) and wave number ($1/\lambda$). Coordinates for the maxima at each frequency were divided by the wave number ($c = \lambda f$) to obtain Lamb wave dispersion curves through a heart cycle [3]. The frequency response of the myocardium was assumed to obey the Voigt model so that the shear modulus $\mu = \mu1+i\omega\mu2$, where μ1 and μ2 are the shear wave elasticity and viscosity.

In vivo open chest measurements of the group velocity show an increase from ~ 1.5 m/s to ~ 4 m/s from systole to diastole. The shear wave elasticity (μ1) and viscosity (μ2) in an open-chest experiment were ~1.0 kPa and ~2.0 Pa*s in systole, and ~9 kPa and ~6.0 Pa*s in diastole. In vivo closed-chest studies show the changes in group velocity and elasticity (μ1) and viscosity (μ2) throughout a heart cycle. Group velocity changed from ~ 1.5 m/s in diastole to ~ 5 m/s at the peak of systole. The values of elasticity (μ1) increased from ~ 2 to ~ 8 kPa, while the values of viscosity (μ2) increased from ~ 2 to ~ 12 Pa*s from diastole to systole.

Discussion and Conclusions

These results demonstrate the feasibility of using LDUV to quantify changes in myocardial mechanical properties through a heart cycle.

2A-2

10:45 am Intracardiac Shear-wave Velocimetry using Acoustic Radiation Force (ARF) excitations: In Vivo Results

Peter Hollender[1], Patrick Wolf[1], Gregg Trahey[1,2]; [1]Biomedical Engineering, Duke University, Durham, North Carolina, USA, [2]Radiology, Duke University, USA

Background, Motivation and Objective

Acoustic Radiation Force (ARF)-based methods are useful for imaging tissue elastic properties. Shear-wave velocimetry has been shown to be able to measure the stiffening and relaxing of myocardial tissue. Dynamic stiffness is an indicator for cardiac disease like diastolic dysfunction and risk of heart failure, but obtaining this measurement has previously required a thoracotomy, limiting clinical application. Intracardiac echocardiography (ICE) catheter-tip transducers, commonly used to monitor ablation procedures and valve replacements, could make this measurement less invasively. While ICE probes gain proximity to the myocardium, their small size means that relative tissue motion may be great. This work elaborates on the techniques used to overcome the challenges of intracardiac ARFI shear-wave velocimetry and presents *in vivo* canine and porcine data showing the effectiveness of this method.

Statement of Contribution/Methods

Sets of shear-waves are generated at up to 40Hz in healthy animal subjects. Specialized imaging sequences minimize acquisition time and motion artifacts while maintaining effective shear-wave tracking. Interspersed B-mode images guide motion compensation and direct the ROI for each velocity estimate.

Results

Repeated ARF-induced shear-waves are imaged in both septal and free wall myocardial tissue, with velocities tracking the cardiac cycle. In the figure are shown typical *in vivo* results across three heartbeats, with velocities of 2.4 m/s in systole and 1 m/s in diastole. Catheter tip placement imposes a limit on how much motion can be compensated for.

Discussion and Conclusions

This work demonstrates the efficacy of using ICE to perform intracardiac ARFI shear-wave velocimetry in vivo, a viable alternative to the open-chest preparations. Enough views are available that both global and regional estimates are possible. Velocimetry studies for pathology diagnosis are feasible in a minimally-invasive manner with this method.

This work is supported by NIH EB001040, NIH 5R37HL096023, and NIH R01EB012484

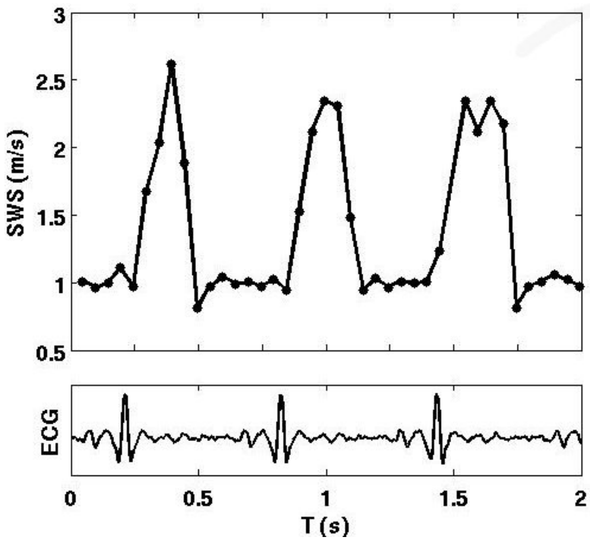

2A-3

11:00 am Direct In Vivo Myocardial Infarct Visualization Using 3D Ultrasound and Passive Strain Contrast

Brett Byram[1], David Bradway[1], Marko Jakovljevic[1], Doug Giannantonio[1], Dongwoon Hyun[1], Anna Lisa Crowley[2], Han Kim[2], Lowie Van Assche[2], Michele Parker[2], Raymond Kim[2], Robert Judd[2], Gregg Trahey[1]; [1]*Duke University, USA*, [2]*Duke University Medical Center, USA*

Background, Motivation and Objective

Previously, methods have been developed to measure active myocardial strain during ventricular contraction. Strain estimates during this period correlate to current heart function but only indirectly and approximately to the efficacy of myocardial tissue. In most clinical scenarios there is a mixture of stunned and infarcted tissue, which to date has not been distinguishable using active strain. A method is evaluated that uses passive strain to directly visualize myocardial infarct.

Statement of Contribution/Methods

A new approach to cardiac imaging using atrial contraction as a passive mechanism for inducing contrast (instead of active ventricular contraction) between tissue types in the ventricles was developed. The algorithm was tested on mongrel canines with chronic myocardial infarcts (MI). Three canines were scanned at volume rates between 80 and 240 Hz based on the anatomical constraint of the heart's location. All subjects also underwent contrast enhanced MR scans--the gold standard for MI visualization.

Ultrasound data were acquired as 3D volumes in baseband format and 30 receive beams-per-transmit configuration using a SC2000 and a 4Z1C matrix array (Siemens Healthcare, Ultrasound Business Unit, Mountain View, CA, USA).

Displacement was estimated using a Bayesian speckle tracking algorithm coupled with a quality guidance algorithm similar to those described by others for use with elastography displacement fields. The displacements are converted to axial strains, and the total normal and shear axial strain magnitude was used constract the ultrasound MI image.

Results

Results from 3 transthoracic scans of mongrel canines are reported. An example comparison of results from the largest canine subject is shown as side by side MR and ultrasound images.

In the ultrasound image, the MI is mapped to dark pixels. The ceMR image maps the MI as bright pixels. The images show qualitative agreement. Additionally, an open-chested canine subject with an ablation lesion (modeling a MI) was also scanned and showed contrast of 5.4 dB and contrast to noise ratio of 7.4 dB.

Discussion and Conclusions

The described approach for infarct visualization shows promise. A larger sample population and more sophisticated methods for MR and ultrasound registration will allow for more comprehensive statistical analysis and make reporting ROC curves appropriate.

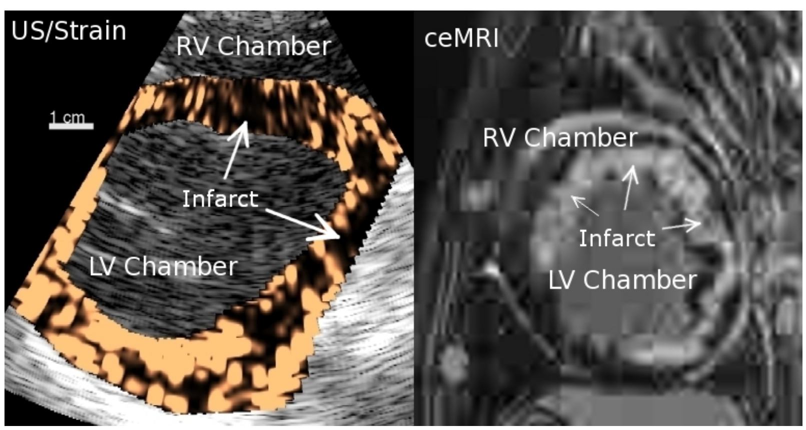

2A-4

11:15 am Mapping Myocardial Structure using Shear Wave Imaging- Comparison with Diffusion Tensor Imaging

Wei-Ning Lee[1,2], Benoit Larrat[1,2], Mathieu Pernot[1,2], Mickael Tanter[1,2]; [1]Institut Langevin, ESPCI ParisTech, France, [2]CNRS, UMR 7587; INSERM, U979, Paris, France

Background, Motivation and Objective

Shear wave imaging (SWI) has been demonstrated its feasibility to noninvasively measure myocardial fiber orientation in both in vitro porcine and in vivo ovine hearts and been validated with histology (Lee et al., IUS 2010). In this study, we further compared SWI with Magnetic Resonance (MR) Diffusion Tensor Imaging (DTI), an extensively-reported non-invasive imaging method for mapping fiber architecture.

Statement of Contribution/Methods

Fresh porcine myocardial samples (n=8; 20x20x30 mm^3) were studied. SWI (Pernot et al., JACC 2011) was firstly performed to generate shear waves and acquire the wave events at ultrafast frame rate (8000 fps). A 8 MHz linear array probe (pitch= 0.205 mm), connected to a prototype ultrasound scanner, was mounted on a customized MRI-compatible rotation device, which allowed both the rotation of the probe from -90° to 90° at 5° increments and co-registration between two imaging modalities. The fiber angle at each myocardial depth was defined by the probe rotation angle at which the maximum shear wave speed occurred (Lee et al., IUS 2010). The myocardial sample was then placed inside a 7T MRI scanner. Diffusion was encoded in six directions. A total of 270 diffusion-weighted images (b = 1000 s^2/mm, FOV=30 mm, Matrix size= 64x60, TR=9 s, TE=19 ms, 24 averages) and 45 b0 images were acquired in 13 h. The fiber structure was analyzed by the fiber tracking module in the software, MedINRIA. The fiber orientation in the overlapped myocardial region which both SWI and DTI accessed was therefore compared thanks to the co-registered imaging system.

Results

The figure below shows the transmural fiber structure of one porcine myocardial sample estimated by SWI in excellent correlation with that obtained by DTI. All experimental data show good correlation between SWI and DTI fiber angle estimates (n=8, r^2=0.83±0.01, p<0.0001). The average difference of 8.7°±20.5° (n=316) in measured fiber angles between SWI and DTI across the wall in all 8 samples was found.

Discussion and Conclusions

For the first time, we have demonstrated that the fiber orientation estimated by SWI, which assesses the shear wave speed (and thus the stiffness) of the myocardium, was comparable to that measured by DTI, which evaluates the water diffusion rate within the myocardium. Further validation with histology is being investigated.

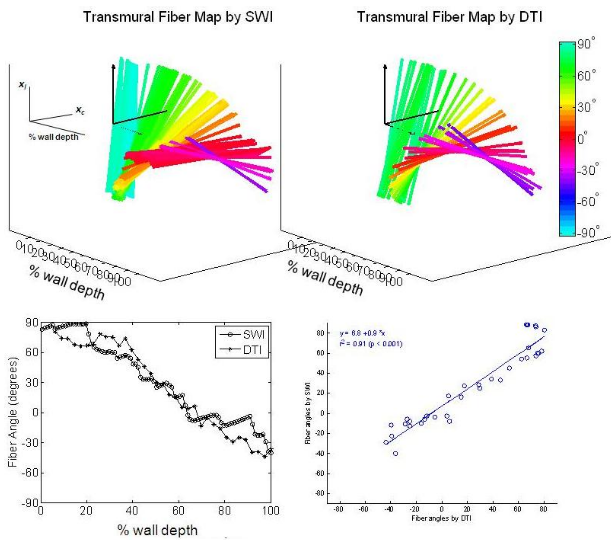

2A-5

11:30 am Non-invasive Electromechanical Imaging of Atrial, Supraventricular and Ventricular Cardiac Conduction Disorders in Canines and Humans

Jean Provost[1], Alok Gambhir[2], Stephane Thiebaut[3], Vu Thanh-Hieu Nguyen[3], John Vest[2], Hasan Garan[2], Elisa Konofagou[3,4]; [1]Biomedical Engineering, Columbia University, New York, New York, USA, [2]Medicine, Columbia University, USA, [3]Biomedical Engineering, Columbia University, USA, [4]Radiology, Columbia University, USA

Background, Motivation and Objective

Arrhythmias are a major cause of death and disability worldwide. However, no non-invasive imaging modality that can map the electrical activation is available to the physician. Electromechanical Imaging (EMI) is a non-invasive imaging method capable of mapping the electromechanical activation in vivo, i.e., the transient deformations occurring in response to the electrical activation of the heart. We have recently demonstrated the close relationship existing between the electromechanical and electrical activations in normal canines and humans [1], indicating that EMI can be used to map the transmural cardiac activation sequence in real time and in all four chambers. In this study, EMI is performed for the first time in patients with arrhythmias usually treated with ablation or pacing therapies.

Statement of Contribution/Methods

EMI was performed using a Sonix MDP system (Ultrasonix, Burnaby, Canada) with a 3.3 MHz phased-array. Axial displacements and strains were estimated at 350-500 Hz with a 4.6 mm cross-correlation window and a 10.7 mm least-squares kernel, respectively, in 3D bi-plane views constructed from 2 and 4-chamber views. In humans, normal sinus rhythm (n = 5) and three types of arrhythmias were studied: (i) atrial flutter (AF, n = 1), (ii) Wolff-Parkinson-White syndrome (WPW, n = 1), and (iii) left-bundle-branch block (LBBB) during cardiac resynchronization therapy (CRT, n = 3). In CRT patients, EMI was performed when pacing the left ventricle (LV), the right ventricle (RV), and during sinus rhythm (SR). A fourth arrhythmia, i.e., ventricular fibrillation (VF, n = 1), was studied in canines induced by fast pacing.

Results

In normals, activation was initiated in the right atrium (RA), and propagated in the left atrium (LA) during the P-wave. During the QRS complex, activation originated from multiple different locations in the ventricles. This corresponded to the expected, normal, synchronous transmural electrical activation sequence. In AF, activation originated at the

LA, indicating the presence of an arrhythmic focus. In WPW, activation propagated from the LA to the ventricular lateral wall prior to the Q-wave, indicating the presence of an accessory pathway. In CRT cases, activation originated from the pacing lead during both RV and LV pacing. In SR, the ventricles were asynchronous with the RV activated before the LV. In VF, fast, small, oscillating deformations were mapped. Frequency analysis of such oscillations could be used to localize arrhythmia foci.

Discussion and Conclusions

Arrhythmia foci and pacing leads were successfully detected in all the cases studied, indicating the capability of EMI to reliably determine the ablation sites prior to treatment and to optimize CRT, across all four cardiac chambers. EMI could thus be used for diagnosis of arrhythmias and monitoring and optimization of their treatment. Supported in part by NIH R01EB006042 and R21HL096094.

[1] Provost et al., Proc. Natl. Acad. Sci., 2011, in press.

2A-6

11:45 am In vivo passive elastic properties of normal and infarcted myocardium using shear wave imaging

Mathieu Pernot[1], Wei-Ning Lee[1], Mathieu Couade[1], Emmanuel Messas[2], Philippe Mateo[3], Bertrand Crozatier[3], Clement Papadacci[1], Alain Bel[2], Mickael Tanter[1]; *Institut Langevin, ESPCI, Paris, France, [2]Hopital Europeen Georges Pompidou, Paris, France, [3]INSERM U769, Chatenay-Malabry, France*

Background, Motivation and Objective

Quantitative imaging of myocardial viscoelastic properties is essential for the evaluation of both passive and active cardiac functions. We have demonstrated previously in vivo that Shear Wave Imaging can assess quantitatively the time-varying myocardial stiffness. Systolic myocardial stiffness was shown to provide non invasively an index of active contractility. Passive diastolic myocardial properties are also important for normal cardiac function and myocardial relaxation. In this study, we investigate the change of passive diastolic myocardial stiffness in ischemic/reperfused myocardium.

Statement of Contribution/Methods

Shear Wave Imaging was performed in vivo on five open-chest sheep using the ultrasound-based technique Supersonic Shear Imaging. A linear conventional ultrasonic transducer (8 MHz, Vermon, France) was positioned on the anterior wall of the left ventricle. Shear waves were generated in the myocardium using the acoustic radiation force induced by the ultrasonic probe. The shear wave propagation was imaged in real-time using an ultrafast scanner prototype (12 000 frames/s). The local myocardial stiffness was derived from the shear wave speed. Each shear wave measurement was achieved in less than 20 ms and was repeated 12 times every 60 ms to measure the stiffness variation within one cardiac cycle. Myocardial stiffness was also assessed invasively in the same region using the pressure-segment length relationship obtained by sonomicrometers (Sonometrics Corporation, Canada). The ligation of one diagonal of the left anterior descending coronary artery was achieved to induce ischemia during 2 hours, and reperfusion was performed during 30 minutes.

Results

The diastolic stiffness was found to increase after 45 minutes of ischemia. The shear modulus increased from 0.7±0.3 kPa to 2.1±0.7 kPa and was stable between 45 minutes and 2 hours. After reperfusion, diastolic stiffness increased even more strongly and diastolic shear modulus reached 14.6±1.5 kPa. The stiffening was confirmed by the stiffness constant of the exponential-fitted end-diastolic pressure-segment relationship which increased from 0.10 to 0.23 mm^{-1}. The peak diastolic strain rate decreased (from 2.43±0.35 s^{-1} to 0.82±0.13 s^{-1}) which showed impaired relaxation of the ischemic segment. Finally, TTC staining performed on the explanted myocardium confirmed the presence of a large infarcted zone.

Discussion and Conclusions

Shear Wave Imaging was able to quantify the increase of passive diastolic myocardial stiffness in infarcted myocardium. The passive diastolic stiffness was found to increase after only 45 minutes of ischemia and to increase strongly after reperfusion. Quantitative mapping of the passive elastic properties could have important clinical applications for early diagnostic of diastolic dysfunctions.

3A - Scattering and Attenuation

Carribean Ballroom VII

Wednesday, October 19, 2011, 10:30 am - 12:00 pm

Chair: **Ernest Feleppa**
Lizzi Center for Biomedical Engineering

3A-1

10:30 am Ultrasound Backscatter Spectral Analysis Provides Image Feedback for Histotripsy Tissue Fractionation

Kuang-Wei Lin[1], Tzu-Yin Wang[1], Ronald E. Kumon[1], Cheri X. Deng[1], Zhen Xu[1], Timothy L. Hall[1], J. Brian Fowlkes[1,2], Charles A. Cain[1,3]; [1]*Department of Biomedical Engineering, University of Michigan, Ann Arbor, MI, USA,* [2]*Department of Radiology, University of Michigan, Ann Arbor, MI, USA,* [3]*Department of Electrical Engineering and Computer Science, University of Michigan, Ann Arbor, MI, USA*

Background, Motivation and Objective

Spectral analysis of backscattered ultrasound is a procedure that can evaluate the scatterer size and acoustic concentration (CQ^2, where C is scatterer concentration, Q is relative acoustic impedance of the scatterers to the surrounding medium). Our hypothesis is that the scatterer size and acoustic concentration will decrease as the level of histotripsy-induced tissue fractionation increases, affecting the corresponding spectral parameters. Therefore, spectral analysis may provide image feedback on the degree of tissue fractionation during therapy.

Statement of Contribution/Methods

Excised canine livers were degassed, dissected, embedded in agar gels, and treated with 10-cycle histotripsy pulses generated by a custom 2 MHz 7-element transducer at PRF = 100 Hz (P+/P- > 25/17MPa). The number of treatment pulses varied from 100 to 2000 to produce varying levels of tissue fractionation. The specimens were then scanned using an ultrasound system (Vevo 770, VisualSonics, 15dB bandwidth: 7-40 MHz). Spectrum analysis of the radiofrequency data was performed using a custom-developed algorithm. The differences of average spectral parameters between treated and background regions were computed along with the effective scatterer size and acoustic concentration. After the scan, the specimens were fixed and processed into histology sections. The number of remaining intact cell nuclei within treated region (nuclei density) was counted by a custom program. [Wang et al, UFFC, 56(5): 995-1005]

Results

1) As the number of treatment pulses increased (N = 3, each), the spectral midband fit and intercept decreased while the spectral slope increased. The corresponding effective scatterer size and acoustic concentration decreased.

2) Cell nuclei density (N = 3) decreased as the treatment pulse number increased.

3) The nuclei density was highly correlated with the acoustic concentration.

Discussion and Conclusions

The scatterer size and acoustic concentration decrease as the level of tissue fractionation increases as demonstrated by the decreasing nuclei density, suggesting that spectral analysis may be a useful image feedback approach for estimating the degree of tissue fractionation. High frequency ultrasound imaging was employed to provide high spatial resolution in this feasibility study. Future work will extend the study to lower frequencies used in diagnostic ultrasound imaging.

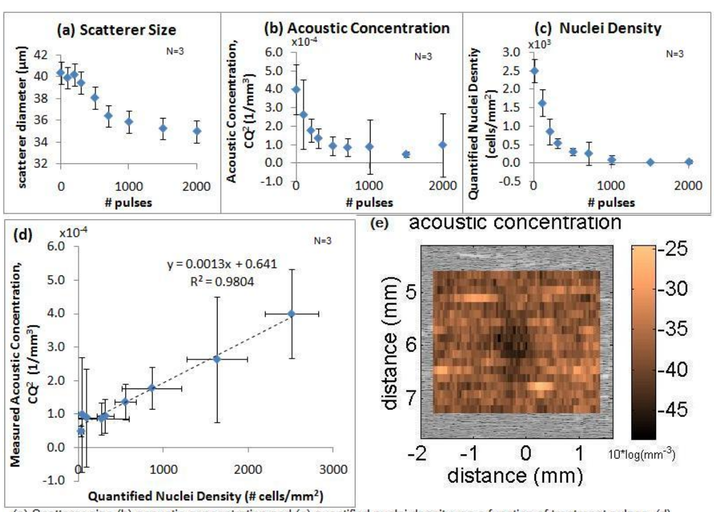

(a) Scatterer size (b) acoustic concentration and (c) quantified nuclei density, as a function of treatment pulses. (d) Correlation between acoustic concentration and nuclei density (e) Sample acoustic concentration image (500 pulses)

3A-2

10:45 am Three-dimensional Quantitative High-frequency Characterization of Freshly-excised Human Lymph Nodes

Jonathan Mamou[1], Emi Saegusa-Beecroft[2], Alain Coron[3,4], Michael L. Oelze[5], Tadashi Yamaguchi[6], Junji Machi[2], Masaki Hata[2], Eugene Yanagihara[2], Pascal Laugier[3,4], Ernest J. Feleppa[1]; *[1]F. L. Lizzi Center for Biomedical Engineering, Riverside Research, New York, NY, USA, [2]University of Hawaii and Kuakini Medical Center, Honolulu, HI, USA, [3]Laboratoire d'Imagerie Paramétrique UMR 7623, CNRS, Paris, France, [4]Laboratoire d'Imagerie Paramétrique UMR 7623, UPMC, Paris, France, [5]Department of Electrical and Computer Engineering, Bioacoustics Research Laboratory, University of Illinois, Champaign, IL, USA, [6]Research Center for Frontier Medical Engineering, Chiba University, Chiba, Japan*

Background, Motivation and Objective

High-frequency quantitative ultrasound (QUS) permits characterization of tissue microstructure using system-independent estimates. In this study, freshly-excised lymph nodes from cancer patients were evaluated using specifically designed QUS methods. The long-term objective was to develop 3D QUS methods for detecting metastases. Detection of metastases is critically important for staging and treatment planning.

Statement of Contribution/Methods

A custom laboratory scanning system was used to acquire radio-frequency data in 3D using a 26-MHz center-frequency transducer. A 3D algorithm based on the watershed transform segmented saline, fat, and nodal tissue. Overlapping 1-mm cylindrical regions-of-interest (ROIs) were processed to yield 13 QUS estimates associated with tissue microstructure. Spectral intercept, spectral slope, scatterer size and acoustic concentration were estimated from system-corrected attenuation-compensated power spectra. Four QUS estimates were obtained by fitting the Nakagami distribution or the more complex homodyned-K distribution to the ROI envelope distribution. Finally, the last 5 estimates quantified how the ROI envelope distribution differs from a Rayleigh distribution. 3D QUS images were generated by expressing QUS estimates as color-encoded pixels and overlaying them on conventional 3D B-mode images

Results

QUS estimates were obtained from more than 250 nodes from more than 120 gastrointestinal- or breast-cancer patients. Classification performance was assessed for individual estimates and linear combinations of estimates. ROC results demonstrated excellent classification. For gastrointestinal nodes, the areas under the ROC curves (AUCs) were above 0.95 (combination of 6 estimates). Slightly poorer results (AUC ~0.89) were obtained for breast nodes (combination of 4 estimates). Images based on QUS parameters also permitted the localization of cancer foci in some micrometastatic cases (Fig. 1).

Discussion and Conclusions

These encouraging results suggest that QUS methods may provide a clinically valuable means of detecting small metastatic cancers in dissected lymph nodes that might not be detected using standard pathology procedures. This capability will enable pathologists to more efficiently focus histological effort on cancer-containing regions of nodes.

(Supported in part by NIH grant CA100183.)

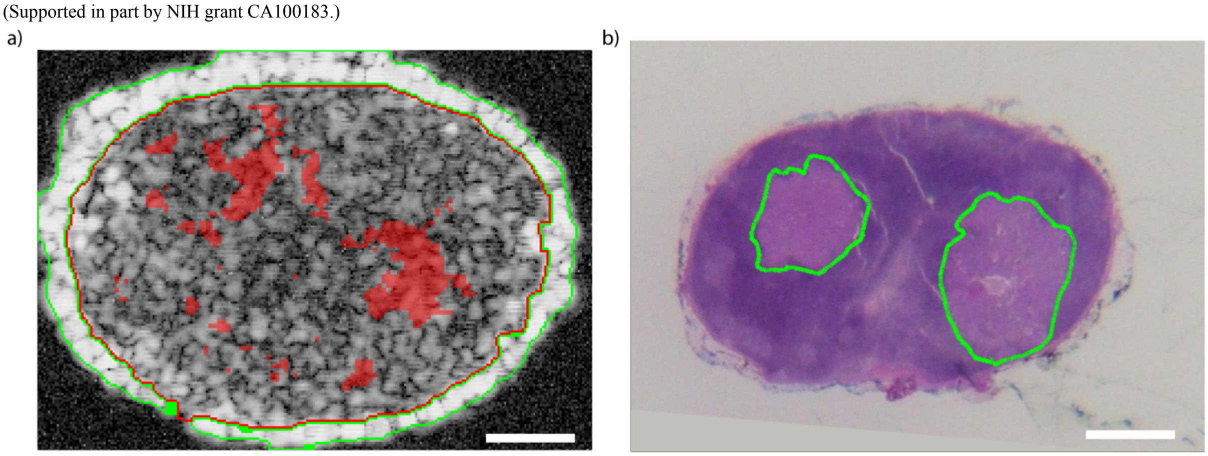

Figure 1: Illustrative breast axillary node containing micromestatic foci. a) QUS image showing regions in red with a detected likelihood of cancer greater than 50% based on linear-discrimnant analysis. b) Coregistered histology image with cancer foci demarcated in green by a pathologist. (Scale bar is 1 mm.)

3A-3

11:00 am computer-aided ultrasound (caus) to determine liver fat content applied in an animal model and in patients

Gert Weijers[1], Geert Wanten[2], Johan Thijssen[3], Marinette van der Graaf [3,4], Chris de Korte[3]; [1]Clinical Physics Laboratory, Radboud University Nijmegen Medical Centre, Nijmegen, Gelderland, Netherlands, [2]Gastroenterology, Radboud University Nijmegen Medical Centre, Netherlands, [3]Clinical Physics Laboratory, Radboud University Nijmegen Medical Centre, Netherlands, [4]Radiology, Radboud University Nijmegen Medical Centre, Netherlands

Background, Motivation and Objective

Obesity is related to our Western World life style and is a growing problem. In obese people, fat is not only accumulated subcutaneously but also in the liver (steatosis). Steatosis is one of the main causes for developing diabetes type-2 in obese populations. Patients on Home Parenteral Nutrition (HPN) are also at risk for developing hepatic dysfunctioning due to steatosis. Developing a cost effective, non-invasive technique for the assessment and follow-up of hepatic fat content in HPN patients.

Statement of Contribution/Methods

We developed and tested a quantitative ultrasound technique (CAUS) for the staging of steatosis using Ultrasound Tissue Characteristics Parameters (UTCPs) from B-mode images. Pre-processing in short: linearization of the Look Up Table (LUT); Back-Scan conversion; correction for the combined skin, fat and muscle layer thickness and attenuation; automatic gain correction (AGC) and finally automatic image segmentation for the removal of large hepatic arteries and portal veins. The following UTCPs were estimated; Mean echo level (Mu), Standard Deviation of mean echo level (SD), Signal to Noise Ratio (SNR), Residual Attenuation coefficient (ResAtt), Axial (Ax) and Lateral (Lat) speckle size.

This method was validated with an extensive animal study in 151 post-partem cows. Transcutaneous images were obtained with a Toshiba PowerVision 6000 with a curved array transducer (C7, fc = 4.2 MHz). Since also biopsies were taken, correlation with triacylglycerol (TAG) content could be investigated. Furthermore, data have been obtained from 15 human patients (3 males) on Home Parenteral Nutrition (HPN, administrated at least 6 times per week) with a mean age of 42 yrs. Five independent US liver images per patient were acquired using a SONOS 7500 (Philips Ultrasound, Andover, MA, USA) with a linear array transducer (L11-3, bandwidth 3-11 MHz) at an inter-costal position. These data was validated using an absolute quantification of liver fat concentration by proton Magnetic Resonance Spectroscopy (MRS, 3T Trio MR system, Siemens, Erlangen, Germany) at the same day.

Results

In the bovine study, high UTCP correlations were found (Mu r=0.7, ResAtt r=0.81, SNR r=0.74) with TAG. The ResAtt parameter was the only selected UTCP in stepwise multiple linear regression analysis, and revealed high predictive values (ROC, Area Under the Curve: AUC=0.95; Sensitivity: 87% and Specificity: 87%) for the classification of the liver fat content into several risk groups. In patients, positive and significant ($p<0.05$) correlations were obtained between several UTCPs and MRS derived liver fat content (Mu r=0.71, ResAtt r=0.84, Lat r=-0.62).

Discussion and Conclusions

In conclusion, high correlation between CAUS parameters and histology (cows) and MRS (patients) were found. Therefore, CAUS has potential in staging and possibly even screening of hepatic steatosis in human liver, thus preventing taking biopsies..

3A-4

11:15 am The impact of different estimator algorithms when obtaining effective diameter estimates from populations of scatterers of different sizes

Roberto J. Lavarello[1], Michael L. Oelze[2]; [1]Seccion Electricidad y Electronica, Pontificia Universidad Catolica del Peru, Peru, [2]Department of Electrical and Computer Engineering, University of Illinois at Urbana-Champaign, USA

Background, Motivation and Objective

Quantitative ultrasound using backscatter coefficients (BSCs) is a potentially powerful tool for estimating micro-structural properties from tissues. However, most scattering models assume distributions of identical scatterers even though actual tissues exhibit different levels of spatial variations. It has been experimentally demonstrated that the use of single-size scattering models may yield effective scatterer diameter (ESD) estimates that are not physically meaningful, i.e., ESDs that do not correspond to the size of actual structures present in the analysis medium. The objective of this study is to analyze three different estimator algorithms when estimating ESDs from media with populations of fluid-like spherical scatterers of different sizes.

Statement of Contribution/Methods

All estimator algorithms used a single-sized fluid sphere scattering model for ESD estimation. The estimators corresponded to minimizing (1) the variance of the ratio in decibels between the estimated BSCs and the scattering model, (2) the root mean square error (RMSE) between the estimated BSC and a scaled version of the scattering model, and (3) the RMSE between the estimated BSC and a linear transformation (allowing for an intercept) of the scattering model. In simulations, the input to the ESD estimators was obtained using band-limited portions of the theoretical BSC (neglecting multiple scattering and coherent scattering terms). The bands were defined by taking a 100% fractional bandwidth of simulated sources with center frequencies between 1 and 40 MHz. BSCs were calculated for several scatterer size distributions ranging between 25 and 100 µm. In experiments, BSCs were estimated from a gelatin phantom with Sephadex spheres ranging in diameter from 70 to 130 µm and 5-, 7.5-, 10-, and 13-MHz focused transducers.

Results

In simulations, ESD estimates obtained with Estimator 1 were approximately inversely proportional to frequency and mostly independent of the underlying scatterer size distribution for sufficiently large analysis frequencies. Estimator 2 also converged to physically meaningless solutions for sufficiently large frequencies, but generally converged at higher frequencies than Estimator 1. Estimator 3, in contrast, produced meaningful estimates for all studied analysis frequencies and all simulated media. In experiments, Estimator 1 produced ESD estimates lower than 70 µm when using both the 10 and 13 MHz data. However, Estimators 2 and 3 produced ESD estimates between 80 and 100 µm from the same experimental BSCs.

Discussion and Conclusions

The results of this work demonstrate that ESD estimates are highly dependent on the algorithm used to produce them. Results from both simulations and experiments suggest that single-size scattering models may produce meaningful ESD estimates for moderately large ka factors with the use of a proper estimator algorithm. This work was supported by NIH Grants R21-CA139095 and R01-EB008992.

3A-5

11:30 am Performance of various spectral estimation methods on acoustic Backscatter Coefficient estimation under data size limitations

Ivan M. Rosado-Mendez[1], Kibo Nam[1], Timothy J. Hall[1], James A. Zagzebski[1]; [1]Department of Medical Physics, University of Wisconsin-Madison, Madison, Wisconsin, USA

Background, Motivation and Objective

The *in-vivo* estimation of the acoustic backscatter coefficient (BSC) can be performed with clinical ultrasound scanners by applying a Reference Phantom method. This involves comparing the power spectra of the radiofrequency (RF) echo signals from a homogeneous region of interest within the sampled tissue to the echo signal power spectrum from the same depth in a reference phantom with known acoustic properties. However, when tissue is highly heterogeneous, the power spectra must be estimated over short duration windows and averaged over a limited number of independent realizations, possibly leading to biased and noisy BSC estimates, particularly when its dependence on frequency is not smooth. Our goal is to compare the performance of various spectral estimation methods when performing imaging system-based estimations of the non-smooth BSC of a previously characterized custom-made phantom under severe constrains of the gating window size.

Statement of Contribution/Methods

The phantom consists of a spherical inclusion (1.58dB/cm-MHz, 75-90µm diam. glass bead scatterers) within a homogeneous background. It was scanned with a SIEMENS S2000 system (Siemens, WA, USA) equipped with the Axius Direct research interface, at a 10 MHz central frequency. The backscatter coefficient was determined offline by applying the Reference Phantom method to the RF echo data supplied by the interface and using the phantom background as the reference. Echo signal power spectra were estimated using four different methods: Short-time Fourier transform with Hann (FT-H) and Blackman-Harris (FT-B) windows, Welch periodogram (WEL) and Thomson's Multi-Taper method (MTM). Spectra were computed for gating window sizes ranging from a maximum of 7mm down to a minimum of 1mm. The performance of these methods was evaluated by computing the Mean Square Error (MSE) relative to predictions from Faran's theory for spherical scatterers, using BSC estimations from 9 randomly scanned frames of the inclusion to get expectation values.

Results

Good agreement was obtained between imaging system-based BSC estimates and predictions from Faran's theory. Below the 2mm window length, the narrower (spectral) main lobe of the FT-B and the FT-H window functions led to smaller MSE values as a result of the smallest bias (by a factor of approx. 0.5 from the MTM and WEL methods). Above the 2.5mm window length, the smaller variance obtained from the MTM and WEL methods (approx. by a factor of 0.7) resulted in smaller MSE than the FT-B and the FT-H methods.

Discussion and Conclusions

Our results indicate that implicitly-averaging spectral estimation methods such as the Welch periodogram and Thomson's multi-taper method can be used to reduce the variance of BSC estimates when using gating windows longer than 2mm. For shorter window lengths, the Short-Time Fourier Transform with either Blackman-Harris or Hann windows could be used instead to reduce the bias at the expense of larger variance.

3A-6

11:45 am Ultrasonic Attenuation Imaging Using Spectral Cross-Correlation and Reference Phantom

Kayvan Samimi[1], Tomy Varghese[2]; [1]Electrical Engineering, Medical Physics, University of Wisconsin-Madison, Madison, WISCONSIN, USA, [2]Medical Physics, University of Wisconsin-Madison, Madison, WISCONSIN, USA

Background, Motivation and Objective

Estimation of ultrasonic attenuation properties of soft tissue provides an additional diagnosis tool that can help distinguish benign from malignant tumors and detect diffuse disease. Previously introduced methods of obtaining attenuation slope estimates using medical ultrasound include the spectral difference method, the spectral shift method, and the hybrid spectral domain method which combines the ideas of using a reference phantom with known attenuation and backscatter properties and using the spectral cross-correlation for frequency downshift estimation from the first two methods respectively. The hybrid method reduces the impact of system dependent parameters including diffraction effects by normalizing the sample power spectrum by the reference power spectrum. Although the hybrid method provides improvements with regard to estimation accuracy and indifference to backscatter level changes, it has resolution limitations when used to produce 2-dimensional attenuation images of the sample.

Statement of Contribution/Methods

In this paper we modify the hybrid attenuation estimation method by using the information from the entire normalized power spectrum to determine frequency downshifts more robustly in smaller ROIs, and using an L1-norm linear regression to fit frequency downshift estimates versus depth to a sloped line with minimum susceptibility to outliers; thus enabling us to construct attenuation maps with better resolution which provide better separation of regions with different attenuation levels.

Results

Attenuation images obtained from phantoms with cylindrical inclusions of different backscatter levels (0, 1, 2, 3 dB with respect to background) and different attenuation levels (0.5, 0.8 dB/cm/MHz with background at 0.5 dB/cm/MHz) indicate that this method provides a better 2-D attenuation map with distinct boundaries between the inclusions and the background material. Figure-1 is an example of a cylindrical inclusion with same backscatter level as background and higher attenuation of 0.8dB/cm/MHz

Discussion and Conclusions

The improved resolution of attenuation maps obtained using this method allows for pathological interpretation of such images and may provide an additional tool for diagnosis of diffuse diseases.

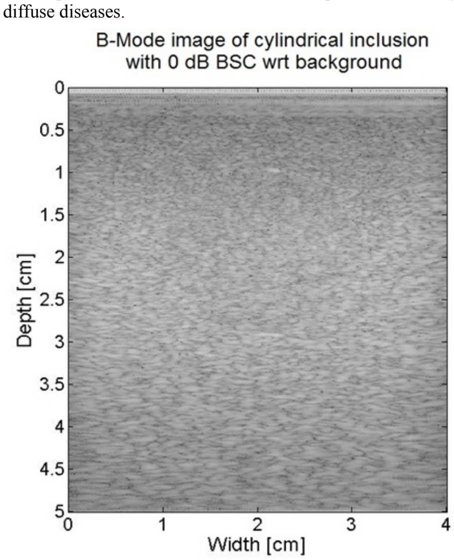

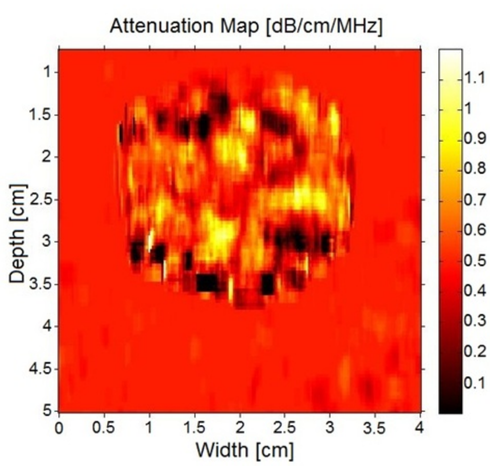

4A. Physical and Biological Acoutic Sensing

Carribean Ballroom I

Wednesday, October 19, 2011, 10:30 am - 12:00 pm

Chair: **John Vetelino**
University of Maine

4A-1

10:30 am Integrated ultrasound sensor for microwave heating and radiometry in medical applications

Yngve Birkelund[1], Frank Melandsø[1]; [1]Physics and Technology, University of Tromso, Tromso, NO, Norway

Background, Motivation and Objective

Microwaves heating have been proposed in different medical applications like e.g. hyperthermia treatment of recurrent breast cancer and heating of urine in a pediatric bladder to detect vesicoureteral reflux of urine into the kidney. Common for these applications is that the skin temperature needs to be kept low to avoid painful burns and/or blisters, which is normally obtained through the use of colder water circulating through a water bolus placed between the microwave heating antenna and the patient skin. To control the applied microwave power, a microwave radiometry can be used to non-invasively measure the tissue temperature in the illuminated volume. The deposited microwave power into the patient tissues is strongly dependent of the water bolus thickness, as the inversion techniques for measuring the temperature using a microwave radiometer is very sensitive to changes in the thickness. To increase the safety for the patient, a dynamic measurement of the water bolus thickness has to be implemented.

Statement of Contribution/Methods

We have investigated the use of an integrated ultrasound sensor to measure the water bolus thickness. The microwave heating in this study is a planar dual concentric conductor microstrip antenna produced on RO4350b hydrocarbon ceramic laminate, and the ultrasound sensor implemented as a PVDF film are fitted under the antenna laminate. An experimental setup with a pulser/receiver card configured in single transducer mode (pulse/echo) and a standard match filter are used to estimate the thickness of the water bolus.

Results

Numerical simulations of the microwave heating system will illustrate the need of an accurate thickness measurement of the water bolus. An experimental setup of the integrated ultrasound measurement system is presented. In-situ results using cheek tissue to mimic the triple-layered skin-fat-muscle tissue outside of the pediatric bladder, shows both the accuracy and limitation of the current ultrasonic sensor setup.

Discussion and Conclusions

The integrated ultrasonic sensor can be used to measure the water bolus thickness. This leads to better control of deposited microwave power in medical applications, and it may improve the non-invasive temperature measurements using microwave radiometry. To avoid electromagnetic interference, the ultrasound and microwave system can be activated separately using an on-off duty cycle. This allows for pseudo-continuous measurements of thickness, and improves the safety of the heating system in case of patient movement. The spatial shape of the PVDF film can be shaped to fit a specific antenna layout, but its size should be optimized to improve acoustic power without interfering with the electromagnetic fields during the microwave mode.

4A-2

10:45 am Acoustic sensor for rapid detection of bacteria in water

Aba Priev[1], Lev Ostrovsky[2], Yechezkel Barenholz[1]; [1]Biochemistry Department, Hebrew University-Hadassah Medical School, Jerusalem, Israel, Israel, [2]Zel Technologies, University of Colorado, Boulder, Colorado, USA

Background, Motivation and Objective

Ultrasonic standing waves can be used to concentrate trace quantities of particles and bacterial cells into equally-spaced bands, thus enhancing real-time water quality monitoring. Particles and bacteria denser than water are driven to a nearby pressure node by acoustic radiation force. This procedure, based on plane standing waves, is restricted to cells of at least a few microns; the larger cell will move faster in the standing wave field than the smaller one (velocity of particles, v, having the same acoustic properties is proportional to the square of the particle radius, R). There are some cells, like bacteria, that are smaller than a micron; such submicron particles cannot be efficiently separated and concentrated using plane standing waves.

Statement of Contribution/Methods

This paper presents the possibility of using acoustic radiation force produced by cylindrical standing waves for rapid detection of submicron-size bacterial cells and particles in drinking water. The cylindrical standing wave system performance was evaluated using E. coli bacteria; the results were compared with the latex test kit for E. coli O157 (Denka Seiken Co., Ltd., Tokyo, Japan).

Results

Theoretical calculations of the acoustic radiation force acting on the suspended particles in the cylindrical ultrasonic chamber show that the main maximum of the force dragging the particle to the central node can exceed the force maximum at the periphery of the cylindrical chamber by about 50 times (Figure 1). Radiation force in a standing acoustic wave field may induce movement of E. coli bacterial cells (density 1.160 g/cm3) with a speed of the order of a few mm/s at a frequency of 2 MHz and ultrasound pressure amplitude of 100 kPa, whereas the speed of bacteria in the plane standing wave does not exceed 0.2 mm/s under the same conditions. Such small forces cannot exceed the viscous drag force on the particle in the flowing buffer solution (Fvisc = kvR).

Discussion and Conclusions

Acoustical radiation forces in the cylindrical chamber were able to concentrate very dilute suspensions of bacteria (100 CFU/ml) by at least two orders of magnitude. Ultrasonic detection of the presence of an indicator microorganism, such as E. coli, in drinking water can be made more sensitive by the enrichment procedure using ultrasonic standing waves.

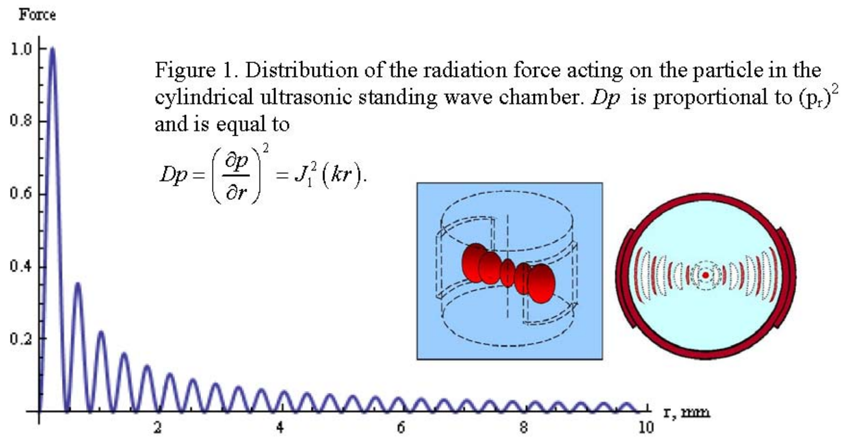

4A-3

11:00 am Numerical analysis of causal and noncausal lossy impulse responses in the far field for a circular piston

Christopher Johnson[1], Robert McGough[1]; [1]Electrical and Computer Engineering, Michigan State University, East Lansing, MI, USA

Background, Motivation and Objective

Accurate models of attenuation and dispersion are required for simulations of transient linear and nonlinear ultrasound propagation. Ideally, these models should be causal, although several models of ultrasound propagation that incorporate the effects of loss are noncausal.

Statement of Contribution/Methods

To determine causality, the arrival time of the lossy impulse response is evaluated on-axis in the far field and compared to the arrival time of the lossless impulse response. Noncausal lossy impulse responses are indicated by nonzero contributions prior to the arrival of the lossless impulse response, whereas causal lossy impulse responses occur strictly after the lossless impulse response arrives. This approach is motivated by the limiting form of the lossless on-axis impulse response for circular and rectangular pistons, which is represented by a delta function in the far field. The delta function describing the on-axis lossless impulse response represents a moving time reference, differentiating between causal and noncausal impulse responses.

Results

This approach is demonstrated for a circular piston with a radius of 37.5 um using time- domain Green's functions derived previously for the power law wave equation. The lossy impulse response is numerically evaluated by superposing point sources, where the corresponding Green's functions are computed in space and time to obtain the impulse response. The Green's functions are evaluated with the stable toolbox. The results are compared to the analytical lossless impulse response evaluated on-axis in the far field, 10 cm from the piston face. For power-law exponents $0<y<1$, the lossy impulse response begins after the arrival of the lossless impulse response. For power-law exponents $1<=y<=2$, the lossy impulse response begins before the lossless impulse response arrives. Results are shown in Figure 1.

Discussion and Conclusions

The power law wave equation, which is closely related to Szabo's wave equation, is causal for $0<=y<1$ and noncausal for $1<=y<=2$. Noncausal behavior, which was previously observed in the nearfield, is also identified in the farfield. By comparing the arrival time of the lossy and lossless impulse responses, causal models of lossy ultrasound propagation are readily distinguished from noncausal models.

Fig 1: Impulse responses of a circular piston evaluated in tissues with power-law attenuation.

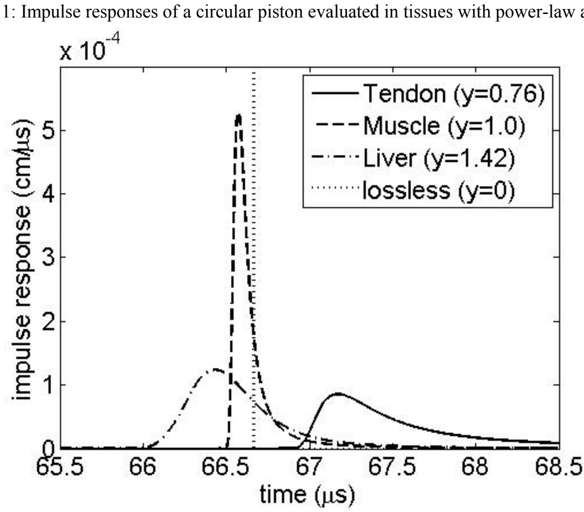

4A-4

11:15 am Design Of Acoustic Lenses For Ultrasonic Human-Computer Interaction

Tobias Dahl[1], Joao Ealo[2], Konstantinos Papakonstantinou[1]; [1]Elliptic Laboratories, Norway, [2]School of Mechanical Engineering, University of Valle, Colombia

Background, Motivation and Objective

Gesture recognition systems in general and touchless gesture systems specifically are gaining popularity in the consumer electronics world. The launch of Microsofts Kinect system, a 3D optical touchless system, is an important driver in this respect. Several less costly and complex systems are approaching mass markets. Some are based on IR or capacitive sensors, yet others on using echo-location ultrasound.

A particular advantage of ultrasonic systems over its competitors appears during product design. It involves creating a flat, robust and aesthetically pleasing front face, while simultaneously creating a wide field of view (≈180°). This is important for end users and designers alike, since one can avoid the dead zones normally associated with optical solutions. Moreover, a flat front end is close to a requirement for most small and medium-sized screen-based consumer devices, like handsets, tablets and notebooks.

Statement of Contribution/Methods

We show how off-the-shelf ultrasonic transducers can be turned into field-of-view maximizing components while keeping a flat front end.

The general idea is derived from the point source model for transducers, i.e. by noting that the behavior of disc-shaped transducer can be modeled by considering every surface point as a point source. A large value of r/λ yields a strongly directive transducer. However, if the point sources further away from the centre could artificially be given a larger delay than the ones closer to it, a more spherical and omnidirectional wavefront arises.

Results

We show that precisely this effect is obtained simply by placing a perforated, twisted, thick lens in front of a disc-shaped transducer (see figure). Excellent directivity characteristics is demonstrated by simulation, and initial verifications provided by building a small-scale prototype. Specifically, using a torsion angle for the twisting lens between 66 and 75 degrees gave the best results for frequencies between 20 and 50 kHz.

Discussion and Conclusions

Most commercially available transducers are highly directive. Whereas custom ones can be envisioned having much lower directivity, we propose to equip off-the-shelf transducer with *a twisted, perforated lens made of plastic*. This gives a low-cost alternative to designing and manufacturing new transducers from scratch.

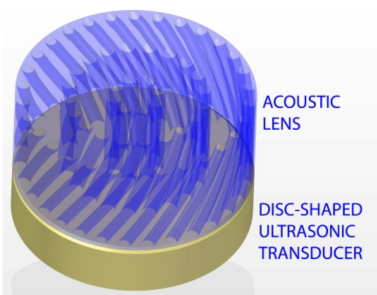

4A-5

11:30 am Quantitative Analysis of Liquids and Emulsions by means of High-Frequency Ultrasound (15-35 MHz)

Michael Vogt[1]; [1]Dept. of Electrical Engineering and Information Technology, Ruhr-University Bochum, Bochum, D, Germany

Background, Motivation and Objective

The analysis of homogeneous liquids and immiscible mixtures of different liquids (emulsions) is of interest in many industrial processes. Ultrasound based methods enable the measurement of various parameters (speed of sound, acoustic impedance, frequency-dependent attenuation), which are suitable to quantitatively characterize liquids and emulsions.

Statement of Contribution/Methods

In this work, a high-frequency ultrasound (HFUS) measurement cell working in the 15 to 35 MHz frequency range is presented. Design considerations for an optimum design of the cell are discussed based on an analytical one-dimensional model for propagating ultrasound waves. Appropriate echo signal processing strategies for parameter extraction and calibration techniques have been investigated, and results of the evaluation of the implemented system are presented.

Results

A HFUS piston transducer (6.3 mm aperture diameter, 25 MHz center frequency, 13 MHz bandwidth) is utilized in the implemented measurement cell. Ultrasound waves are coupled through a water path into a coplanar structure consisting of an acoustic delay line (quartz glass), a measurement chamber for the fluid to be analyzed, and a reflector (stainless steel). Highly sensitive echo measurements of the transducer’s reflectance are performed with an overall dynamic range larger than 100 dB by frequency-domain sampling with a frequency-swept continuous wave (CW) excitation signal by using a 10 Hz to 40 MHz network analyzer. Ultrasound waves, which are reflected at the glass / liquid interface and at the reflector, are separately assessed by time-gating of echo signals obtained by spectral windowing and inverse Fourier transform of the measured reflectance.

In a first implemented measurement approach, echoes from once and twice double-transmissions through the measurement chamber are taken into consideration. As an alternative, a second concept, which advantageously only includes the echo from the first double-transmission, but requires measurements from the liquid to be analyzed and from a reference liquid with known properties (distilled water), is presented and discussed.

Speed of sound (SOS) and dispersion are assessed by cross-correlation of echo signals and analyzing the phase of signal spectra. Furthermore, the acoustic impedance and quantitative parameters describing the frequency-dependent attenuation are calculated from the magnitude of echo signal spectra. The implemented system has been evaluated by measurements with different solutions of water and germ oil, glycerin, ethanol, and salt-water of different concentrations and salinity.

Discussion and Conclusions

A broadband spectroscopic measurement system for quantitative analysis of liquids and emulsions in the 15 to 35 MHz frequency range has been designed and successfully implemented. Highly sensitive measurements are enabled by employing a network analyzer for frequency-domain sampling.

4A-6

11:45 am Acoustic and Optical Investigation of Microbubble Contrast Agents Designed for Oil Exploration at High Pressures

Aleksandr Zhushma[1], Natalia Lebedeva[1], Michael Rubinstein[1], Paul Dayton[2], Sergei Sheiko[1]; [1]Chemistry, University of North Carolina at Chapel Hill, Chapel Hill, NC, USA, [2]Biomedical Engineering, University of North Carolina at Chapel Hill, Chapel Hill, NC, USA

Background, Motivation and Objective

Imaging of underground fluids in porous media is important to the field of petroleum exploration. Microbubbles are widely used as acoustic contrast agents for imaging in medicine, but at physiological conditions. Microbubbles in pressurized microporous systems, e.g. rock formations in subsurface oil reservoirs, exhibit low microbubble stability and poorly understood response to hydrostatic compression. More stable microbubbles are needed, along with acoustic-optical experiments to investigate microbubble echogenicity and stability at high pressures. We present soft and hard shell bubble formulations, a high-pressure cell for simultaneous acoustic and optical imaging under simulated borehole conditions, and finally perform acoustic, optical, and pressure-volume tests on the bubbles under high pressure, high salinity, and varied viscosity.

Statement of Contribution/Methods

Soft and hard shell pressure-resistant microbubbles stable to pressures above 1000 psi were formulated. A steel chamber was designed to withstand 7,000 psi pressure, at temperatures exceeding 100 °C, under a variety of solution conditions. Transparent windows made of sapphire or acrylic polymer provide visualization of material inside the chamber. Acrylic windows are semi-transparent to ultrasound, allowing for acoustic analysis of the contents. During simultaneous acoustic/optical measurements, a still image camera imaged the microbubbles. During optical-only experiments, a microscope was used to image bubbles with higher magnification.

Results

At constant microbubble concentration, confirmed with optical images, as pressure increased (tested up to 5,000 psi) the acoustic scattering signal of soft and hard shell microbubbles decreased. Optical observation experiments on soft shell microbubbles show that during repeated compression/expansion of bubbles, the pressure-volume P(V) relationship of these microbubbles deviated from ideal-gas-law predictions as such: initially microbubbles resisted compression because of shell elasticity, but after some pressure I reached, they shrank much quicker than initially, suggesting gas effusion out of the bubble. This P(V) relationship changed depending on the viscosity and salinity of the solution.

Discussion and Conclusions

Analysis of hard and soft shell microbubbles shows that those with rigid shells (glass) can withstand high pressure, but lack echogenicity; whereas, microbubbles with ultra-soft shells (such as monolayer lipids), are echogenic, but are destroyed at high pressure. We present data on prototype formulations which compromise on these characteristics, demonstrating both echogenicity and the ability to survive high pressures. This is a new application of microbubble acoustics for underground oil exploration.

5A - TCF Reduction

Carribean Ballroom II

Wednesday, October 19, 2011, 10:30 am - 12:00 pm

Chair: **Ben Abbott**
Triquint

5A-1

10:30 am Suppression of Transverse-mode Spurious Responses for Zero Temperature Coefficient of Frequency SAW Resonator on a SiO_2/Al/$LiNbO_3$ Structure

Hidekazu Nakanishi[1,2], Hiroyuki Nakamura[1], Tetsuya Tsurunari[1], Joji Fujiwara[1], Yosuke Hamaoka[1], Ken-ya Hashimoto[2]; [1]Panasonic Electronic Devices Co., Ltd., Kadoma City, Osaka, Japan, [2]Graduate School of Engineering, Chiba University, Chiba City, Chiba, Japan

Background, Motivation and Objective

Band II, III and VIII systems have narrow duplex gap in UMTS. To realize the duplexers for these applications, the SAW resonator having moderate effective electromechanical coupling coefficient (K^2) and small temperature coefficient of frequency (TCF) is required. The authors demonstrated that the SAW resonator with a moderate K^2, a zero TCF, and no Rayleigh-mode spurious response can be realized by optimizing the SiO_2 shape and the SiO_2 thickness h (=0.35λ) above the IDT on a SiO_2/Al/$LiNbO_3$ structure, where λ is the SAW the wavelength[1]. For practical use, it is also necessary to suppress the transverse-mode spurious responses.

Statement of Contribution/Methods

First, we directly applied the SiO_2 selective removal from the dummy electrode region to the current device structure. The technique has already been successfully applied to the resonators with h=0.20λ for the Band I SAW duplexer with wide duplex gap[2]. The experimental result indicated the technique is not effective for the current case: transverse-mode responses remained and spurious responses newly appeared at frequencies lower than the main resonance. Then we investigated to use thinning of SiO_2 on the dummy electrodes and studied how the transverse-mode responses change with remaining SiO_2 thickness H on the dummy electrode region.

Results

Fig. 1 shows measured admittance characteristic of the resonator when H=0.20λ. It is seen that spurious resonances including transverse-mode ones are completely suppressed. Measured TCF was unchanged and almost zero because no structural modification was given to the IDT region.

Discussion and Conclusions

It was demonstrated that the selective SiO_2 removal is effective to suppress transverse-mode responses for SAW resonators employing the SiO_2/Al/$LiNbO_3$ structure for wide range of SiO_2 thicknesses, provided that the SiO_2 thickness at the dummy electrode region is adjusted properly.

References

[1] H. Nakanishi, et al, IEEE Ultrasonics Symp., 2010. (to be published)
[2] H. Nakamura, et al, IEEE Ultrasonics Symp., 2010. (to be published)

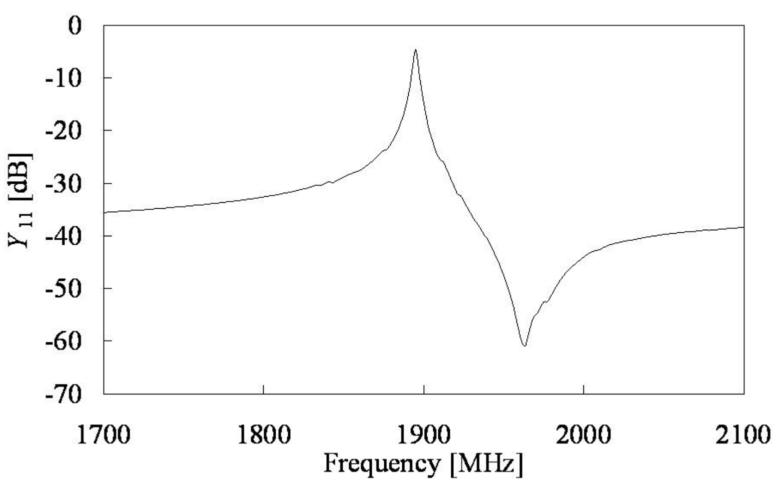

Fig. 1

5A-2

10:45 am Application of Fluorine Doped SiO_2 Films for Temperature Compensated SAW Devices

Satoru Matsuda[1,2], Motoaki Hara[1], Michio Miura[1], Takashi Matsuda[1], Masanori Ueda[1], Yoshio Satoh[1], Ken-ya Hashimoto[2]; [1]*Taiyo Yuden Co.,Ltd., Hyogo, Japan,* [2]*Graduate School of Engineering, Chiba University, Japan*

Background, Motivation and Objective

Temperature compensation techniques are demanded for RF SAW filters to fulfill stringent specifications for a wide temperature range. For the purpose, use of the SiO_2 overlay has been extensively studied, and the SiO_2/$LiNbO_3$ (LN) structure is widely used in mass production. This is owed to a distinctive feature of SiO_2, i.e., positive temperature coefficient of elasticity (TCE). In Ref. [1], the authors pointed out that TCE of SiO_2 films is strongly correlated with peak frequencies and full width of half maxima (FWHM) of the absorption peaks detected by the Fourier transform infrared spectroscopy (FT-IR). Namely, larger TCE is achieved when the peak frequency $\omega 4$ is higher and its FWHM is narrower. This result implies that FT-IR can be used to identify the most appropriate SiO_2 preparation technique and/or to find the most appropriate dopant for developing high performance temperature compensated SAW devices.

Statement of Contribution/Methods

This paper proposes use of fluorine-doped SiO_2 (SiOF) for the temperature compensation of RF SAW devices. The FT-IR measurement indicated that SiOF films exhibit higher $\omega 4$ and narrower FWHM than undoped SiO_2 films, and they change monotonically with the fluorine content r. Thus SiOF was expected to offer better temperature compensation ability than undoped SiO_2. Then we fabricated a series of SAW devices using the SiOF-overlay/Cu-grating/LN substrate structure, and their device performances including the temperature coefficient of frequency (TCF) were evaluated.

Results

The experiments confirmed that TCF increases with r, as we expected from the FT-IR measurement. In comparison with the pure SiO_2 case, F inclusion of r=8.8 at. % improved the TCF by 49.5 ppm/°C when the film thickness h was 0.3 wavelengths (λ). It should be noted that the SAW resonance frequency and effective electromechanical coupling factor K^2 decrease considerably with r. This indicates that better energy confinement in the overlay also contributes to the TCF improvement. When h was set to 0.2 λ so that K^2 was larger than the undoped case with h=0.3 λ, TCF improvement was reduced but still better by 6.5 ppm/°C. Although the Q factor at the antiresonance decreases with r, its tendency is not so obvious.

Discussion and Conclusions

It was demonstrated that the SiOF film is effective for the temperature compensation of RF SAW devices. Of course, SiOF films can be also applicable to the temperature compensation of RF bulk acoustic wave devices. We also showed that the Si-O-Si atomic structure measurable by the FT-IR governs the TCE of SiO_2 films even when dopant is added.

[1] S.Matsuda et al., Proc. IEEE Ultrason. Symp. (2010) [to be published]

5A-3

11:00 am Recent Development of Temperature Compensated SAW Devices

Ken-ya Hashimoto[1], Michio Kadota[2], Takeshi Nakao[3], Masanori Ueda[4], Michio Miura[4], Hiroyuki Nakamura[5], Hidekazu Nakanishi[5], Kenji Suzuki[6]; [1]*Graduate School of Engineering, Chiba University, Chiba, Chiba, Japan,* [2]*Murata MFG Co. Ltd., Nagaokakyo, Kyoto, Japan,* [3]*Murata MFG Co. Ltd., Nagaokakyo, Japan,* [4]*Taiyo Yuden Co. Ltd., Akashi, Hyogo, Japan,* [5]*Panasonic Electronic Devices Co., Ltd., Kadoma, Osaka, Japan,* [6]*NGK Insulators Ltd., Nagoya, Japan*

Background, Motivation and Objective

Although SAW antenna duplexers are mass-produced and widely used in mobile phones, improvement of their temperature stability is strongly demanded without degrading the other performances.

Achievable performances of SAW devices are inherently limited by the employed piezoelectric substrate. On the other hand, use of new piezoelectric materials is not desirable from industrial points of view because long years and investments are necessary to develop technologies and equipment to produce large size homogeneous wafers applicable to the mass use. Their inhomogeneity may badly influence the production yield. Thus possible solutions are limited for this request, and use of a single crystal $LiNbO_3$ or $LiTaO_3$ is mandatory as a member of the device structure.

Statement of Contribution/Methods

This paper reviews current status of research and development of temperature compensated RF SAW devices for the use in antenna duplexers.

Results

Currently two strategies are extensively studied. First one is based on deposition of a SiO_2 layer on IDTs fabricated on a traditional $LiNbO_3$/$LiTaO_3$ substrate. Since the SiO_2 layer influences not only the temperature characteristic but also the SAW excitation and reflection, the device configuration must be chosen properly. Two device structures were proposed: one employs a SiO_2 film with the flattened top surface deposited on heavy electrodes, and another one employs a SiO_2 film with the corrugated top surface deposited on relatively light Al electrodes. When $LiNbO_3$ is used as a substrate, strong spurious resonances are observed, and proper structural design is necessary for their suppression. Another strategy is based on the wafer bonding of a single crystal $LiNbO_3$/$LiTaO_3$ with a stiff substrate having small thermal expansion coefficient. Since influence of the stiff substrate is small except the temperature stability, we can directly apply design and production tools established for conventional SAW devices using a $LiNbO_3$/$LiTaO_3$ wafer to the current purpose. After tight wafer bonding, $LiNbO_3$/$LiTaO_3$ should be thinned as much as possible to make the influence of the stiff substrate obvious. This is the most important hurdle for the device realization. Another important issue is suppression of plate modes caused by the bulk wave reflection at the boundary between the $LiNbO_3$/$LiTaO_3$ layer and stiff substrate.

Discussion and Conclusions

We will show what kinds of technologies are used to satisfy various W-CDMA specifications and how high performances are achieved using these technologies.

5A-4

11:30 am Performances of Monolithic Micro-Oven Heated SAW and STW resonators

Pierre Dufilie[1], Joe Adler[1], Andrew Sawyer[1]; [1]*Phonon Corp., Simsbury, CT, USA*

Background, Motivation and Objective

Frequency stability of resonators used in low noise oscillators is typically achieved by encasing the resonator or the complete oscillator in a temperature-controlled oven. This method is preferred over electrically pulling the resonator which results in a lower loaded Q. The oven approach introduces long warm-up time, increased size, and adds considerably to the total power dissipation of the oscillator. The objective is to develop an oven structure which drastically reduces both warmup time and power dissipation.

Statement of Contribution/Methods

A novel micro-oven heated resonator structure will be presented. The structure includes the resonator, resistive heaters and temperature sensors all formed with the same fabrication process as for a resonator alone. The temperature sensor is formed by meander-connection of groups of reflective grating strips resulting in a direct temperature measurement of the active part of the resonator die.

Results

The micro-oven heated resonator structure and characteristics of both SAW and STW resonators and performances in oscillators will be presented. Warmup times of less than 1 minute at –40C are achieved.

Discussion and Conclusions

Direct heating of the active surface of the SAW resonator chip drastically reduces warmup time and heater power consumption over previous ovenized resonator approaches. The micro-oven electronics requires little additional space resulting in a compact oscillator.

5A-5

11:45 am Design of Surface Acoustic Wave Filters using Layer Diamond Structures with Zero Temperature Coefficient of Delay

Ruyen Ro[1], Ru-Yue Lee[1], Chia-Chi Sung[2], Sean Wu[3], Yen-Hsun Liao[4]; [1]Electrical Engineering, I-Shou University, Kaohsiung, Taiwan, [2]Engineering Science and Ocean Engineering, National Taiwan University, Taipei, Taiwan, [3]Electronics Engineering and Computer Science, Tung-Fang Institute of Technology, Kaohsiung, Taiwan, [4]Electronics Engineering, National Kaohsiung University of Applied Sciences, Taiwan

Background, Motivation and Objective

Piezoelectric films, such as ZnO and AlN, were combined with diamond to be a novel composite surface acoustic wave (SAW) substrate showing high phase velocity, large coupling coefficient, and small temperature coefficient of delay (TCD). Propagation characteristics of SAWs in the (100) ZnO/interdigital transducers (IDTs)/(100) AlN/diamond structure were evaluated using the finite element method (FEM). The extracted coupling-of-mode (COM) parameters were employed to design RF filters for the long term evolution (LTE) wireless communication applications.

Statement of Contribution/Methods

The resonance and anti-resonance frequencies obtained using the FEM are employed to calculate the effective phase velocity, reflectivity, and coupling coefficient of SAWs in the (100) ZnO/Cu IDTs/(100) AlN/diamond structures. A low-dispersion region of zero TCD with high phase velocity and large coupling coefficient is obtained. RF filters using the proposed structure are designed.

Results

The (100) ZnO/Cu IDTs/(100) AlN/diamond structures is presented in this study to retain a zero TCD along with a larger coupling coefficient and a higher phase velocity such that it can be employed for the design of wide-band RF filters. The contour plots of the calculated TCD versus AlN and ZnO films thickness-to-wavelength ratios is presented in the figure. With the optimized AlN and ZnO films thickness ratio of 2.357 and 0.16, and Cu electrode thickness ratio of 0.093, respectively, Sezawa mode in the (100) ZnO/Cu IDTs/(100) AlN/diamond structures possesses the phase velocity of 5753.9 m/s, coupling coefficient of 6.6%, and reflectivity of 0.075. The tailored ladder filter using these COM parameters yields a RF filter operating at 2535 MHz with 3 dB bandwidth of 70 MHz, insertion loss of 2.5 dB, and sidelobe suppression of 55 dB.

Discussion and Conclusions

SAW characteristics in the (100) ZnO/Cu IDTs/(100) AlN/diamond structures were analyzed using the FEM. The composite substrate can be employed for the design of wide-band SAW filters with zero TCD for the LTE wireless communication applications.

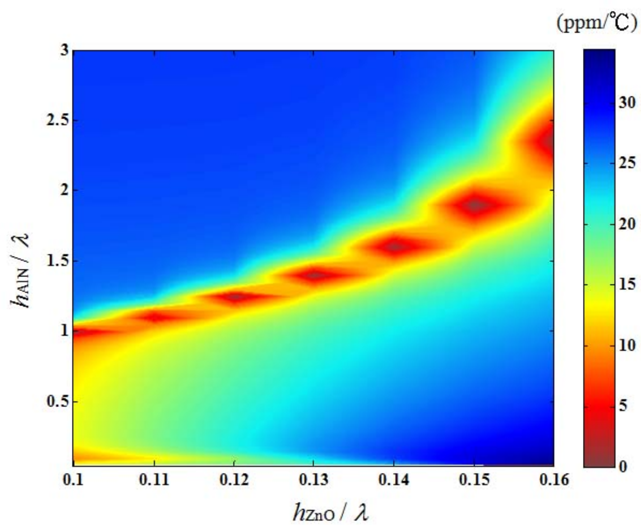

6A. CMUTs I Applications

Carribean Ballroom VI

Wednesday, October 19, 2011, 10:30 am - 12:00 pm

Chair: **Omer Oralkan**
Stanford University

6A-1

10:30 am Interdigitated CMUT Arrays for Low Intensity Focused Ultrasound Drug Delivery

Paul Cristman[1], Omer Oralkan[1], Mike Mandella[2], Olav Solgaard[1], Christopher Contag[2], B. (Pierre) T. Khuri-Yakub[1]; [1]E. L. Ginzton Laboratory, Stanford University, USA, [2]Pediatrics Department School of Medicine, Stanford University, USA

Background, Motivation and Objective

Early stage cancer detection is critical for successful treatment. For this reason there has been a continued effort to detect early stage cancers. One promising advance has been the creation of molecular contrast agents. There is a need to improve the delivery, activation, and uptake of these contrast agents. One option is to apply low intensity focused ultrasound directly to the region to be imaged. Low intensity focused ultrasound has been used for years to aid drug delivery. Here an interdigitated capacitive micromachined ultrasonic transducer (CMUT) array is being combined with a miniature dual axis confocal (DAC) microscope. The DAC microscope is used to image fluorescent contrast agents that bind specifically to cancer cells. The field of view the DAC microscope is limited to a depth of 300 µm making the application of ultrasound energy difficult. In order to overlap the acoustic pressure field with the optical field and not interfere with the lens optics surface waves must be exploited.

Statement of Contribution/Methods

Interdigitated CMUTs have been used for a range of applications including, sensing, mixing, and pumping. For this application a circularly symmetric interdigitated CMUT is used to focus the surface waves into the field of view of the optics. The circular CMUT transducer has the center removed creating a ring shape allowing a clear path for the optics. Finally, the CMUT will be packaged at the end of the miniature DAC microscope inside of a commercial endoscope. The initial purpose of the CMUT was to provide low intensity focused ultrasound for sonophoresis of fluorescent contrast agents. The same interdigitated CMUT array can be used as a photo-acoustic receiver. Photo-acoustic imaging can be obtained using the focused scanning laser already part of the microscope.

Results

A wide variety of interdigitated CMUT arrays have been fabricated. The fabricated arrays have outer diameters of 2.6 and 4.5 mm with inner diameter of 1.2 mm and 2 mm. The pitch of the interdigitated rings ranges from 40 µm to 80 µm. With all the designs a wide range of frequencies are available. One device with 45 µm width rectangular cells biased at 30 V DC and a 12 Vpp 10 cycle 1.5 MHz tone burst was scanned with a calibrated hydrophone. The peak pressure was 6.3 kPa corresponding to a power of 1.4 mW/cm^2.

Work supported by NIH Project: 5U54CA136465

Discussion and Conclusions

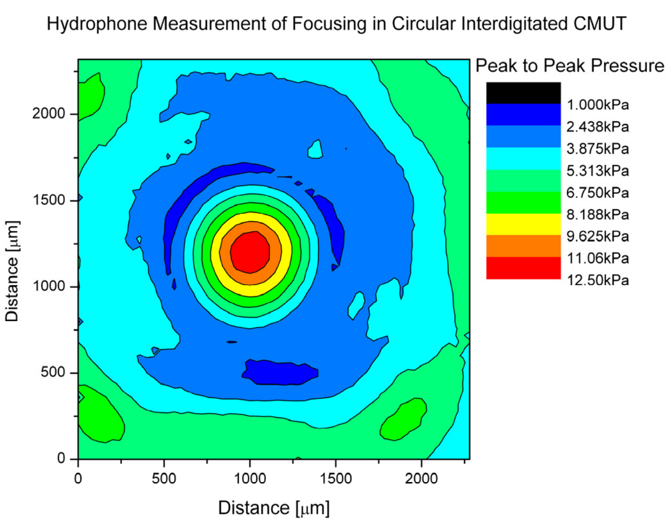

6A-2

10:45 am Comparing the Performance of CMUT and Piezoelectric Transducer Elements for Two-Dimensional Medical Imaging

Ira Wygant[1]; [1]National Semiconductor, USA

Background, Motivation and Objective

The general characteristics of CMUTs relative to piezoelectric transducers are well understood. CMUTs benefit from semiconductor-industry manufacturing methods i.e. the economy of wafer-level manufacturing, excellent control of device properties, and improved solutions for integration with electronics. Conventionally-designed CMUTs are less sensitive than comparable piezoelectric transducers but can have superior bandwidth. While the general characteristics of the two technologies are well-known, a more detailed comparison is needed. This work makes such a comparison by evaluating the performance of the two technologies for a typical 1D 7.5-MHz transducer array element.

Statement of Contribution/Methods

The array element has a 200-µm pitch, 4-mm height, and a nominal center frequency of 7.5-MHz. A ±50-V pulser drives the array. Simulation of the piezoelectric transducer is based on the Redwood model implemented in a circuit simulator. The piezoelectric transducer material stack consists of a backing layer, 1-3 composite PZT-5H, and two matching layers. CMUT simulation is based on a first-order spring-mass-damper model of a conventional silicon-based device with circular cells. The simulation results are validated with measurements of a fabricated CMUT array and a commercially available piezoelectric probe.

Results

Optimization of the piezoelectric transducer yields a 3-MRayl backing layer, 285-µm PZT-5H layer, and two quarter-wave matching layers with 8.1-MRayl and 2.2-MRayl impedances respectively. The CMUT utilizes a 30-µm-radius cell, a 1.75-µm plate, and a 300-nm effective gap. Simulations show that the CMUT has higher impedance (30 pF||2.5 kΩ compared to 35 pF|| 1kΩ), greater fractional bandwidth (150% compared to 81%), and lower output pressure (3.3 MPa compared to 4 MPa). Measurements confirm the relative performance of the two technologies but show a lower than predicted bandwidth and sensitivity for the CMUT.

Discussion and Conclusions

While this work confirms the better bandwidth and lower sensitivity of a conventional CMUT, it also shows that the sensitivity is within reach of piezoelectric transducer sensitivity. The manufacturing advantages of CMUTs and continually improving device design could make CMUTs the preferred transducer for some medical applications.

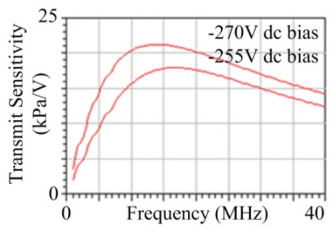

CMUT Simulation

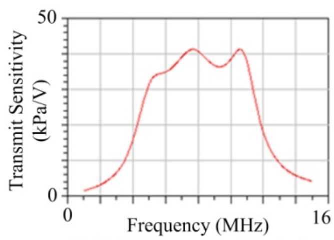

PZT-5H Composite Simulation

6A-3

11:00 am Ultrasonic Sensing Using Thermal Mechanical Noise Recorded on Monolithic CMUT-on-CMOS Arrays

Shane Lani[1], Sarp Satir[1], Gokce Gurun[1], Karim G. Sabra[1], F. Levent Degertekin[1]; [1]*Georgia Institute of Technology, USA*

Background, Motivation and Objective

Monolithic integration of miniature CMUT arrays and CMOS electronics minimizes interconnect parasitics and enables detection of the thermal-mechanical component of the ultrasonic noise field. Consequently, an estimate of the pulse-echo response (or Green's function) between two CMUT array elements can be obtained from the cross-correlation of ambient noise recorded by these two sensors [1]. This provides a foundation for passive ultrasound sensing and imaging using only the thermal- mechanical noise field, without the use of active transmitter elements.

Statement of Contribution/Methods

We designed and fabricated monolithic a 32 element CMUT-on-CMOS array for intravascular imaging with low noise transimpedance amplifiers (TIAs) implemented in 0.35µm CMOS technology. The DC bias was set near the collapse value of the CMUT membrane to maximize receiver sensitivity. Demonstration experiments were conducted by immersing the CMUT array in a water bath to sense/image the water-air interface from noise signals in the frequency band 14MHz-25MHz.

Results

The normalized cross-correlations function computed between selected pairs of receivers show a clear echo associated with the water interface (Fig. 1) consistent with the sensor and target location. Note that each waveform shows two echoes for both positive or negative time-delays which result from coherent thermal mechanical noise propagating one-way from the first sensor to the other and vice versa. These target echoes were found to shift in a consistent symmetric fashion when we reduced the thickness of the water layer from 2.0mm to 1.5mm. Additionally, the large peak centered at t = 0s corresponds to the non-propagating electronic noise and crosstalk components of the recorded noise

Discussion and Conclusions

Using low noise amplifier designs in a CMUT-on-CMOS implementation allows for extracting pulse-echo-like arrivals from thermal-mechanical noise cross-correlations between CMUT array elements. In particular, this totally passive technique could improve ultrasound imaging of near-field targets in the deadzone created by active transmitters biasing the receivers and may lead to imaging using evanescent waves.

[1] Weaver, R. L., and Lobkis, O. I. (2001). "Ultrasonics without a source: Thermal fluctuation correlations at MHz frequencies," Phys. Rev. Lett. 87, 134301

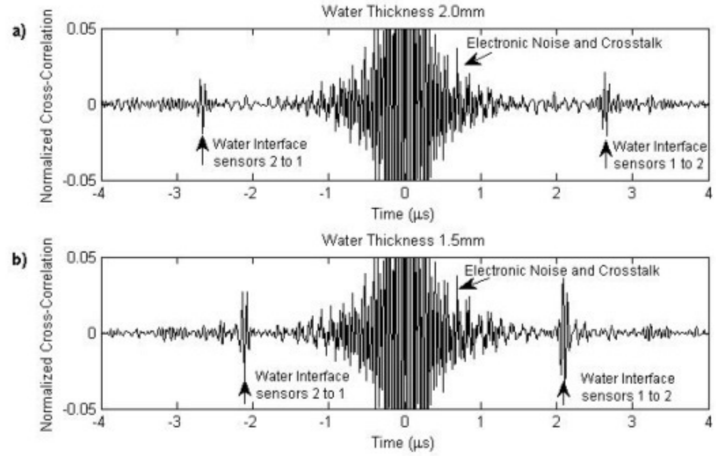

Figure 1: Cross-correlation of ambient noise between two sensors for a.) water thickness of 2mm and b.) water thickness of 1.5mm

6A-4

11:15 am CMUT Array Element Operating in Deep Collapse Mode of Operation

Selim Olcum[1], Yalcin Yamaner[2], Ayhan Bozkurt[2], Hayrettin Koymen[1], Abdullah Atalar[1]; [1]Electrical & Electronics Eng., Bilkent University, Ankara, Turkey, [2]Sabanci University, Istanbul, Turkey

Background, Motivation and Objective

Output power limitations of conventional mode CMUTs have been a major drawback since CMUTs have first been introduced. However, ultrasound applications require high transmitted pressures for an increased penetration and a better signal-to-noise ratio. Collapse and deep collapse mode of operations have boosted the pressure outputs considerably. However, unresolved issues of high voltage requirements and charge trapping hinder a successful application utilizing these modes. In this work, we demonstrate a CMUT element operating in the deep collapse mode with 25V excitation and without charge trapping effects.

Statement of Contribution/Methods

We utilized a surface microfabrication process for producing the CMUT elements. Fabricated CMUT cells have 1.3um thick PECVD grown nitride membranes suspended over a 50nm cavity. The fabricated CMUT element consists of 4 by 4 circular cells with 20μm radius. The overall size of the element is 190μm by 190μm. The collapse voltage is measured to be approximately 3V.

Results

We performed immersion experiments in an oil tank using a calibrated hydrophone. By driving the CMUTs with 25V pulses, we achieved 1.2MPa pressure output on the surface of the CMUT element with a center frequency of 9MHz and more than 100% bandwidth. Such an electrical excitation forces the membrane to go into deep collapse.

One outstanding problem of the collapsed state is the charge trapping in the insulator between the electrodes. By driving the CMUTs with an electrical pulse sequence with alternating polarities we eliminated this effect. We applied 1000 consecutive electrical pulses with alternating polarity to the element and measured no change in the transmitted acoustic pulse as seen in the figure. For the case of 40V electrical pulses with uniform polarity, on the other hand, the amplitude of the transmitted acoustic pulse decreases to half of its maximum value after 50 firings.

Discussion and Conclusions

It is possible to generate high intensity, sharp acoustical pulses at a desired frequency of operation by driving deep collapse mode CMUT elements using ±25V pulses - i.e. compatible with 50V CMOS processes. Furthermore, by utilizing an electrical pulse sequence with alternating polarities as the excitation, the problem of charge trapping is eliminated. We believe such an approach will be vital in designing future ultrasonic probes incorporating CMUTs.

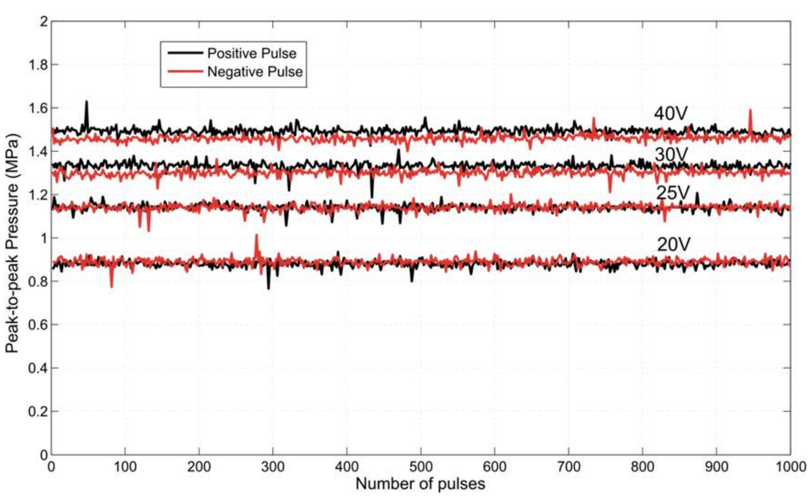

6A-5

11:30 am Gap Feedback Linearization of Capacitive Micromachined Ultrasonic Transducers for Harmonic Imaging

Sarp Satir[1], F. Levent Degertekin[2]; [1]School of Electrical & Computer Engineering, Georgia Institute of Technology, Atlanta, GA, USA, [2]G.W. Woodruff School of Mechanical Engineering, Georgia Institute of Technology, Atlanta, GA, USA

Background, Motivation and Objective

The nonlinear relationship between electrical input signal and electrostatic force acting on the CMUT membrane limits its harmonic imaging performance. Several input shaping methods were proposed in order to compensate for the nonlinearity originating from the voltage square dependence [1]. Here we analyze harmonic generation in CMUTs with a time domain model, verify previous experimental work and propose a feedback based linearization method.

Statement of Contribution/Methods

CMUT is modeled as a parallel plate capacitor in Simulink to obtain the time domain displacement and pressure for arbitrary input signals. The model is verified using experimental data from nonlinearity reduction using predistorted waveforms. Since the square voltage law and inverse gap dependence are the sources of nonlinearity, the model suggests that harmonic distortion in the output pressure can be eliminated by subharmonic AC only excitation of the CMUT while the input voltage is scaled with the instantaneous gap. This method can be simply approximated by addition of a series feedback capacitor to the CMUT capacitance.

Results

The nonlinear equivalent circuit of a transducer with a center frequency of 30MHz and 100% FBW, is modeled as an example. In Fig.1a, it can be seen that for the same pressure output at 20MHz, the harmonic component at 40MHz decreases by only 2 dB with 10MHz excitation of the transducer. This indicates that for large membrane displacements the main contributor to the nonlinearity is the gap dependence of the electrostatic force. With series feedback capacitor and 10MHz excitation, 2nd harmonic is reduced by 6dB for the same output pressure. In addition, one can increase the output pressure with a higher amplitude input signal for given harmonic distortion using a series capacitance by avoiding the membrane collapse [2].

Discussion and Conclusions

A simple model has been used to analyze nonlinearity compensation methods for CMUT. A linearization method is proposed which is based on subharmonic excitation of the transducer with no DC bias and a small series feedback capacitance. The proposed method offers simple input signals and a trade-off between input voltage amplitude and harmonic distortion for a desired output pressure.

[1] A. Novell et al., IEEE Trans. on UFFC, Vol. 56, p. 2733, 2009.

[2] J. I. Seeger, S. B. Crary, 1997 Intl. Conf. on Solid-State Sensors and Actuators, pp. 1133-1136.

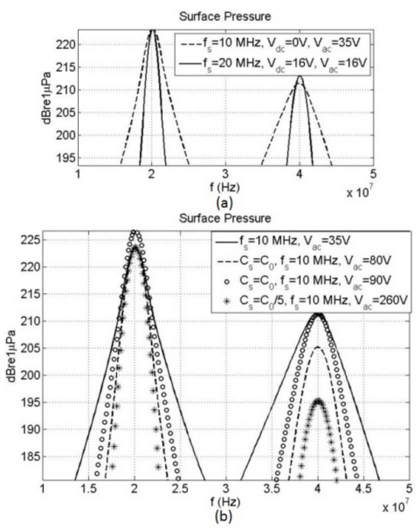

Fig.1

6A-6

11:45 am CMUTs with interlaced high- and low-frequency elements for combined imaging and therapy

Peiyu Zhang[1], Wei Zheng[1], Walied Moussa[2], Roger Zemp[1]; [1]Electric and Computer Engineering, University of Alberta, Canada, [2]Mechanical Engineering, University of Alberta, Canada

Background, Motivation and Objective

There are a number of emerging biomedical applications where it would be advantageous to have anultrasound transducer that could operate at low frequencies (1-2MHz) &high power in a treatment-mode, yet have the ability to image with high frequencies (~10MHz) &large bandwidth in an imaging mode. Potential applications may include image-guided HIFU-ablation therapy, sensitive contrast agent imaging and radiation-force facilitated targeting, image-guided gene &drug delivery, image-guided biomarker release. Unfortunately, such transducers are difficult to fabricate using piezoelectric technology. Capacitive Micromachined Ultrasound Transducers (CMUTs) may offer a viable alternativedue to advances in MEMS microfabrication technologies.

Statement of Contribution/Methods

CMUTs with interlaced low- &high-frequency elements are designed, simulated &fabricated. Our designs are based on the key observation that the acoustic wavelength in water/tissue corresponding to the resonance frequency of CMUT cells is typically significantly larger than the device dimensions. We design CMUT devices with interlaced 2 MHz cells &10MHz cells. One composite cell (with 2- &10MHz CMUT structures) is smaller than the acoustic imaging wavelength in tissue. This design ensures that grating lobe artifactsin ultrasound images will be minimized. Devices are modeled using ANSYS, which is used to predict static and dynamic behavior of large and small CMUT elements. Field II software is used to simulate the therapeutic beam-patterns and imaging point-spread functions. Several different interlacing schemes are proposed. Devices are fabricated using both a double-SOI wafer-bonding technique &a sacrificial-release process.

Results

White light interferometry results show that device deflection as a function of bias voltage is in excellent agreement with predicted values. For example, for 100-um structures, snapdown voltages are measured as 51+/-2 V, compared to the predicted value of 51 V. Fabricated devices have a ~350 nm gap as validated by SEM. A range of fabricated membrane sizes were tested for frequency response. Fabricated devices exhibit resonance frequencies in good agreement with ANSYS simulated design values as measured by laser vibrometry in air.We focus our experimental studies on single-element composite transducers in a 7mmx7mm test area for proof of principle. Fabrication &testing of linear arrays is underway.

Discussion and Conclusions

Simulations of linear arrays using Field II show that image quality is not significantly degraded by the interlaced architectures, since element dimensions are smaller than the acoustic imaging wavelength in tissue. Fabricated devices show promising performance as combined imaging-therapy transducers, however, more work is needed to construct and test imaging-therapy linear arrays.

1B - HIFU Application and Monitoring

Boca Rooms II-IV

Wednesday, October 19, 2011, 2:00 pm - 3:30 pm

Chair: **Ralf Seip**
Philips Research

1B-1

2:00 pm High-Throughput Coagulation by Heating with Laterally Enlarged Focus, Enhanced by Mircobubble Clouds Created by Electronically Scanned Trigger Pulses

Shin-ichiro Umemura[1], Jumpei Okada[2], Keisuke Takada[3], Tatsuya Moriyama[3], Eiko Iwasaki[4], Shin Yosizawa[5]; [1]*Biomedical Engineering, Tohoku University, Sendai, Miyagi, Japan,* [2]*Electrical and Communication Engineering, Tohoku University, Miyagi, Japan,* [3]*Electrical and Computer Engineering, Tohoku University, Miyagi, Japan,* [4]*Biomedical Engineering, Tohoku University, Miyagi, Japan,* [5]*Electrical and Communication Engineering, Tohoku University, Sendai, Miyagi, Japan*

Background, Motivation and Objective

The smallness of an ultrasonic focal spot provides both great geometric selectivity and low throughput of focused ultrasound treatment. We have proposed that the throughput can be significantly enhanced by microbubbles created by extremely high-intensity trigger pulses in prior to heating waves [1]. Because a typical focal spot is longer in the propagation than lateral direction by an order of magniude, its surface/volume ratio can be much more reduced when the focus is enlarged in the lateral rather than propagation direction.

[1] Y. Inaba, S. Yoshizawa, S. Umemura: Japanese J. Applied Physics, 49, 7, 07HF22 (2010).

Statement of Contribution/Methods

The exposure sequence as shown in Fig. 1, consisting of electronically scanned trigger pulses, followed by heating waves with a focus enlarged laterally in two dimensions, was conceived. The surface/volume ratio was reduced approximately by twice compared to the conventional single spot focus, and the heat efficiency should thereby be significantly increased. In vitro experiments with tissue mimicking gel were performed using a 128 ch focused composite array transducer (Imasonic), 100 mm in diameter and focal length, driven by FPGA-controlled 32 ch amplifiers at 1 MHz. Neighboring elements of the 8-track 16-sector array were electrically combined to form a 2-track 16-sector array, each element of which is driven by one of the 32 ch stair-case drive amplifiers consisting of complementary pairs of power MOSFETs (Fairchild). The laterally enlarged focus has four pressure peaks, to each of which the focal position of a trigger pulse was adjusted.

Results

A high-speed camera showed that the microbubble clouds were created by the trigger pulses at about 30 kW/cm2 and survived by the time the heating waves arrived. The observed coagulation volume due to the same heating wave exposure at about 1 kW/cm2 for 10 s was several times larger with than without the trigger pulses.

Discussion and Conclusions

The throughput enhancing potential of the proposed exposure sequence, consisting of electronically-scanned extremely-high-intensity trigger pulses, followed by heating waves with a focus enlarged laterally in two dimensions, was demonstrated with in vitro experiments using tissue mimicking gel. The results clearly suggest that the lateral enlargement of heating focus alone is not enough and microbubbles are needed for enhancing the throughput.

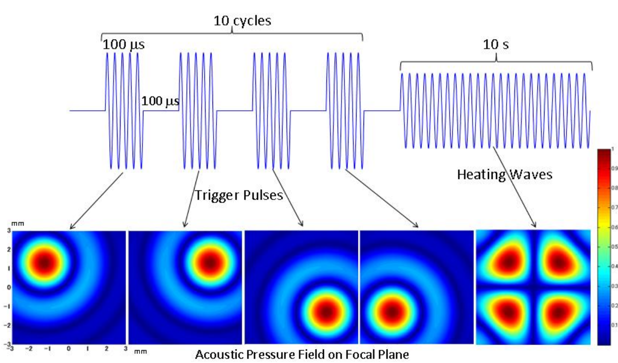

Fig. 1 Triggered HIFU sequence with laterally enlarged focal volume of heating.

1B-2

2:03 pm High amplitude ultrasound pulse generation using time-reversal through a multiple scattering medium.

Bastien Arnal[1], Mathieu Pernot[1], Mathias Fink[1], Mickael Tanter[1]; [1]Institut Langevin, ESPCI ParisTech, CNRS UMR 7587, INSERM ERL U979, Université Paris VII, Paris, France

Background, Motivation and Objective

In histotripsy, the generation of very high pressure pulses allows the fragmentation of soft tissues in a targeted area. However, electronical beam steering of conventional multi-element transducers is limited to a small region around the geometrical focus and requires hundreds of elements to reach cavitational thresholds. The use of time-reversal (TR) cavity has already been shown as a way to generate several virtual acoustic sources allowing reducing the number of emitters. Using 1-bit TR, Montaldo et al. have applied this concept in a solid waveguide where compression and shear waves reverberate in the cavity. Nevertheless, this one meter long heavy device was limited by a poor transmission into water and by limited steering abilities because of the cylindrical geometry.

Statement of Contribution/Methods

We propose here to use a waveguide made of thin steel walls filled with water (dim 14x14x25cm). Inside the waveguide, we add a 2D multiple-scattering medium made of steel rods (diameter 0.8mm) positioned randomly with controlled densities and width (L=0 to 60mm and d=0 to 20rods/cm2). We investigate experimentally and numerically the benefits of TR through a multiple -scattering medium to amplify the focal pressure of a linear probe (Vermon, 128 elements, 1.5MHz) at a target location outside the cavity and to improve the beam steering capabilities. FDTD simulations were performed using a discretization of the 2D acoustic wave equation (Acel).

Results

First, simulations have been performed to find an optimum in rod density for a given width of the scattering medium. A short pulse (3µs, central frequency 1.5MHz) was transmitted at a point outside the cavity and its propagation toward the linear array inside the cavity was computed. The signals recorded by the linear array (total duration of 300 µs) were time reversed and after reemission, it focused back at the initial location. With a multiple scattering width of 30 mm, the time-reversed pressure reached a maximum for a rod density of 10 rods/cm2. Then, this dependence was measured experimentally using a TR mirror and 1-bit TR. The optimal density was similar with simulation results. Compared to a regular focusing with the equivalent aperture, pressure peak amplitude at the focus is multiplied by 6. Beam steering abilities were also improved to an extent of 10 cm.

Discussion and Conclusions

The use of multiple scattering medium and 1-bit TR is of great interest to gain spatial degrees of freedom and amplify acoustic pulses emissions. We found experimentally and numerically that an optimal multiple scattering medium exists resulting from a tradeoff between the gain provided by multiple paths and the loss due to multiple scattering attenuation. This technique requires a TR mirror but no high-power voltage electronics and no particular transducers technology is needed. It could become a potential alternative to expensive high power phased arrays. The extension to 2D phased arrays is under investigation.

1B-3

2:30 pm Thermal ablation by high-intensity-focused ultrasound using a toroidal transducer for the treatment of colorectal liver metastases during an open procedure. First clinical results.

David Melodelima[1], Aurélien Dupre[2], Alessandro Gandini[2], Jean-Yves Chapelon[1], Michel Rivoire[2]; [1]*U1032, INSERM, Lyon, France,* [2]*Centre Leon Berard, France*

Background, Motivation and Objective

In this study an ultrasound device that uses a toroidal HIFU transducer guided by ultrasound imaging was evaluated clinically for the treatment of colorectal liver metastases during an open procedure. Our long-term objective is to associate HIFU with hepatic resection. Here we report the first clinical results obtained on six patients with liver metastases and scheduled for elective surgical resection of their tumors. The principal objective was to validate the effectiveness, tolerance and safety of the HIFU parameters defined during preclinical studies. In addition, the response to HIFU was assessed using the ultrasound imaging probe integrated in the HIFU device and compared directly with histological analysis.

Statement of Contribution/Methods

It was planned to include 6 patients in this Phase I trial. A 85% ablation rate success was required to continue the study (Phase II). Secondary endpoint was preciseness of ultrasound imaging to visualize HIFU ablations. The transducer has a toroidal shape 70 mm in diameter and is divided into 8 radial ultrasound emitters of 4.16 cm2 each. The radius of curvature is 70 mm to enable treatment of the deepest regions of the liver and each of the 8 emitters is divided into 32 individual transducers operating at 3 MHz. A 7.5 MHz ultrasound imaging probe was placed in the centre of the device to guide the treatment. The imaging plane was aligned with the HIFU focal zone. Two single thermal ablations were created in each patient after laparotomy and just before the planned liver resection.

Results

Twelve HIFU lesions were performed. All were visible on ultrasound images. Consistent with our previous experience, the demarcation between ablated and non-ablated tissue was apparent in ultrasound images as a hypoechoic boundary and a large central hyperechoic zone. The dimensions measured on ultrasound imaging were correlated (r=0.92) with dimensions measured during histological analysis. The average coagulated volume obtained from a 40 s total exposure in the liver was 5.6 ± 2.6 cm3 (1.9 – 11.4) with an average diameter of 21.6 ± 4.5 mm (12.0 – 28.0) and an average depth of 28.4 ± 6.3 mm (20.0 – 43.0). The patients have tolerated the treatment well. There was no hemodynamics and respiratory changes. No HIFU-related complications occurred during surgery and 30 days postoperatively. The ultrasound imaging probe integrated in the HIFU device enabled exploration of 88% of the liver.

Discussion and Conclusions

This HIFU treatment using a toroidal transducer is feasible, safe and well tolerated. The HIFU approach presented in this study is characterized by the brevity of the treatment (40 seconds for one single ablation of 5-6 cm3). This device is capable of achieving selective ablation of predefined liver regions. Ultrasound imaging evidence of complete ablation of the target region can be taken to infer histological success.

1B-4

2:45 pm An ultrasonic device with Parabolic Convex Reflector for the Conformal Thermal Ablation of the Ciliary Body

Thomas Charrel[1,2], Florent Aptel[1,3], Alain Birer[1], Francoise Chavrier[1], Jean-Yves Chapelon[1], Fabrice Romano[2], Cyril Lafon[1]; [1]inserm U1032, Lyon, Rhone, France, [2]eyetechcare, Rillieux-La-Pape, Rhone, France, [3]edouard Herriot Hospital, Lyon, Rhone, France

Background, Motivation and Objective

The thermal ablation of the ciliary body (CB) is a common and efficient method to reduce the intra-ocular pressure (IOP), see figure 1. High-Intensity Focused Ultrasound (HIFU) for cyclocoagulation, introduced by Lizzi in the 80's and recently by Aptel (2010), has shown good results to reduce the IOP and to treat glaucoma. This study examines a new HIFU probe based on the reflection of a convergent cylindrical wave (21MHz) on a parabolic convex reflector (PCR) to treat the CB. The efficiency of using acoustic reflection for focusing ultrasonic treatment has been proven by numerous therapeutic applications, such as lithotripsy (Coptcoat 1987) and atrial fibrillation (Meininger 2003). This design allows producing a ring-shaped focus area without undesirable re-focusing effect, see figure 2.

Statement of Contribution/Methods

The acoustic pressure field and the thermal lesions were simulated. A numerical model of the eyeball was developed and the Bio-Heat Transfer Equation (BHTE) was solved to estimate the thermal dose deposition in the CB and adjacent tissues such as cornea, iris, lens and retina. A prototype was made, and the acoustic field was characterized using a 75µm hydrophone and a 3D scanning system. Thermal lesions in heat-sensitive 18% BSA gel were analyzed.

Results

Focal volumes at -6dB, predicted by the model, are in accordance with the measurement (1.5±0.1mm^3). Thermal lesions predicted by the BHTE model are confined in the CB and no undesirable lesions appeared in adjacent tissues. Thermal effects in gel show six lesions conforming with the predicted circle of lesion (13±0.1mm in diameter).

Discussion and Conclusions

Ultrasound PCR device seems to be a promising application for ophthalmic treatment and will be experimented In-vivo. Work funded by EyeTechCare SA.

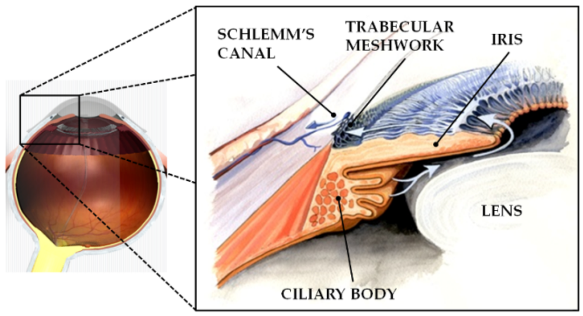

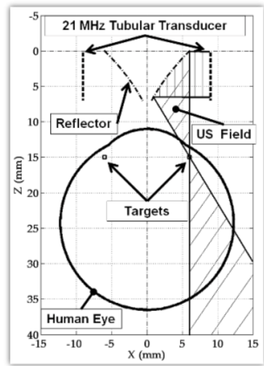

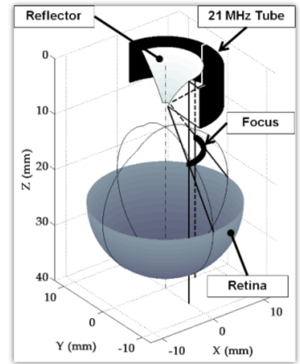

1B-5

3:00 pm Simultaneous temperature and cavitation activity mapping with a transcranial MR-guided focused ultrasound system

Costas Arvanitis[1], Nathan McDannold[2]; [1]Radiology, Harvard Medical School, Boston, Massachsetts, USA, [2]Radiology, Harvard Medical School, Boston, Massachusetts, USA

Background, Motivation and Objective

As focused ultrasound is maturing rapidly with a wealth of novel approaches to treat cancer, neurodegenerative and vascular diseases currently at preclinical evaluation, there is a quest to monitor, optimise and warrant the safety of the treatments. The vast majority of these approaches exploit either acoustic cavitation - a manifestation of mechanical effects, or viscous heating - a manifestation of thermal effects, or both. Here we show the development of a dual modality approach (MR and US) that allows, for the first time, simultaneous assessment and localization of the effects of therapeutic ultrasound.

Statement of Contribution/Methods

A 128-element (82 mm) linear US array (central frequency: 3.5 MHz) was incorporated via an acoustic mirror in a 30 cm hemisphere 1024-channel therapeutic phased array (ExAblate 4000, InSightec, Haifa, Israel) that was developed for MR guided brain surgery using a clinical 3T MRI (GE). The linear array was connected to a research US imaging engine (Verasonics Inc., Redmond, WA) through the MR penetration panel. A brain mimicking phantom placed in the focal region of the therapeutic transducer was sonicated at multiple nonoverlapping locations (20 mm apart) for 10s at acoustic powers from 25W to 100W. The targets were approximately 120 mm away from the US probe and in its imaging plane. MR temperature and passive cavitation maps, were obtained with phase mapping and back-propagation methods respectively. 15 temperature and cavitation maps where collected during each sonication.

Results

Minimal magnetic inhomogeneity and interference/artifacts were observed in the temperature and cavitation maps as a result of crosstalk between the systems. The temperature elevation in the presence of cavitation activity was from 10°C to 40°C and was confined to the targeted locations. The cavitation maps showed consistent cavitation activity. The cavitation location with respect to three targeted locations in the transverse (resolution ≈0.6 mm) and axial (resolution ≈7 mm) directions were 1) -3.1 ± 9 mm 3.5 ± 6.9 mm 2) -0.7 ± 3.8 and -1.6 ±1.8 mm and 3) 6.5 ± 11.3 mm and 1.8 ± 7.8 mm respectively. During the sonication of the last target the cavitation maps revealed cavitation activity at all of the previously sonicated points (same MR and US plane) whereas temperature elevation was observed only at the targeted location.

Discussion and Conclusions

Using MR temperature imaging and passive cavitation maps, we simultaneously assessed and localized the thermal and mechanical effects of focused ultrasound. The results demonstrate that this dual modality approach may enable improved safety monitoring, guidance of cavitation-based therapies, and provide the means to optimize and potentially accelerate ultrasound therapies.

1B-6

3:15 pm **Cavitation Inception and Growth by Dual-Frequency Excitation in High-Intensity Focused Ultrasound Treatment**

Shin Yoshizawa[1], Jun Yasuda[1], Shin-ichiro Umemura[1]; [1]*Tohoku University, Japan*

Background, Motivation and Objective

HIFU treatment with cavitation bubbles has attracted much attention because they enhance the therapeutic efficacy of HIFU. Negative acoustic pressure is known to primarily determine the cavitation threshold. However, it is hard to generate highly negative acoustic pressure over the cavitation threshold by ultrasonic focusing because of the nonlinear propagation. We investigated a new sequence which was superimposed the second harmonic onto the fundamental to trigger cavitation efficiently.

Statement of Contribution/Methods

In this study, 2.28 MHz frequency ultrasound was superimposed to 1.14 MHz ultrasound, and cavitation inception and growth on an aluminum block in water was investigated by high-speed camera observation. An air-backed ultrasound transducer for second-harmonic superimposition consists of two co-focally aligned spherically curved PZT ceramic elements. In the experiments, four different types of sequence were used. The first two employed the second-harmonic which emphasizes either the peak positive pressure (dual-frequency 1) or negative pressure (dual-frequency 2). Both continued for 80 µs. The third employed the second-harmonic emphasizing the peak negative pressure for the earlier 40 µs and that emphasizing the peak positive pressure for the later 40 µs (dual-frequency 3). The fourth sequence employed a single frequency (1.14 MHz) continued for 80 µs (single-frequency).

Results

Figure 1 shows images of cavitating bubbles at an intensity of 3.5 kW/cm^2 in the cases of (a) dual-frequency 1, (b) dual-frequency 2, (c) dual-frequency 3, and (d) single-frequency exposure, respectively. The results showed that cavitation bubbles were generated most efficiently by the third waves. A small amount of bubbles were generated in the earlier 40 µs of negative-peak-pressure emphasized waves, and then the bubbles markedly expanded by the positive-peak emphasized waves.

Discussion and Conclusions

The initiated bubbles may have provided a pressure-release surface and the positive-peak emphasized waves could be converted thereby to ultrasonic waves with highly negative peak pressure. The exposure sequence which uses negative-peak-pressure emphasized waves followed by positive-peak-pressure emphasized waves may have the potential to be used to effectively accelerate HIFU treatment.

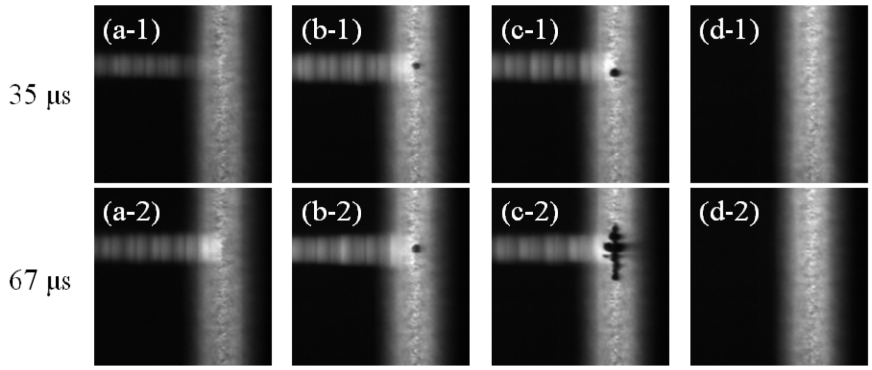

Fig. 1. Images of cavitating bubbles at an intensity of 3.5 kW/cm^2 in the cases of (a) dual-frequency 1, (b) dual-frequency 2, (c) dual-frequency 3, and (d) single-frequency exposure, respectively.

2B - Cardiac Beam Forming

Boca Rooms VI-VII

Wednesday, October 19, 2011, 2:00 pm - 3:30 pm

Chair: **Kai Thomenius**
GE's corporate R&D

2B-1

2:00 pm High Frame Rate Echocardiography Using Diverging Beams

Hideyuki Hasegawa[1,2], Hiroshi Kanai[1,2]; [1]Graduate School of Biomedical Engineering, Tohoku University, Japan, [2]Graduate School of Engineering, Tohoku University, Japan

Background, Motivation and Objective

It has been recently shown that the measurement of propagation of spontaneous vibration of the heart would be useful for evaluation of myocardial function and viscoelasticity (Kanai, IEEE Trans. UFFC, 2005). However, such measurements require a frame rate much higher than that of conventional ultrasonic imaging. In the present study, a method based on parallel receive beamforming was developed to achieve high frame rate echocardiography.

Statement of Contribution/Methods

Spatial resolution realized by parallel beamforming is often degraded due to use of unfocused transmit beams. In addition, ultrasound images in sector format obtained by highly parallelized beams suffer from the discontinuity at the edge of the region imaged by one transmission because the difference between directivities in consecutive transmissions is large due to large angular intervals of steered transmit beams. In the present study, by partially overlapping unfocused transmit beams, spatial resolution was improved by compounding point spread functions (PSFs) created at each point of interest (POI) by several transmissions in different directions. In addition, the discontinuity in the image could be significantly reduced by weighting the PSFs used in compounding. The weights were determined by the angular distance between the POI and the direction of transmission. Furthermore, to realize a wider region imaged by one transmission, ultrasound waves, which were diverging from virtual point sources in an ultrasonic probe, were used because, in sector format, the width of the region imaged by one transmission increases with the range distance.

Results

Spatial resolution of the proposed method was validated using fine nylon wires. PSFs obtained by the proposed method were 0.84 mm (axial) and 0.86 mm (lateral). They were slightly degraded but very similar to those, 0.73 mm (axial) and 0.68 mm (lateral), obtained by conventional beamforming (focusing in both transmit and receive). Furthermore, a heart of a 23-year-old healthy male was measured. The image quality obtained by the proposed method (Fig. (b)) is very similar to that obtained by conventional beamforming (Fig. (a)). But the frame rate was significantly increased to 316 Hz (a) from 39 Hz (b).

Discussion and Conclusions

High frame rate echocardiography at a frame rate of 316 Hz was realized with a full lateral field of view of 90 degrees.

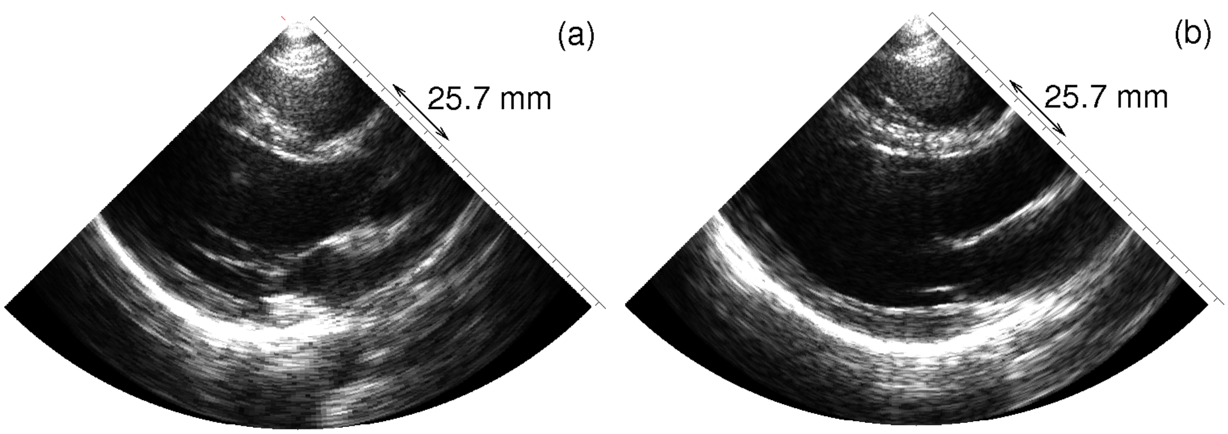

2B-2

2:03 pm Motion compensated Synthetic Transmit Beam technique for real-time echocardiography

Bastien Denarie[1], Hans Torp[1], Geir Haugen[2], Anders Sørnes[2], Tore Bjåstad[2]; [1]MI Lab and Department of Circulation and Medical Imaging, Norwegian University of Science and Technology, Trondheim, Norway, [2]GE Vingmed Ultrasound AS, Horten, Norway

Background, Motivation and Objective

The Synthetic Transmit Beam (STB) technique is a previously published technique for removing image artifacts caused by parallel beamforming. Since it is based on lateral coherent interpolation between overlapping beams acquired from neighboring transmit events, it is vulnerable to motion. Especially in cardiac imaging where high velocities from both tissue and blood in the cavities will result in stripe-shaped artifacts in the image.

The objective of this work was to develop a motion compensated STB algorithm capable of compensating for motion in cardiac imaging.

Statement of Contribution/Methods

The algorithm presented in this work is based on the autocorrelation product between the IQ data of overlapping scan lines from neighboring transmit events, and has a sufficiently small computational demand to be implemented in real-time. The technique was tested by post processing of recorded IQ data, using Field II simulations (DTU, Denmark), and implemented further in real-time on a Vivid E9 scanner (GE Vingmed Ultrasound, Norway).

Results

The proposed algorithm was successful in compensating for cardiac motion and tested with different values of Pulse Repetition Frequency (PRF).

The attached Figure illustrates the effect of the phase compensation algorithm when combining 8 parallel receive beams into 4 STB at a PRF of 1000. Motion of the heart induces an observed intensity variation of up to 18% between the different STB scan lines when averaged over the whole cardiac cycle, while the difference in intensity is below 1.5% with the proposed motion compensated STB algorithm.

Discussion and Conclusions

Applying the proposed motion compensation algorithm, stripe artifacts appearing in the STB images in presence of myocardium and blood motion were removed. The compensation technique can also be adapted to compensate for motion artifacts in other coherent imaging techniques such as plane wave compounding, retrospective transmit beamforming and other variants of synthetic aperture imaging.

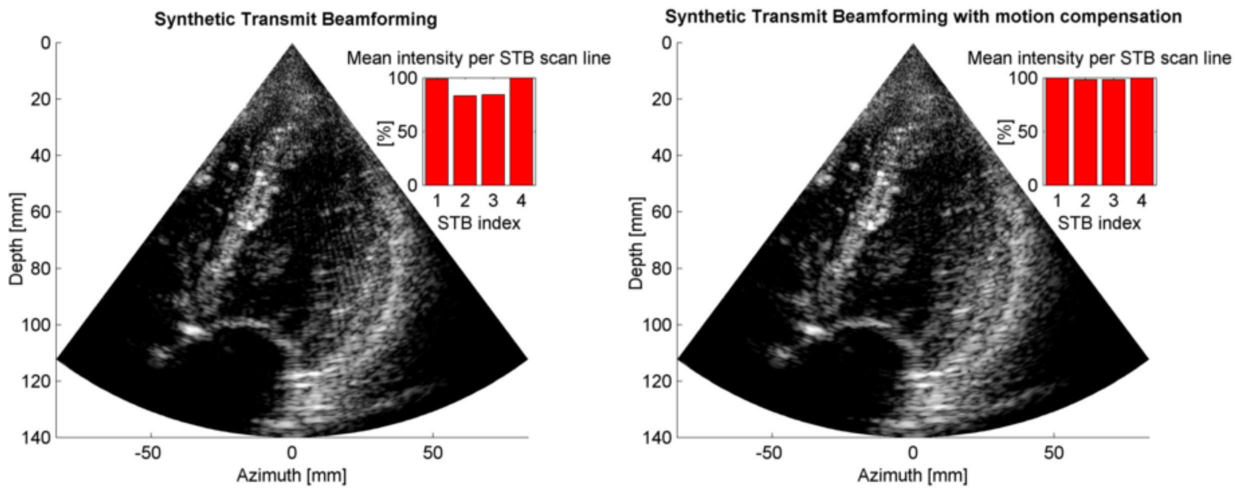

2B-3

2:30 pm Multi-transmit beam forming for fast cardiac imaging

Ling Tong[1], Hang Gao[1], Hon Fai Choi[1], Jan D'hooge[1]; [1]Dept. of Cardiovascular Diseases, Catholic University of Leuven, Leuven, Belgium

Background, Motivation and Objective

A better understanding of short-lived cardiac phases could be of diagnostic value but would require very high temporal resolution. To increase frame rate, as an alternative to parallel receive beam forming, it has been proposed to transmit multiple lines simultaneously (i.e. multi-line transmit (MLT)) although this approach has received less attention due to potential cross-talk artifacts between beams. The aim of this study was to compare the performance of different MLT implementations to conventional beam forming with computer simulation in order to develop a fast cardiac imaging system.

Statement of Contribution/Methods

MLT beams were generated by transmitting different pulses on the individual elements of a phased array. The pulse to be transmitted on an element was defined as the sum of the pulses that would be transmitted on that element when generating conventional, focused single line transmit (SLT) beams along the directions of different MLT lines. Using an in-house developed simulation environment, we simulated the point-spread function (PSF) of a 64-element, 2.5MHz phased array transmitting 1 (SLT), 2, 4 or 6 (MLT) beams at the same time. To reduce the cross-talk, different combinations of transmit and receive apodizations were tested using windowing functions: Rectangular, Hanning, Tukey and Hamming. Finally, phantom images were generated with all systems.

Results

For a 90° sector image, the PSFs produced by the 2MLT system were almost identical to the conventional SLT approach although some cross-talk was present in the near field. With increasing number of MLT beams, this cross-talk became more severe. However, apodizations could significantly reduce these artifacts. In particular a Hanning–Tukey (α = 0.3) combination reduced these artifacts below the -40dB level for all MLT systems tested (cf. Fig.1 a-c). With this apodization scheme, no marked differences between SLT and 6MLT phantom images could be observed (cf. Fig.1 d-e).

Discussion and Conclusions

Based on our simulations, 6MLT has a competitive image quality to SLT but with a 6 times higher frame rate. The MLT approach can be combined with (multiple) parallel receive beam forming to increase frame rate further. With these methods, a 90° sector image can be generated without significant loss in image quality at approximately 420Hz. Implementation of this approach on an experimental system is the ongoing work.

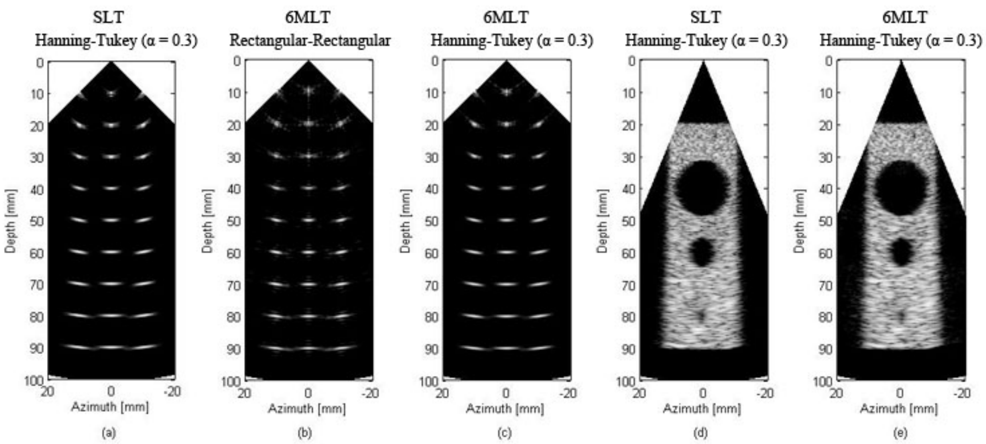

Fig.1 Images generated with different systems

2B-4

2:45 pm Comparison of parallel beam forming with plane wave imaging for cardiac applications: a simulation study

Ling Tong[1], Hang Gao[1], Hon Fai Choi[1], Jan D'hooge[1]; [1]Dept. of Cardiovascular Diseases, Catholic University of Leuven, Leuven, Belgium

Background, Motivation and Objective

Parallel beam forming (i.e. multiple line acquisition (MLA)) is commonly used to increase frame rate for fast cardiac imaging. With 4MLA, the frame rate increases by a factor of 4 but a broadened transmit beam is needed to reduce block-like artifacts. As an alternative, plane wave (PW) imaging could be used allowing – for a typical phased array transducer – for 16MLA. However, different transmits then need to be compounded in order to keep the spatial resolution acceptable. As such, a gain in frame rate similar to the one of 4MLA can typically be obtained. The aim of this study was therefore to directly contrast the performance of a conventional 4MLA system to a plane wave imaging system by computer simulation.

Statement of Contribution/Methods

A 64-element, 2.5MHz phased array was used in this study. Two-way beam profiles of the 4MLA and PW imaging system were simulated and quantified by averaging the following characteristics over depth (10-90mm) and steering angle (0-45degrees): -6dB beam width, main lobe to side lobe energy ratio (MSER), main lobe centralization (warping), and side lobe asymmetry (skewing). Different combinations of typical windowing functions (i.e. Rectangular, Hanning, Tukey and Hamming) were evaluated. Conventional single line acquisition (SLA) with Hanning-Tukey (α=0.3) windowing on transmit and receive respectively and dynamic focusing were included as a reference. Finally, based on the beam profile characteristics, the optimal 4MLA and PW system was used to simulate images of a phantom.

Results

In the near field, 4MLA and PW beam profiles showed almost identical lateral resolution as SLA (~1.47mm), while 4MLA had a better MSER(~10.54dB) than PW (~8.73dB) and SLA(~8.79dB). In the far field, the beam profiles of 4MLA and PW were very similar. Rectangular apodization on both transmit and receive provided the best beam characteristics for both the 4MLA and PW systems while skewing and warping of the 4MLA and PW beam profiles were comparable. The images generated with optimal 4MLA and PW imaging conditions are shown in Fig.1 a-c.

Discussion and Conclusions

Overall, 4MLA and PW imaging seemed to be very competitive approaches for fast cardiac imaging. However, in the near field, 4MLA outperformed PW imaging. Block-like artifacts were not obviously present in our simulations which may be more obvious in dynamic image sequences. This remains the topic of future research.

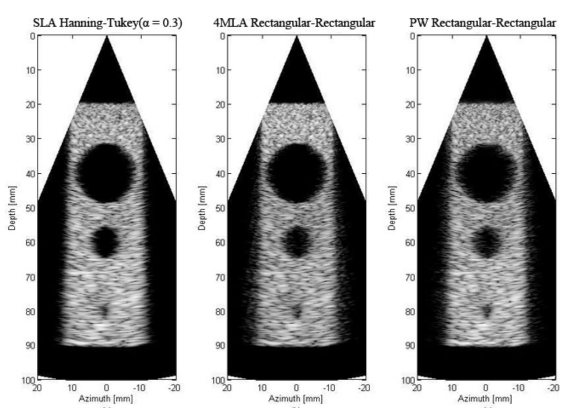

Fig.1 B-mode images of a tissue phantom generated with optimal 4MLA and PW

2B-5

3:00 pm Parallel Transmit Beam Forming using Orthogonal Frequency-Division Multiplexing for Harmonic Imaging

L. Demi[1], M. D. Verweij[1], K. W. A. van Dongen[1]; [1]Laboratory of Acoustical Imaging and Sound Control, Delft University of Technology, Delft, Zuid Holland, Netherlands

Background, Motivation and Objective

Nowadays real-time volumetric ultrasound imaging systems are used for medical diagnosis. To achieve the required data acquisition rate, the system relies on parallel beam forming, i.e. a single wide-angled beam is used for transmission and several narrow parallel beams for reception. When applied to harmonic imaging, the demand for high-amplitude pressure wave fields, necessary to generate the harmonic components, clashes with the idea of using a wide-angled beam in transmission since this results in a large spatial spreading of the energy. To enhance the harmonics' amplitude it is preferable to do the reverse; transmit several narrow parallel beams and use a wide-angled beam in reception. Here it is investigated whether this concept can be used for harmonic imaging.

Statement of Contribution/Methods

The proposed method to achieve parallel beam forming for harmonic imaging relies on orthogonal frequency-division multiplexing (OFDM). OFDM can be used to create distinctive pulses, essential for generating distinctive parallel beams in transmission. In the current situation it means that each beam will have a shifted center frequency, resulting in distinct harmonic components being generated during propagation and received by the receiver.

Results

To test the proposed method, a numerical study has been done using a 32 element linear array as transmitter and a 5 element linear array as receiver. In transmission, the three parallel narrow beams steered over -8°, 0° and 8° have been generated by a Gaussian modulated pulse with center frequency at 0.8, 1.0 and 1.2 MHz respectively. The receiving wide-angled linear array has been centered at 2.0 MHz. To compare with standard parallel beam forming performances, the same arrays have been used in reversed order; the small array as transmitter, the large array as receiver. All transmit, receive and combined patterns have been simulated up to the 2nd harmonic component using the Iterative Nonlinear Contrast Source (INCS) method.

Compared to standard parallel beam forming, application of the proposed method results in a reduction of side-lobe amplitudes and a gain of 23 dB for the main beam.

The proposed technique has also been verified experimentally in water. A single transducer, with center frequency at 1 MHz, has been excited with the same driving signal as the simulations. As receiver, a calibrated hydrophone has been positioned at 80 mm distance from the transmitter. The measurements are in agreement with the simulations and confirm the feasibility of the proposed technique.

Discussion and Conclusions

OFDM has been applied successfully for parallel beam forming during harmonic imaging. Compared with standard parallel beam forming, the method yields a reduction of side-lobe amplitudes and a gain of 23 dB for the main beam amplitude. Finally, experiments confirm the feasibility of the proposed technique.

2B-6

3:15 pm Spatiotemporal Interpolation by Normalized Convolution for 4D Transesophageal Echocardiography

Alexander Haak[1], Marijn van Stralen[2], Gerard van Burken[1], Stefan Klein[1], Josien Pluim[2], Nico de Jong[1,3], Antonius F. W. van der Steen[1,3], Johannes G. Bosch[1]; [1]*Erasmus MC, Netherlands*, [2]*UMC, Netherlands*, [3]*Interuniversity Cardiology Institute of the Netherlands, Netherlands*

Background, Motivation and Objective

For interventional monitoring, we aim at 4D ultrasound reconstructions of structures in the beating heart from 2D transesophageal echo images by fast scanplane rotation, unsynchronized to the heart rate. For such sparsely and irregularly sampled 2D images, a special spatiotemporal interpolation approach is desired. We have previously shown the potential of spatiotemporal interpolation by normalized convolution (NC).

In this work we optimized NC for our application and compared it to nearest neighbor interpolation (NN) and to temporal binning followed by linear spatial interpolation (LTB).

Statement of Contribution/Methods

We have investigated 4D interpolation by 3 different methods on 2 test data sets. The sets consist of 500 2D image slices taken from a moving 3D object for a specific normalized cardiac cycle time point (τ, range: 0-1) and a specific rotation (θ, range: 0-180°) around the vertical central axis. The first set (CUBE, 50x50x50 voxels) contains a synthetic pulsating cube (size 28 to 32); the second set is a fully sampled 4D matrixTEE patient dataset (TEE, 224x208x208 voxels, 30 frames).

For the CUBE set 25 rotation angles were sampled 20 times at random τ (uniformly distributed). For the TEE set 500 2D planes were taken with θ and τ randomly chosen from a uniform distribution. Interpolation to 30 3D sets was performed by NC, NN, and LTB. The NC kernel was a Gaussian function with parameters separately optimized for the sampling of the two sets. Difference from known ground truth was established as the average absolute intensity error per voxel (AEPV).

Results

The AEPV for the CUBE data set was 1.32, 1.7, and 2.1 for NC, NN, and LTB respectively. The NC kernel parameters were estimated to be 0.01 and 2.2° for τ and θ respectively.

For the TEE dataset the AEPV was 9.5, 10.1, and 12.4 for NC, NN, and LTB respectively. NC used 0.05 and 5° as kernel sizes. The figure shows an example of the original TEE (A) data and the NC (B) and NN (C) reconstructions.

Discussion and Conclusions

NC provides a practical solution to spatiotemporal interpolation with a clear improvement over temporal binning interpolations. This work was financially supported by the Dutch Technology Foundation STW.

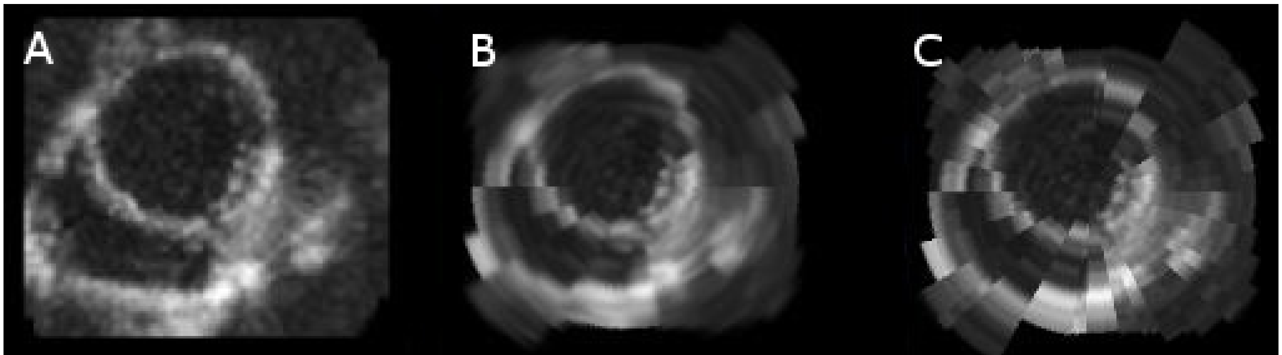

Original TEE image (A) compared to the reconstructed images using NC (B) and NN (C).

3B - Contrast Agents I

Carribean Ballroom VII

Wednesday, October 19, 2011, 2:00 pm - 3:30 pm

Chair: **Katherine Ferrara**
Univ. of California Davis

3B-1

2:00 pmFlow Cytometery to Characterize Ultrasound Contrast Agents

Tom Matula[1], Juan Tu[2], Jarred Swalwell[3], Weicheng CUI[2], Weizhong Chen[2]; [1]Center for Industrial and Medical Ultrasound, University of Washington, Seattle, WA, USA, [2]Nanjing University, China, People's Republic of, [3]University of Washington, USA

Background, Motivation and Objective

Standard methods for characterizing ultrasound contrast agents (UCAs) involve measuring the size and population distribution. The most popular instruments use either electrical sensing (e.g., Coulter Multisizer) or light scattering (e.g., Horiba). However, these instruments do not allow for characterization of shell properties. The shell is a critical component of a UCA: (1) It provides stability to administration and circulation throughout the vasculature; (2) it greatly affects the UCA response to incident ultrasound; (3) it is the backbone for conjugating ligands for molecular imaging and therapy; and (4) its properties are required for models that simulate UCA responses to incident ultrasound. Thus it is critical to understand the physical and rheological properties of shells. Current techniques to measure shell properties are either too cumbersome (imaging), or often provide only average properties (acoustic attenuation, scattering). The objective of this work is to modify an off-the-shelf flow cytometer that can provide shell property information, especially for thin-shelled UCAs.

Statement of Contribution/Methods

An InFlux Cell Sorter (BD Biosciences, San Jose, CA) was modified to include a custom square quartz flow cell with 150 µm flow channel as a measurement chamber in place of the standard nozzle and fluid jet. Acoustic coupling to the carrier sheath fluid and microbubble samples occurred through a 0.7 mm piezoelectric element (PZT) that was bonded to one side of the flow cell with epoxy. The PZT was driven with sinusoidal voltages, leading to a variable pressure within the sensing region (ROI) of the cytometer. PMT signals were digitized by a 12 bit PXI-5105 at a 10 MHz sampling rate with 302 points collected per sampling sequence for the calibration microspheres and at a 25 MHz sampling rate with 1002 points collection for UCAs, then saved to a computer for post processing. The signals were then fitted to the Marmottant UCA model where the shell parameters were the only fitting variables.

Results

Without ultrasound, Definity UCAs passing through the ROI were sized and counted, and the results were consistent with manufacturer specifications (mean diameter 1.8 µm, 99% smaller than 10 µm). With ultrasound, the varying detector signal was analyzed with the Marmottant's model. The shell viscosity increases with increasing UCA size. This is in agreement with high-speed imaging studies. The shell elastic modulus remained constant if the nonlinear Marmottant model was used, 0.70 and 0.46 N/m for Definity and SonoVue, respectively.

Discussion and Conclusions

20,000 UCAs were sized and counted in less than 5 minutes. Shell properties were analyzed with mean and standard deviations at each pressure. The UCAs showed characteristic shear thinning behavior, in agreement with previous reports. Flow cytometry, a commercial high-throughput process, can be used to obtain large data sets for detailed analysis.(Work supported by NIH NIBIB).

3B-2

2:03 pm Parallel Output, Liquid Flooded Flow-Focusing Microfluidic Device for Generating Monodisperse Microbubbles within a Catheter

Johnny L Chen[1], Ali H Dhanaliwala[1,2], Shiying Wang[1], John A Hossack[1,2]; [1]Biomedical Engineering, University of Virginia, Charlottesville, VA, USA, [2]R. M. Berne Cardiovascular Research Center, University of Virginia, USA

Background, Motivation and Objective

Our goal is to develop an ultrasound catheter capable of IVUS imaging and focal drug delivery to the vessel wall. Microbubbles (MB) are dispensed from the catheter tip while ultrasound mediates delivery. Producing MBs in situ at the catheter tip offers several advantages: MB loss during injection is reduced, MB shelf life is not a factor, and exploration of unstable (e.g. oxygen) MBs that enhance safety by dissolving before reaching smaller vascular beds is possible. Flow-Focusing Microfluidic devices (FFMD) are ideal as they produce monodisperse MBs through a continuous process in a small form factor. Current FFMDs are not suitable for catheters as they use rigid backing and require complex 3D manifold-like structures for conveying the liquid (shell) and gas (core) phases to parallel devices.

Statement of Contribution/Methods

We have designed a thin, flexible FFMD that bonds to the inside wall of a catheter. The lumen of the catheter is flooded with pressurized liquid to supply the liquid phase, while gas is supplied via a tube that can feed multiple MB generating nozzles without a 3D manifold. MBs exit directly into the vessel after production. The FFMD is fabricated using PDMS and a custom designed SU-8 mold. The liquid and gas phase are 2% Tween 20 and purified nitrogen, respectively. Flow rates and pressures between 20-70 µl/min and 3-10 psi, respectively, were tested. MB size, polydispersity, and production rate were measured by video microscopy.

Results

The flexible FFMD (14.5 x 2.8 x 2.3 mm bonded inside a 3 mm (ID) tube with gas and liquid channels measuring 35, 50 µm, and orifice width and height measuring 10, 25 µm, respectively) generated 20.4 ± 0.8 µm diameter MB at a peak production rate of 529 MB/s. The minimum MB diameter achieved is 15.2 ± 0.4 µm. A total production rate of up to 25e3 MB/s was achieved by using a three channel parallelized FFMD inside a pressurized catheter. The minimum MB diameter achieved with the parallelized device was 16.7 ± 0.4 µm.

Discussion and Conclusions

We demonstrate the ability to produce monodisperse MBs using a FFMD capable of fitting in a catheter. By feeding the liquid inputs using a pressurized lumen, we are able to significantly reduce the size and complexity of parallelized FFMD. Furthermore, the diameters and production rate are consistent with previous reports of FFMD and may be improved by continued reduction in orifice size and increases in parallelization.

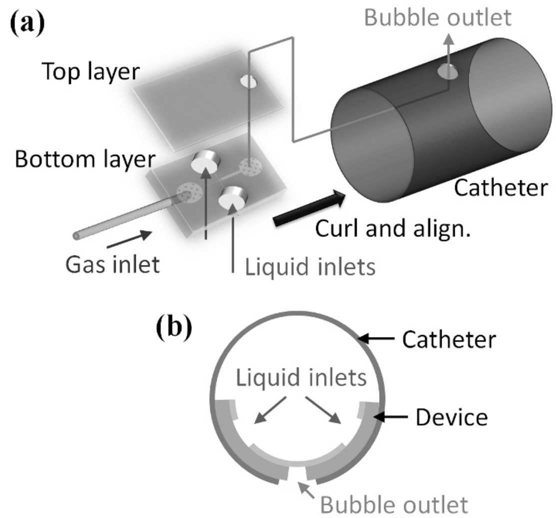

3B-3

2:30 pm **Optimal Microbubble Production Rate from a Flow-Focusing Microfluidic Device as a Function of Orifice Size, Gas Pressure, and Liquid Flow Rate**

Shiying Wang[1], Ali H Dhanaliwala[1,2], Johnny L Chen[1], Alexander L Klibanov[1,3], John A Hossack[1,2]; [1]*Biomedical Engineering, University of Virginia, Charlottesville, VA, USA,* [2]*R. M. Berne Cardiovascular Research Center, University of Virginia, USA,* [3]*Dept.of Medicine - Cardiovascular Division, University of Virginia, USA*

Background, Motivation and Objective

Previous studies have shown that monodisperse microbubbles (mMB) as ultrasound contrast agents have many advantages over polydisperse MBs. mMBs can be tuned to the bandwidth of a given transducer and have better echo-echo correlation. Flow-focusing microfluidic devices (FFMDs) produce low polydispersity MBs with tunable diameters in a continuous process. A major drawback of FFMDs is low mMB production rate. Published rates vary from 1e3 to 1e6 MB/s with loss of monodispersity at the higher production rates. We hypothesize that reducing orifice width will allow increased production rates while maintaining monodispersity.

Statement of Contribution/Methods

FFMDs were fabricated from PDMS and custom designed SU-8 molds. Devices had orifice heights of 25 µm and widths between 5-20 µm. Each device was tested with gas pressures and liquid flow rates ranging from 3-15 psi and 20-140 µL/min, respectively. The gas (core) phase was purified nitrogen. The liquid (shell) phase was either Tween 20 in water (0.002-2%), or phosphatidylcholine and PEG-stearate in water (20 mg/ml each). MB diameter, polydispersity, and production rate were measured by high speed camera video microscopy.

Results

A FFMD with an orifice width of 12 µm produced 15 ± 0.4 µm diameter MBs at a peak production rate of 102e3 MB/s when flow rate and gas pressure equal 90 µL/min and 5 psi, respectively. While MBs of similar diameter can be produced at other flow rate and gas pressure combinations, production rate was less than half at these other combinations. Therefore, only 15 µm diameter MBs could be produced at the peak production rate. With a 5 µm orifice, 7.3 ± 0.7 µm diameter MBs were produced at a peak production rate of 500e3 MB/s when flow rate and gas pressure equal 126 µL/min and 7 psi, respectively. With a 16 µm orifice width, 12.2 ± 0.2 µm diameter lipid shelled MBs were produced at 3.9e3 MB/s when flow rate and gas pressure equal 9 µL/min and 4 psi, respectively. With a 20 µm orifice width at 5 psi gas pressure, MB diameter was reduced by up to 34% but production rate dropped seven-fold when Tween 20 concentration was reduced from 2% to 0.02%.

Discussion and Conclusions

FFMDs operate in three regimes. We found that the flow rates demarcating the transition between these regimes depend on orifice width and pressure. Furthermore, peak productivity occurs when the mMB diameter is close to the orifice width but rapidly falls to zero if flow rate is further increased. By reducing the orifice width to reduce MB diameter rather than increasing viscosity, we were able to reach our highest production rates while producing the smallest MBs. This effect can be seen with the lipid MB. Since the lipid is more viscous than Tween, mMBs smaller than the orifice width can be produced; however, this causes a sharp drop in production rate. We also found that we could reduce MB diameter by reducing Tween 20 concentration, probably due to incomplete shell coverage of the nascent MB. Further reductions in concentration lead to MB coalescence.

3B-4

2:45 pm **Intravascular ultrasound contrast imaging at 20 MHz using radial modulation: a promising approach for coronary vasa vasorum imaging**

Francois T.H. Yu[1], Flordeliza Villanueva[1], Xucai Chen[1]; [1]*Cardiovascular Institute, University of Pittsburgh, Pittsburgh, PA, USA*

Background, Motivation and Objective

There is evidence that vasa vasorum (VV) proliferation is a marker of high risk atherosclerotic plaque. While the histologic components of high-risk coronary plaque are well characterized, methods for imaging them in vivo are scarce. We developed an intravascular ultrasound (IVUS) system based on radial modulation (RM) for VV contrast enhanced imaging. RM is a dual band approach applicable for high frequency microbubble (MB) imaging, where a low frequency (LF) ultrasound pulse is used to manipulate the MB radius while a synchronized high frequency (HF) pulse successively measures MB backscatter in compressed and expanded states. Subtracting both HF signals yields high resolution imaging with contrast enhancement and tissue cancellation.

Statement of Contribution/Methods

Lipid-encapsulated perfluorocarbon MB (3.54 ± 1.76 µm) were circulated in a 6 mm diameter hollow tissue mimicking phantom. A 20 MHz IVUS catheter (Sonicath Ultra 3.2, Boston Scientific, Fremont, CA) was positioned against the wall of the tube and rotated at 1 to 30 frames per second. The radio frequency signal was band-pass filtered, amplified, and digitized at 400 MHz for offline processing. The RM pulse pair consisted of two identical HF imaging pulses (20 MHz, 2 cycles) respectively synchronized at the 4th maximal and minimal MB expansions caused by successive LF pulses (3 MHz, 5 cycles). Bubble concentration, LF pressure amplitude and phase synchronization were varied and optimized in multiple experiments.

Results

Our prototype IVUS system produced RM images at 30 frames per second that selectively enhanced contrast signal while suppressing tissue signal. RM images were analyzed to determine contrast to tissue ratio (CTR) and contrast to tissue enhancement (CTE) relative to the same image in B-mode. CTR and CTE respectively decreased from 12 and 10 dB near the catheter to 3 dB at a radial distance of 4 mm from the catheter. This corresponded to LF pressures dropping from 350 kPa near the catheter to 150 kPa at 4 mm. A 200 µm tube, imbedded in the tissue phantom to mimick a microvessel and perfused with microbubbles, was also imaged successfully while the signals from surrounding tissues were suppressed.

Discussion and Conclusions

It was demonstrated that our prototype IVUS system allows microbubble specific imaging at high resolution. Contrast signal could be detected up to a radial distance of 4 mm from the catheter, which is sufficient for coronary imaging. Compared to previously described sub-harmonic and 2nd harmonic imaging, our RM imaging produced lower CTR and CTE. However, unlike these other technologies, our approach was implemented on a commercially available catheter which provides a significant advantage for clinical translation. A new catheter design that allows more efficient LF delivery would further enhance the performance of RM imaging.

We thank Boston Scientific Corp. for providing hardware and engineering support for this study.

3B-5

3:00 pm Dynamic manipulation of subharmonic response of ultrasound contrast agent microbubbles

TELLI FAEZ[1], Guillaume Renaud[1], Nico de Jong[1]; [1]*Erasmus MC, Netherlands*

Background, Motivation and Objective

There has been a great interest recently to exploit subharmonic (SH) emissions from contrast agents because SH imaging has potentially a larger contrast to tissue ratio compared to other imaging methods. It has been shown recently that the SH amplitude can be amplified by applying an ambient overpressure. In this study we investigate the effect of a 2.5 kHz dynamic variation in the ambient pressure on the SH response of microbubbles at driving frequency of 10 MHz.

Statement of Contribution/Methods

Highly diluted BR14 (Bracco Research S.A., Geneva, Switzerland) microbubbles were filled in a sealed container and mounted in the center of a large water tank. A wide band transducer (3-13 MHz) was used to transmit 25-cycle 10 MHz sinusoidal bursts with a repetition frequency of 16 kHz. The echoes were received by another focused transducer. A low frequency (LF) wave was produced by a glass disk immersed in water and connected to a shaker, in order to create a 2.5 kHz dynamic modulation of the ambient pressure in the container.

Results

FIG. 1 shows that a modulation of the ambient pressure of 15 kPa enhances the SH amplitude up to 200% compared to the atmospheric pressure conditions. Moreover, the SH amplitude modulation as a function of the LF acoustic pressure was asymmetrical.

Discussion and Conclusions

We believe that the modulation of the bubble radius induced by the LF acoustic pressure modulates the efficiency in SH generation since the instantaneous radius is alternatively brought closer and pushed away from the resonant radius at 5 MHz for transmitting frequency of 10 MHz. However, the asymmetry observed in the SH amplitude modulation is related to the shell properties of the microbubbles. If a bubble has an initial surface tension higher than zero, an overpressure compresses the bubble and consequently the surface tension decreases to zero and the bubble enters its so-called buckling state[1]. It is known that buckled bubbles exude the highest SH energy[2]. Therefore the enhancement in the SH amplitude shows an asymmetric trend.

In conclusion, the SH amplitude can be enhanced up to 10 dB by applying a dynamic overpressure of 15 kPa using a secondary LF wave. This method can be used in vitro for characterization and tailoring of contrast agents or in vivo to improve the performance of SH imaging.

1 Marmottant et al. (2005) JASA 118(6), pp 3499-3505

2 Sijl et al. (2010) JASA 128, pp 3239–3252.

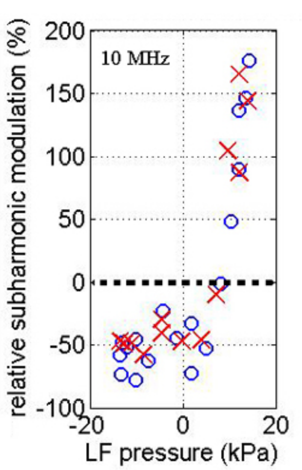

FIG. 1- Relative subharmonic amplitude vs. LF pressure at 10 MHz transmitting frequency. Circles: increasing LF pressure, Crosses: decreasing LF pressure.

3B-6

3:15 pm Noninvasive estimation of dynamic pressures *in vitro* and *in vivo* using the subharmonic response from microbubbles

Jaydev Dave[1,2], Valgerdur Halldorsdottir[1,2], John Eisenbrey[1], Ji-Bin Liu[1], Maureen McDonald[3], Kris Dickie[4], Corina Leung[4], Flemming Forsberg[1]; [1]*Radiology, Thomas Jefferson University, Philadelphia, PA, USA,* [2]*School of Biomedical Engineering, Science and Health Systems, Drexel University, Philadelphia, PA, USA,* [3]*Radiologic Sciences, Thomas Jefferson University, Philadelphia, PA, USA,* [4]*Ultrasonix Medical Corporation, Richmond, BC, Canada*

Background, Motivation and Objective

Instantaneous pressure changes in the heart can be monitored using an invasive catheterization approach, but this is associated with increased morbidity and mortality. The ability of microbubbles' subharmonic emissions (at half the insonation frequency) to respond to changes in ambient hydrostatic pressures *in vitro* has been previously demonstrated using single element transducers and may be applicable to measure cardiac pressures. Thus, the purpose of this study was to develop and validate a noninvasive pressure estimation technique based on subharmonic emissions *in vitro* and test the feasibility *in vivo* using commercially available ultrasound equipment.

Statement of Contribution/Methods

In vitro, ambient pressures were varied in a closed-loop flow system between 0 and 120 mmHg (the clinical range) at a flow rate of 650 ml/min with 0.2 ml Sonazoid microbubbles (GE Healthcare, Oslo, Norway) in 750 ml of isotonic diluent and recorded by a solid state pressure catheter (SPR 350, Millar Instruments, Inc., Houston, TX, USA) as the reference standard. Simultaneously, a SonixRP ultrasound scanner (Ultrasonix Medical Corp., Richmond, BC, Canada) operating in pulse inversion mode and transmitting at 2.5 MHz was used to acquire unprocessed RF data at five different incident acoustic pressures (from 76 kPa to 897 kPa; n=3). The subharmonic data for each pulse was extracted using band-pass filtering with averaging, and subsequently, processed to eliminate noise. The incident acoustic pressure most sensitive to ambient pressure fluctuations was determined; then the ambient pressure was tracked over 20 seconds. Regression analysis was used to compare subharmonic and catheter pressure values. *In vivo* validation of this technique was performed noninvasively for tracking left ventricular (LV) pressures of two canines using similar post processing as *in vitro*.

Results

In vitro the subharmonic signal could track ambient pressure values with $r^2 = 0.922$ ($p<0.001$) for 20 seconds at the most sensitive incident acoustic pressure. *In vivo* the subharmonic signal tracked the LV pressures with $r^2 > 0.790$ ($p<0.001$). Maximum errors in estimating clinically relevant systolic and diastolic pressures ranged from 0.22 to 2.84 mmHg using this subharmonic technique (compared to the pressure catheter reference standard).

Discussion and Conclusions

The efficacy of subharmonic approach to pressure estimation has been demonstrated *in vitro*. *In vivo* tracking of LV pressures in two canines produced errors up to 2.84 mmHg between the pressure catheter and the subharmonic technique. Clinical validation and real time implementation of this technique may ultimately lead to the first noninvasive cardiac pressure monitoring tool.

Work was supported by AHA 0655441U and NIH CA140338

4B - Acoustic Tweezers I

Carribean Ballroom I

Wednesday, October 19, 2011, 2:00 pm - 3:30 pm

Chair: **John L. Larson**
Avago Technologies

4B-1

2:00 pm Ultrasonic Fields for Cell Levitation and Manipulation

Martyn Hill[1]; [1]Engineering Sciences, University of Southampton, Southampton, Hants, United Kingdom

Background, Motivation and Objective

The ability to trap, move and position biological cells is of fundamental importance in a wide variety of life sciences applications. One means of manipulating cells is through the use of ultrasonic standing wave (USW) fields. Within such a field, gradients of pressure and velocity interact with small scatterers, such as cells, to generate time-averaged forces, in addition to the oscillatory acoustic forces. These steady-state radiation forces have a component towards the acoustic velocity maximum for a dense scatterer (relative to the surrounding fluid) and a component towards the acoustic pressure minimum for a relatively stiff particle. The resultant of these components will move the majority of scatterers, such as cells in aqueous suspension, towards the pressure nodes of a plane standing wave.

Statement of Contribution/Methods

This paper discusses the origin of the second order terms that lead to the radiation forces and describes different approaches to modelling the forces, both numerical and analytical. It is shown that the magnitude and scale of the potential wells that can be created within USWs complement alternative approaches such as optical traps and dielectrophoresis, and that USWs are particularly suitable for integration into lab-on-a-chip devices. Data relating to cell viability is also presented and it is shown that the fields are suitable for biological cell handling.

Results

Several applications are discussed including :

- sample processing such as filtration and concentration
- biosensor enhancement through active cell deposition and the acceleration of bead-based assays
- fractionation of particles on the basis of size, material properties and geometry

Discussion and Conclusions

Ultrasonic radiation forces are able to levitate and manipulate cells without impairing their viability and their use is highly compatible with microfluidic devices. The paper concludes with a discussion of emerging areas of importance for the technology, including :

- potential tissue engineering applications
- the combination of ultrasonic forces with other force fields
- the generation of complex, dynamic, three dimensional force fields such as those being investigated within the Electronic Sonotweezers project

4B-2

2:30 pm A Sonic Screwdriver: Acoustic Angular Momentum Transfer for Ultrasonic Manipulation

Christine Demore[1], Zhengyi Yang[1], Alex Volovick[1,2], Han Wang[1], Sandy Cochran[1], Mike MacDonald[1], Gabriel Spalding[3]; [1]Institute for Medical Science and Technology, University of Dundee, Dundee, United Kingdom, [2]InSightec Ltd., Tirat Carmel, Israel, [3]Department of Physics, Illinois Wesleyan University, Bloomington, IL, USA

Background, Motivation and Objective

Helical ultrasonic beams, which carry orbital angular momentum because of inclined wavefronts, can impart this angular momentum to objects. Travelling wave beams, whether optic or acoustic, with topological charge m providing $m2\pi$ phase shift in azimuth, have an amplitude null along the axis due to the superposition of all phases. The beams can be used for strong axial traps, rotation of objects, or many other applications such as aberration correction. Here we demonstrate the controlled transfer of angular momentum to an object as a mechanism that can be incorporated into an ultrasonic manipulation system.

Statement of Contribution/Methods

A 500 kHz matrix array with approximately 1000 elements connected to a focused ultrasound surgery system (ExAblate 2000, Insightec, Israel) was used to generate structured ultrasonic fields that exert both axial and torsional forces on a target. The array was placed at the bottom of a cylindrical chamber filled with degassed water. The target, an 87 g, 100 mm diameter disk of acoustic absorber material (Aptflex F28, Precision Acoustics, Dorchester, UK), was suspended above the transducer. A plastic tube attached to the target added buoyancy and allowed the target to both levitate and rotate about a stabilizing rod attached to a lid on the chamber. Azimuthal phase shifts of $\pm m2\pi$, $0 < m < 12$, were applied to the elements within a circular sub-aperture of the array to transmit a helical beam. The total electric power, P, supplied to the array was $30\ W < P < 70\ W$. The transmitted angular momentum and the levitation force were measured as functions of both m and P.

Results

When $m = 0$, there is no angular momentum in the beam, so the acoustic absorber levitates due to the radiation force but does not rotate. The rotational motion is shown to be due to the angular momentum in the ultrasonic beam by the equal and opposite angular velocity for positive and negative m. The rotation rate increases linearly with m and P, for low driving powers. However, the trend becomes non-linear at higher driving powers due to losses in the system. An angular momentum of $18\ x10^{-3}\ kgm^2/s$ was imparted to the target with $m = -12$, $P = 30$ W, and no focusing phases applied to the array elements. The radiation force on the absorber, calculated from the change in buoyancy required to balance gravity, increases linearly with power, but decreases with increasing value of m.

Discussion and Conclusions

In this work, we have demonstrated the transfer of orbital angular momentum to a large target from a helical ultrasonic beam. The linear relationships between rotation rate and both m and P are as expected for helical beams. The decreasing axial force with m can be explained by the increasing inclination of the beam and corresponding reduction in axial momentum flux. These results provide impetus for developing electronically controlled ultrasonic tweezers to expand the range of objects that can be manipulated and to broaden the applications for manipulation technologies.

4B-3

2:45 pm Two-Dimensional Cell Trapping by Ultrasound Microbeam

Jungwoo Lee[1], Changyang Lee[2], Hyung Ham Kim[2], Anette Jakob[3], Robert Lemor[3], Shia-Yen Teh[4], Abraham Lee[4], Koping Shung[2]; [1]University of Southern California, Los Angeles, CA, USA, [2]University of Southern California, USA, [3]Fraunhofer IBMT for Biomedical Engineering, Germany, [4]University of California at Irvine, USA

Background, Motivation and Objective

Biological experiments in laboratory-on-a-Chip (LOC) type devices have been undertaken on a single-cell basis rather than in a homogeneous batch culture. In this regard, we previously reported that an acoustic trap for a 125 µm lipid droplet was able to be formed by a sharp intensity gradient near the focus. The use of highly focused ultrasound beam at frequencies higher than 100 MHz, referred to herein as ultrasound microbeam, is extremely critical in order to further trap a single cell of a few micron diameter. Hence this paper presents that a 200 MHz microbeam emitted from a zinc oxide (ZnO) transducer was able to individually immobilize a 10 µm leukemia cell suspended in phosphate buffered saline (PBS).

Statement of Contribution/Methods

Cultured human leukemia cells were suspended in a chamber filled with PBS, sitting on top of a microstage. The transducer interrogated the cells from the above, as driven in a sinusoidal burst mode whose peak-to-peak voltage amplitude was as high as 2 V. The duty factor of the burst was 0.025 % and the pulse repetition frequency was set to 1 kHz. A pulse echo test was performed to ensure that the cells were axially positioned at the focus of 0.5 mm. A single cell was then laterally located at 50 µm from the focus while the transducer was switched off. Cell motion was recorded by a CMOS camera equipped with an inverted microscope.

Results

After being turned on, the trap began to attract the cell towards its center through 50 µm (Figs. 1A and 1B) and later immobilized it at the focus (Fig. 1C). The increment of the vertical displacement between successive image frames was plotted in Fig. 1D. Except for a sudden dip in frame #5, the displacement was increased until frame #8 and then decreased afterwards. This approximated a similar pattern when an elastic spring is released after being stretched beyond the equilibrium point.

Fig. 1. Lateral displacement measurement of trapped cell.

Discussion and Conclusions

These results demonstrated that an acoustic trap generated by a 200 MHz ultrasound microbeam immobilized a single leukemia cell in a two-dimensional domain. The lateral displacement of a trapped cell was measured, indicating the cell tended to retract back to the focus as in optical tweezers. As a result, this non-invasive technique was shown to be capable of handling an individual cell without affecting other cells nearby.

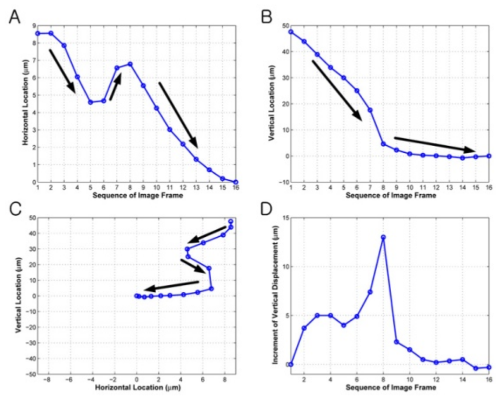

4B-4

3:00 pm Multi-wavelength Ultrasonic Standing Wave Device for Non-invasive Cell Manipulation and Characterisation

Yongqiang Qiu[1], David A. Hughes[2], **Christine Demore**[1], Srikanta Sharma[1], Kees Weijer[2], Sandy Cochran[1]; [1]Institute for Medical Science and Technology, University of Dundee, United Kingdom, [2]Division of Cell and Developmental Biology, College of Life Sciences, University of Dundee, United Kingdom

Background, Motivation and Objective

Cell and tissue mechanics can be investigated through contact mediated interactions such as Atomic Force Microscopy and nano-mechanical tools (e.g. Micro-grippers). However, direct mechanical contact raises problems: damaging the fragile structure of cells and/or difficulty in handling large numbers of cells. Noncontact technologies based on radiation forces, such as optical tweezing and dielectrophoresis, may overcome some of these problems, however it remains difficult to achieve the necessary forces to manipulate cells, with dimensions of tens of microns, or groups of cells across a substrate.

Statement of Contribution/Methods

In this paper, we present the recent progress in the development of an acoustic device which utilises acoustic forces generated by an ultrasonic standing wave to manipulate particles and cells. The device, which is designed to sit in a standard petri dish with the propagation direction parallel to the dish surface and be compatible with an optical microscopy, comprises three parts: a high frequency ultrasonic transducer with a low acoustic impedance transducer mounting, a reflector, and a set of variable thickness precision spacers between the reflector and transducer. The device forms a multi-wavelength standing wave across the fluid chamber, and the acoustic force drives the particles and cells toward pressure nodes.

Results

We report the design, simulations and precision micro-fabrication of this device. The basic design of device was validated with one-dimensional transducer modelling software and finite element analysis (PZFlex, Weidlinger Associates Ltd, CA). A prototype device was fabricated using a Y-36°-Cut lithium niobate wafer, lapped and polished to 135 µm for a resonant frequency of 25 MHz, diced to 2 mm × 5 mm, and set into a block of glass microbubble filled epoxy. MACOR machineable glass-ceramic spacers were lapped and diced to obtain 300 µm - 800 µm chambers. The reflector was polished to obtain a uniform, high reflectivity surface. Quartz wax adhesive was used to easily reassemble the device with alternate components. Electrical impedance spectroscopy of the device demonstrates strong resonances related to the chamber resonant length, agreeing with simulated impedance curves, and corresponding to simulated pressure distributions showing multiples of half-wavelength standing waves. Device performance is demonstrated with manipulation of latex beads and cells on the surface of a standard petri dish.

Discussion and Conclusions

The presented device can generate larger forces than lower frequency devices due to the sharper pressure gradients and the shorter wavelength reduces the width of pressure nodes to the order of cell dimensions. Consequently, the multi-wavelength high frequency resonator will enable life scientists to non-invasively manipulate multiple lines of cells. Potential applications of this device in cell biology, such as measuring motility forces of cells, are discussed.

4B-5

3:15 pm Manipulation of microparticles in two dimensions using counter-propagating ultrasonic waves

Charles Courtney[1], Chun-Kiat Ong[1], Bruce Drinkwater[1], Paul Wilcox[1]; [1]*Mechanical Engineering, University of Bristol, United Kingdom*

Background, Motivation and Objective

Trapping and manipulating micrometer-scale particles in fluids is of interest in the biosciences. The most mature technology in this field is optical tweezing; however, significant progress is also being made in use of ultrasonic waves to manipulate microparticles with the intention of broadening the applications of particle manipulation.

Many applications rely on generating resonances of the device in order to produce particle traps. The dexterity/flexibility of this approach is limited by shape of the ultrasonic field being determined by device geometry. The work reported here uses a method whereby standing waves are generated using counter-propagating ultrasonic waves in order to generate standing waves with nodal positions that can be determined by adjusting the relative phases of the waves. The overall aim is to allow arbitrary translations of trapped particles on a plane.

Statement of Contribution/Methods

Two transducers, acoustically matched to water and backed to reduce reflections, are placed opposing each other and excited to produce a standing wave in a water-filled cavity between them. The acoustic radiation force acts to drive dense particles to nodes of the standing wave. Varying the relative phase of the signals applied to each transducer allows the positions of the nodes, and hence the particles to be varied. Using two pairs of opposing transducers, positioned orthogonally and with appropriate relative phases (determined analytically) applied, allows trapping of particles on a grid and manipulation in two dimensions.

Results

A device, consisting of two pairs of matched transducers, for manipulation, and a resonant stage, to hold particles against gravity, was constructed. The technique was demonstrated using 10-micron-diameter polystyrene spheres in water. The spheres were levitated on planes using the levitation transducer and then 5 MHz signals applied to the four matched transducers. It was shown that by varying the relative phases applied to the transducers the particles could be forced onto a grid pattern, with a half-wavelength (0.15 mm) separation, and then the grid translated with very high accuracy. It was shown that the relationship between phase and position agreed with that expected analytically. The force applied to an individual sphere was measured by recording the response to a step change in field and found to be 30 pN, in reasonable agreement with the value of 37 pN found using analytical expressions for the acoustic radiation force on a sphere and the acoustic field predicted by a finite element model of the device.

Discussion and Conclusions

A method of manipulating in two dimensions microparticles using ultrasonic standing waves with nodes determined by the relative phases of exciting signals has been proposed and demonstrated. This approach represents an opportunity to develop a new class of dextrous/flexible particle manipulation devices facilitates positioning and patterning applications in the biosciences.

5B - Microacoustic Sensors (6J)

Carribean Ballroom II

Wednesday, October 19, 2011, 2:00 pm - 3:30 pm

Chair: **Omar Elmazria**
Nancy University

5B-1

2:00 pm Piezoelectric Thin Films : A Technology Platform For Thin Film Ultrasound Transducer Arrays

Mareike Klee[1], Ruediger Mauczok[1], Chris van Heesch[1], Marco de Wild[1], Henk Boots[1], Wilco Keur[1], Biju Kumar[2], Georg Schmitz[3], Michal Mleczko[3]; [1]*Philips Research, Eindhoven, 5656 AE Eindhoven, Netherlands,* [2]*Philips Lighting, Netherlands,* [3]*Institute of Medical Engineering University of Bochum, Germany*

Background, Motivation and Objective

Piezoelectric thin film technologies get more and more relevance for miniaturized and integrated sensors, actuators and transducers.

Statement of Contribution/Methods

A piezoelectric thin film technology platform has been developed, which processes lead perovskite based piezoelectric thin films by spin-on processing on thin film membranes. Making use of lithographic patterning, piezoelectric thin film ultrasound transducers have been realized operating in the d33 mode.

Results

With the piezoelectric thin film platform, piezoelectric thin film ultrasound transducer arrays have been realized, which dependent on the design are operating at frequencies of 50 KHz up to > 10 MHz. The piezoelectric thin film ultrasound transducer arrays are tested with respect to their performance. The piezoelectric thin film membrane transducer arrays operating at 4 MHz and above show a very good acoustic matching to water. This results in a bandwidth of the transducer arrays, which is equal or even larger than 100%. The output pressure of the thin film piezoelectric ultrasound transducer arrays is linear dependent of the applied voltage. These piezoelectric thin film ultrasound transducer arrays, due to their similar operation conditions as traditional ceramic or single crystal ultrasound transducer, can be operated with standard ultrasound machines. With the piezoelectric thin film ultrasound transducer arrays with 32- 42 elements ultrasound test images of e.g. nylon wires with 0.12 mm diameter in a water tank have been demonstrated.

Discussion and Conclusions

The piezoelectric thin film technology platform developed opens the way to a new class of ultrasound transducer arrays.

5B-2

2:03 pm Sensing Acoustic Properties of Materials Using Piezoelectric Lateral-Mode Resonators

Jonathan Gonzales[1], Reza Abdolvand[2]; [1]Electrical Engineering, Oklahoma State University, Tulsa, OK, USA, [2]Electrical Engineering, Oklahoma State University, USA

Background, Motivation and Objective

Acoustic energy in lateral-mode thin-film piezoelectric-on-substrate (TPoS) resonators is radiated to the supporting substrate from suspension tethers. Previous work has shown that in-plane acoustic reflectors can drastically change the quality factor (Q) of the resonator by reflecting the waves either in-phase or out-of-phase. If such reflectors, which are through-substrate trenches, are filled with different materials then the total reflected energy is altered and, consequently, the Q can be correlated to the material properties. This research aims to use these ultrasonic micro-devices to determine the physical properties of a material without directly contacting the device.

Statement of Contribution/Methods

In this work, we use a high frequency (110MHz)/high quality factor (~10000) resonator to indirectly interact with a fluid to determine the fluid properties, namely acoustic velocity and density.

A Suss Microtech probe station was used with GSG probes to measure the resonator performance (center frequency, quality factor, and electrical loss). An additional manipulator was added to position a 36 gauge beveled micro-needle around the device under test. Shipley 1813 photoresist, which has dynamically changing viscosity, was injected into the reflector trenches and the Q was monitored and recorded during the drying cycle of the resist and also after additional baking.

Results

Two pairs of devices were tested. Pairs were used because the two independent devices were expected to exhibit a reversed reaction to the reflector trench filling. The devices in which the waves are reflected in-phase show a decrease in Q when the photoresist is added (ITC1). In contrast, the devices in which the waves are reflected out-of-phase show an increase in Q with added photoresist (ITC0.5).

Discussion and Conclusions

We have shown that the addition of photoresist into the reflectors of a TPoS ultrasonic resonator can alter the Q of the device based on the photoresist's viscosity. This viscosity change impacts the acoustic velocity of the material which consequently changes the efficiency of the built-in reflectors by allowing more or less acoustic energy to return to the resonator. This method can be expanded to other fluids, notably bio-fluids whose physical properties are helpful in determining health related issues.

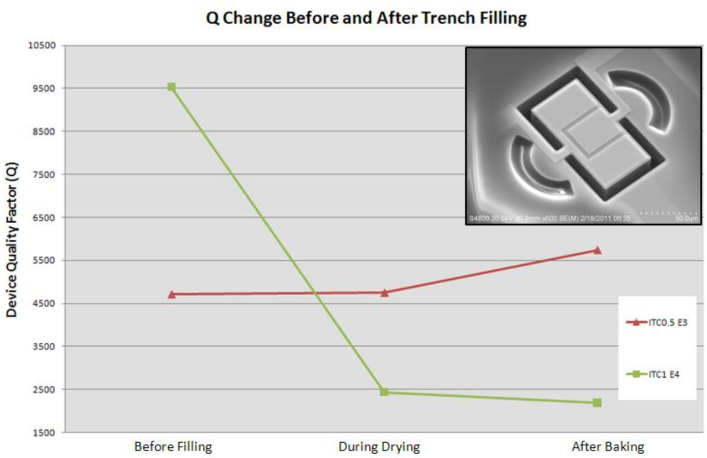

Fig. 1 Quality factor change for contrasting devices before, during and after photoresist filling. SEM of filled device (inset).

5B-3

2:30 pm An Acoustic Microfluidic Platform for Size and Density-Based Cell Separation

Myeong Chan Jo[1], Rasim Guldiken[1]; [1]Mechanical Engineering, University of South Florida, USA

Background, Motivation and Objective

The objective of the present research is to explore a label-free cell separation platform based on surface acoustic waves. The prominent features of the present microfluidic platform are that particle focusing and separation are accomplished simultaneously and the device doesn't require the use of the sheath flow for positioning or aligning of particles. Moreover, our approach is capable of cell separation based on not only size, but also by density.

Statement of Contribution/Methods

We incorporate two separate stages with different functions within a single microfluidic device. The function of the first stage is to align cells on the center of the microfludic channel without introducing any sheath flow. The second stage is responsible from the actual separation process. For the operation of the device, two interdigitated transducer (IDT) pairs are patterned on a piezoelectric substrate to generate the surface acoustic waves and a microfluidic channel is aligned at half way between the IDT pairs. For size or density based separation, in the second stage of the design, the larger cells or the denser cells is exposed to more lateral displacement in the channel towards the pressure node due to the difference in acoustic forces acting on them.

Results

For proof-of-concept experiments, a mixture of fluorescent polystyrene particles with diameters of 3ìm and 10ìm was introduced. When particles entered the first stage, the acoustic forces acting on particles aligned them at the center of the channel where pressure nodes existed. At the second stage, 10ìm particles moved to the pressure nodes while 3ìm particles remained in the center of the channel because the acoustic forces exerted on the 3ìm particles were insufficient to push them into the pressure nodes. As a result, the larger particles were separated to the side channels and the smaller particles were separated to the center channels. This experiment showed that the present device is capable of separating different size particles based on surface acoustic waves without introducing any external sheath flow to the microchannel.

Discussion and Conclusions

The present proof-of-concept experiments does indeed show that the proposed concept works as hypothesized with the non-optimized preliminary device. We will conduct the design optimization studies with the theoretical analysis as well as density-dependant separation experiments.

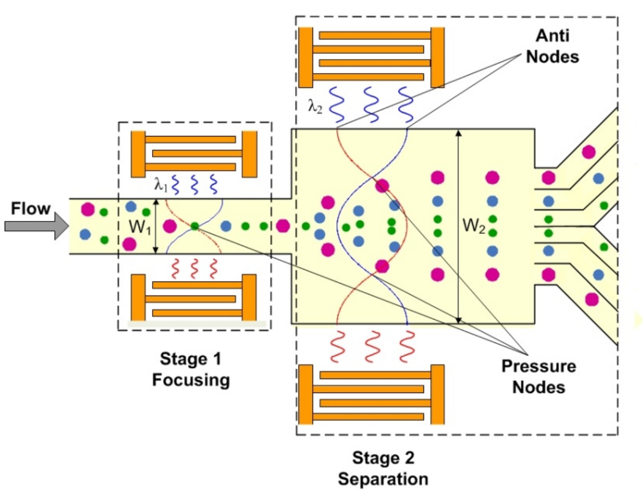

5B-4

2:45 pm Experimental Study of the Biomimetic Artificial Basilar Membrane Fabricated by Piezoelectric Micromachined Beams

Sangwon Kim[1], Hongsoo Choi[1]; [1]Department of Robotics Engineering, Daegu Gyeongbuk Institute of Science and Technology, Daegu, Korea, Korea, Republic of

Background, Motivation and Objective

The human ear is a highly engineered hearing organ that can hear sound in the frequency range of 20 Hz - 20 kHz and able to measure sound pressure as low as 20 µPa. It was found that the passive hearing ability of the human ear is mainly based on basilar membrane (BM) which is in the cochlea. Researchers found that cochlea, which is about 1 cm3 in volume, uses a mechanical process to separate incoming sound waves into about 3500 channels of frequency information. In this work, an experimental study on a biomimetic artificial basilar membrane (ABM) is conducted to mimic the functionality of human hearing, and the ultimate goal is using the developed ABM for the next generation of artificial cochlea.

Statement of Contribution/Methods

Cochlea consists of vestibular duct, cochlear duct and tympanic duct. The organ of corti, which contains auditory sensory cells, is on the BM in the cochlear duct. The base of BM is thick and narrow and the apex of the BM is thin and wide. The base responses to high frequency sound wave and the apex is activated at low frequency sound wave. This is possible because of the different rigidity of the BM at the base and apex. As a result, a specific location of the BM is activated by a certain incoming sound frequency. Hair cells on the locally activated BM generate bioelectrical signal by the vibration of the BM and the generated bioelectrical signal is transferred to the auditory nerve system. Therefore, BM can mechanically separate incoming acoustic sound waves by their frequencies. We defined this mechanism as a passive hearing mechanism and we are working on mimicking the functionality of passive hearing using piezoelectric thin-film structures.

Results

Piezoelectric thin-film structures have found a wide variety of applications in emerging MEMS technologies. For electro-mechanical applications, lead zirconate titanate (PZT) film is commonly used as the actuating or sensing component in these structures due to its high piezoelectric constant, high energy density, and large electrical-mechanical coupling coefficient. We fabricated 1D array type piezoelectric thin-film beam structures with different lengths and widths using MEMS technology. For each array a constant width was used as 100, 200, 300 and 400 µm. The lengths were varied from ~3 mm to ~220 µm. The variation of the beam length is required to make each beam has different resonance frequency, so that each beam will response at different incoming sound frequencies. To characterize 1D array of beams with different lengths, electric impedance measurement will be used and their resonance frequencies will be found. The experiment will be conducted in both air and silicon oil since the cochlea is filled with biological fluid.

Discussion and Conclusions

1D array type piezoelectric thin-film beam structures have been fabricated and the characteristics of the devices are under investigation. This is the starting points of developing ABM using piezoelectric thin-film beam structures.

5B-5

3:00 pm Wireless Physical SAW Sensors for Automotive Applications

Victor Kalinin[1]; [1]Transense Technologies plc, Bicester, Oxfordshire, United Kingdom

Background, Motivation and Objective

Passive wireless sensors emerged as a new branch of SAW technology in the early 90s and almost immediately they were proposed for the use in automotive industry. The paper gives a brief overview of the early research projects devoted to pressure and torque automotive sensors based both on SAW reflective delay lines and resonators. Motivation behind development of the automotive SAW sensors and their advantages and disadvantages in comparison with competing technologies are discussed.

Statement of Contribution/Methods

Further progress of the automotive SAW sensors from the first demonstrators to production-ready systems required a solution of a number of problems, in particular, development of an inexpensive and accurate wireless interrogator, development of compact SAW sensing elements and packages for them suitable for high volume manufacturing. The paper discusses evolution of the sensing elements and interrogation methods with a particular emphasis on the resonant SAW sensors. Packaging methods are also discussed from the point of view of achieving good sensor reproducibility.

Results

A number of SAW sensing systems recently developed for automotive applications is presented: the tire pressure and temperature monitoring systems (TPMS) for sports cars and OTR vehicles, the torque and temperature sensor for the electrical power assisted steering system in off-road vehicles, the flexplate sensor for measuring IC engine output torque, the torque sensor for the F1 kinetic energy recovery system (KERS).

Discussion and Conclusions

Calibration of the wireless SAW sensors makes a significant contribution into the system cost. Methods of reducing complexity of the torque sensor calibration are discussed. A rig suitable for high volume calibration of the TPMS sensors is presented (shown in the figure below).

Further directions of work in the field of SAW automotive physical sensors are related to improvement of packaging and sensor assembly methods, reduction of the interrogation time and combination of sensing and ID functions.

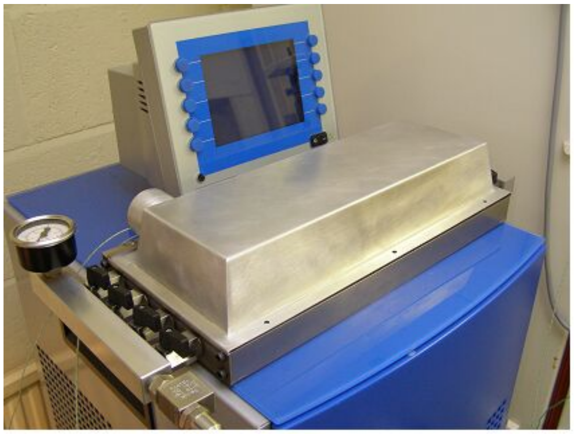

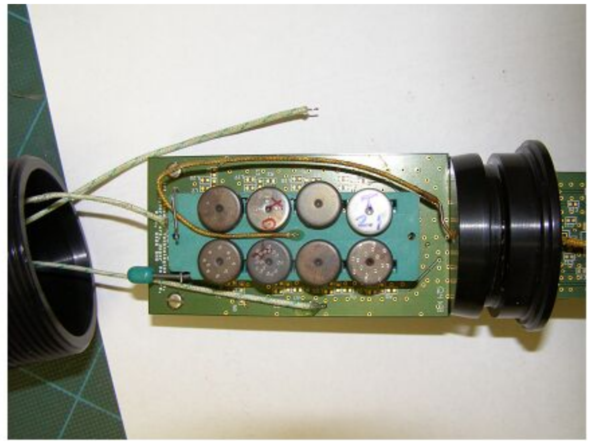

6B - Medical Imaging Transducers

Carribean Ballroom VI

Wednesday, October 19, 2011, 2:00 pm - 3:30 pm

Chair: **Scott Smith**
GE

6B-1

2:00 pm 80 MHz intravascular ultrasound (IVUS) transducer

Xiang Li[1], Wei Wu[2], Youngsoo Chung[2], Wan Y Shih[3], Wei-Heng Shih[2], Qifa Zhou[1], K. Kirk Shung[1]; [1]NIH Ultrasonic Transducer Resource Center and Biomedical Engineering, University of Southern California, Los Angeles, CA, USA, [2]Department of Materials Science and Engineering, Drexel University, Philadelphia, PA, USA, [3]School of Biomedical Engineering, Science, and Health Systems, Drexel University, Philadelphia, PA, USA

Background, Motivation and Objective

Clinically proven Intravascular Ultrasound (IVUS) imaging normally operates in the 20~40 MHz range, providing a resolution no better than 100 μm, which is insufficient for detection of a number of critical microstructures (<65 μm). Increasing the working frequency might be the only feasible solution for higher resolution IVUS imaging. However, it is hard to fabricate miniature transducers working well at 80 MHz or higher, especially considering the limitation of traditional lapping strategy for preparing very thin layers of piezoelectric material down to 20~30 μm. Piezoelectric thin film technology is an effective way to overcome this difficult.

Statement of Contribution/Methods

$[Pb(Mg_{1/3}Nb_{2/3})O_3]0.63[PbTiO_3]0.37$ (PMN-PT) free-standing film of comparable piezoelectric properties to bulk material with thickness of 30 μm has been fabricated using a modified precursor coating approach. Miniature side looking ultrasonic transducers have been fabricated from on this film. *Ex vivo* tests have been conducted on human coronary artery specimens at 80 MHz.

Results

The k_t of PMN-PT free-standing film was measured to be 0.55, which was close to that of bulk PMN-PT single crystal material. The center frequency and bandwidth of the miniature ultrasonic transducer were 82MHz and 65%. Insertion loss was 23 dB. Axial and lateral resolutions were determined to be as high as 35 μm and 176 μm. *Ex vivo* IVUS image acquired on coronary artery is shown in Fig. 1 (scale bar equals to 0.5 mm), which displays superior clarity in differentiating layered structures and plaques.

Discussion and Conclusions

The PMN-PT free-standing film technology simplified the process of preparation of very thin layers of piezoelectric material with satisfactory quality. The penetration depth observed in these experiments could achieve 2~2.5 mm, which could be further enhanced by implementing TGC or coded excitation. Although the resolution of 80 MHz IVUS image is still not comparable to OCT, it does possess a larger depth of penetration.

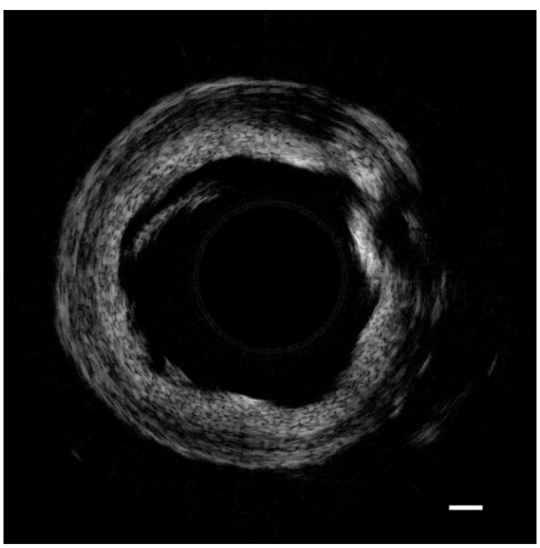

6B-2

2:03 pm 40 MHz piezo-composite linear array for medical imaging and integration in a high resolution system

Claire BANTIGNIES[1], Pascal MAUCHAMP[1], Franck LEVASSORT[2], Tony MATEO[2], Jean-Marc GREGOIRE[2], Remi DUFAIT[1], Frederic OSSANT[2]; *[1]VERMON, TOURS, France, [2]UMRS Imagerie&Cerveau, INSERM U930, CNRS ERL 3106, Francois-Rabelais University, TOURS, France*

Background, Motivation and Objective

The evolution of high resolution ultrasonic imaging is widely dependent on the development of efficient high frequency piezoelectric transducers. Nowadays, efforts are focused on the fabrication of linear arrays in the 40-50 MHz frequency range for dermatology, ophthalmology and small animals imaging. At these frequencies, technological aspects are predominant at several stages of the array fabrication due to typical dimensions of the constitutive elements (few tens of micrometers). The control of all these key parameters (such as efficient piezoelectric material, electrical connections…) is always a challenge. Moreover, the development of the imaging system and associated beamforming specifically adapted is of primary interest to optimize the use of the corresponding array and consequently image quality. The objectives of the presentation is first to detail the performance of a new fully operational 40 MHz linear array from the fabrication to the characterization. Secondly, this array will be coupled with an ultrasonic system developed at the laboratory and skin images are shown.

Statement of Contribution/Methods

On the basis of previous work [1, 2] and more recently with contributions detailed in the literature, new high performance 1-3 piezocomposite was fabricated to be used in the array. This piezocomposite was designed to minimize the effect of lateral modes which is the key points at these frequencies. For this application, the thickness of the piezoelectric material is around 30 µm to deliver a resonance frequency at 60 MHz in air. A 50 µm pitch is used to design 128 elements and a 2 mm elevation aperture is chosen. Fabrication rules of low frequency probes were extended and adapted to the design of this high frequency probe. Matching layers, backing and interconnect method are used to finalize the internal structure of the array. A specific real-time imaging platform with 128 channels using impulse electrical excitation and 100 MHz bandwidth in reception is used to perform human skin images.

[1] E. Lacaze, IEEE Ultrasonics Symp., 1139-1142, 2001

[2] S. Michau, IEEE Ultrasonics Symp., 898-901, 2004

Results

A complete set of measurements are performed on the final array. A center frequency at 40 Mhz is delivered with a relative bandwidth over 50%. All the 128 elements of the probe are active and very good sensitivity homogeneity along the probe is measured. Crosstalk between adjacent elements is also evaluated and the corresponding value is around 30 dB.

Discussion and Conclusions

The very good performance of the new HF40 MHz linear array coupled with the developed imaging system result in high resolution images, as evaluated with specifically designed phantoms. Further evaluation shall be performed to assess the image quality and clinical benefits as compared to lower frequency ultrasonic imaging and other diagnostic techniques.

6B-3

2:30 pm Low Power Embedded Processors for Ultrasonics Signal Chain

Murtaza Ali[1]; [1]Systems and Applications R&D Center, Texas Instruments, Dallas, TX, USA

Background, Motivation and Objective

Ultrasound systems are signal processing intensive. The signal processing for a typical ultrasound system can be roughly divided into three components: the front end which includes digitization of ultrasound signal followed by beam-forming to focus on a particular scan line, the mid end which performs demodulation, envelope detection, compression, and velocity estimation, and finally the back end which performs various image enhancement, rendering functions and user interfaces. In this paper, we describe how the ultrasound signal chain can be efficiently implemented in the class of embedded processors known as Digital Signal Processors (DSP).

Statement of Contribution/Methods

We have characterized the performance of various Ultrasound algorithms in several classes of DSP architectures from Texas Instruments (TI). Specifically we have optimized implementations of mid-end and back end processing needed for B-mode and color flow imaging mode. We have used TI's software framework to put together a demonstration processing systems that shows the capabilities of these devices.

Results

We have demonstrated the operations of ultrasound back-end processing which includes magnitude and velocity estimate from the demodulated data, compression for B-mode magnitude, scan conversion to match the display as well as color flow versus B-mode selection on one of TI's evaluation modules. With only a 430 MHz DSP, we can perform these operations for 30 frames per second, 96 scanlines per frame, 256 samples per scanline and 10 ensembles for velocity estimate with about 84% loading of the DSP. New multi-core platforms run up to 1.2 GHz with 8 of these cores available for processing on a single device. We are now measuring performance including the mid-end processing across these devices and will report on these performance measures at the conference. A very detailed analysis of the capabilities implement the front end functionalities has been submitted for regular paper in this conference as well. We will show how these devices can be put together to develop the digital part of the ultrasonic system. Some of these devices also include reduced instruction set Computing (RISC) processor as well as display units to handle the necessary control, user interface, display, and saving of data to external devices like hard disks or memory cards.

Discussion and Conclusions

DSP based low power embedded processors have revolutionalized the compute platforms for consumer electronics. The same technology is well suited for ultrasound systems. The family of devices available to ultrasound system designers using the architectures analyzed in this paper varies from single core to multi-core devices. These devices thus bring the added advantage of scalability. Portable to high end systems can all be based on same baseline embedded architecture and code.

6B-4

3:00 pm 2D Ring Array Transducers for Real-Time 3D Imaging of Atrial Septal Defect Repair

Edward Light[1], Stephen Smith[1]; [1]Biomedical Engineering, Duke University, Durham, North Carolina, USA

Background, Motivation and Objective

Atrial septal defects (ASD) make up 10% of total congenital heart diseases and as much as 25% of congenital heart disease in adults. ASDs may go undetected for decades. Typical treatments include doing nothing if the ASD is small and the patient is asymptomatic, surgery to repair the hole and transcatheter deployment of an atrial septal occluder. The minimally invasive transcatheter procedure is often preferred by patients. This procedure is typically done under fluoroscopic guidance combined with transesophageal echo (TEE) and Doppler ultrasound. Since the procedure already calls for the insertion of a catheter, we believe a catheter based transducer capable of generating real-time 3D images will reduce the need for the other imaging modalities.

Statement of Contribution/Methods

We used the Volumetrics real-time 3D scanner with a catheter based ring array transducer consisting of 55 elements operating near 5 MHz. The interelement spacing is 0.20 mm and the total device size is 12 Fr. The lumen size is 8 French. Typical – 6dB bandwidth was 20% with a center frequency of 4.7 MHz. We placed the St Jude Amplatzer Septal Occluder and the Gore Helix Septal Occluder in the lumen of our transducer and placed the transducer in a water tank for imaging.

Results

We made real-time 3D images of both Septal Occluders including a 3D rendered view of the Gore device shown below. A photograph of the device is shown on the left for comparison.

Discussion and Conclusions

Using our ring arrays we have now demonstrated feasibility of real time 3D ultrasound guidance of four critical implantable devices including vena cava filters, aortic aneurysm stent grafts, trans-apical heart valves and these septal occluders.

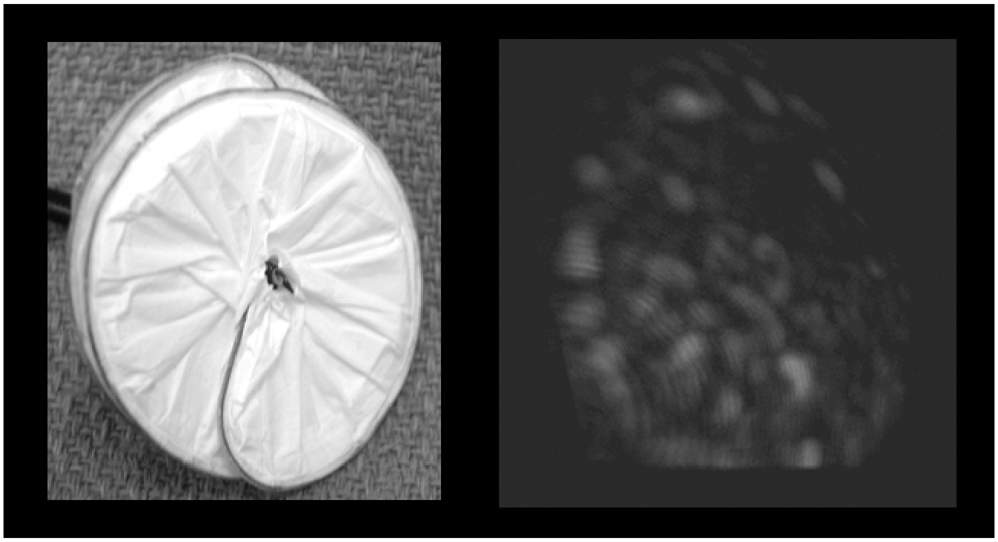

6B-5

3:15 pm Elastomeric photonic crystals for optoacoustic detection of high frequency ultrasound

Daniela Cruz[1], Ammar Khan[2], **Takashi Buma[3]**; [1]California State University Long Beach, USA, [2]University of Minnesota, USA, [3]University of Delaware, USA

Background, Motivation and Objective

Optical techniques are a promising technology for high frequency ultrasound imaging arrays. We have previously demonstrated an extremely thin etalon sensor based on a self-assembled monolayer of polystyrene microspheres. Increased sensitivity is possible with a stronger optical resonance. We are therefore exploring self-assembled multi-layers of microspheres (photonic crystals) as optoacoustic sensors.

Statement of Contribution/Methods

A 2% aqueous suspension of 0.32 um diameter polystyrene microspheres are placed on a glass cover slip. The colloidal suspension is then completely covered with silicone fluid. The fluid controls water evaporation to produce a more uniform crystallization of the microspheres. The entire sample is maintained at 60 degrees Celsius for one day. The crystallized microspheres are then infused with a polydimethylsiloxane (PDMS) matrix and cured. This "photonic sheet" is attached to the side of a water tank containing a 25 MHz spherically focused f/2 transducer. The probe laser is a temperature controlled Fabry-Perot AlGaAs diode laser with a wavelength of 780 nm. The optoacoustic signal is averaged 4 times by a 500 MHz 8-bit digital oscilloscope.

Results

The attached figure shows a scanning electron microscope (SEM) image of a photonic crystal fabricated in our laboratory. The orderly arrangement produces a strong optical diffraction at a resonant wavelength, as shown by the measured reflection spectrum. The peak wavelength is determined by the spacing and refractive index of the microspheres and the refractive index of the surrounding matrix material. The proposed sensing mechanism is the deformation of the microsphere spacing due to the incident ultrasound pressure. The recorded optical signal from the ultrasound transducer is shown below. The photonic crystal and pulse echo data both have peak frequencies of 25 MHz. The corresponding -6 dB bandwidths are 16 MHz and 11 MHz, respectively. The signal-to-noise ratio of the optical signal is 34 dB over a 50 MHz bandwidth.

Discussion and Conclusions

Further experimental investigations (e.g. reducing cracks) are under way to improve photonic crystal quality. Elastomeric photonic crystals can be coated on curved surfaces as well, making it possible to make focused sensors. We believe these encouraging results suggest the potential of optoacoustic detection by elastomeric photonic crystals.

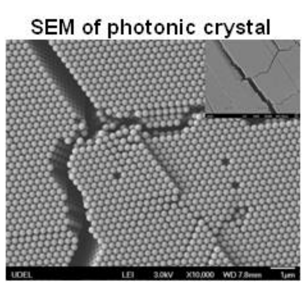

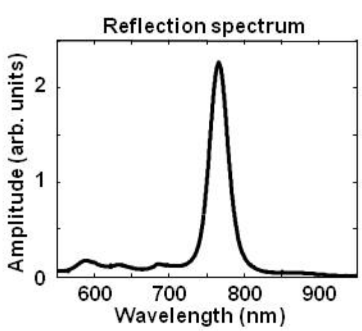

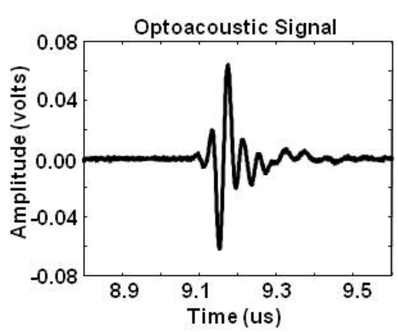

1C - 3D Imaging & Fast Simulation Tools

Boca Rooms II-IV

Wednesday, October 19, 2011, 4:30 pm - 6:00 pm

Chair: **Jian-yu Lu**
Univ. of Toledo

1C-1

4:30 pm Three-dimensional Spinal Bone Imaging with Medical Ultrasound for Epidural Anesthesia Guidance

F. William Mauldin, Jr. [1,2], Kevin Owen[1,2], John Hossack[1]; [1]Biomedical Engineering, University of Virginia, Charlottesville, VA, USA, [2]Rivanna Medical, Crozet, VA, USA

Background, Motivation and Objective

Epidural anesthesia procedures are performed in approximately 75 percent of all childbirths in the United States; however, failure rates for these procedures are as high as 40 percent over all cases and 70 percent in the obese population. Due to the limitations associated with X-ray-based fluoroscopy, including exposure to ionizing radiation and lack of portability, the standard of care is to perform epidurals manually – i.e. without medical imaging. High-quality 3D imaging of spinal bone surfaces using a portable ultrasound device could potentially overcome these challenges and offer physicians a safe imaging tool to increase success rates.

Statement of Contribution/Methods

A 4-channel handheld ultrasound system with custom 3/8" diameter piston transducers focused at 5cm were designed and fabricated. The system was then used to image an excised lumbar spine in a water bath over a mechanically-scanned 90mm x 50mm 2D plane. Positional information regarding the surface of the lumbar spine bone at each point across the 2D plane was estimated in MATLAB by detecting the position of maximum envelope-detected signal above the noise level. 3D topographical images were rendered and qualitatively compared to photographs of the actual spine. Additionally, automated measurements of spinous process and epidural gap dimensions along the axis of the spine were performed and compared to actual dimensions as a means to quantify bone surface depth estimation error.

Results

Three-dimensional bone imaging was demonstrated using a low-cost, portable ultrasound imaging device with hardware exhibiting a footprint of approximately 65mm x 90mm. Images of the excised spine using the handheld ultrasound system illustrated excellent correlation to optical images, as shown by the representative images in the figure below. Automated measurements (performed in MATLAB) of spinous process and epidural gap dimensions across the axis of the spine were within 0.5 mm of the actual dimensions, which represented less than 5% dimensional error.

Discussion and Conclusions

Results in this paper demonstrate the feasibility of a handheld ultrasound device for low-cost, safe, and portable imaging of spinal bone anatomy in 3D, which possesses the potential for improving the success rates of epidural anesthesia procedures. Excellent image quality was demonstrated with dimensional error less than 5%.

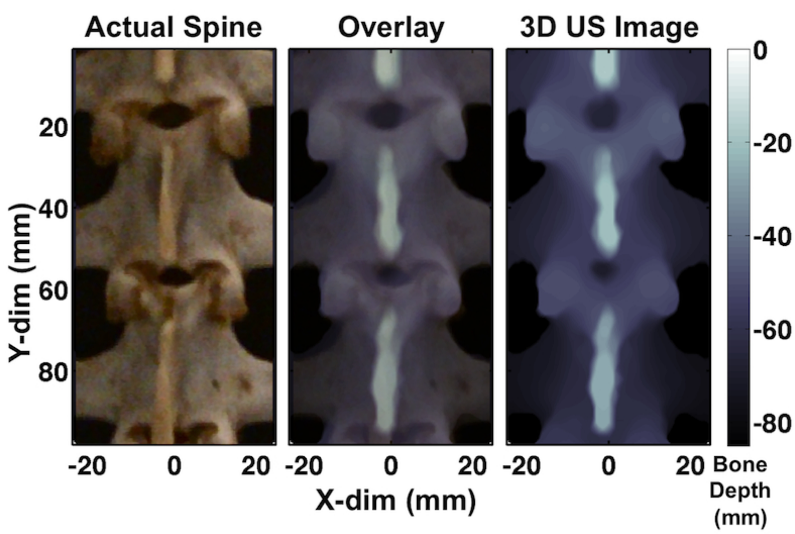

1C-2

4:45 pm Evaluation of 3D Point Spread Function of a Semi-Ellipsoidal Ultrasound Computer Tomography System

Nicole Ruiter[1], Robin Dapp[1], Michael Zapf[1], Hartmut Gemmeke[1]; [1]*Institute for Data Processing and Electronics, Karlsruhe Institute of Technology, Karlsruhe, Baden-Wuerttemberg, Germany*

Background, Motivation and Objective

A promising candidate for breast cancer imaging is ultrasound computer tomography (USCT). However, current USCT systems are focused in elevation dimension, resulting in a large slice thickness. 3D USCT with a 3D aperture, emitting and receiving spherical waves, overcomes this limitation by generating full 3D volumes. We designed and built an optimized 3D USCT, with the aim of nearly isotropic and approx. spatially invariant 3D point spread function (PSF). The objective of this work was to experimentally evaluate the 3D PSF.

Statement of Contribution/Methods

The built 3D USCT has a semi-ellipsoidal aperture with over 2000 ultrasound transducers (628 emitters and 1413 receivers). Approx. spherical wave fronts are generated by emitting with a single emitter at 2.5 MHz (50% bandwidth). Rotational and translational movement of the complete sensor system creates further virtual positions of the ultrasound transducers. The data acquisition is carried out with a FPGA based system which can store up to 40 GB of A-Scans. The read-out is performed by 480 parallel channels (12 Bit @ 20 MHz), enabling data acquisition of one aperture position in 6 s. The left photo in the attached figure shows the 3D USCT system.

In order to evaluate the 3D PSF, a bonding wire much thinner than the expected resolution was twisted into an irregular helix with approx. 2 cm diameter and imaged with the USCT device (four fold averaging, 887,364 emitting-receiving combinations, ROI of 16.7 x 10.2 x 6.7 cm). The PSF was measured at 38 approx. equidistant points along the thread. At each of these points the PSF was evaluated as 2D profile of the full width at half maximum (FWHM) in a plane perpendicular to the current direction of the thread.

Results

In the left image of the included figure a maximum intensity projection of the reconstructed thread is shown. The average maximum FWHM over all profiles was 1.06 mm. The standard deviation (STD) of the FWHM profiles as measure of the isotropy is maximally 0.35 mm (mean 0.21 mm). The variability of the mean FWHM over the points as measure of the spatial variability shows no systematic trend. It has a mean of 0.73 mm with a STD 0.08 mm.

Discussion and Conclusions

The achieved 3D isotropy of the PSF is very satisfactory and fits previously simulated values. The spatial deviation of the FWHM over the ROI is small. As next step the application to breast tissue will be shown.

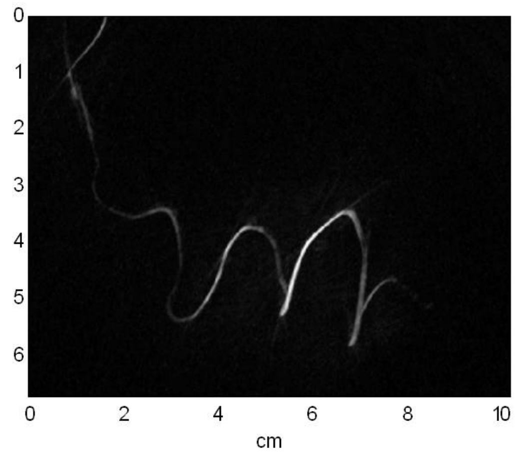

1C-3

5:00 pm High Frequency Doppler Flow Triggering for 75 MHz Ultra-High Frame Rate 3D Ultrasonic Zebrafish Echocardiography

Ting-Yu Liu[1], Po-Yang Lee[1], Cho-Chiang Shih[1], Chih-Chung Huang[1]; [1]Department of Electrical Engineering, Fu Jen Catholic University, Taiwan

Background, Motivation and Objective

Recently, zebrafish has become a new animal model for cardiovascular development and genetics studies. Because adult zebrafish heart has a small size (~2 mm) and high heart rate (80~130 beats/min), an ultrasound imaging requires high resolution and high frame rate. Currently, a commercial high frequency ultrasound scanner is available for monitoring small animal cardiac cycles, which can achieve a frame rate up to 1000 fps using array probe. However, it still needs a trigger signal for 3D cardiac imaging by mechanical scan. In present study, the 75 MHz ultra-high frame rate and high resolution 3D ultrasonic zebrafish echocardiography was proposed by using pulsed-wave (PW) Doppler flow trigger technology.

Statement of Contribution/Methods

Figure 1(a) shows the block diagram of zebrafish cardiac imaging system. A 45 MHz PW Doppler flowmeter was built for measuring the Doppler spectrogram from zebrafish artery, and the timing of peak flow velocity was selected by analog circuits as a trigger signal to synchronize the three-dimension 75 MHz high frequency ultrasound imaging system. The high-frame rate 2D and 3D echocardiography was reconstructed by acquired A-line signals at different cardiac positions with high pulse repetition frequency, as shown in Fig 1(b)

Results

Figure 1(c) shows the typical screenshots of zebrafish echocardiography at different timings during one cardiac cycle from a dynamic video. The dotted line shows the volume of heart. The dynamic motion of cardiac cycle was observed clearly at a frame rate of 2000 fps. The axial and lateral resolution of this imaging system was approximately 23.1 and 66 μm, respectively.

Discussion and Conclusions

The 2D and 3D ultra-high frame rate ultrasonic zebrafish echocardiography was obtained by PW Doppler blood flow triggering in this study. The volume size of heart was changed approximately 12-14% between diastole and systole. Compared with ECG triggering, noninvasive measurement is the main advantage of this design (often uses needle electrode for zebrafish ECG). Even though the single element transducer was used for scanning the zebrafish heart, this technology still can be applied to array system for high frame dynamic 3D imaging.

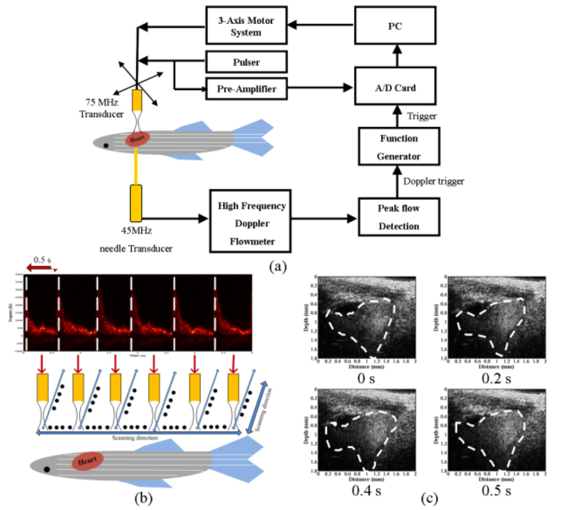

1C-4

5:15 pm 4D Simulation of nonlinear pressure field propagation on GPU with the Angular Spectrum Method

François Varray[1,2], Christian Cachard[1], Piero Tortoli[2], Olivier Basset[1]; [1]Université de Lyon, CREATIS ; CNRS UMR5220 ; INSERM U1044 ; INSA-Lyon ; Université Lyon 1, France, [2]MSD Lab, University of Firenze, Italy

Background, Motivation and Objective

Although several developments are currently running in the field of harmonic imaging, the simulation of nonlinear ultrasound (US) propagation is complex, and still requires long computation times. Using the angular spectrum method (ASM) instead of KZK simulator is a first step to decrease the computation time. Moreover, the involved mathematical background of the ASM is particularly suitable for implementation in the graphic processor units (GPUs), which are capable of massive and parallel computation tasks. In this paper, we propose a new ASM-based mathematical background, allowing to compute the first three harmonics of the US field in media with inhomogeneous nonlinear parameter. The proposed solution was implemented on a GPU to provide a fast nonlinear propagation simulator.

Statement of Contribution/Methods

The ASM is based on the Fourier transform of the propagation equation. Using the quasi-linear approximation, three distinct equations for the fundamental, second and third harmonic components are solved in the Fourier domain, producing a complete 4D (3D+t) pressure field. The proposed formulation, which is valid for any 1D or 2D array, also permits to consider a medium with inhomogeneous nonlinear parameter, by taking into account the increase of the harmonic during the propagation. The simulation was implemented on both CPUs and GPUs, by computing the Fourier transform through a function from an optimized external library.

Results

The ASM results have been first compared with those provided by FieldII for linear propagation, with KZK simulations for nonlinear propagation, and with experimental measurements. The global amplitude error in simulation is $\leq 3.7 \pm 1.9$ %. A difference of 5.4 ± 2.7 % was found with respect to the experimental fields. Secondly, the computation time was measured on two computers with two different GPUs, composed of 8 and 240 processing units, respectively. By using GPUs rather than CPUs, the computation time was reduced by a factor 3.5 and 19.2 depending on the computer.

Discussion and Conclusions

The proposed mathematical background allows for the first time to consider inhomogeneous nonlinear media for the first three harmonics. Moreover, this new formulation of the ASM is particularly suited to GPU implementation and the computation time shows a noticeable speed-up. Since all operations, except the Fourier transform, are made pixel by pixel, GPU programming is very efficient. Using several GPUs in parallel could also permit to further decrease the total computation time. The high level of parallelization could decrease down to a couple of minutes, a computation time now taking hours with the KZK simulator and a single CPU. The proposed mathematical background can be easily generalized to simulate the n^{th} harmonics with a corresponding increase of the global computation time.

1C-5

5:30 pm Multi-modal cardiac image fusion and visualization on the GPU

Gabriel Kiss[1,2], Jon Petter Åsen[1,3], Piet Claus[4], Jan D'hooge[1,4], Hans Torp[1]; [1]MI Lab and Department of Circulation and Medical Imaging, Norwegian University of Science and Technology, Trondheim, Norway, [2]St. Olavs Hospital, Trondheim, Norway, [3]Department of Informatics, University of Oslo, Oslo, Norway, [4]Cardiovascular Imaging & Dynamics, Dept. of Cardiovascular Diseases, K.U.Leuven, Leuven, Belgium

Background, Motivation and Objective

The main motivation of this project is to derive and present an integrated cardiac model, based on information obtained using two different imaging modalities: 3D echocardiography (3D echo) and cardiac magnetic resonance imaging (CMR). Since 3D echo allows for volumetric and functional measurements in real-time, while CMR can produce anatomically accurate recordings of morphology and function (cine imaging), perfusion (first-pass imaging) and tissue characterization (such as edema (T2 STIR) or scar (late enhancement imaging)), combining them should benefit myocardial viability assessment and ischemia diagnosis.

Statement of Contribution/Methods

Ten subjects (7 with myocardial infarction) have been selected for this study. Among them 6 underwent 3D echo and CMR short- long-axis cine the same day, while the remaining 4 patients underwent CMR cine, delayed enhancement and edema imaging at baseline and after 4 up to 6 months, but no 3D echo.

In-house developed breath-hold and diaphragm motion compensation software was applied to the CMR slices as a first step. The 3D echo and CMR datasets were aligned by matching a set of 7 landmarks (apex and 6 mitral attachment points), via linear least square approximation. Afterwards 3D echo slices corresponding to CMR data could be extracted. In order to solve the spatial and temporal mismatch between CMR recordings an image registration algorithm that runs on the GPU (AIRWC) was customized. Using

AIRWC the affine matrix and the non-rigid deformation field between subsequent CMR cine slices can be computed and reapplied to late-enhancement or edema slices to obtain continuous loops similar to the cine recordings.

Results

A good visual alignment between 3D echo and CMR data was achieved for all 6 cases (figure 1.a: 3D echo - red, cine - gray), also a superposition of longitudinal strain values (3D echo speckle tracking) was feasible(figure 1.b). Figure 1.c shows aligned CMR data at end diastole for the same patient at baseline and after 6 months. Average slice to slice registration times were reduced from: 360.78s CPU to 7.74s GPU.

Discussion and Conclusions

Combining multi-modal anatomical and functional information allows for a quick visual assessment of datasets obtained the same day or during longitudinal studies. Current work includes further integration of 3D echo and CMR data and possibly of other imaging modalities (e.g. CT).

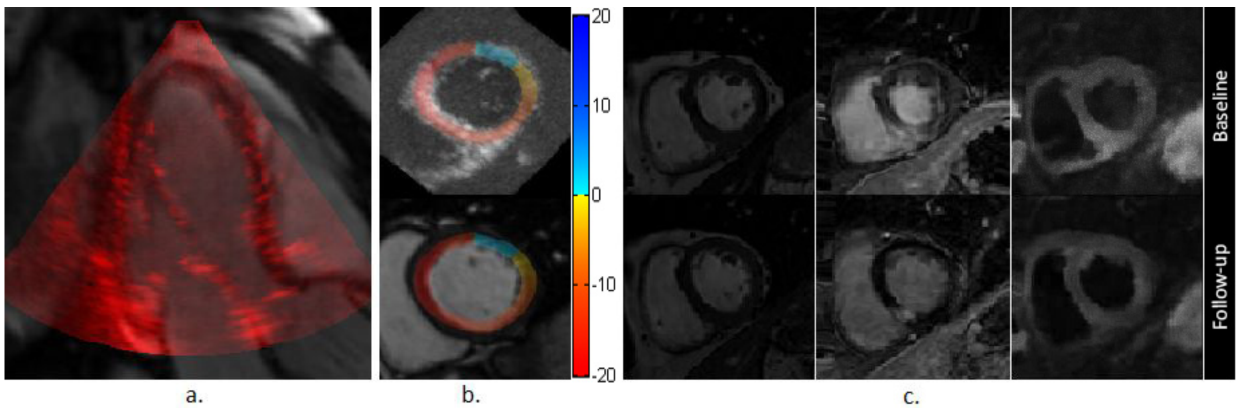

1C-6

5:45 pm Real-time simulation of ultrasound images using the GPU

Sjur Urdson Gjerald[1], Reidar Brekken[1,2], Torbjørn Hergum[1], Jan D'hooge[1,3]; [1]MI Lab and Dept. of Circulation and Medical Imaging, Norwegian University of Science and Technology, Trondheim, Norway, [2]Dept. of Medical Technology, SINTEF, Trondheim, Norway, [3]Lab. on Cardiovascular Imaging & Dynamics, Dept. of Cardiovascular Diseases, Katholieke Universiteit, Leuven, Belgium

Background, Motivation and Objective

In ultrasound training simulators, synthetic ultrasound images have to be generated in real time at a frame-rate close to the actual ultrasound scanner. Patient specific anatomy can be modeled by computed tomography (CT) data, and shadows and attenuation can be added by calculating reflection coefficients and depth-dependent, exponential intensity decay. In order to produce ultrasound speckle at this frame rate, it is typically added as a pre-calculated texture map. We propose to increase the speckle realism by using a physical model of the underlying scattering process.

Statement of Contribution/Methods

The scattering process was modeled as a convolution of the point spread function (PSF) of the ultrasound scanner with a scatterer distribution. The challenge is that a typical field-of-view (FOV) contains thousands of scatterers, which have to be selected by a virtual probe from an even larger body of scatterers and then sampled. In order to do this in real time, we 1) selected and sampled scatterers in parallel on the graphic processing unit (GPU), and 2) avoided searching through the entire body of scatterers by anchoring every scatterer in the body to a regular grid for direct look-up. In order to get depth dependent beam width and increased intensity in focus, the two-dimensional PSF was assumed to be separable, and the sampled scatterer object was convolved with one-dimensional PSFs axially and laterally on the GPU. For testing, a B-mode image for a curvilinear array probe with 5 cm radius, 3.5 MHz center frequency and beam profile from Field II was made with 3760 by 224 samples (70 mm by 60 degrees) and involving 465345 scatterers in the FOV.

Results

The resulting image in beam-space is shown to the left in the figure, and a reference image using Field II to the right. Calculation time using the new method was 7 milliseconds (ms) for sampling and 2.2 ms for convolutions.

Discussion and Conclusions

The method allows for real-time simulation of ultrasound images. Since the method treats individual scatterers, it may be used for simulating e.g. Doppler or tracking methods, thus increasing the scope of ultrasound training simulators.

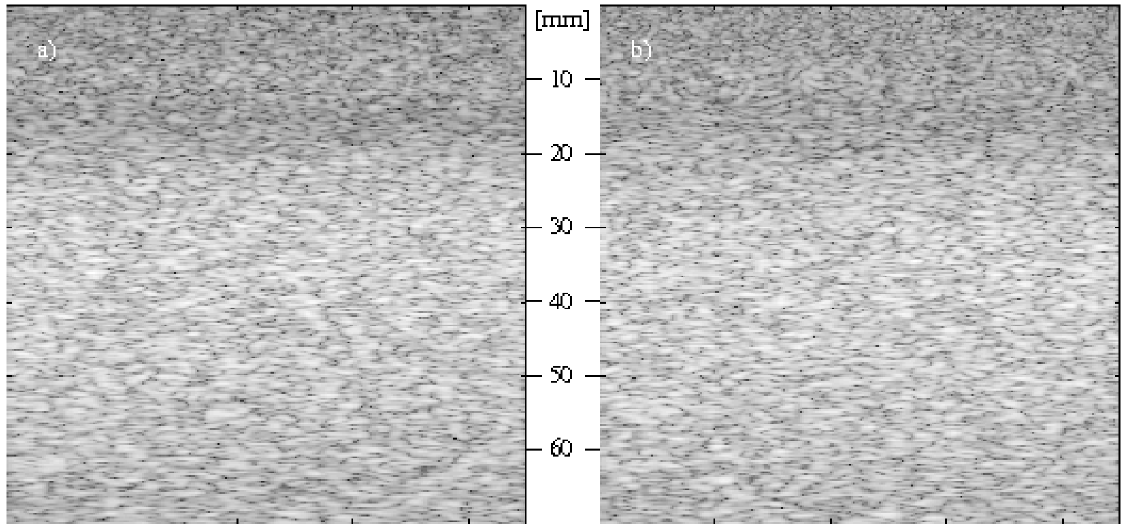
a)
b)
[mm]
10
20
30
40
50
60

2C - Advanced Flow Estimation Algorithms and Functional Imaging

Boca Rooms VI-VII

Wednesday, October 19, 2011, 4:30 pm - 6:00 pm

Chair: **Svetoslav Nikolov**
BK Medical

2C-1

4:30 pm Recent advances in blood vector velocity imaging

Jørgen Arendt Jensen[1]; [1]Center for fast Ultrasound Imaging, Dept. of Elec. Eng, Bldg. 349, Technical University of Denmark, Lyngby, Denmark

Background, Motivation and Objective

Medical ultrasound has for more than 40 years been capable of estimating the blood velocity in the human circulatory system. This is of major diagnostic value for screening and investigating haemodynamic problems. Current commercial systems, however, only estimated the velocity along the ultrasound direction, which often is the least significant velocity component as the major vessels run parallel to the skin. Also at bifurcations, valves, and geometric changes the flow is not uni-directional and varies as a function of space and phase in the cardiac cycle.

Statement of Contribution/Methods

A number of methods for solving this problem are presented in the paper. The transverse oscillation (TO) method can estimate the velocity transverse to the ultrasound beam by introducing a lateral oscillation in the received ultrasound field. The approach has been thoroughly investigated using both simulations, flow rig measurements, and in-vivo validation against MR scans. A range of other methods will also be presented. This includes synthetic aperture imaging using either spherical or plane waves with velocity estimation performed with directional beamforming or speckle tracking. The key advantages of these techniques are very fast imaging that can attain an order of magnitude higher precision than other methods.

Results

The TO method obtains a relative accuracy of 10% for a fully transverse flow in both simulations and flow rig experiments. In-vivo studies performed on 11 healthy volunteers comparing the TO method with magnetic resonance phase contrast angiography (MRA) revealed a correlation between the stroke volume estimated by TO and MRA of 0.91 ($p < 0.01$) with an equation for the line of regression given as: MRA = 1.1•TO-0.4 ml. Several clinical examples of complex flow in e.g. bifurcations and around valves have been acquired using a commercial implementation of the method (BK Medical ProFocus Ultraview scanner). SA flow imaging was implemented on the experimental scanner RASMUS using an 8-emission spherical emission sequence and reception of 64 channels on a BK Medical 8804 transducer. This resulted in a relative standard deviation of 1.2% for a fully transverse flow. Plane wave imaging was also implemented on the RASMUS scanner and a 100 Hz frame rate was attained. Several vector velocity image sequences of complex flow was acquired and demonstrates the benefits of fast vector flow imaging.

Discussion and Conclusions

The flow in the human body is pulsating, complex, and hardly ever laminar. The velocity vector changes over time and space, and current static angle compensation methods are inadequate for quantitative velocity estimation in everything but the simplest cases. The new vector velocity imaging schemes are capable of revealing a wealth of information regarding the human circulation in real time and without the use of contrast agents.

2C-2

5:00 pm **Ultrafast imaging of blood flow dynamics in myocardium**

Bruno-Felix OSMANSKI[1], Mathieu Pernot[1], Gabriel Montaldo[1], Mickael Tanter[1]; [1]*Institut Langevin, France*

Background, Motivation and Objective

Imaging myocardial perfusion could strongly help to achieve better diagnostic of cardiovascular diseases. However, no current imaging modalities allow imaging accurately myocardial blood flow dynamics. In Doppler echocardiography, the large tissue velocities generate strong artifacts that mask the weak signal coming from blood. In this work we used an ultrafast Doppler imaging technique to follow the blood flow and fast tissue motion of the heart walls during a whole cardiac cycle. A special demodulation-filtering process enables us to image the flow dynamics inside the myocardium.

Statement of Contribution/Methods

The experiment is carried out on three anesthetized open-chest sheep. The ultrasound transducer array (8Mhz, 60% Bandwidth) is placed against the epicardium of the left ventricle. The myocardium is imaged at an ultrafast frame rate (3kHz) using plane wave transmits during a complete cardiac cycle (0.5s) generating a set of 1500 images. For each pixel of the 2D image, a Doppler signal of 1500 points is obtained (tissue and blood signal). The spectrum of the tissue signal is not centered at zero due to the fast tissue motion. Before wall filtering we demodulated the tissue motion to center it to zero. After demodulation, we applied a high pass filter to extract the blood signal.

Results

After tissue motion filtering, venous flows are clearly observed (fig 1a) from mid to end systole (from 0.15s to 0.27s (fig 1b)). The arterial network starts while the heart is still contracted and continues during the whole diastole (fig 1c). The mean speed of these flows varies from 10 to 25 cm/s. Finally, after a complete coronary artery ligation, venous and arterial flows were found to completely vanish and to reappear during reperfusion.

Discussion and Conclusions

Our method is able to image small vessels in fast moving tissues using a demodulation process. The temporal resolution of the ultrafast doppler allows imaging the flow dynamics and the vessel network both in systole and diastole. Known from cardiac physiology, myocardial perfusion is inversed respect to the other organs with venous flows occurring predominantly during systole and arterial flows during diastole.

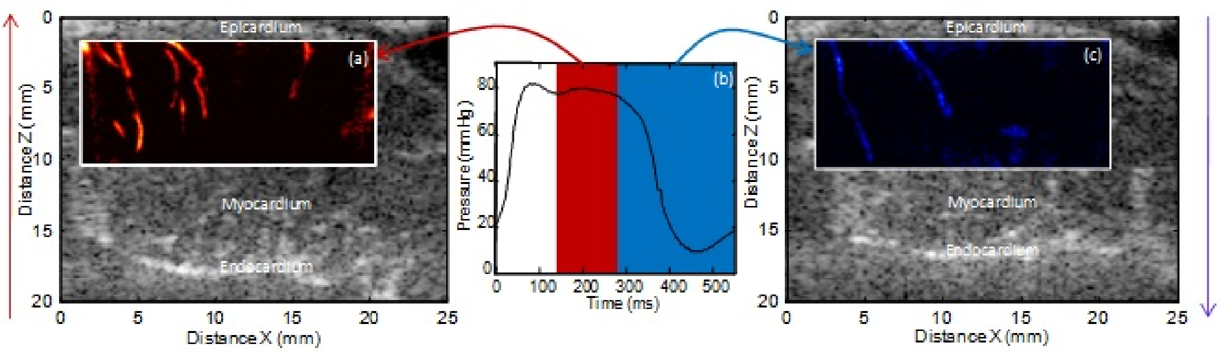

Figure 1: Signed power doppler of venous flow going up (towards the transducer) (a) and of arterial flow going down (away from the transducer) (c). (b) Intra-ventricular pressure.

2C-3

5:15 pm **Peak Velocity Measurement Through Doppler Spectrum: Experimental Verification**

Stefano Ricci[1], Luca Bassi[1], Piero Tortoli[1]; [1]Electronics & Telecommunications Dept., Florence University, Firenze, Italy

Background, Motivation and Objective

The signal backscattered by the blood cells that cross a large sample volume (SV) produces a Doppler spectrum whose frequency content is related to the scatterers velocity distribution. Several methods have been proposed for measuring the maximum velocity component, but they typically propose approximate solutions based on heuristics thresholds applied to the Doppler power spectral density. A new theory that models the Doppler spectrum shape is proposed in the companion abstract #496. This theory locates the peak velocity in correspondence of a precise threshold applied to the descending slope of the measured spectrum. For example, for parabolic velocity distribution, this theory states that the peak velocity corresponds to the half slope frequency. This works reports on the experimental verification of this assertion.

.

Statement of Contribution/Methods

The measurements were made on a phantom. A blood mimicking fluid flowed in a straight pipe between two reservoirs provided with weirs which granted a constant level difference between the reservoirs. The circuit included a reference flowmeter and a valve for controlling the flow rate. Above the straight tube, two non focussed transducers working in a pitch-catch configuration created a large SV centered in the middle of the pipe. A dual-channel research US system was used to produce the excitation bursts, demodulate and save the received echoes. Flow rates were controlled in 20 ml/min steps over a range (100-300 ml/min) which guarantees parabolic velocity profiles in the measurement site.

.

Results

60″ of data were gathered for each flow rate. Data were divided in segments of 1k samples each with 75% overlap. Each segment was windowed and processed through FFT. The spectral data were squared and averaged. The half-slope frequency was converted to velocity through the classic Doppler equation and compared to the reference. The error featured 1% bias and 1.3% standard deviation for all the 15 investigated flow rates. For example, the picture below compares the measured and predicted Doppler spectra for a 250 ml/min flow zoomed in the slope region. Experimental half-slope and reference frequency are also reported. Here the error was 0.7%.

.

Discussion and Conclusions

This work has demonstrated that the peak velocity in parabolic flows investigated with a large SV corresponds to the half-slope frequency of the Doppler spectrum.

.

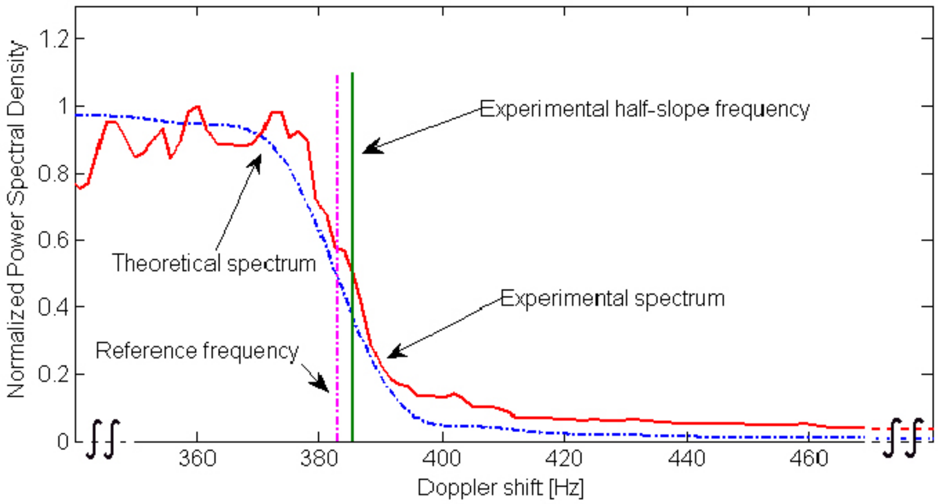

2C-4

5:30 pm Detection of Atherosclerosis from Vessel Wall Vibrations using Non-linear Features

Leili Salehi[1], Parisa Gifani[2], Georg Schmitz[1]; [1]Electronics and Information Technology, Ruhr Universität Bochum, Bochum, Germany, [2]Electrical Engineering, Iran University of Science and Technology, Tehran, Iran

Background, Motivation and Objective

Atherosclerosis is a major cause of mortality worldwide. Circulatory diseases such as cerebral and myocardial infarction are the last symptoms of atherosclerosis. Diagnosis of this disease in the early stages can be helpful for further treatments.

Non-invasive measurement of the mechanical properties of the vessel wall, such as vibratility, is useful for the diagnosis of atherosclerosis, since there are significant differences between vibration characteristics of normal arterial walls and those affected by atherosclerosis.

Here, non-linear features are extracted from vessel wall vibrations and tested for their capability of discriminating between normal and atherosclerotic vessels.

Statement of Contribution/Methods

The small vibrations of vessel walls due to blood flow were extracted from RF ultrasound data using a modified phase-tracking method. For a first test, RF data of aorta and hepatic vein were obtained from a normal 33 year old male in 3 cardiac cycles by a B-K Medical A/S type 3535, 3.2 MHz linear array probe.

A vein is considered here as a model for an atherosclerotic vessel with its less and irregular vibrations compared to a normal artery. All calculations are applied to normalized time signals from 6 windows in the depth direction of the vessel wall.

The ratio of the standard deviation of points in the consecutive maxima map, and a state-space plot (x[n+5] in terms of x[n]) around the 135° line to that around 45° line are considered as numerical time features as well as the spectral entropy.

Results

Table 1 shows the averaged values of three features for 6 windows.

Investigating the time features demonstrates that propagation of points in state-space for the artery is more compact around the 45° line (like a long ellipse) than for a vein (like a circle). Also significant differences in entropies can be observed.

Discussion and Conclusions

Different time and frequency dependent features investigated to discriminate normal vessel from atherosclerotic vessel. It is obvious from the two left columns of Table1 that the dynamic of vessel wall motion in a normal artery is close to a linear dynamic, while that for a vein is non-linear. Also, entropy, which is a measure of non-regularity in a system, is more for vein. In the future we will study the capability to differentiate between diseased and healthy arteries.

Table1. Comparison between mean values of three features for 6 windows in the depth direction of two different vessels

	Consecutive Maxima Map		State-Space Plot		Mean Spectral Entropy	
	Aorta	Hepatic	Aorta	Hepatic	Aorta	Hepatic
Mean$\pm SD$	0.30 ± 0.02	0.52 ± 0.07	0.49 ± 0.08	0.87 ± 0.14	0.58 ± 0.08	0.74 ± 0.08

2C-5

5:45 pm Determination of the depth dependent Fourier spectra of catheter reflections for automatic catheter detection

Anke Poelstra[1], Heinrich Martin Overhoff[1]; [1]University of Applied Sciences Gelsenkirchen, Gelsenkirchen, Germany

Background, Motivation and Objective

The planning of a high dose rate (HDR) brachytherapy of the breast depends strongly on catheter positions. For determining these positions, 3-D ultrasound is a promising alternative to stereotactic mammography and CT but suffers from poor image contrast.

B-mode image pixels relate to short time samples of focused receive raw data (A-lines). In such images, bright, straight lines in different depths z visualize either catheters or tissue structures. Primary investigations had shown, that a parameter set of (1) the threshold of the postprocessed sample amplitude A_{th}, (2) fixed lower (f_l) and upper (f_u) cut off frequency of the sample's bandpass-like Fourier spectrum and (3) the number N of laterally neighbored samples allows to classify A-line samples to ″tissue″ and ″catheters″.

It was hypothesized that (a) depth dependent instead of fixed cut off frequencies improve sensitivity and specifity of the classification and (b) for small depths, the cut off frequencies decrease logarithmically with increasing depth.

Statement of Contribution/Methods

A-lines of 30 image volumes of plastic catheters placed in turkey breast were acquired. Further raw data originated from patients who had undergone lumpectomy and implantation of flexible plastic tubes. The data were analyzed and reconstructed to images using MATLAB; each image consisted of $N_I \times N_J$ pixels with gray scale values $g(i,j)$, with $1 \leq i \leq N_I$, $1 \leq j \leq N_j$, in which $z=i\ \Delta z$ and the gray scale values represent postprocessed A-line samples.

For raw data samples whose corresponding pixels comply with $g(i,j) \geq A_{th}$, the frequency with maximal amplitude $f_{A,max}$ was identified. Its depth dependence was exploited to define the frequency criterion $f_l\ (z) \leq f_{A,max} \leq f_u\ (z)$.

Manually segmented B-mode images were the reference for fourfold tests and ROC curves, by which optimized parameter sets with depth dependent cut off frequencies were determined.

Results

No parameter set generated a ROC curve which approximated sensitifity = specificity =100%. For specitifities >90%, an improve of sensitivity from 30% (fixed) up to 35% (depth dependent cut off frequencies) was gained (a). Parameter sets that maximize the sensitivity of catheter sample detection at a specificity >90% rely on logarithmic frequency decrease at increasing depth up to 4 cm (b).

Discussion and Conclusions

Analyzing depth dependent Fourier spectra of A-lines improves the automatic detection of catheters in B-mode images. The stated logarithmic decrease of cut off frequencies at increasing depth fits well to the expected properties of attenuation coefficients.

3C - Photoacoustics: Applications

Carribean Ballroom VII

Wednesday, October 19, 2011, 4:30 pm - 6:00 pm

Chair: **Michael Kolios**
Ryerson University

3C-1

4:30 pm Simultaneous photoacoustic and high-frequency ultrasound *in vivo* imaging of the mouse embryonic vasculature

Orlando Aristizábal[1], Jonathan Mamou[2], Erwan Filoux[2], Jeffrey A. Ketterling[2], Daniel H. Turnbull[1], Parag V. Chitnis[2]; [1]*Skirball Institute, NYU School of Medicine, New York, NY, USA,* [2]*Riverside Research, New York, NY, USA*

Background, Motivation and Objective

The developing embryonic vasculature system is a morphologically complex structure whose normal development depends critically on the spatio-temporal expression of secreted factors. Furthermore, there is an intimate relation between cell differentiation and proliferation of the central nervous system and normal vascular development. To study this dynamic system *in vivo*, an imaging protocol that integrates photoacoustics (PA) with high-frequency ultrasound (HFU) is presented.

Statement of Contribution/Methods

Three dimensional data sets were acquired by raster scanning a 5-element, 40-MHz, PVDF-TrFE annular-array transducer with a geometric focus of 12 mm in 50 µm increments. A bifurcated fiber-guide assembly with collimating lenses mounted on the transducer illuminated the focal region from opposing sides at an angle of 45° to the imaging plane. A single intact conceptus from an anesthetized mouse was surgically exposed into PBS-filled Petri-dish. Illumination from a pulsed, 532-nm laser was synchronized with a high-voltage impulse excitation of the central array element to facilitate simultaneous HFU and PA data acquisition. All data were gated to the resting phase of the respiratory cycle. The resulting HFU echo and PA signal from each scan location were recorded on all five array channels and post-processed using a synthetic focusing algorithm to enhance the depth of field (DOF).

Results

3D datasets were acquired from mouse embryos at E12.5 and E13.5 days of gestation. The extended DOF allowed morphologically accurate visualization of the embryonic head (Fig. 1a,d). Because the RF line acquired at each scan location contained discrete PA and HFU-echo signals, co-registration of both the anatomy and vasculature is automatic (Fig. 1b,e). The PA data provided a visual indication of the vascular plexus. By adjusting the colormap transparency, individual vessels can be appreciated. Deeper vascular imaging was obtained with the smaller E12.5 embryos attributed to better optical penetration than the E13.5 case.

Discussion and Conclusions

Feasibility of real-time, spatially co-registered, low-cost dual-modality *in vivo* imaging of mouse embryos was demonstrated. This method can be extended to other gestational stages with the possibility of full *in utero, in vivo* imaging, thus allowing for longitudinal embryonic development studies.

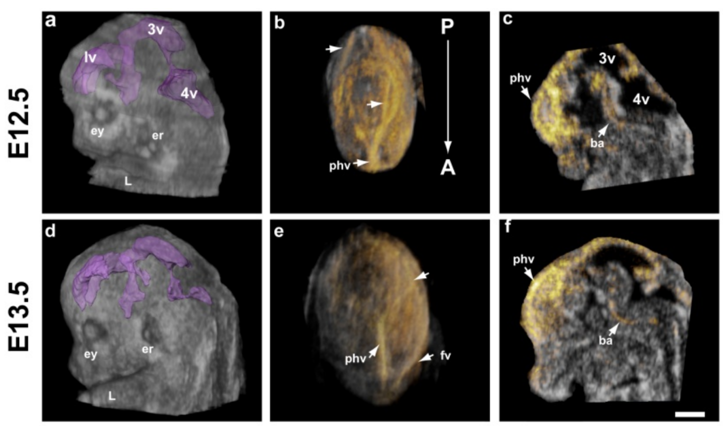

Figure 1. Volumetric reconstructions of the B-mode data sets (a) and (d) reveals facial features such as the eye (ey), the ear canal (er) and the fore-limb (L). High quality datasets also allow for the segmentation of the brain ventricles . Co-registered B-mode and photoacoustic data (b) and (e) reveal major blood vessels in the embryonic head (arrows) including the primary head vein (phv) and facial vein (fv). (c) and (f), mid-saggital orthoslices show the basilar artery (ba) deep inside the head . P-A , posterior to anterior axis. lv, 3v, 4v= lateral, third, fourth ventricle. Scale bar =1mm.

3C-2

4:45 pm Integrated 3-D vascular ultrasound, strain and spectroscopic photoacoustic imaging for noninvasive characterization of atherosclerotic arteries

Iulia Graf[1], Arman Satari[1], Richard Smalling[2], Stanislav Emelianov[1]; [1]Biomedical Engineering, University of Texas at Austin, Austin, Texas, USA, [2]Department of Internal Medicine, University of Texas Medical School at Houston, Houston, Texas, USA

Background, Motivation and Objective

The complex nature of atherosclerosis requires the assessment of various arterial properties to accurately diagnose the severity of the disease. The aim of this study is to develop and test a vascular imaging method combining ultrasound, strain-rate and spectroscopic photoacoustic (PA) imaging to non-invasively diagnose superficial arteries.

Statement of Contribution/Methods

The experiments were performed using balloon-injured New Zealand white rabbit models of atherosclerosis. The system was tested ex-vivo on 5 freshly excised atherosclerotic aortas with 4-6 mm lumen diameters. Each sample was fixed in a water tank filled with saline and flushed with blood at a pulsatile flow (2 Hz, 50 cm/s). The artery was scanned using a 20-MHz linear array transducer surrounded by 20 optical fibers and Vevo 2100 ultrasound system. Ultrasound 3-D data sets were formed from 256 beams and 150 frames. For strain imaging, 40 RF frames (64 beams) were recorded at 210 fps. The 3-D PA images with 256 beams were acquired at 1210 nm, 1220 nm and 1230 nm wavelengths. Offline processing algorithms based on cross-correlation method (for 0.10 mm X 0.24 mm X 10 ms kernel sizes) enabled the derivation of strain rate. A multi-wavelength spectroscopic PA algorithm was developed based on optical absorption spectra to distinguish lipids from surrounding tissue and blood in the range 1210-1230 nm.

Results

Ultrasound images revealed arterial morphology (Fig. 1A), which guided tissue segmentation, such as lumen-intima interface (Fig. 1B-D). Spatial variations in strain rate indicated changes in tissue biomechanics, red and blue corresponding to most compliant and stiffest regions, respectively (Fig. 1B). Strain rate images illustrated the existence of focally stiffer regions, marking both radial and lateral variation in tissue compliance. The spectroscopic PA image overlapping the ultrasound image showed the location of lipids (marked by yellow color in Fig. 1C-D). Using 3-D spectroscopic PA data the volume of the lipid pool were directly derived. The spectroscopic PA imaging results were confirmed by Oil Red O histology staining.

Discussion and Conclusions

The results of our study demonstrate that the proposed method is feasible, and integrated 3-D ultrasound, strain-rate and spectroscopic PA imaging provides localized and global detailed characterization of arterial morphology, biomechanics and composition.

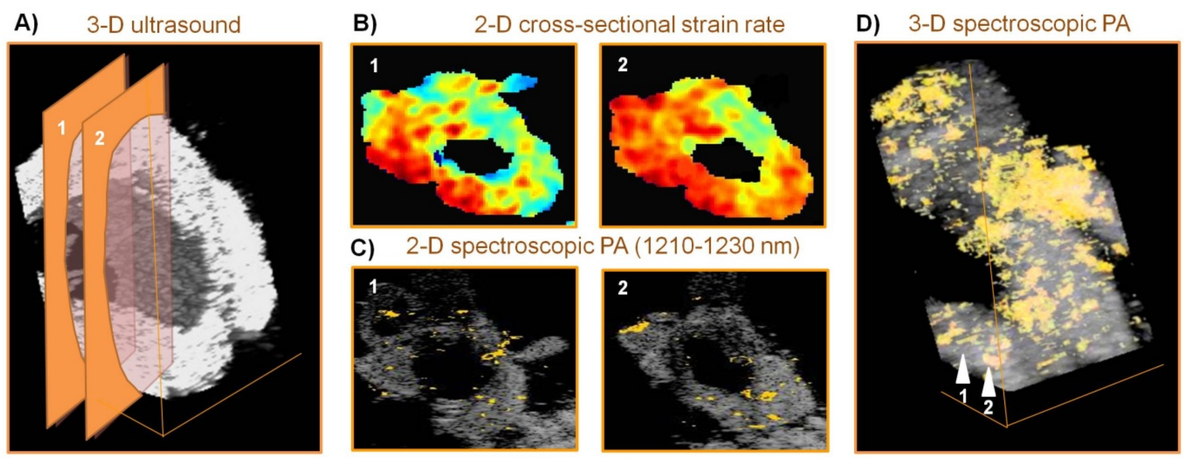

Fig. 1 *A) Ultrasound, B) strain rate and C) and D) spectroscopic photoacoustic (PA) imaging of an atherosclerotic artery using noninvasive imaging modalities covering a volume of 1.5 cm X 2 cm X 2 cm.*

3C-3

5:00 pm Photoacoustic microscopy with a pulsed multi-color source based on stimulated Raman scattering

Mengyang Liu[1], **Takashi Buma[1]**; [1]*University of Delaware, USA*

Background, Motivation and Objective

Photoacoustic microscopy (PAM) provides excellent image contrast based on optical absorption. A very common pulsed optical source is a frequency-doubled Q-switched Nd:YAG laser. However, the fixed 532 nm output is not suitable for spectroscopic PAM. We demonstrate a simple approach to increase the number of wavelengths by using stimulated Raman scattering (SRS) in an optical fiber. A sufficiently intense laser pulse nonlinearly interacts with the internal vibrations of the glass molecular structure to produce a series of down-shifted frequency components (Stokes lines). The number of spectral peaks depends on the fiber length, peak intensity, and polarization of the propagating laser pulse.

Statement of Contribution/Methods

Our Q-switched Nd:YAG microchip laser produces 0.6 ns duration pulses at 1064 nm with 10 uJ of energy at a 7.4 kHz repetition rate. A 10 mm long frequency-doubling KTP crystal produces 2 uJ pulses at 532 nm. After passing through a half-wave plate for polarization control, the laser pulses are coupled into a 6 meter long polarization-maintaining single-mode silica fiber. The multi-color fiber output goes through a band pass filter, where the selected wavelength is sent to a photoacoustic microscopy system employing optical focusing. Detection is performed with a 25 MHz spherically focused f/3 transducer.

Results

The attached figure shows the first three spectral peaks (532, 546, 560 nm) at the output of the multi-color fiber source. The individual pulse energy is over 100 nJ at each wavelength, which is sufficient for in vivo imaging. A scattering phantom consists of colored cotton fibers embedded in polydimethylsiloxane mixed with titanium dioxide. The attached figure shows the resulting PAM images of the red and blue fibers. Both images are shown over a 380 x 260 um region and a 20 dB dynamic range.

Discussion and Conclusions

A major advantage of our technique is the simple arrangement to convert a single-wavelength laser into a multi-color source for spectroscopic PAM. Large-mode area single-mode fiber can be used with higher energy lasers without fiber damage. The discrete number of Stokes lines does not allow arbitrary wavelength selection, but the wavelength spacing is sufficiently close for practical applications (e.g. oxygenation measurements). We believe this multi-color technique can significantly benefit spectroscopic photoacoustic microscopy.

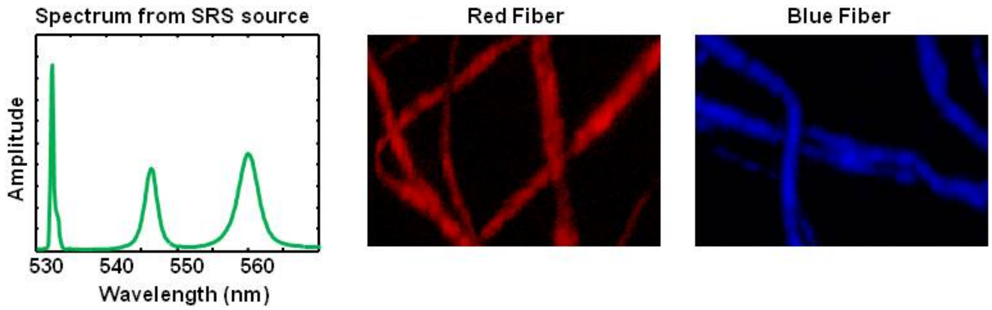

3C-4

5:15 pm Optoacoustic signal amplitude and frequency spectrum analysis laser heated bovine liver ex vivo

Michelle P. Patterson[1,2], Christopher B. Riley[3], Michael C. Kolios[4], William M. Whelan[5]; [1]physics, university of prince edward island, charlottetown, pei, Canada, [2]Biomedical Sciences, university of prince edward island, charlottetown, pei, Canada, [3]Animal and Veterinary Sciences, Adelaide university, Australia, [4]Ryerson University, Canada, [5]university of prince edward island, Canada

Background, Motivation and Objective

Current imaging methods for monitoring thermal therapy suffer from poor image contrast and resolution. Our current research aims to investigate the sensitivity of optoacoustic (OA) signals to heat-induced tissue changes that occur during laser thermal therapy (LTT).

Statement of Contribution/Methods

OA signals were acquired from 20 ex vivo bovine liver samples using a reverse-mode OA imaging system consisting of a pulsed laser operating at 775 nm, and an 8 element annular array transducer (SENO Imagio, San Antonio, TX). LTT was performed using an 810 nm laser at 4 W for five minutes. OA signals were acquired at 0.5 s intervals for two minutes prior to, five minutes during, and seven minutes post treatment .

Treatment induced effects were identified based on the OA signal amplitude in combination with spectral analysis of the OA RF-data. The amplitude of the signal is largely affected by the optical absorption of the target while its spectral components may be related to the physical properties of the absorbing targets, in a similar manner to ultrasound spectral analysis. Since RF data are collected in OA imaging experiments, we hypothesize that the signs and spatial distribution of the absorbing structures contributes to the frequency content of the signal.

Peak to peak and time-window integrated OA signals were determined and used as metrics for comparison with measured tissue temperatures. Spectrum analysis commonly performed on ultrasound backscatter RF data, which identify the spectral midband fit, slope, and intercept of the data was utilized (Lizzi, 1986).

Results

The OA amplitude Peak-Peak and integrated signals increase with increasing temperature by approximately 150% (see Fig. 1a), and remain at elevated values post heating, indicating a permanent tissue change. The spectral midband fit and intercept values increased by approximately 150% and 400% respectively during heating, and continued to increase up to 200% and 500% respectively, post-heating (see Fig 1b). The spectral slope did not show any significant changes.

Discussion and Conclusions

The results of this study support our hypothesis that LTT causes detectable changes in the amplitude and frequency components of detected OA signals. Both of these analytical techniques may provide independent information about the tissue state during and post heating. These results demonstrate the potential of OA monitoring of LTT.

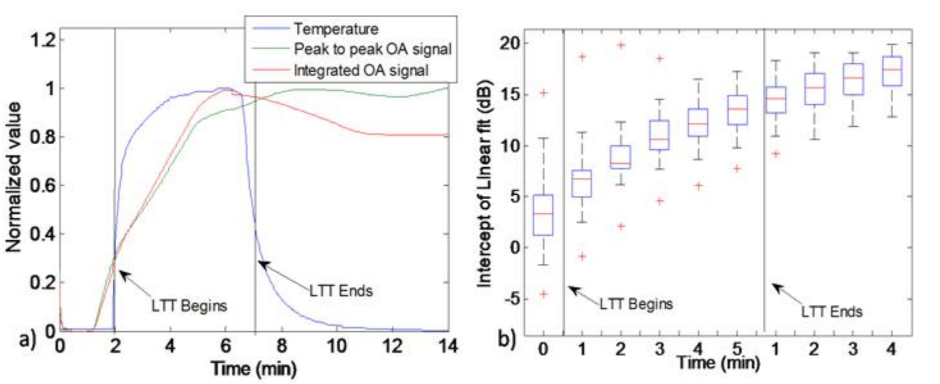

Figure 1: (a) Normalized peak to peak and time window integrated optoacoustic (OA) signals and relative temperature change, and (b) boxplot of the spectral intercept of the OA RF data acquired from 20 liver samples prior to, during and post laser heating performed by an 810 nm laser at 4 W for 5 minutes.

3C-5

5:30 pm Clinical feasibility of duplex photoacoustic and ultrasound pulse-echo imaging using photoacoustic transmit pulses

Michael Jaeger[1,2], David David Birtill[1], Andreas Gertsch[1], Elizabeth O'Flynn[2,3], **Jeffrey Bamber[1,2]**; [1]Joint Department of Physics, Institute of Cancer Research and Royal Marsden NHS Foundation Trust, Sutton, Surrey, United Kingdom, [2]CRUK-EPSRC Cancer Imaging Centre, Institute of Cancer Research and Royal Marsden NHS Foundation Trust, Sutton, Surrey, United Kingdom, [3]Radiology Department, Royal Marsden NHS Foundation Trust, Sutton, Surrey, United Kingdom

Background, Motivation and Objective

Photoacoustic (PA) imaging is an emerging imaging modality offering promise for cancer diagnosis, therapy planning, and monitoring response. The images show optically absorbing tissue structures based on detection of ultrasound signals after laser irradiation. For clinical use, PA imaging is best implemented with freehand pulse-echo scanning in a single device, so that PA signals may be displayed in real-time within the anatomical context. For this purpose, PA frames must be interleaved with pulse-echo frames. This is normally not feasible with commercially available ultrasound imaging systems. For clinical research purposes therefore, we developed a novel approach where both PA and pulse-echo images are generated photoacoustically. Our objective was to evaluate the feasibility of clinical imaging with this technique.

Statement of Contribution/Methods

Combined PA imaging and PA-transmit echography was implemented on a commercial US scanner (Z.one™ Zonare, Mountain View) and a Q-switched Nd:YAG laser at 1064 nm wavelength and 10 Hz pulse rate. In this system, each laser pulse results in a data frame from which both a PA and a PA-echo image is reconstructed; PA signals are generated directly from optically absorbing tissue structures, whereas a transmit pulse for echography is generated by a black absorbing film placed inside an acoustic stand-off that also permits temporal separation of the two types of information. Preliminary clinical evaluations were carried out by scanning the necks and forearms of volunteers, and breast tumours of several consenting patients.

Results

Echograms generated with a PA transmit pulse were of poorer resolution and were noisier than those obtained using a focused transmit pulse. Nevertheless, they corresponded well to conventional pulse-echo images, making them a valuable surrogate and permitting registration of PA images with high quality echograms and colour Doppler images. Strong PA signals were obtained from the skin and various tissue structures to depths of 2-3 cm. Although some of the PA signals corresponded to vasculature as expected, demonstrating vascular pulsations in real time, they frequently did not correspond with obvious colour Doppler signals. There was also strong evidence of PA-clutter in the images.

Discussion and Conclusions

Duplex reflection-mode photoacoustic and ultrasound pulse-echo real-time scanning is currently feasible using photoacoustically-generated transmit pulses. Preliminary results demonstrate the need for further clinical and preclinical evaluation to improve understanding of the origin and significance of the PA signals. Further work is also desirable to develop successful clutter-reduction strategies, since PA clutter appears to limit clinical image quality, particularly at large depths.

3C-6

5:45 pm Intravascular photoacoustic imaging in the presence of luminal blood

Bo Wang[1], Andrei Karpiouk[1], Jimmy Su[1], James Amirian[2], Richard Smalling[2], Stanislav Emelianov[1]; *[1]University of Texas at Austin, USA, [2]University of Texas Health Science Center at Houston, USA*

Background, Motivation and Objective

Detection of the composition of atherosclerotic plaque is critical for the guidance of treatment of atherosclerosis and understanding the disease progression. Intravascular photoacoustic (IVPA) imaging has shown great potential in the characterization of plaque composition based on the optical absorption contrast found in different tissue types. However, clinical application of IVPA is limited by the lack of an integrated catheter for combined IVPA and intravascular ultrasound (IVUS) imaging, and challenged by the optical attenuation of luminal blood. In this study, we demonstrated that coronary stents and lipid deposits inside diseased rabbit aortas can be imaged in vivo in the presence of luminal blood.

Statement of Contribution/Methods

Two excised aorta samples from atherosclerotic rabbits were imaged ex vivo using an integrated IVPA/IVUS imaging catheter. One aorta sample had human coronary stent deployed inside the vessel lumen. The other sample had lipid rich plaques. An integrated catheter composed of a side-fire optical fiber and a 40 MHz conventional IVUS imaging catheter was used to perform combined IVUS/IVPA imaging. The laser beam and electric signals were coupled to the integrated catheter using a custom designed rotation system. During imaging, the aorta samples were immersed inside whole blood. The integrated catheter was inserted inside the lumen of the aorta with a 6F catheter introducer. The coronary stent was imaged using an Nd:YAG laser operating at 1064 nm wavelength. Lipid deposits were imaged using an Nd:YAG pumped OPO laser system operating at 1720 nm wavelength, at which the optical absorption of lipid is stronger than water based tissue.

Results

Combined IVUS and IVPA images showed that both stents and lipids can be successfully imaged in the presence of luminal blood.

Discussion and Conclusions

IVPA imaging in the near infrared range significantly reduced the optical attenuation of light, therefore allowing imaging of stents and lipids in the presence of luminal blood. IVPA was performed in the presence of luminal blood without a flush, which is required in most optical based imaging modalities. The results show that IVPA imaging of atherosclerosis can easily be applied in vivo.

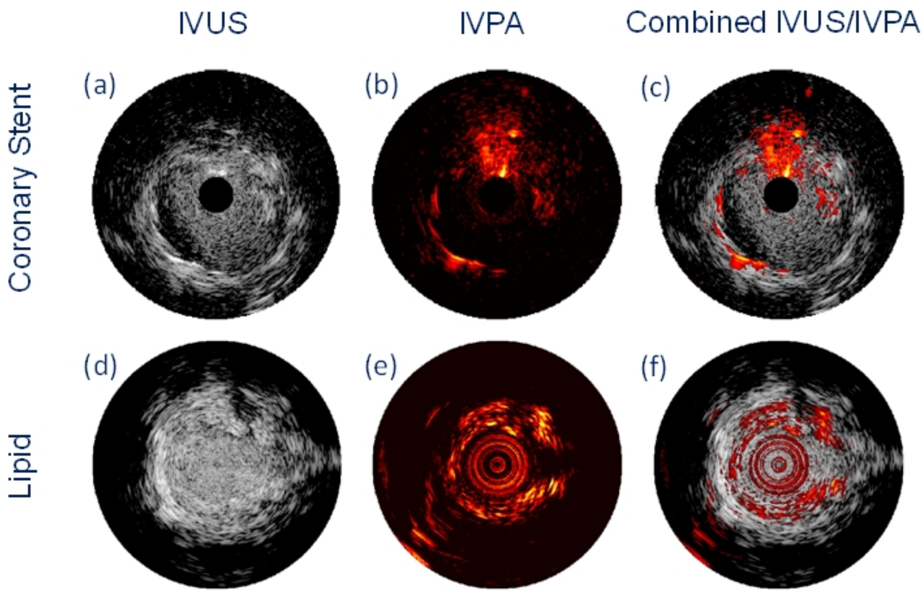

IVUS, IVPA and combined IVUS/IVPA images of coronary stent deployed inside a vessel lumen (a-c), and lipid deposits in a atherosclerotic rabbit aorta (d-f). Images were acquired in the presence of luminal blood.

4C - Bulk Wave Effects and Devices I

Carribean Ballroom I

Wednesday, October 19, 2011, 4:30 pm - 6:00 pm

Chair: **Jan Brown**
JB Consulting

4C-1

4:30 pm Measurement of Dispersion Properties of Active and Surrounding Regions in BAW Resonator

Kimmo Kokkonen[1], Johanna Meltaus[2], Tuomas Pensala[2], Matti Kaivola[1]; [1]Aalto University, Finland, [2]VTT Technical Research Centre of Finland, Finland

Background, Motivation and Objective

In solidly mounted bulk acoustic wave (BAW) resonators and devices, engineering of correct plate-wave dispersion is central to successful device operation. It is therefore of interest to be able to experimentally measure and to verify the dispersion properties of manufactured devices. Furthermore, it would be advantageous to be able to measure the dispersion properties of not only the active, electroded resonator area, but also of other areas of the device, such as the surroundings of the resonator. The characterization of the different acoustic regions is of particular importance in the case of laterally coupled BAW devices.

In this work, we demonstrate laser-interferometric measurements of the plate-wave dispersion properties of a BAW resonator within the active resonator region as well as the sourceless outside region. These two dispersion diagrams are then used to accurately determine the energy trapping frequency range.

Statement of Contribution/Methods

Heterodyne laser interferometer is used to image wave fields excited in a 1.8 GHz BAW resonator. The wave field data is used to calculate the dispersion properties of the resonator and of its surrounding (outside) area via Fourier transform, utilizing appropriate windowing of the measurement data. The dispersion properties are compared to simulated behaviour.

Results

It is demonstrated that, in addition to the resonator area, the dispersion properties of the sourceless outside area can be extracted from measurements, see Fig. 1. The two dispersion diagrams (active area presented with colors and the outside area with shades of gray and a dotted line) allow to directly experimentally determine the lateral energy trapping frequency range of the resonator. This can be seen in our resonator also as a sudden diminishing of the TE1 lateral standing waves and as activation of the outside region.

Discussion and Conclusions

The presented method allows to determine the dispersion properties of the sourceless regions of a BAW resonator by utilizing the acoustic wave leakage from the active area of the resonator. The method can be used to gain further insight into the device physics and to provide feedback in component design. The method demonstrated here is believed to be especially useful in the research and development of laterally coupled BAW resonator filters.

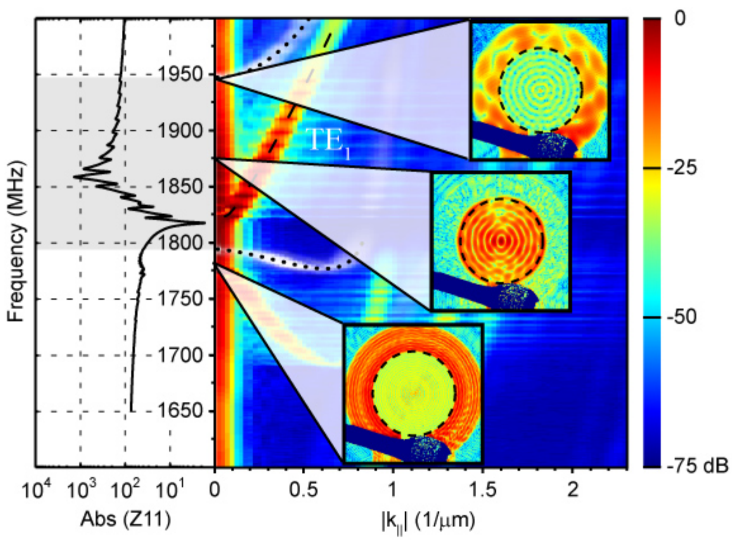

4C-2

4:45 pm Polarizaion-inverted multilayered pure shear mode AlN film resonator

Masashi Suzuki[1], Takahiko Yanagitani[1]; [1]Graduate School of Engineering, Nagoya Institute of Technology, Nagoya, Aichi, Japan

Background, Motivation and Objective

c-axis parallel AlN film is suitable for pure shear mode film acoustic resonators. Polarizaion-inverted multi-layer structure can excite high-overtone mode resonance. This multilayer resonator is expected to have high power handling capability, and if this structure is used to the NDE transducer, electrode area and conversion efficiency can be improved. In this study, we investigated the k15 value of c-axis parallel oriented AlN films. In addition, polarizaion-inverted multi-layered resonator consisting of c-axis parallel AlN films is fabricated.

Statement of Contribution/Methods

Single-layered c-axis parallel AlN film HBARs and polarizaion-inverted four-layered c-axis parallel AlN films HBARs were prepared on silica glass substrate by ion beam assisted deposition. Polarization direction of the layers was alternately inverted by inverting the ion beam irradiation direction. Characteristics of suppression of thickness extensional mode, k15 estimation and high-overtone resonance of the resonator samples were investigated by using an impulse response and a conversion loss of the resonator.

Results

As shown in Fig. 1, single-layered film exited only pure shear wave without any longitudinal wave. k15 of the film was determined to be 0.05 by comparing experimental curve with the curve simulated by Mason's equivalent circuit model as shown in Fig. 2 (a). This k15 value is 63 % of the values expected in AlN single crystal. As shown in Fig. 2(b), we can confirm fourth order mode excitation at 1.9 GHz in the shear wave conversion loss of the multilayered resonator shown in Fig. 2 (b).

Discussion and Conclusions

c-axis parallel AlN film excited pure shear wave without any extensional mode. High order mode excitation was demonstrated in polarizaion-inverted multilayered c-axis parallel AlN film.

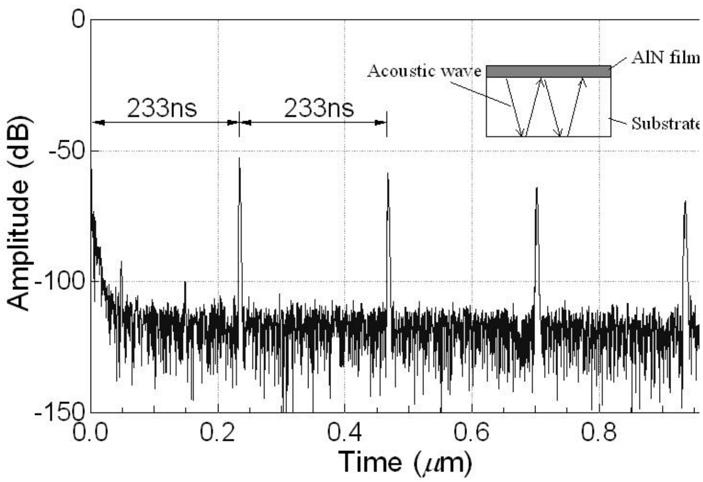

Fig. 1 The impulse response of single-layered film

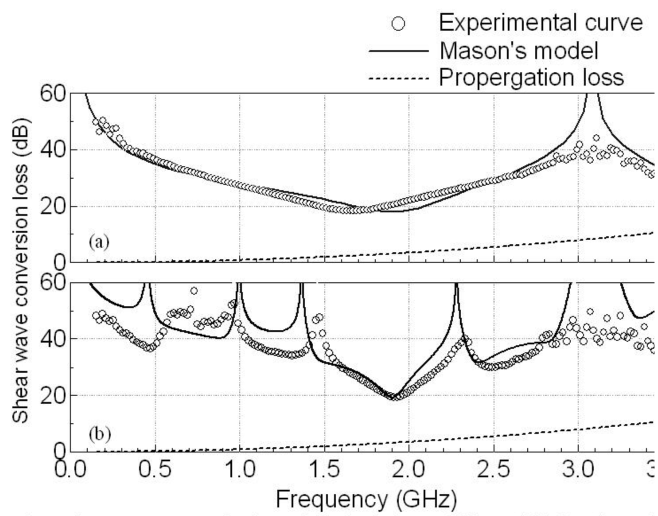

Fig.2 Shear wave conversion loss of (a) single-layered film and (b) four-layered

4C-3

5:00 pm High temperature piezoelectricity in Mn doped ZnO film

Kosuke Imamura[1], Shinji Takayanagi[1], Takahiko Yanagitani[2], Mami Matsukawa[1], Yoshiaki Watanabe[1]; [1]*Doshisha University, Japan,* [2]*Nagoya Institute of Technology, Japan*

Background, Motivation and Objective

New piezoelectric film is required for transducer and sensors operating in high temperature (HT) because piezoelectricity in most of the ferroelectric films deteriorates above 300 ºC. AlN or ScAlN [1] is good candidate for HT piezoelectric film, however, low piezoelectricity or rare Sc metal may be a problem. On the other hand, ZnO has no phase transition point up to melting point, but piezoelectricity deteriorate at HT probably due the increase of carrier concentration.

Statement of Contribution/Methods

Mn doping, which acts as accepter, is one of the way to compensate n-type donor. In this study, piezoelectricity of Mn doped ZnO film in HT were investigated. ZnMnO films were fabricated on Ni/silica glass substrate by using an RF sputtering with ZnO and MnO_2 composite powder target. Resistivities of the films were measured using ohmic liquid Ga alloy electrode to avoid contact resistance.

Results

Figure 1 shows the temperature dependence of resistivity of the pure ZnO film and 5 wt % MnO_2 doped ZnO. We can confirm that resistivity of the film significantly increased by Mn doping. XRD rocking curves showed that Mn doping does not much affect the crystalline orientation. Figure 2 shows temperature dependence of the k15 value in the c-axis parallel oriented 4 wt % MnO_2 doped ZnO film. k15 values of the film were determined by a conversion loss of the HBAR structure [1]. Also plotted is k15 value of the c-axis tilted pure ZnO films for a comparison.

Discussion and Conclusions

k15 value start to decrease at 300 ºC in the pure ZnO film, whereas such a significant decrease of k15 value was not observed in the ZnMnO film. k15 value and crystalline orientation are little affected by Mn doping, therefore, ZnMnO film is promising for HT piezoelectric film.

[1] T. Yanagitani, et al., Proc. 2010 IUS

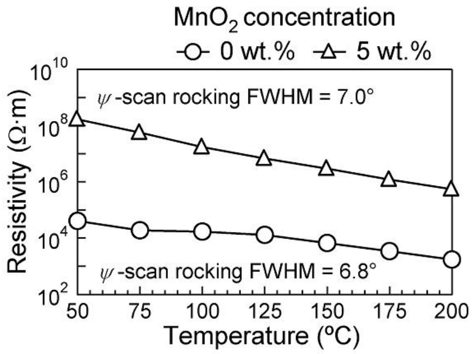

Fig.1 Temperature dependence of resistivity of the ZnO film with 0 and 5 wt% MnO_2 doping.

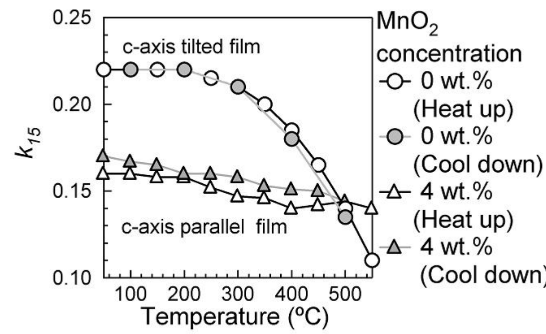

Fig.2 Temperature dependence of k_{15} value of the pure c-axis tilted ZnO film and 4 wt% Mn doped c-axis parallel film.

4C-4

5:15 pm Force-Frequency Effect on the Q-Factor of Thickness-Shear Mode Quartz and Langasite Resonators at High Temperatures

Mihir Patel[1], Bikash Sinha[1]; [1]Schlumberger-Doll Research, Cambridge, MA, USA

Background, Motivation and Objective

There has been a growing interest in langasite (LGS) and its isomorphs owing to their extremely high quality (Q) factors. Q value of LGS that is at least twice that of quartz has been reported. High Q makes LGS an excellent candidate for a stable frequency source operating at temperatures as high as 300 deg C for oil, gas, and geothermal applications. These applications require high resolution frequency measurements on the order of 1 ppm during drilling of deep wellbores. The objective of this paper is to calculate the force-frequency effect for different rotated quartz cuts and LGS at high temperatures. In addition, we calculate the effects of isotropic stresses in the resonator plane on the Q-factor at 25 and 300 deg C.

Statement of Contribution/Methods

A theoretical study was conducted for a 90um thick circular resonator to calculate the force-frequency effect and temperature effect on the slow (C-) and fast (B-) thickness-shear mode for the SC-cut, SBTC-cut, rotated X-cut, and YX-LGS using the 3-D Lagrangian finite-element model (FEM), and Sinha-Tiersten perturbation method. Based on the frequency spectrum analysis, the best aspect ratio for each cut angle was investigated for the force-frequency effect at 25 and 300 deg C. The Q-factor calculations are based on the intrinsic viscosity of crystalline quartz and LGS. The assumption that the effect of intrinsic viscosity on thermal strains is negligible helps to calculate the intrinsic Q-factor as a function of force and temperature.

Results

We report the calculated force-frequency coefficients K_f ($\times10^{-15}$ m.s/N) as a function of the azimuthal angle, which is the angle between the crystalline x-axis of a resonator plate, and the direction of in-plane forces applied to the periphery of the resonator. At room temperature the C-mode for the SC-cut and the B-mode for the SBTC-cut exhibit zero mean K_f value, whereas at 300 deg C they, respectively, exhibit mean K_f values of 1.2 and 1.36. The C-mode for the YX-LGS exhibits mean K_f value of 0.71 and 1.4, respectively, at 25 and 300 deg C. Among the quartz orientations analyzed in this work, the SBTC-cut exhibits highest Q×Freq = 1.64×10^{13} and 1.59×10^{13}, respectively, at 25 and 300 deg C. Interestingly, the YX-LGS has a Q×Freq = 4.48×10^{13}, at 25 deg C, which is about 2.7 times larger than that of the SBTC-cut. Frequency shifts resulting from temperature for the C-mode of the SC-cut and YX-LGS is 0.97 and -32 ppm/deg C, respectively.

Discussion and Conclusions

Results obtained from the FEM and Sinha-Tiersten perturbation method show an excellent agreement of the mean K_f value with the available measured data, and has been used to investigate the force-frequency effect on rotated quartz cuts and LGS for possible applications at high temperatures. Calculated results show YX-LGS and SC-cut as ideal candidates for a stable frequency source operating at temperature as high as 300 deg C.

4C-5

5:30 pm Drive Level Dependency in Langasite Resonators

Yook-Kong Yong[1]; [1]Civil and Environmental Engineering, Rutgers University, Piscataway, NJ, USA

Background, Motivation and Objective

New langasite resonators have a very high Q and ultra stable resonant frequency. However, due to small material nonlinearities in the langasite crystal, the resonator is drive level dependent, that is, the resonator level of activity and its frequency are dependent on the driving, or excitation voltage. Small or miniaturized resonators are in general more drive level dependent than their larger counterparts. The objective of this paper is to study the relationship between the drive level dependency of a fundamental thickness shear langasite resonator and (a) its crystal cut angles, (b) the size of the resonator. The size of these resonators will be reduced to one fourth of their current sizes in the next few years, but the electrical power which is applied will not be reduced as much. Hence, the applied power to resonator size ratio will be larger, and the drive level dependency may play a role in the resonator designs.

Statement of Contribution/Methods

We study this phenomenon using the Lagrangian nonlinear stress equations of motion and Piola-Kirchhoff stress tensor of the second kind. The material constants such as the second and third order elastic constants, dielectric and piezoelectric constants are obtained from published works and employed in programs to yield material properties for singly and doubly rotated cut angles of langasite. Solutions are obtained for the fundamental thickness shear mode using COMSOL for both the singly rotated and doubly rotated cuts of langasite. The phenomenon of the drive level dependence is discussed in terms of the voltage drive, electric field, power density and current density.

Results

It is found that the drive level dependency is best described in terms of the power density. Some results are compared with experimental results on drive level dependency in langasite resonators. Drive level dependency of different sizes resonators, cut angles of langasite are presented.

Discussion and Conclusions

1) The drive level dependence of the resonant frequency of langasite resonators is caused mainly by the nonlinear third order elastic constants.

2) The results obtained from the finite element models for predicting the drive level dependency could be compared to experimental data.

3) Results for different resonator sizes and crystal cut angles are presented. For a given frequency of the fundamental thickness shear mode, there are cut angles for reduced drive level dependency. The effect of resonator size was also presented.

4C-6

5:45 pm The Nonlinear Thickness-shear Vibrations of a Crystal Plate Under a Strong Electric Field

Ji Wang[1], Rongxing Wu[1], Jianke Du[1], Dejin Huang[1], Wei Yan[2]; [1]School of Mech Eng & Mechanics, Ningbo University, Ningbo, Zhejiang, China, People's Republic of, [2]School of Civil & Arch Eng, Ningbo University, Ningbo, Zhejiang, China, People's Republic of

Background, Motivation and Objective

The linear plate theories for vibrations of crystal resonator have been successfully developed by Mindlin, Tiersten and Lee et al and yielded many useful results. Our earlier studies shown neither kinematic nor material nonlinearities are the main factor of frequency shifts and performance fluctuation of quartz crystal resonator. Naturally, we studied nonlinear thickness-shear vibrations of a quartz crystal plate driving by a high electrical voltage and obtained electrical current amplitude-frequency behavior near resonance.

Statement of Contribution/Methods

With the consideration of material and kinematic nonlinearities, a nonlinear system of two-dimensional equations for the coupled thickness-shear and flexural vibrations of piezoelectric plates is established. The nonlinear equation of thickness-shear vibrations in a strong electric field have been solved by combination of Galerkin approximation and successive approximation method.

Results

By successive approximation method, we can obtain nth-order electrical current amplitude-frequency relation. The first-order electrical current amplitude-frequency relation is accurate enough to give some nonlinear characteristics of thickness-shear vibration of quartz crystal plate.

Discussion and Conclusions

The curves of nonlinear amplitude-frequency behavior with different electrical voltages in Fig. 1 are parabolas which are similar with results from three-dimensional equations. Fig. 2 shows that nonlinear frequency of thickness-shear vibrations not only depends on thickness and length of plates but also related to amplitude ratios between thickness-shear and flexural vibrations. The electrical field has a strong effect on nonlinear frequency compared with other factors.

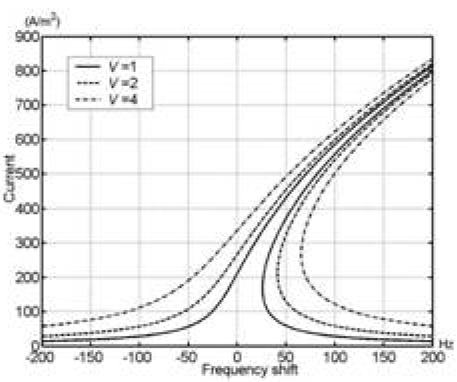

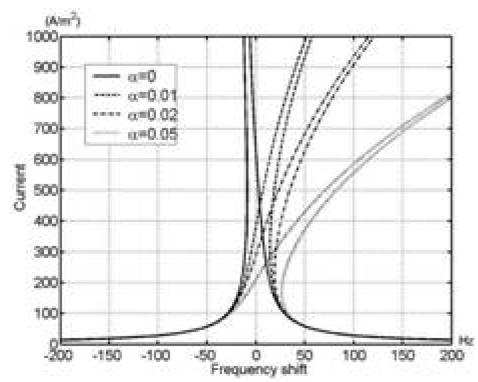

5C - Transverse Modes in SAW (6F)

Carribean Ballroom II

Wednesday, October 19, 2011, 4:30 pm - 6:00 pm

Chair: **Karl Wagner**
TDK-EPC

5C-1

4:30 pm A method to reduce losses in buried electrodes RF SAW resonators

Marc Solal[1], Julien Gratier[2], Kevin Gamble[1], Ben Abbott[1], Taeho Kook[1], Alan Chen[1], Kurt Steiner[1]; [1]*TriQuint Semiconductor, Apopka, FL, USA,* [2]*TriQuint Semiconductor, Chelmsford, MA, USA*

Background, Motivation and Objective

Temperature sensitivity is a major criterion when choosing the substrate for a SAW filter. It is known that a better coupling factor /temperature sensitivity trade off can be obtained by burying the electrodes inside a SiO2 overlay. On lithium niobate substrates, velocities are larger inside the resonator than outside resulting in losses by energy leakage in the busbars .

In practical devices, the electrode end gaps play an important role since they constitute a very fast region and reflect the acoustic waves creating multiple transverse modes. Usually, gap sizes are small and some energy is still leaking by tunneling effect. For apodized transducers, the transverse modes frequencies and shapes vary along the transducer cancelling their effect on the response, but also increasing the losses.

Statement of Contribution/Methods

Guiding conditions need to be created in SAW resonators to obtain good quality factors. It can be done by using large enough gaps sizes. Unfortunately, this leads to even stronger transverse modes. The proposed solution consists in tailoring the shape of the main mode. A “piston mode” shape is obtained by adding a slow region at the edge of the active region. The mode shape is matched to the rectangular excitation and the coupling to the higher order modes becomes negligible.

Results

This method is described and experimentally demonstrated for various devices. Results exhibit low spurious, lower losses and better effective coupling coefficients than apodized devices. Quality factors in the 1500 range are measured on resonators while CRF losses are significantly reduced.

Discussion and Conclusions

By creating guiding conditions and adding a slow region it is possible to both reduce the loss and suppress the transverses modes spurii.

5C-2

5:00 pm Extension of Scalar Potential Formalism for Transverse Mode Analysis of Surface Acoustic Wave Resonators

Ken-ya Hashimoto[1], Tatsuya Omori[1], Chang-Jun Ahn[1]; [1]Graduate School of Engineering, Chiba University, Chiba, Japan

Background, Motivation and Objective

For the realization of high Q SAW resonators, SAWs must be confined well within the device structure toward not only the longitudinal but also transverse directions.

For the analysis of in-plane SAW propagation, the scalar potential (SP) theory has been used, and its effectiveness is well recognized in the SAW community. On the other hand, the coupling-of-modes (COM) theory and the p matrix model are widely used for the one-dimensional (1D) analysis and design of SAW resonators. Several approaches were reported to combine them for the in-plane two-dimensional (2D) and design of SAW resonators. They are intended to use for numerical simulation, and are not feasible for fundamental understandings of SAW properties.

Statement of Contribution/Methods

This paper describes extension of the SP theory using the 2D wave equation for a shear-vertical bulk wave. The equation is fully compatible to the traditional SP theory when variation of acoustic properties is expressed as that of the mass density while the elastic properties are uniform in the structure. When periodic variation of the mass density and stress sources is taken into account, the theory is equivalent to the COM model. Because of the compatibility, primary parameters necessary for the analysis are readily derived from those determined by the SP and COM theories.

Results

The theory is applied to an SH-type SAW resonator on the 15°YX-$LiNbO_3$ substrate. The Cu electrode thickness is assumed to be 8.2λ. Fig. 1 shows the calculated input admittance Y of an infinitely long IDT. Series of transverse resonances are seen at frequencies higher than the main one. Longitudinal resonances are not seen in this case because of the infinite IDT length. The figure also shows Y of a resonator on the substrate. The calculation agrees well with the simulation except longitudinal resonances appearing at frequencies lower than the main one. Small discrepancy is seen in the location and height of the transverse modes. This may be due to variation of the SAW dispersion characteristic in the device structure, which is not taken into account in the present analysis.

Discussion and Conclusions

Since the present theory starts from an ultimately simplified physical model, we can readily apply various well-established calculation techniques. For example, the theory can be used for the 2D FEM analysis of SAW resonators.

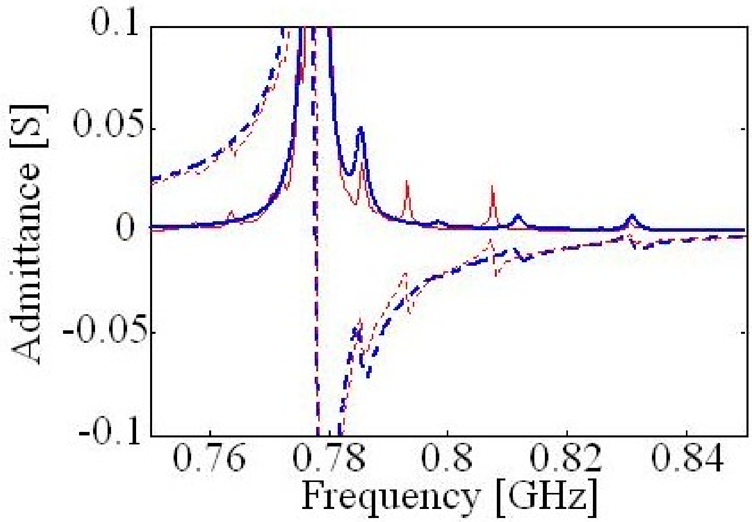

5C-3

5:15 pm Transversal mode orthogonality in SAW waveguides with transversally varying slowness anisotropy within the scalar field approximation

Markus Mayer[1], Thomas Ebner[1], Karl Wagner[1], Ken-Ya Hashimoto[2]; [1]SAW RD, TDK-EPC, Munich, Germany, [2]Department of Electrical and Electronic Engineering, Chiba University, Chiba, Japan

Background, Motivation and Objective

The scalar field approximation is widely employed to describe diffraction and waveguiding in SAW devices. The basic assumption is that the actual vector field of transversal modes can be reduced to a scalar field, like that of a mechanical wave polarized vertically to the surface. Within the 2D P-matrix model the scalar field is identified with a power wave. As has been demonstrated recently, orthogonality of the transversal modes implies power conservation in the 2D P-matrix model [Mayer et al., IUS 2008]. Assuming continuity of the transversal mode profile and its derivative, however, orthogonality is only obtained if the slowness anisotropy is parabolic and constant within the waveguide.

Whereas for standard Rayleigh wave devices on quartz it had been a good approximation to assume a constant slowness in a waveguide, on other substrates slownesses in metalized, unmetalized or partially metalized areas may differ significantly. To account for the resulting anisotropy differences in an orthogonal mode description therefore is crucial for an accurate prediction.

Statement of Contribution/Methods

Orthogonality conditions for transversal modes within the parabolic approximation of slowness are derived for the case of transversally varying anisotropy constants. Thereto the transversal wave equations are identified with the elastic wave equations of a vertically polarized wave. Continuity of the displacement and the stress field at boundaries of transversal sections is required and therefrom orthogonality conditions of the modes are derived. Translating these conditions to the 2D P-matrix model implies discontinuity of the power waves at transversal section interfaces.

Results

The method was implemented into the 2D P-matrix method. The resulting modes are shown to be orthogonal within the parabolic approximation. Energy conservation in the 2D P-matrix framework is achieved.

Discussion and Conclusions

For transversally varying anisotropy of the slowness an orthogonal mode description, fulfilling energy conservation within the 2D P-matrix model, was achieved. The resulting power wave profiles of the modes are discontinuous at boundaries of transversal sections.

5C-4

5:30 pm Miniaturized SAW Designs using High Aspect Ratio Electrodes

Hoi Yan Fong[1], Akifumi Kamijima[2], **Stephane Chamaly[1];** [1]EPCOS Pte Ltd - TDK Corporation, Singapore, Singapore, [2]TDK Corporation, Hong Kong, Hong Kong

Background, Motivation and Objective

The aim of this work is to miniaturize SAW filters using massive high aspect ratio metallic electrodes. These structures are capable of slowing down the surface wave and reduce the wavelength by 10 times. It is therefore expected that the size of devices using such high metal thickness is reduced by a significant amount. In this work, the relationship of the SAW propagation properties to substrate orientation and metallization thickness is studied theoretically using FEM-BIM approach and experimentally in order to achieve designs of a filter demonstrating a size miniaturization by a factor of 2 and a very low loss 20% bandwidth filters both at 40MHz range.

Statement of Contribution/Methods

We have computed the phase and group velocities of varying height/lambda ratios [H/L] and verified with measurements. Investigations on the coupling coefficients using various cuts of Lithium Niobate crystals with a span of H/L have also been made by FEM-BIM periodic software. Optimum working point is chosen to achieve the required filter performances.

Using these parameters, filters have been designed and manufactured. The first filter is using an innovative Transversal Dispersive technique coping with the high dispersiveness of the wave propagation. The second filter is using balanced bridge architecture to obtain very low losses.

Comparison between measurement and simulation using finite FEM-BIM software is performed.

This is first time ever that miniature SAW filters using high aspect ratio electrode are reported.

Results

Theoretical and measurement studies showed that a phase velocity of 2000m/s and group velocity of 590m/s were obtainable with H/L of 25% on Lithium Niobate.

A low loss design 20% bandwidth filter at 36MHz requires a 22% coupling coefficient. This is achievable by using the shear mode on a LN Y cut X propagation substrate with up to 20% H/L.

The results have been demonstrated on LN Y+15 cut with metal thickness of 10um. The active size of the Transversal Dispersive filter is 2.1mm x 0.7mm as compared to a 9.7mm x 0.7mm of a con-ventional TV filter. Furthermore, comparing a transversal filter with identical selectivity, the active size is reduced by more than a factor of 2.

In addition, based on the same metal thickness and substrate, a balanced bridge filter having 13MHz bandwidth at 38MHz center frequency has been designed. The active size of the filter is 3.2mm x 2.5mm. The designs were made using a combined FEM and BEM method.

Discussion and Conclusions

With the selected 20% of H/L metal thickness, it is possible to reduce the die size of a transversal filter with the same selectivity by more than two times. The balanced-bridge filter design is also at the same order of magnitude. Using the information gathered from this work, we can work out the relative metal thickness H/L required for higher center frequencies. It is believed that this work would be a good foundation upon which the same concepts of miniaturization can be used in high frequencies devices.

5C-5

5:45 pm Design of SAW/BAW Ladder type filters with constant group delay

hualei wang[1,2], Jing Chen[1], Yu Shi[2], Tatsuya Omori[1], Changjun Ahn[1], Ken-ya Hashimoto[1]; [1]Chiba University, Japan, [2]University of Electronic Science and Technology of China, China, People's Republic of

Background, Motivation and Objective

Usually RF SAW/BAW filters are designed so as to offer low insertion loss, flat passband, and good out-of-band rejection. Suppression of group delay variation may be also required within the passband for future high speed telecommunications. Here one question arises. How well can we control the group delay as well as the amplitude characteristic of the filters employing the SAW/BAW resonators?

Statement of Contribution/Methods

This paper discusses design of the Bessel-type RF SAW/BAW resonator filter, which gives priority to flatness of the group delay in the passband rather than that of the amplitude. The ladder-type architecture is employed. The design procedure is as follows: (1) the low-pass LC filter is designed for a specific bandwidth, and is converted to the band-pass one, (2) LC resonators are replaced by the SAW/BAW resonators with small capacitance ratio γ, (3) the optimization is applied to recover group delay flatness, which is deteriorated by finite γ of SAW/BAW resonators, and (4) Norton's first transformation is applied to reduce difference among the static capacitances of SAW/BAW resonators.

Results

Fig. 1 shows a typical transmission characteristic of the Bessel-type SAW filter designed by the proposed procedure. It is composed of five resonators and four capacitors, and employs the Cu-grating/15^{o}YX-$LiNbO_3$ structure, which possesses extremely large K^2 close to 30% for the SH-type SAW. With the simulated annealing optimization, the group delay deviation can be reduced to 4 ns over the frequency range of ±20 MHz at the center frequency of 1GHz. It should be noted that the bandwidth giving the flat group delay is inherently limited by γ, and use of resonators with larger γ causes larger ripples in the group delay. The round passband edges are unavoidable when the group delay flatness is required from the passband center to the edges.

Discussion and Conclusions

We presented design procedure of the Bessel-type SAW/BAW filters with flat group delay. This design can be applicable to various specifications, for example, flat group delay only in the passband. We will also show the experimental verification at the conference.

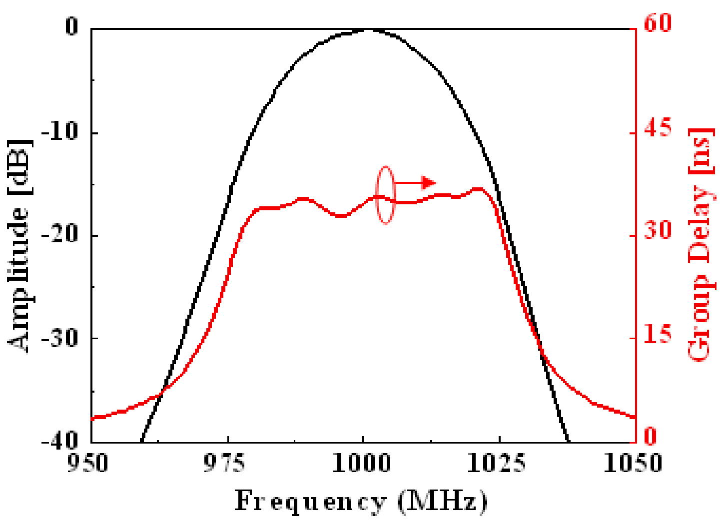

6C - Transducer Modeling

Carribean Ballroom VI

Wednesday, October 19, 2011, 4:30 pm - 6:00 pm

Chair: **Paul Reynolds**
Weidlinger Associates Inc

6C-1

4:30 pm Simulating Quartz Resonators at High Temperature and Pressure: Limitations Regarding Lack of Experimental Data for Temperature Derivatives of Third-Order Elastic Coefficients

Austin D. Beerwinkle[1], Raman P. Singh[1], Goutham R. Kirikera[2]; [1]Mechanical and Aerospace Engineering, Oklahoma State University, Tulsa, OK, USA, [2]Geophysical Research Company, LLC, Tulsa, OK, USA

Background, Motivation and Objective

It is known that the currently available anisotropic material properties of quartz allow for finite element simulations that closely match experimental resonator frequency response with respect to both changes in pressure near ambient temperatures and changes in temperature near ambient pressures. However, as observed in the current work, such models deviate from experimental frequency values when high temperatures and pressures are applied simultaneously to the resonator (up to 200°C and 138 MPa). The current work explores in detail the nature of these deviations, with the objective of defining what new specific constitutive properties are needed to further the material model of quartz to these currently unsupported extreme conditions. Such conditions directly correspond to current uses of quartz resonators as temperature and pressure transducers for the oil and gas industry.

Statement of Contribution/Methods

A three-dimensional finite element model, based on the linear field equations for superimposed small vibrations onto nonlinear thermoelastic stressed media given by Lee and Yong [1], was developed. The frequency response of the model was benchmarked to experimental transducer data with temperature ranging from 50°C to 200°C and pressure from 96.5 kPa to 138 MPa.

Results

The normalized frequency response to the change in external pressure from 96.5 kPa to 138 MPa matched very well with experimental data for lower temperatures, having a maximum deviation of only 8.9% at 138 MPa, when assuming constant 50°C temperature. However, the same deviation grew to about 21.7% at 138 MPa assuming a higher 175°C constant temperature. Similarly, the temperature-frequency response from 50°C to 200°C matched the experimental trend well for lower pressures, but this agreement deteriorated as pressure increased.

Discussion and Conclusions

The nature of the observed frequency deviations suggests that changes in the third-order elastic constants with temperature, a quartz material property that is not currently available in literature, could play a significant role in accurately modeling the frequency response at such conditions, and that the lack of such properties are the primary source of the error in both temperature and pressure response. Varying the currently known (temperature independent) third-order elastic coefficients used within the finite element model yields insights into the expected trends of their unknown temperature derivatives. Specifically, for an AT-Cut quartz resonator, those third-order elastic coefficients which are most relevant to the thickness shear mode vibrations should be shown experimentally to decrease in magnitude as temperature increases.

[1] P.C.Y. Lee and Y.K. Yong, “Temperature derivates of elastic stiffness derived from the temperature behavior of quartz plates”, *Journal of Applied Physics* 56(5), 1984, pp. 1514-1521

6C-2

4:45 pm Empirical Model for Dielectric Charging in Double-SOI-Wafer-Bonded CMUTs: Theory and Experiment

Wei Zheng[1], Douglas Barlage[1], Peiyu Zhang[1], Glen Fitzpatrick[2], Walied Moussa[3], Roger Zemp[1]; [1]Electrical and Computer Engineering, University of Alberta, Edmonton, Alberta, Canada, [2]Micralyne Inc., Edmonton, Alberta, Canada, [3]Mechanical Engineering, University of Alberta, Edmonton, Alberta, Canada

Background, Motivation and Objective

Collapsed mode operation for capacitive micromachined ultrasound transducers (CMUTs) offers improved acoustic pressure output and receive sensitivity compared to conventional pre-collapse operation. However, in collapse mode, the top membrane maintains contact with the dielectric layers and charge accumulates in the dielectric layer. The dielectric charging causes shifts in the effective snapdown and snapback voltages and may even lead to permanent device failure. Significant effort has been expended in the RF-MEMS switch literature to address these effects but comparatively little has been done in the CMUT literature. Modeling the dielectric charging may be important to better understand how to design devices with improved long-term reliability.

Statement of Contribution/Methods

We studied CMUTs fabricated with a unique double-SOI wafer-bonding process using capacitance measurements from a Keithley 4200 Semiconductor Characterization System integrated with a probe-station. Snapdown and snapback voltages are measured over repeated cycles of the bias voltage, with intermediate prolonged high-voltage states (above the snapdown-voltage level) to effectively simulate long-term device operation.

We have built an empirical charging model with time constants that depend on current density (which in turn is a nonlinear function of bias voltage across the dielectric), defect charge-trapping cross-section in the case of bulk charging, and surface roughness in the case of surface charging.

Results

We plot the shifted snapdown/snapback voltage as a function of total snapdown time, and observe charging behavior over short-term and long-term periods. There is a clear fast-charging response with a fitted charging time-constant of seconds and a slower charging behavior with a time-constant of hours. Fast-charging shifts snapdown voltages dramatically, and slow-charging further changes the snapdown voltage by several volts over a time-period of several days. Model parameters are extracted from the fitted data. Bias voltage reversal over a time-scale of minutes is seen to reverse fast-charging effects.

Discussion and Conclusions

The observation of a fast-charging and slow-charging response is novel to the CMUT literature to the best of our knowledge. We hypothesize that the fast-charging response is due to surface charging while the slower response is due to bulk-charge accumulation. The model suggests that surface charging may be minimized by minimizing dielectric surface roughness.

6C-3

5:00 pm Enhancement of the Inverse Method enabling the Material Parameter Identification for Piezoceramics

Stefan Rupitsch[1], Jürgen Ilg[1], Reinhard Lerch[1]; [1]Chair of Sensor Technology, Friedrich-Alexander-University Erlangen-Nuremberg, Erlangen, Germany

Background, Motivation and Objective

Reliable numerical simulations of piezoceramic sensors and actuators ask for precise material parameters of the piezoceramics. Usually, these material parameters are determined according to the IEEE/ANSI standard. Thereby, mono-modal vibrations of various test samples with well-defined geometries are assumed which is strictly speaking an improper simplification. Hence, alternative approaches are required providing precise material parameters of piezoceramics.

Statement of Contribution/Methods

With a view to identifying material parameters of piezoceramics, we developed an appropriate so-called Inverse Method. The non-vanishing entries of the material tensors (elastic, dielectric and piezoelectric) are determined by a comparison of measurements and simulations. Both the frequency resolved electrical impedance and the spatially resolved surface normal velocity serve as input quantities of the method. As presented in our previous work, the consideration of these quantities allows for the determination of the whole parameter set by utilizing only a piezoceramic disc. However, the acquisition of the velocity is time-consuming and requires expensive measurement equipment. In this contribution, we present an enhanced Inverse Method enabling the determination of the whole parameter set by considering only the electrical impedance as input quantity. For the enhanced method, we utilize two block shaped piezoceramics polarized in different directions. Compared to discs, block shaped piezoceramics offer additional resonance-antiresonance pairs in the electrical impedance. Therewith, more significant data is available within the identification procedure.

Results

Figure 1 shows measurements and simulations of the electrical impedance for a block shaped piezoceramics made of PIC255 (PI Ceramic) which was used for the identification of the parameter set. Contrary to the manufacturer's material parameters, the determined parameters lead to reliable simulation results. As Fig. 2 depicts, these identified parameters yield superior simulation results for a piezoceramic disc, too. Note that the disc was not considered within the Inverse Method.

Discussion and Conclusions

The presented results clearly prove the applicability of the enhanced Inverse Method. Currently, the identification procedure is applied to various piezoceramic materials (e.g., PIC155).

Fig. 1: Electrical impedance of a block shaped piezoceramic made of PIC255.

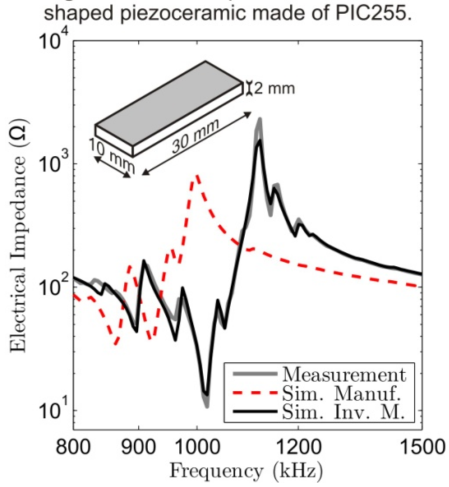

Fig. 2: Surface normal velocity of a disc for the thickness extensional mode.

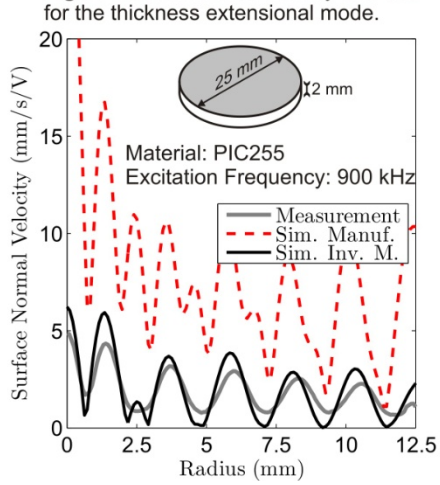

6C-4

5:15 pm Radiation pattern deterioration for phase steered capacitive micromachined ultrasonic transducer arrays due to cross coupling.

Erlend Leirset[1], Arne Rønnekleiv[1], Astrid Aksnes[1]; [1]Department of Electronics and Telecommunications, Norwegian University of Science and Technology, TRONDHEIM, TRONDHEIM, Norway

Background, Motivation and Objective

Cross coupling between neighbor elements in ultrasonic transducer arrays through surrounding fluid is a known effect. Previous work has shown that it can form a mode that is bound to the transducer fluid interface. This paper investigates how cross coupling affects the radiation pattern for finite phase steered arrays of capacitive micromachined ultrasonic transducers (CMUTs).

Statement of Contribution/Methods

A spatially finite 2D model of a 1D CMUT array with 72 CMUTs was constructed for finite element simulations using COMSOL. The simulated transducer array was loaded with a viscous fluid, and excited by phase modulated pressure to form a steered plane wave. To model typical electrical CMUT interconnects groups of two CMUTs were excited with the same phase. This enables, for distinct frequencies, acoustic power to be coupled into the bound mode induced by cross coupling. Simulations were performed for a frequency range of 1-35MHz for different steering angles and viscosities. To relate the simulations to a physical CMUT array, displacement measurements were performed using an optical heterodyne interferometer. It is capable of measuring phase and absolute amplitude up to 1GHz with a noise floor down to 1pm/√Hz. The dispersion relation of the cross coupling induced bound mode was found by exciting one element at the edge of the array, and measuring the displacement amplitude of the CMUTs along the array. These measurements were used to estimate the frequencies where excitation of the bound mode is possible.

Results

The simulations indicated notable effects in the radiation pattern at frequencies where power is coupled into the bound mode. For non zero steering angles, a significant amount of the power is radiated in another direction than intended, as indicated in the figure. The amount of miss-steered power is reduced for larger viscosities. Optical measurements indicated a dispersive bound mode that can be excited at frequencies around 18MHz which is less than the 2D simulations indicated.

Discussion and Conclusions

The simulations indicated that the presence of a cross coupling induced mode can notably affect the power steering capabilities of transducer arrays used in low viscosity fluids. The optical measurements indicated the expected frequencies at which the physical CMUT array has similar disadvantages.

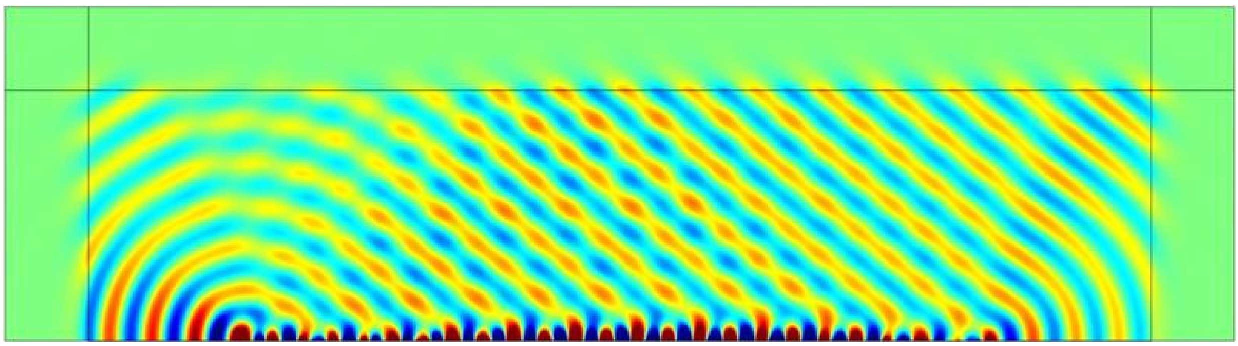

6C-5

5:30 pm Experimental and Finite Element Model Directivity Comparison Between PZT and PMN-PT Kerfless Arrays

Phil Garland[1], Andre Bezanson[1], Rob Adamson[1], Jeremy Brown[1]; [1]School of Biomedical Engineering, Dalhousie University, Canada

Background, Motivation and Objective

When first conceived, kerfless ultrasound arrays offered a promise of a simplified fabrication procedure for high-frequency arrays over the standard kerfed design because one is not required to physically dice the array elements. However, the first linear PZT kerfless arrays showed relatively poor directivity, a fact that essentially made kerfless arrays unsuitable for beamsteering and/or phased arrays. Given that the mechanical and dielectric properties of PMN-PT are very anisotropic we have revisited the kerfless array design using PMN-PT as the transducer substrate hypothesising a dramatically different directivity pattern. Our objectives in this work are to compare the directivity results of PZT-5H and PMN-32%PT kerfless arrays through finite element simulations and experimental hydrophone measurements.

Statement of Contribution/Methods

This paper presents finite element and experimental results of PZT and PMN-PT kerfless arrays. The two arrays were fabricated to have a centre frequency of 8 MHz, 32 elements, 1λ width and no matching layer. The experimental results were obtained by moving the arrays in an equidistant arc over a 40 um needle hyrdrophone (Precision Acoustics Ltd.) while electronically pulsing the centre element with the adjacent elements terminated at 50 ohms. The arrays were moved using a 3-axis staging (Thorlabs, MTS50/M-Z8), and the transmit pulse was provided by a pulser/ receiver unit (Daxsonics 10ers, Halifax, NS). The hydrophone signal was captured using an oscilloscope (Agilent MSO-3502) and transferred to Matlab (Mathworks Inc.) for post-processing. The finite element simulation of the arrays was performed using PZFlex 2.4 (Weidlinger Associates Inc.).

Results

For the PMN-PT array, the finite element simulation predicted that the one-way pulse pressure would drop to -6dB at ±50° and the PZT array would drop to -6dB at ±32°. The experimental results for the PMN-PT array were very similar to the finite element model measuring a one way directivity of ±46° and the one-way measured directivity for PZT was ±22° in agreement with previous work.

Discussion and Conclusions

Both the experimental measurements and finite element model show greatly increased element directivity for a PMN-PT kerfless array element over a PZT kerfless array element. The -6dB full width one-way directivity for PMN-PT was 90° while that for PZT was only 44 °. The unique anisotropic dielectric and mechanical properties of PMN-PT that produce this far superior directivity over PZT for kerfless ultrasound arrays, could greatly simplify the array fabrication procedure making the kerfless design suitable for high-frequency phased arrays.

6C-6

5:45 pm Iterative Inverse Extrapolation for Transducer Characterization

E.J. Alles[1], M.D. Verweij[1], K.W.A. van Dongen[1]; [1]Laboratory of Acoustical Imaging and Sound Control, Faculty of Applied Sciences, Delft University of Technology, Delft, Zuid-Holland, Netherlands

Background, Motivation and Objective

In medical ultrasound, there is a constant demand for images of higher quality and resolution. To fulfill this demand, current ultrasound transducer arrays are composed of large numbers of small elements operating at high center frequencies up to 10 MHz or higher.

Due to the complex construction of these transducers, the motion of and the cross-coupling between the transducer elements are hard to predict. However, the motion of the radiating surfaces determines its radiation pattern and thus the image resolution and quality. A good control over the transducer surface motion is thus of vital importance.

However, direct measurement of the motion under realistic conditions is complicated. Instead of direct measurement, the velocity distribution on the transducer surface can also be derived from pressure measurements at some distance from the radiating source.

Statement of Contribution/Methods

Pressure measurements can be analytically inversely extrapolated to transducer surface velocity distributions using Weyl's representation of the Green's function. However, evanescent waves have been shown to cause instability and thus need to be omitted [1].

Omitting evanescent waves removes the higher spatial frequencies from the problem. Therefore, inversion results are significantly spatially smoothed. To avoid this spatial smoothing, in this work the temporal and spatial behavior of the velocity distribution are reconstructed using an iterative conjugate gradient inversion scheme.

Results

The proposed method has been tested first for a synthetic array with five elements (l x w = 700 µm x 200 µm, kerf = 200 µm), where all the elements are driven simultaneous at different amplitudes using a 10 MHz Gaussian modulated pulse. Synthetic pressure measurements are made at 0.1 and 1 mm distance from the surface. To simulate real measurements, 0.1% white noise has been added to the synthetic data. Using the proposed method, an accurate reconstruction of the vibrating elements is achieved ($error_{no\ noise}$ = 1.4%, $error_{noise}$ = 2.9%) for a measurement distance of 1 mm, which yields a significant improvement over Weyl's representation ($error_{no\ noise}$ = 9.1%, $error_{noise}$ = 50%).

Finally, the proposed method has been tested on an in-house build array with the dimensions specified above. The obtained results are compared with the results obtained using Weyl's representation.

Discussion and Conclusions

An iterative inverse extrapolation scheme for transducer characterization has been developed. The method has been tested on synthetic data and on an in-house build array. In general, the new method works better than Weyl's representation, yielding less spatial smoothing and being less sensitive to noise.

[1] E.J. Alles, M.D. Verweij, K.W.A. van Dongen, "Reconstructing Transducer Surface Motion by Inverse Extrapolation of Measured Pressure Wavefields", proc. of IEEE IUS 2010 San Diego.

Wednesday Poster Sessions

P1Aa - Beam Formation: Computational Aspects and Artifact Reduction

Carribean Ballroom III-V

Wednesday, October 19, 2011, 9:30 am - 1:00 pm

Chair: **Jian-yu Lu**
Univ. of Toledo

P1Aa-1

Synthetic Aperture Beamformation using a GPU

Jens Munk Hansen[1], Dana Schaa[2], Jørgen Arendt Jensen[1]; [1]Dept. of Elec. Eng., Technical University of Denmark, DK-2800 Lyngby, Denmark, [2]Department of Electrical and Computer Engineering, Northeastern University, Boston, MA, USA

Background, Motivation and Objective

For ultrasound imaging, focusing and apodization are an essential part of the signal processing. Together they are referred to simply as beamformation. The focusing part amounts to massive time-of-flight calculations followed by memory look-ups. The apodization part consists of a weighting based on the pixel location and the origin of the ultrasound signals. The GPU is a many-core massive parallel throughput-oriented execution unit. It is ALU heavy and therefore good for massive calculations. An initial implementation, however, will most likely be very slow due to the randomly shifted memory access pattern. The latest GPU generation from Nvidia is equipped with a hardware cache reminiscent to what is found on a CPU. This cache allows for fast random memory access and makes it particularly easy to implement advanced beamformers without having to worry too much on how the memory is addressed.

Statement of Contribution/Methods

A comprehensive synthetic aperture ultrasound beamformer is implemented for the GPU using the OpenCL framework. The implementation supports beamformation of either RF signals or complex base band signals. Transmit and receive apodization can be either parametric or dynamic using a fixed F-number and a direction for directional beamformation. Images can be formed using an arbitrary number of emissions and receive channels. Input data is read from files or memory and processed on the GPU for later investigation using Matlab. The RF and complex base band signals beamformed using the GPU have been simulated using Field II. To validate the performance, the frame rate is measured for continuous beamformation and display.

Results

A large number of different setups has been investigated and the frame rate measured. For all setups, the number of samples is chosen such that each and every sample is used for beamformation. For an image size of 512x512 pixels and 4000 complex 32-bit samples recorded at 40 MHz using a λ-pitch transducer, the following frame rates are obtained.

Discussion and Conclusions

We conclude that the GPU is indeed suitable for advanced beamformation scenarios for both online and offline beamformation. In addition, the large cache on Fermi architecture makes it particular easy to obtain high frame rates.

Table 1: Frame rates for an image size of 512x512 pixels beamformed using 4000 complex samples for each receive channel.

# channels	# emissions 4	8	16	32
192	42.8	23.7	12.5	7.2
128	70.4	39.9	20.0	11.2
96	77.6	44.8	23.8	13.3
64	137.3	75.4	39.7	21.1
48	171.3	80.5	49.7	26.2
24	226.2	143.7	86.1	44.2

P1Aa-2

Conjugate Gradient and Regularized Inverse Problem-based Solutions Applied to Ultrasound Image Reconstruction

Leonardo Zanin[1], Marcelo Zibetti[1], **Fabio Schneider[1]**; [1]*CPGEI, UTFPR, Curitiba, Parana, Brazil*

Background, Motivation and Objective

Computational methods for inverse problems have long been successfully applied in medical imaging such as computed tomography and magnetic resonance as described by H.H. Barrett, and K.J. Myers. Recently, researchers such as R. Lavarello et al., F. Lingvall and T. Olofsson have applied the methodology of inverse problems to ultrasound imaging reconstruction. Inverse problem-based (IPB) solutions for ultrasound image reconstruction are known for potentially suffering from instability and high sensitivity to data perturbation (e.g., noise) to achieve a good image quality. For evaluating the feasibility of using IPB solutions in ultrasound image systems, we have implemented regularized and iterative methods with image quality assessment purposes.

Statement of Contribution/Methods

In this paper, two methods of image reconstruction for ultrasound are discussed, they are alternatives to deal with the ill-posedness through the use of regularization with Euclidean norm penalty and the conjugate gradient (CG) iterative method. Reasonable approximate solutions can often be obtained, especially due to the regularizing property of the iterative methods as applied to magnetic resonance imaging. The experiments in this paper aim to compare mainly the lateral resolution comparing results from a traditional beamforming technique with the resolution achieved with inverse reconstruction. For all experiments we reconstructed a 50×50-pixel image representing a 10×10 mm2 region for which the center is 20 mm apart from the transducer centered in the lateral dimension. A transducer with central frequency of 5MHz and 80% BW was simulated with a 100 MHz sampling frequency. A single set of 64 elements spaced by the wavelength size with focus at 20 mm and no apodization was used.

Results

Gray scale images and 3D plots of the point spread function are shown for 20 and 40 dB ranges considering the three methods. Lateral and axial resolution plots are additionally presented. The -6dB lateral resolution found for traditional delay-and-sum method was around 0.5 mm and the largest side lobe was around -17.8 dB. On the other hand, the values for the regularized method was 0.2 mm with the largest side lobe at around -16.6 dB or with a different regularization factor 0.18 mm and -43 dB were found. For the CG method a 0.25 mm lateral resolution was found for – 6dB with a side lobe of -10 dB. The axial resolution varies from 0.23 mm for the reference beam forming method to smaller than 0.2 mm for the regularized and CG methods.

Discussion and Conclusions

The regularized and CG methods results were similar to those presented by Lavarello et al.. An improvement in lateral resolution can be achieved when using IPB solutions at the expense of side lobe degradation. A correlated paper is presented with a deeper discussion on the effects of regularized factor and the number of iterations for the CG method.

P1Aa-3

Scalable Intersample Interpolation Architecture for High-channel-count Beamformers

Borislav G. Tomov[1], Svetoslav I. Nikolov[2], Jørgen Arendt Jensen[1]; [1]Center for Fast Ultrasound Imaging, Dept. of Elec. Eng., Technical University of Denmark, DK-2800 Lyngby, Denmark, [2]R&D Applications & Technologies, BK Medical, DK-2730 Herlev, Denmark

Background, Motivation and Objective

Using higher number of channels in ultrasound beamformers provides significant benefits, such as higher signal-to-noise ratio, better focusing, and the ability to handle 2-dimensional arrays that allow 3-dimensional (volume) imaging. The higher channel count requires more amplifiers, more A/D and D/A converters and more logic resources to implement the focusing. To achieve precise focusing, interpolation between the acquired echo samples is necessary. Band-pass interpolation produces much better results than the simpler linear interpolation. This paper presents a post-delay band-pass interpolation algorithm, mathematically equivalent to per-channel band-pass interpolation, but requiring much fewer multiplication operations.

Statement of Contribution/Methods

Band-pass interpolation is performed by applying one of several short FIR filters on a set of input samples, chosen by the required rough delay (the integer part of the focusing delay). The choice of filter is determined by the fine delay (the fractional part of the focusing delay). Output samples from each channel are then apodized and summed to produce a focused sample. Achieving a precision of e.g. 1/16th sampling interval requires 16 filters.

In the suggested algorithm, the conventional set of 16 4-tap FIR filters is combined into a filter of length 64. Each coefficient of that filter is to be applied to a data bin / input sample accumulator. Input samples from each channel are added to the appropriate bins according to the current focusing delay profile. The multiplications are then performed, producing a correctly focused sample.

Results

The computational requirements for performing linear interpolation, band-pass interpolation and post-delay band-pass interpolation are calculated. For a 256-channel beamformer, the new approach requires 320 multiplications per output sample versus 768 when using linear interpolation (58.3 % savings) and 1280 when using bandpass interpolation (75 % savings). For a 1024-channel design, the savings are 64.6 % (1088 vs. 3072) and 78.7 % (1088 vs. 5120).

Discussion and Conclusions

The post-delay band-pass interpolation provides the precision of band-pass interpolation, combined with computational requirements that are much lower than those of linear interpolation, making it suitable for use in high-channel-count beamformers.

P1Aa-4

Mitigation of Off-axis Specular Reflection Artifacts in Diagnostic Bone Imaging with Medical Ultrasound Using Mechanically Scanned Piston Transducers

F. William Mauldin, Jr. [1,2], Kevin Owen[1,2], John Hossack[1]; [1]Biomedical Engineering, University of Virginia, Charlottesville, VA, USA, [2]Rivanna Medical, Crozet, VA, USA

Background, Motivation and Objective

Medical ultrasound is a potentially superior alternative to X-ray for bone imaging due to its portability, low cost, and non-ionizing radiation. Unfortunately, conventional ultrasound-based bone image quality is generally poor. A dominant source of image degradation is derived from off-axis specular surface (e.g. bone) reflections, which are enhanced by two attributes of linear transducer arrays: grating lobes and poor resolution in the elevational dimension. Focused piston transducers are not affected by these problems, and therefore, offer the potential for bone imaging with reduced artifact.

Statement of Contribution/Methods

Simulations in FIELD II were conducted to assess artifacts generated for varied transducer parameters and geometries along with varied orientations of specular reflecting surfaces. Experimental images of an excised lumbar spine were collected using the L14-5 linear array on the Ultrasonix RP scanner and a 3/8" diameter mechanically scanned piston transducer. Focal depth for both was 5cm. Bone surface position estimates were rendered from ultrasound image frames, and performance was quantified in terms of estimation error and contrast between on-axis and off-axis reflection energy.

Results

Simulation results demonstrate superior mitigation of off-axis specular reflection artifact using the piston transducer compared to the linear array. Under representative spinal bone imaging conditions, contrast between received echo amplitude derived from on-axis specular reflections versus off-axis reflections were 10.6 dB greater with the piston transducer. Similarly, experimental results with the piston transducer exhibited superior bone image quality with lower off-axis reflection artifacts and enhanced bone surface estimates (see figure below). Automated measurements performed in MATLAB of spinous process and epidural gap dimensions across the axis of the spine exhibited 75% and 40% lower error respectively when derived from images rendered with the piston transducer compared with the linear array.

Discussion and Conclusions

Simulation and experimental data demonstrate that off-axis specular reflections are a dominant source of artifact in bone imaging with ultrasound. These artifacts can be mitigated using transducer geometries, such as focused pistons, that lack grating-lobes and have a tight focus in all dimensions.

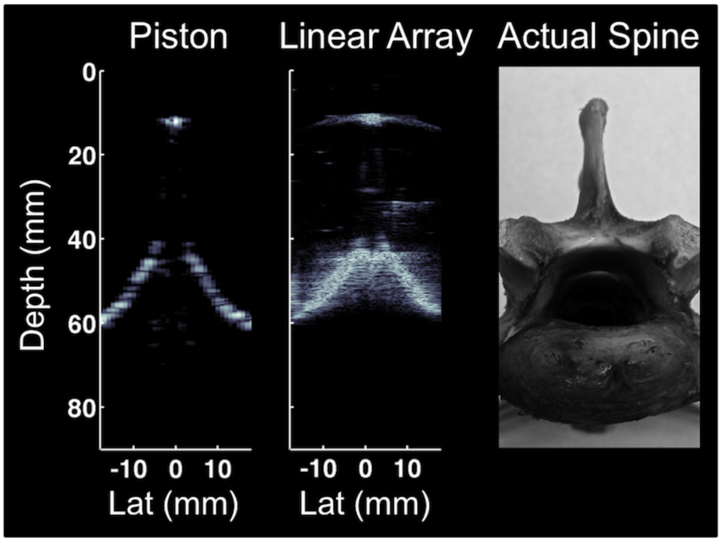

P1Aa-5

A Novel Imaging Method of Coded THI using Multi Chirp Signals

Masayuki Tanabe[1], Takuya Yamamura[2], Kan Okubo[2], Norio Tagawa[2]; [1]*Graduate School of Science and Technology, Kumamoto University, Kurokami, Kumamoto, Japan,* [2]*Graduate School of System Design, Tokyo Metropolitan University, Hino, Tokyo, Japan*

Background, Motivation and Objective

In medical ultrasound imaging, tissue harmonic imaging (THI), coded excitation and a combination of both (coded THI) have been investigated by many researchers. In THI, a spectral overlap occurs between fundamental and harmonic components, and it makes axial resolution worse. Especially, the spectral overlap in coded THI causes a specific artifact which is caused by inappropriate cross-correlation between fundamental component of echo signal and the matched filter for harmonic. To avoid the spectral overlap, the pulse inversion (PI) method, which excites two phase-inverted pulses, has been used. However, the PI is sensitive to tissue motion. In coded excitation especially chirp, a longer coded signal enables a higher signal-to-noise ratio (SNR) imaging However, there is temporal overlap between a transmitted signal and echo signal from near region when the longer coded signal is used.

The objective of this study is to realize high SNR and high axial resolution imaging by removing the time and the spectral overlaps existing in the coded THI.

Statement of Contribution/Methods

In our proposed method, multi chirp signals are used. Each duration time of the transmitted chirp signals is designed not to overlap the transmitted and echo signals from region of interest (ROI). Similarly, each frequency bandwidth of the signals is designed not to overlap the fundamental and the harmonic components. Subsequently, the harmonic components of the echo signals are extracted and vector-correlated with the matched filters. Consequently, the proposed method can acquire high axial resolution images with high SNR.

Results

In proposal, two chirp signals are employed. The each frequency is 2.5-3.7 and 3.6-5 MHz, and each duration is 13.5 µs. As a reference, the conventional coded THI method uses a chirp signal which frequency is 2.5-5 MHz and duration is 24 µs. B-mode images are shown in the figure.

Discussion and Conclusions

The conventional coded THI method causes artifacts, which caused by a cross-correlation between the fundamental component of echo signal and the matched filter for harmonic component. The proposal image is clearer than the conventional one without artifacts. Through the experiment, the availability of the proposal was shown. In a future work, extending the proposed method, a higher frame rate imaging method with a linear array transducer will be examined.

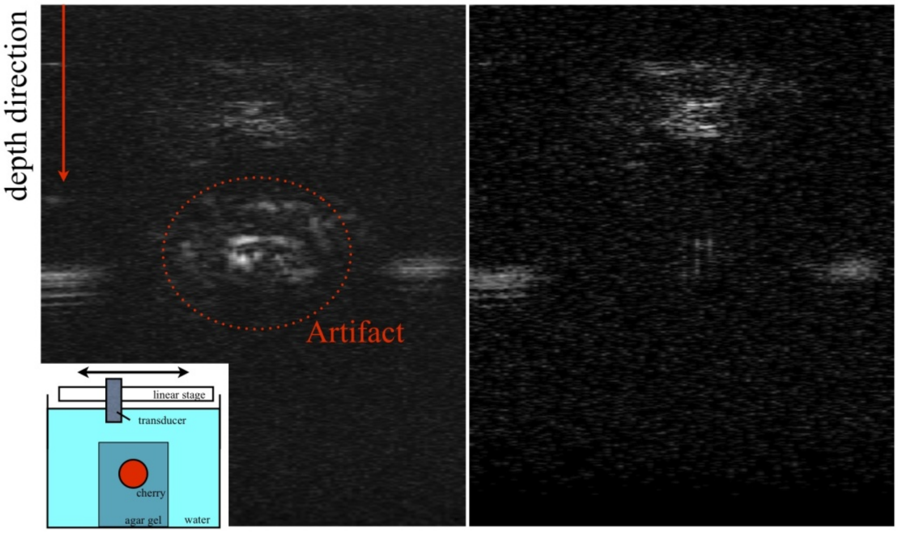

P1Aa-6

Improved Image Quality Using Phase Aberration Correction and Dual Apodization with Cross-correlation

Junseob Shin[1], Jesse Yen[1]; [1]Biomedical Engineering, University of Southern California, Los Angeles, CA, USA

Background, Motivation and Objective

Dual Apodization with Cross-correlation (DAX) is a novel beamforming method which utilizes two distinct receive apodizations in suppressing sidelobes and clutter to improve ultrasound image contrast. Although DAX has been shown to minimize the effects of phase aberration and noise in a highly robust manner, its performance diminishes as aberrator strength increases. In this work, we propose combining DAX with a well-established aberration correction algorithm based on nearest-neighbor cross-correlation (NNCC) to maximize improvement in image quality.

Statement of Contribution/Methods

Field II simulations of a point target and a 3 mm diameter anechoic cyst at a depth of 30 mm were performed. Imaging parameters were chosen to model a 128-element linear array with center frequency of 5MHz, 50% bandwidth, azimuthal element pitch of 308 um. Assuming a near-field phase screen model, phase errors were estimated from simulated RF data using cross-correlation between adjacent elements within the subaperture and were then corrected by time shifting RF lines. Subsequently, DAX was performed on the RF data with phase errors corrected. An 8-8 alternating pattern was used as it has been shown to achieve greatest CNR improvement with minimal amount of artifacts near the transmit focus. The cross-correlation matrices were filtered with a median filter of size 0.6 mm×0.6 mm to remove any artifacts. Results were also obtained with the Generalized Coherence Factor (GCF), a competing method of DAX.

Results

The beamplots show that the NNCC-based correction is most effective in reducing the mainlobe width and suppressing sidelobes that are -20 dB or higher near the mainlobe while DAX is best suited for suppressing sidelobes that are -20dB or lower farther away from the mainlobe. CNR Improvements of 215%, 290%, and 321% were obtained with DAX combined with NNCC-based correction over standard beamforming for aberrators of strengths 25, 35, and 45ns RMS, respectively.

Discussion and Conclusions

Our results show that the combined method achieves greater improvement in image quality than either DAX or NNCC-based correction alone. This is especially true for imaging applications with strong aberrators in which neither yields significant CNR improvement. The proposed method also demonstrates improvement over GCF. Experimental work is underway to validate the improvements shown by simulation results.

	Aberrator Strength	Standard	GCF	DAX	Correction	GCF+ Correction	DAX+ Correction
CNR	25ns RMS	3.50	4.93	10.17	4.03	5.60	11.04
	35ns RMS	2.92	4.09	10.17	3.58	5.16	11.38
	45ns RMS	2.23	2.79	7.49	2.71	3.95	9.38

Table 1: CNR values calculated from the 3mm-diameter cyst.

P1Aa-7

A Multitaper Approach to Speckle Reduction for Medical Ultrasound Imaging

Are Charles Jensen[1], Carl-Inge Nilsen[1], Andreas Austeng[1], Sven Peter Näsholm[1], Sverre Holm[1]; [1]*Department of Informatics, University of Oslo, Oslo, Norway*

Background, Motivation and Objective

The visual quality of images produced by coherent imaging systems is often degraded by the presence of noise-like patterns, stemming from constructive and destructive interference, known as speckle. This phenomenon, however, can be reduced by averaging images with different such speckle realizations. Traditionally, these images have been formed by observing the target region from slightly different angles (spatial compounding) or by varying the involved frequencies (frequency compounding). In this paper we investigate a third option based on Thomson's multitaper approach to power spectrum estimation. In effect, we synthesize a flat, slightly wider, "mainlobe" by a set of orthogonal tapers (windows), each of which extracts a different part

of the spatial spectrum yielding images with different speckle patterns. Furthermore, the windows are designed to maximize the relative power within the mainlobe, minimizing sidelobe leakage.

Statement of Contribution/Methods

When studying speckle reduction, a common figure of merit is the ratio between the produced image's mean value to its standard deviation (μ/σ). Besides using this measure to compare the proposed approach to that of a traditional spatial compounding system, we study how the ratio varies with the number of windows used. A visual assessment of the multitaper approach on real ultrasound phantom data is also provided. Finally, we examine results on simulated scenes of point sources.

Results

The results show that the multitaper approach is capable of reducing speckle. The μ/σ ratio when using two orthogonal windows (a time-bandwidth product of one) is very close to what is achieved by two-way spatial compounding. By increasing the number of windows (increasing the bandwidth / reducing the azimuthal resolution), the ratio can be increased even further.

Fig. 1 shows a cross section of an image created from a synthetic scene consisting of a single point source. We can clearly see that the sidelobe level is reduced when using the multitaper approach.

Discussion and Conclusions

Our investigations verify that the multitaper approach can be used for speckle reduction, and at a rate compared to that of the more traditional method of spatial compounding. Due to the spectral concentration of the tapers (windows), an added benefit is reduced sidelobe levels.

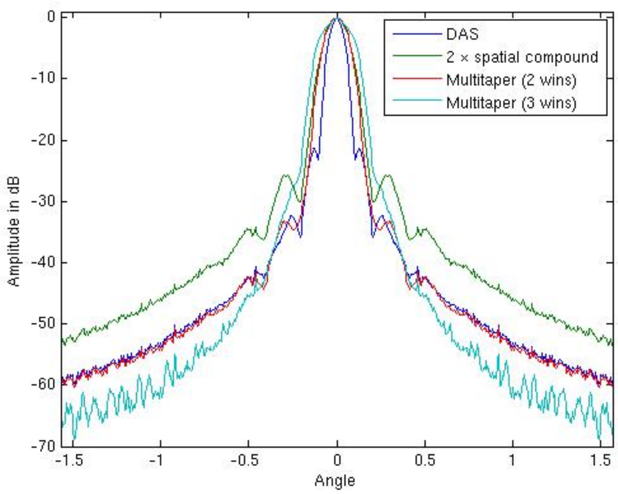

P1Aa-8

A New Extended Range Ultrasonic Synthetic Aperture Tissue Harmonic Imaging System

Moo-Ho Bae[1], Sung-Bae Park[1], Han-Woo Lee[2], Sang-Gyu Nam[2], Mok-Kun Jeong[3]; [1]*Hallym Univ., Korea, Republic of,* [2]*Samsung Medison Co., LTD., Korea, Republic of,* [3]*Daejin Univ., Korea, Republic of*

Background, Motivation and Objective

Recently we reported that tissue harmonic imaging (THI) can successfully be combined with synthetic aperture imaging (SAI). (Bae et al., "A New Ultrasonic Synthetic Aperture Tissue Harmonic Imaging System," IUS 2008)

However, THI has an inherent limitation as follows: The generating of 2'nd harmonic component is mostly concentrated around virtual source, therefore the SNR is high only in the vicinity of the virtual sources. This limits effective imaging range for diagnosis. Even though THI is combined with SAI, this limitation still exists.

Statement of Contribution/Methods

In this work, a new modified SAI method is proposed, which utilizes several different depth virtual sources, in contrast to the conventional SAI method which mostly utilized virtual sources at a single depth. Using these virtual sources with multiple depths, the generation of 2'nd harmonic component can be spread effectively over longer range. Here, as examples, we propose two methods as follows:

Method I: Two different depth virtual sources are located at a same scanline, and transmission to each virtual source is done successively. The received signals from all the transmissions in one frame are synthesized to form a SAI image.

Method II: Even and odd number scanlines have virtual sources with two different depths to each other. The frame rate is doubled compared to that of method I at the expense of slightly degraded image quality.

Results

Proposed methods are simulated by both PZFlex (nonlinear propagation) and Field II. Simulation conditions are as follows: 128 element linear array transducer with f0=4MHz, pitch=0.3mm, medium=water, Tx f number = 3, 7 point targets at depth= 20 - 80mm, depths of virtual sources = 50mm for the previous method(Bae et al., IUS 2008), 30 and 70mm for both method I and II, respectively. Figure shows the simulated results of the proposed methods compared to the previous method: (a) relative SNR vs. depth, (b) point target image comparison. These results show significantly improved field pattern and SNR throughout the imaging range by using the proposed methods.

Discussion and Conclusions

In this work, we proposed new methods which extend the effective imaging range of THI and SAI combination by placing the virtual sources to different depths. This modification needs almost no hardware or software overhead, and almost no sacrification of any performance compared to previous method.

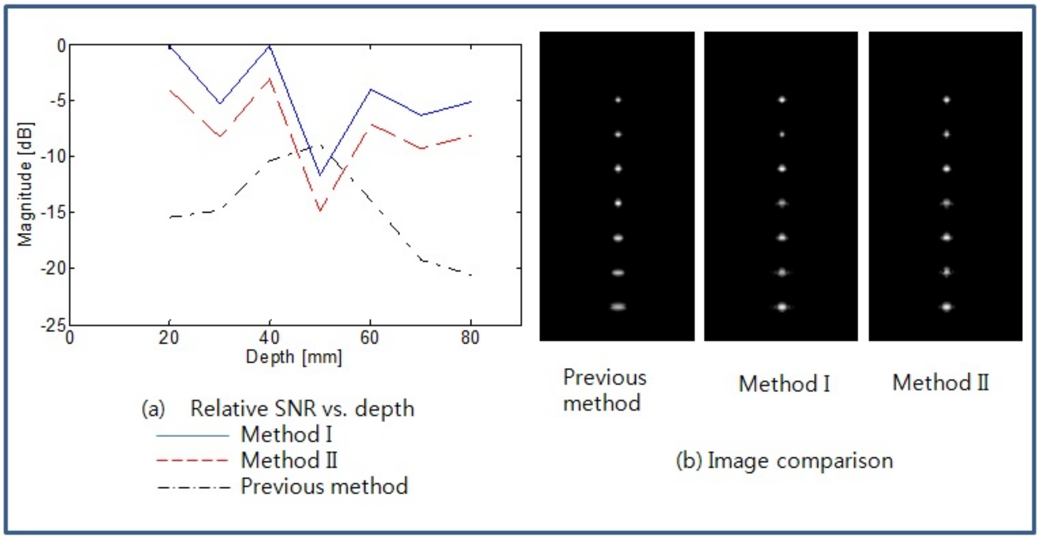

P1Aa-9

Extraction of an Overlapped Second Harmonic Chirp Component using the Fractional Fourier Transform

Muhammad Arif[1], Sevan Harput[2], Peter Smith[2], David Cowell[2], Steven Freear[2]; [1]Ultrasound Research Group, School of Electronic and Electrical Engineering, University of Leeds, United Kingdom, [2]University of Leeds, United Kingdom

Background, Motivation and Objective

In ultrasound harmonic imaging with chirp coded excitation, the axial resolution can be improved by increasing the excitation signal bandwidth. However increasing the bandwidth will cause overlap between the received nonlinear second harmonic chirp component (SHCC) and the fundamental component. In the spectral overlap harmonic condition, signal decoding using the second harmonic matched filter (SHMF) typically produces higher range sidelobes level (RSLL) which reduce the contrast resolution. A multi-pulse excitation scheme such as pulse inversion can be used to extract the overlapped SHCC; however it is susceptible to motion artifacts and reduced system frame-rate. In this paper, fractional Fourier transform (FrFT) is proposed with chirp coded excitation for the extraction of the overlapped SHCC.

Statement of Contribution/Methods

In order to validate the proposed method, experiments were conducted both pitch-catch and pulse-echo configurations. In a pitch-catch configuration, a 2.25 MHz single element transducer was mounted coaxially with a 1 mm needle hydrophone at a distance of 110 mm in a water tank. In a pulse-echo configuration, a 4.8 MHz standard medical probe with 96 elements was used to scan the wire phantom. A Hann windowed linear chirp with duration of 10 µsec, and bandwidth ranging from 1-3 MHz was used as an excitation signal. The nonlinear received signals were processed offline using the FrFT in order to extract the SHCC. Using the FrFT, the time domain signal can be transformed into the fractional domain where the overlapped SHCC is separable and therefore can be extracted by applying a rectangular window around it. The extracted SHCC is then transformed back to the time domain for further processing. The extracted SHCC is then decoded using the SHMF in order to restore axial resolution.

Results

In both experiments, the results indicate at least a 13 dB improvement in the RSLL of the FrFT filtered compressed SHCC when compared with the unfiltered compressed SHCC as shown in the enclosed figure.

Discussion and Conclusions

The FrFT can be used as a filtering tool with a wide bandwidth chirp excitation in order to extract the overlapped SHCC without reducing the system frame-rate. Using the FrFT filtering, the RSLL in the compressed SHCC can be reduced which potentially improve the contrast resolution.

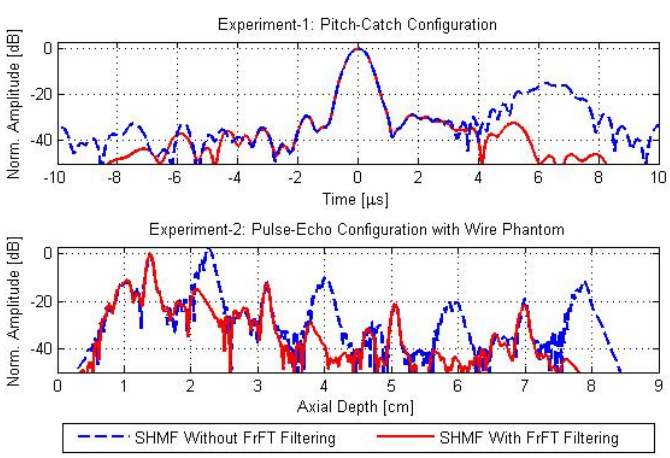

P1Ab - Blood Flow Imaging

Carribean Ballroom III-V

Wednesday, October 19, 2011, 9:30 am - 1:00 pm

Chair: **Lasse Lovstakken**
Nowegian Univ. of Science & Technology

P1Ab-1

High Frame Rate Vector Flow Imaging of Stenotic Carotid Bifurcation: Computational Modeling and Analysis

Donald L. S. Chan[1], Billy Y. S. Yiu[1], Alfred C. H. Yu[1]; [1]Medical Engineering Program, The University of Hong Kong, Hong Kong

Background, Motivation and Objective

Analysis of the complex blood flow pattern in the carotid bifurcation is clinically important to the diagnosis of carotid stenoses. Color flow imaging (CFI) can only provide a biased visualization as it is only sensitive to axial flow and its frame rate is often inadequate for resolving the flow pattern in various cardiac cycle phases. The use of high frame rate imaging methods such as plane wave excitation, together with vector flow estimators like block matching, may potentially overcome these limitations.

Statement of Contribution/Methods

We have investigated the efficacy of high-frame-rate vector flow imaging (VFI) in stenotic carotid bifurcation analysis using Field-II and computational fluid dynamics (CFD). Geometric models of the carotid bifurcation with different eccentric stenosis levels (0% to 70% blockage, in 10% increments) were constructed and their blood flow patterns were computed via Fluent CFD software. Pulse-echo data of these flow models were obtained by simulating the plane-wave imaging technique in Field II (center freq.: 5MHz, PRF: 5kHz, pulse duration: 2 cycles). To obtain vector flow images, the data were first beamformed with dynamic focusing. Axial and lateral velocity estimates were then obtained by performing block matching (kernel size: 2mm x 2mm, search area: 4mm x 4mm) between successive beamformed images using sum of absolute difference as the matching criteria and linear regression fitting as a sub-sample motion estimator. Flow streamlines and velocity magnitudes were computed and displayed on top of the corresponding plane wave images. To facilitate analysis, these images were compared against those obtained from conventional CFI (based on Field-II data generated from the same flow model).

Results

In the high frame rate vector flow images obtained, turbulent streamlines can be readily observed near the stenosis (see attached figure). In contrast, conventional CFI was only able to depict axial velocity increase in the form of color-map aliasing, and it led to misinterpretation of the flow directions in the two branches. The high imaging frame rate (5000 fps) was also found to be crucial to the efficacy of the block matching algorithm.

Discussion and Conclusions

This work demonstrates the complex blood flow visualization capabilities of high frame rate VFI. It has potential to be further developed into a new clinical technique for vascular diagnoses.

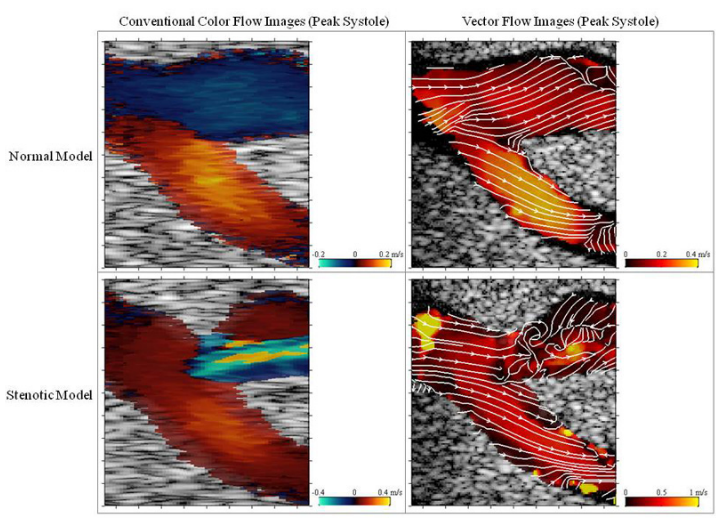

P1Ab-2

Fast, Robust Estimation and a Novel Visualization Method for Vector Doppler Imaging with Planewave Transmissions

John Flynn[1], Ron Daigle[1], Lauren Pflugrath[1], Peter Kaczkowski[2], Ken Linkhart[1]; [1]Verasonics, Inc. Redmond, WA, USA, [2]Applied Physics Laboratory, University of Washington, Seattle, WA, USA

Background, Motivation and Objective

Vector Doppler Imaging (VDI) improves on conventional color Doppler Imaging (CDI) by giving speed and direction of blood flow at each pixel. Multiple angles of planewave transmissions (PWT) conveniently give projected Doppler measurements over a wide field of view, providing enough angular diversity to identify velocity vectors in a short time window while capturing transitory flow dynamics. We present a fast, aliasing-resistant velocity vector estimator for PWT, and show VDI imaging of a carotid artery with a 5 MHz linear array using a novel synthetic particle flow visualization method.

Statement of Contribution/Methods

We partition a PWT measurement model into nonlinear and linear components in a way that simplifies vector velocity computation. Each pixel's velocity vector predicts the IQ measurements at diverse angles of PWT ensembles through a nonlinear model, which we linearize by transforming with conventional CDI processing (clutter filtering and Kasai autocorrelation) to a set of Doppler frequencies. Velocity vector estimation then simplifies as the solution to a small linear weighted least squares (WLS) problem, conditioned on a hypothesized measurement bias due to aliasing. Weights derived from CDI autocorrelation lag variances account for clutter filtering effects. The nonlinearity of the original problem is thus reduced to a discrete search over a finite number of known aliasing bias vectors. Further, the WLS estimator covariance provides information used to qualify pixels.

To visualize the resulting velocity vector image, we use a novel technique which synthesizes a moving field of points representing particles entrained in the fluid. In its creation, each particle is probabilistically generated at a pixel where flow is detected, and imbued with motion proportional to the velocity vector estimate, scaled down so the viewer may easily perceive motion. Particles migrate across the image from frame to frame, under conservation rules that control particle density to the user's preference. The particle motion overlays the detected flow regions, which are color-coded for velocity magnitude.

Results

Using a Philips L7-4 transducer and a Verasonics acquisition system, we demonstrate in vivo VDI on neck vasculature. PWT ensembles collected at seven angles are processed with the VDI algorithm, in a GPU implementation that accommodates the collection rate of 30 fps. Video display reveals dynamics of the flow field and shows good detection of flow during diastole.

Discussion and Conclusions

This vector velocity imaging framework demonstrates acquisition framerates sufficient to capture flow dynamics in the carotid artery. The algorithm is conceptually simple and computationally efficient, and leverages standard CDI processing as its front-end. The particle flow display technique is subjectively informative in conditions of plug, laminar, and turbulent flow.

P1Ab-3

Model-based correction of angle-dependencies in navigated 3-D flow imaging during neurosurgical interventions

Daniel Høyer Iversen[1], Frank Lindseth[2,3], Hans Torp[1], Lasse Løvstakken[1,4]; [1]MI Lab and Department of Circulation and Medical Imaging, Norwegian University of Science and Technology, Trondheim, Norway, [2]SINTEF Medical Technology, Trondheim, Norway, [3]Department of Computer and Information Science, Norwegian University of Science and Technology, Trondheim, Norway, [4]Trondheim University Hospital, Norway

Background, Motivation and Objective

In neurosurgery, knowledge of blood flow can be important to avoid damage to vessels or to identify the feeding arteries of arteriovenous malformations (AVMs). Intraoperative ultrasound imaging has proven useful, as brain deformation after skull opening renders preoperative MR images inaccurate. Ideally the surgeon would prefer to work in a navigation scene that portrays 3-D geometry as well as flow velocity and direction. However, due to Doppler angle-dependencies and the complex vascular architecture, detailed 3-D information of flow direction and velocity is currently not available. In this work we attempt to correct for angle-dependencies using a model-based approach.

Statement of Contribution/Methods

A 3-D model of the neurovascular tree was constructed on the fly from registered free-hand 2-D color flow images using an in-house 3-D navigation software based on optical position sensing. A vessel centerline representation was further extracted and used as *a priori* information of vessel orientation. Combined with the registered orientation of each 2-D image plane this allowed for angle-correction of Doppler measurements, and the true principal flow direction and mean velocity was calculated. Increased robustness was achieved by averaging over vessel segments while avoiding near perpendicular beam-to-flow angles.

Results

The accuracy of the approach was tested *in vitro* in a straight tube flow rig, orienting the probe at varying angles relative to the tube. After correcting for the angle an average velocity of 18 cm/s was estimated, compared to a reference mean velocity of 17 cm/s. *In vivo* data from AVM and aneurysm surgery was further acquired and processed offline. In the Fig, an aneurysm is shown, where both directional and velocity information was reconstructed to provide clinically relevant information.

Discussion and Conclusions

The success of model-based angle correction is dependent on accurate vessel segmentations, and further that image planes are not all near-perpendicular to individual vessel segments. The approach is promising for use during neurosurgery where spatial averaging along vessel segments can be used to ensure robust estimates, however, the approach may also have applications in general cardiovascular imaging. Thereby clinically useful information of the true flow direction and velocity in the complex vascular architecture not previously available can be obtained.

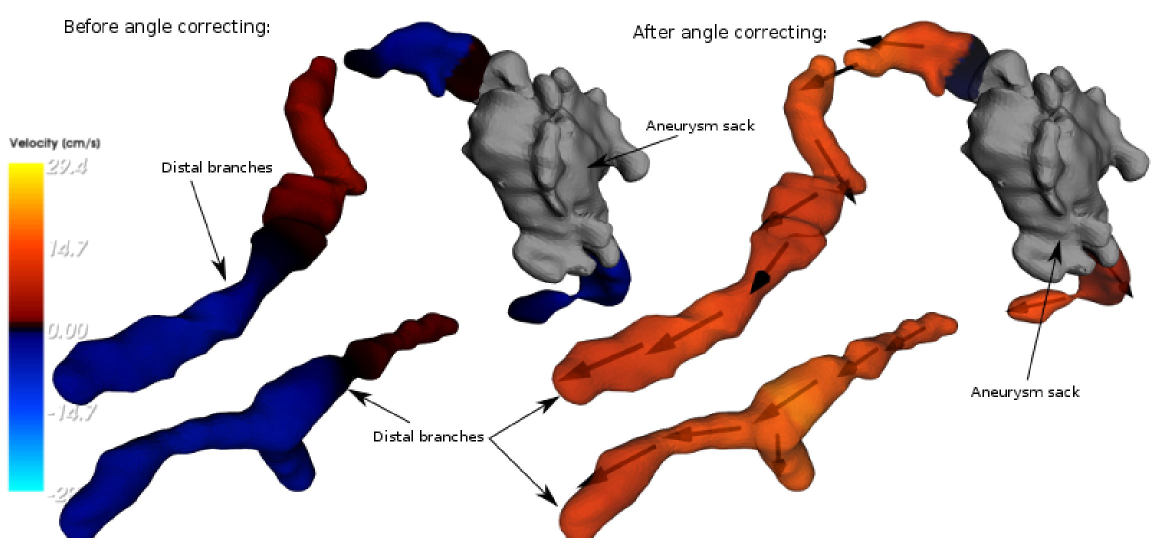

P1Ab-4

Clutter Suppression for Harmonic Doppler Detection in Swept-Scan High-Frequency System

Che-Chou Shen[1], Wu hsin-hsien[1], Chih-Kuang Yeh[2]; [1]Department of Electrical Engineering, National Taiwan University of Science and Technology, Taiwan, [2]Department of Biomedical Engineering and Environmental Sciences, National Tsing Hua University, Taiwan

Background, Motivation and Objective

Swept scanning is commonly utilized in high-frequency Doppler imaging when the array transducer is not available. Conventional swept-scan system suffers from tradeoff between frame-rate and detectability of low-velocity flow. When the lateral scanning speed of the transducer increases to boost the frame-rate, the tissue Doppler signal spectrally broadens and overlaps with the low-velocity flow signal. To remove the tissue clutter, wall-filtering with high cut-off frequency has to be selected that compromises the detection of low-velocity flow. Therefore, the removal or suppression of tissue clutter signal becomes essential in swept-scan system.

Statement of Contribution/Methods

Third harmonic (3f0) transmit phasing utilizes dual-frequency transmission at both fundamental and 3f0 frequencies to reduce tissue harmonic magnitude and thus can provide effective clutter suppression in harmonic Doppler power (HDP) mode. In contrast, the 3f0 transmit phasing can maintain the HDP in the perfusion region when the microbubble contrast agent is used as the harmonic signal source in the blood flow. Reduced clutter signal allows the use of lower cut-off frequency of wall-filtering for detection of low-velocity flow without introducing additional clutter artifacts.

Results

In this study, the swept-scan high-frequency HDP imaging was implemented by transmitting at 16 MHz and 48 MHz and the harmonic signal was received at 32 MHz. The cut-off frequency of wall-filtering varies from full (1) to half (1/2) and quarter (1/4) of its ideal value. Results in flow phantom experiments indicate that the harmonic clutter level is reduced by about 8-dB in 3f0 transmit phasing. Consequently, the resultant HPD image shows reduced clutter artifacts (Fig.(a)) for all cut-off frequencies. With 1/4 wall-filtering, 3f0 transmit phasing already provides comparable signal-to-clutter ratio (SCR) to that of conventional method with full wall-filtering (Fig.(b)). With the low cut-off frequency, 3f0 transmit phasing also improves the color pixel density (CPD) (Fig.(c)) due to the inclusion of more low-velocity flow.

Discussion and Conclusions

This study verifies the clutter suppression can be implemented by using dual-frequency transmit waveform in swept-scan Doppler imaging to reduce clutter artifacts and improve the detection of low-velocity flow.

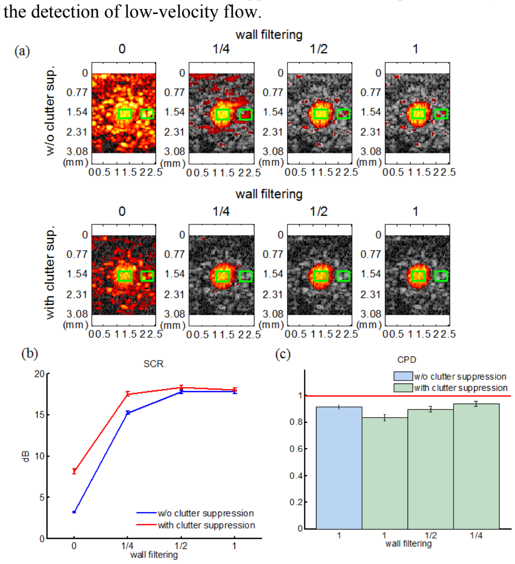

P1Ab-5

Clutter filtering issues in speckle tracking for two-dimensional blood velocity estimation – a potential solution based on compounded imaging

Solveig S. Alnes[1], Abigail Swillens[2], Patrick Segers[2], Hans Torp[1], Lasse Lovstakken[1,3]; [1]MI Lab and Department of Circulation and Medical Imaging, Norwegian University of Science and Technology, Trondheim, Norway, [2]IBiTech-BioMMeda, Ghent University, Ghent, Belgium, [3]St. Olavs Hospital, Trondheim, Norway

Background, Motivation and Objective

Clutter filtering is a major limitation in multi-dimensional blood velocity estimation. For approaches based on the autocorrelation method (ACM), bias is induced in the filter transition region. For speckle tracking (ST), the attenuated signal approach band-pass characteristics which affect speckle appearance. Using ST, only one scan angle is needed to produce an image. A second tilted scan may therefore be added to always ensure a sufficient beam-to-flow angle. In this work, we investigated clutter filter influence on ST, and used these results to set up two tilted scans at minimum angles in order to avoid filter issues with minimum loss of imaging depth.

Statement of Contribution/Methods

Filter influence was studied by simulating scattering from blood following uniform and parabolic velocity profiles with varying angles and velocities (Field II). ST (SAD algorithm) performance was compared to ACM for velocity estimates in the filter transition region (4th order FIR filter). Based on these results a compounded plane wave scan sequence was set up at minimum angles to ensure reasonable ST estimates. By comparing variance and power between the tilted scans, regions obscured by the filter were identified in either scan and avoided in the final 2-D velocity estimate.

Results

Results showed that ST provided reasonable estimates well below the filter cut-off where the ACM had significant bias. At –20 dB attenuation in the transition region, a relative bias of 61% was observed for ACM while 1% for ST (SNR = 30dB). When approaching the filter stop band a significant increase in variance was observed (Figure). Using tilt angles of ±5 deg resulted in a scan setup with twice the image width in depth compared to a typical vector-Doppler setup (±10 deg), and with less clutter filter issues. This was demonstrated for realistic conditions in a simulation of flow in a CFD carotid bifurcation model.

Discussion and Conclusions

A compounded ST setup may be used to provide angle-independent vector-velocity estimates with less clutter filter influence, and without substantially restricting imaging depth in vascular applications. Compared to the ACM, near unbiased estimates were obtained well below the clutter filter cut-off velocity. Further work will focus on implementation on a research scanner for *in vitro* and *in vivo* validation.

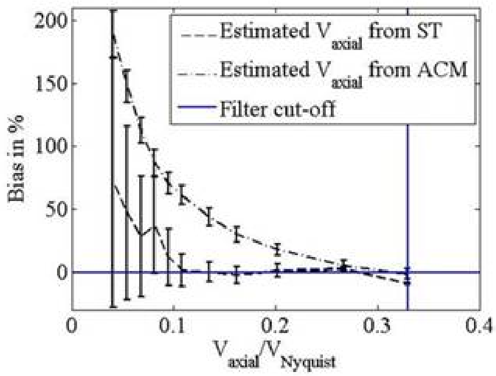

Figure 1: Bias for axial velocity component estimated from ST and ACM

P1Ab-6

3D Velocity Estimation using a 2D Matrix Array

Michael Johannes Pihl[1], Jørgen Arendt Jensen[1]; [1]Center for Fast Ultrasound Imaging, Dept. of Elec. Eng., Bldg. 349, Technical University of Denmark, DK-2800 Lyngby, Denmark

Background, Motivation and Objective

Contrary to conventional methods, the Transverse Oscillation (TO) method is able to estimate the 2D velocity vector of tissue motion and blood flow. The velocity estimates provide new insight in e.g. the disturbed flow patterns in the major arteries; however, the method is currently limited to the 2D velocity components in the scan plane. Therefore, a new method has been developed to measure the 3D velocity vector by use of a 2D phased array matrix transducer. The feasibility of this approach is demonstrated in a simulation study.

Statement of Contribution/Methods

The new method can find the velocity in all directions. In the 3D case, the velocity vector is obtained by estimating the axial velocity component v_z and the two transverse velocity components v_x and v_y. Using Field II, a 3 MHz 64x64 2D matrix array and a 3 MHz 32x32 array are emulated with λ/2 pitch - both employing 1024 channels. Plug flow in a 10x10x10 mm^3 volume centered at (x,y,z)=(0,0,15) mm is simulated with constant speed at 1 m/s at seven different angles in the *XY*-plane: 0, 15, 30, 45, 60, 75, and 90 degrees. Thirty-two emissions at 5 kHz are used per velocity estimate, and the simulations are repeated 10 times for each angle. To evaluate the performance of the method, the mean velocities and the standard deviations, SD, are calculated and compared to the expected velocities.

Results

At a depth of 15 mm, the results for the seven different angles are shown in the figure for the 64x64 and the 32x32 transducer, respectively. The average performance for the 64x64 transducer for all seven angles is: mean speed 0.97 m/s, mean angle difference -0.73 deg, mean SD 0.053 m/s and 0.046 m/s for v_x and v_y, respectively. For the 32x32 transducer, the average performance for all angles is: mean speed 0.93 m/s, mean angle difference -0.64 deg, mean SD 0.11 m/s and 0.11 m/s for v_x and v_y, respectively.

Discussion and Conclusions

The simulations demonstrate that the new method can be used to estimate the 3D velocity vector when using a 2D array. The beamforming is within the capabilities of modern 3D scanners and the estimators for the three velocity components are on the order of the conventional autocorrelation approach with RF averaging making it suitable for commercial implementations.

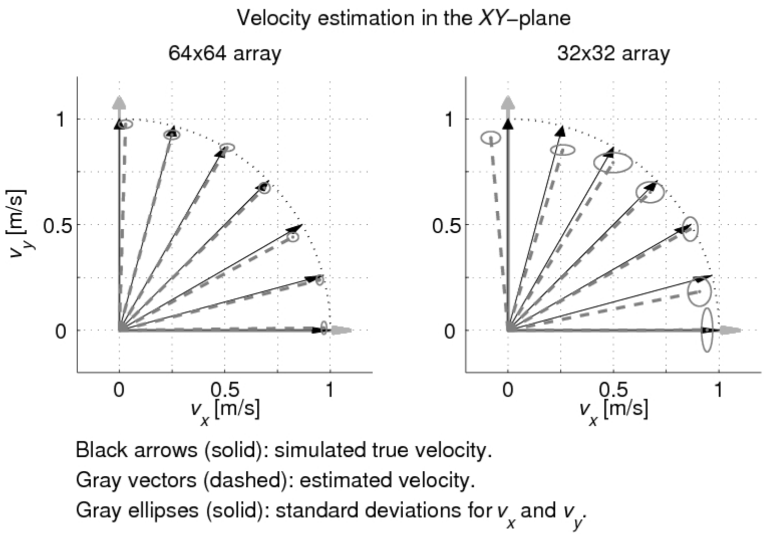

P1Ab-7

Quantification of Mitral Regurgitation Using PW Doppler and Parallel Beamforming

Tonje D. Fredriksen[1], Hans Torp[1], Torbjørn Hergum[1]; [1]MI Lab, Department of Circulation and Medical Imaging, NTNU, Trondheim, Norway

Background, Motivation and Objective

Delayed decision to replace or repair a defective mitral valve may lead to worsening ventricular function. This work takes advantage of the latest developments of ultrasound matrix probes and modern acquisition with many parallel beams to develop a Doppler-based method for quantification of mitral regurgitation.

Statement of Contribution/Methods

We have developed a new method to semi-quantitatively estimate the size of regurgitant jets using spectral Doppler and parallel beamforming. Multiple simultaneous velocity spectra were generated from parallel beams, and combined into a composite, enhanced velocity spectrum. This composite velocity spectrum was colored with a color map representing the number of beams intersecting the jet. A Vivid E9 (GE Vingmed Ultrasound, Norway) equipped with a 4V cardiac probe was modified to acquire 3D high pulse repetition frequency Doppler data with parallel receive beams. Computer simulations and an in vitro model were used for development and testing. The method was also tested on a small number of in vivo data for feasibility.

Results

The figure shows a color spectrum that was generated from an in vivo recording of mitral regurgitation. One plane transmit beam and 16 parallel receive beams were used when recording. The region of interests (ROI) was about 9 x 9 mm. The receive beams had a resolution of 3.6 mm and were equally distributed over the ROI, as shown to the right in the figure. The velocity spectrum is colored red in the low velocity area and green or yellow in the high velocity area. This indicates that all the beams receive signals from slow moving blood during inflow, while only about half of the beams receive signals from the high velocity jet. The algorithm for determining the color of each velocity bin is currently based on thresholding.

Discussion and Conclusions

The spectra give information about the size of the jet, in addition to all the information the cardiologist is used to from a pulsed wave Doppler recording. The thresholding algorithm and the placement of the parallel beams should be optimized in future work. This will be done with the help of computed fluid dynamics simulations together with in vitro recordings.

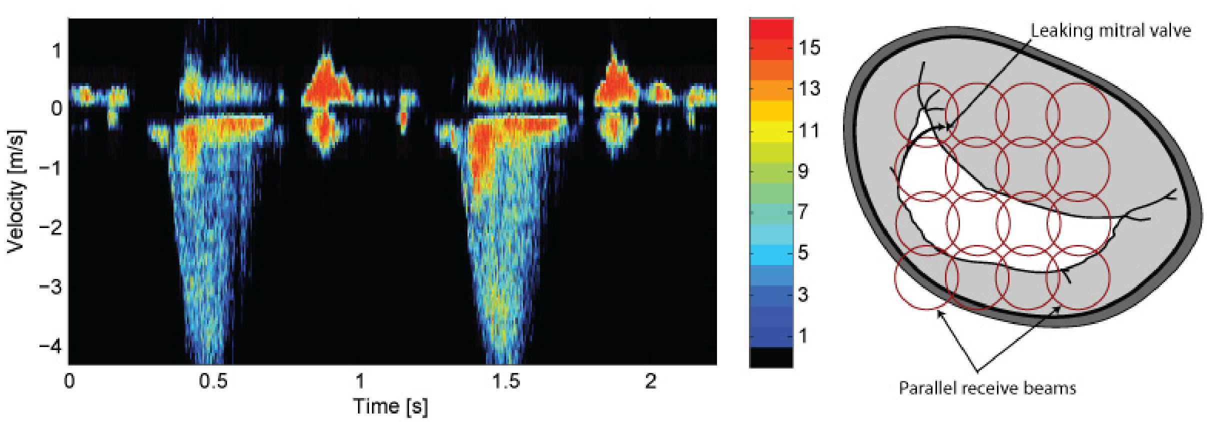

P1Ab-8

Simultaneous quantification of flow and tissue velocities based on multi-angle plane-wave imaging with extended velocity range

Ingvild Ekroll[1], Abigail Swillens[2], Patrick Segers[2], Hans Torp[1], Lasse Lovstakken[1]; [1]MI Lab and Department of Circulation and Medical Imaging, NTNU, Trondheim, Norway, [2]Gent University, Belgium

Background, Motivation and Objective

When quantifying flow velocities or tissue deformation in Doppler imaging, we are often restricted by the limited measurable velocity span. This is particularly challenging when attempting to quantify both simultaneously, as could be of interest in quantitative vascular imaging of arterial disease. Further, angle-dependencies lead to errors that limit the quantitative use of Doppler imaging and make comparisons and follow-up more difficult in patient studies.

Statement of Contribution/Methods

We approach this challenge by using multi-angle plane wave imaging. Utilizing an interleaved packet acquisition with two unfocused transmit pulses separated by 20 deg., high frame rate vector-Doppler estimates are obtained. A high PRF and a large ensemble size allows for a high Nyquist limit while retaining a low clutter filter cut-off frequency. The result is a large measurable velocity span as well as robust vector-velocity estimates. Accuracy of the method was assessed by simulating imaging of a rotating cylindrical phantom (Field II) with varying velocity ranges (0-40 cm/s and 0-4 cm/s), using identical imaging setups (2.5 cycles @ 5 MHz, PRF = 4 kHz, ensemble size = 50). To further demonstrate the potential of the technique, imaging of realistic flow in a CFD model of the carotid artery bifurcation was simulated, where both high and low swirling flows were present simultaneously.

Results

2D velocity fields in both cylindrical and bifurcation phantoms were well depicted (left figure). However, regression analysis of the estimated velocity components in the cylindrical phantom compared to the ground truth indicated a small bias and some underestimation (right figure, SNR of 30).

Slow regime: $v_x = 0.0022 + 0.71 * v_{x,true}$, $v_z = -0.0002 + 0.95 * v_{z,true}$

Fast regime: $v_x = 0.034 + 0.87 * v_{x,true}$, $v_z = -0.0047+ 0.90 * v_{z,true}$

Discussion and Conclusions

Using multi-angle plane-wave imaging and a high ensemble size, robust angle-independent Doppler estimates may be achieved with a wide measurable velocity span at high frame rates. Thus, both tissue deformation and blood velocities may be estimated simultaneously in a 2D region of interest. Further work will focus on *in vivo* implementation and application in a research scanner.

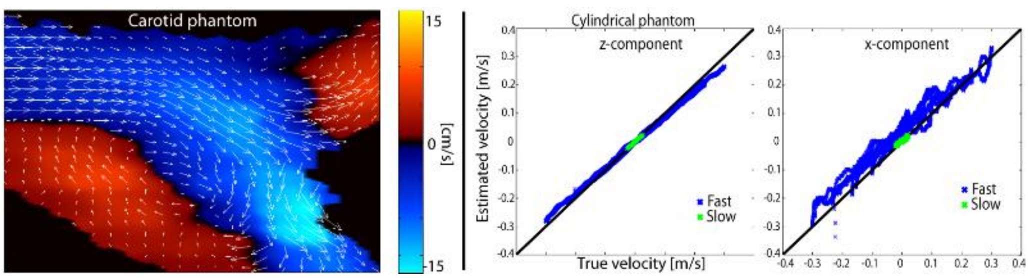

P1Ab-9

Numerical simulation of time for red blood cell aggregation under pulsatile flow with depletion model

Ying Li[1], Tae-Hoon Bok[1], Dong-Guk Paeng[1,2]; [1]Ocean System engineering, Jeju National Univeristy, Korea, Republic of, [2]Interdisciplinary Postgraduate Program in Biomedical Engineering, Jeju, Korea, Republic of

Background, Motivation and Objective

Shear rate is known to be a determining factor for red blood cell (RBC) aggregation and thus has significant effects on ultrasound backscattered power from blood. But shear rate could not fully explain the cyclic variation of backscattered power from blood under pulsatile flow. The flow acceleration was suggested as another hemodynamic factor to enhance the RBC aggregation and thus backscattered power from blood. In this study, two RBCs were placed along a streamline under pulsatile flow, and the time for two RBCs to form a rouleau was numerically simulated with depletion model. It aims to test if the flow acceleration would enhance the RBC aggregation by a numerical simulation.

Statement of Contribution/Methods

Based on the depletion model, an analytical method to describe the interaction energy between RBCs was proposed by Neu and Meiselman (2002), and further developed by Fenech et al. (2009). In this study, the time required for two RBCs to form a rouleau was calculated by the method of Fenech et al. In order to reduce calculation cost, the blood viscosity was assumed as a low value. The blood flow was simulated as a sinusoidal flow with a minimum speed of 20cm/s and maximum speed of 80cm/s. The stroke rate of blood flow was changed from 50 beats per minutes (BPM) to 70 BPM. Two RBCs were placed at a distance of 1μm, 20μm and 100μm. The initial velocity of the two RBCs was set to 0 m/s.

Results

The required times for two RBCs to form a rouleau at different stroke rates and initial distances were summarized in Table 1. It demonstrated that the RBC aggregation time is increasing with the increase of initial distance, but decreasing with the increase of stroke rate. It suggests that the increased stroke rate may enhance RBC aggregation.

Discussion and Conclusions

In our previous in vitro and in vivo studies, flow acceleration is hypothesized to enhance the RBC aggregation under pulsatile flow to produce the cyclic variation of the backscattered power and verified by experiments. This numerical simulation supports that the increased HR may enhance RBC aggregation due to its effects on flow acceleration.

Table 1. Summary of RBC aggregation time for two RBCs

Stroke rate	50 BPM	55 BPM	60 BPM	65BPM	70 BPM
d=1μm	0.083s	0.078s	0.074s	0.071s	0.068s
d=20μm	0.118s	0.111s	0.105s	0.099s	0.095s
d=100μm	0.154s	0.143s	0.134s	0.126s	0.120s

P1Ab-10

Effect of flow gradient, ROI size and random scatterer movement during speckle size estimation based blood flow measurement

Tiantian Xu[1], Gregory Bashford[1]; [1]Biological Systems Engineering, University of Nebraska-Lincoln, Lincoln, NE, USA

Background, Motivation and Objective

Recently, a new method of ultrasonic blood flow velocity estimation was developed by measuring the change in speckle size due to the direction and spatial rate of scanner A-line acquisition. Quantitative investigation on the effect of flow gradient, ROI size and random scatterer movement on the estimation performance was studied to give recommendations on how to optimize blood flow measurement based on speckle size estimation.

Statement of Contribution/Methods

The Field II program was used to simulate blood flow data in the common carotid artery with four flow conditions: plug flow, parabolic flow, plug flow with random scatterer movement and parabolic flow with random scatterer movement. Different ROI sizes (varying from 5 to 60 times the lateral speckle cell length laterally and 1 to 4 times the axial speckle cell widths axially), flow gradients (selected from 7 positions in the parabolic flow profile) and random scatterer movement (Gaussian noise added to the scatterers' positions with a standard deviation as much as one-tenth of the speckle cell size) were used during estimation to evaluate their effect on blood flow measurement.

Results

Fig. (a), (b), (c) and (d) show the relationship between the estimation error and ROI size, showing that the estimation error decreases and approaches an asymptote at the optimal ROI in the flow without a flow gradient. When a flow gradient is introduced, a lateral optimal ROI size exists and the estimation error increases with axial ROI size. Fig. (e) and (f) show the relationship between the estimation error and flow gradient, showing that the estimation error increases with increasing flow gradient and introduction of random scatter movement.

Discussion and Conclusions

When blood flow is relatively stable (little or no flow gradient), the optimal ROI size is about 2.5 axial speckle cell widths axially and 30 lateral speckle cell lengths laterally. When a flow gradient is introduced, the optimal ROI size is about one axial speckle cell width axially and 35 lateral speckle cell lengths laterally. The average estimation error is increased by a factor of three as a result of scatterer random movement. These results permit recommendations of parameter setting when estimating blood flow by speckle cell size changes.

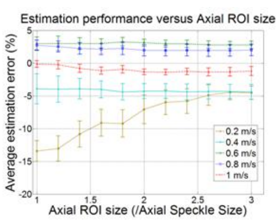

(a)

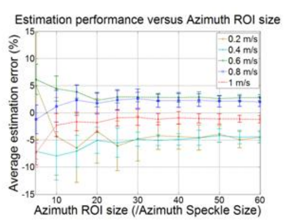

(b)

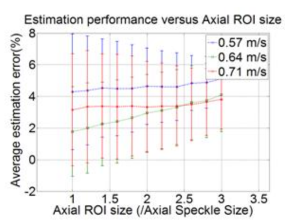

(c)

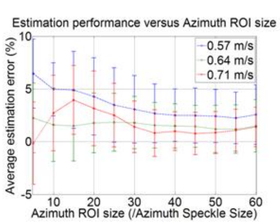

(d)

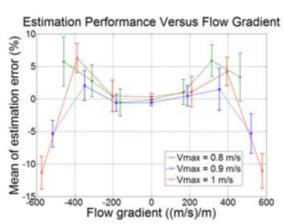

(e)

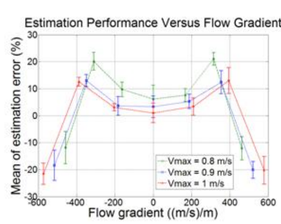

(f)

P1Ac - System Design

Carribean Ballroom III-V

Wednesday, October 19, 2011, 9:30 am - 1:00 pm

Chair: **Andrzej Nowicki**
Polish Academy of Sciences

P1Ac-1

A Digital-Feedback Pre-distortion Technique for Integrated High-Voltage Ultrasound Transmitting Power Amplifiers

Zheng Gao[1], Zao Chen[1], Ping Gui[1], Xiaochen Xu[2], Max Nielsen[2], Ismail Oguzman[2], Karthik Vasanth[2], Jikai Chen[3]; [1]Department of Electrical Engineering, Southern Methodist University, Dallas, Texas, USA, [2]Texas Instruments Inc., Dallas, Texas, USA, [3]Department of Electrical Engineering, University of Florida, Gainesville, Florida, USA

Background, Motivation and Objective

Ultrasound systems require high-voltage (HV) transmitters to excite the transducers. Compared to digital pulsers, class-AB power amplifiers have many advantages, such as lower harmonics and the capability of generating complex arbitrary waveforms for Coded-Excitation Mode and other advanced ultrasound imaging modes. However, the need to suppress cross-over distortion and achieve high slew-rate usually introduces large biasing current. This significantly degrades the power efficiency of the system, limiting the number of integrated channels in a single package.

Statement of Contribution/Methods

This paper presents a digital feedback pre-distortion system for ultrasound HV class-AB PA to reduce the harmonic distortions while at the same time improving the power efficiency. The proposed system searches the error coefficients of the output feedback signal using the least-mean-square (LMS) algorithm, and stores the error data in the look-up table (LUT) memory. On the next cycle the errors are used to equalize the ideal input waveforms with the negative harmonic components to cancel the amplifier's non-linear response. The proposed algorithm applies to both sine-wave with the constant amplitude and the Morlet Wavelet.

Results

The measurement results show that the proposed pre-distortion system reduces the second-order harmonics (HD2) in the output sine-wave signals by 20 dB and the third-order harmonics (HD3) by 15 dB, while increasing the amplifier power efficiency by 18%.

Discussion and Conclusions

The proposed technique reduces the nonlinear higher-order effects of the PA to improve the ultrasound transmitting signal fidelity, relieving the requirement on amplifier biasing current. The system requires zero additional hardware by utilizing the high-speed ADC in the receiver analog front end.

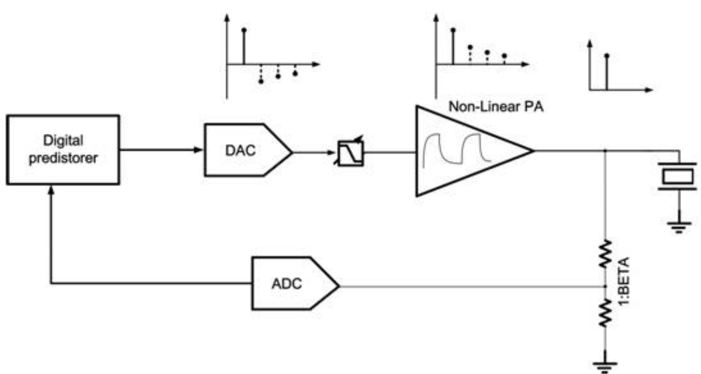

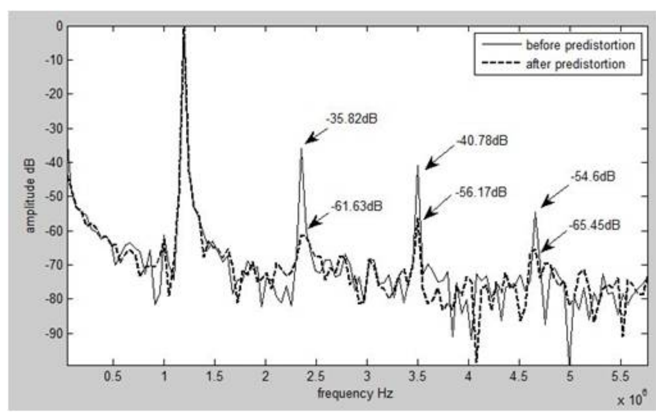

P1Ac-2

Harmonic Cancellation in Switched Mode Linear Frequency Modulated (LFM) Excitation of Ultrasound Arrays

David Cowell[1], Peter Smith[1], Steven Freear[1]; [1]Ultrasound Group, School of Electronic Engineering, University of Leeds, Leeds, United Kingdom

Background, Motivation and Objective

Ultrasound array systems are used in a wide range of applications from non destructive evaluation to medical diagnostics and therapeutics. Excitation signal integrity is critical in demanding applications such as harmonic imaging where the transmitted ultrasound wave must not contain harmonics. Consequently, excitation circuitry typically requires an arbitrary waveform generator and high frequency power amplifier. In array systems containing many channels this presents a significant challenge for the system designer.

Ultrasound pulser integrated circuits (IC) combine low voltage drive circuits with high voltage and current MOSFETs to allow switched mode excitation in a single low cost IC. Switched mode excitation signals contain harmonics that distort the shape of the ultrasound wave, reduce energy at the fundamental frequency and cause additional lobes in the transmitted field. This work presents a method for cancelling harmonics in frequency modulated switched excitation systems using multiple excitation voltages and precise switching timing especially suited to array excitation.

Statement of Contribution/Methods

A multilevel switched excitation scheme is demonstrated exploiting a direct correlation between harmonic cancellation and the number of excitation voltages. Harmonic cancellation in both tone and LFM signals is experimentally demonstrated for two, three, five and nine level switched excitation modes using a custom 48 channel excitation system consisting of MAX4811 high voltage pulser ICs driven by an Altera Cyclone III FPGA. The performance of each switched excitation mode is compared against that of a conventional arbitrary waveform generator and linear power amplifier.

Results

The figure shows excitation waveforms and spectra for each switched excitation mode. All odd harmonics of the fundamental LFM excitation signal are present in the 2 level excitation signal. Harmonics are iteratively cancelled in each excitation scheme until the 9 level signal contains no harmonics below the 11th harmonic.

Discussion and Conclusions

A switched excitation method with reduced harmonic distortion is proposed enabling excitation across multiple channels where high frequency linear power amplifier based systems are impractical. A switched excitation system with 9 levels has been presented with performance comparable to a high frequency linear power amplifier.

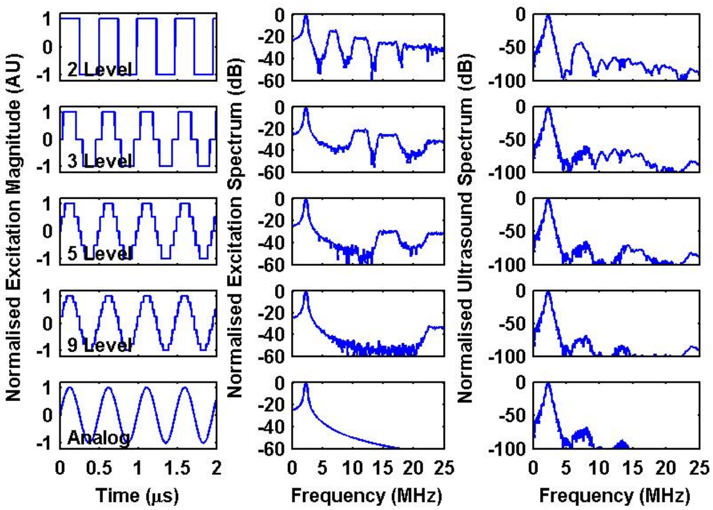

P1Ac-3

A Low-Cost High Frame-Rate Piezoelectric Scanning Mechanism for High-Frequency Ultrasound Systems

Andre Bezanson[1], Robert Adamson[1], Jeremy Brown[1]; [1]Biomedical Engineering, Dalhousie University, Halifax, Nova Scotia, Canada

Background, Motivation and Objective

Although there has recently been a great deal of progress in the development of high-frequency linear array transducers, there is still strong interest in developing imaging systems based on mechanically scanned transducers such as annular arrays and single-element geometrically focused transducers. This is primarily due to the fact that annular arrays and single-element focused transducers can be manufactured at a much lower cost. As annular arrays and single-element transducers can only focus the ultrasound energy down the central axis, a scanning mechanism is required to laterally translate the transducer and collect the parallel lines of sight. Conventional scanning mechanisms in high-frequency imaging systems are based on electromagnetic motors that can achieve lateral translations on the order of a centimeter at frame-rates up to 150 fps. Some drawbacks associated these motors, however, are that they can be expensive, relatively bulky, and typically require an encoder in order to accurately feedback position information.

This work is focused on the development of a small, low-cost scanning system utilizing a piezoelectric bimorph and an in-line lever mechanism. This design can achieve large deflections at high frame rates and has the advantage of being fabricated into a long narrow package. As the scanning is based on a piezoelectric actuator, the position can also be predicted without an encoder at scanning frequencies below the first resonance.

Statement of Contribution/Methods

A prototype scanning mechanism has been designed, fabricated and its performance has been characterized. A single-element focused transducer has been mounted on the tip of the scanning mechanism. The bi-morph actuator was driven through an audio amplifier and the velocity and relative phase of the transducer was measured using a laser Doppler vibrometer (Polytec CLV 3000). Finally, preliminary images were collected by pulsing/receiving the transducer using a high-frequency pulse generator (Daxsonics, Halifax, NS) and capturing the signal through a digitizer card controlled by Labview.

Results

Laser Doppler measurements have shown that our piezoelectric scan head is able to achieve frame rates of up to 220 fps. When driven at the resonance frequency of 110Hz (220 fps) the mechanism can achieve maximum deflections of up to 2 cm. Below resonance, a 1 cm scan width can be easily achieved. Additionally, the transducer phase remains within +/- 2º of the drive signal up to 60 Hz.

Discussion and Conclusions

A low-cost high-frame rate piezoelectric scanning mechanism has been successfully fabricated into a small package. A lateral translation of 1 cm can be easily achieved up to the first resonance of the transducer, resulting in a maximum frame rate of 220 fps. The reliability of the phase shift suggests that a position encoder is not necessary up to a frequency of 60Hz.

P1Ac-4

A Low Cost Receive Beamformer for a High Frequency Annular Array

Holly Lay[1,2], Geoffrey Lockwood[1]; *[1]Queen's University, Canada, [2]Sonavation Inc., USA*

Background, Motivation and Objective

High frequency ultrasound imaging systems can be costly to develop due to the more stringent analog design requirements and higher sampling rates. Advances in consumer electronics and computer processors, however, have allowed the development of beamformers which are low cost and easily adapted to custom applications. We have developed a software beamformer which uses a new interpolation scheme to reduce the sampling rate while maintaining secondary lobes that are suppressed by approximately 60 dB with respect to the main lobe.

Statement of Contribution/Methods

A 7-channel receive beamformer for a 20 MHz annular array was implemented using an Analog Devices AD9272 octal ADC evaluation board and ADC-HSC-EVALC FPGA acquisition board with a total cost of <$1200 (US). Data was sampled at 80 MHz and 12 bits and transferred to a PC using a USB cable. Digital filters and amplifiers built into the AD9272 were controlled using software supplied by the manufacturer running on the host PC. The sampled data was interpolated using a 20 MHz sine-wave. By using look-up-tables and by sampling at four times the centre frequency, the computation cost of the interpolation calculation was similar to that of linear interpolation. The interpolation algorithm and subsequent beamforming were coded in MATLAB, allowing application specific customization.

Results

The software based receive beamformer was evaluated initially using simulated data and the performance of the sine-wave interpolation and linear interpolation were compared. Simulated data for a linear array with a 64-element active aperture focused at f/2 was also processed. A 5 dB decrease in secondary lobes was found for an annular array using the sine interpolation compared to linear interpolation while a 10 dB decrease in secondary lobes were found for a linear array. The software beamformer was capable of 20 frames/sec. To test the hardware, a 7-element 20 MHz annular array was connected to the beamformer and a series of wire targets were imaged in a water tank. The beamformed data displayed 60 dB of dynamic range and the beamformer operated at 10 frames/second, limited only by the USB interface.

Discussion and Conclusions

A real-time software beamformer for a 7-element 20 MHz annular array has been developed which can be implemented using inexpensive commercially available hardware. The system is easy to customize and required very little development time.

P1Ac-5

Implementation of non standard methods with the Ultrasound Advanced Open Platform (ULA-OP)

Enrico Boni[1], Luca Bassi[1], Francesco Guidi[1], Alessandro Ramalli[1], Stefano Ricci[1], **Piero Tortoli[1]**; [1]*Electronics & Telecomm., Università di Firenze, Firenze, Italy*

Background, Motivation and Objective

The ULtrasound Advanced Open Platform (ULA-OP) was recently developed as system specifically dedicated to research (IEEE Trans. UFFC, 56:10, 2207-2216, 2009). In this paper, we report the main results of this development, obtained in the last two years either internally, through the implementation of non-standard working modes, or connected to the collaboration with external partners.

Statement of Contribution/Methods

ULA-OP was developed with the specific goals of enabling: a) arbitrary transmission patterns; b) the implementation of new working modalities (including real-time); c) the access to raw echo-data at each point of the receiver chain. Special efforts were dedicated to maintain small dimensions, so that the system could be duplicated and delivered to external partners.

Three case studies, demonstrating the fulfilment of the initial specifications, will be reported.

The benefits deriving from the decision of making the system available to other laboratories will also be discussed.

Results

An original real-time vector Doppler technique capable of continuously tracking the flow direction was implemented. The technique is currently used in 5 clinical centers participating in the EU SUMMIT project, to identify surrogate markers of vascular diseases in diabetic patients.

Raw brachial artery echo-data concurrently obtained in B-Mode and Doppler multigate-Mode were processed to measure, for the first time, both the stimulus (wall shear stress increase) and the effect (diameter enlargement) in Flow Mediated Dilation (FMD) studies. Significant results were obtained from 15 volunteers, and a larger study is in progress.

A novel frequency domain displacement estimation method, coupled with the high-frame rate imaging modality, was shown to provide improved quasi-static elastograms. The method is presently employed in a clinical study for the investigation of breast lesions.

Finally, the ongoing collaborations with international partners on stimulating topics such as 2D array-based imaging, synthetic focussing, adaptive beamforming and contrast imaging, represent, by themselves, a major result of ULA-OP development.

Discussion and Conclusions

In each of the aforementioned applications, the hardware and software resources of ULA-OP were differently exploited, showing that the system is a nice tool to implement non standard US modalities. As far as we know, ULA-OP represents a rare example of advanced US instrument developed in a University laboratory and made available to the entire scientific community. The latter choice is proven really beneficial, as it is helpful not only to raise the funds necessary for research, but also to facilitate the exchange of ideas with worldwide US experts and to address our efforts to continuously improve the system functionality.

P1Ac-6

Portable 4D Ultrasound Medical Diagnostic Imaging System

Yi-Ting Shen[1], Stergios Stergiopoulos[1,2], Pang Shek[1]; [1]Defence R&D Canada Toronto, Toronto, Ontario, Canada, [2]Department of Electrical and Computer Engineering, University of Toronto, Toronto, Ontario, Canada

Background, Motivation and Objective

Portable real-time 3-Dimensional (4D) ultrasound imaging systems are considered by medical practitioners to be exceedingly helpful for trauma care in austere environments. They have the capabilities to provide rapid diagnosis of non-visible internal injuries and assist in image guided interventions with minimal requirements for training. However, there is a trade-off between system portability and image resolution due to the hardware complexity that is associated with the required large number of transducers in a planar array. The objective of this project is to miniaturize for field deployment an ultrasound system that is field deployable and supports a planar array with 32x32 transducers and with improved angular image resolution to be approximately equivalent to that of a 64x64 planar array. This angular image resolution improvement is based on a proprietary 3D adaptive beamformer that has been implemented in a highly parallelized computing architecture. This paper describes the components of a fully digital real-time 3D ultrasound system, including the transmission functionality, the efficient 3D beamforming implementation, and its mapping into a multi-processor (high-end Field Programmable Gate Array (FPGA)) platform.

Statement of Contribution/Methods

The computational intensity of the standard beamforming process for 4D ultrasound imaging systems is a major limitation for achieving real-time system performance. Algorithms for 3D beamforming present high memory and processing power requirements, and are not inherently given to parallelization. The 3D adaptive beamforming algorithm here presented has been developed for 4D ultrasound systems, and assumes a 2D planar sensor aperture. The method is based on the decomposition of the 3D beamforming process for a regular two-dimensional array into two steps of simpler 2D beamforming of standard linear phased array processing. The proposed decomposition of the 3D beamforming allows for the parallelization of the required processing. The system design consists of a 32x32 element planar phased array and a cluster of eight high performance FPGAs. The digital design of inter-element transmission delays allow for coding multiple frequency regimes to provide transmission focusing at multiple depths on a single firing.

Results

Results demonstrate that the angular image resolution of reconstructed 3D volumes from a 32x32 planar array has an approximately 14% coarser resolution than that of an equivalent 64x64 planar array.

Discussion and Conclusions

The presented results confirm the validity of the proposed methods both for coded phased array energy transmission, and for the efficient real-time 3D adaptive beamforming for a 32x32 planar array, as well as the feasibility of implementing this complex beamforming algorithms on a fully digital real time computing architecture providing 20 volumes per second.

P1Ac-7

Real-Time GPU-Based Adaptive Beamformer for High Quality Ultrasound Imaging

Junying Chen[1], Billy Y. S. Yiu[2], Hayden K. H. So[1], Alfred C. H. Yu[2]; [1]*Dept. of Electrical and Electronic Engineering, The University of Hong Kong, Hong Kong,* [2]*Medical Engineering Program, The University of Hong Kong, Hong Kong*

Background, Motivation and Objective

Whilst the feasibility of applying adaptive beamforming methods to medical ultrasound imaging has been theoretically considered, their practical realization remains a significant challenge that has yet to be overcome because of their high computational demand. Software-based implementation of these methods using multi-core graphics processing units (GPUs) may represent a viable solution, especially since the current ultrasound system design trend increasingly favors software implementation of processing algorithms. This forms the strategic objective of this work.

Statement of Contribution/Methods

We have developed a GPU-based adaptive beamformer that can operate on commercial GPUs targeted for the high-performance, mobile, and sub-mobile markets. In this beamformer, the apodization weights used to form each pixel were adaptively computed using a minimum variance (MV) optimization technique based on the corresponding set of focus-delayed channel-domain data samples (i.e. the channel data vector) in an M-channel aperture. This involved four major processing stages. First, a Hankel data matrix was formed from the channel data for a series of lag-one overlapping size-L sub-apertures. Second, the data covariance matrix was found by computing the outer product of the Hankel matrix and its transpose. Third, the matrix inverse was found using a Gaussian elimination computational algorithm. Lastly, the apodization weights were estimated according to the MV constraint, and the pixel value was calculated as the absolute average of all sub-apertures' individual weighted sum for the corresponding channel data vector segment. To reduce processing latency on the GPU, the channel data vector of each pixel was fetched to the fast-access shared memory allocated to the corresponding computational core. Also, the symmetry of the Hankel matrix was exploited to reduce the actual amount of computational load. As a performance analysis, our adaptive beamformer was evaluated on three different platforms equipped with these GPUs: 1) high-performance class GTX-480; 2) notebook class 9600M; 3) sub-mobile class ION2. Their execution time was analyzed using the built-in timing functions in the GPU application programming interface.

Results

For a 32-channel aperture with 8-channel sub-apertures, real-time processing throughput was found to be achievable with the GTX-480 GPU (~28 fps). The use of 16-channel sub-apertures reduced the performance to 20 fps. The 2 mobile-class GPUs processing throughput were found to be unready for real-time execution unless further optimizations were developed. Such is also crucial for extending adaptive beamforming to larger aperture sizes.

Discussion and Conclusions

As the use of GPUs in ultrasound imaging systems become more prevalent, real-time realization of adaptive beamforming algorithms should eventually become possible. In turn, significant improvements in the quality of ultrasound images can be expected.

P1Ac-8

A 1.5mm Diameter Single-Chip CMOS Front-End System with Transmit-Receive Capability for CMUT-on-CMOS Forward-Looking IVUS

Gokce Gurun[1], **F. Levent Degertekin**[1], Paul Hasler[1]; [1]*Georgia Institute of Technology, Atlanta, GA, USA*

Background, Motivation and Objective

Integration of receive and transmit electronics and transducer array elements on a single chip is critical for successful implementation of a highly flexible forward looking (FL) IVUS imaging catheter. Single chip integration reduces the interconnect complexity significantly, and enables ultimate miniaturization of IVUS arrays. However, it is challenging to fit the transmit and receive circuitry under a tight donut shape with an outer radius of 1.5 mm (Fig 1-left). Here we describe the design and initial testing of a CMOS IC to implement a single chip fully integrated imaging system using CMUT-on-CMOS technology [1].

Statement of Contribution/Methods

We designed and fabricated an IC in 0.35 µm CMOS for monolithic integration with a 1.4 mm diameter 15 MHz center frequency FL-IVUS dual-ring array including 56Tx and 48Rx CMUT elements. The chip fits into a size of 1.5 mm diameter silicon donut with a 430 µm gap left inside for a guide wire (Fig. 1-right). The IC includes 56 pulsers capable of generating 35 V pulses and a low noise receiver transimpedance amplifier for each of the 48 CMUT array elements. The amplifiers are designed with a 55*25 um2 area and with a 0.75 mW per amplifier power consumption. The chip also includes multiplexers, buffers and a digital control circuitry. The chip requires only 12 external connections and provides 4 parallel RF outputs. The average power consumption of the chip is reduced to 20 mW by biasing off the unused receive amplifiers using the digital logic.

Results

The single chip front end system for FL-IVUS has been designed and implemented. Initial measurement results of the amplifiers demonstrated a gain of 800 kΩ with a 20 MHz bandwidth. The input referred current noise level is 260 fF/√Hz with 250 fF CMUT capacitance. This figure is on the order of the thermal mechanical noise of the CMUT elements, critical for the SNR of the system. Further testing and characterization results of the IC after monolithic integration with the FL-IVUS CMUT array will also be presented.

[1]: M. Hochman, J. Zahorian, S. Satir, G. Gurun, T. Xu, M. Karaman, P. Hasler, F. L. Degertekin, “CMUT-on-CMOS for Forward-Looking IVUS: Improved Fabrication and Real-Time Imaging,” IEEE Ultrasonics Symposium, 2010.

Discussion and Conclusions

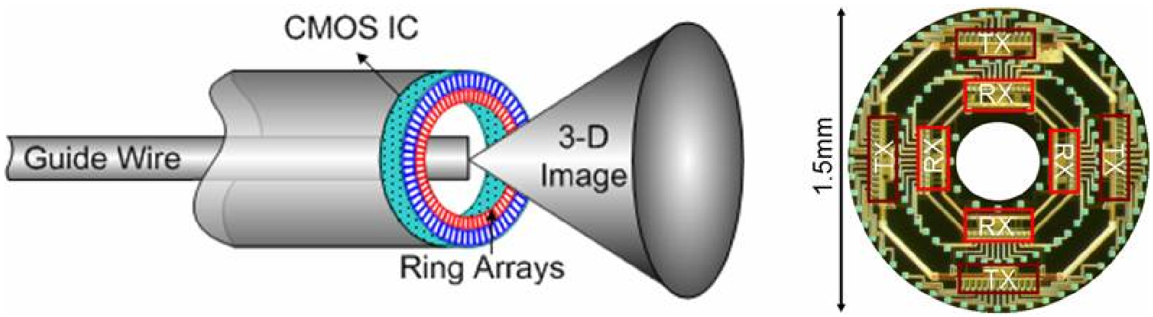

P1Ac-9

A Happy Marriage of Ultrasonography and Near Infrared Spectroscopy in Coronary Imaging

Zhihua He[1], Steve Sum[1], Cory Doucet[1], Brian Gilan[1], Antonius F.W. van der Steen[2,3], James Muller[1]; [1]InfaRedx Inc, Burlington, MA, USA, [2]Biomedical Engineering, Thorax centre ErasmusMC, Netherlands, [3]Interuniversity Cardiology Institute of the Netherlands, Netherlands

Background, Motivation and Objective

Coronary artery disease (CAD) is one of the leading causes of death in developed countries. Histopathological evidence suggests that the rupture of coronary artery plaques with a lipid core and thin cap are the cause of most acute coronary syndromes.

Intravascular ultrasound (IVUS) is useful for structural imaging, but offers limited compositional information. Intravascular near-infrared spectroscopy (NIRS) is ideal for detecting lipid, but provides limited structural information.

The world's first multi-modality intravascular imaging system has recently been cleared by the FDA, it can simultaneously collects NIR and ultrasound data, providing co-registered chemical and structural information in a single pullback.

Statement of Contribution/Methods

We examined NIRS-IVUS pullbacks in a total of 11 blood-perfused coronary artery specimens. Following scanning, histologic sections were prepared at 2 mm intervals. The NIRS-IVUS catheter incorporates fiber optic light delivery and a 40 MHz ultrasound transducer. The core rotates at 960 rpm with pullback speed of 0.5mm/s. Each scan generates a 2D map (chemogram) of LCP composition and sequence of ultrasound transverse images, which were compared with corresponding histology.

Results

Based on histology, the combination of NIRS and IVUS provided a more complete characterization of CAD than would otherwise have been possible with either modality alone.

In Figure: Top: Chemogram map with x-axis the linear location, y-axis the rotation angle. LCP is yellow and outliers (e.g. guide wire) are black. Middle: Transverse IVUS with chemogram overlay at selected linear location. Bottom: Histology slides. Three cases are presented. Left: No LCP by NIRS, Calcium by IVUS, calcified fibrous by histology. NIRS and IVUS each correctly identify components of the plaque. Middle: LCP by NIRS, large plaque with calcium by IVUS, Large LCP with thin cap by histology. This is a plaque that may not have been identified as high-risk by IVUS alone. Right: LCP by NIRS, minor plaque by IVUS, fibroatheroma with thick cap and small volume by histology. NIRS alone may have overestimated the risk of this plaque

Discussion and Conclusions

The combination of NIRS and IVUS in a single catheter allows for simultaneous, co-registered compositional and structural assessment of CAD, enabling an unprecedented ability to characterize coronary artery plaques.

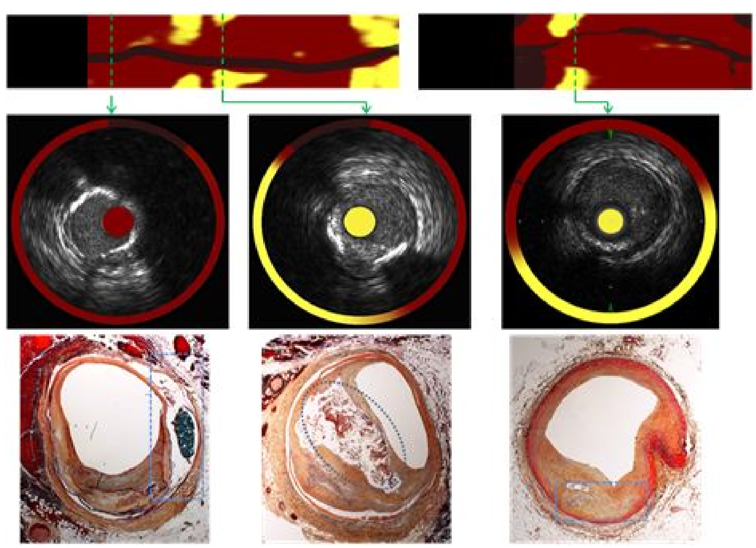

P1Ac-10

Bone scanner for examination of deeply located trabecular bones

Jerzy Litniewski[1], Lucyna Cieslik[1], Marcin Lewandowski[1], Ryszard Tymkiewicz[1], Boguslaw Zienkiewicz[1], Andrzej Nowicki[1]; [1]*Ultrasound, Institute of Fundamental Technological Research, Warsaw, Warsaw, Poland*

Background, Motivation and Objective

The femoral neck fracture often occurs in osteoporosis and leads to severe complications. Therefore assessment of femoral bone microstructure and condition is important and essential for the osteoporosis diagnosis and treatment monitoring. As far the only in vivo measurements were carried out in transmission. Mostly, they concerned the attenuation estimation in the heel bone. We have developed the ultrasonic scanner dedicated for acquiring the RF (Radio Frequency) echoes, backscattered not only from calcaneal bone but from the deeply located bones, as well. This study presents the scanner and preliminary results of the evaluation of attenuating properties of femoral neck bone.

Statement of Contribution/Methods

The bone scanner is based on the concept of absolute minimizing of electronics and computations executed solely on the main computer processor and the graphics card. The electronic module of encoder-digitizer executing all the transmission and reception functions is based on a single low-cost field programmable gate array chip. The scanner was equipped with the probe with mechanically wobbling concave transducer operating at the frequency from 1MHz to 1.7MHz and producing the sector scan within ±14 deg. The applicability of the scanner for the data acquisition from the bones other than the heel bone was validated in in vivo experiment. Data were recorded in trigonum femorale area approaching the bone trough the skin, subcutaneous tissue and the muscles (iliopsoas and rectus femoris). The system gain together with the Time Gain Compensation were carefully adjusted to obtain uniform brightness within the ROI in trabecular bone B-scan image. This procedure highly increased the dynamic range of the registered RF echoes that were farther processed in order to determine the normalized broadband ultrasonic attenuation (nBUA).

Results

The experimental measurements showed that the scanner could be used for collecting the backscatter from the trabecular bones located deep in the body. The calculated averaged nBUA equaled to 4.1 ± 0.55 dB/MHz×cm and it is in the range of the nBUA determined in vitro for trabecular bone of femoral neck using the transmission technique. However, it is relatively low as one would expect considering the useful length of backscattered echoes limited to 15µs - 25µs what corresponds to 11mm - 18mm depth of the bone.

Discussion and Conclusions

The novel versatile ultrasonic scanner dedicated for the bone research was developed. Light and easy to manipulate scanner probe allows the operator for recording the ultrasonic signals from the optimal projection. The ultrasonic data provided by the scanner will be useful in developing the processing techniques designed for the estimation of attenuation including compensation of diffraction, encountered by the wave at the soft tissue/bone interface. This diffraction is probably responsible for the low value of nBUA determined in the presented examination.

P1Ac-11

Novel limiter using bipolar power transistor for high frequency ultrasonic transducer applications

Hojong Choi[1], Hao-Chung Yang[1], Sien-Ting Lau[1], Qifa Zhou[1], K. Kirk Shung[1];[1]NIH Transducer Resource Center and Biomedical Engineering, University of Southern California, Los Angeles, California, USA

Background, Motivation and Objective

Diode limiters have been widely used to protect front-end circuits from high voltage signals from pulsers, but they can sometimes degrade the performance of a receiver [1]. We propose a new limiter design using bipolar power transistors for high frequency ultrasonic transducer applications. These bipolar transistor devices are NPN and PNP silicon power transistors that can provide on-state low impedances and high breakdown voltage capability. The response time of the NPN bipolar transistor is shorter than the PNP bipolar transistor such that one more NPN bipolar transistor is connected on the top of the PNP bipolar transistor in order to reduce the mismatch of response time. Compared to the diode limiter, these devices can be a good alternative providing lower signal distortion.

Statement of Contribution/Methods

The new limiter using NPN(ZTX453) and PNP(ZTX553) power transistors has been implemented in a pulse-echo measurement and its performances is compared to that of the diode limiter (MATEC, DL-1). The Pulser(AVTECH, AVB2-TE-C) was used to trigger the 100MHz single element transducer and the received echo was sent through the limiter and preamplifier. The pulse-echo responses were evaluated using a quartz target in a water tank. The waveforms at time-domain with peak-to-peak voltage recorded in the oscilloscope and the spectra were calculated using Matlab software.

Results

For the new limiter using bipolar power transistor, its -6dB bandwidth has been improved by 6% and peak-peak voltage of echo signals increased 2.6 times compared to the diode limiter.

Discussion and Conclusions

The results show that a wider bandwidth and higher amplitude of the received echoes generated by high frequency ultrasonic transducers than conventional diode limiters can be achieved with this new limiter design. It may find applications in imaging systems where bandwidth and signal to noise ratio requirements are crucial.

[1] Michael I. Fuller, Travis N. Blalock, John A. Hossack, William F. Walker, "Novel Transmit Protection Scheme for Ultrasound Systems" IEEE Transactions on Ultrasonics Ferroelectrics Frequency Control, Vol. 54, No.1, January, 2007, pp79-86.

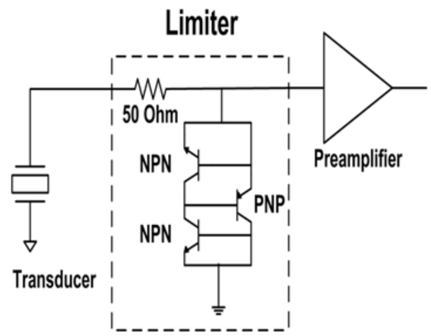

Fig 1. Architecture of novel limiter for high frequency ultrasonic transducer

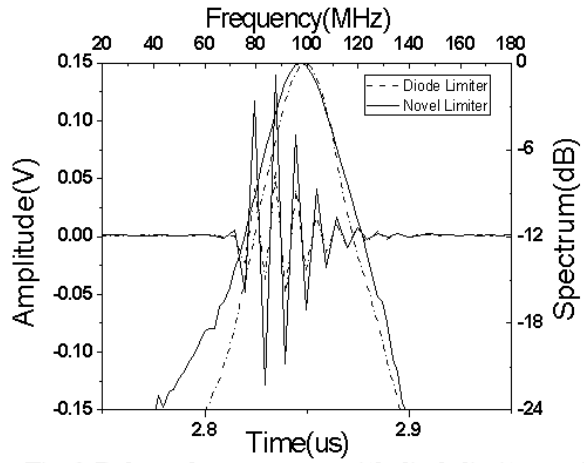

Fig. 2. Pulse-echo responses with diode limiter and novel limiter for 100MHz ultrasonic transducer

P1Ac-12

Detection of Deeply-Implanted Impedance-Switching Devices Using Ultrasound Doppler

Jean Martial Mari[1], Cyril Lafon[2], Jean Yves Chapelon[2]; [1]LabTAU, Unit1032, INSERM, Lyon, France, [2]LabTAU, Unit 1032, INSERM, Lyon, France

Background, Motivation and Objective

The ultrasonic communication and possibly powering up/control with remote devices such as deeply-implanted physiological recorders sets the problem of their localization and the adequate insonification of their piezo electric sensors. Alike RFID devices, rapidly changing their impedance modulates through time their reflectivity, which allows the device to slightly flash periodically and in particular situations to communicate with the exterior.

Statement of Contribution/Methods

A Space Division Multiple Access method is proposed to localize the device by assimilating the flashing to an apparent movement, and enable further accurate focalization, and optimized communication if required. An ultrasound colour Doppler 4.4 kHz PRF sequence is performed using a programmable scanner equipped with a custom probe imaging at 5 MHz a controlled piezo sensor, and the RF data collected at 40 MHz for different excitation lengths and flashing frequencies.

Results

Measurements show that (1) detection can be achieved (see Fig. 1) when the excitation length is at least 100 ns long, with an optimum reached at 400 ns, which is the Doppler processing window length, and that (2) the switching frequency of the device must be in the range of 0.5 kHz and 200 kHz. A brief study of the incidence angle also showed that the sensor of the device can be detected over an angle window of around 34°.

Discussion and Conclusions

Impedance-switching piezo-electric devices can be detected and distinguished from fully passive structures using ultrasound Colour Doppler, which validates Spatial Division Multiple Access as an interrogation process for multiple devices when using steered ultrasound beams to control the interrogation area. Depending on the constrains of the imaging process, there are optimum switching frequencies and ultrasound excitation lengths which will maximize the ability to distinguish a semi passive ultrasonic transponder.

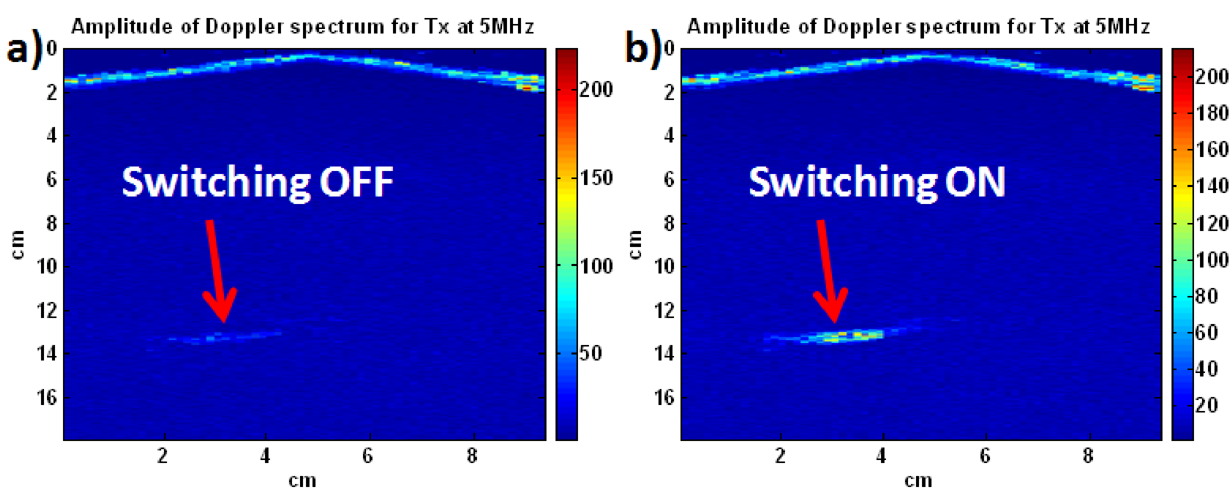

P1Ac-13

A Transmit/Receive 256-Channel Ultrasound Phased Array Driving System Design and Strategy for Transrib Thermal Therapy

Guan-Lu Huang[1], Hao-Yu Chung[1], **Hao-Li Liu[1]**; [1]Department of Electrical Engineering, Chang-Gung University, Taiwan

Background, Motivation and Objective

Ultrasound phased-array system has the capability to steer the energy through the bone so that transcranial/ transrib therapy is feasible. However, ultrasonic energy when passing through the bone can be distorted significantly to fail the focal beam steering, and also cause intervening bone heating. A possible solution is to receive echo-signals from each transmit elements for further correction or dynamically activate/deactivate elements for restoring the focus and preventing from temperature buildup in bone. The purpose of this study is to develop the hardware of a 256-channel ultrasound transmit/receive system in order to achieve transrib liver-tumor thermal therapy.

Statement of Contribution/Methods

The system comprises of PC/MCU/FPGA duplex communication and triggering so that transmit/ receive sequence of each channel can be well controlled. Echo signals received from each element and amplified through a channel-multiplexing circuit. When combining high-speed A/D conversion and USB data transmission, echo signals can be real-time feed into PC for real-time process. The received signals obtained from each element were analyzed and the element obstructing by ribs can be identified. Self-made rib-contained gelatin phantoms were used to validate the accuracy of the algorithm and functionality of the system, and the temperature were feedback from the thermocouple to track the temperature elevation.

Results

Preliminary experiments demonstrated that the implemented algorithm can successfully predict the element been block by ribs via the received backscattered signals, that brings the capability to dynamically activate/ deactivate array elements to avoid rib overheating. We also demonstrated that the temperature rise obtained from the focus can still remain, but significantly reduce the rib over-heating.

Discussion and Conclusions

The proposed multiple-channel transmit/receive phased arrays system provides potential for improving the successful yields when intending to use 2-D ultrasound phased array to transrib treat the liver tumors noninvasively.

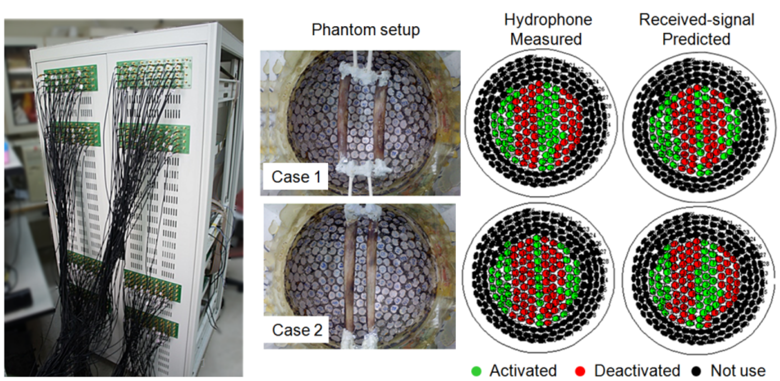

(a) (b)

P1Ac-14

Feasibility of 2D CMUT Arrays with Orthogonal Transmit and Receive Strips for Low-Channel-Count 3D Imaging

Wei Zheng[1], Peiyu Zhang[1], Walied Moussa[2], Roger Zemp[1]; [1]Electrical and Computer Engineering, University of Alberta, Edmonton, Alberta, Canada, [2]Mechanical Engineering, University of Alberta, Edmonton, Alberta, Canada

Background, Motivation and Objective

2D ultrasound array transducers have great potential for 3D imaging but are expensive and typically require high system complexity. Fully wired 2D arrays are cost-prohibitive. Various sparse-array schemes have been proposed to minimize the channel count. CMUTs are an ideal candidate technology for 2D arrays, but wiring is still highly non-trivial. We propose a unique CMUT design that requires only N transmit channels and N receive channels for 3D imaging using an NxN 2D array.

Statement of Contribution/Methods

We use novel CMUT architectures permitting addressability of both top and bottom CMUT cell electrodes. CMUT top electrodes are connected in strips along the x (receive) direction, while CMUT bottom electrodes are connected in strips along the y (transmit) direction. A unique transmit-receive circuit is proposed such that the top electrode strips are tied to DC ground (for patient safety), but permit small AC signals from the device to be received and amplified. Bottom electrode strips are designed to route high-voltage bias signals and carry CMUT transmit driving pulses. Device performance for 3D imaging is simulated using Field II. Bottom strips are actuated using a walking-aperture approach, producing pulsed transmit beams focused in the y-direction but unfocused in the x-direction. Top electrode strips receive backscattered signals and amplified channel data is subjected to dynamic-receive beamforming. Synthetic aperture focusing methods are implemented to additionally demonstrate dynamic focusing in the y-z plane. Fabrication of 2D arrays is underway using a sacrificial-release process. Simple devices are tested to demonstrate proof of principle.

Results

We tested current devices consisting of individual 100-um-wide 3.5 MHz CMUT elements demonstrating addressable top and bottom electrodes. Laser-vibrometer-measured resonance frequencies show good agreement with ANSYS-modeled values. Field II simulations demonstrate the feasibility of dynamically- focused 3D imaging. Because only one-way rather than two-way focusing in each of the x- and y- directions is implemented, simulated images exhibit higher sidelobes and broader mainlobes compared to the focal zone of simulated mechanically-wobbled linear array probes, however, away from the transmit focal zone, image-quality in the x-z planes is comparable, and image quality in y-z planes is better due to synthetic aperture focusing.

Discussion and Conclusions

Our test devices demonstrate the feasibility of the proposed 2D array architecture. Fabricated CMUT devices show good transmit performance, but more work is needed to accurately quantify receive performance. Feasibility of 3D imaging with 2D CMUT arrays using orthogonal transmit and receive strips is demonstrated, and may prove valuable for future 3D ultrasound imaging solutions.

P1Ac-15

Software-based Ultrasound Phase Rotation Beamforming on Multi-core DSP

Jieming Ma[1], Kerem Karadayi[1], Murtaza Ali[2], Yongmin Kim[1,3]; [1]Electrical Engineering, University of Washington, Seattle, WA, USA, [2]Texas Instruments, Dallas, TX, USA, [3]Bioengineering, University of Washington, Seattle, WA, USA

Background, Motivation and Objective

Phase rotation beamforming (PRBF) is a commonly-used digital receive beamforming technique. However, due to the high computational requirement, it has traditionally been supported by hardwired architectures (e.g., application-specific integrated circuits (ASICs) or more recently field-programmable gate arrays (FPGAs)). Programmable processors, e.g., digital signal processors (DSPs), have been used for back-end signal and image processing in clinical ultrasound systems for some time, but not for front-end beamforming. Recently, we proposed a two-stage demodulation phase rotation beamforming method to reduce the amount of computation, which incurred some image quality degradation. With the development of new multi-core DSPs, it might be possible to support both full (not simplified) PRBF and back-end processing on the same multi-core DSP. Our objective is to investigate the feasibility of supporting software-based PRBF on a multi-core DSP.

Statement of Contribution/Methods

Typically, PRBF consists of three main modules (quadrature demodulation, delay alignment and phase rotation). Filtering in demodulation is computationally expensive since it is applied to each one of the pre-beamformed channels. We found that the demodulation module takes nearly 70% of the total PRBF computation time. To alleviate this high computing requirement, the ADC chips in the future could include quadrature demodulation. Under this condition, only delay alignment and phase rotation need to be performed by DSP, reducing the computational load substantially. We implemented the delay alignment and phase rotation modules on a Texas Instruments C6678 DSP with 8 cores.

Results

With a sampling rate of 40 MHz and 2:1 decimation, it takes 200 µs to generate one scanline (2048 samples/scanline) on two cores. With 4 cores, it can support beamforming for 64 channels with 10k scanlines/s, e.g., 200 scanlines/frame and at 50 frames/s. The remaining 4 cores can work on back-end processing tasks and applications, e.g., color Doppler or ultrasound elastography.

Discussion and Conclusions

Our results show that, when quadrature demodulation is performed in ADC chips, software-based PRBF and back-end processing can be supported on an 8-core DSP chip, i.e., C6678. Based on the performance of 64 channels, an 8-core DSP chip could also be used for supporting 128 channels with the beamforming throughput of 10k scanlines/s. With an increased number of cores in the future, the number of scanlines that can be supported per second could increase further and/or more sophisticated front and back-end algorithms could be supported in real time. This unified architecture using one DSP for both front-end and back-end processing will lead to low-power and low-cost ultrasound machines, benefiting ultrasound imaging in general, but particularly portable ultrasound machines.

WEDNESDAY POSTER

P1B Sensing and Signal Processing

Carribean Ballroom III-V

Wednesday, October 19, 2011, 9:30 am - 1:00 pm

Chair: **Erdal Oruklu**
Illionois Institute of Technology, USA

P1B-1

Wideband Time-Reversal Processing for Ultrasound NDE Imaging

Cindy Bernard[1], **Ramazan Demirli[2]**, Cornel Ioana[1]; [1]Signal and Image Processing Lab, National Polytechnique Institute of Grenoble, France, [2]Center for Advanced Communications, Villanova University, Villanova, PA, USA

Background, Motivation and Objective

Time-reversal technique based on the decomposition of the time-reversal operator (TR-DORT) using large arrays of transducers has been used in ultrasound imaging for many years. However, this technique has some known limitations such as the point target assumption, poor target resolution, and large number of array elements with $\lambda/2$ sensor-spacing where λ is the wavelength of the ultrasound wave. In order to overcome these limitations, we investigate two new TR imaging techniques emerged in radar imaging: the WB Multiple Signal Classification (WB-MUSIC) and the Time-Domain (TD-DORT) algorithms.

Statement of Contribution/Methods

We compare the traditional TR-DORT technique to those two emerging techniques which take into account the spectral distribution of the interrogating ultrasonic pulse. TD-DORT uses the projection onto the signal subspace and allows focusing on selective targets. On the contrary, WB-MUSIC uses the projection onto the noise subspace and provides a high resolution image but cannot focus on selective targets. We compare the imaging performances of these techniques to that of the traditional TR-DORT in terms of signal-to-noise ratio (SNR), sensor spacing, and resolution. We also investigated imaging with a non-uniform sparse array where the minimum spacing between two transducers is greater than 4λ, thereby effectively forming a virtual array with 2λ average spacing. It has been observed that WB TR-DORT techniques are more flexible for non-uniform and sparse sensor array configurations while preserving the image quality.

Results

Simulation results show that compared to TR-DORT, WB-MUSIC and TD-DORT are more robust with noise and offer improved target localization. They also enable sparse array configurations, allowing the spacing between two sensors up to 2λ instead of $\lambda/2$ required for the conventional TR-DORT imaging. We tested the imaging performance of these two algorithms using ultrasonic data acquired from a metallic alloy containing artificially drilled flaws. The array data is acquired with an 8-element non-uniform sparse array where the spacing between any two array elements is greater than 4λ. Using such configuration, flaws can be visualized with WB-MUSIC and TD-DORT imaging. WB-MUSIC obtains a compound image of flaws with high resolution while TD-DORT obtains an individual image of each flaw with lesser resolution.

Discussion and Conclusions

The proposed WB TR-DORT algorithms ease the $\lambda/2$ sensor spacing requirement in the traditional TR-DORT method and allow imaging with a fewer number of array elements. They are more robust with noise and offer improved target localizations.

P1B-2

Analysis of Fractional Fourier Transform for Ultrasonic NDE Applications

Yufeng Lu[1], Erdal Oruklu[2], **Jafar Saniie[2];** [1]ECE Department, Bradley University, Peoria, Illinois, USA, [2]ECE Department, Illinois Institute of Technology, Chicago, IL, USA

Background, Motivation and Objective

In ultrasonic NDE applications, backscattered echoes reveal important physical information along the propagation path. These highly overlapped echoes are caused by a combination of close location, irregular boundaries, different sizes, random orientation of scattering reflectors and the contamination of measurement noise. It is inadequate to separate or characterize these echoes by using either time domain or frequency domain analysis. Therefore, alternative signal processing methods capable of analyzing and interpreting the nonstationary ultrasonic signal based on time-frequency distributions for NDE applications are highly sought-after.

Statement of Contribution/Methods

As a generalized Fourier transform with an additional parameter (i.e., transformation order), fractional Fourier transform (FrFT) has been utilized to process nonstationary signals in Radar, sonar, optics, and medical ultrasound applications. In this investigation, FrFT is introduced as a means to decompose and analyze ultrasonic signals in NDE applications. Unlike the conventional time-frequency (TF) analysis, the ultrasonic signals are not decomposed by filtering in time-frequency or time-scale domain. FrFT rotates the spectrum with an arbitrary angle in time-frequency domain. Moreover, chirplet is a type of signal often encountered in ultrasonic applications. A matched-order FrFT of chirplet allows for a more compact support by compressing the signal into narrow peaks. This property contributes to FrFT-based decomposition algorithm when applied to ultrasonic signals. Ultrasonic signal is decomposed into a group of chirplets by iteratively windowing the signal and searching for optimum transform order. Additionally, a grid search is utilized to perform parameter estimation for each chirplet.

Results

In this study, in order to evaluate its performance, we apply the FrFT algorithm to various experimental ultrasonic data sets measured using layered structures and materials with significant microstructure scattering noise. Simulation studies and experimental results show that the FrFT algorithm has a unique analysis quality due to capability to manipulate the transformation order for unraveling complex and interfering echoes often encountered in ultrasonic NDE applications.

Discussion and Conclusions

Numerical and analytical results indicate that the FrFT-based algorithm shows great potential as a very efficient way for ultrasonic signal analysis accounting for narrow-band, broadband, and dispersive echoes. This method can be utilized in the analysis of ultrasonic signals for echo detection, parameter estimation, signal classification, and pattern recognition.

P1B-3

Comparison of Cascade and Concurrent Signal Denoising Methods

Michal Kubinyi[1], Ondrej Kreibich[1], Radislav Smid[1]; [1]Department of Measurement, Czech Technical University in Prague, Faculty of Electrical Engineering, Prague, Czech Republic, Czech Republic

Background, Motivation and Objective

An important issue in ultrasonic NDE is the signal of interest analysis in the presence of background noise created by instrumentation and by clutter noise. We study and develop signal processing methods for Electro-magnetic Acoustic Transducers (EMAT). EMATs use electromagnetic field to generate and receive ultrasonic waves inside the studied specimen. Low transducer efficiency provides a challenging ground for development of advanced signal denoising methods for ultrasonic signals.

Signal averaging, autoregressive analysis, spectrum analysis, matched filtering and the wavelet transform have all been used to filter noise in ultrasonic signals.

The objective of this article is to present and discuss new methods how to extract ultrasonic echoes from signal with amplitudes lower than noise level.

Statement of Contribution/Methods

This article presents novel signal denoising methods developed on ultrasonic signals acquired by EMAT. We propose two methods how to process the signal of interest. We named the methods Cascade and Concurrent signal denoising.

Cascade denosing uses combination of linear and nonlinear filter in cascade. Nonlinear filtering methods often suffer from degraded performance for low Signal to Noise Ratio (SNR). We analysed linear filters which pre-process ultrasonic signal for nonlinear filters. These filters further improve the performance of the processed signal. The cascade combination of the filters was designed to improve the performance over the single element filter.

The second method is called Concurrent denoising. The method is based on fusion of information from multiple domains (time, frequency and the time-frequency domain). The information is extracted from a statistical echo detector, an apriori known frequency characteristics of the transducer and a signal decomposition into packet coefficients. The algorithm suppresses coefficients corresponding to noise and reconstructs denoised signal to time domain.

Results

The proposed methods were analysed by means of Signal to Noise Ratio Enhancement (SNRE) and computation complexity factor. Signals with SNR around 0 were denoised better with concurrent denoising with SNRE 2,5 dB where cascade filtering achieved SNRE 1,2 dB. Computation complexity was for the concurrent denoising 10 times higher than for cascade denoising.

Discussion and Conclusions

The performance of the proposed signal denoising methods was evaluated on artificial and real signals by means of SNRE under various SNR conditions. The experiments proved that the concurrent denoising method achieves SNRE 2,5 dB for the EMAT signal in comparison with Split Spectrum processing or standard wavelet based denoising algorithms. The second proposed method; cascade denoising did not achieve the same performance as the first method but it is less demanding by means of computation complexity.

P1B-4

Numerical and analytical modeling of optical fibers for ultrasound detection

Istvan A Veres[1,2], Gordon Flockhart[3], Gareth Pierce[3], Brian Culshaw[3], Thomas Berer[1,2], Hubert Grün[2], Peter Burgholzer[1,2]; [1]Christian Doppler Laboratory for Photoacoustic Imaging and Laser Ultrasonics, Linz, Austria, [2]Research Center for Non Destructive Testing GmbH, Linz, Austria, [3]Department of Electronic & Electrical Engineering, University of Strathclyde, Glasgow, United Kingdom

Background, Motivation and Objective

Detection of ultrasound by optical fibers has been extensively investigated in the past decades. Due to their small diameter (<250 µm) optical fibers could be applied to detect ultrasonic waves up to the 100 MHz range. The incident acoustic waves introduce changes of the refractive index or birefringence in the optical fiber which is the main working principle of the detection. Their application varies from the detection of ultrasonic waves in fluids (photo acoustics, for example) to the detection of acoustic emission in diverse mechanical components.

Statement of Contribution/Methods

Nevertheless, optical fibers utilized to detect broadband ultrasonic signals their frequency response show a strong frequency dependency. Analytical models based on scattering problems can predict the acoustically induced changes of the refractive index or birefringence in bare, single mode fibers to obliquely incident waves. Optical fibers are, however, usually coated and enclose special structures, such as stress rods of various shapes, to maintain the plane of the polarization of the propagating light within the fiber (PM fiber), which cannot be described by these models. The description and modeling of these cases and the evaluation of the transfer function is the purpose of the presented work.

Results

The classical scattering problem of a homogeneous cylinder submerged in water has been extended to a layered cylinder surrounded by a solid or fluid matrix, which can predict the transfer function of a coated fiber. The modeling of more complex geometries, such as the PM fiber, requires, however, numerical models. A time domain model based on the Finite Element Method has been developed and applied to evaluate the frequency responses of single mode and PM fibers submerged in water. The numerical results are compared to the analytical solutions for single mode fibers and show a good agreement (see Figure). The effect of the stress rods has been investigated with the numerical model for PM fibers showing birefringence also for the hydrostatic case, in accordance with previous observations.

Discussion and Conclusions

New analytical and numerical models have been introduced for single mode and PM fibers. The models show a good agreement and especially the numerical FEM model provides a wide range of opportunities in the modeling of the frequency responses of optical fibers.

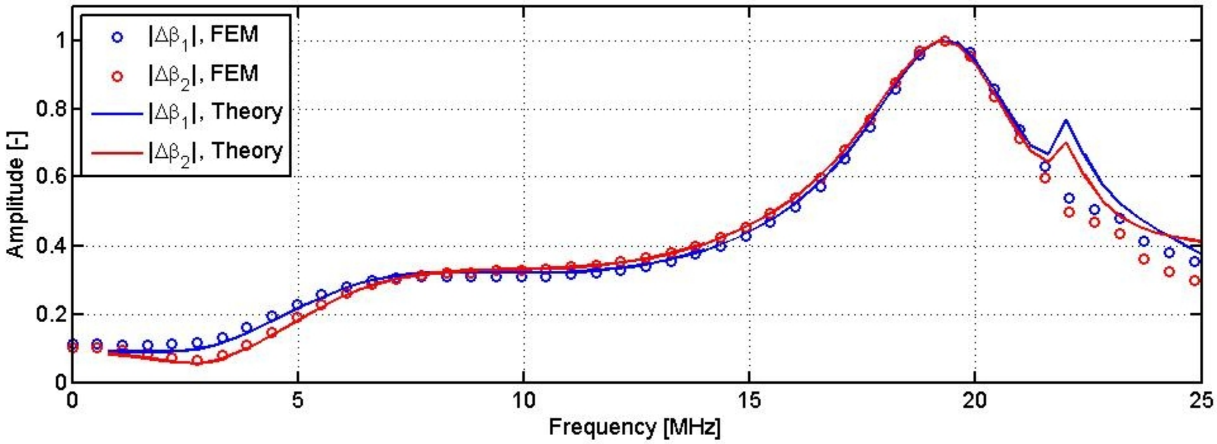

P1B-5

Application of a Programmable Multi-channel Ultrasonic System for In-Line Quality Monitoring of Spot Welds

Anthony Lui[1], Anthony C. Karloff[1], Andriy M. Chertov[1], Roman Gr. Maev[1], Enrico Boni[2], Piero Tortoli[2]; [1]Institute for Diagnostic Imaging Research, Windsor, Ontario, Canada, [2]University of Florence, Firenze, Italy

Background, Motivation and Objective

Spot welding is one of the most commonly used joining methods for metals in the automotive industry. A typical car body contains a few thousand spot welds, many of which are critical for safety. Thus, the development of an advanced ultrasonic monitoring system for non-destructive evaluation (NDE) can greatly improve the quality control of critical spot welds. It has been shown that ultrasonic waves can be used effectively for determining spot weld quality characteristics in a number of inline and offline devices. However, existing in-line systems use only a single-element transducer where a multi-element transducer can provide substantially more information regarding the welding process.

Statement of Contribution/Methods

This paper presents an advanced solution for real-time ultrasonic quality monitoring of spot welds. The new approach is based on a multi-element array transducer controlled by an Ultrasound Advanced Open Platform (ULA-OP). ULA-OP is a fully programmable electronic device capable of reconfigurable phased array imaging and synthetic aperture focusing at high sample rates (12kHz pulse repetition rate and 50 MHz sampling rate). This high-speed processing was essential for real-time imaging of the spot welding process which occurs in less than 200 ms for steel and 66 ms for aluminum. The ULA-OP was combined with a 15 MHz, 52 element, array transducer and was used to analyze a series of spot welds of varying size for preliminary investigations.

Results

Results of real time quality monitoring are presented as C-scan ultrasonic signatures. A number of images have been obtained from different types of defective or fully formed spot welds. This unique device and setup has allowed a set of ultrasonic signatures to be generated in real-time. This showed the complete dynamic process of melting and solidification of a weld nugget during the spot welding process. Using these signatures, an equivalent weld diameter was determined, which is an important parameter for NDE of spot welds. Additionally, indications of internal voids and expulsion events were also observed.

Discussion and Conclusions

The ULA-OP and array transducer set-up presented in this paper provided a method for improving NDE of spot welds by permitting high-speed data acquisition over the weld area. Results have shown that a multi-element array transducer provides more accurate data regarding the geometry of the weld nugget. This setup has also shown a potential to improve sensitivity for detecting internal voids and process disturbances such as expulsions.

P1C - Acoustic Wave Sensing and Transduction

Carribean Ballroom III-V

Wednesday, October 19, 2011, 9:30 am - 1:00 pm

Chair: **Yook-Kong Yong**
Rutgers, the State University of New Jersey

P1C-1

Cavitation Sensor with hydrothermally synthesized lead zirconate titanate poly-crystalline film deposited on Ti cylindrical hollow pipe

Shinichi Takeuchi[1], Michihisa Shiiba[1], Mutsuo Ishikawa[1], Norimichi Kawashima[1], Takeyoshi Uchida[2], Tsuneo Kikuchi[2], Minoru Kurosawa[3]; [1]*Department of Clinical Engineering, Toin University of Yokohama, Yokohama, Kanagawa, Japan,* [2]*National Metrogy Institute of Japan, National Institute of Advanced Industrial Science and Technology, Tsukuba, Ibaraki, Japan,* [3]*Interdisciplinary Graduate School of Science and Engineering, Tokyo Institute of Technology, Yokohama, Kanagawa, Japan*

Background, Motivation and Objective

Recently, ultrasound diagnistic methods, such as color doppler imaging and harmonic imaging, have been used widely. These diagnostic methods irradiate ultrasound pulses high frequently with high intensity. Furthermore, new ultrasound treatment methods with high intensity ultrasound, such as HIFU and sono dynamic therapy are developed and used. Therefore, it becomes important from the view point of safety to measure the acoustic cavitation.

Statement of Contribution/Methods

We developed a cavitation sensor by deposition of hydrothermally synthesized lead zirconate titanate polycrystalline film on a Ti hollow cylindrical pipe. The spatial distributions of acoustic cavitation generated in a vessel of 150 kHz sonoreactor were measured by using our cavitation sensor. We estimated the spatial distribution of acoustic cavitation by using the broad band integrated voltage (BIV) which was calculated from the output signals of our cavitation sensor. BIV were calculated by integrating the output signal from our cavitation sensor in frequency range of 1-10MHz. Measured spatial distribution data of acoustic cavitation was compared with the sonochemical luminescence (SCL) pattern in the sonoreactor Furthermore, we measured the receiving sensitivity inside and outside the hollow space of our cavitation sensor for consideration of the meaning of its output signals.

Results

Similar spatial distributions of the BIV with a sonochemical luminescence patterns could be observed in the water tank of the sonoreactor, when driven with output voltages 300mV and 500mV from the function generator. Our cavitation sensor could be applied to the measurement of sound pressure in a high-intensity ultrasound field with acoustic cavitation for longer than 150 hours without damage.

Discussion and Conclusions

A high-intensity SCL could be observed in the central and peripheral ring shaped areas in the water tank of the sonoreactor when driven with a 300mV output voltage from the function generator. Similar patterns could be observed in the spatial distributions of the BIV and SCL. When the sonoreactor was driven with 500mV, the SCL could not be observed in the central area, because cavitation bubbles were moved to the periphery area by acoustic streaming. A similar spatial distribution of the BIV with CL pattern could be observed under both conditions.

Moreover, it was found that the sensitivity inside the hollow space of our cavitation sensor was about 10 times higher than that outside the hollow space. Therefore, it is considered that the BIV and the cavitation signal included in output signal from our cavitation sensor are based on the acoustic cavitation generated in the hollow of our cavitation sensor.

P1C-2

Improved theory for near-resonance bubble rectified diffusion with applications

Yuning Zhang[1], Shengcai Li[1]; [1]School of Engineering, Warwick University, United Kingdom

Background, Motivation and Objective

Rectified diffusion is an essential phenomenon of oscillating bubbles in sound fields, involved in many biomedical applications. The framework for thermal damping was provided by Prosperetti (1977, J. Acoust. Soc. Am. 61, 17-27). For a complete understanding of rectified diffusion, readers are referred to review article by Crum (1984, Ultrasonic, 22, 215-223) with thermal damping based on Devin (1959, J. Acoust. Soc. Am. 31, 1654-1667). Recently, Zhang and Li (2010, J. Acoust. Soc. Am., 128, EL306-309) has extended the framework in respect of thermal effects into higher frequency regions. The valid regions for formulas derived by Devin (1959) and Prosperetti (1977) are also defined in Zhang and Li (2010) by categorizing bubble behavior into three different regions according to the ratios of bubble radius to wavelengths in gases and liquids.

Statement of Contribution/Methods

In this paper, an approach based on the formulas for thermal damping evaluated in Zhang and Li (2010) for predicting the rectified diffusion near resonance for frequencies at megahertz and above has been proposed. The predictions are compared with others for typical frequencies and bubble sizes involved in biomedical applications.

Results

The accuracy of prediction of bubble rectified diffusion near resonance has been improved by using the proposed approach for frequencies at megahertz and above. The predicted threshold of rectified diffusion is lower while the predicted bubble growth rate and final equilibrium radius are higher and larger.

Discussion and Conclusions

The study and re-evaluation of this fundamental issue has been inspired by our on-going project for crushing kidney stone by using the enormous damaging power from the collapsing bubble cloud that is generated through rectified diffusion process. In early 2008, a dynamic-frequency technique following the resonance frequency of bubbles has been proposed by Li for rapid growth of bubbles in the acoustic fields. Here, we demonstrated some calculated examples with this technique by using the formulas developed by us. Result shows a much more accurate prediction of rapid bubble growth achieved by using the dynamic-frequency technique. The improved theory combined with the dynamic-frequency technique will greatly benefit those biomedical applications that involve the use of acoustic bubbles growing from rectifications in sound field. For example, the operation time for kidney stone crushing will be reduced. The details of this concept are to be disclosed at the coming 3rd WIMRC Cavitation Forum (Li and Zhang, 2011, ¡°Dynamic-frequency technique for speeding up bubble growth in stone crushing by cavitation¡±) during July, 2011.

P1C-3

The Acoustic Resonator Combined with Electrical Discharges

Rudolf Balek[1]; [1]Department of Physics, Czech Technical University in Prague, Faculty of Electrical Engineering, Prague 6, Czech Republic

Background, Motivation and Objective

Environmental applications such as pollution control, volatile organic compounds removal, car exhaust emission control, polymer surface treatment and ozone generation for water purification utilize different chemical reactions. The efficiency of these reactions depends on the temperature, on the reactant residence time and also on the pressure in reaction volume. The change of pressure in this volume can be achieved by application of acoustic field. At the same time many reactions can be enhanced by ionization of the reactant medium, which is frequently performed by electrical discharges. These requirements are easily met by the combination of acoustic resonators with non-thermal electrical discharges.

Statement of Contribution/Methods

The cylindrical acoustic resonator in combination with the electrical discharges was investigated with the aim to clarify the effect of acoustic field to the discharges between radial negative multi-needle electrodes and the earth wire electrode axially placed at the resonator axis.

Results

The main requirements in industrial applications are discharge power and volume. To increase the discharge volume and to prevent a discharge transition into sparks, we designed an acoustic stabilization of multi-needle-to-wire electrode system, which is situated in the pressure node of the resonator. Factors which contribute to the stabilization are: first, the gas particles that are swung on the pressure node plane; and second the acoustic pressure gradient, which strongly influences the discharges breakdown conditions. With the decreasing of pressure, the reduced electric field is increased, and suitable conditions for discharge streamer tracing are established. The streamers are swung into place over the estimated amplitude of acoustic displacement. The discharges are strongly spread and effectively stabilized at all needles placed in one line in the direction of the resonator axis even if they are connected to the same potential.

Discussion and Conclusions

The stabilization of the discharge which is placed in the pressure node of the acoustic resonator is based on homogenization, cooling and spread of the discharge volume in front of each needle of the multi-needle electrode by means of the acoustic standing wave field.

The tips of the electrodes are acoustically cooled without any threat to be burned and without any dilution of the processed gas. The stabilization may be applied to different regimes of discharges, e.g. corona, glow and streamer.

Suitably arranged acoustic resonators with electrical discharges offer the synergy effect of power acoustic field with the discharge volume enhancement and discharge stabilization at all electrodes. It opens new perspectives in many practical environmental applications.

P1C-4

Measurements of the viscosity of liquids in function of pressure and temperature using SH surface acoustic waves

Piotr Kielczynski[1], Marek Szalewski[1], Andrzej Balcerzak[1], Aleksander Rostocki[2]; [1]*Polish Academy of Sciences, Poland,* [2]*Warsaw University of Technology, Poland*

Background, Motivation and Objective

High-pressure research of the physical properties of liquids has been stimulated by the fast development of such technologies as biodiesel production, high-pressure food processing and conservation, modification of biotechnological materials. Viscosity is one the most important parameters of liquids. Monitoring and studying the pressure and temperature effect on liquid viscosity allow insight into the phenomena governing the microstructural modifications occuring in the treated substances. High-pressure phase transitions in liquids can be investigated by the measurements of the viscosity in function of hydrostatic pressure and temperature. The conventional mechanical methods can not be applied in the high-pressure range due to their inherent limitations.

Statement of Contribution/Methods

Due to disadvantages of conventional methods, a need for new measuring methods arose. Ultrasonic methods for the measurement of the viscosity of liquids under high pressure were introduced. The authors have established new ultrasonic methods, the Bleustein-Gulyaev (B-G) wave method and Love wave method (P. Kielczynski et al., 2008 IEEE Int. Ultrason. Conf. Proc., 2154). The B-G wave method is more sensitive than that which employs Love waves. The sensor consists of the B-G wave waveguide made of PZT piezoceramics and sending – receiving PZT transducer. The operating frequency was 2 MHz. Triolein has been selected as an investigated liquid.

Results

The viscosity of triolein was measured in function of pressure and temperature at 10° C intervals from 10°C to 40°C and from atmospheric pressure up to 650 MPa. The pressure was increased until the first-order phase transition began. During the phase transition the drop of pressure and large increase of viscosity were observed. When the temperature during measurements was higher, the pressure, at which the phase transition began, increased. Consequently, the pressure at which transition stopped was also higher. After the termination of the phase transition process, the pressure was increased again, in order to measure the viscosity of the new high-pressure phase of triolein. With the increase of temperature, viscosity of high-pressure and low-pressure phases of triolein diminished.

Discussion and Conclusions

The usefulness of the B-G wave method and established experimental setup for measuring liquid viscosity at high pressure for various temperatures has been stated. The presented method enables measuring viscosity during phase trasnsition, after emerging of the high-pressure phase and during phase decomposition. To the authors' knowledge, the measurement of liquid viscosity under high pressure, for various temperatures (isotherms), during the phase transition were not yet reported in the scientific literature.

P1C-5

Coherent Acoustic Waves Excitation and Detection on Subterahertz Frequencies

Natalia Polzikova[1], Georgy Mansfeld[1], Alexander Raevskii[1]; [1]*IRE RAS, Russian Federation*

Background, Motivation and Objective

The spectrum of acoustic phonons covers frequencies up to some terahertz. So the excitation of coherent acoustic waves (AW) with subterahertz frequencies is a problem of great importance. Recently, the experiments carried out on Nb-AlOx-Nb junction on Si substrate revealed the fine structure of current voltage characteristics (IVC) with steps separation and resistance pointed out on AW generation (V.P. Koshelets, et al, IEEE Trans. on Appl. Supercond., vol. 11, p. 1211, 2001).

Statement of Contribution/Methods

In present paper we analyze coherent phonon radiation and detection due to interaction of Josephson's electromagnetic oscillations with mechanical displacement field caused by piezoelectric effect in barrier layer. We consider AW generation in the long Josephson junction depositing on the rather thick substrate as it is shown in Figure. The basic equations of the problem are: the equation for Josephson phase and the motion equation for mechanical displacement in barrier layer with boundary equations for elastic displacements and stresses at the dielectric layer surfaces.

Results

These equations let to get the dispersion relation for coupled acoustic and electromagnetic oscillations. The IVC of Josephson current under the influence the acousic subsystem was found. The Lorentz form of Fiske step is distorted – the set of peaks over the smuth curve appear. The positions of the peaks correspond to the resonance frequencies of the longitudinal subterahertz acoustic waves exciting and propagating normally to the surface of the substrate as in HBAR. Such a behavior of the IVC have been observed experimentally on the frequencies 300-700GHz with distance between peaks 9MHz.

Discussion and Conclusions

The theory developed explains acoustoelectronic phenomena arising in the long Josephson structures. The superfine resonant structure of IVC indicates the acoustic wave excitation. So the generation and detection of coherent acoustic waves with frequencies up to 700 GHz (the gap frequency of Nb) due to piezoelectric effect in dielectric interface of superconductor junction may be achieved.

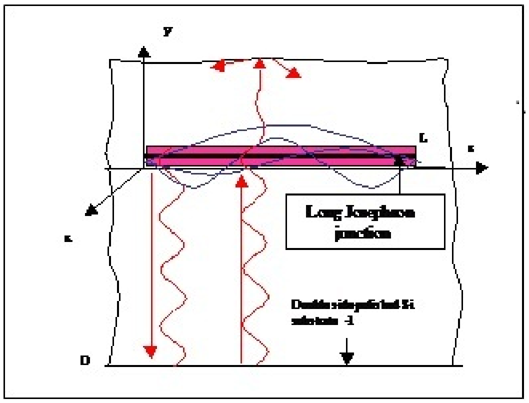

WEDNESDAY POSTER

P1D - SAW Devices and Design

Carribean Ballroom III-V

Wednesday, October 19, 2011, 9:30 am - 1:00 pm

Chair: **Tatsuya Omori**
Chiba University

P1D-1

An Adaptive Thresholding Method for SAW RFID With Large Code Capacity

Along Kang[1,2], Tao Han[2]; [1]*Department of Instrument Science and Engineering, Shanghai Jiaotong University, China, People's Republic of,* [2]*Shanghai Jiaotong University, China, People's Republic of*

Background, Motivation and Objective

In recent years, much attention has been paid on surface acoustic wave (SAW) based radio frequency identification (RFID) research and applications, one of the reasons is the fact that SAW RFID could be used to provide better solutions to the problem of identification in harsh environments where RFID based on semiconductor technologies have been failed to fulfill the needs of high-tech industry.

For the purpose of improving the adaptability and flexibility of SAW RFID systems in most practical applications, it is important to determine the most appropriate identification threshold, which can be used to detect whether a SAW RFID tag enters the interrogating range of the reader. So far, only a few works for SAW RFID applications have been found in the literature, though it is impressive that Gustavo Cerda-Villafana has discussed the optimum thresholds for the identification of wireless SAW RFID tags with binary amplitude shift keying (BASK) based on the minimum error probability criterion. Besides, it is noticeable that several encoding methods with large code capacity, in which the phase information was used to improve the time resolution of SAW RFID systems, have been presented recently for SAW RFID applications. In other words, both the time position information and the phase information have been used for the new generation of SAW RFID encoding systems with large code capacity. However, a detailed discussion over the joint impact of the amplitude and phase information on the adaptive threshold for SAW RFID with large code capacity is still not available. Furthermore, it is necessary to evaluate the role of the risk functions corresponding to some typical applications in the adaptive threshold determination process.

Statement of Contribution/Methods

In this paper, a new adaptive thresholding method for SAW RFID with large code capacity is proposed. In Section I, the time-domain signal model for SAW RFID systems was introduced, especially, some noise source such as wireless channel, the crystal oscillator and sampling etc. have been analyzed. And then, a statistical data model for each encoding bit is acquired by using kernel functions in section II, as a result, the joint probability distribution of the amplitude and phase information for every encoding bit could be used to determine the adaptive identification threshold. Finally, the impacts of several typical risk functions on the adaptive threshold determination have been compared, and then the adaptive thresholds for SAW RFID with large code capacity would be obtained, respectively.

Results

In our experiment, several SAW tags for test have been designed and fabricated, and the proposed adaptive thresholding method was validated by a self-developed SAW RFID reader operating in 920-925 MHz Frequency Band. The experimental results demonstrate that a correct identification rate of 99.97% was achieved using the adaptive threshold proposed.

Discussion and Conclusions

P1D-2

Suppression Mechanism of Transverse-Mode Spurious Responses in SAW Resonators on a $SiO_2/Al/LiNbO_3$ Structure

Hiroyuki Nakamura[1], Hidekazu Nakanishi[1,2], Rei Goto[1], Ken-ya Hashimoto[2]; [1]*Panasonic Electronic Devices Co., Ltd., Japan,* [2]*Chiba University, Japan*

Background, Motivation and Objective

SH SAWs on a $SiO_2/Al/LiNbO_3$ structure are promising for the UMTS Band I application because of their large electromechanical coupling factor and good temperature coefficient of frequency. However, the structure also supports two unwanted spurious resonances due to the Rayleigh-SAW and the transverse-mode. IDT apodization has been used for the suppression of transverse-mode resonances, and the length weighting for dummy electrodes were proposed to scatter higher-order transverse-modes selectively [1]. The authors demonstrated that the transverse-mode spurious responses could be suppressed successfully by the selective removal of SiO_2 at the dummy region [2].

Statement of Contribution/Methods

This paper discusses the suppression mechanism of the transverse-mode spurious responses by the selective removal of SiO_2. The SAW field distribution was analyzed for the $SiO_2/Al/LiNbO_3$ structure, where the SiO_2 and Al thicknesses of are 0.2λ and 0.08λ, respectively, and λ is the SAW wavelength. As the piezoelectric substrate, 5°YX-$LiNbO_3$ was chosen.

Results

The field analysis indicated that the selective removal of SiO_2 enhances the SAW reflection coefficient at the boundary between the interdigital and the dummy electrode regions, and SAW energy tends to be confined well in the active electrode region. It is interesting to note that the boundary behaves like mechanically free because the SAW energy penetrates well into the SiO_2 layer. Thus the fundamental transverse mode in the structure behaves like an electrically active piston mode, while higher-order modes are not active due to phase-inversion in the mode profile.

Discussion and Conclusions

It was shown that the selective removal of SiO_2 confines the SAW energy into the active electrode region, and the transverse-modes can be suppressed in a similar manner to the piston mode resonator. There still remains one thing unclear. Since the evanescent field remains in the dummy electrode region, the phase angle of the reflection coefficient is not zero at the boundary, and this should make the suppression of higher-order transverse modes difficult. This contradicts with our experiment [2]. We expect that the coupling of the SH SAW with the Rayleigh SAW, experimentally observed in [2], plays an important role to cancel the phase angle. In [3], it is shown that when the SiO_2 thickness is large, SiO_2 should not be removed fully but partially from the dummy electrode region for the transverse mode suppression. This result supports the above mentioned hypothesis.

[References]

[1] T. Omori, et al., IEEE Trans. Ultrason., Ferroelec., and Freq. Contr., 54 (2007) pp. 1943-1948.

[2] H. Nakamura, et al, IEEE Ultrasonics Symp., 2010 [to be published]

[3] H. Nakanishi, et al, IEEE Ultrasonics Symp., 2011 [to be presented]

P1D-3

Spurious mode suppression in multiple layer HfO_2/Simax acoustical mirror structure for ILAW on 15°-YX $LiNbO_3$

Sergei Zhgoon[1], Alexander Shvetsov[1], Kushal Bhattacharjee[2]; [1]*MPEI, Moscow, Russian Federation,* [2]*RF MD, USA*

Background, Motivation and Objective

Cavityless wafer level packaging and TCF improvement is possible with isolated layer acoustic wave (ILAW) with an acoustical mirror structure. Meanwhile orientations of $LiNbO_3$ with high coupling factor that are needed for wideband SAW filters are known to possess spurious modes in the working frequency range. Several attempts with useful outcome have been published for orientations around 15°-YX $LiNbO_3$, for example [1], in [2] the cut angle is optimized for reduction of the spurious mode coupling factor. This paper investigates the possibility to use the ILAW supporting structure for suppression of spurious modes by exploiting the difference in propagation properties of the waves with different displacement polarization.

Statement of Contribution/Methods

The multiple layer structure is analyzed with the help of calculations based on the analytical formulas obtained for boundary conditions between adjacent layers. Besides, FEM simulations of the infinite IDT structure are extensively used to identify regions of layer thickness with potentially lower electromechanical coupling of the spurious mode. Experiments are made with continuous in-situ monitoring and registration of a resonator response during the magnetron sputtering of a four-layer HfO_2/Simax/HfO_2/Simax layer over Au/Ti electrodes. Simax is akin to Pyrex.

Results

The analysis confirms different behaviors of the main useful mode and of the spurious mode and the possibility to more or less independently influence their properties by individually changing the thickness of the layers in the structure. FEM simulations of structures with planar dielectric layers over a grating allowed to build a contour map that presents extensive regions where the spurious mode coupling factor is reasonably low and where the velocities of the involved modes vary in usefully extensive limits. Simulations of the structures with corrugated layers (as usually obtained in reality by magnetron deposition over electrodes) predict the existence of some useful cases of acoustically isolated waves. Experimental data validate the modeling approach in a wide range of layers thickness variation.

Discussion and Conclusions

The results show that the mirror structure with ILAW that is aimed for cavityless wafer level packaging and TCF improvement can simultaneously be used for suppression of the spurious mode in wideband filters.

[1] K. Hashimoto et al. Proceedings of 2004 IEEE Ultrasonics Symposium, pp.1330-1334.

[2] N. Naumenko, B.Abbott. Proceedings of 2008 IEEE Ultrasonics Symposium, pp.1013-1017.

P1D-4

Effect of Anisotropy on the Reflection of SAW from Grooves and Strips

Alexander Darinskii[1], Manfred Weihnacht[2,3], **Hagen Schmidt**[3]; [1]Institute of Crystallography RAS, Moscow, Russian Federation, [2]InnoXacs, Dippoldiswalde, Germany, [3]IFW Dresden, Dresden, Germany

Background, Motivation and Objective

Metallic strips and grooves created on the surface of crystals are often used as SAW reflectors. The reciprocity theorem secures the identity of the transmission coefficients of SAW incident from the left and from the right on an obstacle. In contrast, the reflection coefficients for the inverse directions are not constrained by any special relation and therefore can be different because of the crystallographic anisotropy or/and the asymmetry of the imperfection shape. The energy balance is fulfilled in such cases at the expense of the difference in the bulk wave irradiation into the substrate.

Statement of Contribution/Methods

The work studies theoretically manifestations of the above-indicated difference between the reflection coefficients from single grooves and strips for the normal incidence. The substrate is the YZ-LN cut, where the SAW propagates along the z-axis. The positive and the negative directions of this axis are not equivalent, although the SAW velocities are equal. The reflection from asymmetric grooves in an isotropic substrate (fused silicon) is also investigated. Given an incident SAW, the scattered fields are computed by solving the appropriate boundary-value problem by FEM. The grooves/strips are infinitely long so that 2D-simulations are carried out. The computational domain is truncated by the perfectly matched layer (PML). The parameters of PML as well as the method of calculating the amplitude of the reflected SAW are tested by a special series of computations.

Results

The reflection coefficients in YZ-LN are computed for different geometrical characteristics of imperfections and different materials of strips (Al, Cu, Pt). The cross-section of a groove/strip is either symmetric (rectangular) or asymmetric (trapezoid obtained from a rectangular by inclining the left-hand or right-hand side). The strip either overlays LN or is buried into it. Computations reveal that the maximum relative difference of the magnitudes of the coefficients corresponding to the inverse directions strongly depends on the specific situation and can vary from a few percents up to 10 times. As a rule, this difference does not steadily grow with increasing the geometrical parameter which seemingly brings in increasing perturbation and asymmetry. For instance, with deepening the rectangular groove the difference first increases then decreases, vanishes and, having changed sign, increases. The phases of coefficients are different when their magnitudes become equal. The analogous equality of magnitudes takes place for trapezoid grooves with increasing the inclination angle of one side in LN and in fused quartz. In the latter case the asymmetry of the shape is the only factor stipulating the asymmetrical reflection.

Discussion and Conclusions

The obtained results show, in particular, that the characteristics of imperfections affect the reflection of SAW in a fairly involved way so that intuitive estimations can appear to be misleading.

P1D-5

Low propagation loss in the one-port resonator fabricated on single crystal diamond

Satoshi Fujii[1], Tatsuya Odawara[2], Tatsuya Omori[2], Ken-ya Hashimoto[2], Hironori Torii[3], Hitoshi Umezawa[4], Shinichi Shikata[4]; [1]Academic industrial collaboration and Intellectual Property, Chiba University, Chiba, Chiba, Japan, [2]Electrical and Electronic Engineering, Chiba University, Japan, [3]Technology Support & Development, MES AFTY Corporation, Hachioji, Tokyo, Japan, [4]Diamond Research Lab., AIST, Tsukuba, Ibaraki, Japan

Background, Motivation and Objective

The phase velocity of surface acoustic wave (SAW) in diamond is the highest when compared with that for all other materials; this property of diamond has been applied in high frequency SAW devices in the gigahertz rage. Numerous research reports to date have demonstrated SAW devices built on a SiO_2/IDT/ZnO/diamond structure that function in a frequency range of 2 GHz to 10 G Hz; further, the devices have been reported to exhibit outstanding temperature stability. Instead of using a ZnO thin film, we also have reported a SAW device built on a SiO_2/IDT/AlN/diamond structure that functions in the 5 GHz range with better resonance characteristics and higher temperature stability than those obtained in previous studies. In most studies conducted thus far, a polycrystalline diamond thin film, fabricated on silicon wafer by microwave chemical vapor deposition (CVD) or filament CVD methods, has been employed as the SAW substrate. In our study, we examine the effects of the crystalline quality of diamond in the propagation loss of a surface acoustic wave by fabricating a one-port SAW using a single crystal diamond.

Statement of Contribution/Methods

A nitrogen-doped (type Ib) single-crystal diamond that was grown by a high-temperature and high-pressure method was used as the SAW substrate. An AlN thin film of thickness 0.7µm was deposited on the (100) plane of the diamond substrate using electron cyclotron resonance (ECR). A one-port SAW resonator with IDT/AlN/diamond structure and wavelength (λ) of 2.0µm was fabricated using e-beam lithography and the lift-off process. In addition, we fabricated a one-port resonator with a polycrystalline diamond thin film in order to compare its performance with that of the one-port SAW fabricated on a single crystal diamond.

Results

Figure 1 shows the admittance of the one-port resonators with a center frequency of 5.1 GHz. A Q-value of 1700 was obtained for the resonator using the single crystal diamond at a high frequency of 5.1 GHz.

Discussion and Conclusions

From the fitting results, it was determined that the low propagation loss of the one-port SAW using the single crystal diamond was 0.015 dB/λ; this is less than half the value obtained from that using the polycrystalline diamond thin film.

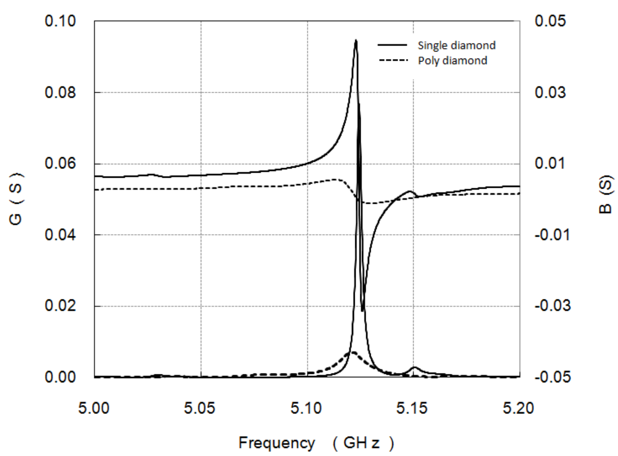

Fig. 1 Admittance of the 1port resonators

P1D-6

Band Pass Type of Tunable Filters composed of Ultra Wide Band SAW Resonators by adjusting Capacitors connected SAW Resonators

Michio Kadota[1], Tetsuya Kimura[2], Yasuyuki Ida[2]; [1]Kadota Laboratory, Murata Mfg. Co., ltd., Yasu, Shiga, Japan, [2]Kadota Laboratory, Murata Mfg. Co., Ltd., Yasu, Shiga, Japan

Background, Motivation and Objective

Recently, a mobile phone with multi-bands and a cognitive radio system require tunable filters with a wide tunable range, which require ultra wide band resonators. Authors realized a ultra wide band one port SAW resonator composed of the grooved-Cu-electrode/4°YX-LiNbO3 with the bandwidth of 17 % and proposed that a band pass (BP) type of tunable filter having the tunable range of 7 % were able to be theoretically realized by using them instead of conventional inductors and adjusting capacitance of capacitors connected them[1]. But the authors didnot report their experimental results.

Statement of Contribution/Methods

The BP type of tunable filter has been attempted to fabricate using their SAW resonators and two kinds of capacitors of Al-electrode interdigital capacitors (IDCs) on the LiNbO3 substrate and Si semiconductor diode variable capacitors.

Results

The center frequency shift of 6.8 % has been obtained by using 3 kinds of IDC sets as shown in Fig.1. On the other hand, when the voltage of 1.2 V to 10V has been applied to the Si semiconductor variable capacitors to adjust the capacitance, the center frequency shift of 6.1% has been continuously obtained for the first time as shown in Fig.2. Their insertion losses were larger than the calculated one using Q=1,000, because the mechanical Q of IDC and the Si diode variable capacitor are low as 5 and 1 at 1.8 GHz, respectively.

Discussion and Conclusions

2 kinds of the BP type of tunable filters have been realized by using two kinds of the capacitors. It is clarified for the first time that the frequency continuously shifts by controlling the applied voltage to adjust capacitance of the variable capacitors. It is considered that a better insertion loss could be obtained,if high Q capacitors are used.

Reference

(1)M. Kadota etal : Jpn. J. Appl. Phys., vol.49, 07HD26(2010).

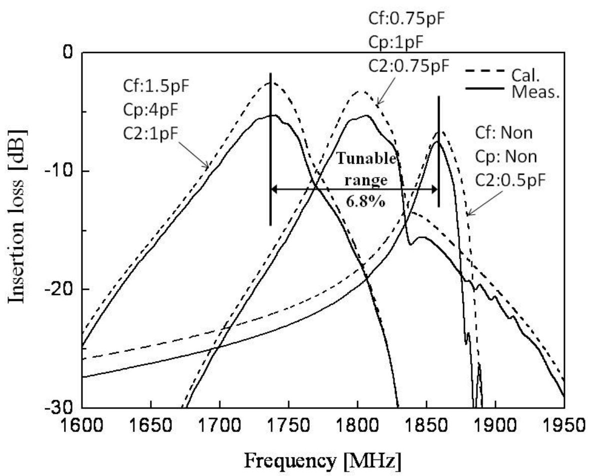

Fig.1 Measured frequency characteristics of BP type of tunable filter using various IDC sets.

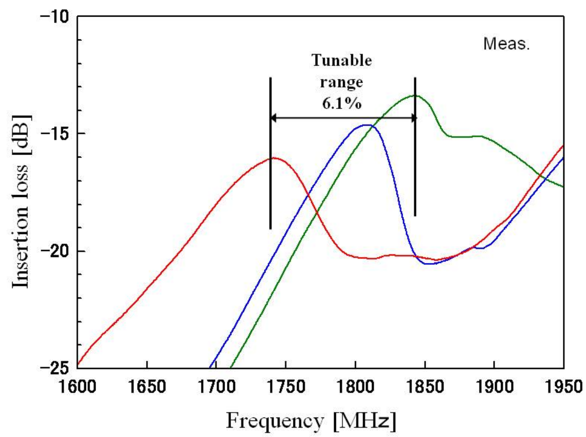

Fig.2 Measured frequency characteristics of BP type of tunable filter using Si diode variable capacitors.

P1D-7

Optimized STW Devices with Buried Electrodes Based on a Mixed FEM/BEM Numerical Model

Pascal Ventura[1], Pierre Dufilié[2]; [1]PV R&D Consulting, Nice, France, [2]Phonon Corporation, Simsbury, CT, USA

Background, Motivation and Objective

STW resonators on quartz are preferred over SAW due to their superior acceleration sensitivity, power handling, improved aging behavior, and 60% higher velocity. The achieved resonator Q at high frequencies using a metallic grating is lower than expected, mainly due to bulk mode scattering losses. The purpose of this study is to find the grating geometry which can reduce the propagation attenuation of the STW.

Statement of Contribution/Methods

STW propagation on α-yx quartz (Euler angles 0,90-α,90) has been examined using a mixed FEM/BEM numerical model developed for buried electrodes for SAW propagation. It was found that by adjusting the a/p of the metal strips and by partially burying the electrodes one obtains SAW-like propagation properties with low propagation attenuation.

For practical device design it is also necessary to be able to predict the turn-over temperature. To this end, simplified assumptions have been made to model the electrode and the piezoelectric substrate dilatations with temperature, and incorporated in the mixed FEM/BEM numerical model PerIDT presented at last year's Ultrasonics Symposium.

Results

The optimized partially buried strip structure is used to obtain STW resonators with increased Q with predicted turnover temperature. Comparison with experiments will be shown.

Discussion and Conclusions

Partially buried electrode STW resonators with improved Q have been developed with the aid of the mixed FEM/BEM numerical model PerIDT.

P1D-8

SAW Resonator-Based Wafer Processing Control

Pierre Dufilie[1], Merle Yoder[1], Jim Jacobs[1]; [1]*Phonon Corp., Simsbury, CT, USA*

Background, Motivation and Objective

The electrical performance of SAW devices is impacted most strongly by metal thickness(h), line width(w) and, at high h/λ , electrode shape. For liftoff processes these key parameters are controlled in the photolithographic and metallization steps. For etching processes the metal etching step also has an impact on the parameters. Controlling the manufacturing process requires an accurate, repeatable method of measuring these parameters.

Statement of Contribution/Methods

A test mask developed to determine these key parameters and their corresponding uniformity over the entire substrate through electrical measurement will be presented. The mask incorporates resonators with 0.5um linewidths, which are used to measure the key parameters of the wafer processing. All of the required resonator parameters are derived from wafer probe measurements within the stopband thereby minimizing interaction with adjacent resonators.

Results

A liftoff process is evaluated by wafer probing quartz wafers processed with the test mask and with 0.12um aluminum metallization. The wafer probe measurements of the resonators are used to determine h and w variations across the wafer. A 2D mapping of the parameters across the wafer is made to assist in adjusting the manufacturing process.

Discussion and Conclusions

Wafer probe measurements of resonator characteristics within the stopband of the resonator effectively eliminates interaction with adjacent resonators. It is found that h and w can be determined by the frequencies of the resonance peaks. This elimates errors encountered by alternate methods such as capacitance and resistance measurements.

P1D-9

Fabrication of high frequency SAW resonators using AlN/Diamond/Si technology

G.F. Iriarte[1], J.G. Rodriguez Madrid[1], R. Ro[2], R. Lee[2], O.A. Williams[3], D. Araujo[4], Pilar Villar[4], F. Calle[1]; [1]ISOM - Universidad Politécnica de Madrid, Spain, [2]I-Shou University, Taiwan, [3]Fraunhofer IAF (Germany) and Cardiff University (UK), United Kingdom, [4]Universidad de Cadiz, Spain

Background, Motivation and Objective

In order to increase the frequency of SAW devices we can either decrease the wavelength, which depends on the size of the interdigital transducers (IDTs), or increase the phase velocity, which depends on the material. The first option entails the introduction of e-beam lithography on the manufacturing process. The alternative choice requires a careful selection of a piezoelectric layer and a substrate with a high phase velocity. The AlN/diamond bilayer system is a perfect combination for high-frequency SAW devices.

Statement of Contribution/Methods

In this report, the room temperature synthesis of AlN thin films by reactive sputtering has been optimized on diamond substrates in order to process high frequency devices. Polished micro and nanocrystalline diamond substrates have been used to deposit AlN. Th-2Th and rocking curve X-ray diffraction analysis were used to determine the crystallographic quality of the AlN thin film. The surface roughness has been measured using an atomic force microscope (AFM). Conventional transmission electron microscopy (CTEM) analysis in electron diffraction mode was performed for structural characterization on cross-sectional prepared samples using a Jeol 1200 EX TEM. Finally, SAW one port resonators have been fabricated. The electrical characterization of these devices (in terms of S11 parameters) is reported. The measured data has been fitted using analytic and FEM based methods.

Results

A critical aspect of the AlN layers deposited by reactive sputtering is their surface roughness, as it may lead to an increase of propagation losses. This roughness is related to the surface roughness of the substrate, in this case CVD (chemical vapor deposition) synthesized diamond. We have studied the influence of the diamond substrate roughness on the AlN growth. The final goal was to optimize these AlN thin films in order to process SAW devices. Figure 1 shows the S11 parameter vs. frequency for one of the SAW resonators manufactured after optimization of the AlN/diamond/Si technology. SAW devices with resonant frequencies above 10 GHz and with more than 45 dB IL (insertion loss) have been manufactured using this technology.

Discussion and Conclusions

High frequency SAW resonators have been fabricated using AlN/diamond/Si technology. These devices exhibit an outstanding performance in terms of IL (insertion loss) and other frequency response parameters.

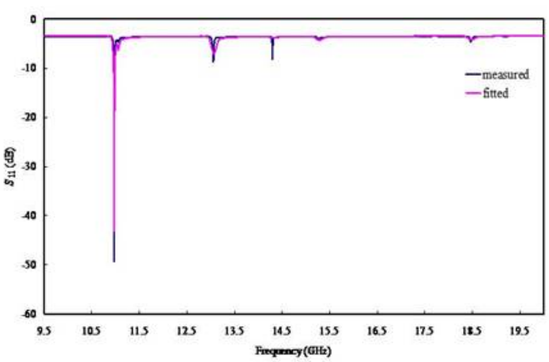

Fig. 1: S11 vs. frequency a SAW resonator based on AlN/Diamond/Si technology.

P1D-10

Temperature effect on the characteristics of Love wave along multi guide layers of SiO2/SU-8

Jiaoli Hou[1], Weng Wang[1], Minghua Liu[1], Shitang He[1]; [1]Institute of Acoustics, Chinese Academy of Sciences, China, People's Republic of

Background, Motivation and Objective

Love wave gas sensor exhibits higher mass sensitivity over SAW sensor, and the waveguide protects the metal interdigital electrodes from oxygenization. However, the stability and the detection limits of love sensor are influenced by the ambient temperature because of the inherent temperature coefficient of the sensor itself. The purpose of this paper is to analyze the temperature effect Love wave propagating along multi-guiding layers of SiO2/SU-8 on ST-90oX quartz substrate, leading to very low temperature coefficient of frequency (TCF), which is significant issue for gas sensor.

Statement of Contribution/Methods

The dispersion characteristics of Love wave propagating along the multi-guide layers structure of ST-90oX quartz/SiO2/SU8 was analyzed by the acoustic propagation theory of stratified media and boundary conditions, the guide thickness versus TCF was described as shown in Fig.1. The extracted optimal waveguide thickness of SiO2 0.2¦Ìm and SU8 near 0.8¦Ìm was confirmed by the experimental result.

Results

Figure.2 shows the measured frequency response of the fabricated 174MHz Love wave delay line with waveguides of SiO2/SU-8 in case of various testing temperatures, the target thickness of the SiO2 and SU-8 are 0.79¦Ìm and 0.78¦Ìm, respectively. Superior temperature stability (TCF of ~2.3ppm) was observed from the fabricated Love wave device.

Discussion and Conclusions

the Love wave device with multi-wave guides of SiO2/SU-8 and very low temperature coefficient (~2.3ppm) was implemented based on establishment of the theoretical model. The validity of the theoretical calculation was confirmed by the experimental results.

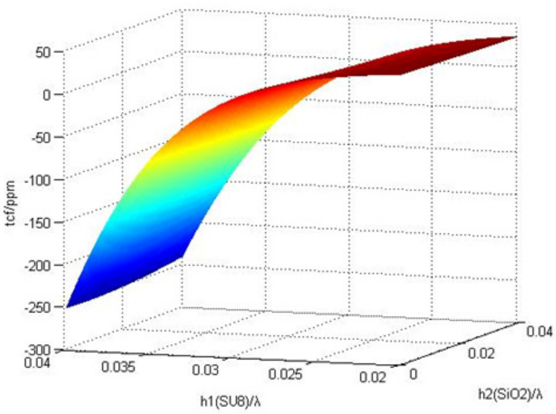

Fig. 1 The calculated TCF depending on various thicknesses of SU8 and SiO_2.

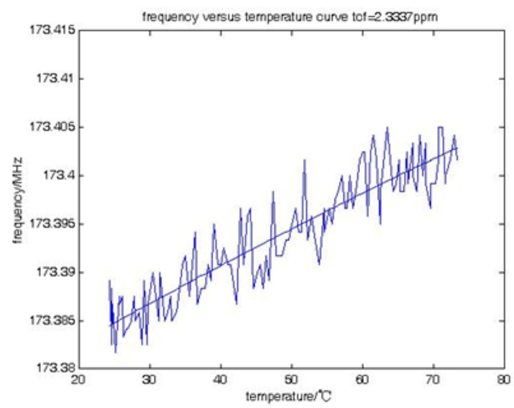

Fig. 2 Measured TCF of the 174MHz- Love wave delay line with multi wave guides

P1D-11

Implementation of Error-Correcting Encoded SAW RFID Tags

Jingchu He[1], Tao Han[1], **Yongan Shui[2];** [1]Shanghai Jiaotong University, China, People's Republic of, [2]Nanjing University, China, People's Republic of

Background, Motivation and Objective

Surface acoustic wave (SAW) based radio frequency identification (RFID) tags are truly passive. The reflected responses are weak and usually been corrupted from the tags to the reader. This severely decreases the decoding reliability of SAW RFID system. A powerful method to enhance the reliability of RFID systems is the data checksum, i.e. a few calculated bits of code added to an ID data block to verify its complete transmission. Apart from the GOST SAW tags using cyclic redundancy checks (CRCs), rare SAW RFID system adopting the error control technique has been reported till now. However, the CRC is an error control technique whereby an error detection scheme is combined with requests for retransmission of erroneous data, which means even the decoding error is detected, the position of error still cannot be determined. The only way to get the original responses of tags is to repeat the interrogation from the reader. Obviously, the retransmission will reduce the efficiency of system.

Statement of Contribution/Methods

In this paper, SAW RFID system employing Reed-Solomon (RS) codes, which can both detect and correct multiple random errors in identifying reflector positions, is presented. The coding methods and error correction algorithms of Reed-Solomon codes for SAW RFID are described. Moreover, Monte Carlo methods are applied to analyze the performance of correction efficiency of the developed SAW tags.

Results

Several SAW RFID prototypes with RS(7, 5, 3), which represents that 5 reflectors of 7 on the substrate are source symbols of data group and the 2 remainders are generated from the source symbols called encoding symbols of correction group, are presented in the experimental results. All the symbols'cumulative sum correspond to the position of adjacent reflector and range from 0 to 2^3-1. And a random error of reflector position can be corrected.

Discussion and Conclusions

The results demonstrate that such error correct method will improve the performance of RFID system.

P1E - CMUTs

Carribean Ballroom III-V

Wednesday, October 19, 2011, 9:30 am - 1:00 pm

Chair: **Levent Degertekin**
Georgia Institute of Technology

P1E-1

An Accurate Model For Fluid Loading On Circular CMUTs

Bichoy Azmy[1], Mourad El-Gamal[2], Adel El-Hennawy[1], Hani Ragai[1]; [1]Department of Electronics & Communication Engineering, Ain Shams University, Cairo, Egypt, [2]Department of Electrical & Computer Engineering, McGill University, Montreal, Quebec, Canada

Background, Motivation and Objective

Capacitive Micromachined Ultrasound Transducers (CMUTs) have gained interest by many researchers over the past two decades, namely for medical applications. A wide range of applications requires tissue or fluid coupled ultrasound measurements. CMUT – fluid interaction is a complex process, and fluid loading significantly affects the performance of CMUTs.

This work introduces an accurate analytical model for fluid loading effects on circular CMUT cells, which enables faster computational evaluation of the radiated pressure spectrum compared to the state-of-the-art FEM-based CAD tools.

Statement of Contribution/Methods

In this work, the exact closed form expression of a CMUT acoustical impedance augments the conventional CMUT equivalent circuit model.

The model replaces the material density in the CMUT acoustical impedance with an equivalent density to account for the distributed fluid loading effect.

Data fitting to FEM models was performed to obtain the dependence of the equivalent density on the CMUT dimensions and fluid density.

The equivalent density is also considered to be frequency dependent to enable the prediction of the parallel resonance frequency. The acoustical impedance of a circular piston radiating into a tube is used to estimate the equivalent density frequency dependence.

Results

Figure 1 compares FEM model results to results from the model suggested here. The small signal radiated pressure spectrum are shown.

Discussion and Conclusions

The results show good agreement between the proposed model and its FEM counterpart. Computationally, the model proposed is 15,000 times faster, making it attractive for design iterations and optimization.

Figure 2 shows how our model can predict the case, where parallel resonance destroys the operation of a CMUT, if not properly designed.

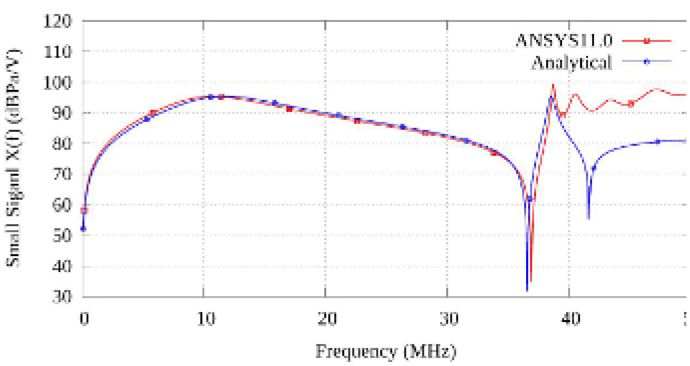

Figure 1: A properly designed CMUT cell. Parallel resonance occurs outside the operational bandwidth.

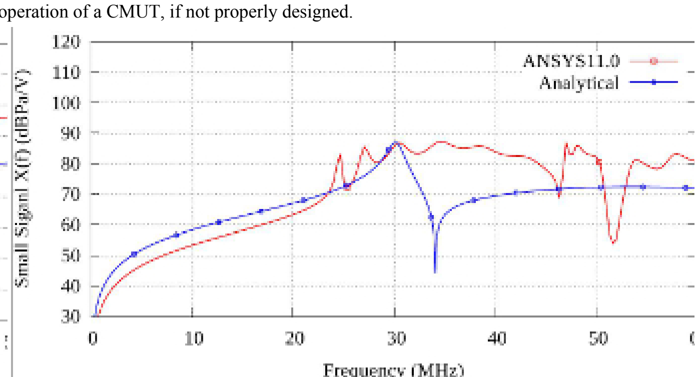

Figure 2: A CMUT cell operational bandwidth disturbed by a parallel resonance.

P1E-2

Improving CMUT Receiving Sensitivity Using Parametric Amplification

Wei You[1], Edmond Cretu[1], Robert Rohling[1]; [1]Electrical and Computer Engineering, University of British Columbia, Vancouver, British Columbia, Canada

Background, Motivation and Objective

An ongoing challenge of CMUTs is the receive sensitivity. Approaches to this problem include operating in collapse-snapback mode, designing non-uniform membranes or dual-electrode structures. Instead of resorting to changes in structural design, we propose a signal control method based on the concept of *parametric amplification* to improve the receive sensitivity of a generic CMUT. The principle is to boost the receive signal amplitude by superimposing the DC receive bias with an AC pump voltage operating at twice the frequency of the incoming acoustic signal.

Statement of Contribution/Methods

During reception, a CMUT cell in an infinite fluid medium is considered as a non-linear oscillator subjected to an external acoustic pressure and an electrostatic force Fe. When an AC pump voltage of twice the incoming signal frequency is superimposed on the DC bias, the nonlinearity of Fe adds a time-varying spring constant. Parametric amplification theory suggests that large gains of the receive signal are possible with proper choice of the phase and amplitude of the pump signal.

We explored the method using both numerical solutions of the CMUT dynamics equation and FEM. We computed the conventional displacement response Xdc to an acoustic source with a DC bias close to pull-in; the mixed response Xdc+ac to the source with a superimposed AC pump voltage; and the response Xac with an AC pump voltage with no acoustic source present. The gain is the ratio between Xdc and the net pumped signal Xpump = Xdc+ac - Xac.

Results

The numerical computation and FEM were carried out assuming the parameters similar to our fabricated CMUT array. Fig. 1 shows the frequency domain average displacement of a CMUT cell in response to a sinusoid acoustic pressure source with the CMUT resonant frequency, and a $\pi/2$ phase shift. The gain for both models is around twofold. The displacement for a pulsed acoustic source was also shown to be amplified. The influence of pump amplitude and phase on the gain was computed to find the optimal phase angles and proper pump voltage.

Discussion and Conclusions

We explored the application of parametric amplification in improving CMUT receive sensitivity by superimposing an AC pump voltage of twice the incoming acoustic signal frequency. The CMUT net displacement during reception shows a twofold increase. This method is a promising alternative to structural designs with the same purpose.

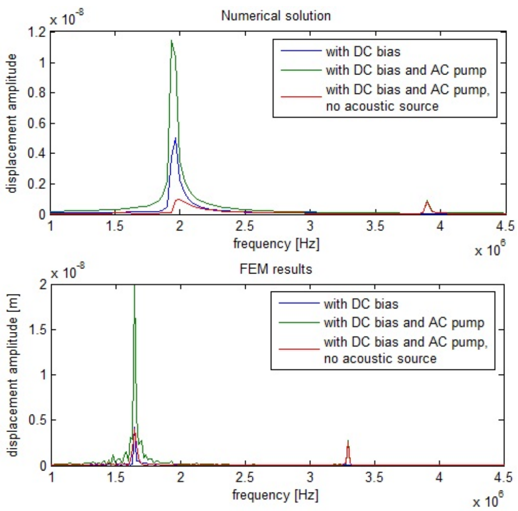

Fig.1

P1E-3

CMUTs for air coupled ultrasound with improved bandwidth

Mario Kupnik[1], **Min-Chieh Ho[2]**, Srikant Vaithilingam[2], Butrus T. Khuri-Yakub[2]; [1]Brandenburg University of Technology (BTU), Cottbus, Germany, [2]Stanford University, CA, USA

Background, Motivation and Objective

We present the design, fabrication and characterization of a multi-purpose capacitive micromachined ultrasonic transducer (CMUT) for air coupled ultrasound (~300-500 kHz), with a focus on improved bandwidth. In wafer-bonded CMUTs, with single-crystal silicon plates from silicon on insulation (SOI) wafers, the bandwidth is low (Q ~ 300 to 500), due to the excellent plate thickness and geometry uniformity between cells. In CMUT-based chemical sensing applications, this is extremely beneficial. In many other applications, however, a wider bandwidth is preferred. This is valid for most applications that require the accurate detection of arrival times of transient ultrasonic pulses. Examples are range finding, ultrasonic transit-time gas flow meters, anemometry, and various other ultrasound-based sensing applications. The focus of this work is to investigate whether wafer-bonded CMUTs can be improved for these applications in terms of arrival time detection.

Statement of Contribution/Methods

The main idea of this work extends the obvious approach to intentionally vary the cell radii across the entire device for improved bandwidth. Because the static deflection is different for each cell of a specific radius, the larger cells inevitably will be closer to pull-in point. The result is a higher transmit and receive sensitivity for larger cells. Thus, we use a calculated sensitivity to estimate an optimum number of cells for each radii group, to avoid an uneven frequency distribution around the center frequency. Further, the larger cells are placed at the perimeter of the device, the smaller one towards the center, for improved acoustic beam profiles. We successfully fabricated two types of circular single-element transducers with a diameter of 12 mm. The device fabrication is based on a previously reported thick buried oxide layer CMUT process (Kupnik, et. al., IUS 2010) for improved reliability. The reference device has 163 circular cells with a radius of 290 µm each, targeting a frequency of ~ 400 kHz. The two new types of devices have cell radii ranging from 280 – 300 µm (20 radii type) and 270 – 310 µm (40 radii type), respectively.

Results

For both impulse response and sinusoidal 3-cycle burst transmit signals, we present time signals and frequency spectra for a pitch-catch configuration. The ring-up time is significantly improved for both types of CMUTs. The bandwidth is higher by a factor up to 30 for the 40 radii type. In all received time signals from both types of CMUTs, we observe a beat frequency oscillation after the first couple of oscillations, which increases the ring-down time.

Discussion and Conclusions

Our approach of varying the cell radii can be used to improve the bandwidth behavior of wafer-bonded CMUTs for airborne ultrasound applications. The observed reduced ring-up time supports the argument that this type of transducer will be beneficial for ultrasonic transit-time detection based applications.

P1E-4

Modeling and Characterization of Thin Film Coatings for High Frequency CMUT Annular Arrays

Jaime Zahorian[1], Sarp Satir[2], Gokce Gurun[2], F. Levent Degertekin[2]; [1]*ECE, Georgia Tech, USA,* [2]*Georgia Tech, USA*

Background, Motivation and Objective

Sub-mm CMUT annular arrays are very attractive for generating high quality imaging beams with small channel count for intravascular imaging. In this work, we analyzed the performance of 840 µm diameter, 40 MHz CMUT annular arrays using analytical and FEA methods in detail, experimentally characterized several types of RTV films at high frequencies as protective and cross talk reducing coatings and evaluated their effect on the annular array performance through FEA.

Statement of Contribution/Methods

The FEA of the CMUT array was conducted using ANSYS and the analytical calculations were based on the Rayleigh integral. To accurately model the effects of RTV layers in ANSYS with the FLUID79 element, the frequency dependent attenuation of ~1 mm thick RTV-60 and RTV-615 samples were measured using two high frequency CMUT arrays in water. The frequency domain and transient pressure fields for focused and unfocused operation were obtained using axisymmetric models. Ideal equal area annular piston array, actual CMUT array with and without cross talk, and RTV coated CMUT arrays were considered. The results are compared with experimental hydrophone data as well as among themselves.

Results

The attenuation of the RTV samples was fit to the relation $\alpha \sim Af^n$ (Np/m) over the frequency range of 5 MHz to 30 MHz with excellent agreement (A= 2.4E-9, n=1.67 for RTV-60, A=2.1E-4, n= 0.956 for RTV-615). With these measurements, attenuation was included in the FEA for 5-15um thick RTV layers and the resulting fields were subsequently propagated into the fluid via post processing in MATLAB. The beam pattern for a Gaussian pulse with 40 MHz center frequency and 50% FBW at F#2 (Fig. 1) show that the CMUT with acoustic cross talk has the same main lobe width but 6 dB higher far side lobe level as compared to an ideal piston array. A 5 µm thick RTV-615 layer reduces the far side lobe level by an additional 7 dBs while also reducing the pressure 3 dBs on the same array and also reduces the center frequency by ~7 MHz.

Discussion and Conclusions

An FEA model that accurately represents the CMUT array behavior with attenuating thin films has been developed. The addition of thin (5-15 µm) RTV layers reduce the cross talk, change the frequency response but do not significantly alter the beam pattern. Therefore, one needs to carefully design the CMUT arrays with higher center frequency to offset the effects of these films.

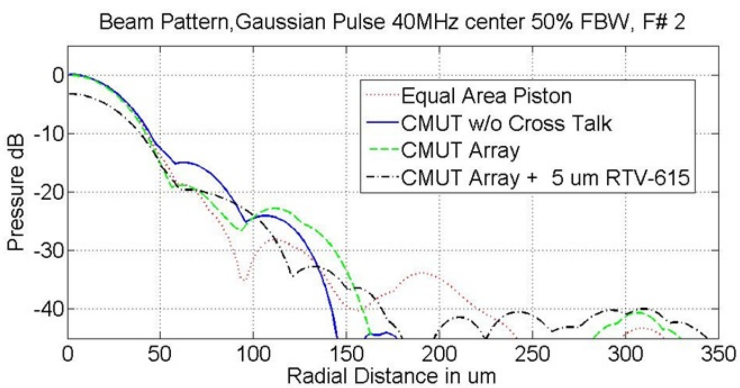

Figure 1. Calculated pressure from an 8 element annular array using a uniform 5 ns delay between elements with a Gaussian pulse centered at 40 Mhz with a 50% fractional bandwidth.

P1E-5

Performance Optimization of a High Frequency cMUT Probe for Medical Imaging

Alessandro Stuart Savoia[1], Giosue Caliano[1], Massimo Pappalardo[1]; [1]Dipartimento di Ingegneria Elettronica, Università degli Studi Roma Tre, Rome, Italy, Italy

Background, Motivation and Objective

The interest by the industry towards the CMUT technology for medical imaging applications is still alive. To date, however, after more than ten years of research and development that led to several cMUT ultrasound probe prototypes, no commercial product based on cMUTs seems to be available on the international market.

In previous works we presented a working prototype of a cMUT probe for medical imaging [1], and the development of a cMUT fabrication technology called "Reverse Fabrication Process" (RFP) [2]. In this work we address the issues related to the performance optimization of a recently developed high frequency cMUT probe, in order to demonstrate the actual usability of cMUT technology for medical imaging purposes.

Statement of Contribution/Methods

We report on the design and fabrication of a 192 element linear array cMUT probe operating in the range 6-18 MHz, designed for vascular, small parts, rheumatology and anaesthesiology imaging applications. By leveraging the advantages offered by our RFP technology, we have developed an efficient and reliable packaging procedure useful for the fabrication of small sized probe-heads, providing the cMUT with specifically designed acoustic backing and lens. The performance maximization has been performed by connecting the cMUT probe-head with multichannel analog front-end electronic circuits housed into the probe. The cMUT and electronics power supplies are internally generated in the probe.

Results

The probe prototypes have been electrically and acoustically characterized and in-vivo ultrasound images have been obtained. A performance comparison between our cMUT probe and its PZT commercial counterpart designed for the same applications, has been carried out. The optimized cMUT probe prototypes show better performances in terms of two-ways sensitivity and bandwidth.

Discussion and Conclusions

We have optimized the electro-acoustic performances of a high frequency cMUT probe by introducing analog front-end electronic circuits in the probe itself and by working on the packaging process and materials of the cMUT probe-head. The prototypes realized within this activity can be used on commercial ultrasound imaging systems without the need of any hardware modification.

[1] A. Caronti, G. Caliano, R. Carotenuto, A. Savoia, M. Pappalardo, E. Cianci, and V. Foglietti, "Capacitive micromachined ultrasonic transducer (CMUT) arrays for medical imaging," Microelectronics Journal, vol. 37, pp. 770-777, 2006.

[2] G. Caliano, A. Caronti, A. Savoia, C. Longo, M. Pappalardo, E. Cianci and V. Foglietti, "Capacitive micromachined ultrasonic transducer (cMUT) made by a novel "reverse fabrication process"," Ultrasonics Symposium, 2005 IEEE , vol.1, no., pp. 479- 482, 18-21 Sept. 2005.

P1E-6

Dual mode cMUTs fabricated with LPCVD sacrificial release process

Certon Dominique[1], Senegond Nicolas[1], Gross Dominique[1], Ferin Guillaume[2], Legros Mathieu[2], Boulme Audren[1], Roman Benoit[1], Teston Franck[1]; [1]*INSERM U930, François Rabelais University, TOURS, France, Metropolitan,* [2]*VERMON, TOURS, France, Metropolitan*

Background, Motivation and Objective

More and more medical ultrasonic applications are strongly interested by the development of dual acoustic sources enable to emit high frequency ultrasound and low frequency pressure field. The use of the piezoelectricity to fabricate such device requires overcoming strong technological bottlenecks. The objective of this paper is to demonstrate that the technology of capacitive micro-machined ultrasonic transducer is able to take up this challenge.

Statement of Contribution/Methods

To design and manufacture high frequency cMUTs, the main technological challenge is the fabrication of devices with low gap height to avoid high collapse voltage values. To contrary, low frequency cMUTs must possess high gap height to produce high amplitude mechanical displacements. The construction of dual mode acoustic cMUTs with high level of performances requires thus manufacturing on the same substrate two populations of cMUTs with two gap heights. In this work, we will show that, up to 20 MHz, acoustic trade-offs can be done in order that the two functions can be realized with one gap height only. Two demonstrators of dual mode transducers were fabricated. The manufacturing procedure was a LPCVD-based sacrificial release process.

Results

The first part of the paper is devoted to the design of low and high frequency cMUTs. The gap height was fixed to 250 nm, and two membrane thicknesses of 400 nm and 600 nm were chosen. For the low acoustic source, a dedicated time domain model was used, taking into account the nonlinearity of the cMUT. Several simulations were conducted to optimize the emitted pressure field intensity at 1 MHz for a set of diaphragm with different sizes (25 µm to 40 µm) and geometries. The high frequency source was designed on the help of a linear model, where output parameters were central frequencies, bandwidths and collapse voltages. The second part is dedicated to the characterization of the manufactured demonstrator. Two low acoustic diaphragms were fabricated (25 µm and 30 µm width) and tested. Two high frequency sources were selected: 13 MHz and 16 MHz. Measurements of electrical impedance, mechanical displacements in oil were done. Acoustic pressure field are reported too.

Discussion and Conclusions

Experimental responses of the cMUTs were compared with theoretical simulations. The displacements and pressures of low frequency cMUTs were well predicted in terms of shapes and amplitudes, as a consequence the radiated acoustic intensity too. We observed that acoustic peak-to-peak pressure amplitude of 1 MPa was achievable. High frequency sources had the expected central frequency with bandwidth of 100 %. Their collapse voltage was lower than 200 Volts, with the same gap height than that of the low acoustic source. The feasibility of dual mode cMUT with one gap is thus demonstrated. This first base of experimental knowledge is finally used to discuss and define new trade-offs to optimize dual-mode cMUTs with a single gap height.

P1E-7

Dynamic and Acoustic Modelization of Capacitive Micromachined Ultrasonic Transducers

Marc Berthillier[1], Patrice Le Moal[1], Joseph Lardiès[1]; [1]*Mécanique Appliquée, Femto-ST, Besançon, France*

Background, Motivation and Objective

The Capacitive Micromachined Ultrasonic Transducers (CMUT) is a very promising alternative to piezo-electric ultrasonic transducers. They are constituted by a very large number of micro-membranes organized in network and electrostatically actuated. The prediction of the radiated acoustic pressure with a finite element model representing all the micro-membranes and the radiation medium is almost impossible. So models have been proposed with various levels of simplification. In most of them crosstalk between membranes is strongly simplified. We propose here a modelization of the complete CMUT network with almost no simplifications that can provide the dynamic displacements of all the membranes as well as radiation pressures within an acceptable computational time.

Statement of Contribution/Methods

The dynamic displacements of the membranes are decomposed on the membranes modes shapes in vacuum. The non linear electrostatic actuation is linearized, around the static equilibrium position. A softening effect is thus introduced. Coupling between membranes is only considered via the radiation medium. As the CMUT is flat and the medium is semi infinite, coupling pressures have been computed by the Rayleigh integral. The dynamic response of the membranes is computed first, in the frequency domain, taking into account crosstalk effects. Then the radiated pressures in the medium are deduced using the Rayleigh integral.

Results

The method has been applied to a network of 300 circular membranes radiating in water. The network is 1D with 6 elements of 50 membranes each. The silicon membranes have a radius of 50 µm and a thickness of 1,5 µm. We present on the figure the displacement on a part of the network, for a phase shift of 36° between elements and at an excitation frequency close to that of the second mode. We can notice the coupling between the first and the second mode that will strongly influence the radiated pressure. Network modes are also observable at other frequencies.

Discussion and Conclusions

We successfully develop a method to predict the displacements and the radiation pressures of CMUT with a model very close to the physics. We can see the strong influence of crosstalk between membranes via mode coupling, network modes and side effects. Computational time is compatible with design constraints.

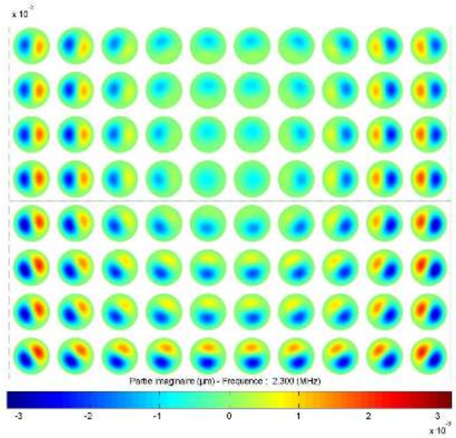

P1E-8

Large area 1D CMUT phased arrays for multi-modality ultrasound imaging

Nikhil Apte[1], Srikant Vaithilingam[2], Ali Fatih Sarioglu[2], Mario Kupnik[3], Butrus T. Khuri-Yakub[2]; [1]Mechanical Engineering, Stanford University, USA, [2]Electrical Engineering, Stanford University, USA, [3]Brandenburg University of Technology, Germany

Background, Motivation and Objective

Capacitive Micromachined Ultrasound Transducers (CMUTs) offer many advantages over conventional piezoelectric transducers including an inherently large bandwidth (in immersion). Unlike piezoelectric transducers, they do not overheat when delivering ultrasound waves over a prolonged period of time. These qualities make CMUTs ideal for use in multi-modality imaging with techniques like harmonic imaging, ultrafast imaging and shear wave elastography. We have designed 1D CMUT phased arrays for cardiac and trans-thoracic multi-modality imaging and are currently fabricating these arrays.

Statement of Contribution/Methods

The arrays were designed to have an element height of 14 mm. Two types of arrays were designed with 64 and 80 elements each and an element pitch of 280 µm and 224 µm respectively. The CMUTs were modeled with an equivalent circuit model and simulated for computation of bandwidth and output pressure. The cables and preamplifier were also incorporated in the simulation to determine the noise performance of the entire system.

The CMUT arrays are currently being fabricated with a modified version of the process based on a thick buried oxide layer, developed by Kupnik et al. In our process the via connections for each cell's electrode with the handle layer are made from the front side. The process starts with an SOI wafer having a 50 µm device layer, 250 µm handle layer and a 1 µm thick buried oxide layer. Individual cells are defined on the front side using DRIE. An intermediary titanium layer is used to bond two SOI wafers together to form the 1.9 µm thick CMUT plate layer. Individual elements in each array are isolated using DRIE on the back side.

Results

Our calculations predict a center frequency of 2.5 MHz and a fractional bandwidth exceeding 200% for these arrays. When biased at 80% of their pull-in voltage and excited by an ac signal of 80 V amplitude, the calculated transmit pressure is 680 kPa. Using a dedicated low noise preamplifier integrated in the probe handle, a minimum noise figure of 7.5 dB can be achieved at 2 MHz.

Discussion and Conclusions

The large simulated bandwidth and transmit pressure for the arrays make them suitable for multi-modality imaging. Since the via connections are made from the front side, further we will be able to fabricate smaller cells for higher frequency.

This research is supported by SuperSonic Imagine, France under the scope of Icare project.

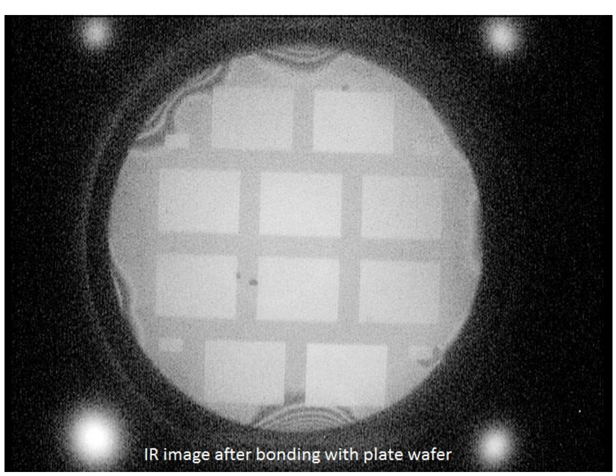

WEDNESDAY POSTER

PS - Student Paper Competition

Carribean Ballroom III-V

Wednesday, October 19, 2011, 9:30 am - 4:30 pm

Chair: **0**
0

PS-1

In-vivo pulsed magneto-motive ultrasound imaging of tumor bearing small animals

Mohammad Mehrmohammadi[1], Seungsoo Kim[1], Min Qu[1], Ryan Truby[1], Pieter Kruizinga[2], Stanislav Emelianov[1]; [1]Biomedical Engineering, University of Texas at Austin, Austin, TX, USA, [2]Thoraxcenter, Biomedical Engineering, Erasmus MC, Rotterdam, Netherlands

Background, Motivation and Objective

Pulsed magneto-motive ultrasound (pMMUS) imaging has been introduced as a novel ultrasound-based cellular/molecular imaging modality. In pulsed magneto-motive ultrasound imaging a high intensity pulsed magnetic field is used to excite the cells labeled with magnetic nanoparticles and ultrasound imaging is then used to monitor the mechanical response of the tissue (i.e. tissue displacement). Here, we investigated the feasibility of pMMUS imaging to identify the presence and distribution of magnetic nanoparticles within a tumor-bearing animal injected with superparamagnetic iron-oxide nanoparticles.

Statement of Contribution/Methods

Superparamagnetic magnetite nanoparticles were used as pMMUS contrast agents. The nanoparticles were synthesized by the thermal decomposition of iron (iii) acetylacetonate in triethylene glycol without a surfactant. By replacing the polyol surface layer with citrate, the magnetite nanoparticles were dispersed in aqueous solutions. Epidermoid carcinoma A431 cells were injected into 10 weeks old Nu-Nu mice for tumor inoculation. When the tumor size reached about 1 cm in diameter, the contrast agents were injected directly into tumor or intravenously. The animal was kept close to a permanent magnet (~ 0.5 T) for 2 hours after the injection to increase the uptake of nanoparticles by tumor cells. The ultrasound and pMMUS imaging were performed using a high frequency array transducer (20 MHz central frequency) and Vevo2100 small animal ultrasound imaging system. The magnetic pulses of 0.8 T were generated using a high power current amplifier connected to a relatively large coil. Both ultrasound (US) and power Doppler (PD) signals were acquired before, during and after application of a 40 msec long magnetic pulse.

Results

Figure 1 represents the US and PD images of a selected cross-section within the tumor region 24 hours after intra-tumor injecting the magnetic contrast agents. The PD signal clearly indicates the induced displacement within the tumor region that corresponds to the presence of magnetic nanoparticles.

Discussion and Conclusions

In summary, we have demonstrated the capability of pMMUS imaging to detect the presence of magnetic nanoparticles in-vivo. Once developed, pMMUS imaging can provide such information in real time, non-invasively and at reasonable imaging depths and therefore can be used to monitor events at the cellular level.

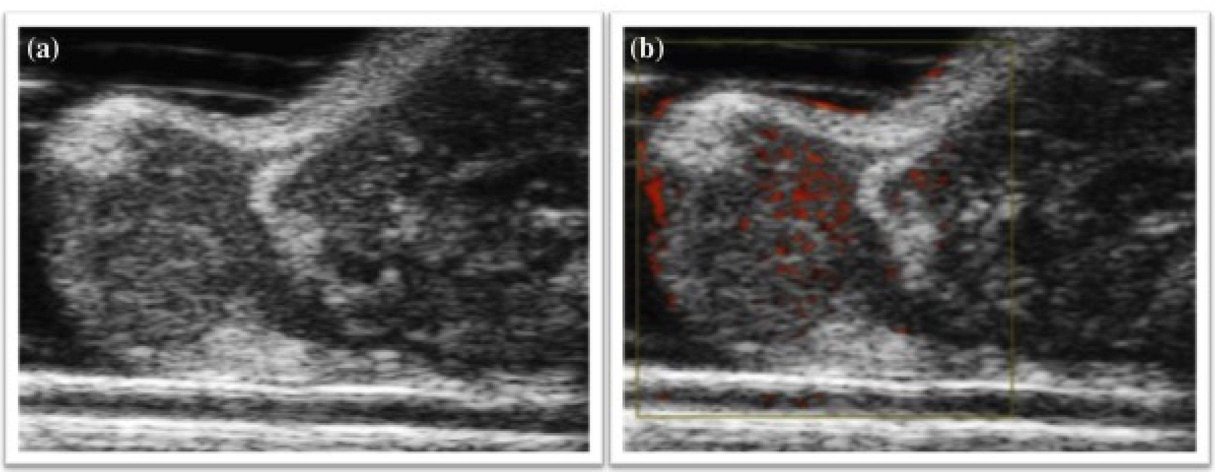

PS-2

Generalized Bayesian Speckle Tracking Applied to Strain and ARFI Displacements

Brett Byram[1], Gregg Trahey[1], Mark Palmeri[1]; [1]*Duke University, USA*

Background, Motivation and Objective

A hallmark of clinical ultrasound has been accurate and precise time-delay estimation (TDE). TDE has numerous clinical uses including blood-flow, elastography, therapeutic guidance and ARFI imaging. In ultrasonic TDE, the fundamental limit on displacement accuracy has been regarded as the Cramer-Rao lower bound (CRLB). The CRLB, more specifically, represents the minimum variance of an unbiased estimator. Unbiased estimators can be useful, but in many cases allowing an estimator to be slightly biased results in a large decrease in variance and overall mean square error (MSE) improvement relative to CRLB limited estimators.

Statement of Contribution/Methods

To create a biased estimator with better performance than a CRLB limited estimator (e.g. normalized cross-correlation (NCC)) a generalized framework is developed for Bayesian speckle tracking. A Bayesian estimator requires a likelihood function and prior probability distribution function (PDF). First, a likelihood function appropriate for ultrasound is derived since the canonical likelihood function used in other fields for TDE requires precise knowledge of the thermal noise power for each estimate which is not currently feasible. Second, prior PDFs are formed using several methods. These methods were evaluated and include both informative and non-informative priors. The informative priors were based on the displacement PDFs at adjacent locations.

The biased estimators were validated using bulk motion simulations and ARFI simulations created with a finite-element model and Field II.

Results

The proposed likelihood function was evaluated and compared against the classic likelihood function by converting both to posterior PDFs using a non-informative prior. Example results are reported for bulk motion simulations using a 6 lambda tracking kernel and 30 dB SNR for 1000 data realizations. The new and canonical likelihood function assigned the true displacements probabilities of .22+/- .16 and .070+/- .020, respectively. For the same tracking parameters and simulated ARFI displacements the new and canonical likelihood function assigned the entire true ARFI displacement profile the log10 probability of -34 +/- 7 and -51+/- 14. These trends hold at least for SNRs greater than 10 dB and kernel lengths between 1.5 and 12 lambda.

The peak displacement of the ARFI response is reported since this position results in the noisiest estimates. Estimates were made with a 1.5 lambda kernel and 20 dB SNR on 100 data realizations. Estimates using NCC and the Bayes estimator had MSEs of 17 and 7.6 microns squared, respectively, contextualized by the true displacement magnitude, 10.9 um. Biases for the NCC estimator and the Bayes estimator are -.12 and -.28 um, respectively.

Visible improvements were also seen in in vivo myocardial canine ARFI and strain images.

Discussion and Conclusions

Bayesian speckle tracking has been tested with simulation and in vivo data. Bayesian tracking outperforms traditional ultrasonic TDE.

PS-3

Improving Shear Wave Speed Estimation Precision in Homogeneous Media by Tracking Shear Wave Propagation in 3D using a Real-time Volumetric Imaging Transducer

Michael Wang[1], Brett Byram[1], Mark Palmeri[1], Ned Rouze[1], Kathryn Nightingale[1]; [1]*Biomedical Engineering, Duke University, USA*

Background, Motivation and Objective

Tissue displacement due to acoustic radiation force impulse (ARFI) excitation can only be monitored in one slice of the anatomy using conventional 1D array ultrasound transducers. As a result, shear wave propagation data in only one direction is available for stiffness estimation. With the recent availability of matrix array ultrasound transducers, acquisition of displacement fields within a volume of tissue in real-time is now possible. The ability to track shear wave propagation in multiple directions allows anisotropic mechanical properties to be estimated, as well as the ability to measure ARFI response over a larger volume. We present a system capable of tracking ARFI induced shear wave propagation in 3D, and show that by monitoring shear wave propagation in multiple directions, the precision of shear wave speed (SWS) estimation in a homogeneous material can be improved.

Statement of Contribution/Methods

An annular focused HIFU piston transducer (H-101, Sonic Concepts, Bothell, WA) is used for ARFI excitation (1.1 MHz, f/1, 60 mm focal depth). A 2D matrix array transducer (4Z1C on an SC2000 scanner, Siemens Healthcare, Ultrasound Business Unit, Mountain View, CA, USA) inserted in the central opening of the HIFU piston was used for monitoring ARFI displacement. Shear waves were induced in a homogeneous phantom (E=4.5 kPa) using a 1000 cycle push pulse with $I_{sppa.7}$ = 1417 W/cm^2. Displacement tracking was performed at a frequency of 2.5 MHz using a 10×12 (lateral × elevation) rectangular grid of receive beams. The spatial extent of this tracking region was 16.5×20 mm at the push focal depth. The push axis was located at one corner of the tracking region. 30:1 parallel receive was used to enable a volume rate of 2 kHz. The effect of tracking beam locations on the precision of time-of-flight (TOF) SWS estimation was investigated using synthetic shear wave arrival time data corrupted by Gaussian noise.

Results

For the very first time, shear wave propagation away from the push within the lateral-elevation plane is observed. It can be shown (and verified by simulation) that by using radially symmetric beam locations about the excitation, the root mean square (RMS) error of TOF SWS estimation in a homogeneous medium can be reduced by a factor of $R=\sqrt{((N+1)(N-N_\theta)/((N-1)(N+N_\theta))}$, where N is the total number of beam locations, and N_θ the number of directions tracked. For N=64 (the number of parallel receive beams available on the SC2000), the greatest reduction in RMS error in this approach is R=0.6, and is obtained when N_θ=32 (i.e., 2 beams per direction at the edges of the reconstruction kernel).

Discussion and Conclusions

Tracking ARFI induced shear wave propagation in 3D is now possible using a matrix array volumetric imaging transducer. By tracking shear wave propagation in multiple directions, the RMS error of TOF SWS estimation in homogeneous media can be reduced.

PS-4

Optical Characterization of Individual Liposome Loaded Microbubbles

Ying Luan[1], Telli Faez[1], Erik Gelderblom[2], Ilya Skachkov[1], Bart Geers[3], Ine Lentacker[3], Antonius van der Steen[1], Michel Versluis[2], Nico de Jong[1,2]; [1]*Erasmus Medical Center, Netherlands,* [2]*University of Twente, Netherlands,* [3]*University of Gent, Belgium*

Background, Motivation and Objective

Liposome loaded microbubbles (lps bubbles) have been newly developed by attaching drug containing liposomes to phospholipid-shelled microbubbles through covalent thiol-maleimide linkages (Figure (A)) [1]. Applied as an ultrasound triggered drug delivery vehicle, it has shown great potential to realize highly efficient and localized drug release. In this study we optically compared individual lps bubbles with standard phospholipid bubbles (bare bubbles) concerning shell properties and ultrasonic response with a high framing camera.

Statement of Contribution/Methods

Lps bubbles and bare bubbles, ranging from diameter of 3 to 8 μm, were insonified with driving frequencies from 0.5 to 4 MHz and acoustical pressures from 5 to 100 kPa. Bubble dynamics were recorded with the ultra-high speed camera Brandaris 128 at 15 Mfs. Resonance curves were constructed from diameter-time (D-t) curves of bubble oscillations and shell elasticity and viscosity were derived (Figure (B))[2]. Laser induced fluorescence imaging were applied before and after ultrasound treatment to acquire morphology and stability of liposomes attachment.

Results

72 lps bubbles and 55 bare bubbles were investigated. Shell elasticity of lps bubbles (0.77±0.1 N/m) was 88% higher compared to bare bubbles (0.41±0.1 N/m) for all investigated bubble sizes. Clear difference of shell viscosity was found for bubbles larger than 6 µm. Averaged viscosity of lps bubbles ($3.2 \cdot 10^{-8}$ kg/s) was 44% higher than that of bare bubbles ($1.8 \cdot 10^{-8}$ kg/s). Moreover, we found an ″expansion only behavior″ among 73% of lps bubbles (Figure (C)), with 60% among them happened at low pressures (<30 kPa). Fluorescence imaging clearly showed stably attached bodipy-labeled liposomes at the surface of microbubbles.

Discussion and Conclusions

Lps bubbles and bare bubbles have different ultrasonic response and shell properties. Results from this study will facilitate applications as well as further comprehension of drug transfer mechanism using ultrasound triggered drug delivery system.

1. Geers, B., et al., Journal of Controlled Release. In Press.

2. Meer van der, S.M., et al., Journal of the Acoustical Society of America, 2007. 121(1): p. 648-656.

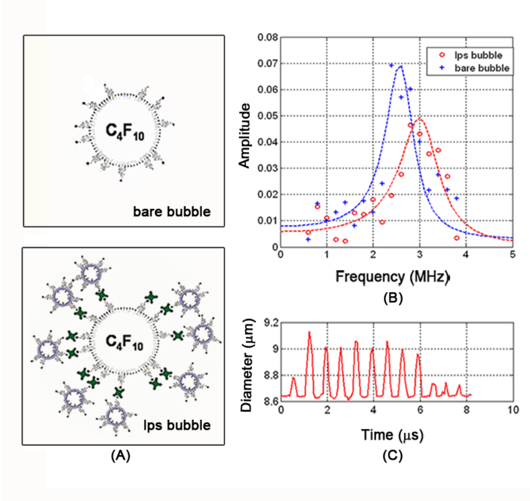

PS-5

In vivo monitoring of nanoparticle delivery using spectroscopic photoacoustic imaging

Seungsoo Kim[1], Geoffrey Luke[2], Yun-Sheng Chen[2], Stanislav Emelianov[1,2]; [1]Biomedical Engineering, University of Texas at Austin, Austin, TX, USA, [2]Electrical and Computer Engineering, University of Texas at Austin, Austin, TX, USA

Background, Motivation and Objective

In vivo monitoring of nanoparticle (NP) delivery is essential to better understand cellular and molecular interactions of NPs with cells. Spectroscopic photoacoustic (sPA) imaging can detect NPs based on optical absorption spectra. The goal of this study was to demonstrate sPA imaging can be used for in vivo monitoring of nanoparticle delivery using a mouse bearing a subcutaneous tumor.

Statement of Contribution/Methods

A431 cancer cells were injected into the flank of a Nu/Nu mouse to produce a tumor mass. The tumor was scanned before and 31 hours after intravenous injection of PEGylated gold nanorods (PEG-Au NRs) using an integrated ultrasound (US) and photoacoustic (PA) imaging system. In order to monitor uptake of PEG-Au NRs within the tumor, three-dimensional (3-D) sPA imaging was performed. Spectral processing based on a minimum mean squared error (MMSE) method was used to determine the similarity between the sPA and NP spectra. The MMSE, along with the sPA signal amplitude, determined the relative NP concentration. Finally silver staining of the excised tumor tissue was used to confirm NP deposition.

Results

Uptake of PEG-Au NRs was ascertained by both 3-D sPA imaging and silver staining. Figures 1 (a) and (b) show combined 3-D US (gray color) and overlaid sPA (green color) images before and 31 hours after the NP injection, respectively. While the US image shows mouse tumor morphology (i.e., tumor size and location) as well as overall outline of the mouse body, the sPA image provides information on NP distribution. The silver staining slide of excised tumor tissue (Fig. 1(d)) clearly confirmed NP deposition, and moreover was highly correlated with sPA image (Fig. 1(c)) at the same cross section as the histological slide.

Discussion and Conclusions

We successfully demonstrated 3-D US and sPA imaging can be used for in vivo detection of NPs using a tumor-bearing mouse. Good correlation of NP distribution between histological slides and sPA images was also demonstrated. The results of our study suggest that sPA imaging is a promising imaging technique to detect NPs in vivo, and therefore can be used for more nanoparticle-related studies such as the effect of using molecular specific targeted NPs on delivery efficiency.

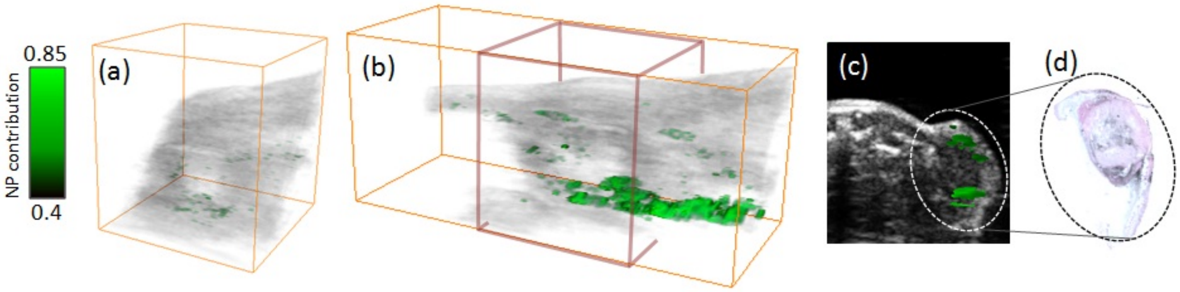

Fig. 1. 3-D ultrasound (US) and spectroscopic photoacoustic (sPA) images of the mouse (a) before and (b) 31 hours after PEGylated gold nanorods injection. Green-colored pixels on the images are nanoparticle contributions obtained from the developed spectroscopic analysis method. (c) The combined US and sPA image and (d) a silver staining slide shows good correlation as well as NP deposition at the tumor.

PS-6

Intravascular Ultrasound Chirp Imaging of atherosclerotic plaque pathology and neovascularization

David Maresca[1], Krista Jansen[1], Guillaume Renaud[1], Wijnand den Dekker[2], Gijs van Soest[1], Xiang Li[3], Qifa Zhou[3], Jonathan Cannata[3], Antonius F.W. van der Steen[1,4]; [1]*Biomedical Engineering, Thorax Centre, Erasmus MC, Rotterdam, Netherlands,* [2]*Experimental Cardiology, Erasmus MC, Rotterdam, Netherlands,* [3]*Resource Center for Medical Ultrasonic Transducer Technology, University of Southern California, Los Angeles, USA,* [4]*Interuniversity Cardiology Institute of the Netherlands, Netherlands*

Background, Motivation and Objective

The detection and identification of vulnerable atherosclerotic plaques, susceptible to rupture and therefore candidates for intervention, remains a central issue in cardiac imaging. Neovascularization within and surrounding plaques is essential to enable lesion growth and plays a central role in rendering it vulnerable to rupture. We investigated how chirp coded excitation could extend intravascular ultrasound (IVUS) imaging depth in order to characterize deeper coronary atherosclerosis and neovascularization.

Statement of Contribution/Methods

A 53 MHz IVUS transducer (-6dB bandwidth 55%, natural focus 3.1mm) was driven with 0.5µs chirp excitations (39-67MHz) or 53MHz full band Gaussian pulses of equal peak negative amplitude. A TPX hollow cylinder containing 4 sub wavelength targets (15µm thick platinum/iridium wires) at 1.5, 3, 5 and 7 mm from the cylinder axis allowed to measure the axial resolution and the signal to noise ratio (SNR). The cylinder was immersed in water and imaged with 360 radio frequency (RF) lines per rotation. Both excitations were subsequently fired at each angular position. The RF data was band pass filtered, the envelope was derived, log compressed and scan converted with a 40dB dynamic range. The chirp compression filter consisted of the Chebyshev tapered chirp excitation. The same protocol was repeated on ex-vivo atherosclerotic rabbit aortas at clinical IVUS frequencies (24 to 44MHz) with another IVUS transducer and no averaging.

Results

We measured from the closest to the farthest wire a gain in SNR of 8.7, 9.0, 9.1 and 9.9dB with the chirp coded excitation. The axial resolutions (-6dB point spread function) were 68, 68, 70 and 68µm for the Gaussian pulse and 97, 92, 93 and 101µm for the chirp excitation after compression. The ex-vivo rabbit aorta results showed a significant gain in SNR and a slight deterioration of the resolution (see figure).

Discussion and Conclusions

We demonstrated that chirp coded excitations of limited temporal lengths can be successfully used for IVUS imaging. We observed a gain in SNR of 10dB at a distance of 7 mm while maintaining a satisfactory axial resolution. These findings were confirmed at conventional IVUS frequencies on the ex-vivo rabbit aortas. Different compression filters will be investigated to reduce compression sidelobe levels and account for frequency dependent attenuation.

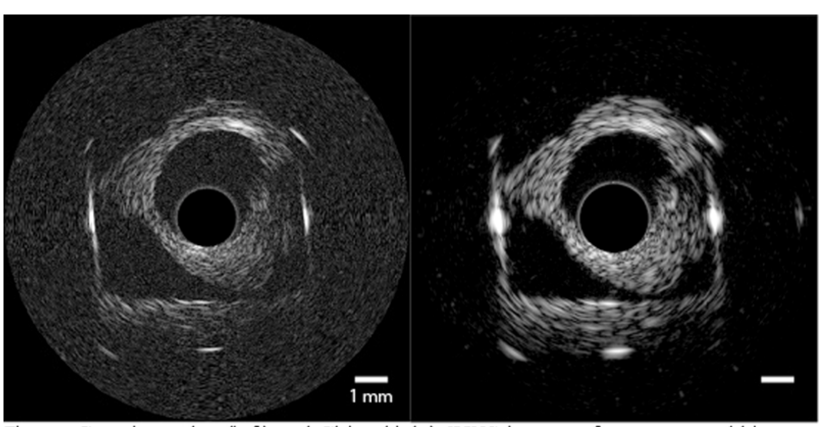

Figure: Gaussian pulse (left) and Chirp (right) IVUS images of an *ex-vivo* rabbit aorta (dynamic range 40dB). The square structure holding the vessel appears around the artery cross section.

PS-7

Real-time Handheld Optical Resolution Photoacoustic Microscopy

Parsin Hajireza[1], Wei Shi[1], Roger Zemp[1]; [1]Electrical & Computer Engineering, University of Alberta, Edmonton, Alberta, Canada

Background, Motivation and Objective

Optical resolution photoacoustic microscopy (OR-PAM) is an imaging technology providing high optically defined lateral spatial resolution to visualize superficial structures in vivo with optical-absorption contrast. OR-PAM is able to quantify morphological parameters and functional parameters down to capillary size (~7µm). Such parameters include microvascular density, total hemoglobin concentration, hemoglobin oxygen saturation, etc, important for studying the earliest stages of tumor angiogenesis. Besides preclinical research applications, OR-PAM could have clinical potential if it could be developed into a portable, real-time imaging technology. Previous systems, however, require long imaging times due to low-repetition-rate lasers and mechanical scanning. They are also typically tabletop systems requiring bulky and expensive laser systems, and providing little flexibility for imaging various anatomical locations. In order to overcome this limitation, we have introduced a unique high repetition rate, inexpensive, compact fiber laser sources for realizing high frame rate photoacoustic imaging.

Statement of Contribution/Methods

In order to extend the potential range of applications to clinical settings, for the first time, we demonstrate a handheld real-time optical resolution photoacoustic microscope (HH-OR-PAM). Using fast scanning mirrors, an image guide with 30,000 fiber pixels, a customized doublet lens and a special probe we managed to reduce the footprint of an OR-PAM system from a stationary table-top system to a portable, 3x5x6cm, probe weighing ~ 500g.

Results

The capability of HH-OR-PAM is demonstrated with phantoms and in vivo (microvasculature in a Swiss Webster mouse ear) studies based on a customized tunable fiber laser with repetition rates of nanosecond-pulses up to 600kHz, enabling near real-time C-scan imaging. Phantom studies indicate 7 µm transverse resolution.

Discussion and Conclusions

The proposed setup keeps many of the powerful properties of previous top-table OR-PAM systems but adds high flexibility due to the nature of the image guide and handheld apparatus. Therefore, the setup may widely improve the usability of OR-PAM from lab experiments to real world clinical applications.

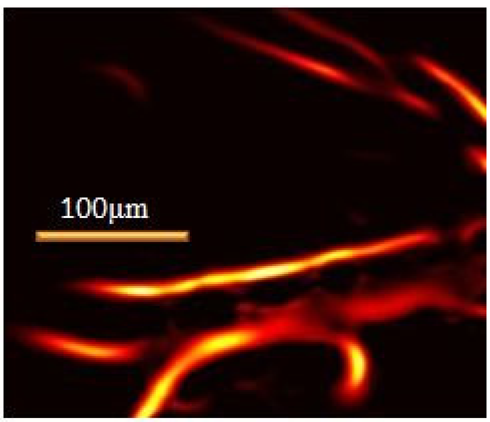

PS-8

Precise Transportation of Single Cell by Phase-shift Standing Surface Acoustic Wave

Long Meng[1], Feiyan Cai[1], Qiaofeng Jin[1], Lili Niu[1], Hairong Zheng[1]; [1]Shenzhen Institutes of Advanced Technology, Chinese Academy of Sciences, China, People's Republic of

Background, Motivation and Objective

Continuous manipulation of single cell in a fluid medium is of crucial interest not only for basic cell biology but also for clinical medicine, cancer research and gene therapy. Available methods for controlling transportation of cells are realized mainly by switching the acoustic pressure, resonant mode and actuation frequency. However, it is challenging to precisely transport and locate the cells. In this paper, a microfluidic device that could precisely transport a single cell by phase-shift standing surface acoustic wave (SSAW) was developed.

Statement of Contribution/Methods

A pair of interdigital transducers (IDTs), having a pitch of 200 µm, was deposited on a 128YX-LiNbO3 substrate. Then, a PDMS microchannel was bonded to the SSAW generator using oxygen plasma treatment. Human breast cancer cell was infused in the microchannel through a pressure driven flow. By modulating the relative phase, Δφ, between two IDTs, the position of pressure nodes in the microchannel changes correspondingly resulting in the transportation of the single cell. Both of the numerical calculation and experiments were carried out to investigate the mechanics and performance of the transportation device.

Results

When there was no phase shift, the cell was retained in the center of the microchannel (dash line), as shown in Fig. 1a. Setting the value of Δφ to -100º, the cell moved upwards for a distance of 27.6 µm, agreeing well with the theoretical value of 27.8 µm (Fig. 1b). While adjusting the value of Δφ to -150º, the cell kept on moving upwards but the displacement reduced by half correspondingly, about 13.85 µm (Fig. 1c). Then, modulating the Δφ to -50º, the cell moved toward the initial position (Fig. 1d). Finally, the Δφ was further modulated to 0º, the cell went on moving downwards, and returned back to the same location (Fig. 1e).

Discussion and Conclusions

The simulation and experimental results reveal that there is a good linear relationship between the relative phase and the displacement. Varying the relative phase continuously, the single cell could be transported precisely in arbitrary location in the microchannel. Furthermore, improving the frequency and structure of IDTs would make it possible to transport the nanoscale bioparticles in two dimensional spatial positions.

WEDNESDAY POSTER

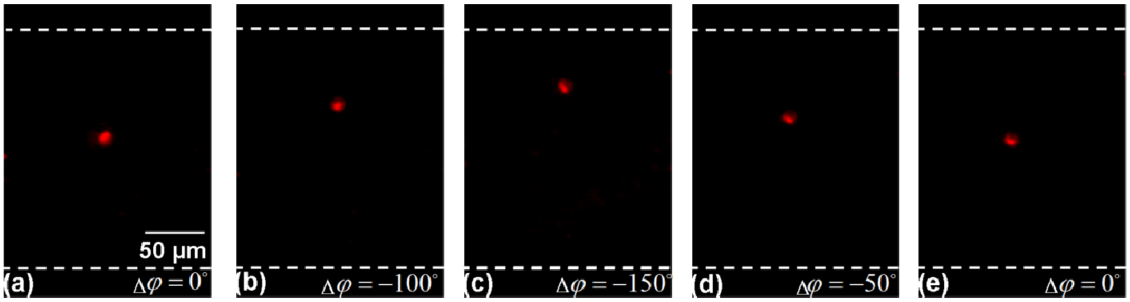

PS-9

Guided wave temperature compensation with the scale-invariant correlation coefficient

Joel B. Harley[1], José M.F. Moura[1]; [1]Department of Electrical and Computer Engineering, Carnegie Mellon University, Pittsburgh, Pennsylvania, USA

Background, Motivation and Objective

Guided wave structural health monitoring systems create complex wave fields that travel through the thickness of a structure and reflect off of damage. However, variations in environmental conditions alter the propagation of guided waves and significantly affect the performance of these systems. Temperature is one of the most prominent of these effects. Variations in temperature change the velocities of modes, which stretch measured signals in time.

Several researchers have proposed methods, such as local peak coherence (LPC) [1], to compensate for temperature by estimating the stretch factor and properly adjusting the signal. In this paper, we propose a new compensation technique, the scale-invariant correlation coefficient (SICC) [2]. We benchmark SICC with the more expensive optimal signal stretch (OSS) [3], which correlates each observed signal with a library of stretched replicas of a single baseline.

Statement of Contribution/Methods

Using experimental data, we compare the robustness and computational performance of the LPC, OSS, and SICC methods. Data is generated and measured from two piezoelectric transducers bonded to a thin 9.8cm by 30.5cm by 0.1cm aluminum plate. Measurements are taken every 2 minutes over a 24 hour period in which the ambient temperature varies between 3.75 °C and 21.67 °C. During that time, a cylindrical mass is placed on the plate to simulate damage.

Results

For every signal measured, we apply each compensation method and compute its associated correlation coefficient with a known baseline. Figure 1 illustrates the changes in correlation during the experiment.

Discussion and Conclusions

Without compensation, the correlation coefficient varies dramatically with temperature. With compensation, the values vary little until the mass is added at 6:53 PM, when they drop and LPC begins to vary erratically. SICC has near identical performance as OSS, but is more computationally efficient.

References

[1] Y. Lu and J. E. Michaels, "A meth. for struc. health mon. with diff. ultrason. waves in the pres. of temp. var.," Ultrasonics, vol. 43, no. 9, pp. 717–31, Oct. 2005.

[2] J. Harley and J. M. Moura, "The scale cross-corr. and its app. to ultrason. temp. comp.," preprint.

[3] T. Clarke and et al., "Guided wave health mon. of complex struc. by sprs. array sys.: Influ. of temp. chng. on perfrm.," J. Sound Vib., vol. 329, no. 12, pp. 2306–2322, Jun. 2010.

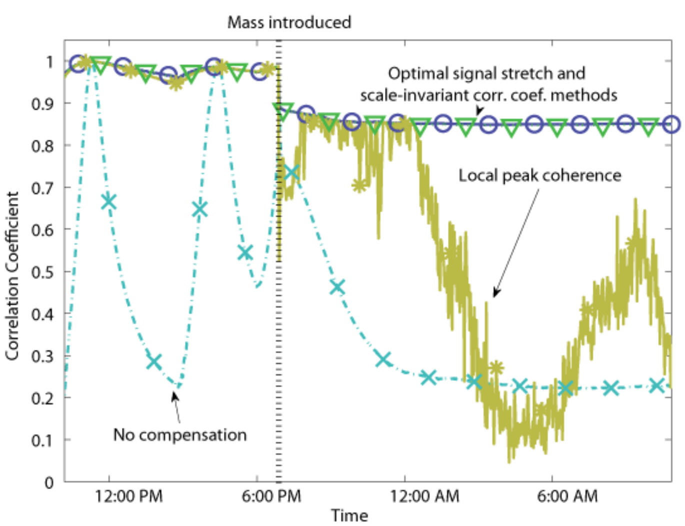

PS-10

Acoustic and Optical Investigation of Microbubble Contrast Agents Designed for Oil Exploration at High Pressures

Aleksandr Zhushma[1], Natalia Lebedeva[1], Michael Rubinstein[1], Paul Dayton[2], Sergei Sheiko[1]; [1]Chemistry, University of North Carolina at Chapel Hill, Chapel Hill, NC, USA, [2]Biomedical Engineering, University of North Carolina at Chapel Hill, Chapel Hill, NC, USA

Background, Motivation and Objective

Imaging of underground fluids in porous media is important to the field of petroleum exploration. Microbubbles are widely used as acoustic contrast agents for imaging in medicine, but at physiological conditions. Microbubbles in pressurized microporous systems, e.g. rock formations in subsurface oil reservoirs, exhibit low microbubble stability and poorly understood response to hydrostatic compression. More stable microbubbles are needed, along with acoustic-optical experiments to investigate microbubble echogenicity and stability at high pressures. We present soft and hard shell bubble formulations, a high-pressure cell for simultaneous acoustic and optical imaging under simulated borehole conditions, and finally perform acoustic, optical, and pressure-volume tests on the bubbles under high pressure, high salinity, and varied viscosity.

Statement of Contribution/Methods

Soft and hard shell pressure-resistant microbubbles stable to pressures above 1000 psi were formulated. A steel chamber was designed to withstand 7,000 psi pressure, at temperatures exceeding 100 °C, under a variety of solution conditions. Transparent windows made of sapphire or acrylic polymer provide visualization of material inside the chamber. Acrylic windows are semi-transparent to ultrasound, allowing for acoustic analysis of the contents. During simultaneous acoustic/optical measurements, a still image camera imaged the microbubbles. During optical-only experiments, a microscope was used to image bubbles with higher magnification.

Results

At constant microbubble concentration, confirmed with optical images, as pressure increased (tested up to 5,000 psi) the acoustic scattering signal of soft and hard shell microbubbles decreased. Optical observation experiments on soft shell microbubbles show that during repeated compression/expansion of bubbles, the pressure-volume P(V) relationship of these microbubbles deviated from ideal-gas-law predictions as such: initially microbubbles resisted compression because of shell elasticity, but after some pressure I reached, they shrank much quicker than initially, suggesting gas effusion out of the bubble. This P(V) relationship changed depending on the viscosity and salinity of the solution.

Discussion and Conclusions

Analysis of hard and soft shell microbubbles shows that those with rigid shells (glass) can withstand high pressure, but lack echogenicity; whereas, microbubbles with ultra-soft shells (such as monolayer lipids), are echogenic, but are destroyed at high pressure. We present data on prototype formulations which compromise on these characteristics, demonstrating both echogenicity and the ability to survive high pressures. This is a new application of microbubble acoustics for underground oil exploration.

PS-11

Confined Acoustic Phonons in Ultra-Thin Silicon Membranes

John Cuffe[1,2], Emigdio Chavez[1,3], Jordi Gomis Bresco[1], Pierre-Olivier Chapuis[1], Francesc Alzina[1], Andrey Shchepetov[4], Mika Prunnila[4], Jouni Ahopelto[4], Olivier Ristow[5], Mike Hettich[5], Thomas Dekosry[5], Clivia M. Sotomayor Torres[1,6]; *[1]Catalan Institute of Nanotechnology (CIN2-CSIC), Bellaterra, Barcelona, Spain, [2]Dept. of Physics, University College Cork, Tyndall National Institute, Cork, Ireland, [3]Dept. of Physics, Universitat Autònoma de Barcelona, Bellaterra, Barcelona, Spain, [4]VTT Technical Research Centre of Finland, Espoo, Finland, [5]Dept. of Physics, University of Konstanz, Konstanz, Germany, [6]Institució Catalana de Recerca i Estudis Avançats (ICREA), Barcelona, Spain*

Background, Motivation and Objective

The acoustic properties of ultra-thin Si layers are important for many areas of nanotechnology, impacting on both structural integrity and thermal transport. The effect of phonon confinement is particularly important, affecting both heat dissipation and charge carrier mobility. The goal of this work is to obtain a deeper understanding of phonon confinement and propagation in materials with dimensions comparable to thermal phonon wavelengths.

Statement of Contribution/Methods

In this work an ultra-fast photo-acoustic pump-probe method, known as Asynchronous Optical Sampling (ASOPS), is used to investigate confined phonon frequencies and lifetimes. The effect of the ~1 nm native oxide layer in such thin systems is also calculated using a three-layer model based on continuum elasticity theory.

Results

The frequency of the first order dilatational mode is measured, and the results show that the frequencies of the measured phonons are consistently ~10% lower than predicted by the continuum elasticity model, and cannot be fully explained by the presence of a native oxide layer or temperature changes within the membrane. The dependence of phonon lifetimes on membrane thickness is also investigated, with the lifetime of a 10 nm membrane found to decrease by over two orders of magnitude compared to that of a 400 nm membrane.

Discussion and Conclusions

The frequencies and lifetimes of confined acoustic phonons in ultra-thin free-standing Si membranes have been measured, and found to deviate from the values predicted by a continuum elasticity theory, including the effects of a native oxide layer and temperature increases within the membrane. A large decrease in phonon lifetimes is also seen for the ultra-thin membranes. The contributions of various attenuation mechanisms are discussed to explain the observed trend.

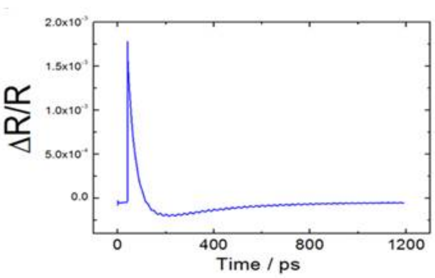

Figure 1: Change in reflectivity vs time for free standing Si membrane

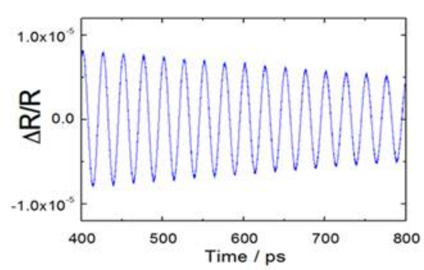

Figure 2: Change in reflectivity vs time for free standing Si membrane after subtraction of electronic response, showing confined acoustic mode.

WEDNESDAY POSTER

PS-12

Experimental evidence of locally resonant sonic band gap in 2D stubbed plates

MOURAD OUDICH[1], Matteo Senesi[2], Badreddine Assouar[1,3], Massimo Ruzzene[2], Jia-Hong Sun[4], Brice Vincent[5], Zhilin Hou[6], Tsung-Tsong Wu[4]; [1]*Institut Jean Lamour, Nancy University - CNRS, Vandoeuvre-les-Nancy, France,* [2]*D Guggenheim School of Aerospace Engineering, Georgia Institute of Technology, USA,* [3]*International Joint Laboratory (UMI 2958), Georgia Institute of Technology - CNRS, ATLANTA, USA,* [4]*National Taiwan University, Taiwan,* [5]*Nancy University - CNRS, France,* [6]*South China University of Technology, China, People's Republic of*

Background, Motivation and Objective

The propagation of an elastic wave in periodic composite material, called phononic crystal (PC), has received much attention over the past decade. The main mechanisms responsible for the opening of acoustic band gap (BG) are based on the Bragg scattering and local resonance (LR). The latter occurs at frequencies which can be almost two orders of magnitude lower than the usual Bragg gap. In this communication, we report on theoretical and experimental studies of 2D LR phononic plates composed of rubber unit resonators squarely arranged on a homogenous aluminum plate.

Statement of Contribution/Methods

We reported recently on theoretical studies concerning 2D LR sonic crystals [1, 2]. Here, besides the theoretical investigation, we point out experimentally the acoustic properties of LR sonic plates. Three LR stubbed plates composed of rubber resonators with different thicknesses (1.5mm, 3mm & 5mm) arranged with a periodicity of a=1cm on aluminum plate (0.5mm thickness) were fabricated. Owing to the different types of silicone rubber, Brillouin spectroscopy analysis was carried out to determine the real elastic constants of the used rubber in our study. These new constants were then implemented in our numerical model to get the true band structure corresponding to the fabricated structures. Scanning Laser Doppler Vibrometer (SLDV) was used to characterize the band gaps of the different LR slabs through a frequency analysis.

Results

Band structure and transmission were computed based on the new elastic constants of silicone rubber measured by Brillouin spectroscopy. Experimental characterization was then performed along the different directions of first Brillouin zone. Very low frequency complete band gaps were clearly obtained for the different structures and a 2 KHz frequency band gap was reached for the 5mm stub thickness plate. The experimental results agree very well with the numerical ones obtained using new measured elastic constants. Fig. 1 shows an example of the band structure and measured transmission of 5mm stub thickness plate.

Discussion and Conclusions

LR band gap at 2 KHz was experimentally evidenced on 2D LR stubbed plates having a periodicity of a=1cm. The use of silicone rubber was carefully considered owing, among other, to its elastic properties frequency-dependent.

1. M. Oudich et al, New. J. Phys. 12 (2010) 083049
2. M. Oudich et al, Appl. Phys. Lett. 97 (2010) 193503

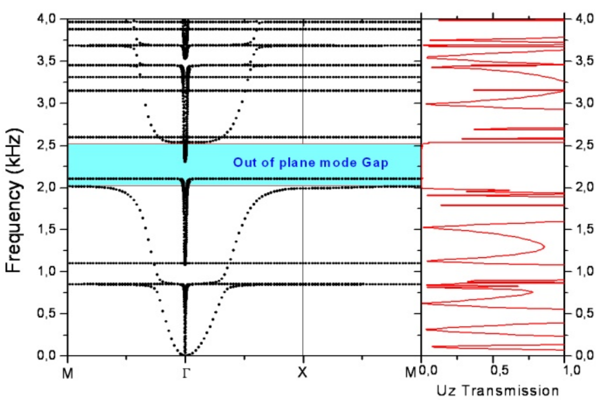

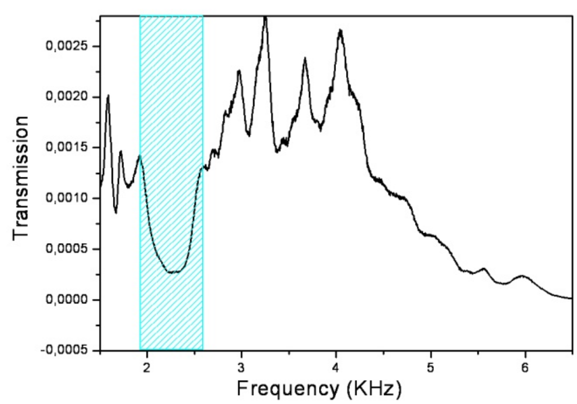

PS-13

Experimental study on high efficiency ultrasonic motors using lubricant

Wei Qiu[1], Yosuke Mizuno[1], Daisuke Koyama[1], Kentaro Nakamura[1]; [1]Precision and Intelligence Laboratory, Tokyo Institute of Technology, Yokohama, Japan

Background, Motivation and Objective

Application fields of ultrasonic motors have been limited due to their low efficiency and short life. Meanwhile, we have found that employing lubricants is an effective way to solve these problems. The feature of lubricants under vibratory preload makes the motor operation close to ideal one to reduce friction loss. In this paper, we investigated in detail the combination of friction materials for rotor and stator, and the characteristics of lubricants using a hybrid transducer type ultrasonic motor. With the good selection of the materials, we succeeded in obtaining high maximum efficiency of over 80% stably.

Statement of Contribution/Methods

The hybrid transducer type ultrasonic motor used in this experiment consisted of two 4-mm-thick torsional PZTs and six 1-mm-thick longitudinal PZTs (Fig. 1a). The effects of lubricants and friction materials were tested using three kinds of oils with two different viscosities and four kinds of ceramics for the contacting surfaces. The load characteristics and the motor efficiency were investigated being based on transient-response measurements with changing the preload applied to the rotor.

Results

The motor efficiency was significantly improved by lubrication at high preloads (Fig. 1b). The contact surfaces were well protected with lubricants so that the motor operation was stable even under high preloads. The combination of alumina for stator and silicone nitride for rotor was the best match of all the friction materials we tested. The maximum efficiency as high as 85% was achieved when high traction fluid of 32 cSt viscosity was used under 100-MPa preload (Fig. 1b).

Discussion and Conclusions

A high efficiency ultrasonic motor was successfully developed by using appropriate lubricant and friction materials. Lubricants and friction materials are both important to improve the efficiency and achieve stable operation. The effects of different lubricants under the same preload will also be discussed in detail as functions of static and dynamic preloads. These results shall lead to a breakthrough for extending the usage of ultrasonic motors.

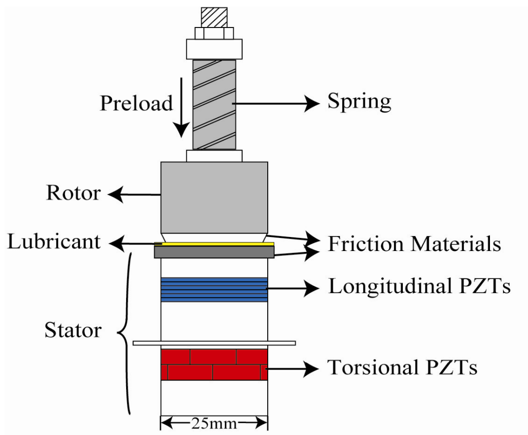

Fig. 1a Schematic configuration of ultrasonic motor using lubricant

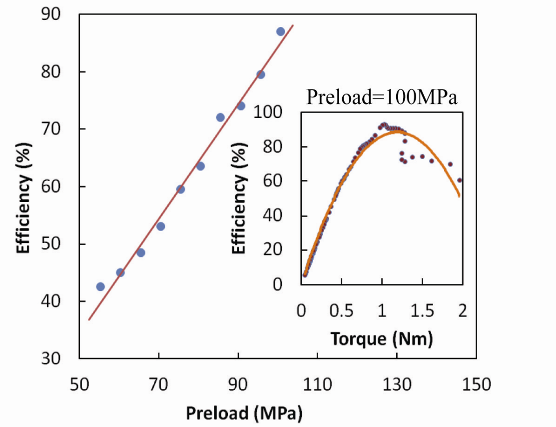

Fig. 1b Motor efficiency as a function of preload. The inset shows the load characteristics of the motor

PS-14

A modular SAW filter design approach for multiband filtering

Xiaoming LU[1], Jeffery Galipeau[2], Koenraad Mouthaan[1]; [1]*NUS, Singapore,* [2]*TriQuint Semiconductor Florida, USA*

Background, Motivation and Objective

The trend in frequency allocation is to release more spectrum for data services. Since many of the band allocations are adjacent to each other, switched SAW filters are well suited to utilize these bands. Traditional switched filter banks are difficult to accomplish in reasonable size and cost. Other research work on switched SAW/BAW/FBAR filters design are reported which use additional elements such as transistors, capacitors or inductors [1, 2, 3]. This paper proposes novel modular SAW filter based topologies which reduce the size and the need of passive elements. A fully packaged feasibility study is presented in the 700 MHz frequency range currently allocated to LTE bands.

Statement of Contribution/Methods

The goal of the current research is to develop practical SAW filters which can switch between adjacent bands or band edges. The design is realized by integrating SAW resonator die and GaAs SPST/SPDT switch die into a common package. During design procedure, parasitic inductances, coupling capacitances, isolation of off state switches are addressed using a linear circuit solver and a 3D EM model which predicts potential problems of degraded shape factor of filter pass bands, decreased coupling coefficient of SAW substrates, etc.

Results

This paper investigates modular ladder type topologies for SAW filters. We achieved a center frequency shift greater than 2.5%, or the lower band edges shifted around 0.6%, with each filter fractional bandwidth around 1.3%, and they maintain typically 12dB return loss and 20dB rejection.

Discussion and Conclusions

Modular SAW filters around 700 MHz are fabricated and tested. The performance in rejection bands can be traded off with the filters' insertion loss which depends on different application requirements. The performance can be improved by compact layout design or different integration technologies to reduce the parasitic effects.

References

[1] N. O. Fenzi et. al, "Multimode bandpass SAW filter using Reconfigurable Resonance Technology", 2010 IUS

[2] S. Aliouane et. al, " RF-MEMS Switchable Inductors for Tunable Bandwidth BAW Filters ", 2010 Int. Conf. on Design & Tech. of Integrated Systems in Nanoscale Era

[3] M. El Hassan et. al, "Tunability of Bulk Acoustic Wave Filters Using CMOS Transistors: Concept, Design and Implementation", 2010 IEEE RFIC

WEDNESDAY POSTER

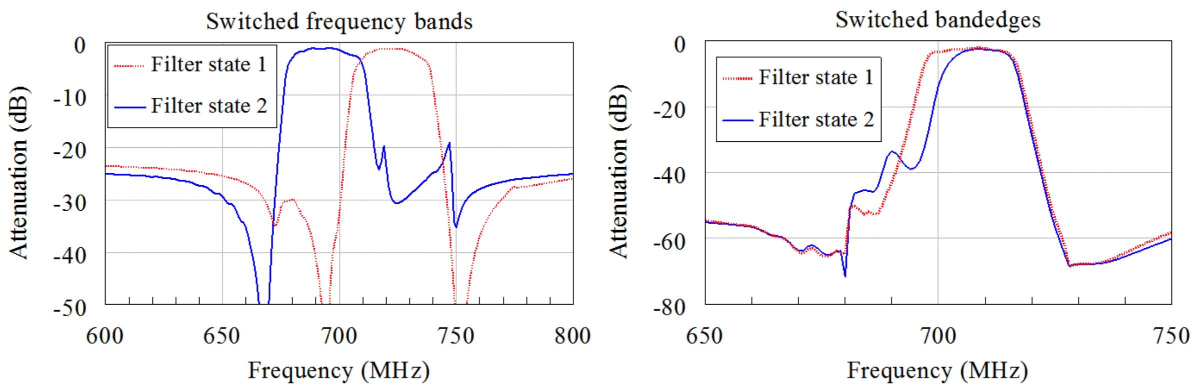

Fig. 1 Two types of performances of insertion loss
by 3D model EM simulation

PS-15

Impact of High-Temperature Dielectric and Piezoelectric Behavior on LGT Acoustic Wave Properties up to 900°C

Peter Davulis[1], Mauricio Pereira da Cunha[1]; [1]Electrical and Computer Engineering Dept., University of Maine, Orono, ME, USA

Background, Motivation and Objective

There is a growing need for frequency control devices and wireless sensors that operate at very high temperatures, 400 to 1000°C, in the aerospace, energy generation, material processing, and oil extraction industries. Langasite (LGS) and langatate (LGT) surface acoustic wave (SAW) devices have demonstrated wireless operation above 900°C. The modeling and design of high-temperature LGT devices requires acoustic wave constants measured throughout the targeted temperature range of operation. Previous work by the authors reported on LGT piezoelectrically-stiffened elastic constants using resonant ultrasound spectroscopy but did not include the temperature variation of the dielectric and piezoelectric constants. This work targets to quantify the dielectric and piezoelectric temperature behavior up to 900°C and verify the impact on the elastic constants and SAW properties.

Statement of Contribution/Methods

In this work, the LGT elastic, dielectric and piezoelectric constants with respective temperature coefficients up to 900°C are reported for the first time. The new set of constants was used to improve the predictions of high-temperature LGT SAW properties such as phase velocity (v_p), temperature coefficient of delay (TCD), and electromechanical coupling (K^2) along multiple orientation sweeps up to 900°C. These predictions were then compared to previous calculations, which ignored the temperature dependence of the dielectric and piezoelectric constants, and to measured data up to 900°C, obtained from delay lines fabricated along 6 orientations in the LGT plane (90°,23°,Ψ).

Results

The average discrepancy between predicted and measured v_p and TCD responses were reduced by 26% and 33%, respectively, up to 500°C and 17% for v_p up to 900°C when the temperature dependence of both dielectric and piezoelectric constants are considered. The extracted LGT piezoelectric constants and temperature coefficients show that e11 and e14 change by up to 11% and 31%, respectively, for the entire 25°C to 900°C range when compared to room temperature values. In addition, this paper uncovers the full set of high temperature LGT elastic, piezoelectric, and dielectric constants and temperature coefficients applicable up to 900°C, including the respective estimated uncertainty.

Discussion and Conclusions

A new set of high-temperature (up to 900°C) LGT acoustic wave constants extracted by RUS technique and which considers the temperature dependence of both dielectric and piezoelectric constants is revealed. The use of these new constants and temperature coefficients resulted in up to 26% and 33% reduction in discrepancies between predictions and measurements for phase velocity and TCD. The reported results verify the relevance of considering the dielectric and piezoelectric temperature behavior for accurate acoustic wave property predictions and device design at high temperatures.

PS-16

c-axis parallel oriented AlN film resonator fabricated by ion-beam assisted RF magnetron sputtering

Masashi Suzuki[1], Takahiko Yanagitani[1]; [1]*Graduate School of Engineering, Nagoya Institute of Technology, Nagoya, Aichi, Japan*

Background, Motivation and Objective

An wurzite film such as ZnO and AlN tends to grow normal to the substrate. In ZnO films, we previously found that c-axis parallel orientation is induced by ion-beam irradiation during deposition. In this study, we investigated the orientation control of AlN films deposited by using ion-beam assisted RF magnetron sputtering.

Statement of Contribution/Methods

The modification of preferential orientation was induced by irradiating 3 kV accelerated nitrogen ion beam from ECR ion source. Ion beam was irradiated 20º with respect to the substrate during RF magnetron sputter deposition. Crystalline orientation of the film was determined by XRD analysis. Next, c-axis parallel AlN film SMR with asymmetric Bragg reflector consisting of W/SiO_2 was fabricated, and k_{15} value and TCF value were measured.

Results

(0002) X-ray pole figure (Fig. 1) and XRD patterns show that c-axis of the film is parallel to substrate and the direction of c-axis corresponded to the ion beam direction. The FWHM value of φ and ψ were found to be 9.8º and 6.3º, respectively. c-axis parallel AlN SMR excited only pure shear mode without thickness extensional mode. Fig. 2 shows temperature dependence of the resonant frequency of the resonator. TCF of -30.2 ppm/ºC found in AlN film SMR was higher than that of -20.3 ppm/ºC measured in AlN single crystal plate resonator. k_{15} of the resonator is determined to be 0.057 from frequencies of series and parallel resonance. This value is 70 % of that in the AlN single crystal.

Discussion and Conclusions

c-axis unidirectional in-plane orientation in the sample was confirmed by X-ray pole figure. Pure shear mode was excited in c-axis parallel AlN SMR. k_{15} of the resonator was determined to be 0.057, and TCF was found to be -30.2 ppm/ºC.

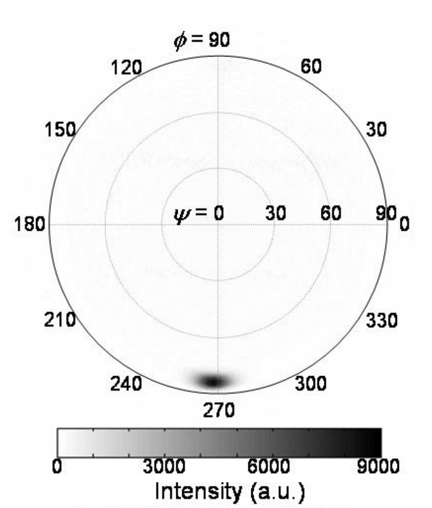

Fig. 1 (0002) pole figure of AlN film

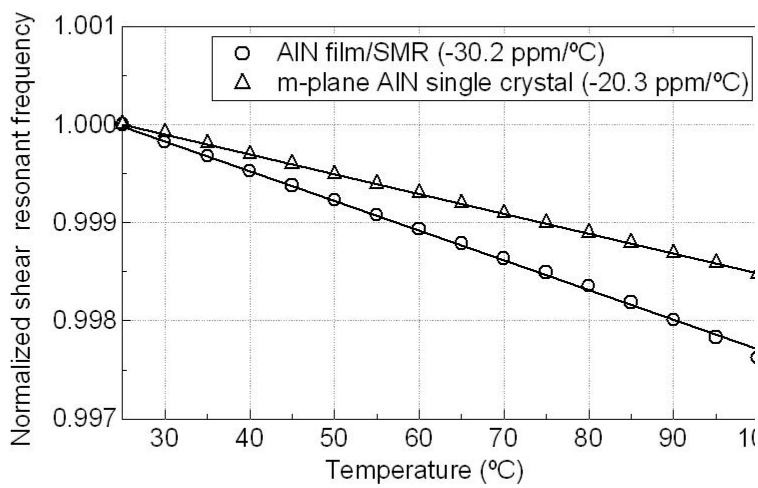

Fig.2 Temperature dependence of the shear resonant frequency of the resonato

PS-17

An All-optical Thin-film High-frequency Ultrasound Transducer

Clay Sheaff[1], Shai Ashkenazi[1]; [1]Biomedical Engineering, University of Minnesota-Twin Cities, Minneapolis, MN, USA

Background, Motivation and Objective

Piezoelectric and capacitive high-frequency ultrasound transducers exhibit excessive noise due to crosstalk, RF interference, and their small capacitance. These factors significantly limit image quality. Devices that optically generate and detect ultrasound avoid these effects by requiring no electrical cabling or interconnections. In this work we have created an all-optical ultrasound transducer by integrating an optically-absorbing thin-film into an etalon sensor.

Statement of Contribution/Methods

2.5μm of polyimide precursor (HD Microsystems PI-2555) was spin-coated onto a 3mm glass substrate. An etalon was then deposited by evaporating a 30nm gold mirror, spin-coating a 10μm layer of SU-8 (Microchem), and evaporating a second mirror. 1.5μm of SU-8 was added for protection (Fig. 1).

The device was probed from underneath the substrate using a 355nm ND:YAG pulsed laser (Continuum) for ultrasound generation and a 1550nm tunable CW laser (HP 8168F) for detection. After tuning the NIR wavelength for maximum sensitivity, a 5ns 4.5mJ UV pulse was used to generate an acoustic signal within the polyimide film which was reflected from a glass slide placed above the device in water. The echo was then detected by the etalon.

Results

Fig. 2 shows the pulse-echo waveform and associated power spectrum. Using a calibrated hydrophone (Onda HGL-0085), the emitted pulse was determined to have an amplitude of 5.9MPa. The transmit/receive response has a -6dB bandwidth of 32MHz centered at 27MHz.

Discussion and Conclusions

The all-optical ultrasound transducer demonstrated here emits and detects signals of a strength and bandwidth suitable for high-resolution imaging. After incorporating fiber optics and beam scanning, potential applications will include endoscopic and intravascular ultrasound.

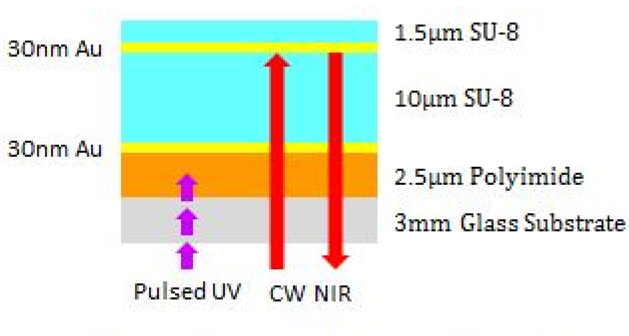

Fig. 1. Layered structure of all-optical transducer.

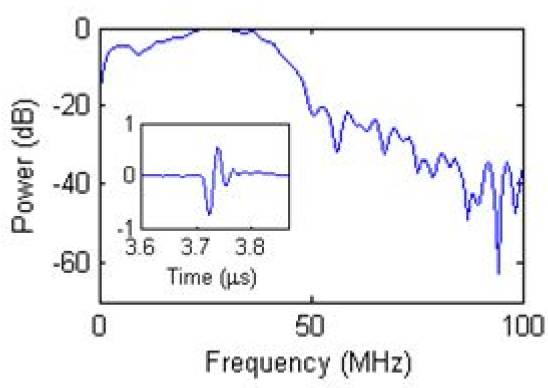

Fig. 2. Pulse-echo and power spectrum.

WEDNESDAY POSTER

PS-18

Radiation Impedance of an Array of Circular Capacitive Micromachined Ultrasonic Transducers in Collapsed State

Alper Ozgurluk[1], Abdullah Atalar[1], Hayrettin Koymen[1], Selim Olcum[1]; [1]Electrical and Electronics Engineering, Bilkent University, Ankara, Turkey

Background, Motivation and Objective

Radiation impedance of an array of CMUT cells is a critical design parameter for achieving high performance cMUT arrays. For conventional (uncollapsed) mode, the radiation impedance of an array of cMUT cells was studied in [1]. However, the radiation impedance of an array for the collapse mode has not yet been investigated.

Statement of Contribution/Methods

In this paper we present the calculation of the radiation impedance of clamped circular CMUTs both analytically and using FEM simulations. First, we model the radiation impedance of a single collapsed cMUT cell analytically by expressing its velocity profile as a linear combination of sufficient number of velocity profiles as given by Porter [2]. For this purpose, 2D-axisymmetric FEM simulations are performed using ANSYS. For an array of collapsed cMUT cells, the mutual impedance between the cells must also be taken into account and is calculated analytically using the formulas given by [2]. In this case, we perform 3D FEM simulations in COMSOL Multiphysics using appropriate symmetry boundary conditions.

Results

Radiation impedances for arrays of 7, 19, 37 and 61 circular collapsed CMUT cells for different contact radii are calculated both analytically and by FEM simulations. A good agreement between the analytical and FEM simulation results is achieved. In the figure below, the results for an array of 7 collapsed circular cells with 20µm radius are given for a contact radius of 8µm. We find that the peak radiation resistance value is reached at higher kd values in the collapsed case as compared to the uncollapsed case where d is the distance between the centers of two neighboring cMUT cells. As the contact radius increases, the radiation resistance becomes smaller for almost all values of kd and reaches a minimum value of 0.4 for a contact radius of 14µm in the deep collapsed case.

Discussion and Conclusions

The radiation resistance of an array reaches to a plateau of certain value between 0.4 and 0.6 depending on the contact radius and maintains this level for a wide kd range. The variation of reactance with respect to frequency indicates a fixed valued inductance behavior in the same kd range. The radiation impedance with these properties is very favorable for the design of wideband arrays.

[1] M. N. Senlik et.al., IEEE Trans. on UFFC , vol.57 (4), pg.969, 2010.
[2] D. T. Porter, J. Acoust. Soc. Am., vol. 36, pp. 1154–1161, 1964.

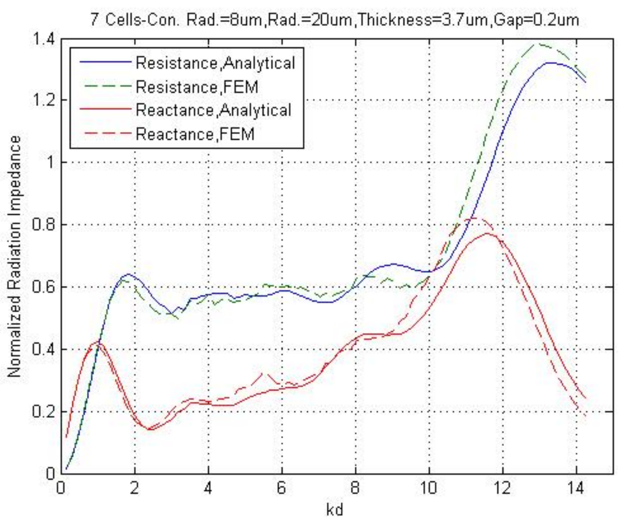

PS-19

Cell Characterization Using High Frequency Ultrasound

Saurabh Bakshi[1], John Williams[2], Xiaoning Jiang[1], Elizabeth Loboa[2]; *[1]Mechanical & Aerospace Engineering, North Carolina State University, Raleigh, NC, USA, [2]Biomedical Engineering, North Carolina State University, Raleigh, NC, USA*

Background, Motivation and Objective

It is known that extracellular physical stimuli can affect stem cell fate and, that malignant cancer cells have different material properties than benign cells. However, it is also known that human cells exhibit extensive variability in their chemical and mechanobiological response due to donor-to-donor variability. Therefore, there is a great need for a sensitive, reliable, and accurate system to characterize cell properties in a high throughput fashion. Time resolved acoustic microscopy is currently used to characterize acoustic and elastic properties of cells using the amplitude and time of the ultrasound (US) backscatter from the cellular membrane. This acoustic microscopy system is bulky and is not practical for characterization of cells in a large population. In this paper, a method of cell detection and characterization based on the use of acoustic impedance of cell material is proposed for cell elastic property characterization in a high throughput fashion.

Statement of Contribution/Methods

Transmit electrical impedance spectrum of a 50 MHz transducer with varied front loading (e.g. cell elastic properties) was modeled using PiezoCAD. Initial cell growth tracking using a 30 MHz transducer was performed to demonstrate that transmit impedance can track elastic property changes in human adipose derived stem cells (hASC) during osteogenic differentiation. In this study, hASC were cultured in complete growth medium (Eagle's Minimum Essential Medium, alpha-modified (α-MEM) supplemented with 10% fetal bovine serum, 2 mM L-glutamine, 100 units/mL penicillin, and 100 µg/mL streptomycin) for 3 days. On day 4, the medium was changed in half the culture wells to osteogenic differentiation medium (expansion medium supplemented with 50 µM ascorbic acid, 0.1 µM dexamethasone, and 10 mM β-glycerolphosphate). Two cell samples were measured for acoustic impedance values on day 1, and an incrementally increasing number of samples, one each from the controlled and differentiating set, were added to the existing set each day for measurement.

Results

Electrical impedance as much as 30 Ω was observed from a 50 MHz transducer model for the case where front load acoustic impedance is changed from 2 MRayl to 4 MRayl. Frequency shift was also observed. Measured transmitting electrical impedance difference (4 Ω) indicated a change in hASC elastic properties within 24 hours (day 5). Interestingly, it was noted that impedance difference began to level off (8 Ω) between days 7-8, indicating that elastic properties were no longer changing.

Discussion and Conclusions

The initial modeling and experimental results suggest that it is feasible to track cell growth by monitoring transmitting electrical impedance change. This may open up a new US cell characterization tool that promises monitoring of a large population of cells in a real time and high throughput fashion.

P2Aa - Bio-effects

Carribean Ballroom III-V

Wednesday, October 19, 2011, 1:00 pm - 4:30 pm

Chair: **Charles Cain**
Univ. of Michigan

P2Aa-1

Biosafety Investigation of Acoustic Cavitation on Cells in the Immune System: Analysis on Human T-Lymphocytes

Wenjing Zhong[1], Wai-Hung Sit[2], Jing Zhang[2], Jennifer M. F. Wan[2], **Alfred C. H. Yu[1]**; [1]Medical Engineering Program, The University of Hong Kong, Hong Kong, [2]School of Biological Sciences, The University of Hong Kong, Hong Kong

Background, Motivation and Objective

The use of microbubbles for imaging and therapeutic purposes has been well-received since its introduction. However, the biosafety of their interaction with ultrasound (acoustic cavitation) remains a central concern that is still subject to debate. Considering that microbubbles are practically used within the vasculature, one specific concern is whether acoustic cavitation would bear cytotoxic effects on cells in the immune system. To evaluate this issue, we have investigated the viability of T-lymphocytes in response to acoustic cavitation, which may introduce sonoporation on these cells.

Statement of Contribution/Methods

T-lymphocytes were freshly extracted from healthy human blood samples through isolation from buffy coat by Ficol-Paque density gradient centrifugation, destruction of red blood cells with lysing buffer, and removal of monocytes by cell adhesion. The extracted cells were then cultured with complete RPMI-1640 medium in the presence of 1% v/v microbubbles, and they were transferred to a four-well plate for ultrasound exposure. They were insonated with pulsed ultrasound for 1 min (0.3MPa and 0.5MPa peak negative pressure, 1MHz freq., 10% duty cycle, 1kHz PRF). Their long-term proliferation was investigated by first re-incubating these cells for 24h, 48h and 72h before harvesting them for multiple target tracing (MTT) analysis. Their post-exposure viability was also analyzed after 4h and 12h using propidium iodide (PI) flow cytometry (loss of viability is evident if high PI fluorescence was detected). To facilitate comparison, a similar analysis was carried out on T-lymphocytes that received sham exposure.

Results

The MTT reduction assay shows that the number of living T-lymphocytes was decreased after 24h in both 0.3 MPa and 0.5 MPa ultrasound exposure groups (respectively 89.8% and 83.8% of the control group). This number remained consistent after 48h and 72h, thereby suggesting that no additional loss of viability had occurred after the first 24h. This was confirmed with the flow cytometry findings, where the dead cell (PI-positive) population was found to be 15.5% and 19.1% respectively after 4h and 12h.

Discussion and Conclusions

Our results show that the loss of cellular viability can indeed be seen in T-lymphocytes that had experienced acoustic cavitation. This warrants further investigation on the issue, especially in cases with mitogen stimulation that would trigger cell-cycle progression of T-lymphocytes.

P2Aa-2

Developing a New Sonoporation Treatment Model Using Plants: Cellular Mechanism Analysis

Peng Qin[1], Lin Xu[2], Wenjing Zhong[1], Alfred C. H. Yu[1]; [1]Medical Engineering Program, The University of Hong Kong, Hong Kong, [2]Shanghai Institute for Biological Sciences, Chinese Academy of Sciences, Shanghai, China, People's Republic of

Background, Motivation and Objective

Plant cells represent a potential experimental model for evaluating the treatment outcome of sonoporation-mediated gene therapy given their totipotency (ability to grow into an adult plant from stem cells) and the relative ease in synthesizing single genetic changes in them. In developing such a model, it is important to investigate whether plant cells undergo similar acoustic cavitation cellular bioeffects as those encountered in mammalian cells considering their evolutionary divergence. There has been validation that the viability of plant cells can be upset by inertial cavitation. The objective of this work is to compare the cellular-level mechanism responsible for the apoptotic response of these cells when exposed to cavitation. Our emphasis is on examining the changes in the plasma membrane and mitochondrial membrane potential of tobacco BY-2 cells after undergoing acoustic cavitation.

Statement of Contribution/Methods

The BY-2 cell suspensions were cultured in MS medium at 27 deg; in darkness and at 120 rpm. They were then transferred to an acoustically-transparent plate, and 1% v/v microbubbles solution was added to promote acoustic cavitation. Pulsed ultrasound (1MHz freq., 10% duty cycle, 1kHz PRF) was applied to the suspension for 1 min. Different peak negative pressure (0.3~0.9MPa) was selected to evaluate the bioeffects of both stable and inertial cavitation. The cells were re-incubated and were collected at 0h, 2h, 4h and 6h after exposure for analysis. Two potentio-dependent fluorescence probes (DiBAC4(3) and TMRE) were used to analyze the changes in the plasma membrane and mitochondrial membrane potential. These changes were monitored by confocal and DIC fluorescence microscopy, and they were quantified using a spectrofluorometer.

Results

The cavitation bioeffects produced on plant cells are found to be similar to those seen previously in mammalian cells. Plasma membrane depolarization was observed immediately following inertial cavitation, as indicated by the 3.5 times increase in DiBAC4(3) fluorescence within the cytosol. The fluorescence remained high over time. As noted by the decrease in TMRE fluorescence, the mitochondrial trans-membrane potential has depolarized and dissipated over time. This is a well-known cytoplasmic event related for the release of some pro-apoptotic molecules from the mitochondria, resulting in apoptosis of plant cells. In the stable cavitation range, the bioeffects were less significant as expected.

Discussion and Conclusions

In ways similar to mammalian cells, cavitation may change the electrophysiological properties of plant cells, alter their cytoplasmic signaling, and affect their ultimate fate. This also indicates mitochontrial signaling pathways may be conserved for cavitation-induced apoptosis of plant and mammalian cells. As such, in using plant cells as a model for sonoporation-mediated gene therapy, the treatment outcomes to be observed should be transferrable to mammalian cells.

P2Ab - Contrast Agents I

Carribean Ballroom III-V

Wednesday, October 19, 2011, 1:00 pm - 4:30 pm

Chair: **Piero Tortoli**
Univ. of Firenze

WEDNESDAY POSTER

P2Ab-1

Subharmonic Aided Pressure Estimation in Patients with Suspected Portal Hypertension

John Eisenbrey[1], Jaydev Dave[1,2], Valgerdur Halldorsdottir[1,2], Daniel Merton[1], Jose Gonzalez[3,4], Cynthia Miller[3], Priscilla Machado[1], Suhyun Park[5], Scott Dianis[5], Carl Chalek[5], Kai Thomenius[5], Daniel Brown[1], Victor Navarro[3], Flemming Forsberg[1]; [1]*Department of Radiology, Thomas Jefferson University, Philadelphia, PA, USA,* [2]*School of Biomedical Engineering and Health Systems, Drexel University, USA,* [3]*Department of Gastroenterology & Hepatology, Thomas Jefferson University, USA,* [4]*Hospital Clinico Universitario de Valladolid, Spain,* [5]*GE Global Research, Niskayuna, NY, USA*

Background, Motivation and Objective

Pressure measurements within the portal vein are clinically useful for treatment and management of a variety of hepatic diseases. Currently these pressures are estimated by the hepatic vein pressure gradient (HVPG), in which the pressure gradient is measured using a wire pressure catheter between free and wedged positions within the hepatic vein. The invasiveness of this measurement places patients at risk while also limiting the frequency of data collection. It has been shown the subharmonic amplitude of microbubble-based ultrasound contrast agents is sensitive to hydrostatic pressures. Hence, a technique using subharmonic aided pressure estimation (SHAPE) may be useful for noninvasively monitoring portal hypertension in patients.

Statement of Contribution/Methods

Portal pressure data was collected from 22 consenting patients (Body Mass Index of 15.5 to 57.2) undergoing transjugular liver biopsy as part of their clinical standard of care. Within two hours post biopsy, patients received a co-infusion of Sonazoid (0.72 uL microbubbles/kg/hour; GE Healthcare, Oslo, Norway) and saline (120 ml/hour). Five minutes into the infusion, subjects were scanned with a modified Logiq9 ultrasound scanner (GE Healthcare, Milwaukee, WI) with a 4C curvilinear probe. The acoustic output of the machine was varied from 1 to 100% acoustic output to determine the acoustic pressure setting resulting in maximal change in the subharmonic amplitude (the point of greatest sensitivity to hydrostatic pressure estimation). After determining the optimal acoustic pressure, RF data was obtained from the portal and hepatic veins for 5 seconds in triplicate. The subharmonic amplitude was then determined off line and compared to both HVPG measurements and the patient's model for end stage liver disease scores (MELD).

Results

RF data was obtained from the portal veins from, while hepatic vein signal was obtained from 20 patients. Subharmonic behavior as a function of acoustic output showed a clear S-curve behavior (consistent with the literature) in the majority of patients, indicating a distinct insonation pressure for optimal SHAPE sensitivity. The differences in hepatic vein to portal vein subharmonic signal (in dB) at this output level were in good overall agreement with HVPGs measured during transjugular biopsy (R = 0.75). Slightly less correlation was seen when comparing this difference in dB to patient MELD scores (R = 0.61), although this correlation was still stronger than the correlation between MELD and HVPG (R = 0.47).

Discussion and Conclusions

Results show a good correlation of subharmonic differences between the hepatic and portal veins to the catheter based reference standard. While these results are based only on raw RF subharmonic amplitudes, future processing of RF data may further improve accuracy. While enrollment is ongoing, preliminary results indicate SHAPE may be a useful tool for the diagnosis and monitoring of portal hypertension.

Supported by NIH RC1 DK087365

P2Ab-2

Dual grayscale and subharmonic ultrasound imaging on modified ultrasound scanner in 2 and 3D

John Eisenbrey[1], Jaydev Dave[1], Valgerdur Halldorsdottir[1], Suhyun Park[2], Scott Dianis[2], Daniel Merton[1], Priscilla Machado[1], Ji-Bin Liu[1], Jose Gonzalez[3], Cynthia Miller[3], Kai Thomenius[2], Daniel Brown[1], Victor Navarro[3], Flemming Forsberg[1]; [1]*Department of Radiology, Thomas Jefferson University, Philadelphia, PA, USA,* [2]*GE Global Research, Niskayuna, NY, USA,* [3]*Department of Gastroenterology & Hepatology, Thomas Jefferson University, USA*

Background, Motivation and Objective

The ability to generate signals at half the insonation frequency is exclusive to ultrasound (US) contrast agents (UCA). Thus, subharmonic imaging (SHI; transmitting at f_0 and receiving at $f_0/2$) provides improved visualization of UCA within the vasculature via suppression of tissue signal. Despite the clinical advantages of this technique, use of SHI is currently limited by a lack of tissue landmarks and the use of a 2D representation of vasculature. Thus, the goal of this work is to implement both dual grayscale/SHI and 3D SHI on a commercial scanner.

Statement of Contribution/Methods

Scanning was performed on a modified Logiq9 US scanner (GE Healthcare, Milwaukee, WI). The machine was modified to provide simultaneous, split screen 2D imaging with both grayscale (f_0 = 4.0 MHz) and SHI (f_0 = 2.5 MHz, $f_0/2$ = 1.25 MHz). 2D imaging was performed with a 4C probe using Sonazoid (GE Healthcare, Oslo) in the portal vein (PV), inferior vena cava (IVC), and hepatic vein (HV) of 4 open chest canines and 4 patients. Preliminary 3D SHI was implemented on this platform (initiated in practice post ROI selection in dual 2D mode) using a 4D10L probe. Imaging of Sonazoid and Definity (Lantheus Medical Imaging, N. Billerica, MA) was performed in a flow phantom to show proof of concept.

Results

Results showed a subharmonic amplitude response as a function of acoustic output to match the S-curve behavior described in the literature. Maximal subharmonic amplitude was found to be 20.8 ± 2.3 dB in canines and 33.9 ± 5.2 dB in humans relative to the noise floor. An example of this imaging is shown below (green arrow = HV; red = PV; blue = IVC). 3D SHI was also successfully implemented on the platform. While imaging parameters are currently being optimized, initial results show 3D volumes of vasculature can be successfully reconstructed from SHI data.

Discussion and Conclusions

Simultaneous grayscale/SHI US benefits from SHI's ability to exclusively image vasculature, while still providing navigation information from grayscale imaging. Additionally, the implementation of 3D SHI post ROI selection provides a complete representation of the vasculature. These improvements should make SHI more readily translatable to clinical applications.

Supported by NIH R21 HL081892, RC1 DK087365 and CA 140338, AHA grant 0655441U and USAMRMC W81XWH-08-1-0503 (VH).

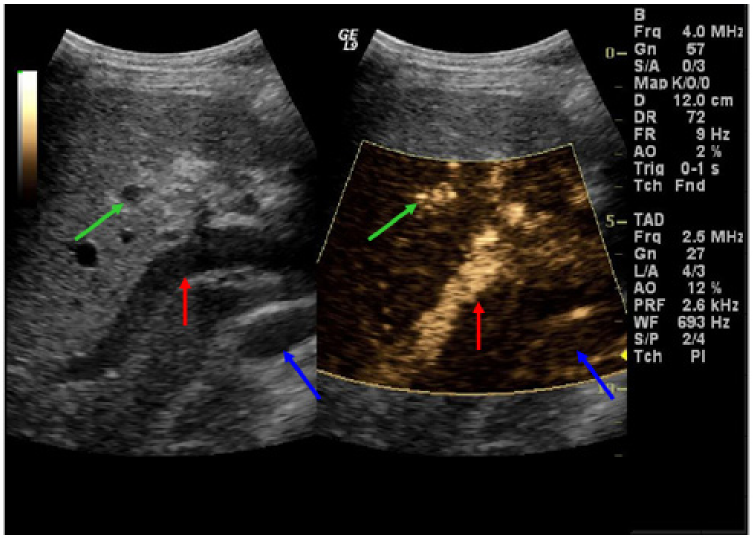

P2Ab-3

In vitro comparative study of the performance of pulse sequences for ultrasound contrast imaging of the carotid artery

Guillaume RENAUD[1], Johan G. Bosch[1], Antonius F.W. van der Steen[1], Nico de Jong[1]; [1]*Biomedical Engineering - ThoraxCenter, Erasmus MC, Rotterdam, Netherlands*

Background, Motivation and Objective

This study intends to identify the best pulse sequences for ultrasound contrast imaging of the carotid artery by comparing a fairly exhaustive list of reported pulse sequences. A good candidate must provide sensitive detection of contrast microbubbles, efficient suppression of echoes arising from linear scattering, prevent artifacts and be simple for high frame rate imaging. Especially the distal wall artifact caused by nonlinear propagation through contrast agent dramatically impairs the detection of microbubbles in any region located behind a vessel.

Statement of Contribution/Methods

Pulse inversion, amplitude modulation, chirp reversal, subharmonic imaging, pulse subtraction time delay imaging, radial modulation and ringdown surf imaging are investigated in vitro. A focused single-element transducer used in pulse-echo mode transmits ultrasound waves and receive backscattered signals in the frequency range of 3 MHz to 8 MHz. Transmitted waveforms are designed with a low mechanical index between 0.1 and 0.2. In a water tank, the transducer acquires a single RF line through a thin-wall tube containing diluted (1:5000) contrast agent (SonoVue, Bracco). A thin metallic wire is placed in front of the tube and a piece of rubber is positioned behind the tube to evaluate the contrast-to-tissue ratio (CTR) and the contrast-to-artifact ratio (CAR), respectively. The contrast-to-noise ratio (CNR) is determined by comparing backscattered signals from contrast agent with that of pure water.

Results

Please see table below.

Discussion and Conclusions

Only subharmonic imaging and ringdown surf imaging are free from the distal wall artifact. Summing CNR, CAR and CTR, ringdown surf imaging (Hansen et al., IEEE Trans. UFFC, vol. 58(2), 2011) turns out to be the best candidate (CNR+CAR+CTR = 18dB).

	Amplitude modulation	Pulse inversion	Pulse inversion-Amplitude modulation	Pulse subtraction time delay	Radial modulation	Sub-harmonic	Chirp reversal	Chirp amplitude modulation	Chirp reversal amplitude modulation	Ringdown surf imaging
CNR (dB)	5.8	4.9	7.1	7.8	2.9	2.8	9.8	12	12	7.3
CAR (dB)	-11	-10	-13	-7.0	-8.8	0.37	-13	-13	-12	5.0
CTR (dB)	3.0	0.62	1.8	4.5	-0.41	0.43	6.2	4.6	5.1	5.2
CNR+CAR +CTR	-1.7	-4.0	-4.0	5.4	-6.4	3.6	3.0	3.6	5.3	18

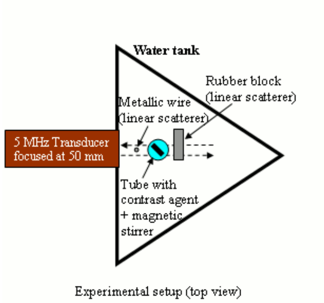

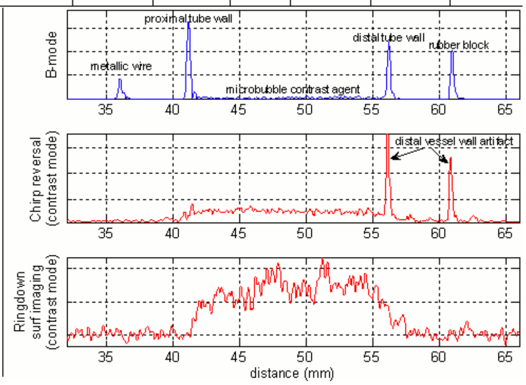

Research supported by the Center for Translational Molecular Medicine and the Netherlands Heart Foundation (PARISk).

P2Ab-4

Chirp reversal power modulation contrast imaging

Anthony Novell[1], Ayache Bouakaz[1]; [1]Inserm U930, CNRS ERL 3106, université François Rabelais de Tours, France

Background, Motivation and Objective

Chirp excitations are known to increase significantly the signal to noise ratio (SNR). Besides, we have shown earlier that chirp reversal approach improves the contrast detection through an increased contrast to tissue ratio (CTR). Chirp reversal consists in transmitting a first up-sweep chirp excitation signal of increasing frequencies with time and a second excitation down-sweep chirp, being a replica of the first signal, but time reversed with a sweep of decreasing frequencies with time. The aim of our study is to evaluate the combination of chirp reversal with power modulation (CRPM) for contrast agent imaging.

Statement of Contribution/Methods

Experiments were performed using a 128 elements PZT linear array probe centered at 4 MHz. The probe was connected to a fully programmable open scanner equipped with analog transmitters (M2M, France). Chirped signals and pulses were transmitted at 2.5 MHz with 55% bandwidth. The chirps had a linear frequency modulation with a length of 8 µs giving thus the same frequency bandwidth as the equivalent transmitted pulse (traditional 2 cycles Gaussian pulse (<2 µs)). A flow phantom was used in which SonoVue® microbubbles at a dilution of 1/2000 was introduced. RF data were recorded and then filtered using a matched filter in order to compress the scattered signals and recover the axial resolution when chirps were used. The compression filter was designed in order to recover both the fundamental and the harmonic components. The transmitted peak negative acoustic pressure was 350 kPa. Traditional multi-excitations schemes such as pulse inversion (PI), power modulation (PM) and their combination PIPM were implemented using pulses and chirps with or without chirp reversal approach. The CTR and SNR were quantified for each transmitted sequence.

Results

In table I are given the CTR and SNR for the different transmit sequences. The use of chirp increases significantly the SNR without degrading the CTR. Compared to other methods, the combination of CR and PM increases both the CTR and the SNR. The CTR using CRPM is 25.3 dB while PM alone and CR alone provided a CTR of 18.7 dB and 21.8 dB respectively.

Discussion and Conclusions

These results demonstrate the ability to increase both the CTR and the SNR when chirp reversal imaging is performed in combination with power modulation technique.

TABLE I
SNR and CTR for different detection strategies

	Pulse			Chirp			Chirp Reversal			
Method	**PI**	**PM**	**PIPM**	**CPI**	**CPM**	**CPIPM**	**CR**	**CRPI**	**CRPM**	**CRPIPM**
SNR (dB)	**30.0**	**31.1**	**32.0**	**38.7**	**40.8**	**40.0**	**43.0**	**43.4**	**45.8**	**43.2**
CTR (dB)	**18.7**	**18.7**	**20.9**	**17.2**	**20.7**	**19.1**	**21.8**	**20.9**	**25.3**	**21.5**

WEDNESDAY POSTER

P2Ab-5

Submicron Decafluorobutane Phase-Change Contrast Agents for Activation with Low Acoustic Intensities Formulated with a Compression-Condensation Method

Paul S. Sheeran[1], Samantha Luois[2], Paul A. Dayton[1], Terry O. Matsunaga[2]; [1]Joint Department of Biomedical Engineering, University of North Carolina and North Carolina State University, Chapel Hill, NC, USA, [2]University of Arizona, Tucson, AZ, USA

Background, Motivation and Objective

Microbubbles (MBs) have the ability to circulate in the vascular space with sufficient scattering ability to be used as an ultrasound (US) contrast agent. However, for the purposes of extravascular ultrasound imaging, MBs are too large to pass through the endothelial gap junctions. Bubbles on the order of 100s of nanometers may extravasate, but may be too small to elicit sufficient backscatter. Previously, we developed stabilized micron-sized decafluorobutane (DFB, bp = -1.1 °C) droplets via extrusion at low temperatures for acoustic droplet activation (ADV). We have extended this by developing a unique method of producing sub-micron sized droplets labile enough to undergo ADV at low acoustic intensities. This method utilizes a simple yet novel technique involving compression/condensation of lipid-coated DFB MBs produced by agitation.

Statement of Contribution/Methods

MBs were subjected to mild cooling and compression with room air, and the condensation of DFB yielded a translucent solution of nanodroplets. Sizing of nanodroplets were conducted using both a Malvern ZS and an Accusizer 780A. Samples were imaged optically and vaporized at 37 °C using 5 MHz US at mechanical indices available on diagnostic machines. Images of resulting bubbles were captured and analyzed.

Results

Sizing of the nanodroplets produced by the DFB MB compression/condensation method showed peaks commonly in the 200-300 nm range. Acoustic activation at 5 MHz and MI = 1.2 and 1.7 resulted in bubble sizes in the micrometer range that were well-correlated to initial droplet sizes through ideal gas law estimations. Preliminary data shows evidence that lipid formulation may be optimized to preserve a greater number of activatable nanodroplets.

Discussion and Conclusions

Stabilized DFB nanodroplets small enough for extravasation can be predictably condensed from pre-formed MBs and in turn, can be activated by low acoustic intensity US back to MBs with a majority between 1 – 2 microns, strongly resembling the initial population. This indicates that the simple methodology works well to preserve the DFB core as the MBs condense into nanodroplets. Furthermore, the stability of the nanodroplets at 37° C bodes well for their potential use as nanodroplets for extravasation outside the vasculature in vivo. Future studies will include generation of targeted US-activatable DFB nanodroplets.

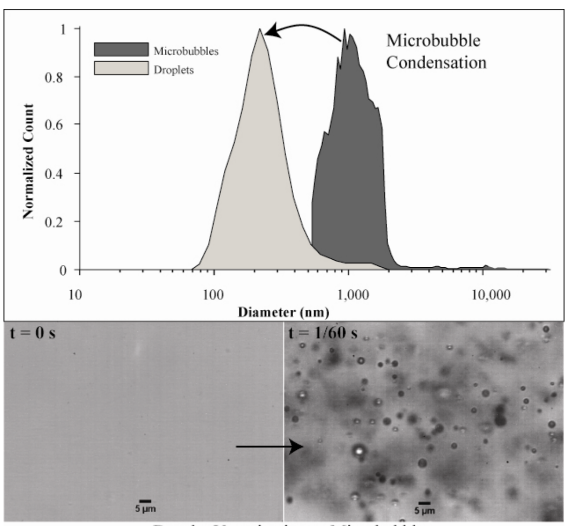

Droplet Vaporization to Microbubbles

P2Ab-6

Quantitative Analysis of Subharmonic Imaging using Microbubbles in Contrast Imaging

Suhyun Park[1], Scott Dianis[1], Kai E Thomenius[1], Carl L Chalek[1], K Wayne Rigby[1], Larry Mo[1], Feng Lin[2], Lihong Pan[3], Anne L Hall[3], Flemming Forsberg[4]; *[1]GE Global Research, Niskayuna, NY, USA, [2]GE Healthcare, WuXi, JiangSu, China, People's Republic of, [3]GE Healthcare, Wauwatosa, WI, USA, [4]Department of Radiology, Thomas Jefferson University, Philadelphia, PA, USA*

Background, Motivation and Objective

Second-harmonic imaging (HI) has been widely used to improve the contrast of microbubbles with respect to tissue since microbubbles have a large second-harmonic response. Unlike tissue, however, microbubbles can also have a response at sub-harmonic frequency under certain conditions [1,2]. This suggests that sub-harmonic imaging (SHI) has the potential of providing a larger contrast-to-tissue ratio (CTR) than does HI. Shankar et al [3] demonstrated this experimentally, but the measurements were limited to a single-element transducer with continuous or long burst insonation. In order to take advantage of sub-harmonics in imaging, it is necessary to evaluate the image quality of SHI through quantitative comparisons with HI.

Statement of Contribution/Methods

Nonlinear tissue response was numerically simulated by solving the KZK wave equation [4] and the response of a microbubble was simulated using the Rayleigh-Plesset equation [5]. Based on the numerical analysis of the tissue and bubble responses, transmit and receive frequencies for sub-harmonic and second-harmonics were chosen. SHI and HI modes were implemented on a Logiq 9 scanner (GE Healthcare, Milwaukee, WI, USA). Images of a flow phantom (ATS laboratories, CT, USA) with Sonazoid (GE Healthcare, Oslo, Norway) microbubbles in the degassed water were acquired as the concentration of the microbubbles was decreased. Pulse inversion was used to suppress the fundamental signal. The vessel tube in the flow phantom was located at various depths. The CTR and signal-to-noise ratio (SNR) were calculated with change of the bubble concentration and the depth of the tube.

Results

The experimental results agree well with the simulations. The SNR of SHI was approximately 10 dB less than of HI. From bubbles at small depths, the CTR at the sub-harmonic frequency can be higher or lower than the value in second-harmonics. However at deeper depths, the CTR for SHI is 5-15 dB higher than for HI. Images from SHI and HI clearly show that the tissue intensity in HI becomes relatively higher than in SHI as the concentration of the bubbles is decreased.

Discussion and Conclusions

With optimum imaging parameters, the contrast of microbubbles using the sub-harmonic signal can be higher than with the second-harmonic. Nonlinear simulations are useful in determining the choice of parameters for SHI and HI. Although the SNR at the sub-harmonic frequency is lower than that at the second-harmonic frequency, SHI can be used at deeper depths with higher CTR. This will be due to the higher generation of second-harmonics in mid-field of the tissue and also the attenuation of second-harmonics when it returns.

[1] J. Chomas, et al, Trans. on IEEE UFFC, 2002

[2] W. Shi, et al, Ultrasound Med in Biol, 2000

[3] P. M. Shankar, et al, Ultrasound Med in Biol, 1998

[4] Y. lee, et al, J. Acoust. Soc. Am., 1995

[5] L. Hoff, et al, Proc. of IEEE UFFC, 1999

This work was supported by NIH grant 1 RC DK087365-01

P2Ab-7

Influence of shell parameters on response of polymer-shelled microbubbles to high-frequency ultrasound

Parag V. Chitnis[1], Jonathan Mamou[1], Sujeeth Koppolu[1], Jeffrey A. Ketterling[1]; [1]F. L. Lizzi Center for Biomedical Engineering, Riverside Research, New York, NY, USA

Background, Motivation and Objective

Polymer-shelled ultrasound contrast agents (UCAs) can undergo a "compression only" behavior leading to shell rupture and nonlinear response of the released gas bubble when excited below 10 MHz. This two-part study investigated their response to high-frequency ultrasound (HFU), and its relation to shell fragility.

Statement of Contribution/Methods

Four types of UCAs with polylactide shells were examined: one from Point Biomedical (diameter 4 µm, shell-thickness-to-radius ratio (STRR) 7.5 nm/µm), and three from Philips Research (all 2 µm diameter, STRRs 40 nm/µm, 65 nm/µm, and 100 nm/µm).

UCA fragility was inferred from their response to slowly increasing overpressure in a glycerol-filled test chamber with reconstituted UCAs added on top of the glycerol surface. A video microscope with a gradient-based dynamic focusing algorithm imaged UCAs while glycerol was pumped at 5 mL/hr to induce overpressure from 2-330 kPa over 1 hour. UCAs were sized in post-processing using Sobel edge detection and generalized Hough transform.

UCA response was examined by streaming individual UCAs through the focus of a 20 MHz transducer using 10 or 20-cycle pulses at negative pressures of 0.2-2.6 MPa. For each exposure condition, 500 UCA-backscatter events were recorded into a matrix, M. The singular-value decomposition of M yielded analyzing vectors (AV) that were sorted in decreasing order of singular value, and the first AV whose Fourier transform (FT) magnitude peaked at 10 MHz (AV10) was selected; a subharmonic score (SHS) was computed by multiplying the average of the decomposition coefficient of M on AV10 by the FT-magnitude of AV10.

Results

UCA rupture induced by overpressure exhibited a sharp threshold that was not size dependent but dependent on STRR (Fig. 1a). UCA-SHS indicated a similarly well-defined pressure regime (0.2-0.5 MPa) of subharmonic activity (Fig. 1b). SHS decayed with increasing acoustic pressure. The SHS of UCAs was not correlated with STRR or the mean rupture pressures; UCAs with STRR of 100 nm/µm produced the highest SHS.

Discussion and Conclusions

The results suggest that the polymer-shelled UCAs examined in this study might not adhere to rupture-based mechanism of nonlinear response at 20 MHz. However, UCAs may be optimized for specific applications that rely on rupture for activation by optimizing the STRR.

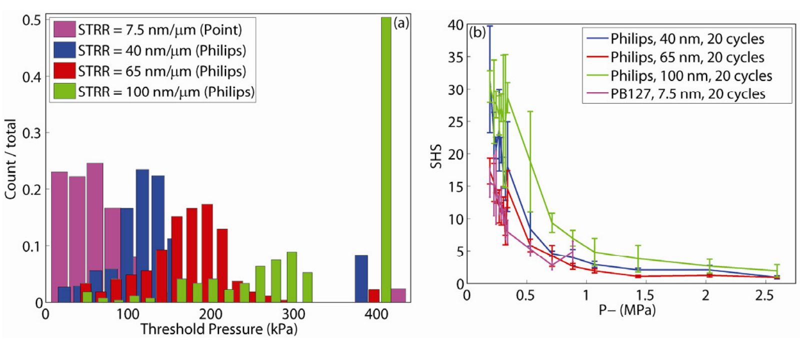

Fig. 1 (a) Rupture-pressure histogram of the four polymer-shelled UCAs. (b) SHS for all UCAs with respect to incident peak-negative pressure. The mean SHS was computed from data accumulated from 3 sets of 500 UCAs; the errorbars show the standard deviation.

P2Ab-8

Modulational Instability and Localized Modes of Ultrasound Contrast Microbubbles Surface Oscillations

Serge Dos Santos[1], Víctor Sánchez-Morcillo[2], André-Pierre Abellard[3], Ayache Bouakaz[3]; [1]U930 "Imagerie et Cerveau" INSERM-CNRS, Centre – Val de Loire Université, BLOIS, France, [2]Departamento de Fisica Aplicada, GANDIA, Spain, [3]INSERM U930 - CNRS ERL 3106, TOURS, France

Background, Motivation and Objective

Microbubble surface modes appear when contrast agents are insonified with specific ultrasound pulses. In this case, the radius is a space-dependent function which can be expanded on the basis of spherical harmonics describing the spatial vibrational modes of the bubble. Modulational Instability (MI) is an instability of the vibration modes in nonlinear systems induced by an external driving, and can be physically interpreted as a nonlinear four-wave (or four-mode) mixing process.

Statement of Contribution/Methods

Starting from the continuous Marmottant model [1] for the vibration of the bubble radius R(t), and a discrete nonlinear model of the discretized radius $R(t,\theta_n)$ with periodic boundary conditions and nonlinear coupling between surface modes, MI in bubbles is investigated numerically. After a first step of Symmetry Analysis [2] applied to the nonlinear equations associated to the models, invariant properties allow an identification of dimensionless similarity variables that link both continuous and discrete models. Thanks to this similarity analysis, the bubble can be studied with a macroscopic mechanical 1D ring chain (diameter =73 cm) using N=52 nonlinearly coupled pendulum of mass m=6g and length =3.2cm, in analogy with [3], but with periodic conditions. The second step consists in studying numerically the MI criterion versus the amplitude of external field applied to the bubble.

Results

The analysis and the experiments reveals the existence of Intrinsic Localized Modes (ILMs), similar to those found in other more generic systems of nonlinearly vibratory lattices. The observation of ILM in 1D chain [3] of coupled oscillators, presenting many similarities with the discrete bubble model, showed to play a role in creating spatio-temporal localized excitations leading to the breaking of the bubble. In our periodic pendulum lattice apparatus describing the macroscopic equivalence of the bubble, the system parametrically driven at 5.4 Hz presents subharmonic behavior and localized modes oscillating at 2.7 Hz.

Discussion and Conclusions

Versus the amplitude and the frequency of the driving, the mechanical ring presents parametric instability surface modes and localized modes oscillating at subharmonics of the parametric excitation. The perspective of this analysis is to define practical optimized ultrasound pulses exciting the bubble and leading to drug delivery applications.

[1] P. Marmottant, S. van der Meer, M. Emmer, M. Versluis, N. de Jong, S. Hilgenfeldt, and D. Lohse, “A model for large amplitude oscillations of coated bubbles accounting for buckling and rupture,” J. Acoust. Soc. Am. 118, 3499 (2005).

[2] A.O. Maksimov, Symmetry in bubble dynamics, Communications in Nonlinear Science and Numerical Simulation, 9, p 83 (2004)

[3] B. Denardo, B. Galvin, A. Greenfield, A. Larraza, S. Putterman, W. Wright, Observations of Localized Structures in Nonlinear Lattices: Domain Walls and Kinks, Phys. Rev. Lett. 68, 1730 (1992).

P2Ab-9

Non-uniform oscillations of deflating bubbles - a pilot study

Jacopo Viti[1,2], Riccardo Mori[1], Francesco Guidi[1], Nico De Jong[2], Piero Tortoli[1]; [1]Electronics and Telecomm., Universita' di Firenze, Firenze, FI, Italy, [2]Biomedical Engineering, ThoraxCenter, Erasmus MC Rotterdam, Rotterdam, Netherlands

Background, Motivation and Objective

The characterization of single ultrasound contrast agent (UCA) microbubbles (µB) is a necessary step to improve contrast detection strategies. Ideally, an optimal detection strategy should fit the physical characteristics of the used µB; however, such characteristics are expected to change during exposure to ultrasound, even when very low pressures are used. In this work, we investigate experimentally the behavior of isolated µB during prolonged US excitation.

Statement of Contribution/Methods

Single Definity® µB, held in a transparent capillary, were positioned in the focal regions of both a microscope and a wideband ultrasound transducer. 15-cycle long tone bursts were transmitted at 60kPa peak-negative pressure. Two pulse schemes were used to excite the µB: in the first, only 2 MHz tones were transmitted to obtain dense sampling of the µB response, in the second scheme the frequency was cyclically changed from 2 MHz to 4 MHz in steps of 500 kHz. The transducer was driven by a custom programmable electronic system. The optical images from the microscope were recorded using the Brandaris-128 camera operating at 12.5 million frames per second.

Results

All imaged µB exhibit a monotonic size decrease; typically, in single-frequency experiments, the µB radius decreases from about 2 µm to about 1.4 µm when insonified 200 times with the 2 MHz pulses. Equivalent results are obtained in the sweeping frequency modality. However, during such a decrease different phenomena were observed. The oscillation shape varies several times during the deflation; non-symmetrical oscillations are observed and in particular, when the µB reach a quasi-stable smallest size, they exhibit compression-only behavior. For several µB it was possible to observe two phases alternating to each other: in the phase A, the oscillation progresses towards compression-only behavior while the resting size is stable; in the phase B, the bubble tends to an expansion-only behavior while a noticeable reduction in the resting size is simultaneously observed.

Discussion and Conclusions

The results of this study show that µB deflation originates, in controlled way, from two phenomena: A. gas losses are dominant, resulting in compression only behavior; B. shell transformations occur, resulting in expansion only. This alternation leads to echo-decorrelation, opening new perspectives for contrast detection methods. Moreover, pushing the µB towards a quasi-stable compression only behavior is an effective method to enhance the generation of higher harmonics.

P2Ab-10

Comparison of the acoustic response of liquid-PFOB and solid-core nanoparticles between 20 and 40 MHz

Sara JAFARI[1], Odile DIOU[2], Nicolas TSAPIS[2], Elias FATTAL[2], S.Lori BRIDAL[1]; [1]Laboratoire d'Imagerie Paramétrique, UMR 7623 Université Pierre et Marie Curie and CNRS, France, [2]Physicochimie-Pharmcotechnie-Biopharmacie, UMR CNRS 8612 and Univ Paris-Sud, France

Background, Motivation and Objective

Liquid-core nanoparticles are promising candidates for targeted ultrasound-controled therapy. Previously, we demonstrated that solutions of polymeric nanocapsules (poly lactide-co-glycolide PLGA, 200 nm diam.) with a liquid perfluorooctyl bromide PFOB core provided detectable acoustic signal between 20 and 40 MHz. To investigate the effect of liquid cores, the current work compares acoustic response from liquid-core PLGA nanocapsules, filled PLGA particles and latex beads.

Statement of Contribution/Methods

Particles were diluted in degassed deionized water (25 mg/mL) and perfused through the lumen of a wall-less flow phantom (5 to 400 mm/s): Liquid-core PLGA particles, 200-nm diam. shell thickness to radius T/R=0.35. filled with PFOB (Boiling point : 142 °C); Filled, 200-nm PLGA particles and 500-nm latex beads (Corpuscular Inc.).

A 35-MHz PVDF transducer (12.5 mm focal length, 110% bandwidth) was placed perpendicular to the lumen axis with the focus in the lumen. Gaussian-modulated sinusoidal pulses (9 cycles, FBW: 20%) were transmitted at 20 MHz and 40MHz. Data were acquired for each solution at matched conditions with conventional; pulse-inversion, PI; multi-pulse inversion, MPI; and sub-harmonic pulse sequences at transmit peak negative pressures from 0.3 -1.3 MPa , ΔP= 0.2 MPa. For each series of measurements, ten sets of independent (N = 256) radio-frequency data lines were recorded, 200Msamples/s. Backscattered echoes were Hamming windowed and Fourier transformed. Average power spectral intensity and standard deviation were calculated for each set of waveforms.

Results

All three types of nanoparticles presented detectable backscattered echoes at transmit pressures above 560 kPa . No significant changes in acoustic response were observed as a function of flow rate in the phantom. Average fundamental Intensity at 20 MHz (560 kPa) for liquid-core PLGA was 8±2.5 dB greater than filled-PLGA and 11 ±2 dB greater than latex beads. Throughout the pressure range, spectra of the average response from filled-PLGA and latex beads presented only fundamental peaks (20MHz or 40MHz). Spectra (560 kPa) from the liquid-core, PLGA particles presented stronger fundamental peaks (17±2 dB above the noise level) and additional ultra harmonic (4±1 dB above the noise level) peaks. Intensity at the ultra-harmonic was improved by 3± 1dB and 4 ± 1.5 dB with the PI and MPI sequences, respectively, relative to the conventional sequence.

Discussion and Conclusions

Filled latex and PLGA particles did not present ultra harmonic response while PFOB-core nanocapsules with a PLGA shell did. Additional measurements with variable T/R should further evaluate the effect of the shell on the acoustic response at high frequency. Results suggest that amplitude and the nonlinear content of the acoustic response (20- 40 MHz) are influenced by the core/shell geometry of these PFOB/PLGA nanoparticles.

P2Ac - Shear Wave Elastography I

Carribean Ballroom III-V

Wednesday, October 19, 2011, 1:00 pm - 4:30 pm

Chair: **Mark Palmeri**
Duke University

P2Ac-1

In Vivo Detection of Bleeding Rate in a Dog Model of Hemophilia and at Human Femoral Arteriotomy by ARFI Ultrasound

Mallory Scola[1], Russell Behler[2], Timothy Nichols[3,4], Melissa Caughey[4], Elizabeth Merricks[3], Robin Raymer[3], Paris Margaritis[5], Katherine High[5,6], Caterina Gallippi[1]; [1]*Joint Department of Biomedical Engineering, The University of North Carolina at Chapel Hill, Chapel Hill, NC, USA,* [2]*GE Healthcare, Milwaukee, WI, USA,* [3]*Department of Pathology and Laboratory Medicine, The University of North Carolina at Chapel Hill, Chapel Hill, NC, USA,* [4]*Department of Medicine, The University of North Carolina at Chapel Hill, Chapel Hill, NC, USA,* [5]*Division of Hematology, Children's Hospital of Philadelphia, Philadelphia, PA, USA,* [6]*Howard Hughes Medical Institute, Children's Hospital of Philadelphia, Philadelphia, PA, USA*

Background, Motivation and Objective

There is currently no validated method for assessing hemostasis in vivo. Such a method would facilitate the development of replacement products for patients with bleeding disorders as well as improve patient care and reduce complications following invasive procedures. We hypothesize that ARFI Ultrasound is relevant for non-invasively monitoring bleeding rates in hemophilic dogs and in human subjects.

Statement of Contribution/Methods

We performed ARFI imaging using a Siemens SONOLINE AntaresTM imaging system (Siemens Medical Solutions USA, Inc. Ultrasound Division) on 20 dogs for 100 min following venous puncture [1]: n=6 normal, 8 naïve hemophilia A, 3 hemophilia A and 1 hemophilia B expressing cFVIIa following gene therapy, and 2 von Willebrand disease (severe type 3 VWD). ARFI imaging was also performed for 15 min on 20 humans following arteriotomy for diagnostic percutaneous cardiac catheterization [2]: n=10 treated by manual compression, and 10 treated with compression augmented by a hemostatic dressing. All data sets were processed with custom software to identify extravasated blood. Bleeding rate, defined as change in blood area v. time, was divided into 10 min intervals, and fit using a linear-least squares approximation; the slope of each segment was recorded as the mean bleeding rate. The mean rate was calculated for the initial 30 min of monitoring in dogs and for 0-4, 5-9, 10-14 min intervals for humans.

Results

Average ARFI-derived venous bleeding rates measured in the dogs during the first 30 min were comparable for normal (0.62 ± 0.33 mm²/min), hemophilia A (0.73 ± 0.47 mm²/min), and canine FVIIa expressing hemophilia A (0.62 ± 0.33 mm²/min) and B (0.69mm²/min), but significantly higher ($p<0.02$, paired t-test) in the VWD dogs (2.13 ± 0.05 mm²/min). Arteriotomy bleeding rates were not statistically significantly different ($p>0.02$) in the first 5 min in human patients treated with manual compression (11.15 ± 6.26 mm²/min) versus manual compression and hemostatic dressing (5.44 ± 3.64 mm²/min), but were significantly higher after 5 minutes ($p>0.02$) in patients receiving only manual compression (5-9 min: compression= 8.15 ± 5.55mm²/min, dressing= 1.43 ± 1.90 mm²/min; 10-14 min: compression= 4.84 ± 2.71mm²/min, dressing= -1.93 ± 2.36mm²/min).

Discussion and Conclusions

Our results, which show significantly higher venous bleeding rates in the VWD dogs consistent with the inherited bleeding phenotype and slower arteriotomy bleeding rates after 5 minutes when a hemostatic dressing is used to augment manual compression, suggest that ARFI imaging is capable of noninvasively monitoring bleeding rates in diverse clinical settings.

[1] Scola, et al, ARFI Ultrasound for In Vivo Monitoring of Soft-Tissue Bleeding and Hemostasis in a Dog Model of Hemophilia, IUS Proceedings, 2010.

[2] Behler, et al, ARFI ultrasound for in vivo hemostasis assessment postcardiac catheterization, part II: pilot clinical results, Ultrason Imaging, vol. 31, pp. 159-71, Jul 2009.

P2Ac-2

Shear wave elastography of in vivo pig kidney: Impact of urinary and vascular pressure on elasticity and viscosity measurements.

jean-luc gennisson[1], nicolas grenier[2], mickael tanter[1]; [1]Langevin Institute, France, [2]Hopital Pellegrin INSERM, France

Background, Motivation and Objective

Chronic kidney disease is a major source of mortality due to an increase of risk factors. Sequential measurement of renal elasticity could help in following the progression of intrarenal fibrosis. However, we know that increased elasticity values can be related to increased fibrotic processes, inflammatory changes or application of an external pressure. Moreover the kidney is a highly compartmentalized organ with a high level of perfusion. The purpose of this study is to evaluate in vivo on pig kidneys how renal anisotropy, perfusion and urinary pressure changes have an impact on measured elasticity values in each renal compartment using Supersonic Shear Imaging (SSI) technique.

Statement of Contribution/Methods

The SSI technique is based on the combination of the radiation force induced by a linear ultrasonic probe (8 MHz), to generate shear waves deep into tissues and, ultrafast ultrasound imaging to catch in real time their propagation throughout the medium (5000 frames/s). Shear wave spectroscopy and time of flight algorithms were applied to recover quantitative tissue viscosity and elasticity respectively. Viscoelastic anisotropy was also studied regarding the axis of kidney pyramids. Investigation of the relationship between viscoelasticity and the urinary or vascular pressure was obtained by filling the kidney with saline solution in the ureter or clamping artery or vein respectively. Measurements were controlled with a pressure sensor through a catheter in the ureter.

Results

6 in vivo pig kidneys were investigated, with the ultrasound axis perpendicular to the pyramid axis, showing strong elasticity differences between outer cortex (OC: 23±7 kPa), inner cortex (IC: 31±6 kPa) and medulla (26±7 kPa) whereas viscosity does not change within the cortex (OC and IC: ~1 Pa.s). The anisotropy ratio was also quantified when the ultrasound axis is perpendicular versus parallel to the pyramids axis (~1.5 for each anatomical zone). Elasticity rise with the urinary pressure by a factor of 4 when 40 mmHg of saline solution are injected. At last, clamping the renal artery or vein change drastically elasticity values within the cortex by a factor of 5 (OC: ~100 kPa) or 0.5 (OC: ~10kPa) respectively.

Discussion and Conclusions

Viscoelastic and anisotropic properties of the kidney were quantified. Separation of outer and inner cortex could be due to perfusion difference. By increasing artificially the urinary pressure we have observed the strong increase of elasticity due to a hydrostatic pressure. This suggests that using the acoustoelasticity theory, it could be possible to recover pressure quantification within the organs through elasticity measurements. Influence of vascular pressure or anisotropy is also extremely important to provide a realistic diagnosis. At last by taking carefully into account these parameters, non invasive identification and follow-up of these processes could improve renal prognosis and help to define adapted targeted therapies.

P2Ac-3

Multi-Push (MP) ARF Assessment of Elastic Properties in a Tissue Mimicking Phantom

Mallory Scola[1], Caterina Gallippi[1]; [1]Joint Department of Biomedical Engineering, The University of North Carolina at Chapel Hill, Chapel Hill, NC, USA

Background, Motivation and Objective

Noninvasively discriminating the viscoelastic properties of tissue has a multitude of diagnostic purposes. In application to muscular dystrophy, imaging viscoelasticity may be useful for delineating the complex and poorly understood disease process. We hypothesize that Multi-Push Acoustic Radiation Force (MP ARF) ultrasound, in which the displacements achieved by successive ARF excitations are compared, can be used to assess viscoelastic tissue parameters. In addition, because MP ARF examines the ratio of displacements achieved by two pushes rather than the absolute displacement achieved by a single push, we hypothesize that MP ARF is less sensitive to depth-dependent variation in force magnitude than ARFI.

Statement of Contribution/Methods

ARF imaging was performed in a soft (11.9 kPa) and a stiff (42.9 kPa) gelatin tissue mimicking phantom using a Siemens SONOLINE Antares™ imaging system and a VF7-3 transducer (Siemens Medical Solutions USA, Inc. Ultrasound Division). MP ARF was implemented using two 300-cycle ARF excitations administered 0.8 ms apart in time and delivered to the same region of excitation. Displacements were compared by calculating marginal peak displacement (MPD), given by MPD = 1 – [PD1 – (PD2 – D)]/PD1 where PD1 is the peak displacement achieved by the first push, PD2 is the peak displacement achieved by the second push, and D is the displacement at the time of the second push. Conventional ARFI and SWEI were also performed to calculate peak displacement (PD), time to 67% recovery, and shear wave velocity (SWV).

Results

In the soft phantom the median PD at the focal depth was 22.43 µm, recovery time was 0.52 ms, and SWV was 1.99 m/s. In the stiff phantom the median PD at the focal depth was 6.57 µm, recovery time was 0.52 ms, and SWV was 3.78 m/s. Fig 1 shows profiles of axial displacement versus time acquired in the soft (left) and stiff (right) phantoms, with PD1, D, and PD2 annotated. Median MPD at the focal depth was 0.92 and 0.65 for the soft and stiff phantom respectively. PD was within 10% of the focal value for 3.21 and 2.73 mm, whereas MPD was within 10% of the focal value for 7.57 and 4.56 mm in the soft and stiff phantoms.

Discussion and Conclusions

Preliminary results indicate that MP ARF differentiates viscoelastic properties in gelatin phantoms and is less depth-dependent than ARFI. Further studies will include phantoms of varying viscosity to show the effect of viscosity on MPD.

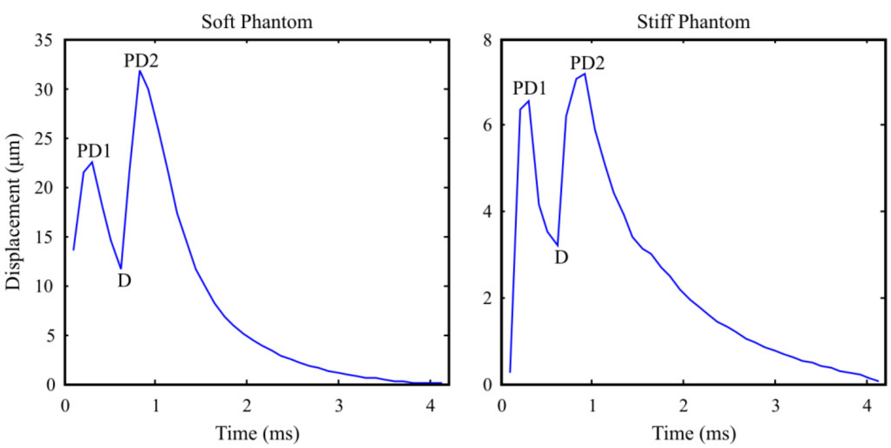

Figure 1. ARF-induced displacement versus time profiles generated by MP ARF

P2Ac-4

Evaluation of Shear Properties in Muscle Tissue via Novel Superficial Elastography Technique

Jeffrey Ballyns[1], Paul Otto[1], Jennifer Hammond[2], Jay Shah[2], Tadesse Gerber[2], Lynn Gerber[1,2], Siddhartha Sikdar[1]; [1]*George Mason University, USA*, [2]*National Institutes of Health, USA*

Background, Motivation and Objective

Noninvasive measurement of the mechanical properties of soft tissue is of significant clinical interest. Recent work has demonstrated the ability of ultrasound (US) elastography techniques to measure shear modulus and shear viscosity of bicep muscle and liver tissue in vivo using specialized equipment. The objective of this study was to evaluate a new elastography technique that can be easily translated to a clinical setting using commercially-available equipment.

Statement of Contribution/Methods

The muscle was externally vibrated at frequencies in the range of 60–200 Hz using a custom massager. The radio frequency (RF) US data were collected using an Ultrasonix SonixRP system and a 5–14 MHz linear array transducer. The phase of the RF data was used to compute the shear wave images (Fig1.B&D) that represent the phase of the externally-induced vibration as it travels through the tissue. The spatial gradient of the vibration phase yielded the shear wave velocity (Fig1.C&D):$C_S=(\omega*\Delta r)/\Delta\theta$, where $\Delta\theta$ is the difference in phase angle (in radians) over distance (Δr), and ω is the shear wave vibration frequency in radians/sec. Shear modulus ($\mu 1$) and shear viscosity ($\mu 2$) were estimated

WEDNESDAY POSTER

using a Voigt-model for soft tissue: $C_S=\sqrt{((2*(\mu1^2+\omega^2*\mu2^2))/(\rho*(\mu1+\sqrt{(\mu1^2+\omega^2*\mu2^2)})))}$, where ρ is the tissue density. We measured shear properties of the bicep (n=5) and trapezius muscles (n=9) in 5 healthy volunteers and the trapezius muscle in 6 symptomatic patients with palpable myofascial trigger points (MTrPs)(n=6).

Results

The bicep branchii muscle had a μ1 of 12.5±3.4 kPa and a μ2 of 7.7±4.0 Pa•s, which matched literature values for this muscle in its relaxed state bent at 90°. MTrPs had significantly higher μ1 (16.0±1.3 kPa) than the palpably normal surrounding muscle tissue (SMT)(11.3±0.6 kPa) and normal trapezius muscle (6.1±2.7 kPa)(P<0.05 for all). SMT was also significantly stiffer in shear that normal tissue (P<0.01).

Discussion and Conclusions

The approach presented here provides a quick and effective method for quantitatively measuring region specific shear properties in both normal and symptomatic muscle tissue using commercially-available equipment.

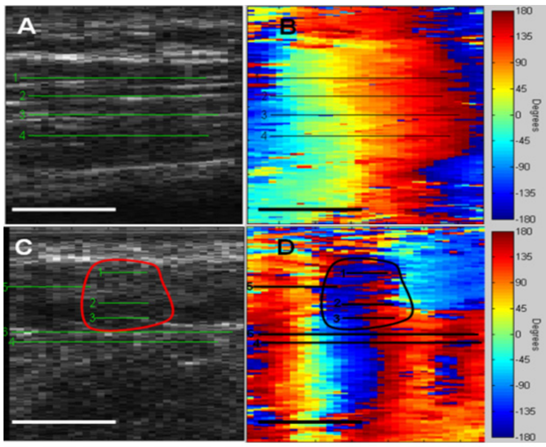

Figure 1. (A) Gray scale image of normal and symptomatic (C) upper trapezius muscle and corresponding phase plot (B&D respectively) with lines denoting paths of interest for μ1 and μ2 measurements and circles denote MTrP. Scale bar = 1cm.

P2Ac-5

Vibro-acoustography beamforming and imaging with a 1.75D array transducer

Matthew Urban[1], Carl Chalek[2], Kai Thomenius[2], Mostafa Fatemi[1], Azra Alizad[1]; [1]Department of Physiology and Biomedical Engineering, Mayo Clinic College of Medicine, Rochester, MN, USA, [2]General Electric Global Research, Niskayuna, NY, USA

Background, Motivation and Objective

Vibro-acoustography (VA) is an ultrasound-based imaging modality that uses radiation force produced by two confocal ultrasound beams separated by small frequency difference, Δf, to vibrate tissue at Δf. An acoustic field is created by the object vibration and measured with a nearby hydrophone. This method has recently been implemented on a clinical ultrasound system using one-dimensional linear array transducers. Beamforming with a linear array transducer produces point-spread functions (PSFs) that are asymmetric, typically wider in the elevation direction as compared to the azimuthal focus. As a result, features in the object can appear elongated or blurred when mechanically scanning the linear array transducer in the elevation direction.

Statement of Contribution/Methods

Different configurations for subaperture design for the two ultrasound beams necessary for VA imaging were analyzed both numerically and experimentally. We used a 1.75D transducer with 12 rows and 70 columns of elements with size 0.9 x 0.9 mm. For our apertures, we used a 12 x 12 element aperture and only 128 elements could be activated. The PSFs for different configurations of the subapertures for the two frequencies centered about 5 MHz were evaluated using a numerical simulation model using Field II. Experimentally, we scanned the pressure field transmitted by the transducer for different configurations using a needle hydrophone with a 0.2 mm active element to evaluate PSF shape and resolution. Also, considering the large element sizes, we evaluated the levels of grating lobes for the different configurations. Lastly, images were formed by scanning a urethane breast phantom and an *ex vivo* human prostate.

Results

We evaluated the PSFs from the simulations and needle hydrophone scans and found good agreement, thereby validating the simulation framework. We quantitatively analyzed the grating lobe levels of the PSFs for the different configurations. We compared images generated using different configurations of the subapertures in the urethane breast phantom and *ex vivo* human prostate. Some "ghost" artifacts were detected in the breast phantom images and will be discussed.

Discussion and Conclusions

The advantage of the 1.75D array transducer is the multiple rows of elements that can be used for improving elevation focus for imaging formation. Artifacts from the grating lobes can create replicas of real objects. These artifacts were observed in the urethane breast phantom, but were not as noticeable in soft tissue images. VA imaging using a 1.75D array transducer offers several advantages including improved image detail and contrast due to better elevation focusing of the imaging point-spread function. [This work was supported in part by grant CA121579.]

P2Ac-6

Optical sensing of shear wave velocity generated by acoustic radiation force

Rui Li[1], Robert Eckersley[2], Chris Dunsby[3], Daniel Elson[4], Meng-Xing Tang[5]; [1]Department of Bioengineering, Imperial College London, United Kingdom, [2]Imaging Sciences Department, Imperial College London, United Kingdom, [3]Depatment of Physics, Imperial College London, United Kingdom, [4]Department of Surgery, Imperial College London, United Kingdom, [5]Department of Bioengineering, Imperial College London, London, London, United Kingdom

Background, Motivation and Objective

The ability to measure shear wave propagation in soft tissue is highly desirable as the shear wave is closely related to the medium elastic properties. Sophisticated super-fast ultrasound imaging techniques have been developed to track shear wave propagation in tissue and reveal tissue elastic properties. We propose an alternative optical sensing technique which can measure the average speed of shear wave propagation.

Statement of Contribution/Methods

A homogeneous tissue mimicking phantom was exposed to a 532nm laser and an amplitude modulated(AM) ultrasound burst generated by a 5MHz focused transducer with a single AM cycle. A CCD camera was placed on the other side of the phantom and was used to record the diffuse transmitted light. One CCD image was recorded before the ultrasound burst as the reference and a series of images were recorded after the burst with an exposure time of 2ms. Image contrast differences before and after the ultrasound burst were calculated and presented as a function of time. In order to sense the shear wave generate by the acoustic radiation force, the ultrasound focus was set at various distances from the centre of the laser radiation area.

Results

The curve of CCD contrast difference over time shows a clear peak during the ultrasound excitation and this peak moves in time as the ultrasound focus moves in space relative to the centre of the laser radiation area. Based on this the average speed of the shear wave was estimated to be 2.5mm/ms, which was in agreement with an independent measurement on the phantom by a SSI scanner (Aixplorer, SuperSonicImagine).

Discussion and Conclusions

An experimental setup with laser and a CCD camera has been proposed which noninvasively measures the speed of shear wave generated by acoustic radiation force. This potentially offers a useful tool for measuring tissue elasticity in vivo.

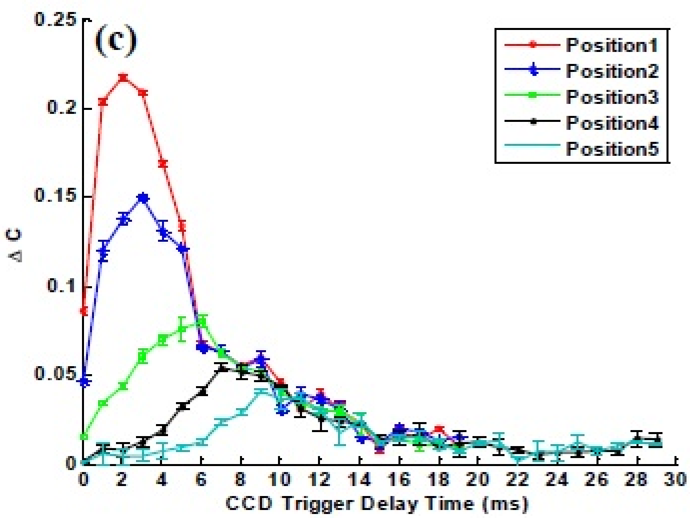

WEDNESDAY POSTER

P2Ad - Image Processing & Measurements

Carribean Ballroom III-V

Wednesday, October 19, 2011, 1:00 pm - 4:30 pm

Chair: **Peter Hoskins**
Univ. of Edinburgh

P2Ad-1

Measurement of Tendon Velocities using Vector Tissue Doppler Imaging and Curved M-Mode in Patients with Cerebral Palsy

Avinash Eranki[1], Paul Otto[1], Lindey Curatalo[2], Laura Prosser[2], Katharine Alter[2], Diane Damiano[2], Siddhartha Sikdar[1]; [1]*George Mason University, USA,* [2]*National Institutes of Health, USA*

Background, Motivation and Objective

Quantitative measurements of muscle and tendon kinematics using ultrasound (US) could be used as an office-based clinical outcome measure or as a research tool in a biomechanics lab. Our goal is to compare two novel methods: vector tissue Doppler imaging (vTDI) and curved M-mode (cMM), to non-invasively measure tendon velocities in children with spastic cerebral palsy (CP) that could be used in neurologic and orthopedic conditions.

Statement of Contribution/Methods

Four ambulatory children with CP were seen in the Functional & Applied Biomechanics Section at the NIH Clinical Center. US data were collected while imaging the tibialis anterior tendon during a seated dorsiflexion task using an Ultrasonix Sonix Touch and a linear array transducer and compared against a Vicon MX 3D motion capture system. vTDI was performed by splitting the array transducer into two transmit and receive apertures steered by 15°. Magnitude of the peak dorsiflexion velocity vector of the tendon was estimated (Fig. 1A). B-mode frames were resampled along a user-defined spline on the tendon to generate a cMM image. The tendon displacement waveform was obtained by speckle tracking and the mean dorsiflexion velocity was estimated (Fig 1C-E). The corresponding peak and mean joint angle velocities were derived from 3D motion capture waveforms (Fig 1B&F).

Results

The peak velocities from vTDI and mean velocity from cMM showed strong correlations with peak and mean joint angle velocities from 3D motion capture (R2 =0.81 and 0.84, respectively) for all four cases over multiple trials. Mean velocities estimated by integrating vTDI waveforms were weakly correlated with corresponding mean joint angle velocities (R2 =0.56).

Discussion and Conclusions

Preliminary results show vTDI and cMM can quantitatively measure tendon velocities in patients with CP and could be a surrogate clinical measure. vTDI overcomes the angle dependence of conventional Doppler, but is not available in conventional US systems. The cMM method can visualize the tendon directly and relies on conventional B-mode imaging, but is operator dependent. vTDI is better suited for peak velocity measurements and fast motion, whereas cMM is better suited for mean velocity measurements and slow motion. Ongoing studies will evaluate the clinical significance of these measures to understand musculoskeletal kinematics in patients with gait related disorders.

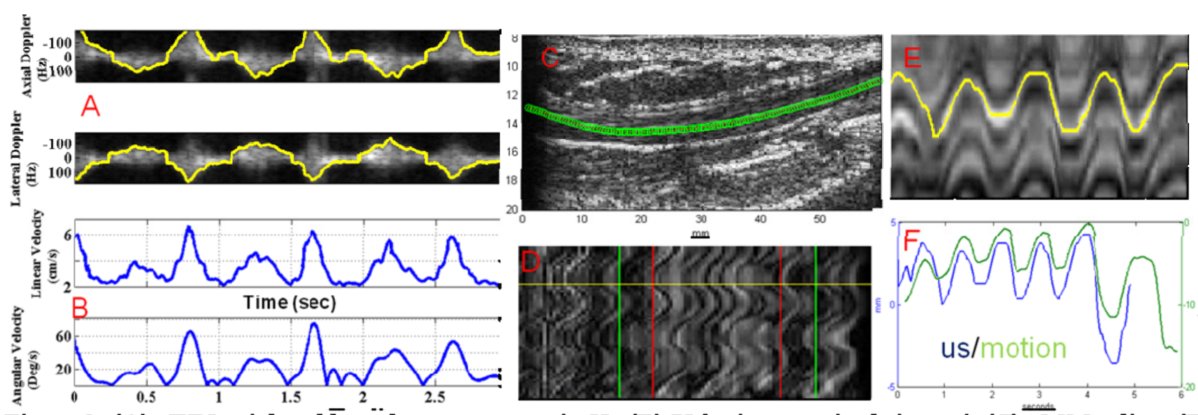

Figure 1. (A) vTDI axial and lateral spectrograms in Hz (B) Velocity magnitude in cm/s (C) cMM spline (D) cMM resampled motion stack (E) cMM correlation track (F) cMM displacement comparison with motion capture

P2Ad-2

Detectability index describes the information conveyed by a sonographic image

Nghia Nguyen[1], Craig Abbey[2], Michael Insana[3]; [1]Department of Electrical and Computer Engineering, University of Illinois at Urbana-Champaign, Urbana, Illinois, USA, [2]Psychological and Brain Sciences, University of California, Santa Barbara, Santa Barbara, California, USA, [3]Bioengineering, University of Illinois at Urbana-Champaign, Urbana, Illinois, USA

Background, Motivation and Objective

We established for the first time a rigorous relationship between diagnostic information and clinical task performance for sonography. This development enables expression of the area under the ROC curve (AUC) in terms of the spectrum of diagnostic features and the system response. Thus ultrasonic imaging systems may now be analyzed like photon imaging systems, where performance is expressed as the product of task spectrum and generalized noise-equivalent-quanta (GNEQ) integrated over the system bandwidth. In sonography, however, we found that GNEQ is replaced by the autocorrelation of a GNEQ-like, due to the nature of acoustic scattering and how sonographic contrast is generated.

Statement of Contribution/Methods

The advancement is to connect the Kullback-Liebler divergence (KLD), quantifying diagnostic information, to the square of the detectability index (sDI) as measured from the AUC during a psychophysical study. For sonography with the quadratic discriminants, the relation is established numerically by relating KLD to the area between detection and false-alarm curves plotted as functions of the decision variable threshold. Comparing KLD to sDI and the square of the detection signal-to-noise-ratio (sSNR), calculated from moments of the decision function, we find that sDI is consistent with KLD but sSNR can under-estimate diagnostic performance.

Results

Figs show performance metrics sDI, KLD, sSNR plotted versus object contrast for three tasks representative of lesion imaging. The task in Fig (a) is to discriminate hypoechoic (S1) from anechoic lesions (S0); in Fig (b) it is to discriminate spiculated (S1) from smooth boundary lesions (S0); and in Fig (c) it is to discriminate elongated eccentric (S1) from circular lesions (S0). Visual tasks are illustrated in Fig (d). In Fig (a), the three metrics are equivalent, whereas in Figs (b, c), sSNR is reduced up to 14% relative to the other two.

Discussion and Conclusions

Results show that sDI found from the AUC describes diagnostic performance based on task-relevant information more accurately than sSNR. This finding has implications for reporting system performance. The equality between sDI and KLD suggests a method for separating the clinical tasks from system performance, which places sonographic system analysis on a parallel footing with photon-based medical imaging modalities, a long-term dream of Robert F. Wagner.

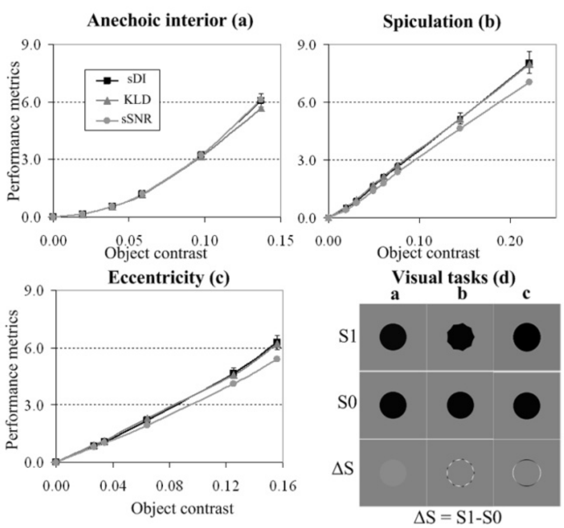

P2Ad-3

Characteristics of the Spatial Coherence Function from Backscattered Ultrasound with Phase Aberration and Reverberation Clutter

Gianmarco Pinton[1], Gregg Trahey[2], Jeremy Dahl[2]; [1]*Institut Langevin, ESPCI, Paris, France,* [2]*Department of Biomedical Engineering, Duke University, Durham, NC, USA*

Background, Motivation and Objective

Clutter, such as multiple reflections by tissue layers, adds acoustic noise that significantly degrades ultrasound image quality however there is currently little characterization of this complex phenomenon. Clutter can be characterized with spatial coherence which measures the similarity of received signals as a function of inter-element distance. The objective of this paper is to characterize the spatial coherence of the backscattered ultrasound signal in realistic diagnostic imaging conditions, where there is a significant amount of multiple scattering and reverberation clutter.

Statement of Contribution/Methods

The backscattered field is determined with a custom finite difference time domain full-wave nonlinear acoustic (FWNA) simulation and in vivo measurements in the human abdomen that include scattering and multiple reflections. To determine the acoustic field at the element locations, the FWNA code was used to propagate a diagnostic ultrasound pulse through a measured representation of human abdominal tissue and the spatial coherence was calculated based on the backscattered signal.

Results

Plot (a) shows that the spatial coherence function predicted by the simulation is consistent with theory for a uniform field of scatterers without reverberation. When only reverberation is modeled, this function a delta function shown in plot (b). A realistic model of the human body is a sum of the uniform scatterer case (a) and the reverberation case (b) and it compares favorably with the measured in vivo spatial coherence of the backscattered signal from the abdomen of 3 volunteers, shown in plot (c). Near-field phase aberration is shown to have a significant effect and scatterer reflectivity is shown to have almost no effect on the spatial coherence.

Discussion and Conclusions

Reverberation clutter from structured tissue introduces random acoustic noise that generates rapid spatial decorrelation. This decorrelation increases with the abdominal layer's impedance mismatch. When the point scatterer brightness is increased there is a small decrease in the spatial coherence, suggesting that the contribution of reverberation clutter introduced by the point scatterers is negligible when compared to ballistic propagation or the reverberation clutter from the tissue layer. These results quantify how tissue properties affect the spatial coherence measured by the transducer.

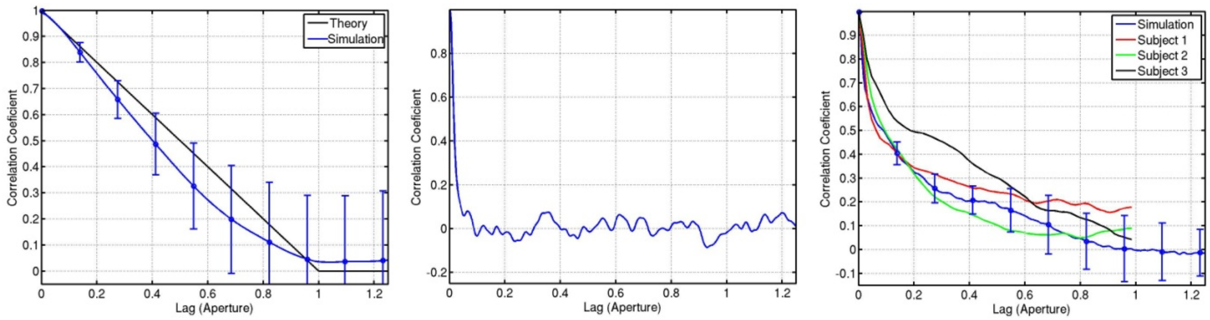

(a) No clutter (b) Clutter (c) In vivo

P2Ad-4

Pulse-Echo Ultrasound Imaging Employing Compressive Sensing

Martin Schiffner[1], Georg Schmitz[1]; [1]Institute of Medical Engineering, Bochum, Germany

Background, Motivation and Objective

Compressive Sensing (CS) is a recently developed concept for the efficient acquisition of compressible noisy signals. Its aim is to minimize the number of physical measurements required to obtain a representation of such a signal in a suitable sparsifying basis. CS has been adopted in different medical imaging modalities, e. g. magnetic resonance imaging and photoacoustic tomography. Maintaining image quality, a significant reduction of the number of measurements and thus of acquisition time was achieved. Using the same number of measurements a reduction of imaging artifacts and noise power was confirmed.

In this contribution we demonstrate the feasibility of CS in two-dimensional pulse-echo ultrasound imaging and discuss potential benefits.

Statement of Contribution/Methods

Our model is based on the linearized wave equation for lossless inhomogeneous fluids subject to the first Born approximation. Assuming plane waves with different angles of incidence as excitation, a sensing matrix relating the scattered velocity potential to the relative deviations in compressibility in a specified field of view (FOV) in the fluid is derived. This matrix is employed in the CS framework to recover the relative deviations in compressibility within the FOV from measurement data by solving a convex optimization problem.

Using data obtained by a SonixTOUCH (Ultrasonix) imaging system with a fixed linear transducer array (L14-5/38, no. of elements: 128, center freq.: 4 MHz) from a wire phantom and a tissue phantom, we validate our model experimentally. We compare the recovered images to those obtained by conventional pulse-echo ultrasound imaging schemes.

Results

The images of the wire phantom are shown in Figures (a) for the CS approach (single plane wave emission) and in (b) for a full synthetic aperture scan (SAFT, 128 emissions, boxcar apodization). In (a) side lobes are completely suppressed. The axial resolution (z-axis) is improved from 0.5 mm to 0.25 mm FWHM. Lateral resolution is comparable. Using wavelets as the sparsifying transform, the tissue phantom is reconstructed from a single plane wave emission as well.

Discussion and Conclusions

Employing our model, the CS approach becomes feasible in pulse-echo ultrasound imaging. It can reduce the required number of emissions significantly and thus lends itself for fast ultrasound imaging. The extension to three-dimensional imaging is simple.

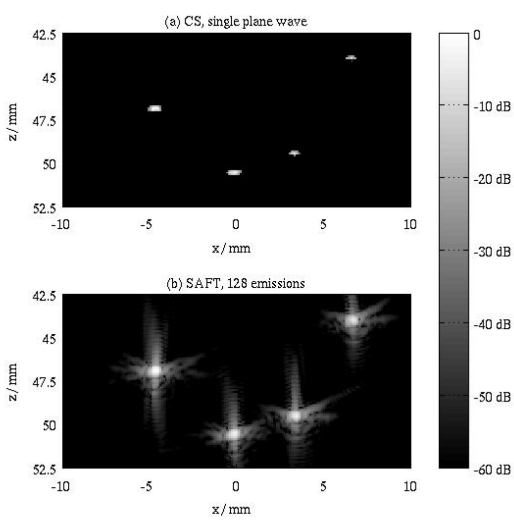

WEDNESDAY POSTER

P2Ad-5

Volumetric Intracardiac Imaging Using a Fully Integrated CMUT Ring Array: Recent Developements

Azadeh Moini[1], Amin Nikoozadeh[1], Omer Oralkan[1], Jung Woo Choe[1], Fatih Sarioglu[1], Douglas N. Stephens[2], Alan de la Rama[3], Peter Chen[3], Aaron Dentinger[4], Douglas Wildes[4], Lowell S. Smith[4], Kai Thomenius[4], Kalyanam Shivkumar[5], Aman Mahajar[5], Matthew O'Donnell[6], David J. Sahn[7], Pierre T. Khuri-Yakub[1]; [1]*Stanford University, USA,* [2]*University of California, Davis, USA,* [3]*St. Jude Medical, USA,* [4]*General Electric Global Research, USA,* [5]*University of California, Los Angeles, USA,* [6]*University of Washington, USA,* [7]*Oregon Health and Science University, USA*

Background, Motivation and Objective

Atrial fibrillation, the most common type of cardiac arrhythmia, now affects more than 2.2 million adults in the US alone. Currently, electrophysiological interventions are performed under fluoroscopy guidance, a procedure that introduces harmful ionizing radiation without providing adequate soft-tissue resolution. Intracardiac echocardiography (ICE) provides real-time, high-resolution anatomical information, reduces fluoroscopy time, and enhances procedural success.

Statement of Contribution/Methods

We have previously developed a forward-looking, volumetric ICE catheter using a ring-shaped, 64-element capacitive micromachined ultrasonic transducer (CMUT) array with a 10MHz center frequency. The ring array was flip-chip bonded to a flexible PCB along with 8 identical custom ICs providing a total of 64 dedicated preamplifiers. The flex was then reshaped for integration with the catheter shaft. 100 micro-coaxial cables were terminated on the flex to provide the connection between the array electronics and the imaging system. We developed several image reconstruction schemes on a PC-based imaging platform from VeraSonics. Beyond real-time, forward-looking imaging capability, the ring catheter provides a continuous central lumen, enabling convenient delivery of other devices such as HIFU transducers, RF ablation catheters, etc.

Several improvements have been made to the first generation ring catheter to improve its performance and reliability and facilitate its use in a clinical setting. We have designed a new flex that requires 72 cables instead of 100, enhancing the catheter's flexibility and steerability. The reduced number of cables also allows us to possibly reduce the catheter shaft size from 12F and/or increase the inner lumen size from about 2.7F. Furthermore, the new flex allows grounding of the top CMUT electrode through proper level-shifting of the IC supplies without additional circuitry. This feature enables complete ground shielding of the catheter, which improves its noise susceptibility and is an important safety measure for its clinical use.

We are fabricating new ring CMUT arrays with a slightly larger gap to improve the transmit pressure capability. We have also designed a new IC that uses charge amplifier instead of transimpedance amplifier architecture to improve the noise performance.

For further clinical convenience, the catheter's required power supplies have been consolidated into one enclosure whose outputs can be monitored from a PC.

Results

We are currently working on the catheter integration and will test the in-vivo imaging performance of the new catheter using porcine animal models in an upcoming animal study.

Discussion and Conclusions

We have implemented several improvements to the first generation ring CMUT ICE catheter to move towards use in a clinical environment.

National Institutes of Health grant NIH/NHLBI R01-HL67647 supported this work.

P2Ad-6

Transmural Myocardial Strain Distribution Measured at High Spatial and Temporal Resolution

Thuy Nguyen[1,2], Andreas Espinoza[3], Espen W. Remme[3], Jan D'hooge[2], Lars Hoff[1]; [1]Falculty of Engineering and Maritime, Vestfold University College, Vestfold, Norway, [2]Lab. on Cardiovascular Imaging & Dynamics, Dept. of Cardiovascular Diseases, Catholic University of Leuven, Leuven, Belgium, [3]Intervention Center, Oslo University Hospital, Rikshospitalet, Oslo, Norway

Background, Motivation and Objective

Cardiac mechanics is complex and remains incompletely understood. Although most studies report increasing strain values from epi- to endocardium, others show the highest values in the mid-myocardium. Recent findings based on FEM simulations of LV mechanics show that the transmural strain gradient may be dependent on regional wall curvature. The aim of this study was therefore to estimate the transmural myocardial strain gradient using a novel ultrasound setup in myocardial segments of different curvature.

Statement of Contribution/Methods

Two custom-build 10MHz single element 3mm-diameter transducers were sutured on the epicardium of the anterior wall of a pig (1 basal-low curvature segment; 1 apical-high curvature segment). Pulse-echo measurements were done for both crystals at a rate of 2.5kHz and sampled at 40MHz. Five recordings were made with simultaneous registration of the ECG and LV blood pressure.

On the reconstructed images, the endocardial border was manually segmented. At end-diastole, the wall was divided into 5 equally sized layers. Tissue velocities were then estimated on the RF signals using a time-delay estimator (SAD; 725µm kernel size; 50% window overlap) after up-sampling the RF by a factor of 10. To avoid outliers in the velocity estimates, the initial estimates were regularized by fitting a snake through the SAD vs. depth data. Next, the position of the individual layers was tracked both forward and backward and a weighted average between both trackings was calculated. Strain rate was then calculated as the spatial gradient of myocardial velocities by linear regression of all velocities within each layer. Finally, strain was obtained by temporally integrating the strain rate profile. At end-systole, 20ms before the maximal rate of LV pressure decay, the mean strain value and its standard deviation were calculated for each layer. The relative strain of each layer was defined by the ratio of its strain value to strain value of endocardial layer.

Results

Radial strain increased from the epi- to endocardium in the apical segment while the highest strain values were observed more towards the mid-myocardium near the base (Figure).

Discussion and Conclusions

Different behavior of the transmural strain distribution was observed for segments of different curvature. These findings are in agreement with FEM results and clarify conflicting data in the literature.

WEDNESDAY POSTER

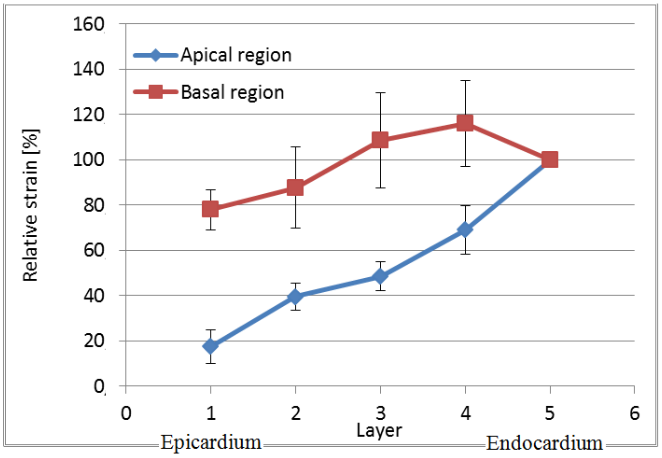

Five layers with their relative strain value at end-systole.

P2Ad-7

Gallbladder Quantification in Ultrasound using GVF Snakes

Ravi Samala[1], Srikrishnan V[1], Michael Washburn[2], **Navneeth Subramanian[1]**; [1]GE Global Research, Bangalore, Karnataka, India, [2]GE Healthcare, Milwaukee, Wisconsin, USA

Background, Motivation and Objective

Ultrasound (US) is typically used as the initial imaging technique for evaluating patients with suspected gallbladder disease. In such an exam, gallbladder wall thickness, fasting volume, ejection fraction and residual volume after ingestion of a test meal are measured to arrive at a diagnosis. Accurate identification of the gallbladder contour is a first requirement towards reporting any of these measures. We propose an active contour based user steered segmentation using region echogenity represented in scale space. The dark blob-like gallbladder is represented in scale space using hessian measure (Frangi's vesselness, FV) which we demonstrate to be a better representative of the gallbladder echogenity. The energy term used in the parametric active contour minimization process is gradient vector flow field (GVF).

Statement of Contribution/Methods

The parameters of the FV is tuned to represent the darker blob-like structures separated by a non-uniform bright edges with missing contours. Since the GVF normalizes the motion field, the magnitude does not play any role in the deformation. Hence, we considered the relative maximum measureness between scales to differentiate the gallbladder from the surrounding structures. Thus the feature image (*f*) is the value of the scale at which the pixel gave the maximum vesselness response ($v(s)_{max}$). In our case, we have considered the measureness between three scales, two to get the relative scale (differentiate gallbladder) and one more to increase the capture range of the structure. This one scale, creates a local minima in the GVF motion field, which helps pull the curve points towards the global maxima.

Results

Quantitative analysis of segmentation accuracy demonstrates a target overlap of 0.93±0.02 and dice coefficient of 0.94±0.01 with the ground truth.

Discussion and Conclusions

We present a semi-automatic method for segmentation of gallbladder on US images. Qualitative results on real-world data show that the proposed approach is capable of segmenting both logitudinal and transverse images of the gall-bladder and found to be comparable with radiologist's delineations.

Figure: (*left*) Initial seed points, (*right*) segmentation in red and ground truth in green.

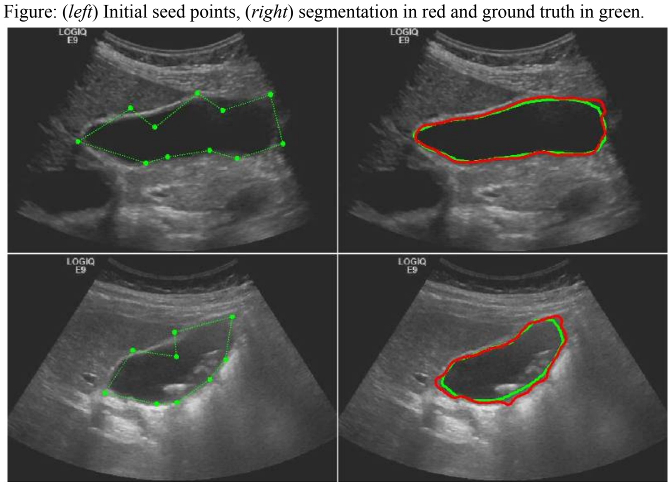

P2Ae - Cardiovascular Elastography

Carribean Ballroom III-V

Wednesday, October 19, 2011, 1:00 pm - 4:30 pm

Chair: **Hiroshi Kanai**
Tohoku University

P2Ae-1

Optical Flow-based B-Mode Elastography: An Application in Hypertensive Rat Models¡¦ Carotid

Roch Listz Maurice[1]; [1]Centre de Recherche, Centre Hospitalier de l'Université de Montréal (CRCHUM), Montreal, Quebec, Canada

Background, Motivation and Objective

Ultrasound elastography is now used worldwide in tissue characterization. The primary premises of elastography are that speckle kinematics reproduces underlying tissue kinematics and that tissue motion can be inferred from speckle tracking. This implicitly assumes that speckle pattern is a material property that can be tracked with respect to time and space. It is then convenient to express the motion of such a material property in terms of total derivative, also known as optical flow (OF) equations.

The present paper introduces a new iterative OF-based elastography (OFBE) method devoted to B-mode data. The first OFBE iteration computes axial and lateral displacement fields. Such displacement fields are used for data rigid registration, prior to the second OFBE iteration which computes the 2D strain tensor.

Statement of Contribution/Methods

The OFBE method was validated in the common carotid artery of rat hypertension models. The effect of aging on carotid stiffness was investigated in female recombinant inbred rats (RI-17, n = 2) in the first experiment. The outcomes of low/high-salt diets were examined in young male Dahl salt-sensitive rats (SS, n = 6; SM12, n = 6; SM9, n = 6) in the second experiment.

Results

Good concordance was observed between left and right carotid axial strain measurements with 11.4% relative error, whereas 4.6% relative error occurred between diastolic and systolic axial strain measurements. Old (80 and 85 weeks) RI-17 carotids were determined to be twice as stiff with 5.70 ¡Ó 0.97% (strain ¡Ó std) as young carotids (30 and 34 weeks) with 13.26 ¡Ó 2.73%, p ƒ¬ 0.001. Carotid axial strain measurement also indicated that salt diets had a significant impact on SS (p = 0.008) and SM12 (p ƒ¬ 0.001) but not on SM9 (p = 0.881) rats.

Discussion and Conclusions

It was demonstrated that Non-Invasive Micro-Vascular Elastography (MicroNIVE) is feasible as a potential tool to phenotype hypertension in rat models (1). It was also determined that OFBE can provide appropriate mechanical markers for investigations with MicroNIVE.

(1) Toufik Zakaria, Zhao Qin, and Roch L. Maurice, Optical Flow-based B-Mode Elastography: Application in Hypertensive Rat Carotid, IEEE Transactions on Medical Imaging, Vol. 29, No. 2, pp. 570-578, February 2010.

P2Ae-2

One-dimensional propagation model of pressure wave in human artery: comparative study of theory and experiment

Masashi Saito[1], Yuki Ikenaga[1], Mami Matsukawa[1], Yoshiaki Watanabe[1], Takaaki Asada[1,2], Pierre-Yves Lagree[3]; [1]*Doshisha University, Japan,* [2]*Murata Manufacturing Co., Ltd., Japan,* [3]*Universite Pierre et Marie Curie, France*

Background, Motivation and Objective

Evaluation of a pulse wave is effective for screening arteriosclerosis. In a previous study, we verified that the waveforms of the pulse waves changed markedly due to the arterial stiffness [M. Saito, Proc. IEEE Ultrason. Symp. (2009) 1934]. However, the pulse wave consists of two components, incident wave and multi-reflected waves. The clarification of complicated propagation phenomenon of the waves is necessary to understand the nature of pulse wave in vivo. In this study, we attempted to build a one-dimensional theoretical model of pressure wave propagating in human artery. To evaluate the validity of the model, we compared the theoretical estimations with measured data obtained from an artificial artery model.

Statement of Contribution/Methods

Experiment: We constructed an artificial human artery model with aorta, femoral, subclavian, radial, and carotid arteries. Soft polyurethane tubes were used for each artery, whose configuration was based on the previous study [Westerhof, J. Biomech. 2 (1969) 121]. The tensile modulus of the tube was about 170 kPa which was similar to the elasticity of aged arteries. A pulsatile flow (ejection time 0.3 s) was input into the human artery model using a controlled pump. Then, the inner pressure wave was measured at the left carotid artery by a pressure sensor. Modelization: We formulated a one-dimensional model derived from the Navier-Stokes equations to characterize the pressure propagation in the tube. The theoretical model includes terms of the nonlinearity, attenuation of the tube wall, and the flow viscosity. Under the same conditions with experiments, the differential equations of the model were computed by MacCormack method.

Results

Figure 1 shows an example of comparison between the measured and simulated pressure waves. The experimentally measured wave was similar to the pulse wave in vivo. The residuals (difference between the two waveforms) became slightly larger in the latter part of the simulated waves. However, the values were less than 10% of maximum amplitude.

Discussion and Conclusions

One possible explanation for the increase of the residuals came from the superposition of complicated multiple reflections from the peripheral points. However, the comparatively small residuals prove the validity of this theory, telling the usefulness for understanding the dynamics of pressure propagation in realistic human artery.

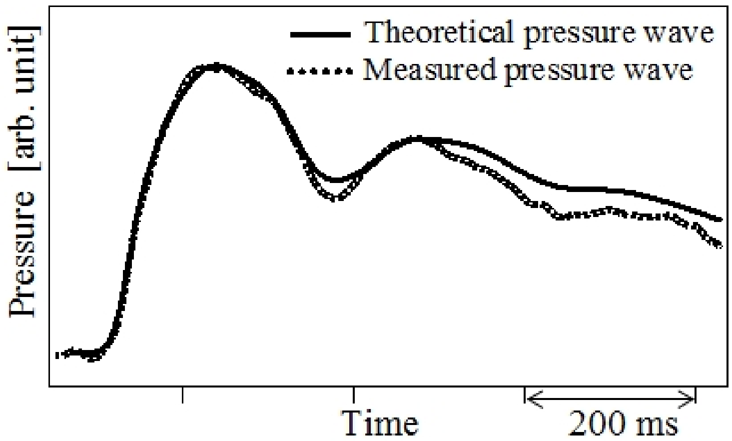

Fig. 1 Result of theoretical and measured pressure waves.

P2Ae-3

3D Tissue Doppler imaging with ultra high frame rate

Birger Brekke[1], Hans Torp[1], Tore Bjåstad[2], Asbjørn Støylen[1], Svein A. Aase[2]; [1]MI Lab and Department of Circulation and Medical Imaging, Norwegian University of Science and Technology, Trondheim, Norway, [2]GE Vingmed Ultrasound, Horten, Norway

Background, Motivation and Objective

Tissue Doppler imaging (TDI) is widely used in echocardiography, and is especially useful for evaluating the function and synchronicity of left ventricle. We suggest a new 3D TDI method based on continuous acquisition and a limited number of transmit beams.

Statement of Contribution/Methods

A GE Vingmed Ultrasound E9 with 4V probe was used for the experiment. ECG trigged acquisition was used to acquire 3D B-mode in one cardiac cycle and 3D TDI in the next. The B-mode data was acquired with a standard setup, while 9 transmit beams and continuous acquisition, i.e. frame rate equals Doppler-PRF, was used for TDI. On receive, IQ data from 16 beams were acquired for each transmit beam. The obtained frame rate was 534 frames per second. Tissue Doppler velocities were obtained by frame to frame autocorrelation in post processing. To generate Figure 1, the left ventricle mesh was calculated, by the GE 4D Auto LVQ tool, based on the B-mode data.

To test our method, the peak velocities of the S-, E-, and A-wave were estimated for 6 positions in the base of the left ventricle. A tri-plan TDI acquisition (A) was first preformed followed by our 3D TDI acquisition (B) and one more tri-plan TDI (C). By using the velocities from acquisition A as reference, we calculated the differences for acquisition B and C. Spatial and temporal smoothing for the 3D TDI were selected to match tri-plane TDI.

Results

The mean difference of A-B over the 6 positions at the S-, E-, and A-wave were correspondingly 0.47 cm/s, 0.87 cm/s, and 0.06 cm/s. The corresponding mean differences of A-C were -0.10 cm/s, 0.72 cm/s, and 0.28 cm/s. The STD of A-B were 0.67 cm/s, 1.36 cm/s, and 0.82 cm/s. And the STD of A-C were 0.75 cm/s, 0.72 cm/s, and 0.92 cm/s. An example anatomic M-mode extracted circumferentially is presented in Figure 1.

Discussion and Conclusions

We have implemented a tissue Doppler imaging modality which cover the entire left ventricle in one heart beat with frame rates at ~500 frames per second depending on depth. In our test case, the peak velocities extracted at the base using this new method are similar to the values extracted using tri-plane TDI. The differences between the new method and tri-plane were comparable to the difference between the two tri-plane acquisitions.

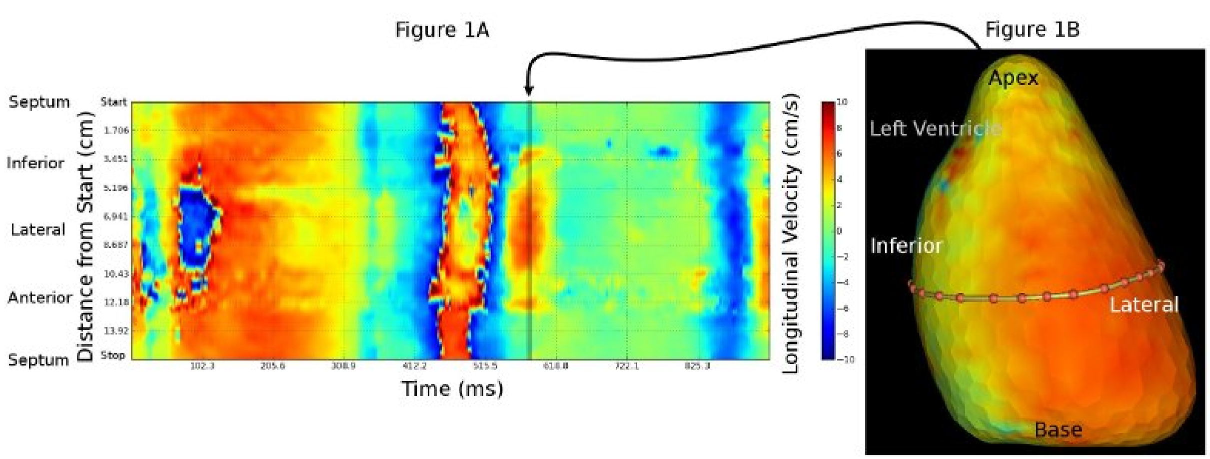

Figure 1: Figure 1A shows the anatomic M-mode corresponding to the curve shown in Figure 1B.

P2Ae-4

3D Ultrafast Elastography Imaging of the Carotid Artery using Sparse Arrays

Sanghamithra Korukonda[1], Marvin Doyley[1]; [1]Department of Electrical and Computer Engineering, University of Rochester, USA

Background, Motivation and Objective

Non-invasive vascular elastography (NIVE) imaging of the carotid artery provides quantitative information on vessel morphology and its mechanical properties. This information is used to detect plaque and characterize its vulnerability to aid cardio-vascular risk assessment. We propose to use sparse arrays to perform 3D ultrafast elastography of the carotid for improved diagnosis and characterization.

Statement of Contribution/Methods

We programmed a SONIX RP system, which was equipped with a linear array, to acquire sparse array data with only 7 active transmit elements and 128 receive elements. To compare with other ultrafast imaging techniques, we acquired plane wave data by transmitting simultaneously with all elements and receiving in parallel with all elements.

We imaged tissue mimicking vessel phantoms at intra-luminal pressures ranging from 4-20mmHg. The transducer was translated along the phantom axis in increments of 2mm for volumetric acquisition. We computed tissue displacements by performing cross-correlation analysis on the reconstructed radio-frequency (RF) images obtained at different pressures. Radial and circumferential strain elastograms were computed directly from gradients of the displacements.

Results

We obtained high quality strain elastograms with both plane wave and sparse array imaging over the range of pressures employed in this study. Fig. 1 shows sample elastograms obtained from a cross-section of a phantom containing a soft plaque (4 o'clock). The plaque, seen as a region of localized high strain, is clearly demarcated in the radial (a) and circumferential (b) strain elastograms obtained with the sparse array. The plaque is also seen in both sets of the plane wave elastograms (c, d), albeit it is less discernable. In the case of the homogeneous elastograms, higher variance was observed in the plane wave elastograms as compared to the sparse array elastograms, particularly in the lateral sectors.

Discussion and Conclusions

Sparse array imaging is a promising elastography technique that can image the carotid artery in real time at ultrafast frame rates. While plane wave imaging has greater speed and higher sonographic SNR, sparse array imaging has greater sensitivity to tissue motion, particularly in the lateral direction. In addition, with the high acquisition speeds, 3D data can be acquired to improve the diagnostic value of this technique.

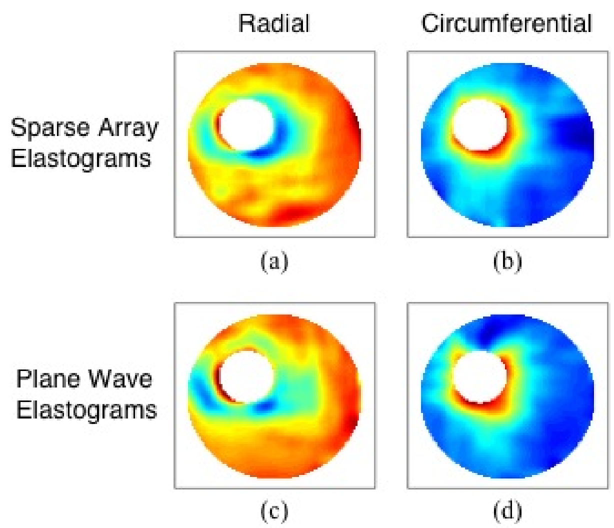

P2Ae-5

Ultrasound-based Speckle Tracking for 3D Strain estimation of the Arterial wall – An experimental validation study in a tissue mimicking phantom

Matilda Larsson[1,2], Florence Kremer[2], Brecht Heyde[2], Lars-Åke Brodin[1], Jan D'hooge[2,3]; [1]Department of Medical Engineering, School of Technology and Health, Royal Institute of Technology, Huddinge, Sweden, [2]Lab on Cardiovascular Imaging & Dynamics, Department of Cardiovascular Diseases, Catholic University of Leuven, Leuven, Belgium, [3]Medical Imaging Lab, Dept. of Circulation and Medical Imaging, Norwegian Institute of Science and Technology, Trondheim, Norway

Background, Motivation and Objective

Arterial stiffness is an important risk factor for cardiovascular disease. As such, ultrasound (US) based methods have been proposed to assess arterial radial strain as a measure of stiffness. We recently proposed a speckle tracking (ST) based approach to further characterize the arterial wall mechanics by estimating the in-plane wall strain tensor. As we previously only tested our algorithm on simulated data sets, the aim of the current study was to validate this algorithm in an experimental setup.

Statement of Contribution/Methods

A solution of 13% polyvinyl alcohol (PVA) and 1% graphite powder was used to construct phantoms mimicking the carotid artery (length: 100mm, inner diameter: 6mm, wall thickness: 3mm). Three phantoms with different mechanical properties were manufactured by varying the number of freeze-thaw cycles (2, 3 and 4 freeze-thaw cycles; 12h freeze+12h thaw). The phantoms were connected to a pulsatile flow pump, programmed to generate a carotid flow profile (peak flows at 7, 14, 21, 28 and 35ml/s). A solution of 40% glycerol and 60% water was used to mimic the blood, whereas 3% agar and 4% graphite powder were used to mimic surrounding tissue. Long and short-axis US images were obtained using a Vivid7 Dimension system (GE Healthcare) with a linear array transducer (12L; frame rate 40Hz). Radial, longitudinal and circumferential strains were estimated throughout three cardiac cycles using the in-house ST algorithm (kernel size: $2.7\lambda\times2\lambda$, normalized cross-correlation; spline-interpolation for subsample motion estimation; 40 % window overlap). Sonomicrometry was used to acquire reference values of radial, longitudinal and circumferential strain in the phantoms.

Results

An example of the estimated and reference strain curves is shown in the figure. Overall, the correlation between the estimated mean peak strain value and the reference strain value for the three phantoms at all flow levels was r = 0.92 (p < 0.001) for radial strain, r = 0.72 (p = 0.006) for longitudinal strain and r = 0.91 (p < 0.001) for circumferential strain.

Discussion and Conclusions

An US-based ST algorithm for strain assessment of the artery wall was validated in an experimental setup. Good agreement was found between the estimated radial, longitudinal and circumferential strain and the acquired reference strain. The application of the proposed algorithm to clinical data is currently ongoing.

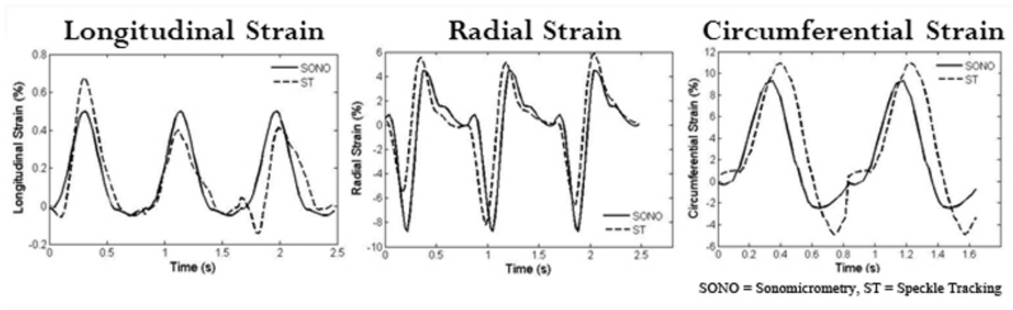

P2Ae-6

In Vitro Experimental System for Ultrasonic Estimation of Myocardial Elasticity

Tomohiko Tanaka[1], Kunio Hashiba[2]; [1]Central Research Laboratory, Hitachi Ltd., Kokubunji, Tokyo, Japan, [2]Central Research Laboratory, Hitachi Ltd., Japan

Background, Motivation and Objective

Myocardial elasticity is a clinically important property closely related to heart event risks, and an effective way to measure it is desired. One potential method for measuring elasticity is cardiac eigenvibration sonoelastometry (CES) (Honda et al., Med. Eng. Phys. 1998, Fig. (a)), but CES may not be accurate enough to diagnose cardiac dysfunction. This is because CES is based on a critical assumption that the left ventricle in diastole is approximated as a spherical shell made of a homogeneous material. Namely, CES does not take into account two key factors: heart-shape complexity and myocardial inhomogeneity, which affect eigenvibrations (EV). To improve the CES, fundamental investigations on the effects of these factors are essential. In this study, an in vitro experimental apparatus was built to examine them, and CES was modified based on the findings of the experiments.

Statement of Contribution/Methods

Fig. (b) shows the apparatus. A heart-shaped silicon shell was created using a mold made from a commercial heart model. An acceleration sensor was attached at the left ventricular wall to measure the cardiac EV generated by a rod. To examine the shape complexity, a heart shell EV was compared with a spherical shell EV reported by Honda et al.. Similarly, to examine myocardial inhomogeneity, the EV of a homogeneous heart shell was compared with that of an inhomogeneous heart shell made of multiple types of silicon.

Results

Preliminary experiments on shape complexity were conducted. Fig. (c) plots typical results of eigenfrequencies (EFs) of two heart shells with the same shape but different elasticities. The harder shell had a higher EF. However, once the EFs are normalized, they are considered to be the same if the shapes are similar. Thus, a normalized EF (NEF) is an essential coefficient in CES. In this experiment, the NEFs for both cases were about the same, but they were two times smaller than that of the spherical shell since complex heart-shape structures lower the EF. This would degrade the CES accuracy.

Discussion and Conclusions

In summary, an experimental system for CES has been built to understand and improve CES. By examining how the shape affected the EFs, we found that the NEF for the heart shell was smaller than that of conventional CES. The NEF correction can improve the CES accuracy. Further results on the complexities and inhomogeneity, and modified CES will be shown in the presentation.

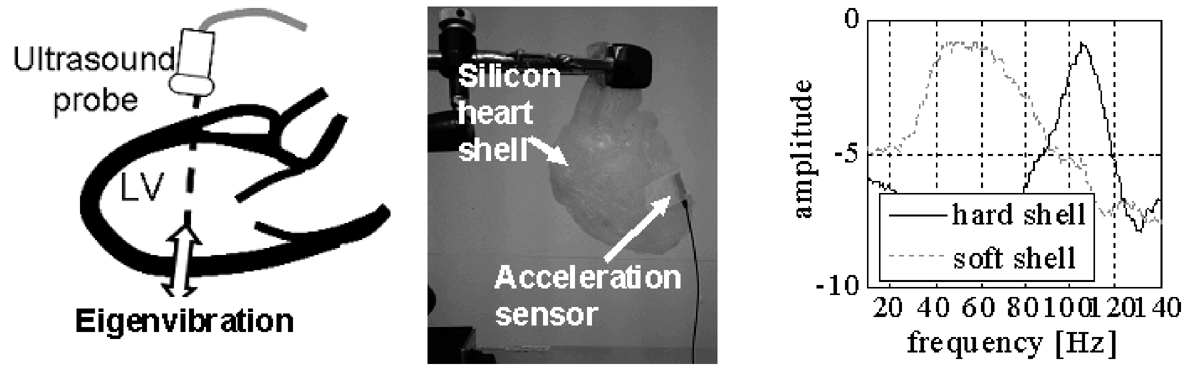

(a) Schematic of shell EF measurements using ultrasound (cited from Tanaka et al. *Proc. IEEE IUS* 2010)

(b) Experimental setup to measure an eigenfrequency of a silicon heart-shape shell

(c) Examples of EFs of two homogeneous heart-shape shells with the same shape, but different elasticities.

Fig. Schematic of in vitro experiments

P2Ae-7

Minimal-path contours combined with speckle tracking to estimate 2D displacements of the carotid artery wall in B-mode imaging

Guillaume ZAHND[1], Maciej ORKISZ[1], André SERUSCLAT[2], Didier VRAY[1]; [1]Université de Lyon, CREATIS; CNRS UMR 5220; Inserm U1044; INSA-Lyon, France, [2]Louis Pradel Hospital, Radiology Department, Lyon, France

Background, Motivation and Objective

Quantifying the dynamic parameters of the carotid artery wall from ultrasound B-mode images can contribute to detect the cardiovascular risk at early stage. Estimating the 2D (radial and longitudinal) movement of the arterial wall with a high accuracy is therefore an important issue. The user-independent method presented here combines contour and speckle tracking (CST). The accuracy of our method is evaluated on in vivo clinical data.

Statement of Contribution/Methods

Our method extracts 2 interfaces of the intima-media layer in both proximal and distal parts of the arterial wall. A priori knowledge of the typical intima-media thickness is used to build a region of interest where the interfaces of interest are transformed to almost horizontal lines.

A cost function is generated by a novel matched filter that also exploits this prior as a shape constraint. Then a dynamic programming algorithm estimates the optimal position of a single skeleton that defines both interfaces. The radial motion of a wall is described by the displacement of its skeleton.

A series of blocks is then automatically positioned along the detected interfaces, and a global operation of 1D longitudinal speckle tracking is performed. The quality of the correlation function of each block is evaluated by a novel outlier removal algorithm, based on the weighting of 3 feature terms that evaluate the intensity, optimal position and distribution. The resulting subset of blocks having the best score is used to determine the longitudinal motion of the wall.

Results

The CST evaluation was done on 10 in vivo clinical sequences, where reference 2D trajectories were established by averaging 9 manual trackings from 3 medical experts (Figure). The errors w.r.t. this reference were calculated for CST, as well as for the conventional block matching (BM) and for each individual manual tracking (MT). The mean longitudinal and radial estimation errors, in µm with a pixel size of 30×30 µm², were 90±55 and 45±30 for MT, 105±65 and 35±20 for BM, and 60±50 and 30±15 for CST.

Discussion and Conclusions

The agreement of the proposed method with the reference is better than for the standard BM as well as for individual observers, especially in the longitudinal dimension, which remains the most challenging and relevant parameter. We conclude that our method robustly and accurately estimates the 2D motion of the arterial wall, and thus can improve the diagnosis.

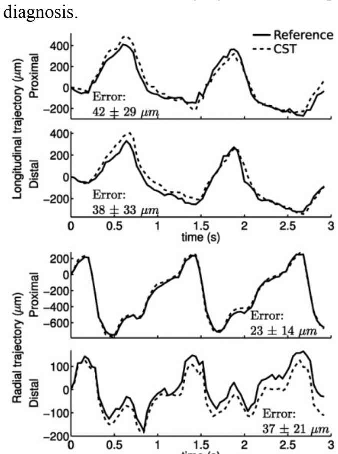

P2Ae-8

Affine phase based motion estimation applied to echocardiography

Florian Douziech[1,2], Hervé Liebgott[1], **Adrian Basarab[2]**; [1]CREATIS CNRS UMR 5220 – INSERM U1044, Université de Lyon, France, [2]IRIT UMR CNRS 5505, Université de Toulouse, France

Background, Motivation and Objective

Motion estimation is an important field of research in echocardiography. Inspired by the techniques introduced for flow estimation and for US elastography, we have recently shown that transverse oscillations (TO) may improve the accuracy of the estimated heart motion [Liebgott et al., IEEE US 09]. We have shown that the TO allowed the development of 2D analytic local rigid translation estimators. They are based on the spatial phases of single-orthant (SO) analytical signals and are more rapid and more accurate than classical cost functions [Basarab et al., IEEE UFFC 09]. However, several studies [Suhling et al., IEEE IP 05] showed the need for more complex local models, such as the affine transformation. In this study, we show how the phases of two 2D SO analytical signals can be exploited to estimate the 6 parameters of the affine model.

Statement of Contribution/Methods

The purpose of our paper is double. First, we show analytically how an affine motion model between two images with TO leads to an affine phase model (for both phases of the two considered SO analytical signals) depending on the six affine parameters. Second, we show that by adding or subtracting the two spatial phases, we obtain two linear models depending on the axial (respectively lateral) affine parameters. This result is very interesting, as it allows the separate estimation of the 6 parameters by two classical least square methods.

Results

A simulation result is given on the figure below: (a) true local affine displacement superimposed to the simulated RF image with TO (SNR=10dB), (b) estimated displacement using our method superimposed to one of the two spatial phases, (c) lateral affine parameter estimation (mean and std, 512 estimations for each level of SNR) in presence of noise. The true values were 0.2, 0.09 and 0.08. Equivalent results were found in the axial direction. Such an estimation is impossible using a phase based method based on rigid translations.

Discussion and Conclusions

This paper presents an affine phase based motion estimation adapted to RF images with TO. Its main advantages are:

- unlike other phase based methods, a local model more complex than rigid translations is considered,
- using the spatial phases of SO analytical signals, we overcome one of the major limitations in US: the non-conservation of pixel intensity along an image sequence,
- 2 phase images are used instead of one single intensity image.

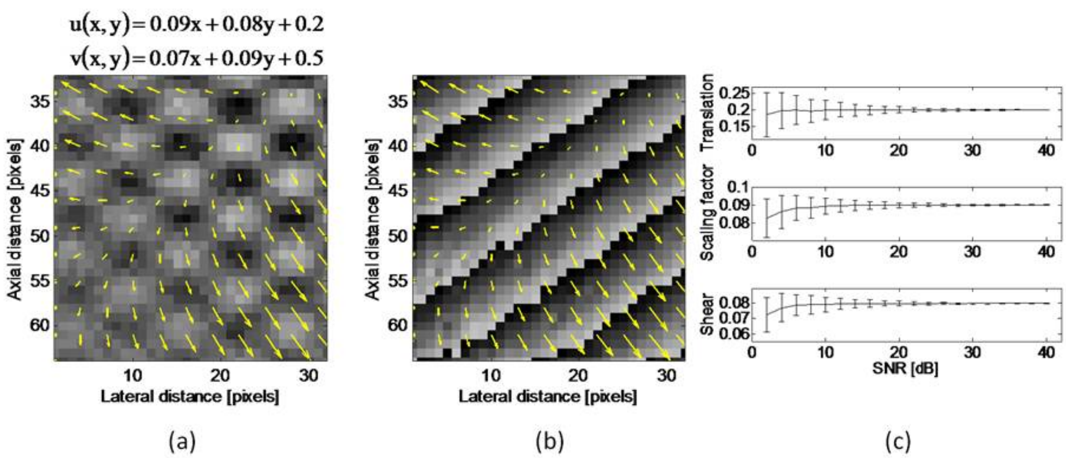

P2Ae-9

3D cardiac strain imaging using plane wave excitation and feature tracking

Lin-Yi Tseng[1], Lung-Chun Lin[1], Pai-Chi Li[1]; [1]*Natoinal Taiwan University, Taiwan*

Background, Motivation and Objective

Evaluation of myocardial motion is important in diagnosis of heart diseases. In particular, myocardial strain imaging is desired when assessing myocardial functions. The purpose of this study is to achieve accurate evaluation of cardiac deformation with ultrasound in real-time 3D imaging using plane-wave excitation and feature tracking. Plane wave excitation can significantly increase the image frame rate, and feature tracking can speed up computations compared to conventional speckle tracking.

Statement of Contribution/Methods

Field II simulations are performed to numerically evaluate performance of the proposed method with a ball-like object mimicking a left ventricle. Clinical data from a 3 months old baby's 3D echocardiography in the parasternal short axis view using a Philips iE33 machine with a 1.9MHz matrix transducer is also used. Feature tracking refers to tracking of selected features only, instead of all image pixels, thus allowing much efficient computations. Both speckle tracking and feature tracking are performed on polar coordinate. Because most of the heart tissue motion is rotational and torsional. Therefore, polar coordinate is more suitable than Cartesian coordinate.

Results

On a personal computer platform, the computation time for specking tracking is 107.5 minutes and it is only 8.96 minutes for feature tracking. In other words, feature tracking is more efficient than speckle tracking by 11 folds. In terms of the tracking accuracy, the average tracking error for speckle tracking is less than 0.05%, and the average tracking error for feature tracking is 0.52%. On the clinical data, the feature tracking is 3.7 times faster than speckle tracking. This is because in clinical data, the number of features increases as generally the correlation coefficient is higher.

Discussion and Conclusions

Feature tracking is more effective for real-time 3D strain imaging with acceptable tracking accuracy on both simulations and real clinical data. There is also a tradeoff between the number of features and its adequacy in representing the entire image.

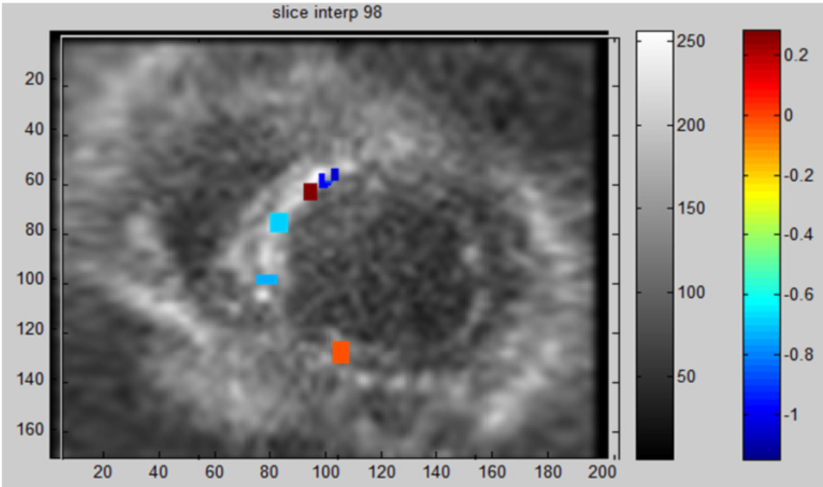

Figure: Strain image of a 3 months old baby's 3D echocardiography acquired by a 1.9MHz matrix transducer (Philips iE33) in the parasternal short axis view The pseudo colors represents tracking results.

WEDNESDAY POSTER

P2B Acoustic Imaging

Carribean Ballroom III-V

Wednesday, October 19, 2011, 1:00 pm - 4:30 pm

Chair: **Ramazan Demirli**
Villanova University, USA

P2B-1

Study on non contact acoustic imaging method for non destructive inspection using SLDV and LRAD

Tsuneyoshi Sugimoto[1], Ryo Akamatsu[1], Noriyuki Utagawa[2], Shuichi Tsujino[2]; [1]Electronics and Information Engineering, Toin University of Yokohama, Yokohama, Japan, [2]Sato kogyo Co. Ltd., Tokyo, Japan

Background, Motivation and Objective

Hammer method is widely used for the examination of the concrete surface such as the tunnel or the bridge girder. However, it is not effective at the place where it is hard to reach. Therefore, we propose a new non-contact acoustic imaging method for destructive inspection using scanning laser Doppler vibrometer (SLDV) and long range acoustic device (LRAD). In this method, Surface vibration, which is generated by air borne sound, is measured using SLDV. This time, the styrofoam board (30x30x10 cm) was buried at 5cm depth in the concrete are used as a substitute of a cavity in the concrete.

Statement of Contribution/Methods

The SLDV (Polytec PSV400-H4) measures the vibration of concrete surface excited by sound wave caused from vibratory source. The vertical direction vibration of the concrete surface is measured by SLDV. LRAD, that have high acoustic pressure and a sharp directivity, is used for a vibration source. Scan area size is about 50 x 40 cm and number of scan points are 15 x 13. A linear chirp wave is used as a emitted sound from LRAD. Start and stop frequencies are 2100 and 2500 Hz, respectively. Duration time is 0.5s. Trigger interval is 2.0s. The sound pressure near the surface of the concrete is about 110dB. Distance with LRAD and the concrete is about 60 cm.

Results

As an experimental result, a styrofoam board is clearly imaged by the vibration velocity of the concrete surface. And also, we confirmed the response range of the frequency of a buried object. Clearer image is formed by the optimum frequency response range (OFR) method.

Discussion and Conclusions

We confirmed the effectiveness of our proposed method. OFR method is also effective for the cavity detection in the concrete. As a future task, we will examine that how long distance can be applied and how much depth can be inspected the cavity in the concrete by this method.

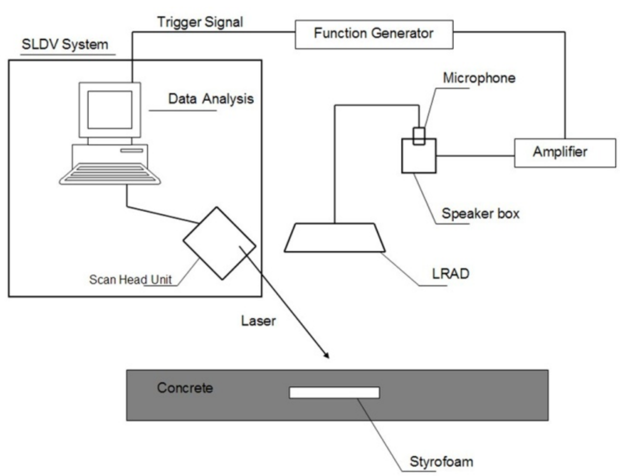

Experimental setup.

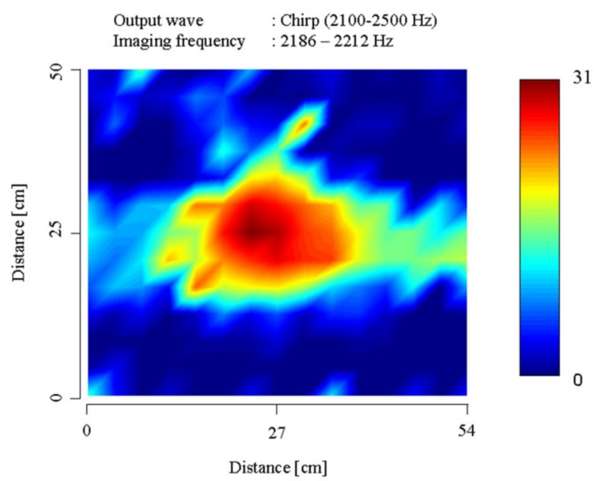

An example of OFR image.
A styrofoam board(30x30cm) is burid in the concrete (depth 5cm).

P2B-2

Basic Study of Water Distribution Measurement in Soil Using SLDV

Tsuneyoshi Sugimoto[1], **Yutaka Nakagawa**[1], Takashi Shirakawa[1], Motoaki Sano[1], Motoyoshi Ohaba[2], Sakae Shibusawa[2]; [1]Electronics and Information Engineering, Toin University of Yokohama, Yokohama, Japan, [2]Faculty of Agriculture, Tokyo University of Agriculture and Technology, Tokyo, Japan

Background, Motivation and Objective

We propose a method of monitoring and imaging of the water content in the rooting zone using a sound vibration and the Scanning Laser Doppler Vibrometer (SLDV). This time, we established the sand which was wetted and difference water content to the sand tank. After that, we study about the influence to the propagation velocity when changing the water-content of the water distribution.

Statement of Contribution/Methods

In this experiment, the water distribution is measured by the change of the propagation velocity. This time, the water-content of the water distribution is 150 ml and 250 ml. Experiment method is shown as follows. Sound vibration is generated by the giant magnetostrictive vibrator that installed in the hole of the sand tank base, it has nine holes which was covered with the rubber for a sound source. SLDV measures the vibration of ground surface excited by sound wave caused from vibratory source. The output waveform uses the burst wave of 2 kHz of sine wave, 300 mVpp, 3 cycles

Results

We can confirm that the speed of sound value becomes fast in the place which is near the position of the water distribution. That is, we can see that the vibration velocity distribution image is reacting very sensitively to the water distribution condition of ground surface. Also, we can confirm that there is a difference in the propagation velocity at 150ml and 250ml

Discussion and Conclusions

This time, we can confirm that the used vibration velocity distribution image was a very effective image method to the water distribution which is in the shallow position near the ground surface. Also, we can see that the difference of the vibration velocity distribution reflected the difference of the water distribution. And, we intend to examine whether our method can apply even in the case that a plant is growing up in soil for gardening.

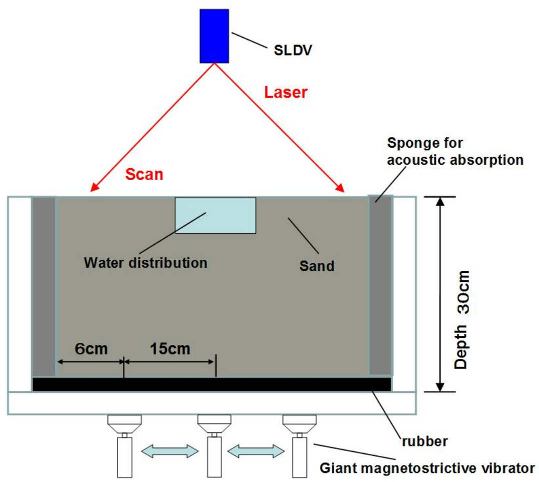

Experimental Setup

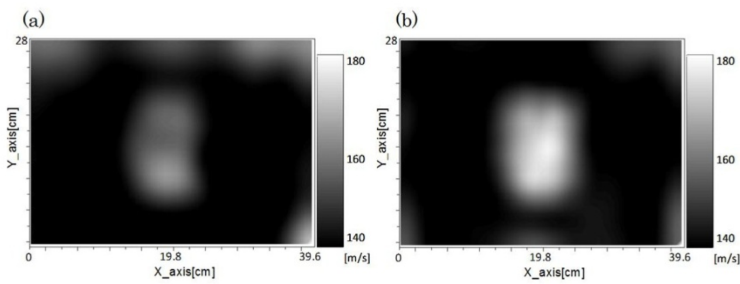

An example of the imaging of propagation velocity
(a) The water-content:150ml (b) The water-content:250ml

P2B-3

Study on the buried object detection method using optimum frequency range method in extremely shallow underground

Tsuneyoshi Sugimoto[1], Touma Abe[2]; [1]Electronics and Information Engineering, Toin Univ. of Yokohama, Yokohama, Japan, [2]IHI Inspection & Instrumentation Co.,Ltd., Tokyo, Japan

Background, Motivation and Objective

Sound wave vibration and a scanning laser Doppler vibrometer (SLDV) are used for a method of exploring and imaging an extremely shallow underground. The target is mainly a plastic antipersonnel land mines at first, but other buried objects are now included. Because our proposed method has potential use for archeological remains. The exploration depth depends on the sound pressure, and it is usually less than about 10 cm. In our previous study, we confirmed that a buried object showed a response range of specific frequency. In this study, the optimum frequency response range method (OFR method) is proposed for detecting the buried object and forming the clearest image.

Statement of Contribution/Methods

The SLDV (Polytec PSV400-H4) measures the vibration velocity of the ground surface excited by a sound wave generated by a vibratory source. In this study, two flat speakers with high directivity are used for a vibration source. The sand tank (110 × 135 × 50 cm3) in our laboratory, which had been filled with sand of uniform particle size (200-300 μm), is used for this experiment. To determine the frequency response range, white noise is used. Plastic containers and stone are buried at 2cm depth.

Results

On the basis of the results for the frequency response range of the buried objects, burst waves are used for buried objects. From the experimental results, we can confirm that the buried object can be detected by the OFR method and, compared with before applying the OFR method, we can see that the effect of the noise is decreased by the OFR method.

Discussion and Conclusions

We confirmed the effectiveness of our proposed method. In particular, a clear image of the buried object was obtained when the SLDV image was unclear. As a future task, we will examine the effectiveness of our method for other materials.

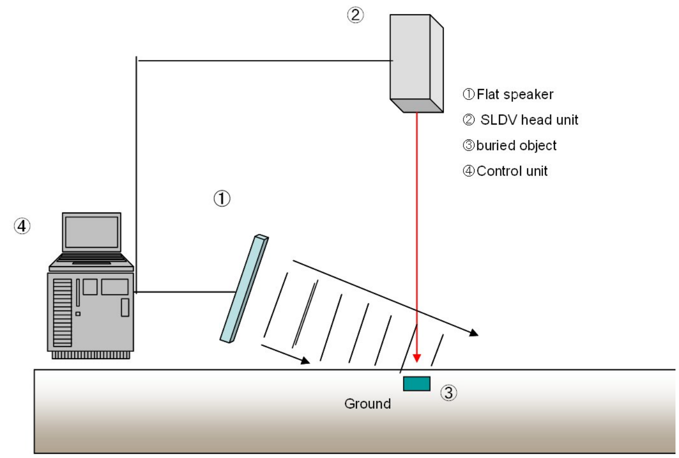

Extreme shallow underground imaging system using flat speaker

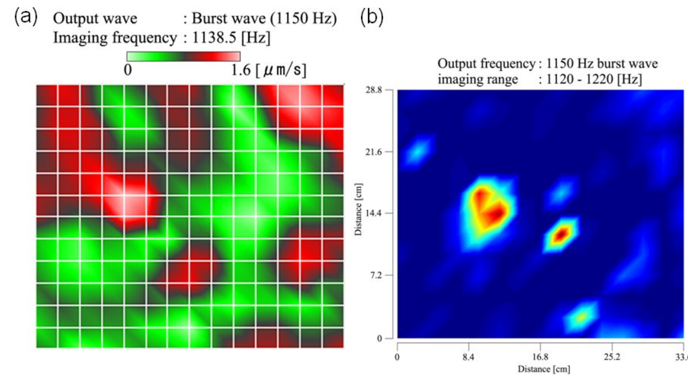

A stone(5.5 × 6.5 × 2.7 cm3, 210g) is buried at 2cm depth.
(a) Imaging result of SLDV, imaging frequency : 1138.5 Hz
(b) Imaging result by OFR method : 1120 - 1220 Hz

P2B-4

3D Direction of Arrival Estimation and Localization Using Ultrasonic Sensors in an Anechoic Chamber

Vitaliy Kunin[1], Weidi Jia[1], Jafar Saniie[1], **Erdal Oruklu[1]**; [1]ECE Department, Illinois Institute of Technology, Chicago, IL, USA

Background, Motivation and Objective

There is currently a significant amount of research on sound and ultrasound based detection applications such as robotic vision, navigation and automation, collision detection, acoustic human-machine interfaces, medical diagnostics, structural failure analysis, or mechanical failure analysis of vehicles. However, there are important challenges to be addressed for practical implementations in real world environments. These include ambient sound and electrical noise, presence of wideband non-stationary source signals, presence of reverberation echoes, and high frequency sources which require higher speed systems. Therefore, this work emphasizes the design and development of ultrasound localization systems. Real world application issues described above are addressed; this includes a presentation of how an anechoic chamber and ultrasonic sensor arrays are used to create a controlled experimental setup in which noise, reverberation echoes, source distance and angles, number and geometry of sensors could be varied.

Statement of Contribution/Methods

Both localization and direction of arrival estimation (DOAE) can be divided into three general steps: collecting data across multiple receivers and/or transmitters, finding the phase difference and/or time difference of arrival, and calculating the direction and distance to the sound source. 2D localization can be performed with 3 receivers using only the time difference of arrival information and 3D localization can be decomposed into two problems of 2D localizations. Geometrically this is the same as finding two circles, the intersection of which is the location of the sound source. For data acquisition, we use an FPGA based MEMS microphone array which is capable of using up to 52 transducers simultaneously. Furthermore, in order to create a controlled environment for acoustic experimentation, a 52”x52”x27” anechoic chamber was designed and built which can isolate the experiment inside the chamber from outside noise and can absorb sound inside the chamber to prevent reverberations.

Results

Both 2D and 3D ultrasound source localization experiments were conducted. Localization technique was based on the delays corresponding to the receiver to the transmitter distances and based on the time difference of arrival between the receivers. The 2D experiments consisted of three 40 kHz ultrasound transducers which acted as receivers and one 40kHz ultrasound transmitter. 3D experiments consisted of six 40 kHz ultrasound transducers, five of which acted as receivers and one of which acted as a transmitter. Both sets of experiments produced accurate ultrasound localization results and collected values were within a 3% of each other.

Discussion and Conclusions

DOAE and source localization experiments with different geometries and with different numbers of sensors have been investigated. Discussion of parameters that influence the sensitivity and accuracy of the results of these experiments are presented.

P2B-5

Air-coupled thickness measurements of steel plates

Grunde Waag[1,2], Petter Norli[2], Lars Hoff[1]; [1]Vestfold University College, Borre, Norway, [2]Det Norske Veritas, Høvik, Norway

Background, Motivation and Objective

Air-coupled ultrasound is attractive in non-destructive testing as it does not require a coupling medium. This enables quick, non-contact measurements at a distance. It has been successfully applied for inspection of several materials, such as aluminium, epoxy, food and textiles.

A broadband acoustic pulse transmitted into a plate will show resonance peaks when the plate thickness is an integer number of half-wavelengths. This is a well-known principle in sound propagation in layered media.

Det Norske Veritas have employed this principle for inspection of steel pipes, using water or high pressure natural gas as coupling medium.

The goal of this paper is to apply this principle to measure the thickness of steel plates with air as coupling medium. The transmission loss from air to steel is extremely high, giving challenges in getting sufficient energy into the steel, and causing strong reverberations.

Statement of Contribution/Methods

The method presented in this paper uses through transmission, where two transducers are mounted on each side of a stainless steel plate. A broad band pulse is transmitted from one side, goes through the plate, and is recorded at the opposite side.

A time window is applied to the recorded signal to gate out the tail coming from multiple reflections inside the steel plate. The spectrum of the windowed pulse is estimated using the periodogram, and it will have peaks at the half-wavelength resonance frequencies of the steel plate. When the speed of sound in the plate is known, the distances between these resonance peaks are used to calculate the thickness.

Results

The method was tested in laboratory experiments on a 10.0 mm thick steel plate. Two sections of the plate had the thickness machined down, one to 9.9 the other to 9.8 mm. A 540 kHz, 12 mm diameter transducer was used as transmitter and a 540 kHz, 6 mm diameter transducer was used as receiver. The transmitted pulse was a 0.1 ms long linear chirp from 250 to 500 kHz. Pulses were transmitted through the regions with different thicknesses.

Resonance peaks in the spectra were observed at 267 and 572 kHz, for 10.0 mm plate thickness, 273 and 584 kHz (9.9 mm), 276 and 592 kHz (9.8 mm). Assuming a speed of sound of 6100 m/s, the measured frequency peaks corresponds to plate thicknesses of 10.0, 9.8 and 9.6 mm.

Peaks found at 465, 475 and 480 kHz correspond to three half-wavelengths of the shear wave in the plate. If confirmed, this can be used to further improve the thickness estimate.

Discussion and Conclusions

We have demonstrated a method to measure the thickness of steel plates in air, using non-contact ultrasound with air as coupling medium.

The relative accuracy of the method could clearly distinguish between steel plates differing 2% in thickness, but selecting the time window is essential to get reliable estimates.

The absolute accuracy of the thickness measurements depends on the uncertainty of the speed of sound in the plate.

P2B-6

A Novel Numerical Simulation of Sound Wave Propagation Using Sub-grid CIP-MOC method

Yuta Ara[1], Kan Okubo[1], Norio Tagawa[1], Takao Tsuchiya[2], Takashi Ishizuka[3]; [1]Tokyo Metropolitan University, Japan, [2]Doshisha University, Japan, [3]Shimizu Corporation, Japan

Background, Motivation and Objective

Numerical analysis for sound wave propagation in time domain has been investigated widely as a result of advances in computer technology. In our past study, we have applied the constrained interpolation profile method with method of characteristic (CIP-MOC) to numerical analyses of sound wave propagation. The CIP-MOC method is a novel low-dispersive numerical scheme.

Statement of Contribution/Methods

In this study, we propose a sub-grid technique for CIP-MOC simulation of sound wave propagation. This technique has an advantage of using a small amount of memory. Thus, we can use suitable multi size grids in an analysis domain according to a calculation model.

Results

We show the numerical results obtained using the sub-grid technique in the CIP-MOC analysis. Figure 1 shows the sound pressure distributions obtained by CIP-MOC analysis with sub-grids. Here, the meshed area is the sub-grid region. This figure confirmed that the boundary in the sub-grids has good permeability characteristics with an extremely low reflection.

Table 1 shows the comparison of calculation time, where the calculation is divided into 500 time steps. The sub-grid model has a much shorter calculation time than the fine grid model.

Discussion and Conclusions

In this study, we examined a sub-grid technique for the CIP-MOC simulation of sound wave propagation. Examination results reveal the following: Correct treatment of the boundary between course grids and sub grids causes no reflection. Use of the suitable multi-size grid reduces the calculation time.

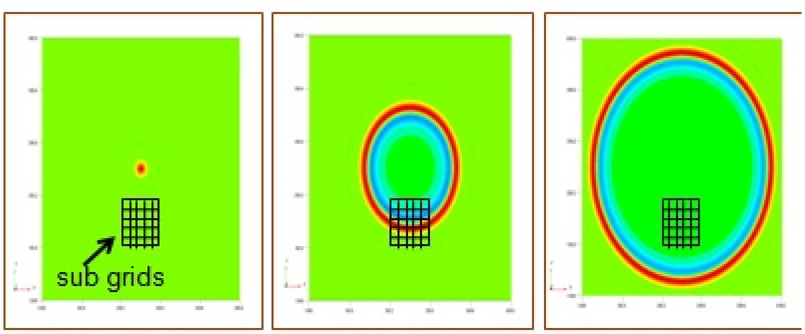

(a) $t = 10\Delta t$ (b) $t = 500\Delta t$ (c) $t = 1000\Delta t$

Model	Grid model	Calculation time [s]
A	Course grid(800 × 800)	37.296
B	Fine grid(2400 × 2400)	323.844
C	Course grid (800 × 800)and sub grid(50 × 50)	38.224
D	Course grid (800 × 800) and sub grid(100 × 100)	41.213
E	Course grid (800 × 800) and sub grid(150 × 150)	48.425

fine grid : (0.02 m)^2, sub-grid: (0.02 m)^2, course grid : (0.06 m)^2

P2B-7

Determination of size and shape of small inclusions from sound-field information

Norbert Gust[1], Elfgard Kuehnicke[1], Mario Wolf[1], Sebastian Kümmritz[1]; [1]*TU Dresden, Germany*

Background, Motivation and Objective

The resolution of scanning ultrasonic systems is limited to the used wavelength and the focus size. Objects smaller than wavelength are always displayed as a convolution of the object with the sound field at this point. Common methods for determination of sizes smaller than wavelength require knowledge of the object geometry and use only amplitude information.

Statement of Contribution/Methods

We present a new approach for obtaining more information from ultrasonic measurements by evaluating sound-field characteristics, such as the shape of the reflected wavefront and amplitude distribution on a spherical focussed array transducer. The sound field information is obtained in dependence of the location of the scanning transducer and the excitation scheme.

For our first studies we use a 10 MHz, 4-element cake-like focussed transducer (Fig. 1). Each element is separately excited and the waveform data is recorded on all 4 elements. The obtained data is evaluated and compared to calibration curves or simulations to determine size and shape of the object(s).

Results

Fig. 2 illustrates the measurement principle on spherical reflectors. The different time t and amplitude a measurement modes (Fig. 1 & 2) are used to identify the shape of the reflector (eg. $a_{11} \ll a_{13}$ for disk, $a_{11} \approx a_{13}$ for ball).

As an example for size determination smaller than wavelength, Fig. 3 shows measured arrival times normalized on the transducer displacement from the center of a 80 µm and a 200 µm ball. The images show that this time-slope is almost independent of the transducer displacement - but dependent on the ball size. Therefore the average time slope of those measurements can be used as size indicator for balls. In Fig. 4 the time-slope is diplayed in dependence of the ball diameters and shows a clear correlation.

Discussion and Conclusions

The example shows that the new method allows extraction of much more information on small objects than with common methods. It is possible to determine the size and the shape of objects smaller than wavelength. The method can also be used for large objects, where the results are very close to simple geometric calculations. For small objects a comparison to calibration curves or ultrasonic simulations can be used to determine size and shape.

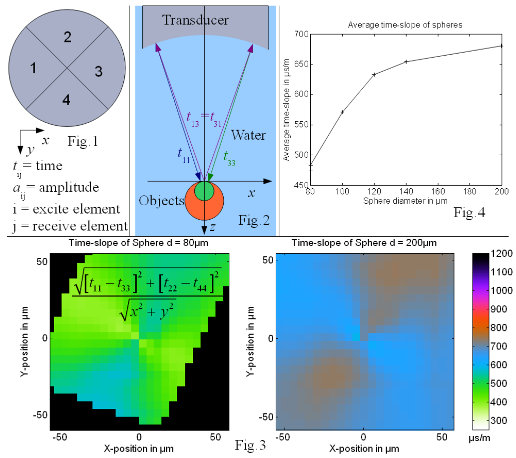

P2B-8

Detection of second harmonic components of Lamb waves passed through fatigue tested magnesium plate

Makoto Fukuda[1], Kazuhiko Imano[1], Hideki Yamagishi[2], Katsuhiro Sasaki[2]; [1]*Akita University, Japan,* [2]*Toyama Industrial Technology Center, Japan*

Background, Motivation and Objective

Magnesium has recently been used for notebook personal computers or parts of cars as weight-saving material. Recently, mechanical behavior of magnesium has been researched, since deformations and cracks result in important accidents. In this paper, Lamb waves are transmitted into pure magnesium plate which is carried out fatigue test and the second harmonic components generated from the plates are detected. Increase of second harmonic components and its possible use for mechanical properties of magnesium are discussed.

Statement of Contribution/Methods

Cracks included dislocations and closed cracks in the magnesium plates were created by the fatigue test. No.1 is before the fatigue test. Number of cycles of No. 2 and No. 3 were carried out the fatigue test by 100 thousand and 200 thousand times, respectively, which were controlled as a stress amplitude σ_a of 56.7 MPa was sinusoidally applied to the magnesium plate, the stress ratio R was 0 and the frequency was 30 Hz by a hydraulic servo fatigue tester at room temperature.

In this study, the each transducer was set 50 mm away from the center of the magnesium plate; i.e. the propagation distance of Lamb waves was 100 mm.

Results

Second harmonic components in No. 2 and 3 plates were increased by 3 dB and 6 dB compared with in No. 1 plate, respectively. Second harmonic components were increased as fatigue test cycles were increased.

Discussion and Conclusions

To determine the Lamb wave mode of the received waveform a wavelet transformation was carried out and was compared with dispersion curves of group velocity. S0 mode Lamb waves were mainly in No. 1, while A1 mode Lamb waves were generated in No. 3. Resulted distribution did not accord dispersion curve of A1 mode Lamb waves, since second harmonic components sources (dislocations and closed cracks) exist halfway through Lamb wave propagation. Thus, it was confirmed that second harmonic components which was generated from magnesium plates were increased by fatigue test.

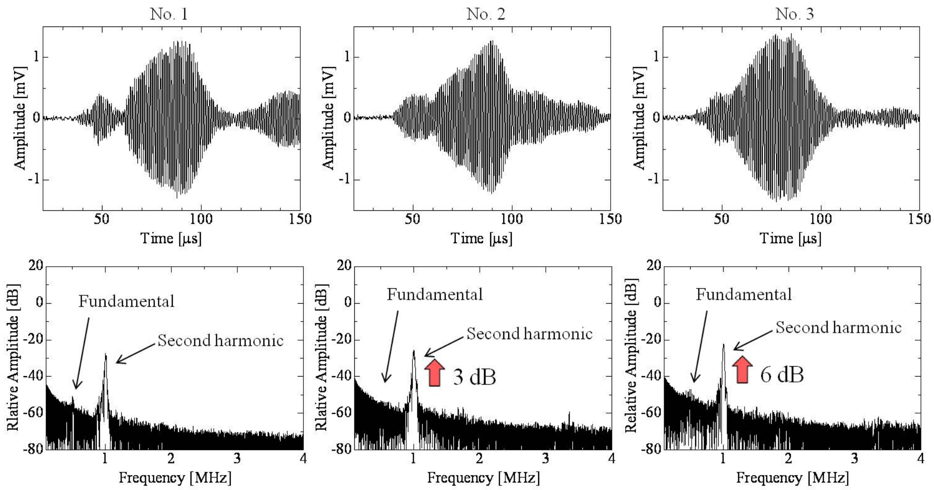

Fig.1 Received waveforms and their spectra after pulse inversion method.

WEDNESDAY POSTER

P2Ca - Optical and Electromagnetic Interations II

Carribean Ballroom III-V

Wednesday, October 19, 2011, 1:00 pm - 4:30 pm

Chair: **Kimmo Kokkonen**
Aalto University, Finland

P2Ca-1

Ultrasonic NDE in a Reactor Core

Bernhard Tittmann[1,2], David Paks[1]; [1]Engineering Science and Mechanics, Penn State University, University Park, Pennsylvania, USA, [2]IEEE-UFFC AdCom, USA

Background, Motivation and Objective

Analyzing radiation effects on materials is desirable for the development of new radiation resistant alloys for components within reactor containment walls and cores. Currently the NRC/DOE Workshop on Plant Life Extension R&D calls for improvements in current NDE methodologies so as to facilitate licensing extensions for exiting plants. In addition, the current lack of a long term waste storage site has necessitated aging analysis of current storage facilities and research into potential improvement to current facilities and protocols. All these applications will be greatly facilitated by the availability of real-time in-situ data obtained via ultrasonic NDE.

Statement of Contribution/Methods

A single crystal of aluminum nitride AlN element was coupled to an aluminum cylinder via mechanical pressure. Aluminum foil was used to eliminate micro-voids between the cylinder and the AlN element, allowing for strong, clear A-scan data to be obtained. The AlN element was loaded on the side opposite the cylinder with a sintered Carbon composite to reduce ringing and improve signal clarity. We present the peak-to-peak amplitude throughout the irradiation as well as the measured gamma heating effects obtained from the time of flight during a typical radiation cycle. The data agree well with the theoretical and cooling curves based on Newton's law of cooling with and withought a constant heat source, respectively. Also presented is a graph of the second harmonic amlitude divided by the first harmonic amplitude squared, which is related to the non-linear parameter.

Results

We have investigated the radiation hardness of piezoelectric AlN. The pulse-echo response of the AlN crystal operating as an ultrasonic transducer was monitored throughout the course of irradiation. In this experiment we obtained a fast neutron fluence of 1.85x10^18 n/cm^2 a thermal neutron fluence of 5.8x10^18 n/cm^2 and gamma dose of 26.8 MGy. We have found that the pulse echo amplitude shows a slight increase over the course of irradiation. Additionally, the Q value of the echo increased linearly with fluence. Transient effects were found to be significant and are thoroughly investigated. The AlN was also utilized to measure gamma heating and second harmonic generation throughout the course of irradiation.

Discussion and Conclusions

In summary, we present data on the irradiation hardness of an AlN transducer operating in a reactor core. Our results provide much needed solid proof of the feasibility of in-situ ultrasonic nondestructive testing of components within intense radiation environment over extended periods of time. The second harmonic can be used to monitor damage created by neutron irradiation because the radiation damage consists of voids, precipitates and dislocation loops. Tests showed that the second harmonics are generated primarily in the propagation medium as opposed to the AlN crystal.

P2Ca-2

Normalization of Magnetic Field Effects: Towards Quantitative Magnetomotive Ultrasound Imaging

Maria Evertsson[1], Magnus Cinthio[2], Sarah Fredriksson[3], Fredrik Olsson[3], Hans W Persson[2], Tomas Jansson[2]; [1]Faculty of engineering, LTH, Lund University, Lund, Sweden, [2]Faculty of engineering, LTH, Lund University, Sweden, [3]Genovis AB, Sweden

Background, Motivation and Objective

Recently we proposed a phase and frequency locked algorithm to reduce motion artifacts in magnetomotive ultrasound (MMUS) imaging, a modality where superparamagnetic iron oxide nanoparticles (NP) are used as a contrast agent. However, the method is not quantitative as the particle movement induced by the external magnetic field is dependent not only on the field strength, but also on the field gradient, plus material parameters. Here we assess the measured nanoparticle movement across the image plane in comparison with simulations of the magnetic force, to evaluate the potential for image normalization of magnetic field effects.

Statement of Contribution/Methods

A 2x1.5x1 cm poly vinyl alcohol-phantom containing 0.45mg Fe3O4/ml (average NP-dia 18 nm incl coating, Genovis AB) and 3% graphite was manufactured and put in a latex wrap. It was scanned using a 21 MHz transducer (VEVO 2100 Visualsonics Inc) while being positioned above a solenoid with a cone shaped iron core. Three measurements each were made at 10, 20, and 30 Vpp solenoid excitation voltages, and at 5, 10 and 15 Hz. IQ image cine loop data was exported to MATLAB, where quadrature demodulation of the temporal phase variation was carried out at twice the magnetic field excitation frequencies to yield the movement. A simulation of the magnetic field for a corresponding situation was performed in COMSOL Multiphysics.

Results

The figure shows (A) a MMUS image of the phantom with movement as color-code. The magnet is located at the bottom center, and the transducer along the top (maximum movement 2.9 µm as white, note the 1mm bar) (B) movement along the vertical axis extending from the tip of the magnet for three voltages, all at 5Hz (solid lines: mean of three measurements). Simulated magnetic force (field times its gradient) is scaled to fit in the figure (scale does not apply).

Discussion and Conclusions

Independent of applied field strength the movement decreases to be zero at the edges of the phantom. This suggests that the transducer and latex wrap act as rigid boundaries for particle movement. Away from the boundaries the magnetic force appears to be dominant. The coefficient of variation between measurements on the homogeneous phantom was typically in the order of 25%, indicating the expected accuracy for quantitative measurements.

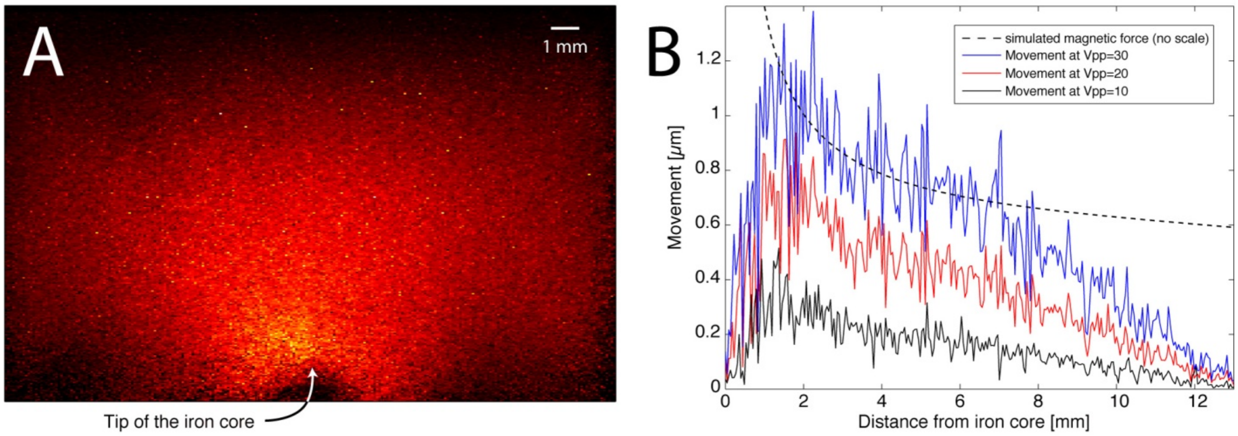

P2Ca-3

Mechanical Characterization of Ultra-thin Films using Colored Picosecond Acoustics

Arnaud Devos[1], Pierre-Adrien Mante[1], Arnaud Le Louarn[1], Sabrina Sadtler[1]; [1]*IEMN CNRS, Lille, France*

Background, Motivation and Objective

The mechanical properties of materials currently used by the microelectronic industry are poorly known. Only a few measurement techniques are able to probe various materials deposited in sub-micron films. Picosecond ultrasonics (PU) is an optical technique which uses a femtosecond laser to excite and detect longitudinal acoustic waves at very high frequencies (100 GHz to 1 THz). Such an optical setup offers an unique way of implementing a sonar at nanoscale. By measuring the time-delay between successive echoes it is basically possible to access to the thickness or to the longitudinal sound velocity. PU is contactless and is a non-destructive technique that is well adapted to mechanical measurements in films whose thickness can be as small as 5 nm. For several years we have shown that the PU capabilities can be enhanced if one uses several laser wavelengths or colors. More parameters are measurable, for example thickness and sound velocity are simultaneously reachable and the measurement accuracy can be significantly enhanced using this so-called Colored Picosecond Acoustic technique (CPU).

Statement of Contribution/Methods

Basically, in picosecond acoustics only longitudinal waves can be emitted by the absorption of the laser pulse. Due to that the measurement of the mechanical properties of a thin layer cannot be complete.

Recently we found a way of producing high-frequency surface acoustic waves using the same experimental setup. Thanks to a nanostructuration of the transducer, we are now able to perform complete elastic measurements namely measuring the Young modulus and the Poisson ratio of thin films.

Up to now this technique was limited to films whose thickness is greater than 200 nm.

Results

In this paper we present some recent results which show that we can extend the technique to thinner films.

We realized 2D lattices of metallic nanocubes using e-beam lithography on top of the thin film to be charaterized. Then we performed picosecond acoustic measurements using an interferometric detection of the probe laser. This way we can detect ultra-high surface acoustic waves and longitudinal waves. From that we show that we can access to the mechanical properties of thin film down to 50 nm.

Discussion and Conclusions

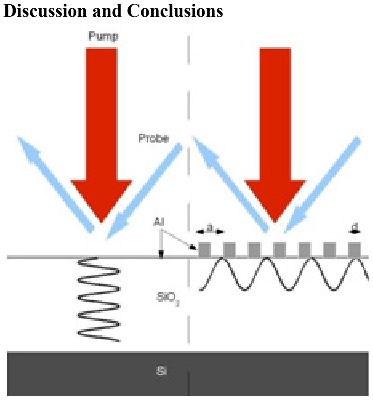

P2Ca-4

Efficient Multi-Beam Density-Tapered Diffraction of Pulse Light by Multi-Frequency Sound

Valery Proklov[1], Sergey Antonov[2], Alexander Vainer[1]; [1]Lab. 254, Kotelnikov IRE RAS, Fryazino, Moscow region, Russian Federation, [2]Lab. 250, Kotelnikov IRE RAS, Fryazino, Moscow region, Russian Federation

Background, Motivation and Objective

Many recent applications have need of a low loss transformation of a single laser beam to a certain multi-beam structure. One way to obtain a high efficiency acousto-optic (AO) light diffraction by multi-frequency sound is based on the poly-frequency signals with use of optimized phase and amplitude inter-frequency relations [1]. However, the question is how it works without frequency equidistance and with a pulse light. So, the present work is the first time investigation of facilities to obtain both a highest AO diffraction efficiency and stability at relevant circumstances.

Statement of Contribution/Methods

The proposal of the work is based on synchronous excitation of a multi-frequency sound wave packet and a short pulse of the light in such a way that the light goes through the AO cell when the acoustic packet fills up the all light aperture. At the first time the modeling and calculations of the AO diffraction efficiency expenses due to inequality of the sound frequency components spacing have been performed and minimized.

Results

The theoretical investigation of the reliable conditions to perform a high efficient and precisely tunable multi-beam AO diffraction of pulse light have been performed. On this basis detailed experimental verifications have been performed with AO cell on TeO2 and laser source with wavelength $\lambda = 1.06$ μm. Particularly for three non-equidistant sound frequencies the summary AO efficiency 80% have been observed. The experimental data have a satisfactory agreement with the theoretical ones.

Discussion and Conclusions

The results of the work demonstrate the ability of the new approach to realize the high efficiency multi-frequency AO diffraction applicable to pulse lightening and non-sensitive to positioning of the sound frequences aside of "equidistant" ones. No doubts it may be used in wide fields of AO applications like fiber optics, laser graving technology and etc.

1. V.V. Proklov, S.N. Antonov, Yu.G. Rezvov and A.V. Vainer, "High-efficiency Multi-beam Bragg Acousto-optic Diffraction", Proceedings of the 2006 IEEE International Ultrasonics symposium. 2006. October 3-6, Vancouver, Canada, C4C-5, pp. 248-251.

This work was supported by the Russian Basic Research Foundation, Project # 10-02-00029.

P2Ca-5

Microstructure-Induced Phonon Focusing Effects and Opportunities for Improved Material Quantification

James Blackshire[1]; [1]AFRL/RXLP, Air Force Research Laboratory, Wright-Patterson AFB, Ohio, USA

Background, Motivation and Objective

It is well known that single-crystal materials such as silicon have anisotropic elastic properties which depend on crystalline direction, causing the characteristic properties of a propagating elastic wave to have spatial and directional dependencies. As a result, variations in the speed and energy flux of an elastic wave propagating in a single crystal material typically produces spatial patterns, which can be used to infer the internal structure of a crystalline material. For polycrystalline materials, similar effects can be manifested when textured or single phase, equiaxed grains are involved, and coherent wave interference processes exist.

Statement of Contribution/Methods

The propagation of elastic waves within single crystal silicon, textured, and polycrystalline materials has been investigated using scanning laser vibrometry in a thru-transmission detection mode, where transverse variations in the phase and amplitude of the propagating energy fields were measured.

Results

Three examples of the scanning laser vibrometry results are presented in the accompanying figure, where phase and amplitude variations provide information regarding the internal microstructure of the materials.

Discussion and Conclusions

It is anticipated that inverse methods can be developed for quantitative evaluation of single crystal and polycrystalline materials based on the proposed methodology.

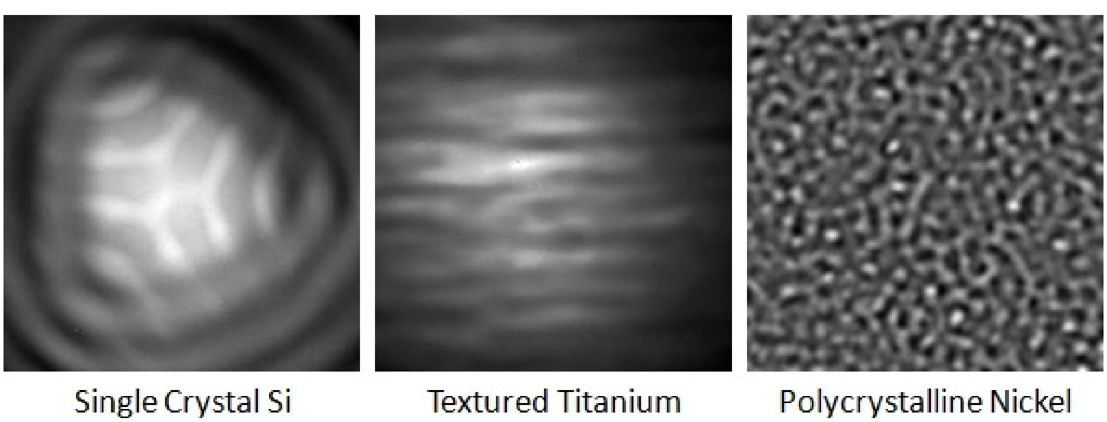

P2Cb - Ultrasonic Motors and Actuators II

Carribean Ballroom III-V

Wednesday, October 19, 2011, 1:00 pm - 4:30 pm

Chair: **Takefumi Kanda**
Okayama University, Japan

WEDNESDAY POSTER

P2Cb-1

Three-dimensional variable-focus liquid lens using acoustic radiation force

Daisuke Koyama[1], Ryoichi Isago[1], Kentaro Nakamura[1]; [1]Precision and Intelligence Laboratory, Tokyo Institute of Technology, Yokohama, Kanagawa, Japan

Background, Motivation and Objective

In compact mobile devices with built-in cameras, the camera lens and its actuator occupy a large volume. We have been investigating the variable-focus liquid lens by acoustic radiation force without a mechanical moving part. Our liquid lens was more compact and had faster response than conventional mechanical lens, and the high-speed focus-scanning at 1 kHz has been realized by exciting with an AM signal. This report describes a liquid lens which can change the focal point in not only the axial direction but also the radial direction.

Statement of Contribution/Methods

The liquid lens consists of an acrylic cylindrical cell with the inner diameter of 10 mm and the thickness of 3 mm, two immiscible liquids with different refractive index (water and silicone oil), and an annular PZT transducer with four-divided electrodes (Fig.1). The center of the transducer and the top of the lens were sealed using circular quartz plates so that light can propagate through the lens in the axial direction. The oil-water interface acting as the lens surface can be deformed by the acoustic radiation force from the transducer, and the lens acts as a variable-focus lens.

Results

The variation of the oil-water interface was observed by changing the driving condition of the transducer and using optical coherence tomography which images differences in the refractive index. The path of the laser beam transmitted through the lens was calculated by ray-tracing simulations. The oil-water interface could be deformed from the oil to water sides and the focal point could changed three-dimensionally by controlling the input voltage of the PZT electrodes (Fig.1). The displacement angle in the radial direction was approximately 3 degrees in the case that only two divide electrodes were excited with the input voltage of 45 V at 1 MHz.

Discussion and Conclusions

Confocal images can be obtained by sweeping the focal point of the lens. The dynamic performance of the lens was investigated by using a high-speed camera. By exciting with AM signals, the hemispherical water droplet oscillated and the focus scanning in the axial and radial directions could be achieved.

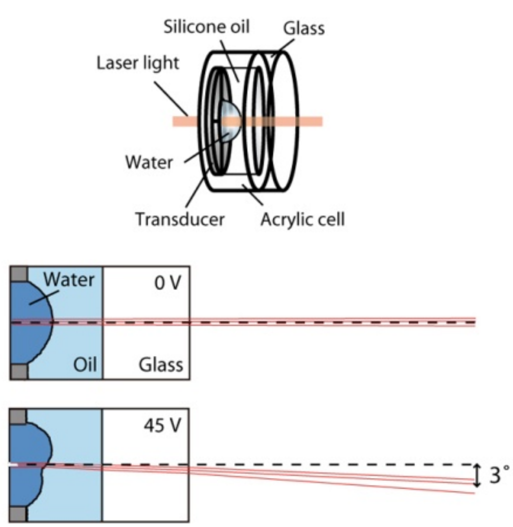

P2Cb-2

Miniaturization of the Traveling Wave Ultrasonic Linear Motor Using Series Connection of Bimorph Transducers

Shuichi Kondo[1], Daisuke Koyama[1], Kentaro Nakamura[1]; [1]Precision and Intelligence Laboratory, Tokyo Institute of Technology, Japan

Background, Motivation and Objective

Small-sized ultrasonic linear motors are highly demanded as an alternative to miniature air cylinders. We aim at realizing the traveling wave ultrasonic linear motor with the diameter less than 10 mm. The target performance of the thrust and the velocity are 1 N and 0.2 m/s, respectively. According to the original design of the traveling wave ultrasonic linear motor, it is difficult to reduce the volume since two balky Langevin transducers are attached vertically to the transmission bar. As a new design for traveling wave motor, we have introduced a single-bar structure consisting of a bending square bar and two bimorph transducers at both ends in line. The thrust was 0.4 N, which is 40 % of the target value, with one transducer for each end.

Statement of Contribution/Methods

We discuss on increasing the number of bimorph transducers in line shown as the Fig.1, for obtaining higher power with keeping the diameter same. The motor consists of a bending aluminum bar, two bimorph transducers for each end, and a slider. The bar end is sandwiched by two pairs of thin PZT plates, which acts as bimorph transducers. The optimal positions of the transducers were investigated through the finite element analysis. The traveling wave can be generated with applying phased voltages to both sides of the transducers. The slider which consisted of two plates whose surface is covered with frictional materials sandwiches the transmission bar.

Results

The distances of two pairs of PZT plates (15×3×8 mm) were designed to be 5 and 25 mm from the end of the bar (200×4×8 mm), respectively. The resonance frequency of the bending vibration was 62 kHz, and the wave length along the bar was 20 mm. The thickness of the bar was designed to be 4 mm for the optimal shape of the elliptical motion exhibited on the surface at the frequency. With the phase difference of ±90 degrees, the traveling wave was perfectly generated along the bar (the standing wave ratio was 1.0). The vibration amplitude of 0.3 µm and the vibration velocity of 61 mm/s are obtained, respectively, with the applied voltage of 350 Vp-p. The thrust of 0.5 N was obtained, which was 20% higher than the former model with one bimorph transducer.

Discussion and Conclusions

Series connection of the bimorph transducers for obtaining higher power with keeping a thinner ultrasonic motor was investigated. A flexural traveling wave was generated along the bar, and motor performance was improved.

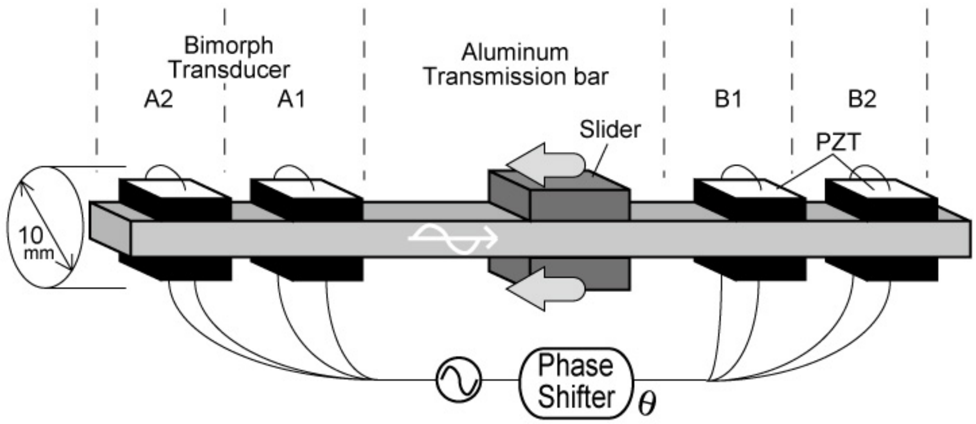

Fig. 1 Structure of the traveling wave ultrasonic linear motor using series connection of bimorph transducers

P2Cb-3

Analysis of Ultrasonic Motor in Air using Fluid Structure Interaction Based Simulations.

Manoj Pandey[1], Sarvani Piratla[2], Amit Lal[2]; [1]Electrical and Computer Engineering, Cornell University, Ithaca, NY, USA, [2]Electrical and Computer Engineerin, Cornell University, Ithaca, NY, USA

Background, Motivation and Objective

Ultrasonic micromotors, driven parametrically by the base vibration using PZT consist of a polysilicon stator and rotor, fabricated using surface micromachining technology [1-2]. These motors are highly stable, free of interconnects and produce high speeds (upto 500 rev/s) and hence can be used as rotating platform for other application. Previously we demonstrated the motor action in vacuum, where generation of circumferential traveling waves in the stator couples to the rotor through direct contact.

Statement of Contribution/Methods

In this work we develop a Fluid structural interaction (FSI) based FEA model by coupling solid mechanics software Abaqus and fluid dynamics software Fluent to numerically study the details of this motor action in air. It is shown that the presence of etch holes in stator, splits certain degenerate, flexural resonant modes, resulting in slightly different frequencies. When the stator is excited close to this resonant frequency, using a piezo drive, circumferential traveling wave is generated on the periphery due to interference of the degenerate modes. This traveling wave on the stator drags the nearby air resulting in steady circulating pattern between itself and the rotor called acoustic streaming [3]. Acoustic streaming between the substrate and the rotor is also the reason for rotor levitation while coupling of the stator motion, results in the rotation.

Results

We are successfully able to capture a challenging effect of acoustic streaming using numerical simulations. Simulations compared well with experiments for a motor running in air. The rotational speed of motors in the two cases is found to be close to each other, after careful calibration. The mode shapes obtained in simulations matched the one obtained by mapping the surface topography of the stator, using a Doppler interferometer (Fig.1).

Discussion and Conclusions

We have successfully modeled the actuation of an Ultrasonic motor in air, using numerical simulations. Acoustic streaming is determined to be the primary effect leading to rotor levitation and motor action. We were able to redesign the stator to achieve better performance of the motor, which was verified experimentally. Stability analysis of the rotor was performed to determine its feasibility as a stable self calibrating rotating platform.

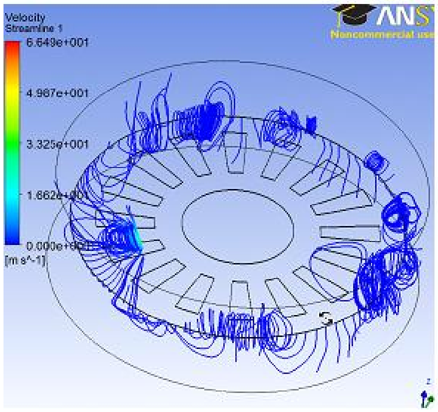
Velocity
Streamline 1
6.649e+001
4.987e+001
3.325e+001
1.662e+001
0.000e+000
[m s^-1]
Noncommercial use

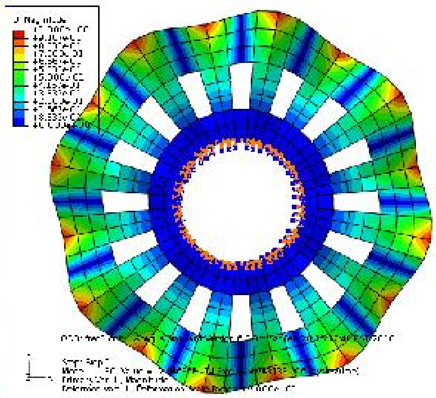

P2D - Novel and Sensor Devices

Carribean Ballroom III-V

Wednesday, October 19, 2011, 1:00 pm - 4:30 pm

Chair: **Ingo Bleyl**
TDK-EPC

P2D-1

Active Mixing in microfluidic systems using Surface acoustic waves

Raimund Bruenig[1], Andreas Winkler[2], Glen Guhr[2], Hagen Schmidt[2]; [1]*IFW Dresden, Dresden, Sachsen, Germany,* [2]*IFW Dresden, Germany*

Background, Motivation and Objective

The growing demand for miniaturization and acceleration in chemical and biological analysis requires new methods for pumping and mixing in Micro Total Analysis Systems or Lab-on-Chip. The interaction of surface acoustic waves with a liquid halfspace atop lead to the excitation of longitudinal pressure waves in the liquid. These high frequency pressure waves generate an acoustic streaming which allows mixing, pumping and even atomization of liquids. However, several issues concerning assembly, signal generation, power durability and handling of such mixing devices turned out to be rather difficult. In this study, we want to present our solutions.

Statement of Contribution/Methods

The experimental setup consists of the piezoelectric substrate (LiNbO3, 128°YX) together with the Interdigital transducer which emits the surface acoustic wave (SAW). A Y-shaped micro fluidic channel casted in PDMS is placed atop. The IDT emits a wavelength of 60µm corresponding to a frequency of approx. 65MHz. The electrical properties of the IDT have been matched to an electrical impedance of 50Ohm. Since the bandwidth for an ideal SAW-excitation is very narrow a newly developed driving device is used. The driving unit continuously monitors the SAW-device and self-tunes to the optimal driving frequency. The output power can be adjusted between 1mW…4W.

A special designed sensor layout based on a meandering electrode inside the microfluidic channel is used to measure the SAW-induced heating effect.

Calculations show the suitability of PDMS for SAW-based microfluidics in regard to parasitic viscous damping of the acoustic wave.

Results

The experiments show that a SAW-induced mixing of fluid streams is possible with streaming velocities in the range of 1-3mm/s in a 0.5x0.5mm channel. A temperature increase of about 10…20°C was monitored for excitation powers of 100…200mW. However an effective mixing was already observed at lower power levels of about 50mW.

Discussion and Conclusions

In microfluidic devices no turbulent mixing is possible due to the low reynold's numbers. However SAW-induced mixing offers a way to split the different fluid streams, recombine them and therefore reduce the necessary distances for diffusion. The acoustic power is able to introduce local heating into the fluid volume. By using our special designed sensors we are able to measure the temperature inside the micro fluidic channel.

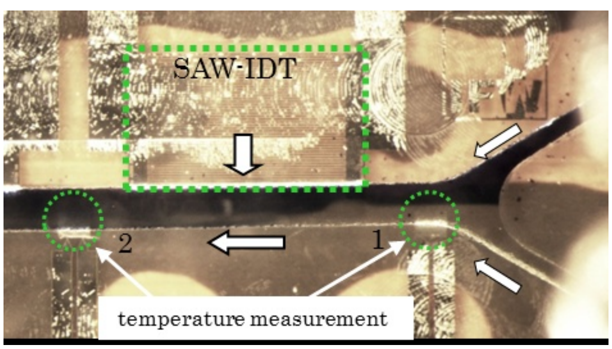

P2D-2

Label-Free Detection of Prostate-Specific Antigen with FBAR-Based Sensor with Oriented Antibody Immobilization

Anderson Lin[1], Yi-Jia Li[2], Lingtao Wang[1], Shih-Jui Chen[1], Mitchell Gross[2], Eun Sok Kim[1]; [1]Department of Electrical Engineering, University of Southern California, USA, [2]Department of Medicine, University of Southern California, USA

Background, Motivation and Objective

Prostate cancer is the most common type of cancer in men in the Western world. The most effective method for early detection of prostate cancer is achieved by measuring the level of prostate-specific antigen (PSA) in blood, where an elevated level is often found in prostate cancer patient. This paper reports a real-time, label-free detection of PSA through mass sensing with film bulk acoustic resonator (FBAR) coated with an oriented antibody layer.

Statement of Contribution/Methods

The FBAR sensor was formed by depositing a gold layer on the backside of an FBAR built on a micromachined silicon nitride diaphragm. PSA antibody was immobilized on the gold surface by sequences of solution treatments, including protein A and antibody solutions. This procedure results in an oriented antibody layer immobilized on the FBAR surface, as protein A binds to the gold surface at the N-terminus and the Fc (fragment crystallizable) region of IgG (immunoglobulin G) antibody on the other end. To achieve an even better orientation in antibody immobilization, DTSSP (3,3´-Dithiobis[sulfosuccinimidylpropionate]) crosslinker was used in later experiments to promote the degree of antibody orientation.

FBAR sensor was measured with a network analyzer, and the resonant frequency was tracked with a LabVIEW program. Second harmonic frequency was tracked, due to its much higher Q of about 70 in liquid than Q of less than 10 for the fundamental resonance.

Results

The first prototype sensor showed clear frequency shifts when exposed to 500 ng/ml and 1 µg/ml of PSA, with a frequency shift of 20 kHz at 1 µg/ml, about 7 ppm of the 2.91 GHz resonant frequency. The sensor's regeneration capability has also been tested to be good by applying 0.1 M glycine pH 2.5, which strips off the antibody-antigen complex, followed by phosphate buffered saline (PBS) washes and subsequent antibody immobilization. Cross-reactivity of the sensor to bovine serum albumin (BSA – variant of a common protein in blood) also has been tested. The sensor showed no cross-reaction with BSA for concentrations up to 0.1 mg/ml.

With DTSSP treatment, the improved sensor showed a frequency shift of 1.2 MHz in response to 500 ng/ml of PSA, corresponding to a frequency change of more than 500 ppm for an FBAR operating at 2.22 GHz resonant frequency. This is an improvement over the first prototype by a factor of more than 70. Assuming a linear relationship between the concentration and frequency shift, we expect the sensor to be able to detect down to ng/ml of PSA.

Discussion and Conclusions

With an oriented antibody immobilization facilitated by DTSSP, we showed that an FBAR-based sensor can potentially detect PSA concentration in the ng/ml range. Also, we demonstrated that the sensor could be regenerated, and had very little cross reactivity to BSA. A label-free detection at such low concentration level with negligible cross-reaction with BSA indicates a high possibility of selective PSA detection in-vivo.

P2D-3

Development of a new wireless surface acoustic wave based gyroscope

Wen Wang[1]; [1]Institute of Acoustics,Chinese Academy of Sciences, Beijing, Beijing, China, People's Republic of

Background, Motivation and Objective

Surface acoustic wave (SAW) gyroscope have many unique properties as superior inherent shock robustness, larger dynamic range, and long working life. This paper develops a new wireless SAW gyroscope on 128o YX LiNbO3 substrate. Wireless measurement and high phase sensitivity were observed experimentally.

Statement of Contribution/Methods

Fig. 1 shows the schematic and the principle of the 434MHz wireless SAW gyroscope, which consists of two parallel reflective delay lines with opposite direction. If the gyroscope is subjected to the counter-clockwise rotation around the y-axis, the Coriolis force acts on the vibrating particles and induces a new running wave shifted a quarter of a wavelength, and coupling the initial SAW, inducing to SAW velocity change, and resulting in phase shifts of the reflected peaks depending on applied rotation. This differential scheme doubles the sensor sensitivity and compensates the temperature effect. By evaluating the phase shifts, the external rotation can be extracted. A fabricated coupling antenna was connected reflective delay line to complete the wireless measurement.

Results

Before rate testing, the S11 of the fabricated SAW devices were measured by the HP 8510 network analyzer, as shown in Fig. 1(b). Then, referring to the network analyzer as the reader unit and using the precise rate table (Fig. 2(a)), the fabricated gyroscope was characterized wirelessly, the sensitivity and the linearity of the SAW gyroscope with rotation in y-axis were measured as 2.42 deg deg−1 s−1 and 0.9568, respectively as shown in Fig. 2(b).

Discussion and Conclusions

A novel wireless SAW gyroscope was developed. The sensor performance was evaluated wirelessly referring to the network analyzer. Meaningful phase sensitivity and linearity were observed experimentally.

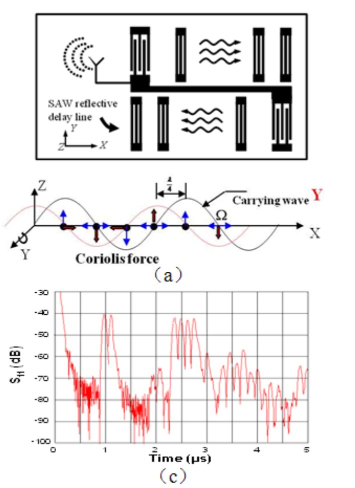

Fig.1 (a)Schematic of the wireless SAW gyroscope, (b) measured S_{11} in time domain

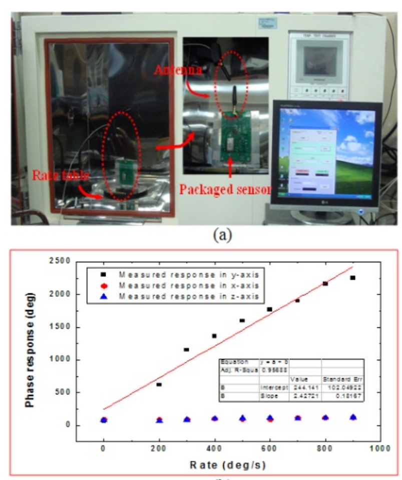

Fig.2 (a) the wireless measurement setup, (b)measured response towards rotation

P2D-4

SAW magnetic sensors composed of various Ni electrode structures on quartz

Michio Kadota[1], Shigeo Ito[1]; [1]*Murata Mfg. Co., Ltd., Japan*

Background, Motivation and Objective

Conventional magnetic sensors such as hall elements and magneto resistive elements require a driving power supply to drive them. On the other hand, sensor systems using SAW resonators such as pressure sensors, torque sensors, and temperature sensors can be applied to the battery-less wireless communication system. A magnetic sensor using SAW for the battery-less wireless communication system was attempted to fabricate.

Statement of Contribution/Methods

The battery-less wireless communication system requires a SAW resonator with high Q. A shear horizontal type of leaky SAW on the high density Ni of magnetostrictive metal electrode/ST-90°X quartz was attempted to fabricate as a magnetic sensor. Fig. 1 shows the calculated coupling factor on 3 kinds of Ni electrode structures/ST-90°X quartz. Their maximum values of the coupling factor are almost same regardless of their structures, though the Ni-film thickness showing the maximum value is different.

Results

Their one port SAW resonators were fabricated. The measured frequency shifts were proportional to the magnetic field strength applied in the vertical direction to SAW propagation one. As shown in Fig. 2, their frequency shifts show similar behavior regardless of their structures. When the SAW magnetic resonator was applied to the battery-less wireless communication system, the sending and receiving of the sensing signal of the magnetic field could be measured.

Discussion and Conclusions

The SAW resonators composed of various Ni electrode structures on ST-90°X quartz were fabricated. Their frequency shifts show similar behavior regardless of their structures. When the SAW resonator was applied to the battery-less wireless communication system, the sending and the receiving of the sensing signal of the magnetic field were measured.

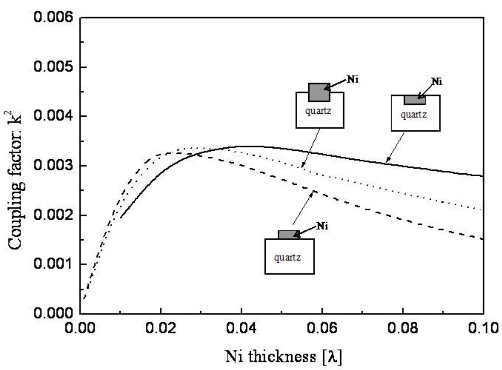

Fig1. Coupling factor on various Ni electrodes structures/ST-90°Xquartz.

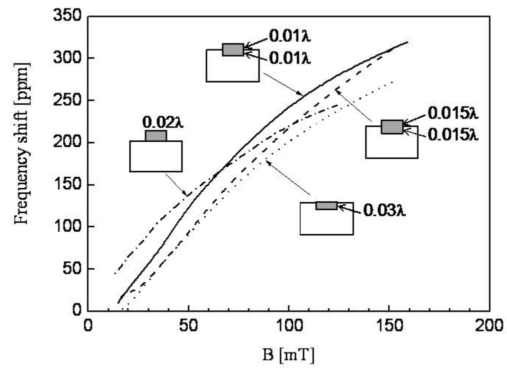

Fig2. Frequency shift of SAW resonators composed of various Ni structures/quartz on magnetic field.

P2D-5

The Thin Film Plate Wave Resonator in view of Sensing Applications

Ventsislav Yantchev[1], Emil Anderas[1], Lilia Arapan[1], Ilia Katardjiev[1]; [1]*Solid State Electronics, Uppsala University, Uppsala, Sweden*

Background, Motivation and Objective

In this work the sensitivities of thin aluminum nitride (AlN) film plate acoustic resonators (FPAR) to various loadings are studied. FPARs represent a class of integrated circuit (IC) compatible micro-acoustic devices operating mainly at the lowest order symmetric Lamb wave (S0). However the first order asymmetric (A1) and symmetric (S1) Lamb wave resonances are found at higher frequencies. FPARs have recently demonstrated Q factors of up to 3000 (S0 mode), 1000 (A1 mode) and 1000 (S1 mode) at a frequencies of 0.9GHz, 1.7GHz and 2.3GHz, respectively. Also, S0 mode based oscillators have exhibited low phase noise, which in turn is a prerequisite for achieving high sensor resolution. Temperature compensation of the S0 mode is readily achieved. The latter motivated us for this study of the S0 mode under various perturbations. Further, sensitivity results for the A1 and the S1 modes are presented.

Statement of Contribution/Methods

The FPARs experimentally tested are having grating pitch of 6µm and AlN thickness of 2 µm. The sensitivities of each of the FPAR modes are experimentally assessed through the relative frequency changes caused by mass, pressure, fluid and temperature perturbations.

Results

Mass sensitivities of the Lamb modes are measured for FPAR loaded by thin SiO2 layers. The highest fractional sensitivity belongs to the A1 mode, although the S0 mode demonstrates still high sensitivity. The highest fractional pressure sensitivity belongs to the S0 mode.

Finally the FPAR has been tested in contact with water. The S0 Lamb wave has shown sufficient performance, further supporting independently published results. The A1 mode attenuated completely, while the S1 mode dissipated its energy limiting the Q to only 13 (in air Q=570). The measured S0-mode FPAR responses, are demonstrated Qs of 1700 (in air), 150 (in water) and 70 (in 50% glycerol solution), respectively. We observed a 9.2 MHz initial (from air to water) and additional 1.3MHz (from water to 50% glycerol) frequency shifts, respectively.

Discussion and Conclusions

The S0 Lamb wave in thin films offers a unique combination of weak dispersion, moderate coupling, low noise as well as high sensitivity to mass and pressure. Its ability to operate in liquid environments could be employed in integrated Bio-sensor applications.

The work is supported by the Swedish Research Council (VR)

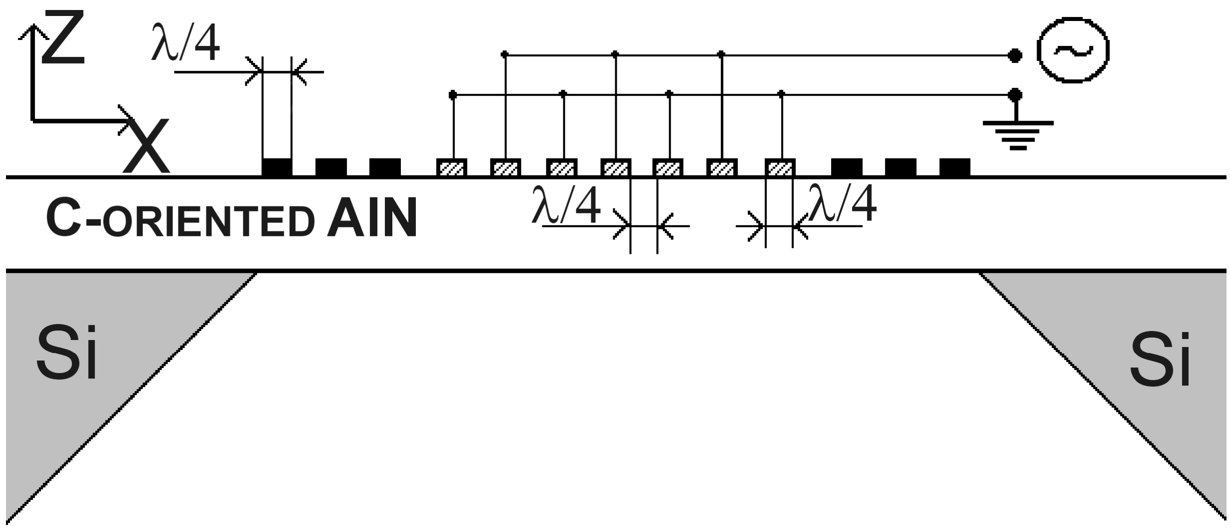

P2D-6

c-axis parallel oriented ZnO film SH-SAW sensor for electrical conductivity measurement in liquid

Yuta Nakahigashi[1], Takahiko Yanagitani[2], Mami Matsukawa[1], Yoshiaki Watanabe[1]; [1]*Doshisha University, Japan,* [2]*Nagoya Institute of Technology, Japan*

Background, Motivation and Objective

The SH-SAW device can be a sensor operating in the liquid, because SH-SAW propagates at liquid/solid interface without energy leakage to the liquid. At electrically conductive interfaces, SAW velocity deceases due to the lack of piezoelectric stiffening effect. The conductivity of the liquid can then be detected as the velocity change. c-axis parallel oriented ZnO film ({11-20} ZnO film) can be one of the best candidates for the SH-SAW liquid sensors on various substrates without the epitaxial technique.

Statement of Contribution/Methods

The performance of the (11-20) ZnO film SH-SAW sensor in liquid was examined. Our numerical simulation proved that the IDT / (11-20) ZnO (0, 90º, 55º) (H / λ = 0.21) / silica glass substrate structure had the highest K^2 value, which directly related to the sensitivity of the sensor. A silicone rubber liquid pool was fabricated on this structure, and SAW velocities were measured in standard conductive KCl solutions from 0.09 to 1.28 S/m.

Results

Figure 1 shows insertion loss of the transversal type IDT sensor. Rayleigh-SAW response disappeared in liquid, whereas SH-SAW response was clearly found. Figure 2 shows phase change of S_{21} as a function of conductivity of KCl solution. The S_{21} phase dramatically changed due to the conductivities from 0.3 to 1.0 S/m. The longer propagation path contributed to the increase of phase sensitivity.

Discussion and Conclusions

If the viscosity of the each solution is assumed to be constant, the decrease of SAW velocity (corresponding to the S_{21} phase) results from the increase of solution conductivity. This is perfectly in good agreement with the data. The (11-20) ZnO film is promising for SH-SAW liquid conductivity sensor on various substrates including curved surface.

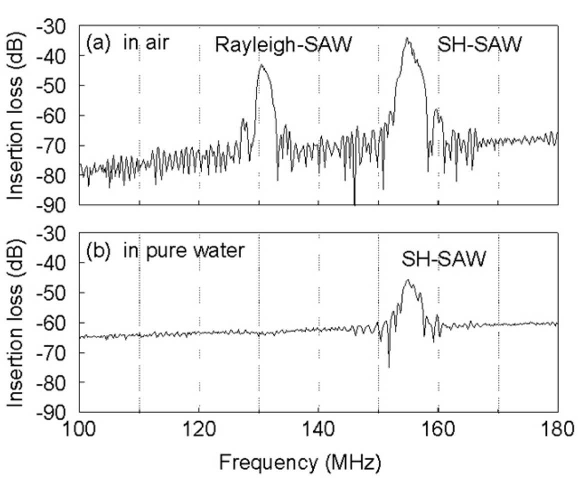

Fig.1 Insertion loss S_{21} of the transversal type IDT sensor (a) in air, (b) in pure water.

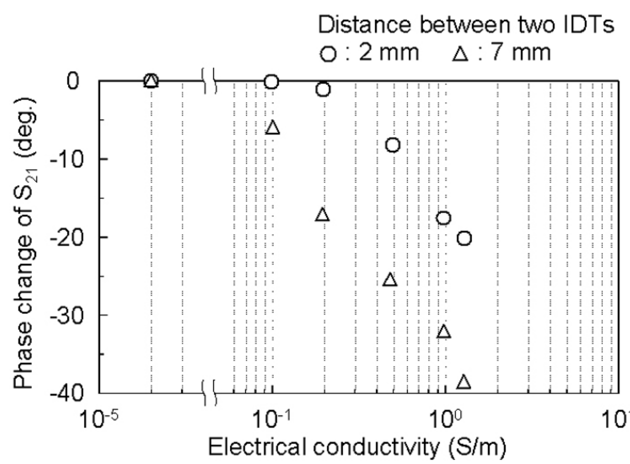

Fig.2 Phase change of S_{21} as a function of electrical conductivity of KCl solution.

P2D-7

High Stable and Sensitive Orthogonal Frequency Coded SAW Tags and Sensors Using Unidirectional IDT and High Coupling Zero TCF Substrates

Hiroyuki Odagawa[1], Donald Malocha[2], Kazuhiko Yamanouchi[3]; [1]Information, Communication and Electronic Engineering, Kumamoto National College of Technology, Japan, [2]University of Central Florida, USA, [3]Tohoku University, Japan

Background, Motivation and Objective

Surface acoustic waves (SAWs) have been applied in various electronic devices, e.g., different kinds of filters, stable high frequency oscillators, real time signal processing devices, convolvers and matched filters used in spread spectrum communication systems.

To obtain the high-performance surface acoustic wave (SAW) devices, it is very important for the interdigital transducer (IDT) to be made unidirectional one (UIDT) together with high-coupling SAW materials.

Statement of Contribution/Methods

OFC is the use of orthogonal frequencies to encode a signal, which spreads the signal bandwidth in a manner similar to a fixed M-ary frequency shift signal. Also, a pseudo noise (PN) sequence can be added for additional coding. The OFC technique provides a wide bandwidth spread spectrum signal with all the inherent advantages obtained from the time-bandwidth product increase over the data bandwidth. To obtain the large time-bandwidth with low loss, the high coupling substrates and UIDT are required. Also the zero TCF materials are very important for the matched filter systems.

In this paper, we propose the new configuration of the internal reflection types of unidirectional IDT of λ/4 electrode width with the highest transduction and new group type unidirectional IDT of λ/4 width using SiO_2/YX-$LiNbO_3$ substrates [1] with k^2=0.3 and zero Temperature Coefficient of Frequency(TCF). The above UDT and substrates are applied to the low loss wide band filter, Tags and Sensors.

Results

The calculation results show the large wide-band width and the very low insertion loss tags and sensors without the degradation of the pulse response over the temperature by zero TCF substrates. Also the experimental results show almost the same of theoretical ones.

Discussion and Conclusions

The new configuration of internal reflection type unidirectional IDTs and group type unidirectional IDTs with the electrode width of λ/4 on SiO_2/YX-$LiNbO_3$, which is described in this paper, will improve the properties of various types of OFC SAW device.

Ref. [1] K.Yamanouchi, et al, Jpn. J. Appl. Phys., 41 (2002) 3480.

P2D-8

Silicon/Periodically Poled Transducer/Silicon resonant devices for the stabili-zation of RF oscillators

Florent Bassignot[1], **Eric Lebrasseur**[1], Gwenn Ulliac[2], Gilles Martin[1], Emilie Courjon[2], Bruno François[1], Jean-Marc Lesage[3], Sylvain Ballandras[1]; [1]*Time & Frequency Dept, Femto-st, CNRS, Besancon, France,* [2]*Mimento, Femto-st, CNRS, Besancon, France,* [3]*CELAR, DGA, Rennes, France*

Background, Motivation and Objective

Surface Acoustic Waves (SAW) resonators are used for the frequency stabilization of electrical oscillators in the range of 50 MHz to 2 GHz. We recently have proposed a new acoustic resonator concept based on a period-ically poled transducer (PPT) in a piezoelectric substrate (LiNbO3 or LiTaO3), embedded between two guiding plates (Si) yielding an acoustic waveguide immune from external pollution.

Statement of Contribution/Methods

In this work, we present the design, manufacture and characterization of a PPT-based resonator based on a Sili-con/PPT/Silicon structure, where the PPT can be built either using LiNbO3 or LiTaO3 ZX cut. These devices are operating as dipole resonators suitable for Colpitts oscillator stabilization. We present the resonator oscillation characteristics, more particularly the phase noise and the frequency stability. Furthermore, we discuss the ad-vantages of thinning down the piezoelectric transducer taking advantage of the dispersion properties of such devices.

Results

Various devices have been manufactured, with period varying from 50µm to 10µm. Si/PPT/Si test vehicles, ex-hibiting a 50µm period and a 30µm thick piezoelectric layer, have pointed out the existence of an isolated mode operating at frequencies near 110MHz for a LiNbO3 PPT and near 90MHz with LiTaO3 PPT. Q factor in excess of 18000 at 130 MHz has been measured for LiNbO3 based devices for which a quasi longitudinal guided mode is excited. These resonators then have been inserted in a Colpitts oscillator and the phase noise was measured (Fig. 1). A value lower than -160dBc/Hz at 50 kHz of the carrier wave has been found, revealing promising ca-pabilities of the resonator for actual application.

Discussion and Conclusions

The phase noise of the oscillator using a Si/PPLN/Si resonator has demonstrated the concept feasibility. The fabrication process and the characterization of resonators based on thinned PPLN or PPLT layers are described and the actual limit of such devices is discussed.

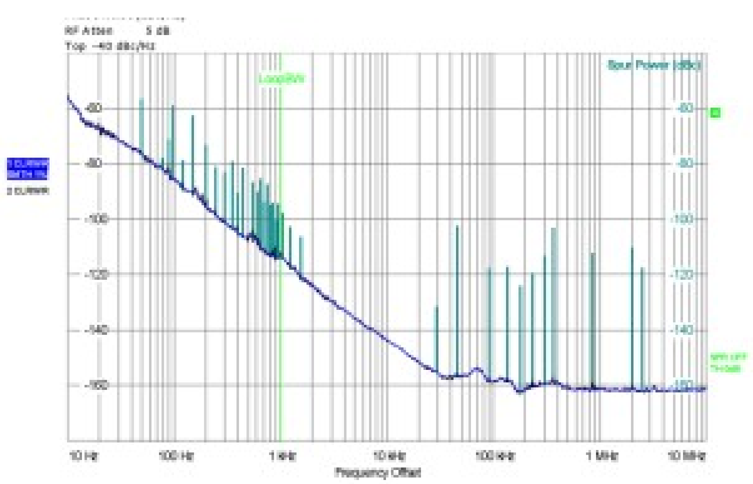

P2D-9

Passive, Wireless Surface Acoustic Wave Radio Frequency Identification (SAW-RFID) Sensors for Temperature and Strain Measurements

Fang Li[1], Dan Xiang[1], Cliff Searfass[2], Bernhard Tittmann[2]; [1]Intelligent Automation, Inc., USA, [2]Penn State University, USA

Background, Motivation and Objective

The testing, validation, and monitoring of aero-structural design and health conditions, require a non-intrusive and in-situ means, in order to provide real time strain/stress and vibration data of turbine engine structures. However, taking such a measurement is difficult, due to the extremely harsh environment that exists in turbine engines. The SAW-RFID sensor, because it takes advantage of being passive, wireless and is high temperature tolerant, provides a promising tool to operate in such a harsh environment. These characteristics, give it the ability to measure the strain and temperature stress on engine blades, in real time. In this paper, we discuss our recent work on the design and development of SAW-RFID sensors for temperature and strain measurements which can be used in harsh environment.

Statement of Contribution/Methods

The modeling and simulation of the surface wave generation, propagation and reflection at the sensor surface were conducted using Finite Element Modeling (FEM). The effects of various parameters in interdigital transducers (IDTs) and reflectors on detected signals were analyzed through simulation. According to the simulation results, we designed and fabricated SAW sensors using LiNbO3 substrate with the lift-off micro-fabrication process. The fabricated sensors were tested at both the wafer and device levels. The developed SAW sensor was tested for temperature measurements up to 400 degree C by putting the senor onto a hot plate. We also performed the strain measurements by attaching sensors to a steel dog bone sample that was mounted in a tensile testing machine.

Results

With our FEM model, we found that the resonant frequency decreases with the mass loading of electrodes and the reflection coefficients for reflectors increase with the their finger number, metallization ratio and electrode thickness. Moreover, the reflection coefficient for open type reflectors is higher than that for short type reflectors. These findings guided our sensor design. The central frequency of fabricated sensors was in the range of 760-800MHz, agreeable with the simulation results. The insertion loss between the input and output signals is around 45dB. The temperature and strain measurements showed that the sensitivity to temperature is around 75ppm/degree C, while sensitivity to the strain is about 1 ppm/micro strain, which is consistent with simulation results.

Discussion and Conclusions

In summary, we designed, fabricated and tested LiNbO3-based SAW-RFID sensors. The developed sensors have decent signal-noise-ratio and have been successfully used to measurement temperature and strain. The results showed that there existed a linear relationship between the time delay shift of the SAW sensor and applied strain as well as temperature changes.

P2D-10

Compact Antennas for Wireless Langasite SAW Sensors

Tao-Lun Chin[1,2], David Greve[2,3], Irving Oppenheim[1,4]; [1]National Energy Technology Laboratory, USA, [2]Electrical and Computer Engineering, Carnegie Mellon University, USA, [3]National Energy Technology Laboratory, Pittsburgh, PA, USA, [4]Civil and Environmental Engineering, Carnegie Mellon University, USA

Background, Motivation and Objective

Wireless langasite SAW temperature and gas sensors have harsh-environment applications. The operating frequency for these sensors involves a difficult tradeoff. Attenuation increases with frequency; however the antenna size is proportional to λ and conventional dipole antennas are impractical at lower frequencies. In this paper we report on possible compact antenna designs for 327 MHz langasite SAW sensors.

Statement of Contribution/Methods

We report on the simulation and experimental demonstration of a capacitively loaded loop. Unloaded, this antenna presents a resistive input impedance when the perimeter is about λ/2. Capacitive loading decreases the resonant frequency and also the radiation resistance. Simulations predict that a square loop with an edge of 6.7 cm (< 0.08λ) resonates at 327 MHz with a loading capacitance of about 0.8 pF.

This antenna design has been tested using a langasite SAW device. The capacitance was tuned for maximum signal but no matching network was used despite the mismatch between the IDT and the antenna radiation resistance. Stable phase difference measurements were observed at a range of up to 14 cm. Wireless temperature sensing was demonstrated at short range. Improved performance is anticipated when a matching network is used.

Results

One design of compact antenna size substantially smaller than λ/2 has been evaluated for wireless langasite SAW sensors. Although simulations predict a small radiation resistance and a poor impedance match, successful operation was demonstrated at short range. A matching network and alternate antenna designs are being developed for further performance improvement.

Discussion and Conclusions

This work was performed in support of research on carbon storage at NETL under RES contract DE-FE0004000.

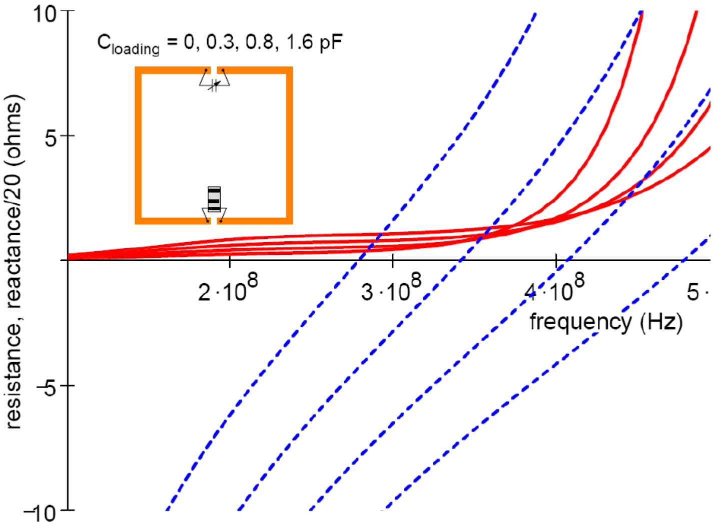

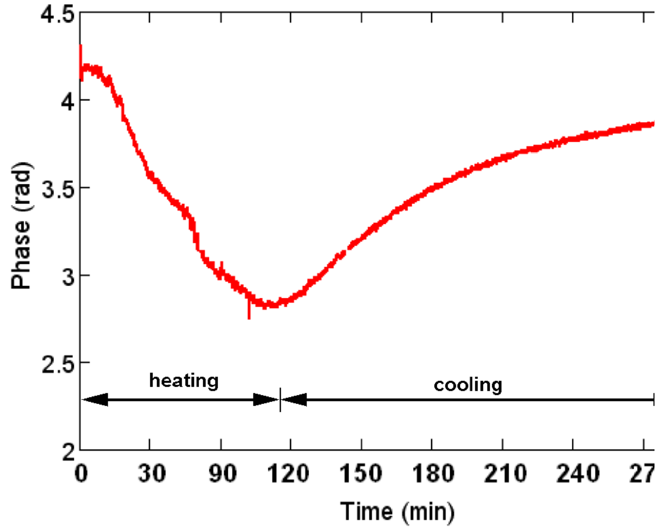

P2D-11

Theoretical Considerations on Suppression Mechanism of Spurious Transverse Mode Resonances in Wideband SAW Resonator on $LiNbO_3$

Tatsuya Omori[1], Takahiro Suyama[2], Kenta Shimada[2], Chang-Jun Ahn[2], Masatsune Yamaguchi[2], Ken-ya Hashimoto[2]; [1]*Electrical & Electronics Engineering, Chiba University, Chiba, Japan,* [2]*Chiba University, Japan*

Background, Motivation and Objective

Ultra-wideband SAW resonators in GHz range are demanded to realise widely variable frequency oscillators, tunable filters etc. The authors have proposed use of the Love-type SAW propagating on the Cu-grating/$LiNbO_3$ structure, and demonstrated how high performances are achievable. In the structure, suppression of spurious transverse modes is mandatory for practical use, because excessive energy confinement traps higher-order modes in the grating. In previous work[1], we showed that the spatially length-weighted dummy electrodes is effective for the suppression. However they were designed empirically without sufficient understanding. This paper analyses SAWs propagation in a multi-layered acoustic waveguide with the weighted dummy electrodes, and the result is extended to a coupling-of-modes (COM) modelling for optimisation of the weighting pattern.

[1] T. Omori et al., Proc. 2006 IEEE Ultrason. Symp., pp. 1874-1877.

Statement of Contribution/Methods

First, the SAW resonator is modelled by an acoustic waveguide, and the dispersion relation of transverse modes is evaluated as a function of dummy length by using the scalar potential (SP) theory. Then mutual coupling between transverse modes is modelled by first order simultaneous linear differential equations based on the COM theory. Coefficients appearing in the equations are determined by fitting the dispersion relation given by the SP theory with that given by the COM theory. Once these coefficients are determined, energy interaction between transverse modes can be analysed evaluated easily even if the dummy electrodes vary their length with position. By using this method, one can seek the appropriate weighting pattern for efficient leakage of spurious modes without deterioration of the dominant response.

Results

Attenuation of the lowest-order spurious mode, which is attributed to its coupling with the higher-order leaky modes, was estimated by the proposed method. When a) triangle, b) ramp, c) smooth pedestal etc., were chosen as the weighting pattern, the estimated attenuation was 8.4, 5.6 and 4.1 dB, respectively, for five round trips in the resonator structure. This indicates that the triangle shaped weighting is the most suitable for suppression of the lowest-order transverse mode. For experimental verification, we fabricated one-port SAW resonators with such weighted dummy electrodes. Measured Q-factor of the lowest-order spurious resonance was 10, 90 and 170 for the weighting pattern a, b and c, respectively. This result agrees with the theory.

Discussion and Conclusions

This work proposes the procedure to analyse transverse mode propagation in the SAW waveguide with weighted dummy electrodes. The proposed method can be used as a powerful tool to understand behaviour of transverse mode propagation and to develop efficient techniques for the suppression of spurious resonances appearing in wideband SAW resonators.

P2E - Transducer Materials

Carribean Ballroom III-V

Wednesday, October 19, 2011, 1:00 pm - 4:30 pm

Chair: **Richard O'Leary**
University of Strathclyde

P2E-1

Reactive magnetron sputtering of piezoelectric Cr-doped AlN thin films

Valery Felmetsger[1]; [1]PVD, OEM Group Inc., Gilbert, AZ, USA

Background, Motivation and Objective

Aluminum nitride (AlN) is the most promising piezoelectric material for new generation of resonators, filters and microsensors working in harsh environment. A well-known issue of these devices is temperature-dependent variation of resonance frequency. A thermal compensation method based on use of additional layer of SiO2 in the device structure reduces temperature coefficient of frequency but introduces additional issues (lower coupling coefficient, spurious resonances). New opportunities to create high-temperature piezoelectric materials have been discovered from studies of pseudo binary alloys, which can combine the excellent properties of pure group IIIA nitrides with the high hardness and temperature stability of transition metal nitrides. Recently the possibility to improve the AlN properties by Cr-doping has been demonstrated experimentally using magnetron co-sputtering technique at high substrate temperature.
In this work, experimental study of AlCrN films deposited at ambient temperature using more advanced ac reactive sputtering technique has been performed with the aim to develop a technology acceptable for implementation in mass production.

Statement of Contribution/Methods

180-3000 nm thick AlCrN films were deposited on 100 mm diameter Si (100) wafers using a dual cathode ac (40 kHz) powered S-gun magnetron equipped with the Al + 5 at.% Cr targets. We investigated an influence of the sputter process conditions on properties (thickness uniformity, crystal orientation, stress, surface roughness) of the AlCrN films deposited on bare Si surfaces and on well-textured Mo bottom electrodes.

Results

X-ray diffraction patterns show that AlCrN films deposited with optimized process parameters have a single c-axis crystal orientation, although AlN (0002) peak position on Theta-2Theta scans is shifted to lower 2Theta values compared to its position for regular AlN films. X-ray rocking curves (RC) around the AlN (0002) peak are typically wider than exhibited by AlN films deposited in the same conditions. Especially it is true for relatively thick AlCrN films. For example, RC of the 180 nm thick AlN film on the Mo electrode had FWHM = 1.8¢ª, which reduced to 1.2¢ª in the 1000 nm thick film, while 180 nm thick AlCrN films had FWHM = 1.6¢ª, which (in contrast to AlN) was not improved with increasing film thickness due to drastically increased surface roughness.

A specific feature of the AlCrN films is a strong tendency to high compressive stress compared to AlN films. In contrast to AlN, reduction of compressive stress by the stress adjustment unit of the S-gun, which reduces ion bombardment of the growing film, leads to worse crystal orientation.

Discussion and Conclusions

Piezoelectric AlCrN films can exhibit potentially improved functional characteristics and stability at elevated temperatures. Preliminary results obtained in this study will help to address technological aspects of the film roughness, crystallinity and stress controlability.

P2E-2

Metal-Polymer Iterative Multilayer Absorber for Ultrasonic Transducers

Minoru Toda[1], Mitchell Thompson[2]; [1]Measurement Specialties Inc, Lawrenceville, NJ, USA, [2]Measurement Specialties Inc, Wayne, PA, USA

Background, Motivation and Objective

Typical wideband ultrasonic transducers are composed of front matching layers and backing absorber attached to surfaces of a piezoelectric layer. The absorber requires appropriate impedance and attenuation. Typical absorber is mixture of metal particles and polymer, and theoretical design of the properties is difficult, and the process control is not suitable for cost-efficient production process because of complexity and lack of consistency associated with mixing and casting. Since the design of two phase material satisfying the requirements is difficult, usually the material is formulated based on experimental trial.

Statement of Contribution/Methods

In the recent paper published on Trans. UFFC Dec. 2010, we have proposed polymer- metal multilayer having function of impedance conversion equivalent to quarter wavelength layer and also proposed design of backing absorber using elastically soft adhesive and metal layer, which were formulated to iterative multilayer absorber. In this work, detailed parameters of materials used for these purpose were investigated and the performance of absorber were experimentally investigated and agreed with design values

Results

Input impedance of copolymer(PVDF-TrFE) with/without copper tape on surface was used for parameter fitting of the added layers, and it was found that mechanical Q of adhesive as 3.5-5.4 and velocity as 1250 m/s at 6MHz. Fig.1 shows transmitted signals from 3.5MHz wideband NDT transducer to 3.2 MHz PZT with 5, 10, 15, 20 layers (25um adhesive and 37um copper). The measured key parameters were determined to be 222dB/cm, 918m/s and 5.28 MRayl. Another example of 10 layers of average 2.5um sprayed adhesive and 38 um stainless steel produced 10MRayl at 7.4MHz. All these measured values are consistent with simple design equations of velocity, attenuation and impedance of iterative multilayer.

Discussion and Conclusions

Basics of acoustic waves in iterative multilayer is same as sequential L/C low pass filter, both of which have pass band, characteristic impedance, propagation velocity and attenuation expressed by the same mathematical formula. The design equations derived from such concept were compared with experimental results and showed fair agreement. The observed attenuation and acoustic impedance are comparable or higher than the conventional most attenuative tungsten-polymer mixture.

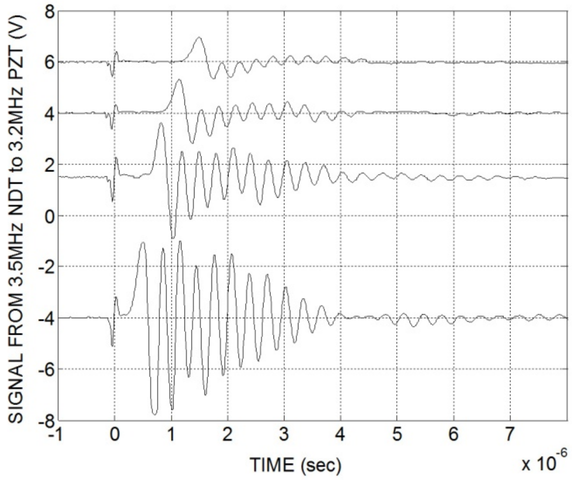

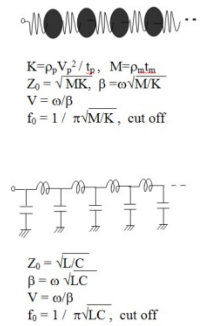

P2E-3

Design of Anti Cavitation Hydrophone by Deposition of Hydrothermally Synthesized Lead Zirconate Ttitanate Poly-crystalline Film on Reverse Surface of Titanium Film Front Layer

Shinichi Takeuchi[1], Mutsuo Ishikawa[1], Norimichi Kawashima[1], Takeyoshi Uchida[2], Masahiro Yoshioka[2], Tsuneo Kikuchi[2], Nagaya Okada[3], Minoru Kurosawa[4]; [1]*Department of Clinical Engineering, Toin University of Yokohama, Yokohama, Kanagawa, Japan,* [2]*National Metrogy Institute of Japan, National Institute of Advanced Industrial Science and Technology, Tsukuba, Ibaraki, Japan,* [3]*Honda Electronics Co.,Ltd, Toyohashi, Aichi, Japan,* [4]*Interdisciplinary Graduate School of Science and Engineering, Tokyo Institute of Technology, Yokohama, Kanagawa, Japan*

Background, Motivation and Objective

It is difficult to measure the high intensity ultrasound field with generation of acoustic cavitaion, since the electrode of hydrophone will be damaged by erosion from acoustic cavitation. Therefore, we developed the original hydrophone by using hydrothermally synthesized lead zirconate titanate poly-crystalline film with thickness of 15 um deposited on a reverse surface of a titanium film front layer with thickness of 50um as protection layer, acoustic receiving layer and GND electrode in order to realize a tough anti cavitation hydrophone. Our hydrophone could be used to measure the high intensity ultrasound field with generation of acoustic cavitation such as focal area of 1.6 MHz high intensity focused ultrasound (HIFU) treatment equipment with acoustic power from 10W to 250 W and in a vessel of a 47 kHz ultrasound cleaner with averaged acoustic intensity of about 0.29 W/cm2 without any damage. However, we observed the output waveform of the hydrophone without nonlinear distortion in spite of measurement in high intensity ultrasound field like focal area of 1.6 MHz HIFU treatment equipment.

Statement of Contribution/Methods

We considered on the cause of above problem and its improving methods by numerical computer simulation with MASON¡¦s equivalent circuit for hydrothermally synthesized lead zirconate titanate poly-crystalline film and one dimensional acoustic transmission model for the titanium front layer.

The effects by thickness of Ti front layer, specific acoustic impedance of backing material on frequency characteristics of receiving sensitivity were calculated for design of optimum structure of the anti-cavitation hydrophone

Results

It was found that the cause of above problem was decrease of its receiving sensitivity in higher frequency region. Furthermore, we could propose two types of structure of hydrophones with improved frequency characteristics of receiving sensitivities. One type hydrophone (TYPE-1) has titanium front layer thinner than 5um and epoxy resin backing material to improve the frequency characteristics. Another type hydrophone (TYPE-2) has 50ƒÝm thickness titanium front layer and backing material of titanium. The hydrothermally synthesized lead zirconate titanate poly-crystalline film with thickness of 15 um was deposited on a reverse surface of a titanium film front layer of both type of hydrophone.

Discussion and Conclusions

We expect to observe the received waveforms with nonlinear distortion and nonlinear harmonic components at focal area of 1.6 MHz HIFU treatment equipment with acoustic power of 250 W by using both types of anti cavitation hydrophones with improved frequency characteristics of receiving sensitivity. It is easier to fabricate the TYPE-2 hydrophone TYPE-2. Furthermore, TYPE-2 hydrophone has 1.5 times higher receiving sensitivity than TYPE-1 hydrophone.

P2E-4

High Frequency Single Element Transducer Based on Pad-printed Lead-Free Piezoelectric Thick Films

Franck Levassort[1], Karsten Hansen[2], Konstantin Astafiev[2], Jean-Marc Grégoire[1], Wanda. W. Wolny[2], Marc Lethiecq[1]; [1]Francois-Rabelais University, UMRS Imagerie & Cerveau, INSERM U930, TOURS, France, [2]MEGGITT A/S, Kvistgaard, Denmark

Background, Motivation and Objective

KNN-based lead free ferroelectric materials are receiving much attention due to their high electromechanical properties that make them promising candidates to replace the lead-based piezoceramics that will eventually be banned by environmental regulations in many countries over the world. Studies include the development of KNN thick films that are particularly well adapted for high frequency applications due to higher wave velocities and a dielectric constant in an acceptable range for single element transducers. In previous work [1], a KNN-LT composition paste was developed to deposit thick films by screen-printing on flat substrates. Here, a KNN-LT based thick film is deposited on a curved substrate by pad-printing in order to be used in a focused high frequency transducer.

[1] K. Hansen, IEEE Ultrasonics Symp., 1738-1741, 2009

Statement of Contribution/Methods

A porous lead-free KNN-LT cylinder was specifically developed to be used as a substrate for the thick film and as the transducer backing. It exhibits the required acoustical properties (acoustical impedance, high attenuation…) and is compatible with the high sintering temperature of the KNN-LT film. This leads to a simplified transducer fabrication and low production costs. This cylinder is machined on the top to have a curved surface with a radius of curvature corresponding to the desired focal distance. The rheological properties of the KNN-LT paste were optimized for pad-printing deposition process. Since this thick film is sensitive to moisture and humidity, an additional coating has been used. It was designed to serve as an acoustic matching layer. Based on this structure, a high frequency transducer was fabricated and the fabrication steps are presented.

Results

Acoustical properties of the backing were measured: an acoustical impedance of 11.4 MRa was observed. Electromechanical properties of the piezoelectric thick film in thickness mode were deduced from the measurement of the electrical impedance: in particular a coupling factor over 30% and a dielectric constant at constant strain of 150 were obtained. For the fabrication of transducer, an f-number of 2.5 was chosen with a focal distance at 10 mm. The center frequency is close to 30 MHz and the -6 dB bandwidth is 55%.

Discussion and Conclusions

The transducer was integrated in a high frequency imaging system and its performance allowed skin images to be produced. Finally its characteristics were compared to those of previously developed PZT-based transducers with similar geometry. To conclude, the replacement of lead-based high frequency transducers by “green” devices is a viable option.

P2E-5

Ultrasonic Properties of Bio-compatible Silicone Rubbers for Matching Transit-Time Piezoelectric Transducers during Blood Flow Estimation in Coronary Vessels

Luis Diez[1], Hector Calás[1], Antonio Ramos[1], **Tomas Gómez Álvarez-Arenas[1];** [1]Ultrasounds for medical and industrial applications (UMEDIA), Spanish National Research council (CSIC), Madrid, Madrid, Spain

Background, Motivation and Objective

Assessment of blood flow in coronary vessels during a bypass surgery is a key issue to assure the proper functioning of the bypass and hence the success of the operation.

Transit-time ultrasonic flow-metering is a good option for this purpose. This is a fast and non-invasive technique with some narrowband commercial solution already on the market and recent proposals in broadband regime. Requirements for the materials selection to couple the piezoelectric element of the probe to the vessels are demanding, especially for the new broadband dproposals: bio-compatibility, good acoustic impedance matching, low attenuation coefficient, low dispersion, low refraction at the probe/vessel interface and precise control of undesired propagation modes. In order to find a material that meets all these requirements it is necessary to measure accurately longitudinal and shear waves velocities and attenuation coefficients, and their variation (dispersion), over the frequency range 1.0-10.0 MHz.

Statement of Contribution/Methods

Seven different commercial silicone rubbers have been studied. Several samples out of each composition have been produced by changing the mix ratio and the curing conditions (gas evacuation, pressure and temperature).

Two different methods have been used, both in a through transmission configuration using normal and oblique incidence. i) Air-coupled resonant ultrasonic spectroscopy that enables us to obtain measurements in the frequency range 1-3 MHz and for incident angles between 0 and 10 degrees by means of the analysis of the thickness resonances. ii) A conventional water immersion method (1-10 MHz). The reason to use these two methods is twofold, first to obtain a better measurement of the attenuation at low frequencies where the attenuation is very low and can be better measured by using a resonant technique and, second, to obtain a comparison between the two methods.

Results

The obtained results are the velocity and the attenuation of ultrasound waves in different bio-compatible silicone rubbers produced under different conditions. These are used to get a viscoelastic model based on a variation of the attenuation coefficient with a power law and to select the best materials and their fabrication routes. A modelisation of the material response as matching material between the active piezoelectric material of the probe and the coronary vessels is produced.

Discussion and Conclusions

The possibility to engineer material properties in bio-compatible silicone rubbers by changing curing conditions to meet the requirement of the matching materials in transit-time probes for the assessment of the blood flow in coronary bypass surgery is discussed. Special attention is paid to impedance matching, refraction, generation of shear waves, attenuation and pulse distortion due to wave dispersion. An optimum solution is proposed and a design of the probe is discussed.

P2E-6

Lead-Free $K_{0.5}Na_{0.5}NbO_3$ and $Bi_{0.5}Na_{0.5}TiO_3$ piezoelectric films for high-frequency ultrasonic transducer applications

Xinwei Yan[1], **Wei Ren[1]**, Lingyan Wang[1], Hongfen Ji[1], Peng Shi[1], Xiaoqing Wu[1], Xi Yao[1], Qifa Zhou[2], Sien-Ting Lau[2], K. Kirk Shung[2]; *[1]Electronic Materials Research Laboratory, Xian Jiaotong University, China, People's Republic of, [2]NIH Transducer Resource Center and Department of Biomedical Engineering, University of Southern California, USA*

Background, Motivation and Objective

Because of outstanding properties of lead-based materials, such as $Pb(Zr,Ti)O_3$ and $Pb(Mg_{1/3}Nb_{2/3})O_3$-$PbTiO_3$, they have been extensively used in various piezoelectric applications. In recent years, concerning the ecological impacts from high Pb concentration in lead-based materials, lead-free materials have attracted much attention. However, there are few reports on the piezoelectric device applications made by lead-free materials.

Statement of Contribution/Methods

In this work, $K_{0.5}Na_{0.5}NbO_3$ (KNN) and $Bi_{0.5}Na_{0.5}TiO_3$ (BNT) thick films have been fabricated by a sol-gel technique. The KNN and BNT films were used to fabricate high-frequency needle transducers.

Results

The KNN and BNT films exhibit the perovskite structure.The dielectric constant, remnant polarization, coercive field are 826, 9.1 $\mu C/cm^2$ and 49.8 kV/cm for KNN film and 1050, 21.9 $\mu C/cm^2$, 71.1 kV/cm for BNT film, respectively. Figure 1 (Left) and Figure 2 (Right) are the XRD patterns and the frequency dependence of dielectric constant and loss tangent of BNT thick films annealed at different annealing temperatures. The performances of KNN-based and BNT-based transducers have been studied.

Discussion and Conclusions

The results suggest that KNN and BNT films are two of the potential lead-free piezoelectric materials for fabricating high-frequency transducers.

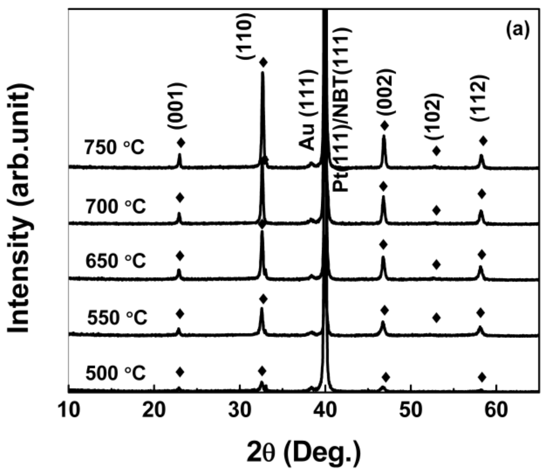

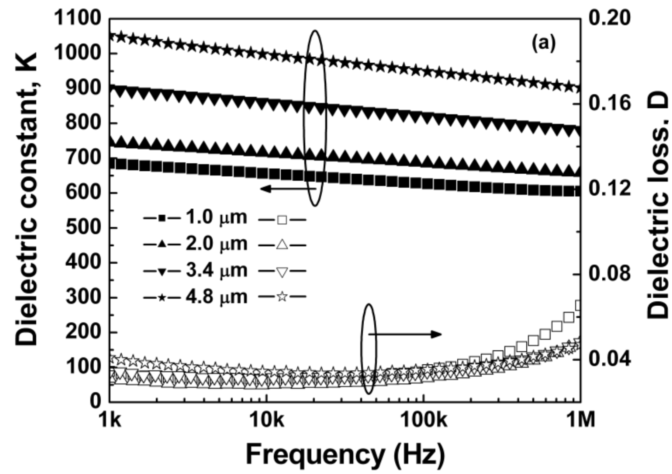

P2E-7

Electro-optical properties of Lead Zirconate Titanate composite films used in flexible high temperature ultrasonic transducers

Jeanne-Louise Shih[1], Maurice Cha-Kiu Cheung[1], Cheng-Kuei Jen[2]; [1]McGill University, Canada, [2]Industrial Materials Institute, National Research Council of Canada, Canada

Background, Motivation and Objective

The development of thick composite ceramic films has been of significant interest for different applications. One is high temperature (HT) ultrasonic non-destructive testing (NDT) or structural health monitoring (SHM) using ultrasonic transducers (UTs) that are non-bulky, flexible and broad in frequency bandwidth. Fabrication of such HTUTs have been demonstrated by a sol-gel spray method using sol-gel PZT. High volume production demands efficient methods of fabrication applicable to a chemical deposition technique such as sol-gel spray. One such may be a photoassisted method. A study of photoinduced properties of the PZT composite (PZT-c) films deposited by the sol-gel spray is presented.

Statement of Contribution/Methods

PZT-c films that had been dried and fired were found to be UV absorbant. Absorbance measurements were performed on PZT-c sprayed on glass and quartz slides and that had been either 1) treated at 350, 450, 550, 650 °C in air, in an oven or 2) exposed to high intensity UV light for several minutes. Measurements were also taken for films deposited on a quartz slide during UV exposure from a Xenon light source, optical chopper and lock-in amplifier centered at 350 Hz. As well, Differential Thermal Analysis and Thermograviometric Analysis (DTA/TGA) was performed under dark and UV illuminated conditions. Photoconductivity of the PZT-c film was measured by a 4-point-probe technique.

Results

PZT-c films that had been dried and fired showed absorbance down to 200 nm in wavelength, with the edge increasing with firing temperature except after 650°C. The absorbance edges of the films heat treated at 350, 450, 550, 650 °C were 375, 425, 440 and 427 nm. The absorbance spectrum of PZT-c film sprayed onto a quartz slide, dried in air and performed before and after several minutes of exposure to UV showed no change; however, that which was dried in air and tested during exposure to locked-in UV light showed a 50 nm shift in the absorbance edge to higher wavelength (450 nm) coupled with a collapse of the absorbance level at a wavelength of 410 nm and lower. The spectrum returned to its original level under dark conditions. DTA/TGA results showed a 10 °C shift to lower temperature in phase transition peak with exposure to UV. A photoconductivity of 107 μohm-1m-1 was measured for a 5 μm thick film.

Discussion and Conclusions

DTA/TGA results indicate mass and heat flow changes occurring at a lower temperature under UV illuminated conditions. Exposure on the PZT-c sol-gel sprayed film, found to be photoconductive, may thus affect the firing and annealing stages of film processing. Explicitly permanent changes in the absorbance of the film resulted from heat treatment, but not from exposure to UV; however a photoresponse during the exposure of film dried in air was detected. The effect of UV may in turn be associated with photoinduced charge effects that occur during exposure, which may be stimulating photochemical reactions associated with firing and annealing stages at lower temperatures.

P2E-8

Air-coupled Piezoelectric Transducer with Active Matching Layers

Tomas Gómez Álvarez-Arenas[1]; [1]Spanish National Research Council (CSIC), Madrid, Madrid, Spain

Background, Motivation and Objective

Optimum matching of piezoelectric transducers to the air to achieve a good sensitivity and a wide-band response is still an open research field. In particular, it is crucial for especially demanding applications as air-coupled pulse-echo operation mode and for one-side materials inspections.

Statement of Contribution/Methods

The approach presented consists of the use an aluminium metallized very low acoustic impedance porous polymer (0.05 MRayl) with an attenuation coefficient not very high (2500 Np/m at 600 KHz) and a stable piezoelectric response to produce the outer quarter-wavelength matching layer of a multilayered piezoelectric transducer. The rest of the transducer consists of a random 1-3 connectivity piezo-composite disk and a stack of two (intermediate) conventional quarter-wavelength matching layers. The transducer can be operated in conventional pulse-echo mode or, alternatively, it is possible to emit using the piezocomposite and to receive using the piezopolymer. This dual configuration is especially well suited for pulse-echo operation to avoid the influence of the electrical noise generated by the electrical excitation, to eliminate the influence of lateral modes and to increase the resolution

Results

First, the thickness resonance of the piezoelectric porous polymer is characterized in order to determine the working frequency of the transducer. Then the transducer is designed and constructed tune to this frequency as mentioned above. The transducer, is tested in conventional pulse-echo operation and in dual mode operation: emitting with the piezocomposite and receiving with the polymer. The figure shows the impulse response (200 V excitation, one semicycle of a square wave, and 10 dB gain in reception) and the amplitude of the FFT. Centre frequency is 300 KHz, and two-way insertion loss is -45 and -70 dB, for conventional and dual mode operation, respectively. 6 dB bandwidth is 21% and 26%, respectively.

Discussion and Conclusions

Sensitivity of the dual mode operation is lower due to the lower piezoelectric response of the polymer. However, the dual mode operation presents the advantage to have a lower level of noise and a larger bandwidth. In addition, both signals can be processed together to increase the temporal resolution of the transducer.

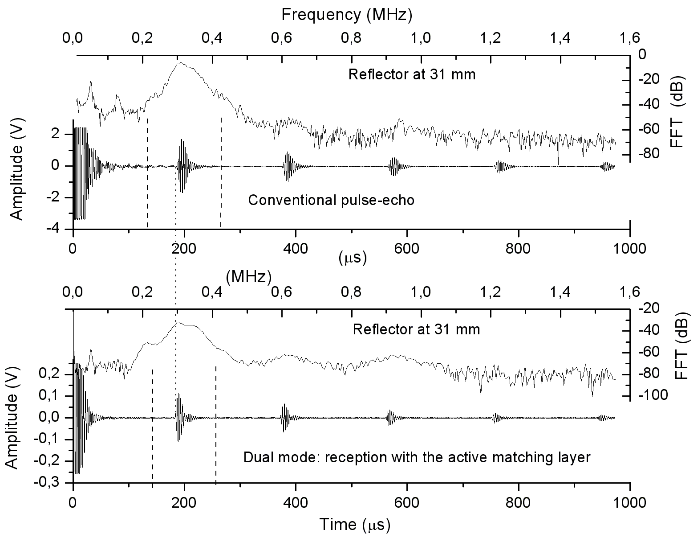

P2E-9

HfO2 High-k Dielectric Layers in Air-Coupled Capacitive Ultrasonic Transducers

Sean Mc Sweeney[1], **William M. D. Wright[1]**; [1]Electrical and Electronic Engineering, University College Cork, Ireland

Background, Motivation and Objective

Capacitive micro-machined ultrasonic transducers, due to tight control over the air gap height and membrane thickness, are highly efficient but difficult to produce with lateral dimensions of more than a few hundred microns due to residual stress in the larger area membranes. Small devices tend to be highly resonant, which compromises their use in certain air-coupled applications, where broadband large area devices are desirable. An effective compromise is to etch well-defined geometric features, such as an array of simple pits, into a silicon backplate electrode using standard bulk micromachining processes, then use a metallised polymer film as the other electrode to produce devices in the mm to cm scale. The capacitance of the device is largely determined by the dielectric constant of the film, and the use of additional dielectric coatings for devices at this scale may have a number of beneficial effects.

Statement of Contribution/Methods

This work investigates the effect of using HfO2 high-k dielectric coatings on the backplate electrodes of air coupled capacitive ultrasonic transducers, both theoretically and experimentally. A range of capacitive ultrasonic transducers consisting of etched silicon backplate electrodes, with a layer of HfO2 high-k dielectric and metallised PET film, were used in through-transmission as either a transmitter or a receiver. A broadband 1MHz transducer was used as the other receiver or transmitter, respectively. A range of HfO2 layers of different thickness were modelled and analyzed. A 1-D lumped element model was used to determine the accuracy in assessing the effect of high-k layer thickness. The selected experimental dependent variables were coating/no-coating, high-k dielectric thickness, polymer film thickness and bias voltage, with the experimental output being the coefficients of the appropriate model and the experimental system response.

Results

Experimental impulse response data for air coupled operation has shown that the sensitivity of the capacitive ultrasonic transducer has been enhanced by the addition of a layer of HfO2 high-k dielectric on the backplate electrode, as expected. The optimum layer thickness was determined to be 0.1μm, for this work with a non-linear relationship between layer thickness and device sensitivity emerging. Magnitude impulse response increases of greater than 15% have been obtained in this work, with simulations showing potential further gains possible. Simulation has also shown that electrical, mechanical and acoustic harmonic alignment allows tuning of the sensitivity/bandwidth trade-off for CUTs with a fine degree of accuracy.

Discussion and Conclusions

It was found that the application of a HfO2 high-k dielectric layer with a high field breakdown strength increased the sensitivity of capacitive ultrasonic transducers and allowed the electrical and mechanical harmonics of the transducer to be appropriately synchronized, leading to an increased device efficiency.

P2E-10

PIN-PMN-PT Piezoelectric Crystals with Increased Rhombohedral-to-Tetragonal Phase Transition Temperature

Jun Luo[1], Shujun Zhang[2], Wesley Hackenberger[1], Thomas Shrout[2]; [1]TRS Technologies, Inc, USA, [2]Pennsylvania State University, USA

Background, Motivation and Objective

Single crystal relaxor ferroelectrics, $Pb(Mg_{1/3}Nb_{2/3})O_3$ - $PbTiO_3$ (PMN-PT), have shown great promise for medical imaging and sonar transducers. Medical ultrasound imaging transducers built upon PMN-PT crystals have been commercialized for several years; meanwhile, broad bandwidth and compact sonar transducers based on PMN-PT crystals have also been demonstrated by NAVY sponsored programs. However, limited by their low rhombohedral-to-tetragonal phase transition temperature (T_{rt} < 100°C), PMN-PT crystals cannot be applied to the transducers operated at the elevated temperature. This work demonstrated that, by increasing PIN concentration in ternary $Pb(In_{1/2}Nb_{1/2})O_3$ - $Pb(Mg_{1/3}Nb_{2/3})O_3$ - $PbTiO_3$ (PIN-PMN-PT) crystals, the usage temperature can be expanded significantly.

Statement of Contribution/Methods

For compositions near the morphotropic phase boundary (MPB), it was reported that binary PIN-PT (PT<32%) ceramics possess T_{rt} larger than 200°C; while our work demonstrated that 46%PIN-PMN-(29-33%)PT ceramics have T_{rt} between 165°C and 180°C. In this work, it was found that perovskite phase PIN-PMN-PT crystals can be grown directly from the melt until PIN reaches a very high concentration. PIN-PMN-PT single crystals with PIN up to 49% have been directly grown from the melt by the Bridgman method. The piezoelectric and dielectric properties of them were measured.

Results

By increasing PIN concentration from 29% to 36% in rhombohedral PIN-PMN-PT crystals (PT~28%), T_{rt} was elevated from 121°C to 139°C, while the piezoelectric coefficient (d_{33}) and electromechanical coupling (k_{33}) of the crystals remained high (1000- 2200pC/N and 88-95% respectively). For crystals grown from PIN-PMN-PT with 49%PIN, volatilization of In_2O_3 and PbO became significant, which shifted the composition too close to the MPB, resulting in decreased T_{rt} (~100°C). Currently, the composition optimization of PIN-PMN-PT with 49% PIN is ongoing. The coercive field (E_C) of above crystals was measured to be about 4-6kV/cm, double the value of their binary counterpart PMN-PT crystals.

Discussion and Conclusions

It was demonstrated that T_{rt} can be significantly increased by adding more PIN into the ternary PIN-PMN-PT crystals; however, it strongly affected by the composition, depending on how close it is to the MPB. Fine tuning of both PIN and PT is critical to achieve high T_{rt} without compromising the piezoelectric performance.

P2E-11

High Frequency (>200 MHz) Focus Transducer with Lead-free KNN-BNT 0-3 Composite Film

Sien Ting Lau[1], Xiang Li[1], Ruimin Chen[1], **Qifa Zhou[1]**, K. Kirk Shung[1], Hongfen Ji[2], Wei Ren[2]; [1]Biomedical Engineering, University of Southern California, USA, [2]Electronic Materials Research Laboratory, Xian Jiaotong University, China, People's Republic of

Background, Motivation and Objective

High frequency (HF) ultrasonic imaging has been extensively used in non-invasive imaging of body tissues. Recently, HF ultrasound may find other significant biomedical applications such as acoustic microscopy for non invasive investigation of living cells and acoustic tweezers for non contact manipulation of microparticles or cells. In this work, we use composite sol-gel method to make good quality piezoelectric film for HF transducer application. The performance of a focus transducer with the center frequency over 200 MHz is presented.

Statement of Contribution/Methods

In this report, a modified 0-3 composite sol-gel technique was used to prepare the K0.5Na0.5NbO3-Bi0.5Na0.5TiO3 (KNN-BNT) films. The KNN ceramic powders were dispersed in the BNT precursor solution to form the uniform slurry which was spin-coated on (111) Pt/TiO2/SiO2/Si substrates. To improve the structure and density of the films, buffer layers and vacuum filtration were used during the deposition process. The structure and electrical properties of the films were evaluated before subsequent transducer fabrication. A focus transducer (with f# ~2) was built by press-focusing method. The pulse-echo response of the transducer was examined.

Results

The KNN-BNT composite film exhibits a well-crystallized perovskite structure without formation of any second phase. The dielectric constant and loss of the composite film measured at 1 kHz are ~ 900 and 0.06, respectively. The film has a remnant polarization Pr of 25 iC/cm2 and coercive field Ec of 100 kV/cm. Using this composite film as the active element, a 230 MHz high frequency focus transducer with a -6dB bandwidth of 65 MHz (fractional bandwidth ~ 30%) has been fabricated as shown in Fig. 1.

Discussion and Conclusions

Lead-free KNN-BNT thick films have been successfully fabricated on Si substrate by modified 0-3 composite sol-gel method. The KNN-BNT films exhibit good dielectric and ferroelectric properties. A press-focus transducer fabrication process utilizing this composite film has been also demonstrated. The center frequency and -6dB bandwidth of the transducer are 230 MHz and 30%. The two-way sensitivity of the transducer is ~ 32 dB. Experimental results imply that this device has a potential on the very high frequency biomedical applications, not only used in imaging systems but also in non-contact manipulation of biological cells/microparticles.

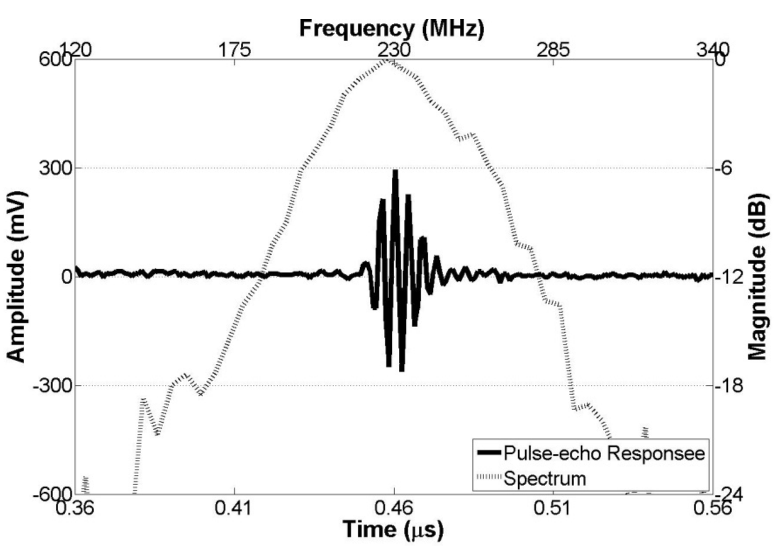

Thursday Oral Sessions

1D - Bio-effects and Dosimetry

Boca Rooms II-IV

Thursday, October 20, 2011, 8:00 am - 9:30 am

Chair: **William O'Brien**
Univ. of Illinois at Urbana-Champaign

1D-1

8:00 AM Dosimetry and Therapeutics

Gail Ter Haar[1]; [1]Institute of Cancer Research, UK

Background

There is increasing interest in the use of ultrasound for its therapeutic potential, whether for increasing drug activation or uptake, or for creating volumes of thermally ablated tissue (High intensity Focused Ultrasound HIFU). These applications entail the use of higher powers and longer pulse lengths than are usual for ultrasound imaging, and thus carry with them different challenges for measurement of the acoustic fields. Therapeutic benefit is obtained through the thermal and mechanical effects induced in tissue. What is important here is to determine the pressure or intensity in the region being targeted, and thus to differentiate between "exposure" and "dose".

Methods

Therapeutic ultrasound fields are usually mapped using piezo-electric or fibre optic hydrophone probes. The pressure distribution can also be visualised using Schlieren or holographic techniques. Intensity distributions can be inferred by imaging the heating of an acoustic absorber using an infra-red camera. Acoustic power is measured using radiation force of calorimetric techniques.

Once the field has been characterised under free field conditions in water, it is necessary to "derate" it to estimate the level at the target site. Here, *in situ* intensity or pressure is usually used, but for HIFU ablation, thermal dose is the parameter most commonly quoted.

Results

Representative field distributions and acoustic power measurements will be discussed, as will the validity of the thermal dose concept at the high temperatures used for thermal ablation.

Conclusions

Existing field characterisation methods are appropriate for many "low power" therapeutic ultrasound applications. However, the small focal regions, on-linear propagation and cavitation that are characyeristic of HIFU fields require new techniques to be developed. No fully satisfactory dosimetric parameter has yet been identified for therapeutic ultrasound applications.

1D-2

8:30 AM Mechanobiologic Acoustics On Bone Cellular And In Vivo Adaptation

Yi-Xian Qin[1], Shu Zhang[1], Suzanne Ferreri[1], Jiqi Zhang[1]; [1]Biomedical Engineering, SUNY Stony Brook, Stony Brook, New York, USA

Background, Motivation and Objective

It is well documented that ultrasound, as a mechanical signal, can produce a wide variety of biological effects in vitro and in vivo. The purpose of the current study was to (1) develop a methodology to allow for in-vitro manipulating osteoblastic cells using acoustic radiation force generated by ultrasound, (2) use this methodology to determine the morphological and biological responses of bone cells to ultrasound, and (3) mitigate bone loss under estrogen deficient osteopenia.

Statement of Contribution/Methods

In Vitro Cellular Manipulation: We used a therapy focused transducer, which has spherical cap with 64 mm diameter and 62.64 mm focal length. A laser guide MC3T3-E1 osteoblastic cells were cultured in α-MEM containing 1% penicillin-streptomycin and 10% decomplemented newborn calf serum. In Vivo OVX Model: 72, 16 w.o. Sprague-Dawley rats were divided into six groups; baseline control, age-matched control, OVX control, OVX + 5 mW/cm^2 ultrasound (US), OVX + 30 mW/cm2 US and OVX + 100 mW/cm^2 US. Low intensity pulsed ultrasound (LIPUS) was delivered transdermally at the L4/L5 vertebrae, using gel-coupled plane wave US transducers. The signal was applied 20 min/day, 5 days/week for 4 weeks.

Results

In Vitro Cellular Response: The developed methodology allowed manipulation of MC3T3-E1 cells by acoustic radiation force. The deformation of cell membranes was observed by the US manipulation, which appeared after 15s treatment of pulsed ultrasound in 6W. We also imaged the movement of primary cilia, which showed corresponding movement when subjected to pulsed ultrasound. In Vivo Response: LIPUS treatment significantly increased BVF compared to OVX controls for the 100mW/cm^2 treated group. Interestingly, the 100mW/cm^2 treated groups showed a significant improvement over the 5mW/cm^2 treated group.

Discussion and Conclusions

Pulsatile focused ultrasound can create local fluid flow nearby cells. The observed primary cilia can be triggered to dynamic movement by the acoustic force as a mechanobiologic effect. In vivo results suggest that low-intensity pulse ultrasound can induced mechanical wave in tissue and initiate bone adaptation. These findings support the hypothesis that LIPUS can inhibit bone loss and preserve bone strength under conditions of estrogen deficient osteopenia.

THURSDAY ORAL

1D-3

8:45 AM Heat Shock Protein Expression in Sonoporated Myeloid Leukemia Cells

Wenjing Zhong[1], Pingping Jiang[2], Hualin Wang[2], Jennifer M. F. Wan[2], **Alfred C. H. Yu[1]**; [1]Medical Engineering Program, The University of Hong Kong, Hong Kong, [2]School of Biological Sciences, The University of Hong Kong, Hong Kong

Background, Motivation and Objective

Much remains unknown over how cells internally respond to the sonoporation stress induced by acoustic cavitation. Although the stress is known to be transient (i.e. cell membrane would reseal quickly), it may upset cytoplasmic signaling and in turn trigger a series of intracellular changes that eventually make cells become unviable. In this work, we investigate the sonoporation-induced stress response of HL-60 leukemia cells using a proteomics approach that allows systematic analysis of the intracellular proteins. Our present focus is on targeting the heat shock proteins (HSP) that play a crucial role in a cell's pro-survival response against an external stress (not necessarily thermal-related).

Statement of Contribution/Methods

HL-60 cells were grown in suspension culture and were prepared in a well plate (10e6 cells/ml). In the presence of 1% v/v microbubbles, the cells were exposed to pulsed ultrasound for 1 min to trigger sonoporation (0.5MPa peak negative pressure, 1MHz freq., 10% duty cycle, 1kHz PRF). The sonoporated cells were then re-incubated and were lysed after 6h to analyze their protein expression using two-dimensional (2D) electrophoresis: lateral dimension depicts the pH gradient and it was carried out after active rehydration and isoelectric focusing; vertical dimension depicts molecular weight and it was performed with 1.0-mm-thick 12.5% polyacrylamide gel electrophoresis. The 2D gels were stained with a SYPRO Ruby dye, and they were scanned to generate gray-scale images. The protein expression level of various spots on the gel images was computationally obtained on using PDQuest 8.0 software and the protein distribution of spots with significant expression were subsequently identified using mass spectrometry. These were compared against those for cells that received sham exposure to facilitate analysis.

Results

Changes in the expression of different HSPs were evident in the sonoporated cells at 6h after exposure. In particular, Hsp70 (HSPs with 70 kDa molecular weight) was found to be up-regulated (high spot intensity, compared with very weak spot expression for control). As Hsp70 is a known suppressor of apoptosis signaling, this observation suggests that pro-survival signaling has been activated within the sonoporated cell. On the other hand, Hsp60 (60kDa-weighted HSPs) was found to be down-regulated (62.8% intensity decrease over control). This directly increased pro-apoptotic activity through mitochondrial release of molecules that enhanced the expression of caspase executor proteins: a finding that helps explain why apoptosis was seen in some sonoporated cells.

Discussion and Conclusions

Hsp60 inhibition seems to take part in sonoporation-induced apoptosis, whilst Hsp70 up-regulation may be related to sonoporated cells undergoing repair. These insights on how cells respond to the sonoporation stress may contribute to the design of advanced strategies for sonoporation-mediated treatment and drug delivery.

1D-4

9:00 AM In Vivo Microbubble Cavitation Imaging

Francois Vignon[1], Jinjin Liu[2], William Shi[1], Jeffery Powers[3], Feng Xie[2], Shunji Gao[2], Lucas Drvol[2], John Lof[2], Carr Everbach[4], Thomas Porter[2]; *[1]Philips Research North America, Briarcliff Manor, NY, USA, [2]University of Nebraska Medical Center, Omaha, NE, USA, [3]Philips Healthcare, Bothell, WA, USA, [4]Swarthmore College, Swarthmore, PA, USA*

Background, Motivation and Objective

Stroke is the #2 cause of death and #1 cause of disability worldwide. Less than 5% of ischemic stroke patients receive the state-of-the art treatment (tPA), and only about 10% of these receive additional benefit from it. Ultrasound (US)-induced microbubble (MB) cavitation has been shown to enhance the efficacy of the tPA drug, and dissolve clots without tPA. Such a Sonothrombolysis (STL) treatment requires monitoring and control of MB cavitation to ensure its reproducible efficacy and safety. In particular it is important to avoid high levels of inertial cavitation, which has been associated with intracerebral hemorrhages. To this end a system has been developed, capable of image-guided STL and cavitation monitoring.

Statement of Contribution/Methods

STL therapy was conducted on 24 pigs in a safety and efficacy study. A US imaging system (iE33 with S51 probe, Philips Healthcare) was modified with capability of sending ensembles of 4 1.6MHz STL pulses of variable lengths (5, 20, or 44µs) transtemporally into 20 directions inside a 57° sector area. A systemic MB infusion was administered (2% Definity; Lantheus Medical). After STL treatment was completed, backscattered data from MBs were spectrally analyzed to image cavitation state: ultraharmonics indicated stable cavitation (SC) and broadband noise indicated inertial caviatation (IC). Low levels of either were classified as Moderate Oscillations (MO).

Results

Cavitation imaging allowed imaging the relative importance of the dominant cavitation states (MO, SC and IC) inside the treatment area and their variations as a function of acoustic amplitude (Figure: MO are color-coded in green, SC in yellow, IC in red; the brightness indicates cavitation intensity). The lateral resolution is ~3mm at 6cm depth, and the axial resolution depends on the pulse length (3cm at 20µs). The temporal evolution of cavitation could also be assessed, showing that one STL frame destroys all MBs in the treatment area at derated peak negative pressures down to 0.6MPa.

Discussion and Conclusions

An ultrasound STL system capable of imaging cavitation states within the treatment area was prototyped based on a commercial ultrasound scanner. Its functionality was demonstrated in living pigs with transtemporal US administration into the brain. Such a system will be critical for the reproducible safe and effective administration of STL treatment of ischemic stroke.

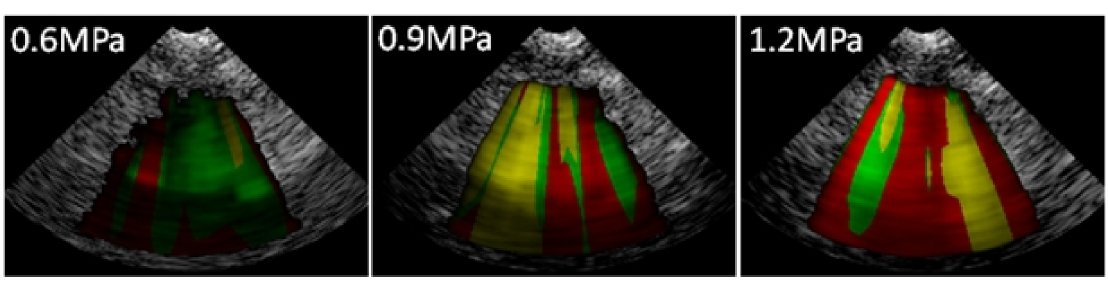

1D-5

9:15 AM Biological Effects of Acoustic Droplet Vaporization in Gas Embolotherapy

Robinson Seda[1], J. Brian Fowlkes[2], Joseph Bull[1]; [1]Biomedical Engineering, University of Michigan, Ann Arbor, MI, USA, [2]Radiology, University of Michigan, Ann Arbor, MI, USA

Background, Motivation and Objective

It is envisioned that selectively formed gas bubbles will function as emboli in a novel cancer treatment called Gas Embolotherapy. These bubbles, formed as a result of acoustic vaporization of encapsulated superheated liquid droplets by focused ultrasound, are sufficiently large to lodge in microvessels, occluding blood flow to tumors causing necrosis. Additionally, these droplets may also be useful as drug carriers. Endothelial cells, lining of the blood vessels are directly affected by the acoustic droplet vaporization process. Consequently, the study of the endothelium-vaporization interactions is particularly important to understanding the potential bioeffects that may result from this approach.

Statement of Contribution/Methods

Endothelial cells were cultured to 90+ percent confluency in OptiCell culture chambers prior to the experiments. Dodecafluoropentane (DDFP) droplets with an albumin shell were introduced inside the chambers and were exposed to a single 20-cycle pulse from a 3.5MHz transducer at different acoustic pressures (7.02, 8.25, 9.14 and 9.78MPa). The chamber was maintained at 37°C. OptiCells were examined through brightfield, phase contrast and fluorescence microscopy after the vaporization process to account for cell damage.

Results

An affected area fraction (affected area/total area) was obtained and compared to our controls: untreated cells and cells treated with ultrasound (US) alone. No cell damage was observed for the case of US alone. Cell damage was induced by all treatments containing droplets, but it was significantly higher ($p<0.05$) when the pressure was 9.78MPa. This pressure accounted for an affected area fraction that was between 2.2 to 3.1 times greater than the affected area fraction generated by the lower pressures studied.

Discussion and Conclusions

This significant increase in cell damage is thought to be caused by the action of inertial cavitation when the pressure is near or above 9.78MPa. Injury to endothelial cells could be reduced if we operate in a pressure regime far below this inertial cavitation regime, but cell damage near vaporization sites may still result in an impairment of important endothelial functions in vivo.

This work was funded by NIH grant R01EB006476.

2D - Cardiovascular Imaging

Boca Rooms VI-VII

Thursday, October 20, 2011, 8:00 am - 9:30 am

Chair: **Chris de Korte**
Catholic Univ. of Nijmegen

2D-1

8:00 AM Performance of elastic image registration against speckle tracking for 2D cardiac motion and strain estimation

Brecht Heyde[1], Ruta Jasaityte[1], Stefaan Bouchez[2], Michael Vandenheuvel[2], Piet Claus[1], Patrick Wouters[2], Jan D'hooge[1,3]; [1]Cardiovascular Imaging and Dynamics, Catholic University of Leuven, Leuven, Belgium, [2]Department of Anesthesiology, Ghent University, Ghent, Belgium, [3]Medical Imaging Lab, Norwegian Institute for Science & Technology, Trondheim, Norway

Background, Motivation and Objective

Two major approaches exist for ultrasound based cardiac strain estimation. One approach is based on RF or envelope-based speckle tracking with *a posteriori* regularization of the block matching output. A second approach is elastic image registration which takes both the image data and a-priori information on the characteristics of the motion field into account *during* the motion estimation process. In this study we compared both approaches directly to a gold standard in an in-vivo setting.

Statement of Contribution/Methods

In 5 open-chest sheep, parasternal short-axis B-mode images were acquired at a mid-ventricular level using a GE Vivid7 (GE Healthcare; 2.5MHz; frame rate 50-70Hz). Images were taken at rest and during acute ischemia induced by ligation of a coronary artery. In 3 animals, data was also recorded during inotropic modulation by infusion of esmolol and dobutamine. Reference radial (eR) and circumferential (eC) strain were obtained using sonomicrometry in the infero-lateral (IL) mid-ventricular wall. Three radial traces were excluded due to poor quality resulting in 16 and 13 data sets for analysis of eC and eR respectively.

All images were analyzed using a well validated and commercially available block-matching based approach (GE EchoPac). After manual myocardial segmentation and subsequent tracking, end-systolic eC and eR values were extracted in the IL wall.

Next, the data sets were processed using an in-house developed elastic registration approach based on a 3rd order tensor-product B-spline multi-resolution transformation model. Inter-frame motion was estimated iteratively using a gradient descent routine and SSD as a similarity. Smoothness of the motion field was imposed by adding a bending energy penalty to the cost function. After manual contouring endo and epicardial boundaries, eC and eR values were calculated from the B-spline motion field in the IL wall.

Results

Correlation coefficients for eC and eR were 0.85 and 0.63 for block matching, and 0.83 and 0.88 for the registration method (Figure).

Discussion and Conclusions

While performance of a validated block matching approach and our elastic registration method was comparable for the eC component (p=0.40), imposing regularization during the motion estimation process (i.e. elastic registration) showed to be advantageous to estimate eR as it improved performance significantly (p=0.02).

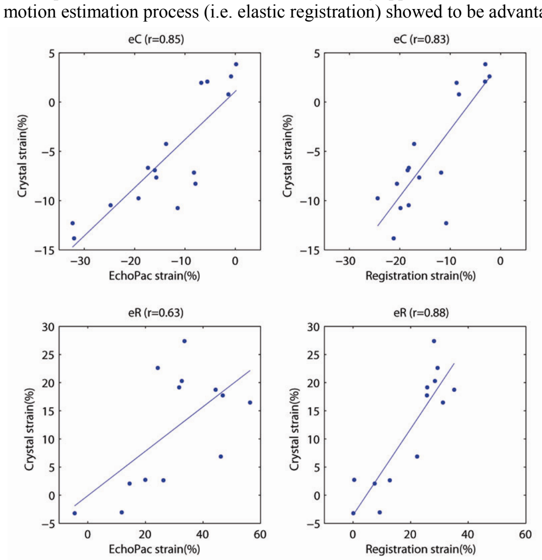

2D-2

8:15 AM Real-time Motion Tracking for Non-invasive Ultrasound Cardiac Therapy

Ryan Miller[1], Yohan Kim[1], Kuang Wei Lin[1], Gabe Owens[2], Charles Cain[1], Zhen Xu[1]; [1]Biomedical Engineering, University of Michigan, Ann Arbor, Michigan, USA, [2]Pediatrics, University of Michigan, USA

Background, Motivation and Objective

The primary motivation is to develop a real-time motion tracking algorithm to use in conjunction with ultrasound cardiac therapy. Cardiac and respiratory motion are significant concerns for achieving high treatment efficiency in cardiac ultrasound therapy. This paper develops a fast target motion tracking algorithm integrated with real-time ultrasound imaging for histotripsy-mediated cardiac therapy.

Statement of Contribution/Methods

Motion tracking is performed by finding the best match in an ultrasound image to a reference target image (5MHz phased array, Verasonics system). A diamond search produces an estimate using the criteria of minimum absolute difference, which is refined by a weighted average with its expected position (Kalman filter). For proof of concept only axial motion was considered, and the axial component of this estimate is transferred to a 1 MHz annular therapy array. Improvement in therapy efficiency was assessed by measuring the erosion rate in a tissue phantom (3% agarose, 2.5% graphite phantom). The 3 to 4mm thick phantoms were displaced in a pulsatile fashion from 3 to 12.5mm along the therapy axis and treated until fully perforated. Erosion rate was calculated as phantom thickness divided by the exposure time necessary to perforate the phantom. The motion tracking system was also tested on ex vivo porcine cardiac tissue with 1 minute exposures and comparison of the resulting lesions.

Results

The motion tracking system operated at an average frame rate of 72 Hz, tracking displacements over 20 mm and peak velocities up to 100 mm/sec. Testing in tissue phantoms showed that the mean erosion rate with motion tracking was maintained within 85% of the control (no target motion) erosion rate for all displacements. This compares to a steady decline in erosion rate to 30% of control with increased displacement without motion tracking (fig 1a). In the ex vivo samples, motion tracking produced greater tissue erosion than without, creating lesions comparable to the control case (fig 1b).

Discussion and Conclusions

Our algorithm has sufficient speed to lock histotripsy therapy onto any physiologically relevant motion, providing significantly higher efficiency than unguided therapy. By replacing our annular therapy array with a 3D steerable phased array, this system has the potential to become a valuable tool for histotripsy therapy of cardiac or any other fast moving tissue.

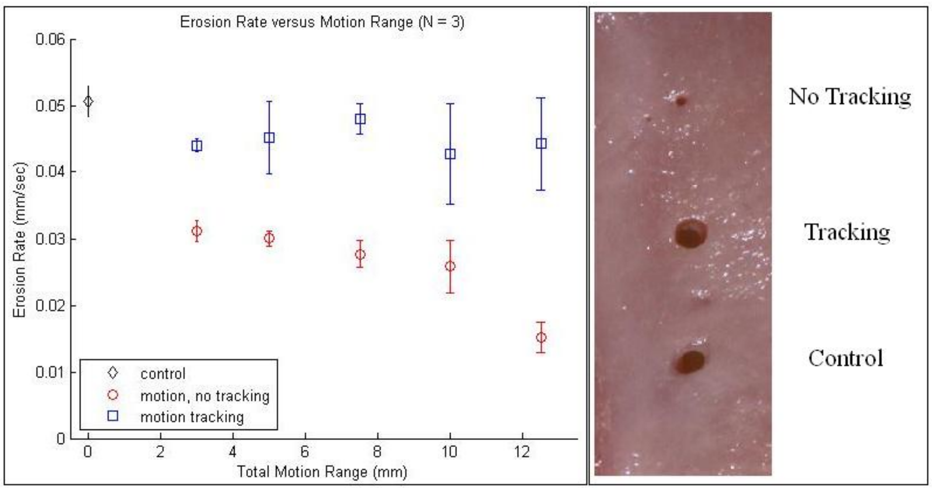

Figure 1: (a) (b)

2D-3

8:30 AM The measurement of layer-specific circumferential strain improves the detection of myocardial viability

Noa Bachner-Hinenzon[1], Offir Ertracht[2], Assaf Malka[2], Marina Leitman[3], Zvi Vered[3], Ofer Binah[2], **Dan Adam[1]**; [1]Biomedical engineering, Technion - Israel institute of technology, Israel, [2]Department of Physiology, Ruth and Bruce Rappaport Faculty of Medicine, Technion - Israel institute of technology, Israel, [3]Department of Cardiology, Assaf Harofeh Medical Center, Israel

Background, Motivation and Objective

The assessment of myocardial viability by echocardiography is of high interest. Since the Myocardial Infarction (MI) injury is inhomogeneous among the myocardial layers, the evaluation of myocardial viability should be separately evaluated for each myocardial layer. To evaluate the contribution of each myocardial layer to the myocardial deformation, a Layer-Specific Speckle Tracking Echocardiography (LS-STE) approach was recently developed. This method is based on a wavelet denoising smoothing process that is applied to the myocardial velocities. In this study the layer-specific strain values, calculated by the LS-STE method, are evaluated against histological analysis for MI size and location. In addition, since a reliable detection of the extent of MI is important, the present study investigated the hypothesis that measurement of layer-specific circumferential strain (SC), instead of the strain across the total-wall-thickness, will improve the detection of MI.

Statement of Contribution/Methods

Thirteen rats underwent occlusion of the left anterior descending artery for 30 minutes, followed by reperfusion. Three short-axis scans, using a VIVIDi system and 10S probe (GE Healthcare, Inc), were obtained at baseline and at 24 hours of reperfusion. The scans were post-processed by the LS-STE program to measure the peak SC at the endocardium, middle layer, epicardium and for the total-wall-thickness. Thereafter, the rats were sacrificed, and the MI size and location were determined by Triphenyltetrazolium Chloride staining method. The specificity and sensitivity in the detection of MI by using layer-specific SC was measured by a receiver operating characteristics method.

Results

The histological analysis results for the apical and papillary muscles levels classified 77 normal segments, 38 non-transmural MI segments and 41 transmural MI segments. MI classification as transmural and non-transmural was more accurate when based on the peak SC of the endocardium or middle layer, compared to the SC of the total-wall-thickness ($P<0.05$). Moreover, the specificity and sensitivity of the peak SC of the endocardium in detecting non-transmural MI was 92% and 87%, respectively, while the peak SC of the total-wall-thickness reached specificity and sensitivity of 76% and 82%, respectively.

Discussion and Conclusions

This validation study shows that evaluation of layer-specific myocardial function is feasible on a rat model by using standard echocardiography. Furthermore, the utilization of layer-specific SC is advantageous over the assessments of SC for the total-wall-thickness in the detection of MI according to the specificity on sensitivity.

2D-4

8:45 AM 2D myocardial strain in the mouse through spatial compounding: in-vivo feasibility study

Florence Kremer[1], Vesselina Ferferieva[1], Hon Fai Choi[1], Jan D'hooge[1,2]; [1]Lab on Cardiovascular Imaging & Dynamics, Department of Cardiovascular Diseases, Catholic University of Leuven, Leuven, Belgium, [2]MI lab, Norwegian Institute for Science & Technology, Trondheim, Norway

Background, Motivation and Objective

Myocardial strain can give valuable information on regional cardiac function. Speckle tracking is often used for this purpose as it can estimate the 2D myocardial strain tensor. However, in the mouse setting, speckle tracking remains challenging due to the high heart rate and the relatively thin wall compared to the typical size of the speckles. We have previously shown with simulated data sets that spatial compounding of axial velocities obtained at 3 steering angles can outperform 2D speckle tracking for 2D strain estimation in the mouse heart. The aim of this study was thus to test the feasibility of this compounding approach in-vivo.

Statement of Contribution/Methods

Five normal mice were anesthetized using isoflurane (1.5%) and placed on a heating pad to maintain body temperature. Mid-level short-axis images were acquired using a GE Vivid7 machine equipped with an i13L linear array transducer emitting at 14MHz. In order to get a stable image plane that allows for proper compounding, the transducer was attached to a mechanical holder. Tissue Doppler images were recorded at steering angles of -20°, 0° and +20° at a frame rate of 200Hz. Next, endo- and epicardial contours were traced at end-diastole on the 0° image and projected on the other data sets. Axial velocities were compounded and the obtained motion field was regularized using a Gaussian. Based on this reconstructed 2D vector field, both contours were updated and the compounding was repeated for the next frame. The myocardium was divided in 6 equally sized segments around the circumference and a plane was fitted through the motion field in order to calculate segmental radial and circumferential strain. Finally, strain curves were drift compensated and temporally smoothed.

Results

Mean radial and circumferential strain curves for each segment are shown below together with their standard deviation. Two segments out of 30 were excluded due to a reverberation artifact.

Discussion and Conclusions

This study shows that applying spatial compounding in-vivo for 2D strain estimation in the mouse heart is feasible. It can be noticed that circumferential strain is more reproducible than radial strain. Regional differences can be seen, especially between anterior regions and inferior regions. Further research is needed to quantify the performance of the algorithm against a reference method in normal and in abnormal animals.

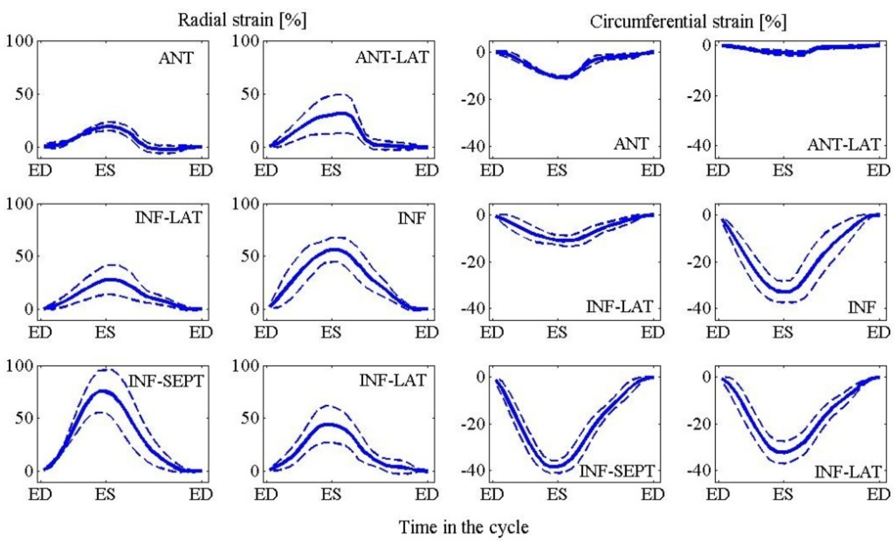

2D-5

9:00 AM 3D Time-Resolved In Vivo Strain Imaging and Elastography of the Human Aorta

R.G.P. Lopata[1,2], H.H.G. Hansen[3], E.M.H. Bosboom[1,2], G.J.L.M. Jongen[1], G.W.H. Schurink[4], C.L. de Korte[3], F.N. van de Vosse[1,2]; [1]Cardiovascular Biomechanics, dept. of Biomedical Engineering, Eindhoven University of Technology, Eindhoven, Netherlands, [2]Biomedical Engineering, Maastricht University, Maastricht, Netherlands, [3]Clinical Physics Lab, Children's Hospital, Radboud University Nijmegen Medical Center, Nijmegen, Netherlands, [4]Department of Surgery, Maastricht University Medical Center, Maastricht, Netherlands

Background, Motivation and Objective

Rupture of an abdominal aortic aneurysm (AAA) is an important cause of death in Western world. Currently, only generic measures such as aneurysm size (> 5.5 cm) and growth rate (> 1 cm/year) are used to decide on treatment to prevent rupture. Surgical intervention, however, carries substantial risk. Mechanical modelling using finite element methods based on CT images was introduced. This promising approach revealed the aneurysm wall stress in a patient-specific way. However, part of the required biomechanical parameters is still literature-based and thus generic. Besides, a less invasive imaging modality is required to monitor aortic wall properties and growth over time. To satisfy both these requirements, 3D ultrasound is proposed. In this study, 3D time-resolved strain imaging and in vivo elastography was explored in normal subjects.

Statement of Contribution/Methods

Three-dimensional radiofrequency data of the abdominal aorta were acquired during one cardiac cycle using a Philips iE33 ultrasound scanner and an X7-2 matrix array probe in 11 normal subjects (age = 22 – 47 yrs). Simultaneously, blood pressure was monitored real-time using a NexFin (BMEYE, NL). Manual segmentation of the aorta was performed by indicating the vessel axis and local radii. The RF data were processed using a 3D coarse-to-fine displacement estimation algorithm. The radial (R), circumferential (C) and longitudinal strain (L) were estimated. Furthermore, the compliance, distensibility and Young's modulus were derived from the 4D displacement data. For the Young's modulus, a thin-walled tube geometry was assumed.

Results

Strains in three orthogonal directions over time were obtained for the aortic over a length of 3 to 6.5 cm. The resulting maximum strains had a median value of R = -5.6% (interquartile range (IQR) = -8.0 – -4.2%), C = 6.5% (IQR = 4.1 – 8.4%) and L = 1.8% (IQR = 1.2 – 2.7%). Results revealed a median compliance per vessel length (m) of 4.5 mm^2/kPa (IQR = 4.0 – 4.7 mm^2/kPa) and distensibility of 22 MPa^{-1} (IQ = 20 – 33 MPa^{-1}). The median Young's modulus was 430 kPa (IQR = 260 – 650 kPa), which is in accordance with our previous 2D work.. The distensibility was found to be significantly larger for the older subjects ($p < 0.03$, $\alpha = 5\%$), but no significant differences in Young's modulus were found.

Discussion and Conclusions

The first results on 3D time-resolved strain imaging and in vivo elastography of the abdominal aorta seem promising despite limitations, such as the field-of-view of the transducer and the differences between the measured brachial blood pressure and the actual aortic blood pressure. In the future, the ultrasonic measurement of biomechanical vessel properties will enable patient-specific modelling of AAAs. This combination of noninvasive functional imaging and mechanical modelling will allow monitoring of AAAs and will help us to understand AAA growth and possibly prevent rupture. The next step will be a patient study.

2D-6

9:15 AM **Arterial elasticity as a predictor for arteriovenous fistula maturation: Preliminary results**

Anna Sorace[1], Kenneth Hoyt[2], Michelle Robbin[2], Mark Lockhart[2], Carl Abts[2], Michael Allon[3]; [1]*Biomedical Engineering, University of Alabama at Birmingham, Birmingham, AL, USA,* [2]*Radiology, University of Alabama at Birmingham, Birmingham, AL, USA,* [3]*Medicine, University of Alabama at Birmingham, Birmingham, AL, USA*

Background, Motivation and Objective

In the United States, chronic kidney disease (CKD) affects 26 million adults. Reliable vascular access is critical for delivery of adequate dialysis and to maintain long-term connections for dialysis. An arteriovenous (AV) fistula is a direct anastomosis between a native artery and vein and is the preferred method for reliable vascular access for CKD patients; however, up to 50% of AV fistulas do not mature. Ultrasound (US) derived elasticity measurements have proven potential in characterizing abnormalities in biological tissues. It is hypothesized that as the preoperative elasticity of the artery is quantified in AV fistula surgery patients, measurements may determine whether the patient will have successful fistula surgery. This will increase the percentage of fistulas maturing to completion, which will improve patient care and decrease the number of unnecessary surgeries.

Statement of Contribution/Methods

US data was collected in the brachial artery of normal subjects and potential AV fistula patients using a Philips iU22 scanner equipped with a L17-5 transducer. The forearm was placed in a custom rest to minimize any patient motion. Simultaneous EKG recordings established 10 cardiac cycles of US data was acquired. Arterial Health prototype software (Siemens) was used to determine intima-media thickness (IMT) of the arterial wall during end systole and diastole. Patient EKG data determined extreme states of vessel distension and contraction. Assuming a linear elastic medium, the modulus of elasticity for the vessel wall was estimated as the ratio of vascular stress to strain. Stress was taken as the difference between systolic and diastolic pressure measurements. Tissue strain was derived from changes in peak IMT measurements and averaged over 6 cardiac cycles. Elasticity measurements were recorded as mean ± SD.

Results

Preliminary results in normal (non-CKD) subjects (mean age of 30, n = 8) were used to establish a database for comparison to AV fistula surgical placement patients. Regarding the latter, fistulas are tracked to either maturation or failure on follow-up clinical examinations and a comprehensive database is currently being compiled. To date, normal patient brachial artery elasticity measurements were found to be 72.6 ± 17.4 kPa. In comparison, elasticity measurements in patients prior to AV fistula surgery (mean age of 52, n = 20) were significantly higher with elasticity measurements of 137.1 ± 56.1 kPa ($p = 0.004$). Comparison to AV fistula outcome and histological measures of vascular fibrosis are pending.

Discussion and Conclusions

The relatively low measurement standard deviation demonstrates feasibility and indicates low variability in healthy brachial artery elasticity. Importantly, US can be used to noninvasively measure the elasticity of the brachial artery in human. A comprehensive database of vascular elasticity measurements has great potential in helping determine whether CKD patients will have complete fistula maturation.

3D - Targeted Contrast Agents

Carribean Ballroom VII

Thursday, October 20, 2011, 8:00 am - 9:30 am

Chair: **Paul Dayton**
Univ. North Carolina/NCSU

3D-1

8:00 AM Probing microbubble adhesion using secondary acoustic radiation force

Tom J.A. Kokhuis[1,2], Valeria Garbin[3], Klazina Kooiman[1], Benno A. Naaijkens[2,4], Lynda J.M. Juffermans[2,5], Otto Kamp[2,6], Michel Versluis[7], Antonius F.W. van der Steen[1,2], Nico de Jong[1,2];
[1]Biomedical Engineering, Erasmus MC, Rotterdam, Netherlands, [2]Interuniversity Cardiology Institute of The Netherlands, Utrecht, Netherlands, [3]Department of Chemical and Biomolecular Engineering, University of Pennsylvania, Pennsylvania, USA, [4]Department of Pathology, VU University Medical Center, Amsterdam, Netherlands, [5]Department of Physiology, VU University Medical Center, Amsterdam, Netherlands, [6]Department of Cardiology, VU University Medical Center, Amsterdam, Netherlands, [7]Physics of Fluids, University of Twente, Enschede, Netherlands

Background, Motivation and Objective

Targeted microbubbles (µBs) are a promising tool for disease-specific contrast enhancement. In this study we investigated a system of 2 targeted µBs. The objective was twofold. First measure the µB binding force using Secondary Acoustic Radiation Force (SARF). Second, model the translation of targeted µBs during and after ultrasound (US) application with a hydrodynamic model.

Statement of Contribution/Methods

Biotinylated µBs (0.8 mol% biotin-PEG-DSPE) [1], were targeted to an avidin coated OptiCell and insonified with 20 cycles at 2.25 MHz at various pressures (0-330 kPa). Dynamics were recorded with the Brandaris128 camera (25 MHz). A hydrodynamic model (including a restoring force) was developed to simulate the translation and recoiling of µBs during and after US application.

Results

Targeted µBs were observed to move towards each other during US application due to the attractive SARF. The left figure shows that the distance in between two µBs (R = 2 µm) decreased up to 700 nm during US application (210 kPa). A high frequency component (2.25 MHz) on top of a net drift towards each other was observed. The right figure shows the effect of US on the inter-µB distance for 5 pressures (inter-experiment time=80 ms). Recovery of the initial inter-µB distance (7.1 µm) after US application due to µB recoiling was observed up to 210 kPa. However, after 270 kPa the inter-µB distance did not fully recover to the initial value, implying that the adhesion of at least one µB was disrupted. Recoiling was not observed with untargeted µBs. Fitting the µB recoiling after US (not shown here) with our model yielded a value for the spring constant k of 2.7 mN/m. With this value for k, the model was able to accurately predict the experimentally observed translation of a targeted µB during US (as shown in the left figure). The product of k and the maximum displacement of a µB just before detachment, gives the maximum restoring force the adhesive belt can resist. For a µB with R = 2 µm the value was 1.1 nN-1.7 nN.

Discussion and Conclusions

A binding force of 1.1nN-1.7 nN was found for µBs with R = 2 µm using a novel method based on SARF. The results are in line with the binding force reported by [2] for larger µBs (same mol% biotin), taken the larger contact area of their system into account.

[1] Klibanov et al. Invest Radiol 39:187 (2004)
[2] Kim et al. Langmuir 16:2808 (2000)

This work was financially supported by the Dutch Technology Foundation STW

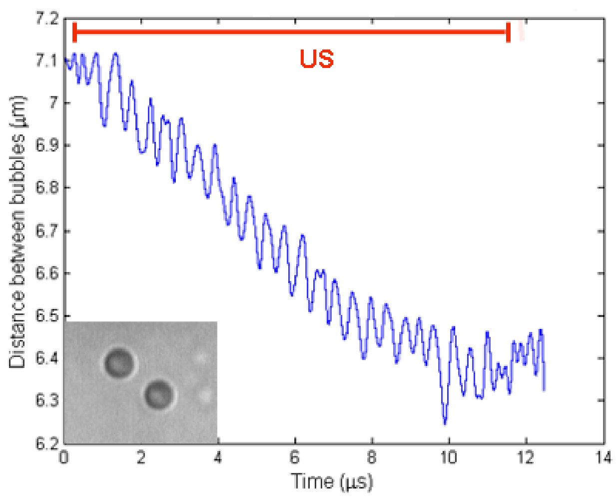

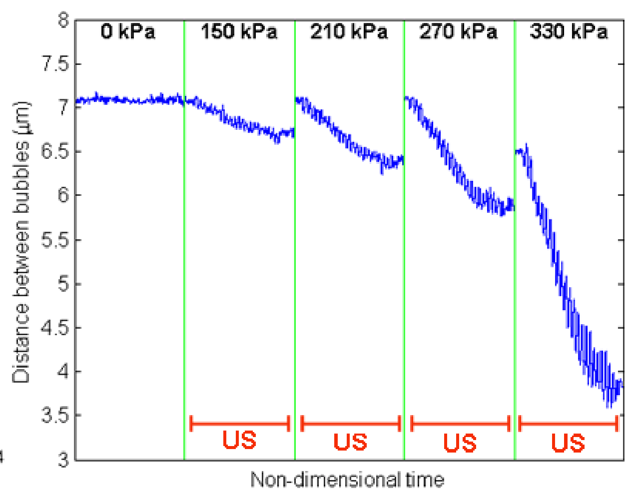

3D-2

8:15 AM Towards a Concentration Independent Readout of Molecular Signals with Micro-ultrasound

Eva Chan[1], John Sun[2], **F. Stuart Foster[1]**; [1]Sunnybrook Health Sciences Centre and University of Toronto, Toronto, Ontario, Canada, [2]VisualSonics Inc, Toronto, Ontario, Canada

Background, Motivation and Objective

The use of targeted microbubbles (MBs) for the detection of specific molecular signals has been established for many years. Yet the use of this remarkable capability has not found widespread application due, in part, to the fact that the quantitative relationship between detected signals and the actual target density has not been well established. In this presentation the quantitative relationship between an important receptor (VEGFR-2)and signals obtained in molecular imaging experiments with targeted microbubbles is explored over a range of concentrations and tumour types. The objective of this work is to derive a quantitative means to evaluate molecular expression patterns.

Statement of Contribution/Methods

Hep3B human hepatocellular carcinoma (HCC), Lewis lung carcinoma (LLC) and 231/LM2-4 breast cancer cells were each implanted in mice, and evaluated in vivo with VEGFR-2 targeted UCA and a VisualSonics Vevo 2100 high-frequency ultrasound imaging system. Blood volume, blood flow and VEGFR-2 targeted UCA binding were obtained from ultrasound contrast intensities from each contrast injection. Four injections of the same concentration ($2.04x10^8$ MB/mL in 50 µL) were used in 231/LM2 2 tumors (n=5) to test the reproducibility of the ultrasound imaging. Next, four targeted UCA concentrations ($1.02x10^9$, $2.04x10^8$, $1.02x10^8$ and $1.02.x10^7$ MB/mL in 50 µL) in three tumor models (n=5 each) were tested to determine the effects on ultrasound imaging blood volume, blood flow and targeted UCA binding. A proposed normalization strategy in which the molecular signal is defined as the ratio of power from bound MB contrast to the peak power of MB contrast at wash-in. The rationale for this normalization is based on the hypothesis that receptor density is proportional to blood volume. Normalized and unnormalized contrast intensities for the 3 tumour types were compared with VEGFR 2 expression from immunohistochemical (IHC) staining.

Results

VEGFR 2 targeted MBs showed significant injection-to-injection coefficients of variation that ranged from 10 to 46% in individual mice. All three tumour types exhibited a linear dependence between bound MB power at t = 4 min. and injected MB concentration (R^2> 0.99). Normalization of these data as described above significantly reduced this correlation resulting in a concentration independent measurement of the molecular signal.

Discussion and Conclusions

The high variability associated with tail vein injections of MB contrast agents illustrates the need for improved contrast delivery as well as better means to suppress concentration dependent artifacts in molecular imaging The proposed normalization strategy studied in this project represents a preliminary step towards accurate quantification of molecular markers such as VEGFR-2 in mouse tumours.

3D-3

8:30 AM The influence of attachment on the nonlinear behaviour of lipid encapsulated microbubbles at high frequencies

Brandon Helfield[1,2], Xuan Huo[1], Stuart Foster[1,2], David Goertz[1,2]; [1]Sunnybrook Research Institute, Toronto, Ontario, Canada, [2]Medical Biophysics, University of Toronto, Toronto, Ontario, Canada

Background, Motivation and Objective

Molecular imaging at higher frequencies (f>10 MHz) has applications in a preclinical context for a range of disease processes and clinically for the detection of vulnerable atherosclerotic plaques. While initial results have demonstrated the feasibility of both linear and nonlinear high frequency molecular imaging, an improved physical understanding of the effects of bubble binding on the generation of nonlinear signals from bound bubbles is required in order to establish a quantitative relationship between signals and molecular expression, as well as to differentiate attached from free bubbles in the presence of substantial tissue motion. Recent work at lower frequencies has shown that binding can affect bubble resonant frequencies, though the impact on nonlinear signals appears not to have been reported. The objective of this study is to investigate the effects of binding on nonlinear (subharmonic - SH) signal generation at high frequencies.

Statement of Contribution/Methods

Individual streptavidin-coated MicroMarker® bubbles were allowed to rest either adjacent but unbound to (UBMM) or bound to (BMM) a compliant agarose/biotin boundary. The bubbles were optically sized and insonified at 25 MHz with pressures from 0.028-1.28 MPa using either 10% Gaussian or tapered rectangular enveloped pulses at 0° and 180° to examine their SH response and effectiveness in pulse inversion (PI) detection strategies. Results were compared to simulations to gain insight into the characteristics of radial oscillations associated with the SH pressure emissions.

Results

The SH response of UBMM (n=53) and BMM (n=57) was found to differ significantly, with BMM exhibiting a narrower active size range and a 21% stronger peak amplitude than UBMM. The bubble state also introduced a shift in active size, from 2.1 µm (UBMM) to 1.9 µm (BMM) in diameter. The propensity for SH generation was observed to be 58% for UBMM and 40% for BMM for bubbles between 1-3.5 µm. Destruction characteristics were also found to differ, with BMM exhibiting a lower threshold of 272 kPa and a 74% disruption rate versus 454 kPa and 55% for UBMM bubbles between 1-3 µm. In addition, for both bubble states a phase offset of 90° was observed between SH responses elicited from a 0° pulse with respect to that elicited from a 180° pulse, resulting in inefficient SH preservation from PI. Applying a phase shift of 90° to SH signals prior to the addition of successive pulse pairs results in an improvement of up to 4.1 dB in residual SH energy, depending on the bubble size. Initial modeling suggests SH emissions in both states are linked to “expansion-dominated” oscillations deriving from asymmetric shell properties.

Discussion and Conclusions

The results show substantial differences in SH response between unbound and bound states, which has implications for differential detection strategies. An understanding of the acoustic signatures from individual bubbles can aid in bubble design and quantification of contrast/molecular images.

3D-4

8:45 AM Insonation of Targeted Microbubbles Produces Regions of Slow Blood Flow within Tumor Vasculature

Xiaowen Hu[1], Azadeh Kheirolomoom[1], Lisa Mahakian[1], Julie Beegle[1], Elizabeth Ingham[1], Charles Caskey[1], Dustin Kruse[1], Katherine Ferrara[1]; [1]*Biomedical Engineering, University of California, Davis, CA, USA*

Background, Motivation and Objective

Previously, the insonation of circulating microbubbles (MBs) by low frequency (1 MHz) ultrasound (US) pulses has been associated with changes in vascular permeability and local changes in blood flow. Here, 5 MHz insonation of bound, targeted MBs using a clinical scanner is demonstrated to locally alter blood flow in murine tumors.

THURSDAY ORAL

Statement of Contribution/Methods

All studies were approved by the UC Davis Animal Use and Care Committee. Peptide-targeted MBs were administrated into murine Met-1 and NDL tumor models via tail vein injection (5×10^7 MBs). Thirty frames of CPS contrast images (Siemens Sequoia 512, 0.09 MI, 10 Hz frame rate) were recorded to assess tumor blood perfusion. Seven minutes after injection, freely-circulating MBs had cleared from the blood stream leaving bound MBs that had accumulated in the tumor vasculature. At this time, 5 MHz, 2 or 4 MPa peak negative pressure (PNP) pulses, with a pulse length of 5 cycles and pulse repetition period of 6.7 ms were transmitted for 1 second. Five minutes after the high pressure pulse sequence, a second dose of MBs was injected and 30 frames of CPS images were acquired. FITC-dextran (MW = 150,000) was co-injected with the first injection of MBs to trace vasculature changes. Tumors were harvested for histological evaluation.

Results

After the insonation of bound MBs with a 4 MPa PNP, additional regions of slow blood flow were observed in 71% of Met-1 tumors (n=26) and 44% of NDL tumors (n=10). In Met-1 tumors insonified with 4 MPa pulses, the area over which slow perfusion was observed increased from 23±7% to 63±11% (p<0.01) of the tumor region of interest. Decreasing the PNP to 2 MPa decreased the percentage of Met-1 tumors with additional regions of slow perfusion from 71% to 24%. Histological analysis of Met-1 tumors after 4 MPa insonation demonstrated that the mean microvascular diameter in insonified tumors was approximately 17±8 µm, compared to 7±4 µm in control tumors (p<0.01). Extravasation of FITC-dextran was observed in 4 MPa insonified, but not in control, Met-1 tumors.

Discussion and Conclusions

The results suggest that high pressure insonation of targeted MBs, which had accumulated at high concentration, may result in changes in vessel diameter and blood flow, although additional studies are required to determine the mechanism.

The authors acknowledge NIH R01CA112356.

3D-5

9:00 AM 3D Radiation Force Enhanced Ultrasonic Molecular Imaging with Clinical System

Jason E. Streeter[1], Ryan C. Gessner[1], Paul A. Dayton[1]; [1]Biomedical Engineering, UNC / NC State, Chapel Hill, NC, USA

Background, Motivation and Objective

For over a decade, acoustic radiation force (ARF) has been proposed as a method to enhance MCA retention in Ultrasonic Molecular Imaging (USMI), since ARF can push microbubbles in contact with the vessel endothelium. However, almost all published data to date has been in-vitro. In this paper, we demonstrate the application of ARF-enhanced USMI of angiogenesis in-vivo using 3D imaging with a clinical US system.

Statement of Contribution/Methods

3D ARF-enhanced MI was performed on 5 rat fibrosarcoma tumors using size selected MCAs fitted with a cyclic RGD peptide targeted to αvβ3 and nontargeted MCAs. 3 different low-amplitude ARF pulse sequences, previously shown to produce non-destructive bubble translation in-vitro, (4.4, 13.4 and 20.6 kPa; Duty Cycle: 25%, Freq: 7 MHz) were tested and compared to passive targeting studies in the same animal. The transducer was scanned 5 times at a constant speed of 1 mm/s across the tumor after MCAs were administered via bolus injection. 3D acquisitions were obtained with a Siemens Sequoia in CPS mode with the same elevational scanning mechanism. The brightness of adherent MCAs was assumed to be correlated with the degree of biomarker expression. 3D data was down-sampled offline at 800 µm intervals to yield independent imaging frames for analysis. Data in each frame was normalized to the mean pixel intensity of the passive targeting data.

Results

The maximum increase in targeting was achieved using the ARF-13.4 kPa setting (Fig.1). On average, ARF at 13.4 kPa yielded 80% greater targeting than with no ARF (13.4 kPa: 1.8 ± 1.1 vs No ARF: 1.0 ± 0.7; $p < 0.05$). Additionally, both the ARF-4.4 (1.4±1.2) and ARF-20.6 (1.4±1.1) settings produced statistically significant increases in targeting relative to the passive targeting case. It is hypothesized that the ARF-20.6 setting may have produced too much radiation force and dislodged bound bubbles, thus a reduction in targeting relative to the ARF-13.4 setting. ARF at 13.4kPa with control MCAs resulted in a slight decrease in non-specific MCA adhesion relative to control MCAs with no ARF (13.4 kPa: 0.7 ± 0.5 vs No ARF: 0.6 ± 0.3; $p > 0.05$).

Discussion and Conclusions

This in-vivo study demonstrates the enhancement of USMI with ARF, as assessed by 3D imaging with a clinical US system. Results show a significant improvement in sensitivity of 80% over traditional non-ARF-enhanced targeted imaging without a corresponding loss in specificity.

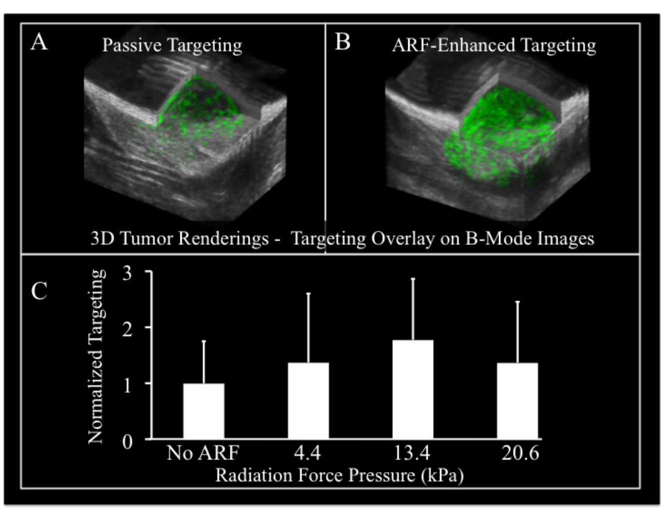

3D-6

9:15 AM A Targeting Therapy Strategy by Aptamer-Conjugated and Drug-Loaded Droplets

Chung-Hsin Wang[1], Ya-Shuan Lee[1], Shih-Tsung Kang[1], Chih-Kuang Yeh[1]; [1]Department of Biomedical Engineering and Environmental Sciences, National Tsing Hua University, Taiwan

Background, Motivation and Objective

The ultrasound-mediated vaporization of droplets enables the loaded drugs to be instantly released from its coated shell. However, the lack of an active targeting capability results in lower accumulation efficiency. Therefore, conjugating the droplets to targeting moieties, aptamer, would enable them to bind to specific cells so as to greatly improve the drug delivery efficiency. Moreover, previous studies also indicated that vaporization process could induce the effect of inertial cavitation which leading to directly kill live cells and enhance the permeability of cell membranes. The purposed therapy strategy includes two pathways to induce tumor cells damage: cavitation effect and drug release after droplets vaporization in different time stages.

Statement of Contribution/Methods

The drug-loaded droplets (perfluoropentane) were achieved by the encapsulation of doxorubicin (Dox) and the conjugation of sgc8c aptamer. Sgc8c is a strong aptamer with a high binding affinity and other advantageous characteristics such as ease of synthesis and modification. The composition of shell materials was regulated to optimize the loading efficiency and the stability for circulation. These droplets fabricated from sonication have the mean size of 758.5 nm and final concentration of 4×10^{10} droplets/mL. The cell targeting ability of conjugated droplets was also showed in figures a-b.

Results

The aptamer conjugation and Dox encapsulation efficiency were both quantified by calculating the changes of fluorescence intensity using spectrophotometer, and results were 37.56±1.02 % and 51.66±2.58 %, respectively. The cell experiments were held to evaluate the targeting performance and the cell viabilities by flow cytometry and MTT analyses from irradiation experiments. The experiments were monitored by using optical and ultrasound images. Figure 1c shows that the optical images acquired by high speed camera and the CEM cells were transiently killed by the explosive vaporization process.

Discussion and Conclusions

The results reveal that targeted droplets can be applied as a therapeutic agent, and released drugs further contribute to therapeutic efficiency in the last few hours. Future works include investigating the correlation between released drug dosage and vaporization signals, exploring the feasibility of embolotherapy, and applying to *in-vivo* studies.

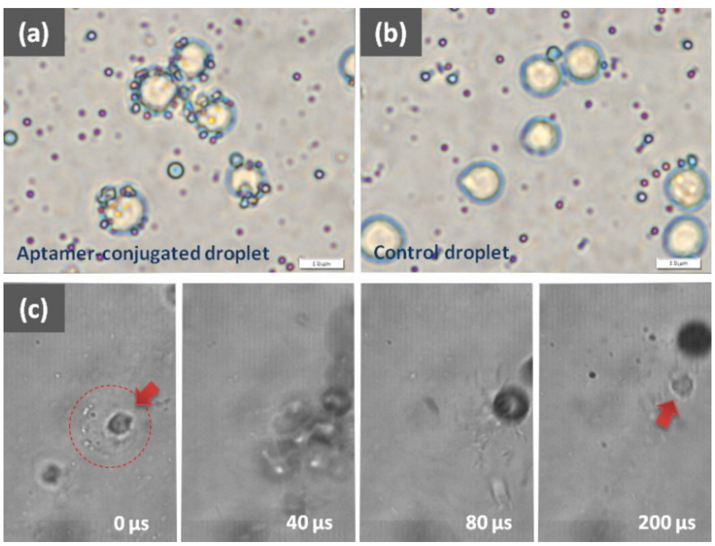

THURSDAY ORAL

4D Phased Arrays

Carribean Ballroom I

Thursday, October 20, 2011, 8:00 am - 9:30 am

Chair: **Paul Wicox**
University of Bristol, UK

4D-1

8:00 AM Development of Conformable Ultrasound Array NDE Transducer

Vishal Kulkarni[1], Fanping Sun[2], Saurabh Bakshi[1], **Xiaoning Jiang[1]**, Zaffir Chaudhry[3]; [1]North Carolina State University, Raleigh, NC, USA, [2]United Technologies Research Center, East Hartford, CT, USA, [3]United Technologies Research Center, USA

Background, Motivation and Objective

Conformable Phased Array ultrasound transducers (CPA) have significant advantages over the conventional phased array transducer for detecting flaws and cracks in non-flat composite structures. They can be enveloped over surfaces of varying curvature without changing wedge adapters, resulting in enhanced volumetric image of defects and more efficient manufacturing inspection. This paper presents development of an 8x8 conformable phased array transducer for NDE of aerospace composite structures with emphasis on its fabrication and characterization.

Statement of Contribution/Methods

A 3 MHz 64 elements (8x8 array) was designed with a mean pitch of 2mm. A 16mm x 16mm PZT-5H 1-3 composite wafer with thickness of 0.47 mm was prepared first. A 2-layer acoustic matching layers were applied next, followed by precision dicing. The top matching layer is conductive and was then epoxy-bonded to a thin gold foil, which acted as the common ground electrode; while the other side with sputtered gold acted as another electrode. Sixty four coax cables were soldered on the sputtered side of each element, and two more cables were bonded onto the common ground electrode. The whole acoustic stack was then potted in a steel fixture with a rubber solution which made it strong yet flexible. The free ends of the wires were soldered onto a printed circuit board (PCB) which was mounted over the steel housing.

Results

The fabricated two dimensional array was successfully tested for its conformability to a 3¡± diameter ball. The capacitance and impedance spectrum value for each element was measured using a precision impedance analyzer (Agilent 4294A). The average capacitance was over 90pF and the impedance value was below 750§Ù at resonance frequency. Pulse-echo experiments demonstrated a average peak-peak echo voltage (Vp-p) of > 231 mV under an input pulse signal with peak-to-peak voltage of 100 V. All 64 elements function properly (Figure 1). The measured average center frequency is 3.3 MHz, average loop sensitivity is -53dB (standard deviation of 2.5 dB), and the average -6 dB bandwidth is 66% (standard deviation of 5%).

Discussion and Conclusions

A flexible 3MHz 64-element 2D array probe was successfully designed, fabricated and characterized. The conformability and performance characteristics are promising for non-flat surface adaptive 2D array ultrasound NDE.

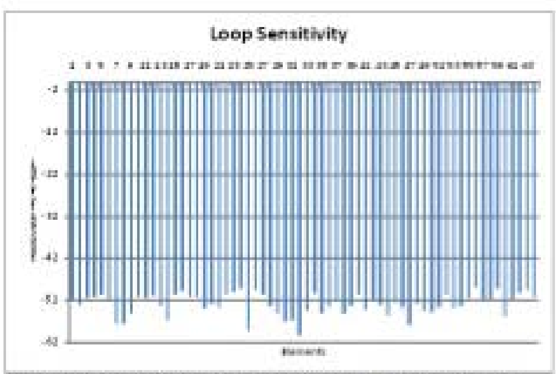

Figure 1. Loop sensitivity of all 64 elements in the prototyped 3.3MHz conformable 2D array

4D-2

8:15 AM Spectrogram remapping based imaging for spiral shaped frequency steerable acoustic transducers

Emanuele Baravelli[1,2], Luca De Marchi[2], Massimo Ruzzene[1], Nicolo' Speciale[2]; [1]Aerospace Engineering, Georgia Institute of Technology, Atlanta, GA, USA, [2]ARCES/DEIS, University of Bologna, Bologna, Italy

Background, Motivation and Objective

Guided Wave based Structural Health Monitoring (SHM) greatly benefits from directional scanning. This is typically achieved through phased arrays featuring a large number of individually controlled elements and hence considerable hardware and software complexity. The novel device concept and the associated signal processing presented in this work enable imaging of 2D areas through the output of a single, dual-channel sensor

Statement of Contribution/Methods

Frequency-steerable acoustic transducers (FSATs) act as spatial filters thanks to their geometry, thus providing a one to one correspondence between the direction of propagation and the spectral content of the actuated/recorded signal. The signal processing methodology proposed here supports sensing operation of a recently demonstrated double-channel, spiral-shaped FSAT [Senesi SPIE Sm. Str./NDE 2011]. Both angular and range distance coordinates required for 2D imaging of acoustic events are encoded in the spectrogram of

FSAT differential output. The travelled distance of an incoming wave can be retrieved through the Warped Frequency Transform [De Marchi TUFFC 2009], which removes dispersion and maps the time axis onto a spatial coordinate (Figs. 1(a-b)). The direction of arrival is indicated by a peak in the signal spectrum, according to FSAT frequency-directivity characteristic: the frequency axis of the warped spectrogram is thus mapped onto the associated angular coordinate. This procedure converts the spectrogram of FSAT output into a polar image of the monitored region, and a Cartesian mapping completes the algorithm (Fig. 1(c-d)).

Results

Correct localization of single or multiple broadband sources (Fig. 1(d)) and scattering events is demonstrated by pitch-catch and pulse-echo simulations as well as experimental validation. This was performed by emulating FSAT behaviour through Scanning Laser Doppler Vibrometer acquisitions, and subsequently by fabricating and testing a polyvinylidene fluoride prototype of the sensor (Fig. 1(e)).

Discussion and Conclusions

A spectrogram remapping strategy has been proposed for processing the signals recorded by spiral FSATs. This approach greatly boosts hardware and software efficiency by enabling SHM of large 2D regions through a single sensor.

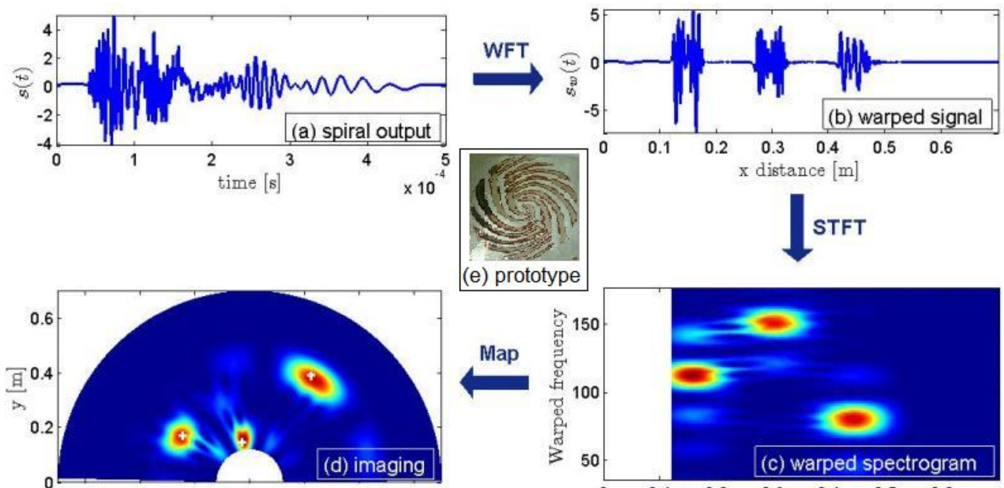

4D-3

8:30 AM **Ultrasonic Synthetic Aperture Focusing Using the Root-mean-square Velocity**

Ruey-Chyuan Shih[1], Young-Fo Chang[1], Chih-Hsiung Chang[2], **Po-Yen Tseng[1]**; *[1]Department of Earth and Environmental Sciences, National Chung Cheng University, Minhsiung Township, Chiayi County, Taiwan, [2]General Education Center, National Chaiyi University, Chiayi City, Taiwan*

Background, Motivation and Objective

The synthetic aperture focusing technique (SAFT) can improve the image resolution of an ultrasonic testing (UT) by applying a delay-and-sum (DAS) technique to the received echoes. The drawback of using the current SAFT for testing a multi-layer medium is that the computation of delays is complicated and time consuming.

Statement of Contribution/Methods

In this paper, we will show that using the approximated delays calculated from the root-mean-square velocity (V_{rms}), we can speed up the process and maintain the resolution of the image, instead of resorting to the calculation of true delays. The difference between the true and approximated delays is minor and can be reasonably ignored by incorporating the magnitude of the emitting amplitude into process. Feasibility of the proposed algorithm is demonstrated by the results of an immersion test as well.

Results

A 20 MHz immersion transducer with 3 mm in diameter is used to transmit and receive the ultrasound. A steel specimen with 5940 m/s in velocity, 7.69×10^{-3} kg/cm^3 in density and three single-side-drilled holes located at different depths was fabricated and scanned (Fig. 1(a)). Water serves as the couplant in the experiment. The distance between the probe and specimen is 20 mm and the scanning interval is 0.5 mm laterally. Fig. 1(b) shows a B-scan image of the steel specimen. Fig. 1(c) is the SAFT image processed by the true delays. Fig. 1(d) is the SAFT image using the V_{rms} to calculate the approximated delays. Since the delays are approximated values, intensities of the flaw images are weaker than those in Fig. 1(c).

Discussion and Conclusions

The error of the propagation time of the ultrasound calculated by the V_{rms} will depend on the offset and the velocity contrast of the median. For a small offset condition, which is common in an ultrasonic NDT, the larger the velocities contrast of the media exist the larger error of the propagation time will be while using the V_{rms}. However, in our case study, the velocity contrast comes up to 0.75, (V_{stell}-V_{water})/V_{stell}, which is very strong but the propagation time error is still small. Therefore the using of V_{rms} of the media to implement the SAFT is successful. The experimental results show that the image resolution of an immersion testing has been successfully improved by this simple and fast SAFT, although the intensities of the flaw images using our method are weaker than those using true delays to implement the SAFT.

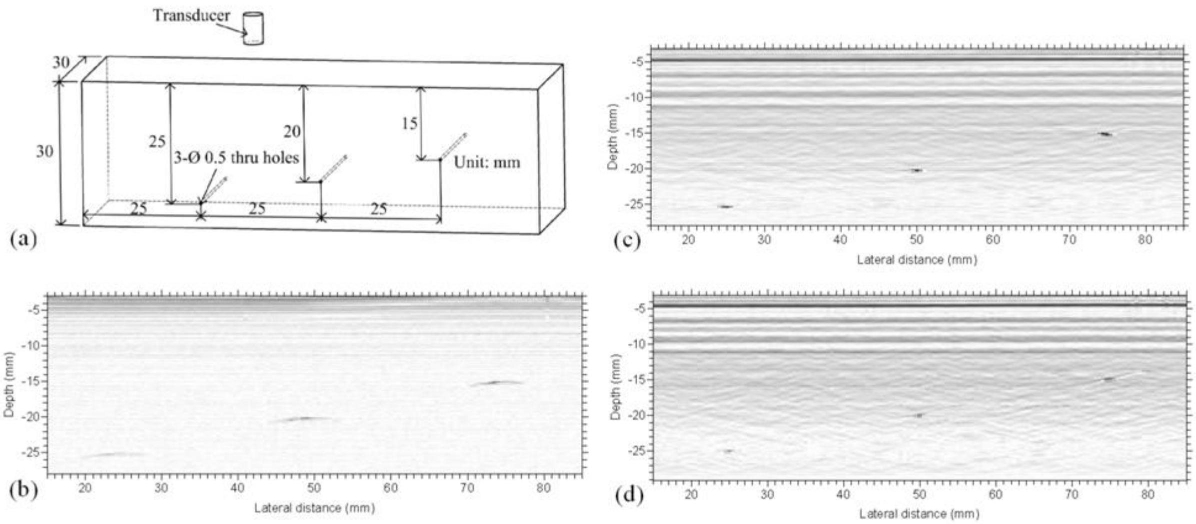

Fig. 1. The SAFT images of testing three single-side-drilled holes at different depths. (a) the configuration of the specimen, (b) the B-scan image, (c) the SAFT image processed with the true delays, (d) the SAFT image obtained using the V_{rms} to calculate the approximated delays.

4D-4

8:45 AM **3D Reconstruction from Adaptive Matrix Microphone Array Signals using Back Projection Algorithm**

Kyohei Mizutani[1], Masanori Sugimoto[2], Hiromichi Hashizume[3]; [1]*School of Engineering, The University of Tokyo, Bunkyo-ku, Tokyo, Japan,* [2]*The University of Tokyo, Japan,* [3]*Information Systems Architecture Science Research Division, Japan*

Background, Motivation and Objective

We propose a new approach for 3D imaging using acoustic signals. Many existing approaches for acoustic imaging are based on spatial division by conducting scan. Generally, beamforming algorithms are used for the scan. The proposed method in this paper is different from these approaches and employs the back projection algorithm to process signals from a static ultrasonic microphone array in spherical polar coordinates. One of the remarkable features of the proposed method is that it can obtain frequency-domain sound-field data that cannot be obtained via conventional beamforming based approaches. We have already tested our method for 2D acoustic imaging and confirmed that the method can achieve higher resolutions than conventional methods [1]. This paper describes extensions from 2D to 3D imaging and shows some initial imaging results using the proposed method.

Statement of Contribution/Methods

We use time distribution of received signal powers obtained by conducting pulse compression and angle distribution of received signal powers obtained through a microphone array, and integrate them with the Radon transform in spherical polar coordinates. A simple back projection algorithm is used for reconstructing 3D acoustic images.

Results

We conducted computer simulations to verify the performance of the proposed algorithm by using 3 point sound sources. The figure shows a cross section of an image perpendicular to the depth direction. This result was obtained by using only time distribution of signal powers. The position of a sound source on this section was [θ,φ]=[0.84 2.68] (unit: radian).

Discussion and Conclusions

Through the simulation results, we verified that the proposed method could identify the sound sources correctly.

One of future works is to conduct computer simulations with angle distribution of signal powers. We also plan to conduct experiments for 3D acoustic imaging in real environments and verify the resolution improvement of obtained images.

1) Mizutani, K., Sugimoto, M., Hashizume, H.: Acoustic Imaging Reconstruction from Adaptive Microphone Array Signals using Back Projection, In Proc. of 31st International Acoustical Imaging Symposium (AI-31), Warsaw, Poland, April 2011 (to appear)

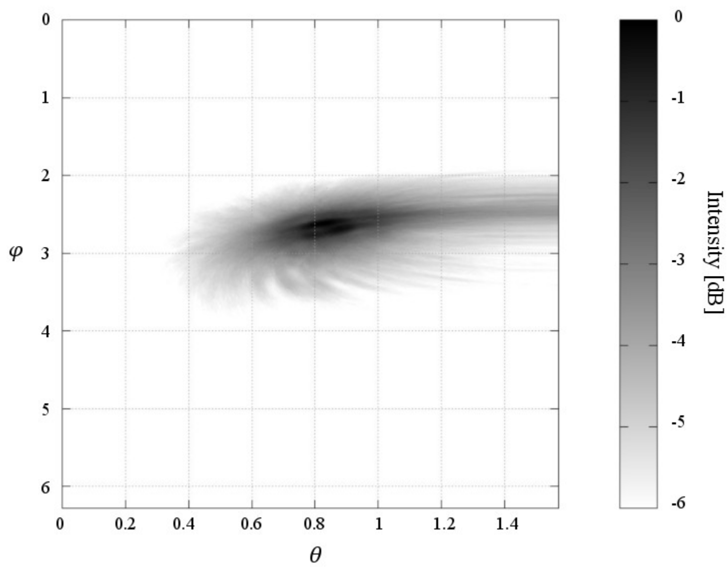

THURSDAY ORAL

4D-5

9:00 AM Synthetic Transmit Aperture 3D Image Reconstruction Using 2D Transmitter Array

Natsuda Laokulrat[1], Yasushige Maeda[2], Masanori Sugimoto[1], Hiromichi Hashizume[3]; [1]Department of Electrical Engineering and Information Systems, Graduate School of Engineering, The University of Tokyo, Bunkyo-ku, Tokyo, Japan, [2]Department of Informatics, School of Multidisciplinary Sciences, The Graduate University for Advanced Studies, Chiyoda-ku, Tokyo, Japan, [3]Information Systems Architecture Science Research Division, National Institute of Informatics, Chiyoda-ku, Tokyo, Japan

Background, Motivation and Objective

Synthetic aperture (SA) imaging has been researched for many years. Recently, a 2D microphone array is used for receiving acoustic signals and reconstructing 3D images using SA technique. However, the conventional arrangement of transmitters in the same horizontal plane or linear array does not give good signal strength all over scanned target space since directivity of transmitted signal is limited to some particular directions, namely directions along the plane of transmitters. As a result, transmitted signals are strong along the plane of transmitters but weak in upper and lower space so it is not suitable for 3D imaging.

In this propose, we focus on effects of the arrangement of the 2D transmitter array and number of transmitters on reconstructed 3D images.

Statement of Contribution/Methods

We are observing 3D acoustic imaging results based on Time-division Synthetic Transmit Aperture (TD-STA) using a 2D transmitter array and a 2D receiver array. The receiver array is composed of 128 MEMS-based ultrasonic microphones aligned in 16x8 planar grids. The transmitter array is virtually constructed by changing a position of a transmitter to 9 different places in a 3x3 planar grids.

The transmitter is placed at one specific position and transmit acoustic signal while the receiver array is ready for capturing signal. After emission, the transmitter is moved to the next position. The process is repeated for all 9 positions of the transmitter. The experiment set up is shown in the figure. In the figure, the transmitter is at position (2, 3). Multi-carrier signal [1] is used for transmission. The received signals are digitized, sampled, and transferred to PC. Matched filtering and TD-STA processes are then performed.

Results

The image has 97(horizontal)x41(vertical)-degree field of view with 1-degree angular resolution. The result shows the improvement of performance in term of resolution and quality, when comparing to conventional beamforming and STA imaging using linear transmitter array.

Discussion and Conclusions

We propose a new arrangement of transmitter array for reconstructing acoustic images by TD-STA technique. More investigation and experiments will be done to confirm the proposal.

[1] Ito, T., Sugimoto, M., Hashizume, H.: High-Resolution Acoustic Imaging Using Multi-Carrier Waveforms Synthesized by Genetic Algorithm, IEEE Ultrasonic Symposium 2009, Rome, Italy, pp. 685-689.

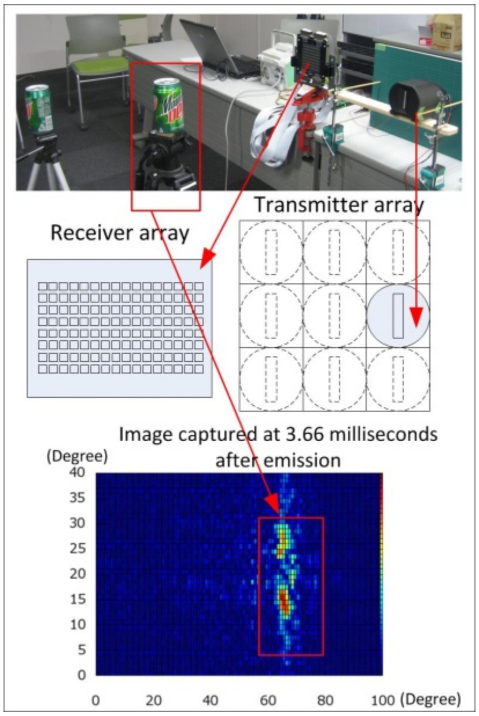

4D-6

9:15 AM Measuring Phase Characteristics of Ultrasonic Microphones for Accurate Ultrasonic Localization Systems

Shigeki Nakamura[1], Masanori Sugimoto[1], Hiromichi Hashizume[2]; [1]Graduate School of Engineering, University of Tokyo, Bunkyo-ku, Tokyo, Japan, [2]National Institute of Informatics, Chiyoda-ku, Tokyo, Japan

Background, Motivation and Objective

We have so far developed and evaluated a 3D ultrasonic localization system using the Extended Phase Accordance Method (EPAM) [1]. The method allows us to measure a 3D position of a transmitter by using a single compact receiver unit whose baseline is 76 mm and shows the satisfactory level of accuracy (13mm standard deviation) for indoor positioning. However, due to the directivity of ultrasonic microphones, a transmitter is not correctly localized if it is placed at different locations but equal distance from the receiver sensor. Ultrasonic microphones show different phase characteristics to different wave incident angles. Since EPAM uses the phase information of received signals for 3D localization, it is necessary to clarify phase characteristics of ultrasonic sensors and compensate them for increasing the positioning accuracy. Therefore, we have conducted experiments to obtain phase characteristics of microphones.

Statement of Contribution/Methods

We placed an ultrasonic receiver at a static position and measured the distance to an ultrasonic transmitter placed at 25×15 different points, which changes wave incident angles in the range of 25 degrees horizontally and 20 degrees vertically. The measurements were conducted 20 times at each point, which was enough to remove thermal noise effects. MEMS-based ultrasonic microphones (SPM0404UD5, by Knowles Acoustics) were used.

Results

The change of the distance measurement error is shown in the attached figure. The error is up to 37 mm in this measurement range, which leads to 200 mm difference in the 3D positioning.

Discussion and Conclusions

We confirmed that the distance measurement error depending on the wave incident angle is a large portion of EPAM measurement errors. Based on this result we are now investigating a compensation method for more accurate 3D positioning. We will achieve about 10-fold improvement in 3D positioning accuracy.

[1] S. Nakamura, T. Sato, M. Sugimoto, and H. Hashizume: An accurate technique for simultaneous measurement of 3D position and velocity of a moving object using a single ultrasonic receiver unit, In Proc. of IEEE IPIN 2010.

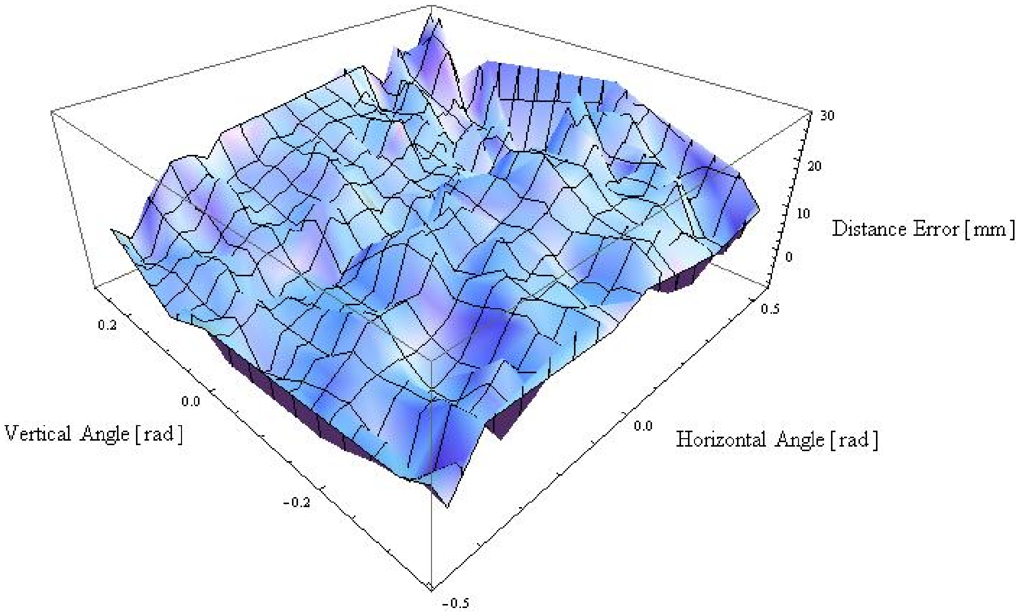
30
20
10
0
Distance Error [mm]
0.5
0.2
0.0
Vertical Angle [rad]
0.0
Horizontal Angle [rad]
-0.2
-0.5

5D - Radio Frequency Phononic Crystals

Carribean Ballroom II

Thursday, October 20, 2011, 8:00 am - 9:30 am

Chair: **Tsung-Tsong Wu**
National Taiwan University

THURSDAY ORAL

5D-1

8:00 AM Micro and Nano Fabricated Phononic Crystals: Technology and Applications

Roy H. Olsson III[1]: Maryam Ziaei-Moayyed[1], Bongsang Kim[1], Charles Reinke[1], Mehmet F. Su[1], Patrick Hopkins[1], Yasser M. Soliman[1], Drew F. Goettler[1], Zayd C. Leseman[1], Ihab El-Kady[1] [1]*Advanced MEMS Department, Sandia National Laboratories, Albuquerque, New Mexico, USA*

Background, Motivation and Objective

Phononic crystals are an emerging field that has applications across a broad range of systems from radio frequency (RF) communications to thermal management and acoustic imaging. Over the past decade phononic crystals have been scaled from large hand assembled balls in acoustically lossy materials such as water and epoxy to micro and nano fabricated 2D structures realized in low loss materials operating at frequencies from 10-10,000 MHz.

Statement of Contribution/Methods

Micro/Nano fabrication of phononic crystals has presented many opportunities and challenges. Batch fabrication and the ability to co-integrate piezoelectric transducers with phononic crystals for rapid electrical interrogation have lead to experimentation on a wide variety of geometries and devices. The ability to suspend 2-D phononic crystals above the substrate using micromachining techniques has allowed for low loss phononic waveguides and cavities to be demonstrated. The wide range of materials available and the implications of finite membrane thickness require careful consideration when designing a phononic crystal for a specific application.

Results

Phononic crystals and devices have been fabricated and studied theoretically and experimentally in several material systems including Si-air, SiC-air, Si-W and SiO2-W. Phononic band gaps at GHz frequencies have been demonstrated in each of these material systems with complete phononic bandgap widths exceeding 10% of the center frequency and band gaps for longitudinal waves in excess of 50%. Solid-Solid phononic crystals realized in Si-W and SiO2-W material systems have demonstrated less sensitivity to membrane thickness and lithography when compared to Solid-Air phononic crystals. Certain devices, such as cavities, requiring very low material damping have been best realized in Solid-Air materials systems using high-Q materials such as SiC. Recently, a nano-fabricated Si-Vacuum phononic crystal with its tailored phonon dispersion has demonstrated over an order of magnitude reduction in thermal conductivity of a Si slab potentially leading to improved performance in thermoelectric devices.

Discussion and Conclusions

While much recent progress has been achieved in realizing micro and nano scale phononic crystals several challenges and opportunities are emerging including: the need for much wider bandwidth piezoelectric transducers for interrogating the phononic crystals, the ability to combine phononic and photonic crystals to increase phonon-photon interactions and for processing light signals in the acoustic regime and the introduction of non-linearity with phononic bandgap materials.

5D-2

8:30 AM Extended band gaps in a GHz aluminum nitride phononic crystal slab

Marie Gorisse[1], Sarah Benchabane[2], Guilhem Teissier[1], Christophe Billard[1], Alexandre Reinhardt[1], Vincent Laude[2], **Emmanuel Defaÿ[1]**; [1]*CEA, Leti, Minatec campus, Grenoble, France,* [2]*FEMTO-ST, Université de Franche-Comté, CNRS, Besançon, France*

Background, Motivation and Objective

Phononic crystals (PC) have known a great interest in the past few years. Microscale phononic crystals are presenting band gaps in the range of several hundreds of megahertz to few gigahertz. As their optical counterparts, photonic crystals, they exhibit interesting physical properties and open the lead to many different applications: reflectors, microcavities, acoustic lenses, …

Following shortly the first demonstration of PCs for surface acoustic waves [1, 2], a great interest has arisen for PC on slabs [3, 4, 5]. Slabs provide isolation from the substrate, which means reaching a three-dimensional confinement of waves in the band gap.

[1] T. T. Wu, L. C. Wu, and Z. G. Huang, J. Appl. Phys. 97, 094916 (2005).
[2] S. Benchabane, A. Khelif, J.Y. Rauch and V. Laude, Phys. Rev. E 73, 065601 (2006).
[3] C.Y. Huang, J.H. Sun and T.T. Wu, Appl. Phys. Let. 97, 031913 (2010).
[4] S. Mohammadi, A.A. Eftekhar, A. Khelif, W. Hunt, A. Adibi, Appl. Phys. Let. 92, 221905 (2008).
[5] Y.M. Soliman, M.F. Su, Z.C. Leseman, C.M. Reinke, I.F. El-Kady, R.H. Olsson III, Appl. Phys. Lett. 97, 193502 (2010).

Statement of Contribution/Methods

In this paper we present the characterization of aluminum nitride phononic crystal slabs fabricated on 200 mm silicon wafers with a lattice spacing of a few micrometers. Two interdigitated transducers were used to excite and detect Lamb waves propagating through the periodical structure. RF measurements were performed and backed up by laser interferometry imaging of the elastic displacement field. FEM simulations were performed to account for the observed experimental results.

Results

AlN phononic crystal slabs have been realized and characterized. Experimental measurements reveal the existence of an attenuation band extending from 600 MHz to 950 MHz (i.e. with around 40% relative bandwidth), much wider than the theoretically predicted band gap (775 MHz to 825 MHz). Laser interferometric measurements confirm the existence of a band gap, while computation of the transmission through FEM simulations are in good agreement with the measurement results.

Discussion and Conclusions

A closer study of the polarization of the waves generated and guided by the membrane reveal that the widening of the gap is due to the presence of deaf bands, corresponding to modes in the crystal exhibiting a polarization orthogonal to that of the source used to test the phononic crystal. For a whole range of frequencies around the gap, no eigenmode is excited or detected by interdigitated Lamb wave transducers. This wider band gap would be interesting in some applications, for example in acoustic mirrors. This work demonstrates that considering the conversion of modes at the boundaries of a phononic crystal complements the band structure analysis and provides more insight into the behavior of the crystal.

5D-3

8:45 AM VHF Phononic Band Gap Band Pass Filters using Coupled Resonator Acoustic Waveguides (CRAW)

Saeed Mohammadi[1], Abdelkrim Khelif[1,2], Ali A. Eftekhar[3], Ali Adibi[1]; [1]*Electrical and Computer Engineering, Georgia Institute of Technology, Atlanta, GA, USA,* [2]*Institut Femto-ST, CNRS, France,* [3]*Georgia Institute of Technology, Atlanta, GA, USA*

Background, Motivation and Objective

Phononic crystals (PnCs) are synthetically-made structures that show extraordinary phenomena such as phononic band gaps (PnBGs). PnBGs are ranges of frequencies in which phonons (or mechanical vibrations) are not allowed to propagate. Recently, there has been a growing interest in micro/nano-fabricated PnC structures that can operate at very high frequencies for wireless communications and sensing applications.

Among the functionalities required in high quality wireless communication devices is filtering. The ability to filter a subset of frequencies with sharp transition bands is one of the most demanding functions that micromechanical structures have a sharp edge over other technologies in wireless communication devices. PnC structures with PnBGs can provide an adaptable and compact platform for implementing such functionalities with high performance.

Statement of Contribution/Methods

In this paper we report the design, fabrication, and characterization a CMOS-compatible VHF filter element based on the PnBG of a PnC structure fabricated in silicon (Si). To our knowledge this is the first demonstration of the possibility of PnC filtering reported at such high frequencies. By coupling PnC resonators, band pass (BP) filters are realized to function within the PnBG of the PnC. It is shown that the bandwidth and the sharpness of the transition regions of the filter depend on the number and the quality factor of the coupled PnC resonators. The BP filter is centered approximately at 140 MHz with a rational bandwidth of 7% and very sharp transition region characteristics.

Among different PnC configurations, we have used PnCs made of an array of void holes etched into a Si slab due to its unique advantages. PnC structure made of a hexagonal array of void holes in a 15 um-thick Si slab. The spacing between the centers of the closest holes is also 15 um, and the diameter of the holes is 12.5 um. Such a PnC structure has a large complete PnBG in the frequency window of 117 MHz < f < 149 MHz, which is appropriate for wide-band applications. We have used a thin (~1 um) stack of transducer made by sandwiching an AlN piezoelectric layer between two metallic electrodes to excite and detect the acoustic signal.

Results

It is shown that by changing the number of coupled resonators and their coupling, the sharpness of the filter and the bandwidth of the filter can be tuned. Also, techniques to suppress the unwanted ripples in the pass band will be discussed and their effectiveness is demonstrated.

Discussion and Conclusions

The demonstration of filtering functionality using coupled PnC resonators with competitive performance as will be shown in this paper opens a new venue in implementing and optimization of filtering functionality for wireless communications not achievable using the conventional micromechanical systems technology.

5D-4

9:00 AM Lithium niobate honeycomb lattice crystals : towards simultaneous photonic and phononic band gaps

Sarah Benchabane[1], Said Sadat-Saleh[1], Roland Salut[1], Gwenn Ulliac[1], Maria-Pilar Bernal[1], Vincent Laude[1]; [1]*FEMTO-ST, France*

Background, Motivation and Objective

The recent demonstrations of the existence of phononic band gaps for guided waves in the hypersonic regime are obviously rising strong interest in the field of radio-frequency telecommunication systems. But the experimental realizations of such periodical structures exhibiting pitches of the order of the micron also open up exciting perspectives in the field of acousto-optics. The dimensions at play are indeed comparable to those usually found in photonic crystals, that allow themselves to open band gaps for electromagnetic waves. It becomes hence conceivable to design and fabricate artificial crystals exhibiting photonic and phononic band gaps where acousto-optical interactions could be enhanced by a simultaneous confinement of both types of waves at a common wavelength scale.

Statement of Contribution/Methods

In this work, we report on the fabrication and acoustic characterization of a 2-dimensional periodical structure theoretically capable of exhibiting a photonic and a phononic band gap. The host material was chosen to be lithium niobate, because of its remarkable piezoelectric and optical properties. A honeycomb lattice based artificial crystal was hence fabricated using focused ion beam (FIB) milling. The phononic properties of the sample were characterized through electrical measurements of surface acoustic waves propagating through the sample.

Results

X-cut optical grade substrates were elected to ensure compatibility with standard processes used in the field of photonics, e.g. optical waveguide fabrication. The geometrical parameters were chosen to allow for both photonic and phononic band gaps. The pitch of the periodic structure, defined as the distance between two adjacent holes, was therefore initially set to be about 1.38 µm for a hole radius of 0.58 µm. The corresponding band gap was hence expected to range roughly from 870 to 1050 MHz. A broadband interdigital transducer (IDT) with an emission band ranging from 560 MHz to 1.25 GHz, encompassing the theoretical band gap, was used to generate surface acoustic waves. Detection was ensured by an identical IDT, located 80 µm away. Electrical measurements of the transmission through the honeycomb phononic crystal were then performed by means of RF probe testing.

Discussion and Conclusions

Transmission measurements performed for (XZ) propagating SAW indicate a clear extinction of the signal above about 640 MHz. This downshift of the entrance frequency of the band gap compared to the theoretically expected value can be easily accounted for by the increased filling fraction of the fabricated structure. Reflection measurements show the appearance of additional oscillations in the signal measured out of the phononic crystal, compared to the one stemming from a reference delay line. The demonstration of a phononic band gap in a structure theoretically supporting band gaps for electromagnetic waves paves the way towards the realization of simultaneously photonic and phononic, or phoxonic, crystals.

5D-5

9:15 AM High efficiency phononic crystal reflective gratings for surface acoustic waves

Jia-Hong Sun[1], Tsung-Tsong Wu[1]; [1]Institute of Applied Mechanics, National Taiwan University, Taipei, Taiwan

Background, Motivation and Objective

Surface acoustic wave (SAW) devices which consist of inter-digital transducer and metal gratings are widely used as filters and resonators for decades. Hundreds of metal gratings are usually employed to have good reflection. Phononic crystals (PCs) consisting of periodic arranged media perform acoustic band gaps and can stop surface acoustic wave propagation efficiently with tens of lattice periods [1, 2]. Thus PC was designed as space-sparing wave reflectors and verified experimentally [3]. In this paper, further analysis of SAW encountering PC is processed and a modified PC structure is proposed to improve the performance of reflective gratings.

Statement of Contribution/Methods

A silicon-based PC in Ref. [3] is adopted in the study. Cylindrical holes form a square lattice on a silicon half space, and the lattice constant is 10 μm with filling fraction of 0.283. Thus the PC has a band gap of 194-223 MHz for SAW along the ΓX direction and the operating frequency is chosen as 210 MHz. Finite element method is used to analyze SAWs incident on the different PC gratings. PCs with gradual increasing radii (called tapered PC) and with finite depth cylindrical holes are considered. By comparing with the amplitude of reflected wave, the efficiency of PC reflective grating is evaluated.

Results

The simulation shows that a great part of incident wave is reflected when SAWs reach the PC gratings. The loss is referred to creeping waves propagating downward along the air cylinders and mode conversion occurring on the boundaries which allows bulk waves to leave away the surface. Thus tapered PCs and PCs with finite-depth cylinders are proposed to reduce the energy loss. In the calculation, the amplitude of SAW reflected from a ten-layer normal PC grating is about 0.8 times of the incident one. The multiplication number becomes 0.9 when the reflective grating is replaced by a three-step tapered PC with a depth smaller than two times of wavelength. Further a SAW resonator is constructed by the improved PC grating, and the maximum amplitude inside the cavity is two times larger than the peak inside the cavity defined by the normal PC grating.

Discussion and Conclusions

In this study, a tapered PC with finite depth cylindrical holes is proposed, designed and studied numerically. The modified air/silicon PC still prohibits the propagation SAW and suppresses the energy leakage resulted from the mode conversion and creep waves on the interface. Thus the modified PC reflects SAW more efficiently and helps to improve the performance of SAW devices.

References:

[1] T.-T. Wu, L.-C. Wu, and Z.-G. Huang, J. Appl. Phys., vol. 97, no. 094916, 2005.
[2] J.-H. Sun and T.-T. Wu, Phys. Rev. B, vol. 74, no. 174305, 2006.
[3] T.-T. Wu, W.-S. Wang, J.-H. Sun, J.-C. Hsu, and Y.-Y. Chen, Appl. Phys. Lett., vol. 94, no. 101913, 2009.

THURSDAY ORAL

6D - CMUTs II Devices

Carribean Ballroom VI

Thursday, October 20, 2011, 8:00 am - 9:30 am

Chair: **John Fraser**
Philips Ultrasound

THURSDAY ORAL

6D-1

8:00 AM Comparison of conventional and collapse-mode CMUTs in 1-D array configuration

Kwan Kyu Park[1], Omer Oralkan[1], Butrus (Pierre) T. Khuri-Yakub[1]; [1]Edward L. Ginzton Laboratory, Stanford University, Stanford, CA, USA

Background, Motivation and Objective

A collapse-mode capacitive micromachined ultrasonic transducer (CMUT) operates beyond a pull-in condition. The center of a circular plate always contacts a substrate and the doughnut-shaped area in the plate acts as a moving plate. Due to a high electrostatic field through a gap and a unique mode shape, the collapse-mode CMUT has better TX/RX efficiency and larger acoustic bandwidth compared to a conventional-mode CMUT. In previous research on the collapse-mode CMUT, the element size of the CMUT is larger than a half-wavelength of the frequency of interest, which is a key feature as an imaging transducer. Our goal is developing the collapse-mode CMUT as a 1-D phased array.

Statement of Contribution/Methods

We fabricated 1-D CMUT arrays which have 70 µm by 2600 µm elements. The collapse-mode CMUT has circular silicon plates with a radius of 30 µm and a thickness of 1 µm. The conventional-mode CMUT has plates with a radius of 15 µm and a thickness of 1 µm to match a center frequency. For a phased array at 10-MHz center frequency, the element-to-element pitch is limited to 75 µm. Therefore, the elements of the conventional and the collapse-mode CMUT are made of two columns and one column of cells respectively (Fig. 1a,b). In addition to the fabrication, we performed finite element analysis (FEA) on the fabricated device.

Results

In the FEA modeling, the conventional-mode CMUT is biased at 111 V, which is 80% of pull-in voltage and the collapse-mode CMUT is biased at 75 V, 105% of the pull-in. A 50-V, 50-ns unipolar pulse is applied, and the conventional-mode CMUT shows 720-kPa (14.4 kPa/V) and the collapse-mode CMUT shows 2-MPa (40 kPa/V) averaged output pressure. The acoustic fractional bandwidth (FBW) is highly affected by the cell configuration. On the assumption of large number of cells, the 3-dB FBW of the conventional-mode CMUT and the collapse-mode CMUT is 106% and 141% respectively, which is much higher than a single-cell CMUT (Fig. 1c).

Discussion and Conclusions

The element configuration of the fabricated CMUT is between the single-cell and the large-number-cell configuration. The frequency response and the output pressure of the fabricated CMUT will be compared to the result from FEA modeling. In addition, the long-term stability of the collapse-mode CMUT will be compared to the conventional-mode CMUT. This work is supported by NIH 1R01CA134720.

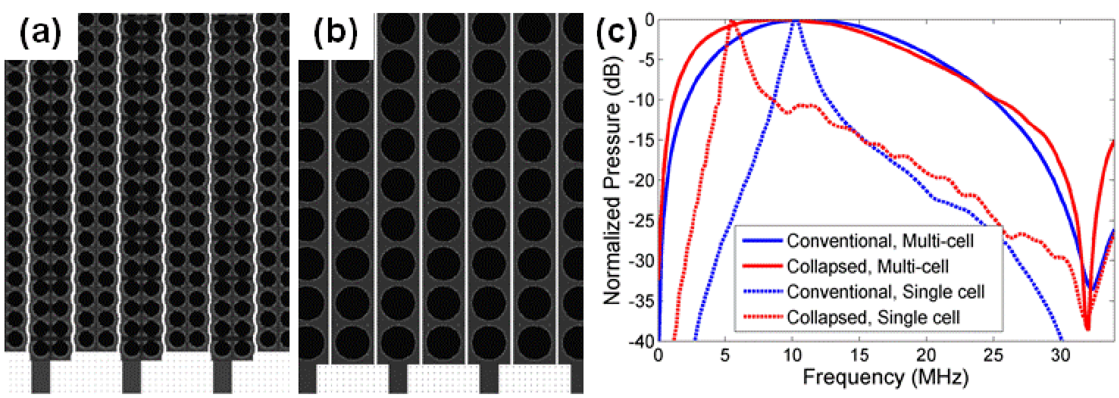

Figure 1. (a) Design of a conventional-mode CMUT and (b) a collapse-mode CMUT. Black color represents CMUT cells and gray color represent CMUT elements.
(c) Frequency response of output pressure of the conventional-mode and collapse-mode CMUT.

6D-2

8:15 AM Measurement of the additional loss due to a grooved bottom structure intended for use in the backing structure for Capacitive Micro machined Ultrasonic Transducers (CMUTs)

Kamal Raj Chapagain[1], Arne Rønnekleiv[1]; [1]Department of Electronics and Telecommunications, Norwegian University of Science and Technology, NTNU, Trondheim, Norway

Background, Motivation and Objective

The backing structure mostly used in CMUTs is a composite of epoxy and tungsten powder. To be able to absorb the acoustic signals, it should have high acoustic impedance that matches with the silicon substrate (on which CMUTs are manufactured) and it should be lossy. If we are able to make this structure thick enough, it will damp out the signal in the backing such that it would not reflect back to the transducer. But if we intend to use the transducer in applications where there is no room for the thick backing, for example in IVUS (Intravascular Ultrasound), a groove structured backing could be used. The grooves give extra loss by scattering the waves so that a thinner backing would be enough. The scattering removes power from the specular reflection from the back surface. This reflection is otherwise harmful for the imaging.

Statement of Contribution/Methods

There may be different ways to create the desired type of grooved structures, such as laser micro-milling, electric discharge machining (EDM), etc. Here an etched silicon wafer is chosen as a mold for making the grooved structure. Wet anisotropic etching of a silicon wafer with TMAH (Tetra methyl ammonium hydroxide) is performed to create the grooves.

If such structure consists of parallel rectangular grooves with equal width and spacing, it gives cancellation of the specular reflection of the waves when the groove depth is 1/4 of the acoustic wavelength at broadside. This will cause strong scattering in a narrow band. The scattering can be extended to a broader frequency range by superimposing grooves with different depths and different periodicities. Cancellation of the specular reflection at two independent frequencies requires four different depths; at three frequencies it requires eight different depths. In this paper, we have implemented a structure that gives cancellation at two chosen frequencies, 16MHz and 25MHz.

We present some experimental results to show that this type of structure reduces the specular reflection and compare the obtained results with theoretical calculations (FEM analysis).

Results

Reflection measurements are performed with the help of network analyzer for the measurement of loss due to grooves. About 40% volume fraction of tungsten powder is mixed with epoxy to get a composite with high acoustic impedance. The composite is cast between the patterned silicon wafers to create the grooves on it. Measurement performed on such structure shows that there is significant additional reflection loss due to the grooves; about 25dB around 16MHz, and about 10dB or more in the frequency range of 14MHz to 24MHz. We would also expect an additional loss at 25MHz, which is another frequency designed to have a null. However we observe only a modest dip at this frequency. We are currently investigating the causes of this.

Discussion and Conclusions

It is shown that the desired reflection level for an imaging application is obtained over a wide range of frequencies around 20MHz using an absorber thickness of 200µm.

THURSDAY ORAL

6D-3

8:30 AM Understanding CMUTs with substrate-embedded springs

Byung Chul Lee[1], Amin Nikoozadeh[1], Kwan Kyu Park[1], Butrus (Pierre) T. Khuri-Yakub[1]; [1]*E. L. Ginzton Laboratory, Stanford University, USA*

Background, Motivation and Objective

A capacitive micromachined ultrasonic transducer (CMUT) with ideal piston-like plate motion provides many benefits over a conventional CMUT having flexural plate movement. The improvements in performance mainly stem from the higher average displacement of the top plate for a given gap height. We previously reported on a new CMUT structure that resembles an ideal piston transducer. We also demonstrated the functionality of the first generation of the devices fabricated using this new structure. In this work, we report on comprehensive 3-D finite element analysis (FEA) models developed to further our understanding of the proposed CMUT structure.

Statement of Contribution/Methods

The proposed CMUT structure is composed of a rigid top plate connected to a substrate using long and narrow posts. The posts provide the spring constant of the structure rather than the top plate as in a conventional CMUT. However, similar to a conventional CMUT, a thin gap is provided under the top plate to achieve a high electric field with the application of a modest DC voltage. The new structure also encourages a single continuous top plate for the whole transducer element compared to a multi-cell design in a conventional CMUT to further enhance the average displacement.

We have developed 3-D FEA models to fully understand the static and dynamic behavior of the structure. To reduce the simulation runtime, we use FEA to separately model a single post and extract its spring constant. Then, the full 3-D model of a transducer element uses ideal springs with the extracted spring constant in place of the actual posts.

To realize a practical device, the top plate should provide a complete encapsulation to preserve the vacuum gap, which can be accomplished by anchoring the top plate at the transducer element edges. For our simulations, we considered two top plate types: a uniform plate, and a non-uniform plate having a thinner edge portion than its center. Comprehensive parametric simulations were performed for both plate types to understand the effect of each parameter on the static and dynamic behavior of the structure.

Results

The non-uniform plate provided better overall performance than the uniform plate type. For the simulated designs the average DC displacement achieved using the non-uniform plate type was over 50% larger than that for the uniform plate type. The FEA simulations also revealed that careful attention must be paid to the engineering of the top plate to assure that unwanted plate modes do not interfere with the normal operation of the device within the desired frequency band.

Discussion and Conclusions

Our FEA simulation results confirm that it is possible to realize a CMUT structure with improved performance. We are currently designing the second generation of devices based on the proposed structure for fabrication in the near future.

This work is supported by the National Institutes of Health under grant 1R01CA134720.

6D-4

8:45 AM Design and Implementation of Capacitive Micromachined Ultrasonic Transducers for High Power

Yalcin Yamaner[1], Selim Olcum[2], Ayhan Bozkurt[1], Hayrettin Koymen[2], Abdullah Atalar[2]; [1]*Electronics Engineering Department, Sabanci University, Istanbul, Turkey,* [2]*Electrical and Electronics Engineering Department, Bilkent University, Ankara, Turkey*

Background, Motivation and Objective

Capacitive micromachined ultrasonic transducers (CMUTs) have a strong potential to compete piezoelectric transducers in high power applications. In a CMUT, obtaining high port pressure competes with high particle velocity: a small gap is required for high electrostatic force while particle displacement is limited by the gap height. On the other hand, it is shown in [1] that CMUT array exhibits radiation impedance maxima over a relatively narrow frequency band. In this paper, we describe a design approach in which CMUT array elements resonate at the frequency of maximum impedance and have gap heights such that the generated electrostatic force in uncollapsed mode, can sustain particle displacement peak amplitude up to the gap height.

Statement of Contribution/Methods

The CMUT parameters are optimized for around 3 MHz of operation, using both a SPICE model and FEM. The optimized parameters require a thick membrane and low gap heights to get maximum displacement without collapsing membrane during the operation. We used anodic bonding process to fabricate CMUT arrays. A conductive 100 µm silicon wafer is bonded to a glass wafer. Before the bonding process, the silicon wafer is thermally oxidized to create an insulating layer which prevents break down in the operation. Then, the cavities are formed on the insulating layer by a wet etch. The gap height is set to 100 nm. Meanwhile, the glass wafer is dry etched by 120 nm and the etched area is filled by gold evaporation to create the bottom electrodes. The wafers are dipped into piranha solution and bonding process is done afterwards.

Results

The fabricated CMUTs are tested in an oil tank. To eliminate the DC voltage which may cause charging problem in the operation, we tried to drive the CMUT array with large continuous wave signals at half of the operating frequency. We observed 1MPa peak to peak pressure with -23 dB second harmonic at the surface of the array (Fig. 1).

Discussion and Conclusions

The proposed design further extends the operation of CMUTs. Observing low harmonic distortions at high output pressure levels, without any charging problem, make CMUT a big candidate for high power applications.

[1] Senlik, M.N.; Olcum, S.; Koymen, H.; Atalar, A.; "Radiation impedance of an array of circular capacitive micromachined ultrasonic transducers", IEEE Transactions on Ultrason., Ferroelect., and Freq. Contr., vol. 57, no. 4, Apr. 2010.

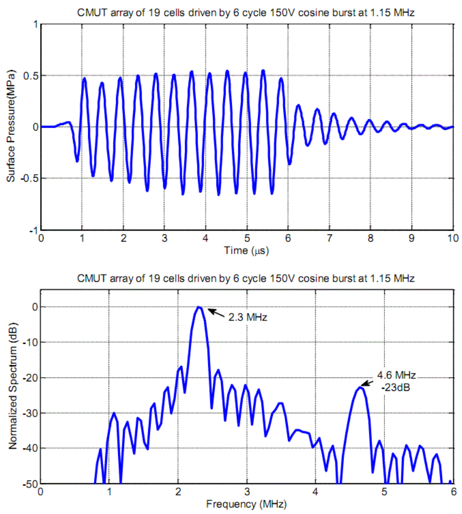

6D-5

9:00 AM Fabrication and model validation for CMUTs operated in permanent contact mode

Min-Chieh Ho[1], Srikant Vaithilingam[1], Mario Kupnik[2], Butrus T. Khuri-Yakub[1]; [1]Edward L. Ginzton Laboratory, Stanford University, CA, USA, [2]Brandenburg University of Technology, Cottbus, Germany

Background, Motivation and Objective

We present the successful fabrication and finite element analysis (FEA) validation of capacitive micromachined ultrasonic transducers (CMUTs), in which each plate is in permanent contact with the bottom of the cavity, even at zero dc bias condition. As presented last year, our calculations indicated that such design has a more stable operating frequency and coupling efficiency over a varying ambient pressure range. The main goal of this research is to provide transducers suitable to operate over a wide and varying pressure range (~1 - 20 atm), targeting applications such as ultrasonic flow metering (UFM) of flare gas.

Statement of Contribution/Methods

The fabrication is based on a thick buried oxide layer CMUT process (Kupnik, et. al., IUS 2010), which uses direct wafer bonding and allows us, in particular for this type of CMUT, the realization of only partially connected bottom electrodes. This means the area beneath the contact region is intentionally not connected, in order to avoid an increased parasitic capacitance value due to the permanent contact. To ensure such a permanent contact, we intentionally varied the cell radii, ranging from 1800 to 2200 um, the gap heights, and plate thicknesses for our first fabrication run. For these CMUTs, the permanent contact happens during the fabrication, i.e. at the release step of the handle layer of the silicon on insulator plate wafer. By using a Zygo white-light 3D surface profiler and Polytec optical fiber interferometer at 1 atm, we were able to validate our FEA in terms of static behavior. From these plate profile measurements we extracted the contact radii for various biasing conditions. In addition, by performing electrical impedance and displacement (optical fiber interferometer) measurements, we were able to validate the FEA in terms of dynamic characteristics as well.

Results

The fabrication was successful and the devices are reliable (no electrical breakdowns). We biased the devices repeatedly up to 500 V over several months. The contact radius measured as a function of applied dc (~ 300 - 400 um for 0 - 200 V) is within 5% from the FEA results. Both impedance and displacement measurements at 1 atm show that for a device with ~34 um gaps and 30 um thick plates, the cells with 1800 um radius operate in conventional mode with resonance frequency of ~ 50 kHz, as predicted by or FEA (+/- 5%). The ones with 2200 um radius operate in permanent contact mode at ~ 75 kHz (first mode, +/- 3% compared to FEA) and ~ 195 kHz for the second mode (+/- 1.5% compared to FEA). In addition, the overall trends of resonant frequency and contact radii as a function of dc bias voltage are both consistent with FEA.

Discussion and Conclusions

The fabrication process for a CMUT operated in permanent contact mode is feasible. Further, the FEA for such a device is suitable for both static and dynamic behavior predictions. For future work, we plan to test the devices under varying ambient pressure conditions.

This research is supported by Fluenta Inc., Norway.

6D-6

9:15 AM Radiation Impedance of an Array of Circular Capacitive Micromachined Ultrasonic Transducers in Collapsed State

Alper Ozgurluk[1], Abdullah Atalar[1], Hayrettin Koymen[1], Selim Olcum[1]; [1]Electrical and Electronics Engineering, Bilkent University, Ankara, Turkey

Background, Motivation and Objective

Radiation impedance of an array of CMUT cells is a critical design parameter for achieving high performance cMUT arrays. For conventional (uncollapsed) mode, the radiation impedance of an array of cMUT cells was studied in [1]. However, the radiation impedance of an array for the collapse mode has not yet been investigated.

Statement of Contribution/Methods

In this paper we present the calculation of the radiation impedance of clamped circular CMUTs both analytically and using FEM simulations. First, we model the radiation impedance of a single collapsed cMUT cell analytically by expressing its velocity profile as a linear combination of sufficient number of velocity profiles as given by Porter [2]. For this purpose, 2D-axisymmetric FEM simulations are performed using ANSYS. For an array of collapsed cMUT cells, the mutual impedance between the cells must also be taken into account and is calculated analytically using the formulas given by [2]. In this case, we perform 3D FEM simulations in COMSOL Multiphysics using appropriate symmetry boundary conditions.

Results

Radiation impedances for arrays of 7, 19, 37 and 61 circular collapsed CMUT cells for different contact radii are calculated both analytically and by FEM simulations. A good agreement between the analytical and FEM simulation results is achieved. In the figure below, the results for an array of 7 collapsed circular cells with 20µm radius are given for a contact radius of 8µm. We find that the peak radiation resistance value is reached at higher kd values in the collapsed case as compared to the uncollapsed case where d is the distance between the centers of two neighboring cMUT cells. As the contact radius increases, the radiation resistance becomes smaller for almost all values of kd and reaches a minimum value of 0.4 for a contact radius of 14µm in the deep collapsed case.

Discussion and Conclusions

The radiation resistance of an array reaches to a plateau of certain value between 0.4 and 0.6 depending on the contact radius and maintains this level for a wide kd range. The variation of reactance with respect to frequency indicates a fixed valued inductance behavior in the same kd range. The radiation impedance with these properties is very favorable for the design of wideband arrays.

[1] M. N. Senlik et.al., IEEE Trans. on UFFC , vol.57 (4), pg.969, 2010.
[2] D. T. Porter, J. Acoust. Soc. Am., vol. 36, pp. 1154–1161, 1964.

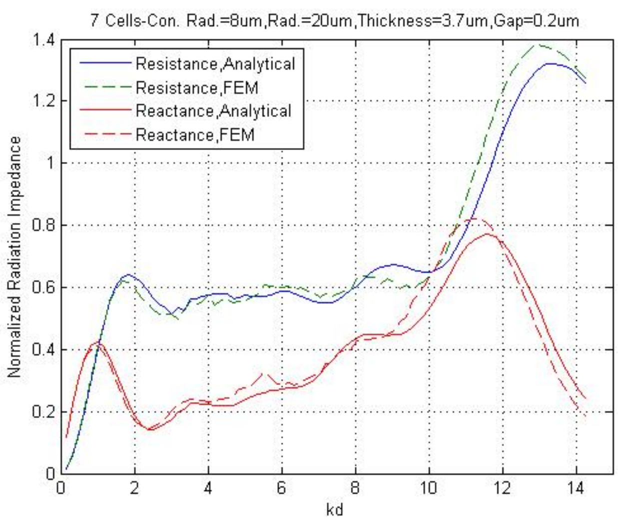

THURSDAY ORAL

1E - Clinical Session

Boca Rooms II-IV

Thursday, October 20, 2011, 10:30 am - 12:00 pm

Chair: **Ton van der Steen**
Erasmus Medical Centre

1E-1

10:30 AM IVUS and IVUS elasticity related imaging

Yoshifumi Saijo1; *1Tohoku University, Japan*

Abstract Not Available

1E-2

11:00 AM OCT, NIR/IVUS and other optical techniques

Evelyn Regar[1]; [1]*Erasmus Medical Center, the Netherlands*

Abstract Not Available

1E-3

11:30 AM Plaque characterization by IVUS, NIR, FFR and other emerging techniques

Akiko Maehara[1]; [1]*Cardiovascular Research Foundation, USA*

Abstract Not Available

2E - Bone

Boca Rooms VI-VII

Thursday, October 20, 2011, 10:30 am - 12:00 pm

Chair: **Pascal Laugier**
Université Pierre et Marie Curie

2E-1

10:30 AM Circumferential waves guided by the femur cortical shell can be used to predict femur strength: in vitro evidence

Julien Grondin[1], Quentin Grimal[1], Sandra Guerard[2], Reinhard Barkmann[3], Claus Gluer[3], **Pascal Laugier[1]**; [1]LIP, UPMC-CNRS, France, [2]Arts et Metiers PARISTECH, France, [3]Medizinische Physik, Klinik fur Diagnostische Radiologie, UKSH, Germany

Background, Motivation and Objective

Quantitative ultrasound (QUS) at the proximal femur shows a good performance for hip fracture discrimination (Barkmann et al. Osteoporos Int 21(6); 2010). QUS measurements at the hip, currently performed in through-transmission using a pair of focused transducers, mostly measures the trabecular bone compartment. However, experiments and simulations (Ultrasound med biol 36(4);2010) showed the existence of an early arriving signal, preceding the signal transmitted directly through cancellous bone. The early arriving signal is most likely associated with the propagation of a circumferential wave guided in the cortical shell. Because cortical bone is a key factor to maintain femur neck mechanical integrity, we hypothesized that the measurement of the propagation time of the first arriving signal in through-transmission at the femur neck could be predictive of femur strength.

Statement of Contribution/Methods

For nine femurs of women donors (mean age 83 y.) we measured: (1) femur strength in one-legged stance configuration with state-of-the-art mechanical tests; (2) bone mineral density (BMD) using dual X-ray absorptiometry; (3) ultrasonic (US) time-of-flight through the neck. US measurements were performed in immersion, in a confocal through-transmission configuration, with cylindrically focused transducers (0.5 MHz central frequency). A 5 mm-thick transverse cross-section of the femoral neck corresponding to the half-maximum beamwidth at focus was interrogated. To account for inter-individual anatomic variations, for each specimen, ultrasonic measurements were performed for a set of nine positions or angles which slightly departed from a nominal position (middle of the neck, perpendicular to the neck axis). The mean time-of-fligth (T) averaged over the nine measurements positions/angles was kept for further analysis.

Results

Significant relationships were observed between T and mechanical parameters: failure load: R2=0.79; elastic energy: R2=0.63; apparent stiffness: R2=0.70; BMD was also well correlated to strength (R2=0.78 for failure load).

Discussion and Conclusions

By measuring nine femurs in vitro with an original and relatively simple method we have proved that probing femur neck cortical bone with ultrasound is possible and brings highly relevant information regarding femur strength. In future works, we shall investigate whether a combination of independent ultrasound measurements of the cortical and trabecular compartments at the upper femur enhance fracture risk prediction.

2E-2

10:45 AM Nonlinear ultrasound monitoring of fatigue microdamage accumulation in cortical bone

Sylvain Haupert[1], Sandra Guerard[2], Paul A. Johnson[3], David Mitton[2,4], Pascal Laugier[5]; *[1]UPMC Univ Paris 6 - CNRS - LIP, PARIS, IDF, France, [2]Arts et Metiers ParisTech - LBM, PARIS, France, [3]Geophysics Group - Los Alamos National Laboratory, LOS ALAMOS, USA, [4]Université de Lyon - Ifsttar - LBMC, BRON, France, [5]UPMC Univ Paris 6 - CNRS - LIP, PARIS, France*

Background, Motivation and Objective

Accumulation of bone microdamage is suspected to lead to severe impairment of mechanical properties with an increase in skeletal fragility and fracture risk [1]. The objective of the study was to evaluate the nonlinear resonant ultrasound spectroscopy (NRUS) technique for measuring micro-damage accumulation in cortical bone using mechanical fatigue

Statement of Contribution/Methods

Sixteen human cortical bone specimens were machined as parallelepiped beams (50*4*2mm) to control damage localization during four-point bending fatigue cycling and to unambiguously identify resonant modes for NRUS measurement. During damage progression, load and displacement curves were recorded to extract secant (Esec), loading (Eload) and linear elastic beam theory (ELEBT) moduli [2]. The latter has been shown previously to reflect microdamage accumulation during four-point bending mechanical fatigue [3]. Before and between each damage step, nonlinear ultrasonic elastic (αf) and dissipative (αQ) coefficients were monitored by NRUS [4]. The experimental setup consists of a piezoceramic emitter bonded with cyanoacrylate at one end of the sample. The longitudinal displacement is measured at the other end by a laser vibrometer. Each bone specimen was probed by a swept-sine around its first compression mode, applying progressively increasing drive levels.

Results

Despite substantial between-sample variability, αf increased significantly (32%) while a significant decrease of 43% was found for ELEBT (See figure 1. Displayed error bars correspond to the 1st and 3rd quartile).With an augmentation of 13%, αQ seems less sensitive to damage. In contrast, results showed no significant variation of the linear elastic moduli (Esec and Eload).

Discussion and Conclusions

The results of this study evidence that micro-damage accumulation in cortical bone can be achieved using nonlinear ultrasound resonant spectroscopy. Next steps will investigate relationships between the magnitude of the nonlinear response and the characteristics of microdamage (e.g., size, density, orientation and localization of microcracks).

[1] P. Zioupos, et al., Journal of Microscopy, 2001.
[2] T. Diab, et al., Bone, 2005.
[3] M. Landrigan, et al., Journal of biomechanics, 2009.
[4] K. E. A. Van den Abeele, et al., Research in Nondestructive Evaluation, 2000.

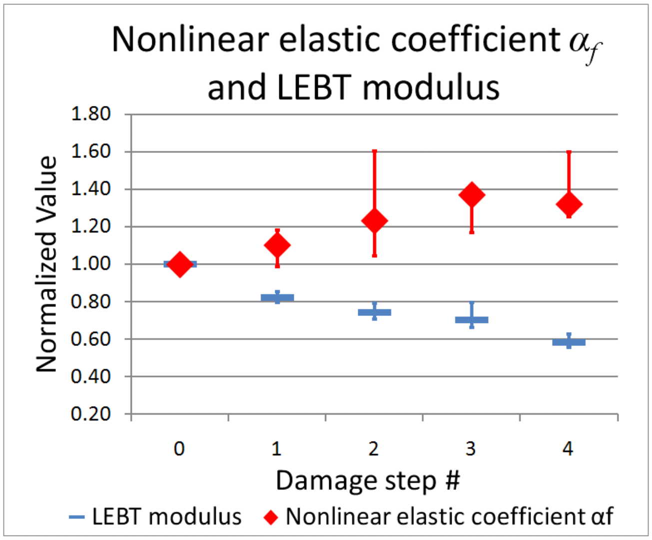

2E-3

11:00 AM Phase Cancellation and Aperture Size on Broadband Ultrasonic Attenuation for Trabecular Bone Assessment using a 2-D Confocal Synthetic Array

Jiqi Cheng[1], Frederick Serra-Hsu[1], Yuan Tian[1], Wei Lin[1], Yi-Xian Qin[1]; [1]*Stony Brook University, USA*

Background, Motivation and Objective

Quantitative ultrasound (QUS), an alternative method for bone status assessment, is inexpensive, portable, highly available, and non-ionizing. Phase cancellation due to large receiver size has been proposed as a contributing factor to the inaccuracy of broadband ultrasound attenuation (BUA). Transducers with aperture size ranging from 2 to 5 mm (themselves are susceptible to phase cancellation) have been used in previous attempts to study the effect of phase cancellation. This study aims to accurately investigate the effects of phase cancellation and receiver aperture size on BUA calculation using an ultra small receiver (aperture size: 0.2 mm) in conjunction with a newly developed 2-D synthetic array system.

Statement of Contribution/Methods

Fresh sheep trabecular bone samples (average sample thickness = 6.26±0.52mm) were harvested from medial and lateral femur condyles (n=54) with a diamond wheel saw under constant water cooling. The bone marrow was removed by water jetting, and the samples were frozen in saline at -20 degree Celsius before testing.

For ultrasound measurement, the ultrasound wave is transmitted by a focused ultrasound transducer and received by a hydrophone. The bone sample is placed in the middle plane vertical to the transmitter and receiver. The receiver scans a plane parallel to the bone sample with a stepping size of 0.25 mm. Both phase sensitive (PS) detection and phase insensitive (PI) detection are performed with different receiver aperture sizes synthesized by one single receiver. A hydrophone with an aperture size of 0.2 mm is used as the receiver, and 2-D scanning (step size of 0.25 mm) is used to synthesize a 2-D ultra-fine array receiver.

Results

When receiver aperture size is the same as transmitter aperture size, the average normalized BUA (nBUA) is 37.60±14.20 dB/MHz/cm and 34.79±10.44 dB/MHz/cm for PS and PI respectively, and PS nBUA is significantly different than PI nBUA (paired t-test, $p<0.0001$). On average, PS nBUA is 8.1% higher than PI nBUA, and linear regression shows that PS nBUA can explain 92.4% of the variability in PI nBUA.

Discussion and Conclusions

With the new system, the major limitations of previous studies are circumvented, and the field distribution of ultrasound waves can be easily identified and visualized. Results show that phase cancellation does have a significant effect on BUA (e.g., PS nBUA is 8.1% higher than PI nBUA). Receiver aperture size also influences the BUA reading for both PI and PS detection and smaller receiver aperture tends to result in higher BUA readings. The results also indicate that the receiver aperture size used in the confocal configuration with PI detection should at least equal the aperture of the transmitter to capture most of the energy redistributed by the interference and diffraction from the trabecular bone. Thus, a correction of BUA calculation based on the phase cancellation factor could significantly improve the accuracy of trabecular bone BUA assessment.

2E-4

11:15 AM Determining the attenuation of overlapping fast and slow waves in cancellous bone using Bayesian techniques

Amber Nelson[1], Joseph Hoffman[1], Mark Holland[1], Katsunori Mizuno[2], Yoshiki Nagatani[3], Mami Matsukawa[2], James Miller[1]; [1]*Washington University in St. Louis, USA,* [2]*Doshisha University, Japan,* [3]*Kobe City College of Technology, Japan*

Background, Motivation and Objective

It is known that cancellous bone can support the propagation of two compressional wave modes, referred to as fast waves and slow waves. Previous studies have demonstrated that performing conventional phase spectroscopy analysis on interfering fast and slow waves can lead to the non-causal negative dispersion sometimes reported in measurements of cancellous bone. The goal of the current study was to investigate the effects of overlapping wave modes on the determination of the attenuation properties of cancellous bone and also to examine the extent to which the choice of analysis method employed effects the attenuation results.

Statement of Contribution/Methods

Using a two-wave mode propagation model, individual fast waves and slow waves were simulated, using Bayesian parameters obtained from 1 MHz experimental data from bovine cancellous bone, for sample thicknesses from 15mm to 6mm in 1mm increments. Two methods of analysis for determining the attenuation as a function of propagation were applied. One was a time-domain method using the amplitude of the first peak of the received mixed-mode waveform. The other was a frequency-domain method applied to the isolated fast wave and slow wave.

Results

As seen in the figure below, the time-domain analysis applied to the simulated unseparated waveforms yielded a fast wave attenuation that decreased with increasing propagation distance. In contrast, the frequency-domain method applied to the separated fast and slow waves yielded attenuation coefficients for each wave mode that were independent of propagation distance and which agreed with the constant-with-distance input parameters of the model. The attenuation coefficients at 0.75MHz are displayed because this frequency is near the center of the received waveforms' bandwidths.

Discussion and Conclusions

Frequency-domain analysis performed on the fast and slow waves separated by Bayesian analysis was shown to be the method least susceptible to artifacts.

Supported by NIH grant R01AR057433

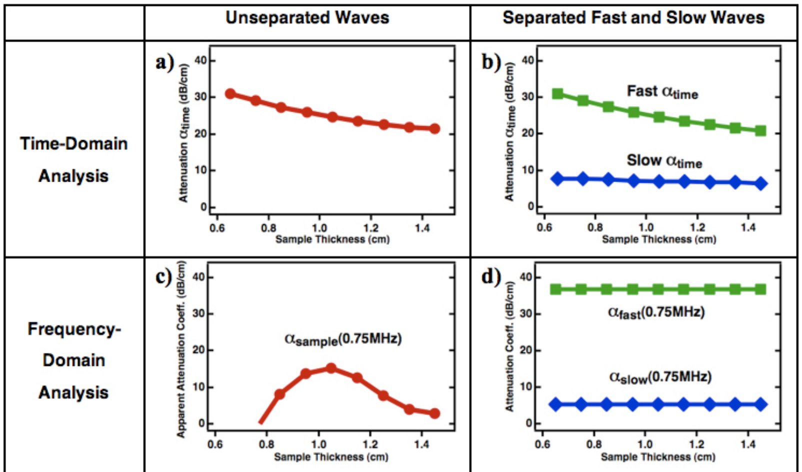

Results as a function of sample thickness for applying: **(a)** the time-domain method to the unseparated fast wave, **(b)** the time-domain method to the separated fast wave and slow wave, **(c)** log-spectral subtraction to the unseparated fast and slow wave, and **(d)** log-spectral subtraction to the individual fast and slow wave.

2E-5

11:30 AM Circumferential guided wave measurement in the femur cortical shell : bone mimicking tube study

Pierre Nauleau[1], Etienne Cochard[2], Jean-Gabriel Minonzio[1], Quentin Grimal[1], Claire Prada[2], Pascal Laugier[1]; [1]Laboratoire d'imagerie paramétrique (UPMC Paris6 - CNRS UMR 7623), Paris, France, [2]Institut Langevin (ESPCI Université Paris7 - CNRS UMR 7587), Paris, France

Background, Motivation and Objective

Previous studies have showed that circumferential guided waves are involved in the ultrasonic propagation at the proximal femur. The frequency-dependent guided wave phase velocities depend on both material properties and geometry (thickness) of the structure in which they propagate. We hypothesize that the measurement of guided waves at the proximal femur could contribute to improve fracture risk prediction. Prada et al. reported that the Lamb mode phase velocities of an air-filled immersed elastic cylinder could be computed from the time-reversal operator recorded with an array of transducers distant from the waveguide using DORT method [Prada and Fink, J Acoust Soc Am, 104, 1998]. The objective of this work was to adapt the method to the case of dissipative cortical bone mimicking tube.

Statement of Contribution/Methods

A cylindrical bone-mimicking phantom made of glass-fiber-filled epoxy material, with typical material properties (elasticity, anisotropy and attenuation) and dimensions of the cortical compartment of human proximal femur was used in the experiments. The scattering response of the phantom immersed in water was measured using a transmit-receive concave 1-D array of 128 transducers of 1MHz-central frequency. The natural focal length of the array was 160mm. The DORT method parameters such as characteristics of the time window, number of singular values, backpropagation distance were optimized to obtain the phase velocity dispersion curves.

Results

For the considered bone-mimicking phantom, three circumferential guided wave modes could be identified as A_0, A_1 and S_1 by comparison with theoretical dispersion curves (Fig.1).

Discussion and Conclusions

This study shows that the dispersion curves of circumferential waves in a bone phantom can be measured with a good precision using the DORT method suggesting that they can be used in an inversion scheme to provide relevant properties such as shell thickness and elastic coefficients to reach the goal of bone strength assessment. Next steps will involve measurements of bone mimicking material with realistic geometries and boundary conditions.

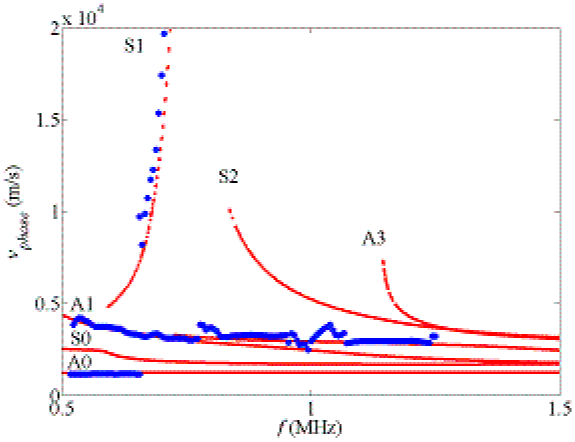

2E-6

11:45 AM Two wave propagation image for investigating the anisotropic structure of cancellous bone

Keisuke Yamashita[1], Katsunori Mizuno[1], Mami Matsukawa[1]; [1]*Doshisha University, Japan*

Background, Motivation and Objective

Two-wave phenomenon in cancellous bone has been reported by several investigators [e.g. Hosokawa et.al., J.Acoust.Soc.Am., 101 (1997) 558.]. Making use of this phenomenon, a new QUS device has been introduced to evaluate the radius *in vivo* [Bréban, et. al., Bone (2010) 46, 1620.]. We have also reported that two waves reflect not only bone mass but also the complex bone structure of cancellous bone [Mizuno et. al., J. Acoust. Soc. Am., 128 (2010) 3181.]. We then propose a new simple imaging technique based on the two-wave phenomenon for investigating the anisotropic structure.

Statement of Contribution/Methods

Cylindrical specimens (diameter: 11 mm) of cancellous bone were obtained from the distal part of a bovine left femur. Longitudinal wave was measured using a conventional ultrasound pulse technique with a focus type transmitter [Mizuno et.al., IEEE Trans. Ultrason. Ferroelectr. Freq. Control., 55 (2008) 1480.]. To investigate the ultrasonic fields after the propagation in the specimen, we rotated the receiver around the central axis of the cylindrical specimen (angle φ), as shown in the figure. The specimen was rotated to check the effect of main trabecular alignment (MTA) (angle θ). The specimen was also moved in the axis direction to change the measurement position in the cylinder. In addition, bone volume fraction (BV/TV), and degree of anisotropy (DA) of the specimen were estimated by 3D-Bon software (Ratoc, Tokyo, Japan) using the X-ray micro CT data.

Results

The image of arrival time of the fast wave was obtained as shown in the figure. Here, MTA direction was not equal to the incident wave direction (θ = 30°). The image clearly showed the effect of alignment. We can find clear ″fast″ wave in the direction of MTA. The arrival time changed due to the measurement position along the axis in the sample, telling the effect of structure variation in the specimen. DA and BV/TV actually changed owing to the position.

Discussion and Conclusions

The ultrasonic field after the propagation in the cancellous bone specimen was observed by rotating the receiver. The image of arrival time clearly reflected the anisotropy, showing ″apparent refraction″. The propagation image is simple and convenient for easy understanding of the anisotropy. The image may become a user-intuitive tool for the future *in vivo* assessment.

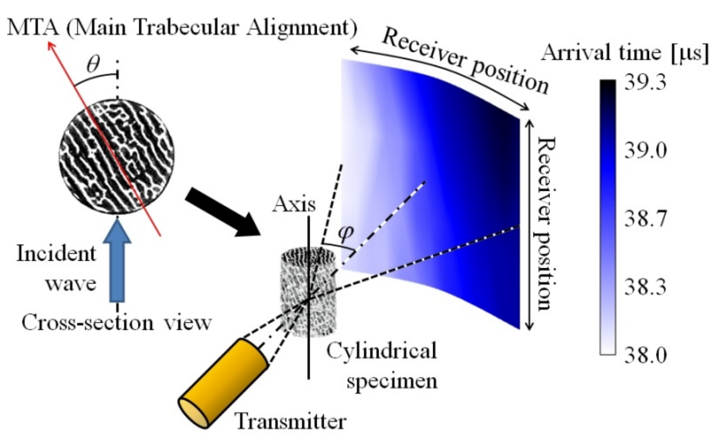

Fig.1 Experimental setup and the propagation image.

3E - Novel Ultrasound Systems

Carribean Ballroom VII

Thursday, October 20, 2011, 10:30 am - 12:00 pm

Chair: **Wilko Wilkening**
Siemens Medical Solution

3E-1

10:30 AM An Architecture and Implementation of Real-time Synthetic Aperture Compounding with SARUS

Matthias Bo Stuart[1], Jørgen Arendt Jensen[1]; [1]Center for Fast Ultrasound Imaging, Dept. of Elec. Eng., Technical University of Denmark, DK-2800 Lyngby, Denmark

Background, Motivation and Objective

Synthetic aperture and compounding are methods for increasing the resolution and decreasing the speckle-noise of ultrasound images. Both methods are computationally very intensive, and no systems in the published literature are capable of implementing both in real-time. The objective of this work is to implement real-time synthetic aperture compounding in the experimental ultrasound scanner SARUS.

Statement of Contribution/Methods

SARUS is constructed with field-programmable gate arrays (FPGAs), which allows the functionality of the system to be modified dynamically. In this paper, the existing implementation meant for real-time synthetic aperture imaging is modified and extended to also implement compounding in receive. The beamformer uses a tile-based algorithm that splits the processing of each line in the beamformed image across the 64 processing boards in the system. Each processing board, thus, hosts the ADCs, DACs, and processing resources for 16 channels of which 4 are processed in real-time in the implementation presented in this work.

Results

The synthetic aperture beamformer is implemented in a Virtex4 FX100 FPGA. The real-time processing produces a low-resolution image consisting of 576 lines (3 angles with 192 lines each) at 1,424 low-resolution images per second. Using 32 low-resolution images to form a high-resolution image, this gives 45 high-resolution images per second, corresponding to 820,224 lines beamformed each second. For comparison, a conventional B-mode image with 192 lines at 45 frames per second only requires 8,640 lines to be beamformed per second.

The synthesized beamformer, including all peripherals, consumes 34,709 (82%) slices of FPGA logic and 242 (64%) of the on-chip block RAMs.

The frame rate scales linearly with the number of lines per image and the number of low-resolution images per high-resolution image. Thus, using only 16 low-resolution images to form a high-resolution image would double the frame rate to 90 high-resolution images per second.

Discussion and Conclusions

This work presents the first implementation of a system capable of producing real-time synthetic aperture compound images at high frame rates.

3E-2

10:45 AM A Programmable and Compact Open Platform for Ultrasound Bio-Microscope

Weibao QIU[1], Yanyan YU[1], Fu Keung TSANG[1], Lei SUN[1]; [1]Department of Health Technology and Informatics, The Hongkong Polytechnic University, Hong Kong

Background, Motivation and Objective

Ultrasound bio-microscope (UBM) has become an important imaging tool to delineate small living structures as its fine spatial resolution on the order of several tens of microns. It has been applied to the diagnosis of human diseases and preclinical research of small animal models. Various studies utilizing UBM requires a truly open imaging platform for flexibility and compactness to satisfy different biomedical investigations. This paper presents the development of a programmable and compact open platform of an UBM capable of high-resolution and real-time imaging (central frequency 20-80MHz).

Statement of Contribution/Methods

Field programmable gate array (FPGA) was employed to process the high-resolution real-time images. Taking advantage of the programmability and high speed of FPGA, flexible and real-time imaging was achieved in this platform with B-mode and pulsed-wave (PW) Doppler imaging. In addition, a novel digital quadrature demodulation algorithm for high frequency ultrasound was implemented to achieve fast and accurate PW Doppler profiling. Moreover, low noise and high speed analog electronics was used to achieve high signal-to-noise ratio and high sensitivity. A 64-bit PCI bus was employed for fast image display or radio frequency raw data storage through DMA operation. Finally, all the electronics were incorporated in a single printed circuit board for compactness and cost-effectiveness.

Results

This open platform offers a minimum detectable signal of 25μV, allowing a 52dB dynamic range at a total gain of 45dB. The image quality of this platform was evaluated by a tungsten wire phantom and a tissue-mimic phantom. Images of the phantoms obtained by this platform are shown in Fig. 1. In vivo sonogram obtained from a vein in human hand is also shown in Fig. 1. The cyclic profile correlates well with the heart rate of the subject (78 beats/min).

Discussion and Conclusions

The development of a programmable and compact open platform for real-time UBM has been described. Both B-mode imaging and PW Doppler imaging had been incorporated with this platform. Such a device could facilitate biomedical researchers with high flexibility to accommodate various investigations in ophthalmic, dermatologic, intravascular, preclinical animal models imaging for normal development and diseases.

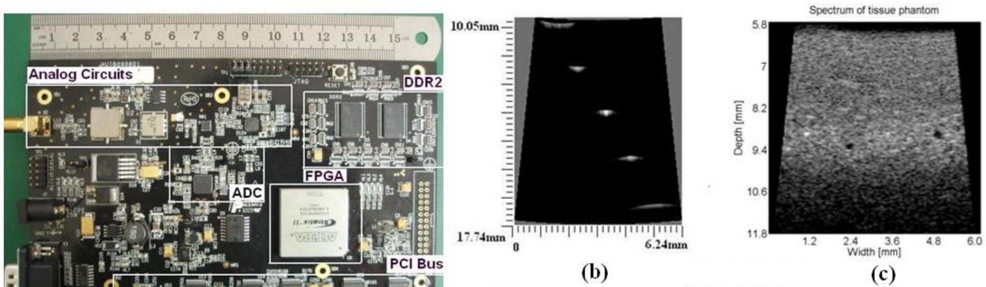

Fig. 1 (a) Photograph of the open platform. (b) Image of wire phantom (20µm tungsten wires). (c) Image of tissue-mimic phantom with ~200um anechoic spheres. (d) Pulsed-wave Doppler waveform of a vein in human hand.

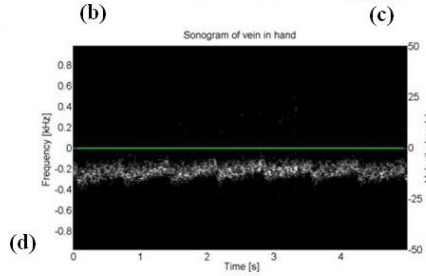

3E-3

11:00 AM Ultrasonic wireless power and data communication for neural stimulation

Je-Yu Tsai[1], Kai-Han Huang[1], Jun-Ru Wang[1], Shen-Iuan Liu[1], Pai-Chi Li[1]; [1]*Natoinal Taiwan University, Taiwan*

Background, Motivation and Objective

Wireless neural stimulation has gained wide interest, as it has potential in several clinical applications such as deep brain stimulation and neuromuscular stimulation. Most of the exiting wireless power and data transmission methods are based on electromagnetic coupling in the radio frequency range. However, the power transmission is often limited at depth. In this study, we propose ultrasound as vehicles for both power and data transmission for wireless, implantable neural stimulation. The main advantage is that ultrasound in the MHz range can focus at depth, thus providing an effective way for power transmission under FDA safety limits. In addition, the weak acoustic scattering in soft tissues also allows accurate data communication with the implantable device using ultrasound.

Statement of Contribution/Methods

We have designed and fabricated a prototype device, which consists of a PVDF transducer (1MHz center frequency and 6mm diameter) and a custom design IC that performs AC-DC conversion and decoding of the ultrasound signals for controlling the neural stimulator. Received power is measured and compared to the power consumption required by the stimulation circuit. Amplitude-shift keying (ASK), frequency-shift keying (FSK) and phase-shift keying are all tested and bit error rates (BERs) are calculated to assess performance of difference coding schemes. A tissue mimicking phantom with speckle generating background and acoustic attenuation at 0.5dB/MHz/cm is also used during measurements.

Results

At an acoustic output power of 112 mW from the transmit transducer, 4.15 mW can be received by the device and the stimulator only consumes a power of 1,8 mW. A BER of 10-6 at 25 kbps data rate is also achieved.

Discussion and Conclusions

The measurements are performed under the FDA safety limits. With the current device, it is possible to increase the transmission power to as high as 19.76mW while still not exceeding the FDA safety limits (Ispta=720mW/cm2). A smaller transducer can also be used to reduce the size of the implantable device. Feasibility of ultrasonic wireless neural stimulation is clearly demonstrated.

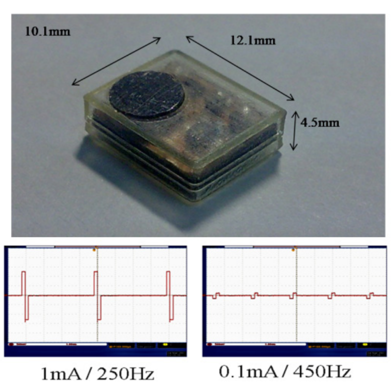

Figure: (Top). Picture of the actual prototype device. Transducer is at the top, and the custom-design IC is on the back. (Bottom). Actual stimulation waveforms measurement from the prototype device.

THURSDAY ORAL

3E-4

11:15 AM Implementation of a Smart-Phone Based Portable Doppler Flowmeter

Po-Yang Lee[1], Pay-Yu Chen[1], Chih-Chung Huang[1]; [1]Department of Electrical Engineering, Fu Jen Catholic University, Taiwan

Background, Motivation and Objective

Recently, portable ultrasound scanner has been introduced for clinical diagnosis. However, it is not convenient to apply Doppler measurement by commercial duplex scanner during exercise or sleeping due to the shape of handheld probe. In addition, most devices used the DSP and/or FPGA chip to process the Doppler signals from flowing blood, however, some attached components are needed such as RF and/or audio ADC, on board memory, programmable timer, and LCD graphic display module and its control circuit (or the connector module for laptop display). In order to simplify these complex circuits, an implementation of a smart-phone based portable ultrasound pulsed-wave Doppler flowmeter is reported in this study.

Statement of Contribution/Methods

A 10 MHz ultrasonic surface transducer was designed for dynamic monitor of arterial blood flow velocity. Figure 1(a) shows the system block diagram. The in-phase and quadrature-phase audio Doppler shift signals were obtained by a portable analog circuits system. After the hardware processing, the Doppler signals were fed directly to an Android based smart-phone for Doppler spectrogram analysis and display in real time. Both in vitro blood flow velocity measurement and in vivo testing were carried out for verifying the performance of portable Doppler flowmeter.

Results

Figure 1(b) shows the prototype of portable device, consisting of the surface transducer, analog circuit system, and smart-phone. In addition to real time display, both audio Doppler signal raw data and Doppler spectrograms can be recorded on the built-in memory card for off-line processing, as shown in Fig 1(c).

Discussion and Conclusions

The entire analog circuits, including the power supply, can be built for less than US$300. The main advantage of this design is the user can attach this analog circuit device to any smart-phone which it allows the user to install and execute advanced application program. All the results demonstrated the potential of using smart-phone as a novel embedded system for portable medical ultrasound applications.

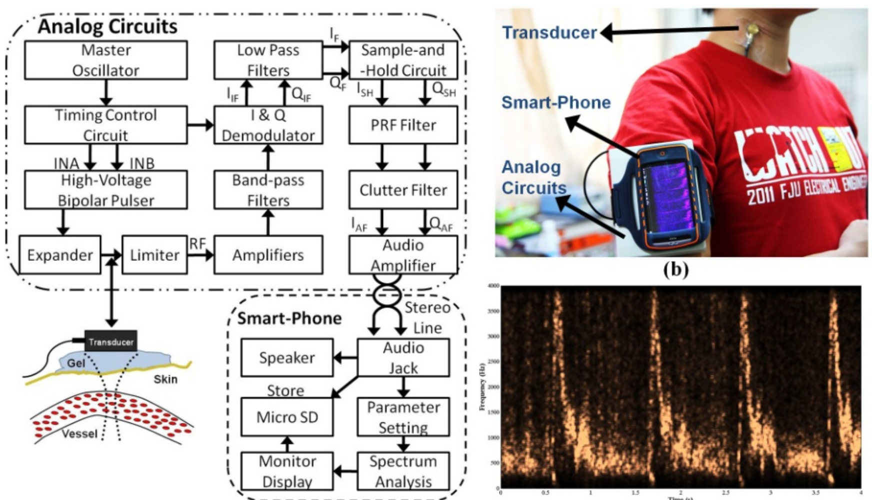

(a) (c)

3E-5

11:30 AM Development of a Low-profile, Wearable, CMUT based, Medical Ultrasound Imaging Probe

Anshuman Bhuyan[1], Jung Woo Choe[1], Byung Chul Lee[1], Omer Oralkan[1], Butrus T. Khuri-Yakub[1]; [1]*Edward L. Ginzton Laboratory, Stanford University, USA*

Background, Motivation and Objective

Ultrasound imaging has been one the most preferred mode of imaging in the medical industry due to its low cost and non-ionizing radiation, which make it suitable for applications that require constant monitoring. Typical ultrasound probes are bulky for such applications. In this paper, we present a wearable ultrasound probe using CMUTs and integrated ICs that can be taped to the patient's body for constant monitoring of human organs / blood vessels.

Statement of Contribution/Methods

This paper describes the assembly of a probe, which consists of the 64-element 5MHz CMUT array and the ICs. The ICs are designed to be closely integrated with the CMUT array for improved SNR. The electronics, which consist of preamplifiers (10 MHz bandwidth) & protection circuitry, directly interface a standard imaging system. Each IC consists of 16 channels and four ICs were used in conjunction with one CMUT array. A flexible PCB was also designed & fabricated to integrate the CMUT array with four ICs. The assembly is encapsulated with a PDMS lens to enable focusing in elevation. The final assembly measures about 6cm x 3.5cm x 0.35cm.

Results

The assembled probe is used to characterize the CMUT array as well as the ICs. The noise figure is 12.5 dB (at the center frequency) and the IC draws 6.72 mW / channel of power. The pulse-echo response of an element is measured from the PDMS – air interface. We also measured the output pressure (584 KPa at its focal depth, Vbias = 50 V = 40% Vpull-in, 40 Vpp) generated by the array, with all elements firing, using a hydrophone. Real-time images were acquired using the phased array technique. Real-time images, using a commercially available piezoelectric probe (with similar pitch), were also acquired for comparison. The CMUT probe showed better resolution due to its wider bandwidth.

Discussion and Conclusions

We have developed a wearable ultrasound probe with a small factor using CMUT technology. ICs were integrated with CMUTs to achieve better SNR using flexible PCBs. Real time images were acquired and showed better resolution than its counterpart, a commercially available piezoelectric probe. Successful acquisition of real time images shows clear feasibility of development of such wearable probes for applications that require constant monitoring of organs / blood vessels. This work is funded by the NIH (grant 1R01CA134720). National Semiconductor provided support for fabrication of the ICs.

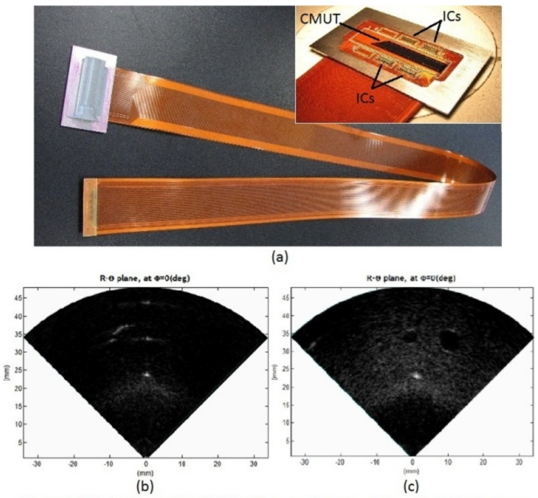

Figure 1a) Probe Assembly, b) Wire Phantom Images, c) Speckle & Cyst Images

3E-6

11:45 AM Real-time Volumetric Ultrasound Imaging System for 2-D CMUT Arrays

Jung Woo Choe[1], Omer Oralkan[1], Amin Nikoozadeh[1], Anshuman Bhuyan[1], Byung Chul (B.C.) Lee[1], Mustafa Gencel[1], Butrus (Pierre) T. Khuri-Yakub[1]; [1]*Edward L. Ginzton Laboratory, Stanford University, USA*

Background, Motivation and Objective

2-D transducer arrays enable 3-D volumetric imaging without a need of mechanical scanning. Recently, 2-D capacitive micromachined ultrasonic transducer (CMUT) arrays with rectangular and annular geometries have been successfully fabricated. We developed a real-time volumetric imaging system for those 2-D CMUT arrays. This system works with multiple imaging methods, such as classic phased array (CPA), synthetic phased array (SPA), and photoacoustic imaging.

Statement of Contribution/Methods

The system we implemented incorporates a Verasonics acquisition system, an FPGA board, and a PC with multi-core CPUs and GPUs. For the probes whose front-end electronics (ASICs) include transmitters and digital circuits, the FPGA controls the ASIC to perform transmit beamforming. The Verasonics system, that we use to acquire the raw data, can also be used as transmitters for up to 128 channels. Custom software we developed runs on the PC to process the raw data and reconstruct real-time images.

Results

For a ring array, SPA with Hadamard coding is a good option for real-time imaging, achieving frame rate of up to 45 frames per second, while obtaining reasonable SNR and excellent resolution. Other imaging methods developed for a ring array include flash, CPA, and CPA with multi-line acquisition (CPA-MLA). For a 2-D rectangular array, photoacoustic imaging was also implemented, as well as flash and CPA with full-transmit full-receive (FT-FR) or full-transmit x-receive (FT-XR) aperture.

Discussion and Conclusions

Besides the ultrasound flight time, practical factors limit the system performance. Data transfer rate from the acquisition system to the PC, being 1.2GB/sec, is lower than the data acquisition rate, which is 5.76GB/sec with 45MHz sampling, and this affects the frame rate in all the imaging methods. In addition, huge computational load reduces the frame rate further in SPA. In CPA with a ring array, we need more than 3,000 beams to cover the volume with 90° field of view, but the system memory allows us to have only up to about 2,000 beams. Some ways to overcome those limitations, including improved data transfer, faster computation, and employing new imaging methods such as flash with multiple angles and parallel beamforming with compensation techniques, are now under investigation and implementation.

This work was supported by the National Institutes of Health (NIH) under grant 1R01CA134720.

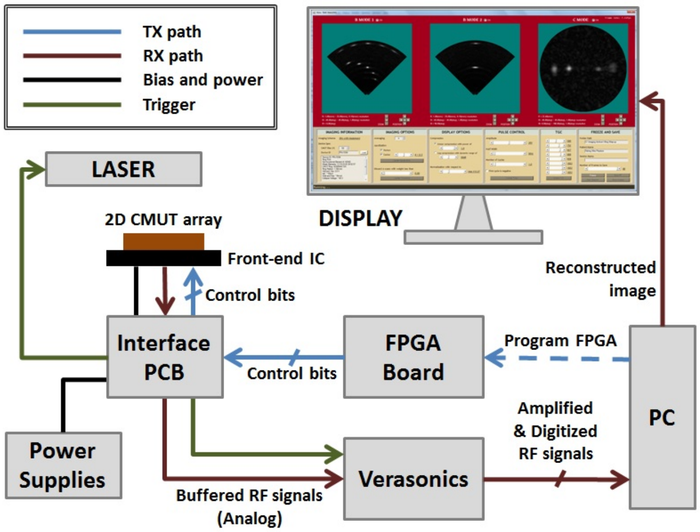
TX path
RX path
Bias and power
Trigger
LASER
2D CMUT array
DISPLAY
Front-end IC
Reconstructed image
Control bits
Interface PCB
FPGA Board
Program FPGA
Control bits
PC
Amplified & Digitized RF signals
Power Supplies
Verasonics
Buffered RF signals (Analog)

4E Imaging and Signal Processing

Carribean Ballroom I

Thursday, October 20, 2011, 10:30 am - 12:00 pm

Chair: **Jafar Saniie**
Illinois Institute of Technology, USA

4E-1

10:30 AM Guided wave temperature compensation with the scale-invariant correlation coefficient

Joel B. Harley[1], José M.F. Moura[1]; [1]Department of Electrical and Computer Engineering, Carnegie Mellon University, Pittsburgh, Pennsylvania, USA

Background, Motivation and Objective

Guided wave structural health monitoring systems create complex wave fields that travel through the thickness of a structure and reflect off of damage. However, variations in environmental conditions alter the propagation of guided waves and significantly affect the performance of these systems. Temperature is one of the most prominent of these effects. Variations in temperature change the velocities of modes, which stretch measured signals in time.

Several researchers have proposed methods, such as local peak coherence (LPC) [1], to compensate for temperature by estimating the stretch factor and properly adjusting the signal. In this paper, we propose a new compensation technique, the scale-invariant correlation coefficient (SICC) [2]. We benchmark SICC with the more expensive optimal signal stretch (OSS) [3], which correlates each observed signal with a library of stretched replicas of a single baseline.

Statement of Contribution/Methods

Using experimental data, we compare the robustness and computational performance of the LPC, OSS, and SICC methods. Data is generated and measured from two piezoelectric transducers bonded to a thin 9.8cm by 30.5cm by 0.1cm aluminum plate. Measurements are taken every 2 minutes over a 24 hour period in which the ambient temperature varies between 3.75 °C and 21.67 °C. During that time, a cylindrical mass is placed on the plate to simulate damage.

Results

For every signal measured, we apply each compensation method and compute its associated correlation coefficient with a known baseline. Figure 1 illustrates the changes in correlation during the experiment.

Discussion and Conclusions

Without compensation, the correlation coefficient varies dramatically with temperature. With compensation, the values vary little until the mass is added at 6:53 PM, when they drop and LPC begins to vary erratically. SICC has near identical performance as OSS, but is more computationally efficient.

References

[1] Y. Lu and J. E. Michaels, "A meth. for struc. health mon. with diff. ultrason. waves in the pres. of temp. var.," Ultrasonics, vol. 43, no. 9, pp. 717–31, Oct. 2005.

[2] J. Harley and J. M. Moura, "The scale cross-corr. and its app. to ultrason. temp. comp.," preprint.

[3] T. Clarke and et al., "Guided wave health mon. of complex struc. by sprs. array sys.: Influ. of temp. chng. on perfrm.," J. Sound Vib., vol. 329, no. 12, pp. 2306–2322, Jun. 2010.

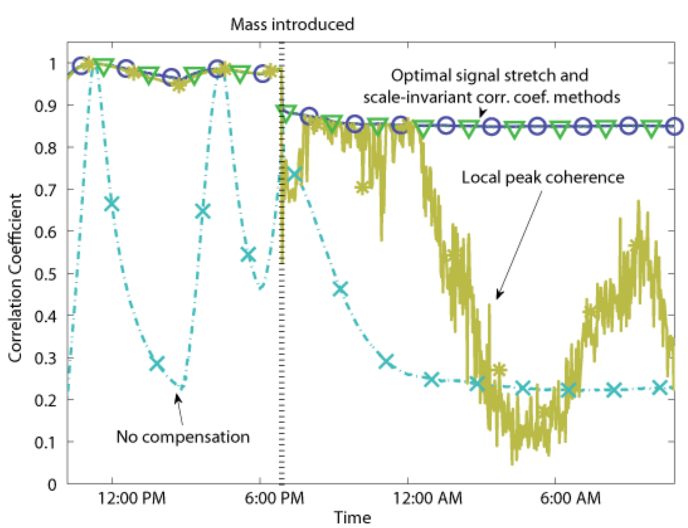

THURSDAY ORAL

4E-2

10:45 AM Acoustic Emission Detection and Classification Using Wavelet-Based Power-Law Detector

Dan Xiang[1], Julia Deng[1], Yexian Qin[1]; [1]*Intelligent Automation, Inc., USA*

Background, Motivation and Objective

Acoustic Emission (AE) techniques have proven to be an effective non-destructive testing method capable of continuously monitoring micro-structural change due to fatigue, stress corrosion, hydrogen embrittlement and creep. Discrimination between true AE signals from a deteriorated structure and noises from rubbing, fretting, mechanical noise, etc. is essential for AE technology. However, it is very challenging to separate noises from true fracture-related AE signals because the detected AE signals vary based on the source and location, structure material and geometry, etc. In this paper, we developed a wavelet-based power-law detector for transient AE analysis.

Statement of Contribution/Methods

A discrete wavelet packet transform (DWPT) was first employed to decompose an acoustic signal into a set of orthogonal wavelet packets. Then an improved power-law detector (PLD) was used to detect and classify a transient AE. The best basis selection (BBS) of PLD was determined based on the prior knowledge of the AE signals and noises. A test setup with a four identical AE transducers mounted on a large steel plate was established. Three types of acoustic events (breaking pencil lead, tapping with a pen, and rubbing with a metallic key) at different locations of the plate were recorded and analyzed. Application software with GUI interface was developed to display the results including the raw four channel signals, AE detection and classification, AE source location, AE event accumulation, etc.

Results

We used the breaking pencil lead source as the “true” acoustic emission, and others (tapping by a pen and a hand) as “faked” acoustic sources to evaluate the performance of DWPT-based PLD. Based on the ROC curves, the combination of Haar wavelet function and Coifman-Wickerhauser entropy yielded a good performance. But the use of Daubechies wavelet function also yielded a very good performance with other types of entropies (Risk, SURE, and Coifman-Wickerhauser). In both cases, when the detection rate was selected to be 100%, the false positive rate was less than 2%.

Discussion and Conclusions

A wavelet-based PLD has been developed and evaluated for AE detection and classification. The PLD along with BBS showed high detection and low positive rates for three types of acoustic signals generated in the lab. Since more than one wavelet function and entropy criteria exist for the DWPT-based PLD, there are rooms for down-selection of the best combinations when we analyze actual AE signals with various background noises for field applications.

4E-3

11:00 AM Acoustic Inspection of High-Density-Interconnects for 3D-Integration

Sebastian Brand[1], Matthias Petzold[1], Peter Czurratis[2], Jason D. Reed[3], Chris Gregory[3], Alan Huffman[3], John M. Lennon Jr. [3], Dorota S. Temple[3]; [1]*Fraunhofer Institute for Mechanics of Materials, IWM, Halle, Germany,* [2]*PVA TePla Analytical Systems GmbH, Westhausen, Germany,* [3]*Center for Materials and Electronic Technologies, RTI International, North Carolina, USA*

Background, Motivation and Objective

The continuing increase in integration rate in microelectronic devices now enters the third dimension. This challenges conventional inspection techniques for ensuring quality related aspects and failure analysis. Today inspection techniques that are applicable for 3D-integraed devices and the adaptation of existing techniques operating non- or semi destructively are of increased interest. Acoustic microscopy remains a powerful tool for investigating opaque samples and there internal structure. However, due to the continued miniaturization of the structures acoustic microscopy has to go to smaller wavelengths in order to provide sufficient resolution. But, as frequency increases other phenomena are of greater importance, which may contradict with the methods applicability. As an example, acoustic attenuation increases exponentially with frequency and thus limits the penetration depth.

Statement of Contribution/Methods

In the current study bonded devices with electrical routings in the bonded interface were inspected using acoustic microscopy applying highly focussed ultrasonic transducers with frequencies ranging from 200 MHz up to 1 GHz. Samples inspected contained high density interconnects forming arrays of 512 x 640 on 10 µm and 15 µm pitch. The devices were thermocompression bonded using Cu/Sn-Cu interconnects at 275°C and a pressure of 50 MPa. For the 10 µm pitch devices, the bottom die consisted of metal links terminated with 6 µm diameter pads plated with 4 µm of Cu and then coated with BCB. The 15 µm pitch devices had the same micropillar dimensions as the 10 µm pitch devices. Vias were etched in the BCB to create openings for bonding to the Cu pads. The BCB sidewalls created a mechanical key to prevent lateral slippage during bonding. Acoustic inspection was performed through the top die of the bonded device with different thicknesses ranging from 200 µm down to 10 µm. Acoustic inspection was also performed through the BCB mechanical key after removal of the top die. Depending on the thickness of the top-layer the acoustic frequency and focal length of the transducer was selected for imaging. With a resolution of approx. 1 µm acoustic imaging of the metal-links behind 5 µm of BCB was performed.

Results

Delaminations of the lateral links were detected without opening the BCB-layer. The delaminated links were confirmed by FIB-cross sectioning and high-resolution SEM imaging. In addition voids in the underfill material have been detected through the top-die.

Discussion and Conclusions

The trade-off between the achievable resolution, acoustic attenuation and the thickness of the top-die has to be taken into account when imaging at a 5 µm scale through opaque materials. It is expected that semi-destructive preparation will be required in practical applications. However, for performing failure analysis the acoustic inspection and the detection of delaminations at the interfaces will be greatly beneficial for guiding additional destructive analyses.

4E-4

11:15 AM Non-linear parametric imaging using an ultrasonic focused transducer.

Guillaume Robin[1], François Vander Meulen[1], Jérôme Fortineau[1], **Guy Feuillard**[1]; [1]Lab. Imagerie et Cerveau, ENIVL-Université de François Rabelais de Tours, Blois, France

Background, Motivation and Objective

Harmonic imaging is now widely used in medicine because of the high contrast enhancement produced by the technique. However, absolute measurement of the local non-linear parameter is not easy because the exact fundamental and harmonic pressure on the front face of the transducer have to be known. In this work, an absolute ultrasonic non linear parameter imaging technique in soft materials is developed. Applications concern both biomedical and industrial imaging.

Statement of Contribution/Methods

Using KZK non-linear equation, the acoustic field of an axisymmetrical focused transducer radiating into water is calculated as a sum of Gaussian beams. When a medium is interleaved in the focal area, the solutions of the KZK equation are modified in consequence. It is shown that the major contribution of the nonlinearity is located in the focal area. As a result, the discrimination of two media with different non-linear properties becomes possible, as well as non-linear parameter imaging.

Based on this theoretical analysis, the ultrasonic non-linear parametric imaging of a phantom was carried out by using a self calibrated method in pulse echo mode. The technique and setup, which were originally developed for planar transducers, were modified to take into account focusing. This allows absolute local measurements of fundamental and harmonic pressures to be obtained. From these, the non linear parameter can be derived. The set up was coupled with an XY scanning system to produce images.

Results

A wideband transducer (center frequency at 5 MHz and f-number at 2.4) was used in the experiments. The operating frequencies are respectively 3 and 6 MHz for the fundamental and second harmonic. The estimated axial and lateral resolutions are 18 and 1 mm for the second harmonic. Local measurements of the non linear parameters are determined for water and ethanol. The method was then applied to a two phase silicon oil/water liquid system. Finally, a non-linear Agar Agar based phantom was fabricated and images were produced.

Discussion and Conclusions

Values of 4.7 and 8 for the non linear parameter are determined respectively in water and ethanol. They are in agreement with data reported in literature. A vertical scanning on the two phase liquid system while measuring the non linear parameter clearly shows the transition between the two media. The non-linear parameter jumps from nearly 12 in silicon oil to around 5 in water. In the phantom, images show the local non-linearities of inclusions. In conclusion, the potential of the technique was demonstrated and future work will focus on increasing the axial and lateral resolutions of the system.

4E-5

11:30 AM Warped-Wigner-Hough Transformation of Lamb Waves for Automatic Defect Detection

Alessandro Perelli[1], Luca De Marchi[1], Emanuele Baravelli[1,2], Alessandro Marzani[3], Nicolò Speciale[1]; [1]Department of Electronics Computer Science and Systems - DEIS, University of Bologna, Bologna, Italy, [2]School of Aerospace Engineering, Georgia Institute of Technology, Atlanta, USA, [3]Department of Civil, Environmental and Materials Engineering - DICAM, University of Bologna, Bologna, Italy

Background, Motivation and Objective

To improve the defect detectability of Lamb wave inspection systems, application of non-linear signal processing was investigated. The approach is based on a Warped Frequency Transform (WTF) to compensate the dispersive behavior of ultrasonic guided waves, followed by a Wigner-Ville time-frequency analysis (WVD) and the Hough Transform (WHT). An automatic detection procedure to locate defect-induced reflections was successfully tested on Lamb waves. The proposed method is suitable for defect detection and can be easily implemented for real application.

Statement of Contribution/Methods

The WFT is a unitary transformation used to match the dispersive structure of a guided mode. Applying the WFT to the excited wave, defect detection is performed automatically through a TFR of the warped signal. Defect-induced reflections appear in the compensated waveform as well-localized spikes, producing vertical maxima lines in the TF plane, whose warped time location is converted to the defect position. The WVD is used to improve localization accuracy. Automatic detection of the lines of energy maxima is performed by applying the Hough Transform (HT) to the WVD. The interference terms induced by the WVD is compensated through the Hough operator.

Results

As a case study, we exploit the tools to locate defects in a 2.54 mm thick aluminum plate where Lamb waves are excited. The equalization algorithm enhances the amplitude of S0 peaks, while attenuating the A0 mode. The HT isolates S0 components and locate defect-induced reflections where the WHT of the equalized warped signal is displayed. Local maxima can be easily detected and the corresponding coordinates provide the distance traveled by the incident and reflected S0 wave.

Discussion and Conclusions

The work describes the application of a Warped Wigner-Ville analysis to improve defect detectability of Lamb wave. The equalization approach effectively enhances the amplitude of relevant peaks in the warped WVD, so local maxima is detected and distance traveled by the incident and reflected mode can be easily recognized. The presence of interference terms is largely compensated by the integration of the Hough operator, making the proposed method a suitable tool to separate overlapping Lamb waves and locate defect-induced reflections.

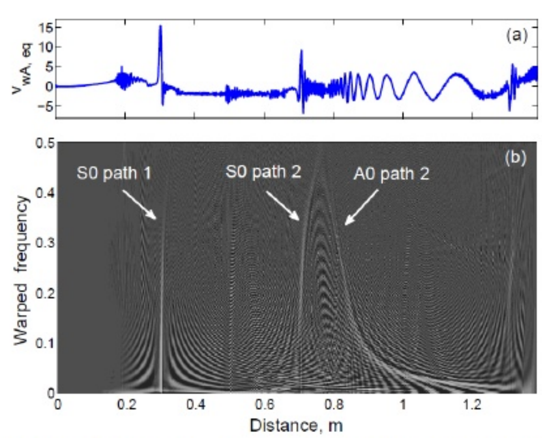

(a) Result of equalization applied to the warped signal.
(b) Wigner-Ville distribution.

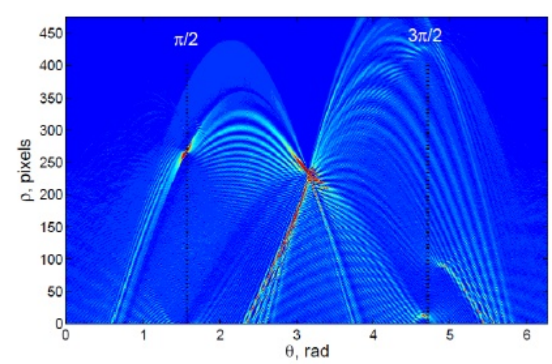

(c) Wigner-Hough Transform of the equalized warped signal with peaks detection.

4E-6

11:45 AM A Computationally Efficient Algorithm for Ultrasonic Signal Decomposition and Flaw Detection

Alireza Kasaeifard[1], Jafar Saniie[1], Erdal Oruklu[1]; [1]ECE Department, Illinois Institute of Technology, Chicago, IL, USA

Background, Motivation and Objective

Characterizing defects in large grain materials is a complex and challenging problem in ultrasonic imaging applications. The complexity is caused by microstructure scattering which often results in interference and masking of ultrasonic flaw echoes. Therefore methods to unravel and decompose these complex signals are advantageous.

Statement of Contribution/Methods

When chirplet excitation is used in NDE and flow measurement applications, the reflected echo will also be a transformed chirplet influenced by the property of materials or the velocity of targets within the object under test. In this study, we developed a computationally efficient algorithm for signal decomposition and target detection. The algorithm is based on ellipse fitting method (EFM) in time-frequency plane. Among existing conic contour fitting approaches, direct least squares ellipse-fitting method demonstrates satisfactory performance for chirplet parameter estimation. The designed algorithm estimates five parameters i.e. time of arrival, center frequency, chirp rate, amplitude and bandwidth factor by template matching on the short time Fourier transform of the signal. All these parameters are critical in characterizing ultrasonic dispersive and attenuative echoes in large grain materials. The fitted ellipse's parameters are obtained by solving a 5 by 5 system of linear equations, which has much lower computational complexity than that of the conventional estimators such as iterative maximum likelihood estimator. Echo detection algorithm is accomplished through successive parameter estimation of individual chirplets.

Results

The EFM algorithm is used to decompose an ultrasonic experimental signal consisting of many interfering echoes acquired from a steel block using a 5 MHz transducer and 100 MHz sampling rate. The comparison between the reconstructed signal (by performing 15 iterations) and the experimental one shows that the decomposition has been successfully performed with the presence of measurement noise and interference from microstructure scattering. After decomposition is performed, the output SNR (i.e. the ratio of the original signal and residual error) is 10.8 dB. For the real-time application and embedded implementation of the proposed method, an FPGA-based hardware/software co-design is developed on XILINX Virtex-5 development board.

Discussion and Conclusions

Using both time-frequency methods in successive manner and MLE algorithms are common in ultrasonic signal decomposition. Although these techniques perform well, their implementation requires excessive computations. A template matching based approach by using ellipse fitting to the chirp components in the time-frequency plane has been presented. The experimental results show that ultrasonic flaw signal can be estimated efficiently and accurately within a few percent with acceptable robustness to presence of microstructure scattering noise.

5E - Optical and Electromagnetic Interactions I

Carribean Ballroom II

Thursday, October 20, 2011, 10:30 am - 12:00 pm

Chair: **Vincent Laude**
Centre National de la Recherche Scientifique

5E-1

10:30 AM Numerical modeling of thermoelastic laser-generation of ultrasonic waves

Istvan A Veres[1,2], Bernhard Reitinger[1,2], Peter Burgholzer[1,2]; [1]Christian Doppler Laboratory for Photoacoustic Imaging and Laser Ultrasonics, Linz, Austria, [2]Research Center for Non Destructive Testing GmbH, Linz, Austria

Background, Motivation and Objective

Laser generation of ultrasound in solids has been extensively used in experimental acoustics in the past decades since it enables the contactless excitation of various elastic waves, such as bulk, surface or guided waves. The description of the generation mechanism by the thermoelastic source has also attracted great attention. Thus, the generation of the elastic waves by laser irradiation of a surface could be described by the coupled heat and wave equations, whereby various coupling terms are taken into account.

Statement of Contribution/Methods

Analytical solutions to the thermoelastic problem are available with different approximations. The thermoelastic source can be replaced with a simple temporal and spatial delta function resulting in an uncoupled problem. The coupled thermoelastic problem is typically solved by a combination of integral transforms. Both solutions have limitations; in the first case the solution approximates only the far field; in the second case the inverse transforms remain a great challenge. Applying numerical solutions to the coupled differential equations in the first place enables the extension of the solutions to the anisotropic case with complex geometries or layers. Moreover, further coupling terms, such as the thermal feedback by the mechanical deformation, can be included.

Results

Numerical solutions of the coupled differential equations are discussed by the Finite Differences Time Domain (FDTD) and the Finite Element Method (FEM). The effect of the coupling is discussed by an implicit-explicit FDTD method and it is shown, that the thermal feedback by the mechanical deformation increases the dispersion. Further results are shown using high-performance time-domain simulations with an implicit-explicit FEM. The temperature distribution is calculated from the heat equation for laser pulses with various temporal and spatial distributions and applied as source term in the wave equation. Numerical results are obtained for the free half space (Figure: vertical displacements of the wave field from a line focused laser by FEM) and for the coated half space. The results are compared to the available analytical solutions.

Discussion and Conclusions

The numerical and analytical solutions show good agreement. Especially the numerical FEM model provides wide range of opportunities in the modeling of the thermomechanical problems.

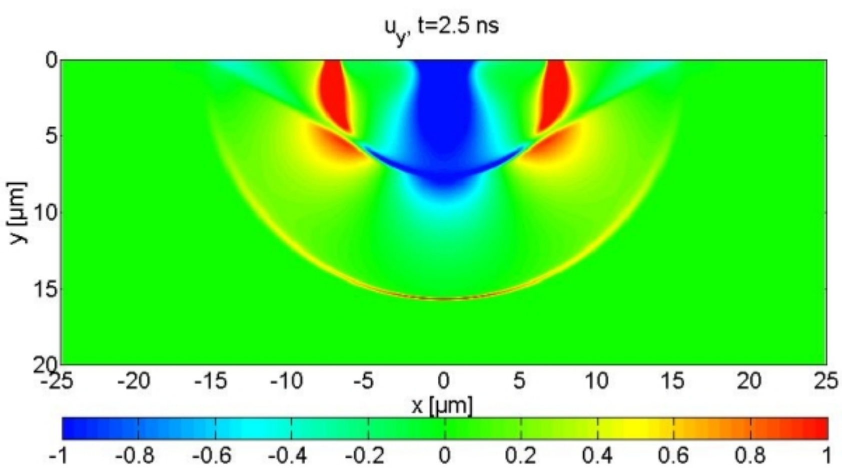

5E-2

10:45 AM Non-perturbing measurement of sound pressure fields by means of laser Doppler vibrometer

Lizhuo Chen[1,2], Stefan Rupitsch[1], Reinhard Lerch[1]; [1]Chair of Sensor Technology, Friedrich-Alexander-University Erlangen-Nuremberg, Erlangen, Germany, [2]Erlangen Graduate School in Advanced Optical Technologies, Germany

Background, Motivation and Objective

The piezo-optic effect can be utilized to collect information about sound pressure fields along an emitted laser beam, for instance, from a laser Doppler vibrometer (LDV). In comparison with hydrophones, this measurement is non-perturbing and inherent omnidirectional. The sound pressure fields of transducer operating in water are reconstructed by means of the computed tomography, which has been developed in the medical area quite well.

Statement of Contribution/Methods

Our previous research was restricted by the assumption of totally axisymmetric sound pressure field. Therefore, we extend the measurement setup so that it is possible to rotate the investigated transducer around its middle axis. Consequently, fields arising from arbitrarily shaped transducers are able to be measured from different perspectives leading to the possibility of full-angle reconstruction. However, the rotation procedure is accompanied by a remarkable measurement effort. In order to obtain a good compromise of measuring efficiency and reconstruction accuracy, we apply non-equidistant spatial sampling. The spatial sampling is determined by means of numerical simulations which are used to predict the pressure field arising from the transducer. Furthermore, these simulations help to identify cut-off frequencies for the filters utilized within the reconstruction procedure. A comparison of different reconstruction methods points out that the filtered back projection (FBP) with Ram-Lak kernel filtered by the tukey-function provides reliable results.

Results

For verification, a simulated sound pressure field with a signal-to-noise ratio of 30 dB was reconstructed. Thereby, the errors were below 6% relative to the maximal pressure. In the measurement experiment, a transducer was excited by a burst-signal of 500 kHz. The figure shows the sound pressure field reconstructed by the optical method as well as measured with hydrophone. The maximal difference between the results is about 10% relative to the maximal pressure.

Discussion and Conclusions

We have applied LDV combined with computed tomography to reconstruct sound pressure fields. Both the simulations and the experiments, show the feasibility of this method. A line-focused transducer without axisymmetric property is now under investigation. The reconstructions of corresponding sound pressure fields will be presented in the contribution.

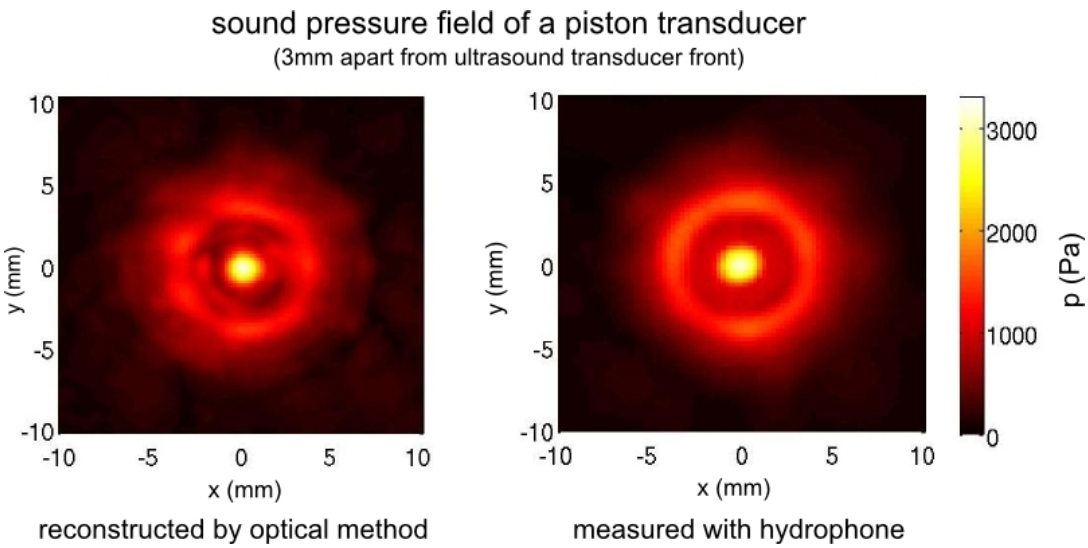

THURSDAY ORAL

5E-3

11:00 AM Brillouin scattering from induced phonons excited by the ZnO piezoelectric thin film with a coaxial resonator

Takeshi Sugimoto[1], Hiroyuki Sano[1], Takahiko Yanagitani[2], Shinji Takayanagi[1], Mami Matsukawa[1]; [1]*Doshisha University, Japan,* [2]*Nagoya Institute of Technology, Japan*

Background, Motivation and Objective

Brillouin scattering is a nondestructive and noncontact technique to measure local longitudinal and shear acoustic velocities in the GHz range. However, the measurements of weak thermal phonons result in the lower measurement accuracy and longer measurement time. To overcome these problems, a technique with artificially induced phonons was developed using a ZnO piezoelectric thin film and a coaxial resonator.

Statement of Contribution/Methods

The acoustic phonons were artificially induced from a ZnO piezoelectric thin film deposited on one side of a silica glass bar with size of 3x10x35 mm^3 [1]. The evanescent wave which was leaked from a coaxial resonator was used to apply an electric field to this film without electrodes. The frequency of the induced phonons is then the resonant frequency of the resonator (2 GHz), which is equal to the Brillouin shift frequency. The Brillouin scattering from the induced phonons was measured using a Tandem Fabry-Perot Interferometer (TFPI), with Ar ion laser at a wavelength of 514.5 nm. The RIΘA (Reflection induced ΘA) scattering geometry was used for the measurements.

Results

Figure 1 shows a spectrum of Brillouin scattering from the induced shear acoustic phonons. The intensity of Stokes peak was about 40000 counts, which was 1000 times as intense as the anti-Stokes peak. The intense scattering of Stokes peak corresponds to the induced phonon and dramatically reduced the measurement time. In this technique, the measurement of shift frequency is not necessary because this frequency is the resonant frequency of the resonator.

Both longitudinal and shear acoustic phonons could be induced in the sample by this technique. We have also observed the Brillouin scattering from induced phonons in the sample with curved surfaces, where ZnO film could be fabricated successfully.

Discussion and Conclusions

The intensity of Brillouin scattering dramatically increased by inducing phonons from ZnO film without electrodes. The measurement accuracy and time of Brillouin scattering were also improved. In this technique, it is not necessary to measure the Brillouin shift frequency. These advantages of this technique indicate the possibility of the future simple measurement system without TFPI and 2D measurements of longitudinal and shear wave velocities.

[1] T. Matsuo, et. al., Proc. IEEE. Ultrason. Symp. (2007), p. 1229.

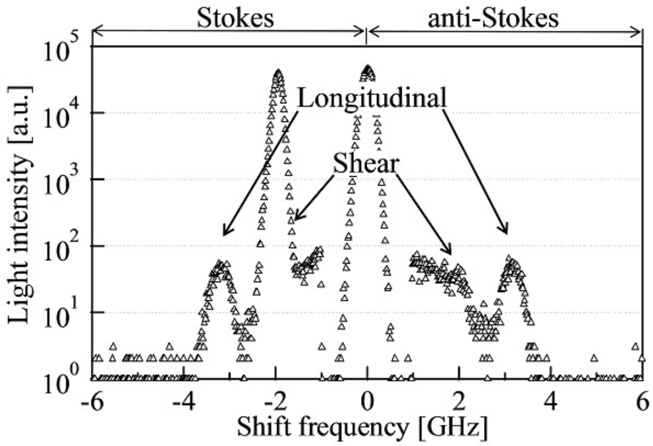

Fig. 1 A Brillouin spectrum of induced shear phonons in the silica glass.

5E-4

11:15 AM Confined Acoustic Phonons in Ultra-Thin Silicon Membranes

John Cuffe[1,2], Emigdio Chavez[1,3], Jordi Gomis Bresco[1], Pierre-Olivier Chapuis[1], Francesc Alzina[1], Andrey Shchepetov[4], Mika Prunnila[4], Jouni Ahopelto[4], Olivier Ristow[5], Mike Hettich[5], Thomas Dekosry[5], Clivia M. Sotomayor Torres[1,6]; [1]*Catalan Institute of Nanotechnology (CIN2-CSIC), Bellaterra, Barcelona, Spain,* [2]*Dept. of Physics, University College Cork, Tyndall National Institute, Cork, Ireland,* [3]*Dept. of Physics, Universitat Autònoma de Barcelona, Bellaterra, Barcelona, Spain,* [4]*VTT Technical Research Centre of Finland, Espoo, Finland,* [5]*Dept. of Physics, University of Konstanz, Konstanz, Germany,* [6]*Institució Catalana de Recerca i Estudis Avançats (ICREA), Barcelona, Spain*

Background, Motivation and Objective

The acoustic properties of ultra-thin Si layers are important for many areas of nanotechnology, impacting on both structural integrity and thermal transport. The effect of phonon confinement is particularly important, affecting both heat dissipation and charge carrier mobility. The goal of this work is to obtain a deeper understanding of phonon confinement and propagation in materials with dimensions comparable to thermal phonon wavelengths.

Statement of Contribution/Methods

In this work an ultra-fast photo-acoustic pump-probe method, known as Asynchronous Optical Sampling (ASOPS), is used to investigate confined phonon frequencies and lifetimes. The effect of the ~1 nm native oxide layer in such thin systems is also calculated using a three-layer model based on continuum elasticity theory.

Results

The frequency of the first order dilatational mode is measured, and the results show that the frequencies of the measured phonons are consistently ~10% lower than predicted by the continuum elasticity model, and cannot be fully explained by the presence of a native oxide layer or temperature changes within the membrane. The dependence of phonon lifetimes on membrane thickness is also investigated, with the lifetime of a 10 nm membrane found to decrease by over two orders of magnitude compared to that of a 400 nm membrane.

Discussion and Conclusions

The frequencies and lifetimes of confined acoustic phonons in ultra-thin free-standing Si membranes have been measured, and found to deviate from the values predicted by a continuum elasticity theory, including the effects of a native oxide layer and temperature increases within the membrane. A large decrease in phonon lifetimes is also seen for the ultra-thin membranes. The contributions of various attenuation mechanisms are discussed to explain the observed trend.

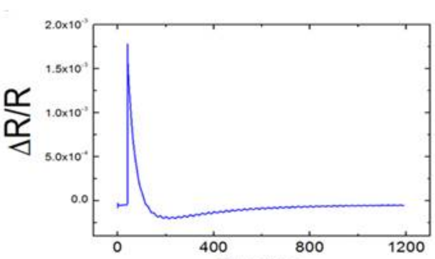

Figure 1: Change in reflectivity vs time for free standing Si membrane

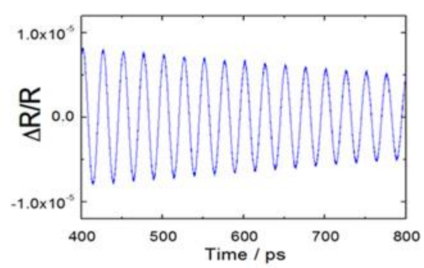

Figure 2: Change in reflectivity vs time for free standing Si membrane after subtraction of electronic response, showing confined acoustic mode.

THURSDAY ORAL

5E-5

11:30 AM Evaluation of thin film coating adhesion with an opto-acoustic technique

Sanichiro Yoshida[1], Mohan Basnet[1], Chiaki Miyasaka[2], **Bernhard Tittmann[2]**, Ik-Keun Park[3]; [1]Southeastern Louisiana University, USA, [2]The Pennsylvania State University, USA, [3]Seoul National University of Science and Technology, Korea, Republic of

Background, Motivation and Objective

Assessment of adhesion of thin film coating is important in many applications. The V(z) analysis is a powerful technique to characterize thin film structures. However, it requires scanning over the area of interest; analysis of localized flaw is relatively easy, but detection of uniform poor adhesion is cumbersome.

Statement of Contribution/Methods

Fig. 1 illustrates our idea to overcome this issue. An acoustic transducer placed behind the substrate oscillates the coated surface, and the resultant displacement is read out with an optical interferometer. The adhesive force is hypothesized to be elastic, as justified by that at the atomistic level the potential is dominantly quadratic. Thus, the relation of the surface displacement to the transducer's displacement (input) represents the transfer function. Analysis on its amplitude and phase reveals the elastic property of the adhesion.

Results

Preliminary experiment was conducted on two specimens of a 1 µm thick polystyrene film coated on a [1 0 0] cut, 100 µm thick silicon substrate of the same diameter (50 mm). These specimens were identical in dimension and different in adhesion strength. The transducer was driven at 50 kHz and a Laser Doppler interferometer measured the displacement. Fig. 2 shows the measured displacement.

Discussion and Conclusions

Fig.2 clearly differentiates the two specimens (A and B) both in the amplitude and phase. Fitting to theoretical transfer function indicates the resonant frequency ω_0 and decay constant γ of these specimens to be ω_0 : γ = 62.5 (kHz): 0.16 (A) and 48.1 (kHz): 0.76 (B). The same experiment at 250 kHz driving frequency along with finite element analysis indicates that the Young's modulus of the adhesion is two orders of magnitude smaller than polystyrene.

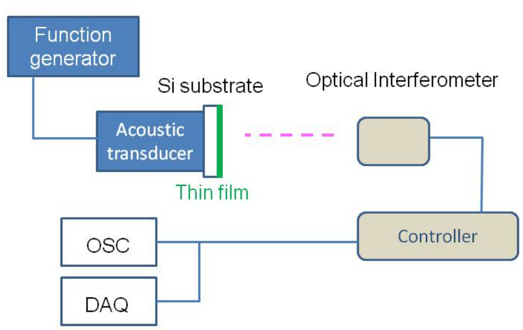

Fig. 1 Experimental Setup. OSC: oscilloscope, DAQ: Data Acquisition

1

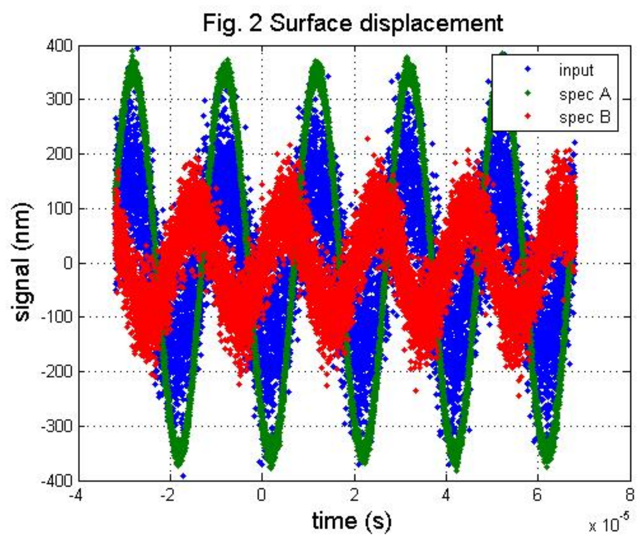

5E-6

11:45 AM Inductive magneto-acoustic technique for viscous fluids monitoring

Nicolas Wilkie-Chancellier[1], Stephane Serfaty[2], Pascal Griesmar[2], Yohan Le Diraison[2], Jean-Yves Le Huerou[2]; [1]SATIE (CNRS - UMR 8029), Université de Cergy-Pontoise, Neuville sur Oise, France, Metropolitan, [2]Université de Cergy-Pontoise, France, Metropolitan

Background, Motivation and Objective

The optimization of new soft hybrid materials elaborated in liquid phase in the industrial domain needs an "on line" characterization of the first steps of their formation. Up to date, few ultrasonic techniques ensure complete tracking of the material requiring a wired excitation unsuited for online monitoring of hidden areas. In our lab various non-destructive ultrasonic techniques have been successfully developed to characterize the rheological evolution of nanostructures. In addition, our lab has also acquired knowledge in RF inductive sensors design.

In order to extract rheological properties of these materials using a wireless technique, an RF inductive magneto-acoustic system is performed to monitor viscous fluids.

Statement of Contribution/Methods

This work presents an ultrasonic sensor remotely controlled. The wireless excitation of this sensor is based on an original RF technique designed to inductive monitored electrical characteristics of the sensor. The interest of this technique is to make possible the online monitoring of hidden complex fluids. The sensor consists of a gold transmission line loop deposited on a piezoelectric substrate inductively coupled with a high quality radiant RF bracelet resonator (Q~700 at 100 MHz). The shape of the sensor used as electro-mechanical transducer is optimized to generate ultrasonic shear waves. In contact with the fluid, the boundary conditions of the piezoelectric loop sensor modify the electrical characteristics of the sensor in accordance with the mechanical and electrical properties of the material. Thus, by mutual induction the input equivalent electrical impedance of the RF bracelet resonator allows us the rheological monitoring of the complex fluid. In order to achieve this monitoring a single loop weakly coupled is connected to an impedance analyzer.

Results

In order to validate this new magneto-acoustic technique various liquids of tabulated viscosity (water – glycerol mixtures) were studied. The appropriate equivalent electrical model used to extract mechanical properties of the material is presented. This model links the resonant frequency shift and the damping of the input impedance, associated with viscoelastic properties of the material, to induced equivalent lumped electrical elements: inductance (Li) and resistance (Ri).

Discussion and Conclusions

We show that the parameters Ri and Li are related to the square root of the product viscosity - density of the liquid. These results are consistent with results obtained using AT cut quartz microbalance loaded by liquids. They suggest that this non-destructive technique can be used to extract the viscoelastic properties of materials.

Thanks to its simplicity, its low cost, its high-resolution mass sensing and its capability to monitor the viscous fluids, this innovative technique is suitable for industrial applications.

6E - Applications

Carribean Ballroom VI

Thursday, October 20, 2011, 10:30 am - 12:00 pm

Chair: **Qifa Zhou**
USC

6E-1

10:30 AM Ultrasonic inspection of nuclear reactor primary components

Jean-Francois Saillant[1]; [1]AREVA - NDE Solutions, Chalon sur Saone, Bourgogne, France

Background, Motivation and Objective

Nuclear industry plays an important role in today's economic activity. It allows to both produce a large amount of energy and to comply with the consensus on climate change regarding the reduction of greenhouse gas emission.

Statement of Contribution/Methods

Safety is an essential aspect of nuclear power plants and a particular attention has been given to inspection techniques deployed to ensure the safe and good operation of our nuclear reactors. Non-Destructive Testing (NDT) techniques based on ultrasound are very commonly used to inspect the integrity of nuclear reactors. This talk aims at introducing some of the techniques that are presently used on site and the R&D that will be needed for the future.

Results

The first part will therefore present some of the automated ultrasonic inspections carried out on the primary components of so called Generation 3 reactors. This kind of reactor consists in the majority of those used in today's nuclear reactor park.

Discussion and Conclusions

The second part of the talk will present the perspectives for NDT in the nuclear industry with tomorrow's Generation 4 reactors. These sodium-cooled reactors will require new ultrasonic transducers capable of surviving in a very severe environment, while still providing quality acoustic performances.

6E-2

11:00 AM Additive Manufacturing of PZT-5H Piezoceramic

Scott Smith[1], Prabhjot Singh[1], Michelle Bezdecny[1], Mark Cheverton[1], Venkat Venkataramani[1], Anthony Brewer[1]; [1]*GE Global Research, USA*

Background, Motivation and Objective

Medical ultrasound is trending toward smaller, lower cost systems based largely on advances in electronics miniaturization. While this has reduced the size, weight, and cost of the console, ultrasound transducer arrays remain largely unchanged and are becoming a high cost and labor-intensive component in an ultrasound scanner. Transducer arrays have been built with semiconductor saws whose serial action is slow. This paper describes the development of a low-cost, high speed manufacturing method for piezoceramic transducer elements.

Statement of Contribution/Methods

A modified multi-layer lithography process is used to additively manufacture high-resolution netshape ceramic structures by photopolymerizing a ceramic-polymer slurry using structured light patterns. The input material is a highly-loaded slurry composed of piezoceramic particles, a photopolymer, and dispersant. This slurry is dispensed as a bead, and is spread to form a thin, uniform layer typically 20-50 micron thick. The layer is selectively photocured with high-intensity broad-spectrum light that passes through a glass mask. The mask comprises a pattern representing the cross-section of the transducer elements. Layer deposition and photocuring operations are repeated till the required geometry is fabricated. Uncured resin is removed and the part is sintered. The paper elaborates on the key features in the development of the process including the selection and optimization of slurry materials for the deposition of PZT 5H materials, optical exposure parameters, debinding/sintering profiles and post-manufacturing processing.

Results

Parts produced by this process are >=95% dense, with a grain size of 2-3 microns. Lead loss during sintering was less than 0.5%. The electromechanical coupling coefficient (kt) was between 0.52-0.53 with a dielectric constant of ~2000.

Discussion and Conclusions

The additive manufacturing process shows promise for the fabrication of 2-2 and 1-3 composite ultrasound transducers in a wide range of frequencies (1-25 MHz). Ongoing work includes optimization to improve the dielectric constant and geometric consistency of the deposited features.

Supported by Award RC2EB011439 from the National Institute Of Biomedical Imaging And Bioengineering. The content is solely the responsibility of the authors and does not necessarily represent the official views of NIBIB or NIH.

PZT-5H Linear Array in Green State

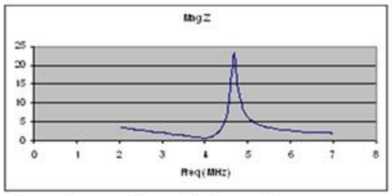

Impedance Magnitude vs. Frequency

6E-3

11:15 AM Cell Characterization Using High Frequency Ultrasound

Saurabh Bakshi[1], John Williams[2], Xiaoning Jiang[1], Elizabeth Loboa[2]; [1]*Mechanical & Aerospace Engineering, North Carolina State University, Raleigh, NC, USA,* [2]*Biomedical Engineering, North Carolina State University, Raleigh, NC, USA*

Background, Motivation and Objective

It is known that extracellular physical stimuli can affect stem cell fate and, that malignant cancer cells have different material properties than benign cells. However, it is also known that human cells exhibit extensive variability in their chemical and mechanobiological response due to donor-to-donor variability. Therefore, there is a great need for a sensitive, reliable, and accurate system to characterize cell properties in a high throughput fashion. Time resolved acoustic microscopy is currently used to characterize acoustic and elastic properties of cells using the amplitude and time of the ultrasound (US) backscatter from the cellular membrane. This acoustic microscopy system is bulky and is not practical for characterization of cells in a large population. In this paper, a method of cell detection and characterization based on the use of acoustic impedance of cell material is proposed for cell elastic property characterization in a high throughput fashion.

Statement of Contribution/Methods

Transmit electrical impedance spectrum of a 50 MHz transducer with varied front loading (e.g. cell elastic properties) was modeled using PiezoCAD. Initial cell growth tracking using a 30 MHz transducer was performed to demonstrate that transmit impedance can track elastic property changes in human adipose derived stem cells (hASC) during osteogenic differentiation. In this study, hASC were cultured in complete growth medium (Eagle's Minimum Essential Medium, alpha-modified (α-MEM) supplemented with 10% fetal bovine serum, 2 mM L-glutamine, 100 units/mL penicillin, and 100 µg/mL streptomycin) for 3 days. On day 4, the medium was changed in half the culture wells to osteogenic differentiation medium (expansion medium supplemented with 50 µM ascorbic acid, 0.1 µM dexamethasone, and 10 mM β-glycerolphosphate). Two cell samples were measured for acoustic impedance values on day 1, and an incrementally increasing number of samples, one each from the controlled and differentiating set, were added to the existing set each day for measurement.

Results

Electrical impedance as much as 30 Ω was observed from a 50 MHz transducer model for the case where front load acoustic impedance is changed from 2 MRayl to 4 MRayl. Frequency shift was also observed. Measured transmitting electrical impedance difference (4 Ω) indicated a change in hASC elastic properties within 24 hours (day 5). Interestingly, it was noted that impedance difference began to level off (8 Ω) between days 7-8, indicating that elastic properties were no longer changing.

Discussion and Conclusions

The initial modeling and experimental results suggest that it is feasible to track cell growth by monitoring transmitting electrical impedance change. This may open up a new US cell characterization tool that promises monitoring of a large population of cells in a real time and high throughput fashion.

6E-4

11:30 AM MEMS-Based Multiple Fourier-Horn Silicon Ultrasonic Atomizer For Inhalation Drug Delivery

Chen Tsai[1,2], Shih-Kai Lin[1], Rong-Wei Mao[1], Shirley Tsai[3]; [1]Electrical Engineering and Computer Science, University of California, Irvine, Irvine, CA, USA, [2]Inst. of Optoelectronics and Photonics, National Taiwan University, Taipei, Taiwan, [3]Chemical Engineering and Materials Science, University of California, Irvine, Irvine, CA, USA

Background, Motivation and Objective

Monodisperse particles and aerosols (particles in air) 2 to 5µm in diameter are ideal for efficient targeted drug delivery to the lung. Tight control of aerosol size can also minimize both local and systemic adverse side effects by minimizing both local deposition and the total dose delivered. Current commercial nebulizers and inhalers all suffer from polydisperse (broad-size) aerosol distribution and/or low throughput, making it difficult to deliver sufficient amount of drugs to the lung rapidly and precisely. This paper reports MHz ul-trasonic atomizers of new and simple nozzle architecture with multiple Fourier horns in reso-nance. The battery-run hand-held inhaler module constructed most recently demonstrated its ca-pability of fulfilling the aforementioned unmet needs in inhalation drug delivery.

Statement of Contribution/Methods

The new centimeter-sized ultrasonic nozzle with operation frequency range of 1.0 to 2.0 MHz was fabricated in silicon using MEMS technology. It consists of a drive section with PZT trans-ducer and a resonator section with multiple (3 or 4) Fourier horns. Each Fourier horn is half-wavelength long with a single-mode longitudinal vibration displacement gain of two. In contrast to our earlier nozzles [1], the new nozzle did not require a central channel for transport of the liquid to be atomized and its fabrication was thus greatly simplified. Resonance of the multiple Fourier horns result in greatly enhanced longitudinal displacement on the nozzle endface upon which the liquid is externally transported. External transport of liquid enabled high throughput be accomplished. As the displacement of the nozzle endface exceeds a critical value, temporal in-stability of the Faraday waves on the liquid surface results in micrometer-sized monodisperse droplets. We developed the theory of temporal instability of Faraday waves for the MHz ultra-sonic nozzles and established the first theoretical formula for the droplet diameter [2].

THURSDAY ORAL

Results

Monodisperse droplets of diameter range 2.2 to 4.6μm have been produced at throughput as high as 500μl/min and electrical drive power as low as 0.3 watt. The low drive power requirement en-abled most recent realization of battery-run hand-held inhaler modules that consists of IC elec-tronic driver, micro pump, and nozzle liquid feed platform.

Discussion and Conclusions

The inhaler modules have demonstrated capability to fulfill the unmet needs in inhalation drug delivery. Other potential applications of the high-throughput MHz ultrasonic nozzles include delivery of lipid-based micro-encapsulated biological entities or therapy, nanoparticles synthesis, 3-D coat-ing, nano-electronic and -photonic device processing.

[1] Tsai et al IEEE Trans. on UFFC, 56 (9), 1968-1979, 2009.
[2] Tsai et al Lab Chip, 10, 2733-2740, 2010.

* Supported by the National Institute of Health (NIH/NIBIB), USA

6E-5

11:45 AM Micro-localized cell lysis by low-power focused acoustic transducer

Lingtao Wang[1], Yi-Jia Li[2], Anderson Lin[1], Youngki Choe[1], Mitchell Gross[2], Eun Sok Kim[1]; [1]Electrical Engineering, University of Southern California, USA, [2]Department of Medicine, University of Southern California, USA

Background, Motivation and Objective

Localized cell lysis with micron precision will provide unprecedented opportunities in cancer diagnosis and therapy at cellular level.

Statement of Contribution/Methods

In this study, we designed and fabricated Self Focused Acoustic Transducer (SFAT) for micron-sized localized cytolysis. Also, we measured the minimum acoustic power intensity for cell lysis within the focal spot, in order to characterize the dependence of a localized cell lysis, acoustic power, and the frequency of acoustic waves. The SFAT-based cell lysis device consists of a Lead Zirconate Titanate (PZT) transducer with an acoustic lens, an acoustic chamber and a cell culture chamber. A monolayer of prostate cancer cell line 22RV1 is grown on the parylene surface of the cell culture chamber. For localized cytolysis, the PZT transducer generates acoustic wave as electric power applied. The Fresnel acoustic lens focuses acoustic waves at the target focal spot. Thus, the concentrated acoustic radiation pressure exerts great shear stresses on the cells and ruptures the cell membranes. To monitor the cell lysis, a cell-impermeant fluorescent nucleic acid dye SYTOX Dead Cell Stain was used. Also, RT-PCR experiments were conducted to compare mRNA amount in cell culture media before and after cell lysis experiment.

Results

Localized cell lysis was obtained with the prostate cancer cell line 22RV1 by various power intensity levels at the transducer's fundamental and 3rd harmonic resonant frequencies (17.3 and 56 MHz, respectively). The cell lysis area was 100 and 50 Âμm in diameter, when the acoustic wave produced by the transducer was 17.3 and 56 MHz, respectively. At the fundamental resonant frequency, the minimum electric power required for the cell lysis was 0.9 W, which produced an acoustic intensity 15 W/cm*cm at the focal spot. The mRNA amount in the culture media was increased more than 10 times when 0.9 Watt power was applied to the fundamental device. For the third harmonic device, when 10 W power (corresponding the focused acoustic intensity of 402 W/cm*cm at the focus spot of 50 Âμm in diameter) was applied to the device, the mRNA amount in the culture media was increased 4.5 times from the case when no acoustic wave was applied. It was 43.6% of the increase obtained by the fundamental device. These PCR results are consistent with the fluorescent images obtained on the small focal areas where the lysis happened. The inertia cavitation phenomena, such as bubble generation and collapsing, were not observed at these power levels that still produced the cell lysis.

Discussion and Conclusions

We demonstrated localized cell lysis at a micron-sized focal spot without any noticeable cavitation. Results showed the cell lysis area was reduced from 100 to 50 Âμm in diameter by using the device designed for the 3rd harmonic frequency operation. The size of cell lysis area depends on the frequency of the acoustic wave, but not on the power applied to the device, as long as the power is above the cytolysis threshold of 15W/cm*cm.

1F - Synthetic Aperture Beam Forming

Boca Rooms II-IV

Thursday, October 20, 2011, 2:00 pm - 3:30 pm

Chair: **Jorgen Jensen**
Technical Univ. of Denmark

1F-1

2:00 PM Experimental Study of Dual-Ring CMUT Array Optimization for Forward-Looking IVUS

Coskun Tekes[1], Sarp Satir[1], Gokce Gurun[1], Jaime Zahorian[1], Michael Hochman[1], Toby Xu[1], F. Levent Degertekin[1], Mustafa Karaman[2]; *[1]George W. Woodruff School of Mechanical Engineering, Georgia Institute of Technology, Atlanta, GA, USA, [2]Electronics Engineering, Isik University, Istanbul, Turkey*

Background, Motivation and Objective

Forward-looking (FL) catheters with guiding and volumetric imaging capability are highly desirable in IVUS applications. With small number of available cables, reduction of firing counts is critical for 3-D real-time imaging with reduced motion artifacts. Recently, we proposed an optimization procedure for dual-ring CMUT based FL-IVUS arrays based on finding an optimal coarray set using simulated annealing algorithm. Here we present the experimental demonstration of the proposed method on dual-ring FL-IVUS arrays based on monolithic CMUT-CMOS integration.

Statement of Contribution/Methods

We used simulated annealing algorithm to optimize the wideband PSF of the array system. The optimal firing set from different transmit (Tx) and receive (Rx) elements eliminates most of the redundant spatial frequencies in the coarray and produces low side lobes and number of firings. The optimization procedure starts with the calculated wideband PSF of the full set coarray including all Tx-Rx firing combinations. In every iteration step, a predefined coarray with only one element change is compared with the previous set in terms of cost function. We obtained optimal reduced set by minimizing the peak side lobe level. For the experiments, we fabricated 0.8 mm diameter dual ring CMUT array which has 32 Rx and 24 Tx elements and operates at 20 MHz with 50% fractional bandwidth.

Results

We used a 0.3 mm spherical target immersed in water tank located 2.5 mm away from the array center to approximate the PSF of the system. For a test case, we obtained a reduced set of 256 coarray elements out of 768 Tx-Rx combinations and reconstructed both the simulated 2-D PSF and cross-sectional images of the spherical target. The simulated PSF of the optimal set has the same parameters with the experimental array and produces an 8-dB reduction in near side lobe level with respect to full set, whereas the experimental results show that the optimal coarray set produces no widening in main lobe width when compared with the full set and it has slightly lower peak near side lobe level.

Discussion and Conclusions

Our experimental results demonstrate that the simulated annealing based optimal firing set achieves similar lateral and contrast resolution performance with only 33% of the full set. The resulting optimal array design can meet the resolution requirements of 3-D real time IVUS imaging with improved immunity to motion artifacts.

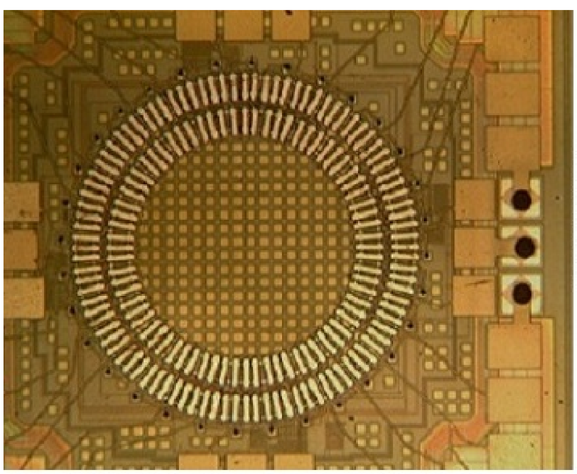

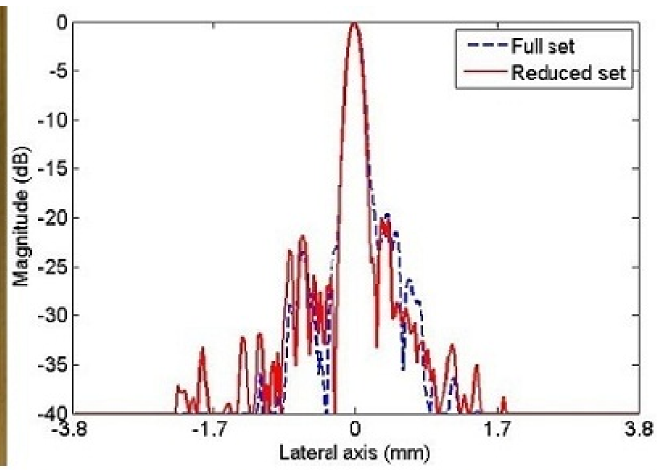

Fig. 1. Picture of CMUT on CMOS dual-ring array (left), Lateral PSF of the spherical target at 2.5 mm on array normal (right)

1F-2

2:15 PM Preliminary In-Vivo evaluation of Synthetic Aperture Sequential Beamforming

Martin Christian Hemmsen[1,2], Peter Møller Hansen[3], Theis Lange[4], Jens Munk Hansen[1], Michael Bachmann Nielsen[3], Jørgen Arendt Jensen[1]; *[1]Dept. of Elec. Eng., Technical University of Denmark, Lyngby, Denmark, [2]R&D Applications & Technologies, BK Medical, Herlev, Denmark, [3]Dept. of Radiology, Copenhagen University Hospital, Rigshospitalet, Copenhagen, Denmark, [4]Dept. of Biostatistics, University of Copenhagen, Copenhagen, Denmark*

Background, Motivation and Objective

This paper presents a preliminary in-vivo study of Synthetic Aperture Sequential Beamforming (SASB) in a side-by-side comparison with conventional imaging. The objective is to evaluate if the image quality using SASB imaging is comparable to conventional imaging in terms of spatial resolution, contrast, and unwanted artifacts

Statement of Contribution/Methods

Data acquisition was performed using a ProFocus ultrasound scanner (BK Medical, Herlev, Denmark) and a 192 element 3.5 MHz convex array transducer (Sound Technology Inc., State College, PA 16801, USA). Conventional and SASB first stage RF data were acquired interleaved, ensuring that the exact same anatomical location was scanned. Data were recorded in real time and processed off-line to generate image sequences. Volunteers were scanned abdominally resulting in 34 image sequence pairs. Each image sequence pair was compared twice with different left-right placement by 5 medical doctors using randomized blinded presentation. For each comparison the doctors gave a score between -50 and 50, where a negative score favored SASB. The statistical analysis of the data was designed to account for two channels of dependencies; the first is the doctor effect and the second is the image effect. The combined effect of these two channels of dependencies is that none of the observations (the individual scores) are independent. To accommodate for this a random effects linear model was used with random effects of image pair, doctor, and side (left vs. right) as covariate. To check the robustness of the findings the analysis was repeated with the square root of the score. In addition a number of Wilcox non-parametric test were performed. All analysis was conducted using the program R version 2.12.2.

Results

There no significant difference between showing SASB images on the left or on the right (p-value: 0.51) and this covariate was therefore dropped from the model in further analysis. In the reduced model it was found that SASB was significantly better than conventional imaging (p-value: < 0.001). The average scores for the comparison were -2.9 with a confidence interval (accounting for the mentioned dependencies) from -4.54 to -1.26. If the covariate “left vs. right” was kept in the model the conclusions were not altered. Analyzing the transformed score did not change the conclusions of the analysis, and likewise did the analysis of the non-parametric tests not change the conclusions of the original analysis.

Discussion and Conclusions

Results show that in-vivo ultrasound imaging using SASB is feasible for abdominal imaging and is statistically significant better than conventional imaging, when evaluating spatial resolution, contrast and unwanted artifacts.

1F-3

2:30 PM A synthetic-focusing strategy for real-time high-frequency annular-array imaging

Jeffrey A. Ketterling[1], Erwan Filoux[1]; [1]Lizzi Center for Biomedical Engineering, Riverside Research, New York, NY, USA

Background, Motivation and Objective

Using a 40 MHz, 5-element annular array, we demonstrated a single-pulsing-channel, 5-pass approach of collecting all transmit-to-receive (TR) echo data and then an arbitrary number of axial focal zones were created with synthetic focusing (SF). This technique is highly effective but limits frame rates due to the 5 passes and large quantity of data that must be passed from the digitizers to the control PC. Here, we examine a beamforming strategy to eliminate the outer receive channels. The technique can be implemented with a single-pass, 5-channel-pulser approach to increase frame rates.

Statement of Contribution/Methods

A spatial-impulse response model was implemented with LabVIEW to simulate the acoustic field of a 5-ring, 40 MHz annular array (6 mm aperture, 12 mm focal length). Acoustic field simulations included lateral beamwidth (LBW) and axial depth of field (DOF) for focusing over the range 8 to 20 mm. In addition, time-domain point spread functions (PSFs) for the 25 TR pair were calculated in 1 mm steps from 6 to 18 mm and Gaussian white noise was added to simulate 40 dB of SNR. Full SF of all 25 TR pairs was then compared to fixed focusing (FF) and to cases with receive channels eliminated. Due to the reciprocal nature of the acoustic path (ring 1to5 = 5to1), it was possible to recover some of the lost aperture by doubling the contribution of the reciprocal TR pair.

Results

The optimal LBW was obtained with all 25 TR pairs. Reducing TR pairs degraded lateral resolution (Fig. 1a). With the inner 4 elements receiving (SF Drop5), resolution dropped by 1% and with the inner 2 elements receiving, by 22%. The -6 dB DOF (5.6 mm) was the same for all focused cases although the absolute magnitude of the DOF profile decreased as TR pairs were removed. SF of PSF data showed that relative to FF, the SNR drastically increased when moving away from the geometric focus and absolute SNR moderately decreased as receive channels were removed (Fig. 1b). The technique was then applied to archived mouse embryo TR data and as receive channels were dropped, SNR slightly decreased and resolution slightly degraded.

Discussion and Conclusions

Simulations show that when using an SF beamforming approach based on individual TR pairs, the outer receive channels of an annular array can be eliminated without drastically affecting LBW, DOF, or SNR. This permits faster frame rates by reducing the amount of data that must be beamformed.

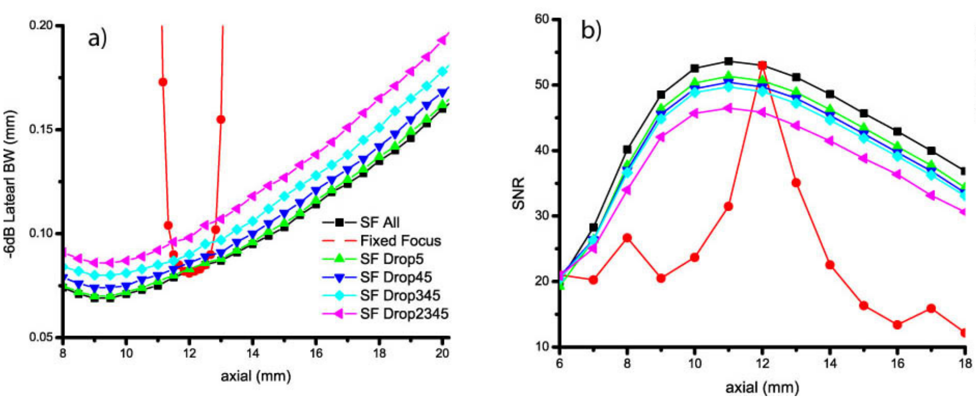

Fig 1: a) LBW vs. axial distance. b) SNR vs. axial distance with simulated PSF and 40 dB SNR.

1F-4

2:45 PM Experimental Verification of a Split-aperture Transmit Beamforming Technique for Suppressing Grating Lobes in Large Pitch Phased Arrays

Zahra Torbatian[1], Rob Adamson[1], Manohar Bance[1,2], Jeremy Brown[1,2]; [1]Biomedical Engineering, Dalhousie University, Canada, [2]Department of Surgery, Dalhousie University, Canada

Background, Motivation and Objective

Conventionally, phased array transducers have used an inter-element pitch of approximately .5λ to avoid grating lobes at large steering angles. This introduces major challenges in the fabrication of high-frequency phased arrays where the wavelength is on the order of 30 µm. We have developed a new transmit beamforming technique in combination with Phase Coherence Imaging (PCI) that can suppress grating lobes in large pitch arrays to make the fabrication of high frequency phased arrays feasible. A method called Phase Coherence Imaging (PCI) was recently introduced in the literature for suppressing grating lobes. In PCI, signals are weighted by a factor proportional to the instantaneous phase coherence of the element echo. This technique is effective for synthetic aperture where the transmit pulse in the grating lobe region is broadband. However, synthetic aperture is often undesirable due to its susceptibility to image distortion from small tissue vibrations. More commonly used in medical ultrasound is transmit beamforming, where all elements are pulsed together. PCI, however, does not fully suppress the grating lobes in this case since the grating lobe echoes have large instantaneous phase overlap between them. We have developed a technique that splits the N element transmit aperture into N/K transmit elements and N receive elements in order to better suppress grating lobes with transmit beamforming. By reducing the size of the transmit aperture, the bandwidths of the grating lobe echoes are increased, making PCI more effective.

Statement of Contribution/Methods

We have used a Vevo 2100 imaging system with a MS70 50 MHz linear array transducer (Visualsonics, Toronto, ON) to experimentally verify our transmit beamforming technique. The system was reprogrammed such that only 64 elements in the array were used. The received echoes could all be collected individually, and transmit beam could be steered off to different angles. Effectively, the array was turned into a 64 element phased array with 1.2λ element pitch. PCI weighting was applied to the echoes offline in Matlab and images were generated of wire phantoms and tissue phantoms.

Results

Images generated of wire phantoms using no PCI processing had large grating lobes only 35 dB below the main lobe. When applying the PCI processing the grating lobe width was shortened but the peak amplitude did not change. By simply splitting the transmit aperture in two, we have shown that the grating lobes can be suppressed to 58 dB below the main lobe. Qualitatively, images generated of tissue phantoms also show a reduction in grating lobe levels using this technique.

Discussion and Conclusions

Based on the experimental measurements and previously presented simulation results, the described split-aperture transmit beamforming method along with PCI effectively suppresses grating lobes in large pitch phased arrays, making fabrication of high-frequency phased arrays feasible.

1F-5

3:00 PM Ring Array PSF Synthesis by Delay Dithering

Scott Dianis[1], Ralph Hoctor[1]; [1]GE Global Research, Niskayuna, New York, USA

Background, Motivation and Objective

A ring array transducer coaxial with an ablation tip combines cardiac ablation and monitoring via ultrasound imaging in a single catheter. Naturally, using single-transmit beamforming methods results in poor image quality due to high side lobes in the ring array point spread function (PSF). In order to reduce peak side lobe levels, use of synthetic aperture has been proposed. Norton proposed a synthetic aperture scheme based on coherent addition of four ring-array Bessel beams. A J_n^2 Bessel beam pattern is generated by applying phase weightings of nθ on transmit and its negative on receive, with θ equal to the polar angle of a ring array element [1].

A broadband implementation of Norton's scheme can utilize time delays to replace phase weightings, with time delays equal to the fraction of a period at the center frequency represented by the phase weights modulo 2π. Thus, Norton's scheme represents a special case of a more general approach, in which the array element delays are dithered: that is, small delays are added to the beamsteering delays to change the sidelobe structure. An approach for designing synthetic aperture schemes based on such dithering is needed.

Statement of Contribution/Methods

Two design methods were investigated.

Using FIELD II, the simulated PSF of two or more firings of the ring array were coherently summed. Dithering delays were varied for the transmit and receive apertures via a simulated annealing algorithm to directly minimize the ratio of maximum side lobe level to main lobe level in the simulated PSF.

An extended coarray formulation was developed to describe the synthetic aperture time-dithering PSF in terms of a single, one-way response. Each point on the coarray is associated with a waveform, representing the coherent superposition of multiple transmits for a single transmit/receive element pair. An alternative design method is used to find an extended coarray with desired PSF characteristics and then to match it using *N* transmits of the ring array.

Results

The best simulated annealing 2-shot result yields a peak side lobe level (PSLL) of -23.2 dB, 3.7 dB lower than the PSLL from Norton's 4-shot scheme, and a 3-shot result yields -26 dB PSLL. Beyond 3-shots, the computational load of simulated annealing becomes too high, and a faster method is needed. We will give examples of PSF design using the coarray, a method that runs much faster than the simulated annealing approach, and which can give even better PSLL results.

Discussion and Conclusions

Using simulated annealing to directly compute dithered time delays to improve synthetic aperture ring array imaging is slow but gives attractive results. The new coarray approach speeds up design of reduced-side lobe synthetic aperture PSFs as well as provides a better understanding of the process.

[1] S. J. Norton, IEEE Trans. on UFFC, 2002.

This work supported by NIH grant R01 HL67647-06A1

THURSDAY ORAL

1F-6

3:15 PM Performance of Synthetic Aperture Compounding for in-invo imaging

Jens Munk Hansen[1], Mads Møller Pedersen[1], Martin Christian Hemmsen[1,2], Jørgen Arendt Jensen[1]; [1]Dept. of Elec. Eng., Technical University of Denmark, DK-2800 Lyngby, Denmark, [2]R&D Applications & Technologies, BK Medical, DK-2730 Herlev, Denmark

Background, Motivation and Objective

Medical ultrasound imaging is a non-invasive method for identifying and classifying cysts and tumors. The identification is impaired because of a poor contrast due to speckle artifacts. A successful approach to remedy the low contrast is spatial compounding, but this at the cost of a reduction in frame rate by the number of directions. With synthetic aperture (SA) data, compounding can be achieved for any number of directions without reducing the frame rate.

Statement of Contribution/Methods

In SA imaging, data are acquired by emitting with a subaperture and receiving with all or a part of the elements. This is repeated for a number of emissions. To make compounding, a large number of transmit beams are synthesized corresponding to imaging each point from many directions. Correspondingly, in receive, a dynamic focus is used for each direction using the same elements that was used for synthesizing the transmit beam. The resulting in-phase and quadrature data are used for computing the envelope and forming an image for each direction. Finally, the images are added to form the compound image. In-vivo images are acquired using an experimental ultrasound scanner, RASMUS, capable of storing 12-bit individual channel data at 40 MHz. For imaging, an 11 element subaperture is used for each emission using a 20 µs FM signal with 90% bandwidth. For receiving 128 channels are sampled. The transducer used is a commercial 5.5 MHz, 128 element convex array with λ pitch (BK Medical)

Results

Compounding images are synthesized using 5 angles with an angular separation of 5 degrees. The figure shows in-vivo images of the abdomen of a healthy 27 year old male with and without compounding. The portal vein branch is in the center of the image and the hepatic veins are located to the left above. The speckle-to-noise ratios (SNR) are calculated in a 10 mm region in the center of the images. For the SA compound image, an SNR of 2.29 is obtained compared to 1.82 for the SA image. Contrast-to-noise ratios (CNR) are computed between regions in the portal and hepatic veins and the surrounding tissue. For the regions in the compound image, CNR values of 1.98 and 3.47 are obtained compared to 3.02 and 1.73 for the SA image, i.e. an average improvement of 15%.

Discussion and Conclusions

The suggested approach for performing compounding using SA in-vivo data reduces the speckle and indeed improves the CNR without a reduction of the frame rate.

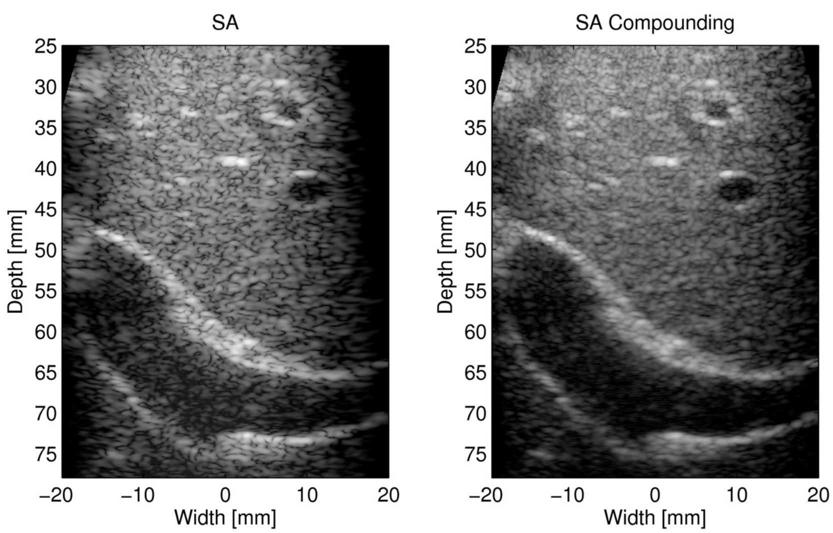

2F - Elastography: New Methods

Boca Rooms VI-VII

Thursday, October 20, 2011, 2:00 pm - 3:30 pm

Chair: **Kathy Nighingale**
Duke University

2F-1

2:00 PM Generalized Bayesian Speckle Tracking Applied to Strain and ARFI Displacements

Brett Byram[1], Gregg Trahey[1], Mark Palmeri[1]; [1]*Duke University, USA*

Background, Motivation and Objective

A hallmark of clinical ultrasound has been accurate and precise time-delay estimation (TDE). TDE has numerous clinical uses including blood-flow, elastography, therapeutic guidance and ARFI imaging. In ultrasonic TDE, the fundamental limit on displacement accuracy has been regarded as the Cramer-Rao lower bound (CRLB). The CRLB, more specifically, represents the minimum variance of an unbiased estimator. Unbiased estimators can be useful, but in many cases allowing an estimator to be slightly biased results in a large decrease in variance and overall mean square error (MSE) improvement relative to CRLB limited estimators.

Statement of Contribution/Methods

To create a biased estimator with better performance than a CRLB limited estimator (e.g. normalized cross-correlation (NCC)) a generalized framework is developed for Bayesian speckle tracking. A Bayesian estimator requires a likelihood function and prior probability distribution function (PDF). First, a likelihood function appropriate for ultrasound is derived since the canonical likelihood function used in other fields for TDE requires precise knowledge of the thermal noise power for each estimate which is not currently feasible. Second, prior PDFs are formed using several methods. These methods were evaluated and include both informative and non-informative priors. The informative priors were based on the displacement PDFs at adjacent locations.

The biased estimators were validated using bulk motion simulations and ARFI simulations created with a finite-element model and Field II.

Results

The proposed likelihood function was evaluated and compared against the classic likelihood function by converting both to posterior PDFs using a non-informative prior. Example results are reported for bulk motion simulations using a 6 lambda tracking kernel and 30 dB SNR for 1000 data realizations. The new and canonical likelihood function assigned the true displacements probabilities of .22+/- .16 and .070+/- .020, respectively. For the same tracking parameters and simulated ARFI displacements the new and canonical likelihood function assigned the entire true ARFI displacement profile the log10 probability of -34 +/- 7 and -51+/- 14. These trends hold at least for SNRs greater than 10 dB and kernel lengths between 1.5 and 12 lambda.

The peak displacement of the ARFI response is reported since this position results in the noisiest estimates. Estimates were made with a 1.5 lambda kernel and 20 dB SNR on 100 data realizations. Estimates using NCC and the Bayes estimator had MSEs of 17 and 7.6 microns squared, respectively, contextualized by the true displacement magnitude, 10.9 um. Biases for the NCC estimator and the Bayes estimator are -.12 and -.28 um, respectively.

Visible improvements were also seen in in vivo myocardial canine ARFI and strain images.

Discussion and Conclusions

Bayesian speckle tracking has been tested with simulation and in vivo data. Bayesian tracking outperforms traditional ultrasonic TDE.

2F-2

2:15 PM Motion Compensation Method for Quantification of Neovascularization in Carotid Atherosclerotic Plaques with Contrast Enhanced Ultrasound (CEUS)

Zeynettin Akkus[1], Johan G. Bosch[1], Guillaume Renaud[1], Gerrit L. ten Kate[2], Stijn van den Oord[2], Arend Schinkel[2], Nico de Jong[1,3], Antonius F.W. van der Steen[1,3]; [1]*Thoraxcenter Biomedical Engineering, Erasmus MC, Netherlands,* [2]*Department of Cardiology, Thoraxcenter, Erasmus MC, Netherlands,* [3]*Interuniversity Cardiology Institute of the Netherlands, Utrecht, Netherlands*

Background, Motivation and Objective

Several studies have linked intraplaque neovascularization (IPN) with progressive atherosclerotic disease and plaque instability. Quantification of IPN may allow early detection of vulnerable plaques. In this study, a dedicated motion compensation method was developed for quantification of IPN in small plaques (<30% diameter stenosis). Motion compensation is a prerequisite to analyze identical regions of interest (ROI). The commercially available motion compensation method (Philips Qlab) was unable to track these small plaques.

Statement of Contribution/Methods

Side-by-side CEUS and B-mode ultrasound images of carotid arteries were acquired by a Philips iU22 system with a L9-3 linear array probe. The motion pattern for the plaque region was obtained from the B-mode images with a tuned speckle tracking method and applied to contrast images. Our drift-free speckle tracking (ST) method uses a fixed template (5 x 5 mm) and normalized cross correlation with 1:10 subpixel peak detection. The ST was validated in-vitro with a phantom, mimicking carotid lumen and wall, moved by a computerized XYZ positioning system with 1mm steps in X and Y directions over 7mm (total #frames N=376). In-vivo validation was done by comparing ST to manual tracking of plaque by two experts for multibeat image sequences (MIS) of 11 patients (N=2750). The ST success rate was visually assessed on 67 atherosclerotic wall plaque MIS (N=7964). The tracking was considered failed if the ST deviated > 2 pixels from true motion in any frame.

Results

In the phantom validation, error was 98.8 ± 30.5 µm (mean ± standard deviation) for X (longitudinal) and -90.0 ±58.1 µm for Y (radial). In-vivo validation, error was 51.4 ± 91 µm for X and 18.7 ± 39.8 µm for Y. Tracking was scored as fully successful in 52 MIS (78%). The range of displacement over these 52 in X and Y was respectively 1.1 ± 0.6 mm (X) and 0.4 ± 0.2 mm (Y). The ST sporadically failed in 15 (22%) MIS due to poor image quality, wall saturation, jugular vein proximity and out of plane motion. Motion correction showed improved lumen-plaque contrast separation as shown below.

Discussion and Conclusions

The proposed motion tracking is sufficiently accurate and successful for in vivo application. Our method allows improved quantification of IPN.

THURSDAY ORAL

This research was supported by the Center for Translational Molecular Medicine and the Netherlands Heart Foundation (PARISk).

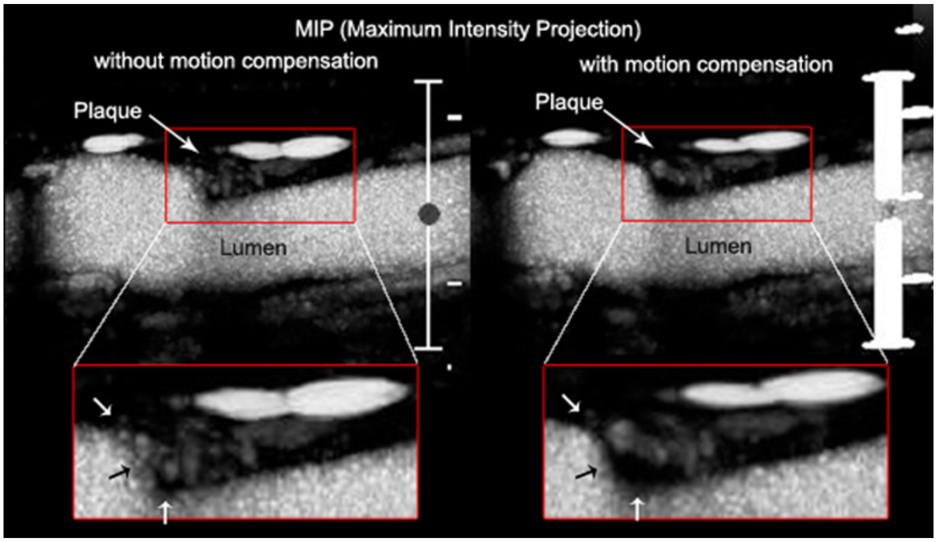

2F-3

2:30 PM Quantitative imaging using Time Reversal Elastography: a feasibility study.

Javier Brum[1,2], Stefan Catheline[2], Nicolas Benech[1], Thomas Gallot[2], Carlos Negreira[1]; [1]*Laboratorio de Acústica Ultrasonora, Instituto de Física,Facultad de Ciencias, Universidad de la República, Montevideo, Uruguay,* [2]*Institut des Sciences de la Terre (ISTerre), Université de Grenoble, Saint Martin d'Heres, Isére, France*

Background, Motivation and Objective

In previous works the authors developed a method for extracting the shear elasticity of soft tissues from a complex reverberated elastic field using spatiotemporal correlations interpreted in the frame of the time-reversal symmetry: Time Reversal Elastography (TRE). By measuring the shear wavelength from the focal width as the wave converges the shear elasticity can be obtained. The feasibility of TRE as an imaging technique has already been shown in vivo in bi-layer mediums (e.g. belly muscle - liver). In this work the authors take a step forward and demonstrate its feasibility as a quantitative imaging technique by detecting small inclusions embedded in a softer medium.

Statement of Contribution/Methods

Experiences in a phantom made of Polyvinil Alcohol Cryogel were performed. The phantom contains a harder cylindrical inclusion of 12 mm diameter. The experiment is the following: a complex elastic field is created inside the sample by randomly tapping with the fingers during 10 s. The displacement field is measured inside the soft solid using a 64 channel array through a speckle tracking technique. Secondly, one displacement line at (xo, zo) is selected and correlated to the others, resulting in a 2D focus in (xo, zo). To gain spatial resolution the focal width at -2 dB is measured for each position. Using the elastodynamic Green function the -2 dB contour can be directly related to the shear wavelength and thus the shear elasticity. The obtained mean shear elasticity will be compared with the one obtained using transient elastography (TE) considered as a reference value.

Results

The image obtained by use of time reversal elastography (TRE) superposed to the B-mode image is shown in Fig. 1(a). The inclusion (marked with the white arrow) is hardly visible in the B-mode image (Fig. 1(b)). Mean shear elasticity values were found to be for both techniques TRE: 19.9+/-0.5 kPa and TE: 18.5+/-5 kPa within the inclusion and TRE: 11.8+/-0.3 kPa and TE: 10.8+/-3 kPa for the background.

Discussion and Conclusions

The inclusion is clearly detected using TRE despite the low elastic contrast. A general quantitative agreement within 8% was found between the different measurements of shear elasticity for the inclusion and the background. The obtained results complete the feasibility study of the shear wavelength tomography as a quantitative imaging technique.

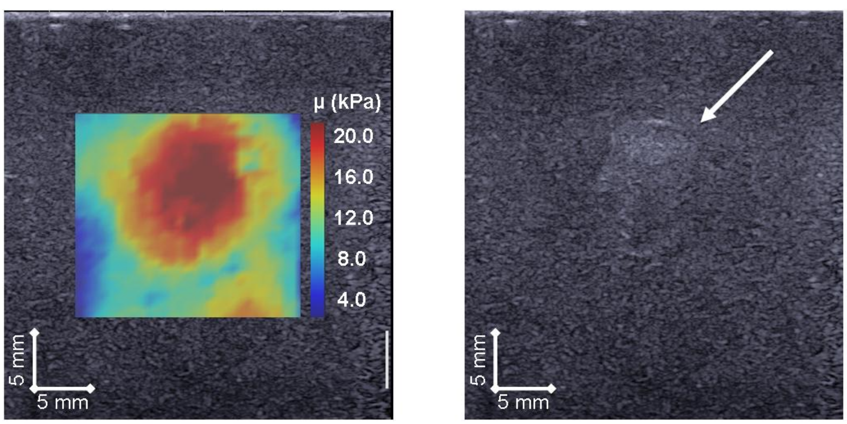

(a) (b)

2F-4

2:45 PM Viscoelastic Characterization of an Elliptic Structure in Dynamic Elastography Imaging using a Semi-analytical Shear-wave Scattering Model

Emmanuel Montagnon[1], Anis Hadj Henni[1], Cédric Schmitt[1], Guy Cloutier[1]; [1]Laboratory of Biorheology and Medical Ultrasonics, University of Montreal Hospital Research Center, Montreal, Quebec, Canada

Background, Motivation and Objective

Most ultrasound dynamic elastography techniques rely on shear wave speed estimation and dispersion curves to assess elasticity and viscosity, but assume one-dimensional displacements and do not consider diffraction of shear waves by a mechanical heterogeneity (i.e., a lesion). Thereby, a two-dimensional (2-D) semi-analytical scattering model of shear vertical waves interacting with elliptical structures is proposed and validated using the finite element method (FEM); then an inverse problem is formulated and validated in-vitro using an agar-gelatin phantom.

Statement of Contribution/Methods

The Helmholtz equation was solved in elliptical coordinates using the separation of variables method (SVM). Solutions were computed by taking into account elastic boundary conditions along the elliptic contour. The stationary 2-D FEM considered the elliptic inclusion embedded in a medium. For experimental validation, an agar-gelatin phantom, containing an elliptic inclusion (3% gelatin, 1% agar) embedded in a surrounding medium (4% gelatin and 3% agar) was used. An inverse problem based on a comparison of displacement profiles was formulated using a non-linear least-mean-square method allowing estimation of viscoelastic parameters of both the inclusion and surrounding medium.

Results

The comparison of displacement profiles obtained from SVM or FEM for various complex shear moduli, incidence angles and frequency highlighted correlation coefficients greater than 0.9. Inverse problem results from 3 distinct positions of the probe along the cylinder axis gave mean shear elasticity moduli of 1.44 ± 0.02 kPa (inclusion) and 17.36 ± 0.84 kPa (surrounding medium), and mean viscosities of 0.13 ± 0.009 Pa/s and 0.9 ± 0.077 Pa/s for the inclusion and surrounding medium, respectively. An example of experimental results is shown in Fig. 1.

Discussion and Conclusions

The proposed model has been validated with both forward and inverse problem approaches, allowing accurate viscoelastic characterization of the inclusion and surrounding medium. Advantages are the absence of spatial derivatives, which are sources of noise in inversion process, and the absence of restrictive assumption about the rheological model of considered materials. The proposed scattering model may be helpful for benign/malign classification of suspected breast lesions with dynamic elastography imaging.

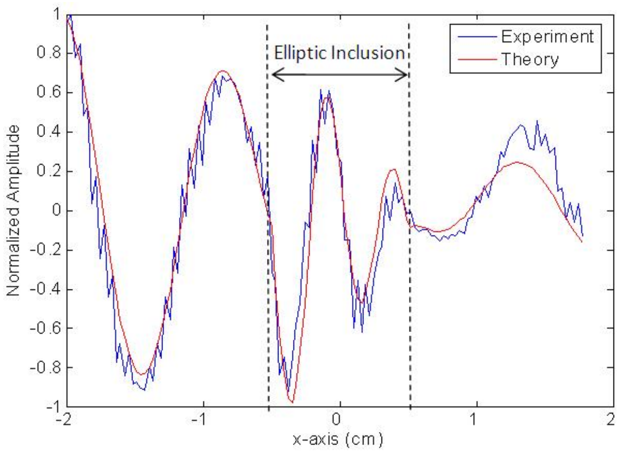

Fig. 1 Solution of the inverse problem compared to experiment results, at 310 Hz (Inclusion: half-large axis: 5mm, half-small axis: 3.8mm).

2F-5

3:00 PM Measurements of Viscoelasticity using the MR Elastography and Lamb wave Dispersion Ultrasound Vibrometry (LDUV)

Ivan Nenadic[1], Sara Aristizabal[1], Kevin Glaser[1], Scott Mitchell[1], Tye Humphrey[1], James Greenleaf[1]; [1]*Mayo Clinic, Rochester, MN, USA*

Background, Motivation and Objective

Changes in tissue stiffness due pathophysiology have been known for centuries. Our group has been investigating the feasibility of using Lamb wave Dispersion Ultrasound Vibrometry (LDUV) method to excite Lamb waves in organs with plate-like geometry to estimate the viscoelasticity of the medium of interest. Two organs, the heart wall and the spleen, can be readily modeled using plate-like geometries. Diastolic dysfunction is the inability of the left ventricle (LV) of the heart to supply sufficient stroke volumes into the systemic circulation and is accompanied by the stiffening of the LV myocardium. It has been shown that there is a correlation between high splenic stiffness in patients with chronic liver disease and strong correlation between spleen and liver stiffness. In this comparative study, we report measurements of viscoelasticity of a gelatin plate, excised porcine spleen and excised porcine LV free wall myocardium using the LDUV method and the Magnetic Resonance Elastography (MRE).

Statement of Contribution/Methods

The samples were embedded in a softer gelatin and placed inside a plastic container. A hole was cut out on the bottom of the container to allow access for a pulse-echo transducer for LDUV studies. A mechanical shaker coupled to a glass rod glued through the thickness of the samples was used to excite harmonic anti-symmetric Lamb waves at several frequencies in the range 100 – 500 Hz. A pulse-echo transducer was used to track the motion along the line of propagation and calculate the Lamb wave velocity. Lamb wave dispersion velocity was used to estimate elasticity ($\mu 1$) and viscosity ($\mu 2$) of the samples by fitting a Lamb wave dispersion equation.

Results

In MRE experiments, a plastic pneumatic driver was used to excite Lamb waves in the samples at several frequencies in the range 100 – 500 Hz. 3-D motion was tracked using a standard MRE protocol. The curl operator was used to filter out compressional wave contributions in the 3D motion data obtained using MRE. Shear wave velocity was fitted with the Voigt model to estimate elasticity ($\mu 1$) and viscosity ($\mu 2$). Mathematical treatment of the Lamb wave displacement and dispersion equations demonstrated that the curl operator acting upon the Lamb wave displacement field cancels out compressional wave contribution.

The obtained values of elasticity ($\mu 1$) and viscosity ($\mu 2$) for the gelatin plate were 3.8 ± 1.1 kPa and 5.3 ± 1.8 Pa*s using MRE, and 2.5 ± 0.5 kPa and 4.7 ± 0.3 Pa*s using LDUV. Elasticity ($\mu 1$) and viscosity ($\mu 2$) for the spleen sample were 2.0 ± 0.6 kPa and 2.8 ± 0.4 Pa*s using MRE, and 1.2 ± 0.2 kPa and 3.8 ± 0.9 Pa*s using LDUV. Elasticity ($\mu 1$) and viscosity ($\mu 2$) for the myocardium sample were 3.6 ± 1.5 kPa and 9.4 ± 2.3 Pa*s using MRE, and 4.3 ± 0.9 kPa and 11.1 ± 1.7 Pa*s using LDUV.

Discussion and Conclusions

The results show that the estimates of elasticity ($\mu 1$) and viscosity ($\mu 2$) obtained using the MRE and the LDUV method agree within one standard deviation, suggesting the validity of the LDUV method.

2F-6

3:15 PM Shear Wave Speed Measurement Using an Unfocused Ultrasound Push Beam

Shigao Chen[1], Heng Zhao[1], Pengfei Song[1], Matthew Urban[1], James Greenleaf[1]; [1]*Mayo Clinic College of Medicine, USA*

Background, Motivation and Objective

Measurement of shear wave speed Cs has important medical applications because it is related to tissue elasticity and pathology. In radiation force based methods, typically a focused ultrasound beam is used to generate shear waves for subsequent cs measurement. Here we study the feasibility of using an unfocused push beam for shear wave production and Cs measurement. Potential benefits are valid Cs measurements over longer axial range, including the transducer near field, for applications in superficial soft tissues.

Statement of Contribution/Methods

A Verasonics ultrasound system with a L7-4 linear array transducer was used in this study. Shear waves were generated by an unfocused push beam transmitted from 8, 12, or 16 elements (628 µs, 4.7 MHz) and were subsequently detected by plane wave "flash" imaging at a PRF of 10 kHz for 10 ms. Shear wave speed was calculated by time-to-peak over a lateral range of 10 mm through linear regression. Three homogeneous phantoms with different Cs calibrated by Magnetic Resonance Elastography (MRE) and 1D Transient Elastography (TE) were studied. Measurements were repeated at 5 different locations within each phantom.

Results

Results in phantom 2 using 16-element transmit aperture are shown as example in the figure below. Panel (a) shows shear wave motions at 15 mm depth along different lateral positions from the push center. Panel (b) is a linear regression of the time-to-peak along lateral direction at 15 mm depth. Panel (c) shows maximum displacements through time at different lateral positions for 3 depths. Panel (d) shows Cs measured at different depths. Means and standard deviations in Panels (c) and (d) were obtained from repeated measurements at 5 different locations. The Cs averaged over all depths shown in (d) were 1.23 ± 0.01, 1.46 ± 0.01, and 1.87 ± 0.01 m/s for phantoms 1, 2, and 3, where MRE results were 1.24 ± 0.01, 1.47 ± 0.02, and 1.80 ± 0.02 m/s, and 1D TE results were 1.23 ± 0.02, 1.48 ± 0.03, and 1.89 ± 0.07 m/s.

Discussion and Conclusions

This study demonstrates the feasibility of Cs measurement using an unfocused ultrasound push beam. Sufficient motion can be generated for reliable Cs measurements along a relatively long axial range. The unfocused push beam has a mechanical index well below 1.9 but maximum depth penetration requires further investigation.

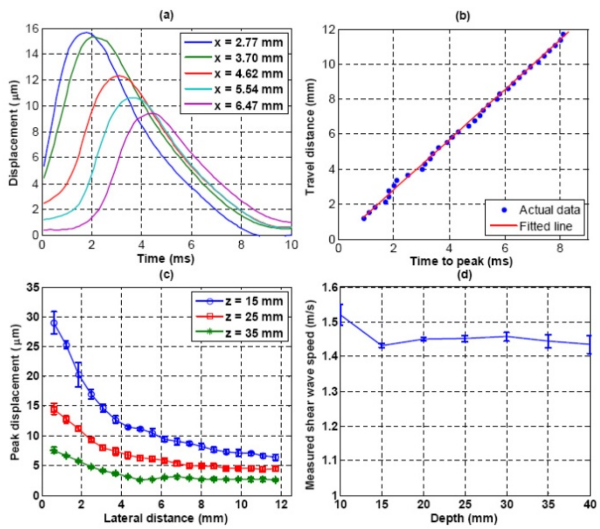

THURSDAY ORAL

3F - Photoacoustics: Technology Development

Carribean Ballroom VII

Thursday, October 20, 2011, 2:00 pm - 3:30 pm

Chair: **Pai-Chi Li**
National Taiwan University

3F-1

2:00 PM All optical generation and detection of acoustic waves for intravascular ultrasound and photoacoustic imaging

Bao-Yu Hsieh[1], Sung-Liang Chen[2], Tao Ling[2], Jay Kuo[2], Pai-Chi Li[1]; [1]*Natoinal Taiwan University, Taiwan,* [2]*University of Michigan, USA*

Background, Motivation and Objective

The combination of intravascular ultrasound (IVUS) and photoacoustic (IVPA) imaging has been proposed for detection of atherosclerotic plaques. Its clinical applications, however, have been hindered by several factors, including the lack of a cost-effective solution for a disposable scanhead. In this study, we propose a new scanhead design for IVUS/IVPA imaging. Specifically, the design is based on optical generation and detection of acoustic waves for both imaging modalities.No conventional piezoelectric device is used and the design is suitable for one-time, disposable use.

Statement of Contribution/Methods

The integrated IVUS/IVPA transducer consists of an optical fiber with an axicon tip for excitation, and a microring for acoustic detection. The axicon tip splits the laser beam so that part of the laser light is directed sideways to tissue for IVPA imaging. The other part of the laser light is directed to the substrate of the microring, at which light is converted to ultrasound based on the photoacoustic response, thus generating ultrasound propagating sideways for IVUS imaging. The microring device is used for detection for both IVPA and IVUS. A grid phantom is used to demonstrate imaging capabilities of this technique. Such a device can simplify configuration of the scanhead and reduce the cost without using any electronic components and conventional piezoelectric devices. The fabrication procedure of microring detectors is a nanoimprint technique, which is possible for mass production.

Results

Images of the grid phantom are shown. The grid consists of lines with a 0.9 mm width and 2.5 mm spacing. -6dB spatial resolution at 305μm/169μm (lateral/axial) is achieved. The US image and the PA image can also be fused into a single representation.

Discussion and Conclusions

An all-optical IVUS/IVPA imaging scanhead has been designed and tested on a grid phantom. It can generate US and PA signals with a single laser pulse. In the present study, US and PA signals are separated by time delays. With the applications of coded excitation and subband imaging, the IVUS and IVPA can be distinguished in the frequency domain.

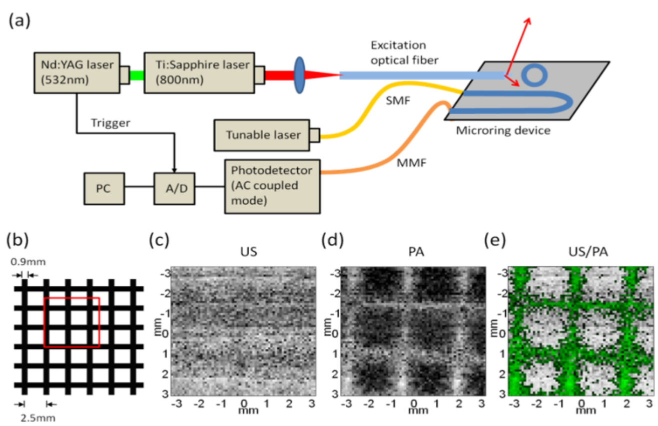

Figure: (a). Schematic of the IVUS/IVPA imaging system and scanhead design. (b). Grid phantom. (c). US image of the grid. (d). PA image of the grid. (e) Fused US/PA image.

3F-2

2:15 PM Photoacoustic Coded Excitation using Periodically Perfect Sequences

Martin F. Beckmann[1], Martin P. Mienkina[1], Claus-Stefan Friedrich[2], Nils C. Gerhardt[2], Martin R. Hofmann[2], Georg Schmitz[1]; [1]Medical Engineering, Ruhr-Universität Bochum, Bochum, Germany, [2]Photonics and Terahertz-Technology, Ruhr-Universität Bochum, Bochum, Germany

Background, Motivation and Objective

Photoacoustic imaging is based on the generation of ultrasound using laser irradiation. Nd:YAG laser systems are commonly employed for this purpose, but cheap and handy pulsed laser diodes can be an attractive alternative. They emit significantly lower pulse energies, but fast averaging is possible due to the high repetition rates of laser diodes in order to improve the Signal to Noise ratio (SNR). Unfortunately, averaging is limited by the time-of-flight of the acoustic signal. Photoacoustic coded excitation (PACE) can be used to overcome this limitation. Strategies exploiting periodic features of sequences can yield improved SNR. Here, we examine the performance of difference set based sequences with perfect correlation properties (periodically perfect sequences, PPS).

Statement of Contribution/Methods

The examined PPS rely on binary sequences constructed from Legendre difference sets. To achieve perfect reconstruction, two different sequences are used for sending and decoding. The sending sequence can easily be realized as a unipolar sequence that can be sent without modification. The code sending time for one repetition must exceed the acoustic time of flight. The gain in SNR compared to averaging (coding gain) was calculated theoretically and compared to previously published sequences. The theoretical results were verified in an experiment. To simulate periodic sending, 3 repetitions of the code were used. A pulsed laser diode (652nm, 31ns pulse) was focused on a sample, photoacoustic signals were detected using a modified Sonix RP clinical ultrasound system (Ultrasonix) and a linear array (Ultrasonix L14-5/38). Both code length and pulse repetition frequency were varied.

Results

For continuous, real-time imaging PPS achieve a coding gain that is equivalent to previously reported sequences. For example, for a pulse repetition frequency of 500 kHz at an imaging depth of 6 cm the coding gain approaches 7.02 dB with increasing code length. For 250 kHz the gain is reduced to about 4.01 dB. This is identical to the coding gain reached by Golay codes and Legendre sequences. As major advantage PPS do not inherently produce side lobes such as Legendre sequences do. The sending procedure is much simpler than for Golay codes or Legendre sequences since only a single unmodified sequence is sent continuously. This also reduces the complexity of data processing.

Discussion and Conclusions

PACE is generally used to improve the SNR compared to averaging. Using PPS for continuous imaging allows for faster artifact free image series generation with a simpler coding procedure than any other previously reported PACE strategy. This is a key advantage, as all other PACE strategies require at least 2 pauses equal to the acoustic time of flight in addition to the code sending time.

3F-3

2:30 PM Quantitative Assessment of Photoacoustic and Ultrasonic Imaging of Prostate Brachytherapy Seeds

Richard Bouchard[1,2], Jimmy Su[2], Andrei Karpiouk[2], John Hazle[1], Stanislav Emelianov[1,2]; [1]*MD Anderson Cancer Center, USA,* [2]*University of Texas at Austin, USA*

Background, Motivation and Objective

Brachytherapy seed therapy is an increasingly common way to treat prostate cancer through localized radiation. The current standard of care relies on transrectal ultrasound (TRUS) for imaging guidance during the seed placement procedure. As visualization of individual metallic seeds tends to be difficult or inaccurate under TRUS guidance, guide needles are generally tracked to infer seed placement. Needle deflections of only 5 deg decrease the minimum target dose by 10%. In an effort to improve seed visualization and placement accuracy, the use of photoacoustic (PA) imaging, which is highly sensitive to metallic objects in soft tissue, was investigated for this clinical application.

Statement of Contribution/Methods

PA imaging properties of bare (i.e., embedded in pure gelatin) and tissue-embedded (at depths of up to 9 mm) seeds were investigated with a multiwavelength (750 to 1090 nm) PA imaging technique. Co-registered PA and ultrasonic (US) imaging (i.e., PAUS imaging) results were compared to assess the angular dependence (i.e., seed orientation relative to transducer) of imaging results and image contrast in excised prostate tissue. Multiwavelength PA imaging was performed on seeds at varied imaging depths (1-9 mm) to assess depth dependent effects (e.g., effect of tissue scattering on local fluence).

Results

Much like US imaging, an angular dependence of the PA signal exists (right figure). PA imaging, however, offers a 22-dB improvement in contrast, over US imaging, of a seed in prostate tissue (left figure). Although the PA signal of a bare seed is greatest for shorter laser wavelengths (e.g., 750 nm), the extinction that results from tissue favors the use of higher wavelengths (e.g., 1064 nm) when the seed is located in tissue.

Discussion and Conclusions

PA imaging promises improved contrast of brachytherapy seeds in tissue. Much like US imaging, there is an angular dependence of a seed's PA signal, with the orientation having the greatest surface area normal to the acoustic beam direction resulting in the greatest signal. With only 9-mm penetration depths investigated, however, greater laser fluences at longer wavelengths (e.g., 1064 nm) will need to be utilized to achieve adequate local fluence in a clinical setting. Combined PAUS imaging shows strong promise in accurately visualizing the seed and surrounding tissue anatomy during brachytherapy seed placement procedures.

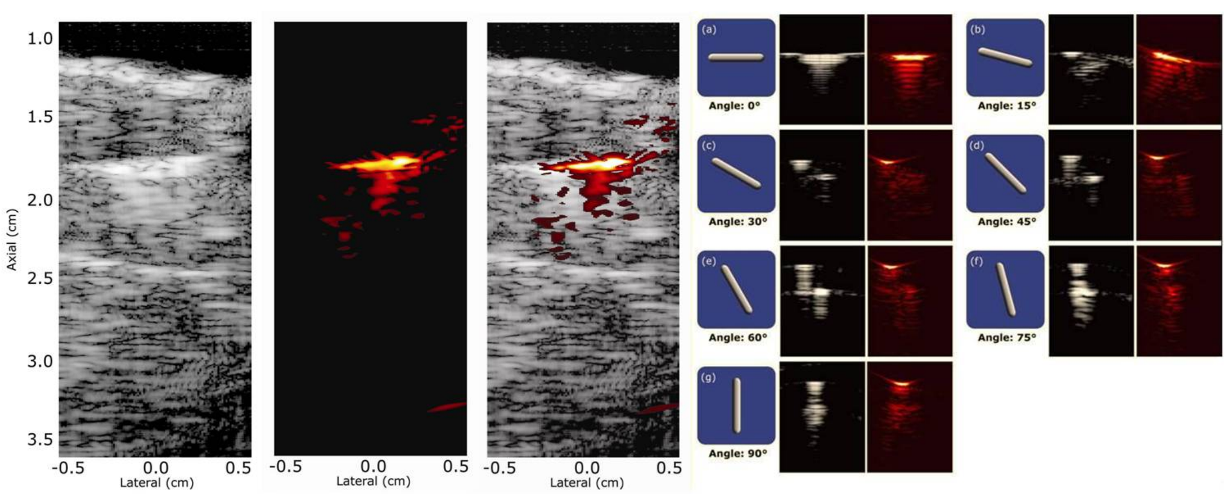

Seed in excised bovine prostate tissue   Angular sensitivity of seed imaging

THURSDAY ORAL

3F-4

2:45 PM Trapping and Dynamic Manipulation of Magnetic Contrast Agent Targeted Cancer Cells in Photoacoustic Imaging: Phantom Study

Chenwei Wei[1], Jinjun Xia[1], Ivan M. Pelivanov[1,2], Xiaoge Hu[1], Xiaohu Gao[1], Matthew O'Donnell[1]; [1]*University of Washington, USA,* [2]*Moscow State University, Russian Federation*

Background, Motivation and Objective

Our previous work on magnetomotive photoacoustic (mmPA) imaging has been extended to address the problem of trapping and manipulating large micro-scale objects, mimicking cancer cells, within a flow stream on the basis of their targeting by coupled contrast agents combining nano-scale magneto-sensitive and highly optically absorbtive components. In addition to magnetic trapping, coupled contrast agents can be manipulated using mmPA imaging to suppress the large background PA signal from blood for sensitive and specific detection of targeted objects. The ultimate application is to identify, accumulate, and kill metastatic cancer cells *in vivo* circulating in the human vasculature.

Statement of Contribution/Methods

The feasibility of trapping and manipulating targeted polystyrene beads in flow with mmPA imaging is demonstrated. Gold nanorods (about 10 nm × 30 nm) were coupled with 15 nm diameter magnetic nanospheres (MNP) to form coupled nanoprobes. They were targeted to 10 µm diameter polystyrene beads (72986, Sigma-Aldrich, MO) to mimick targeting of metastatic cancer cells circulating in the blood. These composite particles recirculated within a water solution inside a 1.6 mm diameter tube at flow speeds up to 50 mm/sec. Two magnets separated by about 4 cm were positioned on opposite sides of the tube to produce a magnetic field of about 0.5 Tesla. The center of the magnet system was changed with respect to the tube to perform dynamic manipulation of the trapped beads for mmPA imaging. The system was illuminated at 730 nm with a tunable OPO laser (Surelite OPO plus, Continuum, CA) with fluence about 1 mJ/cm2. The excited acoustic waves were detected with a linear array transducer (AT8L12-5, Broadsound, Taiwan) interfaced with a Verasonics imaging system (Verasonics, WA).

Results

Fig. 1 shows PA images of MNP-Au nanorods linked beads in the recirculating fluid with flow speed at 50 mm/sec. The accumulated beads trapped by the magnetic force appeared on left or right sides of the tube corresponding to which magnet was closer to the tube.

Discussion and Conclusions

The results clearly demonstrate that polystyrene beads mimicking cancer cells targeted with coupled MNP-Au nanorods can be successfully trapped at a flow speed of 50 mm/sec. With magnetic manipulation, targeted beads can be differentiated from the background even in the presence of large PA signals from blood.

This work was supported in part by (R01CA131797, R01CA140295), NSF (0645080), the Life Sciences Discovery Fund (Grant # 3292512), and the Department of Bioengineering at the University of Washington.

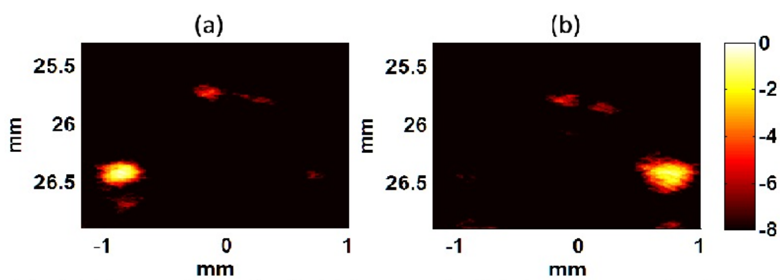

Fig. 1. PA images of accumulated MNP-Au nanoprobes linked to polystyrene microshperes at a flow speed of 50 mm/sec when (a) left, (b) right magnet was closer to the tube.

3F-5

3:00 PM Characterization of Red Blood Cell Aggregation with Photoacoustics: A Theoretical and Experimental Study

Eno Hysi[1], Ratan K Saha[1], Michael C Kolios[1]; [1]Physics, Ryerson University, Toronto, Ontario, Canada

Background, Motivation and Objective

Photoacoustic (PA) imaging combines the molecular specificity of optical imaging and the resolution of ultrasound to probe tissue optical and thermoelastic properties. We hypothesize that PA techniques can differentiate between aggregated and non-aggregated red blood cells (RBCs). The aggregation phenomenon alters the spatial organization of cells forming variable sized rouleaux that changes blood rheology which promotes vascular disorders such as atherosclerosis. Thus, non-invasive detection of RBC aggregation has clinical significance. The objective of this study is to present both theoretical and experimental results showing how PA methods can detect and characterize RBC aggregation.

Statement of Contribution/Methods

2D blood tissue realizations simulating non-aggregating RBCs were generated by employing a Monte Carlo method. Aggregated blood samples were simulated using a hexagonal packing scheme. The PA signals from such samples were computed by employing a frequency domain fluid sphere model for a delta function incident laser pulse. Signal properties such as the envelope statistics and frequency depended power spectra were investigated by varying the hematocrit and aggregate size. *In-vitro* experiments with human RBCs samples were conducted using the Imagio PA imaging system (Seno Medical Instruments Inc., San Antonio, TX) at two laser irradiation wavelengths, 750 and 1064nm. The PA signals from non-aggregated RBCs were collected at varying hematocrits. Aggregation of RBCs was induced with a fibrinogen mimicking macromolecule, Dextran-70. In order to achieve different aggregation levels, Dextran-Phosphate Buffered Saline (wt/vol) concentrations of 1, 3 and 8% were mixed with non-aggregated RBCs.

Results

Theoretical results showed a monotonic increase in PA signal amplitude with increasing hematocrit for non-aggregating RBC. For aggregating samples, the PA signal amplitude and the spectral intensity in the low frequency regime increased as the mean aggregate size increased (e.g. 11 dB at 15.6 MHz for 10.13 µm aggregates). Preliminary experimental results confirmed the monotonic increase in PA signal amplitude for non-aggregating RBCs with increasing hematocrit. Spectral analysis of RBC samples with varying degrees of aggregation exhibited ~10 dB enhancement at 4 MHz for the most aggregated sample compared to the non-aggregated RBCs.

Discussion and Conclusions

Our theoretical results showed a large increase in spectral intensity of the PA signals, specifically 11 dB for the largest aggregate size compared to the non-aggregated sample near 15 MHz. The experimental results also showed an increase ~10 dB at 4 MHz, validating the trends predicted by the theory although on the lower frequency range. This study demonstrates the feasibility of PA methods for the clinical detection and assessment of RBC aggregation.

3F-6

3:15 PM Real-time Handheld Optical Resolution Photoacoustic Microscopy

Parsin Hajireza[1], Wei Shi[1], Roger Zemp[1]; [1]Electrical & Computer Engineering, University of Alberta, Edmonton, Alberta, Canada

Background, Motivation and Objective

Optical resolution photoacoustic microscopy (OR-PAM) is an imaging technology providing high optically defined lateral spatial resolution to visualize superficial structures in vivo with optical-absorption contrast. OR-PAM is able to quantify morphological parameters and functional parameters down to capillary size (~7µm). Such parameters include microvascular density, total hemoglobin concentration, hemoglobin oxygen saturation, etc, important for studying the earliest stages of tumor angiogenesis. Besides preclinical research applications, OR-PAM could have clinical potential if it could be developed into a portable, real-time imaging technology. Previous systems, however, require long imaging times due to low-repetition-rate lasers and mechanical scanning. They are also typically tabletop systems requiring bulky and expensive laser systems, and providing little flexibility for imaging various anatomical locations. In order to overcome this limitation, we have introduced a unique high repetition rate, inexpensive, compact fiber laser sources for realizing high frame rate photoacoustic imaging.

Statement of Contribution/Methods

In order to extend the potential range of applications to clinical settings, for the first time, we demonstrate a handheld real-time optical resolution photoacoustic microscope (HH-OR-PAM). Using fast scanning mirrors, an image guide with 30,000 fiber pixels, a customized doublet lens and a special probe we managed to reduce the footprint of an OR-PAM system from a stationary table-top system to a portable, 3x5x6cm, probe weighing ~ 500g.

Results

The capability of HH-OR-PAM is demonstrated with phantoms and in vivo (microvasculature in a Swiss Webster mouse ear) studies based on a customized tunable fiber laser with repetition rates of nanosecond-pulses up to 600kHz, enabling near real-time C-scan imaging. Phantom studies indicate 7 µm transverse resolution.

Discussion and Conclusions

The proposed setup keeps many of the powerful properties of previous top-table OR-PAM systems but adds high flexibility due to the nature of the image guide and handheld apparatus. Therefore, the setup may widely improve the usability of OR-PAM from lab experiments to real world clinical applications.

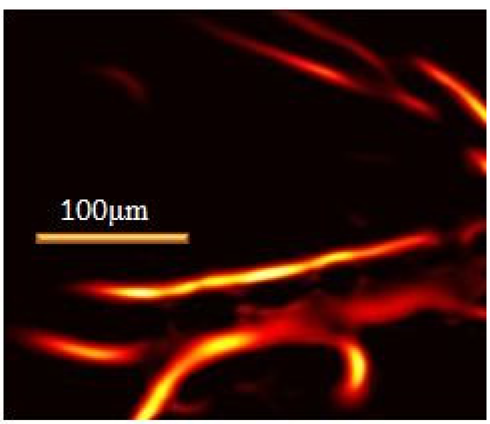

4F Novel Acoustic Wave Sensors

Carribean Ballroom I

Thursday, October 20, 2011, 2:00 pm - 3:30 pm

Chair: **Mauricio Pereia Da Cunha**
University of Maine

4F-1

2:00 PM Recent developments of the thin film electro-acoustic technology in view of biosensor applications

Ilia Katardjiev[1], Ventsislav Yantchev[1]; [1]Solid State Electronics, Uppsala University, Uppsala, Uppland, Sweden

Background, Motivation and Objective

Quartz Crystal Microbalance (QCM) is a popular acoustic transducer for biosensing applications. Recognition takes place on the surface of the QCM resulting in mass and/or viscous loading which in turn results in a shift of the resonant frequency according to the Sauerbrey and Kanazawa-Gordon relationships respectively.

QCM resonators operate in the range 5 to 15 Mhz. The Sauerbrey equation indicates that the mass sensitivity in air is an exponential function of frequency. The losses, however, would increase linearly with frequency which indicates that operating at higher frequencies could provide substantial benefits in terms of resolution, size, cost, multiplexing, integration with the electronics, portability, etc. Similar benefits for biosensors would still apply although gain in resolution would be somewhat mitigated due to the weaker dependence of sensitivity on frequency in addition to increased viscous losses. The frequency of operation can only be increased by decreasing the physical dimensions of the device which, employing existing technologies, would result in a substantial increase in fabrication cost.

Similar cost and performance issues were encountered by the telecom industry at the turn of the century and were eventually resolved by the development of the so called thin film electro-acoustic (TEA) technology. This article analyses recent developments in the TEA technology in view of high frequency acoustic transducers for biosensing applications as well as summarizes the most significant results with emphasis on performance and level of maturity.

Statement of Contribution/Methods

Performance is primarily judged by resolution and sensitivity (in aqueous solutions) which in our specific case refer to both mass and viscosity. Most studies, however, seldom make it to this stage and rightly focus initial attention on the performance of the transducer. In this case and for comparative reasons performance is judged by an overall figure of merit defined as the product kt2xQ, where Q is the Q-factor of the transducer. Nevertheless, an acoustic biosensor is a complex electro-biochemical system and one should always keep in mind other equally important factors such as manufacturability, cost, inherent to the transducer design deficiencies leading to increased parasitic losses in the final system, etc.

Results

The analysis concludes that the thickness excited quasi-shear FBAR technology is long ahead in its development with regard to other alternative approaches in terms of both performance and level of maturity. Consequently, the main aspects of the quasi-shear FBAR technology from film synthesis and fabrication through to performance evaluation and demonstration are reviewed in sufficient detail.

Discussion and Conclusions

The use of the TEA technology leads to transducer miniaturisation, compatibility with the IC technology, possibility for multiplexing, decrease in fabrication cost, reduction of consumables, mass fabrication, etc.

4F-2

2:30 PM An Equivalent Circuit Model for a Liquid Loaded Lateral Field Excited Acoustic Wave Sensor

Lester French[1,2], Michael FitzGerald[3], John Vetelino[1,4]; [1]Laboratory for Surface Science and Technology, University of Maine, Orono, ME, USA, [2]Mainely Sensors, LLC, Orono, ME, USA, [3]Department of Physics & Astronomy, University of Maine, Orono, ME, USA, [4]Department of Electrical & Computer Engineering, University of Maine, Orono, ME, USA

Background, Motivation and Objective

The lateral field excited (LFE) acoustic wave sensor element [1] has been shown to be more sensitive to mass, viscous, and electrical loading than the quartz crystal microbalance [2]. Much of this advantage is due to the bare sensing surface of the LFE sensor element, which has its exciting electrodes on the crystal face that is not exposed to the analyte. Research has demonstrated that the LFE sensor element can effectively detect E coli. O157:H7, phosmet, and saxitoxin [2]. Despite these results, no equivalent circuit exists to model the LFE sensor element under simultaneous mechanical and electrical loading by a liquid. The objective of this work is to present an equivalent circuit model of the LFE sensor element loaded with a Newtonian liquid. The circuit model will predict the sensor response near resonance to mechanical and electrical property changes in the liquid or sensing film due to mechanical and electrical perturbations.

Statement of Contribution/Methods

The LFE sensor is examined by solving the coupled wave equations in the multi-layered LFE sensor structure resulting in an expression for the admittance of the LFE sensor element. The effects of liquid perturbations to the admittance of the LFE sensor element are modeled as discrete circuit elements in an equivalent circuit. The model is verified independently by measuring the sensor response of LFE sensors with a variety of electrode gap separations, (0.5, 1.0, and 2.0 mm), to changes in liquid viscosity, permittivity, and conductivity.

Results

The equivalent circuit model developed results in an accurate, within ±5%, admittance near the resonant frequency for LFE sensors in deionized water. The model predicts the frequency shift of the LFE sensor to perturbations in the density, viscosity, permittivity, and conductivity of the contacting liquid. For example, the predicted frequency shift is within ±5 ppm for viscous loading and ±50 ppm for dielectric loading when compared to measured frequency shifts.

Discussion and Conclusions

The equivalent circuit model for LFE sensors developed in this work is an accurate model for LFE sensors under liquid loading. This equivalent circuit model is the first to model an LFE sensor under liquid loads with lumped elements that relate to the piezoelectric crystal and the material properties of the contacting liquid. The strength of the model is the accurate prediction of the admittance of the LFE sensor under liquid loads with changing density, viscosity, permittivity, and conductivity.

[1] J.F. Vetelino, "Lateral Field Excited Acoustic Wave Sensor," U.S. Patent 7 075 216, 11 July 2006.

[2] D.F. McCann, L.A. French Jr., M.S. Wark, and J.F. Vetelino, “Recent advances in lateral field excited and monolithic spiral coil acoustic transduction bulk acoustic wave sensor platforms,” Meas. Sci. Technol. vol. 20, pp. 124001-124012, Dec. 2009 and references therein.

4F-3

2:45 PM Lateral field excited bulk acoustic wave sensors on Langasite working on different operational modes

Tingfeng Ma[1], Chao Zhang[2], Zhitian Zhang[2], Wenyan Wang[2], Guanping Feng[2]; [1]Tsinghua University, Beijing, China, People's Republic of, [2]Research Institute of Tsinghua University in Shenzhen, China, People's Republic of

Background, Motivation and Objective

It has been shown that bulk acoustic wave devices based on lateral field excitation (LFE) are superior in sensing liquid electrical property changes. Previous research found three operational modes of LFE devices and confirmed that pure-LFE mode and pseudo-LFE mode are suitable for bulk acoustic wave sensors. Recent calculation results showed that (yxl)65° Langasite LFE devices work on pure-LFE mode and (yxl)0° Langasite LFE devices work on pseudo-LFE mode. In this work, sensitivities of Langasite LFE devices working on both modes are investigated and compared.

Statement of Contribution/Methods

In this work, Several 5 MHz Langasite pure-LFE devices and Langasite pseudo-LFE devices were designed and fabricated with the same structure. Two electrodes are semi-circled and separated by a gap of 1 mm. There is no electrode on the sensing surface of the devices in contract with analytes. A crystal sensor holder was used for installing a LFE device and forming a liquid sensing cell. NaCl water solutions and 2-propanol water solutions were used to test the devices′ sensitivities to liquid conductivity and permittivity changes respectively. The devices′ responses were measured using the PLO-10 phase-locked oscillator and a frequency counter.

Results

It was shown that the Langasite pseudo-LFE device is almost 6 times more sensitive to liquid conductivity changes than the Langasite pure-LFE device, which is shown in Fig.1. To liquid permittivity changes, the sensitivity of the Langasite pseudo-LFE device is about 4 times higher than that of the Langasite pure-LFE device.

Discussion and Conclusions

It has been found that Langasite pseudo-LFE devices have superior sensitivities to liquid electrical property changes compared to Langasite pure-LFE devices. The main cause of this phenomenon will be discussed in the full paper. It is suggested that for liquid electrical property measurement, the Langasite pseudo-LFE sensor is a better choice compared to the Langasite pure-LFE sensor.

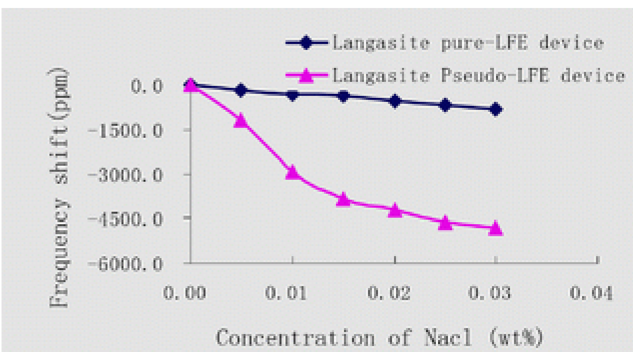

Fig. 1. Frequency shift of two kinds of LFE devices as a function of NaCl concentration in water

4F-4

3:00 PM Development of Acoustic-Wedge-Mode Humidity Sensor Using a Wedge with Hydroscopic Film

Che-Hua Yang[1], **Po-Hsien Tung**[1]; [1]National Taipei Univ of Technology, Manufacturing Technology, Taipei, Not applicable, Taiwan

Background, Motivation and Objective

Acoustic sensor is widely used in the physical, chemical and biological detection. The principle of acoustic sensor is based on mass loading effect influencing the velocity of wave propagating on the sensor surface. Wedge waves are guided acoustic waves propagating along the tip of a wedge. Advantages of wedge-wave-sensor include large motion amplitude at the tip and sensitivity enhancement form the wedge geometry. This research aims at the development of a humidity sensor based on wedge waves with a layer of hydroscopic film.

Statement of Contribution/Methods

In this research, specimen is a 40 degree aluminum wedge with one of its surfaces coated with a layer of hydroscopic film. The wedge sample is placed in a chamber for humidity control with relative humidities of 45%, 65% and 80%. A laser ultrasound technique is employed to measure dispersion spectra of wedge waves propagating in the wedge samples.

Results

Fig. 1 shows dispersion spectra of the fundamental mode of wedge waves with a layer of hydroscopic coating under different humidity. It is found out that wedge wave velocity decreases as the environmental humidity increases. With repeated experiments, this measurement is found out to have good repeatability.

Discussion and Conclusions

Wedge waves travel through hydroscopic coating is sensitive to environmental humidity. The wedge with hydroscopic coating can be a new candidate for humidity sensor and possibly biomedical sensors as well.

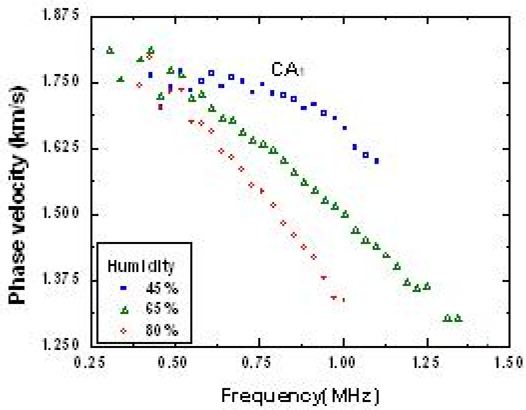

4F-5

3:15 PM A SH-APM Liquid Viscosity Sensor Based on PZT-5H

Zhijun Chen[1], Qianliang Xia[1], Xu Lu[1], Tao Chen[1]; [1]*College of Automation Engineering, Nanjing University of Aeronautics and Astronautics, China, People's Republic of*

Background, Motivation and Objective

Viscosity is one of the characteristic parameters of liquid. The measurement of liquid viscosity is required in many applications. Compared with SAW (surface acoustic wave) device, the APM (acoustic plate mode wave) device has two interfaces. When one interface is deposited with IDTs as acoustic excitation, the other interface can be loaded with liquid sample. Furthermore, when the APM has only SH (shear-horizontal) particle displacement normal to the propagation direction and parallel to the plate surface, the attenuation because of the liquid sample is very small. So the SH-APM device is applicable for liquid viscosity sensing.

Statement of Contribution/Methods

The theoretical model of SH-APM device loaded with viscous liquid is built using the propagation characteristics of acoustic wave in laminated mediums. The liquid viscosity is introduced by adding the imaginary part in liquid elastic tensor. The works are as follows:

(1). The excitation characteristics of SH-APM are investigated, including excitation modes, propagation velocity, excitation efficiency, and vibration displacement, etc.

(2). The influences of liquid viscosity on propagation velocity and attenuation of SH-APM are numerically analyzed.

(3). The changes of SH-APM sensitivity to liquid viscosity with the ratio of the plate thickness to the acoustic wavelength are numerically analyzed.

(4). The optimization design of the SH-APM device is implemented.

Results

(1). Using PZT-5H piezoelectric ceramic as substrate material, the SH-APM device is fabricated. The encapsulation and photo of the SH-APM device are shown in Fig. 1.

(2). Using different ratios of pure water and glycerol as the liquid samples, the experimental results are in agreement with the theoretical analyses.

Discussion and Conclusions

By numerical calculation and experimental analyses, the validity of liquid viscosity sensing by SH-APM device is proved. When the device is used as liquid sensing, not more than one milliliter liquid samples are needed, satisfying the requirement of minim liquid measurement. The measurement process is steady and has good repeatability, without liquid leak. The superiority of the piezoelectric ceramic material used as SH-APM liquid viscosity sensing is testified.

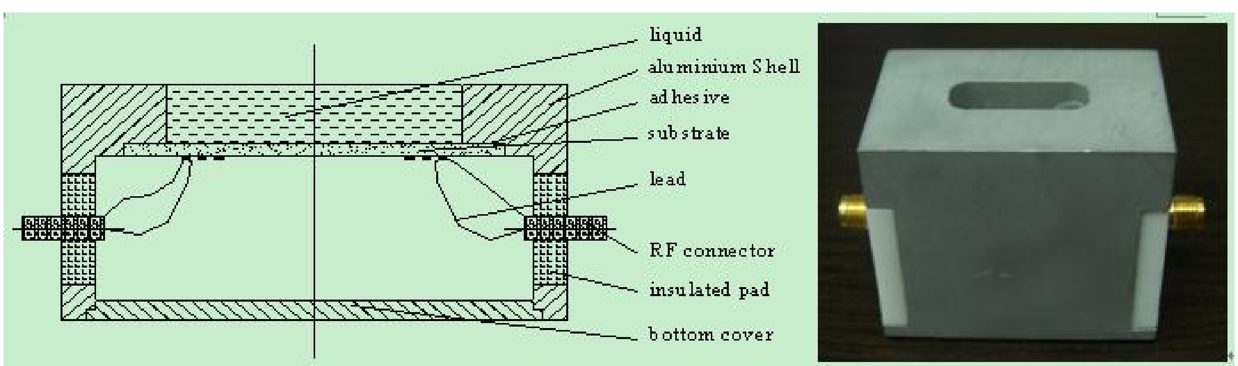

Fig. 1 The encapsulation and photo of the SH-APM device

5F - Ultrasonic Motors and Actuators I

Carribean Ballroom II

Thursday, October 20, 2011, 2:00 pm - 3:30 pm

Chair: **Minotu Kurosawa**
Tokyo Institute of Technology

5F-1

2:00 PM Experimental study on high efficiency ultrasonic motors using lubricant

Wei Qiu[1], Yosuke Mizuno[1], Daisuke Koyama[1], Kentaro Nakamura[1]; [1]Precision and Intelligence Laboratory, Tokyo Institute of Technology, Yokohama, Japan

Background, Motivation and Objective

Application fields of ultrasonic motors have been limited due to their low efficiency and short life. Meanwhile, we have found that employing lubricants is an effective way to solve these problems. The feature of lubricants under vibratory preload makes the motor operation close to ideal one to reduce friction loss. In this paper, we investigated in detail the combination of friction materials for rotor and stator, and the characteristics of lubricants using a hybrid transducer type ultrasonic motor. With the good selection of the materials, we succeeded in obtaining high maximum efficiency of over 80% stably.

Statement of Contribution/Methods

The hybrid transducer type ultrasonic motor used in this experiment consisted of two 4-mm-thick torsional PZTs and six 1-mm-thick longitudinal PZTs (Fig. 1a). The effects of lubricants and friction materials were tested using three kinds of oils with two different viscosities and four kinds of ceramics for the contacting surfaces. The load characteristics and the motor efficiency were investigated being based on transient-response measurements with changing the preload applied to the rotor.

Results

The motor efficiency was significantly improved by lubrication at high preloads (Fig. 1b). The contact surfaces were well protected with lubricants so that the motor operation was stable even under high preloads. The combination of alumina for stator and silicone nitride for rotor was the best match of all the friction materials we tested. The maximum efficiency as high as 85% was achieved when high traction fluid of 32 cSt viscosity was used under 100-MPa preload (Fig. 1b).

Discussion and Conclusions

A high efficiency ultrasonic motor was successfully developed by using appropriate lubricant and friction materials. Lubricants and friction materials are both important to improve the efficiency and achieve stable operation. The effects of different lubricants under the same preload will also be discussed in detail as functions of static and dynamic preloads. These results shall lead to a breakthrough for extending the usage of ultrasonic motors.

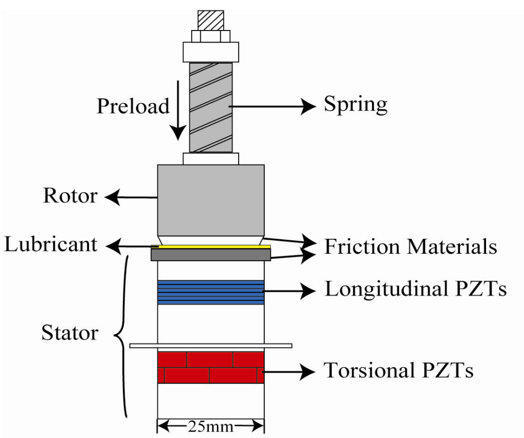

Fig. 1a Schematic configuration of ultrasonic motor using lubricant

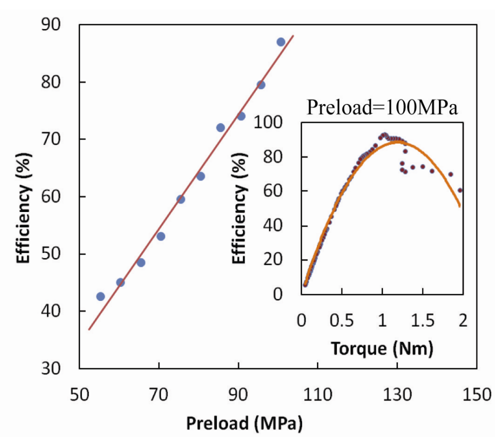

Fig. 1b Motor efficiency as a function of preload. The inset shows the load characteristics of the motor

5F-2

2:15 PM Design and Evaluation of Ultrasonic Motor Located in Cryogenic Temperature Environments

Daisuke Yamaguchi[1], Takefumi Kanda[1], Koichi Suzumori[1]; [1]Graduate School of Natural Science and Technology, Okayama University, Okayama, Okayama, Japan

Background, Motivation and Objective

A cryogenic temperature condition is an important measuring environment for scientific research area. However, previous actuators located in the cryogenic condition had limited application. The purpose of this study is fabrication and evaluation of the cryogenic ultrasonic motor located in the cryogenic environment.

Statement of Contribution/Methods

A bolt-clamped Langevin-type transducer (BLT) for cryogenic temperature has been designed and evaluated. The diameter and height are 6mm and 16mm. The influence of thermal stress to the BLT was estimated by using finite element method analysis with some non-linear characteristics of material at cryogenic temperature. The cryogenic ultrasonic motor using the BLT was fabricated and evaluated. The maximum diameter and height of the motor are 20mm and 30.5mm. The motor was driven in cryogenic helium gas.

Results

In the result of analysis, the thermal stress of the BLT applied the piezoelectric material when the temperature was followed from room temperature to cryogenic temperature. In the result of experiment of the transducer, the pre-load was influenced by thermal stress. In the result of driving experiment, we have succeeded in rotating the motor at cryogenic temperature. The rotation speed was 65.5rpm at 4.5K when the driving frequency and applied voltage were 82.5kHz and 150Vp-p.

Discussion and Conclusions

In the thermal influence, the comparison between the simulation result and experiment result shows a good corresponding value at cryogenic temperature. The design approach of the BLT for cryogenic temperature is confirmed. The motor had higher rotation speed than previous studies.

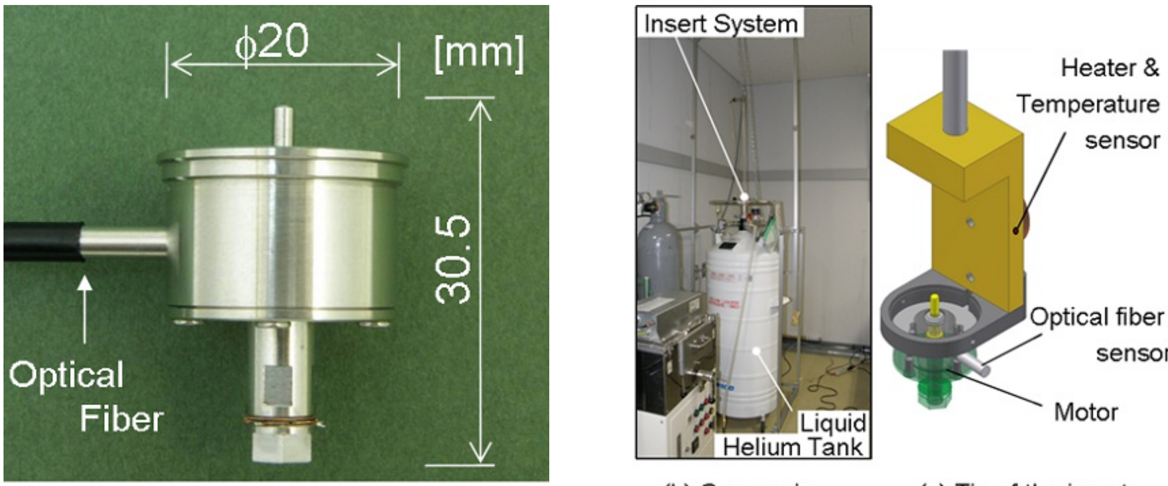

(a) Cryogenic Ultrasonic Motor (b) Cryogenic evaluation system (c) Tip of the insert system

5F-3

2:30 PM Actuation Force Characteristics of Non-contact Ultrasonic Suspension for Minute Objects

Shota CHINO[1], Yasuhiro KATO[1], Masaya TAKASAKI[1], Takeshi MIZUNO[1]; [1]*Saitama Univ, Japan*

Background, Motivation and Objective

Recently, a vacuum gripper equipped on a robotic arm is used for handling small object like electric components. Today, demand of miniaturization of the components is growing with miniaturization of various products. As a result, conventional handling techniques have some problems, such as lacking of positioning accuracy, electrostatic adhesive force preventing release of objects, and so on. They have also possibilities of components damage because of contact with the gripper and dust due to the contact. They should be serious problem for semiconductor substrates or silicon wafers. It is preferable to handle these components by non-contact technique. Previously, we proposed non-contact handling using ultrasonic vibration. This phenomenon is called ultrasonic suspension. A planar object can be suspended vertically downward by non-contact with a gap of tens micrometers from vibrating surface. This handling technique has some merits such as non-contact, independent from material, low cost, easy to release and acting horizontal restoring force.

Statement of Contribution/Methods

In previous research, acting force on the object has been measured during the ultrasonic suspension. Particularly, we observed relationship between acting force and the gap. To measure the acting force, the object was fixed on the tip of cantilever and the force was estimated from deflection of the lever caused by ultrasonic suspension. However this method had problem of leaning of the object according to the deflection. In this research, servo type measuring mechanism was proposed. The mechanism employed VCMs (Voice Coil Motor) as an actuator and PID control on the gap. The acting force could be estimated from input current of actuators because the acting force and output force of the actuator are balanced. Using this mechanism, both horizontal restoring force and vertical suspension force could be measured. Because of servo type, the object can be kept in constant position. The leaning problem can be solved.

Results

Using the proposed measuring mechanism, the vertical suspension force and the horizontal restoring force could be measured simultaneously with the change of gap and relative position of the object. It can be seen that the vertical force changes from repulsive to attractive in near field of vibrating surface, has local maximum value and decrease with increasing gap. It is also observed that the horizontal force has local maximum value, then decreasing. In addition, horizontal force is axially symmetry.

Discussion and Conclusions

Applying PID control to measurement of acting forces in ultrasonic suspension, the circular plate object could be kept in parallel to the vibrating surface and in its original position. Using the mechanism, both the vertical suspension force and the horizontal restoring force could be measured simultaneously. Also, their positional relationship between the object and the vibrating surface could be obtained.

5F-4

2:45 PM The NeuroGlide Actuator: A Multi-Degree-of-Freedom Ultrasonic Micromotor for Neural Microcatheter Navigation

Cheol-ho Yun[1], Leslie Yeo[2], **James Friend[2]**; [1]*MicroNanophysics Research Laboratory, Monash University, Clayton, Victoria, Australia,* [2]*Mechanical Engineering, Monash University, Clayton, VIC, Australia*

Background, Motivation and Objective

The minimally invasive treatment of disease and injury is attractive to the patient for reducing the trauma of surgery and postoperative recovery time, to the doctor for its flexibility, and to society due to its reduced cost. Unfortunately, the lack of microactuators—devices that duplicate typical tasks of the surgeon's hands all while at the end of a catheter and at a scale commensurate with the requirements of confinement in the body—limits the advancement of this field.

Statement of Contribution/Methods

A novel 240-micrometer diameter ultrasonic micromotor, using vibration mode coupling with piezoelectric excitation and with the ability to rotate its end about an arbitrary axis, is presented as a potential solution for an especially difficult task in neurosurgery: navigating a catheter to an injury in the neurovasculature. The technique used here is a substantial improvement in using a tilted structure to reduce the necessary number of electrode wires to only two. Given that space is at a premium, such an improvement is essential to the practical application of these motors for neurosurgical applications.

Results

The peak no-load angular velocity and maximum torque were 600~rad/s and 1.6~nN-m, respectively, and we obtained rotation about all three axes with these performance capabilities. By using a burst drive scheme, open-loop position and speed control sufficient for the neurosurgery application were obtained.

Discussion and Conclusions

The construction method and control scheme proposed in this study removes most of the current limitations in minimally invasive, catheter-based actuation, enabling minimally invasive vascular surgery (MIVS) concepts to be pursued for a broad variety of applications.

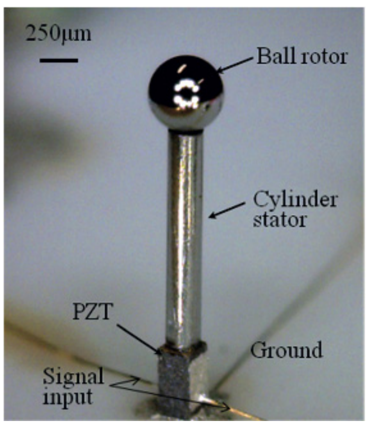

5F-5

3:00 PM Ultrasonic Motors - Past, Present and Future

Jörg Wallaschek[1]: [1]Institute of Dynamics and Vibration Research (IDS), Leibniz University Hannover, Hannover, Germany

Background, Motivation and Objective

Ultrasonic motors are characterized by high force or torque at low velocities or rotational speed, respectively. Most of these motors are based on a two-stage energy conversion. In a first step, electrical energy is transformed into high frequency mechanical vibrations by piezoelectric elements. In the second step friction processes in the interface between the vibrating element and a second body generate the driving force of the motor. A huge number of different designs of ultrasonic motors has been developed over the past decades, but there still is a huge potential for future developments.

It is the aim of the present contribution to give a survey on the field of piezoelectric ultrasonic motors, including a brief desription of their historical development and an outline of current research trends and future perspectives of this interesting drive technology.

Statement of Contribution/Methods

The different types of ultrasonic motors are classified according to their geometry and vibration modes. For each class the most important advantages and disadvantages will be discussed, and finally a comparison of typical motor characteristics of the different designs will be given.

Mechanical models for the different motor types will be presented and the identification of motor parameters based on theoretical and experimental methods will be discussed. Practical considerations, like e.g. the proper choice of materials, control topologies and degradation of motor performance over service life will also be adressed.

Results

Theoretical performance limits of piezoelectric ultrasonic motors will be presented and compared to practically achieved motor performances. The most important motor types are presented and compared based on the demands in various practical applications.

Discussion and Conclusions

Piezoelectric ultrasonic motors have achieved exceptional performances. Many prototypes have been presented and characterized experimentally. Despite this very advanced state of the art, practical applications of piezoelectric ultrasonic motors are still limited to some niche applications. Further research is requred to exploit their full potential.

THURSDAY ORAL

6F - BAW Components and Technology (5B)

Carribean Ballroom VI

Thursday, October 20, 2011, 2:00 pm - 3:30 pm

Chair: **Dave Feld**
Avago Technologies

6F-1

2:00 PM A Feedback-Loop Oscillator stabilized using laterally-coupled-mode narrow-band HBAR filters

Eric Lebrasseur[1], Gilles Martin[1], Dorian Gachon[2], Thomas Baron[1], Alexandre Reinhardt[3], Pierre-Patrick Lassagne[3], Luc Chommeloux[4], Sylvain Ballandras[1]; [1]*Time & Frequency Dept, Femto-st, CNRS, Besancon, France,* [2]*LEAUS, Université de Perpignan, France,* [3]*LCRF, CEA-LETI, France,* [4]*SENSeOR, France*

Background, Motivation and Objective

Radio-Frequency (RF) oscillators are stabilized by various resonating devices. Their stability is conditioned by the spectral quality of the resonator even if the oscillator loop electronics must be optimized to lower the generated noise at best. We have shown the possibility to build temperature compensated High overtone Bulk Acoustic Resonators (HBARs) combining LiNbO3 and Quartz single crystal plates and to develop laterally-coupled narrow-band filters using such structures. Feed-back loop oscillators then are developed on this base as it notably simplifies the fabrication issues for devices operating above 1 GHz.

Statement of Contribution/Methods

In this work, we investigate the use of laterally coupled filters based on thinned single crystal LiNbO3 layers bonded on AT-Quartz substrates for the stabilization of feedback-loop oscillators operating near 1 GHz and above. The resonator exploits dispersion properties as well as the presence of a thick resonating structure (i.e. the substrate) to enhance the lateral coupling between two resonators placed very close one another to favor their modal interaction. (YXl)/163° LiNbO3 cut has been chosen for the excitation of pure shear wave high overtones, taking advantage of its strong electromechanical coupling (about 45%). The AT Quartz substrate is particularly suited for temperature compensation purpose.

Results

Quality factors of about 10 000 are obtained at 1.7 GHz, yielding QF products largely sufficient for the fabrication of oscillators (Fig.1). As a shear mode is exploited here, temperature compensation is obtained, yielding favorable conditions for using the device to stabilize an oscillator loop. The four-port structure is easily looped using a wide band amplifier and the corresponding phase noise is found at –130 dB at 10 kHz from the carrier.

Discussion and Conclusions

This approach allows for a better control of the resonance conditions than dipole-based circuit, as the phase can be efficiently controlled within the loop. Work is engaged to address higher frequency operations.

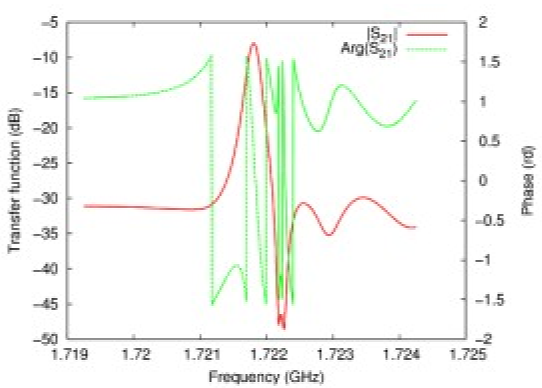

6F-2

2:15 PM A 48 MHz, Small, Hermetic, Chip-Scale Packaged USB3.0 Oscillator Integrating an FBAR Resonator with CMOS Circuitry

Andrew Nelson[1], **Rich Ruby**[2], Martha Small[2], Steve Ortiz[2], Brian Otis[1]; [1]*University of Washington, USA,* [2]*avago technologies, USA*

Background, Motivation and Objective

Most ASIC (Application Specific Integrated Circuits) chips have one common need -- clocking. The clock is usually supplied by the end-user of the ASIC chip and consists of a quartz crystal resonator, two precision capacitors and an on-chip inverter driver. The ASIC supplier that can integrate the clock inside their package will have a product differentiator relative to their competitors.

Statement of Contribution/Methods

We demonstrate a zero drift FBAR Resonator (ZDR) with a native Q of ~3000 and a temperature stability of +/- 50 ppm integrated with a CMOS oscillator core, oscillator buffer, dividers and output buffer). The 0.4 um node CMOS circuitry is integrated in the silicon lid of the microcap'd device. Since many thousands of packaged die are created on each wafer, one can take significant amount of statistics on the effect of frequency shift due to environmental stress tests (HAST, Autoclave, Thermal shock, etc...). This allows us to identify aging specs as well as the most likely forms of device failures in the field.

Results

Phase noise at the divided down frequency (49 MHz) is shown in Figure 1. Jitter was measured to be 120 fsec for the divided output. The far from carrier phase noise was -160 dBc/Hz for both RF and divided down frequencies. The phase noise at 1 KHz offset was -108 dBc/Hz after the divide by 16 frequency (48 MHz). Supply pushing of the frequency over a 2.8 to 5V supply range was < 50ppm. The oscillator with integrated buffer amplifier, divider circuit and output buffer burned 6.9 mW.

Discussion and Conclusions

We present a working USB3.0 oscillator using an all-silicon package. The dimensions are approximately 0.6mm X 0.5 mm by 0.16 mm and use four pads (Vdd, Gnd, Enable and Vosc) with the target of being placed next to or on top of the customers' packaged ASIC chip. Usable frequencies are 24, 48 or 96 MHz with a guaranteed accuracy is +/- 300 ppm or better, uses less than 6.9 MW power when on and <3 uW when disabled. The phase noise is -156 dBc/Hz @ 100 KHz and the output is a square wave driving a 1 pF||10K Ohm load. We believe this is one of the smallest oscillators ever built.

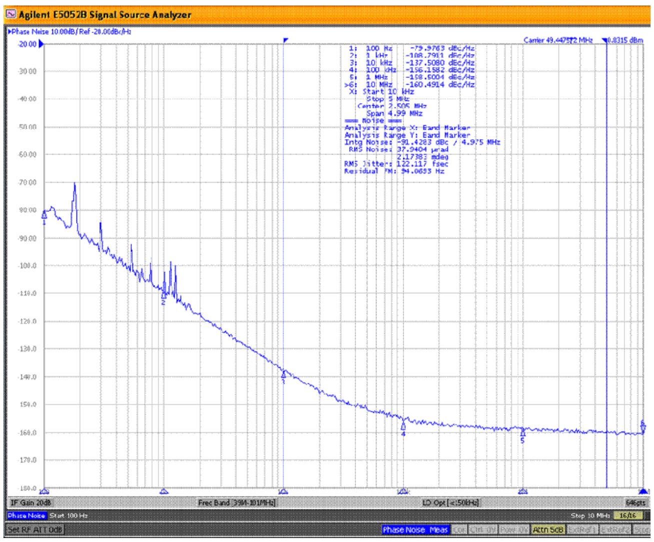

THURSDAY ORAL

6F-3

2:30 PM c-axis parallel oriented AlN film resonator fabricated by ion-beam assisted RF magnetron sputtering

Masashi Suzuki[1], Takahiko Yanagitani[1]; [1]*Graduate School of Engineering, Nagoya Institute of Technology, Nagoya, Aichi, Japan*

Background, Motivation and Objective

An wurzite film such as ZnO and AlN tends to grow normal to the substrate. In ZnO films, we previously found that c-axis parallel orientation is induced by ion-beam irradiation during deposition. In this study, we investigated the orientation control of AlN films deposited by using ion-beam assisted RF magnetron sputtering.

Statement of Contribution/Methods

The modification of preferential orientation was induced by irradiating 3 kV accelerated nitrogen ion beam from ECR ion source. Ion beam was irradiated 20º with respect to the substrate during RF magnetron sputter deposition. Crystalline orientation of the film was determined by XRD analysis. Next, c-axis parallel AlN film SMR with asymmetric Bragg reflector consisting of W/SiO_2 was fabricated, and k_{15} value and TCF value were measured.

Results

(0002) X-ray pole figure (Fig. 1) and XRD patterns show that c-axis of the film is parallel to substrate and the direction of c-axis corresponded to the ion beam direction. The FWHM value of φ and ψ were found to be 9.8º and 6.3º, respectively. c-axis parallel AlN SMR excited only pure shear mode without thickness extensional mode. Fig. 2 shows temperature dependence of the resonant frequency of the resonator. TCF of -30.2 ppm/ºC found in AlN film SMR was higher than that of -20.3 ppm/ºC measured in AlN single crystal plate resonator. k_{15} of the resonator is determined to be 0.057 from frequencies of series and parallel resonance. This value is 70 % of that in the AlN single crystal.

Discussion and Conclusions

c-axis unidirectional in-plane orientation in the sample was confirmed by X-ray pole figure. Pure shear mode was excited in c-axis parallel AlN SMR. k_{15} of the resonator was determined to be 0.057, and TCF was found to be -30.2 ppm/ºC.

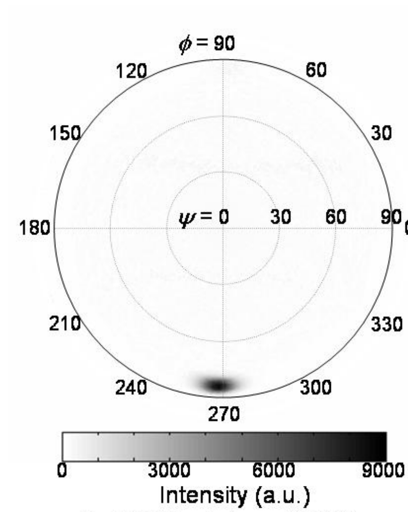

Fig. 1 (0002) pole figure of AlN film

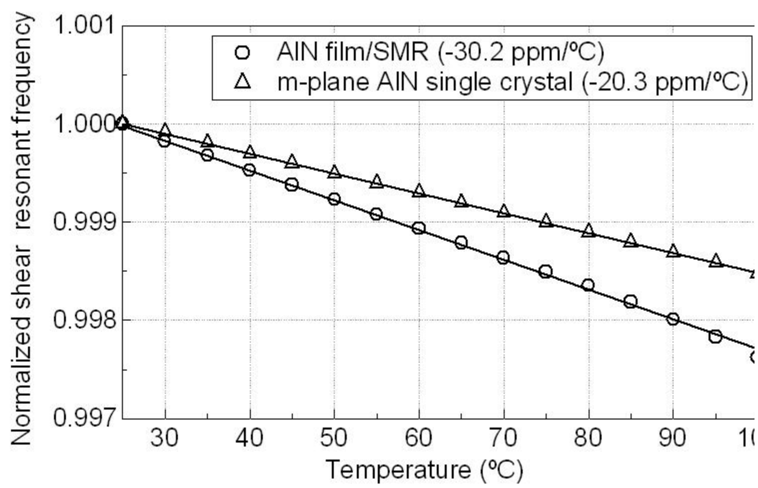

Fig.2 Temperature dependence of the shear resonant frequency of the resonato

6F-4

2:45 PM Experimental investigation of dual wave optimized reflector stacks in solidly mounted bulk acoustic wave resonators

Sumy Jose[1], Ray Hueting[1]; [1]*Semiconductor Components, University of Twente, Netherlands*

Background, Motivation and Objective

Optimizing the reflector stacks for both longitudinal and shear waves is critical in the design of SMRs for high *Quality factor (Q)* filters [1-4]. We recently experimentally verified stop-band theory design approach for SiO_2/Ta_2O_5 reflector stacks [2]. In this work, we experimentally investigate two other design approaches, i.e. novel optimization scheme and Diffraction Grating Method (DGM), applied to a W/SiO_2 reflector stack. The results indicate that these approaches are applicable for any reflector stack combination.

Statement of Contribution/Methods

Various W/SiO_2 stacks were fabricated: one stack using DGM and four others using the novel scheme [2]. In the novel scheme calculations, best reflector and device performance (highest Q) is expected when $1< c <2$ [2]. The oxide in the final reflector layer (below the bottom electrode) was increased until type 1 dispersion was achieved, for the direct implementation of the border region [3-5]. A series of SMRs with varied areas were fabricated to extract the 1D Q_A at anti-resonance [2, 6-7].

Results

Fig. 1 shows $1/Q_A$ vs. perimeter/area for the fabricated novel scheme designed stacks. The extracted 1D Q_A shows the expected trend except for c=1 (the quarter-wave (QW) like stacks). 2D FEM simulations [8] (Fig. 2) reveal that the QW stack with increased top-oxide shows improved shear reflection. Further, the DGM stack showed the highest experimental $Q_A$of 1700.

Discussion and Conclusions

Our design approaches have been experimentally verified. Optimum performance was expected for c=1.5 from the 1D model, however for c=1, QW like stacks with increased top-oxide, showed a higher extracted 1D Q_A. This is due to the coupling between the shear and longitudinal waves in the oxide found from FEM simulations. With DGM stacks the highest experimental Q_A was obtained.

[1]S. Jose et al., Proc. IEEE Ultrasonics Symposium, September, 2009.pp.2111-2114.

[2]S. Jose et al., IEEE Trans. on Ultrasonics Ferroelectric and Frequency Control, Vol.57, No.12, Dec.2010.

THURSDAY ORAL

[3]G.G.Fattinger et al., Proc. IEEE Ultrasonics Symposium, pp.1175-1178, 2005.
[4]S. Marksteiner et al., US patent: 006933807B2.
[5]R. Thalhammer et al., Proc. IEEE Ultrasonics Symposium, pp.456-459, 2006.
[6]J. W. Lobeek, et al., Proc. IEEE Microwave Symposium, pp.2047-2050, 2007.
[7]R. Strijbos et al., Proc. IEEE Electronic components and technology conference, pp.169-174, 2007.
[8]www.comsol.com

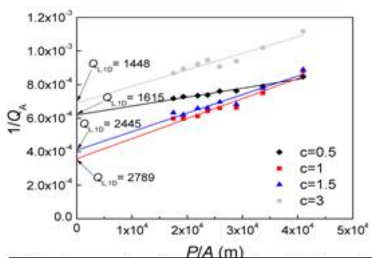

Stack	c=0.5	c=1	c=1.5	c=3
Tlong(dB)	-32	-37.1	-35.2	-26.1
Tshear(dB)	-27.4	-9.76	-22.7	-23.8

Fig. 1. Scaling of Q_A for the fabricated resonators with different novel scheme designed reflector stacks for f_R=1.95GHz. The area was ranging from 100µm² to 550 µm². The extrapolated value at the vertical axis gives us $1/Q_A = 1/Q_{L,1D}$ of the active device. Except for c=1 the extracted 1D Q_A values are in-line with the simulated transmission values from the scheme shown in the table below.

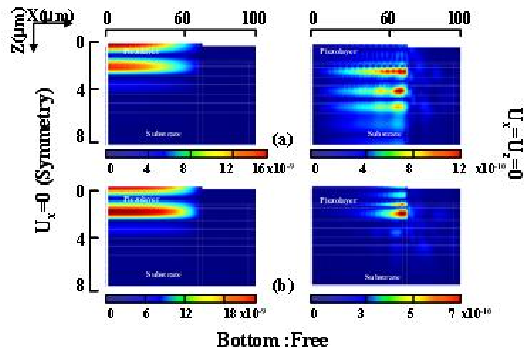

Fig. 2. 2D FEM results for displacement of longitudinal waves (left) and shear waves (right) at resonant frequency in an SMR with five layer W/SiO_2 reflector stack using a QW stack (a) without and (b) with increased top-oxide. Plane of symmetry is defined in the left edge of the device.

6F-5

3:00 PM Synthesis of highly textured w-AlN thin films with a tilted c-axis having good tilt and thickness uniformity

Milena Moreira[1], Johan Bjurstrom[1], Tomas Kubart[1], **Ilia Katardjiev[1]**; [1]Solid State Electronics, Uppsala University, Uppsala, Uppland, Sweden

Background, Motivation and Objective

There is a substantial interest in efficiently exciting acoustic modes in thin film electro-acoustic devices (typically resonators) which exhibit sufficiently low losses in contact with liquids, most notably for biosensor applications. Examples of such modes are the thickness shear or quasi-shear modes, the A1 Lamb mode, etc. So far, the best results in terms of both electro-mechanical coupling and Q-value have been obtained with the quasi-shear mode excited in c-tilted AlN and ZnO thin films. The deposition processes of these films, however, are not quite suitable for industrial fabrication due to tilt non-uniformity in the first instance and very low deposition rate in the second instance. It is the objective of this work to develop a process for the synthesis of highly textured c-tilted thin piezoelectric w-AlN thin films with good tilt and thickness uniformity.

Statement of Contribution/Methods

The method employed here is very similar to the one described by Bjurström et al1, i.e. a two-step process in which a suitable seed layer is grown first followed by a second step in which the directionality of the deposition flux is essential. In this work, the latter is achieved by designing a multi-segmented magnetron sputter source as illustrated in Fig. 1. It is seen that the segments are tilted relative to the substrate normal thus resulting in a uni-directional deposition flux. Thickness uniformity of the deposited film is achieved by translating the substrate over the magnetron source.

Results

The process described above yields highly textured, c-tilted AlN thin films with good tilt and thickness uniformity (Fig. 2).

Discussion and Conclusions

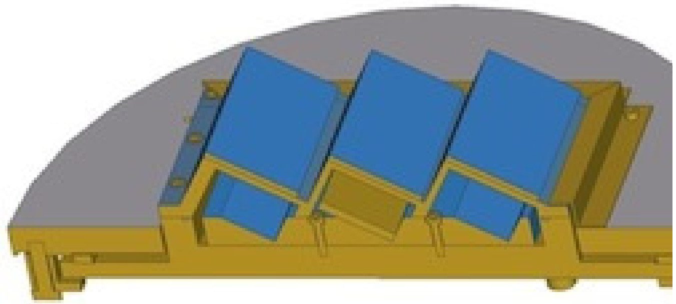

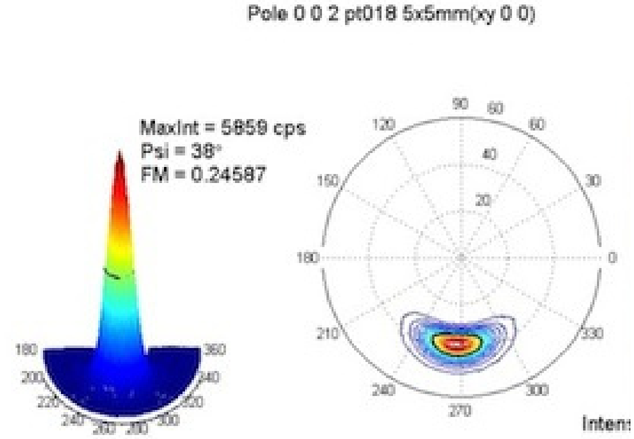

6F-6

3:15 PM Evaluation of Acoustical Properties for AlN Single Crystal by the Ultrasonic Microspectroscopy Technology

Yuji Ohashi[1], Jun-ichi Kushibiki[1], Boris M. Epelbaum[2], Albrecht Winnacker[2], Shunro Nagata[3]; [1]Tohoku University, Japan, [2]University of Erlangen-Nuremberg, Germany, [3]JFE Mineral Company Ltd., Japan

Background, Motivation and Objective

AlN is one of promising materials for ultraviolet optoelectronic devices as well as piezoelectric devices operating at high frequency range. Accurate acoustical physical constants and homogeneous crystals are necessary to develop new ultrasonic devices. We have determined the acoustical physical constants using only two substrates of Y- and Z-cut AlN by the ultrasonic microspectroscopy (UMS) technology [1]. In this paper, we prepared a rotated Y-cut AlN single crystal specimen addition to Y- and Z-cut ones, evaluated basic acoustical properties by the UMS technology, and determined more accurate constants.

Statement of Contribution/Methods

We prepared 67.61°Y-cut AlN single crystal substrate (24×16×2.593 mm^3, amber colored, partially colorless and dark amber) grown on 6H-SiC by physical vapor transport method. For this specimen, we measured leaky surface acoustic wave (LSAW) velocity at 225 MHz using the micro-line-focus-beam ultrasonic-material-characterization (MLFB-UMC) system and longitudinal velocity at 50-450 MHz and shear velocity at 40-200 MHz using the plane-wave (PW) UMC system.

Results

We observed relatively large variations in LSAW velocities at dark amber area of the specimen while there were no differences in those between the amber colored and the colorless areas. Measured LSAW velocities were higher than the calculated ones using the previous constants [1] by 2.1 m/s for X-propagation and by 4.8 m/s for 90°X-propagation. The measured bulk wave velocities were higher than the calculated ones [1] by 7.3 m/s for longitudinal velocity and by 22.7 m/s for shear velocity although there were no velocity dispersions.

Discussion and Conclusions

It is considered that one of the origins of the color difference (amber and colorless) is impurities (mainly oxygen and carbon), but those impurities did not affect to the LSAW velocity. At the dark amber area exhibiting large velocity change, however, it was suggested that the crystal growth orientation was perturbed from the results of the angular dependences of the LSAW velocity. We determined elastic and piezoelectric constants using the above results for 67.61°Y-cut specimen addition to the results of Y- and Z-cut specimens in [1]. Four constants newly determined here were $c^E_{13}=1.011\times10^{11}$ [N/m^2], $c^E_{33}=3.749\times10^{11}$ [N/m^2], $e_{31}=-0.54$ [C/m^2], and $e_{33}=1.66$ [C/m^2]. These values differed from the previous ones by 5.0%, 1.8%, 358%, and -9.8%, respectively. We can obtained more accurate constants using longitudinal and shear velocities for around 60° rotated Y-cut specimen which is particularly sensitive to c^E_{13} and e_{31}.

[1] Y. Ohashi et al., Appl. Phys. Express, Vol. 1 (2008) 077004.

1G - Blood Flow Imaging

Boca Rooms II-IV

Thursday, October 20, 2011, 4:30 pm - 6:00 pm

Chair: **Hans Torp**
Norwegian Univ. of Science & Technology

THURSDAY ORAL

1G-1

4:30 PM Secondary arterial blood flow patterns with vector flow ultrasound

Mads Møller Pedersen[1,2], Michael Johannes Pihl[2], Jens Munk Hansen[2], Peter Møller Hansen[1,2], Per Haugaard[3], Michael Bachmann Nielsen[1], Jørgen Arendt Jensen[2]; [1]*Department of Radiology, Copenhagen University Hospital, Rigshospitalet, Copenhagen, Denmark,* [2]*Department of Electrical Engineering, Technical University of Denmark, Kgs. Lyngby, Denmark,* [3]*R&D Applications & Technologies, BK Medical, Herlev, Denmark*

Background, Motivation and Objective

Previous studies have indicated that rotational flow patterns may play a role in the pathogenesis of atherosclerosis. However, no conventional methods have been able to quantify and visualise these patterns. Rotational blood flow patterns in the transverse plane of the systemic arteries can now be measured with a commercial vector flow ultrasound scanner. A 2D vector field is obtained over time and in the diastole of each cardiac cycle a rotational, secondary blood flow pattern emerges. This study presents the first method that quantifies the rotational frequencies of *in-vivo* secondary blood flow patterns with vector flow ultrasound.

Statement of Contribution/Methods

Vector flow measurements of 10 seconds were obtained from three abdominal aortae, common carotid arteries, and common iliac arteries. The first commercial scanner (ProFocus Ultraview, BK Medical, Denmark) with the vector technique Transverse Oscillation was used with a linear, Multi Frequency Imaging transducer at 5 MHz (8670, BK Medical). The 2D vector fields were obtained over time and the flow patterns were visualised with streamlines using Matlab (Mathworks, USA). For every frame the sum of the angular frequencies were calculated in subareas as ω [rad/s]. The rotational frequency, f, was calculated as $\omega/2\pi$ [Hz] and the subarea with the strongest rotation in each diastolic frame was found. Finally, the mean diastolic rotational frequency and its standard deviation, STD, was calculated for every measurement. A negative f indicates a clockwise rotation, whereas a positive indicates a counterclockwise rotation.

Results

A secondary, blood flow pattern in the abdominal aorta, including the rotational frequencies are shown in the figure. The mean rotational frequency and its STD was calculated for each of the nine measurements from the abdominal aortae {-1.3(0.4); -1.0(0.3); -0.9(0.2)}Hz, the common carotid arteries {-0.4(0.1); -1.0(0.2); -0.4(0.1)}Hz, and the common iliac arteries {0.8(0.3); 1.4(0.3); 0.4(0.1)}Hz.

Discussion and Conclusions

The rotational direction is the same in each vessel type but differs from artery to artery. The identical direction for each vessel and the low STDs indicate that the measurements are reproducible and precise. In conclusion, secondary flow patterns can be visualised with streamlines, and quantified by the angular frequency.

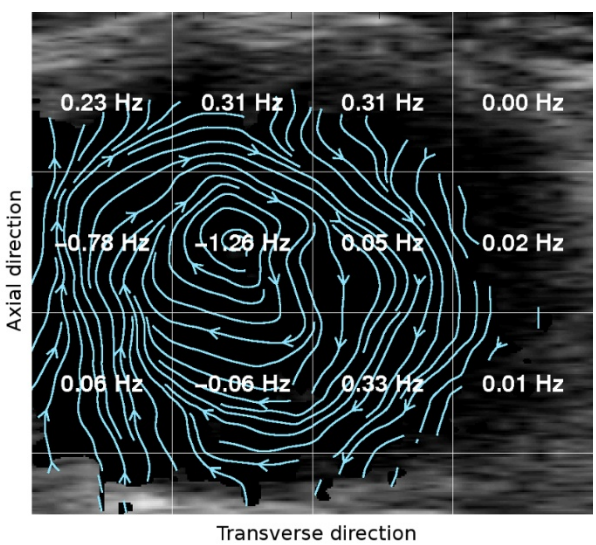

1G-2

4:45 PM Angle-independent quantification of complex flow patterns in congenital heart disease

Lasse Lovstakken[1,2], Siri Ann Nyrnes[1,2], Bjorn Olav Haugen[1,2], Hans Torp[1]; [1]*NTNU, Norway,* [2]*Trondheim University Hospital, Norway*

Background, Motivation and Objective

There is emerging interest in quantifying the relationship between left ventricular flow patterns and left ventricular function. Complex in vivo flow patterns have previously been studied using MR phase-contrast imaging and contrast enhanced ultrasound (echo-PIV). Neither of these approaches are however well suited in pediatric cardiology. In this work we describe an angle-independent flow imaging technique based on speckle tracking without contrast that may quantify complex flow patterns associated with congenital heart disease.

Statement of Contribution/Methods

A custom real-time color flow imaging acquisition was setup based on plane wave (unfocused) emission with 16 parallel receive beams using linear array transducers on a GE Vivid E9 ultrasound system. This allowed for near instantaneous images of flow velocities at high frame rates with dense lateral sampling. In vivo data was acquired from 10 newborns with complex congenital heart disease. IQ-data was stored for offline evaluation of speckle tracking in terms of its accuracy for different interpolation methods, tracking algorithms, and regularization.

Results

Highly complex 2-D flow patterns in congenital heart disease could be quantified and superimposed on traditional color flow images without imposing acquisition trade-offs in terms of the Doppler setup. Similar tracking accuracy could be achieved as for CFI (axial velocities) using IQ data interpolation and envelope tracking (SAD), without imposing substantial computation times (< 30 sec. non-optimized). In the example figures, 2-D flow patterns is visualized as streamlines for jet and vortex flow due to a ventricular septal defect (left), and the abnormal filling of a dilated and hypertrophic heart (right).

Discussion and Conclusions

The presented flow imaging technique may be well suited for imaging and follow up in children. Reasonable tracking accuracy was obtained, however, more smoothing is currently required to obtain similar accuracy as CFI. Further work will focus on improved regularization techniques, as well as a compounded imaging approach to limit clutter filtering influence for near-transversal flow.

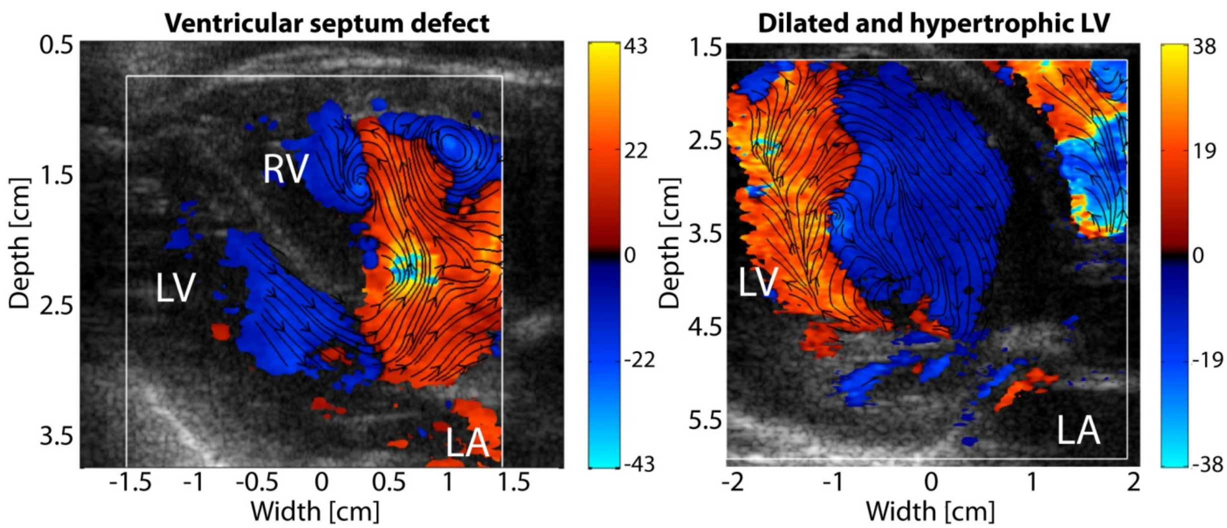

1G-3

5:00 PM Doppler vortography: a new technique for quantification of intracardiac vorticity

Stéphan Muth[1], **Damien Garcia[1]**; [1]CRCHUM - Research Centre, University of Montreal Hospital, Montreal, QC, Canada

Background, Motivation and Objective

A vortex is a fluid pattern that has a rapid swirling motion around its center. The natural swirling flow that occurs in the normal left ventricle (LV) during LV filling is optimized in terms of fluid energy dissipation. In vivo findings revealed the formation of additional counter-rotating vortices in the presence of cardiac disease. Such unnatural vortices may significantly impair the LV function due to important kinetic dissipation. One ultrasound technique has generally been used to quantify the vortices in the LV: optical flow carried out on B-mode frames (echo-PIV). Echo-PIV requires continuous intravenous injection of contrast agents. Due to the unstable property of bubble aggregates in the LV, a complex fine-tuning of the contrast infusion before image acquisition is required. This seriously limits the application of LV echo-PIV in clinical practice. The method that we propose for quantification of intracardiac vorticity (*Doppler vortography*) is based on conventional Doppler images only, which makes this technique clinically-compliant.

Statement of Contribution/Methods

Doppler vortography relies on the centrosymmetric properties of the vortices. Such properties induce specific symmetries in the Doppler flow which can be exploited to describe the vortices quantitatively. For this purpose, a kernel filter was developed to derive a parameter, the *blood vortex signature* (BVS), that reflects the intracardiac vorticity. The reliability of BVS measured by Doppler vortography was first assessed by means of mock Doppler vortical fields. Doppler vortography was also tested in healthy subjects and patients using raw Doppler data acquired with a Vivid (GE) ultrasound scanner (apical 3-chamber view).

Results

The simulation results demonstrated that BVS calculated by Doppler vortography is a highly reliable index of blood flow vorticity (Fig 1). The diastolic BVS measured in the echographic laboratory, at the end of the LV early filling, revealed the presence of counter-rotating vortices in patients with cardiac disease (Fig 2) which may significantly alter the LV relaxation function.

Discussion and Conclusions

Doppler vortography is a promising echographic tool for quantification of vortex flow in the left ventricle. Our findings suggest that Doppler vortography potentially has relevant clinical interest for the quantification of LV diastolic function.

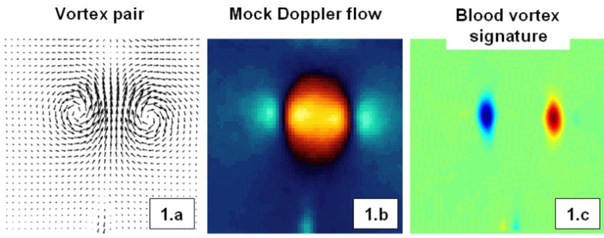

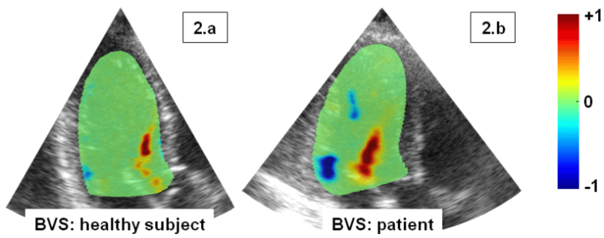

1G-4

5:15 PM Directional synthetic aperture flow imaging using a dual stage beamformer approach

Ye Li[1], Jørgen Arendt Jensen[1]; [1]Center for Fast Ultrasound Imaging, Dept. of Elec. Eng., Bldg. 349, Technical University of Denmark, Lyngby, Denmark

Background, Motivation and Objective

Current ultrasound imaging systems can only measure the flow velocity component along the ultrasound beam. Directional synthetic aperture imaging can solve the problem as the data available from all the channels make it possible to beamform a line in any direction. However, the high demands on processing capabilities makes it very difficult to implement. A dual stage beamformer is proposed to reduce the system complexity and still maintain a beamforming quality sufficient for flow estimation.

Statement of Contribution/Methods

In the first stage, a set of B-mode lines with a single focal point in both transmit and receive are obtained. In the second stage, the output from the first stage is beamformed along the flow direction and focused dynamically. The velocities are found by cross-correlating two pulse echo signals from the same transmission sequence. The method is investigated using both simulations and experimental measurements. A 192-element, 7 MHz linear array transducer with λ pitch is used. The transmission sequence consists of four emissions with 7λ spacing in between and an f_{prf} of 4 KHz. Therefore, only four B-mode lines are processed to achieve the directional image lines in the second stage beamformer. A flow circulation system is used for generating a parabolic laminar flow profile with peak velocity of 0.1 m/s. The signals are transmitted and received by SARUS (Synthetic Aperture Real-time Ultrasound system). The received signals are processed and beamformed afterwards.

Results

In the simulation, the parabolic profile is estimated with a relative standard deviation of [3.9% 3.1%] and a relative bias of [0.6% 0.4%] at flow angles of [70 45] degrees. In the experimental measurement, a relative standard deviation of 7.2% and a relative bias of 4.9% can be obtained for an angle of 70 degrees. Furthermore, varying the number of emission sets used for one estimation from 1 to 12 yields standard deviations ranging from 13.3% to 5.1%. A color flow image for the beam-to-flow angle of 70 degrees is shown in the figure.

Discussion and Conclusions

The performance of the new approach indicates that the two stage beamformer can produce directional synthetic aperture flow images with a low standard deviation. A fixed delay beamformer is needed in the 1st stage and the 2nd stage beamformer has the complexity of a general dynamic receive focusing beamformer.

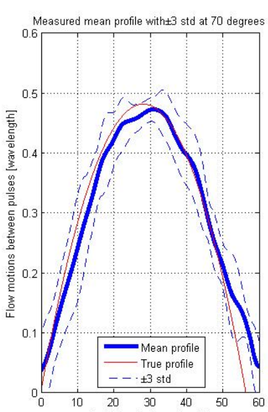

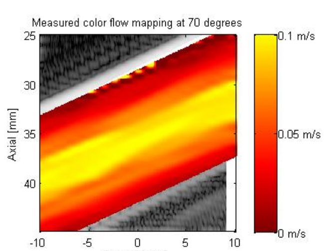

1G-5

5:30 PM Functional micro-ultrasound imaging of rodent cerebral hemodynamics

Martijn van Raaij[1], Liis Lindvere[1], Adrienne Dorr[1], Jianfei He[1], Bhupinder Sahota[1], Bojana Stefanovic[1], F. Stuart Foster[1]; [1]*Imaging Research, Sunnybrook Health Sciences Centre, Toronto, Ontario, Canada*

Background, Motivation and Objective

Quantitative mapping of the brain microvascular hemodynamics is important for understanding brain function in health and disease. High-frequency ultrasound imaging has the spatial resolution, temporal resolution and penetration depth required to image changes in cerebral blood volume (CBV) throughout the rodent cerebrum.

Statement of Contribution/Methods

We have developed a new high-frequency ultrasound imaging technique that enables functional imaging of the hemodynamics of the rat cerebral microvasculature at a spatial resolution of ~100 µm in-plane and 600 µm through-plane and a temporal resolution of 40 ms.

Adult male Sprague-Dawley rats were prepared with a 6 by 4 mm cranial window over the primary somatosensory cortex (S1FL). Ultrasound contrast agent was infused and a near-sagittal plane of view (7 x 10 mm) was imaged using a commercial micro-ultrasound system with a 20 MHz transducer in a nonlinear-contrast imaging mode. In this imaging mode, signal intensity is linearly related to the concentration of contrast agent in each voxel and thus to the local blood volume. The forelimb contralateral to the cranial window was electrically stimulated for either 2 or 10 second intervals while the resulting changes in CBV were recorded.

Results

We obtained detailed maps of vessel topography (panel A, cortical surface at top, anterior to the right). Electrical stimulation of the contralateral forelimb reproducibly induced a hemodynamic response in S1FL with up to 22.7 % change in local CBV in the cortex and 9.8 % in the deep gray region (panel B, color is ΔCBV in %; white lines are manually segmented anatomical regions of interest). A general linear model analysis revealed the presence of regions ranging in size from 100 µm to 2 mm of stimulus-correlated increases as well as decreases in local blood volume. We also detect and quantify differences in the temporal evolution of the blood volume response in deep gray versus cortical regions of the rat brain.

Discussion and Conclusions

The significantly lower cost and higher spatial and temporal resolution of functional micro-ultrasound (fMUS) imaging compared to typical single-slice preclinical fMRI and the much deeper penetration depth compared to two-photon fluorescence microscopy should allow fMUS to become a valuable tool in the study of cerebral hemodynamics.

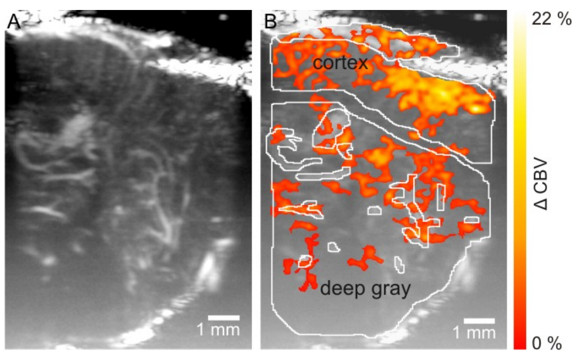

1G-6

5:45 PM Ultrasensitive functional ultrasound imaging of the brain

Emilie Mace[1], Gabriel Montaldo[1], Ivan Cohen[2], Michel Baulac[2], Mathias Fink[1], Mickael Tanter[1]; [1]Institut Langevin, ESPCI ParisTech, CNRS UMR7587, Inserm U979, Paris, France, [2]Institut du Cerveau et de la Moelle épinière, Inserm UMRS 975, CNRS UMR7225, CHU Pitié Salpêtrière, Paris, France

Background, Motivation and Objective

Functional imaging techniques such as fMRI are based on detecting the hemodynamic response to neuronal activity. Interestingly, Doppler ultrasound has never been applied to map brain activation even invasively because its poor sensitivity limited for now its use to major vessels. We aimed at developing the first functional ultrasound imaging technique based on an ultrasensitive Power Doppler sequence to follow hemodynamic changes in cerebral microvascularization and at applying it on rats for imaging task-evoked brain activation.

Statement of Contribution/Methods

Functional ultrasound imaging consisted in repeating over time the acquisition of ultrasensitive Power Doppler images (one every 3s) (a). A Power Doppler image was reconstructed from 200 compound images acquired at 1 kHz, each being computed from 17 tilted plane wave emissions. The gain in sensitivity (x 47) was achieved by the combination of the high number of temporal samples and the high SNR of compound images for estimating the mean Doppler intensity for each pixel. For experimental validation, the functional ultrasound sequence was performed using a 15 MHz linear probe controlled by an ultrafast scanner. Adult rats were anesthetized with isoflurane. The head was placed in a stereotaxic frame and a large cranial window was drilled to expose the somatosensory cortex. Whiskers were excited mechanically at a frequency of 12 Hz. The stimulation pattern consisted in 32 s on / 64 s off repeated 10 times.

Results

A 10 to 20 % increase of mean Doppler intensity was observed during stimulation in the contralateral barrel cortex (b). A map of brain activation was computed by calculating the cross-correlation coefficient between the stimulus pattern and the Power Doppler signal for each pixel. It showed a significant correlation ($r^2>0.6$) in the barrel cortex and the thalamus when all whiskers were excited (c). Moreover, the activation of an individual cortical column was also detected when stimulating a single whisker (d).

Discussion and Conclusions

Ultrasensitive functional ultrasound imaging (ufUS) successfully mapped a task-evoked hemodynamic response on the rat brain with sufficient sensitivity to detect single cortical column activation. Such a mode implemented on an ultrasound scanner paves the way for many applications in neuroscience research but also in clinics during neurosurgery or non invasively on newborns.

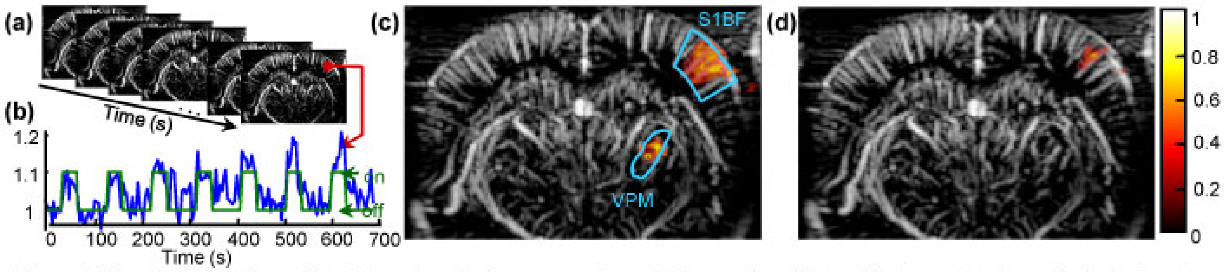

Figure. (a) Acquisition of ultrasensitive Power Doppler images over time. (b) Temporal evolution of the Power Doppler value in the barrel cortex (blue) during the stimulation pattern (green). Correlation map superimposed on a Power Doppler image (c) when stimulating all whiskers (blue lines delineate the barrel cortex S1BF and the thalamus nucleus VPM) (d) when stimulating a single whisker

THURSDAY ORAL

2G - Shear Wave Elastography

Boca Rooms VI-VII

Thursday, October 20, 2011, 4:30 pm - 6:00 pm

Chair: **James Greenleaf**
Mayo Clinic

THURSDAY ORAL

2G-1

4:30 PM Improving Shear Wave Speed Estimation Precision in Homogeneous Media by Tracking Shear Wave Propagation in 3D using a Real-time Volumetric Imaging Transducer

Michael Wang[1], Brett Byram[1], Mark Palmeri[1], Ned Rouze[1], Kathryn Nightingale[1]; [1]*Biomedical Engineering, Duke University, USA*

Background, Motivation and Objective

Tissue displacement due to acoustic radiation force impulse (ARFI) excitation can only be monitored in one slice of the anatomy using conventional 1D array ultrasound transducers. As a result, shear wave propagation data in only one direction is available for stiffness estimation. With the recent availability of matrix array ultrasound transducers, acquisition of displacement fields within a volume of tissue in real-time is now possible. The ability to track shear wave propagation in multiple directions allows anisotropic mechanical properties to be estimated, as well as the ability to measure ARFI response over a larger volume. We present a system capable of tracking ARFI induced shear wave propagation in 3D, and show that by monitoring shear wave propagation in multiple directions, the precision of shear wave speed (SWS) estimation in a homogeneous material can be improved.

Statement of Contribution/Methods

An annular focused HIFU piston transducer (H-101, Sonic Concepts, Bothell, WA) is used for ARFI excitation (1.1 MHz, f/1, 60 mm focal depth). A 2D matrix array transducer (4Z1C on an SC2000 scanner, Siemens Healthcare, Ultrasound Business Unit, Mountain View, CA, USA) inserted in the central opening of the HIFU piston was used for monitoring ARFI displacement. Shear waves were induced in a homogeneous phantom (E=4.5 kPa) using a 1000 cycle push pulse with $I_{sppa.7}$ = 1417 W/cm^2. Displacement tracking was performed at a frequency of 2.5 MHz using a 10×12 (lateral × elevation) rectangular grid of receive beams. The spatial extent of this tracking region was 16.5×20 mm at the push focal depth. The push axis was located at one corner of the tracking region. 30:1 parallel receive was used to enable a volume rate of 2 kHz. The effect of tracking beam locations on the precision of time-of-flight (TOF) SWS estimation was investigated using synthetic shear wave arrival time data corrupted by Gaussian noise.

Results

For the very first time, shear wave propagation away from the push within the lateral-elevation plane is observed. It can be shown (and verified by simulation) that by using radially symmetric beam locations about the excitation, the root mean square (RMS) error of TOF SWS estimation in a homogeneous medium can be reduced by a factor of $R=\sqrt{((N+1)(N-N_\theta)/((N-1)(N+N_\theta))}$, where N is the total number of beam locations, and N_θ the number of directions tracked. For N=64 (the number of parallel receive beams available on the SC2000), the greatest reduction in RMS error in this approach is R=0.6, and is obtained when N_θ=32 (i.e., 2 beams per direction at the edges of the reconstruction kernel).

Discussion and Conclusions

Tracking ARFI induced shear wave propagation in 3D is now possible using a matrix array volumetric imaging transducer. By tracking shear wave propagation in multiple directions, the RMS error of TOF SWS estimation in homogeneous media can be reduced.

2G-2

4:45 PM Shear wave construction with laterally moving radiation force excitations

Matthew Urban[1], Carolina Amador[1], Alireza Nabavizadeh[1], James Greenleaf[1], Shigao Chen[1]; [1]Department of Physiology and Biomedical Engineering, Mayo Clinic College of Medicine, Rochester, MN, USA

Background, Motivation and Objective

Shear wave-based elasticity methods which quantify shear wave speed, V, are becoming clinically relevant as many pathological conditions change values of V in soft tissue. Reliable measurements require shear waves with high signal-to-noise ratio that propagate far enough to measure V. Push tonebursts must have long duration and/or high intensity, but ultrasound exposure regulations limit deposited energy so trade-offs must be made to find new solutions for creating shear waves for clinically reliable measurements.

Statement of Contribution/Methods

We present a method called shear wave construction (SWC) that uses multiple, short tonebursts, transmitted at different times and locations to augment a propagating shear wave. To optimally sustain a propagating shear wave tonebursts must be transmitted at the time-of-arrival (TOA) of the shear wave at different lateral locations. To do this optimally V must be known, but typically is not. We studied SWC using either two or three short pushes of length 100 µs, which resulted in one wave front that is reinforced and in the other direction, multiple wave fronts are created (Fig. 1). We performed simulations with the intensity field used as the force input to a Green's function analysis to analyze the shear wave displacement and also varied the time of the pulses away from the optimal TOA. We performed experiments using a linear array in three elastic phantoms where V values were known. We designed optimal pulse sequences for the phantoms and compared SWC displacement and V results with results from a single push with lengths of 100, 200, or 300 µs. Displacement was measured over a 2 cm lateral extent with plane wave imaging performed at 3.2 kHz. Lastly, we used SWC in an excised porcine kidney to evaluate feasibility in soft tissue.

Results

The displacement generated in the simulations agreed well with the experimental results (Fig. 1). The percent error for V ranged from 3.1-7.1% in the phantoms. The SWC peak displacement through time at each location with two pushes of 100 µs was larger than that generated using a 100 or 200 µs (Fig. 1(c)).

Discussion and Conclusions

The SWC method provided accurate measurements of V in elastic phantoms. This method uses short tonebursts which are less taxing on the scanner power supply, allow for higher detection frame rates without interference from pushing pulses, and have higher displacement bandwidth.

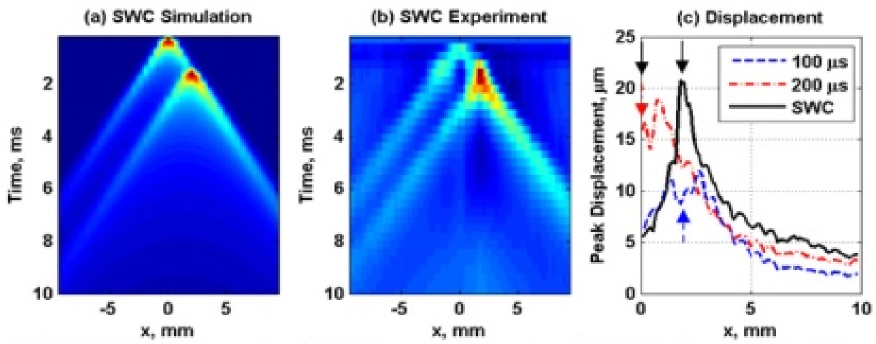

Fig. 1. (a) SWC simulation results, (b) SWC experiment results, (c) Peak displacement for different excitations. Arrows depict location of excitation.

2G-3

5:00 PM Robust Shear Wave Speed Measurement Using Comb-push Ultrasound Radiation Force

Heng Zhao[1], Pengfei Song[1], Matthew W. Urban[1], James F. Greenleaf[1], Shigao Chen[1]; [1]Physiology and Biomedical Engineering, Mayo Clinic College of Medicine, Rochester, Minnesota, USA

Background, Motivation and Objective

Measurement of shear wave propagation speed c_s in tissues has clinical significance of indicating tissue stiffness and health state. Spatially Modulated Ultrasound Radiation Force (SMURF) imaging generates a shear wave of known wavelength in the tested material and measures the temporal frequency of the shear wave to determine c_s (Ultrasonic Imaging 29, 87-104). Detection in SMURF is relatively simple (only requiring A-lines repeated at one location) but beamforming for pushing is rather complicated. In this study we propose a new approach for push beamforming for SMURF.

Statement of Contribution/Methods

A Verasonics ultrasound system with a L7-4 linear array was used to study two homogenous elasticity phantoms with different c_s calibrated by 1D Transient Elastography (TE). The first 84 elements of the L7-4 were divided into 7 groups of 12 elements each. Groups 2, 4, 6 were turned off and groups 1, 3, 5, 7 transmitted simultaneously for 600 is at a frequency of 5 MHz. This produced 4 unfocused push beams like a 4-tooth comb as shown in Fig. (a), which generated shear waves with a prescribed wavelength of 7.4 mm. Shear wave motion was monitored in the region of interest (ROI) next to the comb using plane wave “flash” imaging at 2 kHz, and 1D autocorrelation was used for motion tracking. The center frequency of the slow time signal at each location within the ROI was computed using FFT, and c_s was calculated by multiplying the center frequency with the wavelength.

Results

Figure (b) shows the slow-time axial velocity observed from one location. Figures (c) and (d) are the 2D images of measured c_s in both phantoms which are very stable throughout the entire 25 ×12 mm ROI. Results averaged over the ROI (1.22 ± 0.05 and 1.47 ± 0.06 m/s) are close to results obtained with TE (1.23 ± 0.02 and 1.48 ± 0.03 m/s).

Discussion and Conclusions

This study shows that comb push beams can be used to produce shear waves with prescribed wavelength for SMURF imaging. Shear wave speed measured by this method is stable over a relatively large area. Therefore, traditional ultrasound scanners can obtain reliable c_s measurements over a relatively long axial range using A-lines from only one lateral position. Comb beams with different spatial features can be easily implemented for flexible applications.

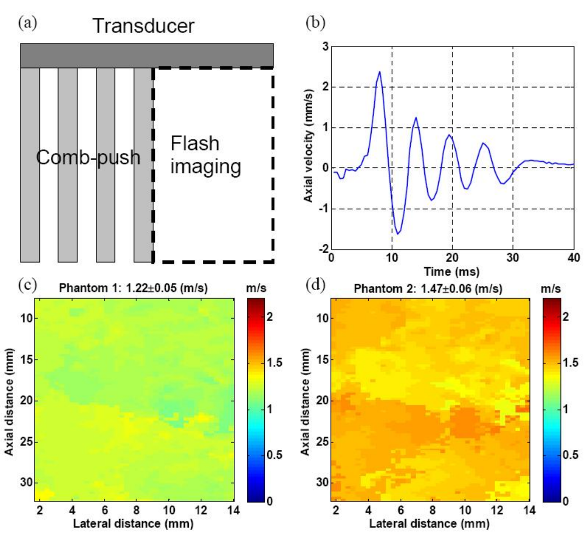

2G-4

5:15 PM Tracking ARFI Induced Shear Wave Propagation by Using Maximum Likelihood Estimation

Liexiang Fan[1], Bob Luick[1], David Duncan[1], Janelle O'Bannon[1], John Benson[1]; [1]*Ultrasound Business Unit, Siemens Healthcare, Issaquah, WA, USA*

Background, Motivation and Objective

Shear wave propagation speed in tissue provides valuable diagnostic information to clinicians and has been increasingly accepted in various clinical studies. While shear velocity measurement based on acoustic radiation force impulse (ARFI) imaging produces reliable results in homogeneous media, it is still a challenge to accurately detect the shear wave propagation velocity in heterogeneous tissue. In prior art, cross-correlation and time-to-peak methods were developed to determine the travel time between spatial locations in order to estimate the shear velocity. Both methods work well in homogeneous media, but become less robust in heterogeneous media. In this work, a maximum likelihood estimation method was developed to overcome the weaknesses of the prior methods and was tested on uniform and heterogeneous phantoms.

Statement of Contribution/Methods

When using ARFI induced shear wave propagation to measure tissue elasticity, there are two common combinations of ARFI excitation and shear wave detection. The first one is to excite the tissue at two different locations and to detect shear wave at one location, the second is to excite tissue at one location and to detect the shear wave at two different locations. In either method, the reflection of the shear wave in heterogeneous media can severely alter the displacement temporal profile shape from location to location, and makes correlation and time-to-peak methods perform poorly when estimating shear wave propagation time. In this work a parametric model was developed to minimize the affect of altered displacement profile on the estimate. The method uses shear velocities between the excitation and detection spaces as model parameters and uses the normalized displacement temporal profiles at detection locations as probability distribution functions. A joint density (likelihood) function is then constructed based on the shear velocities and the displacement profiles. Searching for the maximum value of the likelihood function by using an iterative method produces estimates of the shear velocity which are more robust to shear wave reflections.

Results

This method was applied to an in-vitro phantom which has a background Young’s modulus of 35.6kPa and contains inclusions that have a Young’s modulus from 19.4kPa to 117.6kPa. Signal to noise ratio (SNR) is used to quantify the measurement error in a uniform background, and contrast to noise ratio (CNR) is used to quantify the performance in the region including inclusion and background. Results of the proposed, correlation based and time to peak based methods are: SNR values are 22.5dB, 24.3dB, 17.2dB in background, and CNR values are 13.93dB, 5.04dB, 10.67dB in heterogeneous region embedded with a 78.9kPa inclusion.

Discussion and Conclusions

Our proposed method has similar performance compared with cross-correlation and time-to-peak methods in uniform background, and provides superior performance in heterogeneous material.

2G-5

5:30 PM Assessment of shear anisotropy using Supersonic Shear Imaging with rotating arrays: in vivo evidence of cornea elastic anisotropy.

Thu-Mai NGUYEN[1], Jean-François AUBRY[1], David TOUBOUL[2], Jeremy BERCOFF[3], Mickael TANTER[1]; [1]Institut Langevin Ondes et Images, ESPCI ParisTech, CNRS UMR 7587, Inserm ERL U979, Paris, France, [2]Centre Hospitalo-Universitaire de Bordeaux, Bordeaux, France, [3]Supersonic Imagine, Aix-en-Provence, France

Background, Motivation and Objective

The elastic behavior of soft tissues is known to be linked to their microstructure. The cornea is mainly composed of collagen fibers whose organization determines its biomechanical properties. Understanding these properties has become a crucial issue in ophthalmology to predict the cornea response to refractive surgeries and to avoid post-treatment complications. The Supersonic Shear Imaging (SSI) method is here adapted for the in vivo assessment of the cornea elastic anisotropy using rotating 1D array.

Statement of Contribution/Methods

Tissue shear modulus can be retrieved from the speed of a shear wave propagating in this tissue. In the SSI method, shear wave is induced using a linear ultrasonic array to apply a transient ultrasound radiation force in the tissue. The resulting propagation direction is transverse to the ultrasound beam. The probe is then switched to an ultrafast imaging mode (30 kHz) to follow the shear wave propagation and thus evaluate its local speed. We implemented SSI with specially designed high-frequency rotating arrays (15 MHz, 128 elements) to estimate the tissues elastic anisotropy. 3D scans were performed on human eyes (ex vivo) and porcine eyes (ex vivo and in vivo). Differences in the local shear wave speed for different propagation directions were highlighted.

Results

Elasticity maps of the cornea surface were obtained both ex vivo and in vivo with a good repeatability (standard deviation < 6% of the shear modulus). On both human and porcine corneas, the peripheral part turned out to be 70 ± 10% softer than the central part. Human corneas did not exhibit any strong anisotropy whereas porcine corneas were stiffer along the horizontal meridian (16 ± 2 kPa) than in the diagonal and vertical directions (7.8 ± 0.5 kPa).

Discussion and Conclusions

It is known from X-ray diffraction measurements [1] that the fibers are mainly oriented along the horizontal meridian in porcine cornea, while there are two preferential directions in human cornea (horizontal and vertical). In both cases the fibers are more likely to be circumferential at the limbus. The elastic maps obtained here are consistent with pioneering ex vivo findings [1], proving the sensitivity of SSI to tissue fibers orientation in both ex vivo and in vivo conditions.

[1] S. Hayes et al, “Comparative Study of Fibrillar Collagen Arrangement in the Corneas of Primates and Other Mammals”, The Anat. Rec., 290:1542–1550, 2007

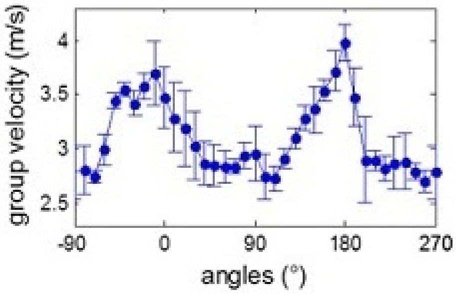

Figure – Shear wave speed as a function of the propagation direction for an *in vivo* porcine cornea. The standard deviation corresponds to the spatial heterogeneity.

2G-6

5:45 PM Development and Evaluation of Pulse Sequences for Freehand ARFI Imaging

Joshua Doherty[1], Douglas Dumont[1], Dongwoon Hyun[1], Jeremy Dahl[1], Gregg Trahey[1,2]; [1]*Biomedical Engineering, Duke University, USA,* [2]*Radiology, Duke University, USA*

Background, Motivation and Objective

Acoustic Radiation Force Impulse (ARFI) imaging techniques can be used to non-invasively evaluate the relative stiffness of tissues; potentially aiding in the identification of cancerous lesions in tissue or vulnerable lipid pools in vasculature. The purpose of this work has been to combine high-frame rate pulse sequences and fast data processing algorithms in the development of a freehand ARFI imaging system capable of providing near real-time feedback to a clinician.

Statement of Contribution/Methods

Several pulse sequences that implement conventional B-mode interleaved with ARFI imaging were developed for various frame rates and scan durations (ranging from 20 fps for 2 sec to 1 fps for 90 seconds). Advanced algorithms using a GPU processor were implemented for data and image processing.

Transducer face heating and acoustic exposure were quantified as a function of frame rate and scan duration for each of the sequences. Image quality of freehand imaging was evaluated in phantoms using SNR and *in vivo* images of the breast, carotid artery, and thyroid of several volunteers were acquired. Spatial and temporal stability of ARFI measurements throughout the swept scan were assessed.

Results

Transducer face heating was <2°C and FDA acoustic exposure limits were not exceeded. In phantoms, little degradation (<10% reduction in SNR) was observed for normal sweep rates (2 to 10 mm/sec). *In vivo* video sequences showed consistent measurements of on-axis displacements across multiple frames and acquisitions. Overall data acquisition, processing, and display frame rates of 1.0 fps were achieved, allowing for low frame rate sequences to provide feedback information during the swept scan. As shown in the example *in vivo* images of the carotid artery, co-registered B-mode and ARFI images depict clear vessel wall definition while swept from the lower common carotid artery up to the bifurcation.

Discussion and Conclusions

We developed a high frame-rate ARFI imaging system with advanced processing power that is capable of acquiring multiple frames of ARFI images using freehand sweeping techniques. Little image degradation was observed during swept scans, both *in vivo* and in phantoms. We demonstrated the ability to measure ARFI displacements continuously for prolonged periods; however transducer face heating will limit increased frame rates and longer duration scans.

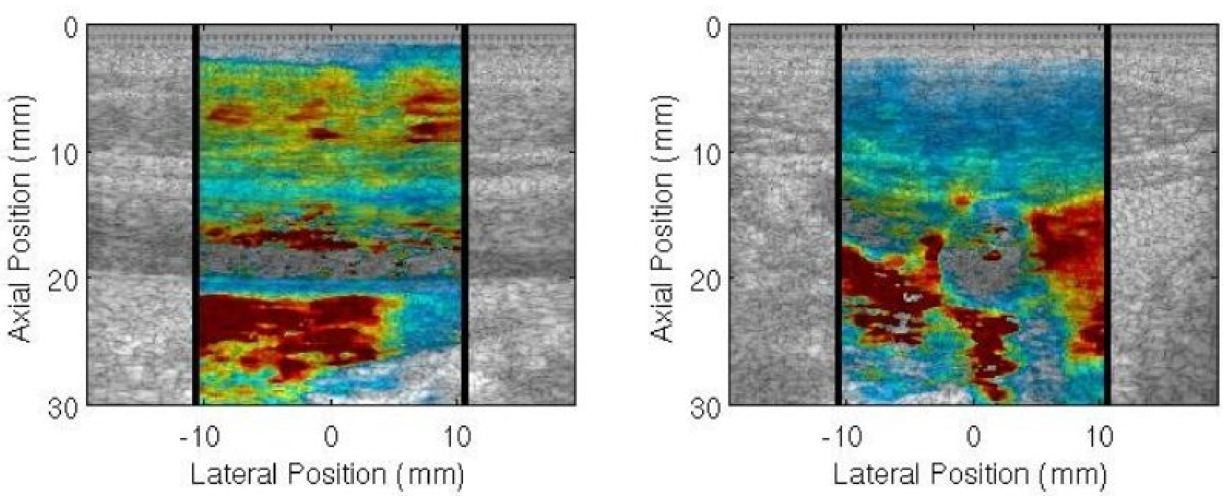

THURSDAY ORAL

3G - Contrast Agents II

Carribean Ballroom VII

Thursday, October 20, 2011, 4:30 pm - 6:00 pm

Chair: **Nico de Jong**
Erasmus Medical Centre

3G-1

4:30 PM Contrast Ultrasound: Recent developments and the battle for regulatory approval

François TRANQUART[1]: [1]Bracco Suisse SA, Plan-les-Ouates, Switzerland

Background, Motivation and Objective

Ultrasound Contrast Agents (UCA) have been approved for clinical use in cardio-vascular and non cardio-vascular indications more than ten years ago. Its introduction prompted tremendous research efforts by clinicians, scientists and manufacturers. The advent of the so-called contrast-specific imaging techniques (e.g. Pulse Inversion, Amplitude Modulation and CPS) helped the field of contrast-enhanced ultrasound (CEUS) to mature and evolve considerably. It has made ultrasound a serious competitor with other imaging modalities, like CT and MR, for which contrast agents have been used for many years. Moreover, CEUS has been recognized as a low cost technique, which is easily available, uses no ionizing radiation, and is relatively safe with the absence of contra-indications such as COPD, renal or liver insufficiency. However, the general acceptance of CEUS still remains poor, and its utilization is limited to expert centers.

Statement of Contribution/Methods

The main problem with CEUS is that some barriers to its use must be overcome, such as: limited number of training programs, lack of approval for new indications (e.g. myocardial perfusion, prostate cancer…), lack of any reimbursement in most countries, limited number of large-scale multicenter trials, limited coordinated efforts from ultrasound and pharma companies to tackle issues like standardization and quantification, cross platform reproducibility, large dominance of radiologists in imaging for non cardio-vascular indications with possible conflicts between the available modalities, lack of workflow standardization for implementing CEUS in an ultrasound department.

Results

Those barriers could be overcome by coordinating efforts in providing evidence to health authorities and physicians, organizing training programs, standardization / automation of acquisition protocols (guidelines), volumetric acquisitions for subsequent analysis etc.

CEUS has proven to be a robust and powerful technique in expert hands but now it has to be translated into routine practice in all ultrasound departments. It will have a significant impact on healthcare cost with a real benefit for developed countries helping to reduce the budget allocated for imaging, but also in developing countries by giving them access to a modern and relatively cheap imaging method.

Discussion and Conclusions

Recent developments have shown new and exciting areas for CEUS, which might have an even greater impact on ultrasound imaging, is in molecular imaging. Microbubbles, or the so-called third generation agents, can be targeted to specific tissue types to delineate pathologies which would otherwise be difficult to detect, or can be used for therapeutic purposes such as drug delivery and gene therapy. The most interesting clinical applications will be in cancer and cardiovascular disease, which are the most prevalent causes of death in humans in developed countries.

3G-2

5:00 PM Super-Resolution Ultrasound Imaging (SRUI) using ultrafast mapping of contrast agents

Olivier Couture[1], Benoit Besson[2], Gabriel Montaldo[3], Mathias Fink[1], Mickael Tanter[4]; [1]*CNRS / ESPCI, France,* [2]*CNRS, France,* [3]*ESPCI, France,* [4]*INSERM, France*

Background, Motivation and Objective

Because of diffraction, the resolution of ultrasound imaging is limited in theory to about a half-wavelength. Below this limit, the echoes of many scatterers are superimposed and become undistinguishable. This leads to a fundamental compromise between resolution and penetration depth. However, if a single scatterer is generated, it can be located with a resolution much beyond the diffraction limit because the point-spread function is known. Our objective is to demonstrate that imaging microbubbles clouds present in the vasculature at very high frame rate (kHz) can create such distinct sources in-vivo, leading to a resolution at the micron-level at low frequencies (1 MHz). This concept is the acoustic analog of fluorescent photoactivation localization microscopy (FPALM), which transformed optical microscopy.

Statement of Contribution/Methods

Firstly, to estimate the resolution limit of SRUI, a 1 MHz array (0.75 mm pitch) was connected to an ultrasound multi-channel system capable of acquiring images at 10000 images / s. A single microbubble (30 um diameter) was generated at a nucleation site and floated toward the array. Images were acquired at 1.3 kHz and the RF signal was further analyzed to detect the summit of the parabola formed by arrival time of the echoes on the 128 channels. Secondly, to demonstrate that single events can be observed within clouds of thousands of clinical microbubbles imaged at high frame rates, experiments were performed by injecting contrast agents in 100um tubes printed in microfluidics systems. Single events were isolated by differential ultrafast imaging of the disruption of bubbles induced by the ultrasonic imaging itself after optimization of the pressure. Thirdly, the same super-localization technique was performed in tumors implanted under the skin of mice after the injection of targeted microbubbles.

Results

The deviation of the floating bubble from a straight path was considered to be the error on the position of the microbubbles as defined by SRUI. When super-resolution is used, most of the events are detected within 6 microns of the trend in the axial direction (wavelength / 250), as compared to 900 um for conventional imaging. For lateral detection, the -6dB resolution of the new method is 40 microns (wavelength / 38). In the microfluidic channels, single events linked to the presence of ultrasound contrast agents were detected within the microfluidic channel, which improved the lateral resolution by a factor of 7. Finally, single events could also be detected in-vivo. They could be used to establish the position of individual contrast agents.

Discussion and Conclusions

By combining ultrafast imaging and disruption sequences, ultrasound can significantly outperform the diffraction-limit if single echoes induced by microbubbles are exploited. Super-Resolution Ultrasound Imaging (SRUI) could potentially map the microvasculature at low frequencies and, hence, deep within tissue.

3G-3

5:15 PM IMPROVED PROSTATE CANCER DETECTION BY CONTRAST-ENHANCED ULTRASOUND PARAMETRIC IMAGE ANALYSIS

Peter Frinking[1], Laurent Mercier[1], Marcel Arditi[1], Hessel Wijkstra[2], Olivier Rouvière[3], Jean-Michel Correas[4], François Tranquart[1]; [1]*Bracco Suisse SA, Plan-les-Ouates, GE, Switzerland,* [2]*AMC University Hospital, Amsterdam, Netherlands,* [3]*Hôpital Edouard Herriot, Lyon, France,* [4]*Hôpital Necker, Paris, France*

Background, Motivation and Objective

Contrast-enhanced ultrasound (CEUS) shows promise of becoming a very useful modality for prostate cancer (PCa) detection. With the help of new perfusion imaging approaches, targeted biopsy under CEUS guidance may substantially increase the detection rate for positive cores, as compared to systematic biopsy approaches. This could result in a major and welcome reduction in patient discomfort and morbidity, and could substantially decrease associated costs. The objective of this work was to develop a new CEUS perfusion imaging approach for improved PCa detection in peripheral zone (PZ) tissue of the prostate, and to evaluate this new method against histopathology of whole-mount prostatectomy samples.

Statement of Contribution/Methods

The new perfusion imaging approach is based on a statistical analysis of parametric images of Wash-in Rate (WiR), a perfusion parameter reflecting the rate of contrast enhancement. The parametric images were generated by analyzing time-intensity curves (TIC), which represent the echo-power as a function of time, on a pixel-by-pixel basis using a CEUS quantification toolbox (Bracco Suisse SA, Switzerland). For each pixel in the parametric image, histograms of WiR were calculated in small regions of interest (ROI), and statistical parameters such as the Mode (most occurring value) and Standard Deviation (SD, dispersion of values) were determined from the histograms. Next, color-coded probability maps of PCa occurrence were constructed using Matlab, based on classification criteria differentiating between cancer and non-cancerous tissues in PZ. These criteria were defined by combinations of Mode and SD of histograms obtained from 42 ROI, located in normal tissue and in biopsy-proven PCa areas in PZ of 16 patients.

The new approach was tested on a new set of CEUS sequences of 21 patients obtained with iU22 (Philips) ultrasound systems and C8-4v probes after 2.4 mL SonoVue (Bracco) bolus injections. In total, 54 areas (29 PCa and 25 non cancerous tissues) were identified in the probability maps and were compared to histopathology of whole-mount prostatectomy samples. The results were also compared to WiR values obtained from TIC analyses in ROI located in the same areas.

Results

Based on the probability maps, PCa detection improved considerably compared to the TIC analyses (sensitivity of 100% vs. 92% and specificity of 90% vs. 84%). Moreover, lesions were much more conspicuous in the probability maps compared to standard CEUS images.

Discussion and Conclusions

This study confirms that the PCa probability maps as obtained from a statistical analysis of WiR parametric images may be useful for improved lesion detection in PZ tissue of the prostate. The approach could also aid in determining the effect of a therapeutic treatment (e.g. HIFU), by assessing tumor response to treatment. Presently, the classification criteria are valid only for PZ tissue and should be adapted for cancer detection in inner gland tissue.

3G-4

5:30 PM Relaxation time course of microvessels deformed by ultrasound-activated microbubble

Hong Chen[1], Andrew A. Brayman[1], **Thomas J. Matula[1];** [1]Center for Industrial and Medical Ultrasound, Applied Physics Laboratory, University of Washington, Seattle, WA, USA

Background, Motivation and Objective

Constrained microbubble dynamics and coupling with surrounding viscoelastic tissues is an important area of research for ultrasound contrast agents. Understanding the dynamics requires knowledge of the tissue parameters, in particular the elasticity and viscosity. Extensive experimental work on microvessels in the mesentery has led to increased need for tissue parameter characterization of these microvessels, for which there is a current lack of good viscoelastic data. Previous research suggests that when a microbubble collapses in a microvessel, the vessel and surrounding tissue is pulled into the lumen [Chen et al, Phys Rev Lett, 106, 034301, 2011]. This process is rapid, only a few microseconds long. The resulting relaxation of the surrounding tissue back to equilibrium can be used to infer the ratio of viscosity to elasticity of the tissue, providing important information to understanding the tissue properties of these tissues.

Statement of Contribution/Methods

Ex-vivo rat mesentery microvessels (approach approved by Univ. of Washington IACUC) were perfused with saline and microbubbles. Under microscopic guidance, specific microvessels were selected. Single ultrasound pulses (1 MHz) of only a few microseconds duration insonified the tissue sample. High speed photomicrography imaged the displacement and subsequent relaxation of the vessel wall. Studies of microbubble-induced deformation and relaxation were performed on vessels with diameters ranging from 20–80 μm. A Voigt model of tissue (parallel spring and dashpot) was used to fit the experimental relaxation time constant τ.

Results

The Voigt model fit the data well. The estimated τ ranged from less than 5 μs to almost 60 μs. No significant difference was found in τ for different diameter microvessels. However, statistically significant variations were shown to occur by changing the syringe pump speed that perfused the tissues with saline. Pump speeds of 10 or 50 mL/hr showed average τ of 26 μs or 10 μs, respectively.

Discussion and Conclusions

These studies are specific to mesenteric venules with flow (and thus vessel integrity) maintained by a syringe pump. Further, the blood in the vessels has been fully replaced by saline. Nevertheless, the measured relaxation time constants are consistent with shear wave measurements of tissue properties at MHz frequencies. In addition, the relaxation time constant is directly associated with the ratio of viscosity to elasticity. The measured ratio provides constraints to possible values for the elasticity and viscosity of this tissue. (Work supported by NIH NIBIB and NIAMS).

3G-5

5:45 PMVolumetric Contrast-Enhanced Ultrasound for Characterizing Tumor Vascularity: Preliminary Studies in an Animal Model

Kenneth Hoyt[1], Anna Sorace[1]; [1]University of Alabama at Birmingham, USA

Background, Motivation and Objective

Contrast-enhanced ultrasound (US) imaging has demonstrated potential as a noninvasive technique for monitoring blood flow in tumor vascularity. However, a limitation of 2D US imaging is that the narrow elevational beamwidth provides information in only a single slice of tissue. The introduction of volumetric (3D) transducers promise to overcome this limitation allowing characterization of the entire tumor burden. Therefore, we developed a volumetric contrast-enhanced US (VCEUS) imaging method for quantitative mapping of tumor vascularity and monitoring of blood flow.

Statement of Contribution/Methods

Imaging was performed using a SONIX RP US system (Ultrasonix Corp) equipped with a broadband 4DL14-5/38 volumetric probe. Using a harmonic imaging mode (transmit at 5 MHz, receive at 10 MHz), acquisition of post scan-converted CEUS data was controlled using the research-based software package Propello (Ultrasonix Corp). The user interface allows customization of US scans to achieve the desired field-of-view and volume rate. Specifically, automatic sweeps were implemented with degrees per frame and frames per volume set to 0.692 and 41, respectively. Given an imaging width and depth of 38.4 and 25.0 mm, respectively, an elevational scan distance of 28.4 mm and volume rate of 1.0 Hz were achieved. Time-intensity curves from each voxel were processed to derive key blood flow parameters (peak and time-to-peak intensity, wash-in slope, and area under the curve). System testing was performed on breast tumor bearing mice (N = 4) during infusion of microbubbles (Definity, Lantheus Medical Imaging) via a surgically placed injection port.

Results

Tumor vascularity parametric maps were generated allowing inspection of blood flow across the entire tumor volume. Given a VCEUS image acquisition, each frame was summarized and plotted as a function of distance from the tumor midsection (reference frame). Deviation in blood flow measurements were computed relative to this reference frame. As results reveal, millimeter-sized deviations in transducer positioning can have profound implications on US-based blood flow estimators with errors ranging from 3.1 to 33 % and dependent on both degree of misalignment (offset) and the particular blood flow estimator. These errors indicate that VCEUS-based blood flow measurements should be considered in tumor analyses (especially longitudinal studies) since they consider the entire mass rather than a representative planar cross-section.

Discussion and Conclusions

A volumetric strategy for characterizing tumor vascularity using contrast-enhanced US was developed. Preliminary results indicate that this imaging method is a promising tool for characterizing and monitoring changes in tumor blood flow in response to drug therapy.

4G Acoustic Micro Fluidics

Carribean Ballroom I

Thursday, October 20, 2011, 4:30 pm - 6:00 pm

Chair: **Donal E. Yuhas**
IMS Inc.

4G-1

4:30 PM Acoustic particle trapping in a microfluidic device using frequency modulated signal

Jong Seob Jeong[1], Jung Woo Lee[2], Chang Yang Lee[2], Shia Yen Teh[3], Abraham Lee[3], K. Kirk Shung[2]; [1]Department of Medical Biotechnology, Dongguk University-Seoul, Seoul, Korea, Republic of, [2]Department of Biomedical Engineering, University of Southern California, Los Angeles, California, USA, [3]Department of Biomedical Engineering, University of California at Irvine, Irvine, California, USA

Background, Motivation and Objective

Recently, several biological cell manipulation techniques using electrostatic, magnetic, optical, and acoustic forces have been developed to precisely control various cell motions within such devices. In our previous research, a 30 MHz lithium niobate single element transducer was fabricated to experimentally demonstrate the feasibility of acoustic trapping, where a droplet could be held stationary in two-dimensional trap. In order to control streaming particles in a fluid in a microfluidic device, it is necessary to generate trapping forces greater than the drag force arising from the surrounding fluid flow. In this paper, a 24 MHz PZT4 transducer was built to immobilize 60 ~ 70 µm droplets flowing in a polydimethylsiloxane (PDMS) microfluidic device. The experimental results showed that the current device may serve as an acoustic switch to direct particle motions in a flow cytometer or similar cell sorting devices.

Statement of Contribution/Methods

A high frequency sound beam was employed to control particle motions in a microfluidic device. A 24 MHz single element PZT4 transducer was built to transmit a focused ultrasound of variable duty factors, and its 1-3 piezocomposite structure established a tight focusing with f-number of one. The transducer was excited by the chirp signal sweeping 18 ~ 30 MHz with a 50% of duty factor, in order to ensure that enough sound beams were penetrated into the device. The device was fabricated from a PDMS mold, and had a main channel composed of three subchannels among which particles flowed in the middle as shown in Fig.1.

Results

In the scenario-A, when the transducer was turned on, the flowing particle with 60 ~ 70 µm diameter was trapped by the transducer located at the sheath flow-A. After a few seconds, the transducer was turned off, and the particle was released and subsequently directed to the outlet-A. In the scenario-B, the particle was trapped by the transducer located at the sheath flow-A. The transducer was then moved to the third channel with the trapped particle by 200 µm. In the sheath flow-C, the particle was released by turning off the transducer and it was directed to the outlet-B

Discussion and Conclusions

The results showed the potential use of a focused sound beam in microfluidic devices, and further suggested that this method could be exploited in the development of ultrasound-based flow cytometry and cell sorting devices.

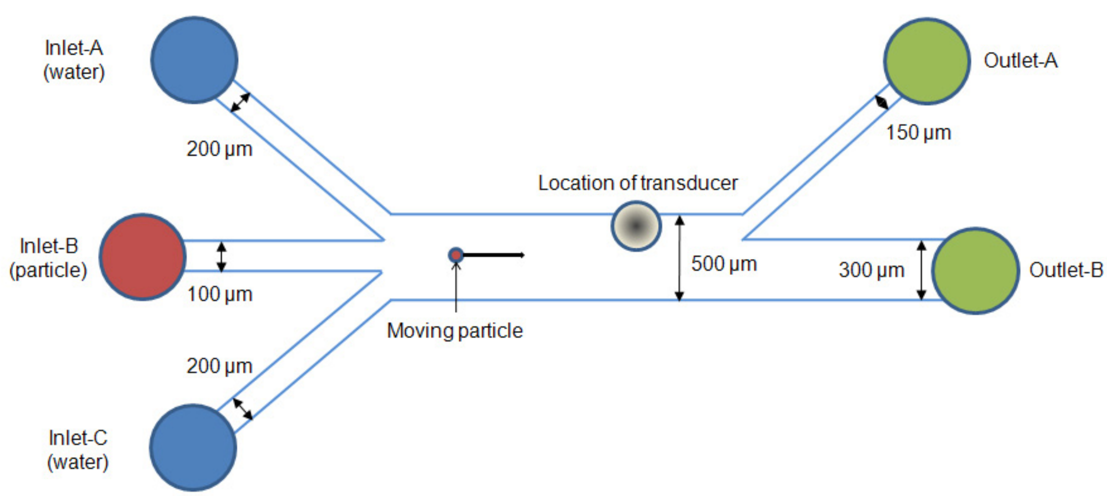

Fig. 1 Schematic diagram for the PDMS microfluidic device

4G-2

4:45 PM Flow-through separation of microparticles of different sizes using ultrasound.

A. K. M. Ariful Haque Siddique[1], CheolGi Kim[1], Bongyoung Ahn[2], SeungHyun Cho[2]; [1]Department of Materials Science & Engineering, Chungnam National University, Yuseong-Gu, Daejeon, Korea, Republic of, [2]Center for Safety Measurement, Korea Research Institute of Standards and Science, Yuseong-Gu, Daejeon, Korea, Republic of

Background, Motivation and Objective

Recently, many studies have been reported on the separation of microparticles in a fluid-flow using ultrasound since ultrasonic standing wave enables particles to align to its pressure nodal or anti-nodal plane (depending on their density and compressibility) due to its acoustic radiation force. However, the existing studies are showing that there still

THURSDAY ORAL

requires more stable and efficient method to separate particles of different sizes. This work concerns an alternative for fast and efficient flow-through separation by using the frequency sweep technique.

Statement of Contribution/Methods

A modulized microchannel comprising steel and acryl with a width of 1.5 mm was manufactured. An ultrasound transducer installed at one side of the microchannel module generates ultrasonic standing wave field inside the channel, where the periodical increasing frequency sweep of the ultrasound can shift all particles nearly to one side of channel wall. Interestingly, in this phenomenon, it is observed that the response time of each particle is not the same due to the difference of the acoustic radiation force. That is to say, large particles moves quickly from large acoustic radiation force. This difference of the response time defines the minimum sweep period (MSP) of the particle, the frequency sweep period of the exciting ultrasound which can move all particles to the last nodal plane close to the wall. The particles can move to the last nodal plane only when the frequency sweep period is over MSP. The different sized particle has different MSP. Then, particles of two different sizes can be separated when the frequency sweep period is chosen between MSP's of two particles since only larger particles can move at that frequency sweep period.

The microchannel has two inlets and two outlets. The mixed particles of different sizes enter one inlets to send particles along one side of the channel and just pure water is flowed to the other inlets to prevent the turbulence effect. Polystyrene microspheres (25 and 6 micron) were used as test particles in this experiments

Results

Figure shows the particle behavior in separation by the ultrasound and the schematic configuration of the microchannel used in the experiment.

Discussion and Conclusions

The experimental results confirm that by choosing the MST of the operational frequency can be one of efficient methods to separate microparticles in fluid-flow using ultrasound.

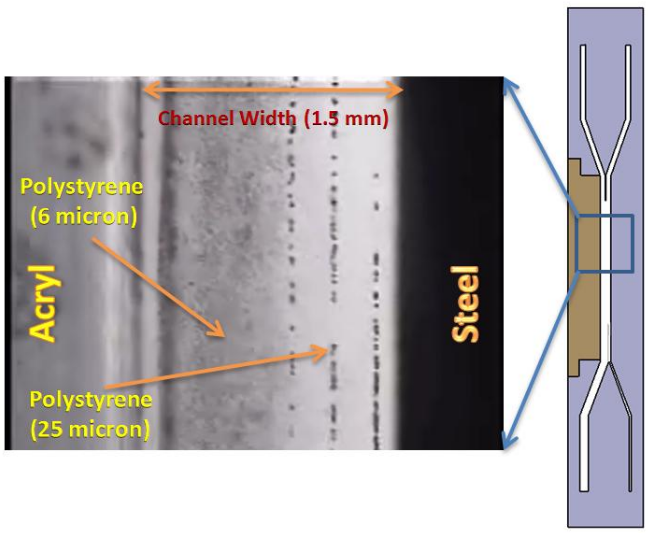

THURSDAY ORAL

4G-3

5:00 PM Microscale Acoustofluidics: Microfluidics via Acoustics and Ultrasonics

James Friend[1,2]; [1]Mechanical Engineering, Monash University, Clayton, VIC, Australia, [2]Melbourne Centre for Nanofabrication, Clayton, VIC, Australia

Background, Motivation and Objective

Microfluidics is a burgeoning new field of research with considerable promise in biomedical applications, yet suffers from a lack of methods for fluid transport, mixing, and manipulation as a consequence of its viscosity and surface tension-dominated behavior at such small scales. The transmission of acoustic waves can be used to solve the problems inherent in microfluidics through acoustic streaming and direct acoustic forces upon particles within. Our objective is to pump fluids in a microchannel containing such particles while demonstrating an ability to mix, concentrate and separate them.

Statement of Contribution/Methods

In this study we have combined several techniques for transmitting surface acoustic waves along the long axis of a microchannel to either pump fluid within with speeds of ~2 cm/s or efficiently mix it on demand. This is accomplished by choosing either the fundamental or a harmonic resonance of the SAW as formed in the lithium niobate 127.68Y-X propagating substrate: the acoustic wavelength can be changed in the fluid in the channel. We cut rectangular and asymmetrically-cut anechoic cross-sectioned channels along the X-axis of lithium niobate with a variety of widths and a depth of 100 micrometers. We generated SAW on the substrate at 30 MHz using a single-phase unidirectional transducer with an elliptically-shaped focus to form a line of intense SAW aligned with the cut channel. For the anechoic cross-sectioned channel, a split interdigital electrode was used with a ground aligned along the X-axis and a "left" and "right" side of the electrode to permit SAW to be generated on one side of the channel and subsequently be transmitted across it.

Results

We find that the transition from weak flow sufficient to manipulate particles in the suspension to strong flow for mixing and pumping is at about 2 nm vibration amplitude for SAW in our system. Using strong acoustic radiation above 1 nm amplitude, uniform (nearly plug) flow is generated if the acoustic wavelength is larger than the width of the channel. Switching to a harmonic so the acoustic wavelength is much less than the width of the channel, the flow changes to a mixing vortex flow in a few milliseconds. Using SAW at less than 1 nm amplitude, suspended particles within can be caused to be organized along lines parallel to the channel's long axis from direct acoustic forces upon them. Using an anechoic asymmetric cross-sectioned channel allows suspended particles to be driven across the channel using a split transducer design to generate traveling waves across it.

Discussion and Conclusions

A complete method for pumping and mixing fluids in a channel and manipulating the particles within will be demonstrated with ample videos and physical explanation of the phenomena. The work demonstrates for the first time a micro-sized device that can perform previously difficult microfluidics operations on a fixed geometry all enabled by SAW.

4G-4

5:30 PM Rotational surface acoustic wave microfluidic motor

Richie Shilton[1], Nick Glass[1], Peggy Chan[2], **Leslie Yeo[1]**, James Friend[1]; [1]Mechanical Engineering, Monash University, Clayton, VIC, Australia, [2]Chemical Engineering, Monash University, Clayton, VIC, Australia

Background, Motivation and Objective

Owing to the inadequacy of current small-scale motor technology, miniaturised motors are increasingly becoming more important for the development of portable devices for a diverse number of applications. Surgical tools, actuators for biological analysis, cells, and diagnostics are a few of the many areas in which microscale actuation is required. Many current micro-motor designs often require complex and precise designs, or are inadequate in either rotation speed or torque for most conceivable lab-on-a-chip applications. *Surface acoustic waves* (SAW) have been shown to be a powerful means for driving fluid actuation to solve this problem.

Statement of Contribution/Methods

A SAW driven fluid-coupled rotary micromotor is reported that can generate high-speed rotation easily incorporated into microfluidics with modest power requirements suitable for a truly portable device. The device consisted of a circular 5 mm disc rotor coupled with a fluid drop contained in a potential well placed asymmetrically in the propagation pathway of two counter-propagating SAWs, as seen in Fig. 1(a). We generate an azimuthally rotating flow throughout a fluid drop via acoustic irradiation of geometrically tailored SAWs to drive the rotary micromotor. This coupled design, the large mass flow that may be induced by acoustic irradiation, and the large amount of power that may be transmitted using SAW, altogether makes it possible to drive the rotation of a thin disc at relatively high rotation speeds.

Results

The rotational speeds of the disc rotor were found to increase linearly with an increase in the average surface displacement up to a maximum of up to 2,250 rpm, with a maximum torque of over 60 nNm. Preliminary findings have shown that reducing the disc rotor size increases the maximum rotational velocities achievable. The rotational velocities achieved after applying the SAW can be seen in Fig. 1(b); the electrical input power applied to each IDT was of the order 0.1-1 W, although the actual power into the fluid is considerably less. As we increase the electrical input power beyond 1 W, the disc rotation becomes unstable with an associated drop in rotational velocity.

Discussion and Conclusions

Providing a simple, miniaturized method for driving efficient and fast rotary motion, the main attraction of the technique is its ability to be incorporated into lab-on-a-chip devices.

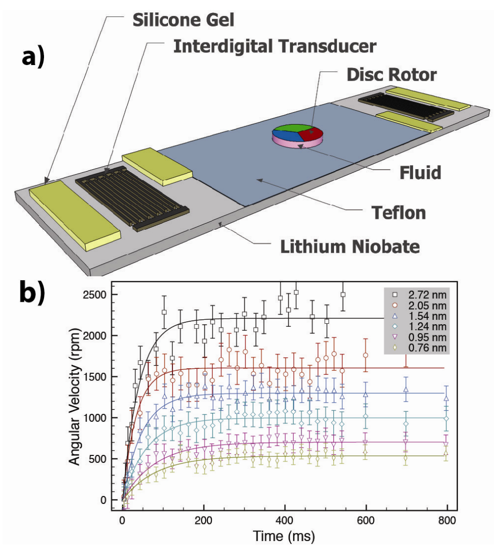

4G-5

5:45 PM Precise Transportation of Single Cell by Phase-shift Standing Surface Acoustic Wave

Long Meng[1], Feiyan Cai[1], Qiaofeng Jin[1], Lili Niu[1], Hairong Zheng[1]; [1]Shenzhen Institutes of Advanced Technology, Chinese Academy of Sciences, China, People's Republic of

Background, Motivation and Objective

Continuous manipulation of single cell in a fluid medium is of crucial interest not only for basic cell biology but also for clinical medicine, cancer research and gene therapy. Available methods for controlling transportation of cells are realized mainly by switching the acoustic pressure, resonant mode and actuation frequency. However, it is challenging to precisely transport and locate the cells. In this paper, a microfluidic device that could precisely transport a single cell by phase-shift standing surface acoustic wave (SSAW) was developed.

Statement of Contribution/Methods

A pair of interdigital transducers (IDTs), having a pitch of 200 μm, was deposited on a 128YX-LiNbO3 substrate. Then, a PDMS microchannel was bonded to the SSAW generator using oxygen plasma treatment. Human breast cancer cell was infused in the microchannel through a pressure driven flow. By modulating the relative phase, Δφ, between two IDTs, the position of pressure nodes in the microchannel changes correspondingly resulting in the transportation of the single cell. Both of the numerical calculation and experiments were carried out to investigate the mechanics and performance of the transportation device.

Results

When there was no phase shift, the cell was retained in the center of the microchannel (dash line), as shown in Fig. 1a. Setting the value of Δφ to -100º, the cell moved upwards for a distance of 27.6 μm, agreeing well with the theoretical value of 27.8 μm (Fig. 1b). While adjusting the value of Δφ to -150º, the cell kept on moving upwards but the displacement reduced by half correspondingly, about 13.85 μm (Fig. 1c). Then, modulating the Δφ to -50º, the cell moved toward the initial position (Fig. 1d). Finally, the Δφ was further modulated to 0º, the cell went on moving downwards, and returned back to the same location (Fig. 1e).

THURSDAY ORAL

Discussion and Conclusions

The simulation and experimental results reveal that there is a good linear relationship between the relative phase and the displacement. Varying the relative phase continuously, the single cell could be transported precisely in arbitrary location in the microchannel. Furthermore, improving the frequency and structure of IDTs would make it possible to transport the nanoscale bioparticles in two dimensional spatial positions.

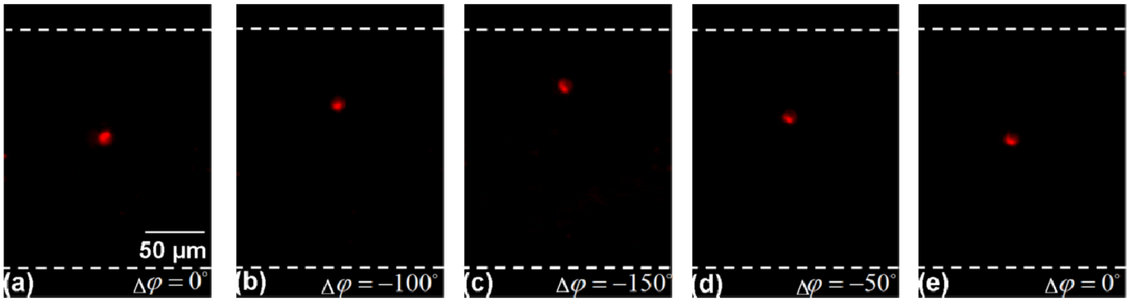

THURSDAY ORAL

5G - Physics of Phononic Crystals

Carribean Ballroom II

Thursday, October 20, 2011, 4:30 pm - 6:00 pm

Chair: **Roy H. Olsson**
Sandia National Laboratories

5G-1

4:30 PM Analysis of deaf bands in phononic crystals

Rayisa P. Moiseyenko[1,2], **Vincent Laude[1]**, Nico F. Declercq[2]; [1]Institut FEMTO-ST, Centre National de la Recherche Scientifique, Besancon, Franche-Comté, France, [2]Unité Mixte Internationale GT-CNRS, Georgia Tech Lorraine, Metz, Lorraine, France

Background, Motivation and Objective

In the analysis of phononic crystals, the occurrence of frequency band gaps is often the sought-after property. Band gaps are frequency regions where wave propagation is forbidden whatever the wave vector, or equivalently where only evanescent waves are allowed. Band gaps can appear either because of Bragg interferences or because of local resonances internal to the periodic unit cell. In this paper, we analyze a different mechanism that also leads to an absence of transmission: deaf bands.

Statement of Contribution/Methods

Deaf bands occur when certain propagative Bloch waves cannot be excited within the phononic crystal because of the excitation symmetry. They have been observed experimentally in recent years. In this paper, we specifically investigate the diffraction of acoustic waves by two-dimensional PCs composed of steel rods in water. The finite element method and appropriate radiation conditions at the boundary of a finite region are used to compute pressure fields generated by a line source. Such field maps are analyzed based on the complex band structure for the infinite periodic PC, i.e., the dispersion relation of both propagating and evanescent Bloch waves.

Results

Our analysis reveals that a deaf band is indeed a result of the absence of modal conversion to a particular Bloch wave at the boundary between the incident medium and the phononic crystal. We give a general numerical criterion to estimate its occurrence and we investigate the sensitivity of deafness with the incidence angle. Furthermore, we find that transmission at a deaf frequency is still an exponentially decreasing function of depth, as in the case of band gaps. The figure shows an example for normal incidence on a hexagonal-lattice phononic crystal of a pressure wave with a deaf frequency.

Discussion and Conclusions

Our finite size computations indicate that the exponential decrease in the transmission at deaf frequencies is much stronger than that in band gaps. The complex band structure, however, reveals that in all cases the decrease is actually multi-exponential, although the evanescent Bloch wave with the smallest imaginary part dominates the transmission. We conclude that at a deaf frequency, transmission is dominated by the excitation of higher order frustrated Bloch waves.

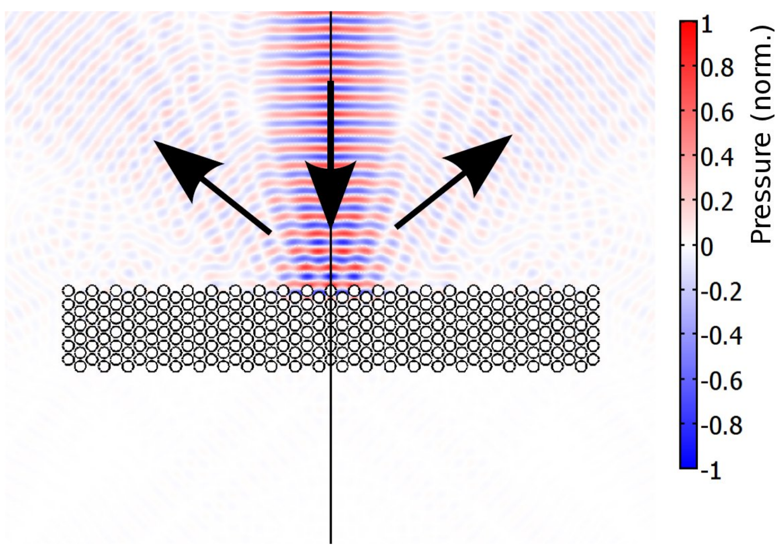

5G-2

4:45 PM Thermal Conductivity Manipulation in Lithographically Patterned Single Crystal Silicon Phononic Crystal Structures

Bongsang Kim[1], Janet Nguyen[1], Eric Shaner[1], C. Thomas Harris[1], Ihab El-Kady[1], Roy Olsson III[1]; [1]*Sandia National Laboratories, Albuquerque, NM, USA*

Background, Motivation and Objective

The thermal conductivity of many semiconductor materials has shown dramatic reductions via micro/nano-scale structuring. In such materials, the dominating heat transfer mechanism is through lattice vibration (phonons). As the dimensions of thermal pathways becomes comparable to the phonon mean-free-path, phonon scattering increases, leading to reduction in heat transfer.

THURSDAY ORAL

Statement of Contribution/Methods

In this work, we demonstrate thermal conductivity manipulation via lithographically defined phonononic crystals in single crystal silicon. Figure 1 shows fabricated bridge-shaped test structures consisting of sub-micron diameter through-holes patterned in a 500nm-thick Si membrane. Heat is supplied via an aluminum serpentine in the membrane center and its temperature change was measured to extract the thermal conductivity.

Results

Figure 2 shows the measured thermal conductivity of phononic crystal samples which were much lower than Maxwell-Eucken predictions which model the volume reduction effect in porous materials. This discrepancy increases as the minimum feature size decreases likely due to enhanced phonon scattering as the size of the thermal pathways shrinks. The device with a limiting dimension of 0.25um showed the highest reduction in thermal conductivity, ~30W/mK, which is half that of the Maxwell-Eucken prediction.

Discussion and Conclusions

Thermal conductivity can be effectively controlled via phonon-scattering enhancement from lithographically defined sub-micron features. This has potential to enhance many micromachined devices. For example, reducing thermal conductivity with much less alteration in electrical conductivity can significantly improve the performance of micromachined thermoelectric coolers, energy harvesters, and ovenized devices.

Fig1. SEM image of a test structure with phononic crystals

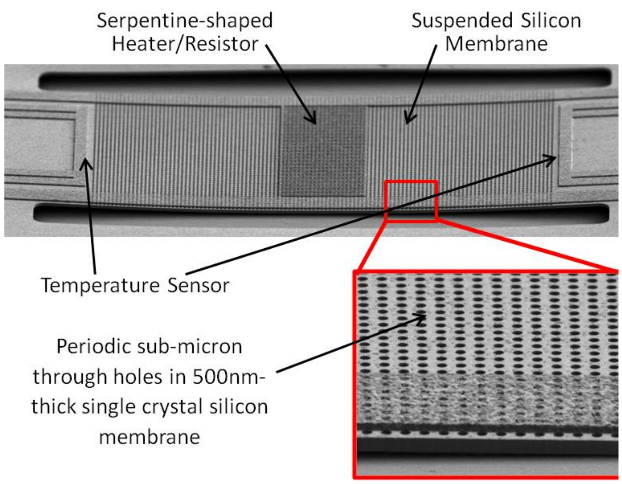

Fig2. Measured thermal conductivities vs. Maxwell-Eucken predictions

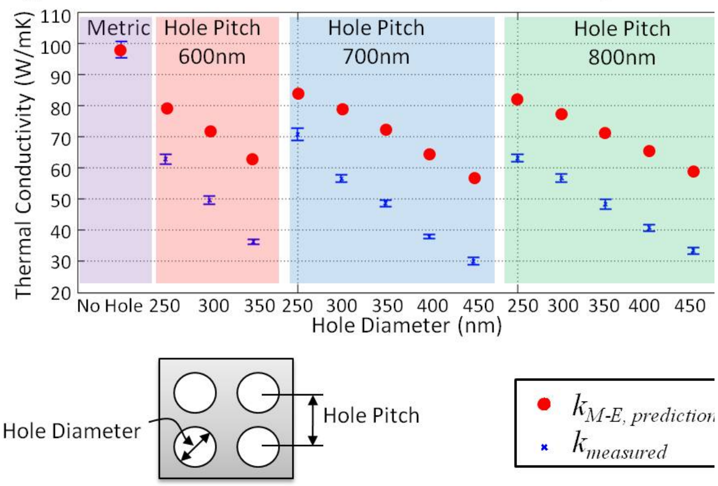

5G-3

5:00 PM Experimental evidence of locally resonant sonic band gap in 2D stubbed plates

MOURAD OUDICH[1], Matteo Senesi[2], Badreddine Assouar[1,3], Massimo Ruzzene[2], Jia-Hong Sun[4], Brice Vincent[5], Zhilin Hou[6], Tsung-Tsong Wu[4]; [1]*Institut Jean Lamour, Nancy University - CNRS, Vandoeuvre-les-Nancy, France,* [2]*D Guggenheim School of Aerospace Engineering, Georgia Institute of Technology, USA,* [3]*International Joint Laboratory (UMI 2958), Georgia Institute of Technology - CNRS, ATLANTA, USA,* [4]*National Taiwan University, Taiwan,* [5]*Nancy University - CNRS, France,* [6]*South China University of Technology, China, People's Republic of*

Background, Motivation and Objective

The propagation of an elastic wave in periodic composite material, called phononic crystal (PC), has received much attention over the past decade. The main mechanisms responsible for the opening of acoustic band gap (BG) are based on the Bragg scattering and local resonance (LR). The latter occurs at frequencies which can be almost two orders of magnitude lower than the usual Bragg gap. In this communication, we report on theoretical and experimental studies of 2D LR phononic plates composed of rubber unit resonators squarely arranged on a homogenous aluminum plate.

Statement of Contribution/Methods

We reported recently on theoretical studies concerning 2D LR sonic crystals [1, 2]. Here, besides the theoretical investigation, we point out experimentally the acoustic properties of LR sonic plates. Three LR stubbed plates composed of rubber resonators with different thicknesses (1.5mm, 3mm & 5mm) arranged with a periodicity of a=1cm on aluminum plate (0.5mm thickness) were fabricated. Owing to the different types of silicone rubber, Brillouin spectroscopy analysis was carried out to determine the real elastic constants of the used rubber in our study. These new constants were then implemented in our numerical model to get the true band structure corresponding to the fabricated structures. Scanning Laser Doppler Vibrometer (SLDV) was used to characterize the band gaps of the different LR slabs through a frequency analysis.

Results

Band structure and transmission were computed based on the new elastic constants of silicone rubber measured by Brillouin spectroscopy. Experimental characterization was then performed along the different directions of first Brillouin zone. Very low frequency complete band gaps were clearly obtained for the different structures and a 2 KHz frequency band gap was reached for the 5mm stub thickness plate. The experimental results agree very well with the numerical ones obtained using new measured elastic constants. Fig. 1 shows an example of the band structure and measured transmission of 5mm stub thickness plate.

Discussion and Conclusions

LR band gap at 2 KHz was experimentally evidenced on 2D LR stubbed plates having a periodicity of a=1cm. The use of silicone rubber was carefully considered owing, among other, to its elastic properties frequency-dependent.

1. M. Oudich et al, New. J. Phys. 12 (2010) 083049

2. M. Oudich et al, Appl. Phys. Lett. 97 (2010) 193503

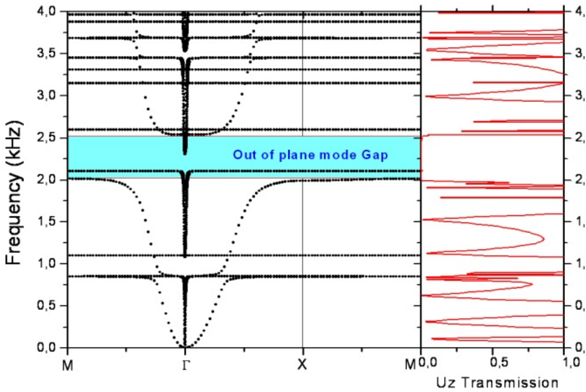

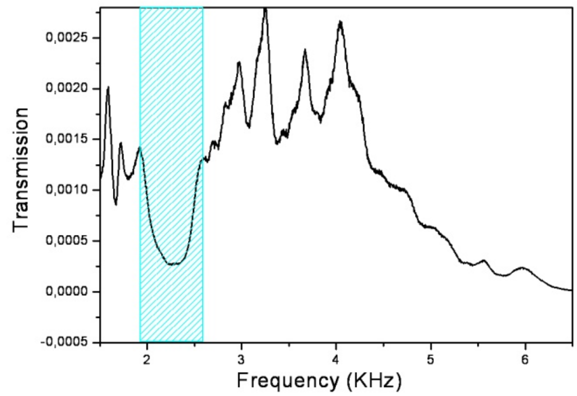

5G-4

5:15 PM **Locally resonant structures for low frequency surface acoustic band gap applications**

Abdelkrim Khelif[1], Younes Achaoui[2]; [1]*CNRS/GeorgiaTech, France,* [2]*Femto-st Institute, France*

Background, Motivation and Objective

Basically, the band gaps can originate from the Bragg reflections resulting from the periodic-ity of the structure. In this case, the spatial period of the crystal is of the same order of mag-nitude than the acoustic wavelength at the central frequency of the gap. Another approach to realize low frequency acoustic band gaps, while utilizing lattice constants much shorter than the acoustic wavelength, is to use an acoustic metamaterial based on locally resonant struc-ture.

Statement of Contribution/Methods

We investigate theoretically and experimentally the propagation of acoustic waves in a two-dimensional array of cylindrical pillars on the surface of a semi-infinite substrate. Through the computation of the band structure of the periodic array and of the transmission of waves through a finite length array, we study the surface propagating modes in the non-radiative region of the substrate, or sound cone, as limited by the slowest bulk acoustic wave. Numeri-cal simulations are based on the efficient finite element method and considering Lithium Niobate pillars on a Lithium Niobate substrate.

Results

In the band structure, guided modes define band gaps that appear at frequencies markedly lower than those expected from the Bragg mechanism. We identify them as originating from local resonances of the individual cylindrical pillars and show their dependence with the geometrical parameters, in particular with the height of the pillars. The frequency positions of these band gaps are invariant with the symmetry and thereby the period of the lattices, which is unexpected in band gap based on Bragg mechanism. The role of the period remains impor-tant for defining the non-radiative region limited by the slowest bulk modes and influencing the existence of new surface mode of the structures.

Discussion and Conclusions

The band structures of square, triangular and honeycomb arrays show that its possess the characteristic of an acoustic metamaterial. Their band gaps are originating from local reso-nances of the individual cylindrical pillars and sensitive to their geometrical parameters. The transmission calculation corroborates very well with the band structure and highlights the ma-jor role of the local resonance of single pillar in the opening the low frequency band gap. In this case, it is valid to expect the same position band gap occurring in any other ordered or disorder structures.

5G-5

5:30 PM Visualization of negative refraction of surface acoustic waves by numerical simulations and experiments

Istvan A Veres[1,2], Bernhard Reitinger[1,2], Thomas Berer[1,2], Peter Burgholzer[1,2], Oliver B. Wright[3], Osamu Matsuda[3]; [1]Christian Doppler Laboratory for Photoacoustic Imaging and Laser Ultrasonics, Linz, Austria, [2]Research Center for Non Destructive Testing GmbH, Linz, Austria, [3]Graduate School of Engineering, Hokkaido University, Sapporo, Japan

Background, Motivation and Objective

Periodic structures form phononic crystals (PCs) for elastic waves. These phononic materials are very promising for applications in the control of sound. Scattering of elastic waves in such structures lead to various effects such as stop bands and negative refraction. The elastic waves are heavily damped in a stop band, whereas negative refraction allows elastic waves to be focused. Negative refraction has been extensively investigated in bulk or slab phononic crystals, but much less so for surface acoustic waves (SAWs).

Statement of Contribution/Methods

We investigate numerically and experimentally the negative refraction of SAWs in two-dimensional PCs (2DPCs) in the MHz range made up of triangular lattices of holes. We performed high-performance time-domain simulations of the propagating broadband SAWs with the Finite Element Method (FEM). Time domain simulations are a powerful tool in the investigation of PCs, since numerical models allow the investigation of the scattering of SAWs in the same geometry as the real phononic crystal sample but with full 3D resolution of the elastic fields. The broadband SAWs are experimentally imaged in the MHz range by means of pulsed optical excitation and contactless, broadband interferometric detection over areas of the order of 10 mm^2.

Results

Real-time simulations and experiments are presented on an air-aluminum 2DPC with cylindrical holes of diameter 440 μm and spacing 600 μm arranged in a triangular lattice. The band structure of the 2DPC is evaluated from numerical simulations by spatial-temporal Fourier transforms. Negative refraction of SAWs is investigated numerically and experimentally by the transmission of the elastic waves through multiple layers of the 2DPC. At particular frequencies the triangular lattice shows negative refraction which results in the focusing of the elastic waves on the opposite side of the PC. The Figure shows the focusing of the 2.6 MHz component of the simulated SAW due to negative refraction after passing through a 2DPC with 7 layers.

Discussion and Conclusions

In conclusion we have imaged the scattering and the focusing of SAWs in a 2DPC. The results show evidence for negative refraction of the SAWs at frequencies where the group and phase velocities are opposite in sign. Good agreement is obtained between experiments and the numerical simulations.

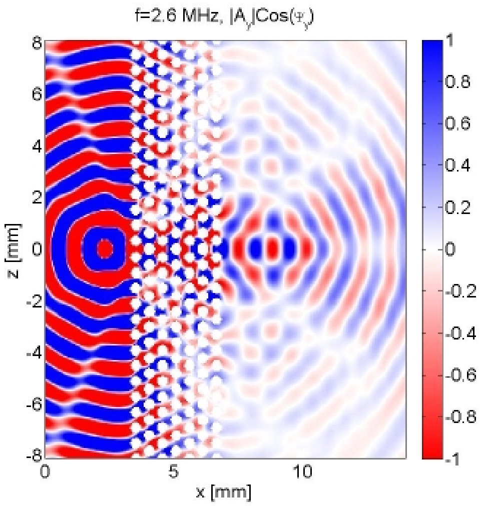

5G-6

5:45 PM Recent advances in the negative refraction of longitudinal waves in an elastic phononic crystal

Anne-Christine HLADKY[1], Charles Croënne[1], K. Raymond Olympio[1], Jérôme Vasseur[1], Bertrand Dubus[1], Bruno Morvan[2]; *[1]IEMN, ISEN Department, Lille, Nord, France, [2]LOMC, Le Havre, France*

Background, Motivation and Objective

Left-handed media are artificial media where acoustic waves propagation exhibits unusual properties: phase and group velocities of opposite sign, negative refraction index, inverse Doppler effect. These kind of phenomena arise for instance in phononic crystals (PC), which are periodic arrangements of several materials, and encouraging results have been obtained with a PC made of stainless rods immersed in a fluid [A. Sukhovich, et al, Phys. Rev. Lett., 154301 (2009)]. Recent studies on left-handed acoustic (fluid) media have shown their capabilities to provide a resolution better than the diffraction limit and to produce real images with a simple flat lens, also called superlens. In the present study, theoretical and experimental results are presented on the development of elastic left-handed materials superlenses.

Statement of Contribution/Methods

Numerical simulations are performed to design left-handed elastic PC in terms of constitutive materials, lattice geometry and filling fraction of the inclusion. The complexity in designing such PC arises from the requirements that the dispersion curves must meet: phase and group velocities of opposite signs for an isolated branch exhibiting quasi-longitudinal behaviour, circular equifrequency contours indicating isotropy of phase velocity, matching of phase velocities in the PC and in the external medium. Moreover, wave injection phenomenon inside the PC is studied and shows the importance of the interface shape between the PC and the external fluid domain to increase the energy transmitted to the PC.

Results

Experiments are performed on ultrasonic longitudinal waves transmitted through a PC and detected by laser vibrometry. Negative refraction angles are measured, demonstrating that the PC behaves as a left-handed elastic material.

Discussion and Conclusions

The negative refraction of a longitudinal wave through an immersed PC has been demonstrated. Results on the development of a flat elastic super-lens and the production of real acoustic images from a point source are given. This work was supported by the French "Agence Nationale pour la Recherche" (SUPREME project).

6G - SAW Design, Integration & Tunability

Carribean Ballroom VI

Thursday, October 20, 2011, 4:30 pm - 6:00 pm

Chair: **Clemens Ruppel**
TDK-EPC

6G-1

4:30 PM **Electrostrictive thin films: an alternative to piezoelectricity**

emmanuel defay[1]; [1]*CEA Leti Minatec, France*

Background, Motivation and Objective

Electrostriction, the second order electromechanical effect, can be seen as dc controlled piezoelectricity. Therefore, an electrostrictive resonator will exhibit resonance only when a dc field is applied. Moreover, the "strength" of this enhanced piezoelectricity is also dc controlled and induces a linear dependency of the piezoelectric coefficient versus voltage. This property gives the ability to dc tune the resonance frequency of electrostrictive resonators. The tuning range can reach several per cent which is very interesting for RF agile applications. In this talk, we will review the best electrostrictive thin films materials (mainly perovskites) and the different techniques to synthesize them. A special focus will be dedicated to agile RF resonators and filters: model, experimental results, main issues and future trends.

Statement of Contribution/Methods

Results

Discussion and Conclusions

6G-2

5:00 PM **Very large bandwidth IF SAW filters using leaky waves on LiNbO3 and LiTaO3**

Mohamed El Hakiki[1], Jacques-Antoine Damy[1], Heiko Hartmann[2], Jean-Michel Brice[1]; [1]*EPCOS Sophia Design center, Sophia-Antipolis, -, France,* [2]*EPCOS, Germany*

Background, Motivation and Objective

It was previously reported that a leaky wave propagating on LiNbO3 Y+41°X or LiTaO3 Y+36°-X substrates has a relatively low temperature coefficient of frequency (TCF) and a large electromechanical coupling factor (K^2), but those substrate are used mainly in conjunction with resonant structure that is limiting the amount of bandwidth that can be reached with reasonable performances.

Statement of Contribution/Methods

In this study, we investigated the performance of wide band IF SAW filters using a fan shaped structure and leaky wave mode.

Results

The optimization of Hanma Hunsinger cell on those substrates enables to have a good reflection coefficient (r) and a large electromechanical coupling factor (K^2) for leaky wave. In addition, those parameters allowed for minimizing the effect of the Raleigh wave.

The experimental results show that large bandwidths (55%) are reached with reasonable losses (13dB) and good return loss (10dB) for an IF SAW filter built on LN Y+41°-X and using fan shaped structure (fig 1).

Discussion and Conclusions

The previous state of the art for the wide bandwidth (55%) IF SAW filter using rayleigh wave and fan shaped structure had loss around 20dB for 5dB return loss, so the results obtained using leaky wave and fan shaped design are very promising.

THURSDAY ORAL

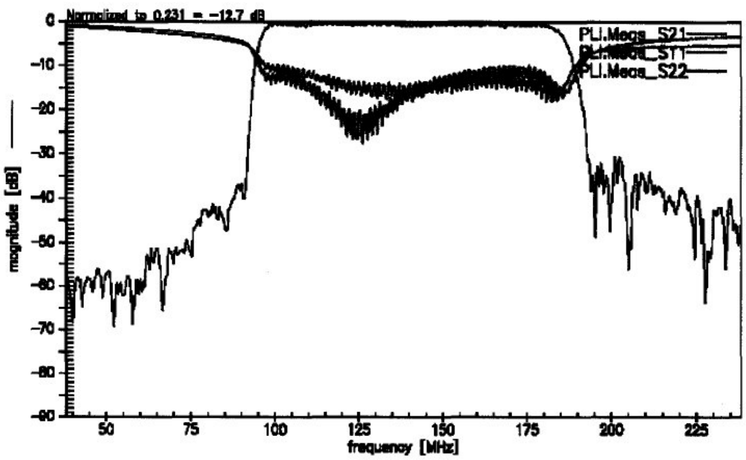

6G-3

5:15 PM Low Loss Wide Band Microwave Filters Using SAW Devices Combined with Microstrip Lines

Hiroyuki Odagawa[1], **Takaoki Taniguchi[1]**, Yoshifumji Shimoshio[1], Yoshitada Iyama[1], Kazuhiko Yamanouchi[2]; [1]Information, Communication and Electronic Engineering, Kumamoto National College of Technology, Koshi, Kumamoto, Japan, [2]Tohoku University, Japan

Background, Motivation and Objective

Recently, traffic in mobile communication has increased remarkably with the development of new mobile systems such as smart phone and cloud computing coupled with new information services. As the results, frequency range and band width of the mobile communication systems are to become higher and wider. Consequently, low loss SAW filters in microwave range with wide band characteristics must be required in the future generation.

Statement of Contribution/Methods

It is known that the band width of low loss SAW devices largely depends on electromechanical coupling coefficient, so that it is difficult to obtain the wide band characteristics using a conventional substrate and IDTs. Therefore, various kinds of research have been conducted, such as investigation of new substrates and SAW modes, development of new IDT structure and so on. In this paper, we propose a new type of low loss wide band microwave filters, in which SAW devices and microstrip lines are combined effectively. Characteristics of this filter in pass band mainly depend on microstrip lines, and cut-off characteristics are mainly realized by SAW devices. Using the configuration that SAW devices are coupled with microstirp lines, we can realize the ultra wide band and low loss characteristics in microwave range.

Results

Simulations using an equivalent circuit model show that wide band and low loss characteristics can be obtained. Also, in experiments, a prototype filter with basic structure achieves excellent characteristics; insertion loss is less than 1dB, bandwidth is approximately 40% and center frequency is 3.5GHz. Shape factor between -1dB and -10dB is about 0.8 for the prototype filter. Moreover, simulation results for improved structure show that the shape factor can be more than 0.9 using properly designed SAW devices.

Discussion and Conclusions

The new type of low loss wide band microwave filters which combine SAW devices and microstrip lines we propose in this paper can apply to higher frequency up to 10GHz range relatively easily. The characteristics of this filter depend on the IDT structure especially in the cut-off region, so that optimization of the IDTs is very important research subject. It will achieve a better cut-off characteristic than obtained one at this stage.

6G-4

5:30 PM A modular SAW filter design approach for multiband filtering

Xiaoming LU[1], Jeffery Galipeau[2], Koenraad Mouthaan[1]; [1]*NUS, Singapore,* [2]*TriQuint Semiconductor Florida, USA*

Background, Motivation and Objective

The trend in frequency allocation is to release more spectrum for data services. Since many of the band allocations are adjacent to each other, switched SAW filters are well suited to utilize these bands. Traditional switched filter banks are difficult to accomplish in reasonable size and cost. Other research work on switched SAW/BAW/FBAR filters design are reported which use additional elements such as transistors, capacitors or inductors [1, 2, 3]. This paper proposes novel modular SAW filter based topologies which reduce the size and the need of passive elements. A fully packaged feasibility study is presented in the 700 MHz frequency range currently allocated to LTE bands.

Statement of Contribution/Methods

The goal of the current research is to develop practical SAW filters which can switch between adjacent bands or band edges. The design is realized by integrating SAW resonator die and GaAs SPST/SPDT switch die into a common package. During design procedure, parasitic inductances, coupling capacitances, isolation of off state switches are addressed using a linear circuit solver and a 3D EM model which predicts potential problems of degraded shape factor of filter pass bands, decreased coupling coefficient of SAW substrates, etc.

Results

This paper investigates modular ladder type topologies for SAW filters. We achieved a center frequency shift greater than 2.5%, or the lower band edges shifted around 0.6%, with each filter fractional bandwidth around 1.3%, and they maintain typically 12dB return loss and 20dB rejection.

Discussion and Conclusions

Modular SAW filters around 700 MHz are fabricated and tested. The performance in rejection bands can be traded off with the filters' insertion loss which depends on different application requirements. The performance can be improved by compact layout design or different integration technologies to reduce the parasitic effects.

References

[1] N. O. Fenzi et. al, "Multimode bandpass SAW filter using Reconfigurable Resonance Technology", 2010 IUS

[2] S. Aliouane et. al, " RF-MEMS Switchable Inductors for Tunable Bandwidth BAW Filters ", 2010 Int. Conf. on Design & Tech. of Integrated Systems in Nanoscale Era

[3] M. El Hassan et. al, "Tunability of Bulk Acoustic Wave Filters Using CMOS Transistors: Concept, Design and Implementation", 2010 IEEE RFIC

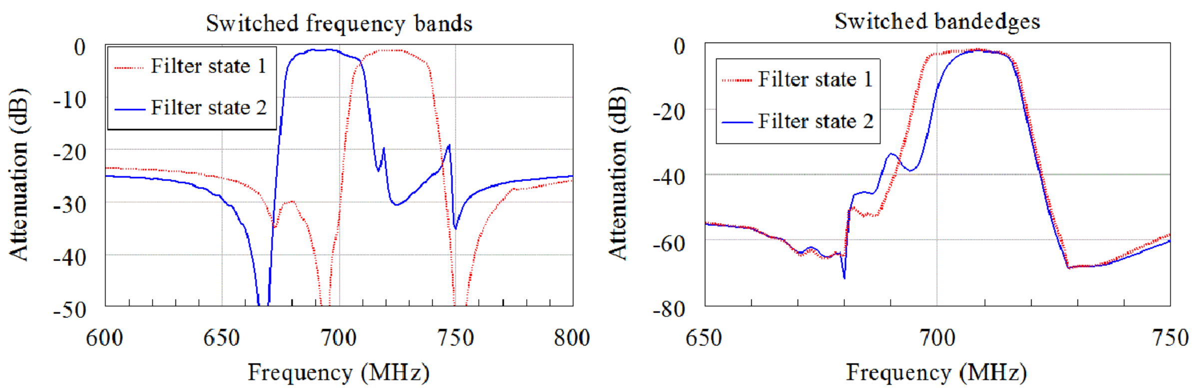

Fig. 1 Two types of performances of insertion loss by 3D model EM simulation

6G-5

5:45 PM SPUDT Cell with One-Wavelength Period and Quarter-Wavelength Electrodes

Sergey Biryukov[1], Guenter Martin[1], **Hagen Schmidt[1]**, Bert Wall[2]; [1]IFW Dresden, Dresden, Germany, [2]Vectron International GmbH & Co. KG, Teltow, Germany

Background, Motivation and Objective

Single-phase unidirectional transducers (SPUDT) on surface acoustic waves (SAW) are important elements for development of low-loss SAW devices. For one-track transducers with a periodic cell width, P, equal to a SAW wavelength several types of SPUDT cells as DART, EWC, Hanma-Hunsinger, FEUDT, and TF are known. A multi-track transducer PMUDT was proposed as well. All mentioned cells include electrodes of one-eighth wavelength width or less. But for 2.45 GHz, standard lithography requires electrode (and gap) widths to be about quarter wavelength. Several SPUDT cells with quarter-wavelength electrodes or wider both for one- and multi- track transducers have been developed by increasing cell period, P, up to 2, 3, or 4 wavelengths. However such a design leads to unavoidable loss of SAW energy to bulk waves. Thus, a new solution is required for high frequencies.

Statement of Contribution/Methods

A novel SPUDT cell with two quarter-wavelength electrodes per one-wavelength period is proposed for the multi-track solution consisting of alternating active IDT tracks and passive reflector tracks. By shifting adjacent tracks relative to each other a phase shift between effective reflection and transduction centers is created. The impact of passive tracks is caused only by diffraction of waves, which are excited in active IDT tracks. To have a good interaction between tracks they should have apertures, which are comparable with wavelength and can be differently wide. The structure is called here active-passive-track unidirectional transducer or APTUDT.

Results

Electrical admittance Y of the APTUDT cell placed on 128 YX $LiNbO_3$ has been simulated by 3D FEM in vicinity of 2.45 GHz for active and passive track apertures equal to P and 1.5 P, respectively, with Al electrode thickness ratio h/P = 0.105. The electrical admittance of APTUDT cell demonstrates a splitting of resonance peak as for any SPUDT cell. Two resonance frequencies and two antiresonance frequencies are clearly seen and allow calculating the phase shift between transduction and reflection centers. The phase shift of 45 degrees, which needs for complete unidirectionality, is achieved. The unidirectional behavior of an APTUDT has been checked experimentally in low frequency range near to 430 MHz by means of test structure on 128 YX $LiNbO_3$, which was not optimized for complete unidirectionality. It included 60 periodic cells and 12 tracks, and two split-electrode IDTs on each side needed as receiving IDTs. The unidirectional effect is clearly visible.

Discussion and Conclusions

A periodic cell forming a multi-track unidirectional transducer on SAW has been proposed. It contains only two electrodes and two gaps with quarter-period width in direction of propagation in each track. That is such a structure has maximal possible dimensions of its elements for cell period equal to one wavelength. It permits to implement SPUDTs for 2.45 GHz in spite of the existing technological limitations.

THURSDAY ORAL

Thursday Poster Sessions

P3Aa - Characterization of Soft Tissue

Carribean Ballroom III-V

Thursday, October 20, 2011, 9:30 am - 1:00 pm

Chair: **Michael Oelze**
University of Illinois

P3Aa-1

Properties of PVA Tissue Phantoms Produced by Directional Solidification

Gideon Gouws[1], Dayna-Maree Kivell[1], Andrew Dawson[2]; [1]*School of Engineering and Computer Science, Victoria University of Wellington, New Zealand,* [2]*Engineering and Applied Physics, Industrial Research Limited, New Zealand*

Background, Motivation and Objective

The use of tissue mimicking materials plays an important part in medical ultrasound research as it allows the development of procedures and callibration of equipment without the need for real tissue samples. Conventional phantom materials are typically produced from polyvinyl alcohol (PVA) solutions in a repeated freeze-thaw process. However, such phantoms have the drawback that they do not accurately represent the important anisotropic properties of real tissue. Recent work from our group has shown that anisotropic phantoms can be produced by a freeze casting process of aqueous PVA solutions, followed by freeze drying to remove the ice crystals. These phantoms showed good agreement in ultrasound velocity and attenuation with real tissue and presented a good starting point for the development of advanced tissue phantoms.

Statement of Contribution/Methods

This presentation describes further development of this phantom production process, aimed at a better understanding of the structural evolution and improved control of the material microstructure and process repeatability. This was achieved by extending the original freeze casting method to a two-zone directional freezing process, facilitating accurate control of both the freeze rate as well as the temperature gradient across the sample. In addition, further control over the microstructure was achieved by the use patterning to control the initial ice nucleation and growth morphology.

Results

Once ice crystals had been removed by sublimation, the horizontal and vertical cross section of the samples were examined by SEM. The remaining PVA shows a porous structure, with irregular tubes aligned along the direction of solidification. Some variation is observed from the first to freeze to the last to freeze ends.

In cross sectional view, three different length scales can be distinguished in this structure:
1. The cells have a typical wall thickness of approximately 10 um, with a spacing of 10 - 20 um between cells.
2. The cell walls contains further microstructure, with typical dimensions < 1 um.
3. The elongated cell walls are alignment over regions with a typical diameter of 1 - 4 mm.

The cell spacing could by controlled by the freeze rate, with smaller cells resulting as the freezing rate is increased. The alignment of cell walls in micro regions was improved by the use of nucleation patterning lines.

Discussion and Conclusions

A directional freezing process is shown to lead to a complex microstructure in aquous PVA, showing significant promise in the application of realistic anisotropic tissue phantoms for ultrasound applications. Factors such as PVA concentration, freeze rate and nucleation patterning on the resultant microstructure were investigated. A simple model will be presented to explain the formation of the observed microstructure. The mechanical and acoustic properties of these samples are currently being measured for comparison to real tissue.

P3Aa-2

Characterization of Tissues in the Pulley System Using High-Frequency Ultrasonic Backscatter Signals

Yi-Hsun Lin[1], Tai-Hua Yang[1], Shyh-Hau Wang[1], Fong-Chin Su[1]; [1]*National Cheng Kung University, Taiwan*

Background, Motivation and Objective

Trigger finger (TF) is a common disease that is usually diagnosed by palpating the first annular pulley region of the hand. The accuracy of palpation examination certainly is largely depending on physician′s clinical experience. Recently, ultrasound images have been explored in an attempt to provide an objective means for assessing TF. However, with an average thickness of around 0.5 mm, the resolution of ultrasound scanners commonly applied in clinics is inadequate to sensitively discern the complexity of tissues in the pulley. To jump over this hurdle, high-frequency ultrasound images incorporated with ultrasonic parameters were implemented to further characterize the annular pulley and surrounding tissues in the hand.

Statement of Contribution/Methods

Ex vivo experiments were performed to respectively measure the skin, fat, annular pulleys, and superficial tendons of the first annular pulley region from 10 cadavers. The excised tissues were immersed in a saline tank and were measured by a 30 MHz high-frequency ultrasound system. In addition to acquiring B-mode images, ultrasonic parameters, including integrated backscatter (*IB*) and Nakagami parameter (*m*), were subsequently calculated from backscattering signals of the corresponding regions.

Results

High-frequency ultrasound images have shown to provide a sufficient resolution able to differentiate variation among each tissue structure. The *IB* of skins, fat, annular pulleys, superficial tendons was respectively measured to be -82.84±1.95 dB, -82.76±1.47 dB, -80.14±1.93 dB, and -78.87±1.89 dB; while the corresponding *m* was 0.50±0.07, 1.03±0.14, 0.91±0.12, and 0.42±0.10. Specifically, the *IB* of the annular pulley was much larger than that of the fat ($p<0.01$). A significant difference of *m* between the annular pulley and tendon ($p<0.01$) also can be found. In addition, *m* of the fat tissue was much larger than that of the skin ($p<0.01$).

Discussion and Conclusions

Although high-frequency ultrasound image can be utilized to readily differentiate the tissue variation, the ultrasonic parameters provide a potential to further quantitatively distinguish annular pulley and surrounding tissues. It is due to that *IB* and *m* vary with the states of tissue composition and arrangement. The probability density distributions of ultrasonic backscattered envelopes between annular pulley and tendon were quite different even though these two tissues consist of similar collagen fiber composition. It could be owing to the difference of collagen fiber orientation between these two tissues. This study has demonstrated that high-frequency ultrasound image in conjunction with ultrasonic parameters are able to characterize the annular pulley and surrounding tissues for further diagnosis on the syndrome of TF.

P3Aa-3

Comparison of Ultrasonic Measurements of Nulliparous versus Mulitparous Cervices

Lisa Reusch[1], Lindsey Carlson[1], Mark Palmeri[2], Jeremy Dahl[2], Helen Feltovich[1,3], **Timothy Hall[1]**; [1]Medical Physics, University of Wisconsin - Madison, USA, [2]Biomedical Engineering, Duke University, USA, [3]Maternal Fetal Medicine, Intermountain Healthcare, USA

Background, Motivation and Objective

Preterm birth costs the US over $26 billion annually and can lead to life-long health complications. Cervical dysfunction plays a large role in preterm birth, but a lack of noninvasive technology sophisticated enough to interrogate the cervical microstructure makes a quantitative assessment of cervical function challenging. Collagen content and alignment gives the cervix its strength and undergoes rearrangement long before gross changes (shortening, softening) are found, so early detection of this rearrangement is important. Additionally, after birth occurs for the first time, the cervix remodels itself, but may be very different from before this first pregnancy. We aim to assess the state of the cervix using quantitative ultrasound (QUS) techniques and acoustic radiation force impulse (ARFI) measurements. Preliminary results indicate that both QUS and ARFI measurements are sensitive enough to detect differences between a cervix that has never had babies (nulliparous) and one that has previously had babies (multiparous).

Statement of Contribution/Methods

Three nulliparous and three multiparous hysterectomy specimens were scanned with a Siemens Acuson S2000 ultrasound machine using a prototype catheter transducer (Siemens Medical Solutions USA, Malvern, PA, USA). Radiofrequency echo data were acquired with the transducer aperture aligned parallel to the endocervical canal. The angle of the acoustic beam was changed electronically between ±40° to assess anisotropic acoustic propagation. The integrated backscattered power was calculated for each angle and compared to normal incidence. Similar data were collected from a phantom with spherical scatterers for system calibration. The shear sound speed of the tissue samples was then measured using ARFI measurements for angles of 0° and ±20°.

Results

There was a clear difference in the backscattered power loss (BSPL; compared to normal incidence) between the two groups. Nulliparous cervices showed a BSPL of about 25 dB at 20° beyond that for a phantom with spherical scatterers. However, the BSPL for the multiparous group was much smaller (5 dB at 20°). Additionally, the BSPL for nulliparous cervices were very symmetric about 0° whereas the BSPL for multiparous cervices were asymmetric about 0°. These results strongly suggest that, not only is the organization different, but also there is greater collagen alignment in nulliparous vs. mulitparous cervices. Finally, we see different shear sound speeds in nulliparous cervices (around 4.5m/s) vs. multiparous cervices (around 3.0m/s).

Discussion and Conclusions

Results suggest a signifficant difference in collagen organization between nulliparous and multiparous cervices. Future studies will aim to quantify this difference and measure the change throughout pregnancy. Early detection of changes in microstructure may open pathways to earlier, more specific interventions for preterm delivery.

P3Aa-4

Attenuation estimation using a synthetic aperture focusing technique

Roberto J. Lavarello[1], Goutam Ghoshal[2], Michael L. Oelze[2]; [1]Seccion Electricidad y Electronica, Pontificia Universidad Catolica del Peru, Peru, [2]Department of Electrical and Computer Engineering, University of Illinois at Urbana-Champaign, USA

Background, Motivation and Objective

Diffraction effects resulting from radiation of ultrasound sources pose problems for ultrasonic exams. In qualitative ultrasound imaging (i.e., B-mode), problems arising from diffraction are related to loss of image quality, (i.e., spatial resolution and contrast). In quantitative imaging, improper diffraction compensation results in loss of accuracy when estimating parameters such as attenuation coefficients (ACs). Although techniques have been developed to correct for diffraction effects for both qualitative and quantitative imaging, these two modalities have largely been treated separately in the specialized literature. The goal of this study is to explore synthetic aperture focusing techniques (SAFT), which have been successfully employed to reduce beamwidth spreading in B-mode imaging, to minimize diffraction effects when estimating ACs from backscatter.

Statement of Contribution/Methods

The ability of SAFT to produce more accurate attenuation estimates was explored experimentally. A flat circular piston with a 0.25" diameter and 3.5 MHz center frequency was used to collect radiofrequency (rf) data. The imaging targets were two agar phantoms with attenuation coefficients equal to 0.4 dB/cm/MHz (phantom A) and 0.7 dB/cm/MHz (phantom B). Both phantoms were raster scanned over a 4 cm by 4 cm area at 0.75 mm steps (i.e., a dataset of 54 rf lines per 54 scan sections). 3D-SAFT volumes were created using conventional delay-and-sum. For both rf and 3D-SAFT datasets, 54 amplitude profiles were obtained by averaging the envelopes of all data lines within each section. The amplitude profiles were gated using 6 mm overlapping rectangular gates centered within the phantom at five depths between 5.2 and 6.5 cm. ACs at all five different depths and 54 sections were estimated in time domain by dividing the slope of the log-compressed gated amplitude profiles vs. depth by the center frequency of the transducer.

Results

The estimated ACs for phantom A using rf and 3D-SAFT data were 0.64 +/- 0.22 dB/cm/MHz and 0.42 +/- 0.22 dB/cm/MHz, respectively. For phantom B, the estimates using unfocused radio-frequency and 3D-SAFT data were 1.00 +/- 0.22 dB/cm/MHz and 0.76 +/- 0.24 dB/cm/MHz, respectively. Therefore, the use of unfocused radio-frequency data resulted in consistent over-estimation of ACs whereas the estimates using SAFT exhibited high accuracy (i.e., maximum estimation bias of 9% for SAFT data vs. 43% for rf data). The precision was comparable for both approaches.

Discussion and Conclusions

The preliminary experimental results obtained in this work indicate that SAFT has potential for simplifying the ability to correct for diffraction effects when estimating attenuation coefficients from backscatter. Further, these results suggest beamforming techniques can be valuable tools for improving the accuracy of quantitative ultrasonic imaging. This work was supported by NIH Grants R21-CA139095 and R01-EB008992.

P3Aa-5

Imaging of Visceral Fat in Living Rabbit by Using Detection of Ultrasonic Velocity Change

Hiromichi Horinaka[1], Toshiyuki Matsunaka[1], Yuya Ohara[1], Yoshinori Maeda[1], Yu Izukawa[1], Kazune Mano[1], Tetsuya Matsuyama[1], Kenji Wada[1]; [1]*Osaka Prefecture University, Japan*

Background, Motivation and Objective

Development of the noninvasive diagnostic imaging equipment of visceral fat in the early stage has been eagerly anticipated because the visceral fat often results in significant impairment of health. It has been known that ultrasonic velocity of each biological tissue shows the different temperature dependence. Therefore, the fat distribution in living body may be determined using temperature dependence of ultrasonic velocity. We already applied the method using detection of the ultrasonic velocity change caused by light irradiation to image the fat distribution in phantoms.

In this study, we performed imaging the visceral fat in living rabbits. The ultrasonic transducer was employed to warm livers of rabbits instead of light irradiation because the ultrasonic wave could reach to deep-lying tissue beneath the body surface.

Statement of Contribution/Methods

The ultrasonic transducer for warming was placed aside of the imaging array transducer. We used two groups of rabbits to characterize levers of living rabbits. Some rabbits were fed on the standard diet and other rabbits were fed on the high fat diet. Ultrasonic echo RF signals from the lever of rabbits under anesthesia were detected by the ultrasonic array transducer before and after the ultrasonic irradiation for warming. The irradiation time was 20s and the irradiation power was $1W/cm^2$ within the sufficient safety. The normal B-mode images and the ultrasonic velocity-change images were constructed from the RF data.

Results

Figure 1 show images of levers of rabbits A and B which were fed on the standard diet and the high fat dietfor, respectively. Figures 1 (a) and (b) show the normal B-mode images of the rabbit A and the rabbit B, respectively. The difference between these B-mode images is not clear. Figures 1 (c) and (d) show the images using ultrasonic velocity-change of the rabbit A and the rabbit B, respectively. Dark portions displaying the region of $+\Delta v$ are dominant in Fig.1 (c). On the other hand, white portions displaying the region of $-\Delta v$ are dominant in Fig.1 (d).

Discussion and Conclusions

It is confirmed that the ultrasonic velocity-change images reflect the fat accumulation level in lever of rabbit fed on the standard diet and that on the high fat diet. The ultrasonic velocity-change imaging method has the possibility of application to a diagnostic monitor of visceral fat in a living human body.

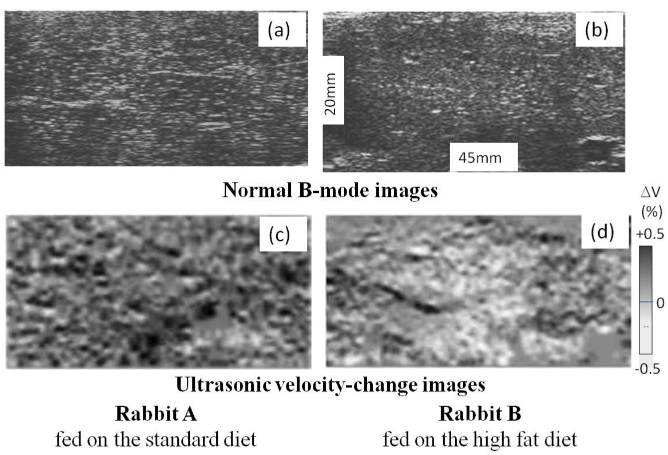

Fig.1 B-mode images and ultrasonic velocity-change images of lever of living rabbits A and B. The rabbit A was fed on the standard diet and the rabbit B was fed on the high fat diet for 4 weeks.

P3Aa-6

Nonlinear Parameter imaging to characterize HIFU ablation: in vitro results in porcine liver

François Varray[1,2], Jérémy Chenot[3], Olivier Basset[1], Piero Tortoli[2], David Melodelima[3], Christian Cachard[1]; [1]Université de Lyon, CREATIS ; CNRS UMR5220 ; INSERM U1044 ; INSA-Lyon ; Université Lyon 1, France, [2]MSD Lab, University of Firenze, Italy, [3]INSERM U1032, Université de Lyon, France

Background, Motivation and Objective

Nonlinear ultrasound imaging is used in various applications such as tissue characterization, harmonic or contrast imaging. For all these methods, the tissue nonlinear coefficient β is responsible for the harmonic components increase. In a previous work (Varray >*et al.*, IEEE IUS 2009), we have proposed a new method to image the nonlinear coefficient in echo mode configuration. Results obtained in simulation showed a good agreement with theoretical values and first experimental images on phantoms were proposed. The present work reports the first *in vitro* results obtained when imaging the nonlinear parameter of porcine liver treated with high intensity focussed ultrasound (HIFU).

Statement of Contribution/Methods

The extended comparative method (ECM) is able to image the relative nonlinear coefficient of an inhomogeneous nonlinear medium by comparing the second harmonic of echoes from different tissue regions. The possibility of using the ECM as imaging technique to characterize HIFU lesions is investigated by estimating the nonlinear coefficient of *in vitro* porcine livers before, after 20 seconds of HIFU therapy, and after complete HIFU ablation. The difference between the nonlinear coefficient maps obtained at different treatment phases is used to estimate the evolution of the nonlinear coefficient.

Results

Fig. 1 presents the different resulting images obtained with the ECM. The yellow dotted line highlights the region where the nonlinear parameter was computed. The difference between the nonlinear coefficient maps obtained after and before the HIFU is shown in Fig 1.d. The red boxes presented in Fig 1 highlight the region where the nonlinear parameter may change due to the HIFU ablation. In this area, the border of the lesion is highlighted with a decrease of the nonlinear coefficient visible in the difference image (Fig 1.d blue color).

Discussion and Conclusions

The ECM imaging can bring new information for characterisation of HIFU treatments. Initial results demonstrate the feasibility of this application that can be combined with other measurements, such as elastography, to provide parametric images that could help the diagnosis and could be a useful complement to conventional sonograms. Further investigation is required to determine the full potential of ECM for visualizing and guiding HIFU therapies *in vivo* as well.

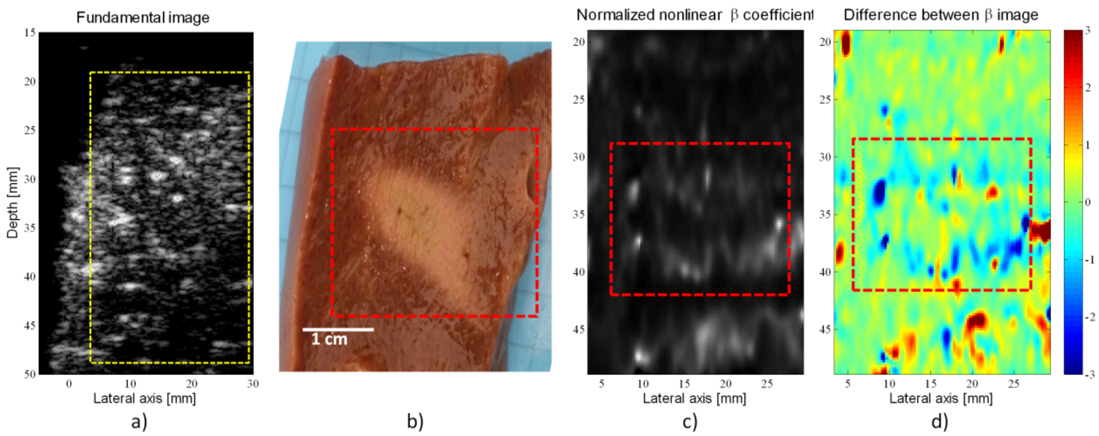

Fig. 1: (a) is the B-mode image, (b) the histological cut of the porcine liver, (c) the nonlinear coefficient map and (d) the difference in nonlinear coefficient map after and before HIFU. In (d), red color represent an increase and blue color a decrease of the nonlinear coefficient after the HIFU ablation.

P3Aa-7

Classifying Ultrasound Image Regions By Using Characteristics of ARFI Induced Tissue Displacement Temporal Profile

Liexiang Fan[1], Paul Freiburger[1], Bob Luick[1], David Duncan[1], Janelle O'Bannon[1], John Benson[1]; [1]*Ultrasound Business Unit, Siemens Healthcare, Issaquah, WA, USA*

Background, Motivation and Objective

Classifying ultrasound image regions with diagnostic information can directly assist clinicians and can also be used as a preprocessing stage in parametric image construction. Methods based on B-mode or Doppler information have been extensively investigated in the past. However these methods are more or less dependent on the imaging parameters configured in data acquisition. Here we present a method to extract information from an Acoustic Radiation Force Impulse (ARFI) induced displacement temporal profile as input features for a linear classifier which assigns each sample to one of either fluid, high stiffness, low stiffness or undetermined categories.

Statement of Contribution/Methods

Immediately after ARFI excitation, tissue displacement was estimated for ~8 miliseconds with a 7 to 10 kHz temporal sampling rate. Three parameters were derived from the displacement profile, 1) signal to noise ratio (SNR), 2) maximum displacement(Maxd), and 3) time-to-peak (TTP). The defined SNR corresponds to two major factors, low SNR in the echo signal and irregular motion of the tissue. A hypoechoic region such as lesions or acoustic shadowing may have low SNR in the echo signal, and fluid tissue has both low SNR and irregular motion due to the acoustic streaming effects. Using the three parameters the classifier assigns the tissue sample to the following categories: a) fluid –- low SNR, median to high maxD, and ignoring TTP; b) high Stiffness –- low TTP, median to high SNR, low to median maxD c) low stiffness – high TTP, median to high SNR, high maxD; d) undetermined – none of the above.

Results

The proposed method was tested both on a phantom which contains a fluid filled cyst and solid inclusions with various stiffness; two diagnostically confirmed human breast simple cysts, and five RF and Microwave ablated thermal lesions in ex-vivo bovine livers. A B-mode image was obtained in each case and was used to manually select the true category of tissues in phantom and human breast cysts. The B-mode image in RF and Microwave ablated thermal lesions did not show clear boundary definition of the lesion, therefore the histological picture of the thermal lesion was used to estimate the area of the stiff region. The performance of the classification was done by calculating the number of matched samples versus the total samples included in the classification. Using 35.6kPa as separation between low and high stiffness, for phantom and breast simple cysts we obtained a mean classification accuracy of 93%,; for thermal lesions, we obtained a mean classification accuracy of 81%.

Discussion and Conclusions

Prior research studies had reported success in detecting cysts or fluid using acoustic streaming imaging based on Doppler shift detection and correlation coefficient thresholding. Our work demonstrated that ARFI induced displacement temporal profiles are also well-suited for differentiating fluid tissue from solid tissue and separating high stiffness from low stiffness regions.

P3Aa-8

Skin lesions assessment using attenuating and statistical properties of backscattered ultrasounds

Hanna Piotrzkowska[1], **Jerzy Litniewski**[1], Elzbieta Szymanska[2], Andrzej Nowicki[1]; [1]Institute of Fundamental Technological Research, Warsaw, Poland, [2]Dermatology Clinic, CSK MSWiA Hospital, Warsaw, Poland

Background, Motivation and Objective

While the needle biopsy is still the gold standard in skin cancer diagnosis there is a growing interest in application of the high frequency ultrasounds for the skin lesions detection and their thickness assessment. The quantitative ultrasound can provide additional information, potentially helpful in diagnosis. The purpose of this study was to assess the usefulness of the attenuating and statistical properties of the backscattered ultrasounds for the skin tissue structure characterization.

Statement of Contribution/Methods

A group of patients (10 cases till now but the clinical research is continued and we expect much more cases in the next month) with diagnosed basal cell carcinoma (BCC) and precancerous lesions (AK - Actinic Keratosis) participated in this study. The ultrasonic data were obtained from pathological and healthy regions of the skin using a high frequency scanner (200 lines per image, 10 frames per second) operating at 30MHz. The transmitted and scattered echoes (sinusoidal or encoded) were sampled at 200MHz frequency with 12bits resolution. The received sequences were envelope detected (prior compressed if necessary) and displayed. Simultaneously, the RF data were stored separately and processed for attenuation coefficient (α) and signal statistics assessment. We have used K distribution to estimate the distribution of the experimental signals envelopes and effective number of scatterers (M). Prior to calculations the influence of diffraction/focusing and attenuation was compensated. Also, the minimal area of the tissue (ROI) necessary to give the results independent of the ROI- size was determined.

Results

For patients with basal cell carcinoma the attenuation coefficient was significantly higher than for the healthy ones (averaged $\alpha = 3.6 \pm 0.3$dB/MHz×cm and $\alpha = 2.2 \pm 0.1$ dB/MHz×cm, respectively). Also, precancerous skin lesions revealed increased attenuation (averaged $\alpha = 3.0 \pm 0.1$dB/MHz×cm). The averaged M parameter for BCC lesions equaled to $M = 1.1 \pm 01$ while for AK lesions and healthy skin was higher and equaled to $M = 1.94 \pm 0.02$ and $M = 1.93 \pm 0.1$, respectively.

Discussion and Conclusions

The results are encouraging however a lot of further study must be performed to assess diagnostic usefulness of the proposed method. Medical description of the remodeling of tissue structure in the BCC and AK lesions explains the experimental results. BCC is characterized by the clusters of tumor cells which are much bigger than the healthy skin cells and AK lesion cells too. The K distribution is sensitive to the number and uniformity of scatterers comprised within the resolution cell. The drop of M parameter of K distribution for BCC can be explained by the lower spatial density of scaterrers (cell clusters) comparing to the spatial density of cells in healthy skin and AK lesions.

P3Aa-9

Development of an agar phantom adaptable for visualization of thermal distribution caused by focused ultrasound

Jungsoon Kim[1], Moojoon Kim[2], Yejoon Park[3], Kanglyeol Ha[3]; [1]Tongmyong University, Korea, Republic of, [2]Physics, Pukyong National University, Korea, Republic of, [3]Pukyong National University, Korea, Republic of

Background, Motivation and Objective

The ultrasound wave has not only been used in medical diagnostics but also in medical treatment. In the case of ultrasound treatment, the high temperatures induced by focused ultrasound treatments necrotize a tumor lesion. Therefore, the ultrasound power and exposure time should be determined precisely. To satisfy of ultrasound treatment, the temperature distribution must be measured. In this study, an agar phantom adaptable for visualization of thermal distribution is developed.

Statement of Contribution/Methods

Cholesteric liquid crystals are used to visualize the thermal distribution in the phantom instead of human tissue. They are quite sensitive to temperature and show a variety of brightness within the temperature range on the order of 1 Deg. Microcapsules filled with the liquid crystals (produced on a commercial basis) were suspended in water with agar powder. Agar in a gel state was used as the phantom of human tissue because its acoustic characteristics are very similar to those of human tissue. A focusing ultrasound transducer was fabricated, and an agar layer mixed with thermochromic particles was molded. Using the transducer on the agar layer, the temperature distribution within the phantom was observed.

Results

Figure shows the pattern with the temperature distribution of the phantom. The degree of brightness corresponds to the temperature difference, as shown in index of the figure.

The bright region on the upper side of the figure is produced by the heat emanating from the surface of the transducer. On the basis of the result, it was found that the focal point in the phantom was heated to about 70 Deg.

Discussion and Conclusions

To investigate the temperature distribution in the phantom caused by the focused ultrasound, we proposed a new visualization method of measuring the temperature distribution. The ultrasound field was focused by a concave-type transducer in an agar layer mixed with thermochromic particles, and the color pattern change with the change in temperature was observed.

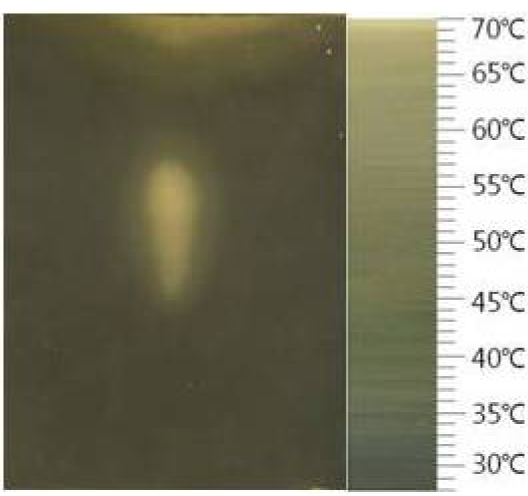

THURSDAY POSTER

P3Aa-10

The acoustic attenuation in an IEC agar-based tissue-mimicking material measured at 12 - 47 MHz

Chao Sun[1], Stephen Pye[2], Anna Janeczko[2], Bill Ellis[2], Mark Brewin[3], Mairead Butler[1], Vassilis Sboros[1], Adrian Thomson[1], Jacinta Browne[4], Carmel Moran[1]; [1]*Medical Physics, University of Edinburgh, Edinburgh, United Kingdom,* [2]*Medical Physics, NHS Lothian, Royal Infirmary of Edinburgh, Edinburgh, United Kingdom,* [3]*Department of Clinical Physics, Royal London Hospital, Barts and the London NHS Trust, London, United Kingdom,* [4]*School of Physics, Dublin Institute of Technology, Dublin, Ireland*

Background, Motivation and Objective

Medical applications of high frequency ultrasound (>20MHz) have increased in recent years with intravascular, superficial tissue, and pre-clinical imaging. Tissue Mimicking Material (TMM) is routinely used in test objects for testing at clinical frequencies as it mimics the speed of sound, attenuation and backscatter properties of soft tissue. This study investigated the attenuation of ultrasound in an IEC agar-based TMM over the frequency range 12 to 47 MHz at 21oC ± 1oC in order to asses its use for high frequency test objects.

Statement of Contribution/Methods

Experiments were performed based on a substitution technique using the Vevo770® pre-clinical ultrasound scanner (VisualSonics Inc., Toronto) and four transducers (nominal centre frequency bracketed): 710B (25 MHz), 707B (30 MHz), 704 (40 MHz), 711 (55 MHz). Thin slices of TMM (mean thickness range: 2.47mm - 3.17 mm) were encased in PVC rings and wrapped in Saran™ PVDC film, placed in a water bath and scanned. The radio-frequency (RF) data was captured. The attenuation coefficient was calculated over the 3 dB bandwidth of each transducer and a power law curve fit was applied to the data. 15 independent positions on each of the twelve TMM samples were measured and average parameters were calculated.

Results

The attenuation in TMM varies nonlinearly over the broad frequency range 12 to 47 MHz and its value with standard deviation is shown in Figure 1. The attenuation coefficients (relative to water) measured by transducers 710B, 707B, 704 and 711 are 0.45 ± 0.03 dB/cm/MHz, 0.53 ± 0.02 dB/cm/MHz, 0.51 ± 0.07 dB/cm/MHz, 0.58 ± 0.04 dB/cm/MHz, respectively.

Discussion and Conclusions

The attenuation in agar-based TMM increases with increasing frequency with a nonlinear relationship of f^1.27 but remains close to the low frequency value of around 0.5 dB/cm/MHz. The mean attenuation value is comparable to the result of Brewin(Brewin MP et al, Ultrasound Med & Biol 2008; 34: 1292-1306) in the frequency range of 17 – 23 MHz. The attenuation of water increases as f^2 and needs to be taken into account at high MHz frequencies for absolute attenuation calculation. This characterisation at frequencies greater than 20 MHz allows for this IEC agar-based TMM to be used with confidence in high frequency applications.

Fig. 1. The attenuation in TMM over the frequency range of 12-47MHz

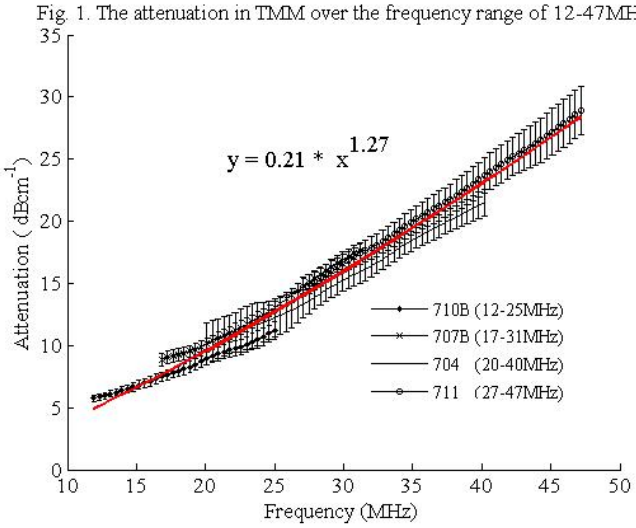

P3Aa-11

Experimental Verification of Blood Characterization Based on Ultrasonic Blood Flow Measurement

Naotaka Nitta[1], Hiroshi Masuda[2], Hidenori Suzuki[2]; [1]Human Technology Research Institute, National Institute of Advanced Industrial Science and Technology (AIST), Tsukuba, Ibaraki, Japan, [2]UNEX corporation, Japan

Background, Motivation and Objective

Blood viscosity is expected as an index for detecting the blood abnormality such as thrombosis and local aggregation of erythrocyte. However, since the viscosity of whole blood depends on the magnitude of shear rate as well as the blood abnormality, it is difficult to detect the blood abnormality by using the only blood viscosity information. Therefore, with the aim of attaining further detailed blood property, a method for extracting the feature parameters of shear rate-viscosity (SV) curve is proposed in this study.

Statement of Contribution/Methods

The feature parameters of SV curve are ultrasonically estimated. First, 2-D distribution of the beam-axis and lateral velocity components are obtained on the basis of the ultrasonic Doppler measurement and the incompressible condition. The obtained 2-D velocity vector distribution is divided into several ROIs. In each ROI, the viscosity coefficient (μ) and the shear rate (ε) are obtained by using a previously-proposed method (Nitta, 2009). The SV curve is obtained by consolidating μ and ε pairs in all ROIs. In order to extract the feature parameters of SV curve considering the non-Newtonian property of whole blood, a model function is introduced as $\mu=\alpha\ \varepsilon^{-\beta}$. Here, α and β are the feature parameters, and determined by the least-square method using the estimated SV curve.

Results

The feasibility of the proposed method was experimentally investigated by using the fresh bovine blood. A circulation system using silicone tube with a diameter of 4 mm was constructed, and a liter of citric acid-added fresh bovine blood was circulated in the circulation system. Mean velocity and temperature of blood were maintained constant at 31.6 cm/s and 37 °C, respectively. In order to mimic the blood property changes, the bovine blood was diluted by saline, and four different blood solutions with different hematocrit were prepared (43.3, 38.8, 35.8 and 32.8 %, respectively). RF signals (8 MHz) for Doppler measurement were acquired on the longitudinal cross section of the tube, by using the ultrasonic diagnosis equipment (UNEX, EF18G). Then, α and β of four different blood solutions were ultrasonically obtained. As the result, the estimated α and β correlated well with the hematocrit (α: $R^2 = 0.81$, β: $R^2 = 0.82$). In addition, α and β of four different blood solutions were measured by a viscometer and compared with the ultrasonically-estimated values. As the result, the ultrasonically-estimated α and β correlated well with those measured by the viscometer (α: $R^2 = 0.88$, β: $R^2 = 0.83$).

Discussion and Conclusions

Experimental results revealed that the changes of blood property could be discriminated by the ultrasonically-estimated feature parameters. In future work, the feasibility for human blood should be investigated.

P3Aa-12

Quantitative Ultrasound Assessment of Thermal Damage in MAT Tumors

Jeremy Kemmerer[1], **Goutam Ghoshal[1]**, Michael Oelze[1]; [1]University of Illinois at Urbana-Champaign, Urbana, IL, USA

Background, Motivation and Objective

High Intensity Focused Ultrasound (HIFU) is a promising means of non-invasive therapy. However, monitoring and assessment challenges for HIFU therapy remain, and conventional B-mode imaging is not reliable for detection and assessment of thermal lesions produced by HIFU. Quantitative ultrasound (QUS) has demonstrated success as a tool for tissue characterization and as a means to detect changes in tissue structure due to therapy. Therefore, it is hypothesized that QUS techniques can be used to assess thermal damage to tissues due to HIFU and to discriminate and quantify treated and untreated tissues.

Statement of Contribution/Methods

Freshly excised MAT tumors were sliced in half. Each half of each tumor sample was either treated in a saline bath at 60 °C for 10 min or remained untreated in 37 °C saline. The tumor slices were then scanned using a single-element 20 MHz f/4 transducer. From the ultrasonic scans, the backscatter coefficient was calculated and parameterized by estimating the effective scatterer diameter (ESD) and the effective acoustic concentration (EAC). Parametric images of QUS estimates were generated for each sample, and histology slides were produced from each sample after fixation.

Results

ESD estimates increased in heated compared to unheated samples by an average of 14%, while EAC estimates decreased by an average of 13%. Additionally, using ANOVA statistically significant differences ($p<0.05$) were observed in both ESD and EAC for heated compared to unheated tumors from the same animal.

Discussion and Conclusions

Changes in tissue structure in MAT tumors induced by heating in a saline bath were evaluated using QUS. Both ESD and EAC changed by an appreciable amount, and statistically significant differences were observed in samples from each animal when comparing heated to unheated tumors. These findings indicate that QUS offers promise for non-invasive assessment of the presence of thermal damage in tissues, which cannot readily be detected and quantified with conventional B-mode imaging. This work was supported by NIH Grant R01-EB008992.

P3Aa-13

A Composite Statistical Model for Ultrasound Applications

Paschalis C. Sofotasios[1], **Sevan Harput[1]**, Steven Freear[1]; [1]School of Electronic and Electrical Engineering, University of Leeds, Leeds, United Kingdom

Background, Motivation and Objective

The backscattered echo from tissue can be modeled as the algebraic sum of the individual reflections from randomly located scatterers. The statistics of the echo envelope contain information regarding the scattering properties of the tissue in which the ultrasound pulse has been propagated. Shankar reported that ultrasonic tissue characterization is possible by matching the probability density function (PDF) of Nakagami-m distribution to the envelope of ultrasonic backscattering from tissue [1]. Likewise, the statistical distributions, such as κ, Nakagami-m/Inverse Gaussian and Rayleigh/Lognormal, are exploited for efficiently detecting the abnormalities in liver, breast and kidney.

Statement of Contribution/Methods

The Nakagami-m/Lognormal (NL) distribution is a generalized composite statistical model that is distinct for its flexibility. It encompasses the Nakagami-m, Lognormal and Rayleigh/Lognormal models while covering the statistics ranging from pre-Rayleigh to post-Rayleigh. Nevertheless, its use has been limited due to the lack of an explicit expression for its PDF. In this study, an explicit expression for the PDF of NL distribution, which has not been reported in the open literature, is derived for ultrasound tissue characterization. The validity of this expression is verified through comparisons with results from numerical integrations.

Results

Agrawal has pointed out that the existing distributions fail to completely match the heavy tails observed in the envelope of backscattered data histogram [2]. The proposed composite distribution can mimic the behavior of the echo envelopes, since the Lognormal distribution is optimum in modeling heavy-tail behavior. This is also verified in the present study where the derived expression is used in fitting simulation results of ultrasound data based on nonlinear-tissue models with different scattering densities. Two scenarios are considered; 675 scatterers/cm^2 and 1350 scatterers/cm^2 in tissue with 0.5 dB/cm·MHz attenuation. The distributions provides fitting for $\mu = 2.1$, $\sigma = 6.9$, $m = 0.6$ and $\mu = 9.2$, $\sigma = 8.8$, $m = 1.0$, respectively. Notably, the overall value of the corresponding absolute error is less than 5%.

Discussion and Conclusions

Various different statistical distributions have been reported for modeling the envelope of the ultrasonic backscattering from tissue as a random process, namely, Rayleigh, Rice, κ, Homodyned κ, and generalized Nakagami distributions. In this work, the Nakagami-m/Lognormal is demonstrated as a more accurate alternative to existing distributions.

[1] P.M. Shankar, A general statistical model for ultrasonic scattering from tissues, IEEE Trans. UFFC, vol. 47, pp. 727–736, 2000.

[2] R. Agrawal, Karmeshu, Ultrasonic backscattering in tissue: characterization through Nakagami-generalized inverse Gaussian distribution, Comput Biol Med, vol. 37, pp. 166–172, 2006.

P3Aa-14

In Vitro Study of Cell-Free Layer in Microvessels by High Frequency Ultrasound Duplex Imaging

Ting-Yu Liu[1], Po-Yang Lee[1], Cho-Chiang Shih[1], Chih-Chung Huang[1]; [1]Department of Electrical Engineering, Fu Jen Catholic University, Taiwan

Background, Motivation and Objective

The cell-free layer is a near wall layer of plasma absent of erythrocytes which has been known the formation of this layer is attributed to the tendency of red cells and aggregates to migrate across the streamlines of the blood flow in microvessels. Most studies used optical microscopy system to measure the blood flow velocity profile across the micro-tube or vessel for assessing the region of cell-free layer. However, the flow velocity profile may be changed due to the effect of red cells aggregation. In addition, it is very difficult to apply this method for larger micro-tube (diameters of 200-500 μm) due to the optical penetration nature. Consequently, a 70 MHz high frequency ultrasound duplex imaging was provided to evaluate this complex rheological behavior in a micro-tube in vitro in this study. The effects of shear rate and hematocrit on cell-free layer were addressed as well

Statement of Contribution/Methods

The experiments were performed on porcine whole blood with different hematocrits from 20 to 60%, and the blood was circulated in the tube with a diameter of 500 μm under different shear rates (2 to 100 s^{-1}). The 70 MHz high frequency ultrasound duplex system was built for this study. The axial and lateral resolution of this system was approximately 23.1 and 66 μm, respectively. Both velocity profile and spatial distribution of erythrocyte from flowing blood were obtained by color/power Doppler imaging for analyzing the cell-free layer phenomenon.

Results

Figure 1(a) shows the typical power Doppler images from different blood hematocrits with various shear rates. The boundary between the cell-free layer and erythrocyte mixing layer is visualized, with the erythrocytes aggregation in the central region due to radial migration. The velocity profiles and spatial distributions of erythrocyte were obtained accordingly, as shown in Fig 1(b).

Discussion and Conclusions

An acoustic method was provided to replace the optical measurements of cell-free layer in a larger micro-tube in present study. The region of cell-free layer was increased with increasing shear rate, however, in general decreased with increasing hematocrit. The power Doppler images provide a better observation for recognizing the boundary between plasma and erythrocyte. In addition, the effect of erythrocyte aggregation is an important factor that enhances the formation of cell-free layer.

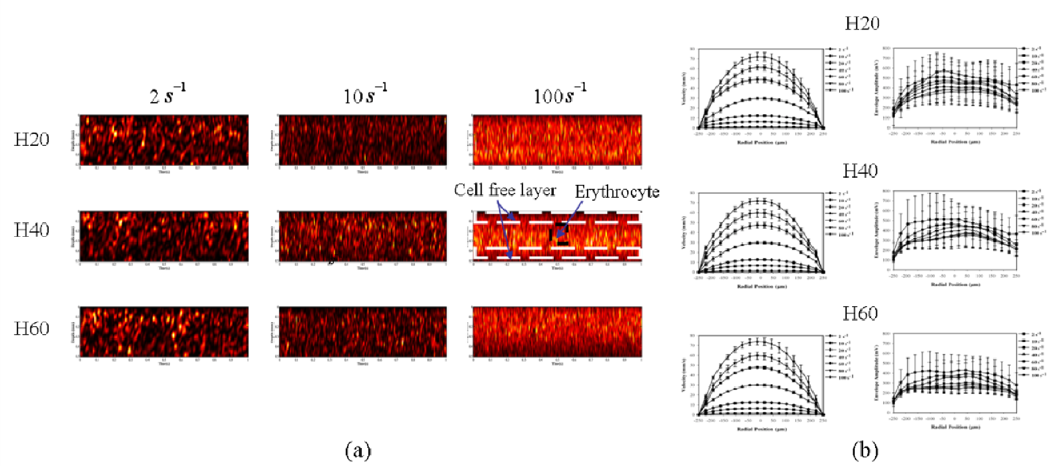

P3Aa-15

Segmentation of Atherosclerotic Plaque Components using a Multiphase Bayesian Level-Set

Jonathan Porée[1], François Destrempes[1], Gilles Soulez[2], Guy Cloutier[1]; [1]Laboratory of Biorheology and Medical Ultrasonics, University of Montreal Hospital Research Center, Montreal, Quebec, Canada, [2]Department of Radiology, University of Montreal Hospital, Montreal, Quebec, Canada

Background, Motivation and Objective

Cardiovascular diseases (CVD) are rated as the leading cause of death in western countries (30% of all deaths each year). Vascular complications are mostly related to atherosclerosis and vulnerable plaque rupture. It was long thought that plaque vulnerability was linked to the stenosis severity but recent studies (Casscells et al., Circulation 2003) have shown that vulnerability depends on plaque composition (fiber, lipid, calcium) and on its biomechanical properties (Finet et al., Coronary Artery Disease 2004). In this context, it is relevant to define imaging tools able to describe and characterize plaque components and their properties. In the present contribution, we propose a fully automated segmentation method, based on statistical properties of backscatter signals, to classify plaque pixels into its main components.

Statement of Contribution/Methods

The proposed algorithm is based on a maximum a posteriori (MAP) formulation of a partition problem. As described by Shankar et al. (UMB 2003), we assume that the first order statistics of the echo envelope of the backscatter signal of each component can be described by a Nakagami distribution. We start with a global plaque segmentation as described in (Destrempes et al., IEEE BME 2011). Next, we estimate the Nakagami mixture using the Expectation Maximization algorithm described by Destrempes et al. (IEEE TMI 2009). Then, we initialize the partition using the maximum likelihood segmentation. Finally, we evolve the partition towards the MAP using a multiphase Bayesian level-set (Samson et al., Int. J. Comput. Vision 2000). This last step alternates likelihood estimation of statistical parameters and partition evolution using a standard level set prior on the contours' smoothness.

Results

The algorithm was tested on several sequences of external ultrasound carotid scans. Our method was able to distinguish plaque components with differences in echogenicity properties with high reproducibility along the sequences (Fig. 1 and Table 1).

THURSDAY POSTER

Discussion and Conclusions

The results showed the feasibility of decomposing a plaque into its main components based on its statistical properties. The future objective of this study is to combine statistical and biomechanical behavior obtained with ultrasound elastography to assess plaque vulnerability.

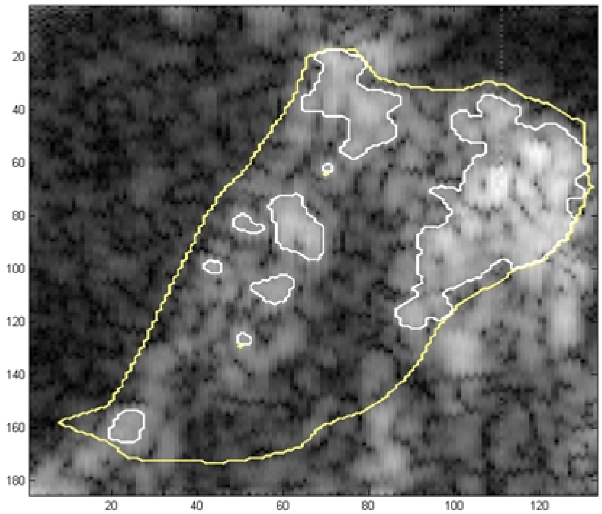

Fig. 1 : Intra plaque segmentation results based on statistical analysis. Global plaque contour (in yellow) and hyper-echoic plaque components (surrounded in white).

Table 1 : Statistical parameter of Hypo- and Hyper-echoic plaque components along a sequence of 50 frames (arbitrary units).

	Mean Intensity	SNR^2 of Intensity
Hypo-echoic	1,3 ± 0,1	0,62 ± 0,02
Hyper-echoic	49,4 ± 2,4	0,75 ± 0,02

P3Aa-16

High Frequency Ultrasound Imaging and Characteriation of Biofilms

Karla Hatfield[1], **Kunal Vaidya[1]**, Maria Helguera[1], Michael Pichichero[2]; [1]CFC Center for Imaging Science, Rochester Institute of Technology, Rochester, NY, USA, [2]Research Institute, Rochester General Hospital, USA

Background, Motivation and Objective

The goal of this study is to develop a high frequency, pulse-echo ultrasound system to non-invasively image and characterize biofilms in children during nasopharyngeal (NP) colonization with potential otopathogens and during acute ear infections (acute otitis media, AOM). This project focuses on biofilms grown in vitro on silastic substrate to determine the feasibility of detecting and characterizing parameters such as biofilm thickness, backscatter coefficient, integrated backscatter, shift of center frequency and reduction of bandwidth. These parameters are needed to understand image properties and design an efficient non-invasive protocol to identify biofilms, map their progression over time, and differentiate between single-species and multiple-species biofilms.

The purpose of this projecy is to launch a systematic study to investigate the feasibility of high-frequency ultrasound as an in vivo biofilm imaging technology and therapeutic tool.

Statement of Contribution/Methods

Three independent batches of Non-typeable Haemophilus influenzae, NTHi, harvested from the middle ear fluid of a case of AOM were studied over a period of 1 week. An experimentally characterized 15MHz piston focused transducer was used to study the acoustic properties of these biofilms. The spectra of the backscattered signals were investigated and changes in the center frequency, bandwidth and amplitude were determined as a function of biofilm maturity. The backscatter coefficient provided a measure of the mean backscatter cross-section per unit volume. The integrated backscatter coefficient (IBC) was used to produce parametric images

Results

Each batch was probed over three phases over the entire span of the study. Results for 'Early', ‘Middle’, and ‘Old’ corresponding to samples that are 1-3 days old, 3-5 days old and 5-7 days old respectively, are presented.

Discussion and Conclusions

Reproducible trends were identified in these batches as a function of time. A downshift in center frequency and narrowing of the bandwidth are indication of attenuation. The IBC was calculated within the -6 dB bandwidth of the transducer. Parametric images were produced while calculating acoustical features locally on a sliding window. Further imaging and quantitative analysis will be conducted with multispecies biofilms, with the goal of effectively quantifying biological and structural properties.

	Batch 1			Batch 2			Batch 3		
	Early	Mid	Old	Early	Mid	Old	Early	Mid	Old
f_0(MHz)	14.3	13.4	11.0	14.0	12.8	11.9	14.1	13.9	13.0
BW(MHz)	4.2	3.9	3.6	3.2	2.4	2.1	3.9	3.2	2.9
IBC(mm^{-1})	1.6	1.7	1.7	3.3	7.3	15.2	0.6	0.9	3.2
Thickness(μm)	n/a	119.0	219.0	10.0	80.0	88.0	18.0	45.0	63.0

P3Ab - Tomography

Carribean Ballroom III-V

Thursday, October 20, 2011, 9:30 am - 1:00 pm

Chair: **Michael Insana**
Univ. of Illinois at Urbana-Champaign

P3Ab-1

An acoustic radiation force assisted ultrasound modulated optical tomography system

Rui Li[1], Robert Eckersley[2], Chris Dunsby[3], Daniel Elson[4], Meng-Xing Tang[5]; [1]Department of Bioengineering, Imperial College London, United Kingdom, [2]Imaging Sciences Department, Imperial College London, United Kingdom, [3]Depatment of Physics, Imperial College London, United Kingdom, [4]Department of Surgery, Imperial College London, United Kingdom, [5]Department of Bioengineering, Imperial College London, London, London, United Kingdom

Background, Motivation and Objective

Optical and mechanical properties of soft tissue are closely related to the tissue function. E.g. cancerous tissue is typically harder and has a higher optical absorption. While techniques for imaging tissue optical and mechanical properties have been studied individually in the past, simultaneous measurement could offer additional benefit. In this work we have developed an acoustic radiation force (ARF) assisted ultrasound modulated optical tomography(UOT) technique which is able to measure and distinguish tissue optical and mechanical properties.

Statement of Contribution/Methods

A mechanical scanning UOT system has been developed including a 532nm laser, an ultrasound system with a 5MHz focused transducer, and a CCD camera. Tissue mimicking phantoms with heterogeneous inclusions of different optical and mechanical properties were exposed to the laser and an ultrasound burst. The CCD camera was positioned on the side of the phantom opposite to the laser to measure the transmitted photons. The phantom was scanned in 1D. Both the timing and the length of CCD exposure were adjusted. By using a short CCD exposure time, the effect of pure ultrasound modulation on the optical signal was recorded which mainly reflects tissue optical properties. By increasing the CCD exposure time, the effect of ARF can be measured which reflects tissue mechanical properties. By adjusting the timing of the measurement, shear wave effects can be minimised.

Results

The following graph shows the scanning results on a phantom with two optical absorbing inclusions, the right one being stiffer than the background. It can be seen that both inclusions were detected, and the signal is sensitive to the CCD trigger delay time.

Discussion and Conclusions

We have demonstrated the capability of an ARF assisted system in detecting and distinguishing tissue optical properties and mechanical properties.

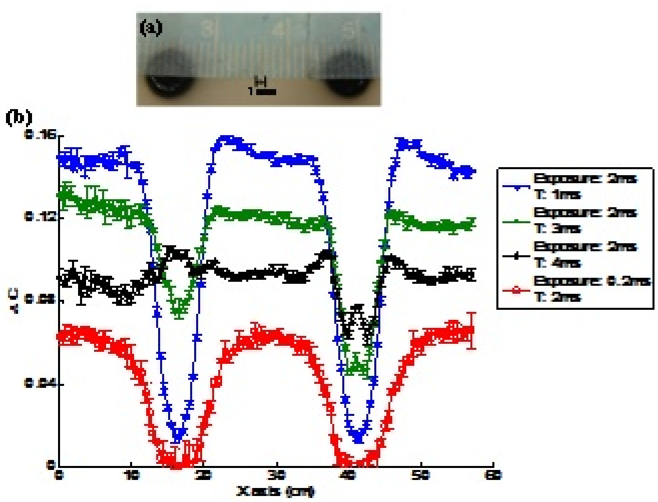

P3Ab-2

Ultrasound mammograph for breast lobe inspection

Serge Mensah[1], Julien Rouyer[1], Philippe Lasaygues[1], Emilie Franceschini[1], Jean-Pierre Lefebvre[1]; [1]*Acoustics and Mechanics Laboratory, CNRS, Marseille, France*

Background, Motivation and Objective

Dense breasts appear “white” on X mammography but are generally ideally contrasted when anatomical views are obtained using ultrasound systems. Ultrasound Computed Tomography (UCT) is an imaging technique recognized for soft-tissue characterization which provides both a high contrast and resolution imaging and a multi-parametric imaging. Our research focuses on the inspection of each of the 15-20 mammary lobes since most lesions develop first in the ductal tree.

Statement of Contribution/Methods

In that purpose, ANAIS (ANAtomical Imaging and Interventional System) prototype which includes a half-ring transducer array was designed. The 200-mm diameter array comprises 1024 active elements in a 190-degree circular arc. The center frequency is 3 MHz and 79% -6 dB bandwidth. The front-end electronics incorporate 32 independent transmit/receive parallel channels and a 32-to-1024 multiplexer unit. SNR and spatial resolution of low contrast objects are enhanced by using pulse compression technique.

Results

Initially, calibration studies are realized with academic objects and a needle hydrophone in order to develop data correction tools and to specify system properties such as speckle distribution, spatial resolution and sensitivity. Tomographic screening is applied on a breast tissue-like phantom (CIRS model 051) containing inclusions emulating solid masses and cysts. Backscattered field (1024 *32 signals in less than 8 sec) is recorded and processed with the correction algorithm. A near-field reconstruction algorithm is used to solve the inverse problem and the resulting images are exhibited.

Discussion and Conclusions

Low frequencies and the numerous elements used in scattering mode blended with our reconstruction procedure provide interesting results as the phantom reconstruction shown herein. The dedicated ultrasonic array and front-end electronics offer interesting resolution (better than 0.185 mm) and an isotropic and homogeneous speckle. In spite of the thickness of the beam which is a limitation for an optimally contrasted 2D imaging; the system versality provides many new potential solutions such as 3D parametric acquisition and tissue characterization.

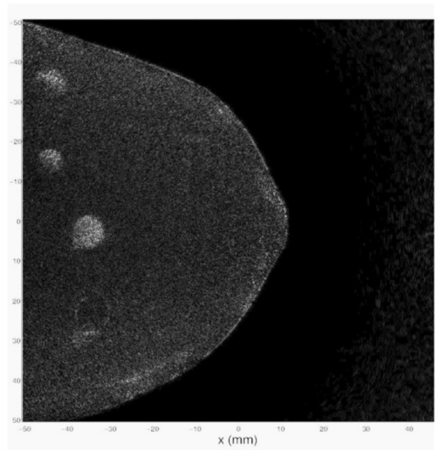

The imaging system dedicated for anatomical inspection (left side) and a tomographic reconstruction of a breast-shaped phantom (right side).

P3Ab-3

Geometry Independent Speed of Sound Reconstruction for 3D USCT Using Apriori Information

Robin Dapp[1], Michael Zapf[1], Nicole Ruiter[1]; [1]*Karlsruhe Institute of Technology, Germany*

Background, Motivation and Objective

We develop a 3D Ultrasound Computer Tomograph (USCT) for breast cancer diagnosis. The 3D USCT I has a cylindrical aperture, while the new optimized 3D USCT II has a semi-ellipsoidal aperture. Both systems have sparse apertures and limited transducer directivity.

For speed of sound (SoS) tomography usually cone-beam algorithms, e.g. Feldkamp-Davis-Kress (FDK), are used. These are not applicable to ellipsoidal or other arbitrary geometries.

The Algebraic Reconstruction Technique (ART) is geometry independent. For sparse apertures however, the sampling density becomes inhomogeneous, posing problems to equation solvers in ART. Our aim is to stabilize and improve ART by including apriori information about our transducers and system parameters to attain the image quality of the FDK algorithm.

Statement of Contribution/Methods

ART traces rays through a voxel grid from emitter to receiver. Due to the discrete nature of the algorithm we can include voxel-specific apriori information in order to improve the reconstruction: We weighted the voxels according to their position in the 3D beam profile.

To alleviate the sampling density problems we modelled the rays' spatial uncertainty by adding spatial noise to them. We also applied 3D interpolation between neighboring transducer positions to increase the available data. In addition we used the measured water temperature to get the initial SoS distribution map.

For the final reconstruction we applied the Compressive Sampling algorithm TwIST with Total Variation regularization which is known to work well in the presence of noise.

Results

We used cone-beam data of 3D USCT I to directly compare the algorithms. The reconstruction quality of our optimized ART method is higher since edges are better preserved and the average SoS is closer to the original. The attached figure shows a comparison of reconstructions with real data of a clinical breast phantom (mean SoS: 1450 m/s).

Reconstruction times were roughly similar for all methods. The mean SoS of the phantom was 1452 m/s with our optimized ART, 1464 m/s with standard ART, and 1457 m/s with FDK.

Discussion and Conclusions

We showed that including apriori information increases the reconstruction quality of ART without adversely affecting the performance. Further work will include utilizing reflection data to further improve the sampling density, and implementing a bent-ray
method.

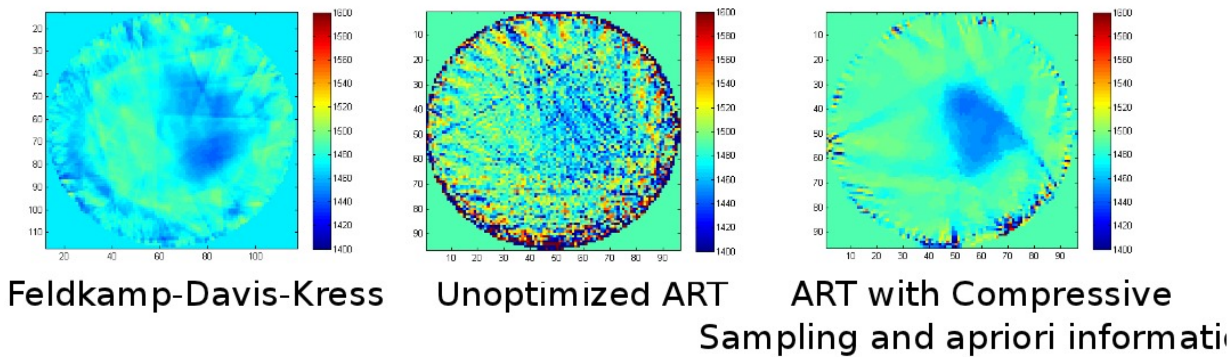

P3Ab-4

A Clinical Experience of a Prototype Automated Breast Ultrasound System Combining Transmission and Reflection 3D Imaging

Paolo Pellegretti[1], Sara Dellepiane[1], Marco Vicari[1], Michele Zani[1], Matthias Weigel[2], Ulrich Saueressig[3], Elmar Kotter[3], Mathias Langer[3]; [1]*Esaote SpA, Genova, Italy,* [2]*Dept. of Radiology, Medical Physics, University Medical Center Freiburg, Freiburg, Germany,* [3]*Dept. of Radiology, Clinical Radiology, University Medical Center Freiburg, Freiburg, Germany*

Background, Motivation and Objective

Breast cancer is the most frequently diagnosed cancer and the leading cause of cancer death among females.

An early detection is demonstrated to significantly improve the chances of success of therapies and consequently of a full recovery.

In the diagnosis workflow a key role is represented by imaging procedures.

None of present imaging breast procedures provides the desired balance between effectiveness, cost of the procedure and safety for the patient.

A successful answer could be new 3D automated ultrasound computed tomography (USCT) proposals.

Purpose of this study was to evaluate the viability of the USCT Warm Bath Ultrasound (WBU) scanner developed by Techniscan Medical Systems, Salt Lake City, Utah, USA, and supported by Esaote.

The WBU system acquires 3D sets of transmission and reflection images simultaneously. They contain information on ultrasound reflection, speed and attenuation of sound (see Figure).

Statement of Contribution/Methods

The clinical study was carried out at the University Medical Center of Freiburg, Department of Radiology, Germany.

Patients were recruited from the undergoing hospital clinical routine.

The results of the WBU were compared to findings from routine mammography, handheld ultrasound and, sometimes, MRI.

In cases of suspected malignancy, vacuum core biopsy was conducted.

Results

A total of 60 patients were included in the study.

After routine examinations, 12 patients were diagnosed with histologically confirmed breast cancer, 13 patients showed cysts, 12 fibroadenomas and 23 cases no significant findings.

10 out of 12 carcinomas could be detected in the WBU examination. In 2 cases, carcinoma close to chest wall lay outside the field of view. Fibroadenomas and cysts were depicted reliably. Lesion characteristics differ markedly from handheld ultrasound. Lesion characterization may be improved by speed of sound and attenuation imaging.

Discussion and Conclusions

The WBU technique offers a new way to examine the breast, combining features of reflection with transmission imaging. This may lead to improved lesion characterization. As an automated examination, objectivity and reproducibility are key features. The difference of image characteristics compared to conventional ultrasound implies a learning curve.

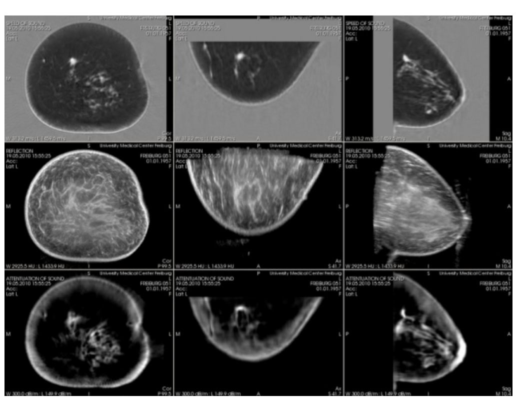

P3Ab-5

Simulation of shadowing effects in ultrasound imaging from computed tomography images

An H. Pham[1,2], Bjarne Stage[1], Bo Lundgren[1], Martin Christian Hemmsen[2,3], Mads Møller Pedersen[2,4], Jørgen Arendt Jensen[2]; [1]National Institute of Aquatic Resources, Technical University of Denmark, Charlottenlund, Copenhagen, Denmark, [2]Center for Fast Ultrasound Imaging, Dept. of Elec. Eng., Bldg. 349, Technical University of Denmark, DK-2800 Lyngby, Denmark, [3]R&D Applications & Technologies, BK Medical, DK-2730 Herlev, Denmark, [4]Dept. of Radiology, Copenhagen University Hospital, Rigshospitalet, DK-2100 Copenhagen, Denmark

Background, Motivation and Objective

Simulation of ultrasound (US) images based on computed tomography (CT) data has previously been performed with different approaches. Shadowing effects are normally pronounced in US images, so they should be included in the simulation. In this study, a new method to introduce shadowing effects has been tested that makes the simulated US images appear more realistic.

Statement of Contribution/Methods

US images of a cod (Gadus morhua) were obtained with a BK Medical 2202 ProFocus US scanner with a dedicated research interface giving access to beamformed RF data. The center frequency of the transmit pulse was 10 MHz. In transmit mode, the F# was 3.6 and the focus point was at 45 mm. 384 US focused beams were emitted to create the image. CT images with a slice thickness of 0.5 mm, and a pixel size of 0.2 x 0.2 mm were obtained with an Aquilion ONE Toshiba CT scanner. CT data were mapped from Hounsfield Units (HU) to characteristic acoustic impedance (CAI) with a new HU to CAI conversion table. The new method uses focused beam tracing to create maps of the transmission coefficient (TRC) and relative transmitted energy (RTE). There were 384 maps of TRC and of RTE corresponding to 384 emissions. Finally an average RTE map was calculated. Multiplication of CAI and RTE created the final scattering strength map. Field II was used to simulate an US image with dimensions of 38.9 mm x 55.3 mm x 4.5 mm, using 10^6 point scatterers.

Results

US images of a slice of the cod are presented in figure 1, where Fig. 1a is the measured US image, Fig. 1b is the direct simulated US image from the CT image, and Fig. 1c is the simulated US image using the new method. In Fig. 1a, the shadowing effects are pronounced due to the differences in the properties of the media. Without the shadowing effects, Fig. 1b does not look realistic. Fig. 1c with the shadowing effects introduced appears more realistic and closer to Fig. 1a. The smallest simulated point spread function is 0.54 x 0.3 mm. It took 3.8 hours using 35 machines to generate Fig. 1c. Since no quantitative method to assess quality of a simulated US image compared to a measured one exists, visual inspection was used.

Discussion and Conclusions

In Fig. 1c the shadows are influenced by the sound waves produced with the transducer and thus, are not sharp, straight lines. The method gives diffuse shadows that are similar to the ones observed in measurements on real objects.

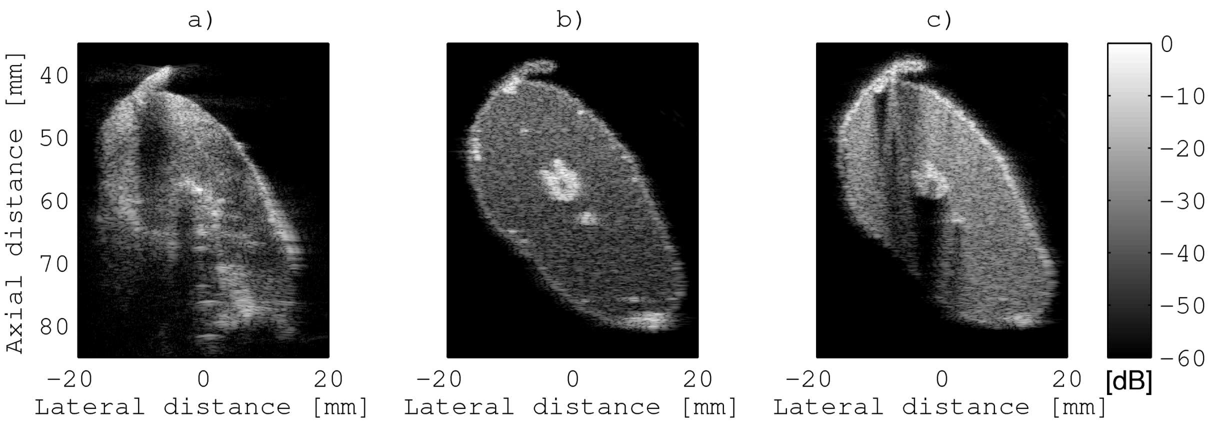

Figure 1. Measured ultrasound image (a), direct simulated US image from CT image (b), simulated ultrasound image using the new method (c)

P3Ab-6

High Frequency Ultrasound Computer Tomography for Small Animal Imaging Applications

Wei-Tsen Chen[1], Cho-Chiang Shih[1], Chih-Chung Huang[1]; *[1]Department of Electrical Engineering, Fu Jen Catholic University, Taiwan*

Background, Motivation and Objective

Ultrasound computer tomography (UCT) has been studied for imaging breast cancer and testicular tumor over the past several decades. Most UCT systems are designed for human used only. Recently, the small animal models (rats, mice, and zebrafish) have been proposed for studying the human diseases, such as cardiovascular pathologies, cancer therapy, and tumor development. However, the traditional UCT imaging systems (ultrasound frequencies from 2.5-5 MHz) can not provide adequate spatial resolution to describe the small internal structures of animal organs. In present study, a high frequency UCT imaging system was proposed for this purpose.

Statement of Contribution/Methods

Because of ultrasound propagation in a tissue is influenced by attenuation, the attenuation UCT image was preformed in this study. Figure 1(a) shows the architecture of high frequency UCT system. The ultrasonic transducers at frequency ranging from 10 to 50 MHz were used in this system. The attenuation of ultrasound was measured at different scan lines by the echo signals from the reflector. The projections of attenuation were acquired from different scan angles. The filtered backprojection algorithm was used to reconstruct the 2D UCT images. The system verification was performed by gelatin phantom and zebrafish.

Results

Figure 1(b) shows the 10 MHz attenuation UCT image of gelatin phantom which an inclusion with a diameter of 3 mm was observed clearly. The phantom was composed of two different gelatins (gelatin concentration of 6% and 9%). Figure 1(c) shows the 50 MHz attenuation UCT image for the cross section of a 0.2 mm diameter micro-tube. Figure 1 (d) shows the 30 MHz UCT image for the cross section of zebrafish trunk (close to tail).

Discussion and Conclusions

A high frequency UCT system was built for high resolution imaging in this study. Even though the difference of stiffness in gelatin phantom is slight, it still can be recognized clearly by UCT image. The reason may be attributed to that the ultrasonic attenuation was affected sensitively by tissue properties. As the ultrasound frequency was increased to 50 MHz, a 0.2 mm diameter micro-tube can be observed in gelatin phantom. Since the dimension of zebrafish spine is small, the cross section of bone structure can be obtained by measuring the high frequency ultrasound attenuation. Future works will apply high frequency UCT to testicular tumor imaging in mice.

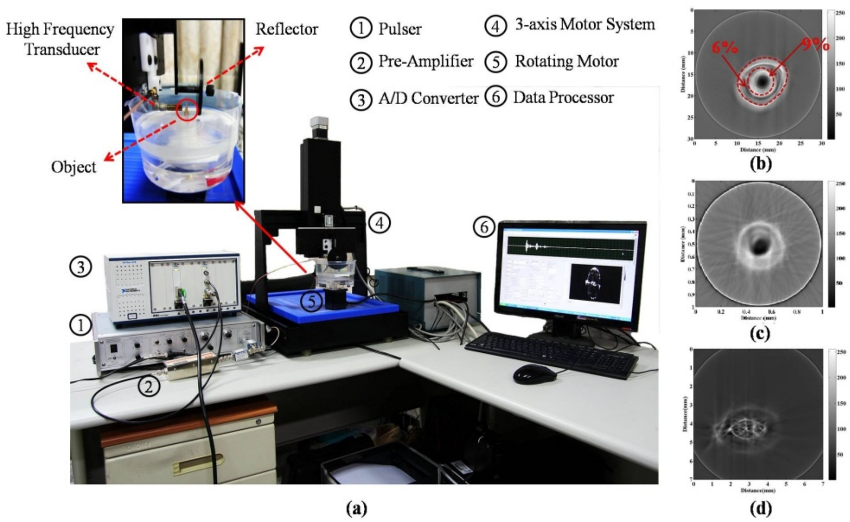

THURSDAY POSTER

P3Ac - Signal Processing

Carribean Ballroom III-V

Thursday, October 20, 2011, 9:30 am - 1:00 pm

Chair: **Kendall Waters**
Silicon Valley Med. Instruments

P3Ac-1

Compressed sensing of ultrasound single-orthant analytical signals

Celine Quinsac[1], François De Vieilleville[1], Adrian Basarab[1], Denis Kouamé[1]; [1]*IRIT UMR CNRS 5505, University of Toulouse, France*

Background, Motivation and Objective

Compressive Sensing (CS) in Ultrasound (US) imaging has been introduced by the authors last year [Quinsac et al., Proc. IEEE IUS, 2010]. This method allows image reconstructions from relatively few samples (below the Nyquist criterion) using the image sparsity in the Fourier domain, leading to a reduced data volume and acquisition time. In this paper, we propose to reduce even further the number of samples (and thereby the acquisition time) using analytical forms of US signals.

Statement of Contribution/Methods

CS in US imaging consists in taking spatial samples at random locations as incoherent linear combinations of the original 2D Fourier transform image. The reconstruction of the US image is then performed via:

$\mathrm{argmin}_M \, \|\Phi F^{-1}M - y\|_2 + \lambda|M|_1$,

where M is the US image k-space, Φ is a sampling mask (uniform random), F^{-1} is the inverse Fourier transform, y are the measurements and λ is a coefficient weighting for the sparsity of M. The original image is then recovered using an inverse Fourier transform. The main contribution of this paper is to reduce the number of samples required to reconstruct a US image. We propose to use the 1D analytical signal (AS) and single-orthant (SO) 2D AS [Hahn et al., Proc. IEEE, 1992] instead of radiofrequency (RF) US images, to increase the sparsity in the Fourier domain by a factor 2 (resp. 4). This should result in a reduction by a factor 2 (resp. 4) of the number of observations needed for image reconstruction.

Results

The results of our method allowed a reconstruction of US images from as little as 5% of spatial samples in simulated images (Fig.1a) and from 16% for mouse kidney in vivo images (Fig.1b). Fig.1 shows results of RF US images (left), US AS (second column), SO US AS (third column) against original images (right). Normalised root mean squared errors of SO were 0.42 in simulation and 0.47 in vivo, vs. 0.75 and 1.04 for RF images.

Discussion and Conclusions

Exploiting the characteristics of the US image AS, the proposed approach allows the reduction of the number of samples by a factor 4 compared with classical CS in US, for a similar reconstruction error. Even if the data volume acquired is equal since the samples acquired are complex and doubled, their spatial locations are the same and the acquisition time can therefore be greatly reduced.

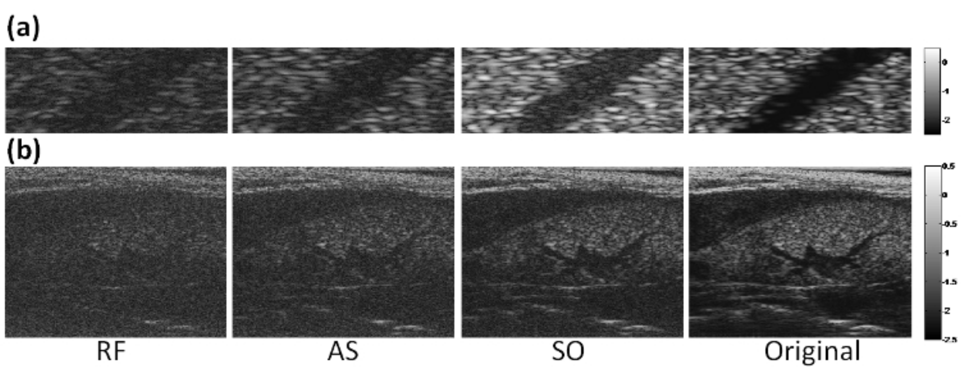

P3Ac-2

Ultrasound RF Channel Data Compression for Implementation of a Software-Based Array Imaging System

Po-Wen Cheng[1], Che-Chou Shen[2], Pai-Chi Li[1]; [1]Natoinal Taiwan University, Taiwan, [2]Natoinal Taiwan University of Science and Technology, Taiwan

Background, Motivation and Objective

Using software for beam-forming in ultrasound systems provides high flexibility, and the large amount of computations required in a software-based system can be performed in real time on a personal computer. However, there is a bottleneck in the very large data transfer rate required from the ultrasound front-end to the personal computer host for real-time operation, which cannot be achieved without appropriate compression. This study utilized MPEG technology to process the ultrasound RF data in order to increase the compression efficiency.

Statement of Contribution/Methods

Previous studies have examined JPEG compression of ultrasound RF channel data, but the schemes do not exploit temporal redundancy between adjacent frames. This study utilized MPEG technology to process the ultrasound RF data in order to increase the compression efficiency. The ultrasound data for MPEG compression were acquired by a Verasonics ultrasound system (Verasonics, WA, USA) with a linear-array transducer (ATL L7-4, Medimtech, CA, USA). The experiments used a multipurpose speckle-generating phantom (Model 539, ATS Laboratories, CT, USA).

Results

Our results indicate that compression ratio of MPEG compression is lower than 0.13, thus making real-time data transfer between data acquisition front-end and the back-end computer to be possible. MPEG compression generally provides a lower compression ratio than JPEG compression, and the compression gain is larger than 48 when the inter-frame displacement is sufficiently low. Moreover, the compression efficiency in different directions also highly depends on the frame-to-frame correlation.

Discussion and Conclusions

It was found that data associated with smaller motion and larger beam widths exhibited a higher frame-to-frame correlation, and that in turns resulted in smaller compression ratio. Therefore, MPEG compression is more suitable than JPEG compression because it is able to exploit the data redundancy between frames. With MPEG, channel data can be effectively transferred to back-end for beamforming and Doppler processing, making a software-based imaging array imaging system possible.

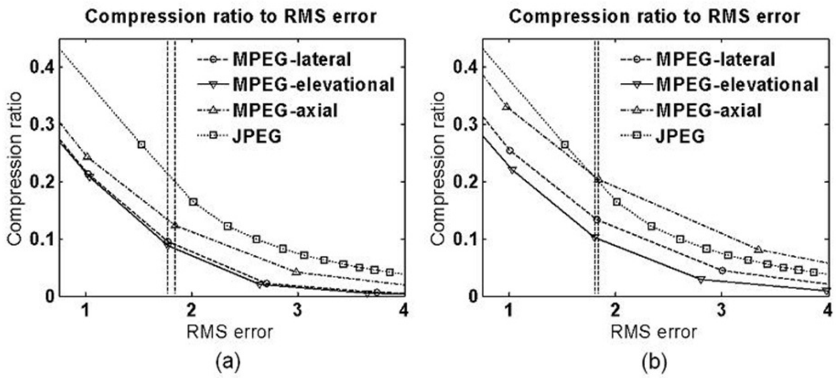

Figure: Comparison between MPEG and JPEG for interframe displacements of 5 µm (a) and 40 µm (b). The vertical dashed line indicates CRF = 15 for MPEG compression.

P3Ac-3

Spectral doppler using compressive sensing

Julien Richy[1], **Hervé Liebgott[2]**, Remy Prost[1], Denis Friboulet[1]; [1]*CREATIS, France,* [2]*CREATIS, Villeurbanne, Rhônes, France*

Background, Motivation and Objective

Doppler exams implies accessing and displaying in real time several types of information:

- the conventional B-mode image in order to navigate through the organs
- the spatial distribution of velocities
- the evolution of blood velocity at one particular point as a function of time (spectrogram) .

Using conventional approaches, this leads to firing strategies that lowers the PRF and, as a consequence, decreases the maximum measurable velocity or leads to spectrograms with missing information

In this framework, several studies attempted to lower the amount of acquired data while maintaining the quality of the displayed information. These studies generally use short acquisition sequences coupled with high-resolution spectral estimation methods.

Compressive sensing (CS) is another candidate to solve this problem that has never been used in this context. This paper investigates the possibility to use CS for spectral Doppler reconstruction.

Statement of Contribution/Methods

CS allows reconstruction of a length n signal x from a small number of measurements $m<n$. At the heart of CS lies the assumption that x has a sparse representation in some model basis. In this work, we propose to perform CS reconstruction using the sparsity of the Doppler signal in the Fourier domain.

Results

Using the Field II program, we simulated the blood flow in a femoralis arteria. The PRF was set to 5kHz for a mean velocity of 0.15 m/s and a beam/flow angle of 60°. The 128-element probe had a center frequency of 3.5 MHz. The simulated cardiac cycle was 1 second long. To simulate CS acquisition, random samples where left out and the signal was reconstructed using 256-sample sliding windows with 50% overlap.

Figure 1 represents the spectrograms obtained from A) the full original signal, B) the CS reconstruction using 60% of the data C) a conventional regular undersampling keeping 60% of the data.

Discussion and Conclusions

This study shows that it is possible to reconstruct the spectrogram with high accuracy from randomly acquired Doppler data even at sampling frequencies where aliasing would appear when using conventional undersampling. As the CS theory is based on sparsity, parts of the signal that have a sparse spectrum are obviously better reconstructed than the others. This represents a first step towards compressive sensing ultrasound flow imaging.

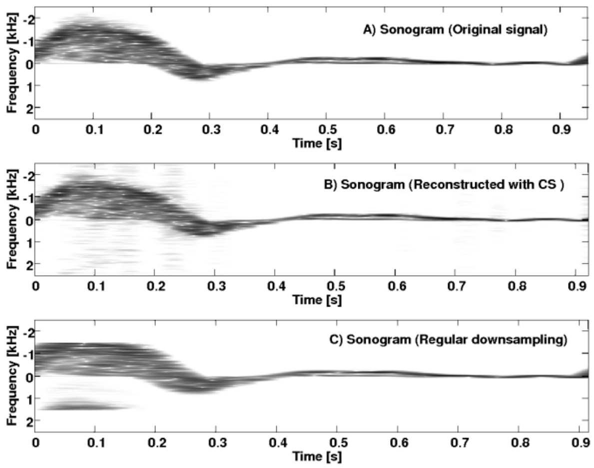

Fig1: Sonograms obtained A) from the original signal, B) from the CS reconstructed signal based on 60% randomly selected samples from the original signal and C) from a signal acquired at 60% of the original PRF

P3Ac-4

Transducer Motion Estimation Using Combined Ultrasound Signal Decorrelation and Optical Sensor Data for Low-cost Ultrasound Systems with Increased Field of View

Kevin Owen[1,2], F. William Mauldin, Jr. [1,2], John A. Hossack[1]; [1]BME, University of Virginia, Charlottesville, VA, USA, [2]Rivanna Medical, Crozet, VA, USA

Background, Motivation and Objective

Precise estimation of transducer position and orientation offers the possibility of expanding an imaging system's field of view without added channels – e.g. performing 3D imaging with a 1D linear array, or 2D/3D imaging with small number of discrete single elements. Phased array ultrasound systems can detect motion in the imaging plane using simple 2D correlation methods; however while out-of-plane motion can be detected using decorrelation measurements, direction of motion cannot be determined. Optical finger navigation (OFN) sensors can be used to detect 2D motion of skin over the surface of the sensor with high resolution. In this paper, we propose a fusion of OFN sensor data with one or more single-element piston transducers to produce an accurate estimate of the position and rotation of an ultrasound device while it is manually translated across the skin, enabling 2D or 3D imaging with a very low-cost handheld ultrasound system.

Statement of Contribution/Methods

A custom board and mechanical housing was designed, with two OFN sensors to estimate rotation in addition to translation, and a housing optimized for general skin contact. This was integrated with a custom ultrasound system to enable capture of both ultrasound and OFN data during translation through a series of 2mm displacements while in contact with a tissue-mimicking phantom. A statistical model was developed using experimental data and was used to form maximum likelihood displacement estimates given the combined sensor data.

Results

The decorrelation function from the piston transducer matched a parameterized Gaussian function to within < 2% RMS error, with a useful estimation range of <1mm. In contrast the OFN sensor is designed for faster translation speeds of 3-15 inches per second. To compare both modalities, 40 successive 2 mm translations were performed, with motion estimated by accumulation of multiple smaller 0.2 mm steps for the ultrasound decorrelation method, and full 2mm steps for the OFN sensor. The decorrelation model gave displacement magnitude estimates with standard deviation and bias of 0.2 mm and -0.064 mm for 2 mm shifts. Estimates using a single OFN sensor had standard deviation and bias of 0.277 mm and 0.015 mm. Using combined data to form maximum likelihood estimates of the 2 mm displacements, the standard deviation dropped to 0.189 mm, with a bias of -0.037 mm. The OFN sensor also demonstrated equally accurate displacement measurements in both X and Y lateral dimensions.

Discussion and Conclusions

Experimental data illustrated in this paper demonstrate that motion estimates from piston transducers and at least two OFN sensors can be combined using a statistical model to estimate position and rotational orientation with enhanced accuracy. Prior work indicates that mechanically scanned piston transducers are capable of forming 3D reconstructions of spinal bone anatomy with dimensional accuracy of ~0.5 mm. This work is a enabling step toward similar freehand 3D reconstructions.

P3Ac-5

Adaptive Frequency Compounding for Speckle Reduction

Il Seob Song[1], Chang Han Yoon[1], Gi Duck Kim[2], Yangmo Yoo[1,3], Jin Ho Chang[2,3]; [1]Electronic engineering, Sogang University, Seoul, Korea, Republic of, [2]Sogang Institute of Advanced Technology, Sogang University, Seoul, Korea, Republic of, [3]Interdisciplinary Program of Integrated Biotechnology, Sogang University, Seoul, Korea, Republic of

Background, Motivation and Objective

Speckle pattern in medical ultrasound images is generally regarded as one of crucial factors degrading contrast and signal-to-noise ratio (SNR). To mitigate the pattern, many commercial ultrasound scanners employ the frequency compounding method in which a radio-frequency (RF) spectrum is divided into two or more sub-bands. A compounding image is produced by extracting envelopes from the sub-bands and subsequently adding these with weighting factors that are generally 0.5 (i.e., averaging). To maximize the compounding effect, the depth-dependent weighting factors determined by assumed attenuation coefficients have been proposed. This method has a limitation because it requires a priori knowledge about the attenuation coefficients of which measurement is difficult in vivo. This paper proposes an adaptive frequency compounding method in which spectral characteristics of RF signals are analyzed and used for the quadrature demodulation (QDM) and the decision of weighting factors.

Statement of Contribution/Methods

In the proposed method, the center frequencies and bandwidths of sub-bands are determined based on spectral energy distribution (SED). Due to the frequency-dependent attenuation, the SED of received echoes varies with imaging depth and tissue types. Therefore, it is reasonable that a RF spectrum should be divided into sub-bands with equal

THURSDAY POSTER

spectral energy, leading to different bandwidths of each sub-band. To obtain envelopes, the QDM is performed with the center frequencies corresponding to each sub-band. The ratios of sub-band energies are used as weighting factors. The performance of the proposed method was evaluated by in vitro experiments with tissue-mimic phantom and measuring the speckle's SNR (SSNR). In the measurement, the region of interest (ROI) was selected and SSNRs of each scanline in the ROI were calculated. The RF signals were acquired by SonixTouch (Ultrasonix Medical Corp) with a 3.3 MHz convex array and divided into two sub-bands by using two band-pass filters (BPFs) lower and upper cutoff frequencies were 1.43 and 3.07 MHz for lower sub-band and 2.56 and 4.9 MHz for upper one. Since the RF spectrum was asymmetric, the ratios of the lower and upper sub-band energies were not equal(i.e., 0.43 and 0.57) and their correlation coefficient was 0.22. For comparison, the conventional frequency compounding image was also constructed two BPFs for the division had lower and upper cutoff frequencies of 1.43 and 3.6 MHz for lower sub-band and 3.0 and 4.89 MHz for upper one. Also, the each weighting factor was 0.5.

Results

The mean and standard deviation of SSNR in the ROI on the original phantom image were 1.83±0.20. The proposed method provided SSNR of 2.46±0.38 while the conventional method improved SSNR to 2.18±0.3.

Discussion and Conclusions

The experimental results indicate that the division of a RF spectrum and the decision of weighting factors based on SED are more suitable to improve SSNR than the conventional one.

P3Ac-6

Improved range resolution and side lobe level of ultrasound echoes using nonlinear frequency-modulated excitation signal and modified compressing filter

Tarcísio Dantas[1], Rodrigo Costa-Felix[2], João Machado[1]; [1]Biomedical Engineering Program - COPPE, Federal University of Rio de Janeiro, Rio de Janeiro, RJ, Brazil, [2]Laboratory of Ultrasound - Division of Acoustic and Vibration Metrology, INMETRO, Duque de Caxias, RJ, Brazil

Background, Motivation and Objective

Modulated, with relative long duration, excitation signals of pulse-echo ultrasound systems are designed with increased frequency bandwidth in order to improve range resolution without compromising the penetration depth into biological tissue. However, when this type of excitation signal is used in imaging systems the contrast is reduced due to temporal lobes generated after pulse compression, to recover range resolution, of received echoes. In this sense, frequency modulated excitation signal is the best recommended for ultrasound systems.

Statement of Contribution/Methods

This work contributes with the synthesis of a nonlinear frequency modulated excitation signal that compensates for losses in the spectral range response of the transducer and all pulse-echo system employed instrumentation, increasing the bandwidth of returned echoes and providing improved results favoring resolution after compression. A compensated frequency modulated (CFM) signal is generated through phase modulation while keeping constant the signal amplitude. The spectrum magnitude of the CFM signal is determined as the n^{th} power of the pseudo-inverted pulse-echo system transfer function magnitude. Minimization of temporal side lobe levels is obtained optimizing the power n. CFM synthesis in frequency domain completes determining its phase spectrum, which is based on the principle of stationary phase and obtained by two successive integrals of CFM spectrum magnitude. An inverse Fourier Transform of CFM in the frequency domain provides the temporal CFM excitation signal. A modified Wiener filter (with amplitude magnitude to the power 1/n') was used for pulse (echo) compression. The pseudo-inversion was implemented over the –10 dB frequency bandwidth of the system transfer function magnitude and a particular combination of n and n' was determined to optimize range resolution with reduced temporal side lobe level. An experimental pulse-echo system setup was used containing of a 2.25 MHz transducer (–3 dB relative bandwidth of 45 %) excited with a CFM signal with a duration of 20 µs and immersed in a water tank containing a flat aluminum reflector.

Results

The best range resolution (normalized to wavelength) of 0.36, measured in –30 dB of the compressed echo envelope, was obtained with n and n' optimized to 3.5 and 1.5, respectively.

Discussion and Conclusions

One of the best results, published in the last four years, for range resolution (normalized to wavelength) measured in –30 dB of the compressed echo envelope is 0.51. It was obtained using a frequency modulated excitation signal and an ultrasound transducer with same center frequency and larger –3 dB bandwidth in comparison to the one used in present work. The CFM excitation signal proposed here, combined with the modified Wiener filter for pulse compression, proved to be superior since the range resolution result is improved by more than 25% over the latest best results.

Work supported by CNPq, CAPES and FAPERJ.

P3Ac-7

Detection of Restoration Faults under Fillings in Human Teeth using Ultrasound

Sevan Harput[1], Tony Evans[2], Nigel Bubb[3], Steven Freear[1]; [1]School of Electronic and Electrical Engineering, University of Leeds, Leeds, United Kingdom, [2]Division of Medical Physics, University of Leeds, Leeds, United Kingdom, [3]Oral Biology, University of Leeds, Leeds, United Kingdom

Background, Motivation and Objective

During the dental restoration process it is important that the insertion reaches the base of the filling. Any cavity present at the base of a restoration can lead to infection requiring repetition of the restoration procedure. In this work, an ultrasound contact imaging technique for detection of restoration faults in human teeth is proposed. Radiography is currently used as a diagnostic technique, but it is not ideal for dental imaging due to its ionizing nature. However, ultrasound can be safely used for dental measurements to locate discontinuities inside the human tooth at low pressure levels.

Statement of Contribution/Methods

A linear frequency modulated chirp signal is used to improve the SNR and increase the penetration depth to allow the detection of the echoes from restoration-tooth boundary using 200 kPa acoustic pressure. Although the detection is improved, it is observed that the duration of the excitation signal is longer than the duration of time of flight in the restoration, which causes signal overlapping between consecutive internal reflections. Due to these reverberations, the applied chirp signals interfere arbitrarily with the successive reflections, where the received signals are not identifiable in the time or frequency domain. In this study, the fractional Fourier transform (FrFT) is used to separate the overlapping chirp signals.

Results

A dentist performed two different restorations on an extracted human molar. For restoration A, a bonding agent is applied before filling the cavity with restorative material. For restoration B, in order to create a poor filling, the cavity is covered with glycerin and no bonding material is used. In order to perform the ultrasound scan, the tooth sample is fixed on a stationary stage and a 14 MHz transducer is held by a computer numerical controlled (CNC) positioning system. The tooth sample is scanned by the automated CNC with a step size of 0.5 mm through the surface of both fillings. A detection threshold for the restoration faults is calculated by taking into account the attenuation and acoustic impedance of the restoration material and tooth layers.

Received signals are windowed in the fractional Fourier domain to filter the reverberations and the pulse compression is performed in time domain after applying inverse FrFT. After cancelling the reverberation effect, the reflected power from the bottom of the filling is measured. The maximum power of reflected echo observed for the restoration A was below the calculated threshold, which indicates no bonding defects. However for restoration B, the level of reflected power from the filling was always above the threshold for each scanning point, which shows an adhesion problem between the filling and tooth.

Discussion and Conclusions

The ultrasonic detection of restoration faults in human teeth using chirp coded excitation together with FrFT was performed. The FrFT was used to filter the received echoes overlapping in both time and frequency domains.

P3Ac-8

Noise Reduction of Tissue Harmonic Images using Information of Fundamental Echo

Takuya Yamamura[1], Masayuki Tanabe[2], Kan Okubo[1], Norio Tagawa[1]; [1]Grad. School of System Design, Tokyo Metropolitan University, Japan, [2]Faculty of Engineering, Kumamoto University, Japan

Background, Motivation and Objective

Tissue harmonic imaging (THI) is used for obtaining high resolution medical ultrasound images. However, it is well-known that the SNR of THI is low, because the amplitude of a harmonic echo is remarkably small and the frequency dependent attenuation is severe with harmonic components. In this study, we propose a method for improving the SNR of THI with keeping its resolution, which can be constructed using the information of a fundamental component.

Statement of Contribution/Methods

We assume that the unknown harmonic echo and the observation noise are weak stationary processes, and hence, we can represent the Wiener filter in the frequency domain. To design the Wiener filter exactly, we have to know the power spectrum of the unknown signal. However, it is generally difficult to know it. In this study, we estimate the power spectrum of a second harmonic echo from the spectrum of a fundamental echo. Specifically, we assume that the fundamental echo is noise free, and by smoothing its spectrum, stretching it twice and shifting it to the second harmonic bands, we can have the estimator of the power spectrum of the second harmonic component. It is expected that this estimator is robust as compared with one derived by simply smoothing the spectrum of the observed second harmonic echo, since the observed harmonic echo includes relatively large noise. By applying the Wiener filter using this estimate of the power spectrum, we can obtain the harmonic signal with high SNR.

Results

In vitro experiments were performed. The broken line in Fig. 1 represents the envelope of the simply extracted second harmonic signal by the rectangular band-pass filter. The transmitted pulse is 5 MHz of the carrier frequency and includes 10 cycles. The solid line represents the estimated second harmonic signal by the proposed method. Figure 1 shows that the noise level can be lowered with approximately 5 - 10 dB with keeping resolution by the proposed method.

Discussion and Conclusions

We proposed a new method to improve the SNR of the harmonic echo using the fundamental echo. In this study, we discuss about one line echo. In the future work, we are going to target multiple scanning lines. In case of this, we will be able to estimate more stable power spectrum using information of multiple lines scaned in advance.

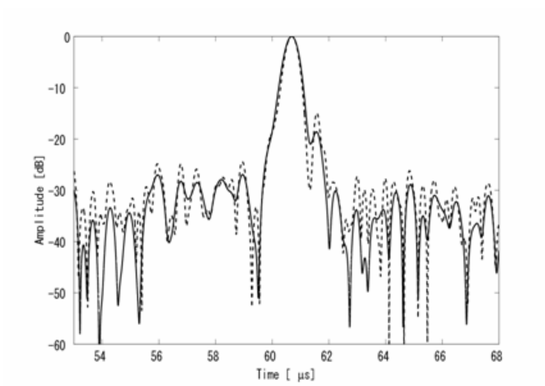

Fig. 1 . Decibel representations of envelopes of proposed signal (solid line) and the harmonic signal simply extracted by band-pass filtering (broken line) in experiment

THURSDAY POSTER

P3Ad - Contrast Therapy

Carribean Ballroom III-V

Thursday, October 20, 2011, 9:30 am - 1:00 pm

Chair: **Tom Thomas**
Boston Scientific

P3Ad-1

Performance evaluation of an automatic controlled sonoporation therapy device

Karin Hensel[1], Georg Schmitz[1]; [1]Electrical Engineering and Information Technologies, Ruhr-Universität, Bochum, Germany

Background, Motivation and Objective

Sonoporation (SP) is the ultrasound induced nonspecific uptake of molecules by cells, which is enforced by the presence of microbubbles (MB). Therapy success strongly depends on the parameters of the acoustic excitation. High sound pressures cause high numbers of dead cells, whereas low pressures result in low SP rates. However, tissue attenuation inhibits reliable prediction of pressure at the therapy site. Consequently, we present a SP device allowing automatic control of therapy pressure by acoustic observation of MB behavior during therapy.

Statement of Contribution/Methods

The SP device employs a custom designed 1 MHz therapy transducer with a central opening for the imaging array of a medical ultrasound machine. Therapy pulses are generated by a function generator and an amplifier. A flow phantom with a constant flow of a SonoVue MB solution in a tube was used. The imaging array allows image guided positioning of the focus of the therapy transducer in the flow phantom. Furthermore, it is used for Phase Inversion imaging during therapy and the observation of the MB response to therapy pulses. The closed-loop control employs the subharmonic to fundamental ratio (SFR) of the MB response as control variable. A PID controller with initial parameters according to Ziegler/Nichols regulates therapy pressure. As a first approach, a calibration curve was used to relate the SFR to the pressure at the therapy site. Control sequences of 150 pulses repeated at 2 Hz were evaluated, while different attenuating layers were inserted between transducer and phantom during pulses 51 to 100.

Results

The SP device successfully compensated for the attenuating layers without steady-state errors by regulating the control variable. Mean rise time and peak overshoot of the step response resulted in 5.3 s and 44%. The sequences' root mean square errors (RMSE) averaged to 0.9%. After adjusting the controller by doubling the integral factor, rise time was significantly reduced to 3.4 s. The most important parameter, however, is the pressure at therapy site, which is derived from the electric excitation of the calibrated transducer and a layer attenuation measurement. Through the effective closed-loop control, a controlled therapy pressure with a mean steady-state error of 21% was achieved. This resulted in a control sequence RMSE of 29%. Thus, the effect of the attenuation layers was successfully reduced, though leaving a steady-state error. The difference in magnitude between control variable and pressure at therapy site indicates an uncertainty in relating SFR to therapy pressure. This is due to SFR being strongly dependent on MB concentration, which can vary significantly during therapy.

Discussion and Conclusions

This study shows the feasibility of the presented SP device to control therapy pressure by acoustic observation of MB behavior. Performance improvement can be expected for a modified control variable, which could combine SFR and information from Phase Inversion imaging.

THURSDAY POSTER

P3Ad-2

Tumor Treatment with Microbubble Enhanced Low-Intensity Ultrasound and Paclitaxel Nanocapsules Reduces Drug Dose Required for Therapeutic Effect

Lee B. Mullin[1], Ping Ma[2], Kennita Johnson[1], Russell J. Mumper[2,3], Paul A. Dayton[1,3]; [1]Joint Department of Biomedical Engineering, University of North Carolina/ North Carolina State University, Chapel Hill, NC, USA, [2]Division of Molecular Pharmaceutics, Center for Nanotechnology in Drug Delivery, University of North Carolina, Chapel Hill, NC, USA, [3]Lineberger Comprehensive Cancer Center, University of North Carolina, Chapel Hill, NC, USA

Background, Motivation and Objective

The development of a drug vehicle that could target a tumor or organ with high specificity and improve therapeutic efficacy, while reducing side effects, is of particular interest for chemotherapy administration. Such targeted therapy would be a significant improvement in standard of care for non-resectable tumors such as pancreatic and hepatic cancer. Prior studies reported in the literature have suggested that applying ultrasound in conjunction with microbubbles at the tumor site can enhance vascular permeability and motivate nanoparticle extravasation. We combine the the addition of low intensity ultrasound (US) and microbubbles (MB) with a drug-bearing nanoparticle to improve the therapeutic index of paclitaxel.

Statement of Contribution/Methods

Lipid MBs were made using DSPC and DSPE-PEG 2000 as the shell components and perfluorobutane as the gas core. Drug delivery nanocapsules (NC) were made with Brij 78, Vitamin E TPGS , Brij78-PEG750, and Miglyol 812, and contained C-22 paclitaxel at a concentration of 0.345 mg/ml.

4T1 mammary carcinoma, a partially resistant tumor, was established in mice. Mice were divided into five groups (each N=8): paclitaxel NC only (NC); paclitaxel NC prior to two minutes of therapeutic US exposure (NC+US); paclitaxel NC co-administered with MB prior to two minutes of therapeutic US (NC+MB+US). The dose of paclitaxel by intravenous injection was 2.5 mg/kg. Therapeutic US was applied using a Sonicator 740 system operated at 1 MHz, 2 W/cm^2, and 10% duty cycle. Treatments were given three times per week for two weeks. Weight and tumor caliper measurements were taken every other day.

Results

Mice treated with NC+MB+US had slower tumor growth compared to treatment with NC or NC+US (figure). A statistically significant difference between NC+MB+US and both NC and NC+US groups was seen on multiple days. No change was seen in animal weight.

Discussion and Conclusions

When compared to treatment with a higher dose of 5 mg/kg (separate study), data suggest treating at a dose of 2.5 mg/kg with NC+MB+US is as effective as treating with NC alone at 5 mg/kg (figure). This finding is significant because lowering a treatment dose may reduce the risk of unwanted side effects. We have demonstrated the potential to use low frequency US in combination with MB and NC to reduce tumor growth in a 4T1 mouse model. Future studies will include more animals and treatment optimization.

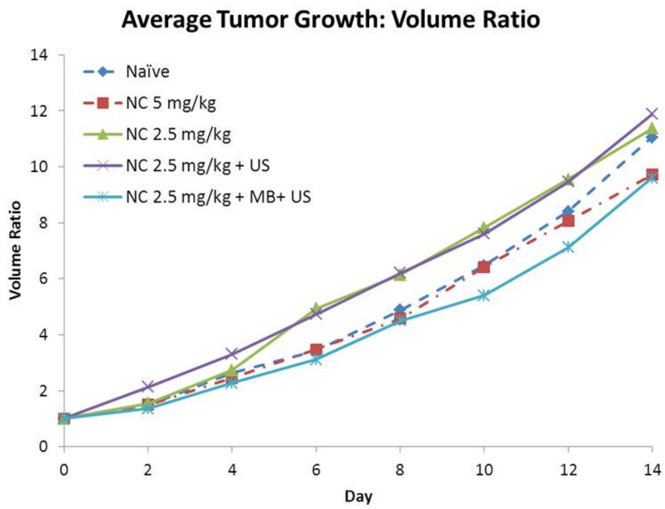

P3Ad-3

Acoustically-Triggered Droplet Vaporization in Macrophages for Hypoxic-Tumor Therapy

Shih-Tsung Kang[1], Chih-Kuang Yeh[1]; [1]Department of Biomedical Engineering and Environmental Sciences, National Tsing Hua University, Hsinchu, Taiwan

Background, Motivation and Objective

Macrophages are potential drug vehicles for tumor therapies since they can migrate toward tumors, and infiltrate avascular and hypoxic areas. The use of macrophages to transport perfluorocarbon (PFC) droplets into hypoxic tumors may enhance efficacy of tumor therapies that utilize acoustic droplet vaporization (ADV). Here we investigated the feasibility and possible physics phenomena of ADV in single macrophages.

Statement of Contribution/Methods

The PFC droplets were composed of perfluoropentane (PFP) and lipids. The macrophages were isolated from the peritoneal cavities of C57BL/6 mice. They were incubated with the droplets for 4 h for ingesting PFP droplets. Flow cytometric analysis showed the cell uptake efficiency up to 87%. Synchronous high speed photography and cavitation detection were conducted in the experiments. A 2-MHz transducer was used to transmit single 3-cycle and 8-MPa ultrasound (US) pulses for inducing ADV. A 40-MHz transducer was used for active cavitation detection (ACD) and passive cavitation detection (PCD) for monitoring bubble generation and inertial cavitation (IC) activity, respectively. One ACD or PCD signal and a series of high-speed images were simultaneously acquired for one ADV event.

Results

The images in Fig. 1(a) show a droplet-loaded macrophage exposed to one US pulse. The vaporized droplets disrupted the cell body at the onset of ADV and then coalesced into a large bubble (~25 μm in diameter). Fig. 1(b) shows a 2.6-fold increase in the amplitude of ACD signal at 1.6 μs for a droplet-loaded macrophage relative to a normal macrophage, indicating the appearance of bubbles at the second-cycle insonation of the US pulse. The time-versus-frequency plot of PCD signal in Fig. 1(c) shows a broadband (20–50 MHz) noise at the same time, indicating the happening of IC when the bubbles appeared. Furthermore, the US image contrast enhanced by the vaporized droplet-loaded macrophages was 10 dB greater than that enhanced by the vaporized free PFP droplets.

Discussion and Conclusions

Here we demonstrated the ADV in single macrophages by insonation with single 3-cycle US pulses. The simultaneously induced IC and bubble coalescence may be beneficial for drug delivery and gas embolotherapy, respectively. We anticipate this technique to increase the efficacy of ADV-based tumor therapies and we are working on in vivo experiments of hypoxic-tumor therapy.

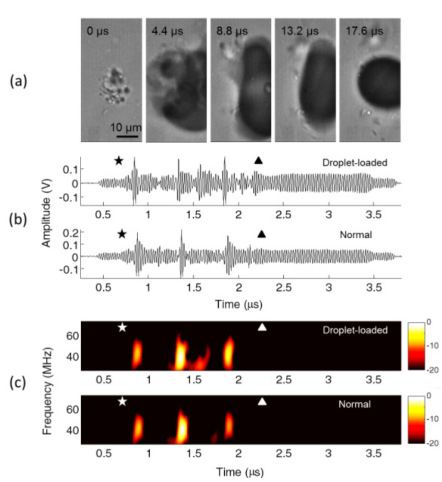

THURSDAY POSTER

P3Ad-4

Ultrasound Therapy with Liposome-microbubble Complex in a Murine Tumor Model

William Shi[1], Talent Shevchenko[2], Balasundar Raju[1], Shriram Sethuraman[1], Zhongmin Du[2], Ralf Seip[1], Eugene Leyvi[1], Alexander Klibanov[2]; [1]*Philips Research North America, Briarcliff Manor, New York, USA,* [2]*University of Virginia, Charlottesville, Virginia, USA*

Background, Motivation and Objective

Localized drug delivery could improve the therapeutic efficacy for treatment of pathological lesions and reduce toxic exposure to healthy organs and tissues. The objective is to develop image-guided, ultrasound-activated tumor chemotherapy with intravenously administrated doxorubicin-liposome-microbubble complexes.

Statement of Contribution/Methods

Decafluorobutane microbubbles were prepared by sonication and stabilized with phosphatidylcholine/PEG stearate/biotin-PEG-PE shell. They were decorated with biotinylated liposomes via a streptavidin link. Liposomes in the complex were loaded with doxorubicin using remote loading ammonium citrate protocol (average drug load 0.6 pg per particle). Subcutaneous murine (C57BL/6) hindleg tumor model (MC38 colon adenocarcinoma cells, provided by J. Schlom, NIH) was used (6 animals per experimental group). After average tumor size reached 5mm, anesthetized mice were subjected to ultrasound treatment (day 1). First, 3 mg/kg doxorubicin entrapped in microbubble-liposome complex was injected intravenously under ultrasound imaging control with imaging system (iE33; Philips). Immediately following injection, entire tumor was insonated in a spiral pattern intermittently (15s on and 10s off, for microbubble replenishment) for 6 minutes with 1.2MHz ultrasound (2MPa, 10000 cycle, 10 Hz PRF, TIPS system with $1\times1\times6$ mm^3 focal zone). Ultrasound treatment combined with 1 mg/kg doxorubicin-liposome-microbubble complex was repeated on day 7. In a control group, animals received doxorubicin entrapped in the carrier without TIPS insonation. Saline-injected animals served as another control. Tumor size and body mass were monitored.

Results

Ultrasound imaging allowed direct observation of the circulating drug carrier. Combination of TIPS ultrasound treatment with doxorubicin-liposome-microbubble complexes resulted in tumor growth suppression, in comparison with both control groups, and showed statistically significant tumor growth inhibition ($p<0.05$) for days 5-9 of the 10-day study, with a maximal tumor size reduction of 31.6% on day 9. Control animals showed unimpeded tumor growth. Relative body mass change during the study was not statistically significant for animals in all groups.

Discussion and Conclusions

Ultrasound activation of the drug-liposome-microbubble complex in the tumor vasculature results in the retardation of tumor growth. The novel liposome-microbubble complex may enable not only localized drug release inside the tumor but also enhanced drug delivery across biological barriers, achieving chemotherapeutic effect. This is a step towards next-generation targeted image-guided therapy.

P3Ad-5

Delivery of drug-loaded microbubbles and disruption of blood-brain barrier by focused ultrasound in a xenograft rat glioma model

Chien-Yu Ting[1], Ching-Hsiang Fan[1], Hao-Li Liu[2], Tzu-Chen Yen[3], Chih-Kuang Yeh[1]; [1]Biomedical Engineering and Environmental Science, National Tsing Hua University, Taiwan, [2]Department of Electrical Engineering, Chang-Gung University, Taiwan, [3]Chang Gung Molecular Medicine Research, Chang-Gung Memorial Hospital, Taiwan

Background, Motivation and Objective

Traditional chemotherapy for treating glioblastoma multiforme (GBM) has limitations such as systemic cytotoxic effects and poor blood-brain barrier (BBB) penetration. Focused ultrasound (FUS) with microbubbles (MBs) has been approved to locally disrupt BBB. In this study, self-made drug-loaded MBs were introduced to delivery the drug of 1,3-bis(2-chloroethyl)-1-nitrosourea (BCNU) and interact with FUS to locally disrupt BBB simultaneously. Thus, local drug-loading release could be increased meanwhile the systemic side effects reducing.

Statement of Contribution/Methods

Cultured C6 glioma cells implanted in twenty-nine Sprague-Dawley rats were used. The BCNU-MBs were fabricated via the thin-film hydration method. The BCNU drug encapsulation efficiency was 68.01±4.35 % by spectrometer. In the study 1-MHz FUS with 0.7 MPa pressure, 5% duty factor, and 2 min sonication were used to minimize the intracerebral hemorrhage. On day 4 and 5 after the implantation of tumor cells, 0.5 ml BCNU-MB was delivered intravenously, following the synergistic effect of FUS. BCNU accumulation in the brain and liver were analyzed by HPLC coupled with an UV detector. Tumor volumes were monitored by MR T2-weighted images to follow outcomes of the treatment.

Results

Typical image of BBB disruption by BCNU-MB with FUS was shown in Fig. A. The HPLC results showed that BCNU-MB delivery system indeed locally release a large number of drugs at FUS-treated hemisphere brains, which reveal 1.5, 2.5, and 4 folds enhancement compared to their own non-treated hemisphere brains corresponding to 1, 2, and 4 number of sonication sites, respectively. (Fig. B) Comparing with only BCNU I.V. direct delivery, the BCNU-MB method performed 3 fold less deposition of BCNU in the liver. The MRI images results show significant reduction in tumor growth (Figs. C and D).

Discussion and Conclusions

In the study, delivery of drug-loaded microbubbles and disruption of blood brain-barrier by focused ultrasound in a xenograft rat glioma model can be achieved at the same time. Future works include modifying specific ligands and SPIO particles on BCNU-MBs surface for targeting therapy and as multimodality contrast agents, respectively.

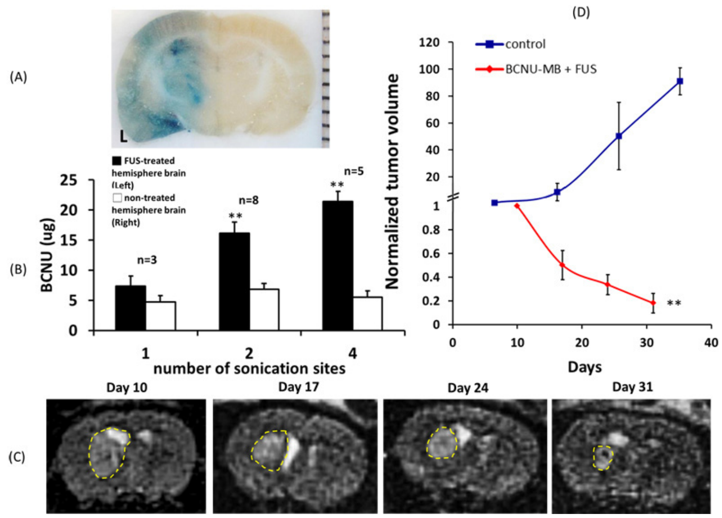

P3Ad-6

Sonoporation of endothelial cells in vivo

Ilya Skachkov[1], Klazina Kooiman[1], Ying Luan[1], Antonius F.W. van der Steen[1,2], Nico de Jong[1,2]; [1]*Erasmus MC, Netherlands,* [2]*Interuniversity Cardiology Institute of the Netherlands, Netherlands*

Background, Motivation and Objective

Ultrasound contrast agents as drug delivery systems are an emerging field [1]. Recently, it was shown that targeted microbubbles (tMB) are able to sonoporate endothelial cells in vitro [2]. This study investigates if tMB can also induce sonoporation in vivo, thereby making it possible to combine molecular imaging and drug delivery. Sonoporation of endothelial cells in the vessel wall were examined without causing rupture of the vessel.

Statement of Contribution/Methods

Live chicken embryos (day 5) were chosen as in vivo model. The lipid-coated MB were made by sonication [3], after which the αvβ3-antibody was conjugated via avidin-biotin bridging [4]. αvβ3 was chosen as target as it is constitutively expressed by the endothelial cells. The model drug propidium iodide (PI) and αvβ3 tMB (~1.8 µm in diameter) were injected in a vitelline vein of the chicken embryo. MB attached to the endothelial wall of the chicken embryo were insonified at 1MHz (1x 1000 cycles) at 200 kPa peak negative acoustic pressure. We studied endothelial cells having between 1 up 10 bubbles attached. Each experiment was repeated 20 times. Sonoporation was studied optically by uptake of PI using a fluorescence microscope.

Results

Endothelial PI uptake was observed in 33% of 120 independently studied MB-vessel wall complexes (n = 32 embryos). All vessels were > 50 µm. Per endothelial cell, 1-19 MB adhered. The uptake of PI as a function of the number of adherent MB is shown in the Figure. We observed 5% PI uptake when 1 or 2 MB adhered, while this increased up to 80% when more than 10 MB adhered. No extravasation of red blood cells and vessel rupture was observed at this low acoustic pressure. Ultrasound or MB alone did not induce PI uptake.

Discussion and Conclusions

This in vivo study reveals that sonoporation can be induced using tMB and low acoustic pressure, without vessel rupture. This unlike previous studies on chicken embryo reporting vessel ruptures using non-targeted MB and 2.5-10 times higher pressures [5]. Further, it was shown that a higher MB concentration on the cell increased the efficiency of sonoporation.

This project is supported by Sonodrugs (NMP-2008-213706).

1. M.R. Böhmer et al Eur J Radiol 2009. 70:242
2. K. Kooiman et al J Control Release, in press
3. A.L. Klibanov et al Invest Radiol 2004. 39:187
4. J.R. Lindner et al Circulation 2001. 104:2107
5. S.M. Stieger et al Radiology 2007. 243:112

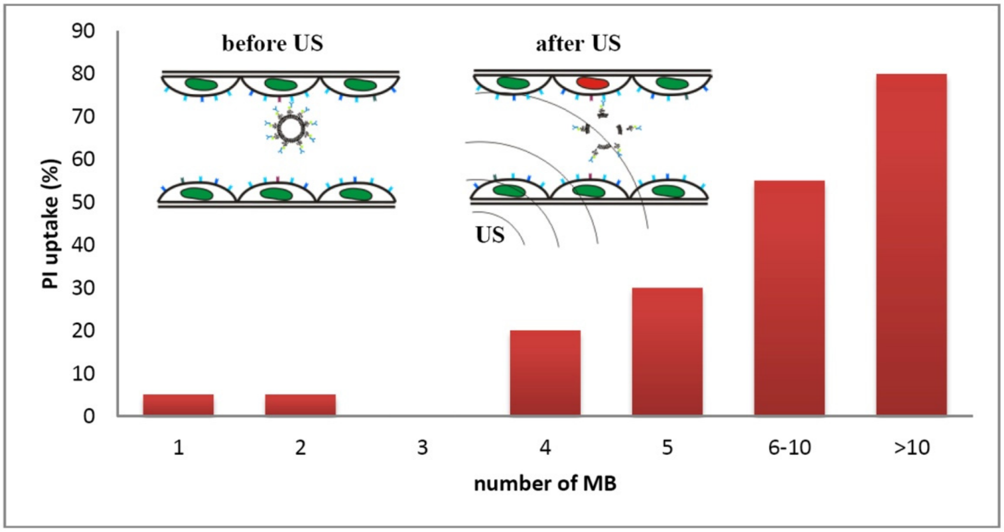

P3Ad-7

The Estimation of Delivery Efficiency of Drug-Loaded Microbubbles in Cancer Cells with US and IVIS

Ai-Ho Liao[1], **Ying-Kai Li[2]**, Wei-Jiunn Lee[3], Hao-Li Liu[4], Ming-Fang Wu[5], Min-Liang Kuo[6], Chih-Hung Wang[7]; [1]Graduate Institute of Biomedical Engineering, National Taiwan University of Science and Technology, Taiwan, [2]Graduate Institute of Biomedical Engineering, National Taiwain University of Science and Technology, Taiwan, [3]Institute of Toxicology College of Medicine, National Taiwain University, Taiwan, [4]Department of Electrical Engineerung, Chang Gung University, Taiwan, [5]Medicine of Animall Medicine Center, National Taiwain University, Taiwan, [6]3Institute of Toxicology College of Medicine, National Taiwain University, Taiwan, Taiwan, [7]Department of Otolaryngology-Head and Neck Surgery, National Defense Medical Center, Taiwan

Background, Motivation and Objective

In combination with drug loaded microbubbles (MBs), increased local concentrations can be achieved by the ultrasound (US) targeted drug release and transiently increased capillary permeability at the site of MBs destruction. To prove the mechanism of US mediated release of drug loaded MBs, this study designs a new model with a method combining the high frequency US image and in vivo bioluminescence imaging system (IVIS). The mechanism of US mediated release of luciferin loaded MBs through blood vessel to targeted cells was investigated.

Statement of Contribution/Methods

The luciferin loaded MBs with a 1591 nm diameter, 2.48x109 bubbles/ml concentration were produced. The concentration of luciferin encapsulated in the shell was 1.48x10-10 mg/bubble. In vitro and in vivo experiments of US mediated release of luciferin loaded MBs with IVIS were performed. The efficiency of US mediated release of luciferin loaded MBs in 4T1-luc2 tumor bearing mice was estimated.

Results

Fig. 1A shows the transmission electron microscope (TEM) image of luciferin loaded MBs. Fig. 1B and C are the IVIS images of luciferin MBs treated cells without and with US energy. Fig. 1D shows the luciferin loaded MBs enhanced US tumor imaging. Fig. 1E and F show the IVIS tumor imaging of luciferin loaded MBs without and with US energy. The photon number of Fig. 1E is 2.475x105 and the photon number of Fig. 1F is 1.040x107.

Discussion and Conclusions

The amount of photon in US mediated release of luciferin loaded MBs is increased obviously and the injection dose of luciferin with US mediated release of luciferin loaded MBs is reduced. The delivery efficiency of US mediated release is higher than non US mediated release with luciferin loaded MBs.

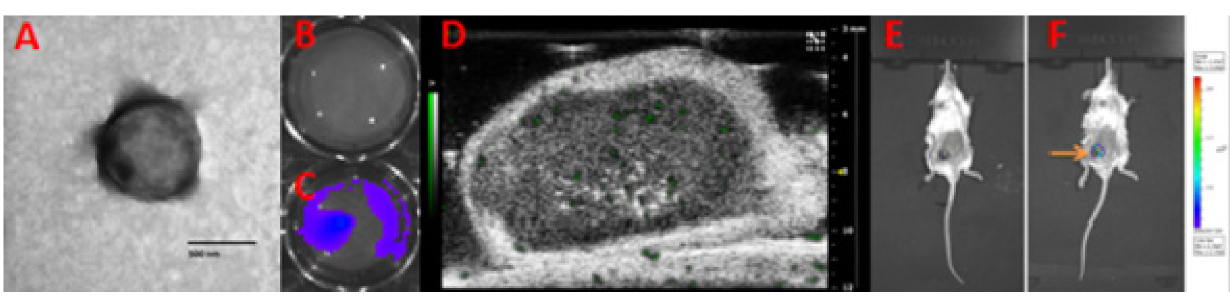

THURSDAY POSTER

P3Ad-8

3D Ultrasonic Molecular Imaging to Assess the Efficacy of an Aurora Kinase Inhibitor in Human Pancreatic Adenocarcinoma

Jason E. Streeter[1], Gabriela Herrera[2], Joey Cao[2], Jen Jen Yeh[2,3], Paul A. Dayton[1]; [1]Biomedical Engineering, UNC / NC State, Chapel Hill, NC, USA, [2]Lineberger Comprehensive Cancer Center, UNC, Chapel Hill, NC, USA, [3]Division of Surgical Oncology, UNC, Chapel Hill, NC, USA

Background, Motivation and Objective

Current therapeutic options towards pancreatic adenocarcinoma (PA) are insufficient. MLN8237 (MLN) is a novel orally delivered aurora kinase inhibitor that stops cell proliferation and has been successful against leukemia and lymphoma. Most early phase trials use the change in tumor volume as a measure for disease response. However, it is difficult to evaluate the true efficacy of drug therapies with tumor size measurements alone due to potentially significant lag times between the time of treatment and change in tumor size. Since ultrasonic molecular imaging (USMI) can provide information prior to the appearance of gross phenotypic changes, it is proposed that USMI can be used to noninvasively assess early response to treatment.

Statement of Contribution/Methods

PA - Patient-derived tumorgrafts (PDTs) were used in this study. This recently developed model is known to better predict therapeutic response in patients relative to traditional cell line models. 10 nude mice with PDTs were used for MI experiments. 5 animals received a dose of 30 mg/Kg of MLN each day over a 48 hour period while the remaining animals were treated with a control vehicle. MI was performed on day 0 and 48 hours after treatment using size-selected microbubble contrast agents (MCAs) fitted with a cyclic RGD peptide targeted to $\alpha v\beta 3$, an angiogenic biomarker. 3D acquisitions were obtained with a Siemens Sequoia in CPS mode by mechanically scanning the transducer across the tumor. The brightness of the targeted MCAs was assumed to be correlated with the degree of biomarker expression.

Results

At 48 hours, mean volumetric targeting decreased by 62% from baseline in treated animals compared to an 8% decrease in targeting for untreated animals (Untreated: 0.92±0.22 vs Treated: 0.38±0.23; $p < 0.05$). Measured volume increased by 3% in treated animals as compared to a 9% increase from baseline in untreated animals (Untreated: 1.09±0.13 vs Treated: 1.03±0.03; $p > 0.05$).

Discussion and Conclusions

3D USMI demonstrated significant changes in expression of angiogenic biomarkers in PA-PDTs in mice, in response to MLN within 48 hours of treatment. In contrast, data showed no appreciable volumetric changes between treated and untreated animals within the same 48 hour time period. Previous studies have shown that over a longer period of time (~2 weeks), treated tumors respond with reduced tumor volume. Monitoring volumetric changes is the “gold standard” for evaluating treatment, however, our data suggests that USMI may provide information about tumor response at earlier timepoints.

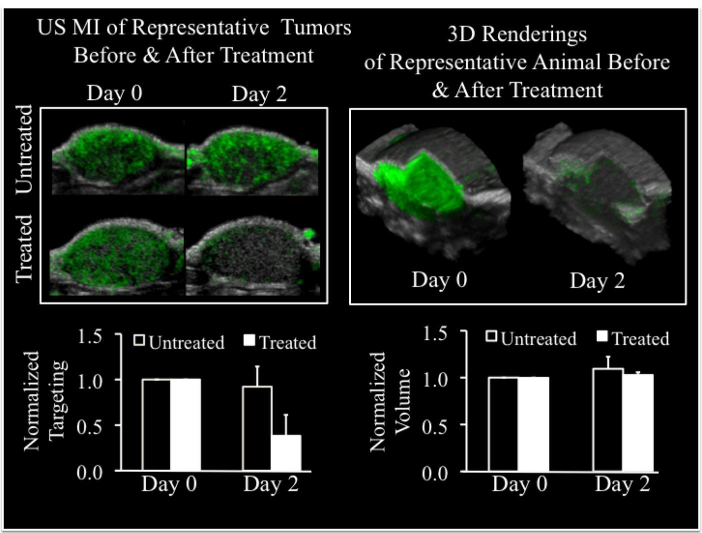

THURSDAY POSTER

P3Ad-9

Ultrasound and microbubble parameter optimization for maximizing sonoporation

Lee Mullin[1], Jun Han[2], Michael Jay[1,2], Paul A. Dayton[1,2]; [1]Joint Department of Biomedical Engineering, University of North Carolina/ North Carolina State University, Chapel Hill, NC, USA, [2]Eshelman School of Pharmacy, University of North Carolina, Chapel Hill, NC, USA

Background, Motivation and Objective

Ultrasound (US) excitation of microbubbles (MB) in proximity to cell membranes can cause sonoporation, which results in enhanced permeability and increased uptake of drugs or other macromolecules. The mechanism behind sonoporation, and the effects of various US and MB parameters, are not yet fully understood and are still being studied. The aim of our study is to optimize cellular uptake through controlling parameter settings including cell-bubble exposure time, pulse repetition frequency (PRF), acoustic pressure, MB size distribution, and MB concentration.

Statement of Contribution/Methods

A549 cells cultured on thermanox cover slips were positioned face down on a stand-off within a FlexCell plate. Calcein, which is too large to normally enter cells, was used as a fluorescent marker to monitor the effects of sonoporation. 1 ml calcein solution (1 mg/ml) with 25 µl of MB was added to the well and incubated (1, 5, 10, or 15 min) before 3 minutes of US exposure with a 1 MHz unfocused transducer. Parameters tested were PRF between 0.150 and 150 Hz, pressures between 300 kPa and 1.2 MPa, number of US/MB exposures from 1 to 3 repetitions, and MB size from 1 – 4 microns mean diameter. After US, cover slips were washed in PBS and fluorescent micrographs were acquired. Images were compared by summing the pixels within areas of intensities above the noise threshold.

Results

Calcein internalization by target cells increased with increasing acoustic pressure, within the range of acoustic pressures tested. Similarly, calcein internalization increased with repeated exposures of the cells to MB and US. Uptake was increased up to 10 fold by increasing pressure from 300 to 1200 kPa and almost by 4 fold by increasing US and MB exposure from 1 to 3 repetitions. Sonoporation as a function of acoustic pressure and exposure repetitions appeared to follow a linear trend. No consistent trend was observed with PRF. Incubation time, which affected the amount of MB that floated into contract with the cell membrane, was observed to result in greater sonoporation after 10 minutes of incubation than 1 and 5 minutes, but data had a large variance and was not statistically significant. MB mean diameter was also observed to affect sonoporation efficiency (data was not statistically significant as of abstract submission, but experiments are being repeated with higher N).

Discussion and Conclusions

Determining optimal US parameters for sonoporation will be beneficial for future studies involving drugs or macromolecules. Challenges for in-vitro studies include selecting parameters that will increase cell permeability, yet not irreversibly damage or detach cells. Increasing pressure and number of US exposures both led to an increase in calcein uptake; however, cells occasionally became dislodged at higher pressures. Preliminary findings suggest there are substantial changes in sonoporation efficiency depending on acoustic parameters, and it is likely that bubble size and bubble concentration also play a role.

P3Ad-10

Theoretical and experimental evaluation of microstreaming created by a single microbubble: application to sonoporation

Anthony Novell[1], James Collis[2], Alexander Doinikov[1], Andrew Ooi[2], Richard Manasseh[3], Ayache Bouakaz[1]; [1]Inserm U930, CNRS ERL 3106, université François Rabelais de Tours, France, [2]Department of Mechanical Engineering, University of Melbourne, Australia, [3]Faculty of Engineering and Industrial Sciences, Swinburne University, Australia

Background, Motivation and Objective

It is well known that a steady vortical flow, referred to as acoustic microstreaming, is generated around a bubble in an ultrasound wave field. It is hypothesized that this phenomenon might play a role in the sonoporation process, inducing shear stresses which create tension and stretching over the cell membrane and likely its transient permeabilization. However, the prediction of the microstreaming and its influence on the sonoporation process is still a complex problem. In this study, the results of microscopic particle-image velocimetry (PIV) for air bubbles are presented and compared to those obtained using a numerical model.

Statement of Contribution/Methods

A PIV system was used to measure the flow generated by oscillating bubbles of different sizes ranging from 238 to 410 µm in diameter. Air bubbles were created in a water solution using the syringe and were then attached to a wall. The microstreaming around a bubble was measured using particles consisting of polystyrene spheres of 2 µm in diameter. For each bubble, the flow was measured over a plane located at a distance of 50 µm from the bubble wall. Bubbles were excited using a single element transducer at 28 kHz and 7 kPa.

The acoustic streaming generated by the air bubble was calculated for the same excitation signal using a theoretical model based on an analytical solution of the time-averaged Navier-Stokes equation. This approach was extended to estimate the acoustic streaming around an encapsulated gas microbubble, such as a contrast agent microbubble, using an excitation signal centered at 2.87 MHz and pressure of 50 kPa.

Results

The mean velocity of the microstreaming was estimated from the PIV system as a function of the bubble size (19 different bubbles). A maximal peak value of 0.25 mm/s occurs near the bubble resonant size (244 µm diameter bubble). For this bubble, the shear stress is also maximal. Our experimental measurements also reveal an additional peak (in the range 280-300 µm) but with a lower amplitude. Theoretical data demonstrate a maximal velocity of 0.15 mm/s for bubbles close to the resonant size (235 µm). The simulations also show an additional peak for bubbles larger than 270 µm. The theoretical model predicts that the second peak arises since the flow velocity changes its direction after the bubble diameter passes through the resonance value. Using contrast agent microbubble model, a maximal flow velocity and shear stress of 4 mm/s and 19 Pa respectively are obtained for a 2.5 µm diameter encapsulated bubble.

Discussion and Conclusions

The measurements and simulations are in a good qualitative agreement which validates the theoretical model. For small contrast bubbles, the theory predicts that shear stresses produced by acoustic microstreaming (19 Pa) are much higher than those produced by normal blood flow (0.5 – 2 Pa). These results suggest that bubbles are capable of exerting significant shear stresses on the cell membrane, affecting likely its permeabilization and thus the sonoporation process.

P3Ad-11

Choice and normalization of contrast ultrasound parameters for detection of anti-angiogenic response

Thomas Payen[1], Aymeric Guibal[2], Michele Lamuraglia[2], Olivier Lucidarme[2], Delphine Le Guillou[3], Sharon Lori Bridal[3]; [1]*Laboratoire d'Imagerie Paramétrique UMR 7623 CNRS UPMC, Paris, Ile-de-France, France,* [2]*Université paris VII, France,* [3]*Laboratoire d'Imagerie Paramétrique UMR 7623 CNRS UPMC, France*

Background, Motivation and Objective

Contrast ultrasound can detect perfusion modifications during anti-angiogenic therapy preceeding tumor size regression. However, assessment is sensitive to injection variability and perfusion parameters choices are not yet standardized. This work compares discrimination of tumors in Sorafenib-treated and placebo mice using contrast ultrasound evaluation of relative blood volume (BV), mean transit time (mTT) and wash in rate (WiR). Results are compared with and without normalization by normal cortex.

Statement of Contribution/Methods

At Day 0, 15 tumors were grafted orthotopically by sub-capsular injection of SK-NEP-1 cells in kidney of nude mice. From D14, 7 mice received sorafenib daily and 8 received corresponding doses of placebo. Contrast ultrasound with destruction-reperfusion was performed prior to and as a function of time after therapy from D12 to D23 with a clinical ultrasound system (Acuson Sequoia 512; Siemens) with a broadband 7- to 14-MHz transducer and cadence contrast pulse sequencing. Retro-orbital injection of 100 µL of Sonovue (Bracco) was performed 25 seconds before destruction of microbubbles in an image plane presenting the tumor and kidney. Then, data were acquired at a mechanical index of 0.25 and a dynamic range of 75 dB. Linearized intensity-time curves calculated in regions of the tumor and adjacent regions of the renal cortex were fit using a sigmoid model. The maximum slope (WiR), the plateau value (BV) and the half-time to the plateau (mTT) were assessed to characterize perfusion. To normalize for injection variability, values calculated in the tumor were normalized with respect to those of an adjacent region of the renal cortex. At D23 the tumor mean weight was measured. A Wilcoxon test was used to compare the results.

Results

Ultrasound estimates of the tumor size increased with time for both groups, but tumor size was never significantly different between treated and placebo groups ($p \geq 0.28$). This was consistent with end-point measurements of the tumor mean weight : placebo 0.45g vs. treated 0.37g (p=0.88). Without normalization, none of the studied parameters was significantly different between the treated and the placebo groups at any time. Even with normalization, neither BV nor mTT discriminated between the two groups. With normalization with respect to the adjacent renal cortex perfusion, however, nWiR was significantly lower for treated than for placebo ($p \leq 0.004$) from D22. The end point values at D23 were 0.007±0.006 treated and 0.06±0.04 placebo.

Discussion and Conclusions

Only nWiR detected anti-angiogenic response in this model. This parameter may be more robust than estimates based on the plateau value or the half-time to the plateau because when tumor filling was slowed complete filling is not always obtained within the recorded time. Normalization with respect to adjacent normal tissue appears to reduce estimate variability and improve functional contrast assessment.

P3Ae - Therapeutical Effects, Microbubbles and Drug Delivery

Carribean Ballroom III-V

Thursday, October 20, 2011, 9:30 am - 1:00 pm

Chair: **Kullervo Hynhynen**
Univ. of Toronto

P3Ae-1

Improving the activation threshold of acoustic droplet vaporization agents through precision formulation using microfluidics

Thomas D. Martz[1], Paul S. Sheeran[2], David Bardin[3], Steven Feingold[2], Abraham P. Lee[3], Paul A. Dayton[2]; [1]Material Science, University of North Carolina, Chapel Hill, North Carolina, USA, [2]Biomedical Engineering, UNC & NCSU, Chapel Hill, North Carolina, USA, [3]Biomedical Engineering, UCI, Irvine, California, USA

Background, Motivation and Objective

Acoustic droplet vaporization has demonstrated potential in areas such as embolotherapy, drug delivery, and contrast enhancement. Traditional methods of formulating perfluorocarbon (PFP) droplets typically have poor size control, both in mean diameter and polydispersity. We hypothesized that microfluidics could be used for precision formulation of PFP droplets, and that resulting uniform sized droplets would have uniform acoustic vaporization thresholds.

Statement of Contribution/Methods

Polydimethylsiloxane microfluidic chips designed with flow-focusing orifices allowed for the uniform creation of PFP droplets over a wide range of diameters. PFP droplets were exposed to 200-cycle, 7.5 MHz, acoustic pulses at varying acoustic pressures, and optically monitored with high-speed imaging to assess vaporization thresholds.

Results

Microfluidic production enabled precision control of PFP droplet diameter, with droplets ranging from 20 microns down to 488 nanometers. Standard deviations of the PFP population were 0.6, 0.3, 0.4, 0.4, and 0.4 respectively for populations of mean diameter of 7.8, 11.3, 13.8, 16.6, and 20.8 µm (Figure 1 A-D). Acoustic studies demonstrated that the activation threshold of these PFP droplets was very consistent; approximately 3.98±0.05, 3.51±0.07, 2.97±0.10, 2.54±0.08, and 2.32±0.04 MPa, respectively (Figure 1 E). Our system could also be adjusted to produce droplets below a micron in diameter (Figure 1 F).

Discussion and Conclusions

The ability to precisely formulate encapsulated perfluorocarbon droplets of specific uniform diameter may enable tailored applications such as vessel-size specific embolotherapy. Additionally, improved size control enables more consistent energy levels for achieving acoustic activation with maximum efficiency.

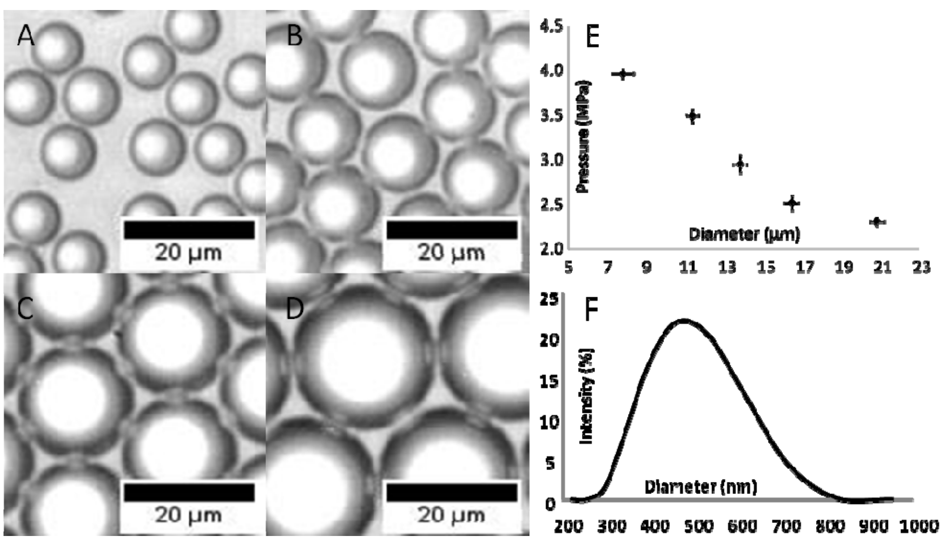

P3Ae-2

ffects of Tissue Mechanical Properties on Histotripsy

Eli Vlaisavljevich[1], Charles Cain[1], Zhen Xu[1]; [1]Biomedical Engineering, University of Michigan, Ann Arbor, MI, USA

Background, Motivation and Objective

Histotripsy is a non-invasive ablation method that depends on a cavitation bubble cloud to mechanically fractionate tissue. Tissue mechanical properties have been observed to affect histotripsy which is often self-limiting at anatomical boundaries such as blood vessels. Understanding the effects of tissue properties is essential to optimize treatment for specific tissues. This work studied the effects of tissue properties on the pressure threshold to initiate the cavitation cloud and the resulting erosion induced by histotripsy.

Statement of Contribution/Methods

Histotripsy pulses were applied by 1 MHz focused transducer (focal distance = 9 cm, f-number = 0.9) inside agarose tissue phantom and fresh porcine tissue. Five cycle pulses at PRF of 10, 100, and 1000 Hz were used as these parameters generated fractionation in vivo. Mechanical properties of the phantom were varied over physiologically relevant range by changing agarose concentration of 0.3-5%. Ultimate stress and density were selected to measure tissue strength. The peak negative pressure at which cavitation cloud was first

THURSDAY POSTER

observed by ultrasound imaging was recorded as the initiation threshold. The extent of erosion at a phantom-fluid interface induced by 5000 pulses was assessed by measuring average lesion depth and diameter. The same studies were also conducted on freshly harvested porcine tissue.

Results

Results demonstrate increased initiation threshold and decreased erosion size with increased mechanical strength (Fig.1). Increases in phantom strength resulted in increased cloud initiation threshold. This trend was verified ex vivo with increased threshold for stronger tissue (skin, tendon, cartilage) in comparison to soft tissue (liver, kidney) and no cavitation in bone. Increased phantom strength also resulted in decreased lesion size indicating stronger tissue is more resistant to histotripsy. This finding was verified ex vivo with no erosion observed for stronger tissue (bone, skin, cartilage) compared to complete erosion for softer tissue (nerve, liver, kidney, heart, brain).

Discussion and Conclusions

This study shows a significant increase in cloud initiation threshold and decrease in tissue damage for higher strength tissue. This work improves our understanding of how tissue properties affect histotripsy and will guide acoustic parameter optimization for histotripsy tissue fractionation.

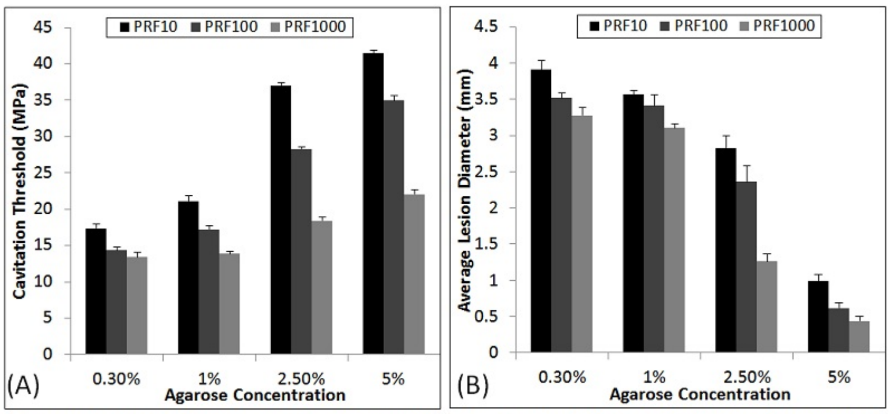

Figure 1. Increased phantom concentration results in increased cavitation cloud initiation threshold and decreased lesion size. (A) Threshold results show significant increase in the peak negative pressure required to initiate cavitation inside higher concentration tissue phantoms. **(B)** Erosion results show a significant decrease in average diameter for higher concentration agarose phantoms. All differences between phantoms were considered significant (p-values<0.05).

P3Ae-3

Permeability and Reversibility Timeline Study of the Focused-Ultrasound Induced Blood-Brain Barrier Opening at Distinct Pressures and Microbubble Sizes *in vivo*

Gesthimani Samiotaki[1], Fotios Vlachos[1], Yao-Sheng Tung[1], Elisa Konofagou[1,2]; [1]Biomedical Engineering, Columbia University, New York, NY, USA, [2]Department of Radiology, Columbia University, New York, NY, USA

Background, Motivation and Objective

Most currently available therapeutic compounds cannot cross the blood-brain barrier (BBB), and their delivery to the brain remains a critical impediment. Focused Ultrasound (FUS) in conjunction with systemically administered microbubbles has been shown to open the BBB locally, non-invasively and reversibly. The objective of this study was to assess the permeability changes and the reversibility timeline of FUS-induced BBB opening using different acoustic pressures, monodispersed microbubbles of different sizes, and the widely used polydispersed Definity® microbubbles, as well as provide quantitative insight to the BBB opening's physiology.

Statement of Contribution/Methods

The acoustic, peak- negative pressures used ranged between 0.30 MPa and 0.60 MPa, the customized, monodispersed microbubbles were 1-2 μm, 4-5 μm and 6-8 μm in diameter while the commercially available Definity microbubbles were 1.1 – 3.3 μm in diameter. Fifty-five mice were sonicated with pulsed FUS which was emitted at a center frequency of 1.5 MHz for 60 s at a burst rate of 10 Hz and 100 burst cycles. Dynamic Contrast-Enhanced MRI (DCE-MRI) and longitudinal T1-weighted MRI images were acquired in order to quantify the permeability changes and the reversibility timeline respectively. Omniscan was used as a tracer to depict the area of opening.

Results

Permeability values (K-trans) maps were found to be proportional to both the pressure and the microbubble diameter. A K-trans plateau of approximately 0.05 min^{-1} was reached at higher pressures for the larger-sized microbubbles (4-5 and 6-8 μm). Smaller bubbles (1-2 μm) yielded significantly lower permeability values (0.01-0.04 min^{-1}), similar to or slightly greater than Definity®. The volume of opening was found to increase with both pressure and microbubble diameter. The reversibility timeline, i.e. the duration required for closing, ranged from 4 h for Definity microbubbles, to 24 h for the 1-2 μm bubbles and, finally, up to 5 days for the 4-5 and 6-8 μm bubbles at higher pressures.

Discussion and Conclusions

The BBB opening volume, permeability values and duration were shown to be dependent on acoustic pressure and microbubble size. There were no significant differences between the 4-5 and 6-8 μm bubble cases. Pressure played a more critical role when using the 1-2 μm and the Definity microbubbles. Closing timeline for 4-5 and 6-8 μm bubbles was much longer than what has been previously reported. Closing timeline for the 1-2 μm bubbles, a size closer to the diameter range commonly used, was shorter. BBB opening reduced daily and radially towards the focal region, to complete reinstatement. Finally, the time required for closing was found to be linearly proportional to the volume of the BBB-opened region and the permeability amplitude on the day of opening.

This study was supported in part by NIH R01 EB9041.

P3Ae-4

Feasibility Study of Using Macrophages as Drug Delivery Carriers for Drug-Loaded Phase-Change Droplets

Ya-Hsuan Lee[1], Chung-Hsin Wang[1], Shih-Tsung Kang[1], Chih-Kuang Yeh[1]; [1]Biomedical Engineering and Environmental Science, National Tsing Hua University, Taiwan

Background, Motivation and Objective

Tumors normally possess irregular vasculature, and tend to outstrip blood supplement and become hypoxia or ischemia. These confer the resistances of the tumor to conventional chemotherapy and radiotherapy. Here, we investigate the feasibility of using macrophages that can infiltrate hypoxic or ischemic areas in tumors, as the carriers of drug-loaded phase-change droplets.

Statement of Contribution/Methods

RAW 264.7 cells were used to ingest the drug-loaded phase-change droplets for 4 h. The droplets were composed of lipid, perfluoropentane and commercial doxorubicin (Dox). For maintaining viability and mobility of macrophages, the stability and cytotoxicity of fabricated droplets were optimized through the composition regulation. Fluorescence spectrophotometer was used to determine drug encapsulation efficiency. Flow cytometric analysis, MTT analysis, and transmembrane cell migration assay were conducted to determine the uptake efficiency, viability, and migration mobility of droplet-loaded macrophages.

Results

The fabricated droplets had a mean size of 1.16± 0.05 µm with a Dox encapsulation efficiency of 51.66±2.58% (51.66 µg/mL). After the 4-hour incubation, the macrophages ingested considerable Dox-loaded droplets and were still adherent on the cell culture plate (Fig. a, b). Flow cytometric analysis showed about 80-90% of cell uptake efficiency. MTT analysis showed that the macrophages were still alive after 24 h (Fig. c), indicating that no cytotoxicity was resulted from the encapsulated Dox. The droplet-loaded macrophages possessed sufficient migration mobility in the transmembrane migration assay (Fig. d). The Dox-loaded droplets were maintained in the liquid phase and stayed in the cell body during the transmembrane movement for at least 6-12 h, showing the promise for achieving the delivery process *in vivo*.

Discussion and Conclusions

These results demonstrate the feasibility of using macrophages to deliver Dox-load phase-change droplets. Ultrasound-triggered vaporization was also performed to investigate the effect of the amount and sizes of ingested droplets on drug liberation efficiency from the droplet-loaded macrophages. Future works include the assessments of the migration ability of droplet-loaded macrophages and the liberated drug payload via ultrasound-triggered vaporization *in vivo*.

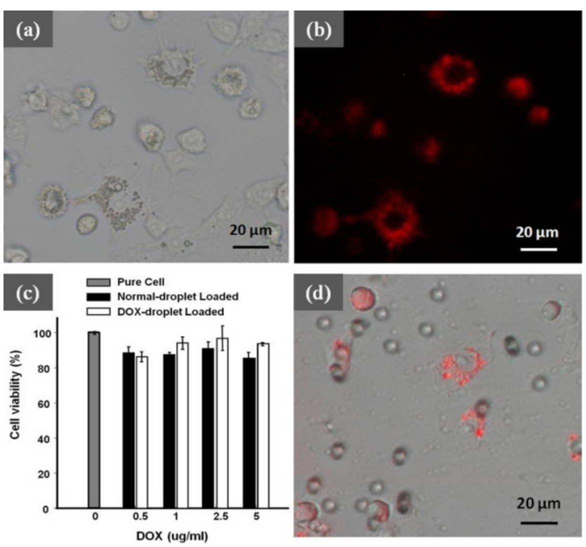

P3Ae-5

Low Intensity Ultrasound Substantially Improves the Efficacy of Bisphosphonate Zoledronic Acid in the Treatment of Breast Cancer Bone Metastases in Animals

David Melodelima[1], Jacqueline Ngo[1], Delphine Goehrig[2], Jean-Yves Chapelon[1], Philippe Clezardin[2]; *[1]U1032, INSERM, Lyon, France, [2]U1033, INSERM, Lyon, France*

Background, Motivation and Objective

Breast tumor cells metastasize to the skeleton and stimulate osteoclast-mediated bone resorption, leading to the formation of osteolytic lesions. Bisphosphonates are potent inhibitors of osteoclast-mediated bone resorption and have demonstrated clinical utility in the palliative treatment of patients with bone metastases. The feasibility of combining the action of a bisphosphonate (zoledronic acid) with low intensity ultrasound was tested in this study. Material and Methods

Statement of Contribution/Methods

Mechanical effects (1.24 MHz) were created using pulsed ultrasound (200 µs) at 40 mW/cm2 (SATA) repeated every 1 ms. Thermal effects (2.85 MHz) were produced using 7 acoustic watts in continuous mode. Fifty-eight mice bearing bone metastases were included and randomized into 8 groups. A single dose of zoledronic acid was combined with a single or daily application of ultrasound (repeated for 15 days). Each ultrasound treatment lasted 30 minutes. These treatment strategies were compared with vehicle, ultrasound alone and zoledronic acid alone.

Results

Radiographic analysis on day 18 after tumor cell injection (the day when treatments start) revealed that all tumor-bearing mice had homogeneous osteolytic lesions. The average osteolytic surface was 0.64 ± 0.14 mm2 (no statistical differences was observed between groups). Radiographic analysis on day 32 after tumor cell injection revealed that ultrasound alone did not have any inhibitory effect on bone destruction when compared to vehicle-treated animals. As expected, zoledronic acid alone reduced bone destruction compared to vehicle. Most importantly, we found a further statistically significant decrease of bone destruction as well as a reduced skeletal tumor burden in metastatic animals that received a daily treatment with ultrasound (thermal or mechanical) in combination with zoledronic acid.

Discussion and Conclusions

The use of low intensity pulsed ultrasound may have produced mechanical effects that increase and accelerate the expression of genes associated with bone formation. This reduce the effect of tumor-derived growth factors on osteoblasts. On the other hand, the use of low intensity ultrasound delivered continuously produces thermal effects up to 43°C. Hyperthermia have produced better intracellular diffusion of the bisphosphonate in the tumor due to a concomitant increase in cell membrane permeability and higher intratumoral blood flow. This increase the bioavailability of the bisphosphonate for tumor cells leading to direct anti-tumoral activity.

Therefore, the combination of low intensity ultrasound with bisphosphonates render the bone a less favorable microenvironment for tumor cell colonization by reducing tumor-derived growth factors released in the bone matrix. In this preliminary work we used clinical doses of bisphosphonates and ultrasounds, suggesting that clinical application of such therapy is conceivable.

P3Ae-6

Intracellular Delivery of Nanoparticles using Ultrasound

Mercy Afadzi[1,2], Svein-Erik Måsøy[2], Yngve Hofstad Hansen[1], Rune Hansen[2,3], Tonni Franke Johansen[2], Bjørn Angelsen[2], Catharina de L Davies[1]; [1]*Department of Physics, The Norwegian University of Science and Technology, Trondheim, Norway,* [2]*Department of Circulation and Medical Imaging, The Norwegian University of Science and Technology, Trondheim, Norway,* [3]*Medical Technology, SINTEF Health Research, Trondheim, Norway*

Background, Motivation and Objective

A prerequisite for successful cancer therapy (drug delivery) is that the cytotoxic agents reach all cancer cells in sufficient concentrations and inactivate them. However, the cellular uptake of chemotherapeutic drugs is restricted by the cell membrane. It has been shown that ultrasound-mediated drug delivery enhances the cellular uptake of these drugs, nevertheless, the mechanism of sonoporation have not been fully understood. In this work, the mechanism of ultrasonic enhancement of the uptake of liposomal doxorubicin (Dox) (88 nm) and FITC-dextran (4–2000 kDa) by Hela cells has been studied using a focused transducer (300 kHz) with varying acoustic parameters.

Statement of Contribution/Methods

The liposomes were labelled with a hydrophobic dye (DiD) in order to separate the cellular uptake of intact liposomes and released Dox. Hela cells in suspension with labelled liposomes or dextran were exposed to different acoustic parameters (0.0 to 1.6 MPa peak negative pressures, 10 and 20%, 120s and 180s insonication time) in the presence and absence of micro-bubbles (MB). After ultrasound exposure, the cellular uptake of nanoparticles and cell viability (determined by cellular uptake of propidium iodide (for dextran)) were measured using flow cytometry. Confocal microscopy was also used to confirm uptake of nanoparticles in cells.

Results

At a constant duty cycle (10%) and insonication time (120s), cellular uptake of Dox and dextran increased (linearly) from 5 to 53.3% and 4 to 65% respectively with increase in acoustic peak negative pressure (0.0 to 0.58 MPa). Uptake was hardly observed without MB even at higher peak negative pressures. In the presence of MB, free dox (but no DiD) was observed in the cells, whereas without MB few cells were observed with DiD as well as Dox. This indicates that, in the presence of MB, ultrasound released the Dox from liposomes before the cellular uptake. Also, dynamic light scattering measurements of liposomes with MB confirmed that ultrasound destroyed the liposomes, and some large aggregates were formed. Futhermore, there was no statistical difference ($p \geq 0.3$) between the uptakes of different sizes of dextran in the presence of MB.

Discussion and Conclusions

The result indicates that ultrasound and MB enhances cellular uptake of nanoparticles (Dox and FITC-dextran) than ultrasound alone. Again, the size of the pores in the cell membrane might be equal or larger than the size of the biggest dextran since cellular uptake was found to be independent of the size of dextran. The improved uptake might be due to sonoporation or endocytosis, which is under investigation. The results show that ultrasound enhances cellular uptake of therapeutic molecules and has the potential to improve cancer therapy.

P3Ae-7

Trapping of solid particles by cavitation-induced acoustic streaming

Adam Maxwell[1], **Simone Park**[1], Charles Cain[1], Zhen Xu[1]; [1]*Biomedical Engineering, University of Michigan, USA*

Background, Motivation and Objective

Cavitation clouds can be generated by short, high-amplitude, focused ultrasound pulses. This cavitation activity can be used to noninvasively remove occlusive blood clots. It has also been observed in-vitro that free clot particles in the blood are attracted, trapped, and eroded by the cloud, even against flow. Such phenomenon may be useful to prevent embolism during cardiovascular procedures such as thrombolysis. This study investigated the mechanism of particle trapping.

Statement of Contribution/Methods

A 6-mm diameter vessel phantom was constructed using a 10% gelatin solution. A peristaltic pump provided flow through the phantom. Spherical agarose beads between 1-4 mm diameter were used to mimic clot particles. A 10-cm diameter, 10-cm focal length 1 MHz focused transducer was used to apply pulses with peak negative pressure of 13 MPa to the vessel. Acoustic pulse durations between 5-20 cycles and repetition rates between 100 – 2000 Hz were applied. The focus was positioned centered in the vessel such that the acoustic propagation was perpendicular to the vessel long axis. High-speed photography and particle image velocimetry were used to image the fluid flow generated by ultrasound in the phantom and the interaction of the flow with particles.

Results

Acoustic streaming velocities at the focus up to 1.2 m/s were generated in the vessel when cavitation was observed. A high-velocity fluid jet was generated through the focus along the direction of propagation, with fluid vortices generated to either side of the focus. Particles were trapped near the edge of the cavitation cloud in the vortex. Acoustic parameters which generated higher streaming velocities were able to trap particles at higher mean crossflow velocity through the vessel, up to 12 cm/s. Streaming reduced the crossflow velocity downstream from the focus, reducing the drag on the particle. Estimation of the fluid pressure field indicated a gradient towards the focus, attracting the particle against the vessel flow.

Discussion and Conclusions

Acoustic trapping of solid particles in a vessel phantom is caused by fluid streaming. Streaming is enhanced by a cavitation cloud generated at the focus. This streaming is accompanied by a region of low pressure near the focus, which effectively traps the particle and provides a counter-force to the drag on the particle caused by the crossflow.

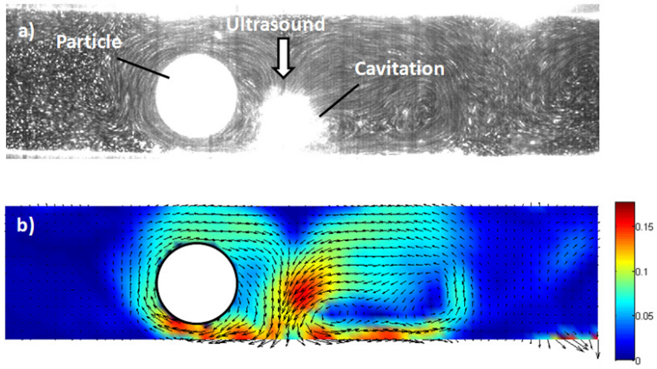

Fig.1. Photograph (a) and fluid velocity map (b) of flow in vessel phantom with particle trapped near the focus in a vortex. Color indicates velocity magnitude in (b).

P3Ae-8

High Frame Rate Imaging of Cavitation Events Using Dual-mode Ultrasound Arrays

Andrew Casper[1], Alyona Haritonova[1], Emad Ebbini[1]; [1]*University of Minnesota, USA*

Background, Motivation and Objective

Modern therapeutic ultrasound systems, especially those using phased arrays, allow for exquisite spatial and temporal control of the HIFU beam(s) to create desired levels of cavitation activity to enhance the therapeutic effect. In practice, real-time monitoring and characterization of the cavitation activity will be the key to controlling the lesion formation trajectory. Dual-mode ultrasound array (DMUA) systems are capable of high frame rate monitoring of cavitation events with both active and passive imaging in water and tissue. The imaging methods were interleaved at a frame rate of 2000 fps allowing both methods to image the same events and track these events over time.

Statement of Contribution/Methods

Using a 64 element, 1 MHz DMUA, together with a 64-channel data acquisition system, we were able to capture discrete cavitation events resulting from short pHIFU beams (~100 uS). This was performed for a variety of electronically steered pHIFU beams. The echoes from these many-cycle initiation pulses were used to form passive images of the cavitation events. In addition, active images were formed by beamforming echo data from imaging pulses generated shortly after pHIFU.

Results

Single focus and multiple focus patterns were used to generated and monitor cavitation events, allowing for localization of distinct cavitation regions. The attached figure shows a comparison between passive and active imaging on a cavitation event in water. The focus was steered to -5 mm laterally and +100 mm axially. This image represents a single frame collected 5 msec after the initial pulse. The entire time series of frames allow for analysis of the cavitation events from inception to dissolution. Gross histology of short-exposure pHIFU (~ 300 msec) in ex vivo tissue showed spotty tissue change consistent with discrete cavitation events.

Discussion and Conclusions

The DMUA provides a clinically relevant platform for imaging cavitation events. The imaging beam is identical to that of the therapeutic beam and does not require registration between imaging and therapy transducers. By combining both passive and active imaging at high frame rates, on a single transducer, both methods can be used to complement the other. Passive imaging allows for long time records useful for identifying signatures of cavitation, while active imaging allows for highly localized spatial maps of cavitation activity.

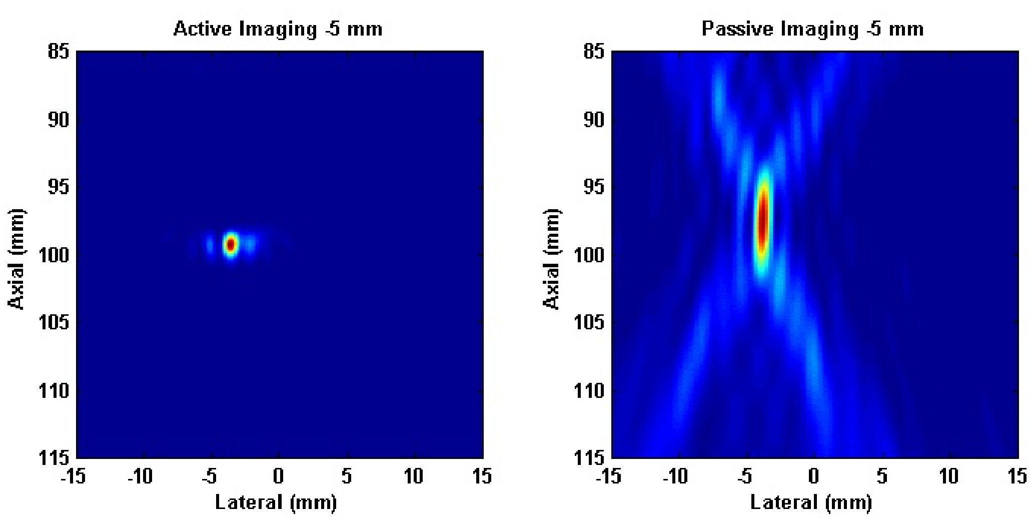

THURSDAY POSTER

P3B Ultrasonics and Fluidics

Carribean Ballroom III-V

Thursday, October 20, 2011, 9:30 am - 1:00 pm

Chair: **Mario kupnik**
Brandenburg University of Technology , Germany

P3B-1

Translocation of microparticles in a fluid-flow by adjusting the operating frequency of ultrasonic standing wave (USW)

SeungHyun Cho[1], A. K. M. Ariful Haque Siddique[1,2], CheolGi Kim[2], Bongyoung Ahn[1]; [1]Center for Safety Measurement, Korea Research Institute of Standards and Science, Yuseong-Gu, Daejeon, Korea, Republic of, [2]Department of Materials Science & Engineering, Chungnam National University, Yuseong-Gu, Daejeon, Korea, Republic of

Background, Motivation and Objective

Recently, many studies have been reported on the non-contact manipulation of microparticles in a fluid-flow using ultrasound since ultrasonic standing wave enables particles to align to its pressure nodal or anti-nodal plane depending on their density and compressibility due to the acoustic radiation force. This phenomenon can be applied usefully to noncontact and rapid manipulation such as trapping and translocation of organic or inorganic microparticles like cells and ceramic powder in many technological fields. The objective of this work is to find an efficient way to translocate microparitcles to one side of a flow channel in the aim of several applications like filtration & separation of particles & cells etc.

Statement of Contribution/Methods

A modulized microchannel comprising steel and acryl with a width of 1.5 mm was manufactured. An ultrasound transducer installed at one side of the microchannel module generates ultrasonic standing wave field inside the channel. Ultrasound within the frequency range of 1.81 MHz ~ 3.14 MHz was applied to concentrate particles at the pressure nodal lines. SiC particles or Polystyrene microspheres mixed in distilled water respectively were used as test particles. The aligned particles at pressure nodal lines can be moved to a certain degree as varying the operating frequency of the ultrasound since the location of the pressure nodes depends on the frequency. The total range of the particle movement by changing only frequency is somewhat limited, but it is possible to shift all particles nearly to the channel wall when using periodical increasing sweep as an actuation signal.

Results

Figure shows the experimental result of translocation of microparticles in a 1.5 mm Steel-Acryl channel.

Discussion and Conclusions

The experimental results confirm that the sweeping of the operational frequency can be one of efficient methods to translocate microparticles in fluid-flow using ultrasound. This method may be successfully utilized in the field of filtration and separation techniques.

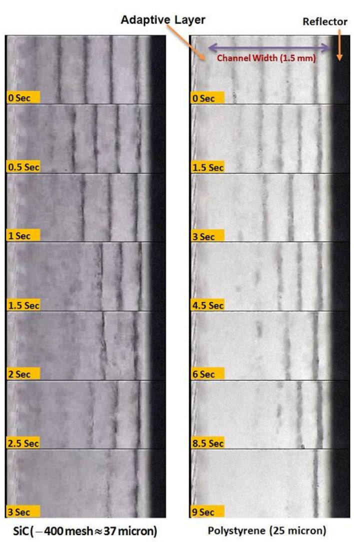

P3B-2

Microrheological monitoring of life cycle of yeast cell Saccharomyces cerevisiae

Emmanuel Caplain[1], Jean-Marie Ringeard[2], Stephane Serfaty[2], Loic Martinez[2], Pascal Griesmar[2]; [1]SATIE (CNRS - UMR 8029), Université de Cergy-Pontoise, France, Metropolitan, [2]Université de Cergy-Pontoise, France, Metropolitan

Background, Motivation and Objective

The conversion of added-value products using cheaper resources such as glycerol could develop the biofuel industry becoming more economically viable. Even if some microorganisms can metabolize glycerol in the presence of external electron acceptors (respiratory metabolism), few are able to do so by fermentation. However some recent works show that engineered Escherichia coli strains can be used for efficient conversion of crude glycerol into ethanol. The simple and harmless eukaryote named Saccharomyces cerevisiae is also able to exploit glycerol as a sole source of carbon. But glycerol fermentation in these organisms is not well-known and described particularly.

Considering this context, NDT can play an important role because its ability to monitor their rheological properties. Commonly rheological monitoring of complex materials give access to dynamical parameters like storage G' and loss G" moduli. These parameters give information of viscoelasticity at macroscopic scale (low frequency 1Hz) which is not convenient for cells investigation. In this study, a simple rheological technique at microscopic scale for S.cerevisiae growth monitoring is proposed.

Statement of Contribution/Methods

This technique uses shear waves generated by an AT-cut quartz crystal in the frequency range 5-9 MHz. This transducer is immersed in a nutrient medium inoculated with S. cerevisiae. During the cultivation process, the rheological measurement at microscopic scale of this complex medium are performed. Using a suitable model including the electrical properties progress during S. cerevisiae cultivation, G'and G" are accurately extracted. In order to optimize growing conditions, the temperature, pH and substrate on which the yeast grows are tightly controlled. This grows is performed under aerobic conditions.

Results

The cells exhibit different morphologies during their life cycle. The high sensitivity of our technique allows the on line monitoring of the different life cycle during the cycles of cell budding. A systematic comparison of viscoelastic evolution with microscopy is performed to link the information of G', G" with number and cells stages. In the production of bioethanol, S. cerevisiae is exposed to significant physicochemical constraints that may affect their physiological state and limit the efficiency of fermentation and the production. Our Online micro-rheometer makes possible its optimization.

Discussion and Conclusions

In addition, sexual reproduction in the yeast S. cerevisae study can be used as a simple laboratory model. This preliminary work will be used to design a new piezoelectric immunosensor for cell biology and genetics investigation in medicine (biomedical research, model organism in genetics, path synthesis of antibiotics), and in environment (pollution, waste recycling, crop protection).

P3B-3

Fabrication of Frequency Scaling circuit Using Phase Locked Loop Synthesizer IC for a Quartz-Crystal Tuning-Fork Tactile Sensor

Susumu Itoh[1], Hideaki Itoh[1]; *shinshu university, Japan*

Background, Motivation and Objective

The frequency of a quartz-crystal tuning-fork tactile sensor in contact with the objects increased as the Young's modulus of them (even soft or hard materials) increased.[1] The increase in frequency of the sensor occurred about 7 Hz in contact with metal plates and from 2 to 3 Hz in contact with silicone rubbers. [2] If its frequency decreases as the liquid level in the acrylic resin vessel, on which the base of the tactile sensor fixed with epoxy resin adhesives, increases, the mass loading effect on its frequency is considered. This frequency change is so small as compared to the longitudinal vibration tactile sensor.[3] Therefore, we fabricated the frequency scaler (scaling circuit) using PLL (Phase Locked Loop) Synthesizer IC to make larger frequency output than the tactile sensor's one.

Statement of Contribution/Methods

We measured the resonant frequency with change of the liquid level from 0 to 12 mm in the vessel filled with water or Japanese liquor (25% alcohol), using the TTL oscillator. Figure 1 shows the fabricated frequency scaler used PLL synthesizer IC for a quartz-crystal tuning-fork tactile sensor.

Results

The measured frequencies for two cases had no difference until the water level 9 mm. However, the resonant frequency for water decreased lower about 5 Hz than that for Japanese liquor (measured density: 0.94 g/cm3) at liquid level 12 mm in the vessel. As for the resonant frequency against the change of water level in the vessel from 0 to 10 mm using frequency scaler made of PLL synthesizer IC, measured frequency was found to tend to decrease as the water level increased.

Discussion and Conclusions

The fabricated PLL synthesizer became more stable as the scaling rate increased. The frequency of quartz-crystal tuning-fork tactile sensor attached on the vessel could be stabilized through PLL synthesizer, except water level 12 mm in the vessel.

Reference

[1] H. Itoh, M. Yamatani, S . Yoshida, Y .Fuzimura, and K. Ishikawa: Jpn. J. Appl. Phys. 43 (2004) 2982.
[2] H. Itoh and N. Hatakeyama: Jpn. J. Appl. Phys. 49 (2010) 07HC03.
[3] S. Omata and Y. Terunuma: Sens. Actuators A 35 (1992) 9.

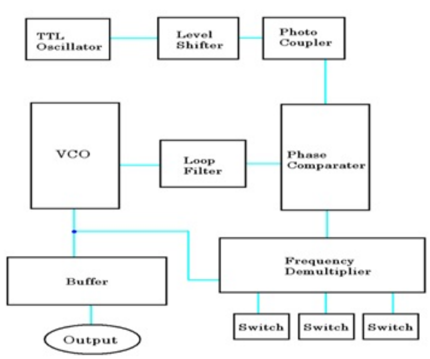

Fig. 1. Diagram of the frequency scaler used PLL synthesizer IC.

THURSDAY POSTER

P3B-4

Use of Inharmonic Modes of Trapped-Energy Resonators for Liquid-Level Sensing

Ken Yamada[1], Shuichi Seto[1], Shuhei Horiuchi[1]; [1]*tohoku Gakuin University, Japan*

Background, Motivation and Objective

The authors have presented a new technique for detecting a small-scale variation in liquid level by using a piezoelectric thickness vibrator operating in a trapped-energy mode [1-4]. Trapped-energy resonators produce inharmonic modes around the main resonance when the central electrode area (conventional type) or the unelectroded gap width (backward-wave type) becomes large compared to the plate thickness. The decay factor, i.e., the imaginary wave number determining the profile of the evanescent field differs between fundamental and inharmonic modes. For inharmonic modes, the decay factor is smaller than that for fundamental modes. This implies that the exponential decay is gentle for inharmonic modes. Therefore, characteristics of liquid-level sensing are considered to be different depending on which of the two modes is employed.

Statement of Contribution/Methods

In order to confirm this prediction, experiments were carried out employing two trapped-energy resonators. One is a conventional trapped-energy resonator composed of a thickness-poled PZT plate (NEPEC-6, TOKIN) of 30 mm diameter and 1 mm thickness, having the electrode of 8 mm diameter (designated as resonator A). In addition to the fundamental resonance at 1.99 MHz, this resonator has an inharmonic overtone resonance at 2.13 MHz. The other is a backward-wave-type trapped-energy resonator[3,4] composed of a $PbTiO_3$ plate of 30 mm diameter and 1 mm thickness (Fuji Ceramics M-6), having the center electrode of 4 mm diameter and the insulation gap of 2 mm width (resonator B). An inharmonic undertone mode is observed at 1.92 MHz, in addition to the fundamental mode at 2.03 MHz.

Results

The resonators were supported vertically by clamping their fringes and dipped in a liquid to be tested[1,2]. Variations in real part G of the electric admittance (or R of the impedance), against the immersion depth h at the resonance (or anti-resonance) point were measured using an impedance/material analyzer.

Discussion and Conclusions

It has been confirmed through the experiments that the variations in G or R are gradual for inharmonic modes, compared to those for fundamental modes. An unexpected small increment in G is observed for resonator A when the liquid level is low (for large h). This might be due to the electrical property of the liquids contacting to the surrounding bare surface of the conventional trapped-energy resonator. This does not occur for the backward-wave type resonator B because the surfaces of the surrounding region are electroded and short-circuited together.

(1) K. Yamada, H. Honda, S. Horiuchi, and T. Kinai: Jpn. J. Appl. Phys. 48 (2009) 07GB08.
(2) K. Yamada, S. Horiuchi, H. Honda, and T. Kinai: Proc. 2009 IEEE Ultrason. Symp., p.2508.
(3) S. Seto, S. Horiuchi, and K. Yamada: Jpn. J. Appl. Phys. 49 (2010) 07HC05.
(4) K. Yamada and S. Seto: Proc. 2010 IEEE Ultrason. Symp. (to be published).

P3B-5

Estimation of the influence of ultrasonic flowmeter structures on their dynamic errors

Vakif Hamidullin[1]**;** [1]State University of Aerospace Instrumentation, St. Petersburg, Russian Federation

Background, Motivation and Objective

The characteristics of flowmeters include important parameters such as measurement error, repeatability and rangeability achieved on flowmetering stands under condition of steady flow. However real flows under industrial conditions are not stationary, pulsating or fast changing. The square-root error depends on the frequency spectrum of flow and dynamic characteristics (bandwidth) of flowmeters. Here dynamic errors may be significant. There tends to be decrease in this error with increases in the bandwidth of flowmeters. The total error may be much more than indicated in the technical documentation. Erroneous invoices amounting to millions of dollars may be saved for firms involved in export / import or use of gas, oil and its products if this error is decreased.

Statement of Contribution/Methods

A distinguishing feature of ultrasonic transit-time instruments for measuring flow is their ability to use only a single pair of electro-acoustic elements in two measurement channels. Therefore the mathematic dynamic models for simulation have been presented as two-channel discrete systems with simultaneous (synchronous) or successive (asynchronous) operation the channels in time. These channels have cross connection between them. The second regime of operation is used usually. These models include the dynamics of medium movement in the test cell, the dynamics of sound signal propagation in moving medium and the measuring scheme and local feedbacks as well. Corresponding discrete transfer functions are derived.

Results

These models enabled to simulate operation ultrasonic flowmeters with intrusive and non-intrusive transducers for two mentioned regimes. The output curves of transient process for dynamic error were calculated and presented in the paper. In case of use asynchronous regime reduced dynamic error may be reached if at least the constant time of the filter connected with the dynamic of medium movement is more than the period switching channels (signal quantization) in 5 times. Minimum of error may be reached in case of use synchronous regime. Simulation with the sinusoidal input influence imitating pulsating flow confirmed this approach as well. Experiments on the dynamic flow metering stand for liquid mediums confirmed fast response of transient process by the flowmeter with optimized structures. The response time was less than 0.1 seconds, the bandwidth – 60 Hz.

Discussion and Conclusions

The presented approach is available for analysis and synthesis of multi-channel measurement systems (including ultrasonic ones) for improvement in the efficiency of combustion driven power generation plants, nuclear power generation stations and pipeline power-carrier communications.

P3B-6

Evaluation of Transducer Configurations and Signal Processing Techniques for Ultrasonic Cross-Correlation Flowmeters

Michael Vogt[1], Helmut Ermert[1]; [1]Dept. of Electrical Engineering and Information Technology, Ruhr-University Bochum, Bochum, Germany

Background, Motivation and Objective

Ultrasound cross-correlation flowmeters are utilized for flow velocity measurement of turbulent flows in pipes. The concept is to assess phase (PM) and amplitude modulations (AM) of ultrasound waves propagating perpendicularly to the flow direction, which are caused by naturally occurring inhomogeneities (speed of sound variations) inside the flowing medium. Pairs of ultrasound transducers are mounted along the pipe, each with one transmit (TX) and receive (RC) transducer. The time interval needed by the 'signature' inside the flow to travel between two pairs of transducers ('channels') is measured by driving the TX elements with continuous wave (CW) signals and cross-correlating the PM and AM signals. Mean flow velocity is estimated as the quotient of the distance between the channels and the measured time interval, corrected for systematic errors by calibration.

Statement of Contribution/Methods

The above concept has been evaluated for flow velocity measurement in small pipes (diameter of some millimeters). Different from flow measurement in large pipes, the challenge is to employ transducers with large apertures compared to the pipe's diameter. Also, a large transducer's aperture angle and a large crosstalk between the channels have to be taken into account. To cope with these problems, different configurations of circular and linear transducers, driven at the same or different frequencies, have been implemented and evaluated. Furthermore, a signal processing strategy for quadrature demodulation and sensitive analysis of the narrowband PM and AM modulations by means of appropriate filtering and sequential sampling frequency down-conversion of digitized RC signals has been developed.

Results

A flow meter (acrylic glass pipe, 8 mm inner diameter, 12 mm distance between channels) with circular (8 mm diameter) and linear transducers (8 mm length, 1 mm width), working at frequencies of 1.4 and 2.0 MHz, has been implemented. Direct TX signal generation and RC signal digitization (D/A- and A/D-converters with 14 bit resolution) is utilized, and a turbine flowmeter has been used for calibration and evaluation. Measurements with degassed water have shown that for highly homogeneous liquids the cross-correlation of PM signals performs best. Furthermore, the best configuration of the implemented flowmeter is using linear transducers, and opposite propagation directions and different frequencies at the two channels. A minimum measurable flow velocity of 0.288 m/s has been found, corresponding to a Reynolds number of 2300, which is close to the theoretic limit. A correlation coefficient of 0.6 has been given at the minimum flow velocity, which proves the validity of the flow measurement.

Discussion and Conclusions

A concept for a cross-correlation flowmeter for flow velocity measurement of highly homogeneous liquids in small pipes has been successfully designed and evaluated by measurements with degassed water and calibration with a turbine flowmeter.

P3B-7

Flow Rate Measurement using an Ultrasonic Beam Radiated Perpendicular to a Pipe when Flow Profile Exists

Juei Igarashi[1], Koichi Mizutani[1], Naoto Wakatsuki[1], Takanobu Kuroyama[1]; [1]Graduate School of Systems and Information Engineering, University of Tsukuba, Tsukuba, Ibaraki, Japan

Background, Motivation and Objective

Conventional ultrasonic Doppler velocimetries are normally based on frequency shift due to Doppler effect occurs on the velocity component parallel to the ultrasonic beam axis. The transducer mounting position relative to the flow pipe typically requires a careful maintenance. Besides, most of the conventional measurement methods of flow profile require plural transducers or combining measurements acquired with different positions. This paper proposes a methodology of pipe flow rate based on the analysis on frequency spectrum of the ultrasonic wave scattered by particles flowing in a pipe and received with a single transducer mounted perpendicular to the pipe.

Statement of Contribution/Methods

Assume a fluid contains particles which scatter ultrasonic wave and it flows in a pipe. A circular planar transducer that is mounted perpendicular to the pipe generates an ultrasonic beam. We consider the cases there is flow profile, which is flow speed distribution over the pipe cross-section. Numerical simulations are performed on the simplified models of different flow profiles. Assume a certain period of data acquisition time to integrate the effect of multiple particles and averaging is applied to analyze the frequency spectrum. The correlation between the integration of the normalized spectrum and the pipe flow rate is evaluated.

Results

In the spectrum of the obtained signal, it is notable that the bandwidth defined as the width between zero drops at the sides of the center peak was consistent among different flow profiles as long as the maximum speed was consistent. Meanwhile, the different flow profiles influenced the shape of the spectrum. The more low flow speed component contained, the narrower the spectrum was obtained. A clear correlation was observed between the flow rate and the integration of the normalized spectra.

Discussion and Conclusions

It is supposed that the spectrum bandwidth is determined by the maximum speed of the profile as the fastest particles cause the maximum Doppler shift. Total flow rate has a correlation with the spectrum shape. Thus, the flow rate could be estimated with the following steps: 1) detect maximum flow speed with the bandwidth and 2) estimate the relative flow rate from the integration of the spectrum. The method may provide a relatively simple measurement system for a monitoring of pipe flow with flow profile changing such as for an oil production.

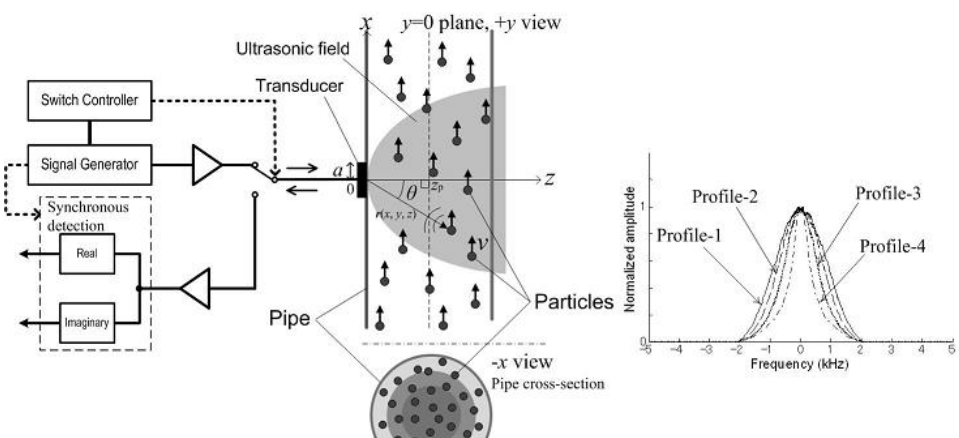

(Left) Geometry and block diagram of the pipe flow measurement system
(Right) Calculated results of normalized amplitude spectra for different flow profile patterns

THURSDAY POSTER

P3B-8

Ultrasonics in enhanced recovery of oil from porous rock

Eimear Neeson[1], Margaret Lucas[1]; [1]*University of Glasgow, United Kingdom*

Background, Motivation and Objective

It is estimated that after primary and secondary oil recovery, up to 85% of the initial oil quantity still remains within the reservoir rock. Secondary and tertiary recovery mechanisms can be costly and invasive, making new alternative methods highly attractive. The effects of vibroseismic reservoir stimulation have been studied over the last 50 years since increased oil and water recovery was observed as a result of cultural noise and earthquakes. Research has confirmed that the mechanisms involved are very complex necessitating further investigation into the processes involved. Ultrasonic waves can be generated due to seismic action as a result of viscoelastic oscillations of the fluid, dry friction at the contacts between adjacent molecules and bimodal wave vibrations. It has been proposed that these resulting weak ultrasonic fields can cause improvements in oil mobility. Strong ultrasonic fields can also be used locally down-hole to stimulate improvements in oil recovery. For both weak and strong ultrasonic fields the mechanisms of improved oil recovery are not well understood.

Statement of Contribution/Methods

To represent the porous stone within an oilfield, sandstone samples saturated with various oils with a range of properties were placed within a water bath and an ultrasonic field applied. This field creates a cavitation region in the surrounding liquid and the regions in the fluid of high negative pressure, most likely to be the cavitation regions, are predicted via finite element modelling. By controlling the presence and locations of cavitating regions, it is possible to characterise its effect on the quantity of oil recovered from the saturated rock samples. Experiments are performed to measure the recovered oil from rock samples at different levels of saturation, for a range of ultrasonic intensities and for a number of different ultrasonic fields.

Results

Increasing the intensity of the ultrasonic source by increasing the amplitude of vibration shows a clear step where the oil recovered increases substantially. This is the cavitation threshold amplitude, above which it can be presumed that cavitation effects dominate.

Discussion and Conclusions

The recovery of oil from saturated rock samples in these experiments is as a result of various mechanisms, including direct mechanical vibration, rock fragmentation and cavitation. The experimental results indicate that, beyond the threshold of cavitation, the presence of cavitation close to the sample results in a step change in the quantity of recovered oil.

P3C - Acoustic Tweezers II

Carribean Ballroom III-V

Thursday, October 20, 2011, 9:30 am - 1:00 pm

Chair: **Christine Demore**
University of Dundee

P3C-1

Particle Trapping of Acoustic Tweezers

Yanyan Yu[1], Weibao QIU[1], Lei SUN[1]; [1]Department of Health Technology and Informatics, The Hongkong Polytechnic University, Hong Kong

Background, Motivation and Objective

The optical tweezers has been found to have many biomedical applications in trapping macromolecules and cells. A recent theoretical study has shown that under appropriate conditions acoustic trapping is also possible [1]. Compared to the optical tweezers, acoustic tweezers are more useful in light opaque media. They can handle larger cells and particles by exerting lager forces. In this paper, we present the region where a particle can be trapped from a 100MHz transducer on various sizes of particles, and demonstrate that the acoustic tweezers can manipulate larger particles.

Statement of Contribution/Methods

The analysis was based on the acoustic intensity field from a 100MHz focused transducer. It was calculated by the radiation pattern generated from a single-element concave circular piston with finite-element model instead of assumed Gaussian intensity distribution [1]. The radiation force was computed by the momentum transfer occurs between the mediums inside and outside the particle. In addition, viscosity of water was also taken into consideration. After motion analysis, the spatial regions where a particle can be trapped were determined in axial and lateral directions, respectively.

Results

The acoustic intensity field of a 100MHz transducer with aperture of 3mm and f-number 1 was shown in Fig.1. Fig.2 shows the radiation force along the beam axis. Assuming acoustic impedance of the particle 1.4 MRayls, sound speed of the surrounding medium and the particle 1500m/s and 1450 m/s, density of the particle 950kg/m3, Fig.3 plots the displacement trajectory of the particle along the axial direction with various diameters. It is noted that particle can be captured quickly within 0.1second. Table 1 summarizes the axial and lateral trapping regions, respectively.

Discussion and Conclusions

The results confirm that acoustic trapping is feasible using the intensity field calculated from a focused transducer. The region where the particles can be trapped along the axial and lateral direction was determined. It demonstrates that the acoustic trapping has the ability to quickly capture large particles in the range of tens of to hundreds of microns. It also shows that the range increases as the increased size of the particles.

[1] J. Lee et al, J Acoust Soc Am 117(5), 2005.

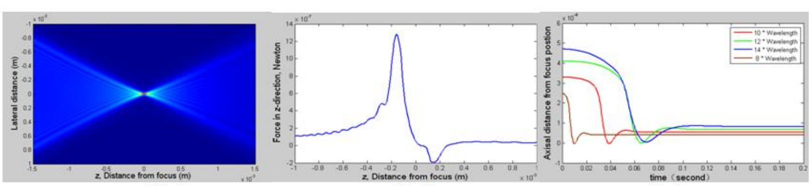

Fig.1 Fig.2 Fig.3

Fig.1 Acoustic intensity field from a 100MHz single-element focused transducer with 3mm aperture and f#/1
Fig.2 Radiation force along the beam axis
Fig.3 Displacement trajectory of the particle along the axial direction with various diameters

Particle diameter	Axial trapping region (μm)	Lateral trapping region (μm)
8*Wavelength	253.3	215.62
10*Wavelength	332	229.44
12*Wavelength	408.28	243.40
14*Wavelength	464.524	257.82

Table 1: The regions where a particle can be trapped in axial and lateral directions, respectively

P3C-2

Acoustic Tweezing in the Nodes or Antinodes of a Heptagonal Multi Piezoelectric Transducer Cell

Anne L. Bernassau[1], David R. S. Cumming[1]; [1]School of Engineering, University of Glasgow, Glasgow, United Kingdom

Background, Motivation and Objective

We present a novel device for acoustically manipulating or sonotweezing micron-scale elements. Such techniques, that allow the micro-manipulation of cells, particles or droplets by non-invasive means, are desired to facilitate biophysical or biological applications such as microarrays and tissue engineering. Non-invasive techniques exploiting the acoustic radiation force have been demonstrated for trapping, separating and moving particles. Most results to date describe acoustic trapping using geometrically fixed standing wave patterns.

However, the concerted action of multiple transducers can be used to generate electronically controlled standing wave patterns. This paper investigates 2-D particle micro-manipulations in a closed system using 2 or 3 transducers. In such systems, wave reflections can be detrimental to performance hence the geometry of the device have a strong impact on the quality of the particle trapping and this is discussed. It is also demonstrated that acoustic trapping can occur at the nodes or antinodes depending on the properties of the particle suspended in the medium.

Statement of Contribution/Methods

A system of 7 transducers was constructed on a flexible substrate that was folded to form a heptagonal cell of ~ 20 mm across. Experiments were performed using 10 µm polystyrene microspheres and emulsions. Trapping occurs at the acoustic nodes or antinodes, respectively. The transducers were excited using a frequency of 4 MHz. In all experiments where two or three transducers were simultaneously excited, the position of the particles could be controlled by shifting the phase of one of the transducers relative to the other.

Results

When two transducers are simultaneously excited, the particles align along a line that bisects the angle formed by the two cell sides on which the transducers are affixed. The distance d between the nodes can be calculated by $d = \lambda/2 \sin(\theta/2)$ where θ is the angle formed between the normal to the planes of the two sides with the active transducers. A 90° phase shift moves the particles by d/4. With three transducers, the microspheres clustered along a clear hexagonal pattern (nodes) whereas the emulsions are trapped at the centre of these hexagonal patterns (antinodes).

Discussion and Conclusions

A scalable sonotweezers device has been fabricated and used to demonstrate the trapping and movement control of various particles. Two transducer configurations allow clustering the particles along lines whereas three transducer configurations allow point type trapping. Solid objects like microspheres tend to cluster at the nodes of the acoustic waves whereas emulsion micro droplets have been shown to cluster at the antinodes.

P3C-3

parallel flow and mass transfer in polymeric ultrasonic microrresonators

Itziar Gonzalez[1], María Tijero[2], Javier Berganzo[3], Victor Acosta[4], Luis Fernandez[5]; [1]Group of Ultrasounds, CSIC Consejo Superior de Invsetigaciones Científicas, Madrid, Madrid, Spain, [2]dpt of microsystems, ikerlan, Spain, [3]microsystems, ikerlan, Spain, [4]CSIC, Spain, [5]Universidad de Zaragoza, Spain

Background, Motivation and Objective

Development of ultrasonic resonators based on the Lab-on-Chip concept demands new low cost constitutve materials for biomedical and clinical applications.

New polymeric microdevices acting as multilayer resonators in an ultrasonic wave show their capability and versatility as particle tweezing tools for selective separation or particle sorting. Combination of parallel flows with ultrasounds perpendicular allow the mass transfer betwen them. The spatial configuration of these plastic resonators, is strongly influent on the establishment of the 3D standing wave and determines the location of the pressure node established inside the channel along which the samples flow in parallel for the mass transfer.

Statement of Contribution/Methods

The group has introduced these polymeric microrresonators for particle separation on flowing samples. For applications of separation of cells in some organic samples the efficiency of separation is not as high as desirable.

New chip configuration are currently being tested to achieve optimal levels of separation, up to 90%.

Direct observations of aqueous suspensions flowing through the channel show this strong influence on their drift motion toward the node of pressure, that shows apparent changes with the spatial configuration of the chip at different frequencies.

In parallel, numerical simulations (COMSOL) to analyse the vibrational behaviour of the chip and pressure distribution inside the channel are under development.

Results

Different chip configurations have been developed to achieve maximal results of cell separation.

Two spatial parameters have been varied in the chip configuration: the distance between the channel and the piezoelectric ceramic and the channel length.

In all of the devices the frequency has been varied about 12% around 1MHz to analyse the stability of the pressure node established inside the channel.

In chips with channel lengths smaller than 1cm the cells require flow rates lower than 100iL/min to to reach the node before leaving. At these low flow rates back flows appear from the outlets of the channel, mixing the samples previously separated by ultrasounds.

In longer channels the experiments show that the increase the flow rate is possible because the cells have longer times inside, compensating it.

Discussion and Conclusions

As conclusion, the polymeric chips require channel lengths longer than 1cm to achieve efficiency levels of cell separation over 70% at flow rates slightly higher than 50microliters/min, from which on the cell samples show stability leaving the device after the acoustic treatment.

The distance of the channel to the ultrasonic actuator seems to be not so influent in the experiments for the particle separation, becase other frequencies within a range of variation of 12% around 1MHz produce a suitable pressure node at the desired location.

P3C-4

Acoustic trapping of particle in the near field of a resonant periodically structured stiff plate

Feiyan Cai[1], Long Meng[1], Xin Cheng[1], Hairong Zheng[1]; [1]Shenzhen Institutes of Advanced Technology, China, People's Republic of

Background, Motivation and Objective

Acoustic manipulation, as providing a noninvasive manipulation method, has been growing rapidly interest in biology and physics. Acoustic tweezers, for example, have proved useful not only for trapping particles but also for assembling objects. However, most of these acoustic fields are standing waves, Gaussian beams, etc. These fields, usually directly generated by acoustic transducer, are hardly to be redesigned. In this paper, we present resonant-induced acoustic trapping of particles in a periodically structured stiff plate. The frequency and the intensity of the resonant-induced trapping force are geometrical dependent on the ratio of the plate thickness to the structural period.

Statement of Contribution/Methods

The near-field trapping system consists of a water-immersed thin brass plate patterned with periodical brass gratings (period d) on one sides, a brass cylinder particle is placed on the other side of the patterned brass plate. In the previous study (PRL 105, 074301 (2010)), we have demonstrated this structure can generate vortex field in the near patterned plate

THURSDAY POSTER

at the resonant frequency. On the basis of the finite-different time-domain method combined with stress-tensor, we theoretically investigate the acoustic force on the particle near the patterned brass plate.

Results

As shown in Fig. 1, the red solid line indicates the normalized acoustic force (Yy) versus normalized frequency on the brass cylinder when it is near the flat side of the patterned brass plate; the black dots show the corresponding normalized acoustic force on the brass cylinder immersed in a plane wave. In addition, the blue short dash dots indicate the power transmission at normal incidence for the patterned brass plate. It is clearly shown that, in the off-resonant frequency, the force on the brass cylinder on patterned brass plate is positive (along the propagation direction of plane wave) and smaller than the case of in plane wave; in the resonant frequency, the force is negative, directing into the field of the surface, and the force amplitude is about ten times larger than that in the plane wave.

Discussion and Conclusions

The particle can be trapped near the surface of patterned brass plate because of the presence of significant gradient forces at the resonance frequency. This configuration may open the possibility of creating arbitrary arrangements of trapping sites for self-assembly.

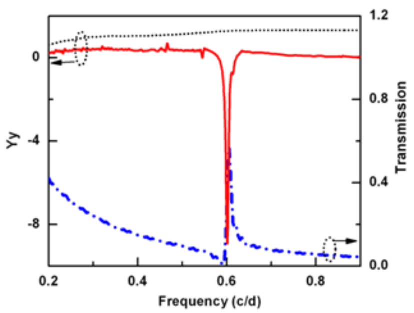

P3C-5

Real time acoustic sensing of flowing microdroplets in a microfluidic device

Changyang Lee[1], Jungwoo Lee[1], Shia-Yen Teh[2], Abraham Lee[2], Hyung Ham Kim[1], K. Kirk Shung[1]; [1]Department of Biomedical Engineering, University of Southern California, Los Angeles, California, USA, [2]University of California at Irvine, USA

Background, Motivation and Objective

Automated and rapid sample preparations have been considered as key components in developing micro total analysis systems (µTAS), for onsite monitoring and diagnosis of various pathogens. Fluorescence-activated cell sorting (FACS), in particular, has allowed fast screening of phenotypically different cells by scanning laser beams, but its implementation is rather complicated and costly. Non-invasive acoustic sensing of a single stationary microparticle isolated by acoustic trapping has been previously reported. This paper presents recent results obtained on rapid acoustic sensing of flowing microdroplets in a PDMS microfluidic device. In conjunction with acoustic trapping or acoustic radiation force from a highly focused high frequency ultrasonic beam or ultrasound microbeam, it is conceivable that cell sensing and sorting may both be achieved acoustically.

Statement of Contribution/Methods

A 30 MHz lithium niobate single element transducer was built for the test. A PDMS device, immersed in a distilled water chamber, consisted of two sheath channels on the side and one main channel providing droplets at the center. The transducer was positioned outside the channel, perpendicularly aiming at the channel wall. Flow rates of the droplet and sheath solutions were 0.5 and 1.5 in µl/min, respectively. Echo signals scattered from these streaming microdroplets of different sizes were acquired through a data acquisition board and the integrated backscatter (IB) coefficient was analyzed by a custom-built LabVIEW panel in real time.

Results

The echoes from moving droplets of 50 and 100 µm in diameter were measured, and their IB coefficients were calculated at the same time. The results shown in Fig. 1 indicate that those droplets can be readily identified by their echo amplitudes and IB values. Typically, the amplitude and the IB coefficient were 7.63 ± 0.55 mVpp and -97.48 ± 0.60 dB for 50 µm droplets, while 17.02 ± 4.00 mVpp and -91.69 ± 1.31 dB for 100 µm droplets. Note that Vpp denotes the peak to peak voltage of an echo amplitude.

Discussion and Conclusions

The results showed that this sensing technique using a highly focused ultrasonic transducer was able to remotely identify flowing microdroplets in microfluidic channels, based on their echo signals and IB coefficients. Hence this acoustic approach may be used to develop much simpler devices than FACS systems and serve as a core element in µTAS.

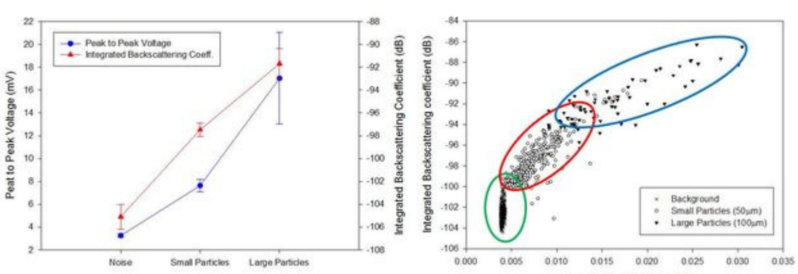

Figure 1. Echo amplitude and backscattering coefficient between 50µm and 100µm microdroplet

P3C-6

Analysis of oscillational instabilities in acoustic levitation using the finite-difference time-domain method

Arturo Santillan[1]; [1]Institute of Technology and Innovation, University of Southern Denmark, Odense S, Southern Denmark, Denmark

Background, Motivation and Objective

Small objects levitated by means of acoustic waves, nowadays using mainly ultrasound, can be affected by rotations and oscillations, which might be undesirable for specific applications.

Under certain driving conditions of a single-axis acoustic levitation device, a suspended sample starts to oscillate vertically around the initial equilibrium position. The amplitude of the oscillations increases with time until the sample is lost or a saturation state is reached where the amplitude of the oscillations remains constant.

A theoretical description of such oscillational instabilities was published in 1990. This approach, however, cannot describe the experimental observation that the instabilities disappear after the amplitude of the sound waves has been sufficiently increased.

The main objective of the project is to investigate the extent to which the finite-difference time-domain method (FDTD) can be used to simulate the onset of oscillational instabilities and their evolution in time.

Statement of Contribution/Methods

The work contributes to further understand the causes of oscillational instabilities, and the physical mechanism involved. For the study, a cylindrical closed cavity with hard walls and a cylindrical solid object in its interior have been assumed for simplicity. In addition, axisymmetric conditions are considered, and the simulations are carried out in an interval of values of the driving frequency around the resonance frequency corresponding to the first axial mode of the empty cavity.

Results

It is shown that the FDTD method can be used to predict the resonance frequency shift in a closed cavity produced by the presence of a solid object in its interior. In addition, the movement of the object as a result of the acoustic force can be simulated together with the onset and evolution of the oscillational instabilities.

The dependence of the oscillational instabilities is obtained as a function of the driving frequency and also as a function of the amplitude of the sound waves. The results of the simulations are qualitatively in good agreement with experimental observations. In addition, the evolution in time of the total acoustic force on the sphere inside the cavity is described.

Discussion and Conclusions

It is shown that the FDTD method can be used in acoustics to describe the force exerted on an object by sound waves, the movement of the object, and the effects of the sound field. Oscillational instabilities can be simulated with the method, given qualitatively good results.

P3C-7

Creating a periodic nanocomposite material structure using nanoparticles in ultrasound standing waves

Farid G. Mitri[1], Dipen N. Sinha[1]; [1]*MPA-11, LANL, Los Alamos, NM, USA*

Background, Motivation and Objective

Many phenomena previously regarded as unachievable, such as sub-wavelength imaging and cloaking, have been realized using metamaterials, which are artificial materials engineered to have properties that may not be found in nature. It has previously been shown that these material properties may be controlled by assembling particles into periodic structures to manipulate electromagnetic or elastic waves. Although new emergent properties have been demonstrated from materials with organized arrays of large millimeter size particles, new fabrication techniques are required to make controllable and tunable (periodicity) arrays of particles in the micron range, which is significantly more useful for practical applications. Thus, an efficient and low-cost approach that precisely controls the arrangement of particles will fill a critical need in the developing field of metamaterials and lead to the discovery of new materials with emergent properties for a host of applications.

Statement of Contribution/Methods

Here, we propose to use the method based on the acoustic radiation force (at 1 MHz) generated inside a resonator cavity to direct the organization of nanoparticle clusters in a host fluid and create periodic arrays that are solidified in a bulk matrix. Gradually, the periodic pattern becomes permanent with full cure of the epoxy matrix so as to form a 3D periodic structure. We also show that the periodicity of the pattern can be changed by selecting a different ultrasound frequency, e.g., 4.2 MHz. Furthermore, x-ray micro-computed tomography is used as a quality control tool to map the internal structure and characterize each nanocomposite.

Results

Nanocomposite structures with different periodicities were synthesized, in which diamond nanoparticle clusters were successfully arranged so as to form 3D periodic structures. Though not investigated here, the ultimate aim is to use the present results as a base for the development of finite-element models which take into account all the structural features to explore the various metamaterial (exotic) functionalities in optical, acoustical, thermal, or even gravitational applications.

Discussion and Conclusions

The fabrication method is a fast, cost-effective, versatile tool and not limited to a particular frequency so as to create metamaterials with different periodicities. The particles may consist of any material (metal, insulator, semiconductor, superconductor, nanowires, or tubes, CNTs, etc.), and other geometries (cylindrical, hexagonal, and other symmetries) may be also possible.

P3E - Transducer Modeling

Carribean Ballroom III-V

Thursday, October 20, 2011, 9:30 am - 1:00 pm

Chair: **Reinhard Lerch**
University of Erlangen

P3E-1

Analysis of beamforming errors from ultrasound sub-array processing

Kangqiao Zhao[1], Tore Bjåstad[1,2], Kjell Kristoffersen[1,2]; [1]Department of circulation and medical imaging, Norwegian University of Science and Technology, Trondheim, Norway, [2]GE healthcare, Norway

Background, Motivation and Objective

Modern real-time 3D ultrasound imaging systems use in-probe processing to cope with the large number of transducer elements from a 2D array. This processing is performed for a cluster of adjacent elements (sub-array), so that the number of system channels can be reduced accordingly.

A practical implementation of a sub-array processor (SAP) is on a tight power and size budget, calling for simplified beamforming methods. Additionally, sub-array processing combined with parallel beamforming introduces errors that are not present in conventional ultrasound systems.

The objective of this work is to analyze the different simplifications in typical SAP-based system, and quantify their impact on image quality.

Statement of Contribution/Methods

An analytical model has been built to investigate the impact of SAP simplifications such as static focusing, delay quantization and delay linearization. Further, this model has been compared to Field II simulations. For evaluation, a new figure of merit (FoM), Ploss, is introduced. This FoM uses losses in main lobe level v.s. ideal processing to evaluate the increased side lobe level, and thus reduction in contrast resolution in the image. A case study has also been performed for an Intracardiac Echocardiography array design.

Results

The results show that SAP delay quantization and static SAP focus are the largest sources of SAP beamforming errors. Mainly, these errors result in raised side lobe levels and reduced image contrast. Quantization may also result in a periodic variation of this side lobe level with steering angle, reducing image uniformity. The influences of the different SAP simplifications are listed in Table 1.

For the case study, lowering the channel count from ~1500 to ~60, a 5x5 SAP with static focus can give good performance for a flat array operating at F-number equals to 2 (element size (λ/2)x(λ/2) assumed). The SAP delay quantization step was suggested not to exceed 20ns (corresponding to 45 degree phase error) in order not to have a significant rise in side lobes compared with other simplifications.

Discussion and Conclusions

This work provides a framework that can be used to optimize SAP probe design parameters and system setup. The introduced FoM, Ploss is shown to be simple and efficient for evaluating the impact of parameter changes. Ploss could also be used to evaluate other beamforming techniques.

Table 1 Impacts of SAP simplifications

Simplifications		Impact on image quality	Importance	Major design choices
Static SAP focusing	Rx DynFoc	Reduction of image contrast outside SAP focal range.	High	Focal depth/strategy
	Parallel BF	Reduction of image contrast and lateral image uniformity.	Medium	Maximum receive steering offset ($\Delta\theta$)
SAP delay quantization		Reduction of image contrast and lateral image uniformity.	High	Quantization step size ($\Delta\tau_{SAP}$)
Linear delay profile across each sub array		Reduction of image contrast	Low	SAP size (N_{SAP})

P3E-2

The use of Fractal Geometry in the design of Piezoelectric Ultrasonic Transducers

Anthony Mulholland[1], Alan Walker[2], Nishal Ramadas[3], Richard O'Leary[3], Anthony Gachagan[3]; [1]Centre for Ultrasonic Engineering, University of Strathclyde, Glasgow, Scotland, United Kingdom, [2]Faculty of Advanced Technology, University of Glamorgan, Pontypridd, United Kingdom, [3]Centre for Ultrasonic Engineering, University of Strathclyde, Glasgow, United Kingdom

Background, Motivation and Objective

The geometry of composite piezoelectric ultrasonic transducers is typically regular and periodic with one dominant length scale. In many applications there is motivation to design transducers that operate over a wide bandwidth so that, for example, signals containing a broad frequency content can be received. The device's length scale will dictate the central operating frequency of the device and so, in order to construct a wide bandwidth device, it would seem natural to design a device that contains a range of length scales. The objective of this paper therefore is to consider one such transducer design and build a theoretical model to assess its performance.

Statement of Contribution/Methods

For the composite geometry a fractal medium is chosen as this contains a wide range of length scales and yields to a renormalisation analysis. Analytic expressions for the electrical impedance, and the transmission and reception sensitivities of this device as a function of the driving frequency are then derived.

Results

Numerical results of this theoretical model are presented. They suggest that this device would have a three-fold improvement in the reception sensitivity bandwidth as compared to a conventional composite design. A preliminary experimental investigation was undertaken, with a Sierpinski gasket fractal transducer design, and good correlation between the simulated and experimentally measured operation was observed.

Discussion and Conclusions

A radically new design for a composite ultrasonic transducer is proposed in this paper. At its heart is the concept of using a wide range of resonators to broaden the bandwidth of the device. As a proof of concept a theoretical model was constructed and analytic expressions for the device performance derived. The model results were used to specify the design of a new hydrophone configuration and encouraging results are presented from both the theoretical and experimental results.

P3E-3

3D-Analysis of Bending-Type Ultrasonic Transducers for Distance Measurement Applications

Mario Jungwirth[1], Manfred Kaltenbacher[2], Michael Rabl[3], Stefan J. Rupitsch[4]; [1]Automation Engineering, University of Applied Sciences Upper Austria, Wels, Upper Austria, Austria, [2]Institute of Smart Systems Technologies, University of Klagenfurt, Klagenfurt, Carinthia, Austria, [3]University of Applied Sciences Upper Austria, Wels, Upper Austria, Austria, [4]Friedrich-Alexander-University Erlangen-Nuremberg, Erlangen, Germany

Background, Motivation and Objective

Ultrasonic sensors are commonly used for a wide variety of non-contact presence, proximity, or distance measuring applications. Since the design process of these transducers (e.g., bending-type transducers) is a challenging task, numerical simulations considering multi-field interactions are utilized. However, the reliability of the simulation results strongly depends on the required material parameters. Therefore, we focus on methods enabling the determination of essential material parameters for such devices.

Statement of Contribution/Methods

The investigated bending-type transducer consists of a piezoceramic disc bonded to a thin, flexible membrane. In order to meet the requirement of impedance matching and resonance frequency at about 60 kHz, the membrane's material should exhibit both, a low density and a high elasticity modulus. Carbon fiber composites (CFC) offer these properties. However, the simulation based virtual prototyping requires precise material parameters for the piezoceramic as well as for the CFC. To obtain the essential material parameters, we first perform measurements of the electrical impedance of the piezoceramic and the spatially resolved mechanical displacement of the membrane. Secondly the whole transducer assembly is simulated in 3D. Finally, we apply the so-called Inverse Method (IM) which is based on a comparison of measurements and simulations for physical quantities. Thereby, the material parameters are adjusted in a convenient way.

Results

Fig. 1a shows preliminary measurement and simulation results for the mechanical displacement of the transducer's membrane made of aluminum. As can be seen, the material parameters resulting from the IM yield reliable simulations. In order to prove the identified parameters, we additionally investigated the acoustic directivity pattern (Fig. 1b) which is decisive for ultrasonic transducers. Although the acoustic directivity was not considered within the IM, the results coincide very well. Thus, the reliability of the utilized material parameters is proven.

Discussion and Conclusions

Based on precise material parameters and numerical simulations, we can predict the behavior of bending-type ultrasonic transducers. Actually, the design of the transducer is optimized for CFC membranes aiming both, a small transducer size and an adequate acoustic directivity.

Figure 1a

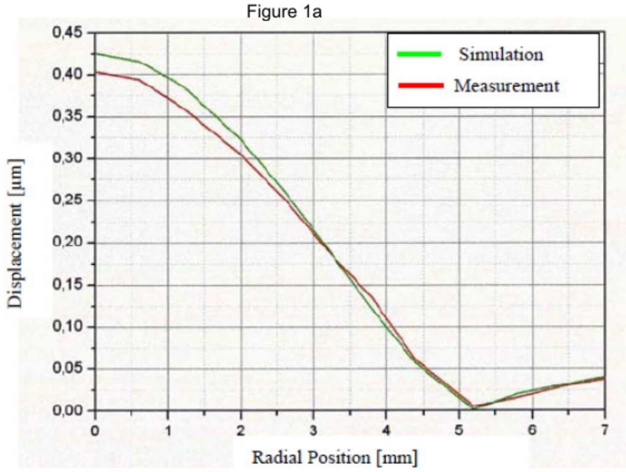

Figure 1b

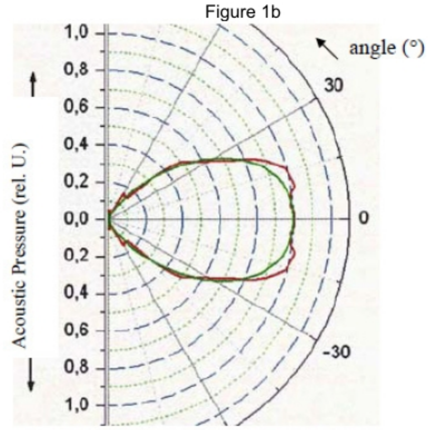

P3E-4

Diffraction correction for precision measurements of sound velocity in gas. Use of an alternative method accounting for non-uniform piezoelectric transmitting transducer vibration

Espen Storheim[1], Per Lunde[1,2], Magne Vestrheim[1]; [1]Department of Physics and Technology, University of Bergen, Bergen, Norway, [2]Christian Michelsen Research AS, Bergen, Norway

Background, Motivation and Objective

Correction for ultrasonic transducer diffraction effects is discussed for realizing a precision sound velocity cell within 100 − 200 ppm relative uncertainty, for use in custody transfer energy measurement of natural gas at high pressures [1]. There is a need for determining the diffraction correction within one degree uncertainty, tentatively, in the 150 − 200 kHz operational frequency range of ultrasonic multipath fiscal flow meters.

THURSDAY POSTER

Statement of Contribution/Methods

As a simplified case to improve the understanding of the complex mechanisms involved in diffraction correction for real piezoelectric transducer vibration modes, a circular piezoceramic disk element vibrating in air is used. The diffraction correction is studied using the SFDC method [1] based on finite element analysis, over the range 0 – 400 kHz.

Results

A Pz27 piezoceramic disk source is considered, with on-axis receiver located 15 cm from the source. In the figure, the traditional uniform piston diffraction correction model is compared with the SFDC calculated diffraction corrections of a baffled and an un-baffled piezoceramic disk element. Significant deviations are found. For the magnitude, these are large near the pressure response minimum which appears in the far field above the first radial mode (R1, occurring at 155 kHz). For the phase the deviations are large for all frequencies above R1. In addition, significant undulations are observed from very low frequencies to above the R1 mode. The results indicate that these are caused by radiation from the sides/rear of the transmitting piezoelectric element, interfering with the front radiation. These undulations are not described by the traditional model.

Discussion and Conclusions

For actual transducer vibration modes in such demanding applications, the traditional uniform piston diffraction correction model is not found to be sufficiently accurate over the frequency band of interest. The deviations are analyzed and explained. Work is in progress experimentally and theoretically to include also a full description of the receiver, to obtain a more complete description and treatment of the diffraction effects.

[1] P. Lunde, K.-E. Frøysa, R. Kippersund, and M. Vestrheim, "Transient diffraction effects in ultrasonic meters for volumetric, mass and energy flow measurement of natural gas", *Proc. 21st North Sea Flow Measurement Workshop* (2003)

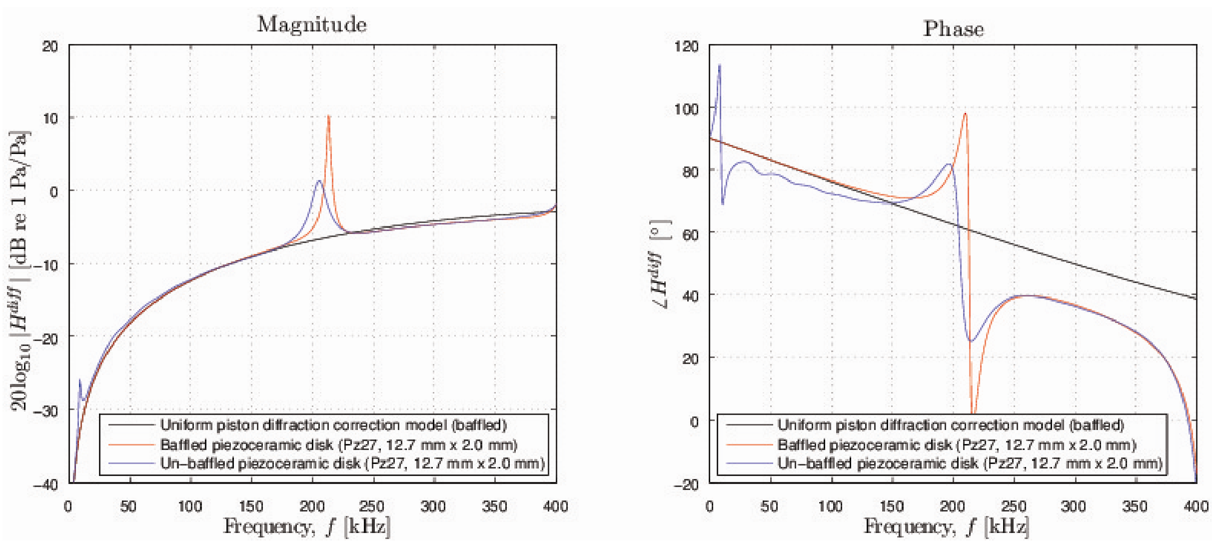

P3E-5

Finite element modelling and design of cymbal transducers for power ultrasonics applications

Fernando Bejarano-Duran[1], Margaret Lucas[1]; [1]School of Engineering, University of Glasgow, United Kingdom

Background, Motivation and Objective

The cymbal transducer consists of an inner piezoelectric disk mechanically coupled to two thin metal end caps on each of its faces by an epoxy adhesive. This miniature flextensional transducer is an emerging technology that has been used principally in underwater applications for large area and restricted volume transmit and receive arrays. This paper is focused on the use of this transducer in power ultrasonic applications where the delivery of high amplitude at a low ultrasonic frquency is essential.

Statement of Contribution/Methods

Cymbal transducers are capable of exciting more than 14× to 40× displacement amplification over the uncapped ceramic alone. Additionally, the resonance frequency of a cymbal transducer can be manipulated simply by selecting the cymbal's end cap material or dimensions. The cymbal is low cost and simple to manufacture, making this transducer a potential substitute for the Langevin transducer in power ultrasonic applications. Using a combination of finite element modelling validated by vibration characterisation measurements, this study demonstrates that power ultrasonic devices based on a cymbal can exhibit comparable performance to those based on a Langevin transducer.

Results

Based on previous studies of cymbals consisting of ceramic bonded to metal end caps, a simplified model has been developed to evaluate the properties of cymbals and to aid in materials selections. For this purpose, different experimental and finite element models have been realized, where loads were applied on each side of the cymbal, evaluating the influence of the geometry characteristics, the stiffness of the metal and the piezoelectric coefficients above the resonance frequency and maximum displacement of the whole device. The study results in a novel double ceramic half- cymbal prototype for power ultrasonic applications.

Discussion and Conclusions

Research involving finite element modelling and experimental vibration characterisation has shown that a novel configuration of a cymbal transducer based device can deliver high displacement amplitude at a low ultrasonic frequency. The device is shown to deliver comparable performance to a Langevin transducer based device for power ultrasonics applications.

P4Aa - Needle Guidance & Simulation Tools

Carribean Ballroom III-V

Thursday, October 20, 2011, 1:00 pm - 4:30 pm

Chair: **Herve Liebgott**
CREATIS, Lyon

P4Aa-1

Quantitative analysis of coated needles for ultrasound guided intervention

Chris de Korte[1], Gert Weijers[1], Dennis Vriezema[2], Hendrik Hansen[1]; [1]Clinical Physics Laboratory, Radboud University Nijmegen Medical Centre, Netherlands, [2]Encapson B.V., Nijmegen, Netherlands

Background, Motivation and Objective

During ultrasound guided interventions like biopsies or local deposition of anesthetics, the visibility of the needle is of crucial importance for accurate positioning. Although a standard needle is clearly visible when the angle between transmitted ultrasound and needle is around 90 degrees, clinically this angle is barely applicable. Therefore, we developed a coating based on small microcapsules to increase the reflectivity over a wide range of angles. We quantified the reflected intensity and needle thickness as a function of the angle using a water tank setup and tested it in real tissue in a chicken breast experiment.

Statement of Contribution/Methods

Needles were coated by dipping the needles into a polyethersulfone coating containing polymeric microcapsules. Three different sizes of capsules were used, 10-25 µm, 25-50 µm and 50-75 µm. Ultrasound data were acquired using a Philips iE33 echo apparatus equipped with an L11-3 linear array transducer. A fixed setting with known look-up table and depth dependent gain was used to allow transformation of the reflected intensity of the ultrasound signal into a dB scale. The needles were positioned in a water tank filled with degassed water and mounted in a rotation arm. Data were acquired for angles from 90° down to 10° in steps of 10°. Data for each angle were rotated to 90° and averaged over all image lines to calculate an average reflection profile. The maximum of this profile was taken as the reflected intensity whereas the distance between the -6dB fall-off points was taken as the thickness. Additionally, a normal and coated needle were inserted in a chicken breast at an angle of 45° to demonstrate differences in performance under clinical circumstances.

Results

The coated as well as the normal needle are clearly visible in the water tank. However, quantitative analysis demonstrates that the intensity of the coated needle is independent of the angle: the reflected intensity is equal for all angles. This effect is observed for all used sizes of the microcapsules. The uncoated needle shows a decay of the intensity for angles smaller than 80° with a decrease of 8 dB for angles smaller than 60°. Although this decrease seems moderate, the chicken breast experiment demonstrates that the normal needle is not visible at all, whereas the coated needle can be clearly depicted. The thickness is overestimated at 90°, but decreases to the actual value for angles smaller than 60°.

Discussion and Conclusions

Coating needles with microcapsules improves the ultrasound visibility and makes the reflected intensity angle independent.

P4Aa-2

Signature-Based Algorithm for Improved Needle Localization in Ultrasound Images: a Feasibility Study

Mohammad I. Daoud[1], Purang Abolmaesumi[1], Septimiu E. Salcudean[1], Robert N. Rohling[1,2]; [1]Department of Electrical and Computer Engineering, University of British Columbia, Vancouver, British Columbia, Canada, [2]Department of Mechanical Engineering, University of British Columbia, Vancouver, British Columbia, Canada

Background, Motivation and Objective

Ultrasound-guided interventions offer the advantage of visualizing patient anatomy and the inserted needle, but localizing the needle in ultrasound images is often a challenging task. An accurate needle localization method is introduced to improve the safety and success rate of the interventions.

Statement of Contribution/Methods

A novel needle detection method is introduced based on the unique needle reflection pattern of circular waves. When a circular wave is reflected by the needle surface, the reflected signal matches a wave transmitted by a virtual point source placed behind the needle with the same orthogonal spacing between the needle surface and the source of the incident wave. Since the wave is reflected by the two needle surfaces, the reflected signal is periodic along the radial dimension with interval matching the needle diameter. Hence, the needle can be located by transmitting circular waves and analyzing the received radio-frequency signals to find the needle reflection pattern. This technique was employed to locate a needle with a diameter of 1.25 mm placed in an agar phantom. The phantom included fishing wires used as fiduciary markers. Ultrasound imaging was performed using a 128 element, curvilinear array with 5 MHz center frequency, 0.625° azimuth element spacing, and 38.96 mm radius of curvature. All elements were actuated pseudo-simultaneously to create an incident circular wave, and the signals received by all elements were recorded using custom parallel receive hardware. The array was oriented such that the needle was placed inside the imaging plane and the angle between the needle and the array central axis was varied between 50° and 90° with 5° increments. The signal received by each element was analyzed along the radial dimension using spectral analysis to find the needle periodicity pattern. The needle radial locations computed for all elements were analyzed based on the needle reflection pattern of circular waves to compute the radial and azimuth coordinates of the needle axis. The needle coordinates computed using the proposed method were compared with the needle coordinates calculated manually using three-dimensional computed tomography scan of the phantom and known wire geometry.

Results

The differences between the (radial, azimuth) coordinates of the needle axis computed using the proposed method and the CT scan are equal to (0.4 mm, 0.7°), (0.3 mm, 2°), (0.2 mm, 0.9°), (0.4 mm, 1.3°), (0.1 mm, 1.4°), (0.2 mm, 1.1°), (0.3 mm, 0.0°), (0.5 mm, 0.3°), and (0.1 mm, 3.1°) when the angle between the needle and the array central axis is 90°, 85°, 80°, 75°, 70°, 65°, 60°, 55°, and 50°, respectively.

Discussion and Conclusions

There is no clear dependency between accuracy and needle angle, unlike needle visibility in conventional ultrasound images. Ongoing research is being conducted to extend the method to also identify the needle tip and perform tests *in vivo*.

P4Aa-3

Imaging Small Targets Using the Time-Reversal with MUSIC Imaging Algorithm: A Phantom Study

Yassin Labyed[1], Lianjie Huang[1]; [1]*Los Alamos National Lab, USA*

Background, Motivation and Objective

In time-reversal (TR) ultrasound imaging, unknown targets embedded in a statistically homogeneous medium are sequentially probed using N transducer elements and the backscattered signals are measured at the N element locations. This system is characterized at each frequency by the Multi-static response matrix Ki,j , with i and j ranging from 1 to N. The transfer matrix is used to compute the Hermitian TR matrix whose non-zero eigenvalues can be shown to correspond to the unknown small targets. If the diffraction impulse response for each element is known for the medium in which the small targets are embedded, an image of the target locations can be generated. Using Multiple Signal Classification (MUSIC) in conjunction with TR processing has been shown to yield images with sub-wavelength resolution for point targets.

Previous experimental studies on TR imaging with MUSIC were conducted only for the case when the targets are much smaller than the wavelength and when the number of targets is much less than the number of transducer elements. The objective of this study is to experimentally test the performance of the imaging algorithm under various conditions where we vary the size of the small targets with respect to the wavelength, and the number of the targets with respect to the number of transducer elements.

Statement of Contribution/Methods

Nine tissue mimicking phantoms are constructed and scanned using a synthetic aperture ultrasound system. Glass spheres are distributed on a plane inside each phantom. For a given phantom, the size of the spheres is either much smaller than the wavelength, approximately equal to the wavelength, or larger than wavelength. Similarly, for a given phantom, the number of small targets is either much smaller the number of elements, or approximately equal to the number of elements, or larger than the number of elements. An investigational synthetic aperture ultrasound system is used to acquire Radio Frequency (RF) data from each phantom. The TR with MUSIC imaging algorithm is then used to image the different phantoms.

Results

The image quality as well as the accuracy in locating the spheres decreases with increasing size and increasing number of spheres due to the decrease in the number of non-zero eigenvalues of the TR matrix. However, significant improvement can be achieved if the image plane is divided into sub-regions, where each sub-region is imaged separately. In this method, the TR matrix is calculated from the windowed backscattered signals originating of the chosen sub-region.

Discussion and Conclusions

We demonstrate using phantoms that the TR with MUSIC imaging algorithm can produce high resolution images of non-pointlike targets embedded in a statistically homogeneous medium. The high resolution of the images is maintained even when there is strong multiple scattering between the targets.

This work was supported by the Breast Cancer Research Program of DoD Congressionally Directed Medical Research Programs.

P4Aa-4

Angular spectrum approach for fast simulation of pulsed non-linear ultrasound fields

Yigang Du[1,2], Henrik Jensen[2], Jørgen Arendt Jensen[1]; [1]Center for Fast Ultrasound Imaging, Dept. of Elec. Eng., Bldg. 349, Technical University of Denmark, Kgs. Lyngby, Denmark, [2]R&D Applications & Technologies, BK Medical Aps, Herlev, Denmark

Background, Motivation and Objective

The non-linear wave equation is usually solved by numerically integrating the KZK or Burgers' equation. This makes the simulation slow and inefficient, since a short iteration step in propagating direction has to be used each time in calculation of the acoustic pressure. The angular spectrum approach (ASA) can solve the non-linear equation analytically and determine the pressure in one step making it fast. A short broadband pulse is usually emitted and ASA calculation with a single temporal frequency is insufficient. The purpose of the paper is to develop the ASA for pulsed non-linear ultrasound field simulation. The source of the ASA is generated by Field II, which can simulate array transducers of any arbitrary geometry and focusing. The non-linear simulation program - Abersim, is used as the reference.

Statement of Contribution/Methods

A linear array transducer (focus: 40 mm) with 64 active elements is simulated. The pitch (0.208 mm) and height (4.5 mm) for each element and its impulse response (f_0 = 7 MHz, bandwidth: 60%) using the data from an existing transducer are used in both Field II and Abersim. The excitation is a 2-cycle sine wave with a frequency of 5 MHz. The second harmonic field in the time domain is simulated using ASA, where Field II calculates the source. Pulse inversion is used in the Abersim simulation to remove the fundamental and keep the second harmonic pulses, since Abersim simulates non-linear fields with all harmonic components.

Results

The comparisons between ASA and Abersim for calculating the pulsed fundamental and second harmonic fields in the time domain at the focal depth 40 mm along the lateral direction are shown in the figure. FWHM of ASA and Abersim are {0.97, 0.95} mm for the fundamental pulses, and {0.56, 0.55} mm for the 2nd harmonic pulses. Full width at -12 dB of ASA and Abersim are {1.27, 1.25} mm for the fundamental pulses, and {0.77, 0.73} mm for the 2nd harmonic pulses. The calculation time, for the 2nd harmonic pulses, using ASA is 12 minutes and using Abersim is 28 hours. This is made by Matlab 7.11.0 (R2010b) using a computer with 2.4 GHz Q6600 CPU and 4 GB memory.

Discussion and Conclusions

The ASA in combination with Field II for simulating pulsed non-linear ultrasound fields has been successfully implemented. Compared to Abersim, the error of ASA for calculating the 2nd harmonic pulses is 1.5% at -6 dB and 6.4% at -12 dB, and the calculation time is reduced by a factor of 140.

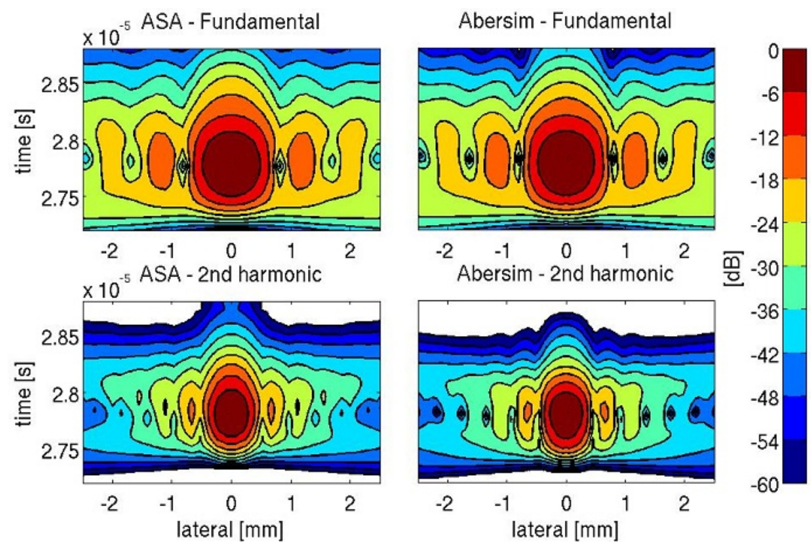

P4Aa-5

Multiphysics modeling in support of ultrasonic image development: integration of fluid-structure interaction simulations and Field II applied to the carotid artery

Abigail Swillens[1], Gianluca De Santis[1], Joris Degroote[2], Lasse Lovstakken[3], Jan Vierendeels[2], Patrick Segers[1]; [1]IBiTech-bioMMeda, Ghent University, Ghent, Belgium, [2]Department of flow, heat and combustion mechanics, Ghent University, Belgium, [3]Department of circulation and medical imaging, NTNU, Norway

Background, Motivation and Objective

Previously, we proposed a multiphysics model coupling computational fluid dynamics and Field II, allowing assessment of the performance of current and new blood flow estimators (e.g. color flow imaging=CFI, PW Doppler, speckle tracking, vector Doppler) in the carotid artery against ground truth information. Important limitations however were the rigid walls and the absence of the arterial wall and surrounding tissue in the simulations. The aim of this study was to improve and expand the model to a more realistic setup of a distensible carotid artery embedded in surrounding tissue.

Statement of Contribution/Methods

Fluid-structure interaction (FSI; simultaneous modeling of the flow and tissue domain by coupling a dedicated flow and structural solver (Fluent & Abaqus)) simulations were performed on a patient-specific carotid model geometry (fig 1-A). Parameters were chosen such that diameter changes of 10% were obtained throughout the cardiac cycle. In Field II, the vascular phantom consists of point scatterers, which were propagated according to the FSI flow field and tissue deformation, a challenging issue due to the complexly layered vascular wall and the temporally changing fluid volume. A realistic carotid imaging setup (linear array probe, center frequency 7 MHz) was modeled.

Results

Realism of the simulations was demonstrated with duplex images (fig.1-B:systolic deceleration), alternating acquisition of B-mode and CFI to meet their dissimilar spatial and temporal resolution requirements. As expected, complex flow was present throughout the bifurcation, appearing as mixed red/blue colored zones in the duplex scans. Specular reflections from the lumen-intima and media-adventitia transitions were mimicked by regularly positioning scatterers at the intima-media and media-adventitia transition, however fading for larger vessel-beam angles and/or non-ideal imaging plane (as e.g. in the internal carotid artery).

Discussion and Conclusions

We successfully expanded our multiphysics model to a synthetic ultrasound image generator of a distensible carotid artery embedded in surrounding tissue. The model produces realistic duplex images and opens up a wide field of vascular ultrasound applications not only for blood flow estimation, but also for the assessment of arterial mechanics.

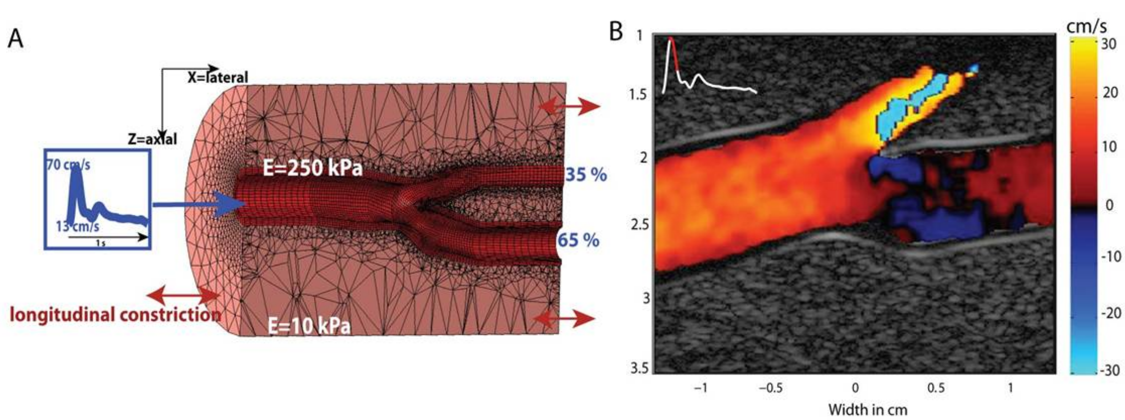

THURSDAY POSTER

P4Aa-6

Frequency Domain Time-Space Decomposition for Efficient Near Field Pressure Computations

Erwin J. Alles[1,2], Koen W.A. van Dongen[2], Robert J. McGough[1]; [1]Department of Electrical and Computer Engineering, College of Engineering, Michigan State University, East Lansing, Michigan, USA, [2]Laboratory of Acoustical Imaging and Sound Control, Faculty of Applied Sciences, Delft University of Technology, Delft, Zuid-Holland, Netherlands

Background, Motivation and Objective

The development of new transducer arrays and beamforming strategies involves repeated simulations of the pressure fields emitted by transducers prior to prototyping. Accurate numerical simulation of nearfield pressures is computationally expensive, especially for arrays populated with a large number of transducer elements. To address the need for faster numerical simulations of transient nearfield pressures, a frequency domain time-space decomposition method has been developed.

Statement of Contribution/Methods

Transient pressures are often computed by convolving the impulse response with an excitation signal using fast Fourier transforms. An even faster transient nearfield simulation method decomposes propagation-delayed excitation functions into products of temporal and spatial functions that facilitate rapid numerical computations with the fast nearfield method [1]. However, the analytic time-space decomposition method is presently restricted to certain classes of excitation functions.

Here, the time-space decomposition method is extended to arbitrary excitation signals with a frequency-domain approach. Frequency domain time space decomposition Fourier transforms the input signal and then discards the least significant frequency components such that the inverse transformed signal has a preset relative error compared to the original. The remaining frequency components are readily time-space decomposed individually at run-time. This enables rapid calculations of transient nearfield pressures for any excitation signal.

Results

Pressure fields have been computed for circular transducers using both the proposed method implemented in MATLAB and Field II [2]. For results accurate to within 1% when compared to analytic and numerical reference solutions, the frequency domain time-space decomposition method is more than 20 times faster than Field II. If a larger error of 6% is permitted, the speed-up is reduced to a factor of 6 in the nearfield.

Discussion and Conclusions

By applying time-space decomposition in the frequency domain, an accurate and efficient method that computes transient nearfield pressures for an arbitrary excitation pulse is demonstrated. For results accurate within 1% when compared to reference solutions, the proposed method is more than 20 times faster than Field II. The efficiency of the frequency domain time-space decomposition approach will be further improved when the Matlab codes are converted to compiled executables.

[1] J. F. Kelly, R. J. McGough, "A time-space decomposition method for calculating the nearfield pressure generated by a pulsed circular piston", IEEE Trans UFFC, vol. 53, no. 6, pp. 1150-1159, 2006.

[2] J. A. Jensen, “Field: A Program for Simulating Ultrasound Systems”, 10th Nordic Baltic conference on Biomedical Imaging, Vol. 4, supplement 1, part 1: pp. 351-353, 1996.

P4Aa-7

2D matrix array optimization by simulated annealing for 3D hepatic imaging

Bakary Diarra[1,2], **Hervé Liebgott**[1], Piero Tortoli[2], Christian Cachard[1]; [1]CREATIS, Université de Lyon ; CNRS UMR 5220 ; INSERM U1044 ; Université Lyon 1 ; INSA-Lyon, Villeurbanne, France, [2]MSDLab,Università degli Studi di Firenze, Florence, Italy

Background, Motivation and Objective

The efficiency of 2D arrays in real time 3D imaging is theoretically proved since many years. They allow beam focusing in both elevation and lateral directions and perform volume scanning without any mechanical displacement. However, these arrays are composed of too many elements; the huge number of elements is a real obstacle to their technological realization because current beamformers do not have so many channels. Limiting the elements number without deteriorating the image quality is an important goal.

This project intends to design an operational 2D arrays probe for use in hepatic biopsy with a low number of connected elements.

Statement of Contribution/Methods

3D ultrasound imaging of liver by means of RF needles is difficult with 2D arrays because acquisitions have to be done through the intercostal window. We propose a 2D arrays probe designed to work at a central frequency of 3.5 MHz to permit a penetration depth of 15 cm. The mean intercostal distance is 5 mm and the distance between neighboring elements (pitch) is 0.22 mm (mid-wavelength). These constraints limit the possible number of elevation rows to 22. We use 16 rows for electronic beamformers adaptability. With 64 lateral rows, the probe contains 1024 (64x16) elements. This number is reduced with the random sparse array technique. The simulated annealing algorithm is used to optimize the beam pattern, the weighting coefficients and the element number.

Results

The simulations are made by FIELD II. The beam pattern of the dense array, used as gold standard beam pattern, is compared to that of our 2D array, sparsely filled and optimized by simulated annealing. The 1024-element initial 2D array was reduced to 267 elements (74%) with good imaging features. The main lobe widening in the sparse array is overcome through the optimization. Its value remains 2 mm (2.86 degrees) in the lateral direction and 6 mm (8.62 degrees) in the elevation direction at -20 dB (Figure). The sidelobes are lower than -40 dB in both directions.

Discussion and Conclusions

The optimized 2D array gives an image quality in the lateral direction equivalent to that of classic 1D probes, with the advantage of a better elevation resolution. Work is in-progress to further improve the elevation resolution to obtain the same quality as in the lateral direction.

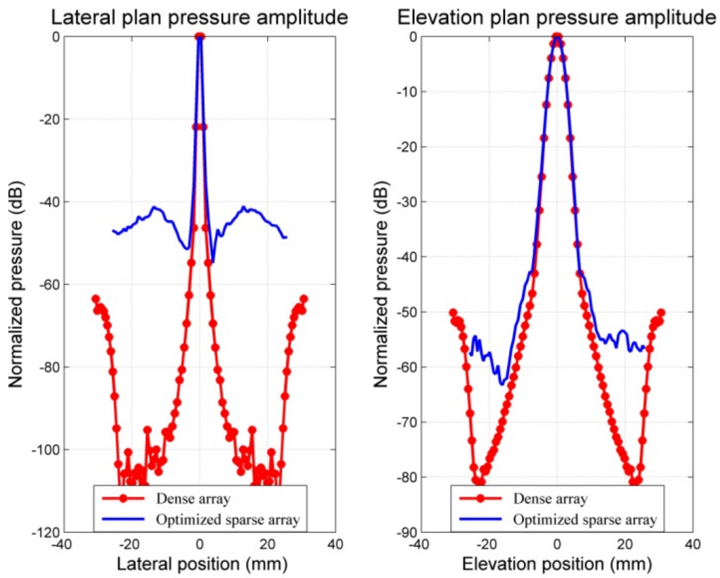

THURSDAY POSTER

P4Ab - Bone

Carribean Ballroom III-V

Thursday, October 20, 2011, 1:00 pm - 4:30 pm

Chair: **Mami Matsukawa**
Doshisha University

P4Ab-1

Assessment of anisotropic elasticity of small bone samples with resonant ultrasound spectroscopy: attenuation does not prevent the measurements

Simon Bernard[1], Quentin Grimal[1], Sylvain Haupert[1], Pascal Laugier[1]; [1]*Laboratoire d'Imagerie Paramétrique, UPMC-CNRS, Paris, France*

Background, Motivation and Objective

Resonant Ultrasound Spectroscopy (RUS) is the gold standard for high precision elasticity measurements of small samples of low damping materials [A. Migliori & J.L. Sarrao, Resonant Ultrasound Spectroscopy, Wiley, 1997]. The frequencies of mechanical resonances of a freely vibrating solid are measured and an inverse problem is solved to recover the stiffness coefficients. The usual implementation of the method fails to measure bone [Lee et al., Biomechan Model Mechanobio., 2002] due to a high damping which causes resonance peaks to overlap. However, large attenuating rock specimens have been measured with a modified RUS method [Lebedev, Acoust Phys, 2002]. In this study, we built a custom RUS setup and adapted the signal processing to handle attenuating materials such as cortical bone.

Statement of Contribution/Methods

A sample (4.05*4.51*4.25 mm3) of bone mimicking material (Sawbones, Pacific Research Laboratories) with similar anisotropic elastic properties and attenuation compared to bone was prepared along the principal directions of the material with dimensions. It has, qualitatively, the same RUS response as bone but was used instead of bone for practical reasons. The sample was placed between two compression PZT transducers (3 mm in diameter, 2 mm in thickness). Mechanical resonances were excited with a swept-sine signal. The signal processing involves converting the frequency response in time domain and finding the best filter to predict time domain data [Lebedev, Acoust Phys, 2002]. Coefficients of the filter give the parameters of resonance peaks. Only linearity of the vibratory system and lorentzian shape of the resonance peaks are assumed a priori, while the number of resonances is found using singular value decomposition of the signal autocorrelation matrix. Reference elastic properties of Sawbone, assessed with an independent validated method, were used for comparison.

Results

In the frequency band 100-350 kHz we were able to measure 10 modes which frequencies are within 1,7% of the frequencies predicted based on the reference Sawbone elastic values. While the first 3 frequencies of the sample spectra and 7 others among the predicted resonances could be measured, 11 frequencies could not be retrieved because (i) of a combination of the increased modal density above 200 kHz and large peak width; (ii) of insufficient excitation of several modes.

Discussion and Conclusions

With an original implementation of RUS we were able to measure several resonance frequencies of a bone mimicking material. The signal processing performs well to find resonance peaks even in cases were the latter are not prominent in the spectrum. Several additional peaks could probably be retrieved with different positioning of the samples or by combining measurements with longitudinal and shear transducers. The results indicate that it should be possible to measure cortical bone with a RUS system. This will open the way for the precise characterization of small-sized bone samples.

P4Ab-2

Quantitative Ultrasound Noninvasive Investigation of Trabecular Organization and Orientation

Frederick Serra-Hsu[1], Stephanie Wang[1], Jiqi Cheng[1], Yi-Xian Qin[1]; [1]Biomedical Engineering, Stony Brook University, Stony Brook, New York, USA

Background, Motivation and Objective

Quantitative Ultrasound (QUS) parameters have shown significant correlation to bone mineral density and fracture risk in patients losing bone mass, as in Osteoporosis. The majority of bone loss and reorganization occurs at the sites dominated by trabecular bone in vivo. QUS measurements greatly vary in trabecular bone due to structural orientation and adaptive anisotropy, both of which are important for overall bone strength. Most work to date focuses on trying to minimize the effect of orientation on QUS parameters. Instead, the current work will focus on the ability of QUS to determine the principal trabecular direction. Prediction of the principal trabecular axis combined with standard QUS measures can more accurately represent changes in trabecular organization and orientation during osteoporotic bone loss.

Statement of Contribution/Methods

Twelve all-trabecular cylinders were scanned at 39µm resolution with a vivaCT80 (SCANCO Medical, Bassersdorf, Switzerland). Our 1MHz QUS device took measurements perpendicular the longitudinal axis of each sample at 5° increments, rotating from 0° to 355°. Structural parameters were obtained from SCANCO software, and included bone volume fraction (BV/TV), Trabecular-Spacing (Tb.Sp) and Degree-of-Anisotropy (DA).

Results

The data show very high dependence of QUS parameters on propagation angle. The correlation between UV and BV/TV varied from 0.12-0.78, depending on the angle of penetration. Other structural parameters, such as DA and Trabecular-Thickness also show dependence upon angle of ultrasound propagation.

Discussion and Conclusions

UV and BV/TV were most highly related when ultrasound propagated along the medial-lateral direction. UV was most highly related to DA at 150 degrees from the medial-lateral axis. Tb.Sp and Tb.N both demonstrated the highest correlation with UV at 160 degrees from the ML axis. The correlation to mean-intercept-length trabecular orientation vector will show predictive capability of QUS on organization of trabecular bone. The combination of standard QUS measures coupled with prediction of organization can provide higher diagnostic capability in osteoporotic fracture risk.

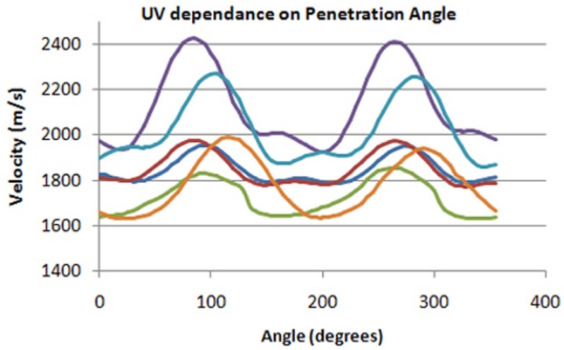

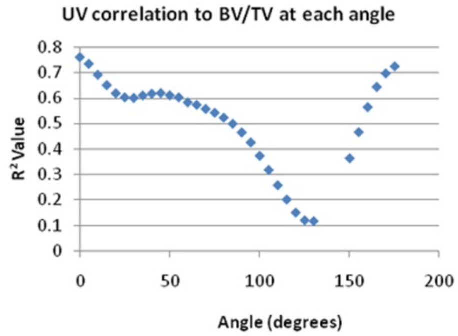

P4Ab-3

Characterization of the fast wave in cancellous bone using the Bayesian probability theory approach

Mami Matsukawa[1], Katsunori Mizuno[1], Joseph Hoffman[2], Amber Nelson[2], Mark Holland[2], Yoshiki Nagatani[3], James Miller[2]; [1]*Doshisha University, Japan,* [2]*Washington University in St.Louis, USA,* [3]*Kobe City College of Technology, Japan*

Background, Motivation and Objective

The two-wave phenomenon (fast and slow waves) often occurs when the ultrasonic wave propagates in the cancellous bone. One important property that might be assessed using the phenomenon is the structural anisotropy obtained from fast wave properties. However, the two waves often overlap in time, making detailed investigation difficult. One interesting solution is a Bayesian probability theory approach [Marutyan et al, J.Acoust.Soc.Am., 121 (2007) EL8]. The objective of this study is to investigate the application of this approach to separating the overlapped waves in cancellous bone.

Statement of Contribution/Methods

Ultrasonic through-transmission data in the MHz range were experimentally obtained using two cancellous bone samples from the distal end of two bovine femora and an ultrasonic pulse technique [Nagatani et al., Ultrasonics, 48 (2008) p.607, Mizuno, et al., J.Acoust.Soc.Am., 128 (2010) p.3181]. The thickness of the specimen was reduced in 1 mm steps from 15 mm to 6 mm, by carefully filing tissue away. A Bayesian analysis was performed on the observed overlapped waves. The speed of sound and attenuation were determined using the fast waves reconstructed from the analysis.

Results

Comparing the experimentally observed wave and the Bayesian-estimated wave in the time domain, we found that residuals (difference between two waveforms) were relatively smaller in the region of the fast wave (Figure). They were comparatively larger in the region of the slow wave. The fast wave attenuations obtained from the initial peak values of the observed waves were in good to moderate agreement with those of the estimated fast waves. The attenuation showed variation among the 1 mm segments of the bone sample, perhaps reflecting the heterogeneity of trabecular bone.

Discussion and Conclusions

The Bayesian approach was useful for investigating the fast wave. The fast wave properties reflect the trabecular structure, which is an important feature of cancellous bone. One possible explanation for the relatively larger residuals of the slow waves is the forward scattering, which has been shown from the wavelet analysis of the experimental waves [Hasegawa, et al., Jpn.J.Appl.Phys., 49 (2010) 07HF28].[NIH grant R01AR057433]

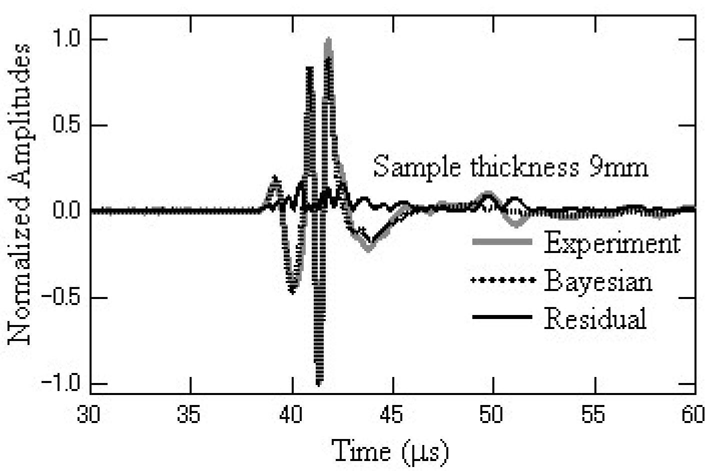

P4Ab-4

The two-wave phenomenon in cancellous bone with the closed-pores on the boundaries: An in vitro study

Katsunori Mizuno[1], Yoshiki Nagatani[2], Keisuke Yamashita[1], Mami Matsukawa[1]; [1]*Doshisha University, Japan,* [2]*Kobe City College of Technology, Hyogo, Japan*

Background, Motivation and Objective

Several experimental studies of the two-wave phenomenon in cancellous bone have been reported using water-immersion ultrasonic techniques [A. Hosokawa et.al., J.Acoust.Soc.Am., 101 (1997) 558-562.]. These two waves were also confirmed by numerical approaches such as 3-D FDTD (finite-difference time-domain) method with reconstructed 3-D CT images. However, the two-wave phenomenon in cancellous bone has always been confirmed under the condition of the open-pore boundaries, which invokes the discussion that the wave can not be separated in the bone (porous medium) with the closed-pore boundaries [P. Rasolofosaon, Appl. Phys. Lett. 52 (1988) 780-782.]. The goal of this study is the investigation of the two-wave phenomeon in cancellous bone with the closed-pore boundaries from the experimental points of view.

Statement of Contribution/Methods

A cancellous bone and two plate-like cortical bones were obtained from the distal part of the left radius of a racehorse. A conventional ultrasonic pulse method was used to observe the longitudinal waves [K. Mizuno et.al., IEEE Trans. Ultrason. Ferroelectr. Freq. Control., 55 (2008) 1480-1487.]. We investigated the propagated waves under two conditions: (i) propagation through the cancellous bone, (ii) propagation through the cancellous bone sealed by the plate-like cortical bones. The structural parameters of the cancellous bone were obtained from the X-ray CT data. The degree of anisotropy (DA), and bone volume fraction (BV/TV) were obtained by "3D-Bon" software (Ratoc, Tokyo, Japan).

Results

Clear separation of the fast and slow waves was experimentally observed under the both conditions with open-pore and closed-pore boundaries, as shown in Fig. 1. However, reflection occurred at the interfaces of cortical plates and cancellous bone, which caused the strong attenuation of the fast (9.8 dB) and slow (10.6 dB) waves.

Discussion and Conclusions

In the cancellous bone sealed by the cortical plates, the two-wave phenomenon was clearly observed experimentally. However, the characteristics of waves with the closed-pore boundaries were different from those with the open-pore boundaries owing to the reflections at the interface of cortical plates and cancellous bone. More precise studies on the effect of the boundary condition are required to investigate the phenomenon for the purpose of in vivo assessment.

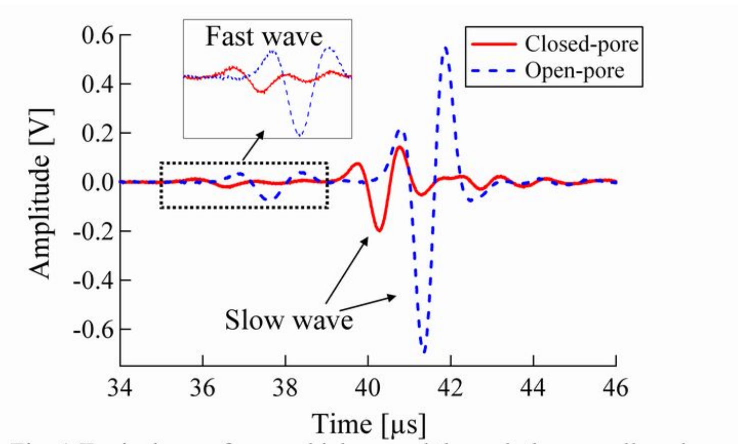

Fig. 1 Typical waveforms which passed through the cancellous bone under the two boundary conditions : solid line was closed-pore and dashed line was open-pore.

P4Ab-5

Guided mode measurement on bone phantoms with realistic geometry

Josquin Foiret[1], Jean-Gabriel Minonzio[1], Maryline Talmant[1], Pascal Laugier[1]; [1]*LIP - UPMC Univ Paris 6 - CNRS UMR 7623, Paris, France*

Background, Motivation and Objective

The project consists in investigating the potential of guided waves in restoring elastic properties and thickness of cortical bone using the axial transmission measurement configuration. The objective of the present study is to assess the method on bone mimicking phantoms with realistic bone geometry.

Statement of Contribution/Methods

Experiments are performed on bone mimicking phantoms (Sawbones, Pacific Research Laboratory Inc, Vashon WA) made of glass fibers embedded in epoxy but with different geometries: a reference flat plate, an empty tube with circular cross section and a radius-shaped sample mimicking forearm bone with a non circular external surface and a cortical layer thickness linearly varying along the bone axis. The material is considered as a transverse isotropic absorbing medium. Its elastic properties have been characterized using ultrasound shear and compression bulk wave transmission measurements in different directions. The 1 MHz broadband axial transmission probe contains a linear array of 5 emitters and 32 receivers. A denoising method based on the singular value decomposition of the time Fourier transformed transfer matrix was developed and was shown to be efficient for low signal to noise ratio cases such as signals on absorbing plates [Minonzio et al. IEEE Ultrasonics Symp. 2010].

Results

Fig. 1 shows comparison between experimental spectrum for the tube and bone phantom and the calculated Lamb spectrum for the plate model. The sample thickness which gives the best adjustment of experimental to calculated Lamb spectrum is respectively 2.3, 2 and 3 mm for the plate, the tube and the bone phantom. These thicknesses match calliper measurements for the plate and the tube. For the bone phantom, the estimated thickness matches the average thickness of the cortical layer under the receivers array.

Discussion and Conclusions

Despite absorption and irregular geometry of the bone shaped sample, the thickness of the cortical layer on radius phantoms was correctly determined, using the flat plate model. This study in controlled conditions is promising for determination of bone properties in in vitro experiments.

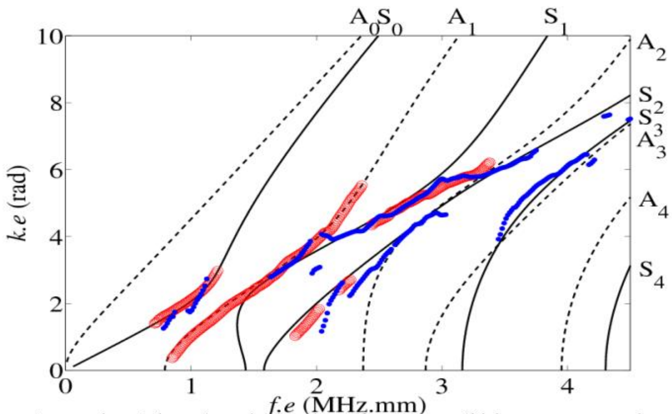

Figure 1: experimental spectrum in the plane (frequency × thickness , wavenumbers × thickness) obtained with the 2 mm thick tube with inner to outer radius ratio of 0.8 (red circle) and the 3 mm thick phantom radius (blue point). Lamb spectrum calculated for transverse isotropic plate is shown as solid and dashed black lines (respectively symmetric S_n and antisymmetric A_n).

P4Ab-6

The slow-wave disappearance owing to the structure at the interface between cancellous and cortical bones - A computational study

Yoshiki Nagatani[1], Katsunori Mizuno[2], **Mami Matsukawa[2]**; [1]Kobe City College of Technology, Japan, [2]Doshisha University, Japan

Background, Motivation and Objective

For the practical use of ultrasonic diagnosis system for osteoporosis, many investigations on the two-wave phenomenon in cancellous bone have been reported [e.g. A. Hosokawa, J. Acoust. Soc. Am. 101 (1997)]. However, P. N. J. Rasolofosaon claimed [Appl. Phys. Lett. 52 (1988)] that the slow wave disappeared in simple porous media with thin coat of paint on both sides. Their report suggested that the effect of the boundary condition between porous portion and sealing material could not be negligible. In this study, therefore, the effect of interface structure between cancellous and cortical bones on the wave propagation was investigated using a simulation technique, especially focusing on the behavior of slow wave.

Statement of Contribution/Methods

The 3-D elastic-FDTD simulation system for the wave propagation in bone was developed by our group. The consistency with experimental measurement has already been confirmed [Nagatani et al., Jpn. J. Appl. Phys. 45 (2006)]. For simulation, a 3-D model was created from X-ray micro-focus CT images of a cancellous bone in distal part of the left radius of a racehorse. The both side of cubic cancellous bone model was virtually sealed with a cortical plate ("closed-pores"), whose thickness was 2 millimeters (left figure). In order to investigate the effect of structure at the interface, the diameter of trabeculae were virtually increased gradually near the interface as shown in the right figure.

Results

The two-wave separation was clearly seen under the condition with clear boundary between cancellous and cortical bones (left figure). When the boundary became ambiguous, the amplitude of slow wave became smaller, then finally disappeared (right figure). On the contrary, the fast wave became larger and propagated faster.

Discussion and Conclusions

The simulated data showed that the slow wave worn away under the conditions with ambiguous boundary. In such conditions, the slow wave seemed to become out of phase during its propagation into cortical bone from liquid portion. The clear boundary, which kept in-phase propagation, resulted in clear separation of two waves. Since human radius bone has distinct boundary between cancellous bone and cortical bone, the slow wave might be observed in vivo. These numerical results support the availability of two-wave information in the practical use of osteoporosis diagnosis system.

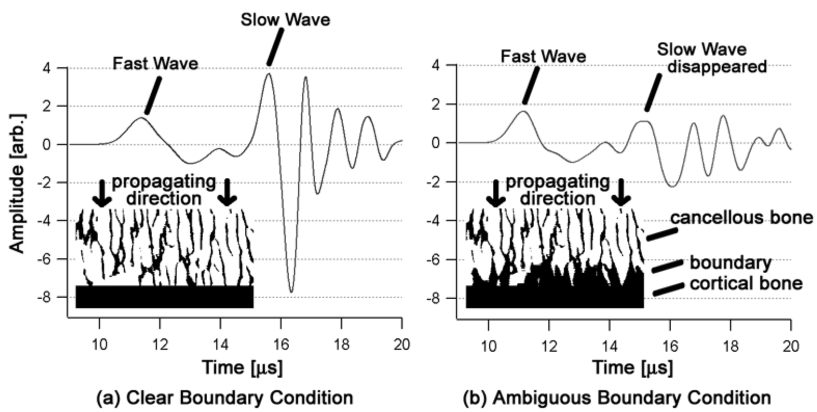

Figure 1: Simulated Waveforms.

P4Ab-7

Ultrasound propagation in random anisotropic media using numerical simulation in 2D: applications to trabecular bone assessment

Marie Muller[1], Emmanuel Bossy[1], Fabien Mézière[1], Arnaud Derode[1]; [1]Institut Langevin- Université Paris Diderot - ESPCI - CNRS, Paris, France

Background, Motivation and Objective

The ultrasonic characterization of bone biomechanical properties can improve bone fracture risk assessment with a non-invasive, non-ionizing and relatively inexpensive method. The relevance of such a diagnostic tool is increasingly important due to the incidence of osteoporosis in an aging population. Currently there are ultrasonic tools available to measure ultrasonic parameters which correlate to bone density. These methods appear to have significant potential and are currently underutilized because the physics of ultrasound wave propagation in bone is still poorly understood. Some phenomena experimentally observed in trabecular bone remain indeed not well understood, such as the possible propagation of two compressional waves with different velocities. This study focuses on determining the conditions necessary to develop two waves on a simple model, and in particular on the influence of guided modes in their occurrence.

Statement of Contribution/Methods

Numerical simulations were conducted using a finite difference (FDTD) tool that can simulate the propagation of elastic waves in heterogeneous anisotropic media with fine control. This simulation tool solves the elastic wave equations with a finite difference scheme and it quantitatively calculates the displacement and stress at all points, across a broad range of frequencies. Trabecular bone was modelled by a binary random medium with fully controlled elasticity and anisotropy. To do so, elliptic-shaped patterns were randomly distributed on 2D maps with an orientation ensuring global anisotropy. The material properties were defined at all points in space. The coherent wave was calculated by averaging over a large number of realizations of the propagation field.

Results

The two waves, which have been reported in the literature under certain conditions, were observed. Two conditions were found necessary for their occurrence: i) the successive arrival of the two waves could only be observed when the propagation was not perpendicular to the ellipses and ii) the existence of shear waves in the solid phase of the medium had to be accounted for. The slow wave had a speed close to that of ultrasound in water (approximately 1500 m/s). The fast wave had a larger speed, which depended on porosity and on material parameters (approximately 3000 m/s), and, more importantly, which was found consistent with the speed of a guided lamb wave.

Discussion and Conclusions

These results suggest for the first time that the occurrence of the two waves reportedly observed in trabecular bone could be attributed to the existence of modes guided by the trabeculae. If this was the case, important bone micro-architecture parameters such as anisotropy and connectivity could potentially be retrieved from ultrasonic measurements, improving the evaluation of fracture risk.

P4Ac - Targeted Contrast Agents

Carribean Ballroom III-V

Thursday, October 20, 2011, 1:00 pm - 4:30 pm

Chair: **Nobuki Kudo**
Hokkaido University

P4Ac-1

A Fast Ultrasound Molecular Imaging Method

Xiaowen Hu[1], Lisa Mahakian[1], Charles Caskey[1], Julie Beegle[1], Dustin Kruse[1], Joshua Rychak[2], Patrick Sutcliffe[1], Katherine Ferrara[1]; [1]*Biomedical Engineering, University of California, Davis, CA, USA,* [2]*Targeson, Inc, San Diego, CA, USA*

Background, Motivation and Objective

Using targeted microbubbles (MBs), ultrasound molecular imaging can selectively and specifically visualize upregulated vascular receptors. In order to acquire bound MB echoes, a delay of ~6 minutes is commonly required for the clearance of freely circulating MBs. In addition, high-pressure destructive pulses are frequently applied to improve the differentiation of free and bound agents.

Statement of Contribution/Methods

We test whether echoes from MBs can be distinguished from the surrounding tissue, based on the transmission of pulses at low (1.5 MHz) and reception at high (5.5 MHz) frequencies (TLRH), without the requirement for destructive pulses. Here, pulses with a peak negative pressure of 200 kPa were transmitted (10 fps) and a 7th order IIR pulse-to-pulse filter was applied to the TLRH radiofrequency (RF) data to distinguish the signature of bound MBs from that of flowing MBs. The resolution and sensitivity of TLRH contrast imaging was compared with CPS imaging, which has been widely utilized in ultrasound targeting imaging. 3D images of the accumulation of intravenously-administrated cRGD- and VEGFR2-targeted MBs (Targeson) in a Met-1 mouse tumor model were acquired.

Results

An *in vitro* study demonstrated that the T2R15 contrast imaging technique has a similar MB detection sensitivity to 2MHz CPS imaging, for a transmission pressure greater than 200 kPa and with an ~2-fold resolution improvement over 2MHz CPS imaging. Applying the 7th order IIR filter to the TLRH RF data acquired at 2 minutes, echoes from flowing MBs in the surrounding tissue region were suppressed by 17±5 dB; while the signal intensity within the tumor was suppressed by 4±2 dB. The targeted images were demonstrated to correctly represent the distribution of bound MBs. After the filter or delay, the signal intensity resulting from cRGD-targeted MBs (a-c) was 30±3 dB higher than that after the injection of non-targeted MBs (d, e). By shortening the acquisition time using TLRH rather than multi-pulse imaging, 3D maps of MB accumulation were rapidly acquired (f).

Discussion and Conclusions

The proposed molecular imaging method, utilizing a 7th order pulse-to-pulse filter and TLRH imaging method, has been demonstrated to be capable of rapidly visualizing targeted MBs *in vivo*.

The authors acknowledge NIH R01CA112356.

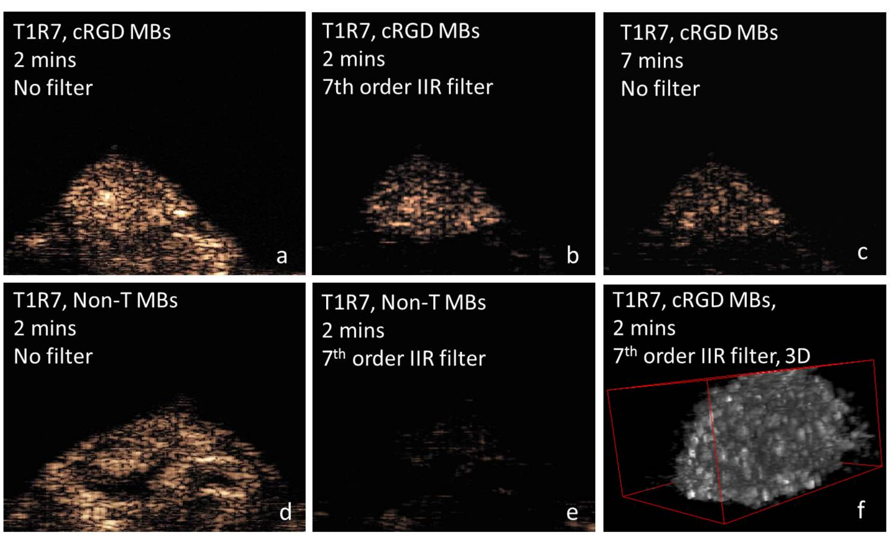

P4Ac-2

Targeted Microbubble-mediated Ultrasound Therapy: A Feasibility Study

Reshu Saini[1], Anna Sorace[1], Kenneth Hoyt[2]; [1]Biomedical Engineering, University of Alabama at Birmingham, USA, [2]Radiology, University of Alabama at Birmingham, USA

Background, Motivation and Objective

Currently, there is a need for improved drug delivery mechanisms to locally increase drug uptake in cancer cells. Microbubble (MB)-mediated ultrasound (US) therapy has been studied as a potential system for enhanced drug uptake due to mechanical perturbation of endothelial cells and subsequent increased permeability. In this study, MB-mediated US therapy was used in conjunction with antibody (Ab) labeled MBs to determine if localization of MBs would improve drug uptake.

Statement of Contribution/Methods

The custom experimental US setup involved single element (0.75 inch) immersion transducer in series (Olympus) with a signal generator (AFG3022B, Tektronix) and power amplifier (A075, Electronics and Innovation). 2LMP cells (1e6) were infected with a replication incompetent adenovirus (Ad) vector containing genes for human somatostatin receptors with an HA tag at a multiplicity of infection (MOI) of 100. Cells were plated on acoustically transparent plates (Opticell). Streptavidin coated MBs (Targeson) were labeled with 100 µg of either biotinylated anti-HA Ab (Sigma-Aldrich) or biotinylated anti-mouse IgG Ab (Southern Biotech). After a 24 hr period to ensure proper seeding, plates were injected with 2 mL of calcein (a membrane non-permeable fluorescent molecule) (1e-3 M concentration) and 50 µL of MBs (anti HA-targeted or IgG isotype control, concentration of 1.5e7 MBs/mL). Cells underwent combination therapy using the following US parameters: transmit frequency of 1.0 MHz, 5.0 min duration, pulse repetition period (PRP) of 0.01 sec, duty cycle of 20% and a mechanical index (MI) of 0.1, 1.0 or 2.0. Fluorescent signal from internalized calcein molecules was quantified for each group using flow cytometer (Accuri C6, Accuri Cytometers Inc). Average fluorescence per cells were recorded as mean +/- SE. Light microscopy images were acquired and matched to fluorescence images to visibly validate targeted MB-mediated US therapy fluorescent uptake.

Results

For each experimental variant, data was normalized by control group fluorescence (calcein dye) and reported as percent control. Results showed a significant increase ($p < 0.001$) in fluorescence at an MI of 0.1 between anti-HA targeted MBs (183.09 ± 4.86) and IgG control MBs (97.51 ± 3.34). At an MI of 2.0, there was a significant increase ($p < 0.001$) in the amount of internalized fluorescent tracer when comparing targeted (41.3 ± 0.79) and control (37.36 ± 0.74) MB-mediated US therapy results. At an MI of 1, however, no significant difference ($p > 0.44$) was seen between targeted (62.07 ± 3.31) and control (59.43 ± 7.27) MBs. These results suggest that low MI US exposure of targeted MBs is more effective at modulating cell permeability and indicate that inertial cavitation may be the dominant mechanism.

Discussion and Conclusions

This study demonstrates that MBs targeted to cellular receptors are a promising addition to MB-mediated US therapy and might further help increase drug uptake in cancerous tumors.

P4Ac-3

Adhesion of targeted microbubbles under pulsatile and steady flow

Charles Sennoga[1], John Seddon[2], Robert Eckersley[3], Meng-Xing Tang[4]; [1]Department of Bioengineering, Imperial College London, United Kingdom, [2]Department of Chemistry, Imperial College London, United Kingdom, [3]Imaging Sciences Department, Imperial College London, United Kingdom, [4]Department of Bioengineering, Imperial College London, London, London, United Kingdom

Background, Motivation and Objective

Background and aim: In ultrasound molecular imaging, microbubbles are engineered to target specific molecules on the endothelial wall and these bubbles can be tracked noninvasively using ultrasound. This technique has great potential in a number of clinical applications including the imaging of atherosclerosis, myocardium infarction, and tumour angiogenesis. A number of studies have investigated the binding efficiency of the targeted microbubbles under various flow velocity and wall shear stress, to our knowledge these studies have used only steady or quasi-steady flow and have not considered pulsatile flow, which is the case in arteries and arterioles. In this study the aim is to investigate the binding of microbubbles under pulsatile flow and compare this with steady flow.

Statement of Contribution/Methods

Homemade biotin coated lipid shell microbubbles were produced through sonication. A flow cell was coated with strapatavidin. A programmable pump was used to produce pulsatile and steady flow in the flow cell. The targeted bubbles were diluted in PBS and flowed through the cell. For both pulsatile and steady flow, the average flow was set at 0.75 ml/minute. The number of bubbles attached to the coated cell surface was observed using optical microscopy and quantified at a number of time points after the flow started.

Results

The initial results show that the number of bubbles attached during pulsatile flow is approximately 20% more than for the steady flow. While the number of attached bubbles increased over time, the rate of increase was reduced gradually over time. No significant difference in the rate of increase between pulsatile and steady flow was observed. Few bubble detachments were observed at the flow rate used.

Discussion and Conclusions

A modest difference in the number of attached bubbles between pulsatile and steady flow was observed. Further studies are needed to confirm this finding and to understand the cause of this difference.

P4Ac-4

A new ultrasound-based approach to visualize target specific polymeric contrast agent

Malin Larsson[1], Anna Bjällmark[1], Matilda Larsson[1], Lars-Åke Brodin[1], Reidar Winter[2], Kenneth Caidahl[3]; [1]School of Technology and Health, Medical Engineering, Huddinge, Sweden, [2]Clinical Physiology, Karolinska University Hospital in Huddinge, Sweden, [3]Molecular Medicine and Surgery, Karolinska University Hospital in Solna, Sweden

Background, Motivation and Objective

Ultrasound (US) contrast imaging is widely used in clinical applications. Advantages of using a polymeric contrast agent (CA) instead of lipids are that particles can be attached to the surface, hence it is possible to produce a multimodal CA, and it also enables introduction of antibodies to the surface making the CA target specific. In the latter case, it is essential to enable detection of a thin layer of CA. However, preliminary results have indicated difficulties in visualizing polymeric CA with present contrast algorithms. The aim of this study was therefore to test a new algorithm for visualization of polymeric CA and to compare it with existing methods.

Statement of Contribution/Methods

US short-axis images of a tissue-mimicking vessel phantom with pulsating flow were obtained using a GE Vivid7 system (12L) and a Philips iE33 system (S5-1), Fig. 1. Repeated (n=34) contrast to tissue ratios (CTR), expressed in times enhancement of the CA signal, were calculated at various MI using the contrast algorithms pulse inversion (PI) and power modulation (PM) at a concentration of 10^5 MB/ml. A subtraction algorithm (SA) was developed based on subtraction of two gray-scale images: a reference image (without CA) and a contrast image (containing CA). The two images were matched spatially by using block-matching with normalized cross-correlation and in time by using the ECG. CTR was then calculated in the subtracted image for the different MI. Moreover, the possibility to detect a thin layer of CA was tested using the SA. The vessel phantom was imaged upside down after 6 hours without flow, where the air filled CA had risen and produced a thin layer at the posterior vessel wall in the image.

Results

The CTRs were 1.05 ± 0.05 (MI 0.1), 2.31 ± 0.16 (MI 0.4) and 1.72 ± 0.11 (MI 0.8) with PI, 1.00 ± 0.12 (MI 0.1), 0.79 ± 0.09 (MI 0.4) and 1.16 ± 0.13 (MI 0.8) with PM and 38.60 ± 2.45 (MI 0.1), 82.63 ± 4.07 (MI 0.4) and 100.55 ± 13.84 (MI 0.8) with the SA. Fig. 1d and 1e show long-axis images of the phantom with a thin layer of CA close to the posterior wall, which has been color-coded using the SA in Fig. 1e.

Discussion and Conclusions

The developed SA showed great improvements in CTR compared to existing contrast algorithms, which improve the possibility of using polymeric CA in target specific imaging. The use of the SA to identify a thin layer of polymeric CA was initially tested, but will be further evaluated in future studies.

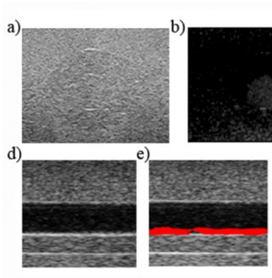

Figure 1. Ultrasound images of a vessel phantom containing blood-mimic and polymeric CA, a) conventional gray-scale image, b) PI image c) SA image, d) zoomed conventional gray-scale image with a thin layer of CA close to the posterior wall, e) image in d after applying the SA and color-coding of the CA.

P4Ac-5

The Periodicity between the Aggregated Microbubbles by Secondary Radiation Force

Sevan Harput[1], Benjamin Raiton[1], Paschalis C. Sofotasios[1], James Mclaughlan[1], Stephen Evans[2], Steven Freear[1]; [1]School of Electronic and Electrical Engineering, University of Leeds, Leeds, United Kingdom, [2]School of Physics and Astronomy, University of Leeds, Leeds, United Kingdom

Background, Motivation and Objective

The *classical* expression for the mutual interaction between oscillating bubbles was first derived by C. A. Bjerknes in 1868. When the secondary radiation force is calculated according to the volume pulsation of bubbles, a negative force engenders attraction whereas a positive one induces repulsion. The sign of the secondary Bjerknes force is directly related to the bubble resonance. Two bubbles excited above or below their resonance frequencies will result in an attractive force, yet if one is below and the other is above resonance, the net force will be repulsive. However, the attractive and repulsive bubble behavior is not always predictable in a microbubble cloud. The sign reversal of secondary Bjerknes force acting on microbubble clusters is observed due to the multiple scattering effects. Regardless of their size, microbubbles attract each other and form stable bubble clusters.

Statement of Contribution/Methods

The aggregation behaviour of Sonovue microbubbles are observed for the frequency range of 2-7 MHz between 25 kPa and 500 kPa peak-negative pressures with flow rates of 0.5 mL/h to 10mL/h. A transparent tube with a diameter of 250 micrometers is placed at the focal point of the transducer where the ultrasound contrast agents are flowing. The onset of microbubble aggregation pattern is captured by a Nikon Eclipse Ti-S inverted microscope (Nikon Corp, Tokyo, Japan) and Fastcam-XLR 1024 (Photron Limited, Marlow, Bucks, UK).

Results

Under certain conditions, the microbubble aggregation pattern is periodic. The attached figure shows the microbubble aggregation pattern for 3 different flow rates and pressure levels. A threshold effect is also observed between the microbubble velocity and secondary radiation force. For the high flow rates, the microbubble aggregation starts at a higher pressure level. The mutual interaction between the microbubbles is observed above 50 kPa for 1mL/h flow rate. However, at 10mL/h the microbubble aggregation starts at 200 kPa.

Discussion and Conclusions

The periodicity between the aggregated microbubble clusters are observed in a small vessel. It is demonstrated that the initial bubble velocity and excitation pressure play an important role on the aggregation pattern.

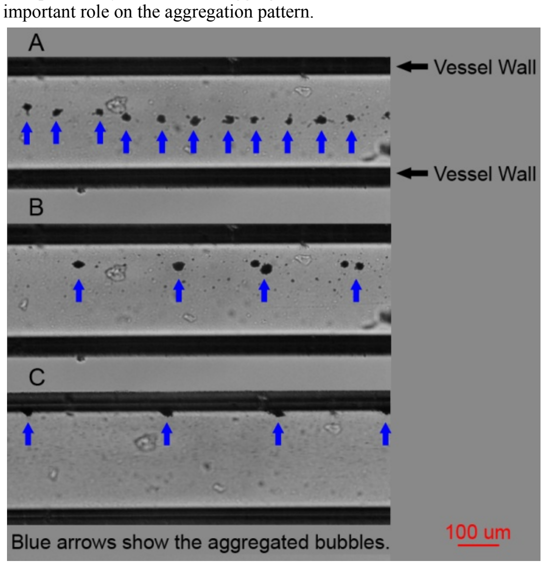

P4Ac-6

Characterization of Acoustically-Vaporized Droplets under Dynamic Flow Conditions

Tung-Yeh Wu[1], Shih-Tsung Kang[1], Chih-Kuang Yeh[1]; [1]Department of Biomedical Engineering and Environmental Sciences, National Tsing Hua University, Hsinchu, Taiwan

Background, Motivation and Objective

Acoustic droplet vaporization (ADV) has been reported to produce gas bubbles to reduce blood flow for gas embolotherapy. However, the evolution of ADV bubbles was mostly investigated using high speed photography in a static fluid that differed from real clinical conditions. In this study, we explored the evolution of ADV bubbles under dynamic flow conditions. Possible physics behaviors of flowing ADV bubbles such as growth, diffusion, and coalescence were characterized based on acoustic and optical observations.

Statement of Contribution/Methods

The experiments were conducted using an integrated acousto-optical system. Diluted lipid perfluoropentane (PFP) droplets with a mean diameter of 1.2 µm were injected into a 200-µm cellulose tube at a flow rate of 16.0 mm/s. A 3.5-MHz HIFU transducer was used to transmit 3-cycle and 8-MPa US pulses at a PRF of 40 Hz for activating the PFP droplets. The ADV bubbles were monitored after they traveled at different distances with respect to the original activation site. M-mode imaging by 40-MHz US and high-speed photography were conducted at downstream from the focus of the HIFU transducer, as depicted in Fig. 1(a). The Doppler power and size distributions of ADV bubbles were calculated from the M-mode and high-speed images, respectively.

Results

Fig. 1(b) shows that the mean Doppler power increased with the travel distance away from the HIFU transducer. The ADV bubbles performed more stable after flowing over 10 mm (travel time of 630 ms). Figs 1(c) and (d) show similar total amounts of ADV bubbles at the distances of 3 and 10 mm, respectively. However, in 10 mm cases, the percentage of larger ADV bubbles (> 15 µm) achieved 35% and the mean diameter of ADV bubbles was 23 µm (both higher than those in 3 mm).

Discussion and Conclusions

The bubble growth can last for hundreds of milliseconds after the onset of ADV under dynamic flow conditions. The stable and larger ADV bubbles far away from the activation site have the potential for gas embolotherapy applications. Different flow rates and acoustic parameters for ADV such as acoustic pressure, PRF, and pulse length were also considered to investigate the generation and evolution of ADV bubbles.

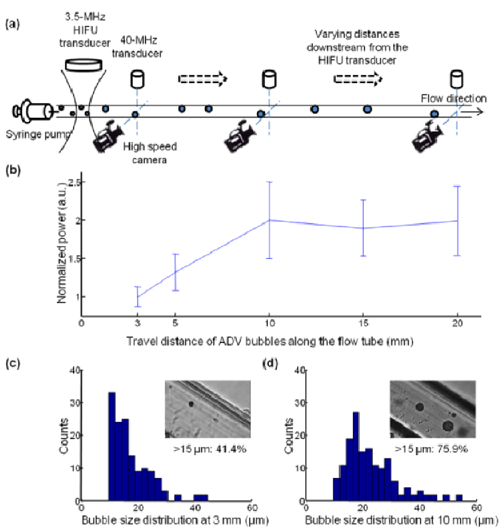

THURSDAY POSTER

P4Ad - Therapy: HIFU, Monitoring, Control, and Quality Assurance

Carribean Ballroom III-V

Thursday, October 20, 2011, 1:00 pm - 4:30 pm

Chair: **Jean-Yves Chapelon**
INSERM, Lyon

P4Ad-1

Todoidal transducer with two large focal zones for increasing the coagulated volume

Jeremy VINCENOT[1], David MELODELIMA[1], Alexandre VIGNOT[1], Francoise CHAVRIER[1], Jean-Yves CHAPELON[1]; [1]Inserm, U1032, Lyon, F-69003, France ; Université de Lyon, Lyon, F-69003, France., France, Metropolitan

Background, Motivation and Objective

Earlier work showed that toroidal HIFU transducer geometry generates simultaneously an enlarged focal zone composed of a first ring-shaped focal plane and an overlap of ultrasound beams behind this first focal plane. This particular focalization allows the creation of one single lesion of 7 cm^3 in 40 seconds. Although these large single lesions contributes to reduce treatment time, it is still needed to juxtapose 4 to 9 single lesions to treat one liver metastases of 2-3 cm in diameter with safety margins. The objective of this work is to combine a new geometry of toroidal transducers and the use of electronic focusing in order to create, in less than 5 minutes, one single HIFU exposure with a coagulated volume sufficient for the destruction of a metastasis of 3 cm in diameter.

Statement of Contribution/Methods

A spindle torus is generated by the rotation of a circle around an axis of revolution with a distance between the axis and the center of the circle lower than the radius of the circle. After rotation, the volume obtained is composed of two envelopes that can be used to create a toroidal transducer. To date, our previous work on toroidal transducers used the outer envelope as a reference surface. A new transducer geometry, based on the interior part of a torus, has been developed. This geometry generate the same focal ring but allows a beams overlap before this focal plane. Therefore, unlike previous toroidal transducers, a second focal zone is created between the transducer and the ring-shaped focal plane. The operating frequency was 2.5 MHz. The radius of curvature was 70 mm with a diameter of 67 mm. An ultrasound imaging probe was placed in a central circular opening of 26 mm. The transducer was also divided into 32 rings of 78mm^2. Using a 32 channels amplifier with a phase resolution of 1.4 degrees, it was possible to change the diameter (0 to 15 mm) and depth (40 to 70 mm) of the focus to maximize dimensions of the lesion.

Results

An ablation volume of 51 cm^3 can be achieved in in vitro liver by electronic focusing with 180 ultrasound exposures of one second without delay between exposures. The ablation is 44 mm large with a depth of 51 mm. It was found that about 1000 single lesions and 170 minutes of treatment are needed to obtain an equivalent volume with a spherical transducer of equivalent characteristics.

Discussion and Conclusions

These results show that if correctly positioned it would be possible to ablate a tumor of 3 cm in diameter with safety margins in 3 minutes of ultrasound treatment. Therefore, this method eliminates the need of juxtaposing single lesions. The rapid creation of one large lesion reduces the risk of inhomogeneous treatment or the lack of safety margins. In conclusion, this approach may have a role in treating unresectable colorectal liver metastases and may represent a powerful technique for large tumors for which there is no therapeutic options.

P4Ad-2

A Unified Approach for Ultrasound-monitored Focused Ultrasound Thermal Therapy: Combination of Temperature Estimation and Nakagami-based Necrosis-Formation Detection

Sheng-Min Huang[1], Hao-Li Liu[2], Meng-Lin Li[1]; [1]Dept. of Electrical Engineering, National Tsing Hua University, Hsinchu, Taiwan, [2]Dept. of Electrical Engineering, Chang-Gung University, Taiwan

Background, Motivation and Objective

It has been well recognized that echo-time shift of the ultrasound radio-frequency (RF) signals can reflect temperature change during focused ultrasound (FUS) thermal ablation, and thus has potential for treatment monitoring and guidance. Nevertheless, temperature estimates based on this approach become uncertain when temperature rises to tissue necrotic level (> 50 °C). Therefore, demand for a monitoring approach, which is valid throughout the whole heating process from temperature rise to tissue necrosis formation, has been raised.

Statement of Contribution/Methods

To address this, we propose a unified approach that exploits the merits of ultrasonic temperature estimation and Nakagami imaging to provide a total solution for monitoring of FUS thermal therapy. Our previous studies demonstrate the potential of Nakagami visualization of FUS-induced thermal lesions. Here ultrasonic temperature estimation is used to locate treatment region before tissue coagulation occurs while Nakagami imaging is applied to track the thermal lesion formation.

Results

Ex vivo experiments on porcine livers were perfomed . A 1.5-MHz FUS transducer was used to perform the thermal ablation and a clinical ultrasound scanner was employed to collect RF data during FUS thermal ablation. The experimental result showed that, in the beginning of heating process, temperature estimation was sensitive to small-temperature change, thus suitable for the identification of the hot spot generation while Nakagami imaging failed to reflect small-temperature change. (first column of the figure). On the contrary, when the temperature elevation reached the tissue-necrosis level, temperature estimation became invalid. Nakagami imaging, however, provided capability to identity the region of tissue necrosis (second column of the figure). Nakagami-image predicted thermal necrosis size was highly correlated to that measured from the tissue section (third column).

Discussion and Conclusions

In this study, we experimentally demonstrated that ultrasonic temperature estimation and tissue necrosis detection by Nakagami imaging can serve as complementary roles; thus their integration can provide a total solution that fulfills the monitoring of the overall heating process. This work may help to improve the current clinical practice, which uses ultrasound to guide the FUS thermal ablation procedure.

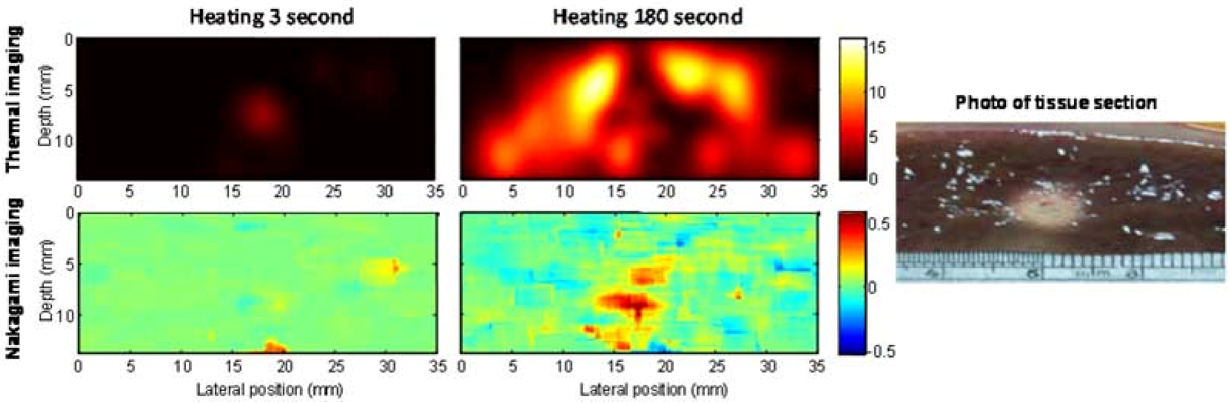

P4Ad-3

MR-Guided High Intensity Focused Ultrasound (HIFU) with Spatial and Temporal Temperature Control for Hyperthermia

Yu Liu[1], Brett Fite[2], Dustin Kruse[1], Lisa Even[1], Erik Dumont[3], Charles Caskey[1], Kathernine Ferrara[1]; [1]Biomedical Engineering, University of California at Davis, Davis, CA, USA, [2]Biophysics Graduate Group, University of California at Davis, Davis, CA, USA, [3]Image Guided Therapy, France

Background, Motivation and Objective

MR-guided High Intensity Focused Ultrasound (HIFU) is a promising non-invasive method for hyperthermia and local drug delivery. Here, we developed a system capable of delivering a controlled 3D acoustic dose during real-time MR thermometry. Our goal was to achieve spatial resolution of ~1 mm with temporal resolution of ~1°C.

Statement of Contribution/Methods

A 3MHz 16-element annular array transducer (F/D=0.8, F=35mm, -6 dB ultrasound focal dimension: ~1×1×2mm^3) (Imasonics), controlled in the lateral dimension with 2D motors (Image Guided Therapy), was integrated with a 7T MR scanner (Bruker Biospin). MR thermometry was validated using a fiber optic thermometer (Luxtron) in a tofu phantom and ultrasonic heating of the tofu phantom was simulated with COMSOL and MATLAB. PID feedback control enabled controlled heating using MR images in Thermoguide (Image Guided Therapy) in real-time. FLASH sequences with TR/TE/FA of 21ms/5ms/10° achieved MRI resolution of 1×1×1mm^3 and a 1 Hz frame rate. The PID feedback control was tested in a Met-1 mouse tumor in real time based on a predefined trajectory and control points.

Results

MR thermometry estimates agreed with fiber optic temperature measurements within 1°C, and simulations of heating in a tofu phantom were in agreement with the MR temperature measurement (Fig. 1a). During PID-controlled heating of an *in vivo* Met-1 tumor, the spatiotemporal mean of the treated region was maintained at 39.1±0.8°C and 40.8±0.8°C for 100.5 seconds, for 2-degree and 4-degree increases, respectively (Fig. 1b). Insonation with multiple control points distributed within a 3 mm circle in a single depth plane produced mild hyperthermia over a volume of 45 mm^3.

Discussion and Conclusions

MR thermometry with real-time feedback was validated by fiber optic measurement. In a Met-1 tumor, real-time PID feedback control is capable of maintaining the desired temperature with high accuracy and will be used to activate temperature-sensitive drugs in a controlled manner.

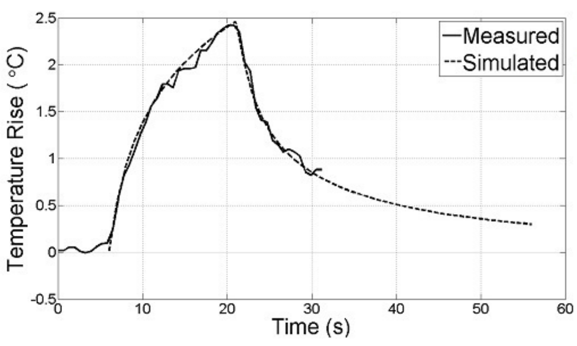

Fig. 1a

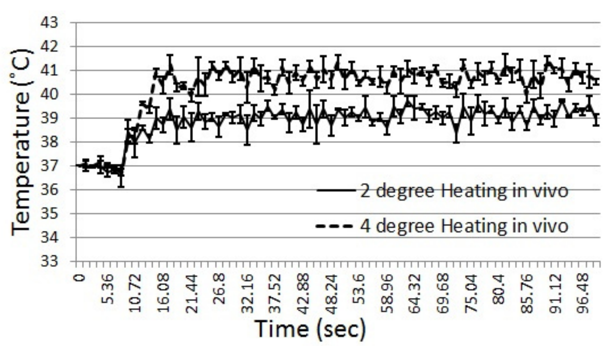

Fig. 1b

P4Ad-4

MR-guided transcranial HIFU treatments in nine human cadaver heads: accuracy of 3D spatial targeting and local temperature elevations based on skull attenuation measurements

Laurent Marsac[1,2], Dorian Chauvet[3], Mathieu Pernot[1], Mathias Fink[1], Jean Francois Aubry[1], Anne Laure Boch[3], Mickael Tanter[1]; [1]Institut Langevin, Paris, France, [2]SuperSonic Imagine, Aix en provence, France, [3]Département de Neurochirurgie, Hôpital Pitié Salpêtrière, Paris, France

Background, Motivation and Objective

Focusing beams trough the human skull is challenging because of its strong attenuation and phase aberrations, especially at the high frequency used here (1 MHz). For intensity maximization at focus the optimal aberration correction is the phase conjugation based on transmission measurement. Previous studies demonstrated non invasive phase

THURSDAY POSTER

conjugation based on high frequency transcranial acoustic simulation. Such 3D finite differences time domain acoustic simulation relies on skull parameters obtained by CT scan. This work is extended here on intact *ex-vivo* human heads and applied to hyperthermia of the thalamic nucleus ventrointermedius located at the center of the brain. The aims of the present study were indeed to estimate the accuracy of the whole procedure, evaluate the simulation-based focusing performance and attenuation of the cranium.

Statement of Contribution/Methods

Nine cadaver heads (consent donors, over 70 years old) were extracted 24 to 72 hours after death. Targeting was done using MR images, a CT scan was done, registered with the MR scan and used to perform the simulation based correction. The HIFU beam was experimentally generated using a MR compatible 512 elements US phased array (1 MHz) dedicated to transcranial human experiments (SuperSonic Imagine). Using a clinical Philips 1.5T MR scanner, a MR temperature sequence (3D, GE, EPI, resolution 1.5x1.5x3 mm^3, 2.5 s) was implemented to measure temperature elevations. Sonications with and without aberration correction were done during 10 s with the same acoustic power and the maximum temperature elevation was recorded. After the treatment the cranium were extracted, cleaned and degassed in water tank for hydrophone measurements of pressure attenuation at focus.

Results

For an emitted acoustic power of 1200 W, temperature elevations of 6 °C to 10 °C were estimated at the targeted location thanks to the sensitive MR temperature sequence. Treatment accuracy in the three directions was 0.4 +/- 1 mm, 0.7 +/- 1.2 mm and 0.5 +/- 2.4 mm. Phase conjugation permitted an increase of the heating by 43 % +/- 9.7 % compared to uncorrected beams. Attenuations measured on extracted craniums were found to be 73 % (-11.4 dB) +/- 7 %. Maximum temperature elevations reached experimentally in the heads were coherent with corresponding skull attenuations (from -16 dB to -8 dB) and simulations based on the 3D discretized bioheat equation (mean error: 16 %).

Discussion and Conclusions

Low temperature elevations presented in nine heads show a precision of the order of the MR temperature voxel. Such sonications are well suited for heating localization and assessment of cranium attenuation prior to tissue necrosis. In order to increase the accuracy, fine electronic steering and future higher resolution MR sequences could be used. Simulation-based correction increased the focalization indeed the temperature elevation was variable because of the cranium attenuation.

P4Ad-5

Dual Frequency Imaging and Therapeutic Transducer Using an Acoustic Band-pass Filter for Application to Endoscopic Surgery

Takashi Azuma[1,2], Hajime Kenmotsu[3], Makoto Hashizume[3], Shu Takagi[1], Yoichiro Matsumoto[1]; [1]Faculty of Engineering, The University of Tokyo, Japan, [2]Hitachi Central Research Laboratory, Japan, [3]Faculty of Medicine, Kyushu University, Japan

Background, Motivation and Objective

A novel endoscopic high intensity focused ultrasound (HIFU) transducer capable of being adapted to an ultrasound (US) imaging guide is described. While endoscopic surgery treats only the inside of the digestive tract, the endoscopic HIFU has the potential to treat outside parts such as the lymph nodes through the tract wall. To minimize the total size of the aperture used for endoscopic application, a bi-laminar structure was adopted. In our previous study, a bi-laminar transducer for sonothrombolysis that involved 2-MHz imaging and 0.5-MHz therapeutic transducers and a polymer layer working as an acoustic band-pass filter (ABPF) between both transducers was developed. Because the layer passes through the 0.5-MHz therapeutic beam and reflects the 2-MHz imaging beam, the imaging array was isolated from the therapeutic transducer.

Statement of Contribution/Methods

In this study, 10-MHz imaging and 3-MHz HIFU frequencies were used. The following three parameters were optimized using a simulation program called PZFlex to realize therapeutic and imaging performance: (1) the covering ratio of the imaging aperture to the HIFU aperture, (2) the thickness of ABPF, (3) the acoustic impedance of ABPF. Based on an optimized design, a prototype transducer was fabricated and tested.

Results

The spherical radius and total aperture width of the HIFU transducer were 40 mm and 15 mm, respectively. The transducer was divided into three parts, arranged, and a 48-ch imaging array was overlaid onto the middle part as shown in Fig.1. The fractional bandwidth at -20 dB of imaging pulses was 100%. The transmittance of the HIFU beam through the imaging array was 0.6.

Discussion and Conclusions

The measured bandwidth of the imaging pulse is sufficient to obtain a high resolution US image. The HIFU beam profile of the prototype was estimated on the basis of the HIFU beam transmittance. The peak intensity of HIFU beam transmitted from the prototype structure was 60% higher than that of the conventional HIFU transducer with a hole to mount the imaging array, whose outer diameter of aperture is the same as that of the prototype structure.

We proposed a novel transducer structure for achieving endoscopic HIFU transducer with US imaging guide. The performance of the prototype demonstrated the practical usefulness of the proposed concept. The actual heating in the transducer will be tested.

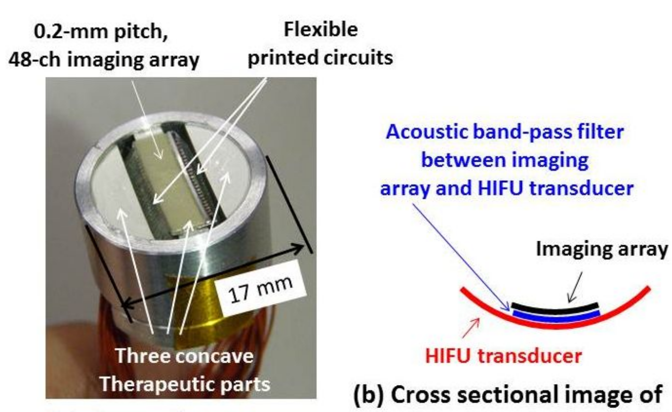

(a) Photo of prototype (b) Cross sectional image of middle part of transducer

THURSDAY POSTER

P4Ad-6

Real-time Monitoring of Thermal and Mechanical Tissue Response to Modulated Phased-array HIFU Beams in Vivo

Dalong Liu[1], John Ballard[2], Alyona Haritonova[3], Jeunghwan Choi[4], John Bischof[4], Emad Ebbini[2]; [1]Electrical and Computer Engineering, University of Minnesota, Minneapolis, MN, USA, [2]Electrical and Computer Engineering, University of Minnesota, USA, [3]Biomedical Engineering, University of Minnesota, USA, [4]Mechanical Engineering, University of Minnesota, USA

Background, Motivation and Objective

Ultrasound thermography based on speckle tracking methods offer the most promise of real-time implementation for minimally-invasive thermotherapy. However, the approach is limited by tissue deformations (e.g. due to breathing and cardiac cycles) that lead to echo and spectral shifts, which can easily mask the temperature-induced echo strains. Our innovative solutions employed a combination of new approaches to data acquisition (M2D mode) and reconstructive temperature estimation to conquer these limitations.

Statement of Contribution/Methods

We have developed an integrated system for real-time ultrasound thermography and strain imaging in monitoring tissue response to phased-array heating patterns. The imaging system is implemented SonixRP scanner (Ultrasonix, Canada) at frame rate up to 500 fps with limited frame sizes covering the vicinity of the HIFU focal spot (M2D mode). With the high temporal and spatial resolution of our strain imaging system, we are able to capture and separate tissue strains due to natural motion (breathing and pulsation) from HIFU induced strains (thermal and mechanical). The post processing that utilizes t-BHTE-based filter and POCS algorithm is effective in removing the motion artifacts while preserving the HIFU induced temperature field. It is also computationally efficient for real-time implementation.

Results

In vivo data was captured using a frame rate of 135 FPS (47 Alines wide). The relatively high frame rate enabled us to capture tissue mechanical/thermal response along with natural tissue motion. Processed result （Figure 1) clearly demonstrated the effectiveness of POCS method with the physics-based regularization filter in removing the tissue motion artifacts. In the meanwhile, the temperature response is preserved with minimal degree of distortion. The result showed that the proposed method has a superior performance compared to regular smoothing filter.

Discussion and Conclusions

We have presented the full *in vivo* demonstration of our realtime thermography system. Results from the in vivo rat experiments show the high frame rate M2D imaging is the key to capture tissue response due to sub-therapeutic application of HIFU beam. We also demonstrated the uses of tBHTE-based filter and POCS algorithm is effective in removing the motion artifacts.

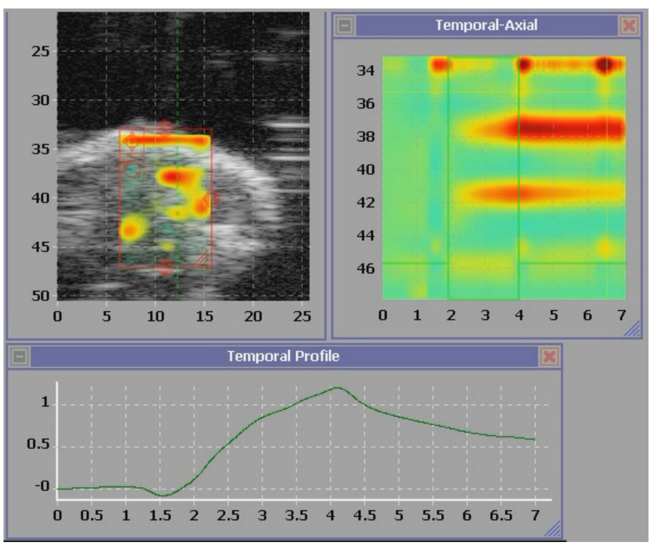

THURSDAY POSTER

P4Ad-7

Multi-parametric analysis of monitoring High Intensity Focused Ultrasound (HIFU) treatment using Harmonic Motion Imaging for Focused Ultrasound (HMIFU)

Gary Y. Hou[1], Fabrice Marquet[1], Jianwen Luo[1], Elisa E. Konofagou[1]; [1]*Biomedical Engineering, Columbia University, USA*

Background, Motivation and Objective

HMIFU is a recently developed high-intensity focused ultrasound (HIFU) treatment monitoring method with feasibilities demonstrated *in vitro* and *in vivo* (Maleke et al., PMB 2008, TBME 2010). Its principle is based on Harmonic Motion Imaging (HMI), a technique for imaging tissue mechanical properties at the same site and during oscillatory acoustic radiation force application. Here, a multi-parametric study is performed to investigate the parameters of strain, phaseshift, and displacement for HIFU treatment monitoring and assessment based on viscoelasticity tissue changes.

Statement of Contribution/Methods

Ex vivo fresh canine liver lobes (n = 3) were excised immediately after animal sacrifice . A focused transducer (f_{center} = 4.7 MHz, Riverside Research Institute, NY) modulated at AM frequency of 25 Hz was used in conjunction with a confocal pulse-echo transducer (f_{center} = *7.5 MHz*, Panametrics, MA) for simultaneous acquisition of RF signals during excitation (PRF = 4 kHz). The extrapolated in situ acoustic intensities were 363 W/cm^2 and 1452 W/cm^2 for imaging and ablation, respectively. The RF signals were filtered through an analog band-pass filter (f_{c1} = 5.84 MHz, f_{c2} = 8.66 MHz) at -60 dB (Reactel Inc., MD) and acquired at 80 MHz. A 1-D normalized cross-correlation (window size of 1 mm, 85% overlap) was used to estimate the HMI displacement and a least-squares estimator was used to estimate the strain. Transverse displacement maps were obtained through raster scans before and after lesion formation. The same method was repeated in 10-, 20- and 30-s HIFU treatments.

Results

Ten thermal lesions were formed and detected. At the baseline, the estimated focal displacement and peak compressive strain were equal to 13.9±4.01μm and -0.62±0.03%, respectively. For the 30-s treatment, the temporal displacement slope changed sign from positive (5.34±3.31 μm) to negative (-14.41±9.09 μm) at approximately 10 sec, indicating tissue softening during initial heating then hardening upon lesion formation, which is consistent with findings in previous studies (Maleke et al., PMB 2008).The estimated displacement change between the baseline and post-ablation was 5.60±3.31 µm for the shorter treatments. Transverse lesion maps corresponded with the size of thermal lesions in pathology.

Discussion and Conclusions

A multi-parametric analysis on HIFU treatment monitoring using HMIFU was hereby presented in ex vivo liver. First, local tissue changes in mechanical properties were detected using both displacement and strain . Secondl, changes of slope in displacement profile were observed, indicating the capability of HMIFU to detect the onset of lesion formation using different motion parameters. Monitoring with the use of the force-strain phase shift and characterization of cavitation effects will also be shown. (Supported in part by NIH R21EB008512)

P4Ad-8

Design of a Focused Ultrasound Array for the Treatment of Stroke: A Simulation Study

Daniel Pajek[1,2], Kullervo Hynynen[1,2]; [1]Sunnybrook Research Institute, Toronto, ON, Canada, [2]Medical Biophysics, University of Toronto, Toronto, ON, Canada

Background, Motivation and Objective

Approved stroke treatments have low recanalization rates [1] and improvements are needed. HIFU is capable of lysing clots via cavitation, but current transcranial arrays, at < 1 MHz, can cause standing waves and hemorrhaging [2]. This study investigates using higher frequency arrays to treat stroke non-invasively through the intact skull.

Statement of Contribution/Methods

Transcranial FUS simulations were conducted with segmented cadaver skulls, using methods presented in [3]. Acoustic coefficients were calculated from CT-derived densities [4] averaged over each beam path. The M1 and basilar (BA) arteries were segmented from CT data [5]. Simulations targeted the array's natural focus and 7 vessel locations. Hemispherical arrays with 1.3, 2.1, and 3.9 mm diameter cylindrical elements (total number of elements ~ 75k, 28k, and 9k, respectively) driven at 37.5 W/cm2 were simulated at 1.5, 1.3, and 1.1 MHz. Simulations were repeated with element amplitudes adjusted to reduce skull surface pressures. From [6], cavitation thresholds of 11-12 MPa were estimated. Focal pressure, gain (skull surface to focus), and -3dB falloffs were calculated.

Results

The 1.5 MHz, 75k array produced gains of 3.3, 3.3, and 2.6, and focal pressures of 12, 13, and 12 MPa at the BA, left, and right proximal M1 locations (see figure). The 28k array produced gains 21±11% lower and focal pressures 21±5% lower, and the 9k array produced gains 47±8% lower and focal pressures 47±11% lower. Amplitude adjustment produced gains 29±12% higher at 1.5 MHz. Simulating at 1.3 MHz produced a 6.3±11% increase in gain and 4.8±2.4% focal pressure increase, and at 1.1 MHz produced a 38±2.5% increase in gain and 23±3.0% focal pressure increase for the 75k array. The largest DOF was 1.4, 1.7, and 2.0 mm at 1.5, 1.3, and 1.1 MHz. Lateral focal widths were all < 1 mm.

Discussion and Conclusions

For the 75k array focal pressures approached the cavitation threshold at 1.5 MHz and exceeded it at lower frequencies, while keeping skull surface pressures below the inertial cavitation threshold. The intensity levels used are achievable with the current technology.

[1] Saqqur et al. Stroke 2007, 38:948-954.
[2] Azuma et al. IEEE Ultrasonics Symposium 2004, 1001-1004.
[3] Sun & Hynynen. JASA 1998, 104:1705-1715.
[4] Picardo et al. Phys. Med. Biol. 2011 56:219-250.
[5] Visible Human Project. NLM, Bethesda, MD.
[6] Vykhodtseva et al. UMB 1995, 21:969-979.

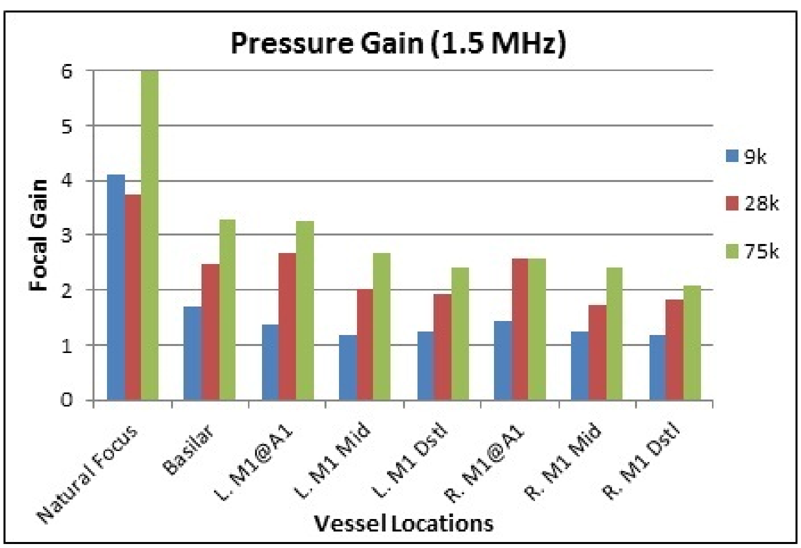

P4Ad-9

Temperature measurement using backscattered ultrasonic power for non-invasive thermometry during HIFU ablation

David Melodelima[1], Jeremy Chenot[1], Jean-Yves Chapelon[1]; [1]*U1032, INSERM, Lyon, France*

Background, Motivation and Objective

The temperature dependence of ultrasonic tissue parameters has been reported extensively. Measurement of velocity changes as a function of temperature was the most investigated parameter. More recently, attenuation changes was also described as a possible ultrasonic parameters that can be taken to infer the temperature distribution during hyperthermia procedures. This paper describes the relationship between changes in ultrasound backscattered power and temperature during HIFU treatments. An analytical model was developed based on attenuation, velocity and thermal expansion to predict temperature changes. In vitro tests were conducted using a HIFU probe guided by ultrasound imaging to confirm that temperature in tissues can be inferred from backscattered power.

Statement of Contribution/Methods

The distribution of speed of sound, attenuation and thermal expansion were first measured in vitro using liver samples. The combined effects of variations in these ultrasound parameters as a function of temperature allows to simulate the effect of tissue heating on backscattered power. HIFU treatments were performed using a focused transducer working at 3 MHz. The radius of curvature and the diameter were both 70 mm. An ultrasound imaging probe working at 7.5 MHz was placed in a circular hole in the centre of the transducer. Long exposure time (120 seconds) were used to observe smooth temperature increase from 30 to 80°C. A duty factor of 90% was used (1s HIFU, 0.1s for ultrasound scanner acquisition). In a first series of tests, a thermocouple was placed at the focal point. A second series of test was performed without the thermocouple to infer the temperature from radiofrequency signals. The thermal dose was deduced from temperature measurements and comparisons were performed with gross pathology.

Results

Simulations predicted that backscattered power increased nearly logarithmically with temperature over the range from 30°C to 80°C. The model predicted a change of +15 dB. An average increase of +12 dB was noted in ultrasound backscattered power during in vitro experiments. The tissue temperature increase correlated well (r=0.79) with thermocouple measurements. A linear relationship between changes in the radiofrequency signal and temperature was observed up to 80°C. 2D temperature measurements correlate with the dimensions of ablations.

Discussion and Conclusions

Changes in backscattered energy have been monotonic in simulations and in vitro in the range of HIFU applications. This behavior enables temperature estimation from ultrasound images. Successful temperature estimation serve as the foundation for the generation of 2D temperature maps in soft tissue as a noninvasive, convenient, and low-cost way to regulate temperature during HIFU treatments.

P4Ad-10

Multiple-frequency Phased Array Pattern Synthesis for HIFU Surgery

John Ballard[1], Dalong Liu[1], Andrew Casper[2], Alyona Haritonova[2], Mohamed Almekkawy[1], Emad Ebbini[1]; [1]Department of Electrical Engineering, University of Minnesota, USA, [2]Department of Biomedical Engineering, University of Minnesota, USA

Background, Motivation and Objective

Modern piezocomposite technology allows for the design and manufacturing of therapeutic arrays with low cross coupling between elements and relatively large bandwidths (>50%). Previously, the increased bandwidth has been taken advantage of for imaging with dual mode ultrasound arrays but therapy has been routinely done at a single frequency. Work by several groups has shown that utilizing multiple frequency excitation from multiple transducers can have enhanced therapeutic effects at the focal point. We present a simulation/experimental study to evaluate and optimize the focusing capabilities of a phased array prototype when excited by multiple-frequency components.

Statement of Contribution/Methods

A multiple-focus multiple-frequency pattern synthesis algorithm for phased arrays has been developed and tested using linear simulations in Matlab. The algorithm maintains the precise phase relationship between the frequency components at each focal spot to achieve a desirable therapeutic outcome. Preliminary simulations indicate that the focal region can be shaped based on the alignment and phase of multiple-frequency components. The pattern synthesis algorithm is experimentally validated with a 3.5 MHz, 64-element prototype designed for small-animal and superficial therapeutic HIFU applications (Imasonic, Inc) which has a 52% fractional bandwidth, allowing for therapeutic output in the frequency range of 2.7-4.6 MHz.

Results

Validation with hydrophone (Precision Acoustics) measurements at the focal locations indicated that there is in increase in harmonic generation at the focal point with the frequency mixed patterns when compared to a conventional single frequency excitation pattern. This increased non-linearity, will allow for increased thermal absorption at the focal point, thus allowing for larger treatment volumes with the same total power or reduced treatment time per shot when compared to the single frequency case. *Ex vivo* experiments with fresh porcine liver were conducted to study the effect of multiple-frequency patterns when compared with conventional single frequency patterns during lesion formation. The lesion size was increased for the multiple-frequency patterns when compared the single frequency pattern at normalized power with respect to each other.

Discussion and Conclusions

Wideband piezocomposite array transducers, together with multi-channel arbitrary waveform generators are enabling technologies which allow for complex, multiple-focus, multiple-frequency HIFU patterns. These patterns can enhanced the focal gain with proper phase alignment. Furthermore, multiple frequency patterns have been shown to be able to increase the harmonic generation at the focal spot, thus improving local absorption. Our early results with *ex vivo* porcine liver indicate that multiple frequency excitation enhances the therapeutic effects at the focal location.

P4B Tranducers for NDE Applications

Carribean Ballroom III-V

Thursday, October 20, 2011, 1:00 pm - 4:30 pm

Chair: **Eric Furgason**
Purdue University, USA

P4B-1

Characterization of two-dimensional hydrophone arrays for instantaneous beamwidth measurements of shockwave lithotripters

Dan Gross[1], Erwan Filoux[1], Jeffrey A. Ketterling[1]; [1]Lizzi Center for Biomedical Engineering, Riverside Research, New York, NY, USA

Background, Motivation and Objective

Characterization of electrohydraulic lithotripters (EHLs) is usually limited to single-point measurements because hydrophone arrays are not readily available and custom hydrophones are too expensive to destroy in a high-pressure acoustic field. Single-point measurements are inaccurate because EHL acoustic fields have high variability and shocks must be averaged to create a beam profile. We previously demonstrated that instantaneous EHL beamwidth measurements with a 1D hydrophone array were 25% lower than averaged, single-point measurements. Here we improve upon our design by fabricating and calibrating hydrophone arrays with a 2D element geometry.

Statement of Contribution/Methods

The hydrophones consisted of twenty 0.5 mm square elements arranged in an 11-by-10-element, plus patterned array, with 2 mm center-to-center spacing. This array pattern was etched onto copper-clad polyimide films that were bonded to a 9 µm thick piezopolymer film. A multi-frequency substitution method was used to calibrate the individual hydrophone elements against a reference fiber-optic hydrophone (FOH). The measurements were performed using a shock tube driven by a 1 MHz, 50 mm diameter, planar PZT transducer. The acoustic field in the shock tube was first characterized with the FOH. Then, the central array element was placed at the peak positive pressure (PPP) location, 1 m from the source, and the sensitivity of all elements were measured simultaneously.

Results

Figure 1 shows the sensitivity curves from 3 hydrophone arrays averaged over 100 shocks. For each array, element sensitivities varied by 30%. Between arrays, mean sensitivities varied by 15%.

Discussion and Conclusions

This study demonstrated that our 2D hydrophone arrays are effective in measuring the instantaneous acoustic field of shock wave sources. The fabrication process provided hydrophones with repeatable characteristics, but it could be improved to reduce the element-to-element variation. Future work will focus on decreasing this variability and then measuring the 2D instantaneous beamwidths of EHLs. Compared to our previous design, the 2D configuration allows for a more accurate localization of the maximum pressure, which is of critical importance in lithotripsy.

THURSDAY POSTER

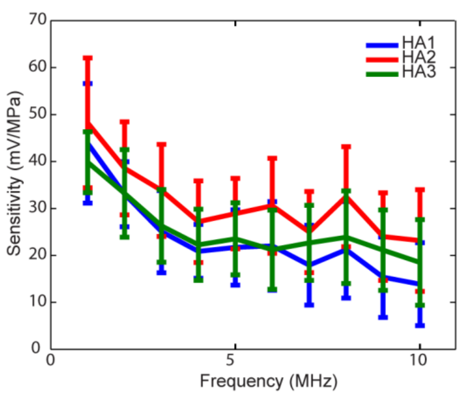

Fig 1: Sensitivity of 3 different hydrophone arrays (HA) measured using multi-position, multi-frequency instantaneous substitution calibration. The error bars reperesent a standard deviation of sensitivity for each element of a single array.

P4B-2

Single-transducer ultrasonic continuous-wave system for transmitting coded sequences

Frank Melandso[1], Svein Jacobsen[1]; [1]Dept of Physics and Technology, The University of Tromso, Tromso, Norway

Background, Motivation and Objective

A major challenge in CW ultrasonic imaging systems is the electrical crosstalk induced during transmission. Standard approaches for reducing this cross talk involve proper shielding of the electronics and setups where the electrodes and/or transducers for transmitting and receiving are separated. Electrical cross talk may also impose problems for pulsed wave (PW) systems, e.g. in near field imaging where the recovery time of the electronics after pulse firing is critical. For single transducer systems these recovery problems can to some extent be solved by increasing the bandwidth or by using an acoustic delay line. It should, however, be noticed that acoustic delay lines often impose unwanted attenuation and dispersion in wide band systems. An electronic setup to improve near field scanning for PW was recently suggested by the authors [1, F. Melandso and S. Jacobsen, Electron. Lett. 47, 5, 2011].

Statement of Contribution/Methods

To reduce the electrical cross talk during ultrasonic transmission, a digital cancellation network shown in Fig. 1 is proposed. In this dual network a reference channel Ch_r, driving a standard capacitance with impedance Z_r, is used to cancel out the capacitive induced current from transducer with impedance Z_x (driven by channel Ch_x). The experimental investigations on PW done in [1] are extended to CW coded sequences that have been transmitted and simultaneously received using only a single PVDF transducer.

Results

Several digital filter methods for current cancellation have been investigated in an experimental test bed for standardized Barker and Golay codes. The most efficient of these are capable of reducing the capacitive induced current with as much as 50 dB, and at the same time provide good preservation of the acoustic information. The need for dynamical resolution of the digitizer unit has also been tested using both an oscilloscope and a high resolution (14-bit) digitizer.

Discussion and Conclusions

We have shown that the proposed network can reduce the electrical crosstalk significantly, and yields a capacitive induced current of the same magnitude as the current produced by relatively weak acoustic backscatters. This equalization will strongly reduce the need for an AD converter with high dynamical range and opens up for new CW applications involving only a single transducer.

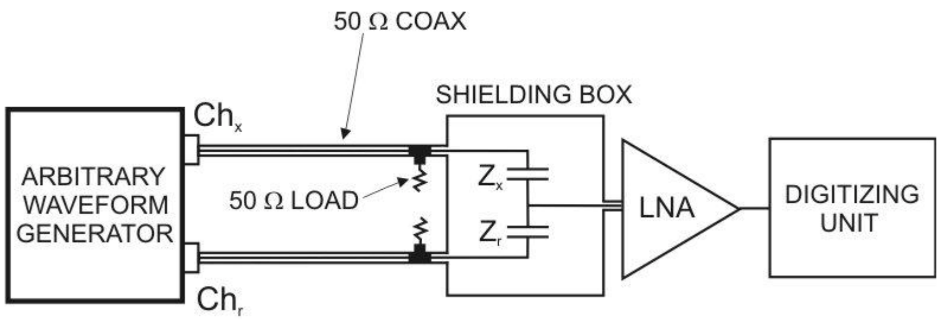

Fig. 1: Ultrasonic cancellation network

P4B-3

An ultrasonic probe and technique for measuring longitudinal and shear properties of viscous liquids

Zhen Qu[1], **Yuu Ono[1]**; [1]Carleton University, Canada

Background, Motivation and Objective

Ultrasonic testing methods of liquids have been widely studied and employed in material science and engineering research. In order to obtain material parameters of a viscous liquid, measurements of its longitudinal (LW) and shear wave (SW) properties are often required. Since a viscoelastic material may be inhomogeneous and its viscoelastic properties are often temperature dependent, accurate and efficient ultrasonic measurements could be conducted if these properties are measured using the same ultrasonic probe. Thus, the objectives of this study are: to develop an ultrasonic probe capable of transmitting and receiving the LW and SW simultaneously; and to demonstrate a technique for characterizing viscous liquids using the probe developed.

Statement of Contribution/Methods

A mode conversion technique was employed in order to generate and receive the SW using a LW ultrasonic transducer (UT). A LW film UT was glued onto a probe substrate having two slanted surfaces, one for transmitting/receiving the LW and the other for the SW. In the probe design, two factors were theoretically investigated: impedance matching between the probe substrate and viscous liquid; and mode conversion efficiency from the LW to SW.

Results

Poly(methyl methacrylate) (PMMA) was chosen as a substrate material because of its good impedance matching with viscous liquids. The angle of the slanted surface of the substrate for the LW was 45° and that for the SW was 63.2° determined from the result of the numerical calculation using the mode conversion theory. The developed probe had a peak frequency and 6-dB bandwidth of 2.3 MHz and 3.0 MHz (130%), respectively, for the LW signal reflected from the probing end and those of 1.5 MHz and 1.8 MHz (120%), respectively, for the SW signal. The peak frequency of the SW was 0.8 MHz lower than that of the LW due to the higher attenuation of the SW than the LW in the PMMA substrate.

Discussion and Conclusions

The probe developed was tested with a silicone fluid (nominal viscosity: 100 mPa·s) at room temperature. The sample was inserted between the probing end and a reflector with the know sample thickness. The time delay of the LW signal that propagated in the sample and reflected from the reflector was measured to determine the LW velocity. In addition, the LW reflection coefficient at the probe/sample interface was measured to obtain the LW impedance using the known impedance of the PMMA substrate. The density was calculated from the LW velocity and impedance measured. The LW velocity and density obtained were 1028 m/s and 996 kg/m^3, respectively, which agreed with the literature values within 5%. Furthermore, the SW complex reflection coefficient was measured to determine the viscosity by the shear reflectance method. The viscosity obtained was 41 mPa·s. In the future study, a temperature controller will be implemented to control and stabilize the temperature environment around the probe and sample, in order to improve the measurement accuracy.

P4B-4

Parameter reproducibility of polypropylene ferroelectret transducers for air-coupled ultrasonic testing

Mate Gaal[1], Joachim Doring[1], Juergen Bartusch[1], Viktor Bovtun[2], Gerhard Brekow[1], Marc Kreutzbruck[1]; [1]BAM Federal Institute for Material Research and Testing, Berlin, Germany, [2]Department of Dielectrics, Institute of Physics ASCR, Prague, Czech Republic

Background, Motivation and Objective

The extremely low acoustic impedance of polypropylene ferroelectret combined with its piezoelectric properties makes this material suitable for construction of air-coupled ultrasonic transducers for non-destructive testing. For the fabrication of transducers with a stable quality, the reproducibility of their key parameters is of interest.

THURSDAY POSTER

Statement of Contribution/Methods

The reproducibility was evaluated by means of dielectric spectroscopy and pulse-echo measurements. Dielectric spectroscopy was applied to identify the resonance frequency, the coupling factor and the acoustic impedance of several nominally identical transducers. Pulse-echo measurements yielded the signal form and the spectrum of these transducers.

Results

The variation of the signal amplitude measured with pulse-echo technique was about 10 dB. A part of this variability is caused by the influence of electrode sputtering and the other part by large-scale variations of ferroelectret properties. This corresponds to the observed variation of the coupling factor, whereas the variation of the acoustic impedance was only about 1 dB.

Discussion and Conclusions

These results indicate that the variability can be reduced by improving the control of electrode sputtering and by optimizing the production technology affecting the reproducibility of material properties.

P4B-5

Homogeneity Evaluation of a Synthetic Silica Glass Ingot by the Ultrasonic Microspectroscopy Technology

Jun-ichi Kushibiki[1], **Mototaka Arakawa[1]**, Yuji Ohashi[1], Yuko Maruyama[1], Hideharu Horikoshi[2], Kenji Moriyama[2]; [1]*Electrical Engineering, Tohoku University, Sendai, Japan,* [2]*Tosoh SGM Corporation, Shunan, Japan*

Background, Motivation and Objective

Synthetic silica (SiO_2) glass is widely used for optical components. Further improvement of homogeneity in refractive index is required. The refractive index of SiO_2 glass depends not only on concentrations of dopants and impurities, but also on the fictive temperature (T_F). We developed a method of evaluating T_F of SiO_2 glasses using the ultrasonic microspectroscopy technology. We applied our method to homogeneity evaluation of a SiO_2 glass ingot.

Statement of Contribution/Methods

A Specimen was prepared in the radial direction from a commercial SiO_2 glass ingot (ES; Tosoh SGM), produced by the direct method, with dimensions of 600 mm (φ) x 600 mm (l) at around positions of 200 mm from the top. Several specimens were also prepared around the central parts for heat-treatment at desired annealing temperatures from 870 to 1150°C, to obtain relationships between acoustic properties and T_F. OH concentrations were 1400 wtppm around the central positions and 1265 wtppm around the edge positions. Distributions of velocities of leaky surface acoustic waves (LSAWs) and longitudinal waves were measured by the line-focus-beam/plane-wave ultrasonic material characterization system. Optical retardations were measured by optical heterodyne interferometry.

Results

Sensitivity and resolution of longitudinal velocity (V_l) to T_F were 7.87°C/(m/s) and 0.4°C, and those of LSAW velocity (V_{LSAW}) were 124°C/(m/s) and 21°C. Measurement results are shown in Fig. 1 as a function of distance from the center. Maximum differences of V_{LSAW} and V_l are 2.31 m/s and 3.10 m/s. T_F distributions can be estimated to be 24.4°C from V_l. Residual stresses were detected around the ingot edge from optical results. V_{LSAW} decreased in the same region, so V_{LSAW} could be influenced by the residual stresses.

Discussion and Conclusions

We demonstrated that T_F distributions of SiO_2 glass ingots can be obtained by V_l measurements and variations caused by the residual stresses could be evaluated by V_{LSAW} measurements. This ultrasonic method is extremely useful for improvement of homogeneity of SiO_2 glass ingots.

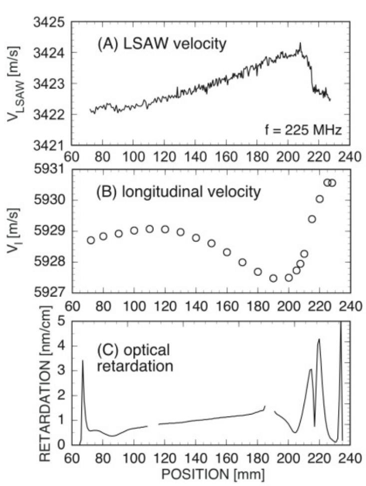

Fig. 1. Distributions of LSAW velocities, longitudinal velocities, and optical retardations measured for a synthetic silica glass specimen.

P4B-6

A track-pad device based on piezoelectric bimorph

Antonio Iula[1], Giosue Caliano[2], Nicola Lamberti[3]; [1]*D.I.F.A., University of Basilicata, Potenza, PZ, Italy,* [2]*University Roma Tre, Italy,* [3]*University of Salerno, Italy*

Background, Motivation and Objective

A trackpad is a pointing device featuring a tactile sensor, able to translate the motion and position of a user's fingers to a relative position on screen. It is a common feature of laptop computers, but it is also found on PDAs and smartphones.

THURSDAY POSTER

In this work a piezoelectric tactile sensor for trackpad applications is proposed, analyzed with Fe methods and experimentally evaluated.

The idea at the basis of the present work relies in the well known property of piezoelectric structures to vary its resonant behaviour depending on the boundary or load conditions

Statement of Contribution/Methods

The tactile sensor analyzed in this work is a commercial membrane composed of a thin piezoelectric disk (radius 11.5 mm, thickness 0.1 mm) glued on a nickel disk of the same thickness but higher radius (15.6 mm). The sensor is clamped all around. A commercial stylus touch pen is pressed on the surface of the membrane in several points and the influence of the pen position and force on a selected flexural resonance frequency of the membrane is investigated.

The pen is fixed on a two dimensional sledge system, one sledge being moved along the radial direction and the other along the z direction to vary the force applied to the pen. For each r-z position, the electric input impedance is measured by means of an impedance analyzer HP4194A. The variation of the frequency of the peak of the impedance (real and imaginary part, modulus etc.) is analyzed and correlated with the pen position variation.

A FE analysis is also performed to analyze the variation of the deformed shape with the pen position.

Results

Several measurements and simulations were carried out varying the position of the pen and the vibration mode selected for analyzing the fequency behavior. The plot shows the relation between the series resonance frequency of the first flexural mode and the radial position of the pen obtained by measuring the maximum of the real part of the electrical impedance; the resonance frequency of the unloaded membrane is 1645 Hz. As can be seen, there is a one-to-one correspondence between the pen position and the measured resonance frequency.

Discussion and Conclusions

The obtained results demonstrate that a device based on this principle could be promising as a tactile sensor in track-point devices in several application. The applicability of the method to two dimensional rectangular structures is described and discussed.

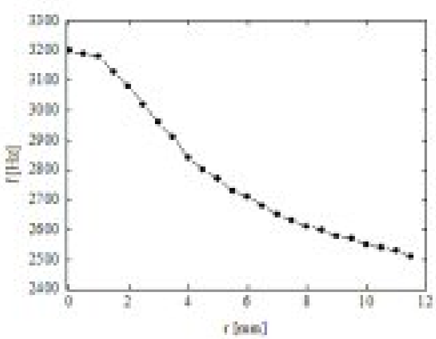

P4B-7

Study on Rotation Speed Control of Coiled Stator Ultrasonic Motor Using Pulse Width Modulation

Tomohiko Omura[1], Masayuki Tanabe[2], Kan Okubo[1], Norio Tagawa[1]; [1]Graduate School of System Design, Tokyo Metropolitan University, Tokyo, Japan, [2]Graduate School of Science and Technology, Kumamoto University, Kumamoto, Japan

Background, Motivation and Objective

We have been developing the Coiled Stator Ultrasonic Motor (CS-USM). In the CS-USM, ultrasound flexural waves are propagated through the helical coiled stator, and frictional force, which arises between the stator and the rotor placed adjacently inside or outside the stator, rotates the rotor. In the previous study, continuous flexural waves are used, and rotation speed is controlled with the amplitude of the flexural wave, i.e. the driving voltage. Since the CS-USM uses no pre-pressure between a stator and a rotor, there is a gap of constant size between them. Hence, it is difficult to rotate the rotor by low voltage, because the frictional force cannot work properly when the amplitude of the flexural waves is small. To avoid this problem, in this study, we apply the pulse width modulation (PWM) to the CS-USM.

Statement of Contribution/Methods

When the PWM is used for an electro-magnetic DC motor, driving energy is adjusted by varying the duty ratio. For the speed control of the CS-USM, phase difference of a carrier between successive ON sections can be used in addition to energy. We can alter the energy with no change of the phase relation by varying the duty ratio using a cycle of the carrier as a unit. On the other hand, it is difficult to alter the phase difference independently with the energy. In this study, we performed the experiments to examine the feasibility of the speed control by the phase adjustment. We adopted the way to change only the phase difference approximately. With keeping ON duration, i.e. the cycle number in an ON section n, fixed, we altered OFF duration d [s] by varying the phase D [deg] with respect to the carrier of frequency f [Hz] as $d = D/(360 f)$ ($0 \le D < 360$ [deg]). By varying D, the phase relation between the both ON sections before and after the OFF section is adjusted.

Results

Under the condition that Vp-p = 40 V, f = 490.6 kHz and n = 23, we measured rotation speed with varying D from 0 to 355 deg by 5 deg. The CS-USM used in the experiments is an outer-rotor type and the outside diameter of the rotor is 0.7 mm. To make a comparison, we used continuous sine wave voltage with 490.6 kHz as the driving source and altered the amplitude of it from 0 to 40 V by 1 V. The lowest speed of the stable rotation is 5 RPS by the PWM with phase adjustment, and 8 RPS by the voltage adjustment with the continuous wave driving.

Discussion and Conclusions

The reason that adjusting the phase difference between successive ON sections can control the rotation speed is because the flexural wave caused by the ON section remains transitionally during the OFF duration, and hence the synchronous phenomenon between this transitional wave and newly arising wave in the next ON section effectively works for speed control. Since decreasing the driving energy by making an OFF duration long may the rotation unstable, the phase adjustment is meaningful for stable rotation, although there are some energy losses.

THURSDAY POSTER

P4C - Wave Propagation III

Carribean Ballroom III-V

Thursday, October 20, 2011, 1:00 pm - 4:30 pm

Chair: **Andreas Mayer**
HS Offenburg, Gengenbach, Germany

P4C-1

Analysis of Frequency Gap of Nanomechanical Antenna Structure Resonator Using Mathieu Equation

Hideaki Itoh[1], Hiroshi Tatebe[2]; [1]Faculty of Engineering, shinshu university, Nagano, Nagano, Japan, [2]shinshu university, Japan

Background, Motivation and Objective

The author already showed that the entire mechanical energy of the antenna structure resonator made of silicon with 40 elements could be approximately reduced to the energy of a harmonic oscillator in the neighborhood of 1.49 GHz, in which the quantum displacement was observed at 110 mK, [1] using Bernoulli-Euler equation applied to the antenna structure resonator.[2] The frequency gap of this antenna structure resonator whose resonant frequency did not exist was already found in the frequency range of 763 MHz ~ 1.197 GHz from calculated results using Bernoulli-Euler equation.[2] The author also elucidated that the frequency gap calculated using the transfer matrix method for travelling flexural wave had approached this frequency gap, calculated using Bernoulli-Euler equation applied to the flexural beam for both the boom and the elements of the antenna structure resonator, [2] and that the frequency gap was intrinsically the physical phenomenon based on the antenna structure resonator consisting of a repeated periodic structure with local vibration.[3]

Statement of Contribution/Methods

By applying the Bernoulli-Euler equation with the harmonic modulated outward axial force with time to the antenna structure resonator, the time term of its vibrational displacement of the antenna structure resonator was found to become the Mathieu equation under a reasonable approximation on the vibrating state of the antenna structure resonator at the frequency of 1.49 GHz.

Results

The author could now obtain the frequency gap of 840 MHz ~ 1.197 GHz, in the case of derivation of the Mathieu equation by applying the Bernoulli-Euler equation with the harmonic modulated outward axial force with time to the antenna structure resonator with 40 elements on both sides of the boom and then by setting the magnitude of the axial force to be 5.58□~10-5 N, which was intermediate between the frequency gaps of 763 MHz ~ 1.197 GHz obtained by Bernoulli-Euler equation [2] and of 927 MHz ~ 1.197 GHz calculated by the transfer matrix method using Bloch theorem of flexural wave based on the periodicity of 40 elements.[3]

Discussion and Conclusions

From the calculated results, the frequency gap, observed in the antenna structure resonator, was found to be realized by the instable vibration of the elements on which the harmonic modulated outward axial force with time was yielded by the movement of the boom driven by Lorentz force as external one from the viewpoint of the Mathieu equation.

Reference

[1] A. Gaidarzhy, G. Zolfagharkhani, R. L. Badzey, and P. Mohanty: Phys. Rev. Lett. 94 (2005) 030402.
[2] H. Itoh, K. Ishikawa, and Y. Kobayashi: Jpn. J. Appl. Phys. 47 (2008) 5734.
[3] H. Itoh and H. Tatebe: Jpn. J. Appl. Phys. 49 (2010) 07HB09.

THURSDAY POSTER

P4C-2

Self-demodulation effects in nonlinear focused beams

Petr Konicek[1], Michal Bednarik[1], Milan Cervenka[1]; [1]*CTU FEE Prague, Czech Republic*

Background, Motivation and Objective

In this work, spatial distributions of acoustic pressure of the nonlinear focused sound beams are presented. Numerical solutions are obtained and analyzed for various types of sound sources. Focused acoustic beams of periodic waves with an initially uniform amplitude distribution and with Gaussian amplitude distribution are considered.

Statement of Contribution/Methods

The numerical algorithm is based on the numerical solution of the nonlinear parabolic Khokhlov-Zabolotskaya-Kuznetsov (KZK) equation. The presented model enables to study the process of nonlinear generation of a low-frequency signal by a amplitude modulated high-frequency carrier wave. The amplitude modulated high-frequency carrier wave is demodulated in the course of its propagation through the near-field domain.

Results

Novel in this work are the pre-prepared single-band modulations of the carrier wave and the comparison with the common modulation techniques.

Discussion and Conclusions

We consider the case of a source which is periodic in time. Hence we seek the solution of the KZK equation in a form of a Fourier series.

The results were obtained on the basis of numerical simulations. The presented model accounts for nonlinearity, thermo-viscous absorption, and diffraction in the directive focused sound beams.

P4C-3

Wave propagation in elastic waveguides with a finite length crack

Mykhailo Semkiv[1]; [1]The Faculty of Mechanics and Mathematics, Taras Shevchenko National University of Kyiv, Kyiv, Ukraine

Background, Motivation and Objective

The topic of wave propagation in elastic waveguides with crack has for a long time been of major interest in acoustic, mathematical physic, engineering. Later on interest in this field arose due to needs in acousto-microelectronics, mainly surface acoustic wave devices, nondestructive evaluation of composite materials. Precise analytical methods for solving boundary value problems, which are used in this article, are major place in acoustics, as are solid foundation for the development of numerical or approximate methods of calculation.

Statement of Contribution/Methods

In the presented work the propagation of SH-wave in elastic waveguides with finite length crack in the case of free boundaries is considered. The complete analysis of diffraction of elastic waveguides with crack of finite length is performed. To solve the problem we used the method of partial areas, which consists of a partition complex field into simple subfields. For these simple subfields can find a solution by method of separation of variable. Matching procedure reduce to the infinite system of algebraic equations for unknown amplitudes. In the general case not possible to construct the solution of system of algebraic equations. This system is solved by the use of method of residues of analytical functions. Residues method is based on calculating of integral as the sums of residues of analytical function f(w) in the complex plane. Properties of function f(w) determined by state of poles and zeros which are chosen so that the residue series coincide with the consideration system of equations. It is possible identify the unknowns in the system of equations with the residues of function. A finite crack in elastic waveguides makes it necessary to solve additional infinite system of algebraic equations, but the solution of this additional system is faster to converge than the original. Conditions at the ends of the crack give opportunity to write the asymptotic behavior of solutions.

Results

In the presented work the analytical solution is built. A displacement components of diffraction fields is obtained. The reflection coefficient (the ratio of power flux incident wave to the power flux reflected wave) as well as transmission coefficient (the ratio of power flux of incident wave to the power flux of transmission wave) are calculated. All of that was obtained for different wavelengths of incident wave. The graphs of reflection and transmission coefficients depending of dimensionless frequency were built.

Discussion and Conclusions

For further investigation is planned to solve this problem for Lamb waves.

P4C-4

Analysis of nonlinear standing waves in two coupled acoustic resonators

Michal Bednarik[1], Milan Cervenka[1], Petr Konicek[1]; [1]Czech Technical University in Prague-FEE, Prague, Czech Republic

Background, Motivation and Objective

The motivation of this work is given by the fact that there are some devices containing an acoustic system which consists of two coupled resonators. The coupled resonators interact which affects the function of the device containing this acoustic system. In addition, a working fluid in the coupled resonators is capable of exerting oscillating force on the structure surrounding it. In such cases, it is important to know the behavior of resulting standing waves.

Statement of Contribution/Methods

For this reason our work deals with the analysis of nonlinear standing waves in two acoustic resonators which are linearly coupled by a narrow half-wave length duct. We assume that the two resonators with the coupler contain air in the same state. The resonators are supposed to be hard-walled and their front walls are harmonically vibrating pistons. To analyze the standing waves in the resonators we found a system of equations in the form of two the inhomogeneous Burgers equations containing coupling terms. This system of equations can be relatively easily solved numerically. The general form of the model equations allows us to analyze various configurations of the studied acoustic system.

Results

Both the numerical and approximate analytical solutions for various configurations of the system model equations gave us interesting results which are not only interesting from a theoretical point of view, but also for their potential use in practice.

Discussion and Conclusions

Each of the considered coupled resonators can be excited by a piston independently, which means that there is a relatively high degree of freedom with respect to the possible configurations. The considered configurations allow us to implement some of the findings and procedures related to the theory of synchronization of nonlinear systems.

P4C-5

Complex Acoustic Doppler Effect in Double Negative Resonance Metamaterials

Ivan Lisenkov[1], Sergey Nikitov[1,2]; [1]Kotel'nikov Institute for Radioengineering and Electronics of RAS, Moscow, Russian Federation, [2]Department of Physical and Quantum Electronics, Moscow Institute for Physics and Technology (State University), Moscow, Russian Federation

Background, Motivation and Objective

Artificial materials with simultaneously negative constitute parameters exhibit properties which are unusual for “ordinary” materials. One of notable examples of such effect is reverse Doppler shift, i.e. a receiver detects a red frequency shift for an approaching source instead of blue one and vice versa. Also it has been shown, that non-linear frequency dispersion is a necessary condition for double negative media. In our work we investigate acoustic Doppler effect in media with resonance behaviour of frequency dispersion with rigid Green function approach.

Statement of Contribution/Methods

A number of attempts were taken to construct double negative acoustic metamaterials during the past decade and most of media were created as continuum composites. But such composites are not suitable for Doppler effect observation, due to technical difficulties to make a source of acoustic waves travel through the matrix with sufficient speed.

In our work we consider a 1D metamatrial as a tube with embedded resonators of two types. The first type are short closed appendixes with pistons on springs attached to a side of the tube, affecting effective bulk modulus of the system. Second type of resonators is a pair of light membranes attached to the pipe in its cross-section with a piston on springs between the membranes. Such resonators are affecting effective density of metamaterial. By using this configuration it is possible to make source move in metamaterial with speed which is necessary for Doppler effect observation.

We theoretically investigate spectrum of a moving acoustic source detected by a steady receiver using Green functions approach.

Results

Parameters of matematerial are adjusted in such way, that there are frequency zones for direct and backward wave propagation and a forbidden gap as well. Two notable particular cases has been investigated. In first case an acoustic source radiates at frequency withing a forbidden gap and travels from a receiver. At low speeds a receiver cannot record a signal, because the emitted wave is decaying. But on greater speeds backward and forward waves can be exited, thus receiver detects two spectrum lines from a monochromatic source: a red-shifted and a blue-shifted. This is a so called a complex Doppler effect. If speed is relatively high no forbidden gap is observed the detector hears the source independently of its self-frequency.

In other case the source is emitting at frequency close to forbidden gap and source travels toward to receiver. At low speed the receiver records a signal, but as speed increases the detector records signal two spectrum lines, but both modes as both forward or backward waves. As speed more increases the source is “cloaked” by the forbidden gap.

Discussion and Conclusions

In our work Doppler effect in high dispersive acoustic media is investigated. Possibility of several modes generation is shown. A device for potential excremental observation is proposed.

The work is supported by GPAD RAS and MSE of RF (П556)

P4C-6

Analytical Solutions of Surface Acoustic Wave Propagation in Functionally Graded Plates with the Homotopy Analysis Method

Liming Gao[1], Zheng Zhong[2], **Ji Wang[3]**; [1]School of Mech Eng, Shanghai Institute of Technology, Shanghai, China, People's Republic of, [2]School of Aerospace Eng & Applied Mechanics, Tongji University, Shanghai, China, People's Republic of, [3]School of Mech Eng & Mechanics, Ningbo University, Ningbo, Zhejiang, China, People's Republic of

Background, Motivation and Objective

Since the governing equations of the propagation of elastic waves in functionally graded materials (FGMs) are differential equations with variable coefficients, it is difficult to solve them with existing analytical methods. In our earlier studies, we have proven that the newly embraced homotopy analysis method (HAM) is an effective approach for exact solutions in power series

.

Statement of Contribution/Methods

In this paper, the homotopy analysis method is used again to study the propagation of surface acoustic waves in FGM plates, which has been solved by many methods such as the layered model, Frobenius method, and the HAM method before. What is different in this paper is that series solutions for the HAM is set as the combinations of exponential functions, which result in different solutions of coefficients. The solution procedure will be more complicated as the solution forms have been changed, and solutions converge in a much fast rate.

Results

With the assumption of wave solutions in series of the product of exponential and power functions, coefficients are determined by taking the standard procedure of HAM implementation. Through the analysis of convergence, accurate solutions are obtained and compared with earlier solutions numerically. The variation of deformation along the thickness, which is the direction of property variation, is proving insightful guidance on the selection of variation pattern for better utilization of FGM in acoustic wave devices.

Discussion and Conclusions

The analytical solutions can be used directly in some cases to support experimental approach and benchmarking numerical approaches we are more comfortable in applications. Fig. 1 shows two surface wave velocities, and Fig. 2 shows the deformation change with the variation of material properties.

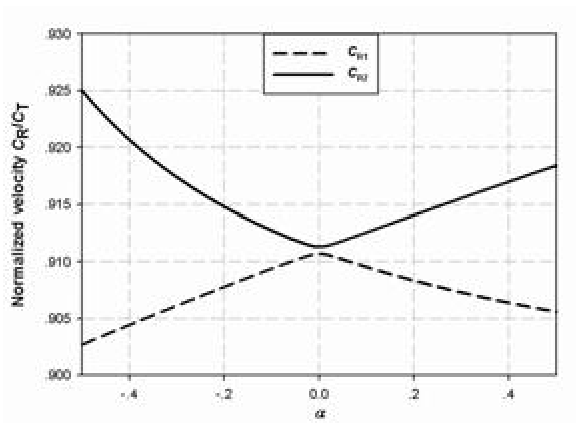

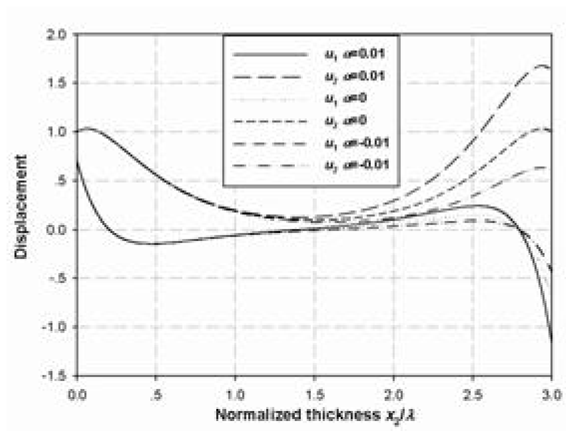

P4C-7

Modeling Acoustic Wave Field Propagation in 3D Breast Models

N. Ozmen-Eryilmaz[1], L. Demi[1], E.J. Alles[1], M.D. Verweij[1], K.W.A. van Dongen[1]; [1]Laboratory of Acoustical Imaging and Sound Control, Delft University of Technology, Delft, Netherlands

Background, Motivation and Objective

Breast cancer is one of the most occurring cancer types worldwide and early diagnoses will significantly increase the survival rate. Nowadays, mammography is the most conventional screening modality despite its drawbacks; e.g. usage of ionizing radiation, painful procedure and bad performance in dense breasts. These drawbacks could be avoided with ultrasound based screening systems. Optimizing the design of these systems requires software which allows one to model the propagation of acoustic wave fields in breasts.

Currently, the modelling of these fields (including multiple scattering) is due to its complexity and problem size not possible with commercially available ultrasound simulation software. Consequently, we investigate the usage of a frequency-domain integral equation approach as full wave modelling technique.

Statement of Contribution/Methods

A frequency-domain integral equation is formulated to model attenuative acoustic wave fields in three-dimensional (3D) breast models. The method allows for multiple scattering caused by inhomogeneities in the speed of sound and attenuation. The latter one is based on a causal compliance relaxation function with a frequency power law, as typically observed in measurements. The resulting integral equation is solved using an iterative conjugate gradient (CG) scheme. Finally, Fourier transforms are used to obtain time domain results.

Results

First, the accuracy of the method has been tested. Results obtained for a plane wave scattering off a homogenous penetrable sphere have been compared with an analytical solution. For simulations, the lossless sphere (sound speed c = 1460 m/s, radius r = 5 mm) is positioned in lossless water (c = 1524 m/s) and illuminated with a Gaussian modulated plane wave with center frequency of 0.5 MHz. Both results are in excellent agreement with each other.

Subsequently, the efficiency of the algorithm has been tested by implementing both a CG and a stabilized BiCG scheme. Results show an improved convergence for the BiCG method.

Next, an MRI scan of a real cancerous breast is used to build a model of a lossy breast submerged in lossy water (volume 154 mm × 154 mm × 154 mm). The breast is illuminated with a Gaussian modulated field with a center frequency of 0.3 MHz. Various simulations have been performed to investigate amongst others the effect of attenuation on A-scan measurements.

Discussion and Conclusions

An integral equation based method has been employed to model the propagation of attenuative acoustic wave fields in breasts and to generate synthetic measured data. First, the accuracy of the method has been confirmed using the analytical solution for a spherical contrast. Next, the algorithm has been tested successfully on a 3D real cancerous breast model. The results clearly show all the typical wave phenomena observed in real data, such as attenuation, refraction, diffraction and multiple scattering.

P4D - BAW and MEMS

Carribean Ballroom III-V

Thursday, October 20, 2011, 1:00 pm - 4:30 pm

Chair: **Jan Kuypers**
Sand 9, Inc.

P4D-1

TaO_x/SiO_2 insulating acoustic mirrors for AlN-based X-band BAW resonators

Jose Capilla[1], Valeriy Felmetsger[2], Marta Clement[3], Jimena Olivares[3], Arnaud Devos[4], Enrique Iborra[3]; [1]Grupo de Microsistemas y Materiales Electronicos, Universidda Politecnica de Madrid, Madrid, Spain, [2]Oem Group Inc., USA, [3]Universidad Politecnica de Madrid, Spain, [4]Département ISEN, France

Background, Motivation and Objective

Solidly mounted resonators (SMR) made with thin aluminum nitride (AlN) capacitors built on top of acoustic reflectors made of metallic high acoustic impedance layers (W, Ir) have been recently developed for high frequency applications. The technology for filter fabrication requires complex technological processes, such as the patterning and planarization of the underlying metallic layers, which could be avoided if insulating reflectors were used. The aim of this work is to investigate the performance of tantalum oxide (TaO_x) as high acoustic impedance layer, compared with that of other insulating material currently used in insulating mirrors.

Statement of Contribution/Methods

We have fabricated acoustic reflectors by alternating low acoustic impedance SiO_2 layers with high acoustic impedance amorphous TaO_x and used them for the acoustic isolation of BAW resonators made of 180 nm-thick AlN layers sandwiched between two Ir and Mo electrodes. The structure of the TaO_x films were previously assessed by X-ray diffraction (XRD) and IR transmittance (T-IR); the acoustic properties were assessed by measuring mass density by X-ray reflectometry (XRR) and acoustic velocity either through picosecond measurements or through the $\lambda/2$ resonance induced in a TaO_x layer inserted between an acoustic reflector and an AlN-based test resonator. The AlN films were deposited by ac (40 kHz) reactive magnetron sputtering of two balanced Al cathodes with stress control by energetic bombardment of the growing film. The frequency response of both high frequency and test resonators was fitted with Mason's model to derive the characteristic parameters (sound velocity, k^2_{eff} and Q).

Results

T-IR and XRD measurements revealed the amorphous nature of the TaO_x films, although films thicker than 400 nm exhibit some nanocrystalline grains in the amorphous matrix. Their mean mass density is 7600 kg/m^3 and longitudinal acoustic velocity varies from 4500 to 5500 m/s. This dispersion has not been correlated with any process parameter (% of O_2 or pressure of the sputtering gas discharge, power, thickness, etc.). 180 nm-thick AlN layers deposited on these acoustic reflectors with bottom Ir electrodes have a pure c-axis orientation and very good crystallinity with rocking curves around the (00•2)-AlN reflection around 2º-wide. BAW resonators operating around 8 GHz with k^2_{mat} of 6.5 % and Q around 500 were achieved.

Discussion and Conclusions

Despite exhibiting some dispersion in acoustic properties, TaO_x sputtered films offer a good performance as high acoustic impedance layer in insulating acoustic reflectors for SMR resonators operating at very high frequency. These results encourage using these mirrors for the fabrication of high frequency SMR filters addressing the X-band.

P4D-2

Comparison of Different Electromagnetic Models of Bulk Acoustic Wave Resonators and Filters

Nermin Selimovic[1], Bernhard Bader[2], Jürgen Kiwitt[2], Maximilian Pitschi[2], Thomas Eibert[1]; *[1]Technische Universität München, Munich, Germany, [2]TDK-EPC Corporation, Munich, Germany*

Background, Motivation and Objective

Constantly increasing performance demands and rapid miniaturization of bulk acoustic wave (BAW) devices require more accurate, and sophisticated design and modeling methods. Different modeling and simulation methods have to be applied depending on the simulated device, its complexity, available computational resources, and required accuracy. In order to model all relevant effects that are important to accurately characterize a device, it is important to know what details to model, how to model them, and at what extent.

This paper presents and compares different electromagnetic models of mirror-type BAW resonators that are simulated with a 3D finite element method electromagnetic solver, whereas the acoustic effects are computed with a 1D solver.

Statement of Contribution/Methods

The electromagnetic analysis conducted in this paper concerns all relevant BAW stack layers, i.e., the influence of the acoustic mirror and piezo layers as well as the meshing effects in these layers. Furthermore, a model with modified piezo dielectric properties is presented, which enables the combined simulation of electromagnetic and acoustic effects.

In the first part, the electromagnetic influence of acoustic mirror layers is investigated. For this purpose, three different electromagnetic BAW resonator models are analyzed: without the mirror layers, with one mirror layer, and with multiple mirror layers. The second part investigates the mesh-cell-density effects in certain regions of the device in electromagnetic simulations. Models with different mesh-cell-densities in the piezo and acoustic mirror layers are considered and analyzed for the mentioned three mirror models. In an additional step, the BAW resonator models were extended by incorporating the acoustic effect into the electromagnetic simulation by applying a frequency-dependent, complex valued, equivalent permittivity for the piezo material.

Results

The electromagnetic effects of the different BAW resonator models are analyzed by comparing the resonance frequencies of the simulated resonators. Frequency shifts of the resonance and anti-resonance frequencies are observable for the different resonator models, which originates from a different effective inductance and static capacitance, respectively.

The resonator model with modified piezo dielectric material properties showed slightly different simulation results in comparison to the simulation method with the standard dielectric material properties. The advantage of this method is that all significant electromagnetic and acoustic effects of BAW devices can be included in only one simulation, avoiding additional and post-processing simulation steps.

Discussion and Conclusions

Different electromagnetic BAW resonator models are presented, their electromagnetic effects, simulation accuracy, computational effort, and applicability are discussed. Finally, the simulation results are compared to measurements.

P4D-3

On the rule of thumb for flipping of the dispersion relation in BAW devices

Sumy Jose[1], Ray Hueting[1], André Jansman[2]; [1]Semiconductor Components, University of Twente, Netherlands, [2]Research, NXP Semiconductors, Netherlands

Background, Motivation and Objective

High-performance solidly mounted bulk acoustic wave resonators (SMRs) can be obtained by employing frame regions, if these exhibit type 1 dispersion ($f_{RTE1} > f_{RTS2}$). The often used piezo-material AlN is a type 2 material ($f_{RTE1} < f_{RTS2}$), for which type 1 dispersion can be enforced by increasing the top low-acoustic-impedance (oxide) layer thickness of the mirror stack [1, 2]. However a criterion for flipping was not investigated. In this work we intent to develop a rule of thumb for flipping dispersion curves, applicable for FBARs and SMRs.

Statement of Contribution/Methods

Our 2D FEM simulations [5] of SMRs with electrodes and mirror stacks below, designed to be just between type 1 and 2 dispersion showed that shear motion is confined to the top oxide. Hence flipping occurs if $t_{ox}=V_{sox}/2f_{RTS1ox}$, with V_{sox} is the shear velocity in oxide. We further explored the dispersion condition [1] for a resonator without physical electrodes and just oxide below it, giving us a rule of thumb for flipping. For type 1 holds: $V_{lpiezo}/V_{sox} \approx > t_{piezo}/t_{ox}$ and type 2 the opposite.

Results

A bi-layer of AlN and SiO_2 was simulated with a fixed and a free (FBAR) boundary condition at the bottom. Table 1 summarizes flipping of dispersion curves for several thickness variations. Indeed, flipping occurs when $t_{piezo}/t_{ox} \geq V_{lpiezo}/V_{sox}$. Fig. 1 shows examples of dispersion curves obtained from FEM simulations.

Discussion and Conclusions

A rule of thumb for flipping dispersion curves is discussed, based on the condition that the shear wave resonates in the top-oxide. The rule is not applicable for flipping type 1 materials to type 2 because its shear confinement is not only in the top-oxide but spreads over the whole bi-layer. However, flipping is observed in a bi-layer of ZnO (type 1 material) with Pt but this is not yet understood.

[1]G.G.Fattinger et al., Proc. IEEE Ultrasonics Symposium, pp.1175-1178, 2005.

[2]S. Marksteiner et al., US patent: 006933807B2

[3]S. Jose et al, Proc. IEEE Ultrasonics Symposium, September, October 2010.

[4]F. Thalmayr et al., IEEE Trans. Ultrasonics, Ferroelectrics, & Freq. Cntrl. 57(12), pp. 2844-2849, 2010

[5]www.comsol.com

Table 1. Flipping of the dispersion curves for (a) t_{piezo}= 1500nm and variable t_{ox} and (b) t_{ox}=300nm and variable t_{piezo}. The flipping takes place when $t_{piezo}/t_{ox} \geq V_{lpiezo}/V_{s,ox}$ = 2.925. In addition this occurs when the full shear wavelength matches the piezoelectric layer thickness (t_{piezo}) as well, hence when $f_{R,TS1ox} \approx f_{R,TS2piezo}$. Fixed bottom boundary condition (BC) was assumed here, more or less applicable for SMRs with quarter wavelength mirror stack. The flipping was also observed with free bottom BC indicating the rule of thumb can be also applied for FBARs.

(a) tpiezo= 1500nm with varying t_{ox}		
t_{ox}(nm)	t_{piezo}/t_{ox}	Dispersion
0	-	Type 2
200	7.5	Type 2
300	5	Type 2
400	3.75	Type 2
500	**3**	**Type 1**
600	**2.5**	**Type 1**
700	**2.14**	**Type 1**
800	**1.875**	**Type 1**
(b) t_{ox}= 300nm with varying t_{piezo}		
t_{ox}(nm)	t_{piezo}/t_{ox}	Dispersion
500	**1.6**	**Type 1**
800	**2.6**	**Type 1**
900	**3.0**	**Type 1**
1000	3.3	Type 2
1200	4.0	Type 2
1500	5.0	Type 2
1700	5.6	Type 2

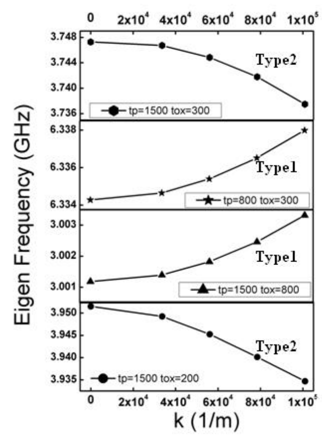

Figure. 1 Dispersion curves obtained from 2D FEM Eigen frequency simulations [5] for the examples cases of type 1 (positive slope) and type2 (negative slope) for both (a) and (b) (see table 1).

P4D-4

Growth of AlN oriented films on insulating substrates

Jimena Olivares[1], Jose Capilla[1], Marta Clement[1], Jesús Sangrador[1], Enrique Iborra[1]; [1]*Universidad Politécnica de Madrid, Spain*

Background, Motivation and Objective

The growth of AlN thin films with good crystal quality and piezoelectric activity on insulating thin films is still a pending matter, as the oriented growth of AlN requires specific surface conditions, which is mainly achieved in metallic layers or single crystal insulating substrates, such as sapphire. However, these layered structures are required in many applications, such as surface acoustic wave (SAW) devices, laterally excited shear mode resonators or bulk acoustic wave (BAW) composite resonators containing insulating layers for temperature compensation.

Statement of Contribution/Methods

In this work we explore the possibility of growing c-axis oriented AlN thin films by pulsed-dc sputtering on insulating glass substrates. The glass substrates are covered with SiO_2, TiO_x and TaO_x seed layers deposited either by dc-pulsed sputtering or by electron beam evaporation. We investigate the influence of the structure and morphology of the different seed layers in the growth of highly textured AlN films, paying a special attention to the influence of their crystalline properties and to the preconditioning of their surface by in-situ ion bombardment just before AlN deposition. The seed layers and the subsequently grown AlN films are characterized by X-ray diffraction, reflection and transmission infrared spectroscopy and atomic force microscopy. The piezoelectric activity of the AlN films is assessed by measuring the frequency response of SAW delay lines using interdigitized electrodes made of molybdenum, which allows deriving the electromechanical coupling factors of the devices, which strongly depend on the piezoelectric coefficients.

Results

Preliminary results point out that the ionic pre-treatment of the underlying seed layer is essential for obtaining a significant piezoelectric activity independently of the material used as seed layer. High substrate bias voltages are required to improve the crystal orientation of AlN films, especially when deposited on SiO_2 seed layers; this causes a significant increase of the compressive stress, which sometimes ends with the delamination of the film. The mechanical stress developed in the AlN film is lower when using TiO_x and TaO_x seed layers; in these cases, electromechanical coupling factors k^2_{SAW} close to 1% are routinely achieved in SAW devices.

Discussion and Conclusions

AlN growth is very sensitive to the nature and morphology of the substrate. The nanocrystalline nature of TiO_x and TaO_x films thick layers seems to promote the oriented growth of polycrystalline AlN and to improve the electromechanical coupling.

P4D-5

Aluminum Scandium Nitride Thin-Film Bulk Acoustic Resonators for wide band applications

Johan Bjurstrom[1], Milena Moreira[1], Ilia Katardjiev[1], **Ventsislav Yantchev[1]**; [1]*Solid State Electronics, Uppsala University, Sweden*

Background, Motivation and Objective

Thin piezoelectric w-Al(1-x)ScxN thin films have been experimentally shown to exhibit a piezoelectric coefficient d33 substantially higher than that of AlN. More specifically, d33 is shown to initially increase monotonically with Sc concentration up to 30 at% Sc. This opens the way for devising electro-acoustic components operating in the microwave region with bandwidths substantially higher than earlier possible with thin AlN films. To verify this possibility, however, one needs to appreciate both the electromechanical coupling (kt2) as well as the Q-value which is the objective of this work.

Statement of Contribution/Methods

Highly c-textured wurtzite Al(1-x)ScxN thin films with a relative Sc concentration x in the range 0 - 0,15 were grown with reactive sputtering from a Sc and an Al targets in an Ar/N2 ambient as illustrated by Fig. 1. Subsequently, standard FBAR resonators were fabricated and their electrical performance measured (Fig. 2).

Results

The above results show that the kt2 of the films increases linearly with Sc concentration and at x=0,15 the observed kt2 exceeds by 100% that of AlN. The Q-value, however, is seen to steadily decrease somewhat with increasing Sc concentration. A maximum FOM, defined as the product kt2.Q, is observed at x=0.09 at which concentration kt2 is around 9.53%.

Discussion and Conclusions

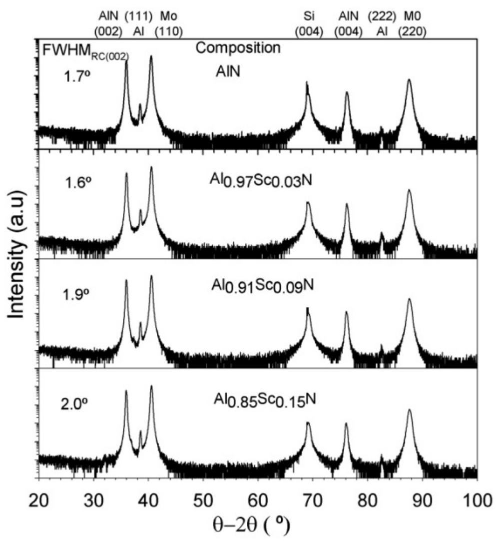

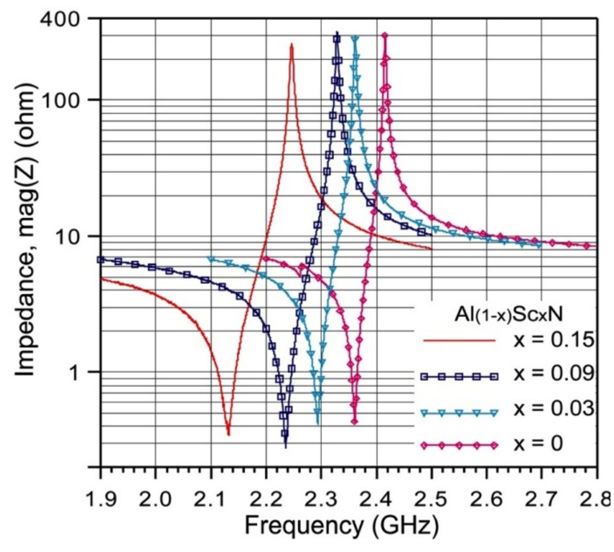

P4D-6

Surface Acoustic Waves on Silicon and the Effect of Electric Current

Lingyao Chen[1], Massood Tabib-Azar[2]; [1]ECE, UoU, USA, [2]ECE, UoU, Salt Lake City, Utah, USA

Background, Motivation and Objective

SAW devices based on piezoelectrics have been extensively used in cell phones as transversal and matched filters. There is a need to implement SAW devices on Si to realize fully integrated systems on a chip (SoC). Recent advances in acoustic crystal waveguides have made Si SAW more attractive for fully programmable filters. The main goal of this study is to examine the effect of electric current flow on SAW in Si and design programmable filters with built-in gain and phase control.

Statement of Contribution/Methods

Figure 1 shows the schematic diagram of the silicon delay line structure. An n-type <100>, 50 Ohm.cm silicon slab was supported by a SiO2 platform resulting in two Si cantilever beams at both ends. Copper electrodes were situated under the Si beams for sensing and actuation. The air gap formed between the Si beam and the Cu electrode was around 50 um. Excitation signal was applied to one of the cantilever beams that excited SAW in the Si slab. The second beam was used to sense the SAW once it reached the other end of the slab. Wires connected to the central part of the silicon delay line (slab) enabled passing dc electric currents.

Results

Figure 2 shows the change of output signal's amplitude under current flow with the electrons directed against the SAW. It can be seen that the SAW amplitude was increased by 5mV (0.46%). To find the velocity change, a lock-in amplifier was used. When electrons were directed against the SAW, the lock-in output decreased by ~ 0.3mV (2.2% and it was increased by ~ 0.5mV (0.43%)when electron flow was reversed.

Discussion and Conclusions

We showed that Si SAW can be excited/detected using cantilever beams and that its parameters (amplitude and velocity) are affected by an electric current. Depending on the direction of the current, the SAW could be advanced or retarded.

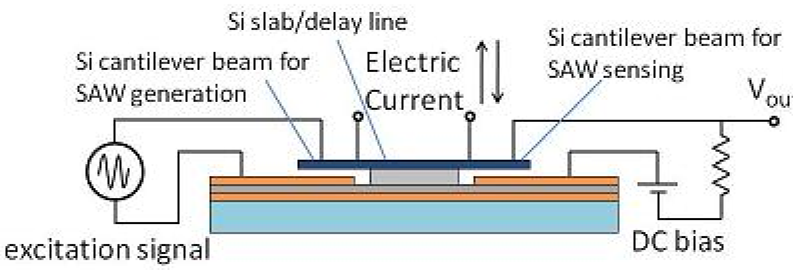

Fig. 1: Schematic diagram of the silicon acoustic wave delay-line structure.

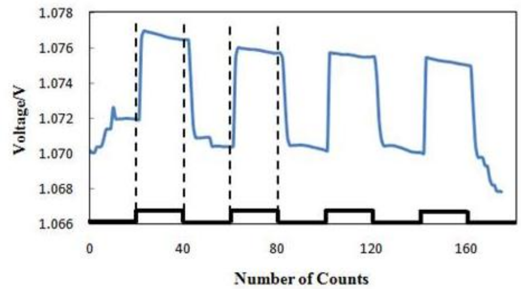

Fig. 2: The amplitude of 1 MHz (twice the excitation frequency) signal detected at the output cantilever beam. Excitation frequency applied to the input cantilever beam was 500kHz and 8.5 mA current pulses were applied along the SAW delay line.

P4D-7

Effect of Lattice Symmetry on the Formation of Phononic Band Gaps in a Silicon Plate with Metallic Stubs

Reza Pourabolghasem[1], Abdelkrim Khelif[1,2], Ali Asghar Eftekhar[1], Saeed Mohammadi[1], Ali Adibi[1]; [1]Electrical and Computer Engineering, Georgia Institute of Technology, Atlanta, GA, USA, [2]Institut FEMTO-ST, CNRS UMR 6174, Université de Franche-Comté, Besançon Cedex, France

Background, Motivation and Objective

Recently, synthetic periodic acoustic structures (i.e., phononic crystals) have attracted significant attention as they enable designers to control the elastic properties of the material. Specific focus of researchers in this field has been on the search for phononic crystal (PnC) structures that support phononic band gaps (PnBGs). It has been shown that 2D structures consisting of an array of cylindrical pillars can produce sizable PnBGs. In this paper, we investigate, theoretically, the existence of PnBGs in different phononic crystal structures composed of 2D array of tungsten (W) pillars on a silicon plate with different lattice structures, namely, triangular and honeycomb lattices.

Statement of Contribution/Methods

Using the finite element method, we show that triangular lattice structure supports multiple wide PnBGs for a wide range of geometrical parameters. On the other hand, honeycomb array of pillars does not support any wide PnBGs with similar dimensions. To further investigate this phenomenon, we have studied the effects of the normalized slab thickness (d/a), and the normalized radius (r/a) and height (h/a) of the pillars on the PnBG.

Results

Figure 1 shows the extent of the PnBG for a honeycomb and a triangular PnC of W pillars on a Si slab for a fixed pillar radius and slab thickness for different values of pillar height. It can be observed that a triangular PnC has wider PnBGs compared to the honeycomb lattice. It can be shown that the first band opening in the triangular structure is due to the periodic perturbation of the slab modes by the pillars. Other PnBGs can be observed for both lattice types with similar center frequencies. Considering the fact that these band gaps are supported in two structures with similar pillars and completely different lattice constants, we believe that the formation of these band gaps are mainly caused by the strong coupling between locally resonant pillar structures through the silicon slab.

Discussion and Conclusions

Theoretical evidence was provided that a triangular lattice of pillars on a Si slab is more likely to provide wide PnBGs in comparison to honeycomb lattice. Comparison of the PnBGs for triangular and honeycomb lattices indicates a trend that suggests PnBGs in these structures are formed because of not only the Bragg reflection but also a strong coupling of resonant modes of the W pillars and slab modes of the Si plate.

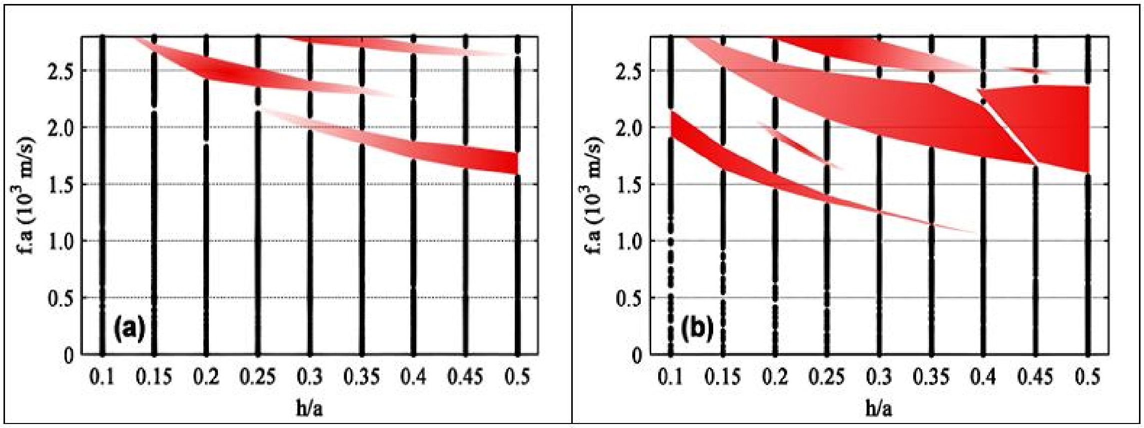

Figure 1 Existence of PnBG openings in (a) honeycomb and (b) triangular array of W pillars (r/a = 0.40) on a Si slab (d/a = 0.5) for different values of h/a.

P4D-8

Theoretical Investigation of Cyclic Mechanically-coupled Contour Mode Filters

Hadi Yagubizade[1], Yung-Yu Chen[2], Miko C. Elwenspoek[1], Niels R. Tas[1]; [1]Transducers Science and Technology Group, MESA+ Institute for Nanotechnology, University of Twente, Enschede, Netherlands, [2]Mechanical Engineering, Tatung University, Taipei 10452, Taiwan

Background, Motivation and Objective

In the last decade, there are increasing investigations on mechanically-coupled contour mode filters for signal processing applications due to promising advantages like small device area and low energy loss. The researches were focused on open-chain configurations, wherein the terminating elements are coupled to a single neighbor and an input or output port. We present a cyclic coupling (closed-chain) architecture for improving the filter performance of contour mode filters.

Statement of Contribution/Methods

A theoretical investigation on mechanically-coupled contour mode filters is presented by using the commercial finite element software COMSOL. First, phase velocities and electromechanical coupling coefficients of Lamb-waves propagating in AlN and PZT plates with different electrical boundary conditions were calculated and compared with experimental results and the transfer matrix method. Further, single contour mode resonators were designed and analyzed. Finally, the frequency responses of contour mode filters of open- and closed-chain configurations are calculated and discussed.

Results

The lowest symmetric (S0-) mode of AlN has a high phase velocity of ~10 km/s and the S0-mode of PZT has a lower phase velocity ~5 km/s. Therefore, AlN is a good candidate material for high frequencies (800 MHz to 2 GHz) and PZT for lower frequencies (50 MHz to 800 MHz) applications. The electromechanical coupling coefficient of PZT is significantly larger than that of AlN, which is in good agreement with experimental results found in literature. Furthermore, single contour mode resonators were analyzed and designed for open- and closed-chain mechanically-coupled filters using PZT and AlN for the ranges of 50 MHz to 800 MHz and more than 800 MHz, respectively. The performance of different kinds of closed-chain coupled filters is compared where design parameters such as thickness of the resonator and its lateral dimensions are varied. Results show that the device performance can be improved effectively by using the closed-chain architecture compared to open-chain architecture.

Discussion and Conclusions

We proposed the use of cyclic mechanically-coupled contour mode filters for the first time. The filters were designed and theoretically analyzed based on finite element method. The obtained Lamb-wave characteristics are in good agreement with results found in literature. It can be concluded that by using the cyclic mechanically-coupled achritecture the performance of a countour mode filter can be improved. The results provide guidelines for designing a contour mode filter.

P5E - Transducer Design and Application

Carribean Ballroom III-V

Thursday, October 20, 2011, 1:00 pm - 4:30 pm

Chair: **Jean-Francois Saillaint**
Areva

P5E-1

A Piezoelectric Acoustic Pump: Design, Mechanism and Characterization

Tao Li[1], Jan Ma[2]; [1]tli@ntu.edu.sg, Singapore, [2]asjma@ntu.edu.sg, Singapore

Background, Motivation and Objective

The piezoelectric pump has been in rapid development in the last decades. Various pumps based on different mechanisms have been proposed. The leading product in current market is the piezoelectric diaphragm pump. Its advantages are the low power consumption and wide range of flow rate that it can facilitate. However, the pressure head is usually within 20-60 kPa, which limits its use in advanced applications. In this paper, piezoelectric acoustic pump, which is able to generate high pressure head (>200 kPa) with low power consumption (1 W), is introduced.

Statement of Contribution/Methods

The pump comprises a piezoelectric transducer and a casing. The transducer is the horn type Langevin transducer, in which a hole is drilled throughout the transducer to work as the flow path. The casing is a hollow cylinder connected to the transducer through the screw. At the bottom of the casing is an energy focusing element, called reflector. Its distance to the horn tip can be adjusted by turning the screw.

Both transducer and pump performance were characterized. Parameters such as resonant frequency, vibration velocity, radiation area, diameter of flow path, distance between horn tip and reflector, were studied. The flow pattern and acoustic field inside casing were investigated theoretically and experimentally. The relation between pump pressure and flow rate were also measured at different conditions.

Results

The vibration velocity of the transducer obtained is about 3.5 m/s when it operates at 30 kHz and at 1 W power input. The radiation area, diameter of flow path and distance of reflector to the horn tip are interlinked together. As the distance decreases, both flow rate and pressure head increase first and then decrease. The optimum distances for flow rate and pressure head are different and they also rely on the radiation area and diameter of flow path. When the distance is flow rate optimum, fluid will be induced into the flow path without repulsion. When the distance is pressure optimum, pressure head of more than 200 kPa can be achieved. The maximum flow rate is about 10 mL/min under this condition.

Discussion and Conclusions

One of the superiorities of the proposed pump is the high pressure head generated. This is mainly due to the transducer and casing design. The transducer generates a large velocity and the casing provides a hard acoustic boundary. Both conditions ensure the generation of a high acoustic pressure inside the casing, which further induces acoustic effects like streaming and cavitation. The cavitation also contains high energy bubbles, which could be used to explain high pressure head generation. The high pressure nature of the pump makes it promising to be applied in the field of microfluidics. Other advantages of the pump include continuous flow, no oscillation, low power consumption and simple configuration.

P5E-2

Fabrication and Characterization of Half-Kerfed LiNbO3_based High-Frequency (>100MHz) Ultrasonic Array Transducers

Jinying Zhang[1,2], Weijiang Xu[2], Julien Carlier[2], Xinming Ji[1], Samuel Queste[3], Bertrand Nongaillard[2], Yiping Huang[1]; [1]ASIC and System State Key Lab, Department of Microelectronics, Fudan University, Shanghai, China, People's Republic of, [2]Departement of Opto-Acousto-Electronics, IEMN, CNRS UMR 8520, Valenciennes, France, [3]Institute FEMTO-ST, CNRS UMR 6174, University of Franche-Comte, Besancon, France

Background, Motivation and Objective

Ultrasonic arrays, benefiting fast electronic scanning, are used in different domains including medical imaging, sonar and non-destructive evaluation. Recently, high-frequency (30-100MHz) ultrasonic array transducers are being developed for high-resolution ultrasound imaging. Very-high-frequency (>100MHz) array has been found potential in biological cell control and in real-time tissue differentiation. However, the fabrication of very-high-frequency arrays requires the patterning of small-scale features in active materials. To reduce the crosstalk, it needs the realization of kerfs with very high depth/width aspect ratio in active materials, which is actually a great challenge using state-of-the-art etching techniques.This work consists of two parts: (1) The theoretical study to design an optimized high-frequency ultrasonic array, especially investigate the influence of kerf depth on the performances of the arrays in focusing and steering; (2) The realization and characterization of half-kerfed LiNbO3 arrays at more than 100 MHz.

Statement of Contribution/Methods

Single crystal LiNbO3 36°/Y-cut is selected as the active material due to its favourable electro-mechanical coupling efficiency and robust crystal structure. To investigate the influences of the kerf depth on the beam performances, finite element simulation (COMSOL) is employed. The numerical results are given in continuous wave beam steering and focusing. It shows that compared with the ideal full-kerfed array, the half-kerfed one can serve an acceptable beam performance. For this half-kerfed array, crosstalk is calculated and presented

.

Results

A thick layer of LiNbO3 is bonded with Cr/In on a silicon wafer, and then precisely thinned by lapping to a desired thickness (16μm). After top electrodes patterning, the array is obtained by ICP RIE etching with CF4/He gas mixture, using electroplated Ni as mask material. The figure below presents the SEM image of the half-kerfed array. Because of LiNbO3 crystal structure, all kerfs are obtained in V grooves with a 75° vertical angle. The realized array is characterized by measuring its electrical impedance and crosstalk, which is consistent to the finite element **results**

.

Discussion and Conclusions

These results demonstrate the half-kerfed array is a promising candidate in development of very-high-frequency ultrasonic array transducers.

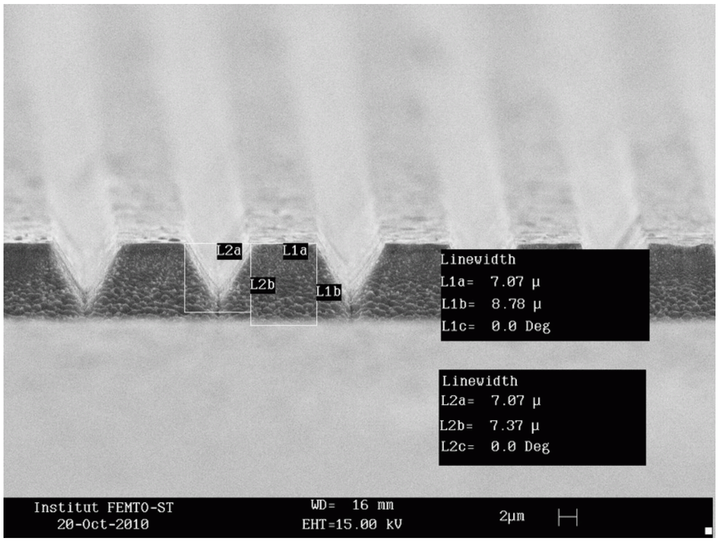

P5E-3

Electrode design and coupling optimization for Aluminum Nitride Tuning Forks

Gabriele Vigevani[1], Fabian T. Goericke[2], Igor Izyumin[2], Albert P. Pisano[2], Bernhard E. Boser[2]; [1]Mechanical Engineering, University of California at Berkeley, Berkeley, CA, USA, [2]University of California at Berkeley, USA

Background, Motivation and Objective

Aluminum Nitride (AlN) has gained an increasing attention for its applications for Lamb Wave Resonators (LWR) [1] and sensors [2]. Due to its post CMOS compatible fabrication process, AlN films can be a promising solution to integrate RF-MEMS and sensors on top of the IC. This integration would not only enable further chip miniaturization, but also improve the circuit performance by eliminating bonding connections between MEMS devices and IC. While AlN has been proven to be a material suitable for LWR and FBARs applications, its use for sensors has been limited.

Statement of Contribution/Methods

In this work we report the dynamic characterization of three Double-Ended Tuning Forks (DETF) with different electrode layouts. An analytical model to design the actuation electrode is proposed. Based on this analytical model three different actuation layouts were designed. The first electrode layout is based on a single port DETF, the second electrode type is a two port asymmetric layout and the third electrode layout is based on a two port symmetric pattern. In order to compare the three actuations, three AlN DETF were fabricated and characterized.

Results

We fabricated three DETF with the same structural dimensions and with three different electrode layouts. The structural AlN layer is 1.8um thick while the top and bottom electrode were created with 0.1um of evaporated Platinum. As we show in this work, the two port symmetric pattern has two advantages: the electrode geometry minimizes feed-through capacitance and having only one electrode on each beam enables further miniaturization of the tines. Our work shows that this electrode layout makes it possible to excite both the symmetric and the anti-symmetric modes of vibration. By means of Finite Element Analysis (FEA) and the device characterization it is possible to demonstrate that the asymmetric mode has higher coupling($k_t^2 = 0.6$) and can be used for strain measurements as shown in [2].

Discussion and Conclusions

This work shows a comparative study on three different electrode layouts for DETF resonators. The characterization performed on the DETF shows the advantages of symmetric electrode layout. As the impedance measurement shows the symmetric layout makes it possible to excite the anti-symmetric mode and operate the resonator with higher coupling coefficients.

[1] J. H. Kuypers, Chih-Ming Lin, G. Vigevani and A. P. Pisano “Intrinsic Temperature Compensation of Aluminum Nitride Lamb Wave Resonators for Multiple-Frequency References” 2008 IEEE International Frequency Control Symposium.

[2] F. T. Goericke, M.W Chan, G. Vigevani,I. Izyumin, B.E. Boser, A.P.Pisano "High temperature compatible Aluminum Nitride resonating strain sensor" to be presented at IEEE Transducers 2011, Beijing,China.

P5E-4

Easy Generation of Airborne Ultrasonic Helical Wavefronts.

Joao Ealo[1], Jose Carlos Prieto[2], Fernando Seco[2]; [1]School of Mechanical Engineering, University of Valle, Cali, Valle del Cauca, Colombia, [2]Centro de Automática y Robótica CSIC-UPM, Arganda del Rey, Madrid, Spain

Background, Motivation and Objective

An acoustic helical wavefront, also known as acoustic vortex (AV), exhibits an screw-type phase distribution singularity. That is, the transverse plane of the wavefront, normal to its propagation axis, shows a phase distribution which linearly increases from 0 to 2π over any circular trajectory around the principal axis. The theory of this phenomenon results the same regardless the field of application, i.e. acoustics, optics or quantum mechanics. For this reason, the AV has been proposed as a tool for the experimental study of its optical and quantum counterpart.

Most of the research and applications of a helical wavefront has been reported in the optics field. Although different methods for AV generation have been proposed (direct generation from a special shaped source, optoacoustic technique, mode conversion from plane wave to AV or using a phase array system) and that the potential of use of AV has been reported, their application in Acoustics has been scarse. This can be attributable, in good part, to the need of a complex instrumentation.

THURSDAY POSTER

The new broadband Ferroelectret technology exhibits interesting properties which makes it an excellent candidate to easily generate airborne ultrasonic vortices thanks to its unprecedented mechanical flexibility, its low acoustic impedance which results in a good adaptation to the air, its wide frequency range of operation (30 kHz to 2 MHz), its easiness of use and its low fabrication cost.

Statement of Contribution/Methods

In this work, we propose a fast and inexpensive alternative to create acoustic vortices by gluing a cellular ferroelectret film on a tangential/helical surface substrate. The high mechanical flexibility of this material, which allows us to fabricate transducers on any developable surface, along with its broadband piston-like response that remains unaltered regardless the radius of curvature, allowed us to create acoustic vortices in air and at ultrasonic frequencies. Up to our knowledge, this is the first demonstration of the generation of AV at ultrasonic frequencies in air. Using broadband ferroelectrets as active material in the vortex generator fabrication process is also a new contribution.

Results

Ultrasonic vortices of topological charge m=-1 were generated using a helical surface with screw dislocation of pitch 3.45 mm (outer diameter 40 mm). Experimental results obtained (both in the nearfield and in the farfield) are in excellent agreement with theoretical estimations using a Gaussian beam model.

Discussion and Conclusions

It is possible to generate high quality airborne helical wavefronts easily and reliably. This paves the way to the potential use of acoustic vortices in engineering applications without using a complicated setup to produce them. In addition to this, the broadband response of the cellular ferroelectrets allows us to create helical beams of different topological charge using the same transducer.

P5E-5

A Novel Method to Fabricate Full-Kerfed High-Frequency (>100MHz) Ultrasonic Array Transducers

Jinying Zhang[1], Weijiang Xu[2], Julien Carlier[2], Bertrand Nongaillard[2], Xinming Ji[1], Yiping Huang[1]; [1]ASIC and System State Key Lab, Department of Microelectronics, Fudan University, Shanghai, China, People's Republic of, [2]Departement of Opto-Acousto-Electronics, IEMN, CNRS UMR 8520, Valenciennes, France

Background, Motivation and Objective

High-frequency (>100MHz) ultrasonic array transducers have gained more and more attentions in recent years for high-resolution ultrasonic imaging. Realization of such high-frequency arrays requires miniaturisation in its geometrical sizes. A number of researchers have focused their efforts on the fabrication methods of high-frequency arrays, and several different approaches are being taken such as dice-and-fill method, Interdigital Pair Bonding (IPB) and laser micromachining. However, all of these fabrication methods are somewhat empirical, have low efficiency, and have correspondingly high fabrication costs. In addition, each small-scale element will induce high electrical impedance, which would be a severe problem in electrical matching.

Statement of Contribution/Methods

We propose a novel method to fabricate full-kerfed high-frequency ultrasonic array transducers. Zinc oxide (ZnO) is selected as the active material because it is easy to be deposited and doped using microelectronic technologies. Thus it has potentials in integration with integrated circuits, which provides opportunities in electrical matching and batch production. Piezoelectric elements are formed by sputtering thick-film ZnO onto etched features of a silicon substrate so that the difficult etching process for ZnO films is avoided by etching silicon. This process is simple and efficient. A 13-μm-pitch ZnO sandwich array (see the figure below) is achieved with a thickness of 8μm for resonating at 300MHz.

Results

The characteristics of the transducer are measured and compared to the finite elemental predictions including electrical impedance (Z) and cross talk. S11 parameter, measured by Network Analyzer, is consistent to the simulation result. It shows the real part of Z is around 200Ω at 300MHz. In order to obtain an efficient wave generation, the electrical impedance should be matched to 50Ω, which will be taken into account in future works. With a 15-element array, the measured scattering parameters S21 are consistent with the calculated results, showing an adjacent crosstalk of -47 dB in air at the resonating frequency. The wave propagation in water is calculated based on this new transducer configuration.

Discussion and Conclusions

All of the results show that this novel method is a promising alternative in development of high-frequency array transducers.

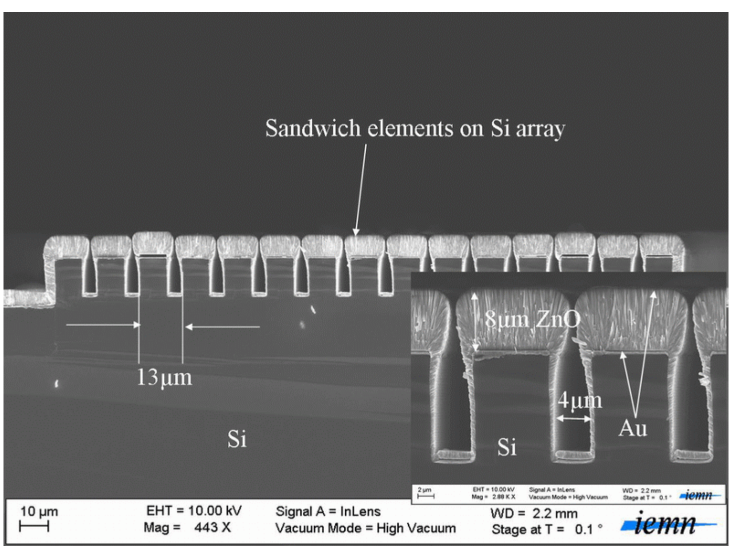

THURSDAY POSTER

P5E-6

A Study of 1-3 Pseudo-Random Pillar Piezocomposites for Ultrasound Transducers

Hao-Chung Yang[1], Jonathan Cannata[1], Jay Williams[1], K. Kirk Shung[1]; [1]Biomedical Engineering, University of Southern California, Los Angeles, CA, USA

Background, Motivation and Objective

The goal of this research was to develop a novel diced 1-3 piezocomposite geometry to reduce pulse-echo ring down and acoustic cross-talk between ultrasonic array elements. It is well known that 1-3 piezocomposites have significant advantages over bulk piezoelectric materials; however, their benefits come at the expense of introducing undesired inter-pillar resonances, which can couple strongly with the fundamental thickness-mode resonance and hence degrade transducer performance. Previous studies have shown that lateral mode coupling could be reduced using a triangular pillar geometry. We believe that a 1-3 pseudo-random pillar piezocomposite (See Fig.1) can enhance composite performance by further reducing the influence of lateral modes on the thickness mode resonance.

Statement of Contribution/Methods

Several 15 MHz 1-3 PZT-5H piezocomposites with different pillar geometries (square (SQ), triangle (TR), and pseudo-random (PR)) were designed to have the same ceramic volume fraction (0.5) and kerf width (14 um). Mechanical dicing was used to fabricate these piezocomposites, which were then made into single element ultrasound transducers. Electrical impedance and pulse-echo measurements were taken to compare their performance.

Results

The thickness-mode electro-mechanical coupling coefficient (kt) for a sample PR was 0.66, which was higher than what was recorded for the other composite geometries (0.50 for TR and 0.64 for SQ), whereas the electrical loss tangent and mechanical quality factors were comparable for all composites. The PR composite transducer displayed the shortest -20 dB pulse length (235 ns), which was 35 ns and 82 ns shorter than that of TR and that of SQ composite transducers, respectively. The PR composite transducer also displayed the highest echo amplitude, which was 4.5 dB and 1.7 dB larger than that of TR and that of SQ composite transducers, respectively.

Discussion and Conclusions

These results demonstrate that a composite constructed with pseudo-random pillars could meet or exceed the performance of other, more common, composite geometries. Therefore, the PR composites may be promising choices for fabricating ultrasound transducers. Our plan is to further analyze use of these composites by modeling and constructing 15 MHz array sub-apertures to see if the PR composite outperforms the others in terms acoustic cross-talk reduction.

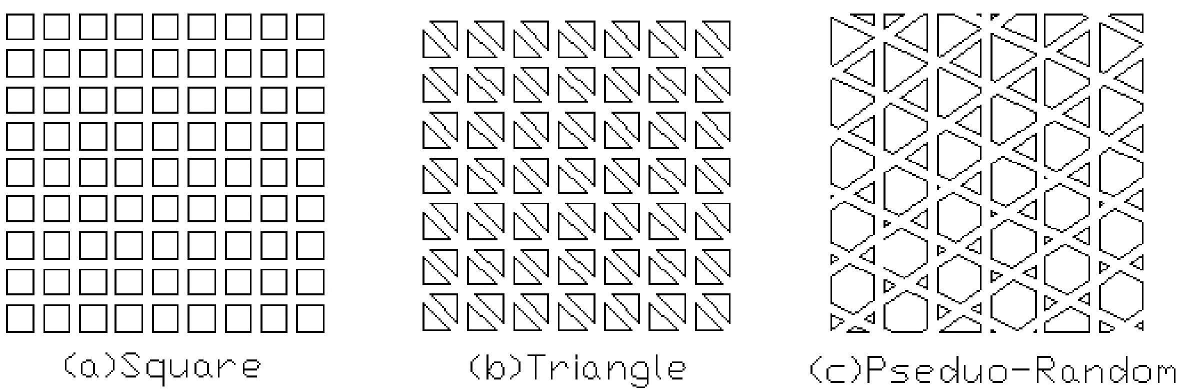

THURSDAY POSTER

P5E-7

Micromachining Techniques in Developing High Frequency Piezoelectric Composite Ultrasound Array Transducers

Changgeng Liu[1], Frank Djuth[1], Qifa Zhou[2], Kirk Shung[2]; [1]Geospace Research, Inc., El Segundo, CA, USA, [2]Biomedical Engineering, University of Southern California, USA

Background, Motivation and Objective

Two-dimensional array transducers have been studied extensively for applications in real time 3-dimensional ultrasound imaging. In this paper, a miniature, high-frequency, PMN-PT composite broadband ultrasonic 2-dimensional array transducer for imaging cellular structure/tissue is presented.

Statement of Contribution/Methods

The array has a total 64 elements with the size of 110 µm by 110 µm. The kerf between elements is 6µm.

PMN-PT/Epoxy 1-3 composite was fabricated by photolithography-based micromachining techniques. A PMN-PT single crystal plate was electroplated with Nickel as a hard mask for dry etching. After etching, the etched kerfs were filled with epoxy and was lapped. 1500 Å of Cr/Au was sputtered and pattered onto the surface forming annular array electrodes. Conductive backing material was then directly applied onto the electrodes and was separated by an insulating material among the elements. Finally, the un-etched side of the sample was lapped until the desired thickness of 22 µm was achieved, serving as the front surface of the array.

A new interconnection method was proposed for connection from the array element electrodes to micro-coaxial cables. A dielectric substrate was patterned with conductive wires and then a thin insulating layer was spread over it with one opening corresponding each array element. Nickel needles were then electroplated and extruded out from the openings. After alignment, the array transducer was assembled with the electric connection board and the elements were electrically connected to the cables through conductive backing material, nickel needles and embedded wires.

Results

The array transducer was fabricated and was assembled to a electric connection board for testing. Pulse-echo response was measured. The central frequency is 60 MHz with the bandwidth of 50%. Figure 1a shows the pictures of an array. Figure 1b shows the pulse-echo response for a typical array element.

Discussion and Conclusions

A micromachined high-frequency, PMN-PT composite, ultrasonic 2-dimensional array transducer is presented. Preliminary results are promising. Dry etching technique demonstrates great promise in fabricating miniaturized complex shape high-frequency ultrasonic transducers. A new electric interconnection method is proposed for fine pitched array elements to array cables.

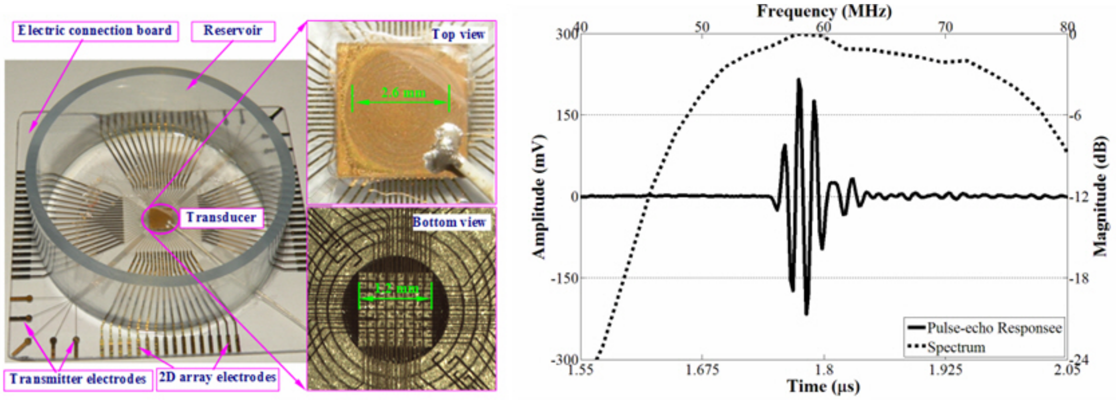

(a) (b)

Figure 1: Micromachined 2-Dimensional ultrasonic array and pulse-echo response for a typical element (a: pictures of 2D array with its closer views of its front and back sides; b: pulse-echo response with the central frequency of 60 MHz and the bandwidth of 50%)

Friday Oral Sessions

1H - CMUT, 3D and Intravascular Imaging Systems

Boca Rooms II-IV

Friday, October 21, 2011, 8:00 am - 9:30 am

Chair: **Stuart Foster**
Univ. of Toronto

1H-1

8:00 AM Seventeen years of CMUTs: A platform technology

B. (Pierre) T. Khuri-Yakub; E. L. Ginzton Laboratory, Center for Nanosale Science and Technology, Stanford University, Stanford CA

The capacitive micromachined ultrasonic transducer (CMUT), in its present most widely used configuration, was first presented at the IEEE International Ultrasonic Symposium in 1994. The last 17 years have seen international adoption of the device and technology, and have seen the realization of CMUT as a platform technology.

This presentation will start with a brief introduction of the CMUT and its merits in comparison to other ultrasound transducers. This will be followed by a summary of the various activities necessary to realize devices: theory (analytic solution, finite element modeling); technology (sacrificial release, direct bonding); modes of operation (conventional, pull-in, permanent pull-in); electronic integration (CMUT on ASIC, flip-chip on ASIC, interposer); packaging (backing, focusing lens); and system integration.

Finally, we present a number of examples of using CMUTs in airborne ultrasound applications such as gas flow (pressure up to 20 atm, and temperature up to 1000 C), non-destructive testing, gravimetric sensing (50 MHz); and immersion application such as medical imaging with ring array catheters, 2-D array for 3-D volumetric imaging, photoacoustic imaging, and high intensity focused ultrasound therapy.

1H-2

8:30 AM Real-time 3D Catheter Localization System Using Ultrasound: Recent in Vivo Results Towards Endovascular Abdominal Aortic Aneurysm Repair

Jay Mung[1], John Moos[2], Fred Weaver[2], Jesse Yen[1]; [1]Biomedical Engineering, University of Southern California, Los Angeles, CA, USA, [2]CardioVascular Thoracic Institute, Keck School of Medicine - University of Southern California, USA

Background, Motivation and Objective

3D localizers are devices that provide the location of tracked objects in 3D space. Surgeons have used localizers for tool guidance in minimally invasive procedures by combining localizer information with anatomical images obtained before or during the procedure. Two types of commercially available surgical localizers are based on optical or electromagnetic (EM) technology. Optical localizers require line of sight between the tool and a set of cameras. Therefore they do not provide a solution for tracking catheters. EM localizers can be prone to error in the presence of metals. This has limited their utility in the operating room. We previously reported an ultrasound based 3D real-time localizer. Here we present recent results towards catheter navigation in the abdominal aorta.

Statement of Contribution/Methods

A single element 3.5 MHz transducer mounted on the catheter transmits a pulse which is received by an array of 7 single element transducers which are placed on the abdomen. A Verasonics system digitizes the signals which provide time of flight measurements to calculate location estimates at 25 Hz. We previously evaluated the system in vitro, showing that the localizer has zero bias and root mean square error as low as 1 mm in water and 3 mm in the presence of tissue and a stent. Here we interfaced the localizer with Slicer3 software for image guided surgery. We report on initial in vivo results deploying an abdominal aorta stent in a porcine model using preoperative CT images.

Results

Preliminary in vivo experience with the ultrasound localizer demonstrated real-time but erratic tracking in the aorta. A vascular surgery resident was able to use the Slicer3 display exclusively to position the delivery catheter. Abdominal aorta explant shows stent deployment within 3 mm of target location (fig).

Discussion and Conclusions

CT images and direct inspection of the abdominal cavity showed bowel gas that likely caused poor signal propagation and thus erratic tracking. Still, tracking was sufficient to navigate the catheter to the target position for stent deployment. Explantation demonstrated that the stent deployment was satisfactorily positioned below the renal arteries. Further in vivo studies are scheduled. The long term goals for this work are to demonstrate feasibility for interventional procedures and show that ultrasound technology may be a viable option for surgical localizer systems.

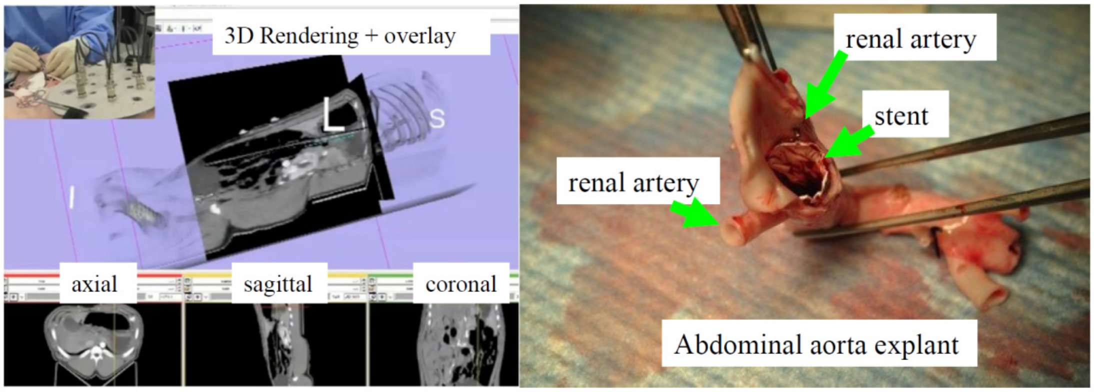

Left: Slicer3 screenshot with preoperative CT data corresponding to catheter location
Left inset: Photo of surgeon placing catheter in porcine model with transducer array
Right: Photo of explant showing renal arteries and stent location

1H-3

8:45 AM A CMUT-based Real-time Volumetric Ultrasound Imaging System with Row-Column Addressing

Albert Chen[1], Lawrence Wong[1], John Yeow[2], Andrew Logan[2]; [1]Systems Design Engineering, University of Waterloo, Waterloo, Ontario, Canada, [2]University of Waterloo, Canada

Background, Motivation and Objective

One of the key design challenges involved in adopting a large 2D array of capacitive micromachined ultrasonic transducers (CMUTs) is how to address the complexity of the front-end analogue electronics. One particular solution would be to use a row-column addressing scheme where only 2N connections are needed for a NXN array instead of N^2. Row-column addressing scheme employs the transmission of a line of focused acoustic pulse in the azimuth direction while receiving a line of beam in the orthogonal direction. The orthogonal relationship allows focusing on the point where the transmitting and receiving lines-of-focus intersect. The CMUT array is fabricated such that each row of elements are connected to a DC bias input and upon toggling of a switch, the row of elements are connected to an output for receiving (i.e. to the digitizer). In addition, each column of elements is connected to a pulser. Due to the simplified connection and circuitry, the size of the front-end electronics can be greatly reduced which correspondingly improves the image reconstruction frame-rate to a large extent.

Statement of Contribution/Methods

In this paper, a 32X32 channel CMUT-based real-time volumetric imaging system built by the AMNDL lab is shown. The CMUTs used were bonded using a silicon-nitride-based wafer bonding process and the arrays are connected such that row-column addressing scheme is allowed. The front-end analogue system is built with off-the-shelf discrete components. The digital-signal processing system is implemented on NI FlexRIOTM FPGA, (NI PXI-7954R), which is designed to conveniently support NI 5752-32-channel-50Mbs digitizer.

Results

The final device has shown pressure at the focal point of slightly above 2 MPa. Furthermore, the system offers dynamic adjustment of aperture through controlling the height of the transducer by feeding in DC bias only to the necessary rows. A sample image depicting four screw heads is shown.

Discussion and Conclusions

From literature review, this is the first time a real-time CMUT-based volumetric imaging with row-column addressing scheme has been demonstrated. With a tolerable loss in image quality, simplified imaging technique such as row-column addressing scheme can provide acceptable quality at a faster frame rate which is desirable in real-time diagnostic such as IVUS/ICE.

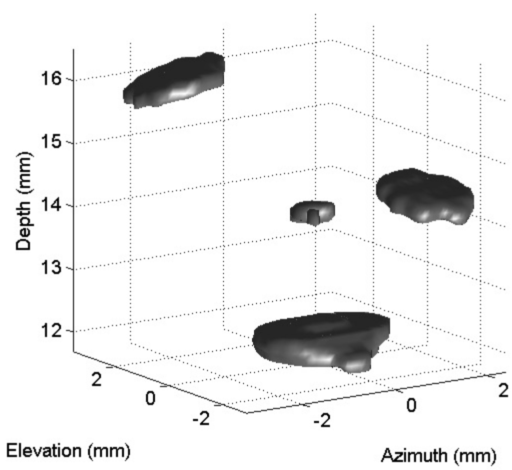

1H-4

9:00 AM Real-time 3D Imaging with a 7.5 MHz Dual-layer Array Transducer – Data Acquisition and Signal Processing

Man Nguyen[1], Yuling Chen[1], Jesse Yen[1]; [1]Biomedical Engineering, University of Southern California, Los Angeles, CA, USA

Background, Motivation and Objective

A 4 x 4 cm2, 7.5 MHz planar dual-layer array has been successfully developed. This array significantly reduces the channel count and fabrication complexity compared to fully-sampled 2D arrays. High frequency (> 5 MHz) 3D imaging can provide more accurate volume measurements, detection of cystic or cancerous masses, and also assist in 3D ultrasound guided biopsy and carotid imaging. We present our work toward real-time 3D imaging with this transducer, including real-time data acquisition with the Verasonics data acquisition system (VDAS) and offline beamforming for volumetric images.

Statement of Contribution/Methods

The transducer consists of 2 separated perpendicular layers of 1D arrays: 1 PZT layer for transmit (Tx) and 1 P[VDF-TrFE]-copolymer layer for receive (Rx). Each array contains 256 elements, and is interfaced with a 4-board VDAS using a set of 128-channel coaxial cable bundle (Prosonics), connecting to 1 scanhead connector (SHC). Since the 4-board VDAS has 2 SHCs, providing 128 Tx/Rx channels each, our setup allows for Tx focusing with 128 PZT elements through 1 SHC and receiving with 128 P[VDF-TrFE] elements through the other SHC. We modified the VDAS sequence program to Tx focus at a depth of 35 mm with a 4-cycle 7.5MHz Tx pulse and with an azimuthal increment of 150 µm. Each Tx event provides an elevational B-scan by beamforming data from128 Rx channels. Azimuthal B-scans and C-scans then can be obtained by selecting corresponding data from the 3D beamformed data. The volumetric frame rate is currently 30 frames/sec with the volume size of 19.2 x 19.2 x 42.2 mm3.

Using this setup, we acquired 3D volumetric data of two custom-made gelatin phantoms. One consists of 5 pairs of 0.1mm-diameter nitinol wire targets and the other consists of an 8-mm-diameter cylindrical anechoic cyst. Generalized coherence factor (GCF) was applied to improve the image quality. Contrast to noise ratios (CNR) and spatial resolution were used as the image quality metrics.

Results

Movies of moving wires and cyst were successfully created. At f# = 3.6, the experimental lateral resolution is 0.88 mm for wires at 35 mm and CNR is 2.9.

Discussion and Conclusions

We have successfully obtained real-time data acquired with Tx focusing and volumetric images. Future work includes implementing the Tx/Rx circuit board to multiplex 512 transducer elements, improving the resolution, CNR, and achieving real-time image display.

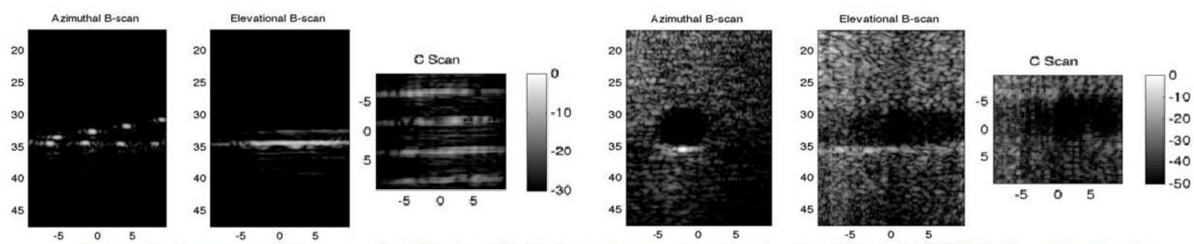

Figure 1. Experimental images of multi-wire (30dB dynamic range) and cyst with GCF applied (50dB dynamic range)

1H-5

9:15 AM Development of a high-definition intravascular ultrasound imaging system and catheter

Kendall Waters[1], Rick Bautista[1], Robert Zelenka[1], Donald Masters[1], Steve Reynolds[1], Steve Nelson[1], Duc Lam[1], Ron Neville[1], Thomas Moore[1]; [1]*Silicon Valley Medical Instruments, Inc., Fremont, CA, USA*

Background, Motivation and Objective

Intravascular ultrasound (IVUS) imaging has been used for over 20 years to facilitate percutaneous coronary interventions. Clinical and investigational uses of IVUS respectively include detection of coronary stent malapposition and thin-cap fibroatheromas. However, current IVUS systems and catheters limit the degree of stent malapposition that can be resolved and are unable to reliably resolve thin fibrous caps. Our goal is to develop a high-definition IVUS system and catheter that is capable of resolving <100 µm stent malapposition and thin (<100 µm) fibrous caps while imaging through a blood pool.

Statement of Contribution/Methods

We have developed an IVUS system and catheter. The catheter includes a mechanically rotating, high-frequency single element transducer. We performed a series of benchtop, in vitro, and pre-clinical studies. We compared pulse-echo measurements off a flat target to two-way excitation responses based on a KLM model. We acquired images of a wire target phantom to evaluate hard-contrast resolution. We performed in vitro imaging of fresh human cadaver diseased coronary arteries. IVUS images were co-registered with histopathology slides. We also performed in vivo imaging of a stented left anterior descending (LAD) coronary artery of an animal model.

Results

A one-dimensional numerical model of our transducer and system agrees reasonably well with experimental pulse-echo measurements, typical results including a center frequency >50 MHz, a fractional bandwidth >50%, and a -20 dB pulse duration <70 ns. We resolved two stainless steel wires having 10 µm diameters with a 50 µm wire separation. Figure 1 shows (A) pulse-echo signal off a flat target, (B) power spectrum of pulse-echo signal in (A), (C) a representative in vitro image of a section of human cadaver diseased coronary artery, and (D) a representative in vivo image of a stented left anterior descending coronary artery of an animal model.

Discussion and Conclusions

An IVUS system and catheter have been developed. Phantom, in vitro human cadaver, and in vivo animal model imaging studies indicate that the system and catheter can provide high-resolution images. In particular, the system and catheter appear to be capable of resolving <100 µm stent malapposition as well as thin (<100 µm) fibrous caps of an atherosclerotic lesion.

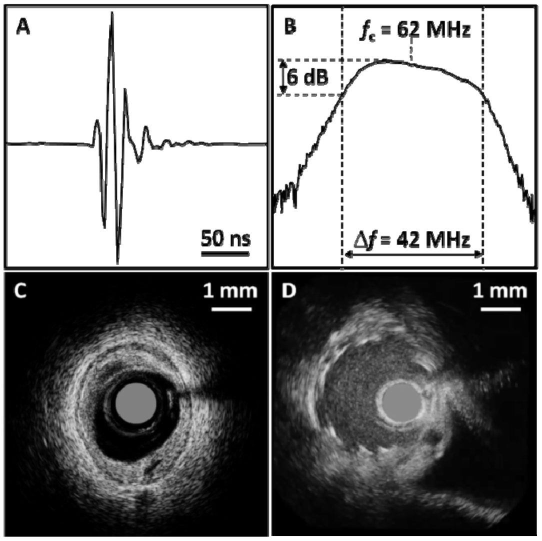
A
50 ns
B
f_c = 62 MHz
6 dB
Δf = 42 MHz
C
1 mm
D
1 mm

2H - Vascular Elastography

Boca Rooms VI-VII

Friday, October 21, 2011, 8:00 am - 9:30 am

Chair: **Stanislav Emelianov**
Univ. of Texas at Austin

2H-1

8:00 AM Strain estimation in the carotid artery from ultrasonic wall tracking: a multiphysics model study

Abigail Swillens[1], Gianluca De Santis[1], Joris Degroote[2], Lasse Lovstakken[3], Jan Vierendeels[2], Patrick Segers[1]; [1]IBiTech-bioMMeda, Ghent University, Ghent, Belgium, [2]Department of flow, heat and combustion mechanics, Ghent University, Belgium, [3]Department of circulation and medical imaging, NTNU, Norway

Background, Motivation and Objective

Non-invasive assessment of (large) arteries is important for cardiovascular screening, with the carotid artery being a preferred measurement location. Ultrasonic (US) wall tracking allows measuring arterial motion and distensibility (~kinematics), but it is unclear to what extent the technique can be used to derive arterial strain (~mechanics).

Statement of Contribution/Methods

We extended our multiphysics simulations (integrating numerical modeling of biomechanics with an ultrasonic simulator (Field II)) to produce synthetic RF-data from blood flow and wall motion in a patient-specific carotid artery embedded in a surrounding tissue. Tissue velocities were estimated with a modified 1D autocorrelation approach. Arterial distension (ΔD) was obtained (from longitudinal scans) in the common and internal carotid (fig 1-A) by tracking paired couples of sample points at 5 equally distributed depths in both the anterior and posterior wall. Circumferential (e_c=ΔD/D) and radial strains (e_r=δΔD/δD) were derived from these data and compared to ground truth (numerical) data.

Results

The coupled simulations provide realistic synthetic US data (see B-mode (1-A) image). At the common carotid, e_c decreases from the intima to the adventitia (see Fig 1-B) with a maximal nominal deviation of 0.4%. However, e_c follows a sigmoidal profile rather than the anticipated monotonic decreasing ($1/D^2$) trend. This error translates into strong deviations in e_r, with maximal nominal deviations of 5.0% (for an average strain of about -5.6%; Fig 1-C). We ascribe these effects to the specular reflections generated on the lumen-intima and media-adventitia transitions (see fig 1-A). In the internal carotid, specular reflections fade (fig 1A), as does the sigmoid shape of e_c. Here, however, errors are induced by the complex 3D motion and non-ideal imaging plane, violating implicit assumptions of axisymmetric deformation of the imaged vessel. Maximal nominal error was 1% for e_c , while e_r differed as much as 6.7% (for a mean value of about -4.9%). We also observed that the phase in the cardiac cycle influences the measurement, with higher wall velocities leading to larger errors.

Discussion and Conclusions

Our data indicate that ultrasonic wall tracking does not allow to derive reliable estimates of –particularly radial - strain in the carotid artery.

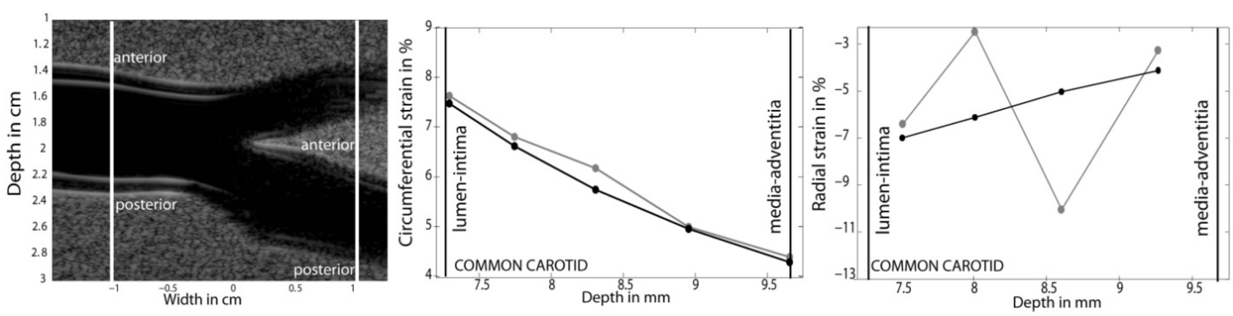

2H-2

8:15 AM In vivo noninvasive multi-angle ultrasound strain imaging of carotid arteries

Hendrik Hansen[1], Gert Jan de Borst[2], Tim Idzenga[1], Suzanne Holewijn[3], Gerard Pasterkamp[4], Richard Lopata[5], Chris de Korte[1]; [1]Clinical Physics Laboratory, Department of Pediatrics, Radboud University Nijmegen Medical Centre, Netherlands, [2]Department of Vascular Surgery, University Medical Centre Utrecht, Netherlands, [3]Department of General Internal Medicine, Division of Vascular Medicine, Radboud University Nijmegen Medical Centre, Netherlands, [4]Department of Experimental Cardiology, University Medical Centre Utrecht, Netherlands, [5]Department of Biomedical Engineering, Eindhoven University of Technology, Netherlands

Background, Motivation and Objective

Rupture of atherosclerotic carotid plaque is a main cause of stroke. Lipid-rich plaques covered by a thin fibrous cap are more prone to rupture than fibrotic plaques. The soft lipids are expected to deform/strain heavily during the pressure cycle. Previously, a noninvasive method was developed to determine the radial strains of the vessel wall using radiofrequency (RF) ultrasound data acquired at multiple beam steering angles. It was tested using phantom experiments. The present study investigates the performance of this multi-angle method in vivo for transverse cross-sections of 5 healthy and 5 severely stenosed carotid arteries. The results are compared to single-angle imaging results and to photographs of the plaque taken after excision.

Statement of Contribution/Methods

RF data of the arteries were recorded for 3 seconds using a Medison Accuvix V10 system equipped with an L5-13 linear transducer (fc = 8.5 MHz) that sequentially stored data for beam steering angles of -26°, 0° and 26° at a frame rate of 129 Hz. 2D displacements were estimated for each steering angle using a coarse-to-fine 2D cross-correlation based algorithm. Projection of the angular axial displacement fields resulted in radial displacements for the multi-angle method. For the single-angle method radial displacements were obtained by rotating the 0° axial and lateral displacement fields. Least squares strain estimation yielded the radial strains. Cumulative strain images were constructed for the diastolic phases of the pressure cycle.

FRIDAY ORAL

Results

In all cases multi-angle imaging provided more accurate strain estimates than single-angle imaging, especially in the regions where lateral information dominated (at 3 and 9 o'clock). For healthy vessels the strains became more circular symmetric which was expected since healthy vessels are homogeneous. For diseased cases multi-angle imaging occasionally revealed strain information that lacked in single-angle images. The images below illustrate this: high strains were observed in a lipid-rich region at 9 o'clock (yellowish in the photograph) which lacked in the single-angle image.

Discussion and Conclusions

These results show that noninvasive carotid strain imaging is possible and promising for detecting lipid-rich plaques. Furthermore, they confirm that multi-angle strain imaging is necessary for accurate strain estimation in the entire vessel cross-section.

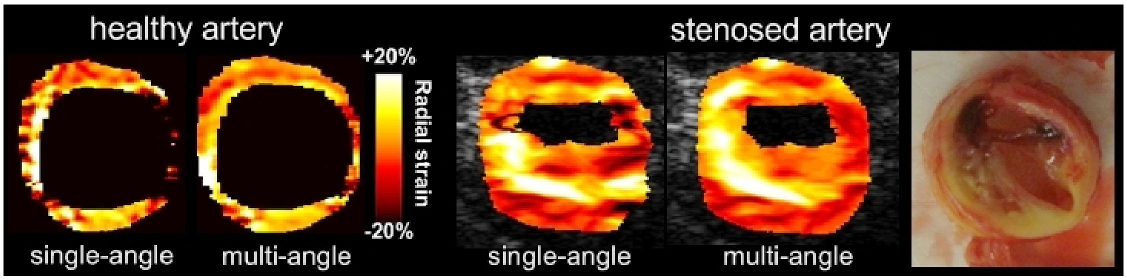

2H-3

8:30 AM Intramural shear strain can highlight the presence of atherosclerosis: a clinical *in vivo* study

Guillaume ZAHND[1], Loïc BOUSSEL[1,2], André SÉRUSCLAT[2], Didier VRAY[1]; [1]Université de Lyon, CREATIS; CNRS UMR 5220; Inserm U1044; INSA-Lyon, France, [2]Louis Pradel Hospital, Radiology Department, Lyon, France

Background, Motivation and Objective

Early detection of atherosclerosis is possible by assessing the mechanical and dynamical properties of the arterial wall, and represents therefore an important issue.

We present here our user-independent framework to estimate the 2D trajectory from ultrasound B-mode sequences of the carotid artery *in vivo*. We also investigate the association between the risk factors of early stage atherosclerosis and several 2D dynamic parameters in a clinical study. The comparative study of the longitudinal Intramural Shear Strain (ISS) represents the major contribution of our work.

Statement of Contribution/Methods

Firstly, the 2D movement of both walls along the cardiac cycle is estimated by our method. The two contour boundaries of the tissue layers, which also describe the radial motion of the walls, are precisely segmented by a dynamic programming approach. From the estimated lumen–intima contour lines, a mesh of kernel blocks is then positioned at different depths within the tissues. The global longitudinal intramural motion is estimated from all the kernels with a pertinent collaboration scheme, through all the covered depth.

Then several 2D dynamic parameters are extracted from the 2D trajectories. The shear index is defined as the ratio between the maximal amplitude of the longitudinal displacement ΔX and the intima-media thickness (IMT). The ISS is described by the attenuation pattern of ΔX within the depth of the tissues.

Results

A clinical study was conducted in which 2 different populations (14 young healthy volunteers and 14 older diabetic patients) were considered. Our method was processed on each sequence (at least 2 cardiac cycles, 29 fps, pixel size 30×30 µm2, 8 blocks of dimension 1.5×0.5 mm2), and the tracking was visually controlled by an expert.

The pathological group presented a significant higher stiffness. The mean shear index of the volunteers and the patients was 104±41% vs 45±24% ($p<0.001$), respectively. The ISS was evaluated from the lumen interface down to 1.5 mm deep in the tissue layers. A distinct pattern is clearly visible between the healthy and pathological carotids (Figure).

Discussion and Conclusions

We presented a robust method to estimate the 2D trajectories of arterial walls in clinical conditions. We also introduced a set of dynamic parameters and studied the ISS, which discriminates with a good accuracy a pathological group from a healthy group.

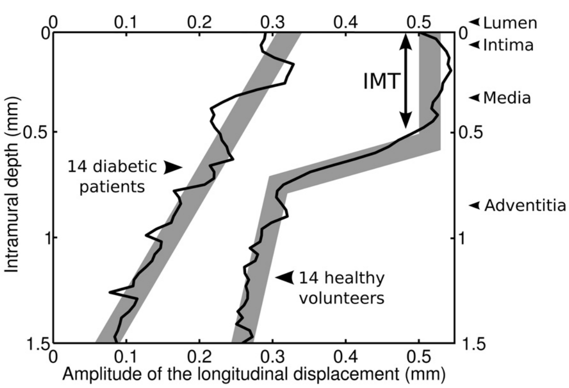

FRIDAY ORAL

2H-4

8:45 AM Feasibility of elastic and compositional characterization of an arterial plaque by dual mechanical strain and thermal strain imaging using a single ultrasound probe

Debaditya Dutta[1], Kang Kim[1,2]; [1]Center for Ultrasound Molecular Imaging and Therapeutics, University of Pittsburgh and University of Pittsburgh Medical Center, USA, [2]Department of Bioengineering, University of Pittsburgh, USA

Background, Motivation and Objective

Vulnerable plaques are often identified with a lipid pool, which is characterized by its mechanical and compositional contrast to the surrounding water bearing tissues. Ultrasound (US) elasticity imaging (UEI) can assess the elastic property by measuring mechanical strain, and US thermal strain imaging (TSI) can determine the lipid contents of the plaque by measuring thermal strain. In this study, the feasibility of dual UEI and TSI using a single US linear array to assess both elasticity and composition of a plaque is demonstrated by in silico simulation and in vitro water tank experiments.

Statement of Contribution/Methods

A numerical tissue thermal model of an arterial plaque under blood flow condition was developed using a finite element (FE) package (COMSOL). An optimized heating beam was designed using US field simulation package (Field II). The designed US beam and tissue thermal model were combined to perform UEI/TSI simulation using a laboratory developed US radio frequency synthesis program. For water tank experiment, an arterial phantom made of polyvinyl alcohol (PVA) with a rubber inclusion seeded with US scatterer was connected to a pulsatile pump. The pressure and US data capturing were synchronized to an external trigger. Two US frames separated by one pulse cycle would exhibit negligible mechanical strain and any strain observed might be attributed to thermal strain. A commercial US probe (6.5 MHz, Sonix TOUCH) was used for both heating and imaging. A standard UEI sequence of 2 seconds was followed by interleaved heating/imaging sequences of total 8 seconds for TSI. 2-D speckle tracking was applied to estimate the mechanical and thermal strains.

Results

In silico TSI image (b) compares well with the FE solution (a), identifying the lipid pool (Panel A) within 8% errors in average strain. Panel B illustrates in vitro (a) B-scan (heating beam shown with dotted lines), (b) TSI with pump on, identifying the rubber inclusion and comparing well with (c) TSI with pump off, indicating successful reduction of motion artifact, and (d) UEI, identifying the rubber inclusion (36.5 kPa) from the surrounding PVA (23.9 kPa).

Discussion and Conclusions

The study demonstrates the feasibility of dual UEI and TSI using a single US probe to simultaneously assess elasticity and composition of the target inclusion. Dual UEI and TSI may be useful to determine the vulnerability of an atherosclerotic plaque.

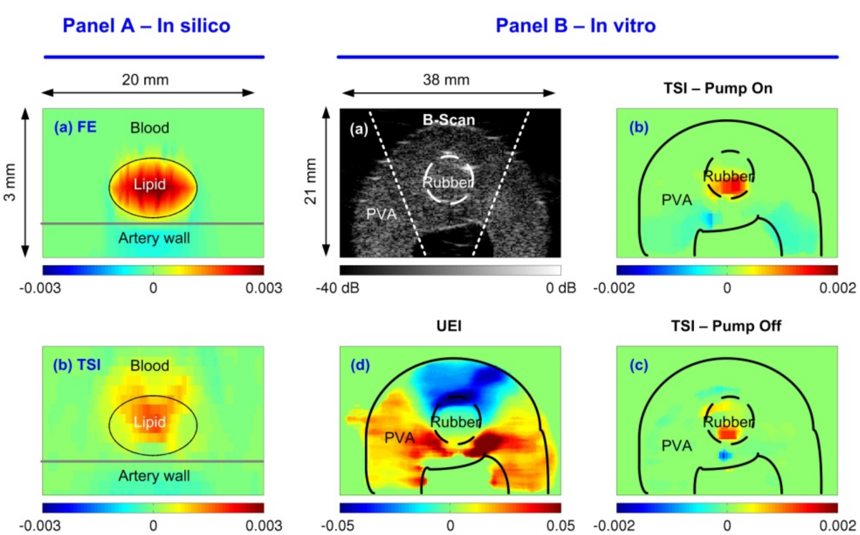

2H-5

9:00 AM Shear Wave Induced Resonance Elastography for Ultrasound Imaging and Mechanical Characterization of Venous Thrombi

Guy Cloutier[1], Cédric Schmitt[1], Anis Hadj Henni[1], Shijie Qi[2]; [1]Laboratory of Biorheology and Medical Ultrasonics, University of Montreal Hospital Research Center, Montreal, Quebec, Canada, [2]Laboratory of Experimental Microsurgery, University of Montreal Hospital Research Center, Montreal, Quebec, Canada

Background, Motivation and Objective

Statistics on venous thromboembolism (VTE) reveal an incidence of 100 per 100,000 persons each year in the United States. About 66% of diagnosed VTE occur in lower limbs where a deep vein thrombus (DVT), usually above the knee, migrates to trigger a pulmonary embolism. Mortality of DVT cases is 6% within one month of diagnosis. Thirty percent of DVT patients will develop recurrent episodes within 8 years, with an associated mortality of 2%. For distinguishing acute from chronic DVT, or more generally to estimate the age of a thrombus, one approach is to determine the mechanical property of the blood clot. In this study, shear wave induced resonance elastography (SWIRE) is proposed for DVT elasticity assessment. This new imaging technique takes advantage of properly polarized shear waves to induce resonance of a confined mechanical heterogeneity.

Statement of Contribution/Methods

Realistic phantoms (n = 9) of DVT total and partial clot occlusions with elasticities from 406 to 3561 Pa were built for in vitro experiments. An ex vivo study was also performed to evaluate the elasticity of two fresh porcine venous thrombi in a pig model. Transient shear waves at 45 to 205 Hz were generated by the vibration of a rigid plate (plane wavefront) or by a needle to simulate a radiation pressure on a line segment (cylindrical wavefront). Induced propagation of shear waves was imaged with an ultrafast ultrasound scanner and a finite element method was developed to simulate tested experimental conditions. An inverse problem was then formulated considering the first resonance frequency of the DVT inclusion.

Results

Elasticity agreements between SWIRE and a reference spectroscopy instrument (RheoSpectris, Montreal, Canada) were found in vitro for total clots either in plane ($r2 = 0.989$) or cylindrical ($r2 = 0.986$) wavefront configurations. For total and partial clots, elasticity estimation errors were $9.0 \pm 4.6\%$ and $9.3 \pm 11.3\%$, respectively. Ex vivo, the blood clot elasticity was 498 ± 58 Pa within the inferior vena cava and 436 ± 45 Pa in the right common iliac vein ($p = 0.22$).

Discussion and Conclusions

The SWIRE technique seems feasible to quantitatively assess blood clot elasticity in the context of DVT ultrasound imaging. This technique is quantitative and may complement qualitative assessment of DVT rigidity with compression-based B-mode ultrasound imaging. An adaptation of the method for in vivo clinical scanning will be discussed.

2H-6

9:15 AM Pulse wave imaging of arteries of healthy subjects and patients with hypertension and abdominal aortic aneurysms

Jianwen Luo[1], Ronny Li[1], Sandhya Balaram[2], Farooq Chaudhry[3], John Lantis[2], Elisa Konofagou[1,4]; [1]Department of Biomedical Engineering, Columbia University, New York, NY, USA, [2]Department of Surgery, St. Luke's-Roosevelt Hospital Center, New York, NY, USA, [3]Department of Medicine, St. Luke's-Roosevelt Hospital Center, New York, NY, USA, [4]Department of Radiology, Columbia University, New York, NY, USA

Background, Motivation and Objective

Pulse wave velocity (PWV) is a significant and independent marker of numerous cardiovascular diseases. Several vascular diseases, such as hypertension, abdominal aortic aneurysms (AAAs) and atherosclerosis, lead to changes in regional aortic wall mechanical properties, resulting in changes in PWV. Pulse wave imaging (PWI) was previously developed by our group to estimate the regional PWV and map the pulse wave propagation along the arterial wall (Luo et al, IEEE TMI 2009, Vappou et al, AJH 2010). In this study, the PWI performance in healthy human subjects, hypertensive patients and patients with AAAs is evaluated.

Statement of Contribution/Methods

The abdominal aortas of 10 healthy, 7 hypertensive and 5 AAA subjects were scanned with a curved linear array at 3.3 MHz (Sonix RP, Ultrasonix, Burnaby, Canada). The beam density of the 2-D echograms was reduced to 24 beams in a 60Â° sector in order to obtain a high frame rate of 180-350 Hz. The common carotid arteries of 5 healthy volunteers were also scanned with a 10-MHz linear array (SonixTOUCH, Ultrasonix) at a beam density of 16 beams within 38 mm and a frame rate of 1127-1284 Hz. The RF data were sampled at 20 MHz. The arterial wall velocities were estimated from the RF data from a 1-D normalized cross-correlation-based, real-time motion estimation method using sum tables (Luo and Konofagou, IEEE TUFFC, 2010). The sequences of 2-D wall velocity images and the spatiotemporal images of the wall velocities accurately depicted the propagation of the pulse wave along the arterial wall. The regional PWV was then estimated from the linear regression fit of the spatiotemporal plot of the pulse wave. The correlation coefficient of the linear fit was also used to indicate the uniformity of the pulse-wave propagation.

Results

In healthy subjects, the PWV was 5-8 m/s in the abdominal aortas and 4-6 m/s in the common carotid arteries. The propagation of the pulse wave was relatively uniform, with a correlation coefficient higher than 0.95, indicating homogenous mechanical properties. In the hypertensive subjects, the correlation coefficient was lower (0.6-0.8) while the PWV in the abdominal aortas was higher (7-12 m/s), indicating higher inhomogeneity than in the normal aortas and stiffening of the abdominal aortas. In subjects with AAAs, the correlation coefficient was much lower (<0.6), suggesting highest vascular inhomogeneity. Therefore, the estimation of PWV in the abdominal aortas exhibited higher variability (6-20 m/s). Peak wall velocities along the aortas were also highly nonuniform, with significantly lower values (0.3-0.8 cm/s) near the saccular region of the AAAs than in the proximal and distal regions (0.7-2.2 cm/s).

Discussion and Conclusions

The PWI technique was shown providing qualitative and quantitative information on the underlying arterial wall inhomogeneity and mechanical properties, and may thus be used as an early detection tool of vascular degeneration. (This work was supported in part by NIH R01HL098830.)

FRIDAY ORAL

3H - Drug Delivery I

Carribean Ballroom VII

Friday, October 21, 2011, 8:00 am - 9:30 am

Chair: **Tom Matula**
Univ. of Washington

3H-1

8:00 AM Dual-Frequency Ultrasound-Mediated Delivery of Rapamycin from Microbubbles Decreases Drug Dose Needed to Reduce Neointima Formation *In Vivo*

Linsey C. Phillips[1], Ali H. Dhanaliwala[1], Alexander L. Klibanov[1,2], Brian R. Wamhoff[2,3], John A. Hossack[1,3]; [1]Dept. of Biomedical Engineering, University of Virginia, USA, [2]Dept. of Medicine - Cardiovascular Division, University of Virginia, USA, [3]R.M.Berne Cardiovascular Research Center, University of Virginia, USA

Background, Motivation and Objective

Non-stent-elution strategies for drug delivery to diseased arteries offer increased control over therapy dose and localization of drug uptake. We have demonstrated local reduction of cells responsible for arterial narrowing (neointima) via delivery of the anti-proliferative drug rapamycin from microbubbles (MBs) by applying 1 MHz ultrasound (US). Our hypotheses are that 1) neointimal formation in a rat carotid balloon injury model is reduced following ultrasound mediated *in vivo* delivery of rapamycin loaded MBs (RMBs), and 2) the combination of radiation force US with focused 'burst' US will decrease the total amount of drug needed to reduce neointima formation.

Statement of Contribution/Methods

MBs generated from phosphatidylcholine and polyethylene glycol stearate contained 29ng of rapamycin per million MBs (or trace amount of DiI for control MBs). Rats underwent carotid balloon injury to induce neointima formation. After injury, a 5 MHz linear array transducer was aligned above the injured artery and programmed to emit 5 cycle, 1.5 MPa (PNP) 'burst' pulses at a PRF of 5 kHz for 3 seconds, paused for 2 seconds, and repeated for the total 8 minute exposure. A model of radiation force US (Dayton et al) was used to select acoustic parameters necessary for pushing MBs out of arterial blood flow without MB rupture. A second, unfocused 1 MHz transducer was concurrently aligned with the injured artery at a 45 degree angle and emitted continuous, 1MHz, 65 kPa (PNP) radiation force US. RMBs at high ($1x10^9$) or low ($1x10^8$) dose were infused through a left jugular vein catheter over 5 minutes. The dual US was applied during infusion plus an additional 3 minutes. Control rats received high or low dose RMBs with or without US. Rats which received RMBs were euthanized 2 weeks after insonation ($n \geq 6$ rats per group). Rats which received DiI MBs ($1x10^9$), with no US, burst US only, or dual US, were euthanized 1 hour after insonation.

Results

DiI delivery was enhanced 3.4 fold in arteries which received burst US ($p < 0.001$). The addition of radiation force US enhanced delivery 1.9 fold over burst US alone, but not significantly ($p = 0.09$). Neointima to media ratios (NI/M) of injured carotid arteries exposed to the high dose of RMBs were reduced by 34.9% and 28.7% ($p < 0.001$) with and without dual US application respectively. Among injured arteries exposed to the low dose of RMBs, NI/M was significantly reduced (by 35.9%, $p<0.001$) only in those treated with US. TUNEL staining revealed no difference in cell death between groups treated with or without US, or RMB.

Discussion and Conclusions

The results suggest that dual frequency US combined with RMB significantly reduces NI formation, and that with US, 1/10 of the dose is sufficient to achieve equal therapeutic effect. This therapy has promise for reducing neointima formation locally using only a fraction of the dose, thereby possibly enabling the use of smaller doses of a more potent drug.

[Funded by NIH HL90700]

3H-2

8:15 AM Potentiating the effects of docetaxel (Taxotere) with ultrasound stimulated microbubbles

David Goertz[1,2], Margarita Todorova[2], Omid Mortazavi[2], Xuan Huo[2], Raffi Karshafian[3], Kullervo Hynynen[1,2]; [1]Medical Biophysics, University of Toronto, Canada, [2]Imaging Research, Sunnybrook Research Institute, Toronto, Canada, [3]Ryerson University, Canada

Background, Motivation and Objective

Docetaxel (Taxotere) is a chemotherapeutic agent in widespread use for a broad spectrum of cancers (breast, prostate, head and neck). At lower dose levels it exhibits antivascular effects through polymerizing endothelial cell microtubules. In recent work we demonstrated that clinically viable concentrations of microbubbles can, at relatively low intensities, cause vascular damage in tumours, shutting down blood flow and inducing growth delays in a prostate tumour models. The objective of this study was to investigate a possible interaction of the antitumor effects of US stimulated microbubble induced vascular damage and docetaxel.

Statement of Contribution/Methods

Tumor growth inhibition studies were performed with the PC3 prostate cancer xenograft model. The four experimental groups were: control, drug (docetaxel), US+MBs, and combined US+drug+MBs (n=4-6 per group). Docetaxel was administered intravenously in the form of a bolus injection 10 minutes prior to US exposure. Treatments were performed on a weekly basis for a total of 4 weeks. The US treatment scheme (1MHz, 860 kPa) consisted of a series of fifty 100 microsecond bursts sent at 1ms intervals, repeated at 20s intervals for a duration of 3 minutes following the bolus injection of an experimental contrast agent (Artenga, Ottawa, Canada). These conditions were found to induce inertial cavitation. Blood flow within the tumors was monitored during the experiments with an imaging transducer operating in contrast mode.

Results

Exposures with US were observed to produce a flow shutdown within tumors. Control tumours grew rapidly and by the 3-4 wk point began to require sacrifice due to tumor burden (>700 mm3). US-only and drug-only tumors had modest but not significant growth delays relative to controls and began to require sacrifice due to tumor burden by week 5. The combined US and drug group had a significantly reduced growth rate and began to reduce in size after week 3 until the study endpoint at week 7. Experiments are continuing to examine longer term effects.

Discussion and Conclusions

The results indicate that the antivascular effects of US stimulated microbubbles potentiate the effects of docetaxel to achieve markedly improved antitumor effects.

FRIDAY ORAL

3H-3

8:30 AM Effects of Acoustic Parameters on Sonothrombolysis with Contrast Microbubbles

Bénédicte Petit[1,2], Emmanuel Gaud[1], **Marcel Arditi[1]**, Feng Yan[1], Peter Frinking[1], Eric Allémann[2], François Tranquart[1]; *[1]Bracco Suisse SA, Switzerland, [2]School of Pharmaceutical Sciences, U. Geneva, U. Lausanne, Switzerland*

Background, Motivation and Objective

Bubble-mediated sonothrombolysis is a promising approach for treating acute ischemic stroke (AIS), as shown by in vitro and in vivo studies. The objective of this work is to elucidate the complex mechanisms at play during lysis, in a variety of acoustic conditions and concomitant use of rtPA, ultrasound and microbubbles. The end-point is the identification of optimal conditions for future clinical use.

Statement of Contribution/Methods

Clots were obtained from incubated human blood and imaged optically, every 5 min in the course of 60 min ultrasound exposures, including the use of microbubbles and rtPA. Diameter profiles were estimated from images using an ad hoc Matlab program. Exposures of p-neg 150-1000 kPa were applied with a focused, single-element transducer, at 1.6 MHz and 33% duty cycle, perpendicular to the clot (n=5). The complex diameter profiles were interpreted with the aid of a model, implemented in Matlab, based on simple assumptions accounting for the effects of the ultrasound beam profile and local bubble concentration (including destruction and replenishment of bubbles during exposure). The model parameters were tuned to match the observed diameter profiles.

Results

The spatial distribution of diameter loss could be directly correlated to the ultrasound beam profile for pressure amplitudes < 300 kPa. For higher amplitudes, lysis increased and the effects of bubble destruction and replenishment of fresh bubbles resulted in complex lysis patterns. An example at 600 kPa is shown in the Figure below, along with the pattern obtained from the model. The highest rate of lysis observed was approx. 6 µm/min.

Exposed and control thrombi were imaged by SEM, which provided insight into the mechanisms at play on fibrin rupture and clot erosion.

Discussion and Conclusions

The results of this study indicate that intermediate acoustic pressures of 300-600 kPa are preferable; at lower values, little or no effects are seen; at higher values, bubble destruction hinders the in-flow of fresh bubbles and sonothrombolysis is less efficient. Furthermore, the SEM observations bring direct evidence of the mechanical action of microbubbles during insonation. Optimization of acoustic and/or rtPA conditions for in vivo applications remains a challenge; but information obtained in vitro represents a small step towards a successful application of sonothrombolysis in the clinical management of AIS.

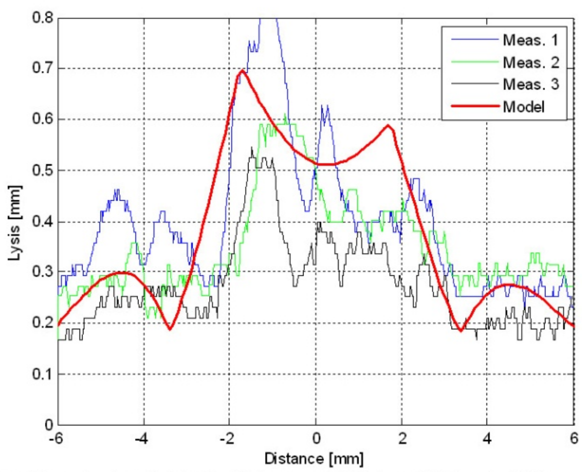

Figure: Diameter loss (in mm) in 3 clots after 60 min exposure, 1.6 MHz beam at 33% duty cycle, 600 kPa $_{p\text{-}neg}$ centered at 0 mm, in presence of 0.3 µg/mL rtPA and microbubbles circulating (left to right) at 45 mm/s

3H-4

8:45 AM Sonoporation-dependent cytotoxicity with toxins subunit

Olivier Couture[1], Estelle Dransart[2], Marine Thiebaud[2], Ludger Johannes[2], Mickael Tanter[3]; *[1]CNRS / ESPCI, France, [2]Institut Curie, France, [3]INSERM, France*

Background, Motivation and Objective

Ideal candidates for tumor-resection exploiting sonoporation would be highly cytotoxic drugs that are incapable of crossing the cell membrane spontaneously. Hence, a cytotoxic effect would be exclusively present at the focus of the ultrasound, which can be controlled with a submillimetric resolution. Existing chemotherapeutic drugs are generally membrane permeable. We therefore turned to the A-subunit of the plant toxin ricin (RTA) as a candidate sonoporation-activated drug. RTA inactivates ribosomes in the cytosol, but lacks the B-subunit which allows the holotoxin to penetrate the cell on its own. Our objective is to exploit the inability of RTA to cross the cell membrane spontaneously to localize cell mortality due to sonoporation only in the target site. Additionally, the experiments compare the sonoporation induced respectively by non-specific and targeted microbubbles.

Statement of Contribution/Methods

Biotinylated STxB, a ligand for the glycolipid Gb3 often present on cancer cells, was incubated at saturating concentrations with avidin-functionalized microbubbles (Bracco Research). Cervix cancer cells C2TA were grown in Opticell culture plates to express, or not, Gb3. STxB-functionalized microbubbles were incubated with the cells for 20 minutes and washed. RTA was then injected within the plates at low concentrations (1ug/mL). The plates were mounted perpendicularly to the axis of a 500 kHz single-element transducer (25 mm focus), which generated 4 cycle pulses at 3 kHz pulse-repetition frequency with peak-negative pressures varying from 0 to 400 kPa for 30 seconds. The surviving cells were counted under microscopy 24 hours after sonoporation.

FRIDAY ORAL

Results

Adherent cells show no significant mortality induced by RTA only (p=0.22). When the majority of the cells lack the target (Gb3-) and in the absence of RTA, sonoporation at maximum pressure (372 kPa) can kill up to 10% of the cells. In the presence of RTA, non-specific microbubbles do not cause additional mortality compared to this baseline. When targeted microbubbles are combined to RTA, mortality is increased to 73% with a threshold at 200 kPa peak-negative pressure.

Discussion and Conclusions

Sonoporation can be exploited to kill cancer cells in-situ with minimal side effects due to its threshold behavior and the low toxicity of RTA outside of the targeted site. Moreover, the effect is enhanced with targeted microbubbles

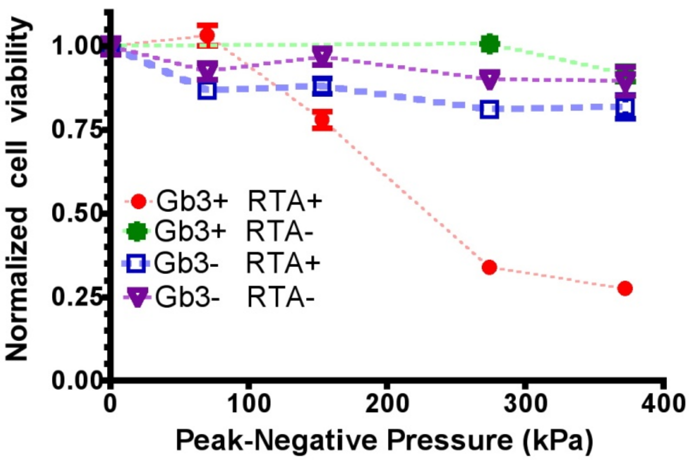

3H-5

9:00 AM Investigating the Interaction Between Acoustically Activated Microbubbles and Fibrin Clots

Christopher Acconcia[1,2], Kullervo Hynynen[1,2], David Goertz[1,2]; [1]Medical Biophysics, University of Toronto, Toronto, Ontario, Canada, [2]Sunnybrook Health Sciences Centre, Toronto, Ontario, Canada

Background, Motivation and Objective

Ultrasound (US) stimulated microbubbles (µBs) are under investigation to promote thrombolysis in the presence and absence of injected enzymes. Despite considerable work to date, the mechanisms by which µBs degrade clots are poorly understood. Blood clots are composed of platelets and red blood cells enmeshed in a fibrin network to which it owes its mechanical integrity and is the target of lytic agents. Clots formed from purified fibrin have been used extensively in thrombolysis drug studies and have the advantage of being nearly optically transparent. The objective of this work was to gain a more fundamental understanding of how acoustically activated µBs interact with fibrin clots, to aid in guiding exposure schemes and contrast agent design to enhance sonothrombolysis.

Statement of Contribution/Methods

Fibrin clots were formed in a chamber with a channel to permit the introduction of contrast agent (Definity®) at clinically viable concentrations. The chamber was situated under a microscope equipped with fluorescent and fast frame cameras (~10kHz). US was applied with a focused transducer (f-# 1) at 1 MHz with 1-4 ms pulse durations over a range of pressures (0.02-2.5 MPa). 200nm fluorescent beads were used to delineate the fluid/clot boundary during and after exposure under widefield and confocal fluorescent microscopy, respectively.

Results

It was found that uBs could readily penetrate into fibrin clots, to a depth related to pulse duration (Figure). At lower pressures (0.27-0.56 MPa), µBs as small as 3µm were observed to penetrate whereas higher pressures (>0.9 MPa) caused the penetration of larger µBs (10-30µm), formed by coalescence prior to entry. In some cases, the path behind penetrating µBs remained patent, an effect termed tunneling. Tunnel diameters ranged between 9-35µm depending on pressure and pulse duration. Confocal microscopy was used to visualize fibrin structure, and indicated paths of disrupted fibers consistent with collapsed tunnels. Fluid flow within the gel was observed to accompany penetrating µBs, which may have implications for lytic enzyme penetration.

Discussion and Conclusions

These results provide direct evidence that µBs can disrupt and penetrate fibrin networks, the primary structural component of thrombus. This approach has relevance in the design of pulsing schemes and determining appropriate µB sizes to perform sonothrombolysis.

FRIDAY ORAL

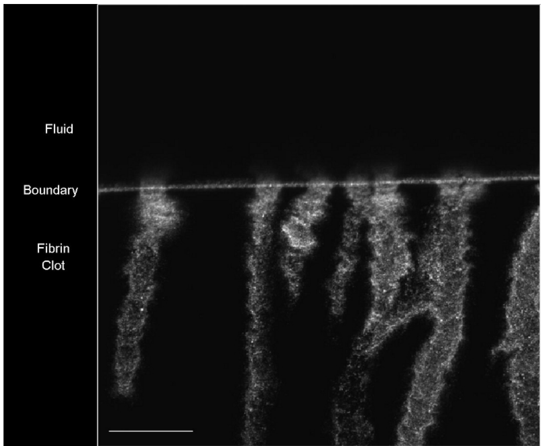

Figure : Confocal microscopy of tunnels generated in fibrin clot using Definity microbubbles at 2500 dilution ratio, 4 ms pulse duration and 2 MPa. Scale bar indicates 100µm.

3H-6

9:15 AM Evaluation of doxorubicin-containing microbubbles for ultrasound-triggered delivery

Jean-Michel Escoffre[1], Bart Geers[2], Ine Lentacker[2], Ayache Bouakaz[1]; [1]Inserm U930, CNRS ERL 3106, université François Rabelais de Tours, France, [2]Laboratory of General Biochemistry and Physical Pharmacy, Ghent University, Belgium

Background, Motivation and Objective

Doxorubicin (Dox) is a potent chemotherapeutic whose severe side effects limit its application. Microbubble-assisted ultrasound has become a promising strategy for non-invasive local drug delivery to increase the drug concentration locally and to reduce systemic side effects. The aim of this study is to evaluate the effectiveness of administration of Dox-liposomes loaded on microbubbles (MB) combined with ultrasound in human U-87MG glioblastoma cells.

Statement of Contribution/Methods

Dox-loaded liposomes containing DSPE-PEG-Maleimide and C4F10 gas were added to vials containing: DPPC and DSPE-PEG-SPDP dissolved in a glycerin:propyleneglycol:H20 mixture and were mechanically activated using a CapmixTM device. This activation gives rise to C4F10 lipid-shelled MBs loaded with liposomes. The liposomes become coupled to the MBs' surface through covalent thiol-maleimide linkages. Experiments were carried out with free Dox or Dox-loaded MBs (final concentration of Dox, 3 µg/mL) on a cell suspension of U-87MG cells. Ultrasound waves were transmitted at 1 MHz frequency with a pulse repetition period of 100µs, 40 cycles per pulse and for 30s. Cell viability was evaluated by Trypan blue assay 24h and 48h later.

Results

Using Dox alone, the cell viability was 63±3% and 26±2% at 24h and 48h later, respectively. The combination of ultrasound at 600 kPa and Dox-loaded MBs induced a 2.5-fold decrease of cell viability compared to the incubation of Dox-loaded MBs alone at 24h and 48h after treatment, respectively. At 24h, this combination was 3 times more efficient than the doxorubicin treatment on its own.

Discussion and Conclusions

The conclusions drawn from this in-vitro study show the potential of this strategy for a controlled, efficient, and safe drug delivery. Indeed, the encapsulation of doxorubicin into liposomes and the ultrasound-triggered delivery would allow reducing the therapeutic dose and the side effects of doxorubicin.

Project funded by the EU Project SONODRUGS (NMP4-LA-2008-213706).

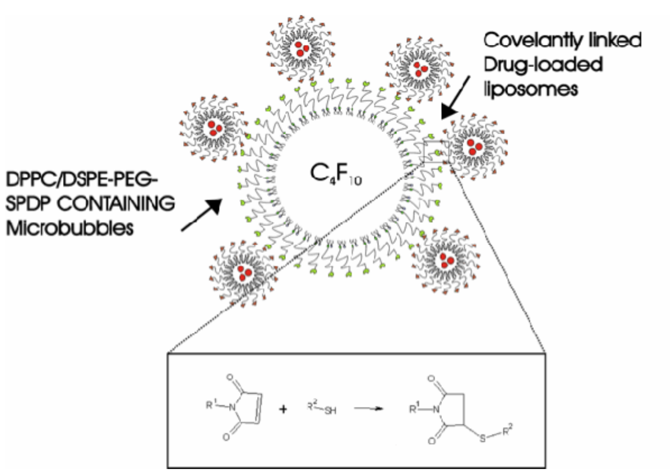

4H Laser Ultrasonics

Carribean Ballroom I

Friday, October 21, 2011, 8:00 am - 9:30 am

Chair: **R. Addison**
Rockwell Science Center, USA

4H-1

8:00 AM Three-dimensional Crack Depth Profile Assessment using Near-Field Surface Acoustic Wave Signal Response

James Blackshire[1]; [1]AFRL/RXLP, Air Force Research Laboratory, Wright-Patterson AFB, Ohio, USA

Background, Motivation and Objective

It has long been the goal of quantitative nondestructive evaluation (QNDE) to characterize key features of cracks such as length, depth, aspect ratio, and orientation. Recent advances in ultrasonic sensor probes, practical numerical models, and innovative analysis methods have led to capabilities for crack characterization with significantly improved measurement capabilities and accuracies, where the 2-D and 3-D reconstruction of cracks and other damage features is becoming possible.

Statement of Contribution/Methods

A method for determining the three-dimensional crack depth profile of a surface-breaking crack is presented based on near-field surface acoustic wave signal responses. Three-dimensional finite element models were used to study the forward problem, where the characteristic near-field scattering of a surface acoustic wave incident on a surface-breaking crack was investigated. Experimental validation of the modeling predictions was accomplished using a wedge transducer for surface wave generation and a scanning laser vibrometry system for surface wave detection.

Results

The characteristic near-field amplitude response in reflection and in transmission was measured and modeled for flat-bottom, angled, and curved-bottom localized notch features and for realistic surface-breaking cracks. A simple linear inversion method was developed, which provides an effective means for characterizing and mapping the three-dimensional depth profile of surface-breaking crack features with depths in the micron to millimeter range.

Discussion and Conclusions

The use of forward numerical models, point-wise detection, and inverse method development have been combined to provide a means for quantifying the local crack depth of a surface-breaking crack.

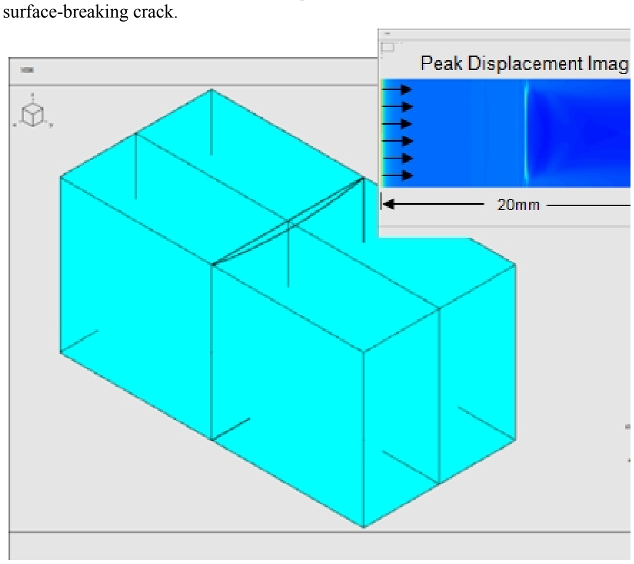

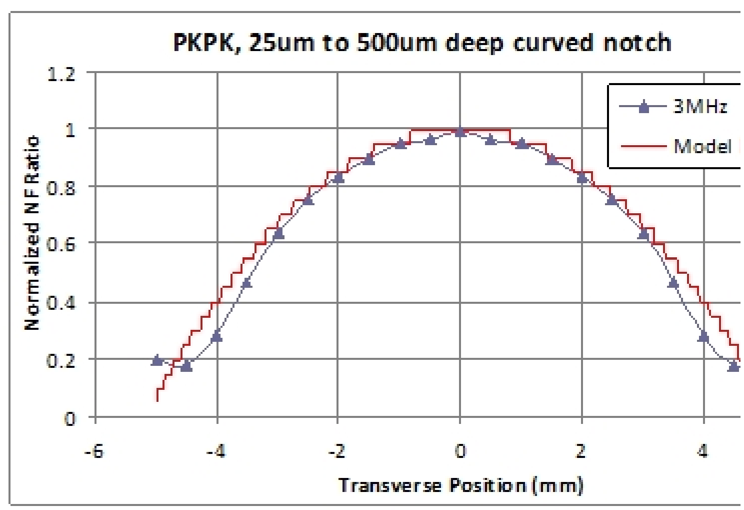

4H-2

8:15 AM Material characterization of thermally sprayed nickel aluminum coatings using a laser ultrasound technique

Cheng-Hung Yeh[1], Che-Hua Yang[1], Cherng-Yuh Su[1], Wei-Tien Hsiao[2]; [1]Graduate Institute of Manufacyuting Technology, National Taipei University of Technology, Taiwan, [2]Material and Chemical Research Laboratories, Industrial Technology Research institute, Taiwan

Background, Motivation and Objective

Nickel-aluminum alloy coatings produced by the thermal spraying process exhibit a wide variation in mechanical properties. Sources influencing the coating properties include the contents of powder material and the processing parameters used in the spraying process. Therefore, characterization of mechanical properties of Ni-Al alloy coatings is an important task. This research aims at nondestructive characterization of thermal spraying coatings.

Statement of Contribution/Methods

A laser ultrasound technique (LUT) is used for the measurements of guided waves dispersion. Theoretical model for surface waves propagating along a multi-layered structure with coating and substrate is used to model the dispersion spectra. An inversion algorism based on shuffled complex evolution (SCE-UA) method is used to extract mechanical properties from the measured dispersions.

Results

Fig. 1 shows three sets of surface wave dispersions measured for three different coatings, namely ANi, ANiBNb, and ANiBNm, which correspond to different sprayed powders and/or powder processing like mixing or balling. Also, Fig. 2 shows calculated theoretical dispersions for surface waves propagating on substrate with coatings of various elastic properties.

Discussion and Conclusions

The method employing LUT and inversion algorism is potentially useful to characterize the mechanical properties of thermal spraying coating in a nondestructive way.

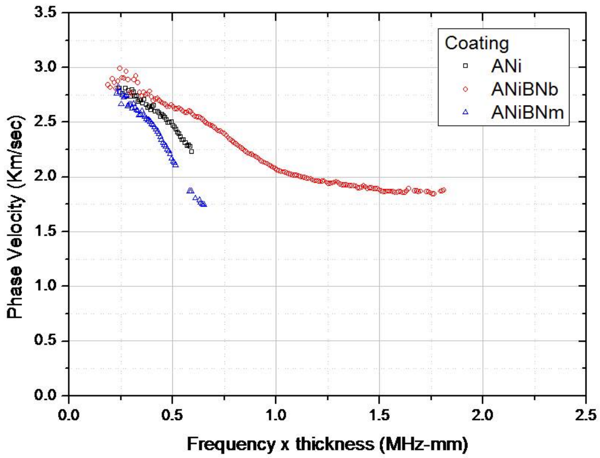

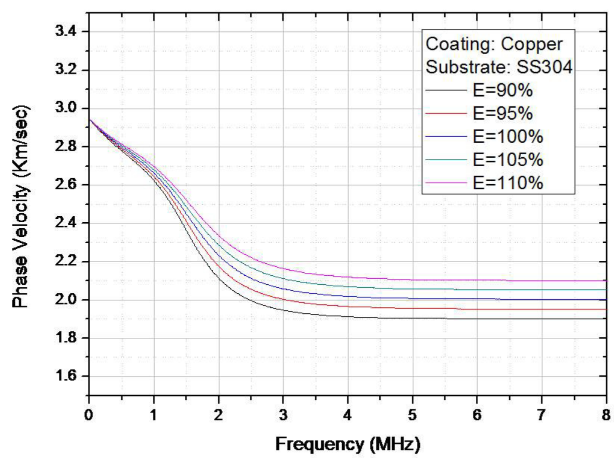

4H-3

8:30 AM Guided waves propagating in plates with temperature gradients

Sheng-Po Tseng[1], Che-Hua Yang[1]; [1]Graduate Institute of Manufacturing Technology, National Taipei University of Technology, Taipei, Taiwan

Background, Motivation and Objective

For the high-power LED, the influence of internal temperature is an important factor of the luminous efficiency and the product lifetime. The internal temperature of high-power LED has gradient distribution due to the multilayered package. This paper focuses on the modeling and measurements on the propagation behaviors of guided waves propagating along plate-like wave guides with temperature gradients along their thickness direction.

Statement of Contribution/Methods

A theoretical model based on recursive asymptotic stiffness matrix (RASM) method with multilayered configuration accommodating temperature gradient profiles is shown in Fig. 1. The RASM model is used to model the dispersion curves of the waveguides with various temperature gradients. Measurements are also conducted using a laser ultrasound technique (LUT). By measuring the dispersion spectra and back-calculating the temperature with inversion algorism, the temperature gradient distribution can be indirectly obtained.

Results

Fig. 2 shows the calculated dispersion spectra for a steel plate with three different temperature distributions, two for uniform distribution and one for temperature gradient. Measure med dispersion spectra are obtained with the laser ultrasound technique in a non-contact manner at elevated temperatures.

Discussion and Conclusions

This method is proved to have better accuracy for plate-like structures with lower thermal conductivity. However, applications for structures with higher thermal conductivity will be also applicable while the measurement accuracy is further improved.

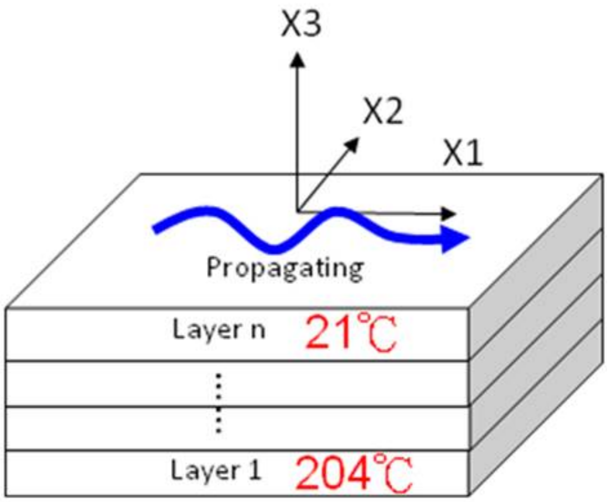

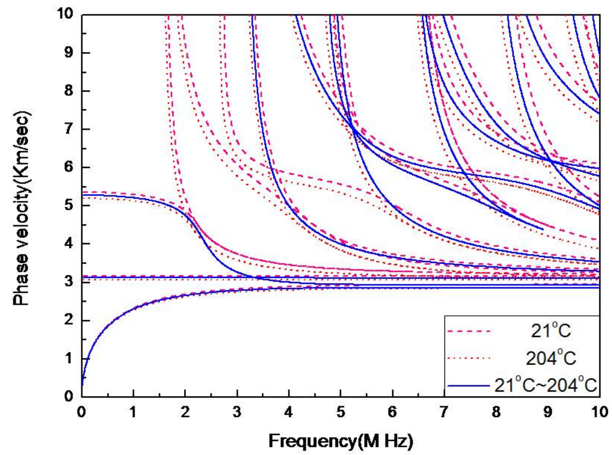

4H-4

8:45 AM Measuring Crystal Orientation by Resonant Ultrasound Spectroscopy

Farhad Farzbod[1], David Hurley[1]; [1]*Idaho National Laboratory, USA*

Background, Motivation and Objective

Resonant Ultrasonic Spectroscopy (RUS) is a technique to characterize the elastic and anelastic properties of materials. It is based on the measurements of the vibrational eigenmodes of a sample with simple geometry such as a parallelepiped. In conventional RUS, a specimen is held between two piezoelectric transducers, one for excitation and the other for detection. The excitation frequency is swept through a wide range. The resonant frequencies measured by the detection transducer represent eigenfrequencies of the specimen. Comparing the measured and calculated eigenfrequencies enables calculation of the complete elastic stiffness tensor. Much information with regard to the microstructural state of the sample can be extracted from the stiffness tensor. This includes the crystallographic orientation of a single crystal material. However, this approach which relies solely on eigenfrequencies is prone to error for elastically anisotropic samples.

Statement of Contribution/Methods

Laser-based RUS can measure eigenfrequencies and eigenvectors and offers an appealing alternative to methods that employ contact transducers. This approach utilizes a pulse laser to thermoelastically excite ultrasound and a photorefractive interferometer to detect ultrasound. By raster scanning the probe along the sample surface, the mode shapes (i.e. eigenvectors) of the individual eigenmodes are formed. These mode shapes along with the eigenfrequencies enable us to accurately calculate the crystallographic orientation of the sample. This technique measures the crystallographic orientation of the bulk sample. In contrast, electron and X-ray diffraction techniques require one to extrapolate the bulk orientation from that of the near surface region.

Results

Experiments have been performed on a high purity single crystal copper sample. Theoretical mode shapes were calculated for various crystallographic orientations. The crystallographic orientation was computed by comparing theoretical and experimental mode shapes. The computed angle is shown to be in a very good agreement with the angle obtained using electron backscatter diffraction.

Discussion and Conclusions

Comparing experiment and theory. (a) Experimental mode shape corresponding to a single crystal copper sample at a frequency of 528 KHz. (b) Corresponding theoretical mode shape for a 13o rotation about the surface normal.

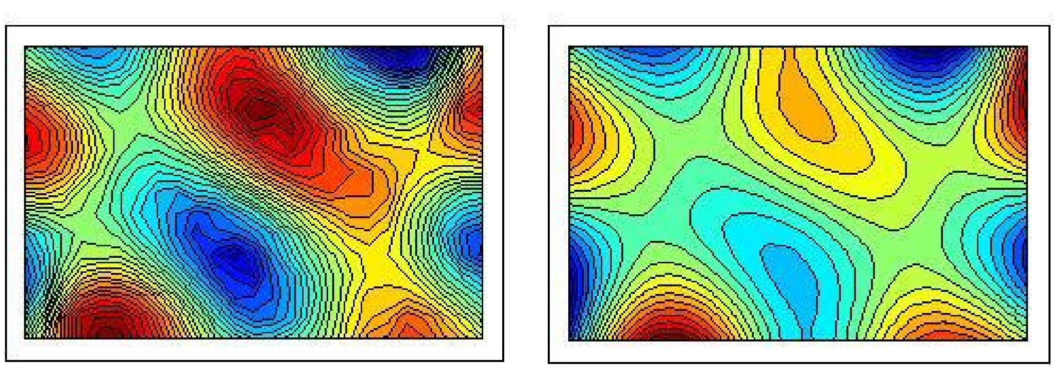

a b

4H-5

9:00 AM Laser ultrasound technique for ray tracing investigation of Lamb wave tomography

Chia Han Wu[1], Che Hua Yang[1]; [1]Graduate Institute of Manufacturing Technology, National Taipei University of Technology, Taipei, Taiwan

Background, Motivation and Objective

The technology involved with Lamb wave tomography (LWT) are continuously been developed for the purpose of various inspections. While Lamb wave data are collected for a large number of specific pitch-catch measurements surrounding interesting region, the image of this region can be reconstructed tomographically. Previous researches emphasized more on the image reconstruction algorithm to discuss the scattering, refractive media and abrupt change in wave velocity. In this research, it is focused in improving LWT image reconstruction method based on a laser ultrasound visulization (LUV) technique.

Statement of Contribution/Methods

In this paper, an iteration reconstruction technique (SIRT) is utilized to reconstruct the LWT image. In the meanwhile, a laser ultrasound visualization technique is employed to collect pitch-catch signals and obtain the Lamb propagating path. The reconstructed image with SIRT is compared with the LUV image for quantitative comparisons for the purpose of improving the reconstruction algorism.

Results

Fig. 1 shows an LUV image in a copper plate with three defects. Also, ray paths of Lamb waves is simulated as straight ray with the SIRT to reconstruct the Lamb wave tomography image as shown in Fig. 2. With this algorism, the velocity map can be obtained quantitatively as well.

Discussion and Conclusions

Tomography reconstruction method for ray tracing with the SIRT algorism is successfully employed to track the defect locations which are verified with laser scanning technique. The laser visualization images provide comparisons to modify the tomography reconstruction algorism or ray tracing algorithms for more supplicated conditions such as refractive or scattering media.

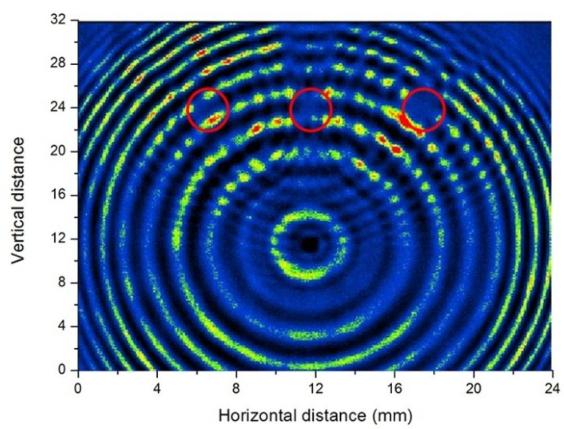

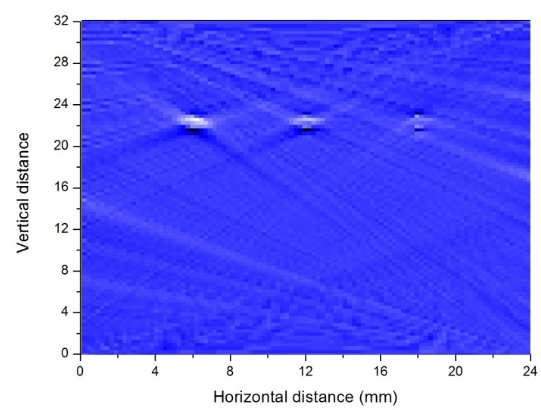

4H-6

9:15 AM Multi-channel random-quarature receiver for industrial laser-ultrasonics

bruno pouet[1], alexis wartelle[1], sebastien breugnot[1]; [1]*bossa nova technologies, USA*

Background, Motivation and Objective

Laser-based ultrasonic (LBU) is now becoming a more mature technology, making the transition from research laboratory equipment to industrial on-line measurement system. The non-contact and remote capability of LBU is an undeniable advantage for high-speed inspection. As LBU competes with other inspection technologies for on-line integration, LBU must retain its performance advantages despite operating in a far from ideal environment. To date, successful LBU industrial integrations have been mostly based on confocal Fabry-Perot interferometers. A new type of interferometers based on multi-channel random-quadrature (MCRQ) detection was recently proposed as a robust and compact solution for industrial inspections.

Statement of Contribution/Methods

A major challenge for interferometers, is to overcome the random phase and intensity distributions (speckles) of laser light reflected off optically rough surfaces. With the MCRQ interferometer, the random phase distribution of the speckled light is taken advantage of to insure a stable output signal. This novel architecture combines a classic interferometric design (Michelson interferometer) with detector arrays and multi-channel parallel processing. No path stabilization is required. The random distribution of the speckled light guaranties that, in average, there is always half of the speckles carrying the information (in quadrature). The ultrasonic information is extracted from the interference signal with simple signal processing based on high-pass filtering followed by signal rectification. Robust behaviour is achieved because the interferometer does not require critical alignment and rejection of unwanted environmental perturbations is set electronically and it can easily be adapted to environment requirements. Its ability to work with speckled light makes it also well suited for being integrated with multi-mode fibres for remote detection.

Results

We will present results demonstrating the system operation and performances. We will also show how we can convert the free-space interferometer to a fibre interferometer, without any losses in performances as the reflection at the fibre-air interface is taken advantage of for generating the reference beam. Measurement on moving samples will be also discussed and examples of measurement on target moving at 3m/s will be shown.

Discussion and Conclusions

We will conclude by a performance review of the developed system. We will discuss the recent improvements being implemented and what we could expect for the next generation of MCRQ interferometers.

5H - Single Crystal Piezoelectrics

Carribean Ballroom II

Friday, October 21, 2011, 8:00 am - 9:30 am

Chair: **Jian Yuan**
Philips Ultrasound

5H-1

8:00 AM Continuous feed growth and characterization of PMN-PT single crystals

Kazuhiko Echizenya[1], Mitsuyoshi Matsushita[1]; [1]Research Laboratories, JFE MINERAL COMPANY, LTD., Chiba, Japan

Background, Motivation and Objective

In recent years, piezoelectric single crystals based on $Pb(Mg_{1/3}Nb_{2/3})TiO_3$ (PMN-PT) have been used for ultrasonic medical transducers to provide better image quality. Commercially PMN-PT single crystals are grown by conventional Bridgman technique. A remaining issue in the crystal growth is the composition variation along the growth direction due to the segregation phenomena. As the variation results in large fluctuations of the dielectric / piezoelectric properties, the crystal portion with the desired properties is only 30% of the crystal length. The low yield in the crystal growth directly leads to high cost for PMN-PT single crystals. Our objective is to improve the composition uniformity and extend the portion which has desired properties.

Statement of Contribution/Methods

Theoretically, continuous feed growth is a promising technique to eliminate the composition variation. Its main feature is to feed raw material into the melt during crystal growth. If the composition change due to segregation can be compensated by fed raw material, the melt composition should stay the same during growth and the grown crystal should have uniform composition. In this study a continuous feed mechanism was installed to a vertical Bridgman furnace and PMN-PT single crystals were grown by the continuous feed technique. The composition and the properties were evaluated.

Results

PMN-PT single crystals of 80 mm in diameter and 200 mm in length have been successfully grown by the continuous feed technique. The crystals show homogeneous composition distribution along the growth direction. TiO_2 concentration variation was only 6% in 80% of the crystal length as shown in fig. 1. As a result of homogeneous composition, the crystal shows uniform and desired properties. The dielectric constants (Kr) and the piezoelectric constants (d_{33}) were 5200 - 6000 and 1300 - 1700 pC/N, respectively.

Discussion and Conclusions

PMN-PT single crystals with uniform properties were successfully grown by the continuous feed technique. The uniform property portion was 80% of the crystal length and much larger than that typically produced using the conventional Bridgman growth method. So the continuous feed technique can deliver more uniform quality and improve the cost-effectiveness of PMN-PT single crystals.

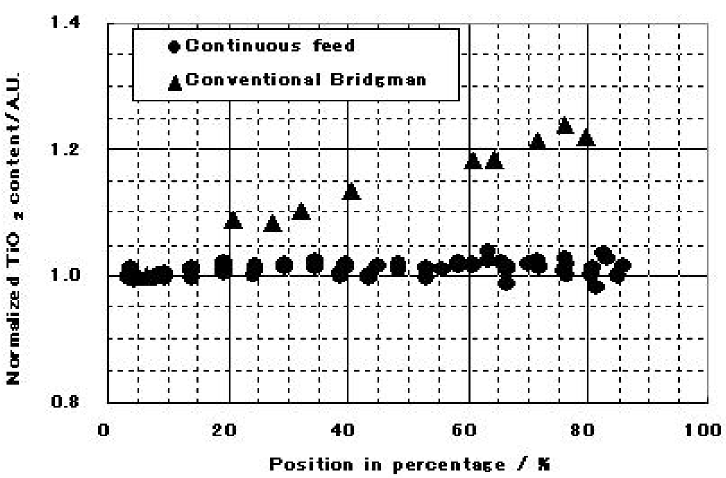

Fig.1 TiO_2 concentration along the growth direction.

FRIDAY ORAL

5H-2

8:30 AM Shearwave Generation of 6MHz 128ch Linear Array using Mn doped PMN-PT Single Crystal for Elastograhpy Imaging.

Sungmin Rhim[1], Jung Ho[1], Deokyoung Kim[1], Ho-Yong Lee[2], Jeong Seok Kim[3]; [1]HUMANSCAN Co., Ltd., Ansan, Kyunggi, Korea, Republic of, [2]Ceracomp Co., Ltd., Cheonan, Chungnam, Korea, Republic of, [3]R&D Dept., GE Ultrasound Korea, Seongnam, Kyunggi, Korea, Republic of

Background, Motivation and Objective

Many elastography techniques depends on radiation force to shearwaves. For getting better image quality, high radiation force is needed. However, if normal imaging transducer is used for this technique, there is the limitation of radiation force due to reliability and mechanical properties of piezomaterial used for transducer. In order to get high radiation force, hard type piezo-material can be used. However, hard type piezo-material has low dielectric constant and electro-mechanical coupling factor. So, it is not easy to get good imaging transducer performance. The purpose of this study is possiblity proof of Mn doped PMN-PT single crystal having better radiation force performance without image quality losing.

Statement of Contribution/Methods

Mn doped PMN-PT single crystal is used for 6.0MHz 128ch linear array. This array performs two functions. One is to generate radiation force and the other is to get ultrasound image. Mn doped PMN-PT single crystal was grown by solid-state single crystal growth method. The size of Mn doped PMN-PT single crystal used linear array is 26mm X 6mm and thickness is 0.175mm. The linear array was made by two types single crystal. One is pure single crystal and the other is 1-3 polymer composite with 70% single crystal volume fraction. The pitch of linear array is 0.2mm and normal double matching layer system is used.

Results

The electrical properties of Mn doped PMN-PT single crystal is almost same as pure PMN-PT single crystal. However, the mechanical quality factor(Qm) is much higher than that of pure PMN-PT. Qm of pure PMN-PT used for imaging transducer is about 50 -100. However, Qm of Mn doped PMN-PT is about 500 without losing electrical properties. The -6dB bandwidth of linear array using MN doped PMN-PT shows about 90% and this is similar with linear array using pure PMN-PT. But the image sensitivity of array using Mn doped PMN-PT is much better than that of pure PMN-PT. We can get similar sensitivity only inducing 50% power. This means higher radiation force can be acquired.

Discussion and Conclusions

6MHz 128ch linear array using Mn doped PMN-PT grown by solid-state single crystal growth method with high Qm is investigated for elastograhpy techniques. Mn doped PMN-PT is good candidate for elastography techniques since the linear array using Mn doped PMN-PT shows good radiation force effect without acoustic performance losing. Therefore, if Mn doped PMN-PT is used for imaging transducer, it is possible to get good image quality with high radiation force to generate shear wave.

5H-3

8:45 AM Advancements in Micromachined PC-MUTs for Medical Devices

Yu Liang[1], Kevin Snook[1], Bradley Dunkin[1], Raffi Sahul[1], Wesley Hackenberger[1]; [1]*TRS Technologies, State College, PA, USA*

Background, Motivation and Objective

Single crystal piezoelectrics such as PMN-PT have shown greater performance and significant improvements in ultrasound imaging over conventional ceramics. Wide bandwidth from high electromechanical coupling (k33) is best achieved through 1-3 composite technology, which has recently been scaled in frequency to >40 MHz through micromachining. Piezoelectric composite micromachined ultrasound transducers (PC-MUTs) provide not only the advantage of less surface damage to crystal posts than conventional dicing, but also provide the ability for irregular patterning and dimensions. In conjunction with the unique resonance modes of PMN-PT due to its anisotropy, novel transducer designs provide more flexibility for acoustic field manipulation and bandwidth improvements. Additionally, new ternary compositions of PMN-PT (PIN-PMN-PT) have been reported to exhibit smaller domain structures, which better maintains bulk crystal properties near microscopic scales. The goal of this work is to evaluate these aspects to provide medical devices with extended capabilities over conventional transducers.

Statement of Contribution/Methods

Anisotropic etching of single crystal PMN-PT and PIN-PMN-PT in multiple orientations, including <001> and <110>, was performed and properties compared between bulk and etched samples. Posts as small as 7µm with 2µm kerfs were achieved at greater than 45µm depth.

Transducers from the crystal composites were fabricated in the frequency range of 35-75 MHz. Properties of the etched material and resulting transducers were compared through in air resonance analysis and in water acoustic measurements.

Other modes of operation were also evaluated to reduce the frequency range for other medical device applications by more than 50%, and will be discussed in more detail.

Results

Both the <001> and <110> electromechanical coupling k33 of PMN-PT were approximately 80-85% in conventional composites (5-10 MHz), but decreased to 70% at frequencies above 35 MHz. Conversely, the coupling of the PIN-PMN-PT showed only a 5% decrease, though variability was higher between samples. 40 MHz transducers showed a 10% increase in bandwidth for the ternary crystal.

Additionally, a transducer design was made which exhibited a bandwidth close to 4 octaves in the low MHz range. The fabricated transducer exhibited a similar bandwidth to modeling.

Discussion and Conclusions

The work suggests that advantages exist for PIN-PMN-PT over PMN-PT, though a larger sample set needs to be evaluated. The domain size appears to make an impact in transducer bandwidth, and allows an increase in frequency while maintaining bulk properties.

The anisotropy in properties provides a distinct advantage for etching of crystal, allowing a significant frequency range to be utilized. Additional results and modifications based on transducer geometry to flatten the response and shape the acoustic beam will be discussed.

5H-4

9:00 AM Piezoelectric Crystal Composite for Low and High Frequency Ultrasound Application

Jian Tian[1], Kevin Meneou[1], Brandon Stone[1], Pengdi Han[1]; [1]*H. C. Materials Corporation, Bolingbrook, Illinois, USA*

Background, Motivation and Objective

The superior properties of piezoelectric single crystal lead magnesium niobate-lead titanate (PMN-PT) have led to the new generation of low frequency medical ultrasound imaging, with greatly improved bandwidth and sensitivity. Recently, ternary piezoelectric crystal lead indium niobate-lead magnesium niobate-lead titanate (PIN-PMN-PT) demonstrated improved electrical and thermal properties as well as excellent dielectric and piezoelectric properties. To fully exploit the excellent properties of piezoelectric single crystals, crystal composite of low and high frequencies using binary PMN-PT and ternary PIN-PMN-PT single crystals were fabricated and evaluated.

Statement of Contribution/Methods

Piezoelectric crystal composite of low frequency was fabricated using traditional dice-and-fill method. Special precautions are needed for the dicing of single crystals. For high frequency crystal composite, kerfs are generally too narrow (<10 um) and posts too fragile (< 20 um) even for the state-of-the-art dicing. Instead, deep reactive ion etching (DRIE) with inductively coupled plasma (ICP) was used to micro-machine the patterns needed for crystal composite. General processing procedures include photolithography, etching mask electroplating, and DRIE. Diced or etched crystal was then filled with epoxy and lapped to final thickness. Chromium/gold electrodes were sputter coated for subsequent poling and property measurement.

Results

Crystal composites with frequencies ranging from 0.5 MHz to 80 MHz were successfully fabricated. Selected materials properties of crystal composites were measured using an Agilent 4294A impedance analyzer. Crystal composite demonstrated significantly improved properties over monolithic crystal. In particular, the electromechanical coupling factor of crystal composite could reach 0.8 or greater, significantly higher than the coupling of monolithic single crystal (~ 0.56).

Discussion and Conclusions

Improved coupling factor of piezoelectric crystal composite enables more efficient conversion between electrical and acoustic energies. During a pulse-echo process, the overall energy conversion efficiency increased by a factor of three (4X) for a coupling factor improvement from 0.56 to 0.8. In addition, the lower acoustic impedance of crystal composite compared to monolithic crystal also improves acoustic matching. Such improvement will lead to further enhanced performance characteristics (e.g., broader bandwidth, higher sensitivity) for transducers based on crystal composite.

5H-5

9:15 AM Characterisation of PMN-29%PT as a Function of Temperature and Pressure

Muhammad Sadiq[1], Zhen Qiu[1], Christine Demore[1], Zhihong Huang[1], Sandy Cochran[1]; [1]*University of Dundee, United Kingdom*

Background, Motivation and Objective

Piezoelectric single crystal relaxor materials, such as $_{(x)}$ $Pb(Mg_{1/3}Nb_{2/3})O_3$– $_{(1-x)}$ $PbTi0_3$ (PMN-PT) have higher performance for ultrasound applications than piezoelectric ceramics. However, phase transitions at relatively low temperatures (T) and external pressures (P) affect their behaviour well within the range of operating conditions of underwater sonar and actuators and in non-destructive testing at elevated temperatures. Single crystals with compositions modified to reduce these problems are under development but application-oriented characterization needs attention to allow robust design practices.

Statement of Contribution/Methods

Single crystal characterization as a function of temperature has been reported extensively but the range of parameters measured is often limited and there have been few reports of the effects of pressure. In our work, an experimental system was set up specifically to characterize single crystals as a function of T, P and electric field biases found in practical use. Characterisation was also possible under drive conditions leading to self-heating.

The experimental setup included a material testing system (Instron Ltd, High Wycombe, UK) with an integrated oven. A high voltage DC source (Glassman High Voltage Inc., NJ, USA) was used for electric field bias and a power amplifier for self-heating (Electronics and Innovation, NY, USA). Electrical impedance data were analysed with PRAP software (TASI Technical, Kingston, Canada) and non-contact measurements used a thermal imaging camera (FLIR Systems UK, Kent, UK) and laser vibrometer (Polytec Ltd, Hertfordshire, UK).

Results

Data were first obtained from bulk thickness-mode PMN-29%PT samples from several suppliers. These demonstrated significant intrinsic variation and not only the commonly reported changes in permittivity with T but also complicated changes with P and bias field. Measurements were repeated on PZ54 ceramic samples (Ferroperm SA, Kvistgaard, Denmark) for comparison. Of particular concern in this comparison was the large variation in parameters such as permittivity of PMN-PT within the range $20 < T < 80°C$; in addition, a variation of 20°C was observed within a sample during self heating. Early measurements on PIN-PMN-PT ternary materials indicated the expected improvement in stability with little reduction in performance.

Discussion and Conclusions

Single crystal PMN-29%PT obtained in small quantities from several suppliers indicated that variation sample-to-sample and between suppliers is still significant. Using a wide range of equipment in a single experimental system allowed detailed characterization, showing significant variations with T, P, and electric field bias within conventional operating limits. Further tests indicated that environmentally-elevated temperature may be a weak model because of spatial non-uniformity in self-heating.

6H - SAW Simulation and Devices

Carribean Ballroom VI

Friday, October 21, 2011, 8:00 am - 9:30 am

Chair: **Don Malocha**
University of Central Florida

6H-1

8:00 AM Ultra Low-Profile Self-Matched HTCC SAW-Duplexer: Manufacturing and Performance Challenges

Robert D. Koch[1], Christian Bauer[1], F. Maximilian Pitschi[1], Juergen E. Kiwitt[1], **Robert Weigel[2]**; [1]*TDK-EPC Corporation, Germany,* [2]*University of Erlangen-Nuremberg, Germany*

Background, Motivation and Objective

Providing the required ability of simultaneously transmitting and receiving RF signals, duplexers are one of the key components in the well established 3G (W)CDMA communication systems. For mobile terminals, duplexers in micro-acoustic filter technology have been used since several years - at the beginning with pure SAW devices, later on also with BAW devices and SAW/BAW hybrids. Generally, these duplexers are composed of two band pass filters and additional passive matching elements to improve the electrical performance. Until today, miniaturization and cost reduction of micro-acoustic duplexers have steadily been demanded by the market. At the same time, the electrical requirements for the duplexers have been become more and more stringent. Therefore, a short design period, a precise simulation of acoustic and electromagnetic effects, and a cost efficient fabrication of such devices have become crucial.

Statement of Contribution/Methods

Based on the experimental packaging approach for the demonstrator of an ultra low-profile self-matched SAW-duplexers which has been published recently, we will present details of the underlying experimental manufacturing process. We will focus on the additional process steps of the process extension of the well established Cu-frame CSSP3 package technology which enables the integration of miniaturized planar copper coils on the top layer of an HTCC package for SAW, BAW and SAW/BAW hybrid filters. Additionally, elaborating on one key process of this technology, we will present investigation results regarding the surface roughness of these coils and its effect on the Q-factor.

Results

In a proof of concept we integrated four spiral coils in a 2520 HTCC package for a Band I (W)CDMA duplexer using the presented process extension of the CSSP3 package technology. The experimental two-stage electroplating process allows the realization of a Cu-frame that is higher than the Cu-coil which prevents the metalization of the flipped filter chip from touching the coils even during molding processes. The surface roughness of these copper coils is determined by surface roughness of the HTCC at the coil/HTCC interface and by the stripping process of the seed-layer. Including the surface roughness in our electromagnetic simulation allows us to determine the resulting Q-factor of the planar coils very precisely. Therefore, using a complete EM-model, we have been able to predict insertion loss of our filters more reliably and accurately.

Discussion and Conclusions

The presented extension of the CSSP3 package technology enables the integration of planar spiral coils in standard CSSP3 packages for micro-acoustic filters. Using an ultra low-profile HTCC package, the resulting SAW/BAW duplexer can be used not only for stand-alone applications but also for module applications. This novel integration approach offers the required miniaturization potential for micro-acoustic duplexers.

6H-2

8:15 AM A Design Technique to Enhance Isolation of Duplexer in Single-Ended and Differential Mode

Jun Tsutsumi[1], **Shogo Inoue[1]**, Masafumi Iwaki[1], Motoaki Hara[1], Hiroshi Nakamura[1], Kazuhiro Matsumoto[1], Masanori Ueda[1], Yoshio Satoh[1]; [1]*TAIYO YUDEN CO.,LTD., Japan*

Background, Motivation and Objective

Complexity of a radio frequency (RF) front-end in current cellular phones is increasing because a number of frequency bands and several standards have to be supported in a single phone. One solution to simplify the RF front-end is to eliminate the inter-stage SAW filters. This solution is so-called "SAW-less" RF front-end and contributes to reduce not only the count of off-chip components but also the cost.

To implement the SAW-less RF front-end for the frequency division duplex system, such as UMTS and CDMA2000, the duplexer's isolation should be higher for compensation. If we focus the elimination of Rx inter-stage SAW filter, the isolation of duplexer in the Tx band should be higher to avoid the flow of Tx leakage into a RFIC.

For the SAW-less RF front-end, the differential Rx output of duplexer is preferred because the second-order inter-modulation distortion in a RFIC, which degrades the receiver performance severely in the direct conversion receiver, can be cancelled out by utilizing the differential operation inside the RFIC. Therefore, the differential-mode isolation of duplexer is important in such RF front-end.

In this paper, the design technique to achieve an extremely high isolation of duplexer in the differential-mode is presented. The presented technique is based on the enhancement of isolation in the single-ended paths with keeping low insertion loss, and fulfills the requirements from an up-to-date RFIC developed using the fine CMOS process.

Statement of Contribution/Methods

The isolation in the differential mode can generally be enhanced by cancelling out the common mode leakages in each single-ended path. Also, the design technique to enhance the single-ended isolation of duplexer has been proposed by the authors. This technique uses the cancellation path to cancel out the single-ended Tx leakage and can also be applied to the duplexer with the differential Rx output to enhance each single-ended isolation. By enhancing the single-ended isolation, the higher differential-mode isolation can also be attained.

Results

The prototype of UMTS Band1 (Tx:1920-1980 MHz, Rx:2110-2170 MHz) duplexer was designed and fabricated in 2.0 x 1.6 mm package. The SAW filter technology was used for both the Tx and Rx filters, and conversion from the single-ended to the differential-mode was realized using the double mode SAW design. The differential-mode Tx band isolation was higher than 65 dB with keeping as small as 1.5 dB insertion loss of Rx filter. Also, each single-ended isolation in the Tx band was higher than 55 dB, due to the utilization of cancellation technique in the single-ended path.

Discussion and Conclusions

The design technique to achieve an extremely high isolation in the differential duplexer by enhancing the single-ended isolation was presented. In the presentation, the detail of the design technique will be shown as well as the experimental results of UMTS Band1 and Band2 (Tx:1850-1910 MHz, Rx:1930-1990 MHz) SAW duplexers.

6H-3

8:30 AM A Nonlinear Elastic Model for Predicting Triple Beat in SAW Duplexers

Shogo Inoue[1], Seiichi Mitobe[2], Motoaki Hara[1], Masafumi Iwaki[1], Jun Tsutsumi[1], Hiroshi Nakamura[1], Masanori Ueda[1], Yoshio Satoh[1]; [1]*Microdevice Research & Development Department, TAIYO YUDEN CO., LTD., Akashi, Hyogo, Japan,* [2]*TAIYO YUDEN Mobile Technology Co., Ltd., Yokohama, Kanagawa, Japan*

Background, Motivation and Objective

SAW and BAW duplexers for recent mobile communication devices are strongly required higher linearity performances. Although the nonlinear behavior in BAW devices has been modeled and characterized in various methods, the analysis of the nonlinearity for SAW devices has been still under exploration due to the complexity of nonlinear phenomena of SAW. This paper proposes a novel nonlinear model for SAW duplexers, which precisely predicts the 3rd order nonlinear distortion, "triple beat (TB)".

Statement of Contribution/Methods

The proposed nonlinear model is based on the nonlinear elasticity, i.e., the nonlinearity of SAW stress vs. strain. First, the linear SAW displacement distributions in all resonators configuring duplexers are calculated by using the coupling-of-modes (COM) theory when the signals from the Tx and antenna ports are applied (under TB test conditions). Afterwards, the nonlinear displacements excited by the linear displacements are calculated on the assumption of the 3rd order nonlinear elasticity of SAW, and then the nonlinear currents in each resonator induced by the nonlinear displacements are calculated. Finally, nonlinear currents at the Rx port from all resonators are calculated and summated, which are converted to the TB level. This model needs just one nonlinear parameter, which represents the nonlinearity of elastic constant.

Results

Figure 1 shows the comparison of the measurement and simulation results of TB test for UMTS Band2 SAW duplexer (1.9 GHz band). These results demonstrate fairly good agreement with the discrepancy of only 1 dB.

Discussion and Conclusions

A precise nonlinear-simulation technique for TB in SAW duplexers has been successfully developed. This simulator can be a powerful tool for designing the highly linear duplexers.

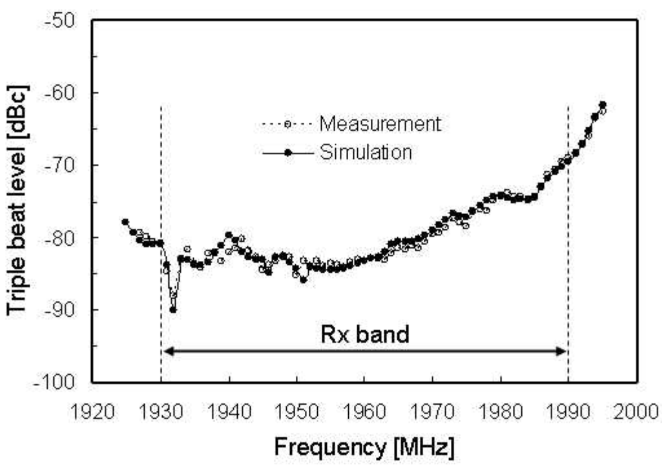

Fig. 1 Measured and simulated triple beat responses.

6H-4

8:45 AM A New Simulation Model of Nonlinearity for SAW Resonator Filters

Katsuhiro Nako[1], Ryo Nakagawa[1], Takanao Suzuki[1], Kazuhiro Takigawa[1], Hiroshi Shimizu[1], Haruki Kyouya[1]; [1]*New Technology & Products Development Group, Murata Manufacturing Company,Ltd., Yasu-shi, Shiga, Japan*

Background, Motivation and Objective

In recent years, IMD (Intermodulation Distortion) characteristic caused by nonlinear effect of SAW (Surface Acoustic Waves) duplexers for WCDMA mobile phone terminals becomes important more and more, because the IMD signals affect the receiving sensitivity of the terminals. Therefore, the prediction technique of its nonlinear characteristics, in the design stage of SAW duplexers, is strongly desired. Generally, current SAW duplexers consist of ladder type filter for TX portion and DMS (Double Mode SAW) filter for RX.

Although Tsutsumi et al. describe a relation between IIP (Input intercept Point) and SAW intensity of DMS filter[1] and Li Chen et al. present a simulation method for the IMD using BVD (Butterworth-Van Dyke equivalent circuit) circuit model[2], the frequency response of nonlinear signals for DMS filters has not been made clear. In this paper, a new simulation method of nonlinear signals applicable for not only one-port SAW resonators but also DMS filters is proposed.

Statement of Contribution/Methods

The calculation model of the nonlinear current is derived by introducing nonlinear terms to the piezoelectric fundamental equation. In the calculation model, the nonlinear current is expressed by the admittance of SAW devices, the voltage applied to electrodes, and nonlinear coefficients. In order to handle the nonlinear current generated from each IDT (Interdigital Transducer) in DMS filter, the admittance is represented as a matrix which has the same dimension as a number of IDTs in the DMS filter.

The admittance matrix and the voltage for each IDT can be obtained by using COM (Coupling of Modes) model and a circuit simulator (like ADS), respectively. Therefore, if nonlinear coefficients are obtained, the nonlinear current generated in the DMS filter can be derived. We obtained nonlinear coefficients by using a fitting method to the measurement results. The nonlinear current generated in one-port SAW resonator's IDT can be derived by the same method of the DMS filter.

Results

In order to verify the simulator, we compared the IMD3 (third order IMD) characteristics of DMS filters with the center frequency of 880MHz, which consists of LiTaO3 substrate and three IDT's configuration.

Good correspondence between the simulation results and the measured results was obtained. Regarding one-port SAW resonator, also good results was obtained.

FRIDAY ORAL

Discussion and Conclusions

A new simulation method for nonlinear effects such as IMD for DMS filters is developed. By using this method, the prediction of the frequency characteristics for designed SAW duplexer is made possible.

[1]J.Tsutsumi et al., "Influence of Linear and Non-Linear Distortions in SAW/FBAW Duplexers on Third-Generation Mobile Phone Systems", Proc. of the European Micro Wave Association, Vol.3, 2007, pp. 120-127.

[2]Li Chen et al., "Third Order Nonlinear Distortion of SAW Duplexers in UMTS System",IEEE Int Ultrason Symp 2010 (to be published)

6H-5

9:00 AM Nonlinear lumped electrical model for Contour Mode AlN Resonators

Jeronimo Segovia Fernandez[1], Augusto Tazzoli[1], Gianluca Piazza[1]; [1]*University of Pennsylvania, USA*

Background, Motivation and Objective

Power handling and intermodulation distortion due to non-linearity in micromechanical resonators play an important role in setting phase noise in oscillators and limit the range of applications for filters. Although significant work has been done to model non-linearity in mechanical resonators, no studies have been performed on laterally vibrating AlN contour-mode resonators (CMR), an emerging class of devices that can enable reconfigurable RF front-ends. Work from others has shown that distributed models based on Mason's equivalent circuits can be adopted for describing mechanical non-linearities in resonators.

Statement of Contribution/Methods

In this work the non-linear parameters were derived by means of 2nd and 3rd order intermodulation distortion (IMD2 and IMD3) experiments. Here we present the use of an equivalent lumped electrical circuit model that is easily integrated into circuit simulators to provide a simple representation of the non nonlinear behavior of AlN CMRs. In addition, we extract the value of the equivalent non-linear parameters by means of a broader set of experiments including not only IMD2 and IMD3, but also amplitude-frequency response analysis.

The non-linear model is represented in the electrical domain by a variable capacitor, whose value depends non-linearly on charge via the 2nd and 3rd order non-linear parameters, C_{M1} and C_{M2}, respectively.

Three different experiments, namely amplitude-frequency measurements, IMD2 and IMD3 were carried out on 3 CMR resonators operating around 200 MHz and formed by a 1.2 µm thick AlN film.

Results

Power levels of 0-6 dBm were applied to the resonators and the amplitude-frequency response was fit to extract a combination of the 3rd and 2nd order non-linear coefficients (C_{M1}^2-C_{M2}). IMD2 experiments were used to reveal the value of C_{M1}, whereas IMD3 measurement were used to further validate the extraction of the combined effect of C_{M1} and C_{M2}. Average values of C_{M1} and C_{M2} are reported in Figure 1.c.

Discussion and Conclusions

The experimental measurements confirm the validity of the proposed electrical model, which lumps all the various non-linear phenomena (mechanical, piezoelectric, and electrical) and offers a rapid method to estimate AlN CMR non-linearity in circuit simulators.

a)

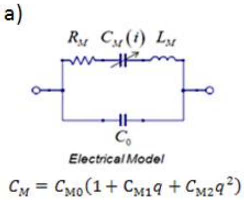

b)

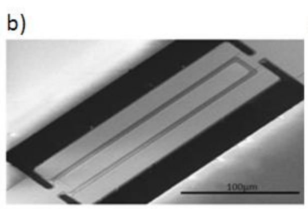

c)

Capacitance Parameters	Max - Min	Average	Experiment
C_{M1} [C^{-1}]	(-4.25e+10) – (-5.2e+10)	-4.68e+10	IMD2
C_{M1}^2-C_{M2} [C^{-2}]	3e+19 – 1e+19	2e+19	IMD3
C_{M1}^2-C_{M2} [C^{-2}]	4e+19 – 2.5e+19	3.3e+19	Amplitude-Frequency

Figure 1: a) Electrical model of nonlinear AlN CMR; b) SEM picture of the tested AlN CMRs; c) Extracted values of non-linear parameters from 200 MHz AlN CMRs.

6H-6

9:15 AM Simulation of complex 2D transducer structures using finite element analysis combined with a canonical Green's function based boundary element method

Thierry Laroche[1], Markus Mayer[2], Xavier Perois[3], William Daniau[1], Julien Garcia[1], Sylvain Ballandras[1], Karl Wagner[2]; [1]Time & Frequency, FEMTO-ST, UMR CNRS 6174, France, [2]EPCOS AG, TDK-EPC Corporation, Germany, [3]EPCOS AG, TDK-EPC Corporation, France

Background, Motivation and Objective

The development of new SAW devices based on complicated electrode patterns or layered excitation transducers has been favored by an intense activity. Devices using IDTs covered by

piezoelectric or dielectric layers are currently fabricated, but their design requires adapted simulation tools. Periodic analysis has been extended to account for any combination of electrodes and passivation layers but it finds its actual limits when considering short transducers with various electrode periods and widths as used e.g. in dual-mode SAW filters.

Statement of Contribution/Methods

The general case of transducers composed of a finite number of electrodes of any shape with full or partial dielectric overlays above a semi-infinite substrate is addressed here. The later condition allows one for exploiting properties of canonical Green's functions, i.e. the spatial distribution determination of any kind of wave generated by the said-transducers at any frequency once for all. Hence, the standard displacement-stress canonical Green's function inverse Fourier transform is combined with finite element (FE) interpolation along a variationnal boundary formulation and the obtained matrix is inverted to express surface stresses vs displacements, the actual FE degrees of freedom. The problem is computed using a direct solver for each frequency, yielding the electromechanical field in the structure from which the electrical admittance is derived.

Results

The computation has been validated by comparing the admittances of a small AT-cut quartz bulk transducer on a semi-infinite anisotropic solid achieved using the proposed approach and a 2D-

periodic computation for which the period was fixed large enough to reject any parasite due to propagation effects. This approach has allowed to demonstrate the agreement between both

computations (fig.1), and therefore to validate the new simulation tool.

Discussion and Conclusions

This approach reveals very flexible and can be extended to 3D in future developments. More work is engaged to accelerate the solving process.

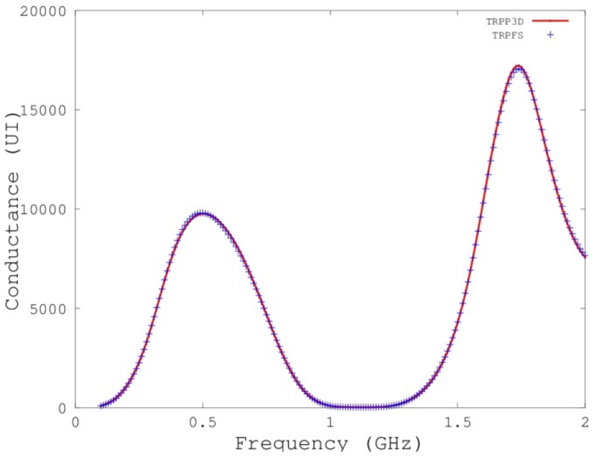

Fig.1 Conductance of a small AT-cut quartz bulk transducer on a semi-infinite anisotropic solid. (Red curve) Periodic method. (Blue crosses) This work.

FRIDAY ORAL

1I - Image Processing

Boca Rooms II-IV

Friday, October 21, 2011, 10:30 am - 12:00 pm

Chair: **Olivier Basset**
CREATIS, Lyon

1I-1

10:30 AM Segmentation of medical ultrasound images

Denis Friboulet[1], Olivier Bernard[1]: [1]Université de Lyon; CREATIS; CNRS UMR5220; INSERM U1044; Université Lyon 1; INSA-LYON, France

Background, Motivation and Objective

The objective of this paper is to present an overview of the current segmentation techniques applied to ultrasound medical images. In the associated talk, we propose to answer some basic questions: What are the specific difficulties raised by ultrasound imaging? What are the main methodological approaches? What is a "good" segmentation? What perspectives can be drawn from the evolution of ultrasound imaging techniques?

Statement of Contribution/Methods

The specificities of ultrasound image formation make them very challenging to segment: diffusion yields speckle noise, attenuation and diffraction yield contrast variation, image properties are orientation dependent and the field of view is often limited. Moreover the ability of ultrasound imaging to perform real-time acquisition sets challenges on the implementation of the algorithms.

Results

A wealth of techniques has been proposed to address segmentation of ultrasound images. Whatever the underlying formulation, these approaches broadly share two common aspects. First, they rely on the proper choice and extraction of image ("low-level") features/properties that characterizes the object to be detected (gradient, texture, etc.). These features alone can however hardly provide reliable segmentation. The second aspect thus consists in introducing a priori information about the object to be detected, i.e. constraints such as shape, volume, motion.

Assessing the quality of a segmentation algorithm is particularly difficult in medical imaging, because defining a ground truth is not straightforward. This evaluation may resort to physical phantom imaging or numerical simulation. The currently available numerical simulations are however not mature enough to serve as a basis for segmentation, and are mainly used as a first prototyping step. Validation is thus usually still performed by comparing the segmentation provided by the algorithm to the segmentation performed manually by medical experts.

We will present in this talk various example borrowed from the field of cardiac imaging, vascular imaging and prostate and breast cancer imaging to illustrate the principle, results and shortcomings of cureent segmentation techniques.

Discussion and Conclusions

One of the most interesting perspectives consists in exploiting new image-based features. To date, the vast majority of the approaches are based on log-envelope images. We will discuss the possibility of processing raw RF data, which has been almost unexploited till now. Another perspective concerns the evaluation of segmentation. The availability of intensive computing resources such as distributed computing infrastructures can provide a way toward more realistic simulations as well a basis for algorithm prototyping. We will exemplify the use of such a validation platform and show some preliminary results.

1I-2

11:00 AM Fast 3D Echocardiographic Segmentation using B-Spline Explicit Active Surfaces: A validation study in a clinical setting

Daniel Barbosa[1,2], Olivier Bernard[2], Denis Friboulet[2], Thomas Dietenbeck[2], Piet Claus[1], Helene Houle[3], Jan D'hooge[1]; [1]Lab on Cardiovascular Imaging & Dynamics, Dept. of Cardiovascular Diseases, Katholieke Universiteit Leuven, Leuven, Belgium, [2]CREATIS, INSA Lyon, France, [3]Siemens Medical Solutions, USA

Background, Motivation and Objective

The evaluation of cardiac morphology and function by ultrasound imaging made a major step forward with the introduction of real-time 3D echocardiography (RT3DE). Several studies have already shown that RT3D is an accurate tool for left ventricular (LV) volume assessment.

However, LV segmentation in RT3DE remains a time-consuming task jeopardizing the use of this modality in routine practice. The automation of this process would thus be of great clinical relevance.

We recently proposed a generic framework for real-time 3D segmentation, based on B-spline Explicit Active Surfaces (BEAS). This method is able to cope with image inhomogeneities, as it uses localized region-based statistics to evolve the contour, while keeping a low computational cost.

The aim of the present study was to evaluate the applicability of our method to clinical 3D RT3DE data and to assess its accuracy in the extraction of volumetric functional parameters used in clinical routine.

Statement of Contribution/Methods

25 RT3DE exams were acquired using a Siemens Acuson SC2000 rev. 1.5 (Siemens Ultrasound, Mountain View, CA). The dataset comprises a blend of healthy individuals and patients with a multitude of conditions, including myocardial infarction and dilated cardiomyopathy. The algorithm was manually initialized by a non-expert user at end-diastole and end-systole with six clicks. As a reference, both end-diastolic and end-systolic volumes were manually contoured by 3 expert sonographers using commercially available tools (eSie LVA). The average of the 3 experts was taken as the reference value. The agreement between the BEAS results and the reference values was assessed using the relative measurement error for end-diastolic, end-systolic and stroke volumes (EDV, ESV and SV), and for ejection fraction values (EF).

Results

The overview is given in Table 1. No statistical significant differences were found between the BEAS values and the ones manually extracted by the experts (unpaired t-test; p=NS). The average CPU time of the proposed method was around 0.25s for each 3D volume, in a MATLAB implementation.

Discussion and Conclusions

The BEAS algorithm is able to accurately extract relevant cardiac functional indexes in a clinical setting. Its low computational burden enables its use in automated LV volumetric quantification tools, where the user input can be integrated in real-time, for optimal clinical usage.

Table 1

	EDV	ESV	SV	EF
BEAS algorithm bias	-1.09ml	1.74ml	-2.83ml	-2.37%
Relative error for the BEAS algorithm (μ±σ %)	8.27±6.66	12.4±7.92	12.5±9.83	9.39±6.38
Inter-observer relative error (μ±σ %)	6.25±6.12	11.5±8.79	10.3±7.95	8.11±6.64
Correlation coefficient (r)	0.97	0.97	0.93	0.90

1I-3

11:15 AM Fine Resolution 3D Displacement Measurements of Mouse Left Ventricle Using Orthogonal Sets of 2D B-Mode Ultrasound Images

Dan Lin[1], Yaqin Xu[1], Brent A. French[1], John A. Hossack[1]; [1]*Biomedical Engineering, University of Virginia, USA*

Background, Motivation and Objective

Ischemic heart disease is one of the leading causes of morbidity and mortality in the developed world. The mouse species provides a well characterized, and widely accepted, model for conducting basic cardiovascular research into the evolution of disease and response to experimental therapy. Consequently, there is significant value in comprehensive and non-invasive 3D quantification of mouse left ventricular (LV) function. Unfortunately, due to the technical challenges in high resolution ultrasound, the vast majority of assessments of LV function in mice rely on M-mode or single-slice 2D analyses.

Statement of Contribution/Methods

We have developed an approach for reconstructing 3D motion that uses a combination of acquired orthogonal 2D imaging planes and mouse heart mathematical model-based fitting to arrive at a finely sampled 3D vs. time displacement mapping. Using orthogonal 2D image sets allows for each of X, Y and Z direction displacement vectors to be detected. Serial short-axis and long-axis images of mouse left ventricle were acquired at 0.5mm intervals using a linear array transducer operating at 30MHz (Vevo 2100) with spatial resolution of 50µm axially and 110µm laterally. Data were acquired for 4 baseline and 2-day post-infarct mice. Approximately 40-50 frames per heart cycle were collected for mice at baseline, and 35-45 frames per heart cycle for infarcted mice. Myocardial motion was tracked using a 2D minimum sum of absolute differences algorithm. In regions experiencing image artifacts or signal dropouts, an incompressible tissue mathematical model was employed, and motion was corrected based on a weighted average of tracked motion and model predicted values. Displacement error was computed based on the ratio of final displacement to the length of the trajectory through the entire heart cycle.

Results

By incorporating an incompressible LV mathematical model, displacement error was reduced from 8.4±1.4% to 5.6±1.2%. 3D analyses of cardiac motion provide a more comprehensive assessment of post-infarct ventricular function than conventional 2D analyses. For example, after evaluating the relative displacement magnitudes of post-infarct hearts, damaged myocardial tissues were determined to be in the apical-anterolateral region of the LV. In the damaged tissue, radial, circumferential, and longitudinal displacements were reduced by 45.1±9.8%, 43.5±8.2%, and 52.4±9.2%, respectively.

Discussion and Conclusions

Acquiring finely spaced 2D image sequences for sets of orthogonal planes allows for reconstruction of 3D displacements, with fine spatial and temporal resolution, in the mouse LV. Significant improvement in tracking results was observed by integrating an incompressible mathematical model of the heart. Finally, accurate reconstruction of 3D displacements allows for precise localization of infarct zone in the LV.

1I-4

11:30 AM Three-dimensional myocardial strain estimation from volumetric ultrasound: experimental validation in an animal model

Brecht Heyde[1], Ruta Jasaityte[1], Stefaan Bouchez[2], Michael Vandenheuvel[2], Dirk Loeckx[3], Piet Claus[1], Patrick Wouters[2], Jan D'hooge[1,4]; [1]*Cardiovascular Imaging and Dynamics, Catholic University of Leuven, Leuven, Belgium,* [2]*Department of Anesthesiology, Ghent University, Ghent, Belgium,* [3]*Medical Image Computing, Catholic University of Leuven, Leuven, Belgium,* [4]*Medical Imaging Lab, Norwegian Institute for Science & Technology, Trondheim, Norway*

Background, Motivation and Objective

We previously proposed an algorithm, referred to as splineMIRIT, for 3D myocardial strain estimation from volumetric ultrasound data based on elastic registration using mutual information. The performance of our approach was previously tested in tissue mimicking phantoms. The aim of the current study was to validate our methodology in an animal model by comparing strain values measured by splineMIRIT with the ones obtained through sonomicrometry.

Statement of Contribution/Methods

In five anesthetized sheep, a median sternotomy was performed. Sonomicrometric crystals were implanted in a tetrahedral configuration in the infero-lateral (IL) wall, resulting in three crystal pairs, providing a reference measure of radial (R), longitudinal (L) and circumferential (C) strain. Ultrasound volumetric data were recorded using a GE Vivid7 equipped with a 3V probe (frame rate: 25-32Hz; ECG gating over four cardiac cycles). Ultrasound and crystal data were acquired at baseline, during positive (dobutamine) and negative (esmolol) inotropic stimulation and during acute ischemia (ligation of the circumflex coronary artery). In-house developed software was used to manually contour the endo- and epicardial borders on the end-diastolic volumes. The resulting myocardial mesh was subsequently tracked throughout the cardiac cycle from which the segmental strain tensor could be estimated in an 18-segment model of the LV. End-systolic strain values measured by ultrasound in the IL wall were correlated against the reference values obtained by sonomicrometry.

Results

Ischemia measurements could not be completed in two animals and esmolol data was lacking in another. Overall, 17 data sets could thus be included. The correlations of all strain components against sonomicrometry are shown in the figure. A correlation coefficient of 0.63 and 0.60 was found for L and C strain respectively. However, no significant correlation for R strain was found.

Discussion and Conclusions

In this study, we demonstrated that L and C strain could be estimated with acceptable accuracy from volumetric ultrasound data sets in an animal model. However, estimates of R strain require further improvement. Currently, the latter component can thus better be estimated from the L and C components through conservation of volume. Data from additional animals will be added to strengthen these preliminary results.

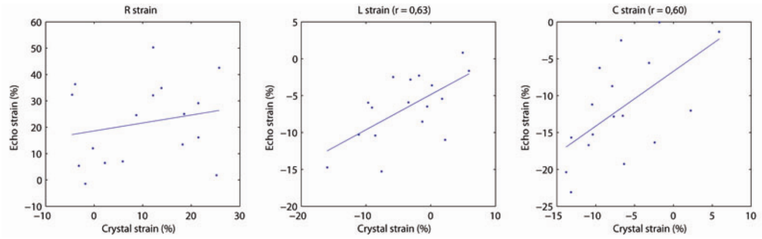

1I-5

11:45 AM Methodology to register prostate B-mode and ARFI images to MR and histology data

Christina Hsu[1], Matthew Davenport[2], Rajan Gupta[2], Thomas Polascik[3], John Madden[4], Mark Palmeri[5], Kathy Nightingale[5]; [1]Biomedical Engineering, Duke University, Durham, NC, USA, [2]Department of Radiology, Duke University Medical Center, USA, [3]Division of Urology, Department of Surgery, Duke University Medical Center, USA, [4]Department of Pathology, Duke University Medical Center, USA, [5]Biomedical Engineering, Duke University, USA

Background, Motivation and Objective

Background: Acoustic Radiation Force Impulse (ARFI) imaging is being developed for guiding needle biopsy and focal therapy of Prostate cancer. We have previously reported in vivo images portraying internal structures in the prostate with higher contrast than matched B-mode images. Given the heterogeneity of the prostate and the poor visualization provided by B-mode, another gold standard for determining what is being visualized in ARFI images is necessary. In the study, we present image processing and registration techniques that facilitate correlation of in vivo ARFI, B-mode ultrasound (US), and MR images obtained prior to radical prostatectomy with whole mount histology data.

Statement of Contribution/Methods

Methods: Data from 7patients were acquired under an ongoing IRB-approved study. Preoperative prostate MR images were acquired using standard sequences in combination with newer DCE and DWI techniques. In vivo 3D ARFI and B-mode US images were obtained immediately preceding radical prostatectomy with an end-fire, mechanical wobbler array (EV9F4) and Siemens Antares scanner. The excised specimens were fixed in formalin for 48 hours; sectioned and processed using whole mount techniques; and digitized.

Images from all modalities were segmented using ITKsnap. The segmented US and MR images were used to form 3D mesh models of the prostate using Hypermesh (Altair Engineering). The node and element information was extrapolated into a 3D image matrix of equivalent size for all modalities using MATLAB. Non-rigid registration of the different models was performed using the ANTs package implemented with a cross-correlation metric. The registered images were evaluated for co-localization of pathology in all modalities.

Results

Results: Initial 3D models demonstrate tissue deformation and dissimilar positions between the multimodality acquisitions due to changes in prostate orientation and different forms of compression. The non-rigid registration methodology successfully co-registered the US and MR datasets, accounting for different geometric distortion between the endorectal MR coil and the transrectal US transducer. Preliminary analysis showed that the co-registered calculated volumes improved in agreement from 92% pre-registration to 97% post-registration. Zonal anatomy (central gland vs. peripheral gland) is clearly portrayed in both T2-weighted MR images and ARFI images, but not consistently in B-mode images.

Discussion and Conclusions

Conclusion: Registration of the data simplified multimodality image comparison. Future analysis will include increasing the field of view and penetration depth for ARFI imaging, and accounting for the expansion of the prostate upon excision and co-registration of the digitized histology slides to the imaging datasets. With its improved anatomical visualization over traditional B-mode imaging, ARFI holds promise for providing targeted image guidance of prostate focal therapy and needle biopsy.

2I - Histotripsy and General Therapy

Boca Rooms VI-VII

Friday, October 21, 2011, 10:30 am - 12:00 pm

Chair: **Georg Schmitz**
Ruhr-Universität Bochum

2I-1

10:30 AM A Dose-efficient Treatment Strategy for Histotripsy By Removing Cavitation Memory

Tzu-Yin Wang[1], Zhen Xu[1], Timothy Hall[1], Brian Fowlkes[1,2], Charles Cain[1]; [1]Biomedical Engineering Department, University of Michigan, USA, [2]Radiology Department, University of Michigan, USA

Background, Motivation and Objective

Cavitation memory effect occurs when fragments of cavitation bubbles persist in the host medium and act as seeds for subsequent events. In pulsed cavitational ultrasound therapy, or histotripsy, this effect may cause cavitation to repeatedly occur at these seeded locations within a target volume, producing inhomogeneous lesions or requiring excess pulses to completely homogenize the target volume. We hypothesized that by removing the cavitation memory, the cavitation bubbles could be induced at random locations in response to each pulse, leading to complete and homogeneous disruption of the target volume with fewer pulses.

Statement of Contribution/Methods

Histotripsy treatments were performed using 10-cycle 1-MHz ultrasound pulses at peak negative/positive pressure of 47/21 MPa. The cavitation memory was passively removed by increasing the time interval between successive pulses, T, from 2, 10, 20, 50, 100, to 200ms. Experiments were conducted on red-blood-cell tissue phantoms and *ex vivo* livers. The former allowed for direct observation of the locations of the cavitation bubbles and the corresponding lesion patterns during the treatments using high speed photography; the latter provided validation of the memory effect in real tissues with histological examinations.

Results

The cavitation bubbles were induced in distinctly different locations in each pulse for T ≥ 100 ms, but they appeared in almost identical locations for shorter T's. The correlation coefficient between cavitation patterns in successive pulses decreased exponentially from 0.5±0.1 to 0.1±0.1 as T increased from 2 to 200ms (R^2 = 0.96, N=10 for each). Correspondingly, the lesion developed more rapidly with increasing numbers of pulses for longer T's (Fig. A). Given the same treatment doses (500 pulses for treatments in red-blood-cell phantoms, and 1000 pulses for treatments in the livers), complete and homogeneous tissue disruption with well-defined lesion boundaries was achieved only for T ≥ 100 ms (Fig. B).

Discussion and Conclusions

Cavitation patterns in successive pulses were highly dependent on the presence or absence of cavitation memory. As the memory was removed, cavitation bubbles occurred in random locations in response to each pulse, resulting in complete and homogeneous tissue disruption with significantly fewer pulses, .i.e., more dose-efficient treatments.

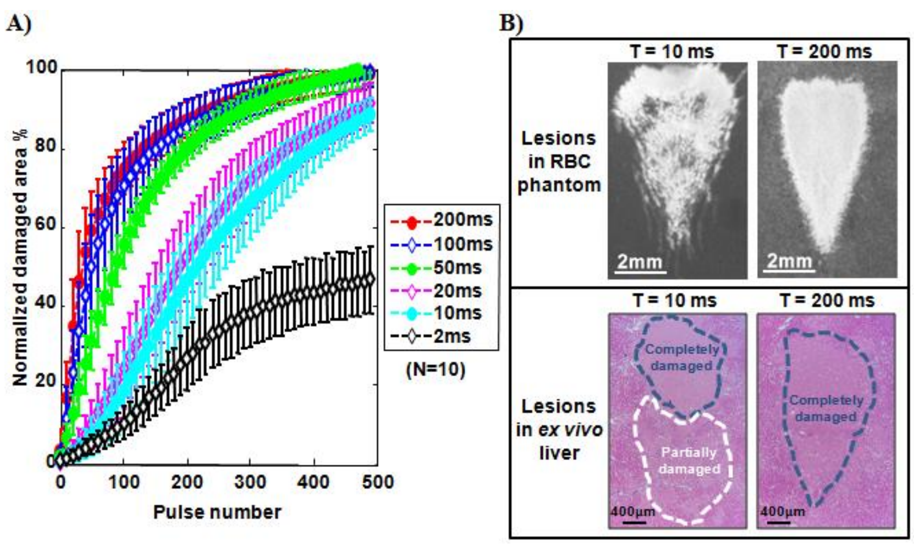

2I-2

10:45 AM Non-invasive Fetal Therapy Using Histotripsy: Safety and Local Impact on Fetal Development

Yohan Kim[1], Carlen Fifer[2], Sarah Gelehrter[2], Gabe Owens[2], Eli Vlaisavljevich[1], Charles Cain[1], Zhen Xu[1]; [1]*Department of Biomedical Engineering, University of Michigan, Ann Arbor, MI, USA,* [2]*Department of Pediatrics, Division of Pediatric Cardiology, University of Michigan, Ann Arbor, MI, USA*

Background, Motivation and Objective

Previous experiments have shown that histotripsy therapy can successfully target and fractionate fetal organs non-invasively in a gravid sheep model. The purpose of this study was to investigate the safety and effects of histotripsy therapy on the fetal development of targeted organs.

Statement of Contribution/Methods

Experiments involved four sheep at 94-102 days into gestation (full gestation period: 150 days). Histotripsy therapy was applied to fetal kidney and liver by a focused 1 MHz transducer acoustically coupled to the maternal abdominal wall. The fetal organs were exposed to 5 µs ultrasound pulses at a 500 Hz pulse repetition rate and 10-16 MPa peak rarefactional pressure. The procedure was guided by real-time ultrasound imaging through a 3 MHz imaging probe coaxially mounted with the therapy transducer. The fetuses were allowed to continue the gestation to live spontaneous birth, and the targeted organs were harvested for histopathological examination.

Results

During each treatment, localized hyperechoic cavitation bubble clouds were successfully generated in fetal kidney and liver and imaged using standard B-mode ultrasound. Volume lesions were created in 8 min by mechanically scanning the transducer focus to cover a region of 125 mm^3. All four treated fetuses survived the treatment and were delivered at full term. The lambs were healthy upon delivery and showed normal behavior. Post euthanasia inspection showed no discernible signs of damage to overlying tissues in the newborn lambs. The external surfaces of the treated kidney or liver appeared intact, although indentations were visualized, indicating that the volume of fractionated tissue may have been reabsorbed. The location of these indentations corresponded well to the regions where the cavitation bubbles were observed. Figure 1 shows the morphological aspect of a kidney harvested from a newborn lamb, 42 days after treatment was administered.

Discussion and Conclusions

Extracorporeal histotripsy therapy successfully created targeted lesions in fetal sheep organs without causing significant damage to overlying structures or impairing fetal development for the remainder of the gestation period. With further refinements and safety analyses, histotripsy has the potential to become an invaluable clinical resource for early fetal intervention.

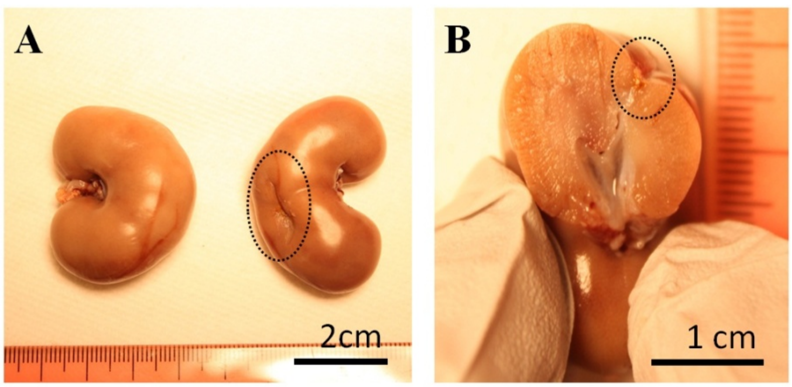

Figure 1. A) Control (left) vs. treated kidney (right) harvested from newborn lambs, with the ablated region indicated by the dashed ellipse. B) Transversal section of the treated kidney detailing the ablated area as shown by the ellipse.

2I-3

11:00 AM The Effect of Acoustic Parameters on a Non-invasive Embolus Trap (NET) Using a Histotripsy-Generated Bubble Cloud

Simone Park[1], Adam Maxwell[1], Gabe Owens[2], Hitinder Gurm[3], Charles Cain[1], Zhen Xu[1]; [1]Department of Biomedical Engineering, University of Michigan, Ann Arbor, MI, USA, [2]Department of Pediatric Cardiology, University of Michigan, Ann Arbor, MI, USA, [3]Department of Internal Medicine, University of Michigan, Ann Arbor, MI, USA

Background, Motivation and Objective

Previous observations during histotripsy-mediated thrombolysis revealed that the generated cavitation bubble cloud attracted, trapped, and eroded free clot fragments near the transducer focus even with background flow. This feature may be used to develop a noninvasive embolus trap (NET) that eliminates clot fragments during thrombolysis therapies. This in-vitro study investigated the effect of histotripsy acoustic parameters on the trapping capability and its safety.

Statement of Contribution/Methods

A closed-loop circulatory system producing flow velocities in between 1-30 cm/s was used. This system included a vessel phantom composed of a 30%-gelatin cylindrical shell embedded within a 10% block of gelatin. A bubble cloud was generated inside this vessel phantom using an 8-element, 1 MHz focused transducer with an elliptical aperture (17.5 cm long axis and 15.5cm short axis) and a 10 cm focal length. To study the trapping ability of the NET, 2-4 mm spherical agarose particles mimicking blood clots were placed in circulation to flow into the bubble cloud. The mean crossflow was increased until the particle escaped from the bubble cloud, at which the velocity was measured. This escape velocity was measured for 5-15 cycle histotripsy pulses at 100-1000 Hz pulse repetition frequencies (PRF), and peak negative pressures ranging from 18-27 MPa. To study the ability of the NET to erode trapped clot particles, 4 mm long cylindrical blood clots with a 3 mm diameter were formed and the time to completely erode the particles was measured. Hemolysis induced by the NET was quantified by exposing human red blood cells with a hematocrit of 0.4 to histotripsy pulses with the same acoustic parameters. Ex-vivo canine blood vessels were also used to look at the degree of damage.

Results

Noticeable trapping was observed only when a bubble cloud was present. Escape velocity increased with pulse length, PRF, and pressures. However, a saturation effect was observed at higher pressures and PRF. Smaller particles had a lower escape velocity compared to larger particles. Degree of hemolysis increased with pulse duration and PRF. With 10 cycle pulses at 21 MPa peak negative pressure and 500 Hz PRF, the escape velocity for a 4 mm particle was 13 cm/s, and the hematocrit of blood changed from 0.4 to 0.38 when circulated once through the system. Ex-vivo canine vein and artery exposed to the same parameters remained structurally intact with damage only to the vessel endothelial lining.

Discussion and Conclusions

These results indicate that a cavitation bubble cloud is required to induce significant trapping. Increased PRF, pulse lengths and pressures improved trapping efficiency but at the same time induced more hemolysis. Strategies are currently being developed to optimize trapping while reducing hemolysis. With further advances, NET has the potential to augment and possibly improve various clinical applications where an embolus filter is needed.

2I-4

11:15 AM Spatiotemporal Electrophysiological Changes during HIFU Ablation in Langendorff-perfused Rabbit Hearts

Ziqi Wu[1], Cheri X. Deng[1], Ronald E. Kumon[1], Yi-sing Hsiao[1]; [1]Biomedical Engineering, University of Michigan, Ann Arbor, MI, USA

Background, Motivation and Objective

High-intensity focused ultrasound (HIFU) has been exploited for thermal ablation of cardiac arrhythmias. However, little is known regarding the spatiotemporal changes in cellular electrophysiology (EP) during HIFU ablation. This study aims to elucidate the HIFU-induced spatiotemporal EP changes.

Statement of Contribution/Methods

Isolated rabbit heart was Langendorff-perfused with 37ºC Tyrode's solution and stained with fluorescent voltage-sensitive dye (FVSD) (di-4-ANEPPS). Simultaneous FVSD imaging (250 frames/s) and infrared (IR) imaging (50 frames/s) were used to measure epicardial EP and surface temperature while HIFU exposure was applied. The maximum fluorescent intensity (FI) change (F_{max}), action potential duration (APD), conduction velocity (CV) were quantified and correlated with surface temperature before, during and after HIFU exposures. These spatiotemporal EP and temperature changes were also correlated with HIFU induced lesions assessed by gross and histological examinations.

Results

1) A shift of the baseline FI was observed during HIFU and was found to depend linearly on HIFU-induced temperature increase with a slope of 0.28±0.07%/ºC (n=3).

2) HIFU ablation generated spatiotemporal changes of EP. For 2KW/cm^2 and 10s exposure duration, F_{max} was reduced by 1.36±0.35%, 0.92±0.16% and 0.02±0.06% in the lesion core, the border zone (0.420~0.84mm from HIFU focus), and non-ablated zone (0.84~1.26mm) respectively, while APD_{50} shortened by 19.17±12.42ms, 19.69±7.41 ms, and 14.16±3.76 ms correspondingly by the end of HIFU exposure. At 20s after HIFU, F_{max} recovered by 0.01±0.34%, 0.03±0.13% and reduced by 0.23±0.21% while APD_{50} further shortened by 18.83±7.52 ms, 2.5±9.83 ms and elongated by 2.5±6.12% in the corresponding zones, respectively (n=5).

3) The EP wavefront was distorted during lesion formation. CV slowed down by 31.78±11.19cm/s and 16.65±15.74cm/s by the end of 10s HIFU application with fitted linear reducing rate of 1.13±0.88cm/s and 0.71±0.31cm/s; CV recovered by 5.75±0.86cm/s and 14.50±18.77cm/s at 20s after HIFU with recover rate of 0.21±0.28cm/s and 0.1±0.05cm/s in lesion core and non-ablated area respectively with CV direction detoured along border zone (n=3).

Discussion and Conclusions

The reduction of AP, shortening of APD, and repatterning of CV within lesion area were correlated with the temperature increase both spatially and temporally. These changes were also correlated with the lesion presence spatially. On-line measurement of EP and temperature during HIFU ablation may provide critical information to guide and assess ablation outcomes.

2I-5

11:30 AM The feasibility of using thermal strain imaging to regulate energy delivery during intercardiac radiofrequency ablation

Chi Hyung Seo[1,2], Douglas Stephens[3], Jonathan Cannata[4], Aaron Dentinger[5], Feng Lin[5], Suhyun Park[5], Douglas Wildes[5], Kai Thomenius[5], Peter Chen[6], Tho Nguyen[6], Alan Delarama[6], Jong Seob Jeong[7], Aman Mahajan[8], Kalyanam Shivkumar[8], Omer Oralkan[9], Amin Nikoozadeh[9], David Sahn[10], Pierre Khuri-Yakub[9], Matthew O'Donnell[2]; [1]*Siemens Healthcare, USA,* [2]*University of Washington, USA,* [3]*University of California, Davis, USA,* [4]*University of Southern California, USA,* [5]*GE Global Research, USA,* [6]*St. Jude Medical, USA,* [7]*Dongguk University, Korea, Republic of,* [8]*David Geffen School of Medicine at UCLA, USA,* [9]*Stanford University, USA,* [10]*Oregon Health and Science University, USA*

Background, Motivation and Objective

Tissue temperature is critically related to the success or failure of catheter ablation procedures. The signal processing methods used here were developed to investigate the feasibility of monitoring ablative therapy by identifying the point at which the slope of the thermal strain curve changes sign caused by speed of sound variations with temperature. Previously, we have demonstrated the feasibility of this method in-vivo using porcine models. In this paper, we present recent results with temperature validation for this method in-vivo using an integrated intracardiac echocardiography (ICE) probe. Also preliminary result of thermal strain imaging using a cMUT array integrated into the ICE probe is presented.

Statement of Contribution/Methods

To ensure that sufficient heat could be delivered for lesion formation, excised porcine heart was prepared in a saline solution. RF data were collected using a prototype integrated ablation catheter array interfaced with a GE Vivid 7 imaging system. Temperatures in the tissue were measured using an implanted fine wire thermocouple. For the in-vivo study, juvenile Yorkshire pigs were used as the animal model. We used a specially designed ultrasound compatible RFA tip integrated into a prototype 9F forward-looking ML ICE catheter array to simultaneously image and ablate the right atrial wall. Additionally, a thermocouple normally residing inside the electrode was pulled out to touch the tissue for thermal strain comparisons. Two-dimensional phase-sensitive correlation-based speckle tracking was applied to RF data to estimate temporal shifts along the axial direction, and the derivative along the same direction was used to estimate temporal strain due primarily to the sound speed change.

Results

B-mode images are overlayed with thermal strain images for both the in-vitro dynamic heating experiment and in-vivo animal study. Thermal strains at positions within the image are plotted against temperature rise. By plotting the slope of the thermal strain curve as a function of temperature, the sign change at around 50 Â°C is clearly observed. In particular, this method appears promising for the case where heating is sufficiently fast to minimize the effects of thermal diffusion. Photographs of the lesions confirm that RF ablation was successful.

Discussion and Conclusions

The potential of monitoring temperature during RF ablation using a slope change in the thermal strain curve has been demonstrated. For both in-vitro and in-vivo experiments, thermal strain curves showed a plateau then slope change at around 50 Â°C. Because only three in-vivo experiments are reported here, additional in vivo studies are needed to better evaluate the robustness of this technique for real clinical applications. Nonetheless, preliminary results look promising and suggest that thermal strain imaging may be a useful tool to guide RF ablations of the heart using intracardiac devices.

This work was supported in part by NIH/NHLBI grant HL-67647

2I-6

11:45 AM Acoustic Radiation Force for Vascular Stem Cell Therapy: an in Vitro Validation

Mehmet Kaya[1], Catalin Toma[1], Michelle Grata[1], Huili Fu[1], Flordeliza S. Villanueva[1], Xucai Chen[1]; [1]Center for Ultrasound Molecular Imaging and Therapeutics, Cardiovascular Institute, University of Pittsburgh Medical Center, Pittsburgh, PA, USA

Background, Motivation and Objective

An important problem in the treatment of coronary disease is the vascular injury following percutaneous interventions. We have previously investigated a novel method for targeted delivery of stem cells to a site of arterial injury using acoustic radiation force (ARF) for therapy in vivo. The objective of this study was to verify and optimize ultrasound (US) parameters for the delivery of stem cells using an in vitro flow model.

Statement of Contribution/Methods

Human mesenchymal stem cells (MSCs) were surface coated electrostatically with cationic lipid microbubbles (MB) of 2.85±0.96 µm diameter. The MB-MSC complexes were withdrawn through a phantom vessel with an inner diameter of 3.5 mm. Flow rates were chosen such that the wall shear stress approximates that of coronary blood flow. An intravascular US catheter (MicroSonic SV, EKOS Corp) placed along the center of the phantom delivered the desired US pulses radially through its tip (2 mm length) at 1.7 MHz. The flow system was placed under a microscope equipped with a highly sensitive EMCCD camera (C9100, Hamamatsu) for optical observation and recording. Images were analyzed for particle trajectory, radial velocity (Vr), and amount of cell adhesion. Numerical simulation of the acoustic radiation force and its effect on the MB-MSC complexes were also performed. Results from in vitro experiments were compared with the simulation.

Results

We sought to explore the optimal combination of US parameters leading to maximal targeted MB-MSC delivery to the vessel phantom wall. Theoretically, this is directly proportional to the amount of acoustic energy delivered, however high levels of US can lead to bubble destruction and thermal injury. We investigated the following parameters on the Vr and adhesion of the MB-MSC complexes: acoustic power (50-500 kPa), duty cycle (DC) (10, 20 and 60%) and pulse length (5, 10, 20 cycles). Vr of the MB-MSCs was found to be proportional to the number of cells adhering to the vessel wall in the time frame explored, and was used a surrogate parameter for the optimization of cell delivery. We found that the maximum Vr and adhesion was achieved at 500 kPa / 20% DC, and this was relatively independent of the pulse length used (5, 10, 20 cycles). This was significantly higher than the Vr and adhesion achieved with lower acoustic pressures, even if longer duty cycles were used. Results from in vitro studies were in agreement with numerical simulations.

Discussion and Conclusions

The use of MB and ARF allows targeted delivery of stem cells. Due to the nature of the coronary flow, there is a very limited time window for the ARF to act on the MB-MSC complexes to facilitate enhanced adhesion. Optimization of the acoustic parameters is essential to maximize the radial translational motion of the MB-MSCs resulting in enhanced adhesion to treatment sites while minimizing the acoustic energy used to avoid undesirable bioeffects such as heating.

3I - Drug Delivery II

Carribean Ballroom VII

Friday, October 21, 2011, 10:30 am - 12:00 pm

Chair: **Ayache Bouakaz**
INSERM, Tours

3I-1

10:30 AM Optical Characterization of Individual Liposome Loaded Microbubbles

Ying Luan[1], Telli Faez[1], Erik Gelderblom[2], Ilya Skachkov[1], Bart Geers[3], Ine Lentacker[3], Antonius van der Steen[1], Michel Versluis[2], Nico de Jong[1,2]; [1]*Erasmus Medical Center, Netherlands,* [2]*University of Twente, Netherlands,* [3]*University of Gent, Belgium*

Background, Motivation and Objective

Liposome loaded microbubbles (lps bubbles) have been newly developed by attaching drug containing liposomes to phospholipid-shelled microbubbles through covalent thiol-maleimide linkages (Figure (A)) [1]. Applied as an ultrasound triggered drug delivery vehicle, it has shown great potential to realize highly efficient and localized drug release. In this study we optically compared individual lps bubbles with standard phospholipid bubbles (bare bubbles) concerning shell properties and ultrasonic response with a high framing camera.

Statement of Contribution/Methods

Lps bubbles and bare bubbles, ranging from diameter of 3 to 8 µm, were insonified with driving frequencies from 0.5 to 4 MHz and acoustical pressures from 5 to 100 kPa. Bubble dynamics were recorded with the ultra-high speed camera Brandaris 128 at 15 Mfs. Resonance curves were constructed from diameter-time (D-t) curves of bubble oscillations and shell elasticity and viscosity were derived (Figure (B))[2]. Laser induced fluorescence imaging were applied before and after ultrasound treatment to acquire morphology and stability of liposomes attachment.

Results

72 lps bubbles and 55 bare bubbles were investigated. Shell elasticity of lps bubbles (0.77±0.1 N/m) was 88% higher compared to bare bubbles (0.41±0.1 N/m) for all investigated bubble sizes. Clear difference of shell viscosity was found for bubbles larger than 6 µm. Averaged viscosity of lps bubbles ($3.2 \cdot 10^{-8}$ kg/s) was 44% higher than that of bare bubbles ($1.8 \cdot 10^{-8}$ kg/s). Moreover, we found an ″expansion only behavior″ among 73% of lps bubbles (Figure (C)), with 60% among them happened at low pressures (<30 kPa). Fluorescence imaging clearly showed stably attached bodipy-labeled liposomes at the surface of microbubbles.

Discussion and Conclusions

Lps bubbles and bare bubbles have different ultrasonic response and shell properties. Results from this study will facilitate applications as well as further comprehension of drug transfer mechanism using ultrasound triggered drug delivery system.

1. Geers, B., et al., Journal of Controlled Release. In Press.
2. Meer van der, S.M., et al., Journal of the Acoustical Society of America, 2007. 121(1): p. 648-656.

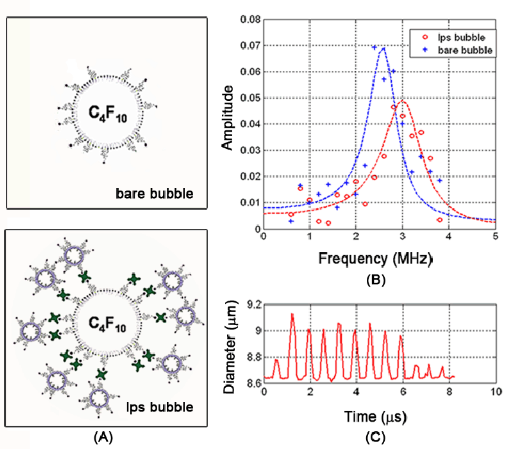

3I-2

10:45 AM Ultrasound and Microbubble Mediated Doxil Delivery in a Murine Breast Cancer Model: Therapeutic Efficacy Dependence on Tumor Growth Rate

Ralf Seip[1], Evgeniy Leyvi[1], Balasundar Raju[1], William Shi[1], Marcel Bohmer[2], Ceciel Chlon[2], Charles Sio[2], Kristin Patterson[3], Terri Swanson[3]; [1]*Philips Research, NA, USA,* [2]*Philips Research Europe, Netherlands,* [3]*Pfizer Global Research and Development, USA*

Background, Motivation and Objective

Localized ultrasound mediated drug delivery could improve the therapeutic efficacy for the treatment of malignant tumors and reduce toxic exposure to healthy organs and tissues. The long term objective of this study is to investigate the usage of ultrasound, microbubbles, and a co-injected anti-neoplastic small molecule drug in a liposomal formulation (Doxil) in a murine breast cancer model to prove this hypothesis.

FRIDAY ORAL

Statement of Contribution/Methods

Two separate studies were performed. In the first study, MDA-MB-231-luc cells were implanted into the lower mammary fat pad of SCID beige mice and yielded a tumor doubling time of approximately 8 days. In the second study, the same cells were implanted similarly, but yielded a tumor doubling time of approximately 13 days. In all other aspects, both studies were identical. Experiment groups included: vehicle-treated control, Doxil treatment only, single ultrasound + microbubbles + Doxil treatment, and two ultrasound + microbubbles + Doxil treatments. Treatments were performed when the tumor size reached 150 mm^3 on average, using a 3 mg/kg Doxil dose (bolus), Definity (Lantheus Medical Imaging) microbubbles (1:1 dilution, constant infusion via tail vein), and focused ultrasound (TIPS, Philips Research NA), at 1MHz, 1MPa, 10ms x 6 sonications/site, 1 cm^2 treatment region covering the entire tumor. Microbubble wash-in was confirmed by low-MI (0.1) ultrasound imaging prior to starting the focused ultrasound exposure. The animals were followed for 15 days after treatment, during which time the animal weight and tumor size (using calipers) was measured. A subset of animals was euthanized at various timepoints for histological and pharmacokinetics (pK) analysis.

Results

At 15 days post-treatment, tumor size was reduced by 3±18%, 8±14%, and 20±10% as compared to control for the Doxil only, ultrasound + microbubbles + Doxil (1 treatment), and ultrasound + microbubbles + Doxil (2 treatments) groups, respectively, in the mice with the slower growing tumors. The mice with the faster growing tumor yielded tumor size reductions of 46±27%, 71±10%, and 61±26%, respectively, for the same groups.

Discussion and Conclusions

Results suggest that the ultrasound mediated treatment efficacy is not only dependent on the drug and microbubble dosages, ultrasound sonication parameters, microbubble composition, and tumor model (as previously shown in the literature), but we hypothesize that it is also dependent on the dynamics of the tumor model itself, even within the same cell line. Additional experiments are needed to validate this hypothesis. Experimental details, including ultrasound setup, tumor model, histology, and pK data findings will be shown.

3I-3

11:00 AM Mechanism Monitoring of Noninvasive Cavitation-Guided Blood-Brain Barrier Opening Using Focused Ultrasound and Microbubbles in Non-Human Primates

Yao-Sheng Tung[1], Fabrice Marquet[1], Tobias Teichert[2], Vincent Ferrera[2], Elisa Konofagou[1,3]; [1]Biomedical Engineering, Columbia University, USA, [2]Neuroscience, Columbia University, USA, [3]Radiology, Columbia University, USA

Background, Motivation and Objective

Most neurological disorders and neurodegenerative diseases, including Alzheimer's and Parkinson's, remain difficult to treat because of the impermeability of the blood-brain barrier (BBB). To date, BBB opening with focused ultrasound (FUS) has been achieved in different animals, including mice, rabbits, rats, and pigs. So far, this method has not been used in primates. It is non-trivial to extend this method to new species due to the thicker skull and more complex brain anatomy involved. Since our group recently demonstrated that the bubble diameter plays an important role in BBB opening, both mono- and poly-dispersed microbubbles were used in order to study the same effect in larger animals and hence infer to the mechanism of BBB opening in primates.

Statement of Contribution/Methods

Six experiments on three monkeys (16 sonications) were each injected intravenously with customized, lipid-shelled, perfluorobutane filled of 4-5-µm in diameter bubbles or commercially available (polydispersed) Definity® microbubbles. The concentration in both cases was 0.05 mL/Kg. The caudate or visual cortex was then sonicated using focused ultrasound (500 kHz frequency; 100 (200 µs) or 15000 cycles (10 ms) pulse length; 2 Hz pulse repetition frequency; 2 minute sonication duration; 0.20 to 0.60 MPa peak-rarefactional pressure). A 7.5-MHz Pulse/Echo transducer was used as the passive cavitation detector (PCD). T1-weighted MRI was used to verify the BBB opening and a spectrogram was generated in order to detect the IC onset and duration.

Results

The BBB was opened in all cases with 4-5 µm diameter bubbles. At 0.30 MPa, the BBB was mainly opened by stable cavitation (harmonics and ultra-harmonics), and very low broadband response was detected. While increasing the pressure to 0.60 MPa, a larger broadband signal was detected and a larger BBB opening area was induced that included the caudate and visual cortex. When using Definity® and targeting the visual cortex, inertial cavitation was induced in all cases, but the BBB was not opened at 0.30 and 0.45 MPa and only opened at 0.60 MPa.

Discussion and Conclusions

The noninvasive and transcranial cavitation detection during BBB opening in non-human primates was shown feasible in this study. In addition, the MRI contrast enhancement were shown to be region and microbubble-size dependent. Inertial cavitation did not result in BBB opening at the visual cortex when the pressure was lower than 0.45 MPa using Definity®. Therefore, this technique might be used for cavitation-guided BBB opening to better monitor the target of sonication and investigate the mechanism of BBB opening in primates. Further studies will be performed to optimize the application in primates and determine the correlation between the location of BBB opening and the cavitation dose.

Supported in part by NIH R01EB009041, NIH MH059244, NSF CAREER 0644713, and the Kavli Institute.

3I-4

11:15 AM Effect of Microbubble Shell Components on Ultrasound and Microbubble mediated Gene Transfection *in vivo*

Richard J. Browning[1], Helen Mulvana[1], Mengxing Tang[2], Jo V. Hajnal[1], Dominic J. Wells[3], Robert J. Eckersley[1]; *[1]Imaging Sciences Department, Imperial College London, London, United Kingdom, [2]Department of Bioengineering, Imperial College London, London, United Kingdom, [3]Department of Veterinary Basic Sciences, Royal Veterinary College, London, United Kingdom*

Background, Motivation and Objective

Ultrasound and microbubble mediated gene transfection is a rapidly advancing field with great potential for the targeted treatment of disease. Protein shelled microbubbles (MB) have been shown to be more effective; however detailed optimisation for transfection has not been reported. Our previous work showed that MB fabricated with a 2% albumin solution displayed greater acoustic scattering and oscillatory behaviour than 5% albumin MB, but transfection was limited by poor MB stability. Here we demonstrate methods to improve MB stability and investigate their bulk acoustic properties and transfection efficiency *in vivo*.

Statement of Contribution/Methods

Albumin shelled MB were produced by sonication of mixed solutions of 2% or 5% human serum albumin, 20% or 40% dextrose and octafluoropropane. The resulting suspensions were sized using optical microscopy.

Acoustic scattering and attenuation measurements of bulk MB suspensions were made.

Acoustic destruction of bulk suspensions was investigated using a Siemens Acuson Sequoia (15L8 probe) between 0.05 – 1.60 MI. Images were processed using custom software developed in MATLAB to recover temporal changes in scattered intensity.

In vivo transfection experiments were performed on the myocardium of 6 week old, female, CD1 mice with the Siemens scanner. A suspension of MB and a luciferase plasmid was administered intravenously with 2 minutes of 6 MHz ultrasound applied. Transfected regions were visualised with bioluminescence imaging.

Results

For 20% dextrose preparations, 2% albumin MB showed greater total and nonlinear scattering (188% and 193% respectively) compared to 5% albumin. Increased dextrose concentration increased scattering for both albumin concentrations with 2% albumin MB still superior to 5% albumin in total and nonlinear scatter (104% and 141%).

At MIs ≥0.92, there was little difference in the rate of MB destruction between albumin concentrations At 0.52 MI, increasing albumin or dextrose reduced the rate of destruction.

An increase in dextrose concentration improved transfection using 5% albumin and 2% albumin MB (287% and 6367%). 2% albumin MB produced less transfection than 5% albumin at 20% dextrose but more at 40% dextrose (6% and 145%). MB with increased dextrose persisted longer in the circulation *in vivo.*

Discussion and Conclusions

MB fabricated using higher dextrose concentration increased *in vivo* transfection. Acoustic investigation indicated that increasing dextrose can be used to improve MB stability without sacrificing the improved shell elasticity achieved by reducing the shell protein concentration. Stabilised 2% albumin MB caused greater transfection than 5% albumin, potentially due to increased oscillatory behaviour as demonstrated during acoustic characterisation. Our work has demonstrated that MB shell components strongly affect acoustic behaviour and functionality, and that oscillatory behaviour affects transfection.

3I-5

11:30 AM Monitoring of Microbubble-mediated Ultrasound Therapy using Fluorescent Imaging: A Feasibility Study

Anna Sorace[1], Reshu Saini[1], Eben Rosenthal[2], Kenneth Hoyt[3]; *[1]Biomedical Engineering, University of Alabama at Birmingham, Birmingham, AL, USA, [2]Surgery, University of Alabama at Birmingham, Birmingham, AL, USA, [3]Radiology, University of Alabama at Birmingham, Birmingham, AL, USA*

Background, Motivation and Objective

Microbubble (MB) contrast agents in the presence of ultrasound (US) have been shown to temporarily enhance cell membrane permeability. They have also been shown to increase extravasation by breaking down gap junctions between cancerous cells. The efficiency of a drug, such as chemotherapy, to be delivered and taken up by cancerous cells, ultimately determines the effectiveness of any systemic treatment. Increased demands for new, noninvasive treatments have led to novel modalities to monitor and evaluate early treatment response. The ability to monitor the effectiveness of increased tumor perfusion from MB-mediated US therapy is extremely beneficial in both monitoring and gaining further understanding on the mechanisms of the treatment.

Statement of Contribution/Methods

Optimized in vitro parameters from previous MB-mediated US therapy studies were used to induce fluorescent tracer tumor uptake in vivo. Nude athymic mice (n = 10) were implanted with 2LMP breast cancer cells (2x106). Mice underwent MB-mediated US therapy in the presence of Cy5.5 fluorescent-labeled IgG antibody and Definity MBs (30 µL bolus via tail vein injection). US parameters included: 1.0 MHz transmit frequency, 5.0 min duration of exposure, 5 sec pulse repetition period, 20% duty cycle and an MI of 0.5. Mice were transiently imaged at 1, 5, 30 and 60 min post therapy using a small animal optical imaging system (Pearl Impulse, LI-COR Biotechnology). The ability to image the tumors progressively over time allowed measurement of any therapy-induced effects.

Results

In vivo fluorescent tracer tumor uptake following MB-mediated US therapy showed a 8.39 % increase at one min post therapy, peaking at a 13.8 % increase five min post therapy over control animal data (p = 0.19). At 60 min, the MB-mediated US therapy group showed an 11.19 % increase in intratumoral fluorescent tracer accumulation over control group measurements. This quantification allowed monitoring direct temporal effects of MB-mediated US therapy on tumor tissue in vivo. This information also gives insight into biological effects into recovery time of the cellular and vascular membranes post MB-mediated US therapy.

Discussion and Conclusions

MB-mediated US therapy has considerable potential for increasing drug uptake in cancer patients. As this novel therapy continues to be studied, it becomes increasingly important to elucidate the effects and mechanisms of this therapeutic adjunct. In this study, we investigated a noninvasive optical imaging method for monitoring the effects of MB-mediated US therapy. This provides insight into the process of increasing extravasation of molecules (such as chemotherapeutic drugs) into target tumors.

3I-6

11:45 AM Imaging Tumor Vascularity by Tracing Single Microbubbles

Monica Siepmann[1], Jessica Bzyl[2], Moritz Palmowski[2], Fabian Kiessling[2], Georg Schmitz[1]; [1]Medical Engineering, Ruhr-University, Bochum, NRW, Germany, [2]Experimental Molecular Imaging, RWTH Aachen, Aachen, NRW, Germany

Background, Motivation and Objective

Assessment of tumor vascularization is an important factor in non invasive detection and characterization of cancer. The usage of contrast enhanced ultrasound to image tumor vessels is therefore subject of ongoing research. In B-Mode image series the flow of single microbubbles (MB) through the vessels can be appreciated. In this work we propose identification of the individual MB as a new approach to assess tumor vascularity. Hereby, the number of MB can be quantified and spatially mapped. Tracing the MB centroids may further yield a more precise estimation of the vessel position. Thus high resolution quantitative images of the vascularization can be obtained.

Statement of Contribution/Methods

Human breast cancer xenografts were induced by injecting 5x10^6 MDA-MB-231 cells orthotopically into the mammary fat pad of CD1 nude mice. A 50µl bolus of 5x10^7 MB of the experimental agent BR38 (Bracco) plus a 20µl saline flush was injected into the tail vein. Ultrasound B-Mode images of the contrast perfused tumor were acquired with a Vevo 2100 ultrasound system (Visualsonics) and a MS550S transducer. A series of 500 frames was acquired, storing the raw IQ data. Image processing was performed on the unfiltered absolute values of the IQ-samples. Consecutive frames were registered by finding the maximum of the cross-correlation. Matched images were then subtracted. Breathing motion resulted in non-rigid transformation of the image in several frames which were therefore discarded. A Difference of Gaussians filter is applied to the subtraction images to enhance structures with the size of the imaged MB. Centroids of spots exceeding a threshold are calculated to estimate the MB position.

Results

Fig. 1 shows the color coded local MB number overlaid on the greyscale intensity image. Tumor vessel structures can be clearly appreciated. While in a standard maximum intensity projection image the perfused area in the tumor was strongly overestimated (68.4%) improved resolution of the new method reduced the area fraction to 10.5% which was in line with results from immunohistochemisty (positive area staining for endothelial marker CD31: 7.7%).

Discussion and Conclusions

Single Microbubble Tracing presents a promising strategy to image the tumor vascularity. It provides quantitative information on the actively perfused vessel surface thus representing a potential surrogate parameter for assessment of early treatment effects.

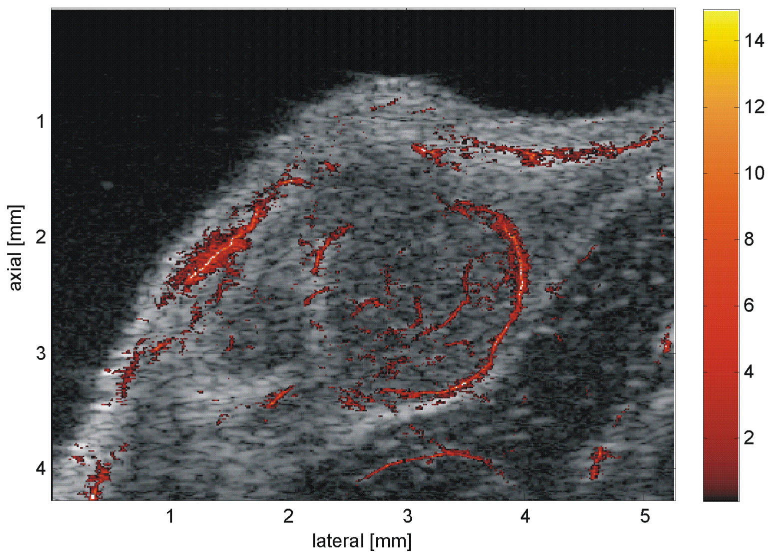

FRIDAY ORAL

4I - Applications and Measurements of Ultrasonic Energy

Carribean Ballroom I

Friday, October 21, 2011, 10:30 am - 12:00 pm

Chair: **Kentaro Nakamora**
Tokyo Institute of Technology, Japan

4I-1

10:30 AM Ultrasonic welding using complex vibration and high frequency vibration - Various vibration sources and frequency characteristics of ultrasonic welding -

Jiromaru Tsujino[1,2]; [1]Kanagawa University, Yokohama, Kanagawa, Japan, [2]Asahi EMS Co Ltd, Yokohama, Kanagawa, Japan

Background, Motivation and Objective

Ultrasonic welding can weld same and different metal specimens directly using ultrasonic vibration. The welding area is limited within very thin layer and possible to weld different metal specimens which have different melting temperature such as aluminum, copper difficult to weld by usual methods. Welding conditions are changed by frequency, dimensions of specimen and especially vibration locus.

Statement of Contribution/Methods

High frequency linear vibration systems up to 1 MHz are designed for metal welding. Complex vibration welding systems with elliptical to circular loci are proposed and the systems are using (1) multiple transducers integrated with a circular disk and (2) longitudinal-torsional vibration converters with diagonal slits driven by a longitudinal vibration source.

For plastic welding, high frequency linear vibration systems up to 180 kHz avoiding radial vibration resonance of the system. Maximum vibration velocity for 180 kHz system obtained is over 5 m/s (peak-to-zero value).

Results

Frequency characteristics of 0.1-mm-diameter aluminum and 1.0-mm-thick copper plate specimens using welding systems of 40 to 800 kHz are shown in Fig. 1. Required vibrations at 15 kHz to 27 kHz for usual specimens are also shown in circular areas. Required vibration amplitude for metal welding decreases as frequency becomes higher, and welding conditions are improved significantly. Using complex vibration of circular locus, required vibration amplitude decreases significantly as shown in Fig.2.

Fig. 3 shows the frequency characteristics of plastic welding in the range of 27 kHz to 180 kHz.

Discussion and Conclusions

For large specimens, two-vibration-system and butt welding methods are effective.

Using complex vibration, required vibration amplitude decreases significantly, and large and uniform weld strength are obtained independent of vibration direction, and multiple and seam welding become possible. For large specimens, two-vibration-system and butt welding methods are effective. Metal specimens were joined directly without any oxide, mutual diffusion and any different structures.

For plastic welding, required vibration velocity and amplitude become smaller as vibration frequency is higher due to larger vibration absorption of plastic materials. The welding method using fundamental and higher resonance frequencies was proposed and shown very effective.

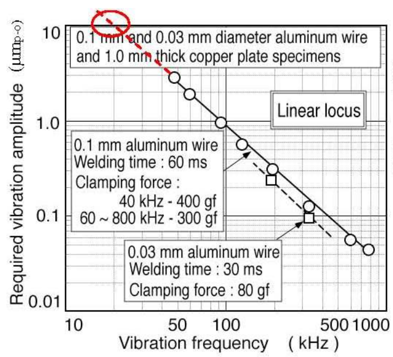

Fig. 1 Frequency characteristics of metal welding: linear vibration.

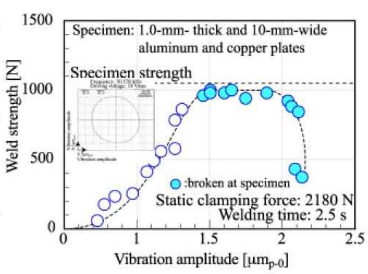

Fig. 2 Welding condition of 1.0-mm-thick aluminum and copper plates using complex vibration welding

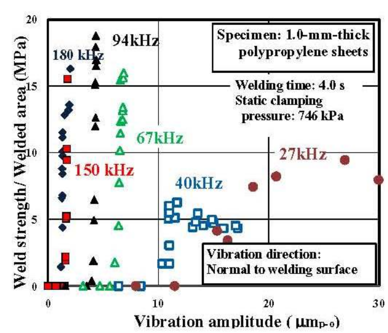

Fig. 3 Frequency characteristics of ultrasonic plastic welding

FRIDAY ORAL

4I-2

11:00 AM Optimization of Friction Stir Welding Parameter for AA 5083 By Radiography and Ultrasonic Technique

Vidya Joshi[1], Krishnan Balasubramaniam[1], Raghu V. Prakash[1]; [1]Department of Mechanical Engineering, Indian Institute of Technology madras, Chennai, Tamilnadu, India

Background, Motivation and Objective

Aluminum (Al) alloy is light weight material and has many industrial application. The Friction stir welding (FSW) is a new and promising welding process which welds the material below its melting temperature. This process is effective for joining difficult to weld material such as various Al-alloy and dissimilar material. Even though various types of defects occurs in the FSW like large mass of flash out, cavity or groove like defect, porosity and kissing bond. These defects reduces the quality of weld. There are several welding parameters taking influence over the final welding quality, namely: vertical force, rotation speed, travel speed, tool geometry, plunge depth and tilt angle between the tool and welding materials. The right choice and application of the welding parameters will result on sound welds and which improves the mechanical properties of material.

Statement of Contribution/Methods

Non-destructive testing (NDT) is based on techniques that rely on the application of physical principles to determine the characteristics of materials and to detect and assess flaws or harmful defects without change of the usefulness or serviceability of materials. Determination of optimum condition is very important in FSW for getting sound weld. In this paper the use of radiography and ultrasonic technique is done for evaluating the effect of welding parameter on the joint quality.

Aluminum AA-5083 is welded by FSW technique with various welding parameter. The material is welded with variation in rotation speed from 100rpm to 800 rpm and travel speed from 50 mm/min to 150 mm/min. The radiography and immersion ultrasonic testing is performed on the welded material for detecting various defects. Along with NDT, metallurgical inspection was performed on the cross section of FSW joint. They were polished and etched in the solution of 4 ml HF, 4 ml H_2SO_4, 2 g CrO_3 in 90 ml water for optical microscopic observation.

Results

Different types of defect are formed depending on the FSW condition : large mass of flash out was ejected outside due to softening of metal by excess heat input i. e. higher rotation speed and lower travel speed, Cavity or groove like defects occur by insufficient heat input i. e. lower rotation speed and higher travel speed. Cavity are caused by abnormal stirring. Kissing bond type defects are observed due to oxide entrapment. At each tool plunge depth sound joints are obtained at appropriate tool rotation speed and welding speed.

Discussion and Conclusions

Various defects in the FSW are observed by the radiography and ultrasonic technique. Thus range of optimum FSW parameter can be determined by using the radiography and ultrasonic technique and the results of NDT is supported by the metallurgical analysis.

4I-3

11:15 AM High Temperature Ultrasonic Transducers for In Service Inspection of Liquid Metal Fast Reactors

Jeffrey Griffin[1], Gerald Posakony[2], Robert Harris[2], David Baldwin[2], Leonard Bond[2]; [1]Applied Physics, Pacific Northwest National Laboratory, Richland, Washington, USA, [2]Pacific Northwest National Laboratory, USA

Background, Motivation and Objective

In service inspections of liquid metal fast reactors require the use of high temperature ultrasonic imaging systems. Building on under-sodium viewing work performed at the DOE Hanford Site in the 1970's, and collaborations with Argonne National Laboratory and the Oarai Research and Development Center, Japan, the Pacific Northwest National Laboratory (PNNL) is developing a new generation of ultrasonic NDE and imaging systems specifically for the high temperature, high radiation sodium environment of fast spectrum reactors.

Statement of Contribution/Methods

The new PNNL transducer designs incorporate high Curie temperature piezo-ceramics such as lead metaniobate and bismuth titanate as well as a rapid-wetting, nickel-alloy faceplate to achieve acoustic coupling to the liquid sodium. Both single-element devices (for sodium wetting studies and thermal bonding materials testing) and 1-3MHz, 12-element linear phased arrays (for under sodium imaging) have been fabricated, and have undergone initial under-sodium testing.

Results

This presentation will summarize: 1) the materials selection process; 2) results of single-element transducer sodium-wetting and under-sodium crack detection experiments; 3) linear phased array performance modeling studies and; 4) under-sodium imaging experiments performed with the high temperature linear (Mark II) phased array.

Discussion and Conclusions

Sustained high-temperature operation of single-element and linear array ultrasonic transducers has been demonstrated in 250C liquid sodium. Pure nickel and nickel alloy (Alloy#48) faceplate materials exhibit rapid sodium wetting and re-wetting thus eliminating the need for sacrificial coating layers.

4I-4

11:30 AM Coupling between flexural and Stoneley modes in cylindrical three-layered media

Hanyin Cui[1], Jon Trevelyan[1], Sherri Johnstone[1], Stuart Millman[2]; [1]School of engineering and computing sciences, Durham University, Durham, United Kingdom, [2]Research Development & Technology, Tata steel, Middlesbrough, United Kingdom

Background, Motivation and Objective

This paper presents a theoretical analysis of guided wave propagation along an ultrasonic transmission rod which is a three-layered cylindrical waveguide that consists of a steel rod, a silica sheath, and steel cladding. The rod is designed to transmit and receive pulses to/from liquid steel for detecting small inclusions. In order to thoroughly understand the signal propagation process, coupling between non-axisymmetric flexural modes and interfacial Stoneley modes is studied for improving the rod design.

Statement of Contribution/Methods

Both dispersion and excitation characteristics are analysed numerically. The dispersion equation of flexural modes with circumferential order equal to 1, termed F(1,m) (m=1,2,…), is solved using the global matrix method. Without considering attenuation, phase velocity dispersion curves are traced by solving the equation applying a bisection technique. Furthermore, group velocity, amplitude spectra, and amplitude distributions along a radial cross section of F(1,m) modes, excited by a radial force source, are investigated.

Results

Typical results are presented. Fig.1 shows the coupling of flexural and Stoneley modes that each of the phase velocity dispersion curves of F(1,m)(m=4,5,…) exhibits a plateau close to the Stoneley velocity 3283m/s.

Discussion and Conclusions

From the numerical results it is concluded that (1) each coupled flexural mode exhibits Stoneley mode properties in a certain frequency range. In the specific range, the mode shows low dispersion with phase and group velocities both around the Stoneley velocity, and its energy is confined to the vicinity of a material interface. (2) The factors influencing the coupling include the shear moduli and the thickness of the sheath layer.

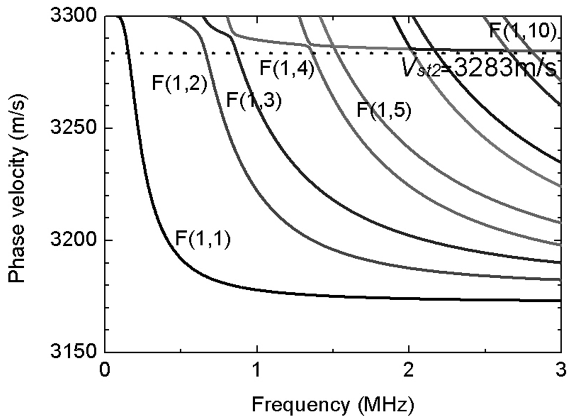

4I-5

11:45 AM Macro energy harvester based on Aluminium Nitride thin films

Thibault Ricart[1], Pierre Patrick Lassagne[1], Sebastien Boisseau[1], Ghislain Despesse[1], **Emmanuel Defay[1]**, Christophe Billard[1]; [1]*CEA/Leti, France*

Background, Motivation and Objective

With the proliferation of ultra low power consumption wireless devices and the green concern, a current trend is to take advantage of energy harvesting. This can be performed from mechanical vibration, electromagnetism, and temperature. Most of the vibration energy is between 50 and 200Hz and the related acceleration is often no more than 1-2 m/s². Besides, for low power communication devices, 10 to 100 µW is considered to be the minimum energy target range to be collected continuously. Therefore, to reach this energy target with such a low acceleration and frequency, the needed device surface lies in the cm² range. This paper reports the fabrication and characterization of cantilevers with Aluminium Nitride (AlN) piezoelectric thin films, adapted to such a kind of weakly vibrating environment (100 Hz – 1m/s²). Moreover, the technology associated must be as simple as possible: 6 process steps in total dedicated to a cheap mass production.

Statement of Contribution/Methods

An analytical model based on piezoelectric equation coupled with mechanical simulation performed with a commercial software was developed to design the cantilevers. AlN films 5.6µm-thick were deposited by dc-pulsed reactive sputtering. One of the key processes is to perform large electrodes (typ. 1 x 2 cm²) to extract the maximum charges from the cantilever vibration. A back side etching is performed to decrease the resonance frequency of this 2.6cm-long cantilever. Moreover, a tungsten mass can be added at the free end of the beam to adjust the resonance frequency. To characterize our device, a vibrating shaker is used to generate a controlled acceleration to the cantilever. The charges generated by the piezoelectric film are collected directly on an oscilloscope to be analysed.

Results

A cantilever resonating at 114Hz harvests 106µW continuously when acceleration is 1.5m/s². This result is in line with our goals to be able to overtake the 100µW desired value. The peak voltage is 14.5V by using 1MΩ as input impedance. By taking into account the volume and the mass of the device, for such low vibrating environment, this works belongs to the best published results for vibrating energy harvesters.

Discussion and Conclusions

The next step is to adjust the input impedance and to optimize the harvested energy by using a dedicated circuit to store energy. Although these devices harvest enough energy for RF transducers, further studies must been conducted. Actually, energy harvesters have to be able to supply a device as long as a battery will. Moreover, study on packaging are currently under way because the mechanical response linked to the piezoelectric effect can be greatly improved if we can decrease the mechanical damping. This in turn should improve the quality factor of the resonance.

5I - Application of Materials

Carribean Ballroom II

Friday, October 21, 2011, 10:30 am - 12:00 pm

Chair: **Steven Freear**
University of Leeds

5I-1

10:30 AM Synthesis and Characterization of PZT Single Crystals

Zuo-Guang Ye[1], Yujuan Xie[1], Alexei Bokov[1], Xifa Long[1]; [1]*Simon Fraser University, Burnaby, BC, Canada*

Background, Motivation and Objective

Single crystals of Pb(Zr1-xTix)O3 [PZT] are of great importance for the characterization of the anisotropic properties, and thereby for the understanding of the origin of the enhanced piezoelectric performance, of this solid solution system near the morphotropic phase boundary (MPB). In this paper, we report on the progress that has been made in the growth and characterization of the PZT single crystals. We have developed an improved top-seeded solution growth (TSSG) technique which resulted in PZT crystals with a wide range of compositions across the MPB, i.e. from x = 0.20 to x = 0.65.

Statement of Contribution/Methods

The availability of PZT crystals has made it possible to investigate the domain structures and phase transitions by polarized light microscopy (PLM) combined with dielectric measurements, and to characterize the piezo-/ferroelectric properties of the PZT crystals with a view to possible applications as ultrasonic transducers.

Results

PZT single crystals were synthesized using improved top-seeded solution growth (TSSG) technique, and it was found that the composition of grown PZT single crystals can be controlled by adjusting chemical, thermodynamic and kinetic parameters of the growth.

By PLM studies of domain structure and phase symmetry, we have found unusual scale-dependent symmetry below the ferroelectric Curie temperature in the PZT crystals of morphotropic phase boundary compositions. The crystals of tetragonal symmetry (from X-ray diffraction experiments) on sub-micrometer scale exhibit a macroscopic (optically determined) cubic symmetry. This peculiar optical isotropy is explained by the anomalously small size of tetragonal ferroelectric domains.

Discussion and Conclusions

The phase transition and critical behaviour of PZT crystals have been studied. Based on the dielectric measurements the phase T-x diagram is constructed. For the compositions with x = 0.5 in the vicinity of this transition, the critical region, recently predicted by the first principle-based calculations, is discovered experimentally for the first time in any ferroelectric systems. The existence of tricritical points in the diagram at xt1 = 0.55 and xt2 = 0.43 is confirmed and an additional tricritical point at xt3 = 0.3 is found. In the concentration range where the second-order phase transition is observed, i.e. at xt2 < x < xt1 and at x < xt3, the behavior is found to be universal. Especially, the temperature dependence of the dielectric susceptibility follows a scaling relation which is valid in a wide temperature range (several hundreds degrees) above as well as below the temperature of the (T) maximum, Tm, except for the narrow interval of several degrees around Tm, where the susceptibility peak is rounded.

The critical behaviour of PZT crystals is compared with the relaxor-based counterparts to provide valuable information on the nature of high piezoelectricity.

5I-2

10:45 AM 1-3 Microfabricated Composite Acoustic Matching Layers for High Frequency Transducers

Tung Manh[1], Geir Uri Jensen[2], Tonni Franke Johansen[3], Lars Hoff[1]; [1]Department of Micro and Nano Technology, Vestfold University College, Borre, Norway, [2]Department of Microsystems and Nanotechnology, SINTEF ICT, Oslo, Norway, [3]Department of Circulation and Medical Imaging, Norwegian University of Science and Technology, Trondheim, Norway

Background, Motivation and Objective

Our goal is to make a composite material for use as acoustic matching layer in high frequency transducers. Previous work in this field has used anisotropic wet etch to make 2-2 connectivity composites, and we have reported the first results from making a 1-3 composite by DRIE, Deep Reactive-Ion Etch.

This paper concentrates on 1-3 composite matching layer made by DRIE. This method is not sensitive to crystal orientation, hence, easier to implement in a mass-production process. Using an SOI, Silicon-On-Insulator, wafer as substrate gives good control of the composite thickness. The method was used to fabricate a 15 MHz transducer, and fabrication and characterization results for this transducer are presented.

Statement of Contribution/Methods

Desired acoustic impedance of the matching layer was calculated by the Mason model, and the corresponding polymer to silicon ratio found from the iso-strain assumption. Dimensions for a ¼ wavelength matching layer were calculated and verified by FEM simulations. A mask for the composite structure was made, and the structure etched out in an SOI wafer using DRIE, the Bosch process. The etching process stopped at the buried oxide layer 83 µm into the wafer, giving a well-defined thickness. Epoxy resin was filled into the kerfs to form the 1-3 silicon-polymer composite.

The resulting structures were characterized by microscopic images. The structures were then bonded to a PZT disc, forming an air-backed transducer. This was characterized by electrical impedance measurements in air. The electrical impedance measurements were compared to Mason model calculations, and used to estimate the composite layer material parameters, using inversion scheme.

Results

Microscopic inspection confirm that we have manufactured a 1-3 silicon-polymer composite with 7µm wide posts, 9 µm kerfs and thickness 83 µm, i.e. the aspect ratio is 10:1 with flat and homogenous bottom. The walls of the posts are not perfectly vertical; the post width at the bottom is reduced by approximately 0.9 µm.

Electrical impedance measurement of the transducer in air gives two resonances at 14.5MHz and 17.5MHz. Compared with theoretical predictions gives an acoustic impedance in the composite of 6.0 MRayl, compared to the expected value 6.5 MRayl.

Discussion and Conclusions

We have successfully fabricated a silicon-polymer acoustic matching layer for a 15 MHz transducer with desired acoustic impedance, using the DRIE process. SOI wafers give good and robust control of the layer thickness, and uniform and flat bottoms. The composite was found to behave acoustically like one effective layer, following the iso-strain model, when the kerf size was kept well below half of the shear wavelength in polymer. Obtaining the desired acoustic impedance requires removing 80% of the silicon during etching. This is considered 'high loading' in a DRIE process and can make it difficult to obtain straight walls, causing the slightly reduced acoustic impedance compared to the ideal theory.

5I-3

11:00 AM Tapered Impedance Matching Section Using PDMS Moulding

Dawei Wu[1], Alan Wright[1], Paul Harris[1]; [1]Medical Device Technology, Industrial Research Limited, Lower Hutt, Wellington, New Zealand

Background, Motivation and Objective

Tapered impedance matching can provide optimum matching over a broad frequency range, however, fabrication is a challenge. Previously we described micromachining high aspect ratio cylindrical tapered micropore sections in SU8 which were electroplated with nickel to fabricate a tapered microrod section. Taper provides a smooth continuous transition in effective porosity and therefore acoustic impedance, which is useful for matching. Finite element modeling shows the tapered microstructure provides high energy coupling (>0.9) when the taper section width is about $\lambda/2$ to $\lambda/5$ and the length >10λ. Coupled with micromachining constraints this restricts the earlier work to frequencies up to ~20 MHz with the cost of fabricating the matching section high. In this paper we use a micromachined section, similar to above, as a mould for casting polydimethylsiloxane (PDMS) which is then electroplated. This simplifies electroplating and greatly reduces cost as the mould is reusable.

Statement of Contribution/Methods

Square base tapered microstructures were first fabricated from a micromachined SU-8 mould which was created using a double sided, dual angle lithographic process. PDMS was cast into the mould under vacuum. After proper curing, the cast PDMS, including small taper tips, can be pulled out of the mould by hand. The mould is reusable so that a high repeatability can be attained. Metal is coated onto the PDMS microstructure which is then used for electroplating.

Results

Figure.1 shows an initial PDMS microstructure with the taper shape having a base width of 10um and height of 50um. In this work, the electroplating occurs easily and reliably as it grows from a sheet which covers the base and microstructures; in the previous work it occurred from the small (<2um) open ended micropores (note closed ended pores do not electroplate). The section can be used with PDMS or it can be peeled from the metal for a fluid filled metal taper section; fluid sections have no shear component providing improved outcomes.

Discussion and Conclusions

A method to fabricate a tapered microstructure for matching is presented. Compared to earlier work it 1) can work at >20 MHz, 2) is easily electroplated, 3) fluid filled sections are possible, and 4) is low cost and repeatable.

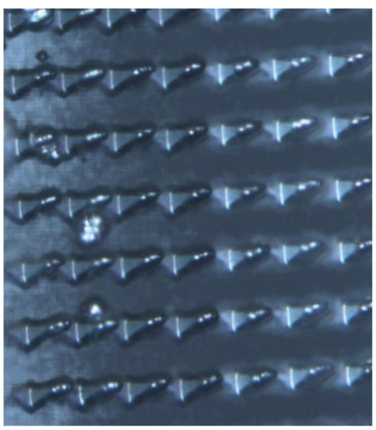

Fig.1 PDMS microstructure

5I-4

11:15 AM Collinear Composite Materials for Impedance Matching

Paul Harris[1], Dawei Wu[1], Matthew Thomson[1], Russell Petherick[1], Frederic Lecarpentier[1], Harry Chen[1]; [1]*Industrial Research Ltd, New Zealand*

Background, Motivation and Objective

Attaining good signal coupling with tissue can be a challenge due to the high impedance of piezoelectric materials, ~35 MRayl. A 1-3 piezocomposite design improves coupling, however, at reduced source power. Matching layers improve coupling, often two layers used for improved bandwidth. A solid with impedance 4 to 10 MRayl is desired but only composites exist e.g. silver loaded epoxy. Rayleigh scattering, having terms k^4a^6, is highly sensitive to frequency (via k^4). As frequency increases above about 10MHz even 2um powder can cause significant scattering. Some researchers use nano (~10nm) powders to reduce scattering (via a^6), but agglomeration can be an issue with high attenuation reported.

We have previously published studies of wave propagation in highly collinear nanoporous alumina (30nm pores, 60nm pitch), a material which for feasible porosities has an impedance covering the desired range. In principle this material does not scatter and, since energy propagates within the solid fraction, absorption is low. Used as a matching layer signal coupling should be very good compared to powder loaded epoxy. Similarly, a material comprised of highly collinear metal rods connecting the layer coupling faces should have low attenuation (scattering and absorption); the rod area fraction chosen for the desired impedance. In this work we explore the use of highly collinear nanoporous and nano/microrod structures for matching with low attenuation.

Statement of Contribution/Methods

2D and 3D PZFlex modeling of nanoporous, microrod and spherical powder loaded epoxy materials was undertaken with varying frequency and structure dimensions to characterize the wave propagation, material impedance and energy coupling.

Varying porosity nanoporous samples of thickness 60um to 400um, nano/microrod samples with rod diameter 200nm to 50um and thickness 0.1mm to 1mm, and 2um powder loaded epoxy samples 0.5mm to 2mm thick were fabricated (sample diameter ~10mm).

A system has been developed to characterize the samples for frequencies ranging from 5MHz to 200MHz.

Results

The nanoporous and microrod modeling shows that energy propagates within the solid fraction (~12:1) as guided waves; wave scattering was not observed. Nanoporous and nano/microrod sample measurements confirms good signal coupling can be attained and that, especially for the nano materials, varying the frequency had no effect on the signal coupled. This is expected since the mode cutoff frequency is high (>1GHz); this criterion sets a frequency limit for the microrod designs. The FEM propagation plots, sample SEM images and measurement system will be presented.

Discussion and Conclusions

Highly collinear composites used for impedance matching can provide low attenuation and be a useful alternative to (spherical) powder loaded epoxy. Nanoporous and nano/microrod materials can provide this functionality at frequencies appropriate for the structure dimensions.

5I-5

11:30 AM An All-optical Thin-film High-frequency Ultrasound Transducer

Clay Sheaff[1], Shai Ashkenazi[1]; [1]Biomedical Engineering, University of Minnesota-Twin Cities, Minneapolis, MN, USA

Background, Motivation and Objective

Piezoelectric and capacitive high-frequency ultrasound transducers exhibit excessive noise due to crosstalk, RF interference, and their small capacitance. These factors significantly limit image quality. Devices that optically generate and detect ultrasound avoid these effects by requiring no electrical cabling or interconnections. In this work we have created an all-optical ultrasound transducer by integrating an optically-absorbing thin-film into an etalon sensor.

Statement of Contribution/Methods

2.5µm of polyimide precursor (HD Microsystems PI-2555) was spin-coated onto a 3mm glass substrate. An etalon was then deposited by evaporating a 30nm gold mirror, spin-coating a 10µm layer of SU-8 (Microchem), and evaporating a second mirror. 1.5µm of SU-8 was added for protection (Fig. 1).

The device was probed from underneath the substrate using a 355nm ND:YAG pulsed laser (Continuum) for ultrasound generation and a 1550nm tunable CW laser (HP 8168F) for detection. After tuning the NIR wavelength for maximum sensitivity, a 5ns 4.5mJ UV pulse was used to generate an acoustic signal within the polyimide film which was reflected from a glass slide placed above the device in water. The echo was then detected by the etalon.

Results

Fig. 2 shows the pulse-echo waveform and associated power spectrum. Using a calibrated hydrophone (Onda HGL-0085), the emitted pulse was determined to have an amplitude of 5.9MPa. The transmit/receive response has a -6dB bandwidth of 32MHz centered at 27MHz.

Discussion and Conclusions

The all-optical ultrasound transducer demonstrated here emits and detects signals of a strength and bandwidth suitable for high-resolution imaging. After incorporating fiber optics and beam scanning, potential applications will include endoscopic and intravascular ultrasound.

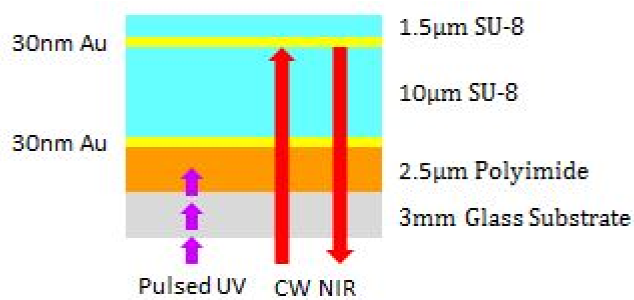

Fig. 1. Layered structure of all-optical transducer.

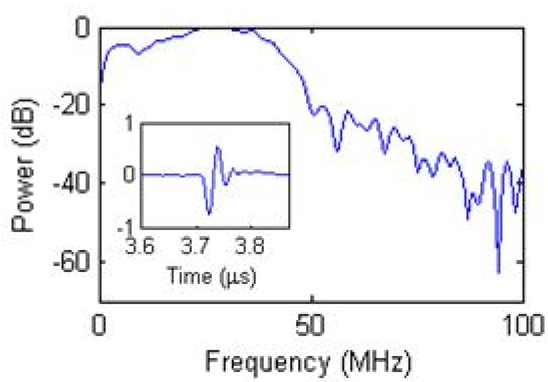

Fig. 2. Pulse-echo and power spectrum.

5I-6

11:45 AM Effect of the crystallographic orientation of Pb(Zr,Ti)O_3 films on the d_{31} transverse piezoelectric coefficient

Matthieu Cueff[1], Marjolaine Allain[1], Julie Abergel[1], Gwenael Le Rhun[1], **Emmanuel Defay**[1], Marc Aid[1]; [1]*CEA-Leti, Minatec Campus, Grenoble, France*

Background, Motivation and Objective

The theoretical prediction that the piezoelectric properties of Pb(Zr,Ti)O_3 (PZT) thin films should be higher for the (001) orientation has been confirmed experimentally for the d_{33} coefficient [1,2]. This orientation can be obtained by means of seeding layers e.g. $PbTiO_3$ [3]. The superiority of the (001) orientation for the transverse piezoelectric coefficient was proved by Ledermann by using the direct piezoelectric $e_{31,eff}$ coefficient [4]. However, for actuators, d_{31} is the right coefficient to be considered. For ceramics, d_{31} reaches -300 pm/V. Calame reported a calculated value of d_{31} = - 156 pm/V from an $e_{31,eff}$ measurement for a (001) oriented thin film with a $PbTiO_3$ seeding layer and gradient engineering [5]. As the relationship between $e_{31,eff}$ and d_{31} involves Young modulus and Poisson ratio ($d_{31} = e_{31,eff} * (1-nu^E)/E^E$) which are still not very well known for PZT thin films, we investigated experimentally (100) and (111)-oriented PZT thin films integrated in micro-cantilevers prepared on SOI 200mm wafers. The objective was to investigate whether it is worth orienting morphotropic PZT films for actuators applications.

FRIDAY ORAL

Statement of Contribution/Methods

We prepared sol gel PZT thin films 2µm-thick. Thanks to the bottom electrode control, we were able to change the PZT crystallographic orientation from (001) to (111), as checked by X-Ray diffraction (XRD). These PZT films were deposited on 5µm SOI/0.5µm SiO_2/TiO_2/Pt 100nm substrate. The 100nm thick Ru top electrode is sputtered before XeF_2 release of the micro-cantilevers. Their deflection is eventually measured by a laser vibrometer. The d_{31} value is extracted from an analytical analysis based on Hsueh's model [6]. FEM was done to estimate the accuracy of this extraction (Comsol).

Results

Experiments clearly confirmed the superiority of the (001) orientation versus (111). Indeed, $d_{31\,(001)}$ = 147pm/V and $d_{31\,(111)}$ = 96pm/V. It is worth noting that this orientation is very uniform on the whole 200mm wafer, as observed by XRD.

Discussion and Conclusions

This paper shows that d_{31} of morphotropic PZT thin films is higher when one can provide the (001) orientation. This was performed without seeding layers and multiple coating solutions by controlling the growth of the bottom electrode. The maximum extracted d_{31} is 147pm/V for (001) PZT.

[1] XH Du *et al.*, Appl. Phys. Lett. 72, 2421 (1998)
[2] D.V. Taylor *et al.*, Appl. Phys. Lett., 76, 1615 (2000)
[3] P. Muralt *et al.*, J. Appl. Phys., 83, 3835 (1998)
[4] N. Ledermann *et al.*, Sens. And Actuators, A 105, 162 (2003)
[5] F. Calame *et al.*, Appl. Phys. Lett., 90, 062907 (2007)
[6] C.H. Hsueh *et al.*, J. of Micromech. Syst. And Microeng., 16, 2509 (2006)

6I - MEMS

Carribean Ballroom VI

Friday, October 21, 2011, 10:30 am - 12:00 pm

Chair: **Sunil Bhave**
Cornell University

6I-1

10:30 AM Temperature compensation of silicon MEMS resonators by heavy p and n type doping

Tuomas Pensala[1], Antti Jaakkola[1], Mika Prunnila[1], James Dekker[1]; [1]*VTT Technical Research Centre of Finland, Finland*

Background, Motivation and Objective

Silicon based MEMS resonators have been investigated for a long time as a replacement for quartz resonators in oscillators and timing circuits. The driving forces have been miniaturization, integration with CMOS, cost reduction, and potentially better noise performance. One of the most serious challenges has been the temperature coefficient of frequency (TCF), typically around -30 ppm/K for silicon, whereas quartz achieves essentially zero linear TCF. In this paper, results on temperature compensation of MEMS resonators based on heavy doping of Si are presented.

Statement of Contribution/Methods

The TCF of an ultrasonic resonator is dominated by the temperature dependence of the stiffness c_{ij} of the resonator material. In a many-valley semiconductor such as Si the free electrons (or holes) have a contribution to the elastic constants, and more importantly, to their temperature behaviour. This is described by the theory of Keyes [1] which was employed to predict the temperature coefficients of the elastic constants. Silicon resonators were fabricated using SOI wafers with heavily doped device layers of both p (B, B+Ge) and n-type (P). The temperature dependence of the resonance frequency of the devices was measured and compared with the theoretical predictions.

Results

The measured TCFs for selected plate resonator vibration modes and various dopings are presented in Table I. Significant reduction from the -30 ppm/K level is observed for several cases, especially the n-type doped 100-oriented Lamé mode resonator the sign of TCF has been inverted with a large margin. Excellent agreement is observed between measurement and Keyes theory in the n-type devices.

Discussion and Conclusions

Significant reduction and even overcompensation of the temperature coefficient of frequency of Si MEMS resonators is demonstrated by heavy doping of Si. This shows the feasibility of reaching zero TCF Si resonators. Especially the n-type doping shows remarkable potential by compensation both shear and extensional type vibration modes.

[1] R. W. Keyes, in Solid State Physics: Advances in Research and Applications, (Academic Press, New York, 1967), vol. 20, pp. 37-90.

Table I: Measured linear TCF for the Lamé and Square Extensional (SE) plate modes. Plate side crystal orientation is indicated.

Doping / Mode	Lamé 110	Lamé 100	SE 100
p++ (B): 5e19cm^{-3}	-3 ppm/K	-10 ppm/K	-20 ppm/K
p++ (B): 2e20cm^{-3} + Ge	-1.8 ppm/K	-10 ppm/K	-20 ppm/K
n++ (P) 5e19cm^{-3}	-32 ppm/K	+18 ppm/K	-0.7 ppm/K

6I-2

10:45 AM Lithium-Niobate-Based Surface Acoustic Wave Device Directly Integrated on LSI

KyeongDong Park[1], Masayoshi Esashi[2], **Shuji Tanaka[1]**; [1]Department of Nanomechanics, Tohoku University, Sendai, Japan, [2]WPI Advanced Institute for Materials Research, Tohoku University, Sendai, Japan

Background, Motivation and Objective

The direct integration of SAW devices on top of LSI enables one-chip wireless systems, high-performance one-chip oscillators etc. This is difficult, however, because SAW devices are often fabricated on piezoelectric crystals such as lithium niobate (LN) with a special cut angle, which have coefficients of thermal expansion considerably different from that of Si. The objective of this study is to develop wafer-bonding-based integration technology for LN-based SAW devices on LSI, and to prototype an integrated high frequency SAW oscillator.

Statement of Contribution/Methods

A 128 ° Y LN wafer is bonded on a Si support wafer covered with sacrificial Ge using UV-cured polymer adhesive, and then thinned by polishing. On it, SAW resonators are fabricated and half-diced into each device. The half-dicing relaxes thermal expansion mismatch between LN and Si during wafer bonding. A simple oscillator circuit is prepared by 0.35 µm BiCMOS technology. On the LSI wafer, Au bumps are formed by electroplating, and their surface is mirror-finished by single point diamond cutting. The SAW/support wafer and the LSI wafer are Au-to-Au-bonded at low temperature (ca. 100 °C), and then the Si support wafer is removed by etching the Ge sacrificial layer in H_2O_2.

FRIDAY ORAL

Results

Figures 1 and 2 show the integrated SAW oscillator and its oscillation characteristic, respectively. The oscillation frequency is 502.6 MHz and the single sideband phase noise (SSB) is ca. 110 dBc/Hz at 100 kHz offset.

Discussion and Conclusions

We have developed new technology for the wafer-level hetero-integration of LN-based SAW devices and LSI. A 500 MHz SAW oscillator fabricated by this technology operated with an SSB of ca. 110 dBc/Hz at 100 kHz offset. This technology is also useful for filters, sensors and optical devices.

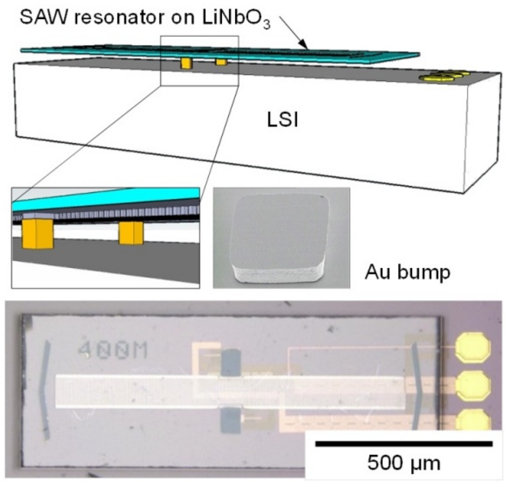

Fig. 1 SAW oscillator integrated on top of LSI

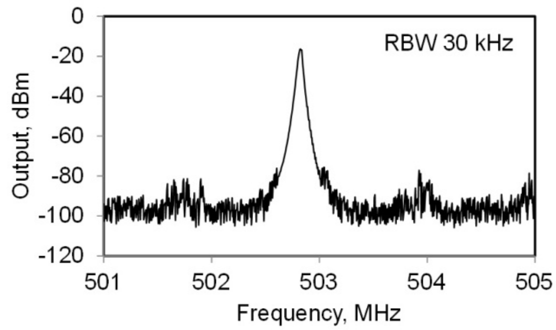

Fig. 2 Oscillation characteristic of integrated SAW oscillator

6I-3

11:00 AM Thin Film Transfer Technology for Tunable SAW Filter Using Integrated Ferroelectric Varactors

Hideki Hirano[1], Toshiyuki Kikuta[1], Masayoshi Esashi[1], Shuji Tanaka[1]; [1]*Tohoku University, Sendai, Japan*

Background, Motivation and Objective

Wide frequency range tunable RF front-end filters with low insertion loss are strongly required for software defined radio and cognitive radio. Recently, a tunable RF filter using variable capacitors (VC) combined with ladder type configuration of wideband SAW resonators has been proposed [T. Komatsu et al., Jpn. J. Appl. Phys., 49, 07HD24, 2010]. A ferroelectric VC is preferable for this use in terms of high tuning ratio, small size and good linearity at GHz range. However, the integration of the ferroelectric VC on a SAW substrate such as lithium niobate (LN) has not been demonstrated, because direct deposition of VC materials (e.g. BST) on LN is difficult due to high growth temperature. Thermal stress due to difference in the coefficient of thermal expansion between LN and BST is also a problem. To directly integrate the ferroelectric VC on the SAW substrate at low temperature, we have developed ferroelectric film transfer technology using sacrificial layer process.

Statement of Contribution/Methods

Figure 1 shows a process for transferring a BST film from a Si substrate to a LN substrate using a Ru sacrificial layer. Ru stands high temperature deposition of BST, and can be removed by ozone at low temperature without damage to both BST and LN. As a result, high-quality BST films can be transferred onto the LN substrate.

Results

Figure 2 shows a tunable SAW filter with transferred BST films. The BST film was transferred as expected. Any deterioration of the composition and orientation of the transferred BST film was not found by XPS and XRD, respectively.

Discussion and Conclusions

This work showed the feasibility of BST film transferring technology for tunable SAW filters. The developed technology is useful for a variety of hetero-integrated devices.

FRIDAY ORAL

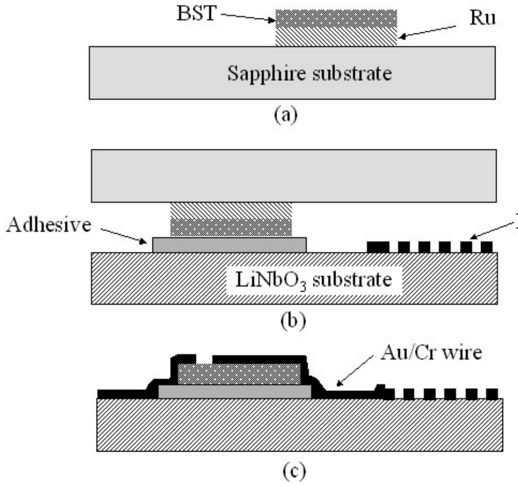

Fig. 1 BST film transfer process.

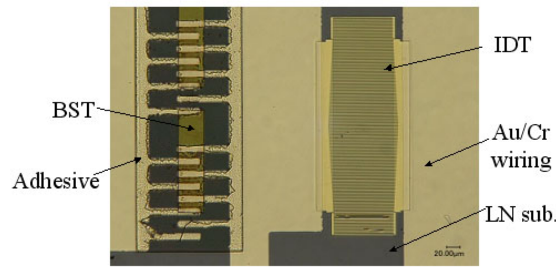

Fig. 2 Tunable SAW filter with transferred BST films

6I-4

11:15 AM Hollow Stems For Higher Uhf Micromechanical Disk Resonator Quality Factor

Lingqi Wu[1], Mehmet Akgul[1], Zeying Ren[1], Yang Lin[1], Wei-Chang Li[1], Tristan Rocheleau[1], Clark T.-C. Nguyen[1]; [1]Department of Electrical Engineering and Computer Sciences, University of California at Berkeley, Berkeley, CA, USA

Background, Motivation and Objective

With Q's already in the vicinity of 15,000 at UHF [S.-S. Li, et al, MEMS'04], capacitively-transduced polysilicon micromechanical resonators are strong candidates for use as RF front-end filtering devices that could revolutionize wireless communications by enabling true software-defined cognitive radio [C. T.-C Nguyen, the 26th Sensor Symp., 2009, plenary talk]. Specifically, if Q's >40,000 are attainable at UHF, the bandwidths of the front-end RF filters in a wireless receiver can be made small enough to select single channels (rather than bands of them), allowing the filters to remove all interferers and pass only energy in the desired channel(s) to the subsequent demodulation electronics, which can now operate with orders of magnitude lower dynamic range, hence substantially lower power consumption. To date, anchor losses have been largely responsible for limiting the Q's attainable by pure-polysilicon capacitively-transduced micromechanical resonators to values lower than 40,000 at UHF.

Statement of Contribution/Methods

This work employs a new hollow stem support, shown in Figure 1(a), and a whispering gallery mode shape to attain a degree of anchor isolation that propels the Q of a pure polysilicon micromechanical resonator to greater than 110,000 at 178 MHz—almost 2× higher than previously achieved by full-stemmed polysilicon disk resonators at the same frequency. At 376 MHz, which is UHF, the Q is 44,000.

Results

With a substantially smaller cross-sectional area compared with a full stem, the hollow stem more effectively suppresses energy loss through the anchor to the substrate—an energy loss reduction that becomes especially favorable when the device operates in a whispering gallery mode, as shown in Figure 1(b), which presents measured plots of identical devices using hollow and full stems, clearly showing the Q advantage of the former.

Discussion and Conclusions

This hollow stem structure provides a simple method with minimal increase in fabrication complexity for achieving the Q >40,000 at UHF required for true software-defined cognitive radio. Work to extend this design method to even higher frequencies that satisfy the full range of cognitive radio bands is ongoing.

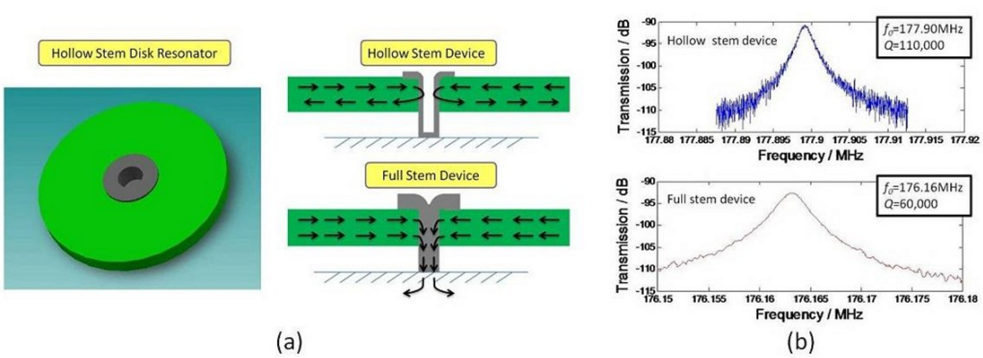

Fig 1. (a) Schematic of a hollow stem disk resonator and comparison of anchor loss mechanism for a hollow stem versus full stem; and (b) Q comparison for hollow stem and full stem polysilicon disk resonators.

6I-5

11:30 AM A Robust Doppler Ultrasonic 3D-imaging System with MEMS Microphone Array and Configurable Processor

Yasushige Maeda[1], Masanori Sugimoto[2], Hiromichi Hashizume[3]; [1]Department of Informatics, The Graduate University for Advanced Studies, Japan, [2]School of Engineering, University of Tokyo, Japan, [3]Information Systems Architecture Science Research Division, National Institute of Informatics, Japan

Background, Motivation and Objective

Since the introduction of micro-electro-mechanical systems (MEMS) technology small MEMS microphone chips became prevalently used for the detectors of airborne ultrasound. To obtain a 3D acoustic image, an imaging system has to be designed to facilitate a large number of sensors placed on a plane and a programmable device running in a high frequency system clock.

In ultrasonic imaging, a moving object causes a substantial Doppler effect on the reflecting sound, and aggravates the cross-correlation value of the transmitting signal and the received ones reflected by the object. Furthermore, the amount of Doppler shift caused by a moving reflector approximately two times larger than that of a moving sound source at the same velocity. We therefore shall pay special attention to the matched-filtering operations on the Doppler distorted signals. Traditional ways to detect Doppler signals has been done by preparing a number of filters that detect the range of signals frequency-shifted by the effect.

Statement of Contribution/Methods

We developed an ultrasonic 3D imaging system, which facilitates 128 microphones and a highly configurable field programmable gate array (FPGA). The sensor array board mounts ultrasonic MEMS sensors precisely positioned with the pitches of 5.08mm x 10.16mm on one side of the printed circuit board, that form 16 x 8 planar grid attaining 112 x 50 degree view angles for wide-band signals with the central frequency 40KHz.

We propose a Doppler imaging method for moving objects by designing the transmitter waveform tolerant for the effect. In this method, we employ a log-step multi-carrier signal as the transmitter sound, in which every two nearest carrier frequencies form constant ratio.

Results

The FPGA has been configured as a sampling and recording machine, achieving 128 channel sampling for the sampling frequency 500KHz, and the duration 128msec. Utilizing this system as a capturing device, we applied the delay-and-sum beamformer and matched filter operations designed accordingly to the proposed method on the captured signals.

While in the matched-filter operation, a traditional linear-sweep chirp signal has inaccurate sensitivity blurred over the bandwidth in the frequency domain, a log-step multi-carrier signal shows multiple steep sensitivity for those signals. A small set of filters, whose base frequencies are previously tuned, has sufficiently detected the Doppler distorted signals of a log-step multi-carrier transmitter sound.

Discussion and Conclusions

The system exemplified suitability of an MEMS sensor array for 3D imaging with wide-band signals involving Doppler effect. We conclude that the validity of the proposed method is shown not only for 3D imaging of static objects but also for 3D and velocity imaging of moving objects. The resolutions of the obtained image and the parameters for the detection of the amount of Doppler shift are also discussed.

6I-6

11:45 AM Novel Template-Free Microfluidic Synthesis and Encapsulation Technique for Layer-by-Layer Polymer Nanocapsule Assembly

Aisha Qi[1], Jenny Ho[2], Peggy Chan[3], Leslie Yeo[2], **James Friend[4];** [1]MicroNanophysics Research Laboratory, Monash University, Australia, [2]MicroNanophysics Research Laboratory, Monash University, Clayton, Victoria, Australia, [3]Chemical Engineering, Monash University, Clayton, Victoria, Australia, [4]Mechanical Engineering, Monash University, Clayton, VIC, Australia

Background, Motivation and Objective

The encapsulation of drugs and therapeutic molecules within biocompatible and biodegradable polymeric excipients offers tremendous opportunities for controlling and targeting the release of drugs in vivo. Furthermore, the scope for manipulating the rate and targeted region at which the drug is released or even the possibility of specifying different release rates and targeted regions has been proposed by encapsulating the drug within nanocapsules with multiple polyelectrolyte coatings. The objective is to demonstrate a method for generating layered nanoparticles suitable for drug delivery via surface acoustic wave atomisation, a unique application of this technology.

Statement of Contribution/Methods

Here, we present a simple microfluidic technique based on surface acoustic wave atomization (see Figure) of polymer solutions as a rapid and efficient alternative to the conventional layer-by-layer assembly of polyelectrolyte multilayer nanocapsules. In contrast to the conventional technique, however, a sacrificial colloidal template over which the polyelectrolyte layers are deposited is not required. Instead, polymer nanoparticles are synthesized by atomizing the solution containing the polymer and suspended within a solution in which the complementary polymer of opposite charge is dissolved. Reatomizing this suspension then produces nanocapsules with a layer of the second polymer deposited over a core comprising the initial polymer. Successive atomization–suspension layering steps can then be repeated over an arbitrary number of times for as many additional layers as desired.

Results

Nanocapsules containing plasmid DNA, itself containing sequences suitable for vaccination against human malaria, were fabricated using the atomization process, layering atop the DNA additional layers of chitosan and carboxymethyl cellulose. Using zeta-potential measurements and in-vitro release profiles of the pDNA from the particles, we found that the pDNA was effectively encapsulated and was released over a period of several days in a manner ideal for vaccination.

Discussion and Conclusions

A new technique for the synthesis of polyelectrolyte multilayer nanocapsules was demonstrated using surface acoustic wave (SAW) atomization.

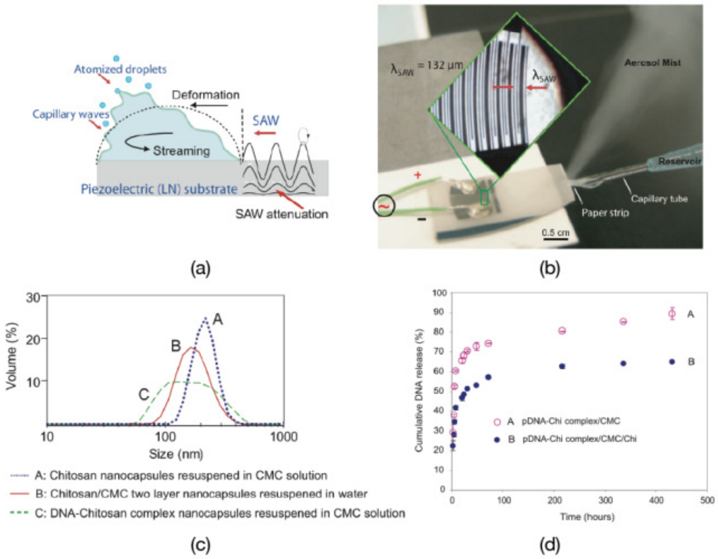

Figure: The process of (a) atomisation of a fluid using a (b) SAW atomiser with special reservoir and fluid supply system to provide a means to generate microdroplets that subsequently evaporate and form (c) polymer/plasmid DNA nanoparticles through multiple atomisation steps. Such particles slowly release the plasmid DNA vaccine (d) over a period of several hundred hours in a manner useful for vaccination.

FRIDAY ORAL

1J- Beam Forming

Boca Rooms II-IV

Friday, October 21, 2011, 2:00 pm - 3:30 pm

Chair: **John Hossack**
Univ. of Virginia

1J-1

2:00 PM Shear Wave Induced Phase Encoding Imaging with Enhanced Resolution

Stephen McAleavey[1], Vaibhav Kakkad[1]; [1]Biomedical Engineering, University of Rochester, Rochester, NY, USA

Background, Motivation and Objective

Conventional ultrasound backscatter imaging relies on geometric focusing of ultrasound echoes across an aperture. In these systems the focal beamwidth, which determines the lateral resolution, is proportional to the ultrasound wavelength and inversely proportional to aperture size. We have presented (McAleavey, IEEE UFFC 58(1) 102-11) a novel method in which lateral resolution of the target is obtained by using traveling shear waves to encode the lateral position of the scatters in the phase of the received echo. In this work we extend the imaging model and demonstrate enhanced image resolution using ultrasound phase modulation harmonics generated by linear propagation of both shear and ultrasound waves.

Statement of Contribution/Methods

Using a Fourier series description of the phase modulation signal, we demonstrate that phase modulated signals at multiples of the shear wave frequency reveal target k-space data at multiples of the shear wavenumber.

These harmonics develop from the non-linear nature of phase modulation, and exist with purely linear propagation of shear and ultrasound waves. A given k-space coefficient can be obtained by probing with a shear wave of the corresponding wavenumber k, or by a detecting the n^{th} modulation harmonic due to a shearwave with wavenumber k/n. We develop an analytical model for determining the optimal shear wave parameters for amplitude and SNR constraints.

Data were acquired using a single element of a 7 MHz linear-array transducer, driven by a spike-excitation pulser-receiver. Shear waves were induced in the phantom using an electromagnetic shaker. Echo signals were recorded with a digital oscilloscope and processed offline. Diffuse and wire targets were embedded in ~ 5kPa shear modulus gelatin.

Results

Images of nylon wires embedded in gelatin were obtained at the fundamental and 2nd harmonic of the shear wave frequency. The expected doubling of resolution was observed. Images of a 1 cm cylindrical inclusion (below) were obtained at the shear wave fundamental. Compounding for speckle reduction was implemented by incoherent summation of images obtained from single transducer elements at several lateral positions.

Discussion and Conclusions

Our results indicate that the lateral resolution achievable with this method is limited by SNR constraints, and not by aperture size and ultrasound wavelength as in conventional imaging.

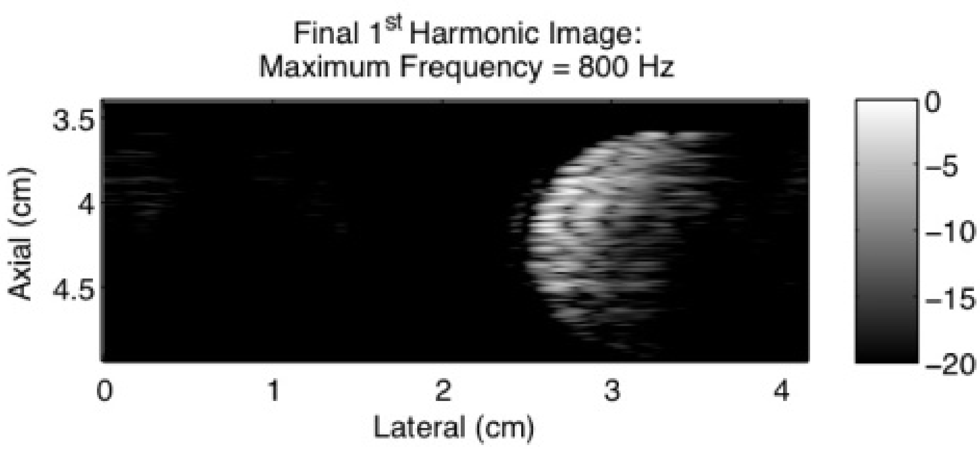

1J-2

2:15 PM Physical Principles for Clutter Reduction in Ultrasonic Imaging via Wavefront Coherence

Jeremy Dahl[1], Gregg Trahey[1,2]; [1]Biomedical Engineering, Duke University, Durham, NC, USA, [2]Radiology, Duke University Medical Center, Durham, NC, USA

Background, Motivation and Objective

There are a variety of factors that contribute to poor image quality in ultrasonic imaging. Numerous algorithms have been designed to compensate for phase aberrations, but recently it was shown that reverberation clutter also plays a significant role in degrading image quality. We have recently developed a novel imaging technique that is capable of differentiating ultrasonic signals corrupted by clutter. We discuss the physical principles of how wavefront coherence can be used to differentiate clutter from signal of interest and how this method can be used to reduce clutter.

Statement of Contribution/Methods

Radio-frequency (rf) element signals were generated using a FDTD simulation of ultrasound propagation through abdominal layers with anechoic lesions as targets. Signal-to-clutter ratio (SCR) was adjusted by modifying impedance mismatch of the abdominal tissues. B-mode and wavefront coherence images were formed from the rf signals, and

FRIDAY ORAL

contrast and contrast-to-noise ratio (CNR) of the lesions were measured. Rf element signals were also acquired from human vascular and cardiovascular tissues to demonstrate WCI *in vivo*.

Results

Measurements of CNR indicated that B-mode imaging degrades linearly with decreasing SCR, while WCI remains relatively flat. WCI yielded an average increase in CNR from 0.9 to 1.7, indicating a significant increase in lesion visibility. WCI also demonstrated better performance than other coherence-based metrics, such as the generalized coherence factor and the waveform similarity factor, although these metrics were not designed for imaging directly. The figure below demonstrates the WCI technique applied to *in vivo* imaging of the human carotid sheath, where visualization of arterioles that surround the common carotid artery are poorly visualized in the B-mode image (left), but are easily visualized in the coherence image (right).

Discussion and Conclusions

The primary mechanism that differentiates clutter from signals of interest in wavefront coherence is the spatial coherence over short distances. In addition, the amplitude of the echoes do not contribute to the coherence. These two mechanisms allow image quality to be maintained over a large range of SCR. The technique demonstrates considerable reduction in clutter and improved visibility *in vivo*, particularly in tasks where high contrast targets are obscured by clutter.

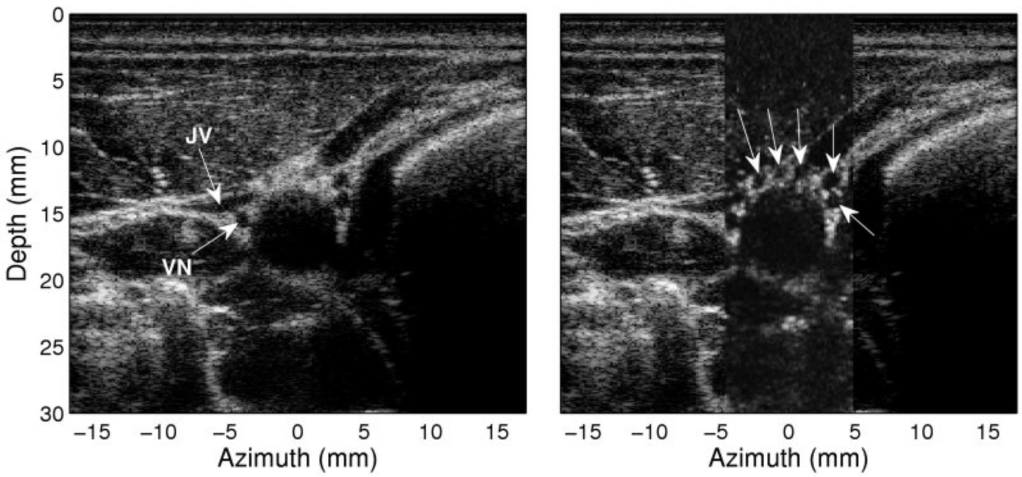

1J-3

2:30 PM Transducers with non-rectangular elements

Svetoslav Ivanov Nikolov[1], Henrik Jensen[2], Terry Kling[3]; [1]RD Applications and Technology, BK Medical Aps, Herlev, Sjæland, Denmark, [2]RD Applications and Technology, BK Medical Aps, Denmark, [3]Sound Technology Inc., USA

Background, Motivation and Objective

The number of elements in a transducer is directly proportional to the cost of the system. To reduce the number of elements, vendors produce transducers with a pitch larger than one wavelength. The contrast of the images created with these transducers is reduced because of the grating lobes. The radiation pattern of the transducer is a product of the radiation pattern of the array and of the individual elements. This work investigates the possibility to reduce the level of the grating lobes by manipulating the shape of the individual transducer elements.

Statement of Contribution/Methods

We consider two design approaches in simulation. We have also produced and tested a transducer with non-rectangular elements. The 2 approaches are: (1) rotation of the transducer elements and (2) interweaving the elements. In (1), the rotation of the elements results in rotation of the radiation pattern, thus pushing the grating lobes outside the imaging plane. The acoustic lens still performs elevation focusing in the imaging plane thus suppressing the grating lobes. Approach (2) emulates transducer elements with width larger than the pitch. The position of the first zero of the radiation pattern of the elements is closer to the main lobe than the first grating lobe. Grating lobes are suppressed at steering angles below 10 degrees.

Results

We present 3 designs: (1) interwoven, (2) diagonal, and (3) wavy, as shown in Sub-figure 1(a). The wavy design has also been manufactured. It was based on a standard transducer, where the metalization was cut by laser in a pattern as shown in Fig. 1(a).All designs have 128 elements, pitch of 300 µm, and height of 4 mm. The center frequency is 8 MHz. Simulations of point spread function are done in Field II. The interwoven design gives highest grating lobe suppression of 20 dB (Fig. 1(b)). The diagonal and wavy designs suppress grating lobes by 8 and 5 dB, respectively. Phantom images with the "wavy" probe are shown in Fig. 1(c) and have higher contrast than images made with a reference probe produced with the same parameters.

Discussion and Conclusions

It is possible to manipulate the position and reduce the level of the grating lobes by using non-rectangular transducer elements. From the presented designs, best results are obtained using interwoven elements. The wavy design can be produced reliably, but the improvement in image quality is only marginal.

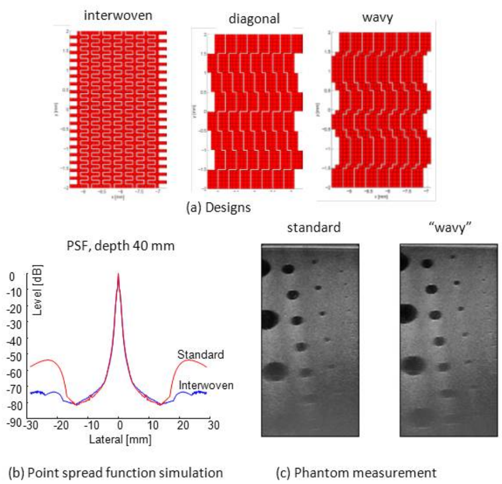

1J-4

2:45 PM Resolution, apodization, and noise considerations in short-lag spatial coherence (SLSC) images compared to B-mode images

Muyinatu Lediju[1], Jeremy Dahl[1], Gregg Trahey[1]; [1]*Duke University, Durham, NC, USA*

Background, Motivation and Objective

Spatial coherence measures the similarity of backscattered echoes received by individual transducer elements, as a function of element separation (or element lag). In short-lag spatial coherence (SLSC) imaging, a novel clutter reduction technique particularly useful in high-noise environments, ultrasonic images are constructed based on local measurements of the SLSC (i.e. the integral of a spatial coherence function over the first few lags). The van Cittert Zernike theorem (VCZT) predicts that spatial coherence is the Fourier transform of the intensity distribution of an incoherent source (or target), scaled by the lateral beam intensity. Challenges with the development of SLSC imaging include target-dependent resolution and optimal beamformer apodization. The objective of this research is to investigate these challenges and compare to B-mode imaging.

Statement of Contribution/Methods

Simulated SLSC images of step targets, sine-like targets, and 2-12 mm lesions with -24 to 6 dB contrast were created using Field II, with a transmit frequency of 2.5 MHz and a focus of 37.5 cm. Simulated B-mode images were constructed with the same data used to create SLSC images by applying a conventional delay-and-sum beamformer. A VCZT-based computation of the SLSC image was compared to simulated images. Resolution was evaluated with the autocorrelation of image texture, the numerical differentiation of a step target, and transfer functions calculated from sinusoidally-varying diffuse targets of varying frequencies. Rectangular, hanning, and one-minus-hanning apodization profiles were applied to the transmit aperture of simulated and theoretical 1 cm lesions. Noise was injected in simulated lesion images.

Results

Measured with the autocorrelation and numerical differentiation techniques, -6dB lateral resolution ranged from 0.46-0.58 mm in B-mode images, and 0.31-0.43 mm in SLSC images. Transfer functions revealed -12dB cut off frequencies ranging from 1-1.5 cycles/mm for B-mode and SLSC images. For the 1-cm, -10 dB contrast lesion, the 3 apodization schemes yielded B-mode images with -10dB contrast and a 1.2 contrast-to-noise ratio (CNR), with and without injected noise. The contrast in corresponding SLSC images was 7-10 dB worse than B-mode. Rectangular, hanning, and one-minus-hanning apodization yielded CNRs of .8-1.3, .02-.1, and 1.4-2.2, respectively. Theoretical calculations agreed with simulation results without noise. The addition of 10 dB noise relative to channel signals improved SLSC image contrast and CNR by 3-25 dB and 0-2.2, respectively. The SNR of SLSC images exceeded that of B-mode images by up to a factor of 30. Contrast, CNR, and SNR in SLSC images varied with lesion size and short-lag value.

Discussion and Conclusions

B-mode and SLSC image resolutions are similar for uniform, step, and sine-like targets. CNR was improved in SLSC images with one-minus-hanning apodization. The addition of noise improved SLSC image contrast and CNR in some cases.

1J-5

3:00 PM Adaptive Spatial Compounding for Needle Visualization

Bo Zhuang[1], Kris Dickie[1], Laurent Pelissier[1]; [1]*Ultrasonix Medical Corp., Canada*

Background, Motivation and Objective

Ultrasound imaging has been increasingly used for the guidance of needle insertion such as nerve blocks, vascular access, biopsy, and therapy procedures. However, visualizing the needles inside the ultrasound image could be challenging due to the small needle footprint and the tissue/speckle pattern surrounding the needles. Spatial compounding has been proposed as one of the methods to enhance the needle visualization. It has been shown that the needle can be enhanced when it's inserted with a small angle (shallow region). When inserting the needle with a large angle (>30 degree to the probe surface), traditional spatial compounding becomes not effective since the noise from large steering images is also combined into the result image.

Statement of Contribution/Methods

In this paper, we propose an adaptive spatial compounding method to enhance the needle visualization not only in shallow but also in deep regions. In our compound scheme, at least two images will have large steering angle (e.g., -20 or 20 degree). These large steering images will pass through an image analysis stage which includes directional filtering to reconstruct the tensor of the image followed by Eigen decomposition. Then an Eigen value remapping technique is employed to suppress the speckle noise patterns while enhancing the strong signal component such as needles. Finally, the processed needle images are merged back to the images with small or zero steering angles.

Results

Fig. 1(a) shows the result of traditional spatial compounding with five imaging angles of -20, -10, 0, 10, and 20 degrees. The result of the proposed method using the same input data is shown in Fig. 1 (b). As shown in the figure, the CNR of the needle was enhanced from 3.64 to 5.78 while the speckle noise pattern from the images with large steer angles (-20 and 20 degrees) was reduced using the proposed method. Real-time implementation was also achieved where a frame with a size of 512x256 can be processed within 15 ms.

Discussion and Conclusions

One of the advantages of the proposed method is enhancing the needle visualization without introducing extra operating procedures. It utilizes a normal spatial compounding process. Although it could also enhance the side lode artifact, we believe the gain of needle CNR could benefit the real-time guidance of needle insertion.

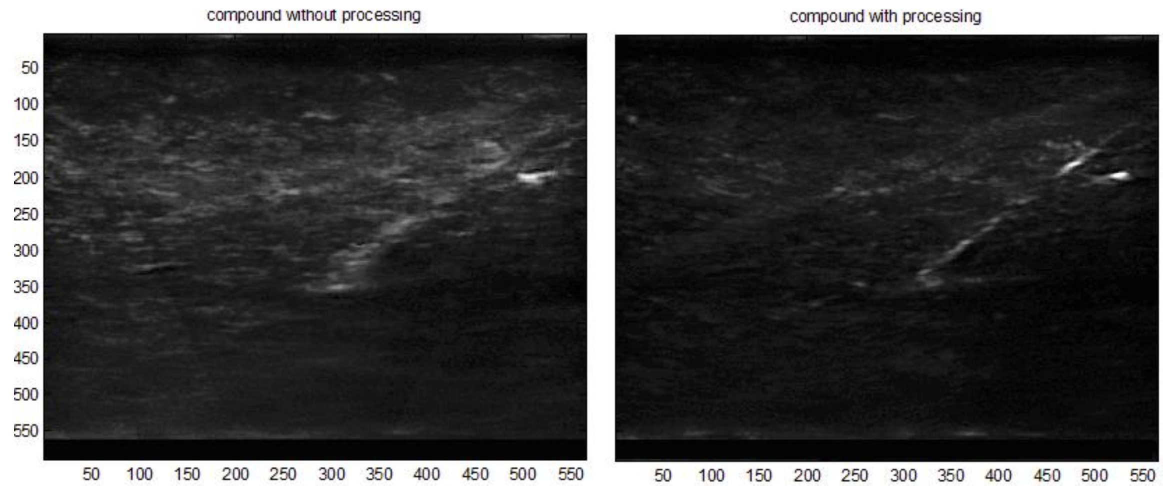

1J-6

3:15 PM Separable 2D Direct-Sampled In-phase Quadrature Beamforming for Greatly Increased Computational Efficiency

Kevin Owen[1,2], Michael I. Fuller[2], John A. Hossack[1]; [1]BME, University of Virginia, Charlottesville, VA, USA, [2]Pocketsonics Inc, Charlottesville, VA, USA

Background, Motivation and Objective

Beamforming in 2D-array ultrasound systems is computationally challenging due to the high channel count and data rate, leading to limits in frame rate or image size. In addition, in handheld 2D-array systems the need for reasonable battery life imposes limits on the energy cost of beamforming. Direct-Sampled In-phase Quadrature (DSIQ) beamforming achieves computational efficiency through sparse sampling and focusing using only phase rotation. However, for real-time frame rates on battery-powered handheld devices, further computational efficiencies are necessary. Separable 2D DSIQ focusing approximates a 2D focusing operation by successive 1D focusing in the X and Y dimensions, providing more than an order-of-magnitude speed increase, enabling real-time frame rates and volume imaging.

Statement of Contribution/Methods

Simulations in FIELD II were conducted to quantify the phase errors introduced by the separable 2D DSIQ approximation. In addition, simulations were used to assess the impact of the approximation on point-spread-functions and anechoic cylindrical void contrast to noise ratios (CNRs). Experimental images were also produced of an anechoic cylindrical void in a phantom, using a prototype 2D array system with and without the separable approximation. The execution time and beamforming energy cost were measured for the standard 2D DSIQ focusing algorithm and the separable algorithm running on two different processors using a range of aperture sizes.

Results

Contrast-to-noise ratios for anechoic cylindrical void images formed with and without the separable approximation were essentially unchanged for both simulated (3.02 dB and 3.04 dB respectively) and experimental (2.04 dB and 2.05 dB) cases. Simulation results indicate the apodization-weighted RMS phase errors introduced by the separable approximation are less than 9 degrees in all relevant cases. The separable approximation phase error produces a worst-case beamplot degradation of only 1.13 dB maximum, 0.21 dB RMS compared to non-separable focusing, with less degradation in typical imaging conditions. When used with a typical 40 x 40 focusing aperture, the separable 2D DSIQ algorithm increased frame rates by a factor of 20 on two different processors, boosting frame rate from 8.8 Hz to 186 Hz on the OMAP 3530 (cell-phone class) processor, and from 32 Hz to 648 Hz on the Intel Core i5 (desktop-class) processor. Energy usage per frame on the OMAP processor reduced from 119.5 mJ to 5.8 mJ using the separable algorithm.

Discussion and Conclusions

Simulation and experimental data illustrated in this paper demonstrate that the separable 2D DSIQ beamforming algorithm enables order-of-magnitude speed increases with no noticeable degradation in image quality. This advance enables real-time frame rates and long battery life for handheld 2D-array imaging systems, and also brings handheld volume imaging within reach.

2J- Ultrasound Therapy of the Brain

Boca Rooms VI-VII

Friday, October 21, 2011, 2:00 pm - 3:30 pm

Chair: **Greg Clement**
Harvard Medical School

2J-1

2:00 PM Optimization of the ultrasound-induced blood-brain barrier opening

Elisa E. Konofagou[1,2]: [1]Department of Biomedical Engineering, Columbia University, New York, NY[2]Department of Radiology, Columbia University, New York, NY

Current treatments of neurological and neurodegenerative diseases are limited due to the lack of a truly non-invasive, transient, and regionally selective brain drug delivery method. The brain is particularly difficult to deliver drugs to because of the blood-brain barrier (BBB). The impermeability of the BBB is due to the tight junctions connecting adjacent endothelial cells and highly regulatory transport systems of the endothelial cell membranes. The main function of the BBB is ion and volume regulation to ensure conditions necessary for proper synaptic and axonal signaling. However, the same permeability properties that keep the brain healthy also constitute the cause of the tremendous obstacles posed in its pharmacological treatment. The BBB prevents most neurologically active drugs from entering the brain and, as a result, has been isolated as the rate-limiting factor in brain drug delivery. Until a solution to the trans-BBB delivery problem is found, treatments of neurological diseases will remain impeded. Over the past decade, methods that combine Focused Ultrasound (FUS) and microbubbles have been shown to offer the unique capability of noninvasively, locally and transiently open the BBB so as to treat central nervous system (CNS) diseases. Four of the main challenges that lie ahead are to: 1) assess its safety profile, 2) unveil the mechanism by which the BBB opens and closes, 3) control and predict the opened BBB properties and duration of the opening and 4) assess its premise in brain drug delivery. All these challenges will be discussed, findings in both small (mice) and large (non-human primates) animals will be shown and finally the case for this technique for clinical applications will be made.

Supported in part by the National Institutes of Health (R01EB009041), National Science Foundation (CAREER 0644713) as well as the Kinetics and the Kavli foundations.

2J-2

2:30 PM Focused ultrasound with submicron bubbles producing inertial cavitation suppression in blood-brain barrier opening application

Ching-Hsiang Fan[1], Hao-Li Liu[2], Tzu-Chen Yen[3], Chih-Kuang Yeh[1]; [1]Department of Biomedical Engineering and Environmental Sciences, National Tsing Hua University, Taiwan, [2]Department of Electrical Engineering, Chang-Gung University, Taiwan, [3]Molecular Imaging Center, Chang-Gung Memorial Hospital, Taiwan

Background, Motivation and Objective

Focused ultrasound (FUS) with microbubbles (MBs) has been validated to induce transient blood-brain barrier disruption (BBBD). Recent evidences have been shown that when MBs interacted with ultrasound in the form of inertial cavitation may cause the appearance of intracerebral hemorrhage (ICH). The aim of this study was to investigate that the use of sub-micron MBs to oscillate at their resonance frequency, thereby suppressing inertial cavitation during BBBD could eliminate ICH.

Statement of Contribution/Methods

Fifty Sprague-Dawley rats were performed craniotomy before FUS irradiation (in the presence of MBs). Two experiments were conducted: (1) 1-MHz FUS exposure with SonoVue, and (2) 10-MHz FUS exposure with self-made sub-micron MBs. FUS were delivered at left hemisphere brain with pressures ranging from 0.5 to 2.5 MPa (PRF = 10 Hz, burst length = 1 ms, exposure time = 60s). Wideband and subharmonic emissions from MBs were both listened to quantity inertial and stable cavitation dosages. BBBD was assessed by quantifying the amount of Evans blue (EB) leakage into the brain. Heavy T2* MRI were acquired to confirm the ICH occurrence.

Results

Figure A exhibited that combing 10-MHz FUS with self-made MBs, BBBD can be produced, and no ICH has been observed even pressure up to 2.5 MPa. In contrast, the 1-MHz FUS with SonoVue elicit BBBD accompanying with ICH when the pressure above 0.5 MPa. The corresponding acoustic emissions showed that for group-1, stable cavitation dominated and the inertial cavitation can be limited, whereas in the group-2 both the stable and inertial cavitation were involved in the BBBD (Fig. B). These indicated that both stable and inertial cavitation can evoke BBBD, however the inertial cavitation are more indicative to responsible for the ICH occurrence. The EB extravasation data performed a high correlation to the stable cavitation dosage, implies that the stable cavitation were directly contribute to the permeability during BBBD (Fig. C).

Discussion and Conclusions

These results revealed that BBBD can be achieved with extensively suppress inertical cavitation using this technique. Besides, subharmonic response from MBs could be a specific imaging index to locate BBBD. We also found that there was no obvious ICH occurrence even FUS exposure duration is longer than 4 min. Potential applications include BBBD with drug-loaded MBs by using 10-MHz FUS in glioblastoma model.

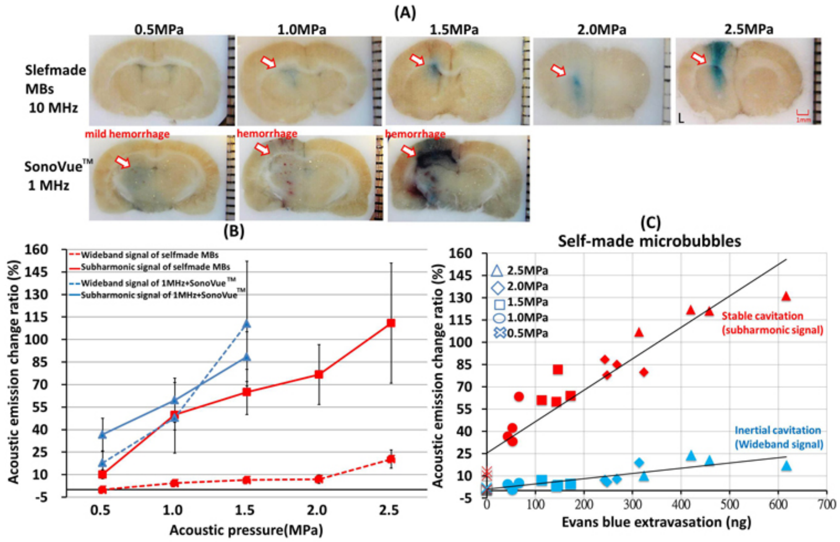

2J-3

2:45 PM Initial In Vivo Feasibility of a Simple, Pre-Clinical Focused Ultrasound System Applied to Blood-Brain Barrier Opening

Fabrice Marquet[1], Yao-Sheng Tung[1], Tobias Teichert[2], Vincent Ferrera[2], Elisa Konofagou[1,3]; [1]Biomedical Engineering, Columbia University, USA, [2]Neuroscience, Columbia University, USA, [3]Radiology, Columbia University, USA

Background, Motivation and Objective

The blood-brain barrier (BBB) is a selective barrier within the neurovascular unit formed by the endothelial cells that line cerebral microvessels. The BBB hinders the effective systemic delivery to the brain of more than 98% of small molecule drugs and nearly all large molecule drugs. Previously, our group has shown, along with others, that microbubble enhanced, focused ultrasound is capable of disrupting the BBB noninvasively, transiently and selectively in small animals. Until now, however, this BBB opening method has mainly been confined to research laboratories because transcranial focusing in large animals has been proven challenging. In this study, operating at intermediate frequencies is selected in order to solve the tradeoff between high aberrations (at higher frequencies) and low inertial cavitation threshold (at lower frequencies). In vitro transcranial focusing targeting clinically relevant targets, especially those involved in Alzheimer's and Parkinson's diseases, is investigated. Initial feasibility in vivo in non-human primates is also demonstrated.

Statement of Contribution/Methods

A PVDF, 500-kHz single-element transducer was used transcranially. A 10-MHz pulse echo transducer was mounted through the central hole of the transducer to ensure targeting. This transducers assembly and a hydrophone were mounted onto two 3D axis positioning system to be able to aim the hippocampus, putamen and caudate locations through the skull. In vivo experiments were conducted in Macaca Mulatta monkeys (16 sonications) using the same setup and Definity or 4-5 µm, custom-made, lipid-shelled, microbubbles. The transducer was mounted on a stereotaxic frame. BBB opening was confirmed using T1-weighted gradient pulse echo MR sequence at 3T and gadodiamide IV injection. Damage was assessed using a T2 sequence.

Results

This study showed acceptable targeting and good focusing quality using a single-element transducer through both the monkey and human skulls (lateral shift below 1 mm and 2 mm, attenuation around 50% and 70%, respectively). BBB opening was achieved in three different monkeys using pressure ranging from 0.2 MPa to 0.6 MPa. The position of the induced BBB opening region was very close to in vitro estimations (in vivo shifts of the focus agree with in vitro measurements within 15%). No damage was detected at pressures below 0.45 MPa.

Discussion and Conclusions

Initial feasibility of noninvasive, highly selective, drug-independent and reversible BBB opening was demonstrated in non-human primates at 500 kHz in vitro and in vivo. The study highlighted the feasibility of achieving BBB opening with a very simple procedure without a complex multi-element transducer or phase aberration correction. High spatial selectivity of this technique was also shown. In vitro and in vivo targeting results were found to be in good agreement regarding the targeting capabilities of the technique.

Supported in part by NIH R01EB009041 and NIH MH059244.

2J-4

3:00 PM MR-guided adaptive focusing of transcranial HIFU beams: a human cadaver study

Laurent Marsac[1,2], Dorian Chauvet[3], Benoit Larrat[1], Mathieu Pernot[1], Benjamin Robert[2], Mathias Fink[1], Jean Francois Aubry[1], Anne Laure Boch[3], Mickael Tanter[1]; [1]*Institut Langevin, Paris, France,* [2]*SuperSonic Imagine, Aix en provence, France,* [3]*Département de Neurochirurgie, Hôpital Pitié Salpêtrière, Paris, France*

Background, Motivation and Objective

Human transcranial focusing of 1 MHz HIFU beams is challenging because of the strong aberrations and attenuation induced by the skull. In order to improve ultrasound focusing through aberrating layers such as fat or bones, adaptive focusing techniques have been proposed, mostly based on the backscattered echoes or simulations using propagation models. We recently proposed energy-based techniques requiring the sole knowledge of the acoustic intensity at the desired focus for different specific US emissions. By measuring displacements induced by acoustic radiation force, we were able to estimate the acoustic intensity in biological tissues. The aberration correction is obtained when the maximal displacement at the focus is reached. In human head, the objective was here to rely on Magnetic Resonance-Acoustic Radiation Force Imaging (MR-ARFI) to rapidly map the displacements induced by a focused ultrasound beam in order to achieve the adaptive focusing.

Statement of Contribution/Methods

Previous proofs of concept were done using numerical phase aberration and *ex vivo* veal brain phantoms. Optimal focusing was then obtained in veal brain through numerical aberrator mimicking the skull phase aberration but without its attenuation effects. For this experiment a cadaver head was extracted 48 hours after death (consent donor, 80 years old). The aim was to focus in the center of the brain of the intact *ex vivo* head where the skull acted as a strong phase and amplitude aberrator. This work was done in a clinical Philips 1.5T Achieva scanner. The HIFU beam was generated using a 512 elements US phased array dedicated to transcranial human experiments and operating at 1MHz (SuperSonic Imagine, France). A motion-sensitized spin echo EPI sequence (TE: 50 ms / TR: 1.2 s, spatial resolution: 2x2x7 mm^3, time: 2.4 s) was implemented to measure displacements induced by the acoustic radiation force of transmitted beams.

Results

MR-ARFI allowed mapping the radiation force at the focus of the array. After the recording of the displacements obtained for different US emissions, the proposed adaptive focusing technique was able to recover the optimal spatial distribution of the phase aberrations. The energy-based adaptive focusing method allowed increasing the intensity at the focus by a factor of 2.18 relatively to emission without correction and 1.49 relatively to the simulation-based correction. SNR of encoded displacement were computed and the minimal SNR for optimal focusing was estimated between 7.7 dB and 9.2 dB. Total acquisition time for 384 US channels correction process was 2 hours.

Discussion and Conclusions

First results in human heads using clinical MR guidance show that energy-based adaptive focusing for high frequency transcranial brain HIFU procedure can be achieved within reasonable time. Ongoing work is aiming at accelerating the MR acquisition and US strategy in order to reach acceptable durations for in vivo protocols.

2J-5

3:15 PM Stationary Waves Arising from Ultrasound Therapy of the Brain: Experimental Measurements, Numerical Computations and Safety Considerations

Gianmarco Pinton[1], Emilie Beaulieu-Ouellet[1], Stephen Meairs[2], Jean-Francois Aubry[1], Mickael Tanter[1]; [1]*Institut Langevin, ESPCI, Paris, France,* [2]*Department of Neurology, Universitätsklinikum Mannheim, University of Heidelberg, Mannheim, Germany*

Background, Motivation and Objective

Therapeutic ultrasound is used in brain therapy for ischemic stroke thrombolysis and thermal ablation. A recent clinical trial, called the Transcranial Low-Frequency Ultrasound Mediated Thrombolysis in Brain Ischemia (TRUMBI), reported a 93% rate of cerebral hemorrhage with ultrasound and thrombolytic drugs, and 41% in the control group. Due to a patient death the trial was halted prematurely. Concerns were raised regarding the procedure's safety and its acoustic intensities. The TRUMBI device is based on an unfocused 300 kHz transducer that transmits a long (765mm) pulse, resulting in multiple reverberations within the skull. During high intensity focused ultrasound (HIFU) therapy, the pulse duration is typically 10 seconds, establishing a permanent regime in the brain. Intensities are larger in areas of constructive interference, affecting transmission safety limits. The objective of this paper is to quantify, with experiments and simulations, the standing wave ratio (SWR) and the contribution of interference to the intensity distribution in the brain during ultrasound therapy.

Statement of Contribution/Methods

A human skull was placed in a degassed water tank and the TRUMBI pulse was recorded with a calibrated hydrophone. Since water is practically non-attenuating, these measurements overestimate the SWR. To obtain a more accurate representation, the acoustic field was modeled with a anatomically accurate 3D finite difference fullwave acoustic code that includes attenuation in tissue. In addition to the non focused thrombolysis geometry, a 1 MHz HIFU therapy array was modeled.

Results

The plot shows the measured maximum pressure as a function of distance to the TRUMBI transducer. It corresponds to the area in the blue circle on the right, which shows the simulated acoustic field. A standing wave pattern, with a SWR of 3.1 is visible. The acoustic intensities are measured for the first time for the TRUMBI protocol (0.16 MPa), confirming the low MI hypothesis proposed by Daffenstoffer.

Discussion and Conclusions

For an unfocused thrombolytic geometry the peak intensities depend on two mechanisms: standing waves and lensing effects from the skull surface. For a focused HIFU array, standing waves result in variations that are small relative to the peak intensity at the focus. These methods will be used to optimize transmission parameters and to reduce standing wave effects.

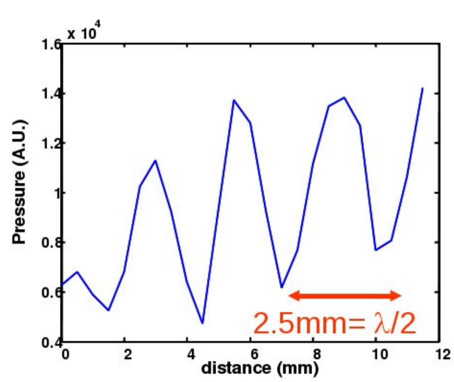

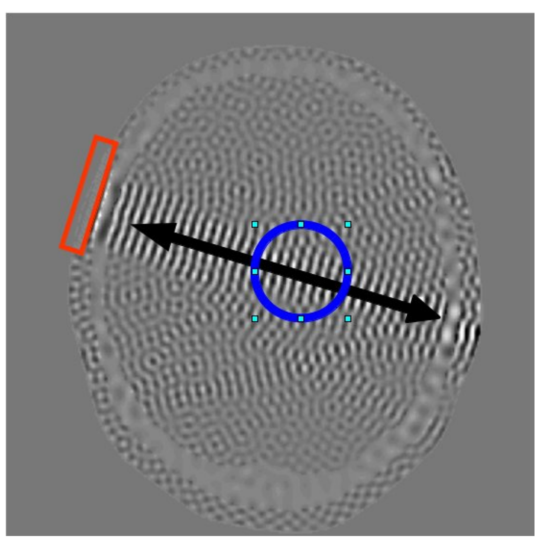

3J - Cardiovascular Tissue Characterization

Carribean Ballroom VII

Friday, October 21, 2011, 2:00 pm - 3:30 pm

Chair: **James Miler**
Washingon University

3J-1

2:00 PM IVUS Is Still Alive - Multi Parameter Analysis for Tissue Characterization of Coronary Atherosclerosis and Interpretation from Acoustic Microscopy Observation

Yoshifumi Saijo[1]; [1]Graduate School of Biomedical Engineering, Tohoku University, Japan

Background, Motivation and Objective

Is IVUS still alive in the era of OCT which provides higher resolution imaging? Besides easier usability, IVUS is superior to OCT from the point of view of tissue characterization of coronary atherosclerosis. In the present study, multi parameter analysis such as integrated backscatter (IB), Virtual Histology (VH), strain rate imaging and newly developed method named ″attenuation imaging″ are compared and discussed the interpretation by acoustic microscopy observations.

Statement of Contribution/Methods

RF signal was obtained from commercial available IVUS systems by the use of fast digitizer card with the sampling frequency of 400 MHz. IB-IVUS image was generated by integrating 128 points of absolute value of RF signal. VH image was generated following the original method proposed by Nair et al. Tissue velocity was obtained by calculating the correlation and displacement of RF signal at the same portion in the consecutive frames. Strain rate was calculated as $(v_k-v_{k-1})/\ d$ where v_n is the velocity and d is the distance of the two points. Assuming that the total power emitted from ultrasound transducer of IVUS is equal in all directions, attenuation is defined as $f\,(R_k/T_{k-1})$ where R_n is reflection and T_n is transmission. Acoustic microscopy data were obtained from autopsied specimen. The tissue was frozen, sliced approximately 10 μm and mounted on a glass slide. A concave ultrasound transducer with the central frequency of 100 MHz was mechanically scanned above the specimen to obtain two-dimensional distribution of attenuation and sound speed.

Results

The figure shows an example of the multi parameter analysis of coronary atherosclerosis. Conventional IVUS and IB-IVUS show homogeneous fibrous plaque but the deeper region is represented as fibrofatty plaque by VH-IVUS, softer region in the strain rate imaging and low attenuation in the attenuation imaging. Acoustic microscopy observation showed that the sound speed of lipid pool was lower than that of the fibrous tissue.

Discussion and Conclusions

Multi parameter analysis showed the region of soft plaque more clearly than conventional IVUS. As ultrasound reflects mechanical properties of the tissue, IVUS provides important information which was not provided by OCT.

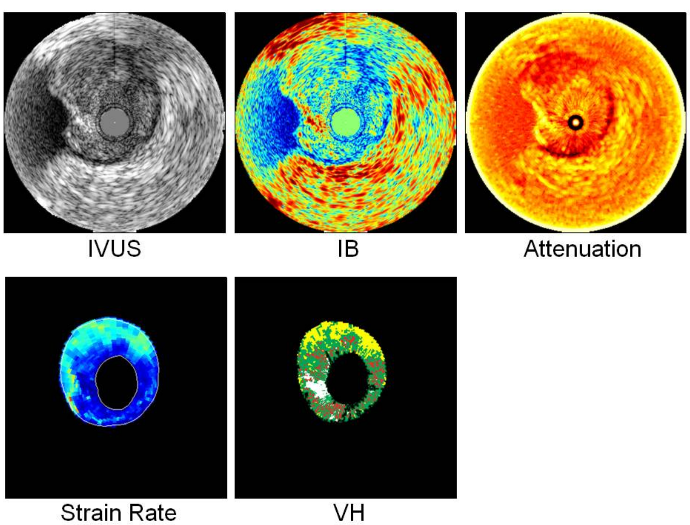

3J-2

2:15 PM Ultrasonic assessment of disease using a quantitative analysis of microvessel morphology

Ryan Gessner[1], Stephen Aylward[2], Elizabeth Bullitt[3], Paul Dayton[1]; [1]Biomedical Engineering, UNC/NCSU, Chapel Hill, NC, USA, [2]Medical imaging, Kitware, Carrboro, NC, USA, [3]Surgery, UNC, Chapel Hill, NC, USA

Background, Motivation and Objective

With the design of new ultrasound techniques which can image microvascular structure with high resolution and high contrast, the opportunity has arisen to apply morphological analysis to assess blood vessel tortuosity characteristics. Previous studies utilizing magnetic resonance angiography in humans have illustrated a relationship between vessel morphological abnormalities and the presence of disease. Moreover, the relationship has predicted effective therapeutic outcomes sooner than conventional clinical methods. In this study, we apply our vessel morphological metrics to 3D US angiography images to distinguish healthy from diseased subjects.

Statement of Contribution/Methods

A transmit-low/receive-high imaging mode was implemented with a custom preclinical probe to create high resolution, high contrast microvascular maps in 3D (Gessner IEEE-UFFC 2010). Images were acquired in-vivo from both control and tumor models (N=8) and the centerlines of over 100 microvessels were extracted from these image data. Vessels either within or near tumor boundaries were selected for segmentation. Similarly, the vessels near the same anatomical location were selected in controls. The morphological metrics used for vessel-structure quantification were the distance-metric (DM) and sum of angles metric (SOAM), which are sensitive to two different types of vessel tortuosity (Bullitt IEEE-TMI 2003).

Results

Using the vessel centerlines extracted from the image data, differences between the tumor and control populations were observed (see figure). The average DM for the tumor population was 1.47±0.34, which was 30% larger than the control population's mean 1.13±0.07. The SOAM was 19% larger in the tumor population, with an average of 16.27±1.36, compared to the healthy population's 13.72±0.36. Using the tumor margins delineated from high frequency b-mode images, a relationship between vessel tortuosity and distance to tumor boundaries could be explored.

Discussion and Conclusions

We have implemented a quantitative vessel morphological diagnostic analysis on high resolution 3D in-vivo US images. Data indicate this analysis approach has allowed us to discriminate and quantify characteristic vascular features in diseased tissue volumes relative to controls.

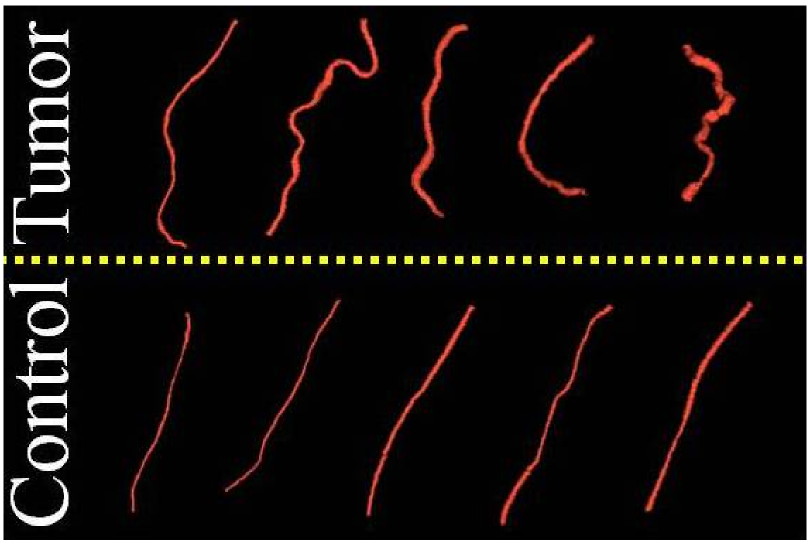

3J-3

2:30 PM Feasibility of Echocardiographic-based Assessment of Myocardial Fiber Structure in Individual Hearts

Michelle Milne[1], Gautam Singh[1], James Miller[1], **Mark Holland[1]**; [1]*Washington University, USA*

Background, Motivation and Objective

Diffusion Tensor Magnetic Resonance Imaging (DT-MRI) represents an established approach for imaging the complex fiber structure of the heart. However, technical limitations, along with the time and expense required for DT-MRI image acquisition, hinder its use as a routine clinical method for obtaining measurements of the intrinsic myocardial structure in individual patients. Methods based on echocardiographic imaging may represent an attractive alternative approach for obtaining intrinsic cardiac fiber structure information that offers the potential for more widespread clinical application. The objective of this study was to explore the feasibility of implementing echocardiographic-based methods for imaging the intrinsic cardiac fiber structure of individual hearts.

Statement of Contribution/Methods

A series of echocardiographic images of excised, whole, sheep hearts, representing two-dimensional apical images acquired in 5-degree rotational increments about the apex, were obtained using a GE Vivid 7 clinical imaging system. The imaging system was configured in a manner that permitted quantitative analyses of the level of ultrasonic backscatter from the images of the myocardium. Radial line profiles representing measured level of backscatter within the ventricular walls of the heart at specific depths from the apex were generated. These backscatter line profiles were combined with data from previously determined relationships between fiber orientation and the relative level of backscatter (anisotropy of myocardial backscatter) to produce images depicting the myofiber structure of each heart. In addition, DT-MRI images of fiber structure of the same intact sheep hearts were acquired for comparison.

Results

Echocardiographic-based images representing myocardial structure exhibit changes in myocardial fiber orientation across the ventricular walls at each depth from the apex investigated. The observed fiber orientation appears consistent with known variations in left-ventricular fiber structure ranging from more longitudinally oriented fibers in the sub-epicardial and sub-endocardial regions and circumferential fibers in the mid-myocardial region. The echocardiographic-derived fiber structure agrees well with the corresponding DT-MRI obtained images of fiber structure.

Discussion and Conclusions

Results of this study suggest that echocardiographic-based methods may represent feasible approach for imaging the intrinsic cardiac fiber structure of individual hearts. The development of this capability could have a significant impact individualized assessment of altered myocardial structure associated with congenital and acquired heart diseases. [Supported, in part, by NIH R01 HL040302]

3J-4

2:45 PM An effective medium model for ultrasound blood characterization

Emilie Franceschini[1], Bloen Metzger[2], Guy Cloutier[3]; [1]Laboratoire de Mécanique et d'Acoustique LMA - CNRS UPR 7051, Marseille, France, [2]Institut Universitaire des Systèmes Thermiques Industriels IUSTI - CNRS UMR 6595, Marseille, France, [3]Laboratory of Biorheology and Medical Ultrasonics, University of Montreal Hospital Research Centre, Montreal, Quebec, Canada

Background, Motivation and Objective

Ultrasonic backscattered echoes from blood contain frequency-dependent information that can be used to obtain quantitative parameters reflecting the aggregation state of red blood cells (RBCs). A Structure Factor Model (SFM) adapted to dense media such as blood has been proposed by Fontaine et al. (Biophysical J 2002). The SFM sums contributions from individual RBCs and models the RBC interaction by a statistical mechanics structure factor. However, the structure factor cannot be analytically computed. That is why Yu and Cloutier (JASA 2007) recently developed the Structure Factor Size Estimator (SFSE) that uses a second-order Taylor expansion of the structure factor. But the SFSE parameterizes the frequency dependent backscatter coefficient (BSC) by two correlated physical parameters. The goal of this paper is to further develop this strategy by proposing a new scattering model that approximates the SFM.

Statement of Contribution/Methods

A scattering model called the Effective Medium Theory combined with the SFM (EMTSFM) is proposed. The EMTSFM assumes that aggregates of RBCs can be treated as individual homogeneous scatterers, which have effective properties determined by the acoustical characteristics and concentration of RBCs within aggregates. Based on this new theory, the RBC aggregation can be acoustically characterized by three parameters: the aggregate radius, internal hematocrit (i.e., volume concentration of RBCs within aggregates) and volume concentration of RBCs in blood.

Results

The accuracy of the EMTSFM was assessed in the frequency range of 4-100 MHz by comparing BSC computed with the EMTSFM and with the SFM (Fig 1). The EMTSFM provided accurate quantitative estimates of the BSC for a product of the wavenumber times the aggregate radius krag≤1.34. The study provided insights into the influence of the aggregate size and internal hematocrit on BSC. The internal hematocrit that has not been studied so far as well as the aggregate size can greatly influence the BSC amplitude.

Discussion and Conclusions

The new EMTSFM theory parameterized the BSC by three physical indices relevant to study the pathophysiological impact of abnormal RBC aggregation. The EMTSFM fitted well BSC computed with the SFM for given ranges of parameterized indices in the frequency bandwidth between 4 MHz and maximum BSC. The EMTSFM provides thus a nice framework for the inversion problem.

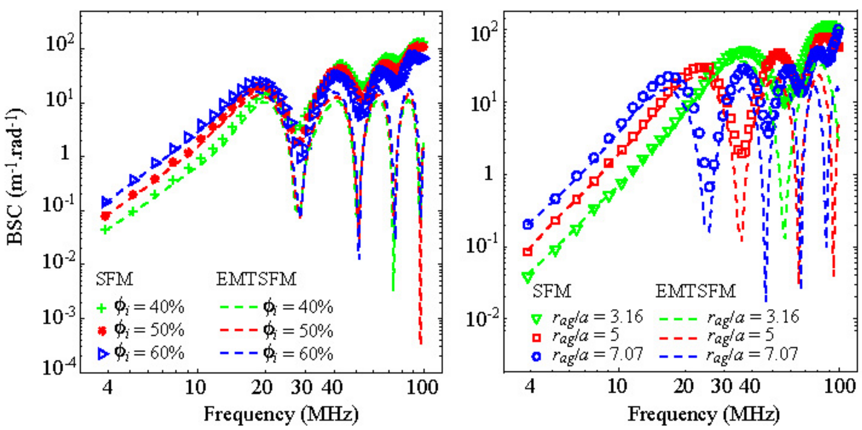

On the left: Dependence of the BSCs for different internal hematocrits ϕ_i and a constant aggregate size r_{ag}/a=6.32 (a being the RBC radius). On the right: Dependence of the BSCs for different aggregatesizes r_{ag}/a and a constant internal hematocrit of 60%. The concentration of RBCs in blood is equal to 20%. The markers represent the BSC computation with the SFM and the dashed lines with the EMTSFM.

3J-5

3:00 PM Experimental validation of the structure factor model on tissue-mimicking phantoms

Nesmah Awad[1], **Emilie Franceschini**[1]; [1]Laboratoire de Mécanique et d'Acoustique LMA - CNRS UPR 7051, Marseille, France

Background, Motivation and Objective

Quantitative ultrasound technique is based on a frequency-based analysis of the signals backscattered from biological tissues. This technique aims to estimate the size and concentration of scatterers in order to diagnose and monitor diseases, such as cancer. The Gaussian Model (GM) and Fluid-Filled Sphere Model (FFSM) have been used for many years but are limited to dilute scattering medium, whereas the scatterers can be densely packed (for example the cells in cancer). A model adapted to dense medium is the Structure Factor model (SFM) used in blood characterization. However, the most often used SFM version is the particle model (PM) using the low frequency limit of the structure factor called the packing factor. The aim of this work is to compare the aforementioned four scattering models with measured backscatter coefficients (BSCs) on tissue-mimicking phantoms.

Statement of Contribution/Methods

The tissue-mimicking phantoms consisted of polyamide microspheres (mean diameter 10 µm) immersed in agar-agar gel. The phantoms had identical scatterer sizes with low impedance contrast (34%) but have different scatterer volume fractions ranging from 1 to 15%. Ultrasonic backscatter measurements were made for frequencies from 5 MHz to 15 MHz. The speeds of sound and the absorption coefficients were also measured.

Results

The sound speeds and absorption coefficients increased with the volume fractions. Good agreement was shown between the measured frequency dependent BSCs and those predicted with the SFM. Figure 1 shows the measured BSC amplitude at 10 MHz versus scatterer volume fraction. Also plotted are the theoretical BSC amplitude computed with the FFSM, PM and SFM. Excellent agreement was obtained at a low volume fraction of 1% for all models. For larger volume fraction (> 5%), the PM underestimated the BSC amplitudes, whereas the FFSM overestimated the BSC amplitudes.

FRIDAY ORAL

Discussion and Conclusions

Most of tissues need to be characterized as dense scattering media. For large scatterer volume fractions, the experimental BSCs agreed with predictions using the SFM in frequency dependence and scattering magnitude. Future works are to extend the study into higher frequencies and to study polydisperse medium.

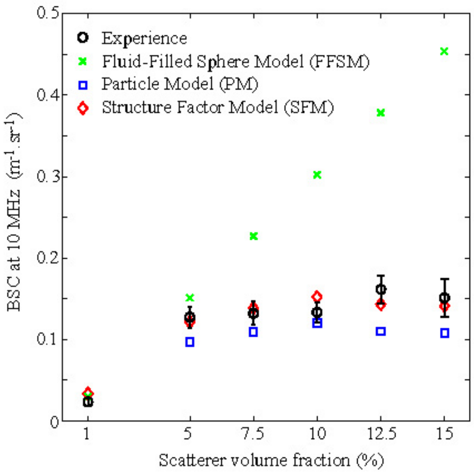

Fig. 1: Theoretical and experimental results of the backscatterer coefficient as a function of scatterer volume fraction at 10 MHz.

3J-6

3:15 PM Experimental study of active control of microbubbles in blood flow by forming their aggregations

Kohji Masuda[1], Ren Koda[1], Nobuyuki Watarai[1], Takumi Ito[1], Nobuhiko Shigehara[1], Takashi Kakimoto[2], Yoshitaka Miyamoto[2], Shin Enosawa[2], Toshio Chiba[2]; [1]*Tokyo Univ of A&T, Japan,* [2]*National Center for Child Health and Development, Japan*

Background, Motivation and Objective

We have previously reported our attempt to propel microbubbles in flow owing to a primary Bjerknes force, which is a physical phenomenon where an acoustic wave pushes an obstacle along its direction of propagation. However, because the primary Bjerknes force is proportional to square of the radius of a bubble, there was a limitation in efficiency to propel bubbles in blood flow when the size of a bubble is as small as red blood cell. On the other hand, microbubbles are known to form aggregation when they are put into an ultrasound field because secondary Bjerknes force, which acts attractive or repulsive between neighboring bubbles, is produced by local condition of oscillation. Thus we consider that forming aggregations of bubbles is effective to be propelled before entering into an ultrasound field to receive more primary Bjerknes force.

Statement of Contribution/Methods

We used the microbubbles, which has a shell made of polyvinyl chloride (PVC) and an average diameter of 4 µm. We also prepared an artificial blood vessel made of polyethylene glycol (PEG), including a Y-form bifurcation, which is placed in the bottom of a tank filled with water. Then we have set two kinds of transducers Tu to form and Tb to propel aggregation, respectively. We have established the conditions of ultrasound emissions of Tu with 7 MHz and 300 kPa, and Tb with 5 MHz and 200kPa to propel aggregations, respectively. Optical image in the observation areas was recorded using a microscope.

Results

When ultrasound was not emitted, each path got uniformly darker. When only Tu was emitted, aggregations of bubbles were clearly observed to make stream but there was no significant difference of amount in both paths. When only Tb was emitted, more bubbles seemed to be propelled to a path but it was not obviously distinguished. When both of Tu and Tb were emitted, stream of aggregations was clearly propelled to a path rather than the other.

To evaluate the amount of bubbles, we extended the two paths using semitransparent tubes and established the evaluation window in a single view. As the result, when ultrasound was emitted to form aggregation, the induction index, which was calculated the area of shadow to pass in the window, was confirmed to improve between 1.3 and 5.5 times more than the time without

forming aggregation.

Discussion and Conclusions

In this study, we realized active control of microbubbles in an artificial blood vessel by primary and secondary Bjerknes force. By using multiple sound sources, we confirmed to be able to change course of aggregations of bubbles at bifurcation of blood vessel.

FRIDAY ORAL

4J High Resolution Acoustic Imaging

Carribean Ballroom I

Friday, October 21, 2011, 2:00 pm - 3:30 pm

Chair: **Roman Maev**
University of Windsor, Canada

4J-1

2:00 PM Implementation of an ultrasound biomicrscopy system by rotational scanning of a high-frequency angled needle transducer

Tae-Hoon Bok[1], Juho Kim[1], Dong-Guk Paeng[1], Jinho Bae[1], Chong Hyun Lee[1]; [1]Ocean System Engineering, Jeju National University, Jeju, Jeju, Korea, Republic of

Background, Motivation and Objective

For high-frequency applications, the mechanical scanning of a single element transducer has been mostly utilized. However, it requires space for both linear and sector scanning. In this paper, an ultrasound biomicroscopy (UBM) system by rotational scanning of a high-frequency angled transducer is designed and implemented and it is applied to obtain the images through a minimal incision hole of 1 mm in diameter for scanning space.

Statement of Contribution/Methods

The rotational scanning UBM system was composed of a high frequency (>40 MHz) angled (45°) needle transducer, and the motion and the signal control divisions. The motion control division consisted of a stepping motor (TS3617-N2E4, Tamagawa, Japan), a motor driver (NMD-2336UD, Tamagawa, Japan), a terminal (UMI-7764, National Instruments, USA) and a motion board (PCI-7332, National Instruments, USA). The signal control division comprised a pulser/receiver (5900PR, Panametrics, USA) and a high speed digitizer (NI-5122, National Instruments, USA). The porcine eye was obtained from a slaughter and set on the holder. The needle transducer was inserted into the eye through a small incision hole of 1 mm diameter for rotational scanning. Ten echo samples from a scan line were collected with 1 kHz of pulse repetition frequency at a reference angle of 0°, and then the transducer was automatically turned to 0.45° for an increment for the next acquisition process which was controlled by a Labview program The total steps were 800 for 360° and the data acquisition time was 10 ms at each step. The data was transferred to a PC and analyzed in Matlab.

Results

The retina with the sclera was visualized in the angel range of 270° ~ 330° and the distance range of 6~7 mm (Figure 1-(a)). The retina and sclera layers were seen as folded layers because the distance from the tip of the angled transducer was not symmetric. The needle transducer was inserted at a certain angle through a hole so that the rotated image was not concentric (Figure 1-(b)).

Discussion and Conclusions

We designed and implemented a rotational scanning UBM system and measured the retina of porcine eye *ex vivo*. The rotational scanning UBM system could be applied to high resolution imaging of the retina and retinal vein by a minimally invasive hole during retinal surgery.

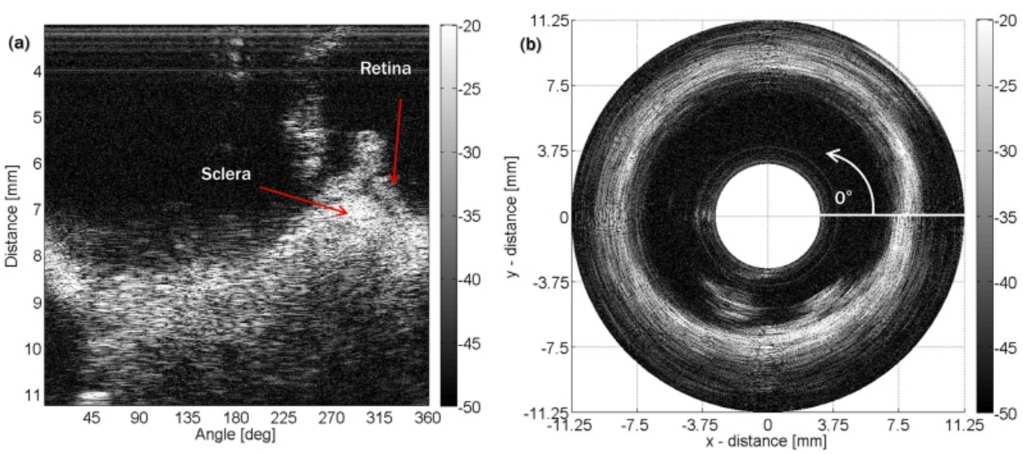

Figure 1. *Ex vivo* posterior image of a porcine eye by the rotational scanning ultrasound biomicroscopy; Rectangular image (a) and polar image (b)

FRIDAY ORAL

4J-2

2:15 PM Adaptive Array Processing for Ultrasonic Non-Destructive Evaluation

Minghui Li[1], Gordon Hayward[1]; [1]Centre for Ultrasonic Engineering, Department of Electronic and Electrical Engineering, University of Strathclyde, Glasgow, United Kingdom

Background, Motivation and Objective

In conventional ultrasound non-destructive evaluation (NDE) imaging systems, the scattering strength of one particular region or point in the imaged medium is estimated using delay-and-sum operations. The data samples that correspond to the time for a wave to travel from the array to the point of interest and back to the different array elements are recorded, and summed to give the intensity of that point. Due to the intersection of different delay curves, the data samples corresponding to the point of interest are loaded with signals backscattered by neighbouring points. This effect can be characterised with the point spread function (PSF), and usually measured by the width of its main lobe and the strength of its side lobes. In NDE practice, most materials like concrete, stainless steel and carbon-reinforced composites used extensively in industries and civil engineering exhibit heterogeneous internal structure. When inspected using ultrasound with delay-and-sum imaging, the signals from defects are significantly corrupted by the echoes form randomly distributed scatterers, even defects that are much larger than these random reflectors are difficult to detect. This is an extremely difficult problem area, for which advanced array processing is potentially able to significantly improve the SNR and enhance defect detection and imaging.

Statement of Contribution/Methods

We propose to apply adaptive beamforming to the received data samples to reduce the interference and clutter noise. Beamforming is to manipulate the array beam pattern by appropriately weighting the per-element delayed data samples prior to summing them. The adaptive weights are computed from the statistical analysis of the data samples. This delay-weight-and-sum process can be explained as applying a lateral spatial filter to the signals across the probe aperture. To the best knowledge of the authors, the application of adaptive beamforming in ultrasonic NDE has not been reported in open literature; however it is highly demanding due to the complex and challenging materials to be inspected.

Results

A 5MHz array with 64 elements and a point reflector located on the array centre-line and at a depth of 20λ are simulated, and imaged with Total Focusing and adaptive beamforming respectively. It shows that the -6dB width of the PSF main lobe is reduced by 50%, and the average background noise level is reduced by 30dB when adaptive beamforming is applied. In experiments inspecting a steel block with side-drilled holes, good quantitative agreement with the simulation results is demonstrated.

Discussion and Conclusions

We present a novel approach for ultrasound NDE imaging. With adaptive filters applied spatially to the data samples, the spurious echoes and clutter noise are significantly reduced. This approach offers a great potential to inspect scattering materials, enhance sensitivity to small flaws, increase imaging resolution and contrast, and improve sizing and classification of defects.

4J-3

2:30 PM Acoustic Tomography: Promise versus Reality

Neb Duric[1]: [1]Karmanos Cancer Institute, Wayne State University, Detroit, MI, USA

Background, Motivation and Objective

Imaging with acoustic waves has made great advances in recent decades. In opposing limits of wavelength, acoustics have played a major role in geophysical applications on the one hand and in medical ultrasound imaging on the other. However, unlike seismic imaging, for example, medical ultrasound has been slow to evolve into the tomographic domain where X-ray imaging still plays a dominant role. In contrast to X-rays, acoustic waves interact strongly with materials through which they propagate, through processes such as refraction, reflection and diffraction. The interactions can be very strong in heterogeneous media such as human tissue. Tomographic reconstructions of ultrasound data therefore require much more sophisticated modeling of acoustic wave propagation often involving highly non-linear inversions. These factors have impeded progress in this otherwise promising methodology.

The advancement of computing power and the rise of high-throughput data acquisition hardware have made ultrasound tomography (UST) feasible in recent years. The objective of this presentation is to relate these developments to practical applications of UST, particularly in the area of medical imaging.

Statement of Contribution/Methods

The major techniques that will be covered include (i) the development of physics-based forward modeling, (ii) the application of new inversion techniques, (iii) the capabilities of modern data acquisition systems and (iv) the current capabilities for signal and data processing in the context of multi-CPU and GPU computing.

Results

Today, a number of laboratory groups are collecting data with UST prototypes and some projects have become commercial ventures. This presentation will review the status of UST imaging, particularly in the area of breast cancer detection, where some of the most recent advances have taken place. Results from these groups will be presented and compared.

Discussion and Conclusions

It is shown that the parallel developments in the four methodologies, noted above, have given rise to exciting new possibilities for UST and for acoustic tomography, at all wavelengths, with potential applications in areas as diverse as seismic exploration, non-destructive testing and cancer detection.

4J-4

3:00 PM Autofocus Imaging in an Anisotropic Austenitic Weld

jie zhang[1], Bruce Drinkwater[1], Paul Wilcox[1], Alan Hunter[2]; [1]Mechanical Engineering, University of Bristol, Bristol, Avon, United Kingdom, [2]TNO, Netherlands

Background, Motivation and Objective

Many industrial welds, such as those in austenitic steels, have inhomogeneous and anisotropic material properties and these can introduce severe distortion to transmitted ultrasonic waves. If left uncompensated these distortions can cause image corruption: blurring, defect mislocation and introduction of spurious artefacts. In this paper a material property autofocus imaging technique is presented, which aims to overcome these image distortions caused by unknown wave velocity variations.

Statement of Contribution/Methods

Material property autofocus aims to estimate the distribution of velocity within a component such as a weld, based on a comparison between measured data and a model. A Monte-Carlo inversion approach is proposed to solve this multi-parameter optimisation problem. Experimental data was collected from a series of active beacons that transmit ultrasound through the unknown weld region. A general forward model based on the Dijkstra fast ray tracing algorithm was used to predict the ultrasonic wave propagation in this inhomogeneous and anisotropic media. The model is then simplified for efficient application to the weld property estimation problem. Using this simplified model, the inherently statistical Monte-Carlo inversion approach determines the unknown weld parameters (i.e. spatial distribution of ultrasonic velocity) using the through-weld travel times between the beacons and a receiver array. Ultrasonic images based on the Total Focusing Method (TFM) are then corrected using these extracted weld parameters.

Results

The weld maps from various thick section steel specimens containing 'V' shaped butt welds are extracted using this material property autofocus technique. Firstly, active beacons are used to transmit ultrasound through the weld and are received at an array placed on the far side of the specimen. Secondly, a Monte-Carlo inversion process then allows the extraction of the weld parameters. Finally, focused images, generated using the extracted experimental weld maps are then compared with images generated using a constant velocity. This scenario is explored both in simulation and through experimental data and the errors and limits of applicability investigated.

Discussion and Conclusions

The performance of the material property autofocus approach has been assessed through simulation and experimental weld map extraction and defect imaging. An important practical application is that the weld maps have been measured within specimens with real industrial welds. Autofocus has been used to improve the location of various defects and in some cases initial mislocation errors greater than 5 mm have been reduced to below 1 mm.

4J-5

3:15 PM Ultrasonic Imaging of Pitting using Multilayer Synthetic Aperture Focusing

Martin Skjelvareid[1,2], Tomas Olofsson[3], Yngve Birkelund[1]; [1]Department of Physics and Technology, University of Tromsoe, Tromsoe, Norway, [2]Breivoll Inspection Technologies, Tromsoe, Norway, [3]Department of Engineering Sciences, Uppsala University, Sweden

Background, Motivation and Objective

Detection and sizing of corrosion damage is vital when assessing the condition of water pipelines. Since the pipes usually are buried in the ground, they have to be inspected from the inside using an inspection robot. Using water inside the pipe as an acoustic couplant, pulse-echo ultrasound measurements can be used to image both the interior of the pipe and the pipe wall itself. Corrosion damage is often present on both the inside and the outside of the pipe, but in this work the imaging problem is limited to outside corrosion only. To accurately determine the size and depth of a corroded area, high spatial resolution is required, and synthetic aperture techniques provide the means for creating such high-resolution images. In this paper, one of the recently proposed multilayer synthetic aperture algorithms is evaluated for imaging of a simulated case of outside corrosion.

Statement of Contribution/Methods

A short summary of the multilayer synthetic aperture algorithm is given. The algorithm can be adapted to both 2D (line scan) and 3D (surface scan) data, and these two variations are tested on a number of artificial pittings in an aluminium plate. The aluminium plate was immersed in water and scanned using a 2.25 MHz, Ø 6 mm transducer.

Results

Comparison of raw and focused images shows that the synthetic aperture algorithm significantly improves the lateral resolution, for both 2D and 3D images. Results from the 2D experiment are shown in the figure. The focused images also show that only the relatively flat sections of the pittings reflect a significant amount of acoustic energy. However, detecting the maximum reflection within the plate for each measurement position still produces a relatively accurate outline of the pitting shape.

Discussion and Conclusions

It has been shown that synthetic aperture focusing is useful for accurate imaging of outside pitting on a plate. A similar technique, adapted for curved surfaces, should be be useful for detection and sizing of outside corrosion on water pipelines.

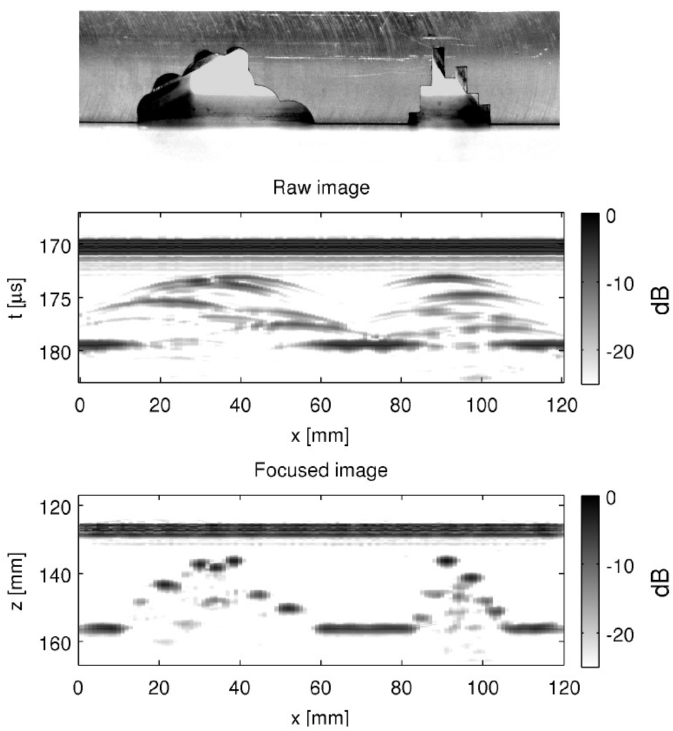

FRIDAY ORAL

5J - Acoustic Wave Propagation I

Carribean Ballroom II

Friday, October 21, 2011, 2:00 pm - 3:30 pm

Chair: **Mihir Patel**
Schlumberger-Doll Research

5J-1

2:00 PM Guided Acoustic Waves Propagating at Surfaces, Interfaces or Edges

Andreas Mayer[1]; [1]HS Offenburg, Gengenbach, Germany

Background, Motivation and Objective

Surface and interface acoustic waves are two-dimensionally guided waves, as their displacement field is plane-wave like regarding its dependence on the spatial coordinates parallel to the guiding plane, while it decays exponentially along the axis normal to that plane. When propagating at the planar surface or interface of homogeneous media, they are non-dispersive. Another type of non-dispersive acoustic waves which is, however, one-dimensionally guided, has displacement fields localized near the apex of a wedge made of an elastic material. In comparison to surface acoustic waves, these wedge acoustic waves have the advantages of being diffraction-less and having lower speeds. In this review, their propagation properties are described and compared with those of surface and interface waves. Also, potential applications will be discussed.

Statement of Contribution/Methods

Apart from work done within the geometrical acoustics approximation, analytic results for the calculation of the velocities and displacement field of these waves have been achieved only for sharp-angle wedges. Numerical approaches will be reviewed that are in use for the treatment of arbitrary wedge angles. It is shown how perturbation theory can be used for a quantitative determination of the dispersion of these waves due to modification of the ideal wedge geometry like truncation or rounding of the wedge tip and coating of the surfaces.

Likewise, an overview will be given of the experimental methods that have been used to excite acoustic waves at wedges and to detect their associated strain fields. These methods involve piezoelectric and interdigital transducers as well as photoacoustic excitation and scanning techniques.

Results

For SAWs in anisotropic elastic media, surface wave existence theory has established a general theorem that guarantees the existence of a subsonic surface wave for almost all propagation geometries. In the case of wedge acoustic waves, such a theory does not exist. However, numerical studies, which will be discussed in this presentation, indicate that the influence of anisotropy is not less pronounced in the case of wedge acoustic waves. For example, these studies reveal that acoustic waves with clearly detectable edge-localisation do not exist for many orientations of rectangular edges in anisotropic media. Furthermore, wedge acoustic waves have specific nonlinear properties as compared to surface or bulk acoustic waves, which will shortly be discussed, too.

Discussion and Conclusions

The potential of wedge acoustic waves for applications has been demonstrated in several fields of technology, including non-destructive testing. In view of the progress seen over recent decades in fabrication techniques for high-quality surfaces and microstructures, it may also be worth reconsidering edge acoustic waves in the context of signal processing devices and sensor applications.

5J-2

2:30 PM Experimental Results on the Pressure Dependence of the Minnaert Resonance Frequency

Bernt Inge Hansen[1], Jarle André Johansen[1]; [1]*Department of Engineering and Safety, University of Tromsoe, Tromsoe, Troms, Norway*

Background, Motivation and Objective

Early detection of subsea gas leaks at depths typical (300m) for the Snøhvit gas field outside Hammerfest, Norway, is of prime importance. Many passive and active (ultra)sonic methods exist for detection and characterization of gas bubbles in water[1]. Here we focus on the passive emission of sound from medium size gas bubbles released in water. The natural oscillation frequency of bubbles in this regime has been shown to follow the Minnaert formula[2]: $\nu=(2\pi a)^{-1} (3\kappa p_0/\rho)^{1/2}$, ν is frequency, a is radius, κ is polytropic index, p_0 is ambient pressure, and ρ is water density.

Very few have presented experimental results on frequency dependence of ambient pressure. Our objective is for the first time to examine this dependence simulating depths down to more than 300m.

Statement of Contribution/Methods

We contribute with new experimental results for the pressure dependence of the natural frequency of the sound emitted from gas bubbles released in water. Measurements are done by use of hydrophones and specially developed near-hydrophone charge amplifiers and low impedance line drivers for low noise and robust signal transport. The water depth is simulated by a controlled pressure vessel. Gas bubbles are released through a nozzle by setting the supply gas pressure slightly higher than inside the vessel. Bubble size is estimated by photographic techniques.

Results

We present the oscillation frequency for medium sized nitrogen gas bubbles, with radius of ca 1.5 mm, released in water. The ambient pressure was varied from 100-4000 kPa, and resulting frequencies ranged from ca 3.4-12.5 kHz. To account for the changes in bubble size at different pressures, and to linearize, we have chosen to plot the product νa versus $\sqrt{p_0}$. Measured data is compared to the Minnaert equation.

Discussion and Conclusions

Our experiment is the first systematic test of the pressure dependence of the Minnaert frequency under the above described conditions. The main uncertainty is estimating the actual size of the bubbles. This is included in error bars in the plot. Clearly our results can be well explained by the Minnaert equation.

[1]TG Leighton, The acoustic bubble, Academic Press 1994.

[2]M Minnaert, On the musical air bubbles and sounds of running water, Phil Mag 1933 16

FRIDAY ORAL

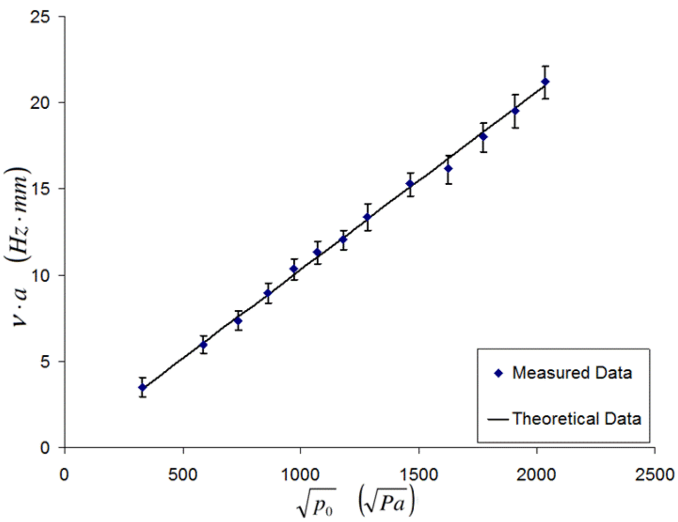

5J-3

2:45 PM Wave Propagation in a Microporous Structure for Angled Excitation

Andrew Dawson[1], Roger Young[1], Paul Harris[1]; [1]Industrial Research Ltd, Lower Hutt, New Zealand

Background, Motivation and Objective

Previously high frequency wave propagation in a collinear fluid-filled microporous material was studied using normally incident plane wave excitation. The work revealed two modes, a fast mode propagating predominantly in the solid fraction and a slow mode propagating mostly in the fluid. That work focused on symmetric modes however we noted that when the source width was reduced 'bow' like waves were observed. In this work finite element modeling (FEM) of angled excitation of the collinear microporous materials is used for a preliminary study of the waves propagating within the bulk and those at the surface. The effect of frequency, microstructure dimensions and material properties are considered.

Statement of Contribution/Methods

2D FEM was performed using PZFlex for a microporous structure consisting of 200 vertically aligned solid columns of width 10 um separated by vertical pores that varied between 1 um and 10 um, the columns being 3 mm long. The solid fraction was typically aluminium and the pores water filled however the material properties were varied to aid the study. Modeling was also performed for a material with similar structure in 3D. To detect propagation of a leaky surface wave the porous microstructure was vertically loaded by a water layer. In addition an immersed single 1 um column was modeled. Vertical (along column), angled, and horizontal (across column) excitation provided preferential generation of symmetric or antisymmetric waves. A Blackman pulse with centre frequency 20 MHz was used.

Results

For vertical excitation propagation was dominated by a fast wave with velocity 5.2 kms-1 along the pillar with small transverse coupling. For horizontal excitation two waves were observed; a very leaky and dispersive wave existing predominantly in the solid but causing large transverse coupling with a velocity range along the pillar of 0.6-2.6 kms-1 (velocity increased with increasing frequency, the frequency range restricted by the pulse spectrum). The second wave traveling across the pillars at 2.7 kms-1 appeared P in nature. Leaky surface waves were only observed for pore widths 3 um or less. The velocity of the surface waves varied between 2.0-2.8 kms-1 with the fastest velocity occurring for the 1 um sized pores; the velocity and displacements suggest a leaky Rayleigh wave.

Discussion and Conclusions

The type of bulk waves propagating in the microporous structure were excitation dependant with transverse coupling a maximum for horizontal excitation. For Rayleigh waves to exist requires P and S components but here the water filled pores should inhibit shear coupling. However we find that sufficient S coupling at small (<3 um) pore widths allows surface wave propagation. By lowering the frequency we find that for larger pore widths a surface wave could be observed to propagate.

5J-4

3:00 PM High-Frequency Wave Propagation in Piezoelectric Semiconductor Plate Under Biasing Electric Field

bernard collet[1]; [1]Institut Jean le Rond d'Alembert, CNRS,UMR 9170, Case 162, Université Pierre et Marie Curie, Paris, Ile de france, France

Background, Motivation and Objective

The piezoelectric materials are either dielectric (insulator) or semiconductor. Semiconductors are materials whose electronics properties are intermediate between those the insulators and metals. These intermediate properties are determined by the crystals structure, bonding characteristics, electronic energy bands, external applied fields and also by the fact, unlike conductor materials a semiconductors has both two carriers of electronic charges (electron and hole) can be controlled by doping the pure semiconductors with appropriate chemical impurities. An ultrasonic wave propagating in a piezoelectric crystals or piezoelectric ceramics is usually accompanied by an electric filed. When the crystals is also semiconducting, the electric field produces electronic currents and space charges which modify the wave speed and attenuation. The interaction between a traveling ultrasonic wave and mobile space charges is currently called acoustoelectric effect. Several interesting phenomena involving the interaction of ultrasonic waves and electrons have been observed in piezoelectric semiconductors. These include in particular the process of ultrasonic amplification and nonlinear harmonic generation. It was shown experimentally and proved theoretically that an ultrasonic wave traveling in a piezoelectric can be amplified by the application of an initial dc electric field. The acoustoelectric amplification of ultrasonic waves have led to the development of acoustic devices.

Statement of Contribution/Methods

Piezoelectric semiconductor devices often have structural design of plates or rods. Here we study the thin piezoelectric-semiconductor plates. In this study we consider the case of piezoelectric semiconductor crystals having one type of majority carriers (electrons or holes). The two-dimensional equations for piezoelectric semiconductor crystal plates with

FRIDAY ORAL

general symmetry and with electroded faces are obtained systematically from the three-dimensional equations by expansion in series of trigonometric functions of thickness coordinate of the plate. A system of approximate first-order equations is extracted from infinite system of two-dimensional equations.

Results

Two-dimensional equations obtained are specialized to crystals of hexagonal (6mm) symmetry. The effects on the spectra of dispersion of electric boundary condition as well as those induced by an initial dc electric field are analyzed. It is shown that the semiconduction induces a dispersion and acoustic loss in the propagation of thickness-shear, flexural, extensional and thickness-stretch waves.

Discussion and Conclusions

The derived first-order equations are shown to give accurate dispersion relations without any correction factors. The equations are obtained are useful to anticipate the high-frequency behaviour of plate structures for acoustoelectric devices.

5J-5

3:15 PM Estimation of Rock Anisotropic Constants using Sonic Data from Deviated Wellbores

Bikash Sinha[1]; [1]Schlumberger-Doll Research, Cambridge, MA, USA

Background, Motivation and Objective

Seismic prospecting for hydrocarbons requires anisotropic velocity model that describes plane wave velocity propagation as a function of direction from the vertical symmetry axis of a transversely isotropic (TI) overburden shale. The anisotropic velocity model for a thick shale layer can be constructed in terms of five TI elastic constants. Generally, these elastic constants are estimated from borehole seismic data analysis. This paper describes a computationally efficient method to estimate all five TI constants using borehole sonic data acquired from boreholes with two different deviations from the vertical TI symmetry axis.

Statement of Contribution/Methods

A new technique for the estimation of all five TI elastic constants consists of measuring the compressional (qP), pure shear (SH) and quasi-shear (qSV) wave velocities along boreholes with two different deviations from the vertical. These velocities can be reliably estimated from a conventional processing of monopole and cross-dipole waveforms. The proposed algorithm is based on weak anisotropy approximation and it successfully inverts the qP, qSV, and SH wave velocities in the two depth intervals in the same lithology with different deviations for all five TI elastic constants. Two modified versions of this workflow can also invert the compressional and shear velocities from (1) a vertical wellbore parallel to the TI-symmetry axis and a deviated wellbore and (2) a horizontal wellbore in the TI-isotropic plane and a deviated wellbore, for all the five TI elastic constants.

Results

Explicit expressions for the compressional and shear wave velocities as a function of propagation direction from the TI-symmetry axis result in an efficient inversion of velocity data to obtain elastic constants of the propagating medium.

Inverted elastic constants from these algorithms agree very well with the actual TI constants used to generate synthetic velocities for three different shale formations. Elastic constants for these shale samples were obtained from laboratory measurements.

Discussion and Conclusions

Thus, we have validated the proposed algorithms using synthetic data for the estimation of all five TI elastic constants. Since these velocity to elastic constants transforms do not require the use of Stoneley data and its associated strong dependence on the borehole fluid compressional velocity in the estimation of Stoneley shear modulus, the proposed method is particularly useful when the compressional velocity of the borehole fluid is not accurately known.

6J - Harsh Environment (5C)

Carribean Ballroom VI

Friday, October 21, 2011, 2:00 pm - 3:30 pm

Chair: **Mauricio Pereira Da Cunha**
University of Maine

6J-1

2:00 PM Iridium interdigital transducers for ultra-high-temperature SAW devices

Thierry Aubert[1,2], Jochen Bardong[1], Omar Elmazria[2], Gudrun Bruckner[1], Badreddine Assouar[3]; [1]Carinthian Tech Research, Villach/St. Magdalen, Austria, [2]Institut Jean Lamour, Vandoeuvre-lès-Nancy, France, [3]Georgia Institute of Technology, International Joint laboratory (UMI 2958), CNRS - GIT, Atlanta, GA, USA

Background, Motivation and Objective

SAW devices have proved to be able of long-term operation at high temperatures up to 800°C, since M. Pereira da Cuhna *et al.* have replaced pure platinum electrodes by innovative co-deposited Pt-10%Rh/ZrO_2 structures to circumvent agglomeration phenomena [1]. Another way to obtain similar results could come from the use of more stable metals than Pt from a physical point of view, i.e. metals with a higher melting point and thus lower self-diffusion coefficients [2]. As it is a noble metal which melting temperature is almost 700°C higher than that of platinum, iridium is a good candidate for such aim.

Statement of Contribution/Methods

10 nm-thick titanium and 100 nm-thick iridium films were deposited respectively as adhesion layer and electrode onto YX-cut langasite substrates, by e-beam evaporation method. SAW delay lines operating at 167 MHz were then fabricated using optical lithography and ion beam etching. These devices were finally characterized (S_{21} parameters) between 20 and 1200°C using a specific setup which description can be found in [3]. Vacuum (10^{-4} mbar of pressure) was chosen as ambient environment because of the tendency of iridium towards oxidation from 700°C on [4].

Results

The very last temperature at which we observed a signal coming from the device was 1140°C (see Fig.). Up to 1000°C (which was reached after 20h of heating) the insertion losses hardly changed. The frequency dependence with temperature was seen to be close to perfect parabola (turnover temperature: 340°C) even if discrepancies were observed for some samples from 900°C on. Optical microscope observations of the devices revealed a strong increase in the surface roughness of the substrate. It also seems that the Ir electrodes vanished.

Discussion and Conclusions

Iridium electrodes proved their suitability for SAW applications up to at least 1000°C. Ongoing experiments should precise their lifetime at such high temperatures. Their major drawback, i.e. oxidation, can be overcome by a correct packaging choice. Further material analysis should also allow explaining the scenario leading to the complete loss of the signal above 1140°C.

[1] M. Pereira da Cunha et al., IEEE Ultrason. Symp., 2008
[2] T. Aubert et al., IEEE Trans. on UFFC, vol. 58 (3), 2011
[3] J. Bardong et al., IEEE Int. Freq. Control Symp., 2009
[4] M. Lisker et al., Surface Coatings Technol., vol. 201, 2007

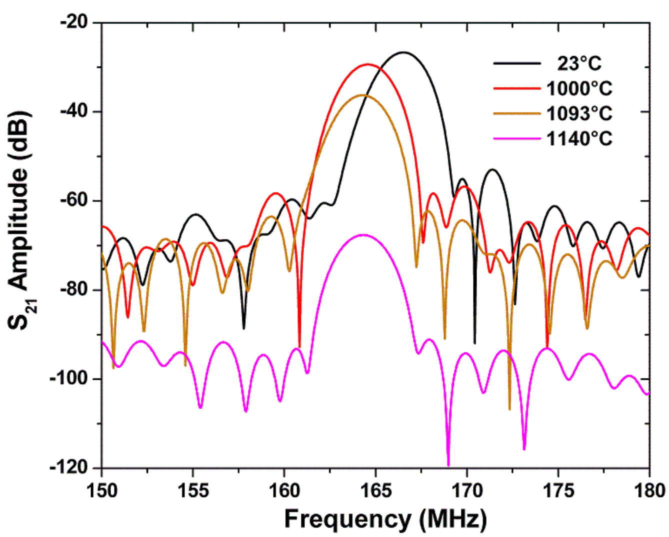

FRIDAY ORAL

6J-2

2:15 PM **SAW Parameters for Langasite at High Temperatures**

Elena Mayer[1], David Eisele[1], Leonhard M. Reindl[1], Victor P. Plessky[2], Gudrun Bruckner[3], Jochen Bardong[3], Thierry Aubert[3]; [1]*IMTEK, University of Freiburg, Freiburg, Germany,* [2]*GVR Trade SA, Bevaix, Switzerland,* [3]*Carinthian Tech Research (CTR), Villach, Austria*

Background, Motivation and Objective

The piezoelectric material langasite has recently attracted a lot of interest in the micro-acoustics community and is currently intensively investigated because of its applicability for wireless SAW sensors at high temperatures. For this purpose it is important to find optimal propagation geometries with regard to thermal stability, electromechanical coupling etc.

The aim of this work is to determine experimentally such acoustical parameters of langasite as velocity under the grating and on a free or metallized surface, the electromechanical coupling coefficient and the reflection coefficient from one electrode with various geometry parameters of the grating. These parameters are measured as functions of temperature up to the highest possible temperature point.

Statement of Contribution/Methods

Three cuts of langsite were investigated with Euler angles (0°, 138.5°,27°), (0°,22°,90°) [1] and (0°,22°,31°). For the acousto-electric characterisation of these orientations, a set of synchronous resonators with five different pitches have been fabricated, covering the frequency range between 250 MHz and 650 MHz. Also, delay lines with free and metallized paths have been designed, operating at four frequencies in a similar frequency range. A Pt metallization with Al2O3-Ti combination as adhesive was used for the electrodes. The parameters of the S-matrix were measured with a network analyser when the samples were slowly heated in the furnace. A high precision signal processing algorithm was applied to the raw data of the delay lines [2] to extract the velocities on free and metallized surfaces.

Results

The temperature dependencies of SAW parameters were obtained up to 800 °C. The results derived from measurements on resonators show good agreement with the results from [3] obtained earlier in a lower frequency range. The metallization has shown good reliability up to 800°C at least for three hours, and after cooling the propagation loss was recovered for lower, but not for high frequencies. Above 800°C, the metallization was destroyed due to de-wetting and decomposition into droplets. The propagation loss shows a local maximum at a temperature around 400°C.

Discussion and Conclusions

The obtained SAW parameters for three cuts of langasite will be useful for the design of SAW devices operating in the investigated frequency range at high temperatures.

This work was performed within the SAWHOT project, funded by the Ministry of Education and Science of the Russian Federation and by the European Community's Seventh Framework Programme (FP7/2007-2013, grant agreement NMP4-SL-2009-247821).

[1] J. Koskela, S. Lehtonen, V. P. Plessky, M. M. Salomaa, Appl. Phys. Lett. vol. 72, no. 21, pp. 2665-2667, 1998.

[2] I. Shrena, D. Eisele, J. Bardong, L. M. Reindl, Proc. IEEE Ultrason. Symp., pp. 863-866, 2009.

[3] S. Sakharov, S. Kondratiev, N. F.Naumenko, A. Zabelin, A. Azarov, S. Zhgoon, A. Shvetsov, Proc. IEEE Ultrason. Symp., 2010.

6J-3

2:30 PM Impact of High-Temperature Dielectric and Piezoelectric Behavior on LGT Acoustic Wave Properties up to 900°C

Peter Davulis[1], Mauricio Pereira da Cunha[1]; [1]Electrical and Computer Engineering Dept., University of Maine, Orono, ME, USA

Background, Motivation and Objective

There is a growing need for frequency control devices and wireless sensors that operate at very high temperatures, 400 to 1000°C, in the aerospace, energy generation, material processing, and oil extraction industries. Langasite (LGS) and langatate (LGT) surface acoustic wave (SAW) devices have demonstrated wireless operation above 900°C. The modeling and design of high-temperature LGT devices requires acoustic wave constants measured throughout the targeted temperature range of operation. Previous work by the authors reported on LGT piezoelectrically-stiffened elastic constants using resonant ultrasound spectroscopy but did not include the temperature variation of the dielectric and piezoelectric constants. This work targets to quantify the dielectric and piezoelectric temperature behavior up to 900°C and verify the impact on the elastic constants and SAW properties.

Statement of Contribution/Methods

In this work, the LGT elastic, dielectric and piezoelectric constants with respective temperature coefficients up to 900°C are reported for the first time. The new set of constants was used to improve the predictions of high-temperature LGT SAW properties such as phase velocity (v_p), temperature coefficient of delay (TCD), and electromechanical coupling (K^2) along multiple orientation sweeps up to 900°C. These predictions were then compared to previous calculations, which ignored the temperature dependence of the dielectric and piezoelectric constants, and to measured data up to 900°C, obtained from delay lines fabricated along 6 orientations in the LGT plane (90°,23°,Ψ).

Results

The average discrepancy between predicted and measured v_p and TCD responses were reduced by 26% and 33%, respectively, up to 500°C and 17% for v_p up to 900°C when the temperature dependence of both dielectric and piezoelectric constants are considered. The extracted LGT piezoelectric constants and temperature coefficients show that e11 and e14 change by up to 11% and 31%, respectively, for the entire 25°C to 900°C range when compared to room temperature values. In addition, this paper uncovers the full set of high temperature LGT elastic, piezoelectric, and dielectric constants and temperature coefficients applicable up to 900°C, including the respective estimated uncertainty.

Discussion and Conclusions

A new set of high-temperature (up to 900°C) LGT acoustic wave constants extracted by RUS technique and which considers the temperature dependence of both dielectric and piezoelectric constants is revealed. The use of these new constants and temperature coefficients resulted in up to 26% and 33% reduction in discrepancies between predictions and measurements for phase velocity and TCD. The reported results verify the relevance of considering the dielectric and piezoelectric temperature behavior for accurate acoustic wave property predictions and device design at high temperatures.

6J-4

2:45 PM Intrinsic Characteristics of Thermally Stable AlN Lamb Wave Resonators at High Temperature

Chih-Ming Lin[1], Ting-Ta Yen[1], Valery Felmetsger[2], Jan Kuypers[1], Albert Pisano[1]; [1]Mechanical Engineering, University of California at Berkeley, USA, [2]OEM Group Incorporated, USA

Background, Motivation and Objective

Piezoelectric microacoustic devices operating in high temperature environments have attracted great interest in various industries, including automotive, aerospace, gas and petroleum exploration, and power electronics. The common piezoelectric materials for high temperature applications are gallium orthophosphate, langasite, langatate, and aluminum nitride (AlN). In addition to operating at high temperature, maintaining the good frequency-temperature stability of the resonance frequency at high temperature is essential for high temperature applications.

Statement of Contribution/Methods

Because silicon dioxide (SiO_2) has the positive first-order temperature coefficients of elasticity (TCE), the thermal compensation for AlN Lamb wave resonators operating at high temperature is achieved using an AlN/SiO_2 composite structure. By varying the thickness ratio of AlN to SiO_2, we can intentionally design the turnover temperatures (To) of the Lamb wave resonators at the high temperature range. As a result, these resonators would have a zero first-order TCF at their turnover temperatures; in other words, they are thermally stable at high temperature.

Results

Three different designs of Lamb wave resonators were compared in this work. As shown in Fig. 1, Design 1 resonator has no SiO_2 film so it shows a linear TCF of -28 ppm/°C. By contrast, design 2 and 3 resonators have the same AlN thickness but design 3 resonator has a thicker SiO_2 layer. Therefore, they exhibit the turnover temperatures at 214 °C and 430 °C, respectively. On the other hand, because the Lamb wave resonators were wire-bonded to a printed circuit board for high temperature measurement, the parasitic inductance and capacitance affect the intrinsic quality (Q) and motional resistance (Rm). Therefore, as shown in Fig. 2, an equivalent circuit is used to extract the intrinsic quality and motional resistance. Figs. 3 and 4 present the intrinsic Q and Rm from room temperature to 600 °C. The experimental results show that Q decreases and Rm increases at high temperature.

Discussion and Conclusions

Lamb wave resonators were temperature-compensated at high temperature using the AlN/SiO_2 composite layer. These results lay the foundation for temperature-compensated Lamb wave resonators for high temperature applications.

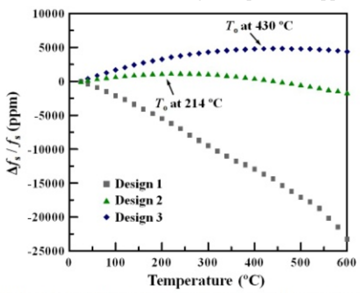

Fig. 1. Plot of the measured frequency variation vs temperature of three Lamb wave resonators.

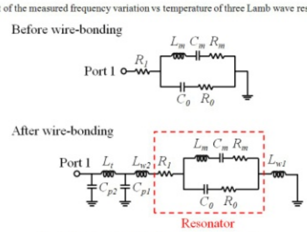

Fig. 2. Equivalent circuit for the resonator and parasitics.

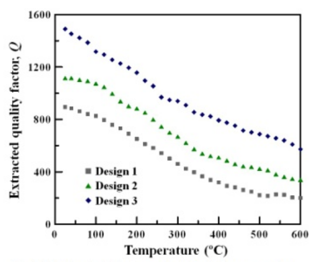

Fig. 3. Plot of the extracted Q vs temperature of three Lamb wave resonators.

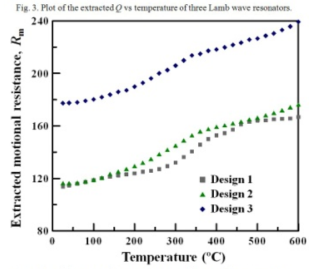

Fig. 4. Plot of the extracted R_m vs temperature of three Lamb wave resonators.

6J-5

3:00 PM Is AlN/Sapphire bilayer structure an alternative to langasite for ultra-high-temperature SAW applications ?

Thierry Aubert[1,2], Jochen Bardong[1], Badreddine Assouar[3], Gudrun Bruckner[1], Omar Elmazria[2]; [1]Carinthian Tech Research, Villach/St. Magdalen, Austria, [2]Institut Jean Lamour, Vandoeuvre-lès-Nancy, France, [3]Georgia Institute of Technology, International Joint laboratory (UMI 2958), CNRS - GIT, Atlanta, GA, USA

Background, Motivation and Objective

Langasite is currently the reference as piezoelectric material for high-temperature SAW applications up to 850°C [1]. However, some drawbacks such as rapidly increasing propagation losses with temperature as well as surface deterioration have been reported [2, 3, 4]. There is clearly a need for alternatives. This paper investigates the suitability of AlN/Sapphire structure for such aim.

Statement of Contribution/Methods

1.2 µm-thick (002) AlN films were grown epitaxially on c-plane sapphire substrate by sputtering method [5]. 10 nm-thick titanium and 100 nm-thick iridium films were then deposited respectively as adhesion layer and electrode by e-beam evaporation technique. SAW delay lines operating at 392 MHz were fabricated using optical lithography and ion beam etching. These devices were characterized (S21 parameters) between 20 and 1050°C using a specific setup [6]. Vacuum (10^{-4} mbar) was chosen as ambient environment because of the tendency of both Ir and AlN towards oxidation from 700°C on [7]. As a comparison, identical delay lines based on YX-cut LGS substrates were characterized in parallel.

Results

The main difference between both kind of devices appeared during the plateau at 1050°C: whereas the amplitude of the signal coming from LGS devices dropped off fastly, the response of the AlN-based delay lines could be observed for 60 hours (Fig. 1). The frequency dependence of the latter is close to linearity (TCF1 = -78 ppm/°C, TCF2 = -12 ppb/°C^2) up to 1050°C. Optical microscope inspections revealed a strong increase in the surface roughness of the LGS substrate, as well as the vanishing of the Ir electrodes. Contrariwise, in the AlN case, the surface seems still smooth, but the Ir electrodes have agglomerated.

Discussion and Conclusions

AlN/Sapphire can be considered for high-temperature SAW applications. Its major drawback, i.e. oxidation, can be overcome by a correct packaging choice. Further material analysis should precise the role of AlN in the aging of the investigated devices.

[1] M. Pereira da Cunha et al., IEEE Ultrason. Symp., 2008
[2] R. Fachberger et al., IEEE Ultrason. Symp., 2004
[3] J. Bardong et al., IEEE Ultrason. Symp., 2009
[4] S. Sakharov et al., IEEE Ultrason. Symp., 2010
[5] T. Aubert et al., J. Vac. Sci. Technol. A, vol. 29(2), 2011
[6] J. Bardong et al., IEEE Int. Freq. Control Symp., 2009
[7] T. Aubert et al., IEEE Ultrason. Symp., 2010

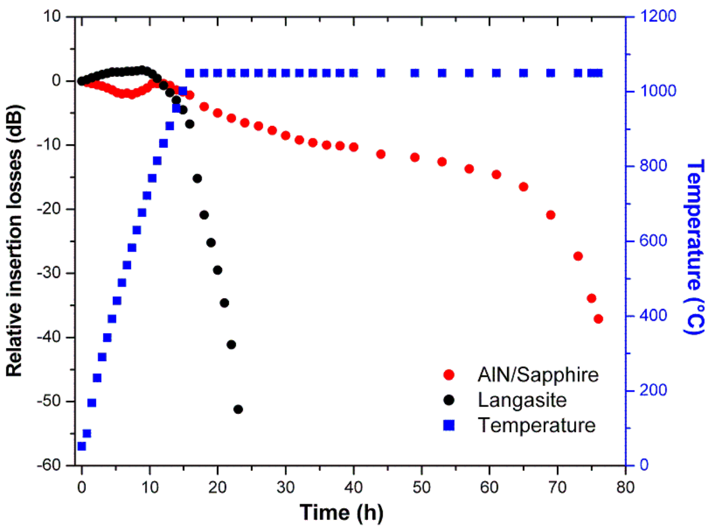

6J-6

3:15 PM Effect of anisotropy on SAW behavior in LGS orientation with Euler angles (0°, 22°, 90°)

Natalya Naumenko[1]; [1]Moscow Technical University of Communication & Information Science, Moscow, Russian Federation

Background, Motivation and Objective

Berkenpas et al[1] reported that LGS cut with Euler angles (0°,22°,90°) is a good choice for high temperature SAW sensors with resonator structure because Bleustein-Gulyaev wave (BGW) propagating in this cut is characterized by sufficient electromechanical coupling and nearly zero TCF. The sensitivity of BGW to variation of electrode thickness enables high coupling when electrodes are sufficiently thick and made of heavy metal, such as Pt, but it can be considered as a drawback for manufacturing SAW resonators with stable electrical parameters. Another specific feature of LGS cut (0°,22°,90°), which was recently confirmed experimentally, is high sensitivity to misorientation, e.g. caused by technological errors. It is much higher than in other BGW cuts and results in splitting of the main resonance into few resonances and degradation of resonator performance. The paper is aimed at clarifying the nature of the observed spurious modes via analysis of anisotropy and its effect on the behavior of BGW and Rayleigh SAW in LGS substrate and in periodic metal grating built on this substrate.

Statement of Contribution/Methods

In LGS orientations with Euler angles (0°,θ, 90°), two degenerate SAW solutions are known to exist: non-piezoactive Rayleigh SAW and piezoelectrically coupled BGW. The velocities of two waves become equal at θ≈22°. Any perturbation of a substrate symmetry eliminates degeneracy and results in strong interaction between the modes. A combination of different numerical techniques was applied to analysis of resonator characteristics and the effect of misorientation on resonator performance.

Results

Two spurious responses deteriorate the resonator performance with misorientation of the third Euler angle less than 0.1° and at 0.5° one resonance is replaced by three comparable resonances. SAW dispersion was calculated and revealed two additional stopbands caused by Bragg reflection of Rayleigh-type SAW and interaction between two SAW modes in the grating when any misorientation occurs. Acoustic fields associated with coupled SAW modes propagating in the grating are visualized. Analysis shows that high sensitivity of resonator performance to misorientation can be reduced by variation of electrode thickness.

Discussion and Conclusions

Investigation of interaction between Rayleigh SAW and BGW, which results from misorientation of LGS cut (0°,22°,90°) helps to estimate the required tolerances for manufacturing substrates and positioning of SAW devices on these substrates. The mechanism of this interaction is analyzed and the ways of reducing sensitivity to misorientation are discussed.

[1] E. Berkenpas, S. Bitla, P. Millard, and M. Pereira da Cunha, IEEE Trans. UFFC-51, 2004, pp.1404-1411.

1K - Abdominal Elastography

Boca Rooms II-IV

Friday, October 21, 2011, 4:30 pm - 6:00 pm

Chair: **Timothy Hall**
Univ. of Wisconsin-Madison

1K-1

4:30 PM Comparison between Acoustic Radiation Force Impulse (ARFI)-based hepatic stiffness quantification in constrained and unconstrained pressurized canine livers

Veronica Rotemberg[1], Mark Palmeri[1,2], Kathryn Nightingale[1]; [1]Biomedical Engineering, Duke University, USA, [2]Anesthesiology, Duke University Medical Center, USA

Background, Motivation and Objective

We have previously reported that Acoustic Radiation Force Impulse (ARFI) based shear wave speed (SWS) estimation can distinguish advanced from moderate hepatic fibrosis noninvasively. Recent studies have suggested that ultrasound-based estimates of liver stiffness increase with hepatic venous pressurization, but the underlying mechanism for this observed stiffening is not understood.

We hypothesize that hepatic stiffening with increased interstitial pressure occurs as a result of a nonlinear material deformation. An experiment was designed to test this hypothesis by comparing SWS estimates from pressurized livers under fixed and free boundary conditions.

Statement of Contribution/Methods

A variable height watertight cylinder was designed with a top acoustic window and water release valves. The liver was submerged under water within the cylinder, the hepatic artery and vein were closed, and the portal vein was connected to the exterior for pressurization. First, liver pressure was increased stepwise from 0-50 mmHg with 6 datasets acquired at each pressurization step while the liver was prevented from expanding. Next, the two valves in the top of the cylinder were opened, and liver internal pressure was again increased stepwise from 0-50mmHg with 6 shear wave datasets acquired at each pressurization state with the liver allowed to expand.

Results

The figure shows initial comparison between SWS in 3 unconstrained (boxes) and constrained (circles) ex-vivo canine liver experiments. Liver stiffness was observed to increase with pressure only in the unconstrained case.

Discussion and Conclusions

These results indicate that the stiffening of liver with increasing pressure requires an underlying tissue deformation. The increase in SWS observed with pressurization in the unconstrained livers to 30 mmHg is similar to that reported in the literature for advanced fibrosis stage. The strain-based nature of this SWS increase supports the hypothesis that this behavior could be described by a nonlinear material model and may provide the basis for distinguishing increases in SWS due to hepatic interstitial pressure from those due to progression of hepatic cirrhosis.

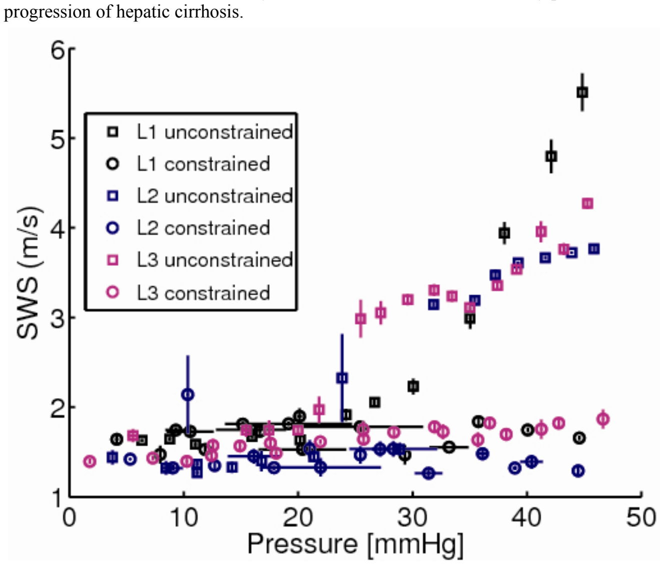

1K-2

4:45 PM Supersonic shear imaging of elastography in obstetrics: quantification of cervix elasticity and uterine contraction.

Jean-Luc Gennisson[1], **Marie Muller**[1], Olivier Ami[2], Valerie Kohl[2], Alexandra Benachi[2], René Frydman[2], Dominique Musset[2], Mickael Tanter[1]; [1]*Institut Langevin- Université Paris Diderot - ESPCI - CNRS, Paris, France*, [2]*Hôpital Antoine Béclère, Université Paris Sud XI, France*

Background, Motivation and Objective

Shear wave elastography based on the Supersonic Shear Imaging method (SSI) is a real-time and quantitative imaging technique that has been proved efficient for tissue elasticity investigation. Very little is known about the physiology of cervix and uterus and SSI could be an efficient tool for a deeper understanding of cervix mechanisms. This could considerably help prevention of premature birth, which consequences on neonate morbidity and pathologies are tremendous. The purpose of this paper is to investigate in vivo the elasticity of the cervix and uterus during pregnancy using SSI with three objectives: the quantification of cervix elasticity, the investigation of uterine anisotropy, and the follow up of uterine elasticity during contraction.

FRIDAY ORAL

Statement of Contribution/Methods

In SSI, radiation force is used to generate shear waves locally within tissue. Shear wave propagation is then followed using an ultrafast ultrasound scanner (5000 frames/s, Aixplorer, Supersonic Imagine, France), and a time-of-flight algorithm is applied to retrieve shear wave displacement, and shear modulus. In this study, remote palpation using radiation force and ultrafast imaging sequences were adapted for the investigation of uterine contraction, as well as for uterine anisotropy estimation. Cervix elasticity was quantified in 30 gravid women using a 7 MHz endocavitary probe (SE 12-3). Uterus elasticity was quantified externally, through the abdomen, using an 8 MHz linear probe (SL 15-4). Changes of elasticity were tracked in real time during uterus contraction. Shear wave tractography (imaging of fibre orientation) was performed with the same probe by assessing shear wave speed variations with respect to probe angle. This allowed the investigation of uterine anisotropy at different depths.

Results

Among all patients, the median Young's modulus value was found to be 8.1 kPa ± 3.1 kPa. Elasticity values were quite homogeneous across the whole cervix. As an example, for one patient, the Young's modulus value was 8.33 kPa ± 1.5 kPa, over a 18 mm diameter region of interest. During contraction, uterus Young's modulus increased by a factor of 10, reaching a plateau (~80 kPa) lasting around 10 seconds. Elasticity values during contraction were correlated to uterine pressure data, which is the gold standard for contraction monitoring. Finally, uterine fibre orientation was observed at different depths.

Discussion and Conclusions

Shear wave elastography allowed the in vivo observation of the consistency of cervix elasticity as well as the monitoring of uterine contraction. This study shows, for the first time, quantitative values of uterine tissue elasticity during contraction, a key parameter in obstetrics. The work presented here could lead to a better understanding of uterine physiology and prevention of prematurity, potentially offering new imaging indicators of threatening signs of pre-term labour.

1K-3

5:00 PM Shear Wave Spectroscopy in liver: initial clinical results and implementation discussion

thomas deffieux[1], Jean-Luc Gennisson[1], Mathieu Couade[1,2], Jeremy Bercoff[2], Laurence Bousquet[3], Simona Cosconea[3], Vincent Mallet[3], Stanislas Pol[3], Mickael Tanter[1]; [1]*Institut Langevin – Ondes et Images, ESPCI ParisTech, CNRS UMR 7587, INSERM U979, France,* [2]*Supersonic Imagine, France,* [3]*Hepatology Unit, Department of Hepato-Gastroenterology, Cochin Hospital, France*

Background, Motivation and Objective

Quantitative elastography is a promising tool for chronic liver diseases diagnosis and staging. By estimating the shear modulus of the liver using shear wave elastography, it is possible to estimate the fibrosis stage and in most cases avoid a liver biopsy. We have recently shown that shear waves could also be used to estimate the full rheological properties of tissue in vivo including viscosity. In this work, we present and discuss the feasibility of the shear wave spectroscopy method in clinical conditions on patients with hepatitis C.

Statement of Contribution/Methods

The shear wave spectroscopy method is applied to a cohort of patients (n>30) diagnosed with hepatitis C with low fibrosis stage (F0-F1) assessed by liver biopsy. Using an ultrafast scanner (Aixplorer, Supersonic Imagine, France) and a 3 MHz curved array (SC 6-1), a quasi plane shear wave is generated inside the liver using acoustic radiation force and is acquired in real time during its propagation. By estimating the phase velocity for each frequency, the dispersion curve is computed and shear modulus and viscosity are estimated assuming the Voigt model. Other approaches including k-space dispersion curve fitting and inversion based on Voigt a priori are also investigated. A method to remove motion artifacts on the acquired data is also presented.

Results

Results show a good reproducibility and the feasibility of the Shear Wave Spectroscopy method in clinical condition (μ_0= 1.6 kPa ± 0.65, η= 1.4 Pa.s ± 0.55). Motion artifacts on the acquisition data due to the presence of veins or respiration movements (up to 10 µm) are successfully removed by the algorithms. As expected, the algorithm taking advantage of the Voigt model a priori performs the best and significantly improves the stability of the viscoelastic measurements in clinical conditions.

Discussion and Conclusions

The quantitative and real time imaging approach provided by the supersonic imaging technique allows inspecting visually and positioning the probe at the best intercostal locations and to provide reliable stiffness estimations over large liver areas. The shear wave spectroscopy can then be used to estimate the liver viscosity, which could be helpful to provide a more complete equivalence to the Metavir scoring system (fibrosis and activity levels) currently only fully assessed by liver biopsies.

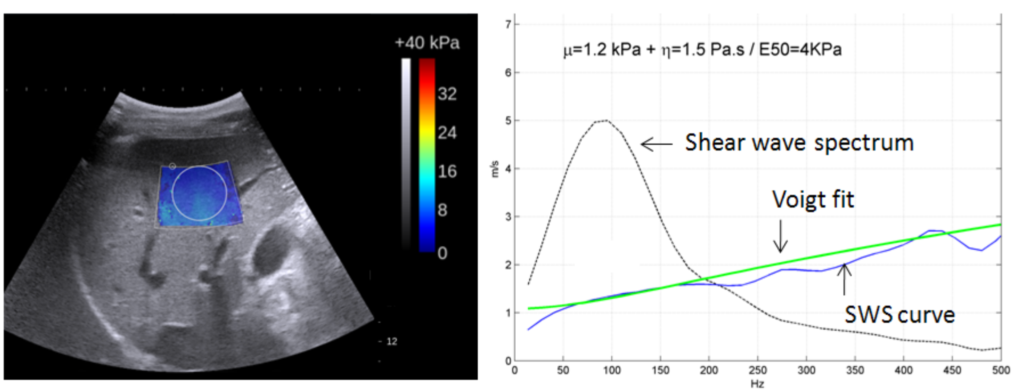

a) A patient liver echography and quantitative stiffness map. b) For each patient, Shear Wave Spectroscopy enables to estimate locally the dispersion curve of the shear wave from 50 to 500 Hz. The shear modulus and viscosity can then be estimated reliably under a Voigt model assumption.

1K-4

5:15 PM Quantitative Assessment of Thermal Lesion Stiffness in the Liver: Initial ex vivo Results

Hua Xie[1], Shiwei Zhou[1], Vijay Shamdasani[2], Yan Shi[1], Jean-Luc Robert[1], John Fraser[2], Shigao Chen[3], James Greenleaf[3]; [1]*Philips Research North America, Briarcliff Manor, New York, USA,* [2]*Philips Healthcare, Bothell, Washington, USA,* [3]*Mayo Clinic College of Medicine, Rochester, Minnesota, USA*

Background, Motivation and Objective

The purpose of this study was to investigate the feasibility of a shear wave-based elastography prototype on Philips' iU22 ultrasound system for measuring liver tissue stiffness before and after RFA (Radio Frequency Ablation) therapy. A special pulse sequence that generates and tracks shear waves was implemented on a curvilinear transducer C5-1, with RF data acquisition and off-line processing. The system was regulated as safe for use in human.

Statement of Contribution/Methods

Two RFA lesions were generated in ex vivo porcine liver by a commercial RF ablation electrode (Rita Medical System). Lesions were created around depth 40 mm beneath the liver surface. The target temperature was set to 90°C and 95°C, and ablation lasted 5 and 6 minutes for two lesions, respectively. Elasticity measurement was made pre-RFA at two sites where lesions were centered. Post RFA, the needle tines were retrieved to prevent interference with the shear wave propagation. To avoid residual bubbles, post-RFA elasticity measurement was performed at an image plane about 1 mm away in elevation from the ablation center plane containing the needle shaft. After the elasticity experiment, the liver was cut open approximately at the imaging plane to confirm the pathological changes caused by RFA. For statistical analysis, shear modulus was estimated and averaged in an 8mm x 4mm area close to the shear wave source.

Results

In the ex vivo study, the shear wave peak displacement at the push focus was about 10 μm pre-RFA. It was significantly reduced to 2 μm post-RFA, signaling the underlying elevated tissue stiffness. Quantitative reconstruction further confirmed the necrosis induced stiffness increase. Pre-RFA, the shear modulus was 1.52 ± 0.13 kPa and 1.02 ± 0.19 kPa for lesion #1 and #2 respectively; post-RFA, the shear modulus was 31.22 ± 10.21 kPa and 27.67 ± 9.52 kPa. An increase of one order of magnitude in shear modulus was observed for both lesions. Similar stiffness contrast also existed between the ablated and neighboring non-treated region post-RFA for both lesions.

Discussion and Conclusions

These early results demonstrate the feasibility of the prototype for quantifying elasticity of thermal lesions in liver. Further technical development such as imaging capability and automated analysis tools are required to enable the visualization of the ablation zone and assessment of the therapy procedure. (Mayo Clinic and Drs. S. Chen and J. Greenleaf have a financial interest in the technology used in this research. That technology has been licensed to Philips Electronics for research purposes, and Mayo Clinic has received royalties greater than the federal threshold for significant financial interest. To date, Drs. Chen and Greenleaf have received no royalties.)

1K-5

5:30 PM *In vivo* assessment of renal tissue viscoelasticity during acute and gradual renal ischemia

Carolina Amador[1], Matthew Urban[1], Shigao Chen[1], James Greenleaf[1]; [1]Department of Physiology and Biomedical Engineering, Mayo Clinic College of Medicine, Rochester, MN, USA

Background, Motivation and Objective

Fundamental material properties of soft tissues are closely related to the state of health of the tissue and can be used as an indicator for medical diagnosis. Although the motivation for developing elasticity imaging techniques relies on the possibility of diagnosing disease process, it is important to study the mechanical properties of healthy tissues under different physiological conditions. For instance, recent studies have observed contribution of augmented hemodynamic factors to tissue stiffness [Investigative Radiology, 2011]. The purpose of this study is to evaluate the effect of acute and gradual ischemia on renal tissue viscoelasticity.

Statement of Contribution/Methods

The right kidney of an anesthetized pig was surgically exposed. A pneumatic vascular occluder was placed on the right renal artery distal to the renal artery bifurcation. An ultrasonic flow meter was placed on the renal artery for continuous monitoring of the renal blood flow (RBF). Shearwave Dispersion Ultrasound Vibrometry (SDUV) measurements were made using a Verasonics V-1 system. A C4-2 curved array transducer was placed in contact with the exposed kidney surface. The push toneburst was 400 μs at a frequency of 2.5 MHz. The detection was performed at 2000 frames/s. Shear wave speeds were measured consequent to RBF reduction by 0, 25, 50, 75 and 100% of baseline. The dispersion of the shear wave speed was fit using a Voigt model to estimate shear elasticity and viscosity.

Results

For each RBF reduction, shear wave speeds were analyzed in two regions of interest within the renal cortex and the mean and standard deviation of shear elasticity (μ_1) and viscosity (μ_2) as shown in Fig. 1. The shear elasticity and viscosity were 6.5 kPa and 1.7 Pa·s at baseline, and 4 kPa and 2.7 Pa·s at 100% RBF reduction.

Discussion and Conclusions

These measurements agree with previous experiment results using a mechanical actuator to generate shear waves instead of radiation force [IUS, 2010]. Although elasticity remained rather constant while RBF was decreased from 25% to 100% reduction, probably due to an increase in vascular resistance as a response to hypoperfusion, renal viscosity increased as RBF was decreasing. Thus, viscosity may be a useful and sensitive variable to tissue damage such as ischemia. However, future studies are needed to test this hypothesis.

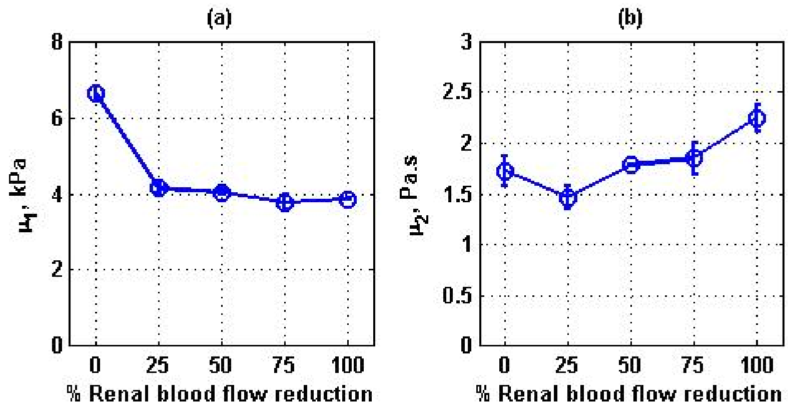

Fig. 1. (a) Variation of shear elasticity (μ_1) with RBF reduction, (b) Variation of viscosity (μ_2) with RBF reduction.

1K-6

5:45 PM Clinical Multi-Push (MP) ARF for Noninvasive, In Vivo Evaluation of Renal Transplant Status

Mallory R. Scola[1], **Leslie M. Baggesen[1]**, Randy K. Detwiler[2], Wui K. Chong[3], So Yoon Jang[2], Lauren M. B. Burke[3], Kristel L. Jernigan[2], Melissa C. Caughey[2], Melrose W. Fisher[2], Sonya B. Whitehead[3], Caterina M. Gallippi[1]; *[1]Joint Department of Biomedical Engineering, The University of North Carolina at Chapel Hill, Chapel Hill, NC, USA, [2]Department of Medicine, The University of North Carolina at Chapel Hill, Chapel Hill, NC, USA, [3]Department of Radiology, The University of North Carolina at Chapel Hill, Chapel Hill, NC, USA*

Background, Motivation and Objective

Invasive biopsy is currently the gold standard for assessment of renal transplant health. The need for biopsy may be reduced as suitable, noninvasive imaging methods become available. An imaging technique that exploits the viscoelastic properties of renal tissue could be relevant as a biopsy alternative, given that normal renal pelvis and cortex have different viscoelastic properties, while renal disease or rejection may result in similar properties between pelvis and cortex. We hypothesize that MP ARF, which qualitatively evaluates the viscoelastic properties of tissue, is relevant for noninvasively assessing viscoelastic similarity between pelvis and cortex in renal transplant patients.

Statement of Contribution/Methods

MP ARF was performed using a Siemens SONOLINE Antares™ imaging system equipped for research purposes and a VF7-3 transducer (Siemens Medical Solutions USA, Inc. Ultrasound Division). Imaging was performed in vivo on the transplanted kidneys of 25 non-biopsied transplant recipients and 19 biopsy patients (9 confirmed rejection). Two 70 µs ARF excitation impulses were administered 2 ms apart in a single region of excitation, with induced motion tracking. Physiological motion was rejected and marginal peak displacement (MPD) was calculated using MPD = 1 - [(P1 - (P2-D)) / P1], where P1 and P2 are peak displacements from the first and second pushes and D is the displacement just before the second push. Regional comparisons of MPD values were made within and between five patient categories: a primary diagnostic group (encompassing acute rejection, chronic allograft nephropathy (CAN), glomerular nephritis, and interstitial nephritis/BK virus diagnoses), vascular disease, tubular/interstitial scarring, and non-biopsied transplant patients.

Results

MPD values measured at the outer edge of the renal pelvis were significantly different ($p < 0.02$, paired t-test) from the MPD values measured throughout the cortex in patients not undergoing biopsy and in those with acute rejection (Table).

Discussion and Conclusions

No significant differences were seen between renal cortex and pelvis in patients diagnosed with CAN, glomerular nephritis, or interstitial nephritis/BK virus. This suggests that MP ARF could be a relevant clinical technique for noninvasively discriminating between diseased, rejected, and healthy renal transplants.

	Cortex Outer Edge	Cortex Center	Cortex Inner Edge
Acute Rejection			
Cortex Outer Edge	1	0.5793	0.0619
Cortex Center	0.5793	1	0.0493
Cortex Inner Edge	0.0619	0.0493	1
Pelvis Edge	**0.0053**	0.0696	**0.0115**
Not Biopsied			
Cortex Outer Edge	1	0.4033	0.1082
Cortex Center	0.4033	1	0.3277
Cortex Inner Edge	0.1082	0.3277	1
Pelvis Edge	**0.0025**	**0.014**	**0.0096**

Table: Regional P-Values in the Primary Diagnostic Group

2K - Vascular Imaging

Boca Rooms VI-VII

Friday, October 21, 2011, 4:30 pm - 6:00 pm

Chair: **Anne Hall**
GE medical systems

2K-1

4:30 PM Intravascular Ultrasound Chirp Imaging of atherosclerotic plaque pathology and neovascularization

David Maresca[1], Krista Jansen[1], Guillaume Renaud[1], Wijnand den Dekker[2], Gijs van Soest[1], Xiang Li[3], Qifa Zhou[3], Jonathan Cannata[3], Antonius F.W. van der Steen[1,4]; [1]*Biomedical Engineering, Thorax Centre, Erasmus MC, Rotterdam, Netherlands,* [2]*Experimental Cardiology, Erasmus MC, Rotterdam, Netherlands,* [3]*Resource Center for Medical Ultrasonic Transducer Technology, University of Southern California, Los Angeles, USA,* [4]*Interuniversity Cardiology Institute of the Netherlands, Netherlands*

Background, Motivation and Objective

The detection and identification of vulnerable atherosclerotic plaques, susceptible to rupture and therefore candidates for intervention, remains a central issue in cardiac imaging. Neovascularization within and surrounding plaques is essential to enable lesion growth and plays a central role in rendering it vulnerable to rupture. We investigated how chirp coded excitation could extend intravascular ultrasound (IVUS) imaging depth in order to characterize deeper coronary atherosclerosis and neovascularization.

Statement of Contribution/Methods

A 53 MHz IVUS transducer (-6dB bandwidth 55%, natural focus 3.1mm) was driven with 0.5µs chirp excitations (39-67MHz) or 53MHz full band Gaussian pulses of equal peak negative amplitude. A TPX hollow cylinder containing 4 sub wavelength targets (15µm thick platinum/iridium wires) at 1.5, 3, 5 and 7 mm from the cylinder axis allowed to measure the axial resolution and the signal to noise ratio (SNR). The cylinder was immersed in water and imaged with 360 radio frequency (RF) lines per rotation. Both excitations were subsequently fired at each angular position. The RF data was band pass filtered, the envelope was derived, log compressed and scan converted with a 40dB dynamic range. The chirp compression filter consisted of the Chebyshev tapered chirp excitation. The same protocol was repeated on ex-vivo atherosclerotic rabbit aortas at clinical IVUS frequencies (24 to 44MHz) with another IVUS transducer and no averaging.

Results

We measured from the closest to the farthest wire a gain in SNR of 8.7, 9.0, 9.1 and 9.9dB with the chirp coded excitation. The axial resolutions (-6dB point spread function) were 68, 68, 70 and 68µm for the Gaussian pulse and 97, 92, 93 and 101µm for the chirp excitation after compression. The ex-vivo rabbit aorta results showed a significant gain in SNR and a slight deterioration of the resolution (see figure).

Discussion and Conclusions

We demonstrated that chirp coded excitations of limited temporal lengths can be successfully used for IVUS imaging. We observed a gain in SNR of 10dB at a distance of 7 mm while maintaining a satisfactory axial resolution. These findings were confirmed at conventional IVUS frequencies on the ex-vivo rabbit aortas. Different compression filters will be investigated to reduce compression sidelobe levels and account for frequency dependent attenuation.

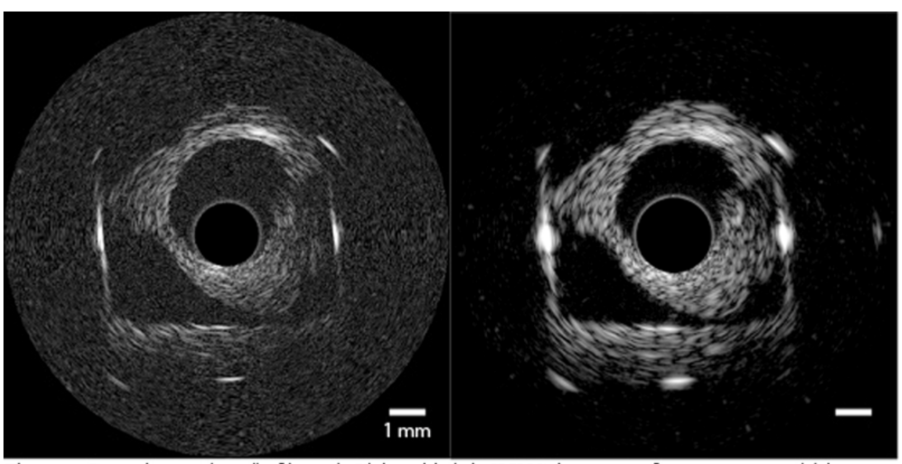

Figure: Gaussian pulse (left) and Chirp (right) IVUS images of an *ex-vivo* rabbit aorta (dynamic range 40dB). The square structure holding the vessel appears around the artery cross section.

FRIDAY ORAL

2K-2

4:45 PM A Hybrid Intravascular Ultrasound and Optical Coherence Tomography Catheter for the Imaging of Coronary Artery Disease

Brian Li[1], **Amandeep Thind**[2], Annie Leung[1], Alan Soong[3,4], Chelsea Munding[5], Hyunggyun Lee[6], Nigel Munce[7], Bradley Strauss[8], F. Stuart Foster[1,6], Brian Courtney[4,6]; [1]*University of Toronto, Canada,* [2]*Colibri Technologies, Toronto, ON, Canada,* [3]*Sunnybrook Research Institute, Toronto, Canada,* [4]*Colibri Technologies Inc, Canada,* [5]*University of Toronto, Toronto, Canada,* [6]*Sunnybrook Research Institute, Toronto, ON, Canada,* [7]*University of Toronto, Toronto, ON, Canada,* [8]*Sunnybrook Health Sciences Centre, Toronto, ON, Canada*

Background, Motivation and Objective

IVUS provides information about plaque and lumen area and can assist with stent sizing and apposition. Aside from detecting calcium, IVUS has limited ability to identify tissue composition. OCT has better resolution and tissue contrast than IVUS, enabling it to identify plaque features. However, OCT has limited tissue and blood penetration. The objective of this study was to develop and test an imaging catheter capable of simultaneously generating co-planar IVUS and OCT images to further assess the potential synergies of these two modalities.

Statement of Contribution/Methods

A custom hybrid IVUS-OCT imaging catheter using a 42MHz ultrasound transducer and an OCT imaging fiber was housed in a 4F sheath (Fig 1). Co-planar images were acquired with both modalities in an ex-vivo setting in 31 segments from 11 human coronary artery samples. Images were acquired at 0.25mm intervals. N=13 segments were selected based on the appearance of IVUS and OCT images as representative of a diverse set of pathological findings. The selected segments were further imaged with X-ray or micro-CT, processed for histological analysis and compared with the corresponding IVUS and OCT images (Fig 2).

Results

Images of coronary disease using hybrid IVUS and OCT demonstrated a range of vascular pathology including intimal thickening, fibrous plaques, fibroatheroma, fibrocalcific plaques, complex plaques. The advantages of each modality was apparent from a qualitative perspective, including the deeper tissue penetration of IVUS and superior contrast, resolution and near-field quality of OCT.

Discussion and Conclusions

A hybrid IVUS / OCT system has been built at a scale suitable for use in human coronary arteries. Such a system may overcome many of the limitations of either system individually by providing complementary information.

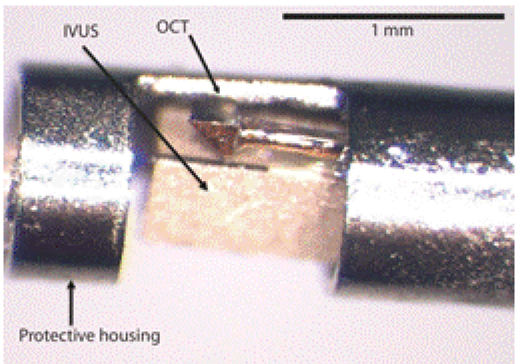

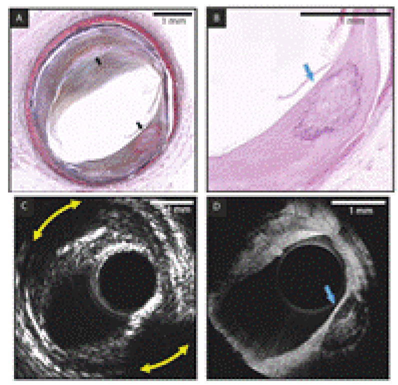

2K-3

5:00 PM Hybrid Method For Restoring the Fidelity of Ultrasound Images of Vessels

Thomas Szabo[1], Caroline Smith[2], Betty Chan[2], Brian Harvey[2]; [1]Biomedical Engineering, Boston University, Boston, MA, USA, [2]Boston University, USA

Background, Motivation and Objective

Distortions in ultrasound images of vessels can be significant even though these effects are negligible at larger scale imaging. System and propagation effects operate on a scale comparable to the dimensions of thin walls and features in longitudinal views. As a result, diagnostic inferences based on observed geometric features in the image such as lumen diameter and wall thickness may be in error. Also, these distortions can vary from imaging system to system as well as the settings and spatial locations within the same system.

Statement of Contribution/Methods

A hybrid approach combines measurements with wave models to reduce system and propagation effects on the image. First, a simulation model was developed that accounted for the effects of reflections, reverberations, absorption, and causal phase velocity dispersion, as well as system transmit characteristics. Second, a sequence of measurement and modeling steps was used to extract data for correction and inverse filtering.

Results

The methodology was tested on a disk-shaped tissue mimicking phantom material and verified by independent physical measurements. Raw RF beamformed data was captured from a Terason 3000 ultrasound imaging system connected to a 5-12 MHz linear array. The thickness obtained from outer surface to outer surface (as is usually done in edge detection algorithms for vessel walls) from RF data gave a value of 1 .00 cm or 5% error compared to the corrected result of 0.987 cm, an error of 0.7%. Half-amplitude pulses lengths from the top and bottom surfaces, originally 0.106 and 0.130 cm, were reduced by 32 and 46% to 0.072 and 0.070 cm, respectively, after correction. Data from a more relevant thinner sample, 0.5mm thick, provided an uncorrected value of 0.37 mm (26% error) and a corrected value of 0.493 mm (1.6% error). A bovine bronchial airway, mounted in a tank filled with Krebs solution and subjected to doses of acetylcholine to simulate asthma like reactions, was observed to appear to close down at higher doses. Early results showed that corrected images indicate the inner diameter was still open.

Discussion and Conclusions

A combination of correcting for propagation effects and inverse filtering has resulted in higher resolution images that are significantly more accurate representations of vessels and has the capability to provide ultrasound measured tissue parameters of absorption and sound speed for the vessel walls.

2K-4

5:15 PM Quantitative analysis of flow behavior of carotid plaque neovasculature

Assaf Hoogi[1], Hans Bosch[2], Antonius.F.W Van der steen[2], Dan Adam[1]; [1]Biomedical engineering, Technion, Israel, [2]Biomedical engineering, Thorax center, ErasmusMC, Netherlands

Background, Motivation and Objective

Vulnerable plaques in the carotid artery have high probability to rupture and cause cardiovascular events as stroke and TIA. Intra plaque inflammation and neovascularization are considered as indications for plaque vulnerability. Thus, analysis of neovasculature flow and reconstruction of the intra-plaque arterial tree enable risk evaluation of plaque vulnerability.

Statement of Contribution/Methods

Clinical examinations of carotid plaques were performed using contrast enhanced ultrasound on a Philips iU22. An algorithm based on Multidimensional Dynamic Programming was developed to track slow moving contrast particles within the plaque, and to map the intra-plaque neovascularization. It took into account correlation values and XY displacement of the examined objects between sequential frames (i.e. during the time). Differentiation between in-plane vessels' flow, out-of-plane oriented flow and saturation artifacts was performed, based on their motion and temporal intensity pattern characteristics. Algorithm validation was done by visual analysis. Parameters as length of a path, its direction and the contrast particle velocity were calculated.

Results

20 different contrast objects were examined in 6 plaques (plaque and objects are presented in fig. 1a). In 17, in-plane, out-of-plane vessels and saturation artifacts were successfully distinguished. Average gray level of saturation artifacts, as its SD values, were significantly higher during the time than the equivalent values of contrast particles. XY path length of in-plane vessels was 3.7± 1.08 mm while the path length of out-of-plane vessels or saturation artifacts was only 0.62 ± 0.11 mm. Thus, saturation artifacts (group1, fig. 1b), out-of-plane vessels (group2, fig. 1b) and in-plane vessels (group3, fig. 1b) could be distinguished. Flow velocity of contrast particles within in-plane vessels was 3.25 ± 0.82 mm/s, its direction during the time was 62.37 ± 5.59 degrees.

Discussion and Conclusions

The proposed method allows 2D reconstruction of intra-plaque neovascularization and can distinguish between different vessel orientations and artifacts, potentially serving as features of vulnerability of the carotid plaque. The method is applied to 150 patients in the CTMM-ParisK trial in which the value of these parameters as an indicator for risk of stroke will be assessed.

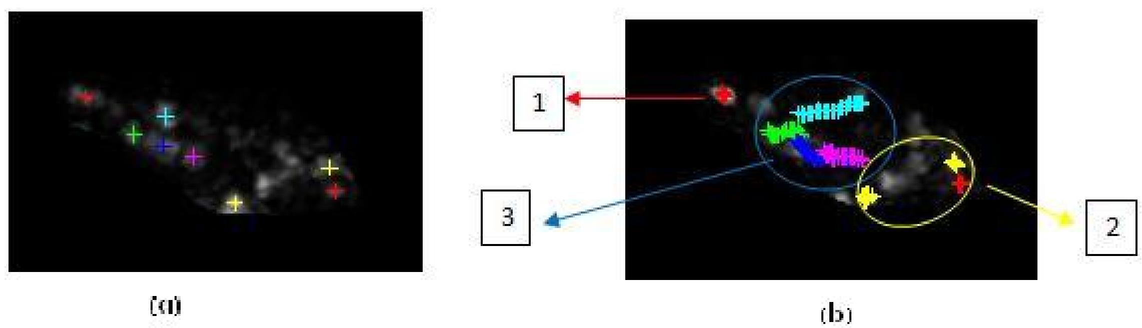

Figure 1: (a) Carotid plaque and some chosen objects which were suspected as neovasculature
(b) Track after those objects and divide them to artifacts (marked as 1), out-of-plane blood vessels (marked as 2), and in-plane vessels (marked as 3).

2K-5

5:30 PM Pulse Wave Ultrasound Manometry (PWUM): Measuring central blood pressure non-invasively

Jonathan Vappou[1,2], Jianwen Luo[1], Kazue Okajima[3], Marco Di Tullio[3], Elisa Konofagou[1]; [1]Department of Biomedical Engineering, Ultrasound and Elasticity Imaging Laboratory, Columbia University, New York, NY, USA, [2]Currently at: LSIIT - UMR 7005 CNRS-Strasbourg University, France, [3]Department of Medicine, Columbia University, USA

Background, Motivation and Objective

As it has been widely established using invasive methodologies, central blood pressure (CBP) has a strong clinical relevance. Despite its significance, CBP is particularly challenging to measure in standard clinical practice. Pulse Wave-based Ultrasound Manometry (PWUM) is a simple-to-use, non-invasive ultrasound-based method that combines Pulse Wave Imaging (PWI) and vessel diameter measurements for quantitative and regional measurement of the central pulse pressure. The objective of this study is to assess the feasibility of the proposed method in human and to compare PWUM to noninvasive arterial tonometry.

Statement of Contribution/Methods

Arterial wall displacements were estimated using radiofrequency ultrasound signals at high frame rates using a Sonix Touch (Ultrasonix) system at 3.3 MHz. This allowed for (1) the estimation of the Young's modulus of the arterial wall, based on the measurement of the Pulse Wave Velocity, and (2) the estimation of the vessel distension waveform over the cardiac cycle. These two measurements allowed for the computation of the pressure waveform under assumption of linear elasticity. The PWUM method was tested on the abdominal aorta of 11 healthy subjects (age 35.7± 16). PWUM pulse pressure measurements were compared to those obtained by radial applanation tonometry that estimates the CBP based on peripheral radial pressure measurements.

Results

The average intra-subject variability of the pulse pressure amplitude was found to 4.2 mmHg, demonstrating good reproducibility of the method. Excellent correlation was found between the waveforms obtained by PWUM and by tonometry in all subjects ($0.94 < r < 0.98$). Fig. 1 illustrates an example of results obtained in one subject. An average, significant bias of 4.7 mmHg was found between PWUM and tonometry regarding pulse pressure amplitude.

Discussion and Conclusions

The feasibility of the PWUM method was demonstrated in this study. PWUM is a noninvasive ultrasound-based method that provides a direct measurement of the pulse pressure waveform at the imaged location. This can represent an important alternative to current, clinically used methods that are either invasive (catheterization) or based on empirical transfer functions between peripheral and central pressures. Future developments include the validation of the method against invasive estimates and application to other central arteries.

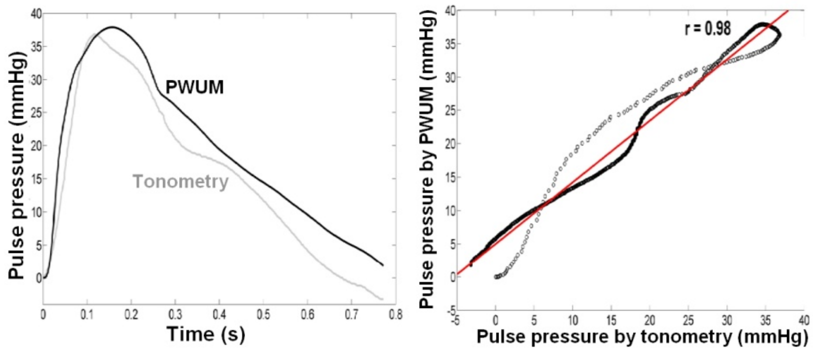

2K-6

5:45 PM A method for measuring the variation of intima-media thickness during the entire cardiac cycle using B-Mode images

Tobias Nilsson[1], Åsa Rydén Ahlgren[2], Tomas Jansson[1], Hans W Persson[1], Kjell Lindström[1], Jan Nilsson[2], Magnus Cinthio[1]; [1]*Faculty of Engineering, LTH, Lund University, Sweden,* [2]*Lund University, Sweden*

Background, Motivation and Objective

The intima-media thickness (IMT) of the arterial wall has been extensively studied and proved to be a biomarker for cardiovascular disease. However, the variation of IMT during a cardiac cycle had gained less attention. In this study we evaluated a new method for measuring IMT and intima-media compression (IMC), defined as the maximum difference in thickness during a cardiac cycle, using B-Mode images. The method compensates for both angle variations and longitudinal movement and uses information from previous frame.

Statement of Contribution/Methods

The maximum intensity of the intima and adventitia echoes was located for each line in an 8 mm region of the common carotid artery. In the first frame (end-diastole) the IMT was defined as the mean distance between the located intima and adventitia positions. The IMT was angle-corrected relative the orientation of the arterial wall in the image. Sub-pixel accuracy was achieved by solving the equation of a straight line at the zero-crossings in the differentiated data. In subsequent frames also the longitudinal movement, of both the intima and the adventitia echoes, was measured. The located intima and adventitia positions in one frame were coupled with the positions in the following frame at the lines corresponding to the measured longitudinal movement of each layer. Finally the difference in IMT between frames was defined as the mean difference in thickness between coupled positions. The method was evaluated in vivo on 20 healthy volunteers (mean age 38 years, 25-57) using the coefficient of variability (CV). Scans were acquired using a HDI 5000 (Philips Medical Systems) with a resulting spatial resolution of 50-75µm.

Results

The figure shows the variation of IMT during four cardiac cycles of a healthy 49 year-old man. Note that the total compression is in the range of the distance between two samples. The IMT in diastole (IMT_{dia}) was 717±69µm and the IMC was 66±21µm corresponding to a 9.2±2.6% compression. The CV was 3.5% for IMT_{dia} and 9.9% for IMC.

Discussion and Conclusions

The new method can efficiently measure both IMT and IMC during several cardiac cycles. Compared to existing methodologies the accuracy was improved by compensating for both angle variations and longitudinal movement and by using information from previous frame. As a result compressions corresponding to less than one pixel could be resolved.

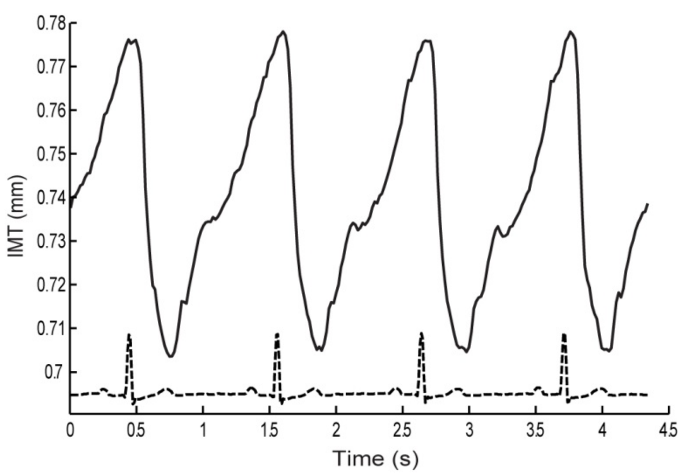

3K - Functional Imaging & Image Quality

Carribean Ballroom VII

Friday, October 21, 2011, 4:30 pm - 6:00 pm

Chair: **Mickael Tanter**
INSERM, Paris

3K-1

4:30 PM Spatiotemporal dynamics of epileptic seizures followed by ultrasensitive functional ultrasound imaging

Emilie Mace[1], Gabriel Montaldo[1], Ivan Cohen[2], Michel Baulac[2], Mathias Fink[1], Mickael Tanter[1]; [1]*Institut Langevin, ESPCI ParisTech, CNRS UMR7587, Inserm U979, Paris, France,* [2]*Institut du Cerveau et de la Moelle épinière, Inserm UMRS 975, CNRS UMR7225, CHU Pitié Salpêtrière, Paris, France*

Background, Motivation and Objective

Imaging transient cerebral activity remains a challenge using fMRI because its poor signal to noise ratio requires significant averaging. For that reason, little is known on the localization of onset and propagation of epileptic seizures in particular in deep structures not accessible to optical imaging. We investigated the potential of ultrasensitive functional ultrasound imaging (ufUS) to image such events on rat models.

Statement of Contribution/Methods

Two rat models of epilepsy were studied: an acute model by cortical injection of a channel blocker (4AP, 15 nmol) and a genetic model of absence seizures (WAG/Rij). Animals were anesthetized with isoflurane and a large cranial window was opened. Cortical electrodes were implanted in the imaging plane of a 15 MHz linear ultrasonic probe controlled by an ultrafast scanner. Functional imaging was performed during 2 h by acquiring every 3s an ultrasensitive Power Doppler image (computed from 200 compound images, 17 tilted plane wave emissions each). EEG and trigs of ultrasonic events were simultaneously recorded for identifying epileptic seizures.

Results

We successfully imaged the increase in blood supply induced by epileptic seizures for both models. An example is given in (a) of the onset of a seizure and in (b) of a later propagation to the thalamus in the case of the acute model. The increase in Power Doppler, up to 50% compared to baseline for both models, was proved to be highly correlated with epileptic neuronal activity (r^2=0.87 with EEG envelop) (c). From the 3D Power Doppler data I(x,z,t), we separated distinct seizing patterns matching well-defined brain structures (cortex, thalamus, hippocampus) using a principal component analysis and measured the velocity of epileptic activity spreading within these structures (3 to 7 mm/min) using a time-of-flight algorithm.

Discussion and Conclusions

For the first time, the transient dynamics of generalized epileptic seizures was imaged in “real time” and in depth using ufUS. No actual functional imaging technique can reach the same sensitivity, penetration and spatiotemporal resolution. Therefore, ufUS imaging provides new information for identifying epileptic foci and pathways in vivo on animal models of human pathologies mainly studied for now by electrode implantation. In clinics, ufUS is also foreseen to be applied directly on epileptic patients during neurosurgical procedures.

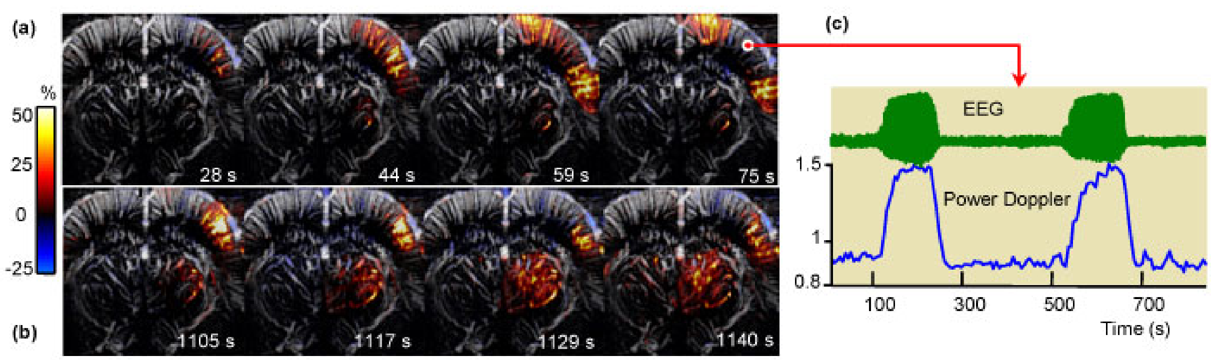

Figure. (a) and (b) Relative changes of Power Doppler superimposed on a control image at different times after seizure induction by 4AP injection. (c) Comparison between electrical activity (green) and Power Doppler signal (blue) at the same cortical location

FRIDAY ORAL

3K-2

4:45 PM In-vivo pulsed magneto-motive ultrasound imaging of tumor bearing small animals

Mohammad Mehrmohammadi[1], Seungsoo Kim[1], Min Qu[1], Ryan Truby[1], Pieter Kruizinga[2], Stanislav Emelianov[1]; [1]Biomedical Engineering, University of Texas at Austin, Austin, TX, USA, [2]Thoraxcenter, Biomedical Engineering, Erasmus MC, Rotterdam, Netherlands

Background, Motivation and Objective

Pulsed magneto-motive ultrasound (pMMUS) imaging has been introduced as a novel ultrasound-based cellular/molecular imaging modality. In pulsed magneto-motive ultrasound imaging a high intensity pulsed magnetic field is used to excite the cells labeled with magnetic nanoparticles and ultrasound imaging is then used to monitor the mechanical response of the tissue (i.e. tissue displacement). Here, we investigated the feasibility of pMMUS imaging to identify the presence and distribution of magnetic nanoparticles within a tumor-bearing animal injected with superparamagnetic iron-oxide nanoparticles.

Statement of Contribution/Methods

Superparamagnetic magnetite nanoparticles were used as pMMUS contrast agents. The nanoparticles were synthesized by the thermal decomposition of iron (iii) acetylacetonate in triethylene glycol without a surfactant. By replacing the polyol surface layer with citrate, the magnetite nanoparticles were dispersed in aqueous solutions. Epidermoid carcinoma A431 cells were injected into 10 weeks old Nu-Nu mice for tumor inoculation. When the tumor size reached about 1 cm in diameter, the contrast agents were injected directly into tumor or intravenously. The animal was kept close to a permanent magnet (~ 0.5 T) for 2 hours after the injection to increase the uptake of nanoparticles by tumor cells. The ultrasound and pMMUS imaging were performed using a high frequency array transducer (20 MHz central frequency) and Vevo2100 small animal ultrasound imaging system. The magnetic pulses of 0.8 T were generated using a high power current amplifier connected to a relatively large coil. Both ultrasound (US) and power Doppler (PD) signals were acquired before, during and after application of a 40 msec long magnetic pulse.

Results

Figure 1 represents the US and PD images of a selected cross-section within the tumor region 24 hours after intra-tumor injecting the magnetic contrast agents. The PD signal clearly indicates the induced displacement within the tumor region that corresponds to the presence of magnetic nanoparticles.

Discussion and Conclusions

In summary, we have demonstrated the capability of pMMUS imaging to detect the presence of magnetic nanoparticles in-vivo. Once developed, pMMUS imaging can provide such information in real time, non-invasively and at reasonable imaging depths and therefore can be used to monitor events at the cellular level.

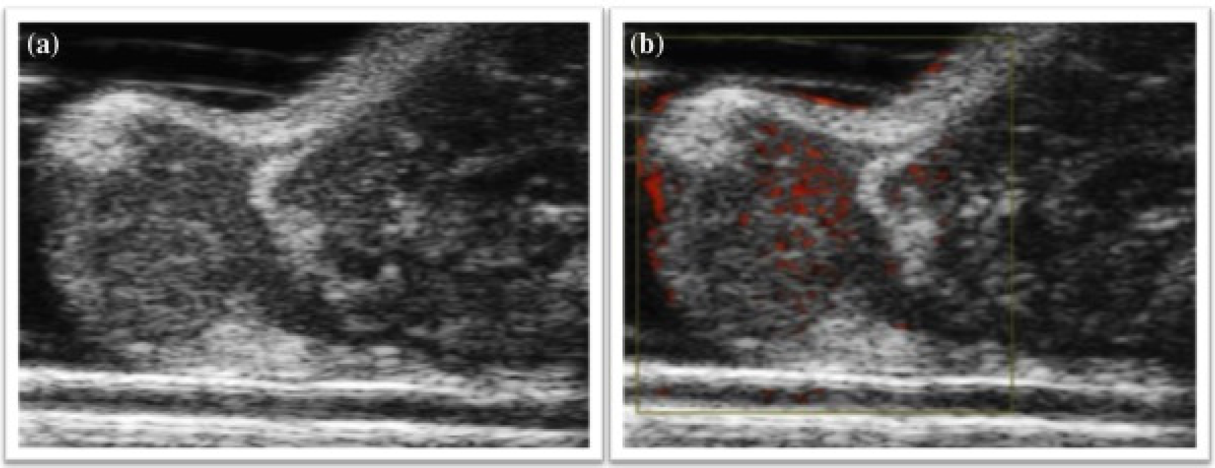

3K-3

5:00 PM Reduction of Reverberation Artifacts with Superharmonic Imaging

Mikhail G. Danilouchkine[1,2], Frits Mastik[1], Robert Beurskens[1], Paul L.M.J. van Neer[1], Guillaume M. Matte[1], Wim Vletter[3], Christian Prins[4], Folkert J. ten Cate[3], Johan G. Bosch[1], Antonius F.W. van der Steen[1,2], **Nico de Jong[1,2]**; *[1]Biomedical Engineering, Erasmus Medical Center, Netherlands, [2]The Interuniversity Cardiology Institute of the Netherlands, Netherlands, [3]Cardiology, Erasmus Medical Center, Netherlands, [4]Oldelft BV, Netherlands*

Background, Motivation and Objective

Echocardiographic assessment of cardiac function appears to be problematic in 15-20% patients because of a poor acoustic window. The suboptimal image quality is mainly caused by artifacts, stemming from reverberations between the transducer and ribs. Those artifacts are significantly reduced with tissue harmonic imaging (THI), which is based on the selective imaging of the 2nd harmonic component. Rcently our group postulated and theoretically proved that the further improvement in image quality can be achieved with superharmonic imaging (SHI). The new method selectively images 3 spectral bands starting from the 3rd harmonic. In this study we perform a qualitative comparison of the THI and SHI modalities on in-vivo cardiac images and quantify suppression of reverberation artifacts with SHI.

Statement of Contribution/Methods

Five healthy volunteers between 25-32y.o. without prior history of cardiovascular disease underwent a clinical examination on commercial (iE33, Philips, NL) and experimental scanners. The latter consisted of a dedicated SHI dual frequency probe (Oldelft, NL) and a programmable ultrasound system (LeCoeur Electronique, FR). The cardiac acquisitions were made in the parasternal long-axis and apical 4-chamber projections. The best imaging mode was selected on the commercial system (either 1.4-2.8 or 2.1-4.2 MHz), while for the experimental one the transmitted and receiving frequencies were 1 MHz and between 3-5 MHz, respectively. All images were acquired by an experienced sonographer.

Results

All volunteers had comparable image quality in the parasternal view on both scanners. The THI images of 2 volunteers in the apical 4-chamer view demonstrated suboptimal visualization of the septal wall in the apical and midventricular segments (Fig A). The use of SHI resulted in a clear improvement in cardiac definition through a significant reduction of the reverberation artifacts (Fig B).

The intensity difference between the ventricular septum and left ventricular blood pool was estimated to quantify the artifact reduction and amounted to 4.8 dB and 18.7 dB for THI and SHI, respectively.

Discussion and Conclusions

An artifact reduction is about 14 dB for patient with a poor acoustic window. The results convincingly demonstrate, that the image quality improvement with SHI as compared to THI, and facilitate use of SHI for cardiac function assessment.

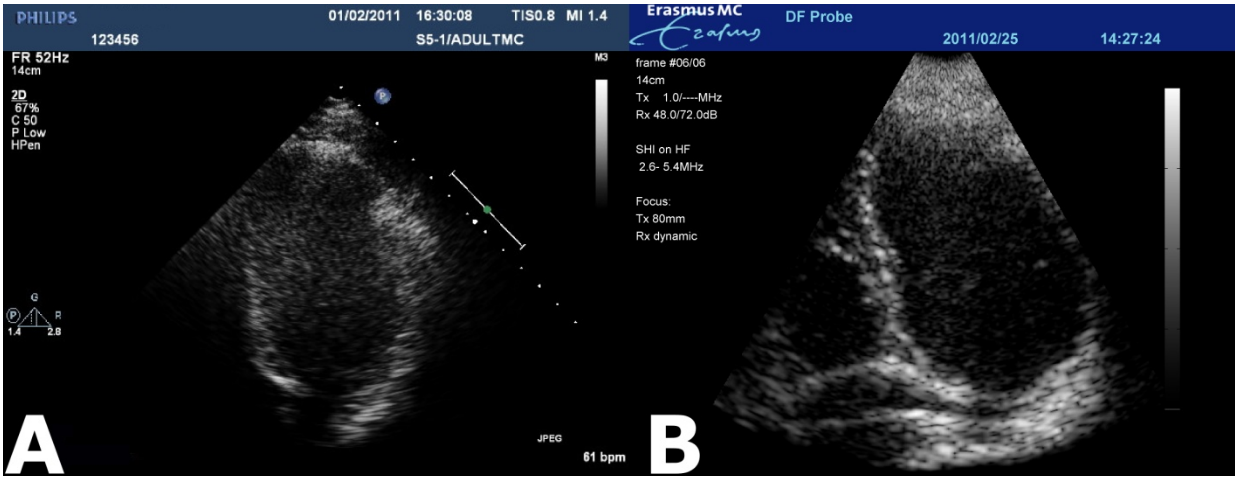

3K-4

5:15 PM *In Vivo* Application of SLSC Imaging in Human Liver

Marko Jakovljevic[1], Gregg Trahey[1], Jeremy Dahl[1]; [1]Biomedical Engineering, Duke University, Durham, North Carolina, USA

Background, Motivation and Objective

We have developed a novel beamforming technique called short-lag-spatial-coherence (SLSC) imaging that is based purely on the spatial coherence of backscattered echoes. We evaluate the effectiveness of SLSC imaging in reducing clutter by comparing the matched SLSC and B-mode images of *in vivo* human liver.

Statement of Contribution/Methods

At the heart of SLSC imaging is the spatial coherence function which is evaluated from the individual-channel data. We collected individual-channel data *in vivo* on the liver vasculature, common bile duct, and other hepatic structures of interest in ten human subjects using a conventional ultrasound scanner and a custom synthetic aperture sequence. Matched B-mode and SLSC images were then formed and the contrast and contrast-to-noise ratio (CNR) of the structures were calculated for each image to assess relative image quality.

Results

Contrast and CNR values vary with the level of clutter present in each patient. For B-mode contrast and CNR range from 0.2 to 0.5 and from 0.52 to 2.93 respectively. For SLSC images contrast and CNR range from 0.44 to 0.92 and from 1.04 to 6.47 respectively. Quality metrics of matched B-mode and SLSC images show that SLSC brings significant improvement in target detection for high and medium image quality and moderate improvement for low quality images. A sample pair of matched B-mode and SLSC images is shown in the figure below. In the SLSC image, a structure in the center of the FOV was visualized and identified as the common bile duct by an experienced sonographer; this structure is not visible in the B-mode image. Contrast and CNR values of the bile duct were found to be 0.47 and 3.2 respectively for B-mode and 0.8 and 6.18, respectively, for the SLSC image.

Discussion and Conclusions

SLSC improves target visibility in the presence of acoustical clutter by suppressing incoherent components of the signal. SLSC images show better visualization of liver vasculature in the presence of clutter while in some cases they indicate the presence of the structures not visible in the B-mode images. We discuss the potential applications, limitations, and trade-offs of SLSC imaging.

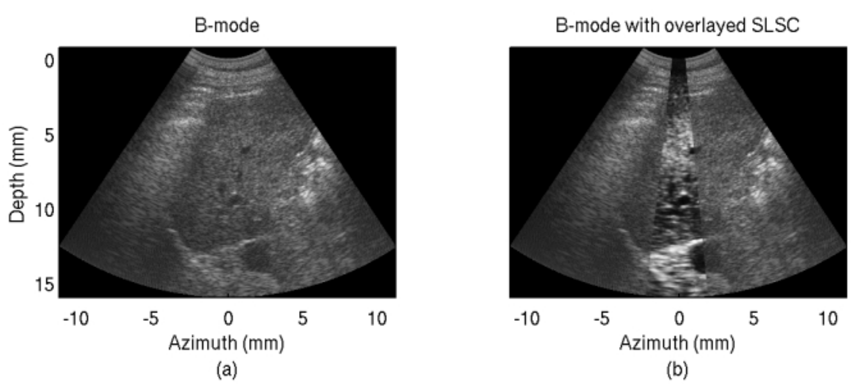

3K-5

5:30 PM Dual sided automated ultrasound system in the mammographic geometry

Paul Carson[1], Fouzaan Zafar[1], Sacha van der Spek[1], Gerald LeCarpentier[1], Fong Ming Hooi[2], Sumedha Sinha[2]; [1]Radiology, Univ. of Michigan, Ann Arbor, MI, USA, [2]Radiology and BME, Univ. of Michigan, Ann Arbor, MI, USA

Background, Motivation and Objective

Implementation and initial testing of an automated ultrasound system to achieve improved coverage in the mammographic geometry was undertaken by with simultaneous imaging from the top and bottom of the compressed breast.

Statement of Contribution/Methods

An Instrumentarium mammography system was modified to hold two Parker two-axis positioning systems with micron resolution above and below mesh compression paddles. The ultrasound probes were mounted rigidly to the positioning systems which were controlled by a Parker 6k4 motor controller. The controller handles trigger sequences that alternate between linear arrays on two GE Logiq 9 systems to acquire a 3D volume dataset with 0.4 mm elevational separation between images. The user interface and control software were developed in MATLAB to allow for cross platform compatibility and easy modification. The scanning algorithm and control circuitry were optimized to provide for the most efficient acquisition time given current hardware. Two 6.4 cm thick breast phantoms and one volunteer were studied.

Results

The system allowed a two sided ultrasound sweep of 10 cm (250 scan locations with a separation of 0.4 mm) in less than 5 minutes using nine angle compounding. As both transducers were carefully aligned and moved together, they saw the same internal structures within the limits of attenuation, depth dependent beam shape, and refraction/diffraction.

Fig. 1. Dual-sided images of compressed breast of a volunteer taken using two mechanically scanned, GE M12L matrix array transducers at 10 MHz setting. Co-registration was performed by eye.

Discussion and Conclusions

Being able to efficiently image the breast from both sides increases the usable frequency, attendant resolution, and sensitivity to small scatterers. The compressed thickness is typically 2-8 cm, half of which is usually imaged well with 12 MHz arrays in all but the most attenuating breasts. Scanning from both sides provides detailed images spanning the entire thickness of the breast and filling in many shadowed areas.

This work was supported in part by NIH Grants CA91713 and CA115267 and performed with guidance and collaboration of Kai Thomenius, Carl Chalek and Robert Wodniki, GE Global Research, Niskayuna, NY.

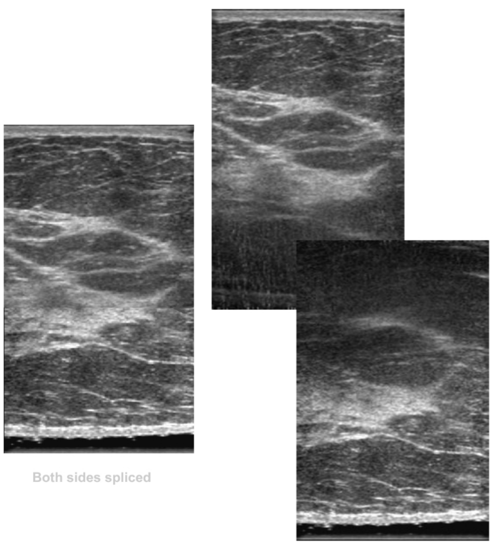

3K-6

5:45 PM Optimizing frequency and pulse shape for ultrasound current source density imaging

Yexian Qin[1], Zhaohui Wang[1], Charles Ingram[1], Qian Li[1], Russell Witte[1]; [1]*The University of Arizona, USA*

Background, Motivation and Objective

Electric field mapping is commonly used to identify irregular conduction pathways in the heart (e.g., arrhythmia) and brain (e.g., epilepsy). Conventional mapping is usually invasive and requires a large number of electrodes to reconstruct a field distribution. To overcome these limitations, we developed Ultrasound Current Source Density Imaging (UCSDI) based on the acoustoelectric (AE) effect, in which high frequency AE voltage is generated when a focused ultrasound beam intersects a current field. The AE signal can be detected by only one electrode and a reference ground to produce an electrical measurement confined to the ultrasound focus. A 3D current density distribution can, therefore, be imaged noninvasively by scanning the ultrasound beam. The goal of this study was to optimize the ultrasound parameters and examine the tradeoff between UCSDI spatial resolution and sensitivity, which are both affected by the ultrasound frequency and beam shape.

Statement of Contribution/Methods

Modeling (Field II™ and Comsol™) and experiments were both used to examine the effects of ultrasound frequency and pulse parameters on UCSDI. A time-varying dipole was produced by injecting current (~20mA) through a pair of electrodes placed in physiologic saline. UCSDI maps of the current distribution were formed by scanning transducers (with different center frequency) laterally and detecting the AE signal at each position.

Results

UCSDI maps (lateral vs. depth) the current dipole at different ultrasound frequencies are presented in Fig 1. The top and bottom rows represent images obtained with the 1MHz and 2.25 MHz transducers, respectively. The left and right columns denote experimental and simulated results. The 2.25 MHz probe is able to resolve the edges of the dipole, but the detected signal is smaller in amplitude (scale bar in mV).

Discussion and Conclusions

The results illustrate the ultrasound frequency and beam size strongly affect UCSDI resolution and sensitivity. Choice of the ultrasound parameters can fulfill different requirements for imaging current flow in the heart and brain. Further control of the ultrasound pulse shape will optimize sensitivity and facilitate UCSDI to the clinic for the diagnosis and treatment of arrhythmia and epilepsy.

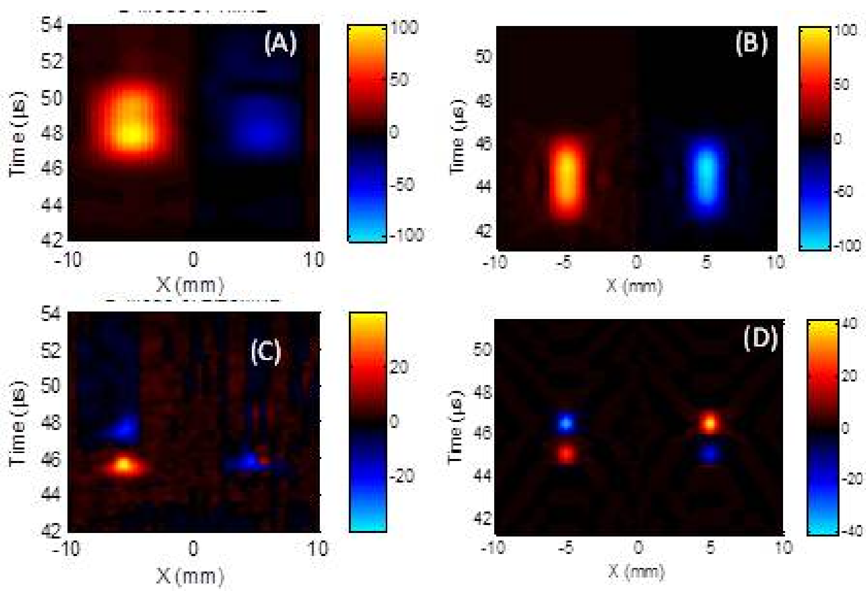

4K - NDE Methods and Analysis

Carribean Ballroom I

Friday, October 21, 2011, 4:30 pm - 6:00 pm

Chair: **David Greve**
Carnegie Mellon University, USA

4K-1

4:30 PM Dependency of Signal to Noise Ratio on Transducer Diameter and Buffer Diameter in Guided wave Time Domain Reflectometry

Håkon Viumdal[1,2], Kuo-Ting Wu[3], Saba Mylvaganam[1]; [1]Telemark University College, Porsgrunn, Norway, [2]Tel-Tek, Porsgrunn, Norway, [3]Industrial Materials Institute, National Research Council, Montreal, Canada

Background, Motivation and Objective

Ultrasonic measurements in high temperature environments are possible either with special piezoelectric elements with high Curie temperature, or piezoelectric elements in combination with acoustic waveguides, also called buffer rods (BRs). In harsh industrial applications the buffer rod concept might be the only feasible method. Different geometrical properties of the buffer rod and ultrasonic transducer (UT) will affect both the signal amplitude and the signal to noise ratio (SNR) of the sensor system. The end diameters of the BRs and the UTs are of main concern for researchers working with BR based ultrasonic measurements. The main consideration in this paper is on how the SNR is affected by the diameter ratio of the UT and the BR.

Statement of Contribution/Methods

Experiments with 9 different titanium double tapered BRs (see figure) in combination with 10 different UTs have been performed. The UTs are categorized into 4 groups, based on the labeled frequencies and bandwidth. Both the amplitude and the SNR of the reflected signal have been considered, for the different combinations of BRs and UTs using a standard time domain reflectometry. The experimental results are analyzed and compared with corresponding simulation results.

Results

Based on the experimental data, there is a distinct trend between the SNR and the ratio between the diameter of the UT element d_{UT} and the end diameter of the BR d_{Be}. The trend is more pronounced as the taper angle α is increased, as seen in the figure. The simulated waveforms show smaller variations for different UT/BR combinations.

Discussion and Conclusions

The SNR-trend of the BRs with taper angle α=1.7 is supported for all the four categories of UTs utilized in the experiment, i.e. individual variations of transducers are not likely the reason for this distinct trend. Uncertainties in the BRs geometrical properties, like divergent parallelism of the two end surfaces can also contribute to variations, but machining of the rods have been performed, thus almost eliminating this as an influencing factor. All the three peaks seen for taper angle α=1.7 are achieved for the thickest BR, whereas the troughs are associated with the thinnest and medium sized BRs. However, the combination of UT element diameter and BR end diameter affects the SNR of the experimental rods considerably.

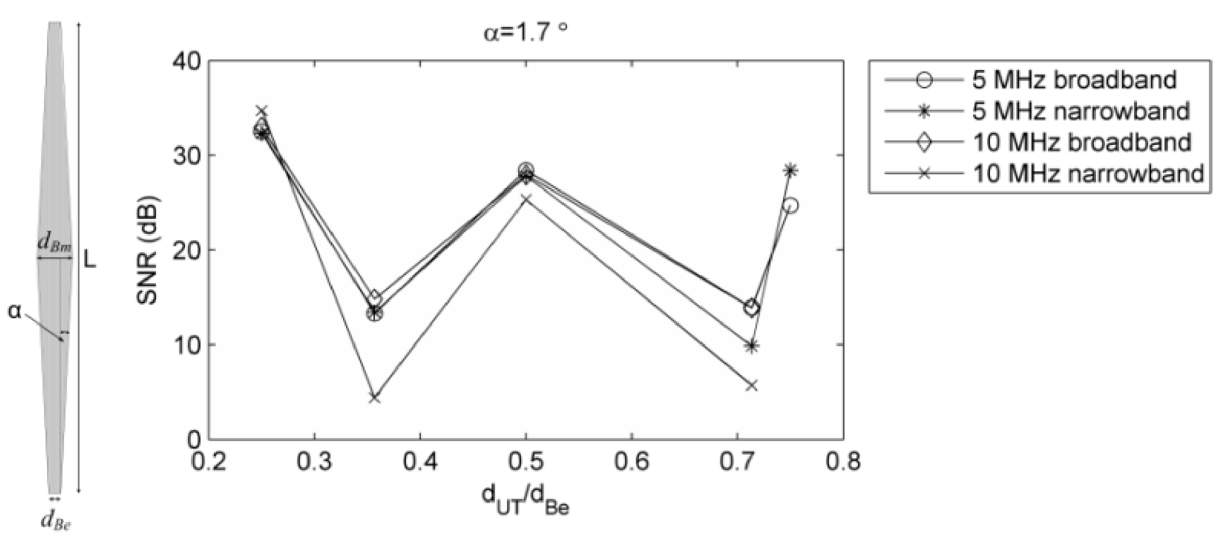

4K-2

4:45 PM Ultrasonic Characterization of Polymer Infiltration into Foam Materials

James Blackshire[1], Ray Ko[2], Ming-Yung Chen[3]; [1]AFRL/RXLP, Air Force Research Laboratory, Wright-Patterson AFB, Ohio, USA, [2]University of Dayton Research Institute, Dayton, Ohio, USA, [3]AFRL/RXBC, Air Force Research Laboratory, Wright-Patterson AFB, Ohio, USA

Background, Motivation and Objective

The development of advanced multi-material systems has become increasingly complex with regard to performance requirements, tailorable material options, and recent innovations in manufacturing technologies. The increased development and use of engineering foam material systems, for example, has recently led to significant improvements in the weight, cost, and performance of materials used in insulating, thermal protection, sound deadening, and lightweight structural materials. An important aspect of such complex multi-material systems includes the ability to effectively join two or more materials and characterize the processing results.

Statement of Contribution/Methods

In the present effort, the use of ultrasound for characterizing the infiltration of a polymer material into a foam is investigated using computational models and experimental validation studies. Characteristic pulse-echo signal responses utilizing time-of-flight reflection and attenuation were used to provide an effective means for estimating the fill-factor of the polymer into a foam material, where thermal and structural performance of the material system could be optimized.

Results

Results for a polymer-aluminum foam infiltration study are provided in the accompanying figures, where backscatter signals were collected in a pulse-echo measurement process. Although scattering effects from the foam are present, a distinct reflection from the polymer-air interface was present in the measurement providing evidence of its location based on signal amplitude levels and signal arrival times as depicted in the figures.

Discussion and Conclusions

The results are consistent with reflection and attenuation/scattering predictions from analytic considerations.

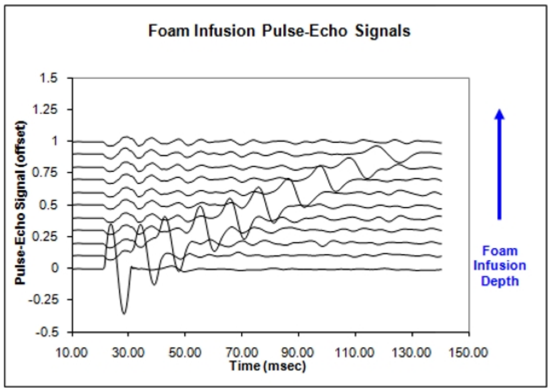

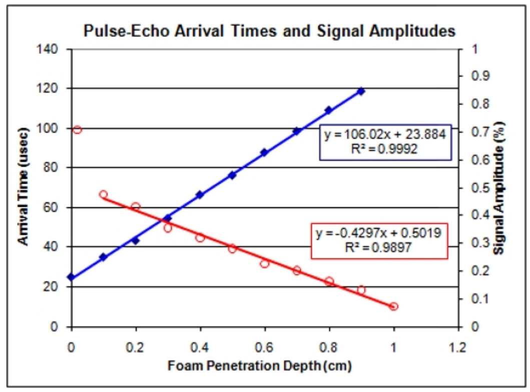

4K-3

5:00 PM Ultrasonic Visualization for Water Flooding in PEM Fuel Cells Using Guided Wave Linear Arrays

Ching-Chung Yin[1], Yu-Shyan Liu[2,3], Yu-Tai Wang[4]; [1]Deaprtment of Mechanical Engineering, National Chiao Tung University, Hsinchu, Taiwan, [2]Deaprtment of Mechanical Engineering, National Chiao Tung University, Taiwan, [3]Center for Measurement Standards, Industrial Technology Research Institute, Hsinchu, Taiwan, [4]National Chiao Tung University, Taiwan

Background, Motivation and Objective

Visualization of proton exchange membrane fuel cells (PEMFC) is an important technique to explore the phenomenon of water flooding in the cathode flow channels. A transparent PEMFC was previously reported to be used to optically visualize the transport of reactants and condensed water. However, its performance was very different than a real, opaque fuel cell. This work presents an ultrasonic visualization method using linear arrays and acoustic guided waves to gain insight into two-phase flow and water transport in a PEMFC.

Statement of Contribution/Methods

A 2 mm thick aluminum alloy plate with a number of parallel serpentine flow channels was used as a test mock-up. The groove type flow channels have a rectangular cross section of dimensions 1 mm wide by 1 mm deep. Two linear arrays of 16 piezoelectric elements were surface mounted at the opposing borders of the flow field plate and regarded as transmitter-receiver. The induced guided waves propagate parallel to the flow channels. The phase velocities of the guided waves traveling in the moist-free flow channels or those filled with water have been investigated numerically and experimentally. The synthetic aperture focusing technique was utilized to establish the B-mode images of water transportation in the flow channels. The image reconstruction scheme involves a two dimensional fast Fourier transform and transfer matrix method for acoustic wave propagation in the flow field plate.

Results

Both numerical and experimental results indicate that the fluid coupling effect retards the guided wave propagation in flow field plate. The direct arriving guided wave signals were interfered by the edge reflected echoes provided the mock-up was small. Different apodization functions were applied to improve the edge diffraction effects. In this work, the B-mode images of water transport in the flow channels can be clearly visualized using linear array transmitter-receiver in the frequency range between 1 to 1.5 MHz.

Discussion and Conclusions

Ultrasonic visualization for water flooding in a real PEMFC has been developed using an integrated technique involving linear arrays and guided waves. Though the B-mode images have not been real time reconstructed, the performance still satisfies the need for visualization in fuel cell. This technique will be applied to an operational PEMFC in the near future.

4K-4

5:15 PM Higher Order Modes Cluster (HOMC) based Guided Wave Technique for Hidden Corrosion NDT

Krishnan Balasubramaniam[1], Krishnamurthy C.V.[2]; [1]Mechanical Engineering, IIT Madras, Chennai, Tamil Nadu, India, [2]Department of Physics, IIT Madras, Chennai, Tamil Nadu, India

Background, Motivation and Objective

This paper reports the use of dispersive Higher Order Modes Guided Waves Higher order modes cluster guided waves (HOMC-GW) which are highly non-dispersive over some distance of propagation. The HOMC-GW technique is a recently explored phenomenon which appearsction o to have greater potential for medium range (approximately of the order of few meters) NDT. This HOMC-GW phenomena occurs at very high frequency-thickness product i.e. around 20 mm. MHz. The current effort will be towards understanding the formation, propagation and dispersion characteristics of HOMC-GW. The application of the new HOMC technique for the detection of corrosion in hidden regions in pipelines and above ground storage tanks bottom.

Statement of Contribution/Methods

Modes in this regime are found to have small differences between their group velocities and small differences in the associated angles of excitation. HOMC-GW appears to have several attractive features for NDE applications. These are (i) tighter envelope that improves the temporal resolution (ii) shorter wavelength that improves the spatial resolution, (iii) The vanishing surface displacements of the out-of-plane component that is insensitive to surface loading, and (iv) sub-surface defect detectability with out the effect of the surface conditions.

Results

The A-scan signals obtained using the 1 MHz conventional (circular transducer of 25 mm diameter) and the 2.25 MHz linear phased array transducers were normalized to the reflected signal from the largest defect. The expected/estimated theoretical amplitude of the smaller defects is taken to be 20%, 40%, 60% and 80% of the reference amplitude. The estimated theoretical amplitude of the signals was compared with the experimentally obtained amplitudes from the respective notches and the percentage errors were estimated.

Discussion and Conclusions

The HOMC guided waves were found to be unique in several ways and found to be useful in detecting corrosion type damage in pipeline and storage tank bottom plate inspection, particulalry in difficut conditions where access to the region for conventional NDT was not feasible. The wave modes were found to have unque displacement characteristics that allow for the wave to detect defects under weld pads, flanges, etc. The sizing of the defects was also found to be feasible.

4K-5

5:30 PM Noncontact Ultrasonic Characterization Techniques for Fibrous Materials Analysis

Thamizhisai Periyaswamy[1], Karthikeyan Balasubramanian[2], Chistopher Pastore[3]; [1]Human Environmental Studies, Central Michigan University, Mount Pleasant, Michigan, USA, [2]Electrical and Computer Engineering, Temple University, USA, [3]Textiles and Materials Technology, Philadelphia University, USA

Background, Motivation and Objective

Fibrous materials are highly complex structures, where discontinuity, heterogeneity and multi-scale porosity are inherent to structural arrangements. Characterizing the mechanical and thermal properties of such materials is a time consuming process and needs a range of testing equipments. The non-uniform, inhomogeneous structure, bulkier and easily compressible forms, different pore structures (fabric porosity and yarn porosity), complex deformations, nonlinearity, and multiphase interactions are some of the structural and behavioral complexities that hinder ultrasonics-based analyses of fabric materials. This research proposes a noncontact ultrasonic based characterization system that can determine the key properties of flexible, porous materials based on their ultrasound frequency response.

A novel characterization technique for fibrous ensembles, based on non-contact ultrasonic waves is presented. The instrumental setup comprises ultrasonic transducers (500 kHz), data acquisition setup and an artificial intelligence mapping system. Ultrasound signals transmitted through fibrous materials were feature extracted and mapped with low-stress mechanical properties and thermal properties.

Statement of Contribution/Methods

(a) Characterization of fibrous ensembles using acoustic signals was not successfully attempted before. This research uses a novel approach that maps the transmitted ultrasound features to an existing standard method for low stress mechanical properties and thermal properties.

(b) A combination of time, frequency and attenuation domain features was extracted for superior characterization.

(c) The artificial engine allows complex non-linear properties mapping that are inherent with most of the fibrous materials.

Results

A total of 80 fibrous samples were used for testing. Ultrasonic signals were transmitted through the samples and acquired at a sampling rate of 5 MHz. The sampled signals were analyzed for five features, i.e., time of flight, signal transmission velocity, power spectral density, signal power and rate of attenuation of signal amplitude. Seventeen low stress mechanical properties, air permeability and thermal conductivity were measured for these samples. The correlation of mapping between the ultrasonic features and the standard measured properties were greater than 0.92 (standard deviation 0.06).

Discussion and Conclusions

Materials behave uniquely for a characteristic pressure wave. This research characterizes fibrous materials based on their response to acoustic frequencies, especially at ultrasound ranges. The characteristics derived from a transmitted ultrasound were mapped towards standard characteristics such as low stress mechanical properties and thermal conductivity, using a model-free algorithm. The strong correlation between ultrasonic measurements and fabric performance properties show that ultrasonic systems are potentially suitable for fabric analyses.

4K-6

5:45 PM Generic hybrid models for two-dimensional ultrasonic guided wave problems

Manoj Reghu[1], **Prabhu Rajagopal**[1], Krishnamurthy Chitti Venkata[1], Krishnan Balasubramaniam[1]; [1]*Centre for Nondestructive Evaluation, Indian Institute of Technology - Madras, India*

Background, Motivation and Objective

Ultrasonic guided waves form the basis of a number of popular Nondestructive Evaluation (NDE) methods that have emerged in recent years. A thorough understanding of guided wave behaviour in structures is essential for the application of existing technologies, as well as for the development of new methods. However, the analysis of guided wave phenomena is challenging because of their complex dispersive and multimodal nature. Although numerical solution procedures have proven to be very useful in this regard, the increasing complexity of features and defects to be considered, as well as the desire to improve the accuracy of inspection often imposes a large computational cost. Hybrid models that combine numerical solutions for wave scattering with faster alternative methods for wave propagation have long been considered as a solution to this problem. However past effort was often focused on particular problems or particular combinations of solution procedures and hence is not easily accessible.

Statement of Contribution/Methods

Recently generalized hybrid modelling procedures that allow combination of any two modelling methods are being developed for bulk ultrasound. Here we seek to extend these concepts to the guided wave case. We first argue that conditions leading to such modularity in treating the total problem can also be found in the guided wave case. We consider the scattering of plane-crested fundamental guided wave modes in a homogenous isotropic plate. Wave generation, scattering and reception are represented by computationally efficient, but converged Finite Element (FE) models with fine meshing. These modules are mutually connected through a wave propagation ‘interface’ module. Different strategies to construct such an interface module are considered.

Results

A hybrid interface module is proposed, which can be used as a generalized 'propagator' between models representing wave generation, scattering and reception. An engineering solution, consisting of a coarse mesh FE model is examined against a more rigorous solution making use of mode orthogonality and plate Green’s functions. With the help of absorbing regions and the hybrid interface, model dimensions can be reduced dramatically. Results from an example hybrid model constructed using the two approaches are compared with those from a full FE model. Although the purely numerical implementation of the interface can work well for rapid visualization, the rigorous analytical approach is more efficient.

Discussion and Conclusions

It is shown that generalized hybrid models can be realized for ultrasonic guided waves, in the same manner as for bulk ultrasonic waves.The applicability and limitations of the methods are discussed using convergence and validation studies. We discuss the smallest size of the 'scattering' module that can be used with the analytical interface approach. Extension of the procedure to other two- and three-dimensional problems is discussed.

5K - Acoustic Wave Propagation II

Carribean Ballroom II

Friday, October 21, 2011, 4:30 pm - 6:00 pm

Chair: **Ji Wang**
Ningbo University

5K-1

4:30 PM Non-invasive measurement of sound velocity profiles

Elfgard Kühnicke[1], Michael Lenz[1], Martin Bock[1]; [1]Fakultät Elektrotechnik, Institut für Festkörperelektronik, Technische Universität Dresden, Dresden, Germany

Background, Motivation and Objective

In ultrasonics, the time of flight to the object interfaces is often the only information that is considered. From this information, one can either determine distances or sound velocities if the other value is known. A combined determination of the sound velocity and the distance of the scattering particles to the transducer makes it possible to measure sound velocity profiles. Possible applications of velocity profiles are tissue characterisation and noninvasive temperature monitoring during hyperthermia for cancer therapy.

Statement of Contribution/Methods

To determine distance and sound velocity simultaneously, we use the focus position as a second piece of information beside the ultrasonic time of flight. The focus position can be determined, because the echo becomes strongest when the scattering particle is located within the maximum of the sound field. Thus the position of the averaged echo signal amplitude indicates the time of flight to the focus (Fig.a).

Results

i.) The presentation gives proof of concept by sound velocity measurements with a focussing transducer in four fluids covering the wide velocity range between 1116 and 2740 m/s (Fig.b). To determine accuracy, a second experiment was carried out, where the sound velocity of water was varied between 1431 and 1555 m/s by heating with a thermostat. The calibration curve derived from this experiment yields a statistical uncertainty of only 1.4 m/s (0.1%).

ii.) To measure a velocity profile, the focus position, i. e. the distance of the sound field maximum from the transducer, is varied by beam forming with an annular array. By using adequate calibration curves, the sound velocity on different points of the axis can be determined in dependence of the chosen set of time lags used for focusing and the time of flight corresponding to the maximum of the averaged echo signal amplitude. First measurement results are given for a sound velocity profile with local resolution in water with a temperature gradient.

Discussion and Conclusions

The examples show the high potential and accuracy of the new method. To bring the measurement method into diagnostic appliance, it is necessary to extend its scope of application to biological tissues (i. e. "fluids" containing stationary scattering particles), to consider attenuation effects and to eliminate interfering signals caused by inhomogeneities and septa.

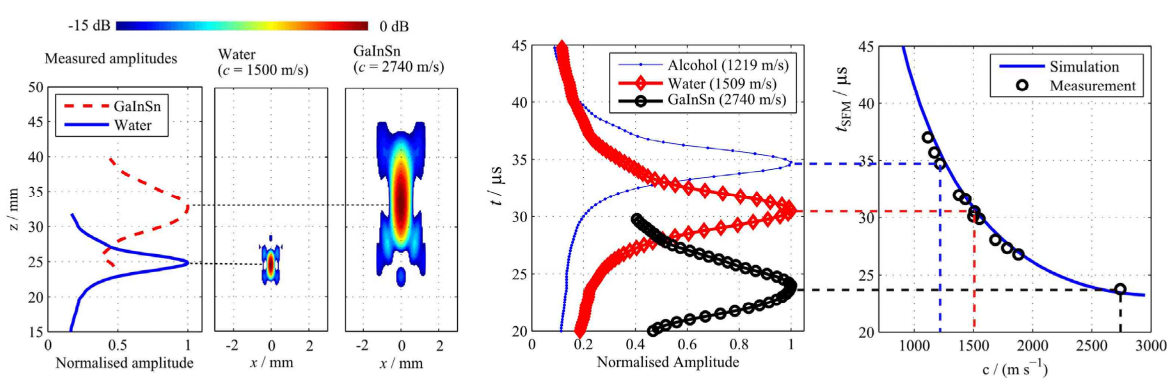

a) Comparison between measurements and simulated sound fields; (*z* - coordinate of acoustic axis)

b) Generation of calibration curves; (*t* - time of flight, t_{SFM} - time of flight to the sound field maximum, *c* - sound velocity)

Fig. Determination of the sound velocity from the averaged echo signal amplitude with a focusing transducer.

5K-2

4:45 PM Modeling Nonlinear Pressure Fields in Inhomogeneous Attenuative Media Using a Lossy Green's Function and a Contrast Source

L. Demi[1], N. Ozmen-Eryilmaz[1], K. W. A. van Dongen[1], M. D. Verweij[1]; [1]Laboratory of Acoustical Imaging and Sound Control, Delft University of Technology, Delft, Zuid Holland, Netherlands

Background, Motivation and Objective

Attenuation or loss forms an important phenomenon in medical ultrasound. At ultrasonic frequencies, attenuation is mainly due to absorption. Experimental data reveals that attenuation acts according to a frequency power law. For a given penetration depth, this effect limits the frequency, and hence the attainable resolution, that can be utilized. Attenuation is also crucial for therapeutic applications where high intensity focused ultrasound fields are used for ablation and hyperthermia treatment. Modeling attenuative nonlinear pressure fields in inhomogeneous media is therefore of great importance for the development of new ultrasound modalities and the optimization of treatment protocols.

Statement of Contribution/Methods

A compliance memory function is included in the linear wave equation to model attenuation. This function consists of two parts; a spatially independent and a spatially dependent part. The former accounts for the lossy background medium, the latter for variations in the attenuation parameters with respect to the background medium. The first part is accounted for by deriving the Green's function of the lossy background medium, whereas the second part results in the formulation of attenuative contrast sources.

The resulting equation is solved with an iterative Neumann scheme. Each step involves the convolution of the attenuative contrast sources with the lossy Green's function. Finally, nonlinear contrast sources are included to apply the method to nonlinear acoustics, resulting in a new version of the Iterative Nonlinear Contrast Source (INCS) method.

Results

The presented method is compared with the version of the INCS method in which attenuation is modeled solely via a contrast source approach. The comparison first concerns the results for the linear propagation of a 1 MHz Gaussian modulated plane wave in the range 0 mm to 100 mm. The medium is lossy heart muscle with a lossy blood slab extending from 20 mm to 40 mm. Next, the same configuration is used to compare the result when nonlinear propagation is taken into account. In this case, the acoustic nonlinearity parameter is inhomogeneous as well.

The results show excellent agreement between the two methods. Moreover, the new method shows an improved convergence rate and a reduction of artificial reflections from the boundaries of the numerical domain.

Discussion and Conclusions

A method has been developed that models attenuative nonlinear pressure waves by using a lossy background Green's function, together with distributed contrast sources to include inhomogeneities in the attenuation and coefficient of nonlinearity. The obtained results are in excellent agreement with those obtained with the use of contrast sources only. Moreover, the new method has an improved convergence rate and generates less artifacts due to spatial domain boundaries.

5K-3

5:00 PM Carbon nanomaterials as broadband airborn ultrasound transducer

Maxim Daschewski[1], Jens Prager[2], Marc Kreutzbruck[2], Andrea Harrer[2], Asmus Meyer-Plath[2], Matthias Guderian[2]; [1]Federal Institute for Materials Research and Testing, Berlin, Germany, [2]Federal Institute for materials research and testing, Germany

Background, Motivation and Objective

The demand for airborne ultrasound techniques for material testing as well as medical applications has increased remarkably in recent years. However, one has to face the problem of the lower coupling efficiency of air-coupled ultrasound compared to conventional liquid coupling due to the impedance mismatch between transducer material and adjacent air. Therefore, an efficient method for the generation of airborne ultrasound would be of great benefit for many ultrasound applications.

Statement of Contribution/Methods

In this contribution we present a novel method for the generation of airborne ultrasound using the thermoacoustic effect and investigate the applicability of micro- and nanoscale carbon materials as airborne ultrasound transducer.

We show that supplying such conductors with an alternating current leads to periodic heating of the conductor and the surrounding air. The resulting adiabatic expansion of the air leads to the generation of a propagating sound wave.

In order to avoid a low-pass effect due to the characteristic time constant of heat conduction effects, materials with high thermal conductivity and low heat capacity should be used to enter the high kHz-regime.

Results

We tested the acoustic performans of different electrographic nanomaterials, such as carbon fibers and carbonized electrospun polyacrylonitrile (PAN) nanofibers and measured the generated sound pressures in a frequency range up to 350 kHz using laser vibrometry.

Our last experiments with a PAN-nanofiber tissue (1x1cm) show, in 3 cm distance from transducer, the sound pressure levels of about 86 dB by 0.175 Watt electrical input power.

Discussion and Conclusions

The experimental results show good agreement with the theoretical prediction and FEM simulations. The presented method is shown to be a promising approach for the generation of airborne ultrasound in a broad frequency range.

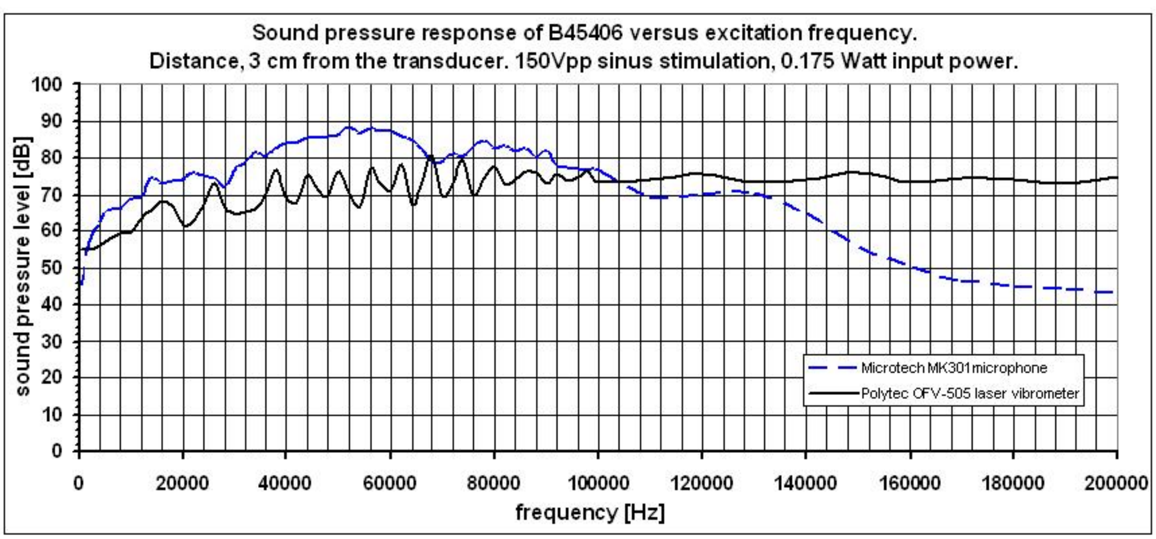

FRIDAY ORAL

5K-4

5:15 PM Experimental validation of a method for the simulation of backscatter signals from finite, shaped scatterers

Martin Salzle[1], Jan D'hooge[1,2], **Marco M. Voormolen[1]**; [1]MI Lab and Department of Circulation and Imaging, Norwegian University of Science and Technology, Trondheim, Norway, [2]Cardiovascular Imaging and Dynamics, Catholic University of Leuven, Leuven, Belgium

Background, Motivation and Objective

Existing simulation tools for diagnostic echography use random distributions of infinitely small point scatterers to model scattering media. Human tissue however, often exhibits a fibrous structure with a varying orientation, such as the myocardium. Modeling tissue with a distribution of finite, shaped scatterers could therefore improve the authenticity of simulated ultrasonic images. The goal of this study is to implement and validate a simulation method for finite, shaped scatterers.

Statement of Contribution/Methods

To calculate backscatter signals from finite, shaped scatterers a method based on the time-domain first-Born approximation was incorporated in a pulse-echo spatial impulse response scheme. The method was adapted from similar methods, previously presented by D.A. Lee et al. (J. Acoust. Soc. Am., 79(3), 1986, p. 681) and J.G. Mottley et al. (J. Acoust. Soc. Am., 83(2), 1988, p. 755).

To validate the method, backscatter signals from single cylindrical scatterers were measured and compared with simulation results. Cylindrical scatterers with different lengths and diameters were interrogated with circular piston transducers under various angles and frequencies. The scatterers could be placed in the ultrasonic field without a support mechanism using a very low concentration agar solution. The orientation of the scatterers was determined with orthogonal biangular photography. Pencil lead (graphite with a polymer binder) or copper was used as scatterer material.

Results

Cylindrical scatterers with a length ranging from 2 to 9mm and a diameter ranging from 0.4 to 0.9mm were interrogated with 0.3, 1 and 3.5MHz. Frequency spectra and backscatter signal strength were found to be in close agreement with the simulation results (see figure 1), as long as the length of the scatterer remained smaller than half the wave length. Above this limit the backscatter signals showed oscillatory behavior under specific angles.

Discussion and Conclusions

A pulse-echo spatial impulse response method for the simulation of backscatter signals from finite, shaped scatterers was developed and validated. With an average myocyte length of 120um, the limits of validity were found to be sufficiently high to make the method suitable for the modeling of myocardial fiber orientation in the echocardiographic frequency range.

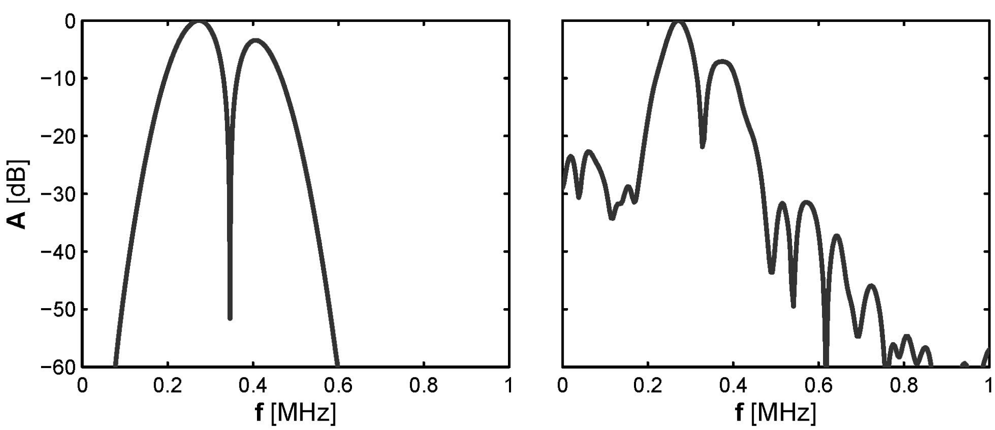

figure 1: Simulated (left) and measured (right) backscatter spectra from a cylindrical copper scatterer with a diameter of 0.5mm and a length of 2.22mm.

5K-5

5:30 PM The influence of the ultrasonic strain on the polarization of quantum-well heterolasers emission

Liudmila Kulakova[1]; [1]Russian Academy, Ioffe Physico-Technical Institute, St.Petersburg, Russian Federation

Background, Motivation and Objective

An ultrasonic strain can influence the process of optical wavelength emission in laser heterostructures, thus providing fast time response and precise wavelength adjustment [1] and the modulation of a laser emission direction [2]. In this paper we shall present first results of our experimental study of ultrasonic strain influence on hole states in quantum-well of InGaAsP/InP laser heterostructures.

The ground states of localized holes in quantum wells of most of the cubic semiconductors are differed in the projection of the angular momentum. The elastic strain both changes the energy separation between the states and mixes their wave functions. It can result in change of the laser emission polarization. Introduction of ultrasonic strain can lead to an additional change of the emission polarization with periodicity of the sound. The effect is of interest not only from fundamental point of view but can also be utilized for the information processing and storage.

Statement of Contribution/Methods

The static pressure influence on luminescence of passive heterostructures limits received information. The study of the phenomenon dynamics by acoustic solitons at the temperature of liquid helium is very complex and so has enough exclusive character.

We have begun researches of influence of ultrasonic strain on polarization characteristics of InGaAsP/InP heterolasers emission at room temperature. Such experiments attract both by the relative simplicity, and possibility of realization of uniaxial strain in a quantum well of an active heterostructure at different orientations with respect to a quantization axis. In addition it's of great importance that such experiments allow to observe processes in the scale of real time.

FRIDAY ORAL

Results

The analysis has shown that sound introduction leads to arising of an alternating component I ~, having periodicity of the sound: 1) near to a threshold its polarization is linear and coincides with polarization of equilibrium emission; 2) the angular (direction of polarization) dependence is changed with the increase of the operating currents, and at transition of angle 90grad. modulation phase of I~ is changed by opposite one. The explanation is possible if to assume that with increase of the operating currents a second alternating component arises in the laser emission.

Discussion and Conclusions

The obtained results, besides the expected effects, have revealed a number of additional unexpected ones which put some questions to the theory. In particular, it is the fact that polarization of alternating components (at large operating currents) essentially differs from the polarization direction of the equilibrium emission.

We are thankful to N. S. Averkiev for discussions and to the OFR_m (No. 09-02-12413) and RFBR (No.11-02-00729) for financial support.

References

[1] Liudmila A. Kulakova Appl. Optics, v.48, pp.1128-1134 (2009).

[2] Kulakova L. A., Lyutetskiĭ A. V. and Voloshinov V. B. Technical Physics Letters, v.3651, pp. 563-565 (2010).

5K-6

5:45 PM Numerical study of low-frequency sound beams

Milan Cervenka[1], Michal Bednarik[1]; [1]Czech Technical University in Prague, Faculty of Electrical Engineering, Czech Republic

Background, Motivation and Objective

This paper is concerned with study of low-frequency highly-directional sound beams. As it is well-known, these sound beams can be generated with use of parametric arrays, where nonlinearity of fluid is utilized to convert acoustic energy of high-amplitude and high-frequency (ultrasonic) primary wave into low-frequency secondary wave retaining directivity of the primary wave. So far, paraxial KZK equation has widely been used for numerical prediction of evolution of the primary as well as the secondary sound fields accounting for effects of nonlinearity, thermoviscous attenuation and diffraction.

Statement of Contribution/Methods

Within this work, numerical calculations of self-demodulated secondary fields reneging the condition $ka > 1$ (k being the wavenumber and a the transmitter radius) are performed. As a model equations, KZK equation and Higher-order parabolic equation (HOPE) [Kamakura, T., Masahiko, A., Kenicii, A, Acoust. Sci. & Tech. 25, 2, (2004)] are used and respective numerical results are compared.

As the numerical calculations in this case require treating extremely wide range of frequencies including higher harmonics of the primary field as well as the low-frequency self-demodulated field, an efficient frequency-domain numerical algorithm based on the operator-splitting method is proposed. Linear parts of the differential operators are integrated using Crank-Nicholson-like implicit scheme assuring numerical stability, whereas the nonlinear parts are integrated using the third-order Runge-Kutta method. Using this approach, solution of sets of coupled nonlinear algebraic equations is avoided. Moreover, integration of the nonlinear part of the operators is suitable for efficient massive parallelization, so that the algorithm implemented on a mainstream GPU allows accomplishing of the numerical calculations in reasonable time span.

Results

Numerical results obtained using KZK equation and HOPE show that the KZK equation overestimates amplitude of the low-frequency secondary wave in the near-field of the primary wave at the axis of symmetry. Both the equations provide the same results in the far-field and at the off-axis for both primary and secondary fields.

Discussion and Conclusions

The numerical results indicate that it is preferable to utilize higher-order parabolic equation for study of low-frequency demodulated acoustic fields. Considerable computational requirements connected with these calculations can be resolved by using of mainstream GPGPU hardware and massively-parallelized algorithms for numerical integration of the model equations.

6K - Medical Therapy Devices

Carribean Ballroom VI

Friday, October 21, 2011, 4:30 pm - 6:00 pm

Chair: **Sandy Cochran**
University of Dundee

6K-6

5:45 PM An Electronically-Scanned CMUT-in-CMOS Transducer for Hemodialysis Vascular Access Monitoring

David F. Lemmerhirt[1], Xiaoyang Cheng[1], Grant Kruger[2], William F. Weitzel[2]; [1]Sonetics Ultrasound, Inc., Ann Arbor, MI, USA, [2]University of Michigan, Ann Arbor, MI, USA

Background, Motivation and Objective

Frequent surveillance of vascular access health is essential for reducing complications in hemodialysis treatment for end-stage renal disease. Our team uses a variable flow "VF Doppler" method that allows accurate volume flow monitoring during dialysis with no angle or vessel size information. This demands a compact low cost array that is electronically reconfigurable to allow reliable operator independent volume flow measurements.

Statement of Contribution/Methods

We present a MEMS ultrasound array with on-chip circuits that control the size/position of a single-output RX aperture to maintain a reliable Doppler flow signal during dialysis. The array was fabricated using a CMUT-in-CMOS approach, which allows CMUT manufacturing in an unaltered foundry CMOS process augmented with just two release/sealing steps with no photolithography. The array output is demodulated, digitized, and relayed to a PC using a ~5 x 10cm board verified (initially w/PZT elements) in phantom/clinical pulsatile and constant flow measurements.

Results

A 20x2mm 1D array with 120 elements at 165um pitch (<lambda for 5-9MHz) has been fabricated. 90 28um-radius cells are clustered to form RX elements whose outputs connect to on-chip transimpedance amplifiers with capacitive feedback to reduce noise. Early single element + circuit prototypes in the same process gave a min. detectable pressure of 6.1mPa/rtHz. 120 CMOS switches, controlled by a serial shift register, select channels to sum together at the input of an analog adder, which provides a single RF output. For B-mode imaging, a parallel output mode is available. To steer TX beams along the vessel, cell lower electrodes are combined into 90 TX elements (grouped again off-chip for early planar TX experiments) oriented orthogonally to the RX elements. Doppler measurement results from phantoms will be presented, showing relationships between signal strength and RX aperture size/position and TX angle.

Discussion and Conclusions

This work demonstrates the feasibility of using CMUT-in-CMOS for highly reconfigurable arrays that directly integrate CMUTs with amps & switches with no added cost or fab complexity. This enables selectable RX summing and orthogonal TX beam steering, appropriate for vascular access monitoring. In the future, demodulation and ADC circuits can be incorporated on the array itself, creating a low cost device with direct digital output.

6K-1

4:30 PM Triple Function Imaging, Radiation Force, and Therapeutic IVUS for Microbubble Based Drug Delivery

Joseph P. Kilroy[1], John A. Hossack[1]; [1]Biomedical Engineering, University of Virginia, Charlottesville, VA, USA

Background, Motivation and Objective

Intravascular ultrasound (IVUS) is widely used to characterize arterial vessel disease. Combined with microbubble-based drug delivery, IVUS has the potential to provide image guided, site-focal therapy. Acoustic radiation force has been previously demonstrated to translate microbubble drug carriers to the vessel wall, while low frequency therapeutic ultrasound can oscillate microbubbles, releasing the drug and enhancing drug delivery via sonoporation. In order to perform all of these functions, a triple function IVUS catheter was designed, fabricated, and tested.

Statement of Contribution/Methods

The IVUS catheter transducer elements were designed and modeled using Finite Element Analysis (PZFlex, WAI) for the purpose of microbubble translation, rupture, and imaging, with center frequencies of 3 MHz, 1.5 MHz, and 9 MHz, respectively. Two transducer elements were created for these three operating frequencies and combined into a single catheter. The radiation force element is a subdiced, 'hard' PZT-4 device designed for the high duty cycle operation required for microbubble translation. The element is 3 mm long to increase the transit time insonation for a microbubble in flow, as compared to a conventional short IVUS transducer. The imaging element is a 1 mm square 'soft' PZT-5H with a thickness mode of 9 MHz and a width mode of 1.5 MHz.

The fabricated IVUS device was characterized with a hydrophone in a water tank for comparison to PZFlex results. An annular image was collected by incrementally rotating the catheter with a motion controller while pulsing with a pulser/receiver. Additional experiments were conducted by optically measuring microbubble displacement during insonation with the radiation force element.

Results

A 0.5 mm thick ceramic was selected for the radiation force element with a simulated center frequency of 2.7 MHz, based on the resonant frequency of the microbubbles. The measured device center frequency was 3.27 MHz with a correlation coefficient of 0.84 when compared with PZFlex results. The imaging and therapeutic element was designed with a 0.24 mm thickness and exhibited a thickness mode frequency of 8.2 MHz with a 43% one way -3dB bandwidth and a width mode frequency of 1.66 MHz.

Insonating with a 270 kPa 3 MHz 20 cycle Gaussian ramped sinusoid at a 50 Hz PRF displaced a 5.3 micron diameter lipid shelled microbubble at an average velocity of 0.089 mm/s, based on optical measurements. Increasing the duty cycle 20 fold is anticipated to increase the velocity to 1.8 mm/s, yielding velocities sufficient to move a microbubble from catheter port to vessel wall (<1 mm) in less than a heart beat.

Discussion and Conclusions

The fabricated IVUS is a multi-functional device that provides for: 1. imaging guidance capability 2. translation of microbubbles and 3. microbubble-based drug delivery. The use of a width mode resonance provides low frequency insonation for therapeutic effect without increasing the number of elements required in the catheter.

6K-2

4:45 PM Tissue Ablation Using Multi-frequency Focused Ultrasound

Sijia Guo[1], Xiaoning Jiang[2]; [1]Mechanical and Aerospace Engineering, North Carolina State University, Raleigh, NC, USA, [2]Mechanical & Aerospace Engineering, North Carolina State University, Raleigh, NC, USA

Background, Motivation and Objective

Focused ultrasound (FUS) has recently been successfully demonstrated in several clinical trials, including the treatment of uterine fibroids, breast, liver, prostate, and brain cancer and the palliation of pain in bone metasis. FUS has also showed great potential for enhancing targeted drug delivery or gene therapy by modifying vascular or cell membrane permeability. However, unwanted heat dissipation, lack of imaging guidance and limited ablation volume have hindered the full realization of its benefits. Dual frequency FUS with frequency difference of less than 50 kHz was demonstrated to be effective to enlarge the lesion volume. In this paper, tissue ablation using multifrequency FUS is studied to enhance controllability of FUS therapy.

Statement of Contribution/Methods

Experiments and simulations on tissue ablation were performed to investigate the effectiveness of multi-frequency ultrasound ablation using FUS with greater frequency differences (950 kHz, 1.5 MHz and 3.3 MHz FUS). Temperature rise and lesion volume were recorded when chicken breast tissue was ablated by FUS with controlled ultrasound power and exposure time at a single frequency and multi-frequencies. Simulations were conducted to verify the temperature change and temperature distribution as well as ablation volume in these tests. Prediction of the ablation is based on tissue properties, ultrasonic heat deposition and perfusion.

Results

It was found that under the same total input power dual frequency ablation can generate 5°C to 20°C higher temperature rise than using each one of them along. Also, the diameter of thermal lesion induced by dual frequency transducers in 15 seconds is 10mm which is almost twice of that by one single transducer; the depths of lesions are similar in both single frequency and dual frequency tests, indicating about 4 times lesion volume increasing by using dual frequency ablation.°

Discussion and Conclusions

Tissue ablation test using multi-frequency FUS can generate a higher temperature rise and a larger lesion volume comparing with ablation using a single frequency under the same exposure condition, which will lead to a more effective FUS ablation. Furthermore, the multi-frequency ultrasound ablation using FUS with a greater frequency difference could result in promising imaging guided therapy using one multi-frequency probe.

6K-3

5:00 PM Novel Concept of Array Transducer Element Using Combined Resonance Between Oscillations of Hemispherical Piezoceramic Shell and Bulk Water

Kenji Otsu[1], Shin Yoshizawa[2], Shin-ichiro Umemura[1]; [1]Department of Biomedical Engineering, Tohoku University, Japan, [2]Department of Electrical and Communication Engineering, Tohoku University, Japan

Background, Motivation and Objective

For therapeutic array transducers, it is required to reduce the electrical impedance of their elements so that the transducer can produce high ultrasonic power at a relatively low drive voltage.

Statement of Contribution/Methods

A new concept of piezoceramic element using its breathing mode has been proposed for a therapeutic array transducer. High acoustical coupling was achieved without impedance matching layer by utilizing the combined resonance between the breathing-mode oscillation of the hemispherical piezoceramic shell and the volume oscillation of a water sphere in simulation. The air-backed concave piezoceramic shell has an element aperture of 4.0 mm and a shell thickness of 0.3 mm. The behavior of such a transducer element has been numerically analyzed based on finite element method.

Results

Figure 1 shows the acoustic waves emitted from the hemispherical transducer driven by continuous sinusoidal voltage at the resonance frequency of 0.50 MHz for 24 µs. Compressive and expansive motions of a spherical bulk of water enclosed by the hemispherical shell and hemispherical waves emitted from it are observed. The transducer element produced more than several times higher acoustic power output than a conventional thickness-mode element at the same drive voltage in simulation.

Discussion and Conclusions

To confirm that the coupled resonance between the piezoceramic shell and water sphere was obtained, virtual materials having the same acoustic impedance as water but different longitudinal velocities were used to replace water in simulation. Figure 2 shows the impedance curves of concave hemispherical elements, which was very sensitive to the longitudinal velocity of the virtual material, whereas those of the convex elements remained unchanged. These results strongly support the hypothesis.

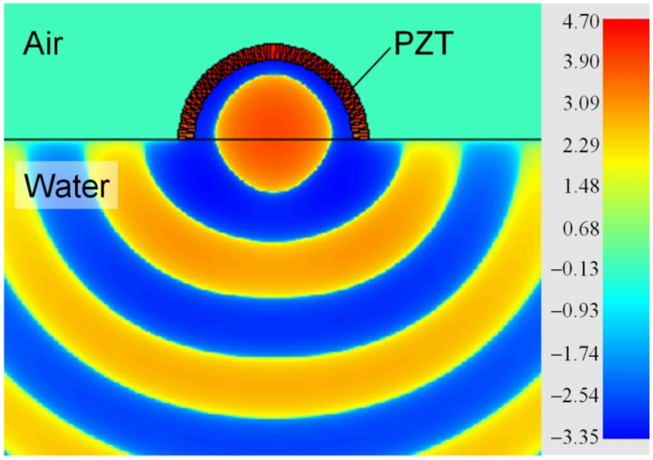

Figure 1 Acoustic waves emitted from breathing-mode piezoceramic element.

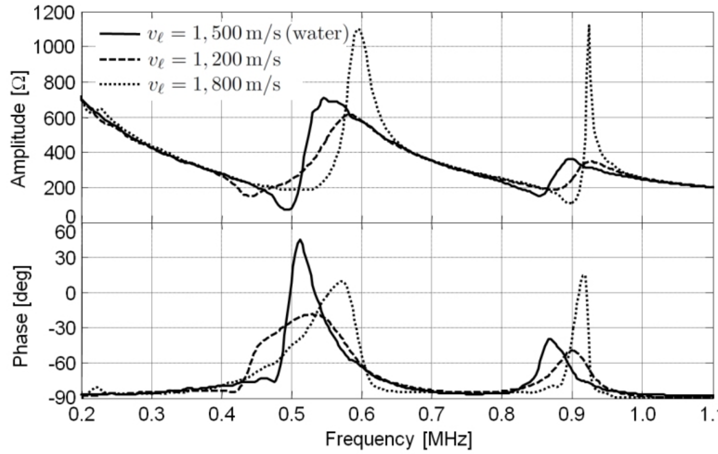

Figure 2 Electrical impedance curves of virtual materials having the same acoustic impedances as water.

6K-4

5:15 PM Intracranial Dual-mode IVUS and Hyperthermia Using Circular Arrays

Edward Light[1], Carl Herickhoff[1], Vivek Patel[1], Mark Palmeri[1], Gerald Grant[2], Gavin Britz[2], Stephen Smith[1]; [1]Biomedical Engineering, Duke University, Durham, North Carolina, USA, [2]Neurosurgery, Duke University Medical Center, Durham, North Carolina, USA

Background, Motivation and Objective

Our goal is minimally-invasive, image-guided ultrasound hyperthermia treatment of tumors in the brain using IVUS catheters placed immediately adjacent to a tumor for targeted control of drug release from thermosensitive liposomes. Therefore, the intravascular transducer must be able to both image and achieve a temperature rise of at least 4°C in tissue. Previously we described 10-13 Fr linear and matrix array catheters for 2D and 3D image guided brain therapy. Last year we modified commercial 3.5 Fr rotating piston IVUS catheters substituting a 9 MHz transducer for the 40 MHz piston. We achieved minimally invasive brain imaging in the pig model and more than 10 degree heating of a human glioblastoma in the flank of a mouse model. However our 9 MHz images were not satisfactory and it is difficult to stop the beam of a rotating IVUS catheter for hyperthermia mode. Therefore, this year, we investigated the feasibility of modified circular IVUS phased arrays for dual mode intracranial applications.

Statement of Contribution/Methods

In a series of in vivo experiments using the pig model we evaluated the quality of IVUS brain images using the Volcano In Vision scanner and 3.5 Fr IVUS catheters each consisting of a circular array of 64 elements operating at 20 MHz. First, the catheter was passed from the femoral artery to the vertebral artery in the brain. In another trial, the IVUS catheter was inserted through a burr hole in the skull to image brain parenchyma through the dura. For hyperthermia experiments, the circular array catheters were hardware modified by short circuiting fractions of the circular array elements to produce fixed beam-widths varying from 30 to 360 degrees. A power amplifier delivered 2 Watts continuous wave electrical power at 20 MHz into the modified IVUS catheters positioned 2 mm above tissue mimicking material with a hypodermic needle thermocouple inserted 1 mm beneath the surface for heating measurements.

Results

The imaging experiments produced high quality real-time echo and color flow circular images of the brain to a depth of 7 mm including vascular structures such as a hematoma and parenchymal gyri and sulci. Multiple hyperthermia trials heated tissue mimicking material by 4-6 degrees in less than 2 minutes.

Discussion and Conclusions

Our hardware IVUS catheter short circuits have mimicked modifications which can already be implemented in IVUS scanner software. Thus our results demonstrate that development of intracranial dual-mode IVUS arrays may be feasible.

6K-5

5:30 PM Ultrasonic Cutting with a d31-mode PMN-PT-driven Planar Tool

Muhammad Sadiq[1], Yang Kuang[1], Zhihong Huang[1], Sandy Cochran[1]; [1]*Mechanical Engineering and Mechatronics, University of Dundee, Dundee, Scotland, United Kingdom*

Background, Motivation and Objective

Ultrasonic cutting tools are widely used in surgery. However, the weight and self-heating of mass-spring configuration of drive transducer are weaknesses. An alternative approach is to use a planar tool to which piezoelectric drive components are bonded directly. This approach, explored previously with silicon tool blades, has significant advantages in simplicity and bulk. Furthermore, by utilising PMN-PT relaxor single crystal materials cut optimally for the d31 mode, efficiency can be increased and electrical impedance matching achieved simply by reconfiguring the material through selection of its width and number of layers.

Statement of Contribution/Methods

The work reported here is mainly theoretical comparison of different planar cutting tool configurations, with early experimental results. Comprehensive data for both PZ54 piezoceramic and PMN-PT single crystal materials (from Ferroperm SA, Kvistgaard, Denmark and Sinoceramics, State College, PA USA, respectively) were obtained from tests as a function of temperature. For PZ54, d31 = 200 pC/N while for PMN-PT d31 = 1300 pC/N. These data were utilised in finite element analysis (Abaqus, Dassault Systemes Abaqus Inc., France) which also allowed detailed design of the planar tool shape, such as nodal mounting.

Results

Simulation was used as the basis for a tool design resembling a dagger, with a triangular blade acting in the same way as an ultrasonic horn, nodal mounting resembling the hilt of the dagger, and a rectangular extension beyond the hilt resembling the handle. A total tool length of 34 mm and maximum triangular width of 12 mm were found to correspond with piston-like amplified longitudinal motion of the tip of the triangle at an excitation frequency of 80.6 kHz. Unlike previous work on silicon planar tools, the blade was made of steel; in future work, medical compatibility will be realised with other materials. The piezoelectric material was mounted towards the top of the triangle. In simulation, a direct interface between the piezoelectric material and the tool was assumed. Ag-loaded epoxy bonding was used in experimental work. Both PZ54 and PMN-PT are effective in this configuration with the better tolerance of elevated temperatures and lower cost suggesting PZ54 as the better choice at present. Nevertheless, tip velocity, $v > 120$ mm/s was achieved experimentally with single-sided PMN-PT in a simple test setup with laser vibrometer measurement.

Discussion and Conclusions

The cumbersome nature and complicated internal structure of a mass-spring transducer in ultrasonic cutting tools contrasts with the elegance of the planar design. Furthermore, the enhanced value of d31 for PMN-PT suggests that an efficient realisation is possible. Our work has confirmed the feasibility of the use of this material with steel blade. Further work will explore modifications in the PMN-PT for direct electrical impedance matching, double-sided PMN-PT, enhanced tool shapes and payloads such as an anaesthetic needles.

P5Aa - Beam Formation: Resolution Improvement

Carribean Ballroom III-V

Friday, October 21, 2011, 9:30 am - 1:00 pm

Chair: **Pai-Chi Li**
National Taiwan University

P5Aa-1

A beamforming strategy dedicated to ocular posterior segment imaging at 20MHz

Tony Matéo[1], Yassine Mofid[1], Jean-Marc Grégoire[1], Dominique Certon[1], Frédéric Ossant[1,2]; [1]Université François-Rabelais, UMRS U930-CNRS ERL 3106, Tours, France, [2]CHRU de Tours, Tours, Indre et Loire, France

Background, Motivation and Objective

Ultrasound biomicroscopy has taken an important place in ocular imaging, mainly to image the anterior segment (20 - 60 MHz) and then the posterior segment (10 - 20MHz) when OCT is ineffective due to cataract or hyalopathy asteroid. Especially, displaying the posterior segment is of clinical importance to diagnose pathologies such as macular degeneration or detached retina.

However, the posterior coat resolution is poor and B-mode imaging underestimates axial dimensions with a mean bias of 400 µm [1]. This bias is mainly due to the influence of the crystalline lens where US celerity (about 1660 m/s in porcine eyes) is around 10% higher than in the surrounding medium (aqueous/vitreous humor), introducing a wave aberration responsible of wrong echo localization.

An original beamforming (BF) method is therefore proposed to optimize the posterior coat imaging beyond the lens.

Statement of Contribution/Methods

An open US device (ECODERM, 20 MHz linear array, 128 elements), capable of generate a large panel of BF strategies with a 100 MHz band pass in reception was used.

The lens was modeled as a biconvex lens with 2 radii of curvature (anterior: ρ_a & posterior: ρ_p) so as to correct its effects. A line beamformed by firing 32 elements centered on the eye axis allowed the detection of the axial lens echoes. Knowing the celerity inside the lens, its real thickness (e) was deduced.

Secondly, a BF derived from Synthetic Transmit Aperture (STA [2]) was implemented: knowing the lens geometry and according to Fermat's principle, the right TOFs beyond the lens were computed, thus taking into account refraction.

Results

Thanks to our model, the mean relative angular deviation of a wave before and after going through the lens has been quantified to 24.8% for an eye with 2.5 mm diameter, ρ_a=10 mm, ρ_p=6mm and e=5mm which implies a mean mislocation of the echoes in the retina around 810 µm (± 910 µm) without refraction correction.

The BF method presently developed was validated ex-vivo on 5 porcine eyes demonstrating images with significant spatial fidelity enhancement beyond the anterior segment.

Discussion and Conclusions

The eye was modeled as a heterogeneous medium (humor + lens) taking into account velocity differences in order to perform a good biometric evaluation not only of the crystalline lens but also of the posterior chamber.

Good resolution and fidelity to the real anatomic dimensions were obtained by our synthetic BF method. As the resulting image suffers from a lack of contrast due to the mono-element emission, a defocalised multi-element emission is currently under study. With further improvements of the contrast, normal and pathologic structures affecting the posterior coats of the eye would be identifiable.

[1] W.A. Hamidzada & al. "Agreement between A-mode and B-mode ultrasonography in the measurement of ocular distances", Vet Radiol &Ultrasonography, 1999

[2] J.A. Jensen & al., "Synthetic aperture ultrasound imaging", Ultrasonics, 2006

P5Aa-2

High range resolution ultrasound imaging of a human carotid artery using frequency domain interferometry

Hirofumi Taki[1], Takuya Sakamoto[1], Kousuke Taki[2], Makoto Yamakawa[3], Tsuyoshi Shiina[4], Motoi Kudo[2], Toru Sato[1]; [1]Graduate School of Informatics, Kyoto University, Kyoto, Kyoto, Japan, [2]Department of Anatomy, Shiga University of Medical Science, Otsu City, Shiga, Japan, [3]Advanced Biomedical Engineering Research Unit, Kyoto University, Kyoto, Kyoto, Japan, [4]Graduate School of Medicine, Kyoto University, Kyoto, Kyoto, Japan

Background, Motivation and Objective

Carotid intima-media thickness (CIMT) is a sensitive measure of atherosclerosis, a surrogate marker for cardiovascular diseases. The improvement of range resolution in ultrasound vascular imaging is desirable for accurate measurement of CIMT. We have proposed an ultrasound vascular imaging method using frequency domain interferometry (FDI) with Capon method, and confirmed that the method succeeds to acquire a high range resolution image of a swine femoral artery in vitro. In this study we extend the previously proposed method to apply it to a living human carotid artery.

Statement of Contribution/Methods

The ultrasound vascular imaging method based on FDI assumes that the waveform of an echo returned from each target is similar to that of a reference target. Therefore a reference target and each target in the region of interest (ROI) should be similar in shape. Since the slope angle of the human artery wall interface varies, we employ 6 flat interfaces as reference targets, where the slope angles of the interfaces are 0, 2, 4, 6, 8 and 10 degrees. 6 images are depicted separately using the 6 references, and then they are averaged. We call this process as reference compound.

Results

We applied the proposed FDI imaging method with reference compound to a single frame IQ data of a living human carotid artery acquired by a commercial ultrasonographic device, where the center frequency is 7.5 MHz (Fig. 1). The proposed method succeeded to acquire a high range resolution image of the human carotid artery, as shown in Fig. 2.

Discussion and Conclusions

We propose a novel ultrasound vascular imaging method using FDI, and confirmed the potential of the method to acquire a high range resolution image of a living human carotid artery.

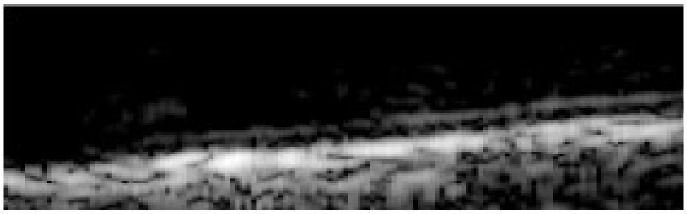

Fig.1 B-mode image of posterior wall living huma carotid artery. The size of the ROI is 5 x 30 mm.

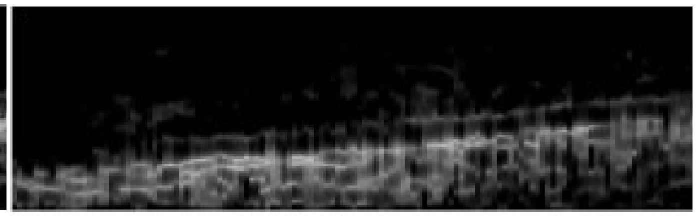

Fig. 2 Image of posterior wall living human caroti artery acquired by the proposed method. The size the ROI is 5 x 30 mm.

P5Aa-3

Mean Sound Speed Estimation with Focusing Quality Evaluation for Medical Ultrasound Imaging

Seok Joon Park[1], Jaejin Lee[1], Woo Youl Lee[1], Yangmo Yoo[1,2]; [1]Department of Electronic Engineering, Sogang University, Seoul, Korea, Republic of, [2]Interdisciplinary Program of Integrated Biotechnology, Sogang University, Seoul, Korea, Republic of

Background, Motivation and Objective

In ultrasound receive beamforming, a fixed sound speed (e.g., 1540 m/s) is assumed for calculating focusing time delays. However, due to the variations of sound speeds incurring in soft tissues, phase distortions are introduced, leading to defocusing and consequent degradation in image quality. The phase distortion becomes severe when imaging fatty tissues and obese patients. The various sound speed estimation methods have been proposed, but these methods require the substantial amount of the computer complexity.

Statement of Contribution/Methods

In this paper, a new mean sound speed estimation method, in which focusing quality is examined by computing the minimum average sum of the absolute difference (MASAD) of raw radio-frequency (RF) data during receive beamforming, is presented to enhance spatial and contrast resolution. The proposed MASAD method was evaluated with the in vitro data from a tissue mimicking phantom (Model 040GSE, CIRS, Norfolk, VA, USA) with the sound speed of 1540 m/s ¡¾ 10 m/s by using a 7.5-MHZ linear array transducer with the Ultrasonix¡¯s SonixTouch research platform connected the SonixDAQ parallel data acquisition system. For quantitative evaluation, the lateral resolution was measured with contour maps of -3 dB, -6 dB and -12 dB.

Results

Figure 1 shows the ultrasound B-mode image from the phantom data with the region of interest (ROI) box chosen at the transmit focal point when the sound speed was assumed to be 1540 m/s. The ASAD values from the ROI are plotted against the sound speed changing from 1400 m/s to 1640 m/s in Fig. 1(b). The MASAD value is found with the sound speed of 1550 m/s matched to the reference value (i.e., 1540 m/s ¡¾ 10 m/s). The -3-, -6-, and -12-dB contour maps for 1500 m/s and 1550 ms/ are shown in Figs. 1(c) and 1(d). The contour map from the estimated 1550 m/s shows the substantial improvement in lateral resolution over that from 1500 m/s (i.e., 0.2 mm vs. 0.9 mm, respectively).

Discussion and Conclusions

From the in vitro phantom experiment, the proposed mean sound speed estimation method accurately estimates the sound speed. Moreover, the proposed method requires the minimum hardware resource since it only utilizes the computationally efficient sum of the absolute difference operations. This result indicates that the MASAD method could be used for enhancing spatial and contrast resolution while minimally increasing the hardware complexity.

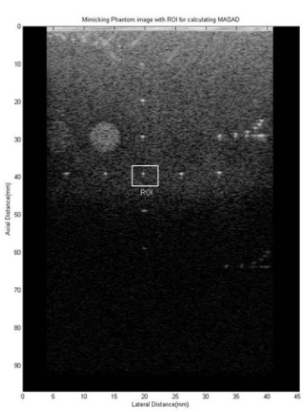

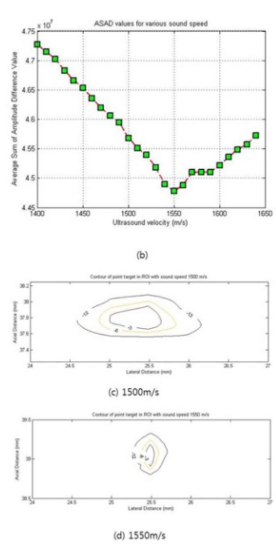

Figure 1.

(a) Mimicking Phantom image with ROI for Calculating MASAD

(b) ASAD values for various sound speed

(c) Contour of ROI with sound speed 1500m/s

(d) Contour of ROI with sound speed 1550m/s

FRIDAY POSTER

P5Aa-4

Improved Depth of Focus for Single Element Annular Transducers

Kai-Han Huang[1], Jian-Hung Liu[1], Pai-Chi Li[1]; [1]*Natoinal Taiwan University, Taiwan*

Background, Motivation and Objective

The design and evaluation of a high-frequency single-element transducer was previously reported. The transducer has an annular geometry, with the thickness of the piezoelectric material increasing from the center to the outside. This single-element annular transducer (SEAT) can provide a broader frequency range than a conventional single-element uniform transducer (SEUT) with a uniform thickness. The SEAT can be used for imaging applications that require a wider transducer bandwidth, such as harmonic imaging. In this study, we further explore its potential in extending the depth of focus (DOF), which is another critical factor in determining image quality.

Statement of Contribution/Methods

The SEAT has a diameter of 6 mm and comprised six subelements of equal area whose thickness ranged from 60 µm (center) to 110 µm (outside), which results in the center frequency of the subelements varying from 61MHz to 33MHz. The overall center frequency is 42.4 MHz. The annular pattern is constructed using an ultrasonic sculpturing machine that reduces the surface roughness. Since the frequency response of the transducer depends on its location relative to center, coded waveforms (e.g., linear chirps) can be used that effectively excite different subelements of the transducer at different times. By properly designing the coded waveforms, one can adjust the transmit focal depths and therefore improve the depth of focus. Two kinds of excitation waveforms are used in this study. One is a coded waveform with an instantaneous frequency from 33MHz to 61MHz and the total duration is 18 cycles. The other is fixed at 40MHz sine wave with 18 cycles for benchmarking. An ultrasonic beam analyzer (S-12D, Onda Corporation, Sunnyvale, CA) is used to measure the ultrasonic beam patterns in water.

Results

Beam patterns, their axial and lateral projections are all shown. With the coded excitation, the DOF (-6dB) is increased from 1.6mm to 2.0mm. In other words, a 25% improvement is achieved without noticeable change in lateral resolution.

Discussion and Conclusions

We demonstrate the ability to improve DOF of a SEAT. Along with its broader bandwidth that we previously demonstrated, the design clearly shows potential of such design methodology. The SEAT can be further extended to increase the DOF on the receive by performing filter-based dynamic focusing, which will be assessed and demonstrated in a future study.

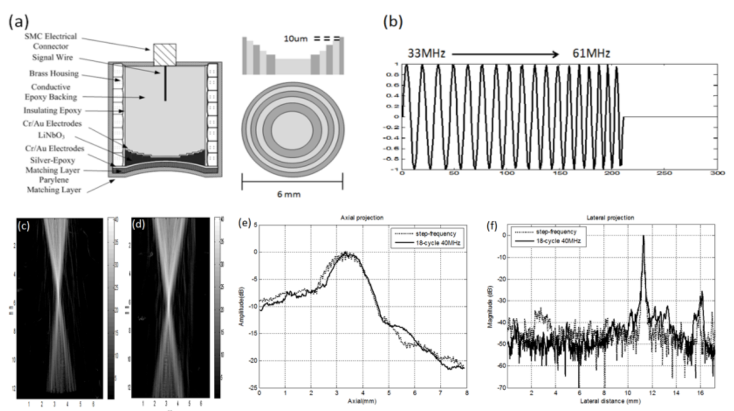

Figure: (a). Schematic of SEAT. (b). Coded excitation waveform. (c). Measured beam pattern in water: 40MHz/18 cycles. (d). Measured beam pattern in water using coded waveform shown in (b). (e) Axial projection shown 25% improvement (dotted vs. solid). (f). Lateral projection showing no noticeable change.

P5Aa-5

Fresnel Beamforming and Dual Apodization with Cross-Correlation for Curvilinear Arrays in Low-cost Portable Ultrasound Systems

Man Nguyen[1], Jesse Yen[1]; [1]Biomedical Engineering, University of Southern California, Los Angeles, CA, USA

Background, Motivation and Objective

New ultrasound system architectures with fewer channels than standard cart-based systems are desired for portable applications. In previous work, we showed that a Fresnel-based beamforming (BF) technique yields comparable performance to conventional delay-and-sum (DAS) BF using a linear array. Here, we present results of a modified Fresnel BF method using curvilinear arrays commonly used for abdominal and obstetrics imaging. This modified beamforming method incorporates dual apodization with cross-correlation (DAX) for improved contrast-to-noise ratio (CNR).

Statement of Contribution/Methods

The primary advantage of Fresnel BF technique is a system with only 4-8 transmit (Tx) and 2 receive channels can be used to focus an array having 64 elements or more. The convex shape of a curvilinear array results in larger time delay differences among elements. These large delay differences translate to larger numbers of wavelength offsets due to wrapping phase shifts, which can degrade the performance of Fresnel BF.

DAX was used to improve the performance of Fresnel BF in terms of contrast-to-noise ratio (CNR). This method uses cross-correlation coefficients as a pixel-by-pixel weighting to pass mainlobe dominated signals while suppressing sidelobe or clutter dominated signals. For Fresnel BF, these coefficients are obtained by cross-correlating the RF signals from the 2 receive channels.

We performed Field II simulations to characterize the performance of the system in terms of -6 dB beamwidths. Subsequently, we imaged an ATS tissue-mimicking phantom consisting of 6-mm-diameter cylindrical anechoic cysts and a 0.1-mm diameter custom-made nitinol wire target. Full synthetic aperture RF data sets sampled at 20 MHz were collected using a Verasonics system with an ATL C4-2 CLA and 2-cycle 3.3 MHz Tx pulse. Offline DAS BF was performed using Matlab to serve as a gold standard. Next, the RF data were beamformed using Fresnel BF, with and without DAX. CNR and lateral wire target size at f#=2 were used as image quality metrics.

Results

In the Field II simulations, the -6dB lateral beamwidths are 0.91, 1.17, and 1.33 mm for DAS BF, 4-phase BF, 8-phase BF, respectively. In experiment, without DAX, these values are 0.93, 1.27, and 1.24 mm and the CNRs are 5.58, 3.21, and 3.33, respectively. With DAX, the experimental -6 dB lateral beamwidths are 0.91, 1.27, and 1.21 mm and experimental CNRs are 10.34, 5.45, and 5.69, respectively.

Discussion and Conclusions

The results show that using DAX on Fresnel BF improved the CNRs by about 50%. In fact, the performance of Fresnel BF combined with DAX is similar to that of DAS BF in terms of CNR. Future work will involve improving the -6dB beamwidth and developing a prototype Fresnel BF system.

P5Aa-6

Reduction of Coherent and Incoherent Image Quality in Rectangular Boundary Arrays Due to Misalignment of Boundary Elements

Christian Coviello[1], Richard Kozick[2], Penny Probert Smith[1], Constantin-C. Coussios[1]; [1]Institute of Biomedical Engineering, Department of Engineering Science, University of Oxford, Oxford, United Kingdom, [2]Department of Electrical Engineering, Bucknell University, Lewisburg, PA, USA

Background, Motivation and Objective

Ultrasound imaging with a two-dimensional (2D) array can provide greater resolution in both transverse and axial dimensions compared to more common one-dimensional (1D) arrays. This advantage comes at a cost of not only greater expense but also system complexity arising from the squared increase in number of channels required for a fully filled 2D array. Using linear imaging techniques, sparsely populated arrays that have elements only on the boundary can be shown to synthesize arrays with fully populated interiors using the concept of the coarray. This is advantageous to transducer designers working to develop new arrays for ultrasound therapy - whether the application is targeted drug delivery or high-intensity focused ultrasound (HIFU) surgery - as both coherent and incoherent ultrasound imaging are often desired. One key design issue facing the transducer designer using this approach is the effect on imaging performance due to misalignment of the boundary subapertures of the array sides relative to each other. In a rectangular boundary array, this is the deviation of the array from a perfect rectangle. This misalignment can occur in the manufacturing process of the array due to misalignment of the top and bottom electrical contact layers that join to the piezoelectric material creating the array elements, anomalies in the dicing process, or alternatively due to misalignment between different piezo-materials if individual subapertures are constructed using separate piezoceramics or piezopolymers.

Statement of Contribution/Methods

In this work after introducing the concept of coarray design, we explore the degradation in performance caused by such misalignment through simulation examples. This is evaluated through the change in the beam shape of point-spread function (PSF), growth in sidelobe levels, and steered and unsteered beam patterns.

Results

Even small misalignments between the subapertures can cause distortion from the ideal PSF when using synthetic aperture techniques. If one side of rectangular boundary array is pivoted on a corner by a maximum of half a wavelength for example, the mainbeam can experience 5% growth along the axis of that pivot. Further results indicate that greater misalignment of subapertures by either rotation or displacement causes unexpected grating lobes and main beam distortion.

Discussion and Conclusions

A study of performance degradation when using rectangular boundary arrays is presented relating misalignment of subapertures to reduction in imaging quality for both coherent and incoherent imaging. Future work will focus on novel uses of boundary arrays for ultrasound therapy applications.

P5Aa-7

Capon Beamforming Applied to Second-Harmonic Ultrasound Experimental Data

Sven Peter Näsholm[1], Andreas Austeng[1], Are Charles Jensen[1], Carl-Inge Colombo Nilsen[1], Sverre Holm[1]; [1]*Department of Informatics, University of Oslo, Norway*

Background, Motivation and Objective

Capon beamforming, or minimum variance beamforming, is an adaptive method shown to increase the medical ultrasound image quality.

Tissue-harmonic imaging improves the image quality in many clinical situations. It relies on image formation by use of receive signals at the second-harmonic (2h) frequency band caused by nonlinear propagation effects.

Since the beginning of the last decade, several papers are published on adaptive ultrasound medical imaging. Primarily, simulated datasets generated e.g. by Field II are used, but to a minor extent experimental data has been exploited. However, presented results are only based on fundamental frequency data.

In this work, experimental ultrasound channel data was collected within the fundamental and 2h frequency bands. Both conventional delay-and-sum (DAS) and Capon beamforming are applied to the datasets, and the generated images are evaluated.

Statement of Contribution/Methods

Data acquisition was performed by a specially adapted GE Vivid E9 scanner. A 1.5D phased array probe was used for pulse transmission with f0=1.7 MHz focused at 8 cm depth. Receive IQ channel data was stored for filtering around the fundamental f0 as well as 2f0. The transmit beam was swept within +-45 deg.

This way 4 different images of a tissue mimicking phantom were generated since DAS and Capon were applied to both the fundamental and 2h datasets.

Results

Fig. 1 displays cross-sectional max-projection plots of the 4 produced images for a selected depth interval, within a selected azimuth angle interval. This phantom section covers a hollow cyst on the left and a strong point scatterer on the right. The gain of each image was adjusted to get the same average amplitude within the specular region between the cyst and the point scatterer.

Discussion and Conclusions

As expected due to the double receive frequency, the result plot indicates better point resolution and improved cyst edge detection for the 2h images than for the fundamentals. As published in other works, the fundamental Capon presents a similar enhancement relative to the fundamental DAS.

In addition to these confirmations, this work presents the novelty of Capon on experimental 2h data. The point resolution is enhanced and the cyst edge detection is improved for Capon as compared to DAS.

Analysis work is underway of an ex vivo pork dataset. The initial look suggests similar relations between Capon and DAS images.

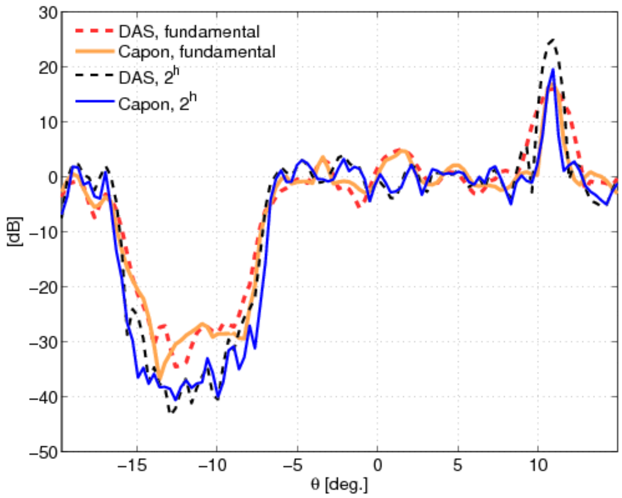

P5Aa-8

High frame rate imaging with diverging beam transmission and Fourier reconstruction

Jian-yu Lu[1], Hong Chen[1]; [1]Bioengineering, The University of Toledo, Toledo, Ohio, USA

Background, Motivation and Objective

The high frame rate (HFR) imaging method developed previously by the authors uses either steered plane waves or limited-diffraction array beams in transmissions and Fast Fourier transform in beamforming to reconstruct 2D or 3D images [1]. Although the method can achieve a high image frame rate, the image width obtained from each transmit beam is about the same as the dimension of the transducer aperture. To obtain a fan-shaped imaging area of a large viewing angle (such as -45 to 45 degrees), the number of transmission beams is increased or the image frame rate is reduced as the depth of image increases. To overcome such a problem, a diverging transmit beams is needed.

Statement of Contribution/Methods

In this paper, we conducted an experimental study using a diverging transmit beam in the HFR imaging method and compared it with the result obtained with steered plane wave transmissions. In the experiment, a home-made high frame rate imaging system [1] and a 2.5-MHz, 19.2 mm aperture, and 128-element broadband phased array transducer were used to obtain RF echo data. A commercial ATS539 tissue-mimicking phantom was used as a test object. Images reconstructed have a +/-45 degree field of view and 120-mm depth. The images were obtained with 11 transmissions at an image frame rate of 486 frames/second. Steered plane waves and diverging beams of a 6-degree diverging angle (using virtual focuses) were used in transmissions. Images were reconstructed with the HFR fast Fourier transform method [1].

Results

Results show that the quality of images reconstructed with the diverging beam (Fig (b)) with a 6 degree diverging angle is similar to that obtained with steered plane wave transmissions (Fig. (a)).

Discussion and Conclusions

Although the high frame rate imaging method introduced in [1] was developed based on transmissions with steered plane waves, the experiment shows that the method can also be used with a diverging beam of a small (6 degrees) diverging angle. This allows the high frame rate imaging method be used to image a large area at a deep depth, which is particularly useful for cardiac imaging where the size of available acoustic windows is small.

[1] Jian-yu Lu, Jiqi Cheng, and Jing Wang, "High frame rate imaging system for limited diffraction array beam imaging with square-wave aperture weightings," IEEE Transactions on Ultrason., Ferroelect., and Freq. Contr., vol. 53, no. 10, pp. 1796-1812, October 2006.

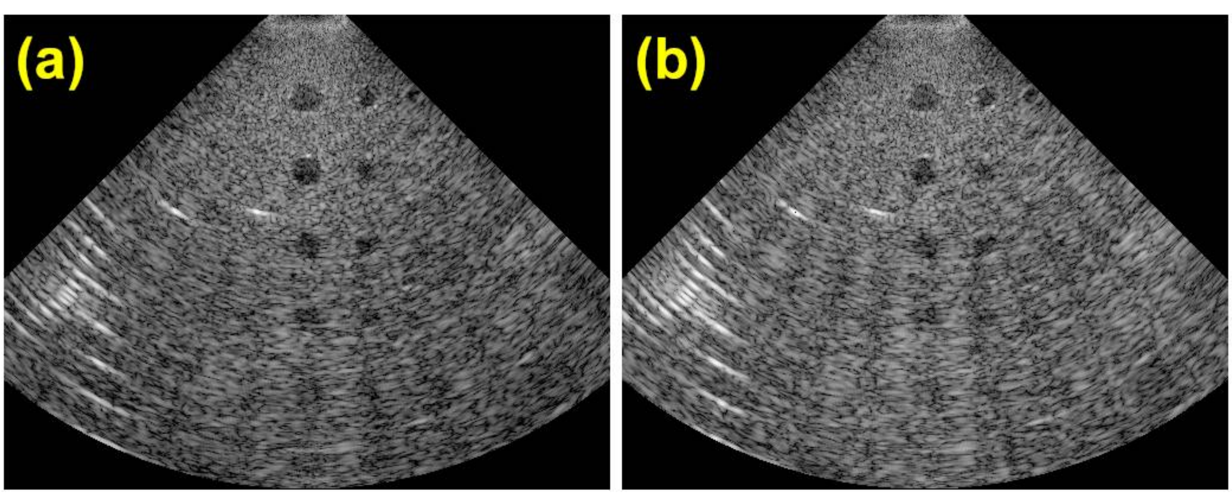

FRIDAY POSTER

P5Ab - Elastography: Clinical Applications

Carribean Ballroom III-V

Friday, October 21, 2011, 9:30 am - 1:00 pm

Chair: **Richard Lopata**
Eindhoven University of Technology

P5Ab-1

Quantifying Local Stiffness Variations in Thermal Ablations Using Dynamic Nanoindentation

Ryan DeWall[1,2], Tomy Varghese[1,2], Chris Brace[2]; [1]Department of Medical Physics, University of Wisconsin-Madison, USA, [2]Department of Biomedical Engineering, University of Wisconsin-Madison, USA

Background, Motivation and Objective

Strain imaging provides a qualitative measure of tissue stiffness and has shown success in monitoring thermal ablation procedures because of stiffness increases in ablated tissue resulting from tissue coagulation and dehydration. However, several studies have shown that strain images underestimate ablation area when compared to the area estimated from gross pathology images. Confident determination of the ablation boundary is essential to ensure complete treatment of the pathological target; misinterpreting the boundary could lead to tumor recurrence. Area underestimation on strain images may be a result of low modulus contrast at the ablation boundaries, as thermal ablation heating is more intense near the center of the ablation than at the periphery. Previous studies have elucidated the bulk mechanical properties of ablated volumes using dynamic compression testing, but local variations in the Young's Modulus have not been investigated. In this study, we use dynamic nanoindentation to quantify the storage modulus in radiofrequency ablations locally in order to better understand stiffness changes at the periphery of ablated volumes and how these might influence area underestimation on strain images.

Statement of Contribution/Methods

Local variations in the stiffness of ablated volumes were investigated using a dynamic nanoindentation approach. Regions of interest in eleven slices from radiofrequency ablations formed in porcine liver tissue in vivo were indented at 18 to 24 locations each, including the central zone of complete necrosis and more peripheral transition zones including untreated tissue. Each point was dynamically indented at 1 Hz to estimate the storage modulus, which approximates the Young's Modulus at low testing frequencies. The opposite face of the ablation was stained to reveal cell viability.

Results

At the ablation periphery, the storage modulus and modulus contrast with the untreated tissue were 3.1 ± 1.0 kPa and 1.6 ± 0.4, respectively. The stiffness and rate of stiffening increased moving towards the center of the ablation. Inside the "white zone" of the ablation, the region of complete cell necrosis, the storage modulus and modulus contrast were 36.2 ± 9.1 kPa and 18.3 ± 5.5, respectively.

Discussion and Conclusions

This study has provided insights into stiffness distributions within radiofrequency ablations by spatially mapping the storage modulus. The stiffness at the ablation periphery was close to that of the untreated tissue, which may explain the area underestimation of thermal ablations observed on strain images. Understanding ablation representation on strain images is crucial for accurate boundary delineation.

This work is supported in part by NIH grants R01 CA112192-04, R01 CA112192-S103, and T32 CA09206-31.

P5Ab-2

Ultrasound observation of the 4D (spatio-temporal) strain distribution in poroelastic media under sustained uniform and localised compressive loading

Jeremie Fromageau[1], Leo Garcia[1], Nigel Bush[1], Gary Berry[1], Jeffrey Bamber[1]; [1]Joint Department of Physics, Institute of Cancer Research and Royal Marsden NHS, Sutton, Surrey, United Kingdom

Background, Motivation and Objective

It is known that the response of a poroelastic material to a sustained applied unidirectional strain is an internal strain that varies with position and time in a manner that is characteristic of the capacity of the fluid to diffuse through the elastic porous structure. We have shown previously, with finite element analysis(FEA), that knowledge of the volume change, or equivalently the time-varying 3D deformation, is necessary to estimate poroelastic parameters of the medium. In addition, when the compression is applied with the ultrasound transducer, as is typical in clinical quasi-static elastography, strain in a homogeneous poroelastic medium will only mainly occur in the directions orthogonal to the load. This is not optimum for ultrasound strain measurement. In the current work we verify experimentally the capacity to observe 3D poroelastic strain relaxation during compression with a 3D ultrasound probe.

Statement of Contribution/Methods

FEA software (MARC Mentat, MSC Software) was used to model a cylinder with homogeneous poroelastic material constants. Two different loads and boundary conditions (BC) were simulated: i) a uniform constant displacement was applied to the whole top surface and only circumferential boundary was permeable, ii) a constant displacement was applied to a limited region of surface (i.e. indentation) and the sample was impermeable on all boundaries, simulating the pitting test used in the clinical evaluation of oedema. Experiments with similar geometry and BC were performed using a poroelastic matrix consisting of a mixture of agarose and cellulose, and water as the fluid. The phantom was observed with an ultrasound scanner (DIASUS, Dynamic Imaging), using a 7 MHz 3D probe, which was also used to apply the compression. The probe was connected to a mechanical test instrument (Instron, Inspec 2200), to record the applied force. The strain in the phantom was estimated from the RF echo signals using cross-correlation speckle tracking methods. To improve lateral and elevation strain estimations, both RF interpolation and beam steering were used.

Results

Experiments were in a good broad agreement with the FEA, showing a shrinking of the sample volume during the sustained compression. However the detailed behaviour differed between experiment and simulation in that time varying axial strains were observed. For the indention case, all strains were concentrated circularly around the region beneath the indentor, showing a similar shrinking of the volume with the time.

Discussion and Conclusions

It is the first time to our knowledge that the complete time-varying 3D deformation has been experimentally measured to characterise a relaxing poroelastic medium, demonstrating that, unlike the elastic case, the response to a sustained axial compression is a shrinking of the volume. The surprisingly small lateral and elevational strain that were measured are currently unexplained but may have been due to lack of homogeneity in phantom porosity.

P5Ab-3

Noninvasive Measurement of Bladder Muscle Activity Using Radiofrequency Ultrasound Strain Imaging

Tim Idzenga[1], Fawzy Farag[2], John Heesakkers[2], Wout Feitz[2], Chris de Korte[1]; [1]Paediatrics, Radboud University Nijmegen Medical Centre, Nijmegen, Netherlands, [2]Urology, Radboud University Nijmegen Medical Centre, Nijmegen, Netherlands

Background, Motivation and Objective

Lower urinary tract symptoms (LUTS) are divided into storage, voiding or post micturition phase symptoms. Bladder outlet obstruction (BOO) is characterized by increased detrusor pressure with decreased urine flow rate during voiding. Twenty five percent of men >60 y require surgical treatment for BOO. Pressure flow studies and filling cystometry are currently the standard diagnostic urodynamic tests for BOO. However, these tests are invasive with potential morbidity. A non-invasive method to diagnose BOO could make diagnostic procedures more patient friendly. With radiofrequency (RF) ultrasound it is possible to estimate deformation (strain) in biological tissue.

Statement of Contribution/Methods

In 7 asymptomatic volunteers and 1 symptomatic patient (all subjects signed an informed consent) we acquired RF ultrasound data of the detrusor muscle during the onset of voiding using a linear array transducer (11-3L, fc = 8.7 MHz, pitch = 135 um) and a Philips iE33 ultrasound system (Philips Medical Systems, Bothell, WA, USA) with a custom designed RF-interface. In each subject appr 8 s of data was acquired retrospectively (including the onset of voiding). In the patient this was done simultaneous to a pressure flow study. Axial strain was estimated using a coarse-to-fine 2D cross-correlation based algorithm and corrected for movements using a tracking algorithm. On the first acquired B-mode image a Region-Of-Interest (ROI) was drawn and the mean axial strain in this ROI was calculated, see figure.

Results

In all subjects axial strain in the detrusor muscle showed a decrease (indicating compression of the detrusor muscle) preceding urine flow. Prior to urine flow the isovolumetric intravesical pressure increases due to detrusor muscle activation. This suggests a negative correlation between strain and isovolumetric intravesical pressure in asymptomatic volunteers. In the symptomatic patient the correlation coefficient was -0.67, $p < .05$.

Discussion and Conclusions

Strain in the detrusor muscle during voiding can be estimated using RF ultrasound strain imaging. The estimated strain varied with the detrusor pressure. This suggests that strain imaging could be used in real-time monitoring of detrusor muscle activity. RF ultrasound monitoring of strain in the detrusor muscle can be a new imaging modality to study the pathophysiology of functional lower urinary tract disorders.

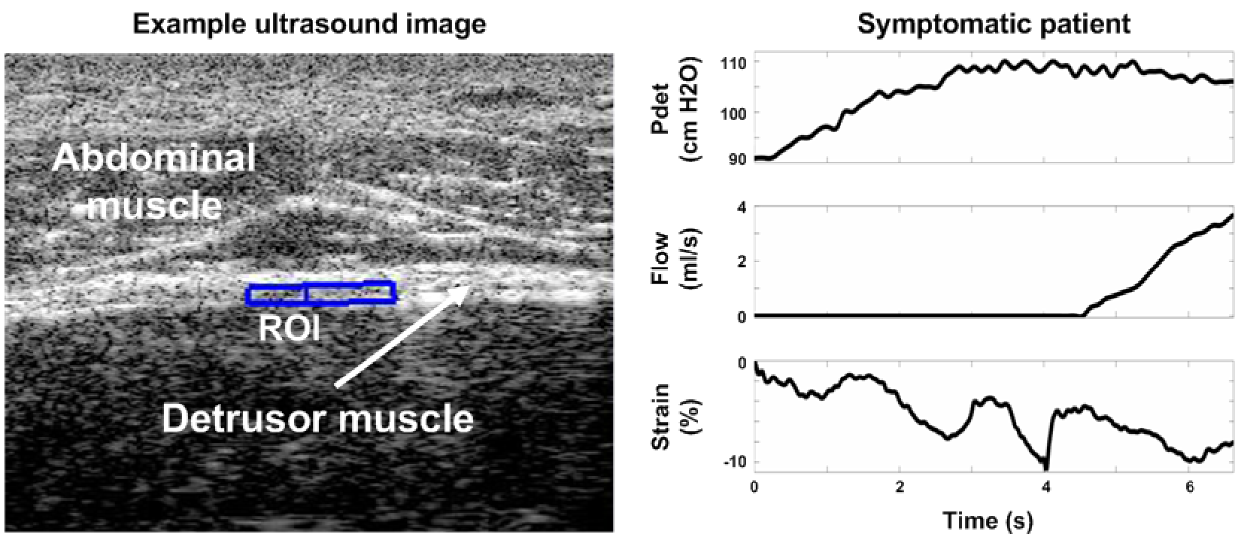

P5Ab-4

Imaging Feedback of Histotripsy Treatments With Ultrasound Transient Elastography

Tzu-Yin Wang[1], Timothy Hall[1], Zhen Xu[1], Brian Fowlkes[1,2], Charles Cain[1]; [1]Biomedical Engineering Department, University of Michigan, USA, [2]Radiology Department, University of Michigan, USA

Background, Motivation and Objective

Histotripsy is a cavitation-based therapy that mechanically fractionates soft tissues using high intensity short ultrasound pulses. During the treatments, the tissues progressively transform from soft solids to fluid-like debris. This paper investigates the feasibility of imaging this transformation with ultrasound transient elastography, and using the measured elasticity as a feedback metric for treatment progression.

Statement of Contribution/Methods

Histotripsy treatments were performed on 0.8% agar tissue phantoms and *ex vivo* kidneys using 3-cycle 750-kHz ultrasound pulses delivered by a therapeutic array at peak negative/positive pressure of 17/72 MPa and a repetition rate of 50 Hz. Lesions with different degrees of fractionation were generated by varying the treatment doses at 0, 100, 200, 300, 500, 1000, 1500 and 2000 pulses per treatment location. The lesion elasticity was measured with transient elastography, where a quasi-planar shear wave was first induced by three 200-µs focused ultrasound pulses generated by the therapeutic array at 5 MPa, and then tracked with ultrasound imaging. The image channel data were collected with a 5-MHz imaging probe at 3000 frames per second and processed offline. Based on the shear wave velocity calculated from the sequentially captured frames, the Young's modulus in the lesion area was reconstructed.

Results

The lesions were clearly identified on the elasticity images as an area whose Young's modulus progressively decreased with increasing doses (Fig A). The size and shape of the lesions detected on the images matched well with those of the lesion morphology (Fig B). As the lesions were fractionated with increasing numbers of pulses from 0 to 2000 pulses, the Young's modulus decreased exponentially from 22.1±2.7 to 2.1±1.1 kPa in the tissue phantoms (R^2=0.99, N=9 each), and from 34.9±6.1 to 4.0±1.6 kPa in the kidneys (R^2=0.98, N=5-9 each). Correspondingly, the tissues transformed from completely intact to completely fractionated with no recognizable structures as examined via histology (Fig C).

Discussion and Conclusions

Lesions produced by histotripsy can be detected with high sensitivity on elasticity images. As the decrease in the tissue elasticity corresponded well with the morphological and histological change, this study provides a basis for predicting the local treatment outcomes with transient elastography.

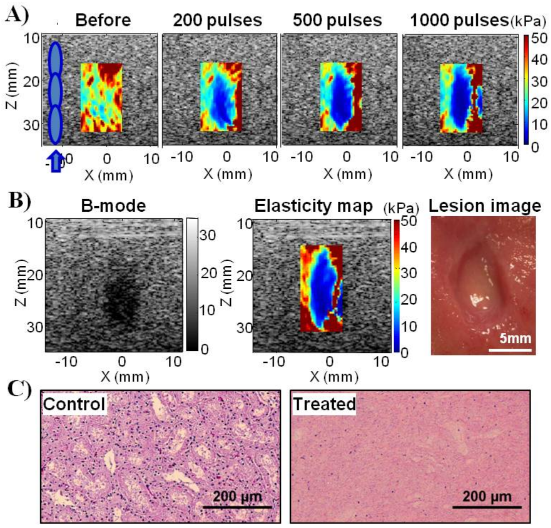

P5Ab-5

Feature based analysis of axial-shear strain imaging for breast mass classification

Haiyan Xu[1], Tomy Varghese[1,2], Jingfeng Jiang[2], Timothy Hall[2]; [1]Department of Electrical and Computer Engineering, University of Wisconsin-Madison, Madison, WI, USA, [2]Department of Medical Physics, University of Wisconsin-Madison, Madison, WI, USA

Background, Motivation and Objective

The feasibility of utilizing the normalized axial-shear strain area (NASSA) feature from axial-shear strain images to differentiate benign from malignant breast masses has been previously demonstrated for in-vivo studies. In this paper we utilize a larger radiofrequency (RF) data set acquired from different hospitals and scanned using different transducers to further investigate the classification performance. In addition to the NASSA feature, other features extracted from the axial-strain images such as the size ratio and stiffness contrast are also evaluated to test the discrimination performance.

Statement of Contribution/Methods

We report on results obtained using109 radiofrequency data sets acquired from three different hospitals with a benign/malignant (B/M) ratio 58/51 established via biopsy results. Of these data sets 38 (B/M: 30/8) were acquired from University of Wisconsin Breast Center using a Siemens SONOLINE Antares real-time clinical scanner equipped with a VFX13-5 linear array transducer with a center frequency of 5 MHz; 48 sets (B/M: 22/26) were from Charing Cross Hospital and 23 sets (B/M: 6/17) were from the Mayo Clinic that used a Siemens SONOLINE Elegra equipped with VFX 13-5 multi-row linear array transducer with a center frequency of 10 MHz. Free-hand palpation was performed for acquiring pre- and post-deformation RF data to generate the axial- displacements using a multi-level pyramid based two-dimensional cross-correlation motion tracking algorithm. The axial- displacement of best pre- and post- RF data frame pair selected based on the normalized cross correlation maps was utilized to estimate both the axial strain and axial-shear strain images. Since the mass boundaries on 19 of the B-mode images were isoechoic, the combined feature analysis was only performed on 90 data sets

.

Results

Receiver operating characteristic (ROC) analysis demonstrated the feasibility of using the combination of strain features in the classification, where the area under the curve (AUC) of the NASSA feature alone is 0.905, size ratio is 0.853, stiffness contrast is 0.728. The overall AUC of the combined features is 0.942 using a linear discriminant with leave-one-case-out approach for classification.

Discussion and Conclusions

The leave-one-case-out classifier provides conservative results since the case being tested is not included in the training set. Our preliminary results demonstrate the potential to utilize multiple features from both axial-strain and axial-shear strain images to improve breast tumor classification.

Acknowledgements: This work is supported by Komen grant BCTR0601153 and NIH-NCI grants 5R21CA140939 and R01CA112192-S103.

P5Ab-6

Fourier Domain and High Frame Rate based Elastography for Breast Nodules Investigation

Alessandro Ramalli[1,2], **Stefano Ricci[1]**, Elisabetta Giannotti[3], Dalmar Abdulcadir[3], Jacopo Nori[4], Olivier Basset[2], Christian Cachard[2], Piero Tortoli[1]; [1]*Electronics & Telecommunications, Università di Firenze, Italy,* [2]*Université de Lyon, CREATIS ; CNRS UMR5220 ; Inserm U1044 ; INSA-Lyon ; Université Lyon 1, France,* [3]*Department of Radiology, Careggi University Hospital, Firenze, Italy,* [4]*Senology Diagnostic Unit, Careggi University Hospital, Firenze, Italy*

Background, Motivation and Objective

The malignant/benignant characterization of breast nodules represents a main concern in current senology diagnostic practice. B-mode imaging plays a major role, but the specificity is still too low. Several studies show that elastography could help reducing false positive cases. A new freehand elastography method, based on a Fourier domain displacement estimator and a high frame-rate (HFR) averaging technique, has been recently shown to produce robust estimates on phantoms (Ramalli et al. 2010 Ultrasonics Symposium). In this study the proposed method is applied to the in-vivo investigation of breast nodules.

.

Statement of Contribution/Methods

At the senology diagnostic unit of the Careggi hospital (Florence, Italy), patients with breast nodules were investigated through B-mode and the proposed elastography method. The ULtrasound Advanced Open Platform (ULA-OP), recently developed in the MSDLab, was programmed to alternatively transmit focused beams for real-time B-mode imaging and plane waves for HFR imaging. The physician roughly located the nodule through B-mode scanning and then, gently moving the probe, applied a tissue compression while the radio-frequency (RF) ultrasonic echoes were acquired from the 64 central elements of the probe. HFR images were off-line obtained through the Fourier method (J-y. Lu, UFFC Trans, 44: 839-856, 1997). The axial displacement was obtained by comparing the phases of the RF signal spectra. An average displacement estimate was obtained from the HFR images.

.

Results

Elastography movies were obtained for 1 malignant and 6 benignant nodules. The lesions were clearly visible in all elastograms. A sample screenshot acquired in a 33-year old patient with a benign nodule is reported in the picture below. The lesion, highlighted by the arrow in the zoomed B-mode image (left), is clearly detected as harder region in the elastogram (center). The combined B-mode and elastography image is reported on the right.

.

Discussion and Conclusions

This study shows that the proposed method is capable of providing easily interpretable deformation images in clinical conditions, and is suitable, in particular, for breast nodules investigation.

.

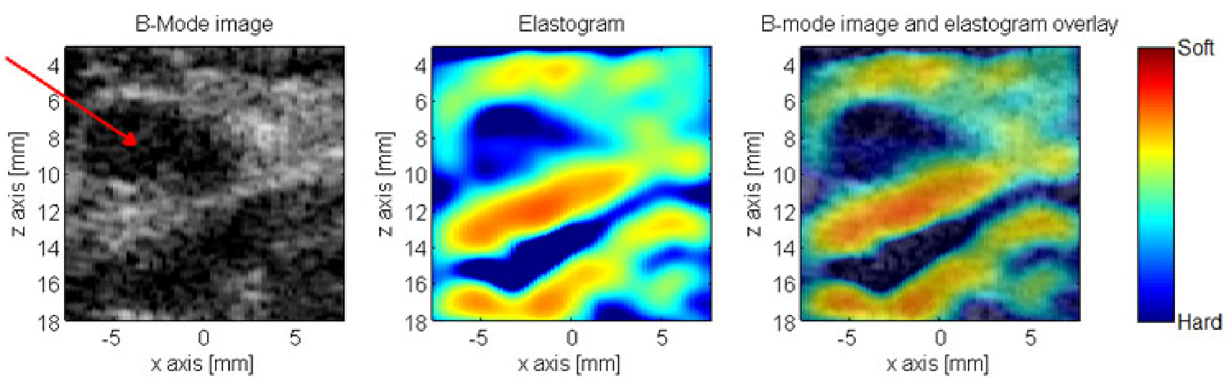

P5Ab-7

Non-invasive assessment of mechanical property changes with cell growth in a polymer-based vascular graft using ultrasound elasticity imaging

Debaditya Dutta[1], Keewon Lee[2], Jiao Yu[1], Yadong Wang[2], Kang Kim[1,2]; [1]Center for Ultrasound Molecular Imaging and Therapeutics, University of Pittsburgh and University of Pittsburgh Medical Center, USA, [2]Department of Bioengineering, University of Pittsburgh, USA

Background, Motivation and Objective

Mechanical strength is a key design factor in engineered vascular grafts for maintaining high burst pressure while preserving compliance of the native vessels. To date, most assessments are made invasively at the end of cell culture and hence such measurements cannot be correlated with cell growth. Therefore, non-invasive monitoring of the changes in mechanical properties as cells grow is essential to optimize the functionality of engineered vascular grafts. In this study, the mechanical property change of a cell-seeded polymer-based scaffold in a bioreactor is monitored using ultrasound (US) elasticity imaging (UEI).

Statement of Contribution/Methods

A porous tubular scaffold (6 mm dia., 0.6 mm thick) was fabricated from a biodegradable elastomer, poly(glycerol sebacate) (PGS) using salt fusion method. An ultrasonically compatible bioreactor was designed for culturing vascular cells on the scaffold in vitro. Fibroblasts were seeded in the abluminal space of the tubular scaffold with a density of 2M cells/sq. cm and cultured in a bioreactor for 10 days. On day 7, smooth muscle cells (SMC) were seeded in the lumen of scaffolds with a density of 2.7M cells/sq. cm and co-cultured for 3 days. The flow rate was maintained around 10 mL/min and the pressure was recorded. At the end of days 0, 5 and 10, US radio frequency frames were captured over 2 seconds (~ 6 cycles of flow motion) at 40 fps using a commercial US probe (6.5 MHz, Sonix TOUCH). 2D phase-sensitive speckle tracking was applied to estimate strain. Tensile stress measurements were performed on the excised construct using a mechanical testing device (MTS Insight).

Results

Along with time, gradual stiffness increase was observed. The axial displacement maps indicating overall distension of the graft wall next to B-scans after days 0, 5 and 10 are presented in the figure below. The average axial strain in the areas circled in the displacement maps demonstrate the decrease of compliance with time as fibroblasts and SMC grow. UEI results compare well with mechanical stretch test results.

FRIDAY POSTER

Discussion and Conclusions

With a limited number of samples and end points, the feasibility of non-invasive monitoring of the changes in mechanical properties with cell growth in a vascular graft was demonstrated. The stiffness increase with multiplication of flibroblasts and SMC agrees well with the mechanical measurements and previous scientific observations.

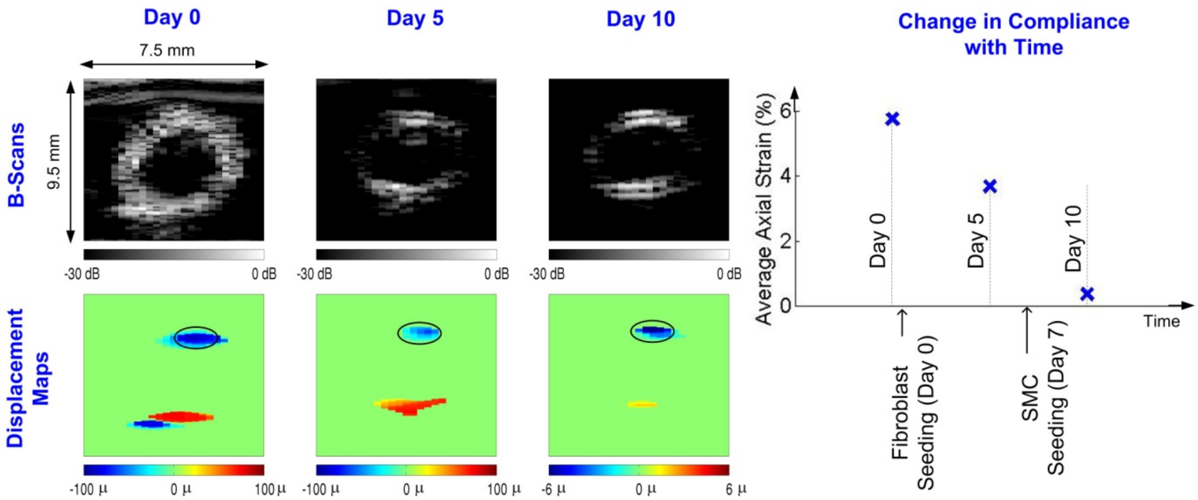

P5Ac - Harmonic & High Frequency Imaging

Carribean Ballroom III-V

Friday, October 21, 2011, 9:30 am - 1:00 pm

Chair: **Jeff Ketterling**
Riverside New York

P5Ac-1

Tissue Harmonic Imaging with CMUTs

Mathieu Legros[1], Anthony Novell[2], Ayache Bouakaz[2], Guillaume Férin[1], Rémi Dufait[1], Dominique Certon[2]; [1]*Vermon, Tours, France,* [2]*Université François Rabelais, UMR Inserm U930, CNRS ERL 3106, Tours, France*

Background, Motivation and Objective

For more than a decade, CMUTs have been widely investigated for conventional ultrasound imaging. Broad bandwidth and low noise capabilities of CMUTs are also attractive features for harmonic imaging. However, electrostatic nature of CMUTs is supposed to be a barrier for nonlinear imaging, since an inherent harmonic component is generated in the emitted signal and can be hardly differentiated from the nonlinear propagation part.

We propose to investigate the feasibility of tissue harmonic imaging with CMUTs and to explore and quantify the possible gain for image quality and diagnosis.

Statement of Contribution/Methods

A 5MHz 1D array CMUT probe with 128 elements was designed and developed for nonlinear imaging. The probe is compatible with an open system equipped with analog transmitters.

First, the harmonic levels of the CMUT probe was estimated through hydrophone measurements in the axial direction (0.4 to 70 mm), and confronted to the components of nonlinear propagation. The harmonic levels were measured for different values of bias voltage (0 to 80V), burst amplitude (20 to 80Vpp) and for 2 cycles excitation at both 2.5 MHz and 3.5 MHz. Compensation approaches were then applied to decrease the undesirable harmonic components of the CMUT probe.

Finally, harmonic images of a tissue mimicking phantom were realized with the optimal set of transmit parameters. A piezoelectric probe with an equivalent design was used to fulfill a benchmark of the harmonic imaging features.

Results

The maximum peak negative pressure obtained was 1.12MPa at 2.5MHz and 1.16MPa at 3.5MHz with all elements focusing at 40 mm. In all cases, the harmonic levels of the CMUT are in agreement with the electrostatic pressure applied on the electrical port of the probe and its transfer function. The compensation approach allows a significant reduction of the Harmonic to Fundamental Ratio, and the harmonic level generated by the CMUT could be reduced down to 15dB with the appropriate waveform excitation.

Using the compensation method, the ultrasound images realized at the optimal transmit parameters showed better details and a contrast improvement of 10dB. Furthermore, the SNR and the penetration depth have not been impacted by the applied technique.

Discussion and Conclusions

We found an optimal way to limit the undesirable harmonic components of the CMUTs to perform tissue harmonic imaging. In comparison with piezoelectric probes, figures of merit of the harmonic images obtained with CMUTs and compensation approach are similar. The method improves harmonic image quality and could be exploited with no loss in frame rate.

P5Ac-2

High Frequency Pulse Inversion Chirp Coded Tissue Harmonic Imaging

Jinhyoung Park[1], Ying Huang[2], Ching-Ling Lien[2], Kirk Shung[1]; [1]Biomedical Engineering, University of Southern California, Los Angeles, California, USA, [2]Surgery, Saban Research Institute of Children's Hospital Los Angeles, Los Angeles, California, USA

Background, Motivation and Objective

Pulse inversion chirp coded harmonic imaging that enhances signal to noise ratio (SNR) and contrast resolution has been implemented in an ultrasonic biomicrosope (UBM). The approach has been used to image amputated zebrafish heart. Zebrafish heart regeneration has attracted great interest in recent years. Soon after ventricular amputation, a blood clot forms immediately and it transforms to a fibrin clot which is replaced by regenerating myocardium. The clot has been traced histologically. However, these methods require sacrificing the fish and the comparison must be made on results from different samples obtained chronologically.

The approach was developed to allow non-invasive serial assessment of clot size. Previous studies suffered from poor image quality and did not allow clear boundary delineation between the heart and clot because the echogenicity of the heart and the background tissue is similar. In order to do so, an improved signal to noise ratio (SNR) and contrast resolution are desired. A pulse inversion based chirp coded tissue harmonic imaging (PI-CTHI) may be a promising for achieving this goal.

Statement of Contribution/Methods

The standalone frontend system was implemented on a prototype UBM. The beam sequence for the PI-CTHI is programmed into the system. Zebra fish with amputated heart was imaged with a 40MHz single element transducer.

Results

The clot can be better identified in the figures showing the PI-CTHI images. The blood clot size 3days after amputation has been deduced and compared to 7days. The clot was observed to disappear from the outer boundary showing the regeneration of epicardium.

Discussion and Conclusions

A standalone frontend system with PI-CTHI has been demonstrated in serial imaging of clot formation and dissolution following ventricular amputation in zebra fish.

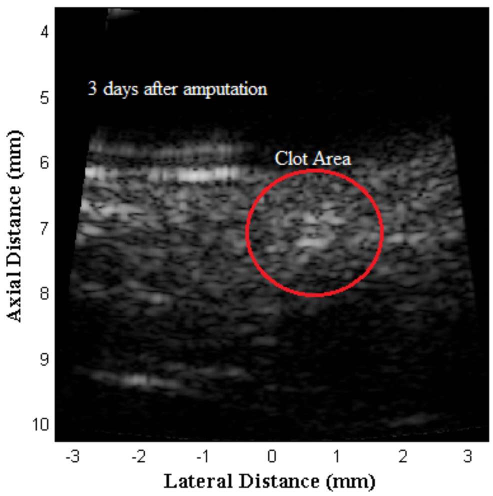

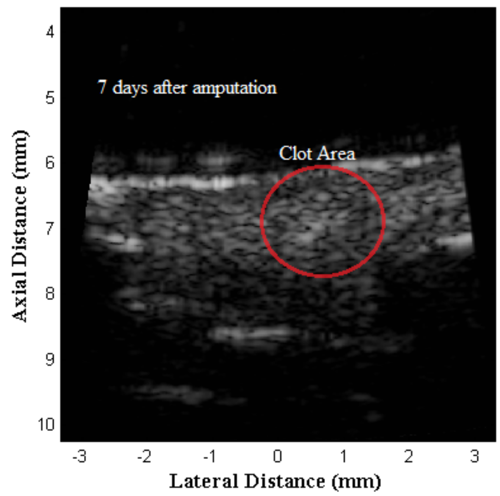

P5Ac-3

High-Frequency (75MHz) Ultrasound based Tooth Digitization using Sparse Spatial Compounding

Stefan Heger[1], Thorsten Vollborn[1], Joachim Tinschert[2], Stefan Wolfart[2], Fabrice Chuembou[1], Klaus Radermacher[1]; [1]Chair of Medical Ingineering, RWTH Aachen University, Aachen, Germany, [2]Clinic of Prosthodontics and Dental Materials, University Hospital Aachen, Aachen, Germany

Background, Motivation and Objective

Intraoral optical chair side scanners for computer integrated manufacturing of dental implants have been introduced to overcome the disadvantages of error prone and time-consuming conventional impression taking followed by gypsum based restoration. However, the presence of saliva and blood influence the accuracy of optical digitization and powder is often required to optimize the contrast level. Since optical scanners cannot penetrate gingiva, subgingival preparation limits need to be uncovered invasively (electrosurgery, retraction cords) prior to digitization. High frequency ultrasound (HFUS) based micro-scanning could be an alternative since it is less influenced by saliva, blood and gingiva. However, for accurate reconstruction of the tooth's surface, a time-efficient scanning concept yielding a sufficiently high and homogenously distributed data coverage is required.

Statement of Contribution/Methods

Whereas the occlusal surface as well as parts of the preparation boundary will be most probably covered by an occlusal scanning direction, scattered echoes from the posterior tooth surface are expected to be weak and diffuse due to the flat beam angle. As one solution to this challenge, missing information can be supplemented by superimposition of a limited number of additional scanning directions (sparse spatial compounding, SSC). In a laboratory set-up, a prepared molar has been scanned (30x30µm) using a calibrated 4-axis robot (3 trans., 1 rot.) and a single element HFUS transducer (75 MHz, f/# = 2) in tempered (37°C) degassed water. Three scanning concepts have been compared: a) occlusal (0°) scan, b) ±30° scan, c) a+b. Lateral resolution has been improved by adjusting the transducer's focal range to the entire depth of field (1mm steps).

Results

As expected, data coverage of the posterior surface is limited in mode a). This can be compensated by superimposition of two ±30° scans (mode c)) whereas in mode b) parts of the preparation limits are not entirely digitized (fig. 1). A threshold based image segmentation of the surface is shown in fig. 1 d).

Discussion and Conclusions

HFUS in combination with SSC is suggested to be a patient friendly alternative for intraoral data acquisition of prepared teeth. The development of a prototype scanner and the consideration of techniques for lateral resolution improvement (e.g. synthetic aperture focusing) are part of our on-going work.

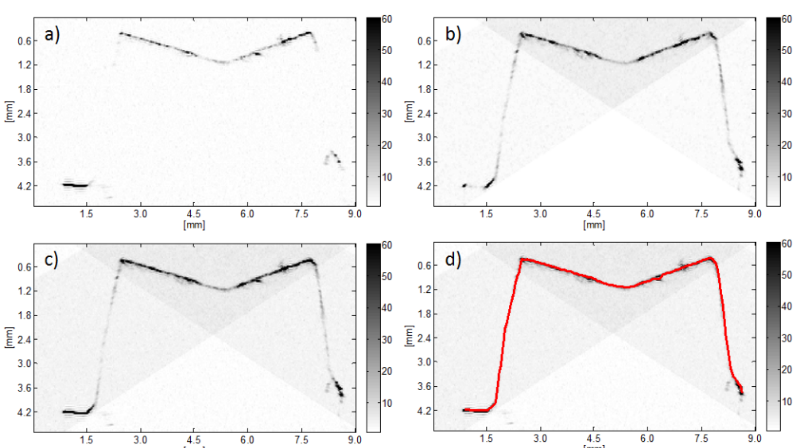

Fig.1: (a) occlusal scan, (b) ±30° scan, (c) superimposition a&b, (d) threshold segmentation of c)

P5Ac-4

Second harmonic imaging using synthetic aperture sequential beamforming

Yigang Du[1,2], Joachim Rasmussen[1], Henrik Jensen[2], Jørgen Arendt Jensen[1]; [1]Center for Fast Ultrasound Imaging, Dept. of Elec. Eng., Bldg. 349, Technical University of Denmark, Kgs. Lyngby, Denmark, [2]R&D Applications & Technologies, BK Medical Aps, Herlev, Denmark

Background, Motivation and Objective

Synthetic Aperture Sequential Beamforming (SASB) is a two-stage technique. The first stage obtains a set of conventional B-mode image lines with the same fixed transmitted and received focal point. Then the image is made by synthetic aperture focusing using the B-mode image lines in the second stage. A dynamic focus in both transmit and receive is achieved. The advantage of SASB is that the lateral resolution is improved independently of image depth. Second harmonic imaging can be made using the Pulse Inversion (PI) technique. With this method, two inverted pulses are transmitted to the same target subsequently and the signal is obtained by summing two received RF lines. Thus, the fundamental component of the signal is canceled out and the second harmonic component is doubled. The objective of the paper is to investigate the ultrasound imaging by combining SASB and PI.

Statement of Contribution/Methods

The investigation is made by an experimental Synthetic Aperture Real-time Ultrasound Scanner (SARUS). A linear array transducer (BK8804, from BK Medical Aps) is used to transmit and receive data from a wire phantom in water. There are 4 wires as point targets at the image depth of {22.5, 47.5, 72.5, 97.5} mm, respectively. Three different experiments are made using three different transmit foci, which are 10 mm, 25 mm and 50 mm, respectively from the transducer surface. A 2-cycle sine wave with a center frequency of 5 MHz is used as the excitation. The data received with and without PI from SARUS are beamformed using Dynamic Receive Focus (DRF) and SASB by a Beamformation Toolbox.

Results

The Full Width at Half Max (FWHM) (-6 dB) in both the lateral and axial directions for these four wire targets using different imaging algorithms (DRF, DRF+PI, SASB and SASB+PI) are calculated and shown in the figure. The average FWHM of these four points for each method is shown in the bracket of each legend in the figure. The Full Width at One Tenth Max (FWOTM) (-20 dB) is also investigated. The mean FWOTM of the four points, for DRF is 2.95 mm, for DRF+PI is 1.77 mm, for SASB is 2.01 mm and for SASB+PI is 1.43 mm.

Discussion and Conclusions

The combination of SASB and PI results in a much better resolution in the lateral direction than other imaging methods. The improvement for FWHM is 66%, 35% and 46%, for FWOTM is 52%, 19% and 29%, compared to DRF, DRF+PI and SASB, respectively. The axial resolution is also improved 24% on average by PI.

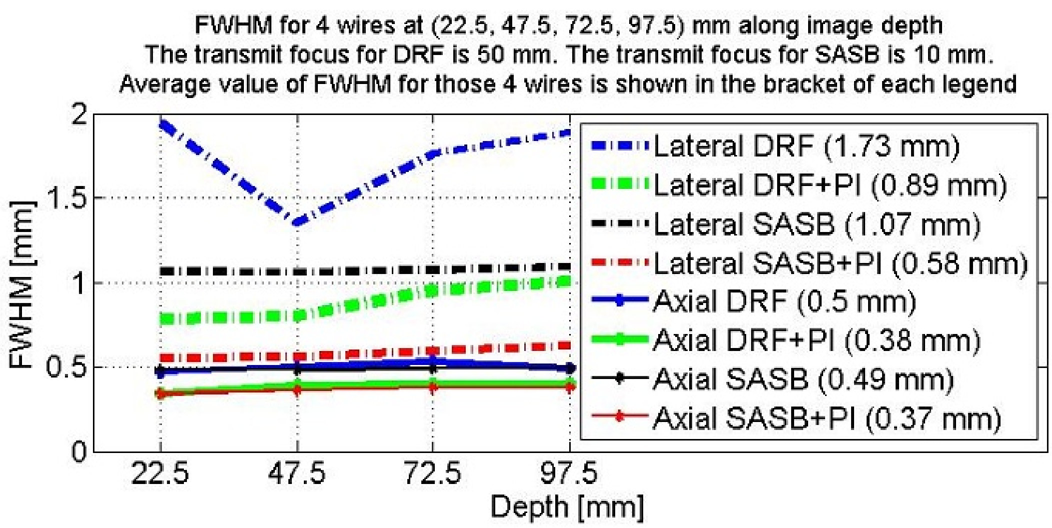

P5Ac-5

In vivo endoluminal ultrasound biomicroscopic imaging of colon lesions in mouse models of cancer and inflammation

Kelly Alves[1], Rossana Soletti[1], Marcelo de Britto[2], Dyanna Matos[3], Helena Borges[3], Mônica Soldan[4], João Machado[1,2]; [1]Biomedical Engineering Program - COPPE, Federal University of Rio de Janeiro, Rio de Janeiro, RJ, Brazil, [2]Post-Graduation Program in Surgical Sciences - Department of Surgery from School of Medicine, Federal University of Rio de Janeiro, Rio de Janeiro, RJ, Brazil, [3]Biomedical Science Institute, Federal University of Rio de Janeiro, Rio de Janeiro, RJ, Brazil, [4]Division of Gastroenterology, Endoscopy Unit, Clementino Fraga Filho University Hospital, Federal University of Rio de Janeiro, Rio de Janeiro, RJ, Brazil

Background, Motivation and Objective

Colorectal cancer (CRC) is the third most common cancer in the world and the third leading cause of cancer-related mortality in United States. Besides the bad prognosis of stage IV CRC, most malignant tumors are cured if diagnosed and properly treated during the disease early stage. CRC risk increases in patients with inflammatory bowel disease (IBD), a chronic inflammatory condition affecting about five million people worldwide. Mice models of CRC and IBD are used to understand the pathogenic mechanisms, to establish therapeutic and preventive measures and to evaluate diagnostic tools. Despite the great number of studies related to ultrasound biomicroscopy in small animals, very few images acquired from murine colon are presented in the literature. The development of minimally invasive tools to detect and monitor colon diseases could improve the studies in mice models for IBD and CRC. This has motivated the use of minimally invasive endoluminal ultrasound biomicroscopy (eUBM) to image colon lesions in mice, in vivo.

Statement of Contribution/Methods

This work contributes with a diagnostic imaging modality of the gastrointestinal tract of mice models for IBD or CRC. The eUBM uses a 40 MHz commercial transducer (Atlantis® SR Pro Imaging Catheter; Boston Scientific Corporation, Natick, MA) attached to a microcomputer controlled front-end electronics. The transducer rotates inside a catheter and ultrasound cross-sectional colon images are obtained with the catheter inserted into the working channel of flexible bronchofiberscope (FB 120-P; Fujinon, Tokyo, Japan). Water, injected through the catheter, was the ultrasound coupling medium. Colonic inflammation was obtained treating 6-7 weeks 129/SvJ mice with 3% dextran sulfate sodium (DSS) in the drinking water for 7 days. Colon tumors were induced treating the mice with a single i.p. injection of the carcinogen azoxymethane (AOM), followed by 3% DSS treatment.

Results

All colonic tissue layers in control mice (mucosa, muscularis mucosae, submucosa and muscularis externa) were detected by eUBM. Regarding DSS-treated mice, the eUBM images show a diffuse wall thickening that was undetected by colonoscopy performed simultaneously. Small adenomas and invasive adenocarcinomas were well visualized in eUBM images of AOM+DSS-treated mice. All eUBM images correlated well with the post-mortem colon histology sections.

Discussion and Conclusions

High frequency ultrasound imaging of large bowel has been used in humans with good results concerning the evaluation of deep penetration in early-stage neoplasic tumors. In mice, the goal is also to improve the accuracy between tumoral and non-tumoral lesions that are sub-epithelial lymphoid hyperplasia, undistinguished from adenomas and adenocarcinomas by colonoscopy alone. In this scenario, the eUBM system is a diagnostic imaging tool applicable to gastrointestinal tract of live small animal models for IBD or CRC.

Work financed by CNPq, CAPES and FAPERJ

P5Ac-6

Third Harmonic Imaging using a Pulse Inversion Technique

Joachim Rasmussen[1], Yigang Du[1,2], Jens Munk Hansen[1], Martin Hemmsen[1,2], Jørgen Arendt Jensen[1]; [1]Department of Electrical Engineering, Technical University of Denmark, Kgs. Lyngby, Denmark, [2]BK Medical Aps, Herlev, Denmark

Background, Motivation and Objective

Tissue harmonic imaging is used in the clinic to improve both lateral and axial resolution in B-mode images. In harmonic B-mode imaging, however, an overlap between the harmonic components in the received signal is often seen making filtration and separation of a harmonic component difficult, thus degrading the image quality. In this study a pulse inversion technique is used to suppress neighboring harmonic components for a more efficient separation enabling for a purely 3rd harmonic component B-mode image.

Statement of Contribution/Methods

Two pulses (regular pulse, 180° phase shifted pulse) are transmitted in turn for each image line. To suppress the even order harmonics each correlated pair (regular and phase shifted) of received responses are subtracted. This separates and enhances the 3rd harmonic component of the received responses, which in turn are matched filtered for displaying an image consisting of only the 3rd harmonic component. Raw channel data from an experimental synthetic aperture real-time ultrasound scanner (SARUS) is used to obtain image data of a water-filled wire phantom. A BK8820e 192 element convex array transducer is used with a transmit focal point set to 60 mm, an f-number of 1.5, and 65 active elements for transmit and receive. The excitation pulse is a 4-cycle sinusoid with a center frequency of 2 MHz. A total of 64 emissions are made enabling for 32 image lines. B-mode images are made for beamformed raw data and matched filtered fundamental, 2nd, and 3rd harmonic components. Full Width at Half Max (FWHM) values in the lateral and axial directions are measured for each detectable wire in all B-mode images.

Results

The lateral FWHM values for the raw B-mode, fundamental, 2nd harmonic, and 3rd harmonic component images for the wire at 67 mm depth close to the transmit focal point are {1.92 mm, 2.39 mm, 1.69 mm, 1.59 mm} respectively. The axial FWHM values are {0.52 mm, 1.64 mm, 1.41 mm, 1.36 mm} respectively. The results show that both lateral and axial FWHM values decrease as the order of the imaging component increases. For the 3rd harmonic component image the lateral FWHM value is 33% lower than the fundamental component image and 6% lower than the 2nd harmonic component image. A similar 17% and 4% decrease is seen respectively in the axial FWHM values. The 3rd harmonic component image shows a 17% decrease in the lateral FWHM and a 160% increase in axial FWHM compared to the FWHM values of the raw B-mode image.

Discussion and Conclusions

The ratio between the lateral and axial FWHM values is 1.17 for the 3rd harmonic component and 3.69 for the raw B-mode image. The ratio describes the appearance of the wire in the B-mode image. A ratio close to 1 indicates that a round dot is seen (as in the 3rd harmonic component image) whereas a higher ratio indicates a disc is seen (as in the raw B-mode image). The overall resolution is, thus, improved by using the pulse inversion technique to isolate the 3rd harmonic component for imaging.

P5Ad - Multimodality Image & Image Quality

Carribean Ballroom III-V

Friday, October 21, 2011, 9:30 am - 1:00 pm

Chair: **Jorgen Jensen**
Technical Univ. of Denmark

P5Ad-1

Imaging ultrasound field and shear wave with a CCD camera

Yi Cheng[1], Lipei Song[2], Rui Li[1], Daniel Elson[2], Meng-Xing Tang[3]; [1]Department of Bioengineering, Imperial College London, United Kingdom, [2]Department of Surgery, Imperial College London, United Kingdom, [3]Department of Bioengineering, Imperial College London, London, United Kingdom

Background, Motivation and Objective

Measurement of an ultrasound field is typically done with a hydrophone in a point by point manner. The measurement of shear waves has been done using either a sophisticated fast speed scanner, interferometric methods, or the decorrelation of CCD camera images. Here we propose a new method to use a CCD camera setup and image contrast to measure both the ultrasound field, and the shear wave generated by Acoustic Radiation Force.

Statement of Contribution/Methods

Tissue mimicking phantoms were exposed to a 532nm laser and a 2ms ultrasound burst generated by a 5MHz focused transducer. The ultrasound focus was aligned laterally with the edge of the phantom so it bisected the ultrasound beam. A CCD camera was used to record images with the edge of the phantom in focus and the difference in CCD image contrast before and after the ultrasound burst was obtained. The timing and the length of the CCD exposure were varied.

Results

By using a short CCD exposure time (0.1ms) and acquiring images at the beginning of the ultrasound burst, a map of the ultrasound field was obtained (Figure1a). By delaying the timing of CCD measurements and using a longer exposure time (2ms), the shear wave generated by the ultrasound burst can be visualised as a function of time (Figure1b&c).

Figure 1 CCD images of ultrasound field and shear wave propagation

(a) The near field is on the left, the far field is on the right;(b) Image taken 0.5 ms after the ultrasound burst;(c) Image taken 4.5 ms after the ultrasound burst

(b)

Discussion and Conclusions

The proposed method provides a new way of charactering the ultrasound field and shear wave propagation in vitro. It has the advantage of mapping the whole field in one go. The measurements reflect the real local field at the presence of tissue attenuation. The measurement of shear wave propagation is also able to provide tissue elastic properties.

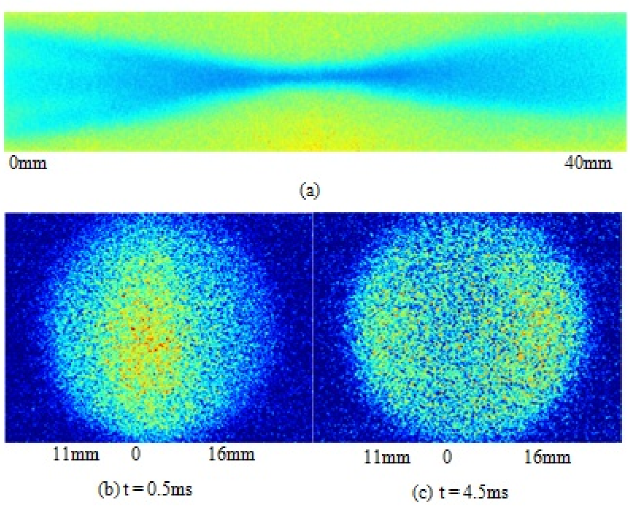

P5Ad-2

Multi modality fusion imaging technique for laparoscopic surgery guiding

Satoki Zenbutsu[1], Tadashi Yamaguchi[1], Tatsuo Igarashi[2]; [1]Research Center for Frontier Medical Engineering, Chiba University, Japan, [2]Graduate School of Engineering, Chiba University, Japan

Background, Motivation and Objective

A new laparoscopic surgery method was proposed at Chiba University. In this method, the inside of an abdominal cavity of the patient is filled with physiological saline instead of gas. An advantage of this method is that the internal structures can now readibly be imaged during surgery using a conventional ultrasound machine. The doctor and operators can easily monitor the progress of the surgery by using overlapped ultrasound and laporascopic images.

Statement of Contribution/Methods

The 3-D registration of the two different imaging modalities is performed using an iterative closest point (ICP) algorithm based on the surface shape of the internal organs. The 3-D optical image is formed from two laparoscopic images obtained from two different view angles. Then, the surface shape of the internal organs is formed by a nonlinear deformation of these images. The 3-D ultrasonic image is acquired from the body surface by imaging the inside of the abdominal cavity using adjacent scans. A morphological operation was applied to reduce speckle and facilitate the detection of surface shape of the organ. The ICP algorithm is implemented by initially selecting corresponding landmrak voxels in both 3-D images. Then, the rigid transformation (i.e., rotation and translation, 6 degrees of freedom) minimizing the Euclidean distance between the landmarks points is found by iterative optimization.

Results

The proposed fusion technique was evaluated in an in vitro experiment with a tissue mimicking phantom (Fig. 1a). The size of each optical laporoscopic image was 50 * 50 mm (640 * 480 pixels, Fig. 1b). The 3-D ultrasonic data was obtained from 300 B-mode images (50 mm in depth by 38 mm laterally) acquired every 0.2 mm with a linear array probe (9.3 MHz center frequency). The fusion of the 3-D optical and US images permitted to display the surface and internal structure of the phantom with a maximum error of 2.6 mm (Fig. 1c). Total processing time was 4 min on a personal computer (Intel Pentium 4 processor, 3-GHz CPU).

Discussion and Conclusions

The surgeon confirmed that the internal organ structure was accurate and could be obtained from arbitrary imaging planes during the operation using the proposed method. Therefore, this method provides a valuable tool to improve the safety and the precision of laparoscopic surgeries. Fture works will focus on reducting the processing cost to permit real-time use in the operating room.

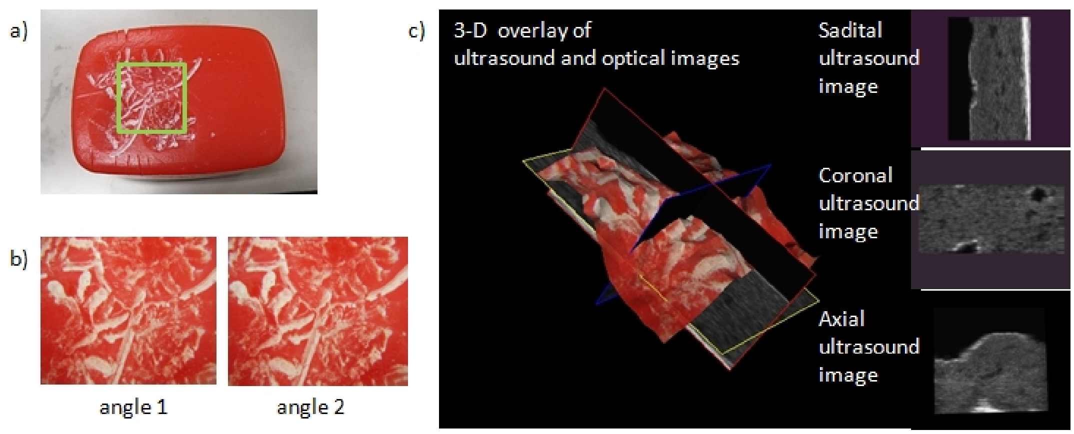

Figure. 1 (a) Tissue mimicking phantom made of agar.
(b) Two laparoscopic images obtained from two different view angles.
(c) Fusion image obtained using the ICP algorithm.

P5Ad-3

Compound imaging using Synthetic Aperture Sequential Beamformation

Casper Bo Jensen[1], Jonas Jensen[1], Martin Christian Hemmsen[1,2], Jens Munk Hansen[1], Jørgen Arendt Jensen[1]; [1]Center for Fast Ultrasound Imaging, Dept. of Elec. Eng., Technical University of Denmark, DK-2800 Kgs. Lyngby, Denmark, [2]R&D Applications & Technologies, BK Medical, DK-2730 Herlev, Denmark

Background, Motivation and Objective

Synthetic Aperture Sequential Beamforming (SASB) is a technique with low complexity and has the ability to yield a more uniform lateral resolution with range. However, the presence of speckle artifacts in ultrasound images degrades the contrast. In conventional imaging speckle is reduced by using spatial compounding at the cost of a reduced frame rate. The objective is to apply spatial compounding to SASB and evaluate if the images have a reduced speckle appearance and thereby an improved image quality in terms of contrast compared to ordinary SASB.

Statement of Contribution/Methods

Using the simulation software Field II, RF data are acquired for a phantom with cysts at different sizes and scattering levels. 192 scanlines are recorded for five steering angles (0, ±2, ±4 degrees) using a 192 element linear array transducer. SASB is performed for each angle using a rectangular grid in the second stage beamformation. After envelope detection the five second stage images are added to form the compounded image. Using a ProFocus scanner and the 8804 linear array transducer (BK Medical, Herlev, Denmark) measurements of a phantom containing water cysts are obtained to validate the simulation results. The setup is the same as in the simulations and SASB second stage beamformed data are processed offline for each of the five angles. Contrast-to-noise ratio (CNR) and speckle-to-noise ratio (SNR) are extracted for the compounded image and the reference image (ordinary SASB).

Results

CNR was calculated for the simulated cysts at depths of 40, 50, 60, 70 and 80 mm. On average the CNR was improved by 33.2% compared to the values obtained from the reference image. For regions of increasing depth SNR was on average increased by 9.3%. Results from the simulation were confirmed by calculations on the measured data. CNR of cysts at depths from 18 to 78 mm with a separation of 10 mm was on average improved by 45.9%. On average an improvement of 16.6% in SNR was obtained. The calculations along with visual inspection revealed larger improvements in deeper regions, and the compounded image for the measured phantom showed a 3 mm diameter cyst not detectable in the reference image.

Discussion and Conclusions

Compounding applied to SASB improves CNR and SNR results in images with a reduced speckle appearance. This was shown for simulations and confirmed on measured data.

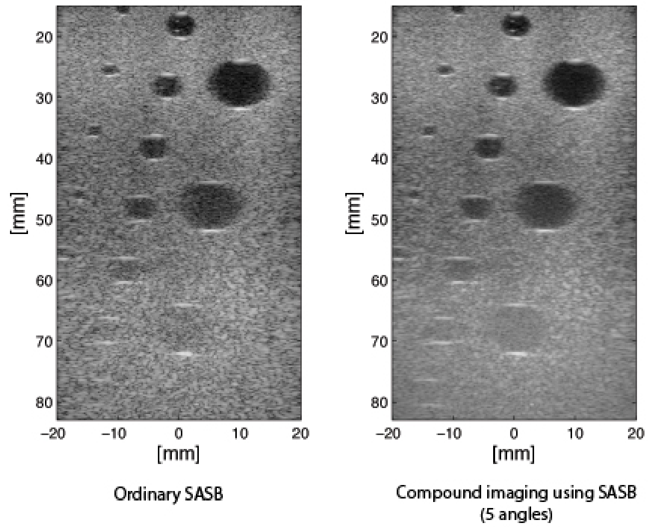

P5Ad-4

Characterize the vasculatures distribution of murine tumors between center and peripheral regions based on Doppler ultrasound and immunofluorescent analysis

Jia-Jiun Chen[1], Chi-Shiun Chiang[1], Ji-Hong Hong[2], Chih-Kuang Yeh[1]; [1]Biomedical Engineering and Enviromental Sciences, National Tsing Hua University, Hsinchu, Taiwan, [2]Department of Radiation Oncology, Chung Gung Memorial Hospital-Linkou, Taoyuan, Taiwan

Background, Motivation and Objective

The change of tumor vasculatures is sensitive to the prognosis of clinical chemotherapy because the efficiency of anticancer drugs delivery relies on the perfusion of tumor vasculatures. However, the heterogeneity of tumors leads to the insufficient drug concentration in tumor center; reducing the curability of chemotherapy. Therefore, investigating the spatial flow information in tumors is helpful for understanding of the progression of tumor vasculatures. In this study we propose a method for characterizing the vasculatures distribution within center/peripheral tumor regions.

Statement of Contribution/Methods

Eight mice with murine prostate tumors on 7th (early stage) and 11th (late stage) days after inoculation were introduced to monitor dynamic changes of vasculatures. The tumor perfusion was examined with power Doppler images by 25-MHz ultrasound and afterward vasculatures patterns were also estimated by immunofluorescent CD31staining. To quantify the spatial distribution of tumor vasculatures, vasculature signals with different fractions of periphery area were cumulated (Figs. (a-d)) and the power-law transformation model was applied to fit the outcome data. The rising rate (γ) equal to 1 means the homogenous perfused tumors, and inversely rising rate lower than 1 represents the most vasculatures in the presence of tumor periphey region.

Results

Figures (a-b) show the spatial distributions of tumor vasculatures at early and late stages by power Doppler images, and the corresponding immunofluorescent results are shown in Figs. (c-d). In Fig. (e), the rising rates in figures a-b are 1.13±0.19 and 0.66±0.10, respectively. However, there was no significant difference in immunofluorescent results between early (1.14±0.21) and late tumors (1.09±0.04). The results revealed that in early stage the perfusion in early stage of tumor growth was homogenous, whereas, in late stage was heterogeneous with evenly vasculature distribution.

Discussion and Conclusions

In conclusion, the rising rate of power-law transformation model can be used to depict the changes in tumor microenvironment. Potential applications include exploring the mechanism of tumor vasculature growth and evaluating of therapeutic responses after chemotherapy.

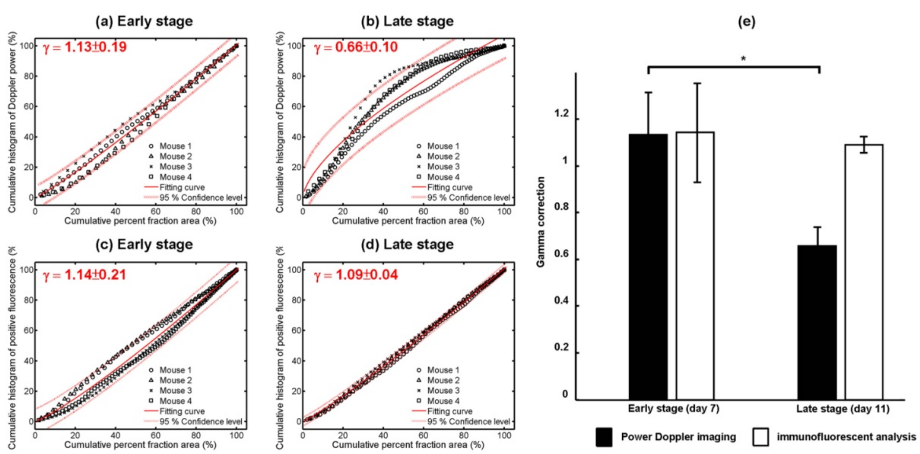

P5Ad-5

White Light Correction in Ultrasound Imaging

Kajoli Krishnan[1], Johan Kirkhorn[2]; [1]Diagnostic and Biomedical Technologies, GE Global Research, Bangalore, Karnataka, India, [2]GE Healthcare, Norway

Background, Motivation and Objective

Resolution with penetration in the field of view (FOV) is key to high quality diagnostic ultrasound. In principle, this can be attained through a uniformly narrow main beam with low side-lobes over maximum depth of tissue. However, in a clinical setting, image quality is ultimately limited by the absence of apriori knowledge of frequency and depth dependent attenuation. The echo signal spanning several magnitudes is compressed into an appropriate gray scale for visual acuity. While several post-processing methods have been proposed to meet the end-user's perceptual demands, there continues to exist a need to both design and quantify physics-based corrections to image quality.

Statement of Contribution/Methods

Drawing from frequency domain methods and motivated by the near-similar propagation of the frequencies of white light in pure water at small depths, we have devised a white light correction (WLC) to compensate for frequency-dependent propagation effects in cardiac ultrasound. WLC determines the frequency content of the complex time domain IQ data at every depth interval with resolution that is permissible by the Nyquist sampling rate, identifies the dominant frequency in the FOV, equalizes the effect of attenuation and aligns the position of impedance mismatch at all frequencies to that of the dominant frequency through an incoherent frequency and depth dependent scale factor. The modified signal is finally inverse Fourier transformed back into a time domain signal, envelop detected, log compressed and scan converted to generate a WLC image. WLC has been applied to the 2nd harmonic band of nine frames of two self-scanned parasternal long axis acquisitions of the heart. The readings were taken several weeks apart. Received noise without any transmit firing was also acquired. WLC has been evaluated for distance-to-noise (DTN) at every frequency and depth point in the FOV, signal-to-noise ratio (SNR) in the left ventricle (LV), right ventricle (RV), septum (IVS) and posterior wall (PW) and contrast-to-noise ratio (CNR) between these regions.

Results

A comparison of the distribution of signal in array sizes 20X10 placed in the LV, RV, IVS and PW shows an enhancement of SNR ranging from 0.7 – 4.3 dB and corresponding reduction in CNR between cardiac chambers and walls by 3% - 31% compared to the 2nd harmonic images. Likewise an analysis of DTN performance of WLC shows up to 22% mean improvement over depth for the less dominant frequencies compared to the 2nd harmonic signal.

Discussion and Conclusions

The experiments suggest that WLC signal extends the dynamic range, improves penetration and beam uniformity at the cost of contrast. Enhancement of dynamic range gives the appearance of improved contrast to the WLC images despite the reduction of contrast in the WLC signal compared to the 2nd harmonic. WLC images are well visualized at small scales. Improvements in mapping the WLC signal to images could enhance their perceptual quality for standard sized displays.

P5B Surface Acustic Wave Sensors

Carribean Ballroom III-V

Friday, October 21, 2011, 9:30 am - 1:00 pm

Chair: **Pierre Khuri-Yakub**
Stanford University, USA

P5B-1

Low-loss SAW gas sensor with self-temperature-compensation characteristics for sensor network

Jun Hosaka[1], Mitsutaka Hikita[1]; [1]Faculty of GE, Kogakuin University, Shinjuku-ku, Tokyo, Japan

Background, Motivation and Objective

We developed the novel SAW gas sensor with self-temperature-compensation characteristics assuming -40 to 80 degree C for garage use (Ref. 1). However, the sensor network requires losses less than 3dB for gas sensors. We have proposed a new structure based on a lattice-type circuit to meet the requirement.

Statement of Contribution/Methods

In the developed structure (upper figure) shown in Fig. 1, D-1 is the sensor delay line, while D-2 and D-3 provide the standard phases with pi/2 difference. The 1st- and 3rd-harmonic frequencies can offer wide dynamic range, and ideal phase characteristics at both frequencies can be achieved at wide temperature range, as shown in the lower figures in Fig. 1. However, extreme low-loss characteristics are necessary for use in the sensor network. A new low-loss resonator-type delay line has been invented to meet this requirement to replace the ones in Fig. 1.

Results

Resonators with spaces of P and P+wavelength/4 whose impedances are Z1(1) and Z2(1) are connected in a lattice circuit as shown in the upper figure in Fig. 2. Z1(2) and Z2(2), whose spaces are shorter by wavelength/8 than Z1(1) and Z2(1) respectively, are also connected as shown in the lower figure. Simulation results shown in right figures show that the low-loss characteristics and phase difference of pi/2 between two delay lines can be achieved, which is essential characteristics for the proposed self-temperature-compensation SAW sensor.

Discussion and Conclusions

When we introduce the lattice-type delay lines shown in Fig. 2 to the structure in Fig. 1, we can achieve not only self-temperature-compensation characteristics but also dramatic loss reduction. Balanced input and output can also be very useful for low-power operation due to their noise-cancelation characteristics. Experimental results will be presented.

1. M. Hikita, K. Kato, et al. in IEEE Ultrason. Symp. Proc., pp. 2496-2499, 2009.

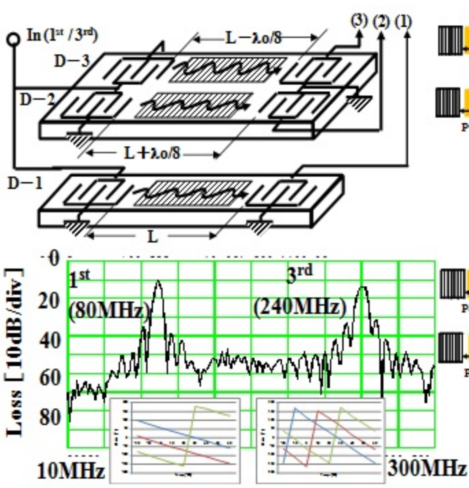

Fig.1 The developed sensor

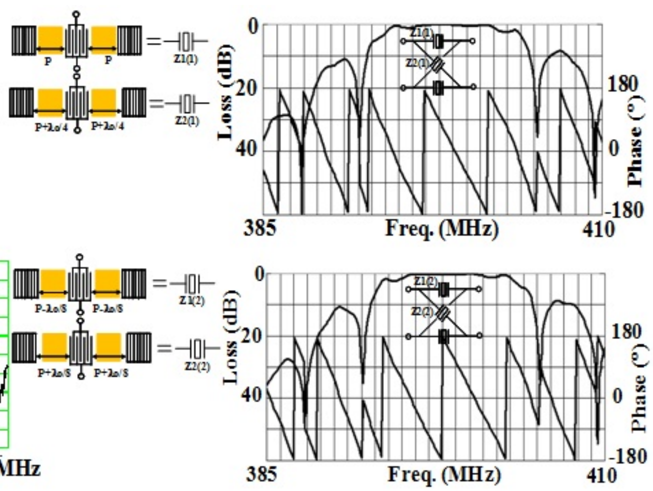

Fig.2 New low-loss delay lines for sensor

P5B-2

Characterization of Langasite for Application in High Temperature SAW Sensors

S. Sakharov[1], **N. Naumenko**[2], A. Zabelin[1], S. Zhgoon[3]; [1]Fomos-Materials, Moscow, Russian Federation, [2]Moscow Technical University of Communication & Information Science, Moscow, Russian Federation, [3]Moscow Power Engineering Institute, Moscow, Russian Federation

Background, Motivation and Objective

Langasite (LGS) is considered as the most promising material for wireless high temperature sensors utilizing SAW resonators. These applications require accurate characterization of LGS in a wide range of temperatures, up to 700°C. Previously reported sets of LGS material constants comprise the first- and second-order temperature coefficients. Our preliminary investigation of SAW resonators with W, Pt and Ir electrodes built on different orientations of LGS in a wide interval of temperatures has revealed that these constants are able to provide good agreement with experiments only up to 250°C. This paper reports on the results of further experimental and theoretical investigation of LGS as material for high temperature SAW sensors and is aimed at characterization of LGS in the temperature interval from 25° to 700° C based on comparison of experimental data with simulations performed with different published sets of material constants.

Statement of Contribution/Methods

For experimental investigation of LGS temperature behavior, the resonators with iridium electrodes of different thickness were fabricated on few orientations of LGS and resonant frequencies were measured as functions of temperature, in the temperature interval from 25° to 500-700°C. The measured dependences were compared with simulations performed with two material data sets. One of these sets was found to provide much better agreement with experimental temperature dependences for all analyzed orientations. In addition, we found that the function, which characterizes the difference between experimental and simulated temperature deviations of frequency, looks similar for few analyzed orientations and can be referred, for example, to temperature dependence of Ir constants. The nature of this difference is discussed.

Results

Due to improvement of fabrication quality of SAW resonators with Ir electrodes and measurements of resonator parameters within wide interval of temperatures, we were able to adjust the temperature coefficients of material constants for better agreement between simulated and measured temperature dependences of resonator parameters.

Discussion and Conclusions

The refined temperature coefficients can be used for more accurate prediction of temperature characteristics in other orientations of LGS, which are potentially attractive for SAW sensors. Since for high temperature applications Pt is better material than Ir, we also compared the simulated temperature characteristics of SAW resonators using these two electrode metals.

This research has been performed within the SAWHOT Project, a corporate project of European and Russian Universities and Industrial partners. The research leading to these results was partially funded by the Ministry of Education and Science of the Russian Federation and by the European Community's Seventh Framework Programme [FP7/2007-2013] under Grant Agreement [NMP4-SL-2009-247821].

P5B-3

Resonance Properties of Surface Acoustic Wave Resonator in Supercritical CO_2

Shoji Kakio[1], **Katsuhiro Hayashi[1]**, Eiichi Kondoh[1]; [1]Interdisciplinary Graduate School of Medicine and Engineering, University of Yamanashi, Kofu, Yamanashi, Japan

Background, Motivation and Objective

A supercritical fluid is a fluid at a temperature and pressure above its critical point (31.1 °C and 7.29 MPa for CO_2) in which a gas phase and a liquid phase coexist. Supercritical CO_2 functions as a moderate solvent, has zero surface tension, and has high permeability in fine structures. These properties are regarded as ideal for processing nano- and microscale substances. A potential problem of supercritical fluid processing is density fluctuations. By utilizing a surface acoustic wave (SAW), it may be possible to realize a sensor for measuring the density fluctuation. In this study, the resonance properties of a shear-horizontal-type SAW (SH-SAW) resonator was measured in high-pressure CO_2.

Statement of Contribution/Methods

The SH-SAW resonator consisting of an interdigital transducer with the wavelength λ of 20 µm, and 30.5 finger pairs and grating reflectors with 50 metal strips was fabricated using an aluminum film on 36°Y-X $LiTaO_3$. A flow of liquid CO_2 was induced into a chamber in which the sample was set using a liquid feed pump. The resonance property was measured using a network analyzer as a function of the pressure in the chamber, which was controlled from 0.1 to 10 MPa by a back-pressure regulator. The temperature in the chamber was monitored by a thermocouple. Furthermore, to measure the change of the resonance property due to only pressure, N_2 gas instead of CO_2 was also induced into the chamber.

Results

The resonance frequency f_r and antiresonance frequency f_a decreased with increasing pressure, and rapidly decreased between the pressures of 5 and 6 MPa. The rates of change of f_r and f_a reached -1,020 and -560 ppm, respectively. Marked changes in the resonance impedance and antiresonance impedance were also observed between the pressures of 5 and 6 MPa. The monitored temperature in the chamber was stable at approximately 18 °C.

Discussion and Conclusions

From the comparison with the changes in the case of the N_2 pressure, it was clear that the abrupt changes were not caused by pressure itself. To discuss the causes of the abrupt changes, the density and viscosity of CO_2 were calculated. A small change in pressure or temperature results in large changes in density and viscosity in high-pressure and supercritical CO_2. In the subcritical state slightly below the critical point, the density and viscosity change discontinuously between the gas and liquid phases. Since the temperature at which the density and viscosity change discontinuously between 5 and 6 MPa is approximately 20 °C, there is a possibility that the abrupt changes in the resonance properties were mainly due to changes in density and viscosity. In the future, an investigation of the resonance properties in supercritical state will be reported.

P5B-4

SAW Phase Modulation by Optical Illumination of Graphene Composite Films deposited on LiNbO3

Venkata Chivukula[1], Daumantas Ciplys[2], Jin-Ho Kim[3], Romualdas Rimeika[2], Jimmy Xu[4], Michael Shur[5]; *[1]Rensselaer Polytechnic Institute, Troy, NY, USA, [2]Vilnius University, Vilnius, Lithuania, [3]jin_ho_kim@brown.edu, Providence, RI, USA, [4]Brown University, USA, [5]Rensselaer Polytechnic Institute, USA*

Background, Motivation and Objective

Recent developments in material synthesis and fabrication technology enabled growth of graphene flakes with variable sheet resistance (on the order of several Ohms to kOhms) by varying the layer thickness. We investigated the effect of illumination on SAW propagation in graphene composite films and propose a model of this effect based on opto-thermal SAW phase modulation. Our research reveals possibility of optothermal spectroscopy of graphene films using surface acoustic waves.

Statement of Contribution/Methods

Graphene composite films of thickness around 200-900 nm were prepared from aqueous solution of graphene oxide obtained from synthesis of purified natural graphite by Hummer's method . The SAW transmission characteristics before and after deposition of graphene film on YZ LiNbO3 were measured at the center frequencies of 54 and 108 MHz. The SAW phase response was monitored by measuring the S-parameters. The He-Ne laser with a beam diameter 2 mm and the power 6.7 mW was used as an illumination source.

Results

The SAW phase response obtained by scanning He-Ne laser along the SAW propagation path is shown in Fig. 1A. Reduction in transmitted optical power in the region covered with graphene was measured and correlated to observed phase shift using opto-thermal model as shown in Fig. 1B. The time characteristics of the SAW phase response were investigated by illuminating the sample with the laser beam modulated using a mechanical chopper.

Discussion and Conclusions

We investigated the response of surface acoustic waves to optical irradiation of graphene composite film consisting of randomly stacked flakes deposited on a surface of piezoelectric substrate. The SAW phase change under illumination from He-Ne laser is attributed to the sample heating due to optical power absorbed by the graphene layer.

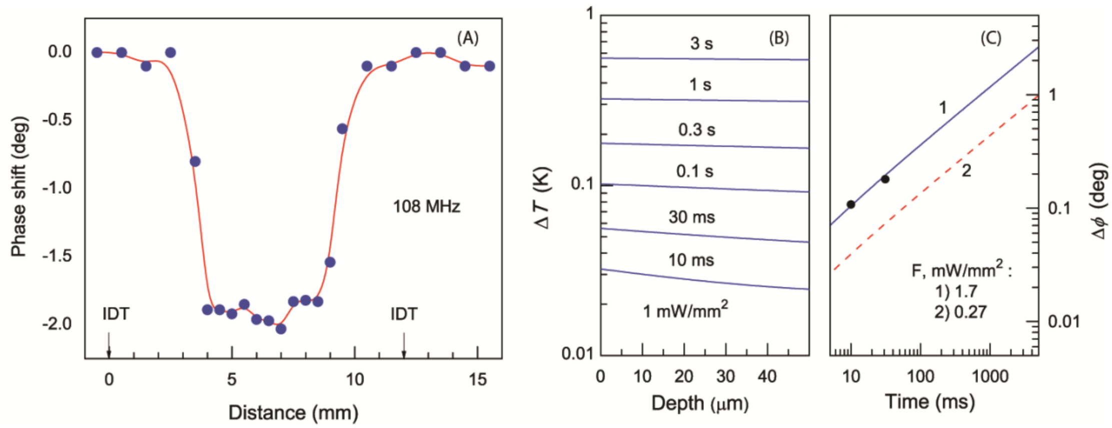

Fig. 1 A) Transmitted SAW phase shift under illumination as a function of light spot position. B) Calculated temperature distributions in $LiNbO_3$ substrate at different surface heating durations normalized to heating power density of 1 mW/mm^2. C) Time dependencies of the magnitude of SAW phase change calculated without (1) and with (2) lateral heat spreading by the graphene film; experimental values of phase change magnitude.

P5B-5

The System Design of a Love Wave Sensor for Measuring Liquid Dielectric Constant

Qianliang Xia[1], Zhijun Chen[1], Mengyang Wang[1]; [1]College of Automation Engineering, Nanjing University of Aeronautics and Astronautics, China, People's Republic of

Background, Motivation and Objective

The precise measurement of the liquid dielectric constant is of great importance. The acoustic sensor meets the requirements of small volume, high precision, minim sample, and quick response. Compared with other acoustic sensors, the Love wave liquid sensor has obvious advantages.

Statement of Contribution/Methods

(1) The design of a Love wave device: By the methods of the partial wave theory and the surface effective permittivity, a three-layer structure model of a Love wave device is established. The delay-line type device is optimized according to the sensitivity and the electromechanical coupling coefficient.

(2) The design of the measurement circuit:In correspondence to the change of the propagation velocity and the resonant frequency, the measurement methods are also classified into the following two types:

1)Phase difference measurement: The propagation velocity can be obtained by measuring the time delay of the Love wave. For the Love wave with a given frequency,the time delay corresponds to the phase difference.

2)Amplitude-frequency characteristic measurement: The Love wave device can be regarded as a two-port network device.Therefore, the resonant frequency can be measured by the frequency sweeping circuit and the amplitude ratio measurement circuit.

Results

(1) As shown in Fig. 1, a Love wave device consisting of 36¡ãYX LiTaO3 and the SU-8 photoresist film is made.

(2) With AD9912 as a signal source, and the phase difference and the amplitude ratio being measured by AD8302, the phase difference measurement circuit and the amplitude-frequency characteristic measurement circuit are shown in Fig. 2.

Discussion and Conclusions

The Love wave device and the two measurement circuits achieve good test results by different ratios of pure water and alcohol as the liquid samples.

Fig. 1 Love wave device

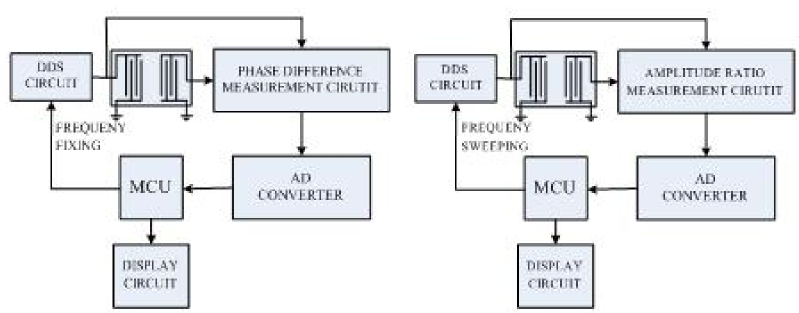

Fig. 2 The two measurement circuits

FRIDAY POSTER

P5C - Bulk Wave Effects and Devices II

Carribean Ballroom III-V

Friday, October 21, 2011, 9:30 am - 1:00 pm

Chair: **Bikash Sinha**
Schlumberger-Doll Research

P5C-1

Influence of Nanocomposite Polymeric Layers on Efficiency of Radiation of Bulk Acoustic Wave in Liquid by Antisymmetric Lamb Wave in Thin Piezoelectric Plate

Iren Kuznetsova[1], Boris Zaitsev[1], Irina Borodina[1], Vladimir Kolesov[2], Anatolii Sknarya[2]; [1]*IRE of RAS, Saratov Branch, Russian Federation,* [2]*IRE of RAS, Russian Federation*

Background, Motivation and Objective

The investigation of acoustic waves in liquids has a great practical significance for the development of the new hydroacoustic technologies and methods of monitoring the underwater objects. For the excitation and reception of bulk waves in liquids one may use the antisymmetric Lamb waves of zero order (À0). However until now the problem of the matching the piezoelements with liquid is urgent. Everybody knows that acoustic impedance of the nanocomposite polymeric materials is significantly less than one of piezoelectrics. So it is possible to use such materials for effective matching the piezoelectric crystals with liquid.

Statement of Contribution/Methods

In this work the theoretical study of À0 wave in the structure "piezoplate – nanocomposite layer –liquid" was performed. For analysis of wave propagation we used the motion equation, Laplace's equation, and constitutive equations for piezoelectric medium, polymeric film and liquid, and appropriate mechanical and electrical boundary conditions. The dependencies of the velocity, attenuation and bulk wave propagation in liquid on the ratio of thicknesses of plate and layer were found. As for nanocomposite material we investigated films with different concentrations of CdS and Fe nanoparticles embedded into high pressure polyethylene matrix.

Results

It has been shown theoretically and experimentally that using the layer of nanocomposite material based on the matrix of low density polyethylene and nanoparticles of cadmium sulfide between plate of 128YX LiNbO3 and water allows improving the efficiency of radiation. In this case the ratio of the thicknesses of the layer and plate is equal d/h=0.154 for the frequency f=1.3 MHz. We also investigated the influence of electrical conductivity of liquid on À0 wave in aforementioned structure. It has been shown that the use of nanocomposite layers allows effective screening the conducting liquid from the piezoelectric plate and keeps the possibility of wave radiation.

Discussion and Conclusions

The obtained show the availability of the use of nanocomposite layers based on the low density polyethylene for developing the effective transmitters/receivers of acoustic wave in liquids. These devices may be used for development of liquid flow meters and as main elements for underwater communications. The work is financially supported by Foundation of Minobrnauka of RF 14.740.11.0645, ÃÊ 14.740.11.0077.

P5C-2

A Mindlin Plate Theory Based Parallel Two-dimensional Finite Element Analysis for Quartz Crystal Resonators

Ji Wang[1], Rongxing Wu[1], Jianke Du[1], Dejin Huang[1], Wei Yan[2]; [1]School of Mech Eng & Mechanics, Ningbo University, Ningbo, Zhejiang, China, People's Republic of, [2]School of Civil & Arch Eng, Ningbo University, Ningbo, Zhejiang, China, People's Republic of

Background, Motivation and Objective

The finite element method is an ideal tool for the analysis and design of quartz crystal resonators. The two-dimensional finite element analysis based on the Mindlin plate theory has been developed more then two decades and has been useful in resonators design. Since resonators are climbing to higher frequency and shrinking to smaller size, the software needs to be paralleled with some new algorithms and libraries for large size problems.

Statement of Contribution/Methods

The 2D program is implemented with the higher-order Mindlin plate theory and integrating thermal and piezoelectric effects into the analysis. The standard finite element formulation and procedure is demonstrated briefly. Then we highlight the distributed parallel algoritms, which include the eigensolver and linear solver combined with PARPACK, SuperLU_DIST, Aztec and ParMetis for performance improvements.

Results

We tested our software on a Linux cluster with 16 processors. We also examined the convergence with different meshes with largest DOF more than 1 million. Our new results are presented into frequency spectrum (Fig. 1), frequency-temperature relations (Fig. 2), displacement solutions and electrical properties for visual examination and interpretation.

Discussion and Conclusions

Finite element analysis is an important tool for resonators design. 2D and 3D analyses based on our own development and commercial software have their own advantages and draw backs, but it is always desired to reduce the problem size and using smaller computing power. We shall extend our program to consider nonlinear effects as the current analytical functions have been built up.

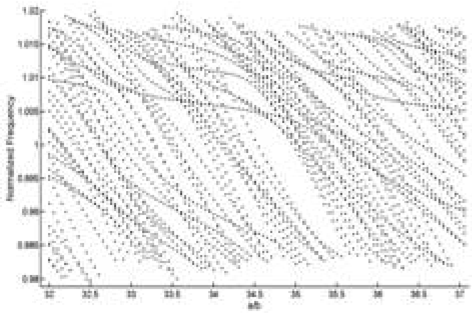

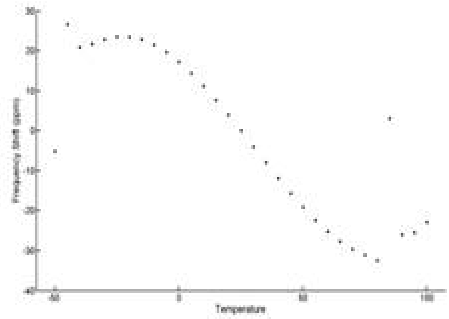

P5C-3

Analysis of Capacitances of Electrical Equivalent Circuit of Quartz-Crystal Tuning Fork in Consideration of Electric Field Distribution using Conformal Mapping Method

Takahiro Ishikawa[1], Hideaki Itoh[2]; [1]*Shinshu University, Japan,* [2]*shinshu university, Japan*

Background, Motivation and Objective

The formulas of capacitances of the equivalent circuit of a quartz-crystal tuning fork were derived for only free-free bar model in consideration of the electric field distribution and the potential ratio in the section of its arm using conformal mapping method and Fourier series in Ref. [1]. We analyzed the same problem for both free-free and clamped-free bar models and compared the calculated values with measured ones of the capacitances of the tuning forks which were available in practical wrist watch application.

Statement of Contribution/Methods

As for the equivalent circuit of the quartz resonator, we derived the formulas of dynamic and static capacitances based on the fact that the ratio of dynamic capacitance to static one was equal to the square of the dynamic electromechanical coupling coefficient, and the square of the dynamic electromechanical coupling coefficient was the product of the coefficient which showed the efficiency in vibration and the square of the static electromechanical coupling coefficient. We derived the formula of static capacitance from the parallel electrode problem obtained by applying Schwarz-Christoffel and Möbius transformations to the 1/4 section of the actual arm. By comparing the relationship between the capacitance ratio and the square of the dynamic electromechanical coupling coefficient, we derived the formula of dynamic capacitance using the potential ratio obtained by applying Fourier series to Poisson's equation standing for the right half section of the arm.

Results

In the case of the practical tuning forks, the calculated values for static capacitance were ranging from 0.17 to 0.41 times of measured ones. The calculated values for dynamic capacitance were ranging from 0.3 to 0.5 times of measured ones using the bimorph flexure model in Ref. [2], and from 0.6 to 0.8 times of measured ones using the method of considering electric field distribution. Next, it was found that the calculated coefficient, which showed the efficiency for free-free bar model, explained the predicted peak of measured Q-values well.

Discussion and Conclusions

We could obtain more accurate calculated values of dynamic capacitance using the method of considering electric field distribution than the bimorph flexure model. It was found that the boundary condition of free-free ends was suitable to calculate the values of dynamic capacitance close to the measured one from the relationship between the length ratio v(the ratio of the electrode length to bar's one) and the measured Q-values.

Reference

[1] J. Herman: Pro. 29th annual FCS, (1975) pp.26-34.

[2] H. Itoh and N. Hatakeyama: Jpn. J. Appl. Phys. 49 (2010) 07HC03.

P5C-4

Deposition of Crack-Free 30 µm AlN on IDT/ZnO/Si for Wave Guiding Layer Acoustic Wave Applications

Ouarda Legrani[1], Omar Elmazria[1], Philippe Pigeat[1], Ausrine Bartasyte[1], Sergei Zhgoon[2]; [1]Institut Jean Lamour, CNRS-Nancy University, France, [2]Moscow Power Engineering Institute, Moscou, Russian Federation

Background, Motivation and Objective

The combination of surface acoustic wave (SAW) and wave guiding layer acoustic wave (WLAW) can offer dual functionality, possibility to compensate temperature or other external parameter effects and to be packageless leading to the extreme miniaturization of devices [1]. AlN/IDT/ZnO/Si structure (IDT – inter digital transducer) was chosen due to the compatibility with CMOS technology and the availability of industrial process for AlN and ZnO deposition. However, the fabrication of correctly operating AlN/IDT/ZnO/Si structure for SAW-WLAW devices is still a challenge. The aim of this work was to provide an efficient AlN/IDT/ZnO/Si structure for SAW-WLAW sensors.

Statement of Contribution/Methods

AlN/IDT/ZnO/Si structure parameters operating at 520MHz have been optimized by a finite element method (FEM) [2] (λ = 10 µm, thickness (ZnO) = 2 µm, thickness (AlN) > 20 µm). Smooth and high quality crystalline c-axis oriented ZnO films were deposited on Si (100) by magnetron RF sputtering. The AlN layer was then deposited by magnetron sputtering, at 345 K, under conditions specially optimized for the growth of crack-free layers. During AlN layer deposition, in-situ measurements of the frequency response were performed by a network analyzer. Real-time AlN thickness was monitored by interferential reflectometry method.

Results

FWHM of rocking curve and surface roughness of ZnO films were 0.9° and 3 nm, respectively.The optimized deposition conditions at relatively low deposition temperature allowed the growth of crack-free AlN films of at least up to 30 µm thickness. The columnar growth of AlN was affected by the surface relief resulted from IDTs (Fig. 1). The electron diffraction attested the (00l) orientation of the individual columns and good crystalline quality of AlN films (Fig. 1). As expected from simulation, the in-situ characterizations of WLAW devices confirmed the confinement of acoustic wave at AlN thicknesses ≥ 17 µm.

Discussion and Conclusions

WLAW device based on AlN/IDT/ZnO/Si structure has been realized. Evolution of the frequency response of WLAW device was monitored during the deposition of 30 µm thick crack-free. Good agreement between experimental and theoretical results was obtained. To improve the performance of devices, possibilities of the flattening of the IDT/ZnO surface before deposition of AlN layer are under investigation.

[1] O. Elmazria et al. Appl. Phys. Lett. 95 (23), pp 233503;(2009)

[2] O. Legrani et al., Procceding COMSOL, nov17-18(39)

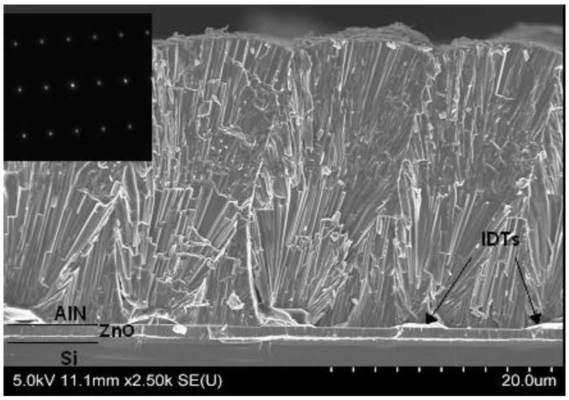

P5C-5

Quantitative analysis of the effect of energetic particle bombardment during deposition on (11-20) ZnO piezoelectric films

Shinji Takayanagi[1], Takahiko Yanagitani[2], Mami Matsukawa[1], Yoshiaki Watanabe[1]; [1]Doshisha University, Kyotanabe, Kyoto, Japan, [2]Nagoya Institute of technology, Nagoya, Aichi, Japan

Background, Motivation and Objective

c-axis parallel-oriented piezoelectric films such as (11-20) textured ZnO film are suitable for shear mode film bulk acoustic resonators (FBARs) and surface horizontal (SH) type SAW devices. In previous studies, we pointed out that (11-20) texture formation was induced by the ion bombardment during RF magnetron sputtering deposition[1]. However, quantitative information of the relationship between ion energy and amount of ion irradiation are not clear.

Statement of Contribution/Methods

In this study, we measured the energy distribution of positive and negative ions which enter the substrate during sputtering deposition by using energy analyzer (Hiden, PSM003). ZnO film was prepared under the same deposition conditions as the measurement conditions of ion energy distributions. Crystalline orientations of the film were measured by XRD analysis.

Results

Figure 1 (a) and (b) shows the energy distribution of positive ions (O_2^+) and negative ions (O^-), at 30 mm from the anode center, respectively. Positive ions have low ion energy and large flux. On the other hand, negative ions have high energy and small flux. Figure 2 shows XRD patterns of the sample. High intensity of (11-20) peak was observed at 30 mm from the anode center.

Discussion and Conclusions

Strong (11-20) preferred orientation was observed at 30 mm from the anode center, probably because the high energy negative ion bombarded to the substrate. This area was above the erosion region oh the sputtering target. Further results on ion energy distribution measurements of the distance distribution will be presented.

[1] T. Kawamoto, et. al., Jpn. J. Appl. Phys., 46, 4660, (2007).

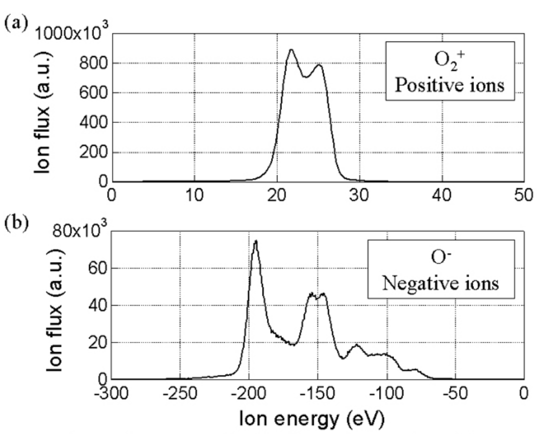

Fig. 1 The energy distributions of (a) O_2^+ positive ions and (b) O^- negative ions.

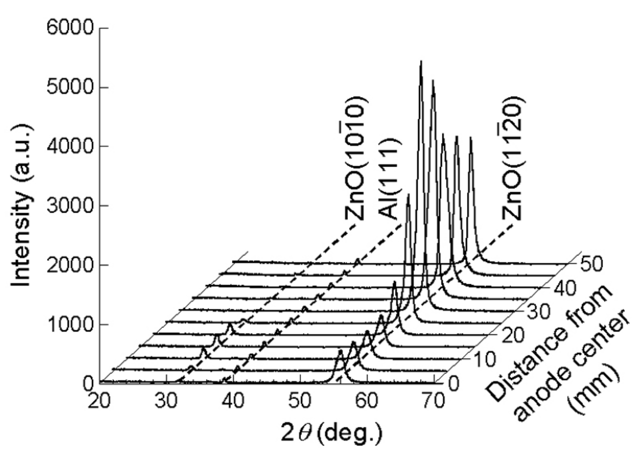

Fig.2 2θ-ω scan XRD patterns of the ZnO film.

FRIDAY POSTER

P5C-6

Effective precipitation method of NaCl using a focused ultrasound

Moojoon Kim[1], **Jungsoon Kim[2]**, Kanglyeol Ha[1], Choonghwa Lee[3]; [1]Physics, Pukyong National University, Busan, Busan, Korea, Republic of, [2]Media Eng., Tongmyong University, Busan, Busan, Korea, Republic of, [3]Physics, Pukyong National University, Korea, Republic of

Background, Motivation and Objective

Ultrasonic cavitation with high power can generate shock wave with high pressure and temperature in the water. Even though the chemical and physical reaction of the phenomena has been studied, the role of the ultrasound has not clarified enough. In this study, a method of NaCl precipitation is suggested using the shock wave. An effective NaCl precipitation method could be applied to the various fields, such as the seawater desalting process for drinking water production, and the salinity control for various chemical processes.

Statement of Contribution/Methods

The shock waves from the ultrasonic cavitations decompose water molecule into hydrogen radical and hydroxyl radical. The radicals react with nitrogen molecule included in the air, and it can induce nitric acid by ultrasound. This process changes pH on the solution of NaCl. It precipitates the NaCl crystal by combining the Na ion and Cl ion. For the precipitation of NaCl without heating, an effective method is suggested by using focused ultrasonic field from cylindrical piezoelectric vibrator.

Results

Figure shows the pH value change in the distilled water with ultrasonic exposure time. The value has decreased from 7.0 to 4.1 according to the exposure time. It means the distilled water is changed to the acid water. To confirm the precipitation of NaCl, the concentration of the NaCl solution is investigated in the cylindrical transducer. As the results, the concentration was changed from 40.1 ¡Æg to 37.2 ¡Æg during 70 minutes and it caused the precipitation of NaCl crystals.

Discussion and Conclusions

An effective precipitation method of NaCl is suggested. Using a focused ultrasound with cylindrical piezoelectric transducer, the ultrasonic cavitation with high power can be generated in the center of the cylinder. The precipitation of NaCl was confirmed by the change of the concentration in the solution.

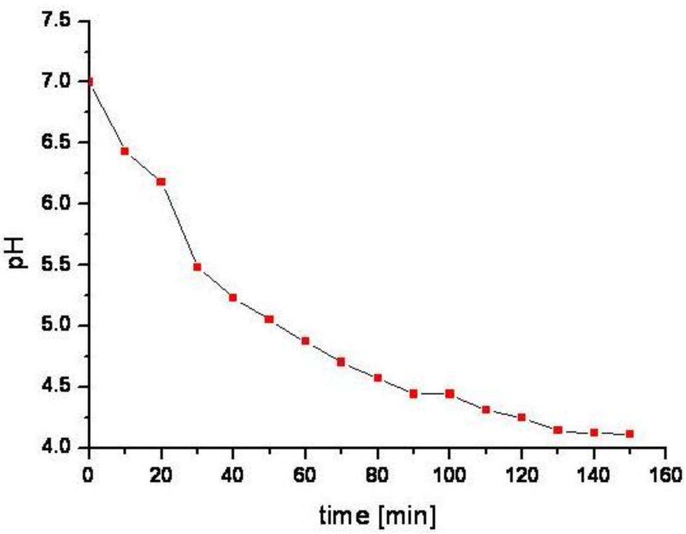

FRIDAY POSTER

P5E - Medical Transducers

Carribean Ballroom III-V

Friday, October 21, 2011, 9:30 am - 1:00 pm

Chair: **Geoff Lockwood**
Queen's University

P5E-1

Extended Necrosis by Using Dual-Curved Therapeutic Transducer for Noninvasive HIFU Surgery

Jong Seob Jeong[1], Jonathan M. Cannata[2], K. Kirk Shung[2]; [1]Department of Medical Biotechnology, Dongguk University-Seoul, Seoul, Korea, Republic of, [2]Department of Biomedical Engineering, University of Southern California, Los Angeles, California, USA

Background, Motivation and Objective

In noninvasive HIFU (High Intensity Focused Ultrasound) surgery, a treatment time can be reduced by using a therapeutic transducer capable of enlarging a coagulated lesion per sonication. Currently, most of studies have been focused on the expansion of necrosis in the lateral direction than the axial direction. In this paper, we present a novel HIFU transducer with a dual curved aperture which can extend DOF (Depth of Focus) resulting in a broad necrotic region in the axial direction. A prototype dual-curved transducer was fabricated and its performance was successfully tested by conducting simulation of bioheat transfer/thermal dose, hydrophone measurement, and in vitro test with a beef liver. Although several design parameters for the transducer were not optimized, the DOF of the proposed method was 3.4 times larger than that of the conventional single element transducer with the same dimension. Thus, the dual-curved therapeutic transducer may be a potential method to reduce treatment time of HIFU surgery.

Statement of Contribution/Methods

The proposed transducer is composed of a disc- and an annular-type element of different radii of curvatures to generate two focal zones. Each transducer can transmit ultrasounds with different center frequencies considering attenuation, i.e., the inner transducer can transmit high frequency (4.1 MHz) ultrasounds at the near field and the outer transducer can transmit low frequency (2.7 MHz) ultrasounds at the far field. The electrodes for two elements are connected together, and thus they can be simultaneously activated using a single transmitter capable of generating a dual-frequency mixed signal.

Results

The simulation results of bioheat transfer for the designed dual-curved transducer showed a temperature range of 60°C ~ 83°C in the extended DOF, and thermal dose simulation also exhibited an extended coagulated necrosis. A prototype dual-curved transducer was fabricated using PZT4 material with a high Curie temperature and a low dielectric/mechanical loss. In hydrophone measurement experiments, the high frequency components were increased at the near field and subsequently reduced as the depth was increased while the low frequency components were conversely increased. The measured -6 dB DOF was almost similar to the sound field simulation results, which was 3.4 times larger than a conventional single element transducer with the same dimension. The in vitro test with a beef liver showed a large coagulated region corresponding to the extended DOF.

Discussion and Conclusions

It was experimentally demonstrated that the dual-curved HIFU transducer can increase the necrotic region per sonication. If several factors affecting the length and the uniformity of DOF are optimized, more improved results can be obtained. Therefore, the proposed scheme may be a promising approach to achieve reduced treatment time and to treat a deep seated target in HIFU surgery.

P5E-2

Automated Transducer Testing and Calibration with a Dynamic Phantom

George Corner[1], Florian Riedel[2], Alex Valente[3], Joyce Joy[4], **Sandy Cochran[5];** [1]Ninewells Hospital, NHS Tayside, United Kingdom, [2]Ilmenau University of Technology, Germany, [3]St Andrews University, United Kingdom, [4]University of Dundee, United Kingdom, [5]Institute for Medical Science and Technology, University of Dundee, Dundee, Dundee and Angus, United Kingdom

Background, Motivation and Objective

Variation in transducer array performance for biomedical imaging and non-destructive testing (NDT) is inherent in manufacturing and performance degradation also occurs in service. It is already straightforward to determine basic device functionality through transmit and receive sensitivity measurements and from electrical impedance. However, this requires special equipment likely to be inaccessible to end users. Nevertheless, validation of transducer performance is of increasing importance as the use of array systems grows for NDT and for medical diagnosis by non-specialist users.

Statement of Contribution/Methods

Phantoms have been developed previously to allow repeatable testing of medical transducers and the production of quantitative parameters, such as the "resolution integral" (RI) [1]. However, this still requires time-consuming manual scanning, the cost of which reduces its utility. Our work aimed to overcome the limitations of manual testing with a dynamic system that allows rapid setup and automatic operation with results generated in the form of the RI.

The system is based on imaging two filamentary targets positioned under computer control in a tank of liquid tissue-mimicking material (TMM) for medical devices or water for NDT. This mechanism has been designed to be reliable and inexpensive, with the filaments coupled magnetically through the wall of the tank containing the liquid.

Images produced by the transducer array under test are captured and analysed to assess if the targets are resolved. The control program is incorporated in a feedback loop for completely automated beam profiling and RI calculation. The method requires only a few minutes set up time by an unskilled user before running autonomously and producing easily interpreted results.

Results

The dynamic phantom has been tested on a total of 20 medical ultrasound imaging transducer arrays working with systems in clinical use. Results were repeatable and consistent compared with those produced using manual testing and with qualitative assessments and clinical experience. Furthermore, RI calculation successfully differentiated recent, high quality transducers from lower quality and obsolete ones and also differentiated linear flat and convex transducer arrays.

Discussion and Conclusions

The new system is intended to allow quantitative assessment of ultrasound imaging transducers in a way that is accessible for devices in service rather than in specialised labs, producing results that can be interpreted by non-experts to characterise their devices. It allows low cost manufacture and needs minimal manual intervention. In further work, it will be developed to benchmark transducer arrays for imaging research, prior to equipment introduction to service, and to assess aging in service.

[1] S.D.Pye, W.Ellis and T.MacGillivray, "Medical ultrasound: a new metric of performance for greyscale imaging", Advanced Metrology in Medicine, J. Phys.: Conf. Series 1, 2004, pp. 187–192.

P5E-3

High Intensity Focused Ultrasound Array Transducers for Sonochemistry Applications

Chuangnan Wang[1], **Tony Gachagan[1]**, Richard O'Leary[1], Alison Nordon[2]; [1]Electronic and Electrical Engineering, University of Strathclyde, Glasgow, Scotland, United Kingdom, [2]Department of Pure and Applied Chemistry and Centre for Process Analytics and Control Technology, University of Strathclyde, Glasgow, Scotland, United Kingdom

Background, Motivation and Objective

High power ultrasound has been employed as catalysis in chemical processes for many years. This is typically based on the ability of the system to produce cavitation, through which the high temperatures and pressures released during the cavitation process accelerates the chemical reaction. The ultrasonic system used in Sonochemistry is traditionally based on a distributed configuration of single frequency transducers. However, these designs can result in complex reactor design and significant power supply demands. In this work, high intensity focused ultrasound (HIFU) is consider as an alternative transduction solution due to its steering and focusing capabilities. Importantly, the steering ability can manipulate the cavitating field within reactor vessel.

Statement of Contribution/Methods

Currently, HIFU is mainly used in clinical applications, with high frequency ultrasound utilized to provide accurate focusing and prevent tissue damage out with the target region. In this work, the fundamental HIFU transducer design principles are maintained, but as Sonochemistry is the desired application field, lower frequency array transducer designs are investigated. PZFlex has been used to design linear array transducers incorporating 1-3 connectivity piezoelectric composite as the active material.

Results

Three low frequency, high power array transducers have been fabricated, with operating frequencies of 210 kHz, 270 kHz and 400 kHz and each device comprising 16 array elements. Preliminary characterization of these devices, including electrical impedance and surface displacement measurements, correlates well with the predicted performance through PZFlex. A comparison of the ability of each device to generate a cavitating field, at a number of focal positions, was conducted using a NPL cavitation sensor and conventional aluminum foil experiments.

Discussion and Conclusions

The 210kHz array was used to assess its' suitability for process intensification through the application of high power ultrasound on Weissler's reaction. Importantly, the dosimetry results indicate the potential of this technique for Sonochemistry applications.

P5E-4

Design of 15-MHz Concave Array Transducers for Ophthalmic Imaging

Jung Hyui Cha[1], Tai-Kyong Song[2], Jin Ho Chang[1,3]; [1]*Interdisciplinary Program of Integrated Biotechnology, Sogang University, Seoul, Korea, Republic of,* [2]*Department of Electronic Engineering, Sogang University, Korea, Republic of,* [3]*Sogang Institute of Advanced Technology, Korea, Republic of*

Background, Motivation and Objective

Ophthalmic imaging is among the most popular applications in high frequency ultrasound imaging. Conventional ophthalmic imaging has commonly employed single element transducers to diagnose ocular diseases such as glaucoma and retinal detachment. While transducers in the range of 30 MHz to 100 MHz have been used for imaging the anterior segment of the eye, the frequency range of 7 to 20 MHz is suitable for imaging the retinal area of the posterior segment, considering acceptable penetration, spatial resolution, and field of view, simultaneously. The current ophthalmic imaging systems equipped with the single element transducers have limitations in diagnosis of the eye diseases because of its relatively slow fame rate and incapability to provide color flow images. Although not only the linear but also the convex array transducers have been recently suggested to overcome those problems, they suffer from high refraction on the cornea due to the disparity between their footprint and the inherent spherical shape of the eye. As a remedy, a 15-MHz concave array transducer is proposed in this paper.

Statement of Contribution/Methods

The human eye is spherical in shape and about 25 mm diameter in size. Since the concave array transducer fits well with the structure of the eye, both reflection and refraction from the cornea are expected to be minimized, in contrast with the conventional array transducers. Also, the concave array can provide a large field of view beyond the center of the curvature that is placed in the center of eyeball filled with vitreous humor. Another advantage of the concave array is that a larger pitch can be allowable because beam steering is not required. Thus, a 15-MHz, 128-element concave array transducer was designed for the imaging of posterior segment of the eye. The 15 mm radius of concave curvature, 7.5 mm element height for the 30 mm elevation focus, and 1.44λ pitch were chosen to secure the best field of view while suppressing the levels of grating lobes to less than -50 dB. In this design, the 1-3 composite of PMN-PT with high coupling coefficient (k_t = 0.78) and low impedance (Z = 16.3 MRayls) were selected as an active material based on KLM modeling. Epo-Tek 301 was chosen as a single matching layer as well.

Results

The one element KLM modeling demonstrated that the designed array provided -6 dB fractional bandwidth of 81.1 %, -20 dB pulse length of 0.127 μs, and sensitivity of -45.2 dB re 1V/V. Also, The Field II simulation showed that the -6 dB lateral beam width was 200 μm at the depth of 29.1 mm and the -6 dB depth of focus was 6.6 mm. The maximum view angle was 72.3° at the center of the curvature, which corresponded to the field of view of 36.7 mm at the depth of 30 mm.

Discussion and Conclusions

The concave array transducer was proposed for ophthalmic imaging. We believe that the array transducer with concave shape has fair advantages over the other counterparts in posterior segment ophthalmic imaging.

P5E-5

LFE Transducers based on Inversion Layer for Medical Imaing

Jin Chen[1], Chao Zhang[2], Zhitian Zhang[2], Guanping Feng[1]; [1]Tsinghua University, Beijing, China, People's Republic of, [2]Research Institute of Tsinghua University in Shenzhen, China, People's Republic of

Background, Motivation and Objective

The resolution of the ultrasonic imaging relies on the frequency and bandwidth of the ultrasonic transducer.

The Lateral-field-excited devices can provide higher fundamental frequency than Thickness-field-excited devices for the same plate thickness. The inversion layer devices can excite even harmonic waves which can broaden the bandwidth of the transducers with appropriate matching layers.

An LFE transducer based on inversion layer has been designed and fabricated to achieve the high frequency and broad bandwidth performance.

Statement of Contribution/Methods

An X-cut LiNbO3 plate with the thickness of 0.152mm was treated to get a 28.6% proportion inversion layer. Two chrome-gold electrodes were sputtered on the same side of the inversion layer plate. Two matching layers have been fabricated.

Results

Two resonance peaks at about 20MHz and 40MHz relative to the fundamental and second harmonic frequencies can be seen in the frequency spectrum. However, the line dropped down below -6dB in a short frequency range, decreasing the center frequency to only 24.7MHz with a bandwidth of 62.8%.

Discussion and Conclusions

It's the first time to combine the advantages of the inversion layer materials and the LFE structure. The results proved that the lateral electrodes could also excite the inversion layer to generate the even harmonic waves. It¡¯s believed that a center frequency of 30MHz with the broad bandwidth as much as 80% can be achieved with better matching layers, compared to the reported bandwidth of 34% for LFE transducer with normal X-cut LiNbO3.

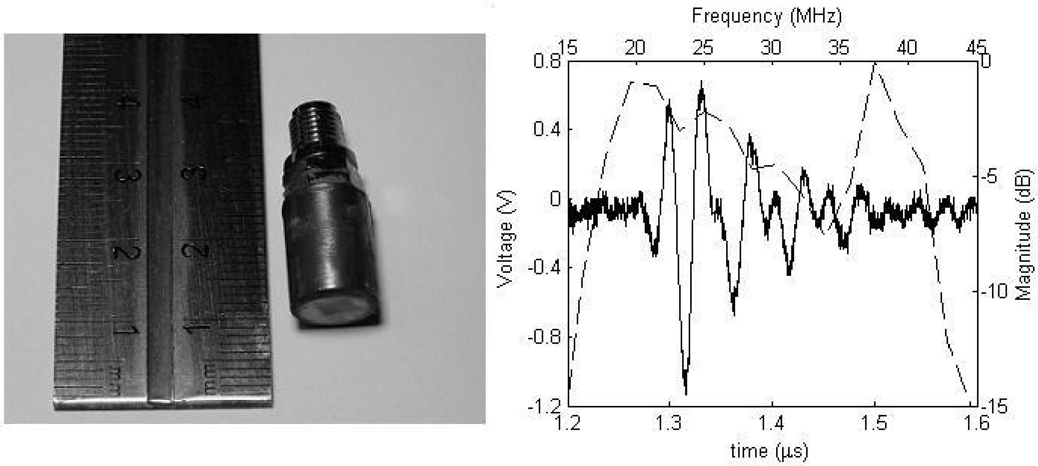

Fig. The LFE transducer based on inversion layer and its pulse-echo characteristic

P5E-6

A matrix transducer for 3D Transesophageal Echocardiography with a separate transmit and receive subarray

Sandra Blaak[1], Charles T. Lancée[1], Johan G. Bosch[1], Christian Prins[2], Antonius F.W. van der Steen[1,3], Nico de Jong[1,3]; [1]Thoraxcenter, Biomedical Engineering, ErasmusMC, Rotterdam, Netherlands, [2]Oldelft Ultrasound B.V., Delft, Netherlands, [3]Interuniversity Cardiology Institute of the Netherlands, Netherlands

Background, Motivation and Objective

Three-dimensional (3D) transesophageal echocardiography (TEE) visualizes the 3D anatomy and function of the heart. For 3D imaging an ultrasound matrix of thousands of elements is required. Since the gastroscopic tube of a TEE probe can accommodate a limited number of cables, smart signal processing with integrated circuitry in the probe head is required. To ensure separation of the low voltage integrated receive circuits from the high voltages required for transmission, our design features a separate transmit and receive subarray. For sufficient frame rate to visualize the movement of the heart valves, wide beam are transmitted (3MHz) and in receive (6MHz) pre-steering is applied in the probe head and parallel beam forming in the mainframe [1]. In this paper we investigate beamforming with the separate transmit and receive array configuration.

Statement of Contribution/Methods

The pressure field emitted by the transmit subarray (4×32 elements, 0.31mm pitch) is measured using a hydrophone setup, for steering angles between -45° and 45°. Results are compared to Field II simulations. The -6dB beam width of the second harmonic field is approximated by taking the -3dB beamwidth of the fundamental field. The receive subarray is square and consists of ~ 2000 elements with a 0.2mm pitch. For each steering angle in transmission the angles of the parallel receive beams for maximal overlap with this transmitted beam are determined.

Results

Simulations and measurements matched well. Figure 1 shows a transmit beam with the overlapping parallel receive beams for varying depths. The transmitted beam is completely overlapped from a depth of 15mm, by adapting the beam forming in the main frame, without changing the pre-steering settings. To insonify a cone with top angle of 90º, ~200 transmit beams are required. Considering a pulse repetition frequency of 5kHz and an imaging depth of 150mm, a frame rate of ~25 frames can be achieved. On average 9 parallel beams are required to scan a single transmit beam.

Discussion and Conclusions

The separate subarray configuration, which has significant advantages in the design of the electronics, has appropriate beam forming capabilities for use in 3D TEE imaging.

[1] S. Blaak, Z. Yu, G. Meijer, C. Prins, C. Lancée, J. Bosch, and N. De Jong, "Design of a micro-beamformer for a 2d piezoelectric ultrasound transducer," in Proc. IEEE Ultrasonic Symp., Rome, Italy, 2009.

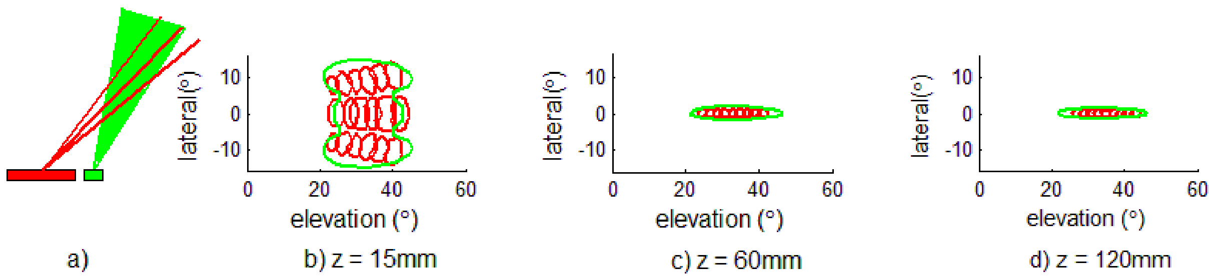

Figure 1: a) A schematic of the two subarrays and the beamforming. b) c) d) The transmit beam (green), steered to 35°, at varying depths. The receive array is presteered to 37°. With parallel beamforming in the main frame and without changing the presteering settings on chip, the transmit beam can be completely overlapped by receive beams (red).

P5E-7

Time Reversal Ultrasound Focusing with Electromagnetic Feedback

Armen Sarvazyan[1], Gaurav Gandhi[1], Alexander Sutin[2]; [1]Artann Laboratories, Ewing, NJ, USA, [2]Stevens Institute of Technology, Hoboken, NJ, USA

Background, Motivation and Objective

Remote recharging of batteries of internal implants, such as cardiac pacemakers, implantable electrical stimulators of all kinds including neurostimulators, urinary tract control devices, and deep brain neurostimulators among others is an important problem to which there is no adequate solution. Present day devices contain an internal battery, which can last for 5-10 years, after which they are surgically replaced. Noninvasive recharging of the implant's battery would help avoid periodic surgical procedures. There were numerous attempts to use focused ultrasound for battery recharge, but conventional focusing means cannot accurately concentrate high levels of acoustic energy on the implanted device without affecting surrounding tissues. The objective of this study is to explore the possibility of using a novel technique of ultrasound focusing based on the principle of Time Reversal Acoustics (TRA) with Electromagnetic (EM) feedback to deliver acoustic energy precisely to the piezoelement for charging.

Statement of Contribution/Methods

TRA method of focusing acoustic energy requires placing a transducer (a beacon) to provide an initial feedback signal from the target focal region. To eliminate the need for the leads connecting the beacon with the TRA electronic unit we propose to use EM feedback signal generated by a miniature piezotransducer mounted in the implanted device.

Specifically, 1 MHz piezotransducer coated with epoxy and equipped with a compact antenna was buried between two 15 mm thick layers of meat. A TRA emitter was placed on the meat to emit an initial binary sweep (0.9-1.1 MHz). A fine insulated copper wire loop placed beneath the meat layer and connected to a band pass preamplifier was used to detect EM feedback from the beacon. The received EM signal was time-reversed and applied to the TRA emitter to generate focused ultrasound signal.

Results

Comparable focusing was achieved on the beacon using wireless EM induction and a conventional cable connection. Wireless focusing amplitude was lower by appx 2dB Vpp and was still able to provide 2.8 Vpp signal on the beacon. We also tested the focusing quality; moving the emitter by 1 mm resulted in a decrease in amplitude of about 3 dB.

Discussion and Conclusions

We demonstrated feasibility of the TRA focusing systems with EM feedback. The main advantage of such system over conventional ultrasound focusing is in its ability to precisely deliver ultrasound energy to the chosen region and avoid exposure to surrounding tissues regardless of the heterogeneity of the propagation medium. Remarkably, scattering and reflections from boundaries, which greatly limit conventional focusing, improves TRA focusing. TRA focusing may be used to deliver acoustic energy precisely to the piezoelectric element incorporated into the implanted device and used for the implant battery charging using an EM feedback.

P5E-8

Design and Fabrication of High frequency Ultrasound Imaging Arrays Integrated into Medical Interventional Tools

Robert Ssekitoleko[1], Jack Hoyd-Gigg Ng[2], Christine Demore[3], David Flynn[2], Marc Desmulliez[2], Sandy Cochran[3]; [1]Department of Bioengineering, University of Strathclyde, Glasgow, United Kingdom, [2]MIcroSystems Engineering Centre, Heriot-Watt University, Edinburgh, United Kingdom, [3]Institute for Medical Science and Technology, University of Dundee, Dundee, United Kingdom

Background, Motivation and Objective

Transducer arrays operating above 15 MHz enable real time high resolution imaging of tissue, capable of resolving features below 200 µm. Clinical applications such as oncology and gastroenterology could significantly benefit from the improved resolution for HFU characterization of tissues. However, this is presently challenging due to the limited penetration depth of HFU and limited access. Since the device dimensions scale with imaging wavelength, it becomes feasible to integrate HFU arrays with interventional tools such as biopsy needles. Although there are many design and fabrication challenges associated with incorporating a transducer with interventional tools such as biopsy needles, it creates opportunities for timely and accurate characterisation of tissue, leading to *in vivo* pathology.

Statement of Contribution/Methods

In this paper we report progress in the development of fabrication processes for miniature linear arrays suitable for integration with biopsy needles. While patterning high frequency transducer arrays based on piezocomposites has been shown to be feasible, there remain many challenges to miniaturize the interconnect and cabling of an ultrasound probe suitable for *in vivo* pathology. Microfabrication and precision micromachining processes have been developed to overcome the technical challenges in fabricating miniature arrays operating up to 25 MHz. Array elements are defined by precision dicing and the necessary external flex circuit cabling is fed through the needle.

Results

Designs for a 15 MHz linear array and 2 mm diameter needle suitable for *in vivo* pathology are presented. The transducer substrate is a 1-3 piezocomposite of 49% volume fraction PMN-29%PT. Matching and backing layers of loaded epoxies are cast on the electrode front and back surfaces of the piezocomposite. A flexible printed circuit is connected to back surface electrodes using low-temperature bonding methods. A 15 MHz PMN-PT single crystal 1-3 piezocomposite with 60 µm pitch has been fabricated using standard dice-and-fill techniques. A flex circuit connected to the 1-3 piezocomposite has also been diced with 60 µm pitch to define array elements suitable for a 25 MHz linear array. The polyimide flexible printed circuit, with fine pitch traces, has been twisted into a helical structure so that it can fit within the core of the biopsy needle and permit large numbers of elements and electrode traces. The fabrication process has been validated initially with a single element transducer in a needle.

Discussion and Conclusions

The fabrication process development and testing demonstrate the feasibility of a linear array integrated into a biopsy needle. The extension of the fabrication processes to higher frequency arrays, and limitations in the processes are discussed. The recent advances in high frequency and miniature ultrasound imaging probes are significant steps toward the development of *in vivo* pathology diagnostic systems.

P5E-9

One-dimensional optoacoustic array employing chirped excitation and GPU-based beamforming

Ya Shu[1], Xinqing Guo[1], Mengyang Liu[1], **Takashi Buma[1]**; [1]*University of Delaware, USA*

Background, Motivation and Objective

Optical techniques are a promising technology to realize high frequency ultrasound arrays. High sensitivity and broad bandwidth have been demonstrated with thin film etalon sensors. We have previously demonstrated a 256-element etalon array with true parallel detection. A disadvantage of this approach is lower signal-to-noise ratio (SNR) due to the use of a linear CCD array. We are also exploring a serial approach where the optical probe beam is rapidly scanned to produce a 500-element etalon array. Higher SNR is achieved with photodiode detection and high optical probe power.

Statement of Contribution/Methods

The optoacoustic sensor is a thin film etalon consisting of a parylene layer with gold coatings on a glass substrate. A fiber coupled 785 nm diode laser is focused on the etalon, where the beam is rapidly scanned over a 5 mm line at a 50 Hz rate. The reflected beam is coupled into a multimode fiber and sent to an AC-coupled photodetector. The 25 MHz source transducer is driven with a 4 us duration chirped waveform at a 50 kHz repetition rate. A 500 MHz 8-bit oscilloscope records the signals from all 500 elements before transfer to a workstation. Pulse compression, beamforming, and image display are performed with a graphics processing unit (GPU). The object is a wire target placed approximately 3 mm below the etalon surface.

Results

The attached figure shows the time-domain data after pulse compression, clearly showing the curved wavefront of the scattered ultrasound. The chirped excitation provides an SNR increase of over 18 dB with respect to traditional impulse excitation. The wavefield is displayed over a linear scale, 1 us time window, and 5 mm lateral extent. The reconstructed image is shown over a 20 dB dynamic range and 4 x 4 mm region. The wire target is clearly visible, where the -6 dB width is 95 um.

Discussion and Conclusions

An advantage of the serial approach is higher SNR, since the entire probe laser power is used to acquire the signal from an individual element. Sensitivity drop-off at the array edges is not a major concern since all 500 elements receive the same optical power. However, uniform detection sensitivity is still limited by variations in the etalon thickness across the array aperture. We are currently improving the system to provide B-mode images at video frame rates. We believe these results suggest the potential of optoacoustic arrays for video-rate ultrasound biomicroscopy.

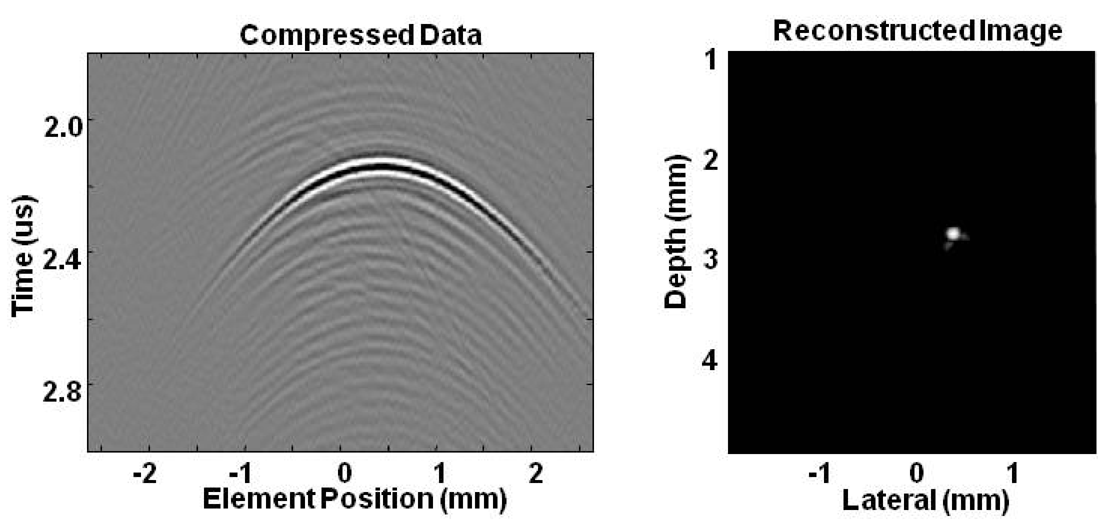

P5E-10

High-Intensity Focused Ultrasound by Optoacoustic Generation from Carbon-Nanotube Polymer Composite Layers

Hyoung Won Baac[1], Jong G. Ok[2], L. Jay Guo[1]: [1]Department of Electrical Engineering and Computer Science, University of Michigan, USA, [2]Department of Mechanical Engineering, University of Michigan, USA

Background, Motivation and Objective

High-intensity focused ultrasound (HIFU) has been widely utilized to address scientific interests on cavitation and give remarkable impactson therapeutic applications. Conventional HIFU has been generated by using piezo-based transducers. However, these transmitters have limited bandwidths and center frequencies typically lower than 10 MHz for HIFU purposes. As they have large focal spot sizes in the range of several 100 μm to millimeter, it is difficult to satisfy needs for high-resolution applications which require tighter focal zones.

Statement of Contribution/Methods

Thin-film optoacoustic generation is an effective way for making broadband and high-frequency ultrasound pulses. Nanosecond laser pulses are commonly used to generate the acoustic pulses which have almost identical frequency spectra with those of laser pulses. While they have excellent frequency characteristics, their pressure amplitudes were usually weak because of poor optoacoustic energy conversion. Recently, we developed highly efficient optoacoustic generation sources based on carbon-nanotube (CNT) polymer composite which have high optical absorption and large thermal expansion. Composite thin-films could generate high-frequency (>100 MHz) and very strong pressure (25-dB stronger than that in a Cr reference film) [Baac et al., Appl. Phys. Lett. 97, 234104 (2010)]. Here, we propose focused optoacoustic transmitters using the CNT-polymer composite. Multi-walled CNTs were directly grown on fused silica concave lenses. Then, composite layers were formed by coating polymer films over the CNTs.

Results

Due to the excellent optoacoustic conversion in the composite, we could successfully obtain HIFU of several MPa at focal point. Such high level of pressure could not be achieved in conventional optoacoustic sources such as thin metal and dye-doped polymer. The frequency spectra of the measured HIFU confirms the broadband characteristic which is required for tight focal zones especially in the axial direction.

Discussion and Conclusions

The CNT-based optoacoustic transmitters were demonstrated. This scheme enables broadband ultrasound generation together with high pressure amplitude. Such strong pressure could be achieved due to the efficient optoacoustic conversion and high damage threshold in the composite. Due to simple fabrication process, the HIFU transmitters with high numerical aperture could be easily produced. The pressure strength can be further enhanced by changing lens dimensions and polymers.

P6Aa - Photoacoustics

Carribean Ballroom III-V

Friday, October 21, 2011, 1:00 pm - 4:30 pm

Chair: **Parag Chitnis**
Riverside New York

P6Aa-1

In vivo monitoring of nanoparticle delivery using spectroscopic photoacoustic imaging

Seungsoo Kim[1], Geoffrey Luke[2], Yun-Sheng Chen[2], Stanislav Emelianov[1,2]; [1]Biomedical Engineering, University of Texas at Austin, Austin, TX, USA, [2]Electrical and Computer Engineering, University of Texas at Austin, Austin, TX, USA

Background, Motivation and Objective

In vivo monitoring of nanoparticle (NP) delivery is essential to better understand cellular and molecular interactions of NPs with cells. Spectroscopic photoacoustic (sPA) imaging can detect NPs based on optical absorption spectra. The goal of this study was to demonstrate sPA imaging can be used for in vivo monitoring of nanoparticle delivery using a mouse bearing a subcutaneous tumor.

Statement of Contribution/Methods

A431 cancer cells were injected into the flank of a Nu/Nu mouse to produce a tumor mass. The tumor was scanned before and 31 hours after intravenous injection of PEGylated gold nanorods (PEG-Au NRs) using an integrated ultrasound (US) and photoacoustic (PA) imaging system. In order to monitor uptake of PEG-Au NRs within the tumor, three-dimensional (3-D) sPA imaging was performed. Spectral processing based on a minimum mean squared error (MMSE) method was used to determine the similarity between the sPA and NP spectra. The MMSE, along with the sPA signal amplitude, determined the relative NP concentration. Finally silver staining of the excised tumor tissue was used to confirm NP deposition.

Results

Uptake of PEG-Au NRs was ascertained by both 3-D sPA imaging and silver staining. Figures 1 (a) and (b) show combined 3-D US (gray color) and overlaid sPA (green color) images before and 31 hours after the NP injection, respectively. While the US image shows mouse tumor morphology (i.e., tumor size and location) as well as overall outline of the mouse body, the sPA image provides information on NP distribution. The silver staining slide of excised tumor tissue (Fig. 1(d)) clearly confirmed NP deposition, and moreover was highly correlated with sPA image (Fig. 1(c)) at the same cross section as the histological slide.

Discussion and Conclusions

We successfully demonstrated 3-D US and sPA imaging can be used for in vivo detection of NPs using a tumor-bearing mouse. Good correlation of NP distribution between histological slides and sPA images was also demonstrated. The results of our study suggest that sPA imaging is a promising imaging technique to detect NPs in vivo, and therefore can be used for more nanoparticle-related studies such as the effect of using molecular specific targeted NPs on delivery efficiency.

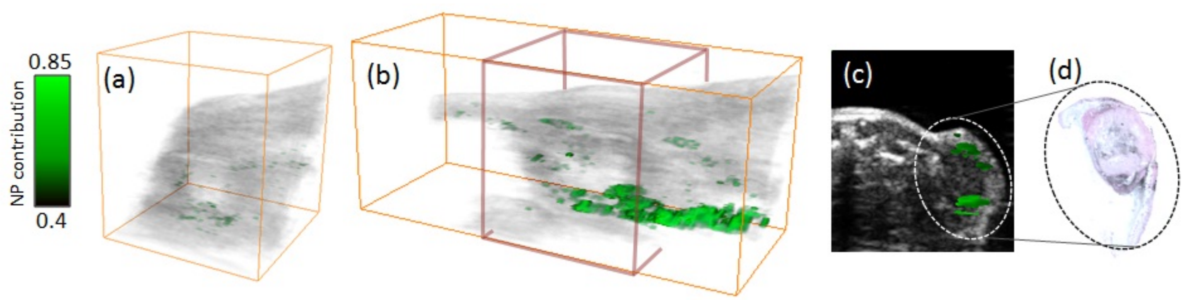

Fig. 1. 3-D ultrasound (US) and spectroscopic photoacoustic (sPA) images of the mouse (a) before and (b) 31 hours after PEGylated gold nanorods injection. Green-colored pixels on the images are nanoparticle contributions obtained from the developed spectroscopic analysis method. (c) The combined US and sPA image and (d) a silver staining slide shows good correlation as well as NP deposition at the tumor.

P6Aa-2

Applying ultrasound beamformers to photoacoustic imaging

Tyler Harrison[1], Roger Zemp[2]; [1]Electrical and Computer Engineering, University of Alberta, Canada, [2]University of Alberta, Canada

Background, Motivation and Objective

Photoacoustic (PA) imaging offers optical contrast and ultrasonic spatial resolution, and is providing new opportunities for functional and molecular imaging. Ultrasound (US) array transducers offer advantages of electronic scanning and dynamic focusing. Clinical use of PA imaging would be greatly facilitated by implementation on commercial ultrasound systems, however, challenges may exist. Commercial array US systems traditionally use hardware-based beamforming which is not easily adapted for PA imaging because dynamic delays are designed for two-way rather than one-way ultrasound propagation. We propose a technique to implement PA beamforming on these systems.

Statement of Contribution/Methods

Many US array systems offer the ability to adjust the speed of sound, *c*, used in reconstructions. Typical US beamformers are based on a second-order approximation of delays that are used to refocus the incoming data. Using analytical methods, we show that by adjusting *c*, PA images can be properly beamformed in the linear scanning case. Sector scanning is shown to require further modifications. Using simulations and parallel-channel data from a Verasonics research-oriented US acquisition system, we reconstruct images with both

FRIDAY POSTER

a traditional US beamformer (using modified *c*) and its PA counterpart. A pulsed Nd:YAG laser pumping a wavelength-tunable optical parametric oscillator was used to excite optically absorbing targets, including resolution phantoms and live subjects.

Results

Scaling *c* by a factor of sqrt(2), we find that a US beamformer reduces to a PA beamformer in a linear-scanned approach, and offers resolution advantages of up to 20x over an unmodified US beamformer (an method previously attempted in the literature). When sector-scanning is required, PA focusing using a *c*-scaled US beamformer is not optimal but provides reasonable results for small scan angles. In both cases image coordinate re-mapping is required. Simulated data agrees well with experimental point-spread function reconstructions. Using a 128-element L7-4 transducer we attained ~500 µm lateral and ~390 µm axial PA resolution. In vivo PA images reconstructed via both US- and PA-beamformers are acquired at 5 frames per second and co-registered with US B-scans to demonstrate clinical viability.

Discussion and Conclusions

We have demonstrated a method for adapting US beamformers for use in PA systems by *c*-scaling and image coordinate warping. This technique may be used to implement a PA system with minimal hardware modification and will be most beneficial when massively parallel beamformers are used. We believe that this and related techniques may speed the adoption of PA imaging by clinicians by decreasing the costs and amount of effort associated with PA imaging.

P6Aa-3

Clinical demonstration of reflection-mode photoacoustic image clutter reduction using tissue deformation

Michael Jaeger[1], David David Birtill[1], Andreas Gertsch[1], Elizabeth O'Flynn[2], **Jeffrey Bamber[1]**; [1]Joint Department of Physics, Institute of Cancer Research and Royal Marsden NHS Foundation Trust, Sutton, Surrey, United Kingdom, [2]CRUK-EPSRC Cancer Imaging Centre, Institute of Cancer Research and Royal Marsden NHS Foundation Trust, Sutton, Surrey, United Kingdom

Background, Motivation and Objective

In photoacoustic (PA) imaging, optically absorbing tissue structures, heated by illumination with a short (ns) laser pulse, expand and generate pressure transients that can be measured at the tissue surface with an ultrasound (US) transducer and used for reconstructing an image of the PA sources. A multi-wavelength approach may further assist the identification and characterisation of disease and optical contrast agents. Reflection-mode PA imaging is expected to be possible to depths of several centimetres but image quality deteriorates rapidly with depth due to PA clutter, which can arise from acoustic scattering of PA transients. It has been shown in simulation and in phantom experiments that PA clutter can be reduced by deforming the medium with ultrasound probe pressure, as in elastography, then averaging multiple images following a global transformation that corrects for the applied deformation. Our objective was to determine whether this technique of deformation-compensated averaging (DCA) can be applied successfully in the clinic.

Statement of Contribution/Methods

Duplex PA imaging and PA-transmit echography was implemented on a commercial US scanner (Z.one™ Zonare, Mountain View) as described in a companion paper. A photoacoustically generated US transmit pulse allowed echograms to be acquired simultaneously with PA images at 10 Hz. Initial clinical images of necks, forearms and breasts, demonstrated loss of PA signal-to-noise ratio due to the existence of a PA-clutter background. For application of DCA, image sequences were acquired during a dynamic freehand shear deformation of the tissue, applied by a lateral motion of the US-PA scan-head at the skin surface. Echographic speckle tracking was then used to derive a transformation that characterised the tissue deformation, which was then used to create a deformation-compensated PA image sequence for subsequent averaging.

Results

The echograms created photoacoustically were found to suffer from echo clutter which caused the speckle to decorrelate rapidly with deformation. This necessitated the development of a spatially and temporally regularised speckle tracking technique. Nevertheless, when used to produce deformation-compensated PA image sequences, this worked well enough for direct PA signals to show good temporal stability while the PA clutter decorrelated. Averaging of these sequences thus produced significant and useful PA clutter reduction in all cases.

Discussion and Conclusions

It has been shown for the first time that deformation-compensated averaging leads to improved clinical PA imaging of human vasculature in vivo, providing significant reduction of PA clutter and allowing blood vessels to be seen at 2 cm depth which were otherwise not visible. The future application of the method, using conventional (transmit-focused) echo images to characterise the tissue deformation, should lead to improved performance.

P6Aa-4

Thermoacoustic imaging and spectroscopy for enhanced breast cancer detection

Daniel Bauer[1], Xiong Wang[2], Hao Xin[2], Russell Witte[1]; [1]Department of Radiology, University of Arizona, USA, [2]Department of Electrical and Computer Engineering, University of Arizona, USA

Background, Motivation and Objective

Microwave-induced thermoacoustic imaging (TA) combines the excellent resolution and deep penetration of ultrasound imaging with the high contrast of microwave imaging. Previous studies have demonstrated that breast tumors produce strong thermoacoustic signals at GHz frequencies due to their high water content. However, clinical studies at 0.45 GHz failed to reliably discriminate malignancy from normal and benign tissue. We hypothesize that limitations in TA technology severely limited the capability and performance of previous imaging systems. This study demonstrates multiwavelength thermoacoustic spectroscopy for discriminating soft tissue and exogenous agents based on the magnitude and slope of the TA signal between 2.7 and 3.1 GHz.

Statement of Contribution/Methods

A narrowband, tunable microwave oscillator (Epsco PG5KB, 2.7 to 3.1 GHz, >300 nsec pulses, 5 kW/pulse) was used to acquire spectroscopic thermoacoustic images. The system was capable of simultaneously acquiring TA and traditional pulse echo ultrasound signals using a 2.25 MHz single element focused transducer with a resolution of approximately 1 mm. The transducer was raster scanned to produce B Mode images. We used the system to evaluate the microwave absorption properties of various samples, including fresh bovine fat, muscle, saline and ethanol. Whereas water has a strong positive microwave absorption slope between 2.7 and 3.1 GHz, ethanol has a published negative slope within this range.

Results

Figure 1 presents the B Mode pulse echo (1a) and co-registered thermoacoustic image (1b) acquired at 2.7 GHz (700 ns and 4 kW/pulse) of the ethanol-filled syringe denoted by the white circle (cross section). Although it is difficult to distinguish water from ethanol based solely on the magnitude of the TA signal, the negative slopes from ethanol is clearly distinct from the positive slopes of the surrounding water above the opening of the waveguide (dashed oval). The average TA slopes of ethanol and water in a 5.8x2.0 mm (441 pixels) rectangle region of interest were -6.08 dB/GHz and 7.99 dB/GHz, respectively.

Discussion and Conclusions

Thermoacoustic spectroscopy has great potential for helping classify different types of soft tissue, as well as identify microwave absorbing contrast agents. This technology potentially enhances the capability of TA to discriminate healthy from malignant breast tissue.

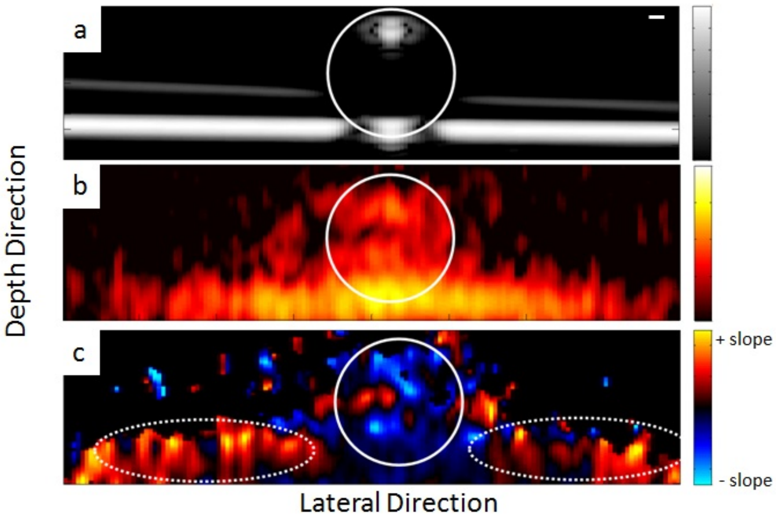

P6Aa-5

Sound velocity and attenuation measurement of perfluorocarbon liquids using photoacoustic methods

Eric Strohm[1], Michael Kolios[1]; [1]Physics, Ryerson University, Toronto, Ontario, Canada

Background, Motivation and Objective

Several methods exist for measuring the sound velocity and attenuation of liquids and biomaterials using reflection or transmission ultrasonic methods, however most studies were limited to narrow frequency ranges or have complex configurations requiring extensive calculations. Our group has developed novel perfluorocarbon droplets for photoacoustic imaging and cancer therapy, yet the acoustic properties (such as sound velocity as attenuation) are largely unknown for the frequencies of interest in our studies (100-1000 MHz). A method to determine the sound velocity and attenuation of liquids was developed using a photoacoustic technique, requiring as little as 20 µL of liquid.

Statement of Contribution/Methods

A scanning photoacoustic microscope was used for all measurements. A 1064 nm laser was focused to a 8 µm spot size onto a glass slide containing a thin (<1 µm) gold layer. Using water as a coupling fluid, the photoacoustic signal was recorded as a function of transducer position away from the gold in 0.5 µm steps (similar to a V(z) curve). The water was replaced with the liquid sample and the measurements repeated. Using the ratio of the time of flight data and the spectral phase and amplitude from the measurements of each liquid, the sound velocity and attenuation were calculated in reference to the known sound velocity and attenuation of water. Three transducers with center frequencies of 200, 375 and 750 MHz, each with approximately 45% bandwidth, were used to give a frequency range of approximately 100-1000 MHz.

Results

Castor oil was used to validate the methodology. The sound velocity was 1489±10, 1542±10 and 1593±10 m/s at 200, 375 and 750 MHz, respectively. The attenuation followed a power law, $\alpha(f) = 0.6\ f^{1.66}$. Two perfluorocarbon liquids commonly used in our droplet research were also measured, perfluorohexane (PFH) and FC-77. For PFH, the sound velocity was 485±8 and 479±8 at 200 and 375 MHz, with an $\alpha(f) = 1.2\ f^{1.55}$. For FC-77, the sound velocity was 555±1, 560±1 and 569±8 m/s at 200, 375 and 750 MHz respectively, with an $\alpha(f) = 0.8\ f^{1.50}$.

Discussion and Conclusions

A new method was developed to measure the sound velocity and attenuation of small samples using the photoacoustic signals generated by the light absorption of a gold layer, acting as an ultrasound source. Castor oil sound velocity and attenuation measurements agreed with previously published data. Many acoustic and photoacoustic models assume a constant sound velocity when probed with wideband high frequency transducers. The sound velocity of FC-77 increased 3% from 200 to 750 MHz, indicating that sound velocity measurements measured using commonly used clinical frequencies are not accurate for high-frequency studies. Due to the small liquid volume required, many applications using this method exist, which include measuring the ultrasonic properties of expensive or rare liquids, or extracted cellular material such as cytoplasm or DNA solution.

P6Aa-6

A Monte Carlo study on the effects of erythrocyte oxygenation on photoacoustic signals

Ratan K Saha[1], **Michael C Kolios[1]**; [1]Department of Physics, Ryerson University, Toronto, Ontario, Canada

Background, Motivation and Objective

The photoacoustic (PA) technique can provide a non-invasive method to monitor tissue oxygenation. Quantitative estimation of this parameter for brain tissue can play significant roles for treating patients with traumatic brain injury and for making clinical decisions during surgeries (e.g. cardiopulmonary bypass). A number of experimental studies have been carried out recently to examine the potential of the PA technique to monitor blood oxygenation for different clinical conditions. However, the effects of blood oxygenation on PA signals have never been studied theoretically. The aim of this work is to present simulation results investigating erythrocyte oxygenation dependent PA signals based on a recently proposed theoretical model.

Statement of Contribution/Methods

A Monte Carlo algorithm was used to simulate spatially random distributions of red blood cells. For such a configuration, the oxygen saturation level of some randomly chosen cells (N_O) was assumed to be 100% and that was 0% for the other cells (N_D). Accordingly, the oxygen saturation of the blood sample was obtained by defining, $SO_2 = N_O/(N_O+N_D)$. The oxygen saturation state of a RBC defines its optical absorption properties and thus controls the strength of the PA emission. The PA field generated by a cell

FRIDAY POSTER

approximated as a fluid sphere and characterized by its oxygenation state was obtained by solving the wave equation in the frequency domain and by implementing the appropriate boundary conditions. The linear superposition principle for the pressure waves emitted by the cells was then used to obtain the resultant PA signal from such a mixture of oxygenated and deoxygenated cells. The signal envelope statistics and spectral features were examined at two laser wavelengths (700 and 1000 nm) for blood samples at different SO_2 levels.

Results

The simulation results showed that the mean PA signal amplitude decreased monotonically as the SO_2 level increased for the 700 nm laser radiation. In contrast, the same quantity exhibited a monotonic rise as the SO_2 level increased for the 1000 nm optical source. The PA amplitude demonstrated nearly 7 fold decrease and 5 fold increase, respectively at those wavelengths when SO_2 level varied from 0 to 100%. Spectral intensity in the low frequency range (< 10 MHz) also decreased for the first laser and increased for the second laser with increasing SO_2. However, these trends were not observed between 10-100 MHz at SO_2 levels > 50%.

Discussion and Conclusions

The simulated trends are in accordance with those of experiments. For example, a nearly 5 fold increase of PA amplitude was measured at 1064 nm wavelength when SO_2 level varied from 10 to 99%. This agreement suggests that the model is capable to describe experimental observations and would be able to predict PA signal behaviors at different SO_2 levels.

P6Aa-7

The use of optically activated nanoparticles to enhance controlled lesion formation from high intensity focused ultrasound exposures

James McLaughlan[1], Todd W. Murray[2], Ronald A. Roy[3]; [1]Electronic and Electrical Engineering, University of Leeds, Leeds, West Yorkshire, United Kingdom, [2]Mechanical Engineering, University of Colorado Boulder, Boulder, CO, USA, [3]Mechanical Engineering, Boston University, Boston, MA, USA

Background, Motivation and Objective

Light-absorbing nanoparticles can be used to improve the signal-to-noise ratio of the thermoelastic emissions from tissue that are used in photoacoustic tomography (PAT) and microscopy (PAT). Nanoparticles can be functionalized to selectively target and, through the formation of vapor bubbles, destroy cancerous cells. It has been shown that simultaneously heating the nanoparticles with a laser whilst they are under tension from a high intensity focused ultrasound (HIFU) field, results in a significant reduction in the fluence and pressure thresholds for bubble formation. The localized heating from HIFU exposures in tissue is believed to be increased through the presence of bubbles, or specifically inertial cavitation, in the focal region. Thus an ability to nucleate vapor bubbles from nanoparticles using laser light combined with a HIFU field presents a unique opportunity for imaging and therapeutic applications.

Statement of Contribution/Methods

A 532 nm pulse laser was used to illuminate nanoparticle-doped tissue-mimicking phantoms (polyacrylamide with bovine serum albumin) in conjunction with ultrasound pulses generated by a 1.1 MHz HIFU transducer. The exposure timing was such that each 10 ns laser pulse occurred during a peak rarefaction period of the HIFU field. The HIFU exposure was either a 3-cycle burst or a 60 s 'quasi' continuous wave exposure (98% duty-cycle) for either imaging or therapeutic applications, respectively. A 7.5 MHz focused transducer, was confocally aligned with the HIFU transducer and used to detect broadband emissions generated by inertial cavitation during exposures.

Results

Figure 1 shows that for imaging (a) applications, broadband emissions associated with inertial cavitation were only generated from exposures where both laser and HIFU pulses were simultaneously used. This was also true for the therapeutic applications but in addition to the detection of broadband emissions, lesions were only observed in the phantoms for these conditions (b).

Discussion and Conclusions

This study demonstrates that optically-activated gold nanoparticles can be used to enhance lesion formation in a controlled manner when simultaneously exposed to light and ultrasound for both imaging and therapeutic applications.

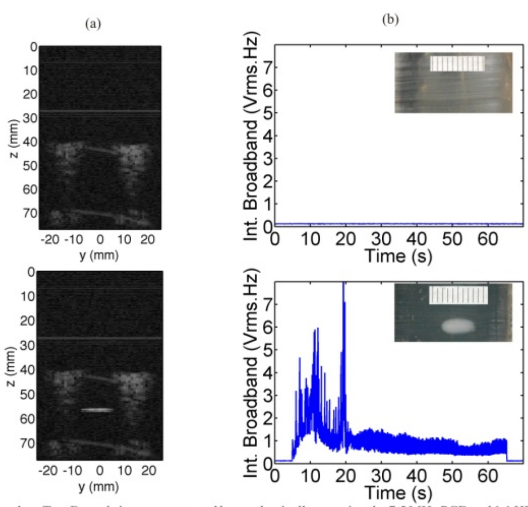

Figure 1. **Imaging**: Two B-mode images generated by mechanically scanning the 7.5 MHz PCD and 1.1 HIFU transducers over a 50 mm range without (top) and with (bottom) the laser on (a). For both of these images a 3-cycle HIFU burst was used. **Therapy**: Two plots showing the filtered, integrated broadband emissions detected during a 60s HIFU exposure with a peak negative pressure of 4.3 MPa, without (top) and with (bottom) the laser on (b). The inset photographs shown in (b) show the exposed region of the phantom (HIFU propagated from left to right).

FRIDAY POSTER

P6Aa-8

Photoacoustic imaging using narrow laser beam scanning

Jinjun xia[1], Chen-wei Wei[2], Lingyun Huang[2], Ivan Pelivanov[2,3], Matthew O'Donnell[2]; [1]bioengineering, University of washington, seattle, wa, USA, [2]bioengineering, University of washington, USA, [3]International Laser Center, Moscow State University, Russian Federation

Background, Motivation and Objective

Current systems designed for deep photoacoustic (PA) imaging typically use a low repetition rate, high power pulsed laser as the acoustic excitation source. The overall imaging frame rate is restricted by the laser repetition rate. An alternative is to fast scan a region of interest using a very high repetition rate fiber laser. A PA image is produced from the summation of individual PA images reconstructed at each laser beam position. This configuration can produce PA images with much higher frame rates than current systems.

As an initial proof of concept, we compare conventional broad beam illumination to a scanned beam approach in a simple model system.

Statement of Contribution/Methods

Two teflon tubes with diameters of 1.6 mm and 0.8 mm were filled with ink with 5 cm-1 optical absorption. They were buried within a chicken breast at a depth of 12 mm below the tissue surface. They were separated by 3 mm edge-to-edge to test spatial and contrast resolution for the two scan modes. The excitation source is a traditional OPO pumped by a Q-switched Nd:YAG laser. Photoacoustic images were reconstructed using signals from a scanned PVDF transducer. Two different illumination configurations were compared: one was 15 mm x 10 mm in cross section and acted as the broad beam; the other was 5 mm x 2 mm in cross section and was scanned over an region equivalent to broad beam illumination. Multiple images obtained during narrow beam scanning were added together to form one PA image equivalent to the single-shot broad beam one.

Results

Fig.1 shows beamformed RF images (i.e., bipolar presentation) for two different illumination modes. (A) was reconstructed from single-shot broad beam excitation; (B) was reconstructed by summing all individual narrow beam excitations scanned through the same region as the single-shot broad beam case.

Discussion and Conclusions

Our results indicate that narrow-beam scanning excitation can achieve equivalent SNR and spatial resolution as single shot broad beam excitation at 12mm depth within a model chicken breast medium. Results of the phantom study suggest that fast narrow-beam laser scanning can be used for deep tissue PA imaging.

This work was supported in part by the Life Sciences Discovery Fund (Grant # 3292512), and the Department of Bioengineering at the University of Washington.

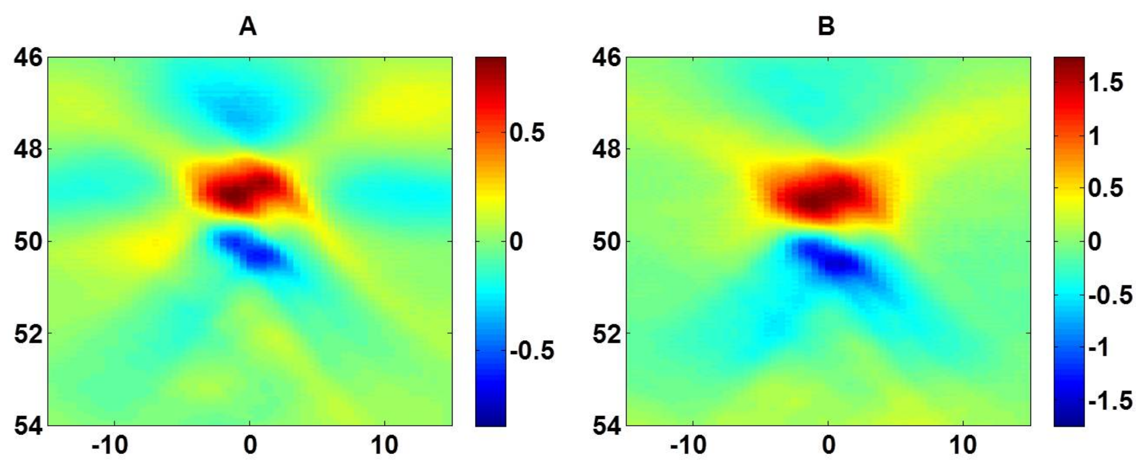

Figure 1. (A). Broad-beam excitation; (B). Narrow-beam excitation

P6Aa-9

Fabrication of Dye-Loaded Submicron Perfluorocarbon Droplets for Contrast Enhancement in Photoacoustic Imaging

Rei Asami[1], Ken-ichi Kawabata[1]; [1]Central Research Laboratory, Hitachi, Ltd., Tokyo, Japan

Background, Motivation and Objective

Acoustic vaporization of superheated perfluorocarbon (PFC) droplets is actively investigated for their use in contrast enhancement in ultrasonography and therapy [1][2]. We aim to provide optically vaporizable droplets for the purpose of photoacoustic (PA) contrast enhancement. Recent studies have shown that PA signals can be obtained from fluorocarbon droplets loaded with gold nano-particles [3]. We seek to incorporate a dye into fluorocarbon droplets as a chromophore, because its relatively small molecular size gives structural flexibility. More importantly, with an appropriate choice of dye spices, laser wavelength for triggering vaporization can be tuned to 700-1100 nm, the wavelengths known as "tissue transparent window" where penetration depth is optimal. In this study, dye-loaded submicron sized perfluorocarbon droplets were prepared and their PA characteristics were investigated. Also droplets' stability, a critical factor for volatile superheated PFC droplets, was evaluated.

Statement of Contribution/Methods

PFC mixture was combined with surfactant containing erythrosine B spirit and emulsified at high pressure to produce photosensitive droplets. Particle distribution was evaluated by laser diffraction method and monitored as droplets were shaken at 37 ºC. Droplets were suspended in an acoustically and optically transparent gel. The gel was placed in a water tank for PA characterization studies using a second harmonic wave of Nd:YAG laser (λ:532 nm). Vaporization was monitored with a clinical ultrasound scanner while photoacoustic signals were acquired with a broadband hydrophone. Droplets without a dye were used for a control study.

Results

Average particle diameter of photosensitive droplets was 385 nm and there was only 10 % increase in diameter after 24 hours of shaking. A significant increase in echo signal intensity was observed immediately after irradiation of laser pulse of 80 mJ/cm^2. A characteristic broadband acoustic signal was observed simultaneously. At lower laser pulse energy, the broadband signal was acquired with hydrophone while no change in echo intensity was observed. Neither a change in echo signal intensity nor a characteristic acoustic signal was observed among control group.

Discussion and Conclusions

Stable hydrophobic dye-loaded droplets were successfully fabricated. The droplets were optically vaporized and resulted in a significant PA signal. A PA signal from a thermal expansion was still present below the pulse energy threshold for vaporization. The study suggests a possibility of PA contrast enhancement for any wavelength by simply substituting a dye with one with a desired absorption spectrum. Further improvements must include increasing optical sensitivity of droplets.

[1] Kripfgans, O., et al., Ultrason. Med. and Biol., 26 (2000), 1177-89

[2] Kawabata, K., et al, Jpn J Appl Phys, 44 (2005), 4548-52

[3] Wilson, K., et al, Proc. SPIE, 7564 (2010), 75642P1-5

P6Aa-10

Improved Synthetic Aperture Focusing Technique for Acoustic-resolution Photoacoustic Microscopy

Meng-Lin Li[1], Yi-Chieh Tseng[1], Po-Hsun Wang[1]; [1]Dept. of Electrical Engineering, National Tsing Hua University, Hsinchu, Taiwan

Background, Motivation and Objective

Acoustic-resolution photoacoustic microscopy (AR-PAM) capable of imaging micro-vessels with high resolution and high contrast has shown its potential in functional neuro-vascular imaging, dermatology and related cancer research. In AR-PAM, A mechanically scanned, single crystal transducer with a fixed focus is commonly used, which causes the image quality to deteriorate significantly in the out-of-focus region. A virtual-detector based synthetic aperture focusing technique (VD-SAFT) was used previously to extend the depth of focus of the AR-PAM where the focal point of the transducer is treated as a virtual point detector. However, the performance of VD-SAFT is impaired by its high sidelobes.

Statement of Contribution/Methods

Such high sidelobes result from over-simplified virtual-point-detector approximation of the focal point. To solve this problem, we introduce an improved synthetic aperture focusing technique (ISAFT) for AR-PAM, which considers diffraction effect in the vicinity of the VD, i.e., the focal point. This technique is based on a linear, discrete model of the AR-PAM system developed using matrix formalism. Using this model, a spatiotemporal optimal filter in minimum mean square error sense is designed to deconvolve the spatial impulse responses associated with the focused transducer at every imaging point; thus retrospective focusing can be achieved.

Results

The performance of the proposed ISAFT is verified using simulation data. A 25-MHz AR-PAM with a single element transducer which has a 6-mm diameter and a 12-mm focal depth (i.e., f-number = 2) is simulated. The figure shows the original, VD-SAFT, and ISAFT images of a point target at the depth of 10 mm, and their projected beam profiles, respectively. The images are displayed on 30-dB dynamic range. The improvement in spatial resolution of ISAFT is superior to that of VD-SAFT because the full geometry of the VD, instead of the simplified virtual-point-detector approximation, is taken into consideration.

Discussion and Conclusions

It is demonstrated by simulation that the proposed method effectively improves the degraded lateral resolution in the out-of-focused region for AR-PAM. Future work will focus on the phantom and in vivo experimental verifications and the study of the effect of signal-to-noise ratio on the ISAFT.

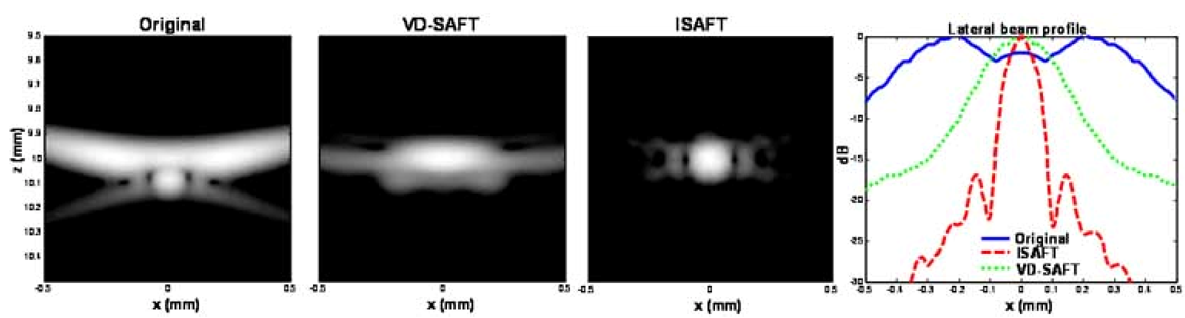

FRIDAY POSTER

P6Ab - Shear Wave Elastography II

Carribean Ballroom III-V

Friday, October 21, 2011, 1:00 pm - 4:30 pm

Chair: **Emad Ebinni**
Univ. of Minnesota

P6Ab-1

Real-Time Quantitative Elastography on Standard Ultrasound Using Mechanically Induced Vibration: System Design and Initial Results

Reza Zahiri Azar[1], Kris Dickie[1], Benjamin Kerby[1], Sergio Bernardo[1], Chris Cheung[1], Laurent Pelissier[1]; [1]*R&D, Ultrasonix Medical Corporation, Richmond, BC, Canada*

Background, Motivation and Objective

Vibration elastography VE has been well established in the literature as a mean of assessing the elasticity of the liver which correlates with fibrosis stages. Previous studies have focused mainly on single element transducer, ultrafast scanners, and magnetic resonance imaging. In this work, we report implementation of a VE system on a standard ultrasound scanner that enables quantitative assessment of tissue elasticity in real-time.

Statement of Contribution/Methods

In order to induce vibration, a linear actuator has been designed and mounted on an ultrasound transducer. A programmable signal generator and an amplifier has also been integrated into the mount to drive the actuator. In addition to B-mode imaging for real-time targeting, two custom imaging modes have been implemented to provide fast RF acquisition rate for elastography. In the first mode, a 1D window of RF signal from a single scan line is acquired at 5kHz for 100ms. In the second mode, by relaxing the requirement for high acquisition rate, a 2D window of RF signals that consists of a small group of scan lines is acquired at 1kHz. Following data acquisition, axial wave images were estimated from the sequences of RF signals. Algebraic Helmholtz inversion of the wave equation was then used to estimate the absolute tissue elasticity from these wave images. Finally, the estimated elasticity value was displayed on the screen along with the wave image and B-mode image at an overall refresh rate of 2 to 6 frames per second.

Results

In the experiments on a commercial elasticity phantom (CIRS, VA, USA), the reported Young's moduli of 25±4 kPa were estimated to be 27±7 kPa for 10 subsequent measurements, in both 1D and 2D modes. Current interface of the VE system on the SonixTouch ultrasound machine is show in Figure 1.

Discussion and Conclusions

The proposed VE system can be implemented on most ultrasound systems with small overhead. It can also be combined with compression elastography to provide quantitative elastograms for better characterization of liver tissue. Initial *in-vivo* results on healthy volunteers were promising. In future, the system will be used in clinical setup for noninvasive staging of liver fibrosis. The results will also be compared with the result of the biopsy as a gold standard.

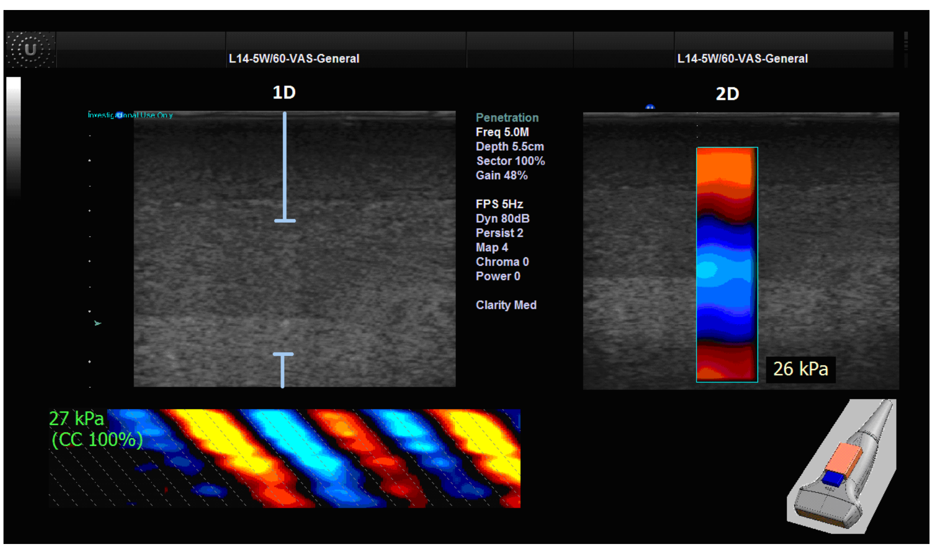

P6Ab-2

Shear Wave Speed Measurements Using Ultrasound Radiation Force Can be Depth Dependent

Heng Zhao[1], Pengfei Song[1], Matthew W. Urban[1], Randall R. Kinnick[1], Meng Yin[2], James F. Greenleaf[1], Shigao Chen[1]; [1]Physiology and Biomedical Engineering, Mayo Clinic College of Medicine, Rochester, Minnesota, USA, [2]Radiology, Mayo Clinic College of Medicine, Rochester, Minnesota, USA

Background, Motivation and Objective

Measurement of shear wave propagation speed c_s has important clinical applications because it is related to tissue stiffness and health state. Shear wave speed can be measured by tracking the lateral propagation of shear waves generated by a focused ultrasound push beam. This study evaluates if c_s thus measured depends on measurement location and the transducer being used.

Statement of Contribution/Methods

Three homogenous elasticity phantoms with different c_s calibrated by Magnetic Resonance Elastography (MRE) and 1D Transient Elastography (TE) were used in this study. Measurements of c_s were made with a curvilinear transducer C4-2 (3 MHz center frequency) and a linear array transducer L7-4 (5 MHz center frequency) using a Verasonics ultrasound system in each phantom. The focal point of the push beam for each transducer was positioned at 5 different depths without steering. Three transmit aperture sizes (32, 64, and 96 elements) were used to produce shear waves at each focal depth, and measurements were repeated at 5 different locations within each phantom for each of the setup combinations. Propagation of shear waves was monitored using plane wave imaging at a frame rate of 4 kHz. Shear wave displacement was calculated using 1D autocorrelation. Shear wave speed (group velocity) was then estimated from the arrival time of the shear wave peak at different lateral locations through linear regression.

Results

Figure 1 shows the representative results from phantom 2. Shear wave speed measured by the C4-2 was depth dependent but not sensitive to transmit aperture size. Results obtained with the L7-4 were close to those obtained by MRE and TE, and were not sensitive to focal depth and aperture size. Results in two other phantoms showed similar trends.

Discussion and Conclusions

The intensity field of the push beam from the C4-2 was measured and found to have two split peaks in the elevational plane when focusing at 30 mm (also confirmed by Field II simulation). Implications of such undesired beam shape for c_s measurements and possible correction options will be discussed. In conclusion, shear wave speed measured using focused push beams may be transducer and depth dependent requiring careful monitoring or correction for clinical applications.

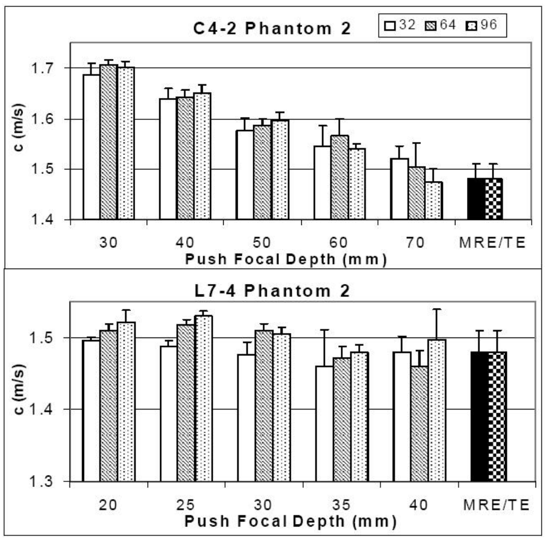

P6Ab-3

High Frequency Acoustic Radiation Force Elastography for Imaging the Elastic Properties of Tissues

Cho-Chiang Shih[1], Chih-Chung Huang[1]; [1]Department of Electrical Engineering, Fu Jen Catholic University, Taiwan

Background, Motivation and Objective

Recently, acoustic radiation force impulse (ARFI) imaging has been shown its potential to detect the elastic properties of soft tissues. The acoustic radiation force can be applied to create localized tissue displacement, and that this displacement can be directly related to the localized tissue elastic properties. However, most ARFI imaging systems can not provide high resolution elastography for some microstructure tissues, such as ocular and skin. In present study, a high frequency acoustic radiation force elastography was proposed for this purpose.

Statement of Contribution/Methods

The experimental setup is shown in Fig. 1(a). A confocal ultrasonic transducer (Fig. 1(a)) was fabricated for imaging the phantom which within two different gelatin stiffnesses. The acoustic radiation force was generated by 20 MHz outer element (PZT-4, 1-3 composite) to create the tissue displacement, and this displacement was detected by 50 MHz inner element (PMN-PT) using pulse-echo algorithm. Two types of gelatin phantom were used for system verification. 2D elastography was obtained via the mechanical scan under different depths.

Results

Figure 1 (b) shows the 50 MHz B-mode image with corresponding high frequency acoustic radiation force elastography from gelatin phantoms. Each phantom contains two different gelatin stiffnesses (2% and 6%) but the similar carbon fiber concentration. Since both sides of phantom had the same particle concentration, the B-mode image has similar speckle pattern. However, the difference of gelatin stiffness was observed clearly from high frequency acoustic radiation force elastography.

Discussion and Conclusions

The difference of gelatin elastic property within a dimension of 1×1 mm was determined by high resolution acoustic radiation force elastography. The elastic modulus for 2% and 6% gelatin was assessed approximately 0.4 kPa and 1.8 kPa, respectively. The result shows the potential of using high frequency ARFI imaging for characterizing the elastic properties of cornea and skin in the future.

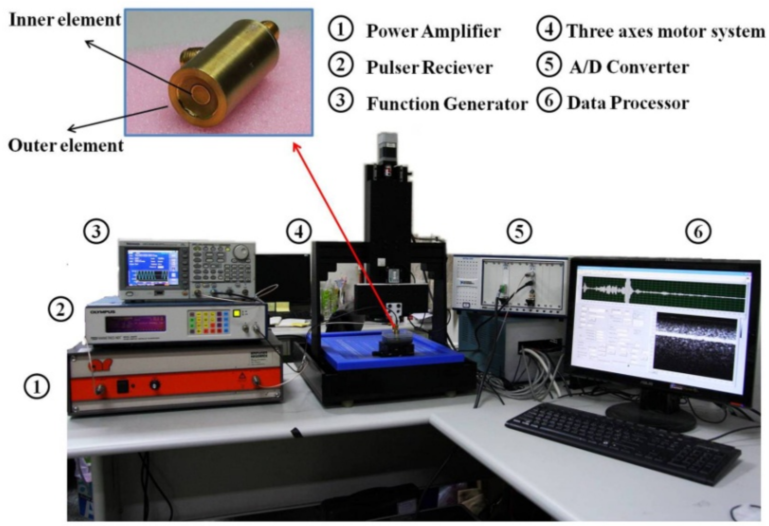

(a)

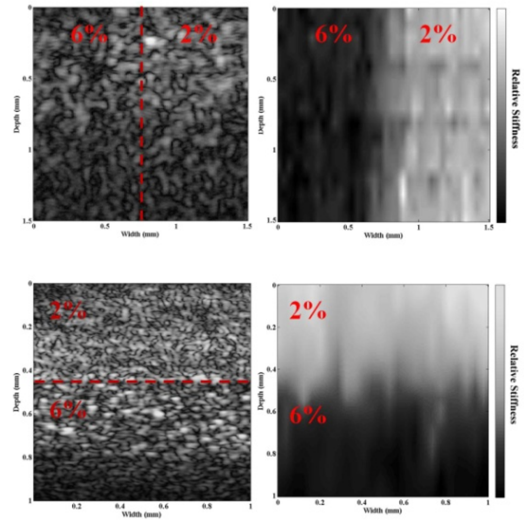

(b)

P6Ab-4

Finite Element Modeling for Shear Wave Elastography

Shiwei Zhou[1], Jean-Luc Robert[1], John Fraser[2], Yan Shi[1], Hua Xie[1], Vijay Shamdasani[2]; *[1]Philips Research North America, USA, [2]Philips Healthcare, USA*

Background, Motivation and Objective

Shear wave elastography is an important imaging modality to evaluate tissue mechanical properties and supplement the conventional ultrasound diagnostics imaging. A finite element model has been created for simulating and understanding shear wave generation by the acoustic radiation force, and its propagation through different media.

Statement of Contribution/Methods

A 3D finite element model was built in PZFlex (Weidlinger Associates Inc, CA), and the simulation settings were based on a shear wave elastography prototype using Philips iU22 scanner with C5-1 curvilinear probe. The modeling process was divided into two steps. In the first step, the acoustic field of the ultrasound probe was calculated and the output acoustic radiation stress (ARS) result in the 3D volume was saved. In the second step, the ARS data was applied as a boundary condition to generate shear wave. The shear wave displacement time profiles in the region of interest were recorded at the end of the second step.

Results

The simulation was performed for different media, including uniform tissues with various shear modulus (2KPa ~ 8KPa) and viscosities (0PaS ~ 8PaS), as well as uniform tissue background with embedded stiffer inclusion. Clear differences were observed on the shear wave displacement time profiles, as the displacement peak was attenuated and widened by the higher shear modulus and viscosity. The simulation result was also cross-checked with elasticity reconstruction algorithms based on wave equation (WE), Voigt model (VM) and time-to-peak (TTP) method. For a medium similar to normal liver tissue with 2KPa shear modulus, all three reconstruction methods reported shear modulus approximately the same as input value when the viscosity was negligible (WE: 2.05KPa, VM: 1.93KPa, TTP: 1.87KPa). With increased viscosity in the medium (2KPa, 2PaS), TTP seemed to under-estimate shear modulus in the near-field (WE: 2.44KPa, VM: 1.84KPa & 2.04PaS, TTP: 1.36KPa). For a uniform medium with an embedded spherical inclusion, all three methods successfully detected the inclusion and reconstructed stiffness maps.

Discussion and Conclusions

The results suggested that the finite element modeling could provide valuable insight in simulating and understanding shear wave generation and propagation. It could also be an important tool to evaluate and analyze stiffness reconstruction algorithms for shear wave elastography.

P6Ab-5

Precise Tracking of Impulsive Acoustic Radiation Force Induced Small Displacements for Shear Wave Speed Estimation

Yang Shen[1], Feiyan Cai[1], Yang Xiao[1], Tao Ling[1], Chengzhi Zeng[1], Qiaofeng Jin[1], Xin Liu[1], Hairong Zheng[1]; [1]Paul C. Lauterbur Research Center for Biomedical Imaging, Shenzhen Institutes of Advanced Technology, Chinese Academy of Sciences, China, People's Republic of

Background, Motivation and Objective

Impulsive acoustic radiation force (ARF) generates localized small displacements (typically less than 20 microns) in soft tissues and induces shear waves which travel perpendicular to the pushing direction. The shear wave speed determined by tissue elasticity can be estimated using time-of-flight method. The small displacements need to be accurately calculated, commonly by phase-shift estimation, to obtain the Displacement-to-peak (DOP) time. This work proposes a novel phase-shift based algorithm being able to track the small displacements (even smaller than sample distance) in a more precise and quick way.

Statement of Contribution/Methods

The new phase-shift algorithm was developed based on Hilbert Transform (HT) approach using adaptive gradient of the phase angle to extract phase-shifts. The experimental RF lines on both axial and off-axial were acquired simultaneously to track the displacements induced by a single pushing pulse in tissue-mimicking phantom with calibrated shear wave speed (0.6 ~ 1 m/s). 8 groups' data acquisitions were performed. The displacement field was calculated based on HT method and the shear wave speed was obtained by means of the lateral DOP time. The method was compared with Kasai's algorithm (C. Kasai et al., IEEE Trans. Sonics Ultrason., 1985) which uses I/Q data with a fixed center frequency to determine the displacement, and Loupas' algorithm (T. Loupas et al., IEEE UFFC Trans, 1995) that also uses I/Q data but with corrected RF center frequency along each axial extent.

Results

For very small displacements (several microns), the HT approach showed the best performance compared with the two I/Q methods. As the displacement increase, Loupas's algorithm and HT method performed comparable. The error for Kasai's algorithm was significantly larger than that of the other two methods. The DOP time at the focal point on axial were 5±0.25ms and that time at the foci offset laterally increased. At the lateral offset of 1 cm, the DOP time reached to 18.6±0.6ms. The DOP time does not changed with pushing time and input power, which is in accordance with that the time is only determined by the parameters of the transducer and the tissue features (A. P. Sarvazyan et al., UMB, 1998). The shear wave speed was computed as 0.7353±0.05m/s.

Discussion and Conclusions

Shear wave speed can be estimated based on the lateral time-of-flight approach in the displacement field. Kasai's method uses the center frequency of the transducer as that of the received RF echo to acquire the small displacements. However, the center frequency of RF line decreases along the axial depth. Loupas' algorithm corrects the mean RF frequency along each axial extent that yields more accurate estimates. The modified HT method presented in this work uses adaptive gradient of the phase angle to calculate the phase-shift time, which improves the precision and reduces the computational load as there is no need for calculating center frequencies.

P6Ab-6

Phase Aberration in Shear Wave Dispersion Ultrasound Vibrometry

Yan Shi[1], Hua Xie[1], Vijay Shamdasani[2], John Fraser[2], Jean-Luc Robert[1], Shiwei Zhou[1], Matthew W. Urban[3], Shigao Chen[3], James F. Greenleaf[3]; *[1]Philips Research North America, Briarcliff Manor, NY, USA, [2]Philips Ultrasound, Bothell, WA, USA, [3]Department of Physiology and Biomedical Engineering, Mayo Clinic College of Medicine, Rochester, MN, USA*

Background, Motivation and Objective

Shear wave Dispersion Ultrasound Vibrometry (SDUV) is an acoustic radiation force-based technique that measures tissue shear elasticity and viscosity by characterizing shear wave speed dispersion. The technique has been prototyped on the Philips iU22 ultrasound system with a C5-1 probe. We previously reported findings from an animal study where larger variations in reconstructed liver shear modulus and viscosity were observed for in vivo versus ex vivo cases.

Statement of Contribution/Methods

This study investigates two major causes of such increased variations, namely attenuation and phase aberration. Our hypothesis is that phase aberration is the most likely reason due to substantial fat/muscle layers in studied animals (pigs). To validate this, a series of experiments were conducted using a custom phantom with known shear modulus (2 ± 0.7 kPa) and very little viscosity. Initially, the phantom was imaged directly with varying push power by setting system transmit attenuation at different levels from 0 dB to 6 dB. The second set of experiments utilized different pieces of pork bellies as aberrators between the probe and the phantom, while maintaining the push power at 0 dB. For each dataset, SDUV reconstruction algorithms yield shear moduli within a ROI of 10 mm x 4 mm close to the push focus (~45mm).

Results

The results are summarized in Table 1. It shows that decreasing push power led to slight increases in shear modulus variation and greater deviation from the ground truth. The pork bellies caused varying degrees of degradation in reconstruction results, ranging from mild to significant. The variations were typically much higher than those from pure attenuation. In particular, some datasets manifested significant variations even when displacements were similar to those achieved at 3 dB attenuation.

Discussion and Conclusions

This work indicates that beam distortion due to inhomogeneous fat/muscle layers is the main cause of elevated variations and should be considered when optimizing SDUV reconstruction performance.

(Mayo Clinic and Drs. S. Chen and J. Greenleaf have a financial interest in the technology used in this research. That technology has been licensed to Philips Electronics for research purposes, and Mayo Clinic has received royalties greater than the federal threshold for significant financial interest. To date, Drs. Chen and Greenleaf have received no royalties.)

Table 1: Reconstructed shear modulus under different conditions. For each measurement, the mean and standard deviation within ROI are listed.

Attenuation	0 dB	1 dB	2 dB	3 dB	4 dB	5 dB	6 dB
Shear Modulus (kPa)	2.25 ± 0.41	2.41 ± 0.51	2.37 ± 0.46	2.10 ± 0.45	1.97 ± 0.56	3.00 ± 0.72	4.11 ± 3.10
Pork Belly (3.5cm)	**Pos1**	**Pos 2**	**Pos 3**	**Pos 4**	**Pos 5**	**Pos 6**	**Pos 7**
Shear Modulus (kPa)	2.23 ± 1.92	2.21 ± 1.44	1.66 ± 0.36	1.93 ± 0.48	3.91 ± 6.41	3.01 ± 7.38	5.19 ± 7.50

P6Ab-7

Improving Shear Wave Velocity Imaging of Thermal Ablations by Assuming Bidirectional Shear Wave Propagation

Ryan DeWall[1,2], Tomy Varghese[1,2]; [1]Department of Medical Physics, University of Wisconsin-Madison, USA, [2]Department of Biomedical Engineering, University of Wisconsin-Madison, USA

Background, Motivation and Objective

Abdominal thermal ablation procedures provide a minimally invasive treatment option for hepatic malignancies, and ultrasound is often used for real-time guidance of the ablation needle into the malignant target. However, B-mode imaging has been shown to be a poor modality for monitoring ablation procedures because of the similar echogenic characteristics of ablated and untreated tissue. Electrode vibration elastography (EVE) is a recently developed technique used to monitor ablation procedures, whereby shear waves are generated via internal mechanical vibration and tracked with ultrasound, and shear wave velocity is reconstructed using the time-to-peak algorithm. EVE provides good lateral boundaries but more ambiguous axial boundaries, which may result from assuming lateral shear wave propagation. In the case of shear wave generation via external mechanical vibration, diffraction effects lead to a longitudinally polarized component. In this study, we reconstruct shear wave velocity assuming both axial and lateral propagation with internal vibrations and investigate the effects on ablation representation on shear wave velocity images.

Statement of Contribution/Methods

Bidirectional shear wave velocity reconstruction was investigated in finite element simulations, tissue mimicking phantoms, and ex vivo ablations. A finite element model of EVE simulating a hard inclusion in a soft background and a corresponding tissue-mimicking phantom were created. EVE was performed using a piezoelectric actuator and custom beam sequencing programmed on an Ultrasonic SonixTOUCH scanner. Finally, EVE was performed on a radiofrequency ablation formed in ex vivo bovine liver tissue. Gradients of the time-to-peak displacement image were taken axially and laterally. For each pixel location, the larger of the two gradients was used in a combined gradient image, the inverse of which yields the combined shear wave velocity image.

Results

Shear wave velocity reconstructions from finite element data showed a decrease in artifacts above and below the ablation when assuming bidirectional wave propagation. A tissue mimicking phantom confirmed this. Area was overestimated in the phantom inclusion by 13.4% with the purely lateral propagation assumption because of artifacts above and below the inclusion; however, area overestimation was reduced to 3.6% when assuming bidirectional propagation. Artifacts were similarly minimized in an ex vivo bovine ablation; area overestimation was reduced from 9.1% to 0.8%.

Discussion and Conclusions

Assuming bidirectional shear wave propagation has shown to minimize artifacts in shear wave velocity images using EVE, particularly above and below the inclusion. Boundary delineation was improved, and the shape of the inclusion in both phantoms and ex vivo tissue more closely resembled the actual inclusion shape.

This work is supported in part by NIH grants R01 CA112192-04, R01 CA112192-S103, and T32 CA09206-31.

P6Ab-8

Impacts of the Capsule on Estimation of Shear Viscoelasticity of Livers

Yi Zheng[1], Ke Chen[1,2], Aiping Yao[1], Eugene Zheng[3], Tianfu Wang[4], Siping Chen[4]; [1]Electrical and Computer Engineering, St. Cloud State University, St. Cloud, MN, USA, [2]Biomedical Engineering, Sichuan University, Chengdu, Sichuan, China, People's Republic of, [3]Dartmouth College, Hanover, NH, USA, [4]Biomedical Engineering, Shenzhen University, Shenzhen, Guandong, China, People's Republic of

Background, Motivation and Objective

Recently, liver tissue properties of shear viscoelasticity were investigated by several research groups. Those studies apply ultrasound radiation force in tissue regions of livers, measure the phase velocities of shear wave up to a few hundred Hertz, and inversely solve the Voigt model with an assumption that liver local tissue is isotropic without considering boundary conditions. The primary objective of this research is to study the impact of the capsule of livers as a boundary on the estimation of the shear viscoelasticity of livers with increased frequencies of shear wave.

Statement of Contribution/Methods

In vitro experiments were designed and conducted to investigate shear moduli of superficial tissue below capsule of livers (0.4 mm) to deeper tissue of livers (7 mm) using the method of Shearwave Dispersion Ultrasound Vibrometry (SDUV). The experiments and liver phantoms are carefully designed and constructed to increase the efficiency of the transmission and the sensitivity of the receiving at higher frequencies. Both binary and specially designed pulses with a center frequency of 3.3 MHz are transmitted to induce shear wave that has high harmonics ranging from 100 Hz to 1.2 kHz. Pulse echo ultrasound, with a center frequency of 7.5 MHz and a pulse repetition frequency of 4 kHz, is used to detect the phase shifts over a distance of 4 to 8 mm away from the center of the radiation force. Using measured phase velocities, Voigt, Maxwell, and Zener models are inversely solved for the shear moduli with a procedure that provides the initial values for robust inverse solutions.

Results

The distributions of measured phase velocities are significantly different from the deeper tissue to superficial tissue when the shear waves at higher frequencies are included. The phase velocities of higher frequencies in the superficial tissue are increased at a rate significantly lower than that in the deeper tissue. It leads large fitting errors when the Voigt model is applied to the shear wave measured in the superficial tissue. Given the same liver, estimated shear elasticity and viscosity are widely ranged and can be different by a factor of two for the superficial tissue and deeper tissue. On the other hand, the Voigt model fits well for the phase velocities measured from deeper tissue and the Zener model fits well for both superficial tissue and deeper tissue of the livers.

Discussion and Conclusions

The capsule of livers has significant impacts on the estimation of shear moduli of the liver tissue that is close to the capsule. The Voigt model only works well for the deeper tissue, not the superficial tissue. While the Zener model fits well for both superficial tissue and deeper tissue of livers, cautions are needed to interpolate the fitting results.

This work is supported in part by China Scholarship Council and a grant from Chinese Natural Science Foundation.

P6Ac - Contrast Agents II

Carribean Ballroom III-V

Friday, October 21, 2011, 1:00 pm - 4:30 pm

Chair: **Lori Bridal**
Univ. Pierre and Marie Curie

P6Ac-1

The Effect of Vial Activation Temperature on the Acoustic Properties of Definity

Xuan Huo[1], **Brandon Helfield[1,2]**, David Goertz[1,2]; [1]Imaging Research, Sunnybrook Research Institute, Toronto, Canada, [2]Medical Biophysics, University of Toronto, Toronto, Canada

Background, Motivation and Objective

Definity® is a widely used clinically available contrast agent. The manufacturer's instructions indicate that the vial should be allowed to reach room temperature prior to the 45s mechanical activation process. Activation results in a heating of the vial, and we have previously observed that 'smaller' bubbles are formed later in this process (>10s) when the vial temperature is elevated. The objective of this work was to examine the potential effects of initial vial temperature on the frequency dependent acoustic response of Definity®. In practice, vials may not always activated at room temperature which may be a significant source of measurement variability. Further, if initial temperature has an effect it may provide a simple means by which to alter the active frequency range of Definity®.

Statement of Contribution/Methods

Experiments were conducted with vials at refrigerator temperature (2°C), room temperature (22°C), or 37°C at the outset of the activation procedure. In all cases agent was extracted from the vials 15 minutes after activation, after cooling to room temperature. Size distribution measurements were performed with a Coulter counter. Attenuation measurements were performed to provide insight into the frequency dependent (2-27 MHz) response of the agent at low pressures. Nonlinear imaging performance was assessed for agent within a wall-less vessel phantom using a Phillips C5-1 probe at a low mechanical index (0.05).

Results

The size distributions were found to be strongly dependent on initial vial temperature. Most notably, the 2° and 37° cases had respectively 2.02 and 0.51 times the number density of the 22° case for bubbles in the 2-5μm size range. The attenuation results indicated considerable differences in the frequency response of the agent, in particular the appearance of a peak at 3-4 MHz for the 2° case (Figure). Nonlinear imaging results indicated that 2° vials produced an enhancement 4.6 dB greater than for 22° Definity®.

Discussion and Conclusions

These results indicate that not permitting the vial to reach room temperature has a considerable impact on the imaging performance of Definity® and may be a source of variability in clinical work. Alternatively, controlling the initial vial temperature may provide, to some extent, a means by which to intentionally modify the active frequency range.

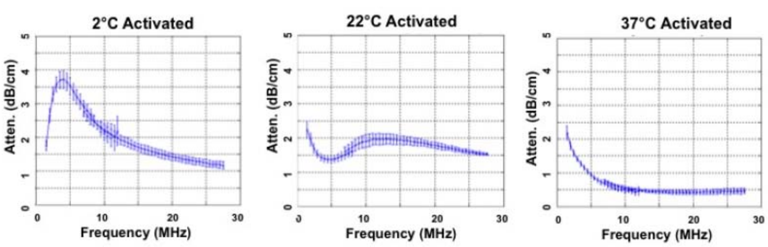

Figure. Frequency dependant attenuation results for the three vial activation temperatures show substantial differences. In particular, a pronounced peak in the 3-4 MHz range is evident for the refrigerator temperature vial.

P6Ac-2

Optical Fluorescence Studies of Perfluorocarbon Droplet Vaporization

Nikita Reznik[1], Minseok Seo[1,2], Ross Williams[2], Naomi Matsuura[1,2], Peter Burns[1,2]; [1]Medical Biophysics, University of Toronto, Canada, [2]Sunnybrook Research Institute, Toronto, Canada

Background, Motivation and Objective

Sub-micron droplets of liquid perfluorocarbon (PFC) can be vaporized into gas bubbles in vivo by externally applied ultrasound, with potential application to diagnosis and therapy. However, little is known about the mechanisms of droplet vaporization and the composition of the bubbles so produced. Here, we observe droplets with fluorescent labels associated either with the PFC liquid or the lipid shells, before and after vaporization, using optical imaging techniques.

Statement of Contribution/Methods

These studies examine the relationship between the components of the bubble and the droplet that produced them. Droplet emulsions were labeled with DiIC-18 fluorescent marker by combining the dye with phospholipid to produce fluorescent shells or with PFC and diethyl ether to produce fluorescent liquid droplets. Micrometer sized PFC droplets were vaporized with a single 50-cycle pulse at 10 MHz. Optical observation was performed under a microscope in either fluorescence or brightfield mode with a 60x microscope objective (NA = 1.0).

Results

Optical images of droplets before and after vaporization show the fluorescent label prior to ultrasound excitation, with sharp contrast between the droplet and surrounding liquid. Confocal microscopy of the droplets using a 100x objective (NA = 1.0) with 0.5 µm slice thickness confirmed that the dye was localized to the shell or liquid before vaporization. Following vaporization, the bubbles exhibit a rapid decrease in overall fluorescence signal. However, non-fluorescent droplets with fluorescent shells are shown to retain the signal around the bubble edge in some cases.

FRIDAY POSTER

Discussion and Conclusions

The results show that it is possible to create emulsions of liquid PFC droplets with fluorescently labeled liquid PFC bulk or lipid shell material, which can be vaporized with applied ultrasound. Loss of fluorescence suggests dissolution of fluorescent marker from the vaporized droplet, yet, retention of fluorescent signal at the edge of the bubble suggests the possibility of the presence of encapsulating shell material. This model may provide insight into the presence of a coating around the bubble after vaporization, facilitating the study of stability of the bubbles after vaporization, and will be a valuable tool in the study of droplet vaporization mechanisms on microsecond timescales.

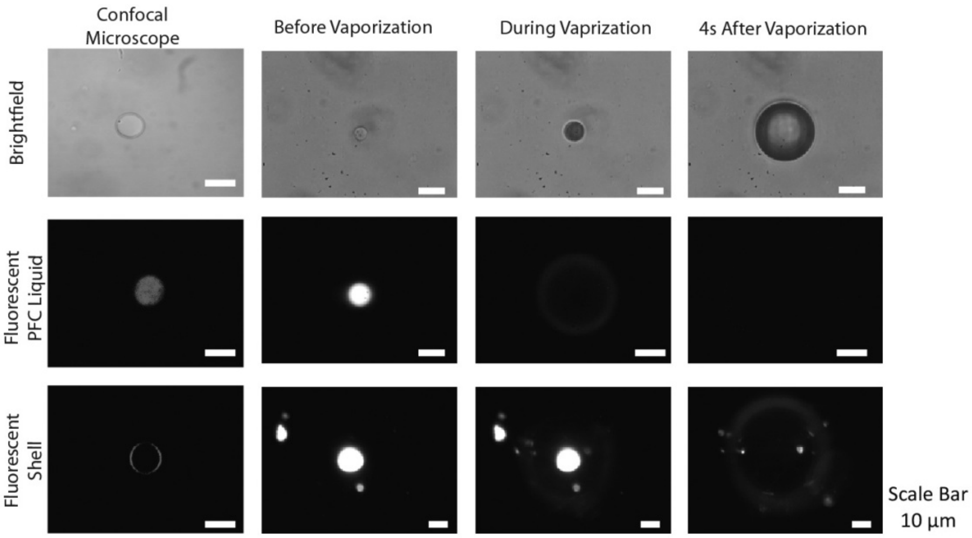

P6Ac-3

Using Fluidity Regulation to Control Size Distribution of Lipid-coated Bubbles

Chung-Hsin Wang[1], Chih-Kuang Yeh[1]; [1]Department of Biomedical Engineering and Environmental Sciences, National Tsing Hua University, Taiwan

Background, Motivation and Objective

The high flexibility of coated lipid shells makes lipid-based bubbles highly echogenic and ideal for the detection of nonlinear oscillation responses. Compared with imaging unbounded bubbles, the detection of targeted ones in molecular imaging presents new challenges due to sparse bounded bubbles. The effectiveness of ultrasound molecular imaging could be further improved by making the resonance frequency of bubbles correspond to scanning systems. Nevertheless, the resonance frequency is critically affected by bubble radius. Thus, we aimed to develop a size-controlling technique that could adjust the size distribution of fabricated bubbles.

Statement of Contribution/Methods

We have used three materials with diverse initial fluidities and phase behaviours to investigate the feasibility of size control via fluidity regulation. The PEG40S emulsifier, whose miscibility has been widely discussed, was mixed with DPPC and DSPG materials that exhibit distinct main phase transition temperatures to demonstrate the regulation. Several formulations were compared by analysing size distribution data in order to elucidate the relationship between size and regulation. Further, the fluidities at different temperature were measured through fluorescence anisotropy to identify the hypothesis of this concept.

Results

The increasing level of PEG40S enlarges the bubbles but enhances the foaming and thermic side effects. Introducing DSPG reduced the mean size and limited the foaming effect, behaviours that were totally different from those for PEG40S. Moreover, DSPG extended the tailoring range of this fluidity regulation technique. Adjusting both the ratio of DSPG and the level of PEG40S simultaneously allowed refined and continuous changes in the bubble distribution shown in figure 1. The ratios listed in figure 1 were the compositions of each formula (DPPC:DSPG:PEG40S).

Discussion and Conclusions

Controlling and maintaining the bubble size in each formation process are the important issues for researchers, especially in high-sensitivity required and size-dependent applications. The results indicated the size distribution could be naturally controlled by modifying the coating compositions. Even though using different fabrication systems results in totally different distributions, we claim that fluidity regulation can be used to adjust the mean size in different systems.

FRIDAY POSTER

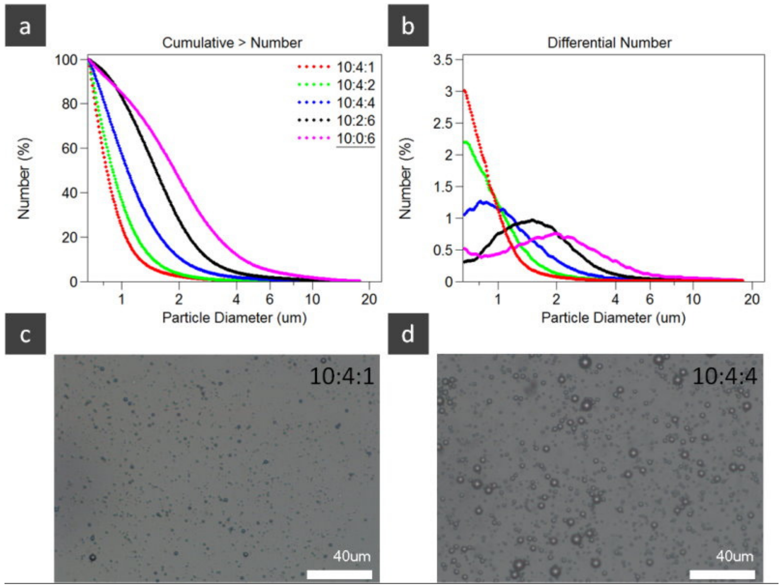

P6Ac-4

Counter flow microbubble channeling using acoustic radiation force funnel

Benjamin Raiton[1], **Sevan Harput[1]**, Dr James Mclaughlan[1], Dr Steven Freear[1]; [1]Ultrasound Group, School of Electronic and Electrical Engineering, University of Leeds, Leeds, West Yorkshire, United Kingdom

Background, Motivation and Objective

The key advantage when employing acoustic travelling waves to manipulate microspheres is the ability to penetrate biological tissues. Other techniques such as optical tweezers or standing-wave traps are limited by their working distance. Previous publications reported on the use of Gaussian focused ultrasound to translate 125 µm lipid droplets and an opposite phase induced pressure black spot to align flowing particles. When microbubbles (MB) are used as drug carriers, a single element transducer is commonly used to emit a plane pressure wave. The effect, referred to as primary radiation force, is a translation of the MB away from the vessel lumen and towards the vessel wall to facilitate bonding to the endothelium. The axial primary radiation force (APRF) is calculated here according to Dayton et al. [1] along with the lateral primary radiation force (LPRF) following the simplified equation by Gor'kov [2].

Statement of Contribution/Methods

Lipid MB used in the experiment have a size distribution of 1-10 µm. The MB are flowed through a 1 mm wide channel with a height of 100 µm, at a rate similar to that of venules. A low peak-negative-pressure (PNP) pulse of 200 cycles is emitted every 6.25 ms. The 96 elements of a standard medical imaging probe are focused at the channel centre at 24 mm. Each half of the array transmits the same tone burst, but out of phase by 180°.

Results

In the figure, captured from beneath the vessel, the fluid is flowing from left to right. A clear formation of 3 parallel channels, flowing in the opposite direction, is observed as predicted by the simulation. The thin grey trails are made up of unaggregated MB whilst the larger and darker dots indicate MB clustering. The clusters break up as soon as the ultrasound source is switched off.

Discussion and Conclusions

Thanks to the use of a 1D linear array the spacing between the channels can be dynamically varied by altering the focal depth or number of elements used. The center of the three channels can also be shifted up and down by steering the focal point of the array.

[1] P.A. Dayton et al., UFFC IEEE Trans, vol.44, no.6, pp,1264-1277, 1997

[2] L.P. Gor'kov, Sov. Phys. 6 (9), 773-775, 1962

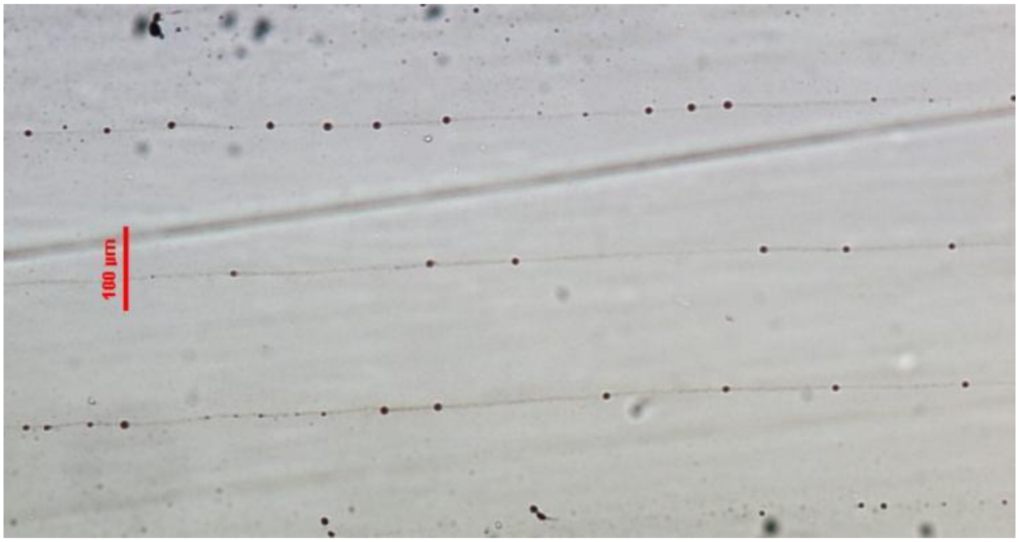

P6Ac-5

Single bubble Acoustic Characterisation and Stability Measurement of Adherent Microbubbles

Jonathan Casey[1], Helen Mulvana[1], Jo Hajnal[1], Mengxing Tang[2], Robert Eckersley[1]; [1]Imaging Sciences Department, Imperial college london, London, London, United Kingdom, [2]Bio-engineering Department, Imperial college london, London, London, United Kingdom

Background, Motivation and Objective

The detection and utilisation of targeted ultrasound contrast agents for molecular imaging and targeted drug/gene delivery can be improved by making use of acoustic phenomena arising as a result of targeting or proximity to the target area. Due to low microbubble (MB) concentration at the target site and signal masking by bubble sub-populations of varying size, these differences are small and difficult to deduce from standard bulk acoustic methods used for the characterisation of MBs. To better understand how the dynamics of whole populations of MBs are affected by factors such as, sub-population size, shell chemistry and targeting it is essential to first understand the acoustic response of single MBs.

The objective of this study was to examine the effect that MB targeting and adhesion has on the acoustic response and stability of MBs

Statement of Contribution/Methods

Acoustic measurements were performed on single in-house produced phospholipid MBs ranging in diameter from 1-10µm. The testing rig consisted of a pair of focussed transducers and an objective lens co-focally aligned on a capillary fibre. MBs in three regimes were examined: 1) MBs functionalised with Biotin and a capillary fibre coated with Streptavidin. 2) Functionalised MBs in an un-coated capillary fibre. 3) Un-functionalised MBs in an uncoated capillary fibre. The MBs were insonated with 2 MHz, narrowband, 100 KPa peak negative pressure pulses to establish the resonant characteristics. Subsequently the MBs were exposed to broadband pulses of increasing amplitude interspersed by the same 2MHz pulse to determine the bubble stability as a function of driving pressure.

Results

Data was collected for a number of MBs within each testing regime (N=41, 44, 47 for the three groups respectively). The resonant behaviour of the MBs in all three testing regimes was broadly similar. Within the same testing regime significant variation in acoustic response (total scattering, harmonic scattering) for MBs of similar size was observed meaning that the subtle changes expected as a result of MB adhesion could not be discerned i.e. changes in resonance frequency due to increased damping and scattering power. Furthermore the variation in harmonic response was far greater for the bound MBs than for the untargeted ones, again masking the expected suppression of 2nd harmonic signal from bound MBs.

The stability of the MBs was heavily influenced by resonance. At the resonant size (1.8±0.3 µm at 2 MHz) significant reduction in stability was measured. This effect was amplified with increasing driving pressure. Interestingly the adherent MBs showed an overall greater signal reduction and increased MB destruction indicative of poorer stability in comparison with the unbound MBs.

Discussion and Conclusions

The major effect that adherence has on MB response is to do decrease the MB stability. This could have wide ranging impications for both targeted imaging as well as MB mediated drug/gene delivery in the design and application of MBS

P6Ac-6

Improving the quantitative ability of contrast enhanced ultrasound perfusion imaging: effect of contrast administration rate and imaging plane orientation

Kennita Johnson[1], Paul Kogan[1], Steven Feingold[1], Nicholas Garrett[2], Ismayil Guracar[3], William Arendshorst[2], Paul Dayton[1]; [1]Biomedical Engineering, UNC/NC State, Chapel Hill, NC, USA, [2]Cell and Molecular Physiology, UNC, Chapel Hill, NC, USA, [3]Siemens Medical Solutions, Mountain Veiw, CA, USA

Background, Motivation and Objective

Contrast-enhanced ultrasound (CEUS) has demonstrated utility in the monitoring of blood flow in tissues, organs, and tumors, but current CEUS methods typically provide only relative image-derived measurements, rather than quantitative values of blood flow in milliliters/minute per gram of tissue. The purpose of this study is to validate CEUS-derived measurements of renal blood flow (RBF) with absolute values of milliliters/minute per gram of tissue based on a calibrated flow probe. New information is provided about the effects of parameters such as microbubble contrast agent infusion rate (IR), transducer positioning: coronal or parasagittal orientations on two different image-derived measurement methods: parametric or wash-in methods.

Statement of Contribution/Methods

Male Sprague-Dawley rats were surgically prepared in order to place a transit-time flow probe on the left renal artery to measure volumetric RBF. Two methods of CEUS RBF measurements described in the literature, the parametric and "wash-in curve" methods were performed on the left kidney with an Acuson Sequoia 512 system using two 15L8 linear array transducers positioned in the coronal and parasagittal orientations. For each method and orientation, IRs from 13 to 78 microliters/minute per gram were tested. Angiotensin II was administered to alter RBF in the rat. For the wash-in method, β values were calculated from the wash-in curves. For the parametric method, a reperfusion rate (RPR) was determined from the image data. Linear regression of CEUS RBF (β or RPR) vs. flow probe RBF was performed for every orientation and IR combination.

Results

CEUS measurements of RBF correlated well with the transit-time flow probe (all $R > 0.9$) at all MCA infusion rates, indicating that both imaging methods produced data that was linear with true flow. However, data illustrates that the wash-in method was less sensitive than the parametric method in detecting changes in RBF. Also, the wash-in method was less sensitive to changes in IR than the parametric method. Coronal plane imaging suggested a higher sensitivity in detecting RBF changes than the parasagittal plane in the kidney.

Discussion and Conclusions

Results indicate that the method of estimating perfusion should be chosen based on the desired sensitivity to flow changes, and whether or not the contrast agent infusion rate can be maintained within an appropriate range. Most importantly, the data illustrates that under appropriate conditions, CEUS can be used as a calibrated quantitative measurement of tissue perfusion to obtain flow values of milliliters/minute per gram of tissue in-vivo.

P6Ac-7

Experimental Implementation of the Second Harmonic Inversion Imaging on an Open Ultrasonic Scanner

Fanglue Lin[1], François Varray[1], Aymeric Guibal[2], Christian Cachard[1], Olivier Basset[1]; [1]CREATIS; Université de Lyon; CNRS UMR5220; INSERM U1044; INSA-Lyon; Université Lyon 1, Villeurbanne, France, [2]Hospices Civils de Lyon, Hôpital Edouard Herriot, Service d'Imagerie Digestive, Lyon, France

Background, Motivation and Objective

Ultrasound harmonic imaging has been proved to be suitable for imaging contrast agents. However, it is limited by the harmonic components which are produced during wave propagation because of the native nonlinearities of the tissue. Several approaches have been proposed to reduce these tissue-made harmonics. A newly proposed method, named Second Harmonic Inversion (SHI)[1], suggests to transmit successively two pulses with the same frequency, the same amplitude and 90° phase difference to reduce the second harmonic generated by tissue.

Statement of Contribution/Methods

This newly proposed SHI method is carried out on an open system equipped with a bipolar square-wave pulser (Ultrasonix RP) and a linear probe (L14-5W/60). Measurements from water, a general purpose ultrasound phantom (CIRS 054GS) and a tissue mimicking phantom (5% agar and 1% silice) with circulating contrast agents (SHU 508A) are investigated. Experimental results acquired with SHI method are compared with standard second harmonic imaging and Pulse Inversion (PI) method to verify the effectiveness of second harmonic suppression of SHI.

Results

SHI method can be easily implemented on an open system. Both radio frequency signals analysis and displayed ultrasound images show that SHI method decreases significantly the native second-harmonic tissue components existing in standard harmonic images. Experimental results also show that contrast-to-tissue ratio (CTR) of SHI image is improved by 4.6dB when compared to standard harmonic image and improved by 3.6dB when compared to PI image, proving that the specificity of contrast agent with SHI method is the best among these three methods.

Discussion and Conclusions

The newly proposed SHI method is successfully and easily implemented on an open clinical system. We demonstrate that SHI method enhances CTR through effective tissue generated second harmonic suppression. Moreover, the easy implementation procedure and the better specificity make SHI an interesting alternative to PI method.

[1] Mirza Pasovic et al, Physics in Medicine and Biology, In Press

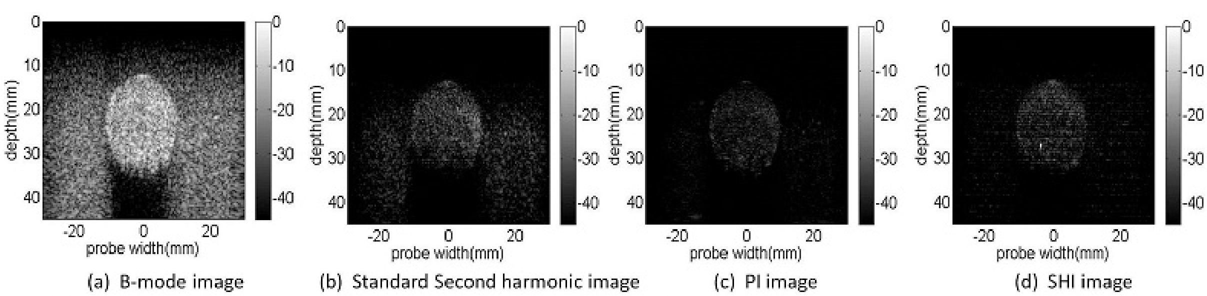

Figure 1 Ultrasound images of the tissue mimicking phantom with contrast agent acquired with different transmitted pulses, with a transmitted frequency of 5MHz. Filter applied for (b) and (d) is an 8 order 9MHz-11MHz bandpass Butterworth filter

FRIDAY POSTER

P6Ad - Adaptive Beam Forming

Carribean Ballroom III-V

Friday, October 21, 2011, 1:00 pm - 4:30 pm

Chair: **Sverre Holm**
University of Oslo

P6Ad-1

Analysis of minimum-variance and Wiener-filtered beamforming strategies

Nghia Nguyen[1], Craig Abbey[2], Michael Insana[3]; [1]Department of Electrical and Computer Engineering, University of Illinois at Urbana-Champaign, Urbana, Illinois, USA, [2]Psychological and Brain Sciences, University of California, Santa Barbara, Santa Barbara, California, USA, [3]Bioengineering, University of Illinois at Urbana-Champaign, Urbana, Illinois, USA

Background, Motivation and Objective

The performance of a beamformer must be evaluated in the context of the clinical task - the reason for acquiring the image. A rigorous approach to task-based assessment is available by employing methods of signal detection theory and the concept of the Ideal Observer (IO). In this research, we explore the IO and derive minimum-variance (MV) and Wiener-filtered beamforming (WB) strategies with the aim of discovering conditions when each strategy excels.

Statement of Contribution/Methods

IO analysis was extended to each receive channel of the transducer. First, the delay-and-sum (DS) beamforming was found to be approximated by matched filtering, a sufficient statistical combination of data; therefore DS preserves diagnostic information. While information will be lost by demodulation, some beamforming strategies are better than others at preserving clinical feature information. Beamformers are viewed as approximations to the IO strategy. The MV and WB strategies are evaluated through the Smith-Wagner observer to predict human observer responses for the five tasks representing lesion visualization. The results are shown in term of visual detection efficiency η - the percentage of signal energy for the IO to match human observer performance.

Results

The psfs from select receive channels are shown in Fig a, generated with Field II with parameters of the Siemens Antares system and transducer VF10-5. The B-mode images for a circular lesion with three beamformers are shown in Fig b. Among them, the WB has the smallest speckle but the lowest contrast resolution. Efficiencies for five typical features are plotted (log scale) in Fig c. Visual detection efficiency is improved significantly with MV and WB over DS for the first four tasks, in agreement with IO analysis predictions. The WB significantly outperforms MV except for task 5, where η for WB is only 10% to compare with 21% for the MV beamformer.

Discussion and Conclusions

The poor performance of the WB in Task 5 suggests the approximation is deficient for this clinical task (anechoic/hypoechoic lesion discrimination), and hence underscores the task dependent nature of performance. The WB excels at producing fine, uniform spatial resolution and yet it requires accurate prior knowledge of the system in the form of element impulse responses and corresponding eSNR. Meanwhile, the MV beamformer is more tolerant of system uncertainties.

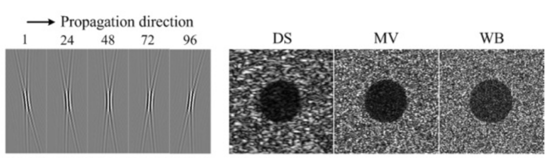

(a) psfs from transducer elements generated with Field II program

(b) The B-mode images of a circular lesion with three different beamformers including DS, MV and WB.

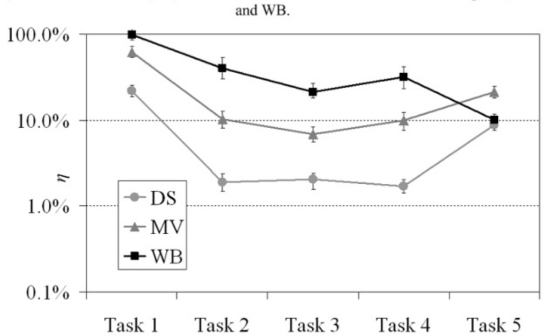

(c) Efficiency

P6Ad-2

Coherent Plane-Wave Compounding and Minimum Variance Beamforming

Andreas Austeng[1], Carl-Inge C Nilsen[1], Are FC Jensen[1], Sven Peter Näsholm[1], Sverre Holm[1]; [1]*Department of Informatics, University of Oslo, Oslo, Oslo, Norway*

Background, Motivation and Objective

Coherent plane-wave compounding has recently been proposed (Montaldo et al., *"Coherent plane-wave compounding for very high frame rate ultrasonography and transient elastography,"* TUFFC, 56, 3, 2009) as a method to produce very high-framerate ultrasound imaging. In the method, multiple low-resolution subimages are formed by transmitting plane waves into the medium. High-resolution images are formed by summing the subimages.

This second stage corresponds to classical delay-and-sum beamforming. As an alternative, it is possible to use an adaptive beamformer. Adaptive beamformers may provide a significant increase in resolution and the possibility to trade-off resolution and frame rate by requiring fewer subimages.

Statement of Contribution/Methods

In this work we have investigated how the subimages can be combined by using the Minimum Variance (MV) beamformer, i.e.\ we have implemented a weighted sum, where the complex weights for each pixel are found using a MV criterion. The performance of the MV beamformer is quantified with respect to speckle intensity as well as point and edge resolution.

Results

We have simulated ultrasound data using Field II from a 4.5MHz 124-element linear array transducer with one wavelength pitch. For each dataset, subimages for a total of 124 different plane waves are formed. Some or all of the subimages are combined using either ordinary summing or a MV weighted sum.

Montaldo et al. showed that the summing of a subset of 70 subimages was required to obtain the same image quality as ordinary focusing. In this case, the MV weighted sum gives a point response with a width of 1/3 of that of DAS measured at the -10dB point. It also has reduced close-in sidelobes. This implies improved cyst contrast and better edge detection.

To increase the framerate, fewer subimages can be combined at the cost of a widened summed point response. As an example, when combining 22 subimages, the response at the -20dB point is more than twice as wide as with 70 subimages.

Our new method using the MV weighted response and 22 subimages gives performance comparable to Montaldo et als method with 70 subimages, i.e. the use of MV means that we can both form high quality images and get an increased frame rate at the same time.

Discussion and Conclusions

Our investigations show that the MV beamformer improves the image quality of the coherent plane-wave compounding method for small subsets of subimages. The method opens for retaining high image quality and high framerate simultaneously.

P6Ad-3

SNR-Dependent Coherence Weighting for Minimum Variance Beamforming

Yu-Hsin Wang[1], Pai-Chi Li[1]; [1]Natoinal Taiwan University, Taiwan

Background, Motivation and Objective

The coherence factor (CF) has been proposed to suppress sidelobes and enhance the contrast in ultrasound imaging. Recent research also investigated minimum variance based coherence factor methods (CFMVDR) to achieve adequate resolution for high frame rate applications. However, performance of CF-based weighting is susceptible to variations in signal-to-noise ratio. On the other hand, a Wiener filter that estimates the SNR of the channel data has better robustness but worse performance. Thus, with the knowledge of SNR, it is the purpose of this study to investigate a modified version of the CF weighting method that combines the CFMVDR method with a Wiener filter approach.

Statement of Contribution/Methods

The proposed solution is applied to the high frame rate imaging that has synthetic transmit aperture and MVDR beamformer. Before finding the MVDR solution, the channel data are used to estimate the SNR in the aperture domain with a Wiener filter. Then, the SNR value determines the CF weighting with a sigmoid function. Specifically, in the high SNR region, the CF or CFMVDR is modified by lowering their noise weighting. Thus, for the region requires higher resolution, e.g. point targets, MVDR beamformer can retain its performance.

Results

A cyst phantom is simulated with a linear array that has a center frequency of 4.37MHz. When the SNR is -10 dB, the CR and CNR from the original CF/CFMVDR methods are 39.01/15.43 dB and 2.08/1.74, respectively. With the proposed method, the CF/CFMVDR is improved to 47.45/29.17 dB and 2.26/2.01 in CR and CNR. On the other hand, simulations of two point targets close to each other are also included to test the spatial resolution. Only when the channel SNR is set to a very poor condition at -20 dB, the 10 dB beam widths are slightly affected (30µm wider than the original width of 550µm).On the other hand, the beam width in the CFMVDR case is improved, which is 9µm narrower than the original.

Discussion and Conclusions

A robust method designed for low SNRs is presented. The SNR estimation of channel data can be effectively implemented with a Wiener filter or conventional CF estimator. This method is an improvement over previous methods that typically perform poorly when SNR is low.

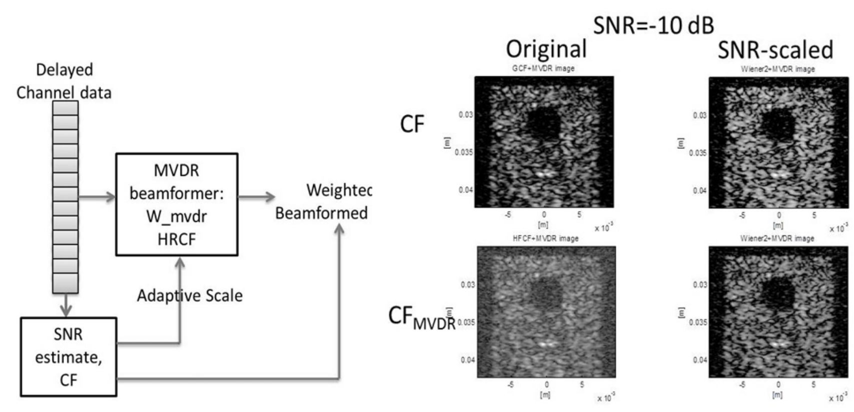

Figure: (Left) Block diagram of the proposed method. (Right) Images of a cyst when SNR is at -10 dB. Top row is for the CF method and bottom row is for the CF_{MVDR} method.

P6Ad-4

Pitch-catch phase aberration correction for 3D ultrasound brain helmet

Brooks Lindsey[1], Stephen Smith[1]; [1]Biomedical Engineering, Duke University, Durham, NC, USA

Background, Motivation and Objective

Motivated by the time-sensitive nature of stroke, we have previously constructed a prototype transcranial ultrasound imaging system and conducted a human trial in which two 3D volumes of echo + color flow data were simultaneously acquired from both sides of the head and fused off-line. This system uses custom sparse matrix array transducers on short cableless flex circuits.

The mismatch in longitudinal velocities of the skull (~2650 m/s) and the brain (~1530 m/s) constitutes a well-known source of image degradation in transcranial ultrasound imaging and has the effect of reducing spatial and contrast resolution as out-of-phase signals are summed by the beamformer. The geometry of having sparse matrix arrays positioned on both temporal bone windows presents an opportunity to correct aberrations using each array to transmit a plane wave received by the opposing array.

Previous work in our lab has used a pulse-echo technique to correct on echoes from diffuse scatterers. However, the use of a pitch-catch approach provides a correction beacon that can potentially improve the quality of the phase map estimate, as the correlation coefficient decreases less rapidly as a function of distance than predicted by the van Cittert-Zernike theorem. Thus signals from elements having greater spatial lags may be correlated.

Statement of Contribution/Methods

Nine central elements of one array are fired to produce a plane wave received by the opposing array. Received single-channel radiofrequency signals for all elements are cross-correlated on a PC adjacent to the scanner, yielding an overdetermined system which is approximately solved using least squares to generate an arrival time estimate for each element.

The computed map is passed to the scanner and used to update the receive delays for all elements in both echo and Doppler modes. Testing has been performed by assessing the brightness of 8 wires in a water tank in the presence of either an electronic aberrator (100 ns RMS, 3 mm FWHM autocorrelation length) or a physical aberrator: a polymer casting of a human temporal bone.

Results

The described approach has been implemented on both commercial arrays (f0=2.5 MHz) and custom cableless arrays (f0=2.3 MHz). Using the commercial transducers, we have observed mean increases in target brightness of 34% with a 100 ns electronic aberrator and 8% with a measured 53.5 ns, 2.5 mm autocorrelation length physical aberrator (temporal bone casting). Results using the custom arrays are incomplete, though we have observed a 17% increase in brightness for a 100 ns electronic aberrator and have also measured a 45 ns RMS applied aberrator with a 10 ns RMS error.

Discussion and Conclusions

While the general applicability of a pitch-catch technique is limited to those imaging situations in which an active source may be positioned outside of the body, such a technique is capable of producing improvements in image quality with modest hardware requirements: only a single point source is needed to correct a single array.

P6Ad-5

Performance of Adaptive Beamformers for Ultrasound Imaging of a Partially Shaded Object

Saeed Mehdizadeh[1], Andreas Austeng[2], Tonni Franke Johansen[1], Sverre Holm[1,2]; [1]Department of Circulation and Medical Imaging, Norwegian University of Science and Technology, Trondheim, Norway, [2]Department of Informatics, University of Oslo, Oslo, Norway

Background, Motivation and Objective

Ultrasound imaging of tissue involving a bone structure is prone to poor image quality due to obstruction of the ultrasound beams by the acoustically hard tissue. The shadowing effect can lead to significant difficulties in the detection of some important anatomic features, e.g., nerves, as the imaging beams are distorted. In this study, we investigate the potential of the adaptive beamforming techniques such as minimum variance (MV), and projected minimum variance (PMV) methods to suppress the shadowing effect in terms of the resolution and sensitivity. In the PMV, the minimum variance weights are projected on the signal subspace constructed from the eigenvectors corresponding to the largest eigenvalues of the covariance matrix.

Statement of Contribution/Methods

Initially, a binary apodization model is proposed to simulate the effects of the shaded aperture on the image of point scatterers located in a vertebra shadow. This model is applied to Field II to modify the apodization function in the imaging system model. Then, we simulate 2 columns of point scatterers located at different distances from the vertebra wall. The right-hand column is closely located to the wall affected by shadowing, whereas the left-hand column is completely unaffected. The shadowing effect increases with the depth for the right-hand column. We employ the MV and PMV techniques to image these point scatterers. The images are compared with delay and sum (DAS) beamforming which is more robust but has lower resolution. Further, in a water tank experiment, these adaptive techniques are employed to image a needle tip located in the shadow of a vertebra specimen. In this experiment, the channel data are acquired using an Ultrasonix scanner, and a 128 element, 5 MHz transducer.

Results

The adaptive beamformers retain the high resolution property as long as less than half of the aperture is shaded. Increasing the shadowing beyond this causes point spread function lateral shift and signal attenuation in the MV image of the point scatterers (Fig.1b). The shifting artifact is compensated for in the PMV image (Fig 1c), but the signal attenuation becomes worse.

Discussion and Conclusions

The MV beamformer can result in a distorted image when the imaging aperture is highly obstructed by the bone. This distortion can be compensated for in the PMV beamformer. However the sensitivity decreases for highly shaded point scatterers.

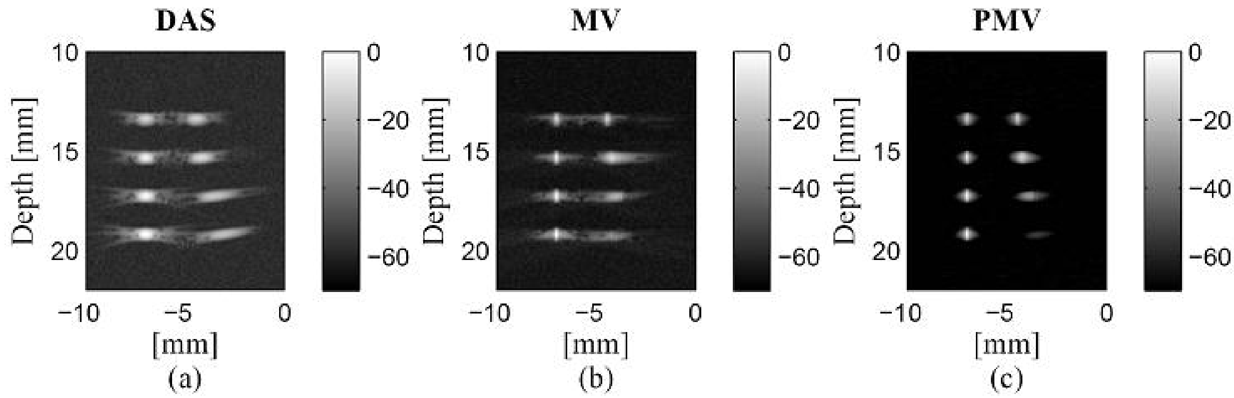
DAS
MV
PMV
10
15
20
Depth [mm]
0
−20
−40
−60
−10
−5
0
[mm]
(a)
(b)
(c)

P6B NDE Methods and Transducers

Carribean Ballroom III-V

Friday, October 21, 2011, 1:00 pm - 4:30 pm

Chair: **Michal Bezdek**
Endress+Hauser Flowtec AG, Switzerland

P6B-1

Detection of Discontinuities in Contact Pressure Between Rough Surfaces

Anthony C. Karloff[1], Andriy M. Chertov[1], Roman Gr. Maev[1]; [1]Institute for Diagnostic Imaging Research, Windsor, Ontario, Canada

Background, Motivation and Objective

Ultrasonic reflection and transmission at rough solid-solid interfaces has been a subject for extensive investigation primarily in geophysical systems, and more recently in non-destructive evaluation (NDE). It has been shown that ultrasonic responses at these interfaces can be quantitatively characterized in terms of interfacial stiffness, which varies with applied pressure. These responses have been described as non-linear by using ultrasonic spectroscopy, which results in the generation of harmonics and frequency dependent attenuation for different contact conditions.

Statement of Contribution/Methods

In this paper, a single broad-band ultrasonic pulse was used to detect sudden changes in contact stiffness over time for two rough solid surfaces under pressure. The process involved ultrasound pulse-echo inspection of the contact interface using a 10 MHz center frequency transducer with 80% bandwidth. Changes in the reflected pulse frequency spectrum and phase over time were analyzed using moments (variance, skewness and kurtosis) in order to detect significant discontinuities in the non-linear interface properties including: frequency attenuation, appearance of harmonics, and changes in phase. This process was applied specifically to monitor the contact stiffness between a copper welding electrode and a steel plate for resistance spot welding. Sudden changes in contact pressure/stiffness at this interface were used to assure process quality and detect process disruptions, such as expulsion.

Results

The contact interface between copper and steel was analyzed for a series of spot welds of varying sizes. Significant changes in interfacial stiffness resulted from pressure due to thermal expansion of a liquid weld nugget below the steel surface. These changes were detectable by observing subtle shifts in the frequency spectrum of the broad-band pulse. Changes in stiffness resulting from elastic deformation of the heated surfaces were present, but negligible when examining higher order moments of the frequency spectrum difference in time. This allowed sudden disruptions such as rapid melting, cooling, and expulsion events to be precisely identified.

Discussion and Conclusions

In this paper, the non-linear characteristics of reflected broad-band pulses resulting from the stiffness of rough contacting surfaces were exploited to detect discontinuities in pressure on the interface. This was applied to resistance spot welding where the contact between copper welding electrodes and steel samples provides important information regarding process quality. It was shown that evaluating changes in the spectrum and phase of reflected signals by second, third, and forth order moments allowed for accurate detection of process discontinuities and weld quality assurance.

P6B-2

Analysis of Subharmonic Resonance in Ultrasonic Testing of a Closed Crack Based on Gap-Width-Dependent Property of Interfacial Stiffness

Kenji Kurihara[1], Keiichi Naitou[1], Toshihiko Sugiura[1]; [1]*Mechanical Engineering, Keio University, Japan*

Background, Motivation and Objective

Nowadays nondestructive testing is becoming quite beneficial for maintenance of structures. Of particular interest is nonlinear ultrasonic testing that detects superharmonic or subharmonic responses occurring when ultrasonic waves propagate through a crack. This study investigates a possible mechanism causing subharmonics at a closed crack and dependence of subharmonics generation on the input amplitude.

Statement of Contribution/Methods

In this study a closed crack is regarded as a nonlinear spring, and nonlinear analysis and numerical simulation were carried out. Numerical simulation was carried out using the Runge-Kutta method. This modeling is based on the fact that, when the gap between the crack surfaces decreases, the contact pressure increases nonlinearly due to the asperity of the crack surfaces.

In experiment, two aluminum specimens strongly pressed were used in place of a metal block with a closed crack. Vertical ultrasonic transducers were used for transmitting and detecting waves.

Results

According to results of our nonlinear analysis, subharmonics can occur if the input amplitude is above a critical level and the input frequency range generating subharmonics can be expanded if the input amplitude increases, as shown in Fig.1. We found that numerical results are in good agreement with the above analytical results, showing generation of subharmonics and expanding of the subharmonic resonance range. Generation of subharmonics was observed in experiment. Experimental results are in good agreement with analytical and numerical results.

Discussion and Conclusions

In our nonlinear analysis, numerical simulation, and experiment, subharmonics can generate if the input frequency is twice the natural frequency and if the input amplitude is above a certain level. The input frequency range generating subharmonics can be expanded if the input amplitude increases.

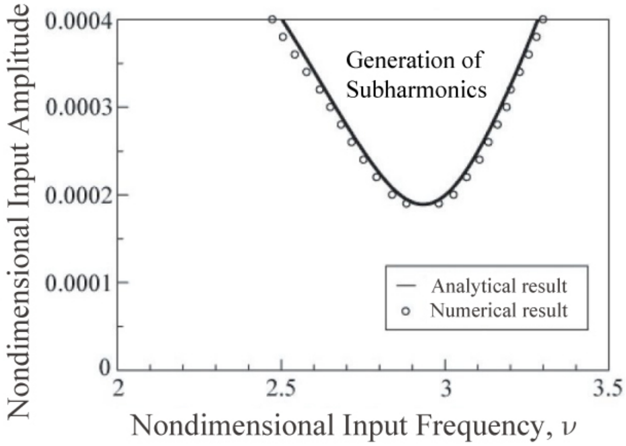

Fig.1 Conditions for subharmonics generation

P6B-3

Rapid prototyping technologies for ultrasonic beam focussing in NDE

Duncan Billson[1], Christopher Purssell[2], Simon Leigh[3], David Hutchins[2]; [1]Engineering, University of Warwick, Coventry, Coventry, United Kingdom, [2]School of Engineering, University of Warwick, United Kingdom, [3]Engineering, University of Warwick, United Kingdom

Background, Motivation and Objective

The motivation for the developments described in this abstract is to produce a series of simple, effective and inexpensive devices that can be used with conventional (commercial) ultrasonic transducers to focus the ultrasonic beam by varying amounts. Focussing the ultrasonic field (within the near-field) will enhance the resolution of a transducer and the ability to vary the focus of the field from a transducer (within physical limits) allows the NDE practitioner to optimise the resolution of the scan for each application. The devices reported in this paper are designed to simply attach to the body of a commercial transducer, and modify its acoustic field either by refraction, reflection or diffraction (or a combination thereof). They are fabricated using what is essentially a rapid-prototyping technology, but with a higher than normal resolution. Such technology is referred to as micro-stereo-lithography (MSL). They are designed to be effective, inexpensive, simple to use, and interchangeable (between, for example transducers of different frequencies), so that the NDE practitioner can rapidly change them to optimise the NDE system.

Statement of Contribution/Methods

The devices were mathematically modelled using a basic ray-tracing methodology, and then designed and fabricated using MSL. For some applications, the acoustic properties of the MSL photopolymer are inappropriate, and the system was then used to produce a mould of the desired shape, which was then be used to cast the device from a more suitable material. After the devices were fabricated, their acoustic focussing properties were determined experimentally in immersion (although it should be noted that contacting transducers can also be fabricated). A needle hydrophone was used to scan and plot the acoustic field. This procedure was repeated for several devices, and for several transducers.

Results

The paper will show the designs of several devices, together with scans of their acoustic fields, and a number of scans of common objects (e.g. coins) performed by the devices to show their effectiveness. These will be repeated using transducers of different frequencies, and the effectiveness, advantages and disadvantages of each type of device will be discussed.

Discussion and Conclusions

This paper will present a new type or class of device that can be used in conjunction with conventional, commercial transducers to provide a simple, and highly versatile ultrasonic inspection tool that can greatly extend the range of standard equipment for minimal financial outlay. Furthermore, a variety of beam-modification devices will be discussed that can produce testing regimes that can be very difficult to produce in other ways (for example using line-focussing).

P6B-4

Effect of Angle Errors in Conical Tip Buffer Rods

Javier Garcia-Alvarez[1], Miguel Garcia-Hernandez[1], Juan Antonio Chavez[1], Antoni Turo[1], Jordi Salazar[1]; [1]*Electronic Engineering, Universitat Politècnica de Catalunya UPC, Barcelona, Barcelona, Spain*

Background, Motivation and Objective

Buffer rods are widely used in the ultrasonic inspection of materials. For the analysis of some liquid-like substances, such as food liquids and beverages, the buffer rod can be terminated in the form of a conical tip in order to avoid trapping external air bubbles on its surface as it enters into the sample. If the angle between the axis and the generatrix of the conical tip is accurately set to 45º, all the components of the ultrasound wave reflected at the buffer tip go along acoustic paths of equal length, being them all received in phase at the transducer and obtaining thus the maximum reflected signal amplitude. On the contrary, if the cone angle differs from 45º, each reflected wave component follow an acoustic path of different length so they are received out of phase at the ultrasound transducer, composing thus a weaker reflected signal. Thus, machining errors of the conical tip can affect the sensitivity and accuracy of the measurements. In this work, the effect of the angle errors of conical buffer rods on the ultrasound measurements has been analysed.

Statement of Contribution/Methods

A finite differences tool was used to simulate the acoustic waves coming from the buffer conical tip, considering diverse cone angles. Then, a bunch of aluminium buffer rods with the same cone angles than the defined for the simulations were constructed and the signals reflected at the buffer tip were obtained experimentally.

FRIDAY POSTER

Results

Waveforms of both simulations and experiments are given for the different cone angles considered. The amplitude of the reflected signal in the conical tip with the angle error, for aluminium buffer rods glued to a 1 MHz/25.4mm ultrasonic transducer, can be seen in Fig.1. The obtained results in simulations and experiments offer a good agreement, showing a progressive loss in the reflected wave amplitude in buffer rods as the cone angle differs from 45º.

Discussion and Conclusions

The finite difference simulation results have provided a general good agreement with the measurements. The significance of the angle errors of conical buffer rods has been related to the transducer frequency and diameter, and the buffer rod material.

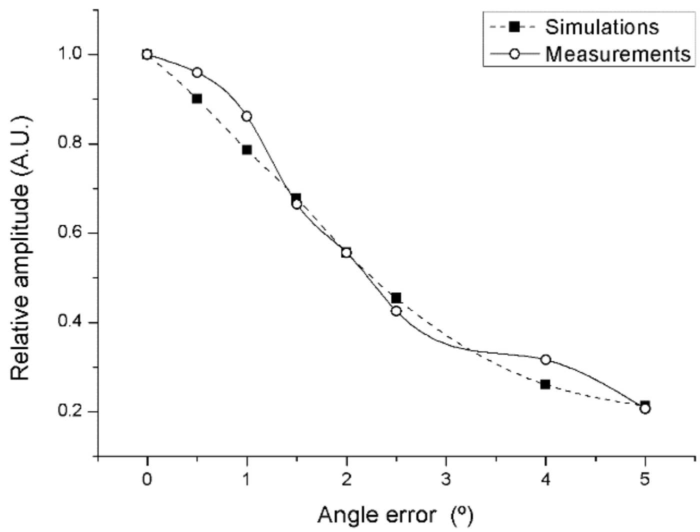

P6B-5

Guided Waves in a Seven-Wire Strand under Vertical Load

Isamu Oguma[1], Toshihiko Sugiura[1]; [1]Mechanical Engineering, Keio University, Yokohama, Kanagawa, Japan

Background, Motivation and Objective

Guided waves are expected as an efficient method for nondestructive testing of long structures. Recently there have been active research and development in applications of guided waves to pipes used in pipelines or power plants and to wire ropes used in elevators or bridges. However, understanding of wave propagation in wire strands is insufficient to put it to practical use. For example, wire ropes are often used partially under load perpendicular to their longitudinal axes when being embedded underground or contacting joining points, though effect of such boundary conditions on wave propagation is not yet clear. Our research aims to examine effects of such vertical loading on propagation of guided waves in a seven-wire strand whose each wire is further composed of nineteen-stranded fine wires.

Statement of Contribution/Methods

Our two specimens were an aluminum rod and a stainless steel seven-wire strand whose each wire is further composed of nineteen-stranded fine wires. Electromagnetic Acoustic Transducers (EMATs) for the rod and magnetostrictive transducers for the seven-wire strand were used for transmitting guided waves. They were effective in the point that they can equally generate ultrasonic waves in these circular structures. Different conditions of vertical loading were applied to these specimens. Receiver signals of ultrasonic waves propagated under these loading conditions were measured. Wave propagation in the rod was analyzed and its velocity dispersion curves were theoretically obtained. On the other hand, optimum frequencies for wave propagation in the seven-wire strand were obtained experimentally. Using these optimum frequencies obtained from the theory and experiments, less-damped modes propagating in the specimens partially under vertical load were investigated in experiment.

Results

First of all, wave reflection at the edges of the specimen did not happen in the wire strand unlike that in the rod. Its reason may be that energy of ultrasonic waves is scattered at the edge of each stranded fine wire. Secondly, effect of the loading conditions on the attenuating rate of waves was examined. The most specific difference between the seven-wire strand and the rod was attenuation of ultrasonic waves propagating through them. There was apparent attenuation in the seven-wire strand caused by external loading perpendicular to its longitudinal direction.

Discussion and Conclusions

Our results suggest that guided waves in a seven-wire strand whose each wire is further composed of nineteen-stranded fine wires are different from those in a rod. In the wire strand, guided waves show larger attenuation under load perpendicular to its longitudinal direction. Nondestructive testing using guided waves for wire ropes needs more consideration for their environments such as embedment or contact to obtain efficient propagation.

P6B-6

Ultrasound based system and methodology for in-line, real time, process monitoring and control

Johan Wiklund[1], Mats Stading[1]; [1]Structure and Material Design, SIK-The Swedish Institute for Food and Biotechnology, Gothenburg, Västra Götaland, Sweden

Background, Motivation and Objective

The trend within fluid industry is towards continuous production, leading to an increasing demand for new and improved methods that allow real-time monitoring of quality parameters and fast process control. The consistency and viscosity can be described by fluid rheology and are frequently used as quality control parameters. Rheological properties can be correlated with product microstructure, they govern the performance of unit operations and detailed knowledge is fundamental for the design of new process equipment and for predicting e.g. heat transfer. The determination of rheological properties in-line, in real time, thus has a great economical impact and is important from a quality perspective for the development of innovative and competitive products and a prerequisite for efficient process control within modern fluid industry. Rheological properties are, however, mainly measured off-line using conventional rheometers, whereas the availability of reliable in-line methods has been limited. The objective of this work was to develop an ultrasound based system and method for in-line, real time, combining the Doppler-based Ultrasound Velocity Profiling (UVP) technique with Pressure Difference (PD) measurements that meets industrial requirements.

Statement of Contribution/Methods

Many publications and several patents exists describing different apparatus for rheological measurements based on the UVP-PD concept but no commercial instrument has been introduced on the market. An industrial system and method with new transducer technology for in-line, real time, flow visualization and rheological characterization of complex fluids has been developed at SIK-The Swedish Institute for Food and Biotechnology. The UVP-PD system gives data in real-time, it is non-invasive, robust and is applicable to complex fluids, such as, opaque, non-Newtonian and inhomogeneous dispersions.

Results

The number of possible industrial applications for the UVP-PD method is already very large and increases rapidly (food, oil, cement, mineral processing and paper pulp etc.). The UVP-PD system developed by SIK has so far successfully been used in well over 30 national and international research and industrial projects, including recent EU-Projects. The UVP-PD method has been validated extensively and excellent agreement was found in comparisons with conventional methods. A portable system and two complete customized industrial instruments have been installed in the production line in two large multi-national companies.

Discussion and Conclusions

The UVP-PD system give access to new valuable real-time information, which is of great value for environmentally friendly and cost effective production through enhanced process monitoring and control. Different versions of the UVP-PD system is anticipated to be used for enhanced process monitoring and control in many branches of industry as well as for increasing the academic understanding of fluid products.

P6C - Phononic Crystals

Carribean Ballroom III-V

Friday, October 21, 2011, 1:00 pm - 4:30 pm

Chair: **Abdelkrim Khelif**
Centre National de la Recherche Scientifique

P6C-1

Reducing Anchor Loss in Micromechanical Resonators using Phononic Crystal Strips

Feng-Chia Hsu[1], **Jin-Chen Hsu[2]**, Tsun-Che Huang[1], Chin-Hung Wang[1], Ping Chang[1]; [1]Microsystems Technology Center, Industrial Technology Research Institute -South, Tainan 709, Taiwan, [2]Department of Mechanical Engineering, National Yunlin University of Science and Technology, Douliou 64002, Yunlin, Taiwan

Background, Motivation and Objective

In modern communication systems, high-frequency micromechanical resonators play an important role in frequency references and filters. To have high frequency selectivity for such applications, micromechanical resonators should exhibit high quality (Q) factors. As a result, energy losses in the resonators must be minimized. In practice, micromechanical resonators are anchored to the substrate, and radiation of elastic waves via anchors (anchor loss) occurs. At high frequencies, anchor loss has been reported as the dominate energy loss mechanism in deciding Q values. The objective of this research is to propose a design of anchor loss-free micromechanical resonators for increasing the Q factors.

Statement of Contribution/Methods

In recent years, elastic waves in periodic structures called phononic crystals (PCs) have received great attention [1, 2]. PCs can give rise to complete frequency band gaps in which the elastic waves are stopped, which show their capability of acting as an elastic-wave barrier. Moreover, some of the PC pass bands may exist as the so-called deaf bands that certain types of incident waves also can not effectively transmit energy into the PCs. In this case, the deaf bands can be used to reduce elastic wave transmission. We use PC structures as supports to eliminate the anchor loss in micromechanical resonators. Finite-element (FE) method is used to give a full wave dynamic analysis and to determine the device performance of our design.

Results

We demonstrate a design of extensional wine-glass mode ring resonators supported by PC strips and show the increase in the Q factors. The PC strips effectively stop the leaky waves and isolate the wave energy with the band-gap and deaf-band effects. We present detailed numerical analyses of resonant characteristics of the ring resonators, as well as the dispersion relations, eigenmodes, and transmission properties of the PC strips. The band-gap and deaf-band properties are fully characterized. Design guidelines of the anchor loss-free micromechanical resonators with PCs are given. With the proposed resonator architecture, FE simulations further show that the leaky energy is effectively reduced and the stored energy inside the ring resonators is enhanced simultaneously as operating frequencies of the ring resonators are within the band gap or deaf bands of the PC strips (102-238 MHz).

Discussion and Conclusions

In conclusion, we propose a method for reducing anchor loss in ring resonators by using a PC structure, which can be extended to general micromechanical resonators. Leaky energy is reduced and stored energy is increased simultaneously in the resonators. Realization of a high-Q micromechanical resonator with minimized support loss is expected.

[1] F.-C. Hsu et al., Appl. Phys. Lett. 96 051902 (2010)
[2] J.-C. Hsu and T.-T. Wu, Phys. Rev. B 74, 144303 (2006)

P6C-2

Isolation of acoustic waves in a sensor array utilizing phononic crystals

Yung-Yu Chen[1], Li-Chung Huang[1], Tsung-Tsong Wu[2], Jia-Hong Sun[2]; [1]Department of Mechanical Engineering, Tatung University, Taiwan, [2]Institute of Applied Mechanics, National Taiwan University, Taiwan

Background, Motivation and Objective

In recent years, multiple bulk acoustic wave sensors have been fabricated on a single AT-cut quartz substrate to develop a sensor array for the detection of multiple analyte parameters. Two primary methods, well structure and crystalline inversion, were used to minimize the crosstalk between adjacent sensors. Phononic crystals are synthetic structures with periodic variation of elastic property. The main property is the possibility of having acoustic band gaps. A phononic crystal with band gaps forbids acoustic waves within the frequency ranges of band gaps to propagate through the structure. In this paper, phononic crystals are utilized for isolating acoustic energy of individual bulk acoustic wave sensor and suppressing interference.

Statement of Contribution/Methods

A theoretical investigation on a sensor array consisting of multiple quartz crystal microbalances (QCMs) surrounded by phononic crystals is presented. The resonance responses of a QCM were calculated by finite element analysis. Then a phononic crystal structure of square lattice of air cylinders in quartz substrate was designed to have an complete band gap covering the QCM¡¦s resonance frequency. Finally, QCM sensor arrays with/without six rows of phononic crystals were analyzed to exhibit the isolation performance of the phononic crystals.

Results

Results show that the QCM¡¦s resonance frequency is around 10.11 MHz when the thickness of the AT-cut quartz substrate is 165 £gm. The designed phononic crystal structure, whose lattice constant and filling ratio are 220 £gm and 0.47, has a complete band gap from 9.66 to 10.80 MHz. As shown in Fig. 1, the sensor array with six rows of the designed phononic crystals has a more centralized mode shape. The attenuation of total displacement on the edge of a QCM unit caused by the phononic crystals is about 50 dB.

Discussion and Conclusions

In this paper, we propose a sensor array consisting of multiple quartz crystal microbalances surrounded by phononic crystals. The phononic crystals are utilized to isolate QCMs in the sensor array. Simulation results show that phononic crystals indeed contribute to a confinement of acoustic energy of individual QCM. Accordingly, phononic crystals are verified to be capable of suppressing the crosstalk between adjacent bulk acoustic wave sensors.

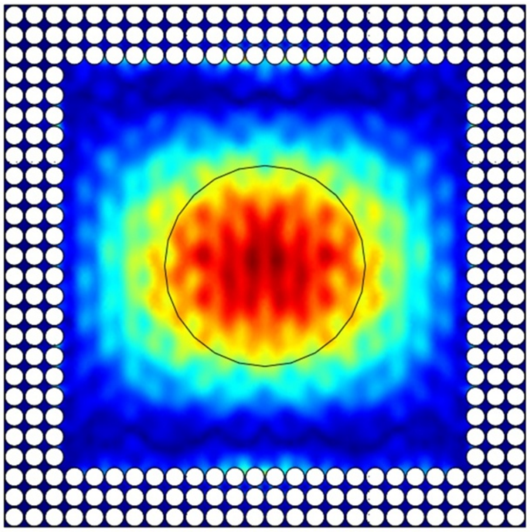

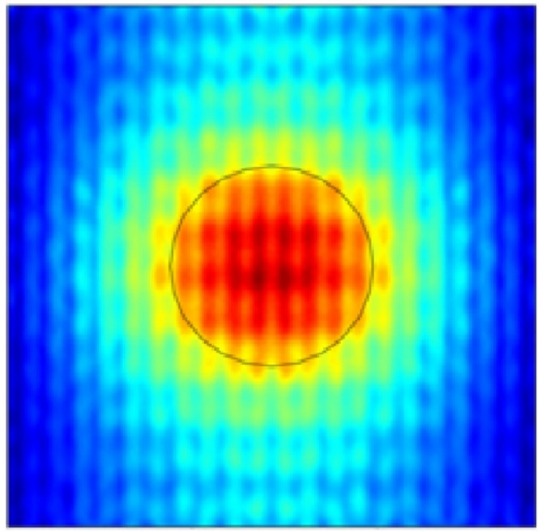

P6C-3

Complex band structure and evanescent Bloch waves in two-dimensional phononic plates

MOURAD OUDICH[1], Badreddine Assouar[1,2]; [1]Institut Jean Lamour, Nancy University - CNRS, Vandoeuvre-lès-Nancy, France, [2]International Joint Laboratory (UMI 2958), Georgia Institute of Technology - CNRS, ATLANTA, USA

Background, Motivation and Objective

Phononic crystals (PC) are periodic structures that consist of two materials with a different elastic constants exhibiting absolute band gap under specific geometrical conditions. Because of the existence of the acoustic band gaps (BG), the PC structure can have many potential applications such as acoustic mirror, waveguides ... Band structures are generally used to describe infinite and finite PC, as they provide one with all propagative waves in the periodic medium, or Bloch waves. The objective of this study is to cope with the evanescent Bloch wave in tree dimensional PC and especially in the finite PC plate.

Statement of Contribution/Methods

Based on a modified plane wave expansion (PWE) method [1, 2], we have dealt with the evanescent Bloch waves in finite phononic plate. We have extended the modified PWE method we developed in our previous work [2] so that it includes complex wave vectors in the direction of propagation at a fixed frequency. The complex PWE method has been used to generate complex band structures for 2D finite PC, especially to deal with phononic slabs. To do so, it is necessary to consider a fixed frequency and to solve for the wave vector.

Results

The complex PWE method for 2D PC plate was developed and used to obtain the complex band structure. Here, we discuss the case of two PC slabs; air holes drilled in silicon plate and gold cylinders embedded in epoxy matrix. Fig. 1 shows an example of band structures related to both structures. Both propagative and evanescent solutions are found at once. The polarization of the evanescent waves was studied to understand the different modes (in-plane and out of plane) coupling occurring in PC slabs and their physical origin. In addition, eigenfrequency contours are obtained which are essential to understand negative and positive refraction in PC.

Discussion and Conclusions

The complex PWE dealing with 2D PC plate allows the obtaining of complex band structures including propagative and evanescent waves. The polarization of the modes involved in the phononic slabs will be discussed. The study of evanescent waves in PC is expected to be incontrovertible to cope with the scattering phenomena, and on the other hand to figure out their behaviour in acoustic metamaterials.

1 V. Laude, Y. Achaoui, S. Benchabane, A. Khelif
Phys. Rev. B., 80 (2009) 092301
2 Z. Hou, M. B. Assouar
Phys. Lett. A, 372 (2008) 2091

FRIDAY POSTER

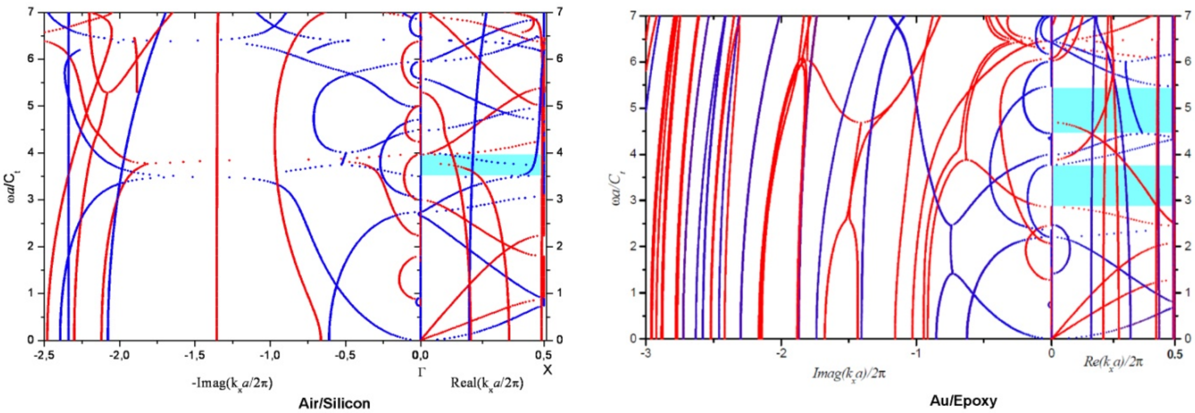

P6C-4

Experimental exploration of imaging properties of a two-dimensional flat lens made of phononic crystals

Etoungh Dimitri Manga[1,2], Lionel Haumesser[1,2], Bruno Morvan[2,3], Anne-Christine Hladky-Hennion[2,4], Emmanuel Le Clézio[1,2]; [1]Laboratoire Imagerie et Cerveau, Equipe Caractérisation Ultrasonore et Piézoélectricité, Blois, France, [2]Fédération Acoustique du Nord Ouest, FR CNRS 3110, France, [3]Université du Havre, Laboratoire Ondes et Milieux Complexes, Le Havre, France, [4]Institut d'Electronique, de Microélectronique et de Nanotechnologie, ISEN, Lille, France

Background, Motivation and Objective

Since it was demonstrated that negative refraction occurs at the interface between two media of different handness in Electromagnetism, researches on phononic crystals which present negative refraction effect grew considerably and lead to interesting results. It was recently proved in an experimental exploration that a phononic crystal slab which has an Effective Refractive Index (ERI) absolute value equal to 1 can achieve a subwavelength resolution (0.35λ) for acoustic imaging.

Statement of Contribution/Methods

In the present paper, this property is applied to evaluate the phononic crystals abilities to medical imaging. In particular, we investigate negative refraction of acoustic waves in a two-dimensional phononic crystal made of stainless steel rods arranged in a triangular lattice and immersed in methanol. The theoretical dispersion curves exhibit a branch with group velocity and phase velocity in opposite directions, and the band are circular around Γ point in the first Brillouin zone which makes the ERI well defined for all incident angles. For experimental investigation, a plane wave transducer is used as acoustic source and the refracted acoustic fields are studied from 0 to 30° incident angles.

Results

The deviation of the incident wave through the phononic crystal slab for incident angles sampling the Brillouin zone is measured experimentally and cut-off angles are defined as functions of the frequency. The equi-frequency contours are deduced from ERI values for all incident angles and allow the determination of the transmission coefficients.

Discussion and Conclusions

For high quality images, acoustic imaging may be done in the regime of All-Angle-Negative-Refraction. In the present study, the final image quality is discussed considering the angular range of the incident beam taken into account by the flat phononic crystal lens.

P6C-5

Ultrasonic Transmission through Plates Perforated with Compound Hole Arrays

Hector Estrada[1,2], Daniel Puig[1], Vicente Gómez-Lozano[1], Antonio Uris[1], Pilar Candelas[1], Francisco Belmar[1], Francisco Meseguer[1,2]; [1]*Centro de Tecnologías Físicas, Valencia, Spain,* [2]*Instituto de Ciencia de Materiales de Madrid (CSIC), Madrid, Spain*

Background, Motivation and Objective

Preliminary results on the measurement of underwater ultrasound transmission through plates perforated with compound hole arrays. Numerical results obtained using rigid solid assumption are presented for complex arrays and compared with a simple rectangular hole lattice measurement.

Statement of Contribution/Methods

Angle dependent transmission calculations are presented for a compound hole array. Measurements at normal incidence for a simple rectangular array (lattice period 6 and 4 mm, hole diameter 3 mm and brass plate thickness 2 mm) are compared with the numerical results. Single point and synthetic aperture technique (SAT) are used.

Results

Calculated sound power transmission τ (gray scale) as a function of the parallel (Q) and incident (k_0) wave numbers is depicted in Figure 1. The compound hole array is showed in the inset at the left whereas the inset at the right shows the path followed by the parallel wave vector (Q_x,Q_y) in the reciprocal space. Complex interplay between Wood anomaly minima, resonant interference minima and resonant full transmission is to observe in the transmission dispersion plot. Figure 2 shows τ as a function of the frequency for a brass plate drilled with a rectangular array of holes measured using a single receiver and using SAT.

Discussion and Conclusions

Complex interference and resonant phenomena take place in compound hole arrays. Preliminary measurements on rectangular arrays show that SAT is required to cope with the large size of the hole array. Differences between SAT and the theory can be explained as due to the finite impedance mismatch between water and brass. More sophisticated numerical models are needed to properly address this issue.

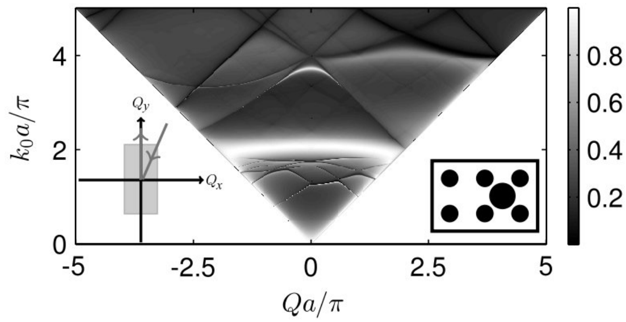

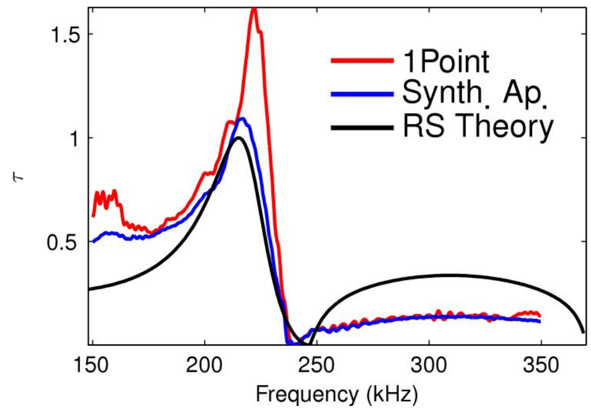

P6C-6

Two-Dimensional Tunable Phononic Crystals

Sz-Chin Lin[1], Tony Huang[1]; [1]Engineering Science and Mechanics, The Pennsylvania State University, University Park, PA, USA

Background, Motivation and Objective

Phononic crystals (PCs) are engineered periodic structures that can manipulate the propagation of acoustic waves. Their versatility in controlling acoustic wave propagation is very useful in wide applications such as ultrasonic imaging, acoustic therapy, and nondestructive evaluation. Explicit control of a phononic band gaps yields desirable operation parameters and improves overall performance in PC-based applications. To further explore the functionalities of PCs, we comprehensively studied the tunability of phononic band gaps in two-dimensional (2D) PCs.

Statement of Contribution/Methods

We present a comprehensive study on the tunability of phononic band gaps in 2D PCs consisting of anisotropic cylinders in an isotropic host, where control of the phononic band gaps results from the reorientation of the anisotropic cylinders. The anisotropic materials considered in this study include cubic, hexagonal, trigonal, and tetragonal materials. A 2D plane wave expansion (PWE) method was used to calculate the variation in phononic band gaps of bulk acoustic waves due to the reorientation of the anisotropic cylinders.

Results

Figure 1 shows the calculate results for a 2D GaAs/epoxy PC. The rotation and slowness curves of GaAs cylinders are illustrated in (a) and (b), respectively. The dispersion curves of bulk acoustic waves propagating in this 2D GaAs/epoxy PC at θ=0° and 45° are presented in (c) and (d), respectively. The shaded areas denote the complete band gaps. We found that we can control the width and position of complete band gaps of this GaAs/epoxy PC, and thus tune the wave blocking and guiding effects, by simply rotating the anisotropic scatterers.

Discussion and Conclusions

We numerically observed that the dispersion relations for bulk acoustic waves propagating in such heterogeneous structures were greatly deformed upon rotation of the anisotropic cylinders. From our theoretical investigations, we suggest that the reorientation of anisotropic cylinders can be a simple and effective way to obtain selective filtering and waveguiding for acoustic metamaterial applications such as acoustic imaging, high intensity focused ultrasound, and NDE.

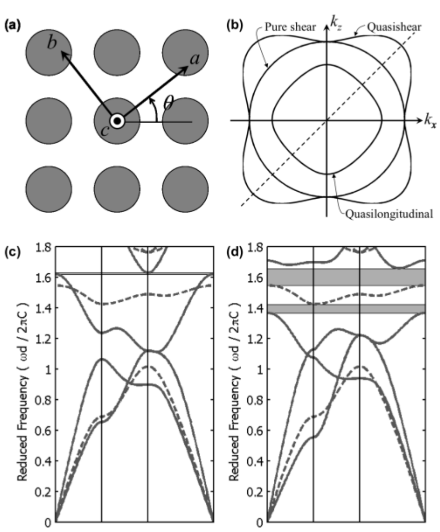

FRIDAY POSTER

P6C-7

Propagation of Surface Acoustic Waves in Two-Dimensional Periodic Structures

Sergey Nikitov[1], Valery Grigorievskii[1], Iosif Kotelyanskii[1], Sergey Suchkov[2]; [1]*IRE RAS, Russian Federation,* [2]*Saratov State University, Russian Federation*

Background, Motivation and Objective

One-dimensional periodic structures of metal electrodes or grooves on crystal surfaces are widely used in modern SAW devices to localize the wave energy in resonators and band pass filters, or to provide desired propagation characteristics from input to output transducers as in dispersive delay lines. The localization of SAW energy in a limited area on the substrate surface similar to wave localization in two-dimensional "photonic" or "phononic" crystals can be interesting from the point of view of application in SAW devices. Recently in [1] there was a theoretical study of interaction of four SAWs in two-dimensional periodic structures of shallow surface corrugations. At the synchronous frequency the analytical solution of COM equations for distribution of wave amplitudes in a rectangular region occupied by two-dimensional periodic structure was found. Also it has been shown that there occurs a reflection of the incident SAW from a rectangular two-dimensional periodic structure due to double Bragg 90°-reflection. The present work was undertaken to investigate experimentally the basic characteristics of SAW propagation in two-dimensional periodic structures.

Statement of Contribution/Methods

Two-dimensional periodic structures of surface corrugations were made by ion etching of the surface of YZ-cut of $LiNbO_3$. Frequency dependencies of transaction and reflection coefficients for Rayleigh SAW propagating in a rectangular region occupied by the two-dimensional periodic structure were measured. To calculate the distribution of wave amplitudes as well as transaction and reflection coefficients a new method based on 2D-transaction matrices was developed. This method can be applied to calculate the wave amplitudes inside the periodic structure at arbitrary distribution of incident wave amplitudes.

Results

Using the measured and calculated results the coupling coefficient for waves propagating along Z and X crystallographic axes was determined. Also it has been shown that if the width of incident acoustic beam is quite narrower than the width of periodic structure, then a resonant enhancement of transaction coefficient arises at the center of the Bragg stop band.

Discussion and Conclusions

The enhancement in transaction coefficient near the center of Bragg stop band can be explained by back reflection, similar to predicted in [1], from the parts of periodic structure, which are not exposed by the narrow acoustic beam. Exactly at the center of Bragg stop band, in accordance with the analytic solution of [1], piecewise-flat distributions of the incident and all scattered SAWs inside the periodic structure are observed.

[1] E. Mayer, V. Plessky, L. Reindl, A. Mayer "Four-Wave Interaction in 2D Periodic Structures," 2010 IEEE Ultrason. Symp. Proc., pp. 1660-1663

P6C-8

Basic Study of Property of Planate Acoustic Lens Constructed with Phononic Crystal Structures

Takenobu TSUCHIYA[1], Tetsuo ANADA[1], Nobuyuki ENDOH[1], Sayuri MATSUMOTO[2], Kazuyoshi MORI[3]; [1]Faculty of Engineering, Kanagawa University, Yokohama, Japan, [2]The Port and Airport Research Institute, Yokosuka, 239-0826, Japan, [3]National Defense Academy, Yokosuka, Japan

Background, Motivation and Objective

The imaging system with acoustic lens was applied in the research of underwater field. The final goal in this study, we develop the acoustic imaging system in Ocean using planate lens with phononic crystal structure. For obtain the basic property of the acoustic lens, we produced the prototype of the planate lens constructed by stainless steel.

In this study, we measured convergence field by planate acoustic lens in water tank. In addition, we simulated convergence field by planate acoustic lens using finite difference time domain method.

Statement of Contribution/Methods

Figure 1 shows schematic diagram of measuring system to obtain convergence field of acoustical lens in water bath. The plate with circular slit that is produced point source fixed forward acoustic lens as sown in Fig. 1. A 5 cycle burst-pulse of 0.7 MHz is radiated from the transmitter. The sound pressure is measured by hydrophone using automatic controlled xyz-stage. In calculation, acoustic parameters of water and stainless steel decide same as experimental data of it.

Results

Normalized sound pressure on propagation axis is shown in Fig.2 for measurement and analysis. It is clearly shown that measured sound pressure almost agrees well with analysis results in Fig. 2. Focal point for measurement and analysis is about 16.5 mm and 17.1 mm, respectively. Measured -3 dB transverse beam width at 4.7 mm is not good agrees with analysis result at 2.2 mm.

Discussion and Conclusions

As a result, Focal point for measurement and analysis is good agreement. However, beam width at -3 dB has different value between measurement and analysis. In further work, we clarify the cause of the difference of beam width of planate acoustic lens constructed by phononic crystal structures.

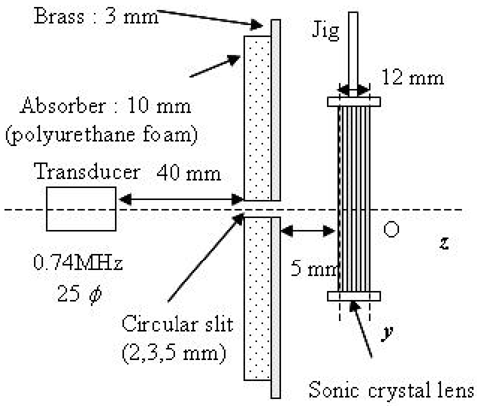

Fig. 1 Model of sound propagation to acoustical lens through sonic crystal structure.

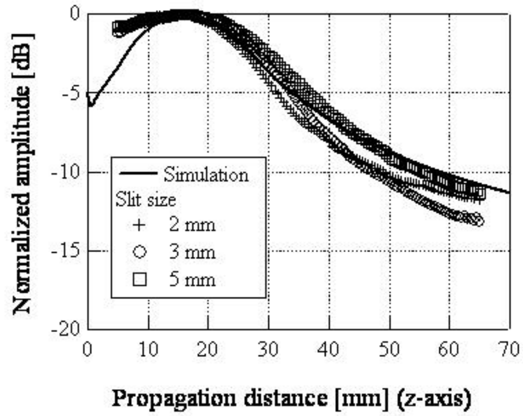

Fig. 2 Measurement and calculation results of sound pressure distribution on axis.

P6C-9

Propagation Characteristics of Surface Acoustic Waves under Hexagonal Phononic Gratings

Ventsislav Yantchev[1], Victor Plessky[2], Ilia Katardjiev[1]; [1]Solid State Electronics, Uppsala University, Uppsala, Sweden, [2]GVR Trade SA, Switzerland

Background, Motivation and Objective

Dispersion characteristics of surface acoustic waves (SAWs) propagating under tungsten hexagonal gratings are initially studied using eigen-frequency finite element analysis (COMSOL Multiphysics).

Statement of Contribution/Methods

A 2D hexagonal grating with a 10μm distance between masses is considered on an isotropic substrate having acoustic properties close to that of the c-oriented Aluminum Nitride (AlN) (see the figure). Frequency stopband SAW characteristics are studied for SAW incidence angles 0 rad and $\pi/6$ rad with respect to the grating structure. Both Rayleigh SAW and surface transverse wave (STW) characteristics are studied.

Results

For hexagonal tungsten gratings with thickness above a critical value (about 900 nm in this case) RSAW stopbands for 0 rad and $\pi/6$ rad incidence penetrate in each other, respectivelly, thus forming a forbidden SAW frequency band lying between the upper stopband edge of the 0 rad incident SAW and the lower stopband edge of the $\pi/6$ rad incident SAW. The lower frequency stopband edge of the STW appeared in close vicinity to its RSAW counterpart, while the upper STW sopband edge seemed to prematurely degrade due to shear wave radiation in to the substrate bulk.

Discussion and Conclusions

In view of the above findings the existence of an omnidirectional frequency stopband is discussed.

This work is supported by the Swedish Research Council (VR)

Session Chairs

Author Index

A

B

C

D

E

F

G

K

L

M

N

O

P

T

U

V

W

X

Y

Z

Floor Plan

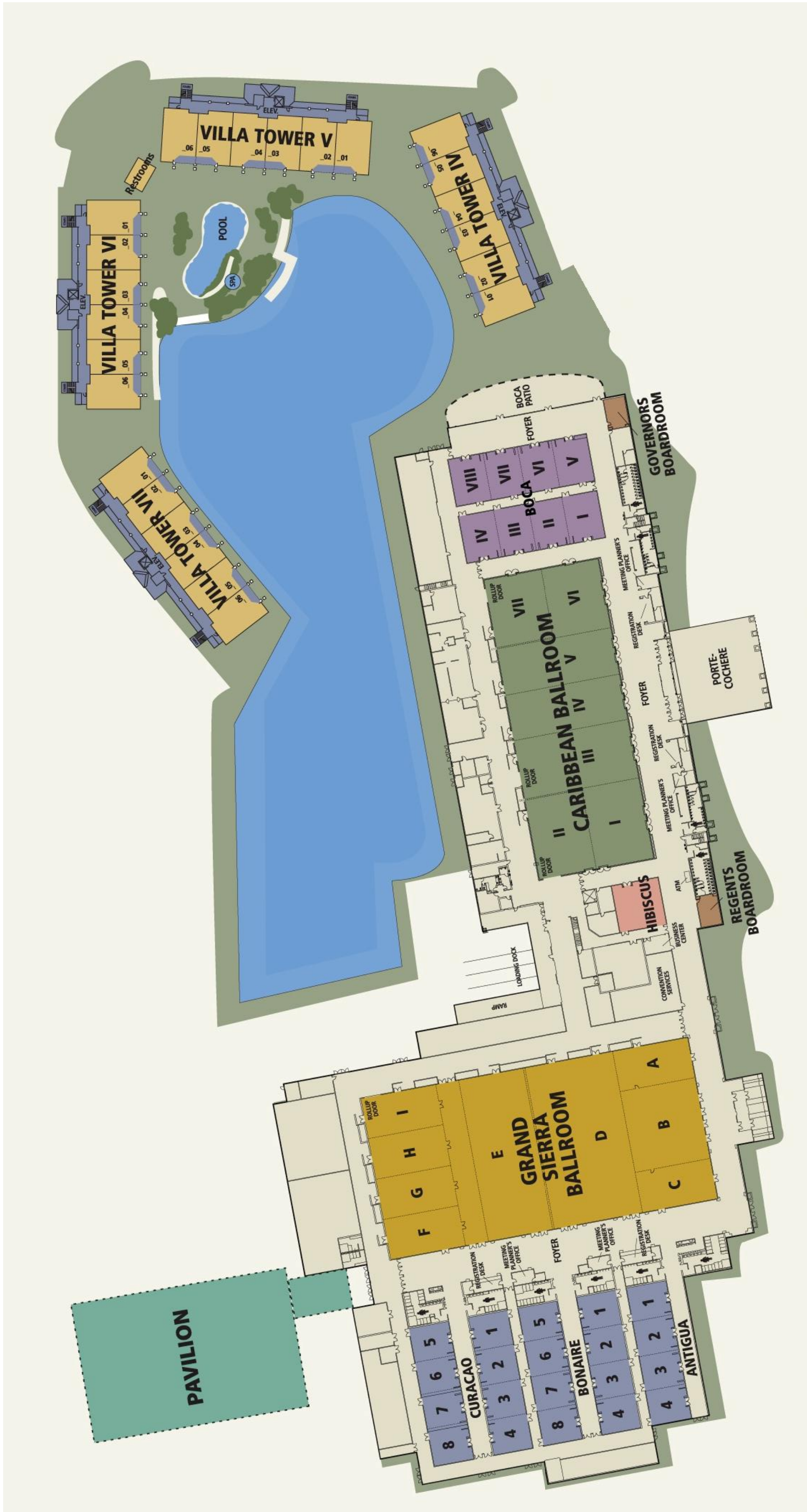
VILLA TOWER V
VILLA TOWER IV
VILLA TOWER VI
VILLA TOWER VII
Restrooms
POOL
SPA
BOCA PATIO
FOYER
BOCA
VIII VII VI V
IV III II I
GOVERNORS BOARDROOM
MEETING PLANNER'S OFFICE
REGISTRATION DESK
CARIBBEAN BALLROOM
VII VI V IV III II I
ROLLUP DOOR
PORTE-COCHERE
HIBISCUS
ATM
BUSINESS CENTER
REGENTS BOARDROOM
CONVENTION SERVICES
LOADING DOCK
RAMP
GRAND SIERRA BALLROOM
A B C D E F G H I
PAVILION
CURACAO
BONAIRE
ANTIGUA

Condensed Program (Tuesday)

Tuesday, Oct. 18	Boca Rooms IV	Boca Rooms V	Boca Rooms VI	Boca Rooms VII	Boca Rooms VIII
Symposium Registration 07:00 – 18:00					
8:00 . - 12:00	**Short Course 1A** Ultrasound Contrast Agents: Theory and Experiment	**Short Course 2A** Ultrasonic Motors: Vibration Generation, Friction drive and Energy Harvesting	**Short Course 3A** Medical Ultrasound Transducers	**Short Course 4A** Phonoic Crystals	**Short Course 5A** Elasticity Imaging: Methods and Applications
12:00 - 13:00	Lunch				
13:00 . - 17:00	**Short Course 1B** Acoustic Microfluidics: Microscale Acoustics and Ultrasonics for Driving Fluids	**Short Course 2B** Ultrasonic Signal Processing for Detection, Estimation and Compression	**Short Course 3B** Processing and Characterization Challenges for Integrated Ferroelectric/Piezoele ctric Devices	**Short Course 4B** Ultrasound Imaging Systems: from Principles to Implementation	**Short Course 5B** Quantitative Ultrasound, Theory and Practice

Condensed Program (Wednesday)

Wednesday, Oct. 19	Boca Rooms II-IV	Boca Rooms VI-VIII	Caribbean Ballroom VII	Caribbean Ballroom I	Caribbean Ballroom II	Caribbean Ballroom VI
	Symposium Registration 07:00 – 18:00			**Exhibits** Caribbean Ballroom III-V, 09:00 - 17:00		
8:00 – 9:30	**Plenary Session**					
9:30 – 13:00	**Refreshments**					
	Poster Session P1 (Caribbean Ballroom III-V)					
10:30– 12:00	Session 1A. Ultrasound Drug Or Gene Delivery and Enhancement	Session 2A. Cardiac Visco-Elasticity and Strain Imaging	Session 3A. Scattering and Attenuation	Session 4A. Physical and Biological Acoutic Sensing	Session 5A. TCF Reduction	Session 6A. CMUTs I Applications
12:00 – 14:00		**Lunch**				
14:00 - 15:30	Session 1B. HIFU Application and Monitoring	Session 2B. Cardiac Beam Forming	Session 3B. Contrast Agents I	Session 4B. Acoustic Tweezers I	Session 5B. Microacoustic Sensors (6J)	Session 6B. Medical Imaging Transducers
13:00 – 16:30	**Refreshments**					
	Poster Session P2 (Caribbean Ballroom III-V)					
16:30 – 18:00	Session 1C. 3D Imaging & Fast Simulation Tools	Session 2C. Advanced Flow Estimation Algorithms and Functional Imaging	Session 3C. Photoacoustics: Applications	Session 4C. Bulk Wave Effects and Devices I	Session 5C. Transverse Modes inSAW (6F)	Session 6C. Transducer Modeling

Condensed Program (Thursday)

Thursday, Oct. 20	Boca Rooms II-IV	Boca Rooms VI-VIII	Caribbean Ballroom VII	Caribbean Ballroom I	Caribbean Ballroom II	Caribbean Ballroom VI
	Symposium Registration 07:00 – 18:00			**Exhibits** Caribbean Ballroom III-V, 09:00 – 17:00		
8:00 – 9:30	Session 1D. Bio-effects and Dosimetry	Session 1D. Bio-effects and Dosimetry	Session 3D. Targeted contrast Agents	Session 4D. Phased Arrays	Session 5D. Radio Frequency Phononic Crystals	Session 6D. CMUTs II Devices
9:30 – 13:00	**Refreshments**					
	Poster Session P3 (Caribbean Ballroom III-V)					
10:30– 12:00	Session 1E. Clinical Session	Session 2E. Bone	Session 3E. Novel Ultrasound Systems	Session 4E. Imaging and Signal Processing	Session 5E. Optical and Electromagnetic Interactions I	Session 6E. Applications
12:00 – 14:00		**Lunch**				
14:00 - 15:30	Session 1F. Synthetic Aperture Beam Forming	Session 2F. Elastography: New Methods	Session 3F. Photoacoustics: Technology Development	Session 4F. Novel Acoustic Wave Sensors	Session 5F. Ultrasonic Motors and Actuators I	Session 6F. BAW Components and Technology (5B)
13:00 – 16:30	**Refreshments**					
	Poster Session P4 (Caribbean Ballroom III-V)					
16:30 – 18:00	Session 1G. Blood Flow Imaging	Session 2G. Shear Wave Elastography	Session 3G. Contrast Agents II	Session 4G. Acoustic Micro Fluidics	Session 5G. Physics of Phononic Crystals	Session 6G. SAW Design, Integration & Tunability

Condensed Program (Friday)

Friday, Oct. 21	Boca Rooms II-IV	Boca Rooms VI-VIII	Caribbean Ballroom VII	Caribbean Ballroom I	Caribbean Ballroom II	Caribbean Ballroom VI
	Symposium Registration 07:00 – 13:00			**Exhibits** Caribbean Ballroom III-V, 09:00 – 13:00		
8:00 – 9:30	Session 1H. CMUT, 3D and Intravascular Imaging Systems	Session 2H. Vascular Elastography	Session 3H. Drug Delivery I	Session 4H. Laser Ultrasonics	Session 5H. Single Crystal Piezoelectrics	Session 6H. SAW Simulation and Devices
9:30 – 13:00	**Refreshments**					
	Poster Session P5 (Caribbean Ballroom III-V)					
10:30– 12:00	Session 1I. Image Processing	Session 2I. Histotripsy and General Therapy	Session 3I. Drug Delivery II	Session 4I. Applications and Measurements of Ultrasonic Energy	Session 5I. Application of Materials	Session 6I. MEMS
12:00 – 14:00		**Lunch**				
14:00 - 15:30	Session 1J. Beam Forming	Session 2J. Ultrasound Therapy of the Brain	Session 3J. Cardiovascular Tissue Characterization	Session 4J. High Resolution Acoustic Imaging	Session 5J. Acoustic Wave Propagation I	Session 6J. Harsh Environment (5C)
13:00 – 16:30	**Refreshments**					
	Poster Session P6 (Caribbean Ballroom III-V)					
16:30 – 18:00	Session 1K. Abdominal Elastography	Session 2K. Vascular Imaging	Session 3K. Functional Imaging & Image Quality	Session 4K. NDE Methods and Analysis	Session 5K. Acoustic Wave Propagation II	Session 6K. Medical Therapy Devices
18:30 – 19:30	**Closing Ceremony** (Caribbean Ballroom)					

Closing Ceremony
Caribbean Ballroom, Friday, October 21, 2011
06:30 p.m. - 07:30 p.m.

Final remarks by
Ken-ya Hashimoto and Clemens Ruppel, General Co-Chairs

Invitation to IUS 2012 in Dresden
Manfred Weihnacht, General Chair

2011 UFFC-S Plenary Speaker
William D. Hunt, Ph.D., Acoustic Based Biosensors—A Window Into the Soul of Biology

Abstract: There are a variety of biosensor approaches in the literature—all with the express intent of transducing some biochemical interaction into an electrical signal. A typical embodiment requires that one first immobilize a molecular recognition element, e.g. an antibody, onto the device surface. When an antigen binds to the antibody the surface physical properties of the device are perturbed, resulting in a change in the electrical signal from the device. For optical biosensors, such as surface plasmon resonance or fiber optic sensors, the operative physical property is the dielectric permittivity of the antibody-antigen space. For acoustic-based biosensors the physical properties perturbed can include mass attachment and stiffness changes in the antibody-antigen space. If we look more closely into the world of biology, we find that **every** biomolecular event has three essential components: i) molecular recognition, ii) conformational change and iii) ATP (adenosine triphosphate) as an energy source. The beer you will be drinking during this talk would not be possible if the yeast (e.g. *Saccharomyces cerevisiae*) involved in the brewing did not actively engage in the use of molecular recognition, conformational change and ATP. Acoustic wave biosensors inherently probe i) and ii) of this canonical set of molecular biology. In this talk we will present more on the underlying molecular biology. In addition we will discuss work from our lab at Georgia Tech as well as from labs around the globe where acoustic-based biosensors are being used to tease out information regarding the details of biomolecular events. The seeds of this approach have been laid in theoretical work within the UFFC community as well as those who have delved into digital radio in such areas as QAM (quadrature amplitude modulation) systems.

Biography of the speaker

William D. Hunt, Ph.D. is Professor of Electrical Computer Engineering at the Georgia Institute of Technology and is Adjunct Professor in the Department of Hematology and Oncology at the Emory University School of Medicine. He runs the Microelectronics Acoustics Group at Georgia Tech and has a diverse collection of graduate students which has included students from Electrical Engineering, Biomedical Engineering and Chemistry.

He joined the electrical engineering faculty at Georgia Tech following completion of his Ph.D. degree. Special recognitions he has received include the NSF Presidential Young Investigator Award in 1989, the DuPont Young Faculty Award in 1988, the University of Alabama Distinguished Engineering Fellowship in 1994. Dr. Hunt was a Rhodes Scholar Finalist in 1975. His "dog on a chip" invention which is a chip which can do specific molecular recognition of compounds in the vapor phase garnered world-wide press culminating in Dr. Hunt's appearance in the January 12, 2004 issue of Time Magazine in their inaugural article on Innovators. His area of expertise is in the area of Microelectronic acoustic devices for wireless applications as well as chemical and biological sensors based on this technology. He has published over 70 papers in refereed journals and conference proceedings. He holds 8 US patents and 6 provisional patents. He is a Senior Member of the IEEE and served as a Distinguished Lecturer for the IEEE Sensors Council from 2006 to 2008 and is currently serving as a Distinguished Lecturer for the IEEE Ultrasonics, Ferroelectrics and Frequency Control Society.

Notes